frontiers | Research Topics

Novel biomarkers for anticancer therapy

Edited by
Hongtao Xiao, Zhe-Sheng Chen, Liang Ouyang,
Ting Wang and Chen Shi

Published in
Frontiers in Pharmacology
Frontiers in Oncology

FRONTIERS EBOOK COPYRIGHT STATEMENT

The copyright in the text of individual articles in this ebook is the property of their respective authors or their respective institutions or funders. The copyright in graphics and images within each article may be subject to copyright of other parties. In both cases this is subject to a license granted to Frontiers.

The compilation of articles constituting this ebook is the property of Frontiers.

Each article within this ebook, and the ebook itself, are published under the most recent version of the Creative Commons CC-BY licence. The version current at the date of publication of this ebook is CC-BY 4.0. If the CC-BY licence is updated, the licence granted by Frontiers is automatically updated to the new version.

When exercising any right under the CC-BY licence, Frontiers must be attributed as the original publisher of the article or ebook, as applicable.

Authors have the responsibility of ensuring that any graphics or other materials which are the property of others may be included in the CC-BY licence, but this should be checked before relying on the CC-BY licence to reproduce those materials. Any copyright notices relating to those materials must be complied with.

Copyright and source acknowledgement notices may not be removed and must be displayed in any copy, derivative work or partial copy which includes the elements in question.

All copyright, and all rights therein, are protected by national and international copyright laws. The above represents a summary only. For further information please read Frontiers' Conditions for Website Use and Copyright Statement, and the applicable CC-BY licence.

ISSN 1664-8714
ISBN 978-2-83251-385-9
DOI 10.3389/978-2-83251-385-9

About Frontiers

Frontiers is more than just an open access publisher of scholarly articles: it is a pioneering approach to the world of academia, radically improving the way scholarly research is managed. The grand vision of Frontiers is a world where all people have an equal opportunity to seek, share and generate knowledge. Frontiers provides immediate and permanent online open access to all its publications, but this alone is not enough to realize our grand goals.

Frontiers journal series

The Frontiers journal series is a multi-tier and interdisciplinary set of open-access, online journals, promising a paradigm shift from the current review, selection and dissemination processes in academic publishing. All Frontiers journals are driven by researchers for researchers; therefore, they constitute a service to the scholarly community. At the same time, the *Frontiers journal series* operates on a revolutionary invention, the tiered publishing system, initially addressing specific communities of scholars, and gradually climbing up to broader public understanding, thus serving the interests of the lay society, too.

Dedication to quality

Each Frontiers article is a landmark of the highest quality, thanks to genuinely collaborative interactions between authors and review editors, who include some of the world's best academicians. Research must be certified by peers before entering a stream of knowledge that may eventually reach the public - and shape society; therefore, Frontiers only applies the most rigorous and unbiased reviews. Frontiers revolutionizes research publishing by freely delivering the most outstanding research, evaluated with no bias from both the academic and social point of view. By applying the most advanced information technologies, Frontiers is catapulting scholarly publishing into a new generation.

What are Frontiers Research Topics?

Frontiers Research Topics are very popular trademarks of the *Frontiers journals series*: they are collections of at least ten articles, all centered on a particular subject. With their unique mix of varied contributions from Original Research to Review Articles, Frontiers Research Topics unify the most influential researchers, the latest key findings and historical advances in a hot research area.

Find out more on how to host your own Frontiers Research Topic or contribute to one as an author by contacting the Frontiers editorial office: frontiersin.org/about/contact

Novel biomarkers for anticancer therapy

Topic editors

Hongtao Xiao — University of Electronic Science and Technology of China, China
Zhe-Sheng Chen — St. John's University, United States
Liang Ouyang — Sichuan University, China
Ting Wang — Sichuan Cancer Hospital, China
Chen Shi — Huazhong University of Science and Technology, China

Citation

Xiao, H., Chen, Z.-S., Ouyang, L., Wang, T., Shi, C., eds. (2023). *Novel biomarkers for anticancer therapy*. Lausanne: Frontiers Media SA. doi: 10.3389/978-2-83251-385-9

Table of contents

07 Editorial: Novel biomarkers for anticancer therapy
Ting Wang, Zhe-Sheng Chen, Chen Shi, Liang Ouyang and Hongtao Xiao

10 Survival Prediction of Patients Treated With Immune Checkpoint Inhibitors *via* KRAS/TP53/EGFR-Single Gene Mutation
Shui Liu, Shuai Geng, Ning Shi, Lili Zhang, Wenxin Xue, Yiwen Li and Kai Jiang

19 LncRNA ENST869 Targeting Nestin Transcriptional Region to Affect the Pharmacological Effects of Chidamide in Breast Cancer Cells
Xiuyan Feng, Han Han, Yarui Guo, Xue Feng, Shanchun Guo and Weiqiang Zhou

31 Efficacy and Safety Evaluation of Sintilimab for Cancer Treatment: A Systematic Review and Meta-analysis of Randomized Controlled Trials
Ziqi Ye, Wenchao Yang, Bixia Xuan, Xiaofang Li, Jiana He, Haiyan Si and Wenhua Ma

39 lncRNA PRADX is a Mesenchymal Glioblastoma Biomarker for Cellular Metabolism Targeted Therapy
Can Xu, Jixing Zhao, Jia Song, Menglin Xiao, Xiaoteng Cui, Lei Xin, Jianglong Xu, Yuhao Zhang, Kaikai Yi, Biao Hong, Fei Tong, Shaohui Tian, Yanli Tan, Chunsheng Kang and Chuan Fang

53 Long Noncoding RNA HAGLROS Promotes the Malignant Progression of Bladder Cancer by Regulating the miR-330-5p/SPRR1B Axis
Shiwei Xiao, Yigang Zuo, Yanan Li, Yinglong Huang, Shi Fu, Dongbo Yuan, Xuhua Qiao, Haifeng Wang and Jiansong Wang

65 Advances in Research on the Effects and Mechanisms of Chemokines and Their Receptors in Cancer
Jing Xu, Jing-quan Li, Qi-lei Chen, Elena A. Shestakova, Vsevolod A. Misyurin, Vadim S. Pokrovsky, Elena M. Tchevkina, Hu-biao Chen, Hang Song and Jian-ye Zhang

76 Programmed Cell Death Protein 1/Programmed Cell Death Protein Ligand 1 Immunosuppressants in Advanced Non-Small Cell Lung Cancer Research Progress in Treatment
Feng Li, Binchi Liao, Ting Wang, Tingting Qi and Yixin Wang

86 Chemotherapy Combined With Immunotherapy as a First-Line Treatment Brings Benefits to Patients With Lung Squamous Cell Carcinoma but Different Risks of Adverse Reactions: A Systematic Review and Meta-Analysis
Qian Chen, Zhen Zhang, Xiaoli Li and Lingbiao Bu

98 Clinical Significance of Serum Haptoglobin and Protein Disulfide-Isomerase A3 in the Screening, Diagnosis, and Staging of Colorectal Cancer
Yajin Niu, Jun Xue, Xueliang Wu, Ming Qu, Likun Wang, Weizheng Liang and Tian Li

109 Therapeutic Implications of FABP4 in Cancer: An Emerging Target to Tackle Cancer
Naihui Sun and Xing Zhao

118 Comparison of Adverse Reactions Caused by Olaparib for Different Indications
Yujing Zhou, Shengwen Zhao, Tong Wu and Han Zhang

128 ACSL4 as a Potential Target and Biomarker for Anticancer: From Molecular Mechanisms to Clinical Therapeutics
Jun Hou, Changqing Jiang, Xudong Wen, Chengming Li, Shiqiang Xiong, Tian Yue, Pan Long, Jianyou Shi and Zhen Zhang

138 RAB39B as a Chemosensitivity-Related Biomarker for Diffuse Large B-Cell Lymphoma
Cong Xu, Ting Liang, Jing Liu and Yunfeng Fu

151 A Multicenter Study of 239 Patients Aged Over 70 Years With Diffuse Large B-Cell Lymphoma in China
Chunli Yang, Qiaoer Li, Ke Xie, Yakun Zhang, Dania Xiang, Yunwei Han and Liqun Zou

160 A Novel Anti-Cancer Therapy: CRISPR/Cas9 Gene Editing
Xin-Zhu Chen, Rong Guo, Cong Zhao, Jing Xu, Hang Song, Hua Yu, Christian Pilarsky, Firzan Nainu, Jing-Quan Li, Xin-Ke Zhou and Jian-Ye Zhang

170 Novel GIRlncRNA Signature for Predicting the Clinical Outcome and Therapeutic Response in NSCLC
Qiangzhe Zhang, Xicheng Liu, Zhinan Chen and Sihe Zhang

189 The role of NPC1L1 in cancer
Renshuai Zhang, Jun Zeng, Wenjing Liu, Jingsen Meng, Chao Wang, Lingyu Shi, Shanbo Yang, Jing Chang and Dongming Xing

198 Significant metabolic alterations in non-small cell lung cancer patients by epidermal growth factor receptor-targeted therapy and PD-1/PD-L1 immunotherapy
Chen Yan, Dan Wu, Lingling Gan, Jun Wang, Wenyu Yang and Bei Xu

212 The expression and significance of efferocytosis and immune checkpoint related molecules in pancancer samples and the correlation of their expression with anticancer drug sensitivity
Lin Cheng, Bangbi Weng, Changsheng Jia, Lin Zhang, Bin Hu, Li Deng, Nan Mou, Fengjun Sun and Jing Hu

224 Whole-exome sequencing and bioinformatics analysis of a case of non-alpha-fetoprotein-elevated lung hepatoid adenocarcinoma
Yao Yao, Xiaojiao Guan, Guangyao Bao, Jie Liang, Tian Li and Xinwen Zhong

237 Cathepsin L promotes chemresistance to neuroblastoma by modulating serglycin
Xiaohuan Du, Leyun Ding, Shungen Huang, Fang Li, Yinghui Yan, Ruze Tang, Xinyuan Ding, Zengyan Zhu and Wenjuan Wang

250 Exploring the oncogenic roles of LINC00857 in pan-cancer
Xiaomin Ren, Jing Liu, Rui Wang, Xinling Liu, Xiaolin Ma, Zhong Lu, Zhenbo Hu, Mingzhu Zheng, Jingang Ma and Jiaqiu Li

273 Identification and verification of hub genes associated with the progression of non-small cell lung cancer by integrated analysis
Xie Mengyan, Ding Kun, Jing Xinming, Wei Yutian and Shu Yongqian

287 RSK2 promotes melanoma cell proliferation and vemurafenib resistance *via* upregulating cyclin D1
Hai-Zhou Wu, Lan-Ya Li, Shi-Long Jiang, Yi-Zhi Li, Xiao-Mei Shi, Xin-Yuan Sun, Zhuo Li and Yan Cheng

298 A novel small molecule RK-019 inhibits *FGFR2*-amplification gastric cancer cell proliferation and induces apoptosis *in vitro* and *in vivo*
Jun Zeng, Kai Ran, Xinyue Li, Longyue Tao, Qiwei Wang, Jiangtao Ren, Rong Hu, Yongxia Zhu, Zhihao Liu and Luoting Yu

318 Effects of PPIs use on clinical outcomes of urothelial cancer patients receiving immune checkpoint inhibitor therapy
Lilong Zhang, Chen Chen, Dongqi Chai, Chunlei Li, Tianrui Kuang, Li Liu, Keshuai Dong, Wenhong Deng and Weixing Wang

327 Comprehensive analysis of FRAS1/FREM family as potential biomarkers and therapeutic targets in renal clear cell carcinoma
Ganggang Wang, Zheng Wang, Haiquan Lu, Zhiqun Zhao, Liqiang Guo, Feng Kong, Aizhen Wang and Shengtian Zhao

347 Insights into the roles and driving forces of CCT3 in human tumors
Jingang Ma, Ping Song, Xinling Liu, Changgeng Ma, Mingzhu Zheng, Xiaomin Ren, Rui Wang, Wenshan Liu, Zhong Lu and Jiaqiu Li

366 Short-chain L-3-hydroxyacyl-CoA dehydrogenase: A novel vital oncogene or tumor suppressor gene in cancers
He Fang, Hanyang Li, Hang Zhang, Shu Wang, Shuang Xu, Li Chang, Yongsheng Yang and Ranji Cui

378 Identification of a novel ferroptosis-related gene signature associated with prognosis, the immune landscape, and biomarkers for immunotherapy in ovarian cancer
Yilong Liu, Suya Du, Mengying Yuan, Xia He, Changyu Zhu, Ke Han, Yuyan Zhu, Qianwen Yang and Rongsheng Tong

398 miRNAs in anti-cancer drug resistance of non-small cell lung cancer: Recent advances and future potential
Hang Yan, Shengjie Tang, Shoujun Tang, Jun Zhang, Haiyang Guo, Chao Qin, Haiyang Hu, Chuan Zhong, Li Yang, Yunhe Zhu and Haining Zhou

414 SLC11A1 associated with tumor microenvironment is a potential biomarker of prognosis and immunotherapy efficacy for colorectal cancer
Yiming Ma, Lei Zhan, Jun Yang and Jingdong Zhang

frontiers | Frontiers in Pharmacology

TYPE Editorial
PUBLISHED 06 January 2023
DOI 10.3389/fphar.2022.1109761

Check for updates

OPEN ACCESS

EDITED AND REVIEWED BY
Dianwen Ju,
Fudan University, China

*CORRESPONDENCE
Hongtao Xiao,
xht927@163.com

SPECIALTY SECTION
This article was submitted to Pharmacology of Anti-Cancer Drugs, a section of the journal Frontiers in Pharmacology

RECEIVED 28 November 2022
ACCEPTED 12 December 2022
PUBLISHED 06 January 2023

CITATION
Wang T, Chen Z-S, Shi C, Ouyang L and Xiao H (2023), Editorial: Novel biomarkers for anticancer therapy.
Front. Pharmacol. 13:1109761.
doi: 10.3389/fphar.2022.1109761

COPYRIGHT
© 2023 Wang, Chen, Shi, Ouyang and Xiao. This is an open-access article distributed under the terms of the Creative Commons Attribution License (CC BY). The use, distribution or reproduction in other forums is permitted, provided the original author(s) and the copyright owner(s) are credited and that the original publication in this journal is cited, in accordance with accepted academic practice. No use, distribution or reproduction is permitted which does not comply with these terms.

Editorial: Novel biomarkers for anticancer therapy

Ting Wang[1], Zhe-Sheng Chen[2], Chen Shi[3,4], Liang Ouyang[5] and Hongtao Xiao[6]*

[1]Department of Clinical Research, Sichuan Cancer Hospital and Institution, Sichuan Cancer Center, School of Medicine, University of Electronic Science and Technology of China, Chengdu, China, [2]Department of Pharmaceutical Sciences, College of Pharmacy and Health Sciences, St. John's University, Queens, NYC, United States, [3]Department of Pharmacy, Union Hospital, Tongji Medical College, Huazhong University of Science and Technology (HUST), Wuhan, China, [4]Hubei Province Clinical Research Center for Precision Medicine for Critical Illness, Wuhan, China, [5]State Key Laboratory of Biotherapy, Sichuan University-University of Oxford Huaxi Joint Centre for Gastrointestinal Cancer, West China Hospital, Sichuan University, Chengdu, China, [6]Department of Pharmacy, Sichuan Cancer Hospital and Institution, Sichuan Cancer Center, School of Medicine, University of Electronic Science and Technology of China, Chengdu, China

KEYWORDS

biomarker, anticancer, non-coding RNAs, chemoresisitance, gene mutation, metabolic reprogramming

Editorial on the Research Topic
Novel biomarkers for anticancer therapy

Cancer is a serious chronic disease that poses a great threat to human health worldwide. Despite the rapid development of targeted therapy and immunotherapy in recent years, the diagnosis and treatment of cancer are still facing huge challenges due to high tumor heterogeneity, a lack of typical biomarkers, and therapeutic resistance. Therefore, it is of great significance to reveal novel and reliable biomarkers in cancer; illustrate the mechanisms of cancer occurrence, development, and therapeutic resistance; and develop new anticancer drugs with high efficacy and low toxicity. The Research Topic titled "*Novel Biomarkers for Anticancer Therapy*" was opened between 21 January 2022 and 21 July 2022. Finally, a total of 32 articles (8 reviews, 5 systemic reviews, and 19 original articles) were accepted in 90 submissions, providing a new and promising direction for future anticancer therapy.

Non-coding RNAs (ncRNAs) are emerging RNA molecules that have been found to play essential roles in cancer progression and therapeutic resistance. In recent decades, ncRNAs have gradually attracted the attention of researchers worldwide. In this Research Topic, five articles focus on lncRNAs, an ncRNA that has more than 200 nucleotides and various functions (Tan et al., 2021). Feng et al. found that the lncRNA ENST869 was upregulated in MCF-7 and MDA-MB-231 cells treated with chidamide. Subsequent experiments suggested that lncRNA ENST869 could promote nestin transcription by binding to the nestin transcriptional region, thus affecting the sensitivity of breast cancer to chidamide. Xiao et al. explored the role of lncRNA HAGLROS in bladder cancer (BC) and discovered that HAGLROS could facilitate BC progression by modulating the miR-330-5p/SPRR1B axis. Additionally, the upregulation of lncRNA PRADX induced by the UNX1-CBFβ complex can accelerate energy metabolism, leading to expediting mesenchymal glioblastoma (GBM) development and poor prognosis in mesenchymal GBM patients (Xu et al.). A pan-cancer analysis revealed that LINC00857 was upregulated in various tumors and associated with an immunosuppressive microenvironment, implying that LINC00857 might serve as a valuable biomarker and therapeutic target for immunotherapy (Ren et al.). Zhang et al. identified genomic instability-related lncRNAs (GIRlncRNAs) in non-small cell lung cancer (NSCLC) and

subsequently constructed a risk-scoring model based on a GIRlncRNA signature, contributing to the future of personalized treatment for NSCLC. In addition to lncRNAs, another essential class of ncRNAs, microRNAs (miRNAs), also have momentous effects on the proliferation, migration, and invasion of tumor cells. Yan et al. summarize the latest advances of miRNAs in therapeutic resistance in NSCLC and discuss their potential clinical values.

Chemotherapy, as an important cancer treatment, can effectively reduce the recurrence and metastasis of many malignant tumors. However, many negative factors, such as larger adverse reactions and drug resistance, seriously hinder the clinical use of chemotherapeutic drugs. Zhou et al. compare the adverse reactions of olaparib in the treatment of three types of cancer *via* meta-analysis, showing that the adverse reactions of olaparib in the treatment of different cancers are themselves different and suggesting that clinicians should conduct a specific analysis of the treatments of different cancers. Recent evidence uncovered by Du et al. suggests that cathepsin L could reduce the sensitivity of neuroblastoma to cisplatin and doxorubicin by elevating the expression of SRGN. In addition, Xu et al. found that the overexpression of RAB39B could augment doxorubicin and vincristine resistance in diffuse large B-cell lymphoma (DLBCL). Yang et al. conducted a multicenter study to predict the clinical characteristics, survival outcomes, and prognosis of elderly patients with DLBCL. This study could help doctors to provide more appropriate treatment options for elderly patients with DLBCL. Nine hub genes, which may modulate NSCLC progression and cisplatin resistance, were identified by Mengyan et al., but more experiments are needed to verify their conclusion.

In recent years, tremendous advances in targeted therapy and immunotherapy have brought hope of survival to many cancer patients. Vemurafenib, a targeted anticancer drug, has been approved for the treatment of BRAF-mutated melanoma patients (Kramkimel et al., 2016). Wu et al. found that RSK2 could interact with FOXO1 to elevate cyclin D1 expression, resulting in the upregulation of cell proliferation and vemurafenib resistance in melanoma. It was found that fibroblast growth factor receptors (FGFRs) are potential targets for gastric cancer. Notably, Zeng et al. synthesized a novel FGFR inhibitor RK-019 and demonstrate its anticancer activity *in vitro* and *in vivo*.

Furthermore, Cheng et al. performed a comprehensive analysis of 15 efferocytosis-associated molecules and 12 immune checkpoint-related molecules in 16 cancer types, including the construction of a protein-protein interaction network, differential expression analysis, correlation analyses with overall survival (OS), tumor microenvironment, and anticancer drug sensitivity. Finally, they conclude that targeting these molecules might be instrumental to overcoming drug resistance and improving patient outcomes. Immunotherapy based on immune checkpoint inhibitors (ICIs) has seen rapid development in the field of clinical cancer treatment. Li et al. reviewed the action mechanisms and clinical trials of PD-1/PD-L1 inhibitors and approved PD-1/PD-L1 inhibitors in advanced NSCLC. Additionally, four meta-analyses about the clinical use of ICIs were included in our Research Topic. In one of these studies, the clinical outcomes of urothelial cancer patients who were simultaneously treated with ICIs and proton pump inhibitors (PPIs) were predicted, showing that concomitant PPI use led to increased progression and death risk and a decreased objective response rate (Zhang et al.). Moreover, Ye et al. clarify that sintilimab could significantly improve OS and progression-free survival (PFS) compared with other anticancer drugs. Sintilimab might become a promising treatment strategy for cancer. Many studies have shown that chemotherapy was not only cytotoxic but also had an effect on activating the anti-tumor immune response, implying that chemotherapy, combined with immunotherapy, may be an effective strategy for the treatment of malignant tumors (Wu and Waxman, 2018). Chen et al. unveil that chemotherapy combined with immunotherapy brings better survival benefits but a higher risk of adverse reactions for squamous NSCLC patients compared with the chemotherapy group.

An altered tumor microenvironment (TME) is highly likely to affect tumor progression, such as tumor metastasis and immunotherapy efficacy. Solute carrier family 11, member 1 (SLC11A1), related to TME, was reported to be positively correlated with immune cell infiltration, including macrophage and fibroblast, and its high expression could reduce immunotherapy benefits in colorectal cancer (CRC). At the end of the article, the authors conclude that SLC11A1 may serve as a promising biomarker and therapeutic target in CRC (Ma et al.). In another study analyzed from a pan-cancer perspective, Ma et al. found that CTT3 depletion could promote immune cell infiltration and some immune checkpoint gene expressions, including CD274, PDCD1, and CTLA4. Additionally, TP53, KRAS, and some epigenetic factors were found to play essential roles in the high expression of CTT3. Interestingly, accumulating studies have shown that a novel form of cell death called ferroptosis could influence immunotherapy efficacy by regulating TME. Therefore, the identification of ferroptosis-related prognostic genes in ovarian cancer (OV) could help to improve prognoses and promote precision immunotherapy, posing benefits to OV patients (Liu et al.).

Gene mutation exerts a critical role in carcinogenesis and cancer development. A comprehensive and deeper understanding of gene mutation exerted in cancer aids cancer diagnosis and treatment. A study performed by Liu et al. explores the correlation between KRAS/EGFR/TP53 single gene mutation and the survival benefits of cancer patients treated with ICIs. Their results show that the OS and PFS of patients with KRAS, EGFR, or TP53 mutation were substantially elevated, suggesting that the detection of genetic mutations in patients will help to predict the clinical benefits of patients receiving ICIs. Hepatoid adenocarcinoma of the lung (HAL) is an infrequent tumor and lacks unified diagnostic standards, resulting in late diagnosis and poor prognosis. Yao et al. discovered two driver mutation genes and nine potential driver mutation genes in HAL, providing a guide for the diagnosis and treatment of this rare malignant tumor for future use. CRISPR/Cas9, as a novel and efficient gene editing technology, has motivated the rapid development of research about cancer initiation, progression, and drug resistance. Ongoing clinical trials based on CRISPR/Cas9 are providing therapeutic strategies for cancer related to gene mutation (Chen et al.).

Metabolic reprogramming is one of the vital hallmarks of cancers. Tumor cells are able to meet their survival needs in some adverse environments by altering their metabolism. Research focused on energy metabolism is currently ongoing. Yan et al. performed a metabolomics analysis in NSCLC patients receiving epidermal growth factor receptor tyrosine kinase inhibitors (EGFR-TKIs) or PD-1/PD-L1 inhibitors and found that EGFR-TKIs and PD-1/PD-L1 inhibitors could promote lipid and amino acid metabolism alterations, providing a new direction for elucidating the antitumor

mechanisms of targeted therapy and immunotherapy. Lipids not only act as biological membrane components but also as signaling molecules in many key signaling pathways and essential sources of cellular energy (Bian et al., 2021). A lot of regulatory molecules, which participate in lipid metabolism, exhibit significant roles in the proliferation, migration, and invasion of tumor cells. Four reviews respectively summarize the roles of fatty acid-binding proteins (Sun et al.), acyl-CoA synthetase long-chain family 4 (Hou et al.), Niemann-Pick C1-like 1 (Zhang et al.), and hydroxy Acyl-CoA Dehydrogenase (Fang et al.) in cancer, including their structures, distribution, functions, and clinical significance. Thus, these molecules might be ideal therapeutic targets in cancer treatment.

Early screening, diagnosis, and treatment of tumors can greatly improve prognoses and reduce mortality. Therefore, it is vital to identify typical and reliable biomarkers in malignant tumors. Niu et al. discovered two markers (haptoglobin and protein disulfide-isomerase A3) in the serum of patients with CRC. They may become ideal tumor markers like traditional carcinoembryonic antigens and carbohydrate antigens (19-9) in CRC. Furthermore, Wang et al. reveal the roles of Fraser syndrome protein 1(FRAS1)/fras1-related extracellular matrix protein (FREM) family members in kidney clear cell renal cell carcinoma. As described by them, FRAS1/FREM family members could act as dependable predictors of cancer progression and targeted therapeutic drug response in kidney clear cell renal cell carcinoma. Xu et al. sum up the effects of chemokines and their receptors in cancer and look at them as significant markers in the future of screening, diagnosis, and treatment of tumors.

In summary, the "*Novel Biomarkers for Anticancer Therapy*" Research Topic collects studies focused on finding novel biomarkers and therapeutic targets in cancer, paving the way for developing novel therapeutic strategies and overcoming therapeutic resistance. We hope that accumulating research associated with carcinogenesis, cancer progression, and therapeutic resistance will help improve survival outcomes and prognoses for cancer patients in the future.

Author contributions

TW and HX contributed to the writing and reviewing of this editorial. All authors contributed to the article and approved the submitted version.

Funding

This work was mainly supported by the Sichuan Science and Technology Program (2022ZYD0092, 2021YFH0144 and 2020JDTD0029).

Conflict of interest

The authors declare that the research was conducted in the absence of any commercial or financial relationships that could be construed as a potential conflict of interest.

Publisher's note

All claims expressed in this article are solely those of the authors and do not necessarily represent those of their affiliated organizations, or those of the publisher, the editors and the reviewers. Any product that may be evaluated in this article, or claim that may be made by its manufacturer, is not guaranteed or endorsed by the publisher.

References

Bian, X., Liu, R., Meng, Y., Xing, D., Xu, D., and Lu, Z. (2021). Lipid metabolism and cancer. *J. Exp. Med.* 218 (1), e20201606. doi:10.1084/jem.20201606

Kramkimel, N., Thomas-Schoemann, A., Sakji, L., Golmard, J., Noe, G., RegniEr-RosEnchEr, E., et al. (2016). Vemurafenib pharmacokinetics and its correlation with efficacy and safety in outpatients with advanced BRAF-mutated melanoma. *Target Oncol.* 11 (1), 59–69. doi:10.1007/s11523-015-0375-8

Tan, Y. T., Lin, J. F., Li, T., Li, J. J., Xu, R. H., and Ju, H. Q. (2021). LncRNA-mediated posttranslational modifications and reprogramming of energy metabolism in cancer. *Cancer Commun. (Lond).* 41 (2), 109–120. doi:10.1002/cac2.12108

Wu, J., and Waxman, D. J. (2018). Immunogenic chemotherapy: Dose and schedule dependence and combination with immunotherapy. *Cancer Lett.* 419, 210–221. doi:10.1016/j.canlet.2018.01.050

frontiers in Pharmacology

SYSTEMATIC REVIEW
published: 23 March 2022
doi: 10.3389/fphar.2022.878540

Survival Prediction of Patients Treated With Immune Checkpoint Inhibitors *via* KRAS/TP53/EGFR-Single Gene Mutation

*Shui Liu[1†], Shuai Geng[2†], Ning Shi[2†], Lili Zhang[1], Wenxin Xue[1], Yiwen Li[1] and Kai Jiang[3]**

[1]Department of Pharmacy, Emergency General Hospital, Beijing, China, [2]Department of Pharmacy, Strategic Support Force Medical Center, Beijing, China, [3]Department of Gastroenterology, Traditional Chinese Medical Hospital of Zhuji, Zhuji, China

Background: Immune checkpoint inhibitors (ICIs) have become an effective treatment option for cancer. KRAS, EGFR and TP53 are common mutated oncogenes in cancer whose single gene status may predict the therapeutic effect of clinical ICIs. In this efficacy evaluation, we aimed to clarify whether the single gene mutation status of KRAS, EGFR or TP53 affects the survival benefits of ICIs in cancer patients.

Methods: We used PubMed, Cochrane Library, web of science, and clinical trials Gov database to retrieve qualified documents, the time was up to January 2022. Hazard ratios (HRS) and 95% confidence intervals (CIs) were used to determine the single gene mutation status and no progression of KRAS, EGFR or TP53.

Results: A total of 19 studies included 7029 cancer patients treated with ICIs. The results showed that KRAS, EGFR or TP53 single gene mutation could significantly improve PFS and OS in patients receiving ICIs, but the degree of improvement was different. The risk of prolongation of PFS (HR = 1.48, 95% CI = 1.19-1.85, $p = 0.0004$) and OS (HR = 1.68, 95% CI = 1.36-2.07, $p < 0.00001$) caused by TP53 single gene mutation was relatively high, the risk ratio of prolongation of PFS (HR = 1.38, 95% CI = 1.21-1.57, $p < 0.00001$) and OS (HR = 1.56, 95% CI = 1.20-2.04, $p = 0.001$) caused by EGFR single gene mutation was the second, the risk ratio of prolongation of PFS (HR = 1.33, 95% CI = 1.12-1.57, $p = 0.001$) and OS (HR = 1.39, 95% CI = 1.18-1.63, $p < 0.00001$) caused by KRAS single gene mutation was relatively low, and the results were significantly different.

Conclusion: In cancer patients, KRAS, EGFR or TP53 single gene status is correlated with the benefits of immunotherapy PFS and OS, which suggests that gene sequencing should be carried out in time in the process of clinical treatment to determine the gene mutation of patients and better predict the clinical treatment effect of ICIs.

Keywords: immune checkpoint inhibitors, cancer, gene mutation, progression free survival, overall survival, survival benefit

OPEN ACCESS

Edited by:
Ting Wang,
Sichuan Cancer Hospital, China

Reviewed by:
Mingming Wu,
Harbin Medical University, China
Mattia Riefolo,
University of Bologna, Italy

****Correspondence:***
Kai Jiang
zjjiangkai@163.com

[†]These authors have contributed equally to this work

Specialty section:
This article was submitted to Pharmacology of Anti-Cancer Drugs, a section of the journal Frontiers in Pharmacology

Received: *18 February 2022*
Accepted: *08 March 2022*
Published: *23 March 2022*

Citation:
Liu S, Geng S, Shi N, Zhang L, Xue W, Li Y and Jiang K (2022) Survival Prediction of Patients Treated With Immune Checkpoint Inhibitors via KRAS/TP53/EGFR-Single Gene Mutation. Front. Pharmacol. 13:878540. doi: 10.3389/fphar.2022.878540

INTRODUCTION

With the advent of the era of tumor immunity, significant progress has been made in the treatment of cancers. In recent years, immune checkpoint inhibitors have become an effective treatment option and means for the treatment of cancer (Ferlay et al., 2015). Programmed death ligand 1 (PD-L1) is an immune checkpoint protein expressed on cancer cells or cancer infiltrating immune cells. PD-L1 binds to the programmed death 1 (PD-1) receptor on activated T cells and induces tumor immune escape by down regulating the function of antitumor T cells (Alexandrov et al., 2013; Brahmer et al., 2015). Therefore, inhibition of PD-1/PD-L1 pathway can induce immune response to cancer by restoring T cell activity (Moore et al., 2020).

Immune checkpoint inhibitors (ICIs) refer to antibodies against PD-1/PD-L1, which block the inhibition signal mediated by PD-1/PD-L1 (Dong et al., 2017). Many clinical trials involving patients with cancer tumors have shown that ICIs can achieve better survival outcomes than standard chemotherapy (Ozaki et al., 2020).

Tumor mutation load has been considered as a potential marker of cancer response to ICIs. High mutation load may be related to the increase of new antigens recognized by T cells to increase antitumor T cell response (Dong et al., 2017). KRAS, EGFR or TP53 are the most common mutated oncogenes in cancer (Dong et al., 2017). However, it is unclear whether the efficacy of ICIs in cancer patients is related to KRAS, EGFR or TP53 single gene mutations. We conducted this meta-analysis to investigate whether KRAS, EGFR or TP53 single gene mutation status affects the survival benefits of ICIs in cancer patients.

MATERIALS AND METHODS

Systematically search the domestic and foreign literature on the efficacy of ICIs in cancer patients and KRAS, EGFR or TP53 single gene mutations, and evaluate whether KRAS, EGFR or TP53 single gene mutations affect the survival benefits of ICIs in cancer patients.

Search Strategy

We performed multiple retrieval tools: 1) Computer literature database search: 1) Retrieval of computer literature database: ① Chinese search terms include immune checkpoint inhibitors, cancer, gene mutation, etc; ② English search terms include ICIS, cancer, KRAS, EGFR, TP53, etc; ③ PubMed, Cochrane Library, EMBASE and EBSCO evidence-based medicine databases are searched in different combinations. The search items include title, abstract and keywords. The search time limit is from the establishment of the database to January 2022. 2) Manual retrieval of ASCO conference related literature as a supplement to computer retrieval.

Study Selection

Immunotherapy is used more and more in many cancer patients. Some research results show that KRAS, EGFR or TP53 single gene mutation leads to the reduction of PFS and OS in cancer patients using ICIs. In order to further systematically evaluate the correlation between gene mutation and survival benefit of ICIs patients, We used inclusion and exclusion criteria for this regimen: inclusion criteria were: 1) confirmed solid tumor; 2) Overall survival (OS) or progressionfree survival (PFS) data can be used to evaluate the efficacy of immune checkpoint inhibitors; 3) KRAS EGFR or TP53 single gene mutation status; 4) Literature type: prospective or retrospective studies, randomized controlled trials, whether blind or lacking, also included animal studies reviews editorial reviews or case reports were excluded duplicative studies, unbalanced matching procedures, or incomplete data were excluded.

Data Extraction and Quality Assessment

We used the Newcastle Ottawa scale (NOS) to evaluate the quality of the included studies (Lazarus et al., 2019). The inclusion studies were evaluated according to the following criteria: 1) whether they were representative; 2) determination of blind method; 3) whether the random method is determined; 4) Completeness of outcome events; 5) Comparability of included studies; 6) Assessment of outcome events; 7) Whether there is follow-up; 8) Completeness of follow-up. High quality literature is rated 7-9, medium quality literature is rated 4-6, and low quality literature is rated 3 or lower. Data were extracted independently by two reviewers according to specified selection criteria. Differences of opinion are resolved by discussion between authors or by obtaining input from a third evaluator.

Statistical Analysis

We extracted key data from the preliminary study and analyzed it using Review Manager 5.4. The results are expressed as odd risk with 95% confidence interval (CI), and the continuous results are expressed as weighted mean difference. In the absence of statistical heterogeneity, fixed effect models were used to aggregate data. If there is statistical heterogeneity ($p < 0.05$, $I^2 \geq 50\%$), the random effect model is used.

RESULTS

Search Results and Patient Characteristics

125 relevant literatures were obtained through database retrieval, excluding 90 duplicates, case reports, reviews and irrelevant contents. 36 literatures were screened in strict accordance with the above screening process. Finally, 19 (Facchinetti et al., 2017; Fujimoto et al., 2018; Garassino et al., 2018; Lin et al., 2018; Ahn et al., 2019; Assoun et al., 2019; Cho et al., 2019; Guibert et al., 2019; Jeanson et al., 2019; Ng et al., 2019; Gianoncelli et al., 2020; Lyu et al., 2020; Marinelli et al., 2020; Morita et al., 2020; Motzer et al., 2020; Schoenfeld et al., 2020; Xiang et al., 2020; An et al., 2021; Kartolo et al., 2021) studies were included, which met the quantitative analysis, involving 7029 cancer patients, as shown in **Figure 1**.

A total of 7029 cancer patients who met the requirements were included in 19 literatures, including 3058 patients with KRAS, EGFR or TP53 single gene mutation and 3971 patients without this gene mutation. All 19 literatures are high-quality literatures, as shown in **Tables 1**, **2**, **3**.

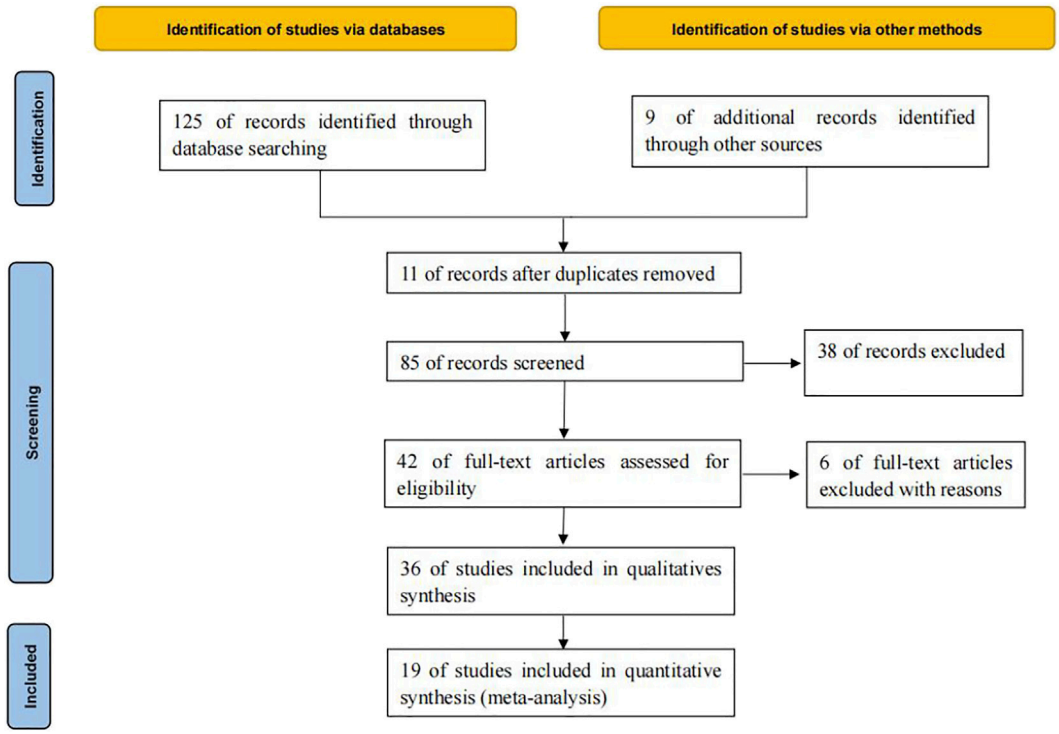

FIGURE 1 | PRISMA Flow chart of article selection.

TABLE 1 | Basic characteristics of included studies with KRAS status.

Author	Year	Type of Cancer	Treatment	Line	KRAS Status	NO.of Patients	HR for PFS(95%CI)	*p*-Value for PFS	HR for OS(95%CI)	*p*-Value for OS	Quality
Luo CL (Xiang et al., 2020)	2020	LUAD	PD-1/PD-L1 inhibitor	First line	MT WT	207 539	NA	NA	1.515(1.172-1.960)	0.0015	7
Adi Kartolo (Kartolo et al., 2021)	2021	NSCLC	Nivolumab	First line	MT WT	54 24	1.184(0.571-2.455)	0.651	0.901(0.417-1.946)	0.791	7
Arnaud Jeanso (Jeanson et al., 2019)	2019	NSCLC	PD-1/PD-L1 inhibitor	First line	MT WT	162 93	0.93 (0.71-1.21)	0.584	0.93(0.68-1.29)	0.682	7
Lin SY (Lin et al., 2018)	2018	NSCLC	Nivolumab, Pembrolizumab	First line	MT WT	10 30	0.73(0.32-1.66)	0.457	1.28(0.49-3.38)	0.614	7
Terry L. Ng (Ng et al., 2019)	2018	NSCLC	PD-1/PD-L1 inhibitor	First line	MT WT	77 112	0.502(0.303-0.806)	0.004	NA	NA	7
Nicolas Guibert (Guibert et al., 2019)	2019	NSCLC	PD-1/PD-L1 inhibitor	Second line	MT WT	31 66	0.46	0.11	NA	NA	8
Letizia Gianoncelli (Gianoncelli et al., 2020)	2020	NSCLC	PD-1/PD-L1 inhibitor	First line	MT WT	43 117	0.89 (0.59-1.34)	0.58	0.81 (0.50-1.31)	0.38	7
Adam J. Schoenfeld (Schoenfeld et al., 2020)	2020	LUAD	PD-1/PD-L1 inhibitor	First line	MT WT	527 1059	0.42(0.31-0.60)	<0.001	0.50(0.31-0.80)	0.003	7
D. Marinelli (Marinelli et al., 2020)	2020	LUAD	PD-1/PD-L1 inhibitor	First line	MT WT	26 173	NA	NA	1.40(0.85-2.31)	0.188	7
Josiah An (An et al., 2021)	2021	NSCLC	PD-1/PD-L1 inhibitor	First line	MT WT	14 56	1.10(0.50-2.42)	0.81	NA	NA	7

LUAD, lung adenocarcinoma; NSCLC, Non-small cell lung cancer; PFS, progression free survival; OS,overall survival; MT, mutant-type; WT, wild-type; HR,Hazard ratio; NA, Not available.

TABLE 2 | Basic characteristics of included studies with TP53 status.

Author	Year	Type of Cancer	Treatment	Line	TP53 Status	No.of Patients	HR for PFS(95% CI)	*p*-Value for PFS	HR for OS(95%CI)	*p*-Value for OS	Quality
Luo CL (Xiang et al., 2020)	2020	LUAD	PD-1/PD-L1 inhibitor	First line	MT WT	84 123	NA	NA	1.618(1.128-2.505)	0.0108	7
Nicolas Guibert (Guibert et al., 2019)	2019	NSCLC	PD-1/PD-L1 inhibitor	Second line	MT WT	31 66	NA	NA	0.36	0.011	7
Adam J. Schoenfeld (Schoenfeld et al., 2020)	2020	LUAD	PD-1/PD-L1 inhibitor	First line	MT WT	701 885	0.62(0.44-0.89)	0.006	0.65(0.43-0.99)	0.04	7
Josiah An (An et al., 2021)	2021	NSCLC	PD-1/PD-L1 inhibitor	First line	MT WT	21 49	1.02(0.52-1.99)	0.96	NA	NA	7
Qiong Lyu (Lyu et al., 2020)	2020	BLCA	PD-1/PD-L1 inhibitor	First line	MT WT	99 111	NA	NA	0.65(0.44-0.99)	0.041	7
Sandra Assoun (Assoun et al., 2019)	2019	NSCLC	Nivolumab	NA	MT WT	41 31	0.53(0.30-0.95)	0.03	0.48(0.25-0.95)	0.04	7
Robert J. Motzer-1 (Motzer et al., 2020)	2019	RCC	Avelumab	First line	MT WT	27 329	0.96 (0.51-1.83)	0.9065	NA	NA	7
Robert J. Motzer-2 (Motzer et al., 2020)	2019	RCC	Avelumab	First line	MT WT	39 336	1.47 (0.95-2.27)	0.0858	NA	NA	7

LUAD, lung adenocarcinoma; NSCLC, Non-small cell lung cancer; BLCA, bladder cancer; RCC, renal cell carcinoma; PFS, progression free survival; OS, overall survival; MT, mutant-type; WT, wild-type; HR, Hazard ratio; NA, Not available.

TABLE 3 | Basic characteristics of included studies with EGFR status.

Author	Year	Type of Cancer	Treatment	Line	EGFR Status	No.of Patients	HR for PFS(95% CI)	*p*-Value for PFS	HR for OS(95%CI)	*p*-Value for OS	Quality
Lin SY (Lin et al., 2018)	2018	NSCLC	Nivolumab, Pembrolizumab	First line	MT WT	25 49	2.00(1.11-3.62)	0.022	1.07(0.50-2.26)	0.867	7
Adam J. Schoenfeld (Schoenfeld et al., 2020)	2020	LUAD	PD-1/PD-L1 inhibitor	First line	MT WT	465 1121	0.75(0.38-1.48)	0.36	0.79(0.36-1.73)	0.53	7
Francesco (Facchinetti et al., 2017)	2017	NSCLC	PD-1/PD-L1 inhibitor	First line	MT WT	NA NA	NA	NA	0.45(0.26-0.81)	0.002	7
Marina Chiara Garassino (Garassino et al., 2018)	2018	NSCLC	Nivolumab	First line	MT WT	102 1293	1.38 (1.11-1.72)	0.004	1.11 (0.84-1.47)	0.46	7
Ryo Morita (Morita et al., 2020)	2020	NSCLC	Nivolumab	First line	MT WT	116 641	1.11 (0.84-1.45)	0.4634	1.74(1.41-2,15)	<0.0001	7
Beung-Chul Ahn (Ahn et al., 2019)	2019	NSCLC	PD-1/PD-L1 inhibitor	First line	MT WT	23 113	NA	NA	2.230(1.352-3.676)	0.002	7
Daichi Fujimoto (Fujimoto et al., 2018)	2018	NSCLC	PD-1/PD-L1 inhibitor	First line	MT WT	95 410	1.45 (1.12-1.86)	0.006	NA	NA	7
Jang Ho Cho (Cho et al., 2019)	2019	LUAD	Nivolumab	First line	MT WT	38 140	1.75(1.11-2.75)	0.02	NA	NA	7

LUAD, lung adenocarcinoma; NSCLC, Non-small cell lung cancer; PFS, progression free survival; OS, overall survival; MT, mutant-type; WT, wild-type; HR, Hazard ratio; NA, Not available.

Meta-Analysis Results

Comparison of KRAS, EGFR or TP53 Single Gene Mutation on PFS in Cancer Patients Using ICIs

Eight studies can obtain KRAS single gene mutation. For the PFS data of cancer patients using ICIs, $I^2 = 43\%$, $p = 0.09$. There is no statistical heterogeneity among the studies. The fixed effect model is used for analysis. The results showed that HR = 1.33 (95% CI = 1.12-1.57, $p = 0.001$), suggesting that KRAS single gene mutation can significantly improve PFS in cancer patients using ICIs, as shown in **Figure 2**.

Six studies can obtain EGFR single gene mutation. For PFS data of cancer patients using ICIs, $I^2 = 0\%$, $p = 0.42$. There is no statistical heterogeneity among studies. Fixed effect model is used for analysis. The results showed that HR = 1.38 (95% CI = 1.21-1.57, $p < 0.00001$), suggesting that EGFR single gene mutation can significantly improve PFS in cancer patients using ICIs, as shown in **Figure 3**.

Six studies can obtain TP53 single gene mutation. The heterogeneity of PFS data of cancer patients using ICIs was analyzed, with $I^2 = 0\%$, $p = 0.58$. There was no statistical heterogeneity among the studies. The fixed effect model was used for analysis. The results showed that HR = 1.48 (95% CI = 1.19-1.85, $p = 0.0004$), suggesting that TP53 single gene mutation can significantly improve PFS in cancer patients using ICIs, as shown in **Figure 4**.

The above univariate analysis results showed that KRAS, EGFR or TP53 single gene mutation can improve PFS, but the

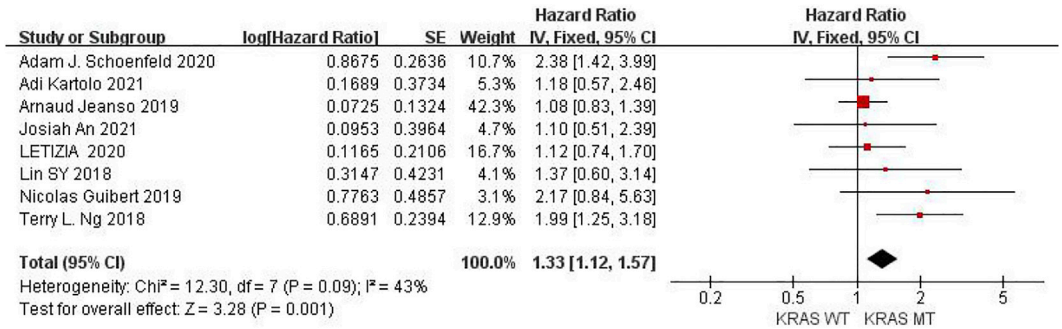

FIGURE 2 | Meta-analysis of objective responses according to KRAS status of PFS in cancer patients treated with ICIs.

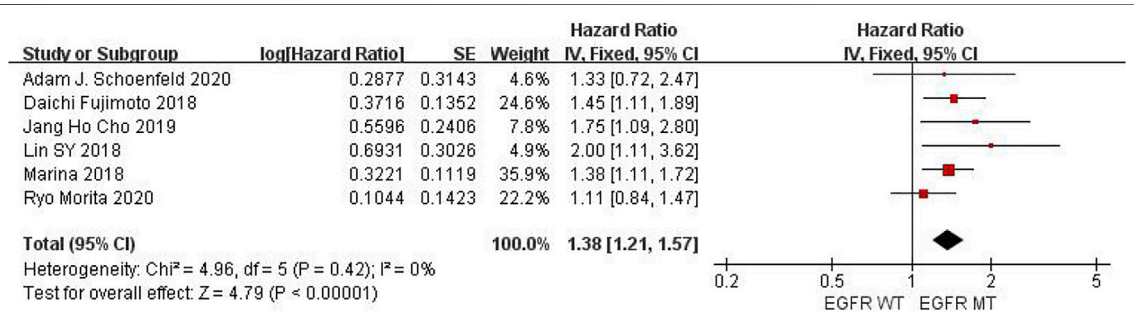

FIGURE 3 | Meta-analysis of objective responses according to EGFR status of PFS in cancer patients treated with ICIs.

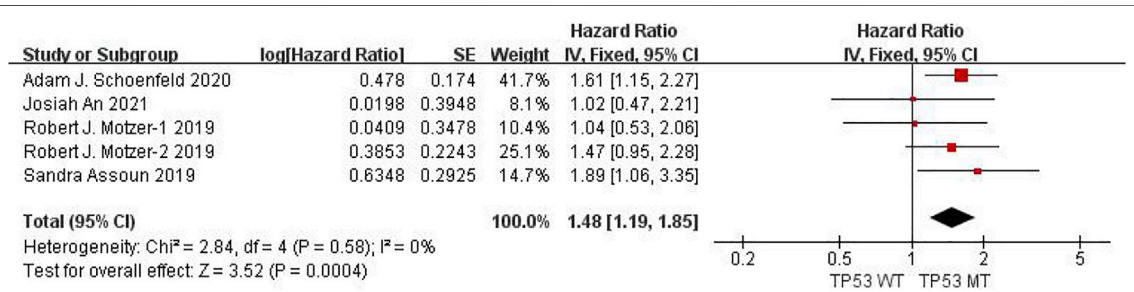

FIGURE 4 | Meta-analysis of objective responses according to TP53 status of PFS in cancer patients treated with ICIs.

extended HRS is different. Compared with no mutation, the risk ratio of KRAS single gene mutation prolonging PFS is 1.33, EGFR single gene mutation prolonging PFS is 1.38, and TP53 single gene mutation prolonging PFS is 1.48. The results suggest that TP53 single gene mutation leads to more significant prolongation of PFS in cancer patients using ICIs.

Comparison of KRAS, EGFR or TP53 on OS in Cancer Patients Using ICIs

Seven studies can obtain KRAS single gene mutation. For OS data of cancer patients using ICIs, $I^2 = 0\%$, $p = 0.47$. There is no statistical heterogeneity among studies. Fixed effect model is used for analysis. The results showed that HR = 1.39 (95% CI = 1.18-1.63, $p < 0.00001$), suggesting that KRAS single gene mutation can significantly improve the OS of cancer patients using ICIs, as shown in **Figure 5**.

Six studies can obtain EGFR single gene mutation. For OS data of cancer patients using ICIs, $I^2 = 58\%$, $p = 0.04$. There is statistical heterogeneity among studies, which is analyzed by random effect model. The results showed that HR = 1.56 (95% CI = 1.20-2.04, $p = 0.001$), suggesting that EGFR single gene mutation can significantly improve the OS of cancer patients using ICIs, as shown in **Figure 6**.

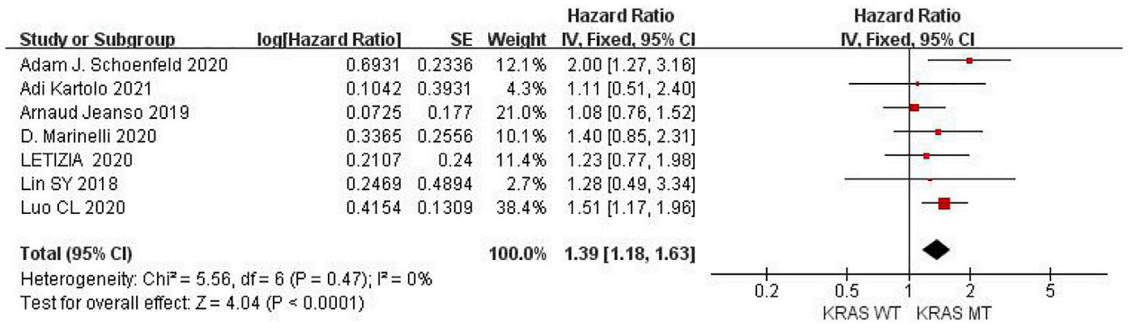

FIGURE 5 | Meta-analysis of objective responses according to KRAS status of OS in cancer patients treated with ICIs.

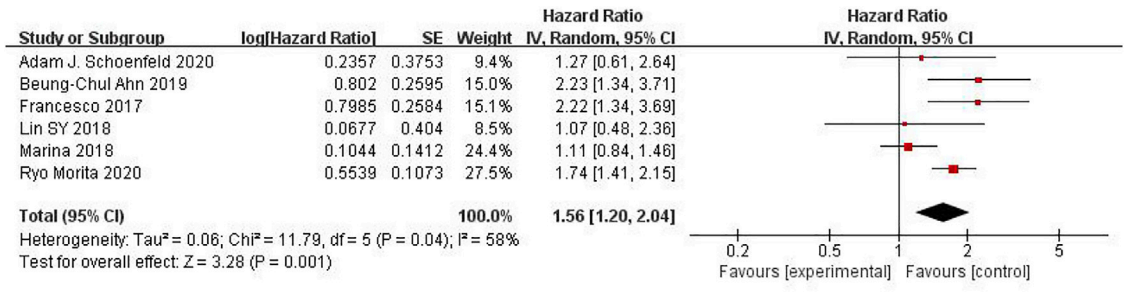

FIGURE 6 | Meta-analysis of objective responses according to EGFR status of OS in cancer patients treated with ICIs.

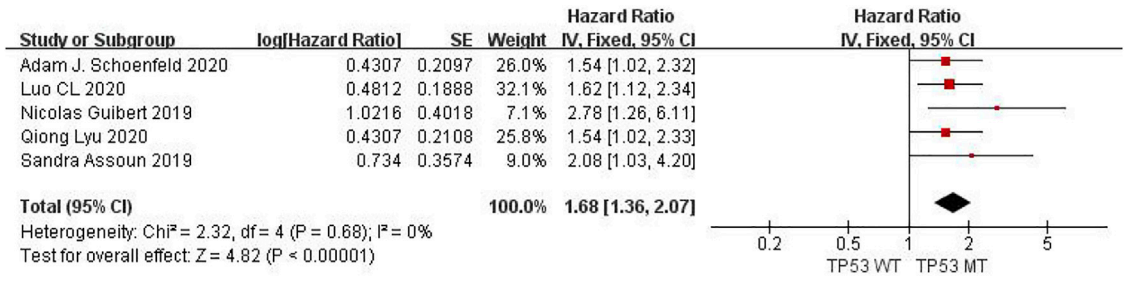

FIGURE 7 | Meta-analysis of objective responses according to TP53 status of OS in cancer patients treated with ICIs.

Five studies can obtain TP53 single gene mutation. For OS data of cancer patients using ICIs, $I^2 = 0\%$, $p = 0.68$. There is no statistical heterogeneity among studies. Fixed effect model is used for analysis. The results showed that HR = 1.68 (95% CI = 1.36-2.07, $p < 0.00001$), suggesting that TP53 single gene mutation can significantly improve the OS of cancer patients using ICIs, as shown in **Figure 7**.

The above univariate analysis results show that KRAS, EGFR or TP53 single gene mutation can significantly improve OS, but the extended HRS is different. Compared with no mutation, the risk ratio of KRAS single gene mutation prolonging OS is 1.39, the risk ratio of EGFR single gene mutation prolonging OS is 1.56, and the risk ratio of TP53 single gene mutation prolonging OS is 1.68. The results suggest that TP53 single gene mutation leads to more significant OS prolongation in cancer patients using ICIs.

Publication Bias

At the same time of meta-analysis and comparison of PFS and OS data indicators, the inverted funnel diagram was drawn for the included studies. The results show that OS with EGFR single gene mutation has small publication bias. Individual studies may have less rigorous design and poor research methods, which lead to the asymmetry of inverted funnel diagram and small bias. Other PFS and OS funnel patterns are symmetrical, as shown in **Figure 8**.

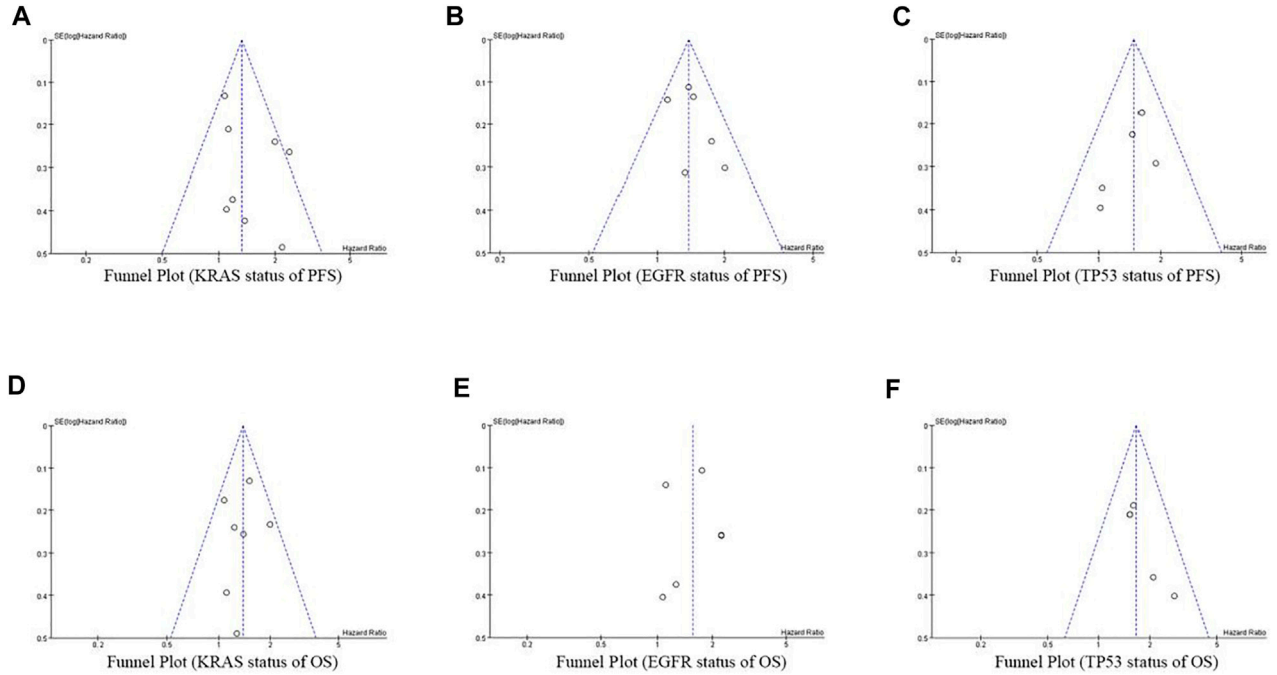

FIGURE 8 | Funnel Plot of objective responses according to KRAS/EGFR/TP53 status of PFS and OS in cancer patients treated with ICIs.

Sensitivity Analysis

In the sensitivity analysis, the sensitivity analysis of meta-analysis results was carried out by excluding one study at a time and then making statistics again. The combined hrs of PFS and OS showed no difference. There was no significant difference in the analysis results before and after elimination, suggesting that all meta-analysis results were stable.

DISCUSSION

A large number of research data show that the emergence of immune checkpoint inhibitors has significantly affected the clinical treatment strategies of most cancer subtypes, especially non-small cell lung cancer, renal cell carcinoma, melanoma and so on. Programmed cell death-1 (PD-1) inhibitors, such as neruzumab or pemilizumab, and programmed cell death ligand-1 (PD-L1) inhibitors, such as atezolizumab, significantly improved progression free survival (PFS) and overall survival (OS) in cancer patients. Compared with platinum based standard first-line chemotherapy or docetaxel based second-line chemotherapy, excellent disease control time is achieved (Borghaei et al., 2015; Le et al., 2017).

Some studies have shown that tumor mutation burden (TMB) can predict the potential activity of immunotherapy in a variety of tumor types, including NSCLC, RCC, etc. (Song et al., 2020). By producing damaged cell proteins recognized as new antigens by immune cells, the resulting genetic instability can enhance the immunogenicity of tumors, so as to optimize the antitumor cytotoxicity of T lymphocytes recovered by ICIs treatment. For example, in colorectal cancer, mismatch repair status predicts the clinical benefit of anti-PD-1 antibody pamumab (Van Allen et al., 2015). In non-small cell lung cancer, a mutation feature associated with smoking predicts anti-PD-1 efficacy (Hollern et al., 2019). In melanoma, TMB and neoantigen load predict patients' response to CTLA-4 treatment (Pauken et al., 2016). The presence of CD8 + T cells and the expression of immune checkpoint genes such as PD-1 ligand (PD-L1) and CTLA-4 can also predict the efficacy of ICIs (Wang et al., 2019). These data show that TMB has a significant effect on predicting the response of ICIs, and it is clinically needed.

KRAS is a guanine nucleotide binding protein that regulates the mitogen activated protein kinase (MAPK) pathway. When it is activated, it promotes downstream signaling pathways, leading to cell growth and proliferation (Nagasaka et al., 2020). KRAS mutation rate in patients with non squamous NSCLC is 20–30% (Nagasaka et al., 2020). So far, there is no therapy for KRAS mutation. Although some targeted drugs (such as G12C inhibitors) are being evaluated in clinical trials, the effective drug targeting of KRAS mutation is also an unprecedented challenge. By studying the correlation between KRAS mutation status and TMB, it was found that TMB was associated with tumor immunogenicity and greater survival benefit of ICIs treatment (Adderley et al., 2019). Recent studies reported that compared with chemotherapy patients, OS and PFS were improved in patients with KRAS mutant NSCLC after ICIs treatment, and KRAS mutant tumors showed stronger PD-L1 expression and T cell infiltration (Adderley et al., 2019). Epidermal growth factor receptor (EGFR) mutation is a good predictor of the efficacy of EGFR tyrosine kinase inhibitors. EGFR mutation is common in cancer, especially in non-small cell lung cancer. EGFR mutations are found in 32% of non-small cell lung cancer cases worldwide, of which 39% of tumors occur in Asian ethnic

groups and 17% in Caucasian ethnic groups (Zhang et al., 2016). The prevalence of EGFR mutation in lung adenocarcinoma is high; 51% of East Asian lung adenocarcinoma patients have EGFR mutation (Shi et al., 2014). The high prevalence of EGFR mutations makes it more important to evaluate whether EGFR mutations are really negative predictors of PD-1/PD-L1 efficacy. The prognostic role of tumor suppressor gene TP53 mutation in predicting the efficacy of ICIs is highly controversial. An early study (Xiao et al., 2018) showed that TP53 mutation was associated with relatively short PFS and shorter OS in 110 patients receiving CTLA-4 blocking treatment. However, inconsistent results were observed in another group of patients with non-small cell lung cancer treated with PD-1 + CTLA-4 block. The study found that TP53 mutation was enriched in responders, suggesting that TP53 may be related to the enhanced response of combination therapy. In addition, Dong et al. (Ozaki et al., 2020) confirmed that patients with lung adenocarcinoma had a relatively good response to TP53 mutation when treated with PD-1 inhibitors, suggesting that TP53 may help to guide the decision of clinical use of ICIs.

In addition, many cancers show different patterns of genomic changes. In the development of cancer, KRAS, as a driving oncogene, has a high mutation frequency. However, it has recently been found that cancers with KRAS mutations also express TP53 mutations. TP53, as a core cancer suppressor gene, encodes p53 protein in humans and mice to prevent mutations in a stable state. Notably, TP53 mutations drive lung cancer, with a higher frequency of TP53 mutations than EGFR or KRAS mutations in LUAD. Studies have shown that tumors with co-mutations of KRAS/TP53 usually show significant upregulation of PD-L1 expression and accumulation of tumor-killing T cells. In this regard, in addition to PD-L1 expression, TP53 mutations will hopefully guide the clinical application of immune checkpoint blocking therapy for KRAS mutated lung adenocarcinoma. However, the prognostic effect of TP53 mutation on EGFR mutant lung cancer is controversial. TP53/EGFR co-mutations may be associated with treatment resistance and shorter survival in lung cancer patients, the study showed. On the other hand, Labbe et al. (Zhang et al., 2019) studied 105 egFR-mutant NSCLC patients, and among the patients undergoing surgery, progressionfree survival (HR 0.99, 95%CI: 0.56-1.75) and overall survival (OS, HR 1.39, 95%CI: 0.70-2.77) was unrelated to TP53 status. Therefore, considering these controversial findings and evaluating the prognostic value of TP53/EGFR co-mutations in lung cancer will also be the focus of our subsequent studies.

In this meta-analysis, we investigated whether the survival benefits of ICIs in cancer patients vary according to KRAS/EGFR/TP53 single gene mutation status. We found that the PFS and OS of patients with KRAS/EGFR/TP5 single gene mutant tumors were significantly improved and the degree of improvement was different when treated with ICIs. TP53 mutant showed a better effect than KRAS mutation and EGFR mutation. These results suggest that KRAS/EGFR/TP53 single gene mutation status may be a potential biomarker of the survival benefits of ICIs. In the future, ICIs may play an important role in the treatment of early cancer. After radiotherapy and chemotherapy, immunotherapy has become the standard treatment of cancer, regardless of its mutation status. Even in the early stages of the disease, molecular characteristics will become the basis to determine the optimal treatment strategy and its combination with local regional treatment, especially in oncogene addiction diseases.

Considering the limited amount of data based on this meta-analysis, further research is needed to evaluate the effect of KRAS/EGFR/TP53 single gene mutation on the efficacy of ICIs in cancer patients. We also expect that the latest progress of next-generation sequencing technology will help to identify more accurate biomarkers and bring clinical benefits to ICIs immunotherapy.

DATA AVAILABILITY STATEMENT

The original contributions presented in the study are included in the article/Supplementary Material, further inquiries can be directed to the corresponding author.

AUTHOR CONTRIBUTIONS

SL, SG, and NS searched the database and analysed the data. LZ, WX, and YL selected the study and extracted the data. SL and SG wrote the manuscript. The manuscript was reviewed by KJ.

REFERENCES

Adderley, H., Blackhall, F. H., and Lindsay, C. R. (2019). KRAS-mutant Non-small Cell Lung Cancer: Converging Small Molecules and Immune Checkpoint Inhibition. *EBioMedicine* 41, 711–716. doi:10.1016/j.ebiom.2019.02.049

Ahn, B. C., Pyo, K. H., Xin, C. F., Jung, D., Shim, H. S., Lee, C. Y., et al. (2019). Comprehensive Analysis of the Characteristics and Treatment Outcomes of Patients with Non-small Cell Lung Cancer Treated with Anti-PD-1 Therapy in Real-World Practice. *J. Cancer Res. Clin. Oncol.* 145, 1613–1623. doi:10.1007/s00432-019-02899-y

Alexandrov, L. B., Nik-Zainal, S., Wedge, D. C., Aparicio, S. A., Behjati, S., Biankin, A. V., et al. (2013). Signatures of Mutational Processes in Human Cancer. *Nature* 500, 415–421. doi:10.1038/nature12477

An, J., Yan, M., Yu, N., Chennamadhavuni, A., Furqan, M., Mott, S. L., et al. (2021). Outcomes of Patients with Stage III Non-small Cell Lung Cancer (NSCLC) that Harbor a STK11 Mutation. *Transl Lung Cancer Res.* 10, 3608–3615. doi:10.21037/tlcr-21-177

Assoun, S., Theou-Anton, N., Nguenang, M., Cazes, A., Danel, C., Abbar, B., et al. (2019). Association of TP53 Mutations with Response and Longer Survival under Immune Checkpoint Inhibitors in Advanced Non-small-cell Lung Cancer. *Lung Cancer* 132, 65–71. doi:10.1016/j.lungcan.2019.04.005

Borghaei, H., Paz-Ares, L., Horn, L., Spigel, D. R., Steins, M., Ready, N. E., et al. (2015). Nivolumab versus Docetaxel in Advanced Nonsquamous Non-small-cell Lung Cancer. *N. Engl. J. Med.* 373, 1627–1639. doi:10.1056/NEJMoa1507643

Brahmer, J., Reckamp, K. L., Baas, P., Crinò, L., Eberhardt, W. E., Poddubskaya, E., et al. (2015). Nivolumab versus Docetaxel in Advanced Squamous-Cell Non-small-cell Lung Cancer. *N. Engl. J. Med.* 373, 123–135. doi:10.1056/NEJMoa1504627

Cho, J. H., Jung, H. A., Lee, S. H., Ahn, J. S., Ahn, M. J., Park, K., et al. (2019). Impact of EGFR Mutation on the Clinical Efficacy of PD-1 Inhibitors in Patients with Pulmonary Adenocarcinoma. *J. Cancer Res. Clin. Oncol.* 145, 1341–1349. doi:10.1007/s00432-019-02889-0

Dong, Z. Y., Zhong, W. Z., Zhang, X. C., Su, J., Xie, Z., Liu, S. Y., et al. (2017). Potential Predictive Value of TP53 and KRAS Mutation Status for Response to

PD-1 Blockade Immunotherapy in Lung Adenocarcinoma. *Clin. Cancer Res.* 23, 3012–3024. doi:10.1158/1078-0432.CCR-16-2554

Facchinetti, F., Bluthgen, M. V., Tergemina-Clain, G., Faivre, L., Pignon, J. P., Planchard, D., et al. (2017). LKB1/STK11 Mutations in Non-small Cell Lung Cancer Patients: Descriptive Analysis and Prognostic Value. *Lung Cancer* 112, 62–68. doi:10.1016/j.lungcan.2017.08.002

Ferlay, J., Soerjomataram, I., Dikshit, R., Eser, S., Mathers, C., Rebelo, M., et al. (2015). Cancer Incidence and Mortality Worldwide: Sources, Methods and Major Patterns in GLOBOCAN 2012. *Int. J. Cancer* 136, E359–E386. doi:10.1002/ijc.29210

Fujimoto, D., Yoshioka, H., Kataoka, Y., Morimoto, T., Kim, Y. H., Tomii, K., et al. (2018). Efficacy and Safety of Nivolumab in Previously Treated Patients with Non-small Cell Lung Cancer: A Multicenter Retrospective Cohort Study. *Lung Cancer* 119, 14–20. doi:10.1016/j.lungcan.2018.02.017

Garassino, M. C., Gelibter, A. J., Grossi, F., Chiari, R., Soto Parra, H., Cascinu, S., et al. (2018). Italian Nivolumab Expanded Access Program in Nonsquamous Non-small Cell Lung Cancer Patients: Results in Never-Smokers and EGFR-Mutant Patients. *J. Thorac. Oncol.* 13, 1146–1155. doi:10.1016/j.jtho.2018.04.025

Gianoncelli, L., Spitaleri, G., Passaro, A., Radice, D., Fumagalli, C., Del Signore, E., et al. (2020). Efficacy of Anti-pd1/pd-L1 Therapy (IO) in KRAS Mutant Non-small Cell Lung Cancer Patients: A Retrospective Analysis. *Anticancer Res.* 40, 427–433. doi:10.21873/anticanres.13970

Guibert, N., Jones, G., Beeler, J. F., Plagnol, V., Morris, C., Mourlanette, J., et al. (2019). Targeted Sequencing of Plasma Cell-free DNA to Predict Response to PD1 Inhibitors in Advanced Non-small Cell Lung Cancer. *Lung Cancer* 137, 1–6. doi:10.1016/j.lungcan.2019.09.005

Hollern, D. P., Xu, N., Thennavan, A., Glodowski, C., Garcia-Recio, S., Mott, K. R., et al. (2019). B Cells and T Follicular Helper Cells Mediate Response to Checkpoint Inhibitors in High Mutation Burden Mouse Models of Breast Cancer. *Cell* 179, 1191–1206. doi:10.1016/j.cell.2019.10.028

Jeanson, A., Tomasini, P., Souquet-Bressand, M., Brandone, N., Boucekine, M., Grangeon, M., et al. (2019). Efficacy of Immune Checkpoint Inhibitors in KRAS-Mutant Non-small Cell Lung Cancer (NSCLC). *J. Thorac. Oncol.* 14, 1095–1101. doi:10.1016/j.jtho.2019.01.011

Kartolo, A., Feilotter, H., Hopman, W., Fung, A. S., and Robinson, A. (2021). A Single Institution Study Evaluating Outcomes of PD-L1 High KRAS-Mutant Advanced Non-small Cell Lung Cancer (NSCLC) Patients Treated with First Line Immune Checkpoint Inhibitors. *Cancer Treat. Res. Commun.* 27, 100330. doi:10.1016/j.ctarc.2021.100330

Lazarus, G., Audrey, J., and Iskandar, A. W. B. (2019). Efficacy and Safety Profiles of Programmed Cell Death-1/programmed Cell Death Ligand-1 Inhibitors in the Treatment of Triple-Negative Breast Cancer: A Comprehensive Systematic Review. *Oncol. Rev.* 13, 425. doi:10.4081/oncol.2019.425

Le, D. T., Durham, J. N., Smith, K. N., Wang, H., Bartlett, B. R., Aulakh, L. K., et al. (2017). Mismatch Repair Deficiency Predicts Response of Solid Tumors to PD-1 Blockade. *Science* 357, 409–413. doi:10.1126/science.aan6733

Lin, S. Y., Yang, C. Y., Liao, B. C., Ho, C. C., Liao, W. Y., Chen, K. Y., et al. (2018). Tumor PD-L1 Expression and Clinical Outcomes in Advanced-Stage Non-small Cell Lung Cancer Patients Treated with Nivolumab or Pembrolizumab: Real-World Data in Taiwan. *J. Cancer* 9, 1813–1820. doi:10.7150/jca.24985

Lyu, Q., Lin, A., Cao, M., Xu, A., Luo, P., and Zhang, J. (2020). Alterations in TP53 Are a Potential Biomarker of Bladder Cancer Patients Who Benefit from Immune Checkpoint Inhibition. *Cancer Control* 27, 1073274820976665. doi:10.1177/1073274820976665

Marinelli, D., Mazzotta, M., Scalera, S., Terrenato, I., Sperati, F., D'Ambrosio, L., et al. (2020). KEAP1-driven Co-mutations in Lung Adenocarcinoma Unresponsive to Immunotherapy Despite High Tumor Mutational burden. *Ann. Oncol.* 31, 1746–1754. doi:10.1016/j.annonc.2020.08.2105

Moore, A. R., Rosenberg, S. C., McCormick, F., and Malek, S. (2020). RAS-targeted Therapies: Is the Undruggable Drugged? *Nat. Rev. Drug Discov.* 19, 533–552. doi:10.1038/s41573-020-0068-6

Morita, R., Okishio, K., Shimizu, J., Saito, H., Sakai, H., Kim, Y. H., et al. (2020). Real-world Effectiveness and Safety of Nivolumab in Patients with Non-small Cell Lung Cancer: A Multicenter Retrospective Observational Study in Japan. *Lung Cancer* 140, 8–18. doi:10.1016/j.lungcan.2019.11.014

Motzer, R. J., Robbins, P. B., Powles, T., Albiges, L., Haanen, J. B., Larkin, J., et al. (2020). Avelumab Plus Axitinib versus Sunitinib in Advanced Renal Cell Carcinoma: Biomarker Analysis of the Phase 3 JAVELIN Renal 101 Trial. *Nat. Med.* 26, 1733–1741. doi:10.1038/s41591-020-1044-8

Nagasaka, M., Li, Y., Sukari, A., Ou, S. I., Al-Hallak, M. N., and Azmi, A. S. (2020). KRAS G12C Game of Thrones, Which Direct KRAS Inhibitor Will Claim the Iron Throne? *Cancer Treat. Rev.* 84, 101974. doi:10.1016/j.ctrv.2020.101974

Ng, T. L., Liu, Y., Dimou, A., Patil, T., Aisner, D. L., Dong, Z., et al. (2019). Predictive Value of Oncogenic Driver Subtype, Programmed Death-1 Ligand (PD-L1) Score, and Smoking Status on the Efficacy of PD-1/pd-L1 Inhibitors in Patients with Oncogene-Driven Non-small Cell Lung Cancer. *Cancer* 125, 1038–1049. doi:10.1002/cncr.31871

Ozaki, Y., Muto, S., Takagi, H., Watanabe, M., Inoue, T., Fukuhara, M., et al. (2020). Tumor Mutation burden and Immunological, Genomic, and Clinicopathological Factors as Biomarkers for Checkpoint Inhibitor Treatment of Patients with Non-small-cell Lung Cancer. *Cancer Immunol. Immunother.* 69, 127–134. doi:10.1007/s00262-019-02446-1

Pauken, K. E., Sammons, M. A., Odorizzi, P. M., Manne, S., Godec, J., Khan, O., et al. (2016). Epigenetic Stability of Exhausted T Cells Limits Durability of Reinvigoration by PD-1 Blockade. *Science* 354, 1160–1165. doi:10.1126/science.aaf2807

Schoenfeld, A. J., Rizvi, H., Bandlamudi, C., Sauter, J. L., Travis, W. D., Rekhtman, N., et al. (2020). Clinical and Molecular Correlates of PD-L1 Expression in Patients with Lung Adenocarcinomas. *Ann. Oncol.* 31, 599–608. doi:10.1016/j.annonc.2020.01.065

Shi, Y., Au, J. S., Thongprasert, S., Srinivasan, S., Tsai, C. M., Khoa, M. T., et al. (2014). A Prospective, Molecular Epidemiology Study of EGFR Mutations in Asian Patients with Advanced Non-small-cell Lung Cancer of Adenocarcinoma Histology (PIONEER). *J. Thorac. Oncol.* 9, 154–162. doi:10.1097/JTO.0000000000000033

Song, P., Yang, D., Wang, H., Cui, X., Si, X., Zhang, X., et al. (2020). Relationship between the Efficacy of Immunotherapy and Characteristics of Specific Tumor Mutation Genes in Non-small Cell Lung Cancer Patients. *Thorac. Cancer* 11, 1647–1654. doi:10.1111/1759-7714.13447

Van Allen, E. M., Miao, D., Schilling, B., Shukla, S. A., Blank, C., Zimmer, L., et al. (2015). Genomic Correlates of Response to CTLA-4 Blockade in Metastatic Melanoma. *Science* 350, 207–211. doi:10.1126/science.aad8366

Wang, X., Wang, G., Wang, Z., Liu, B., Han, N., Li, J., et al. (2019). PD-1-expressing B Cells Suppress CD4(+) and CD8(+) T Cells *via* PD-1/pd-L1-dependent Pathway. *Mol. Immunol.* 109, 20–26. doi:10.1016/j.molimm.2019.02.009

Xiang, L., Fu, X., Wang, X., Li, W., Zheng, X., Nan, K., et al. (2020). A Potential Biomarker of Combination of Tumor Mutation Burden and Copy Number Alteration for Efficacy of Immunotherapy in KRAS-Mutant Advanced Lung Adenocarcinoma. *Front. Oncol.* 10, 559896. doi:10.3389/fonc.2020.559896

Xiao, W., Du, N., Huang, T., Guo, J., Mo, X., Yuan, T., et al. (2018). TP53 Mutation as Potential Negative Predictor for Response of Anti-CTLA-4 Therapy in Metastatic Melanoma. *EBioMedicine* 32, 119–124. doi:10.1016/j.ebiom.2018.05.019

Zhang, R., Tian, P., Chen, B., Wang, T., and Li, W. (2019). The Prognostic Impact of TP53 Comutation in EGFR Mutant Lung Cancer Patients: a Systematic Review and Meta-Analysis. *Postgrad. Med.* 131 (3), 199–206. doi:10.1080/00325481.2019.1585690

Zhang, Y. L., Yuan, J. Q., Wang, K. F., Fu, X. H., Han, X. R., Threapleton, D., et al. (2016). The Prevalence of EGFR Mutation in Patients with Non-small Cell Lung Cancer: a Systematic Review and Meta-Analysis. *Oncotarget* 7, 78985–78993. doi:10.18632/oncotarget.12587

Conflict of Interest: The authors declare that the research was conducted in the absence of any commercial or financial relationships that could be construed as a potential conflict of interest.

Publisher's Note: All claims expressed in this article are solely those of the authors and do not necessarily represent those of their affiliated organizations, or those of the publisher, the editors and the reviewers. Any product that may be evaluated in this article, or claim that may be made by its manufacturer, is not guaranteed or endorsed by the publisher.

Copyright © 2022 Liu, Geng, Shi, Zhang, Xue, Li and Jiang. This is an open-access article distributed under the terms of the Creative Commons Attribution License (CC BY). The use, distribution or reproduction in other forums is permitted, provided the original author(s) and the copyright owner(s) are credited and that the original publication in this journal is cited, in accordance with accepted academic practice. No use, distribution or reproduction is permitted which does not comply with these terms.

frontiers | Frontiers in Oncology

ORIGINAL RESEARCH
published: 04 April 2022
doi: 10.3389/fonc.2022.874343

LncRNA ENST869 Targeting Nestin Transcriptional Region to Affect the Pharmacological Effects of Chidamide in Breast Cancer Cells

Xiuyan Feng[1†], Han Han[2†], Yarui Guo[3], Xue Feng[3], Shanchun Guo[4] and Weiqiang Zhou[3*]*

[1] Medical Administration Division, The Second Affiliated Hospital of Shenyang Medical College, Shenyang City, China, [2] Department of Biochemistry and Molecular Biology, Shenyang Medical College, Shenyang City, China, [3] Department of Pathogen Biology, Shenyang Medical College, Shenyang City, China, [4] RCMI Cancer Research Center, Xavier University of Louisiana, New Orleans, LA, United States

Breast cancer is one of the leading threats to the health of women. It has the highest incidence and mortality in women worldwide. Although progress has been made in the development and application of anti-breast cancer drugs such as Chidamide and others, the occurrence of drug resistance limits the effective application of chemotherapies. The purpose of this study is to explore the role of LncRNA in the pharmacological effect of Chidamide in breast cancer therapy. The human breast cancer MCF-7 or MDA-MB-231 cells were used as the research cell models. The RNA library screening and high-throughput sequencing comparative analysis was conducted. The binding of LncRNA and its downstream target genes in RNA and protein levels was tested. The results showed that the expression of LncRNA ENST869 in cells treated with Chidamide increased significantly, as demonstrated by real-time PCR and cell viability assay. RNAplex analysis showed that LncRNA ENST869 and Nestin mRNA may interact. RNA interference and Western blot analysis indicated that LncRNA ENST869 could target and regulate the expression of Nestin. Luciferase assay and RNA-protein pulldown showed that LncRNA ENST869 affected Nestin transcription. There might be a highly active binding region of LncRNA ENST869 in regulating Nestin transcriptional activity within the site of 250 bp upstream of the transcription starting point of Nestin. In addition, LncRNA ENST869 did not directly interact with Nestin protein to affect its activity. In conclusion, our results demonstrated that LncRNA ENST869 could affect the function of Nestin in breast cancer cells treated with Chidamide. Nestin is a key player in influencing the pharmacological activity of Chidamide and an essential factor in drug resistance of breast cancer cells.

Keywords: biomarker, LncRNA, Chidamide, Nestin, anti-cancer drug resistance

OPEN ACCESS

Edited by:
Zhe-Sheng Chen,
St. John's University, United States

Reviewed by:
Xiaochuan Chen,
Shenzhen Geno-Immune Medical Institute, China
Aiping Du,
Children's Hospital of Philadelphia, United States
Zheng Huachuan,
China Medical University, China

***Correspondence:**
Weiqiang Zhou
zhouwq@hotmail.com
Shanchun Guo
sguo@xula.edu

†These authors have contributed equally to this work

Specialty section:
This article was submitted to Pharmacology of Anti-Cancer Drugs, a section of the journal Frontiers in Oncology

Received: *12 February 2022*
Accepted: *07 March 2022*
Published: *04 April 2022*

Citation:
Feng X, Han H, Guo Y, Feng X, Guo S and Zhou W (2022) LncRNA ENST869 Targeting Nestin Transcriptional Region to Affect the Pharmacological Effects of Chidamide in Breast Cancer Cells. Front. Oncol. 12:874343. doi: 10.3389/fonc.2022.874343

INTRODUCTION

The incidence of breast cancer ranks the highest among all cancers in women worldwide (1, 2). With the intensive study on the structure and function of the human genome, it was found that histone acetylation regulation is an important epigenetic modification, which regulates the dynamic balance between histone acetyltransferase (HAT) and histone deacetylase (HDAC) and plays an important role in the occurrence and development of breast cancer (3–5). The gene transcription activity instead of DNA sequence mutation and stable genetic expression regulation has gradually become an intriguing topic of current research (6).

Chidamide is a third-generation histone deacetylation inhibitor (HDACi) (7). It has better efficacy than the second-generation HDACi anti-cancer drugs such as TSA and SAHA (8). However, its clinical application has inherent defects similar to other common anti-tumor drugs such as drug resistance (9).

Long non-coding RNA (LncRNA) is a kind of RNA molecule that does not encode protein and has a length of 200–10,000 nucleotides (10–12). At present, there are thousands of LncRNA genes involved in mammalian gene activities. The mechanism of LncRNA in regulating gene expression is mainly achieved *via* epigenetics, transcriptional regulation, and post-transcriptional regulation (13, 14). In particular, the transcription regulation of LncRNA can interfere with the expression of its downstream genes and impact the activity of other transcription factors. Moreover, some LncRNAs can form double-stranded RNA complexes with targeted mRNAs to mask the cis-acting elements of mRNA and regulate its gene expression (15).

In this study, Chidamide is applied to estrogen receptor (ER) positive MCF-7 and triple-negative MDA-MB-231 breast cancer cells in order to explore the role of LncRNA in the regulatory mechanism in breast cancer growth inhibition. The goal is to provide a theoretical basis and experimental data for further clarifying the molecular mechanism of action of LncRNA and distinctive factors.

MATERIALS AND METHODS

Cell Lines and Reagents

Human MCF-7 or MDA-MB-231 cells were obtained from American Type Culture Collection (ATCC) (Manassas, VA). Leibovitz's L-15 medium, RPMI-1640 medium, Fetal Bovine Serum (FBS) and, Penicillin–streptomycin Cocktails were purchased from Life Technologies (Austin, TX). Chidamide was supplied by Sigma-Aldrich (St. Louis, MO). Luciferase Assay System and CellTiter 96® AQueous One Solution Cell Proliferation assay were from Promega (Madison, MI). Muse Count & Viability Kit was from Millipore (Darmstadt, Germany). High Pure RNA Isolation Kit and Transcriptor First Strand cDNA Synthesis Kit were given from Roche Diagnostics GmbH (Mannheim, Germany). 5'RACE System for Rapid Amplification of cDNA Ends, LightShift Chemiluminescent RNA EMSA Kit, Power SYBR Green PCR Master Mix, RIPA Cell Lysis Buffer and BCA Protein Assay Kit were from Life Technologies (Austin, TX). Polyclonal anti-Nestin antibody and polyclonal anti-β actin antibody were obtained from Abcam Inc. (Cambridge, MA). LncRNA ENST869 siRNA candidates were designed and synthesized by RiboBio (Guangzhou, China). Nestin siRNA(h) was purchased from Santa Cruz Biotechnology (Santa Cruz, CA). Other chemicals were from Sangon Biotech (Shanghai, China).

Cell Culture

MCF-7 or MDA-MB-231 cells were grown in Leibovitz's L-15 medium or RPMI-1640 medium, respectively, with supplementation of 15% fetal bovine serum (FBS), 100 U/ml penicillin and 100 μg/ml streptomycin. All the cells were maintained at 37°C with 5% CO_2 and 95% humidity. The cells were seeded at a density of 1.0×10^4 cells/ml in a 96-well plate, 5.0×10^5 cells/ml in a 6-well plate and 1.5×10^7 cells/ml in a 100 mm dish. The cells were grown to 70–80% confluence and starved for 24 h in basal medium (with DMSO) without FBS and treated with different compounds.

MTT and Cell Viability Assay

MCF-7 or MDA-MB-231 cells were plated in a 96-well plate (5.0×10^3 cells/ml). After 24 h of starvation, the cells were treated with different concentrations of Chidamide (0, 20, and 100 μM) for 48 h incubation. The same concentrations of DMSO were added as a control. The CellTiter 96® AQueous One Solution Cell Proliferation Assay (MTT) was used, and absorbance was measured at 490 nm on a microplate reader.

Muse Count & Viability Reagent was used to assess cell viability. Approximately 2×10^5 of harvested cells (50 μl cell suspension) was added with 450 μl Count & Viability reagent. The results were obtained using the Muse Count & Viability software module in Muse Cell Analyzer, and the statistics showed the concentrations and percentages of viable and dead cells.

Breast Cancer Tumor Xenograft Models

The female nude mice were subcutaneously injected with 1×10^7 MDA-MB-231 cells suspended in 100 μl PBS. Length (L) and width (W) of the tumor were determined by a vernier caliper. The tumor volume (V) was calculated according to the equation: $V = L \times W^2/2$.

Once the tumor reached 50 mm^3, tumor-bearing mice were randomized into treatment groups. The mice were intravenously administrated with Chidamide (12 mg/kg Chidamide) and saline as a negative control for every two days (total of 12 injections). The tumor size and body weight of the mice were monitored every 2 days. On day 23, the mice were sacrificed. The tumors were harvested and weighted.

siRNA Transfection

siRNAs were transfected into MDA-MB-231 or MCF-7 cells maintained in 6-well plates using Lipofectamine 3000 transfection reagent. Approximately 6.6 μl siRNA was mixed with 125 μl medium without serum for 5 min, and the 3.75 μl Lipofectamine 3000 reagent was mixed with 125 μl medium

without serum for 5 min. These two reagents were mixed and incubated at room temperature for 5 min. The cell culture medium was removed from each well of the 6-well plates, and the mixture of siRNA and Lipofectamine 3000 was added to each well. Approximately 1 ml medium without serum was added with cells for 12 h of incubation. Finally, the transfection mixture was removed and the cells were cultured with 2 ml of medium with serum for 24 h.

Luciferase Assay

MDA-MB-231 cells were treated with Chidamide or siRNAs as described before. Growth medium was carefully removed, and the cells were rinsed with PBS. Approximately 300 µl 1× lysis buffer was added to cover the cells. After rocking the dishes several times, attached cells were scraped from the dish. Cells were then transferred to a 1.5 ml tube and kept in ice for 1 min. The luminometer was programed to perform a 2-second measurement delay followed by a 10-second measurement read for luciferase activity. Approximately 20 µl cell lysate was then mixed with 100 µl luciferase assay reagent. The samples were analyzed on Glomax® 96 luminometer and initiated reading.

cDNA Synthesis and Real-Time PCR Analysis

Total RNA was extracted from MCF-7 or MDA-MB-231 cells using High Pure RNA Isolation Kit according to the instructions of the manufacturer. RNA quantitation was performed *via* real-time PCR. The total RNA was reverse-transcribed with Transcriptor First Strand cDNA Synthesis Kit and amplified by Power SYBR Green PCR Master Mix in an Applied Biosystems 7500 real-time PCR system. The primers were designed by Primer 3 suit and libraries. The sequences of primers are shown in **Table 1**. Data normalization was based on correcting all C_t values for the average C_t values of GAPDH gene present in the reaction. Three independent biological replicates were performed.

Nestin Forward primer: 5'-GCTGAAGCCCTGGGGAAAGT-3'.
Reverse primer: 5'-CCAGGGGAGTGGAGTCTGGA-3'.
GAPDH Forward primer: 5'-ACAGTCAGCCGCATCTTCTT-3'.
Reverse primer: 5'-ACGACCAAATCCGTTGACTC-3'.

Western Blot Analysis

The MCF-7 or MDA-MB-231 cell pellets collected from 6-well plates were incubated in RIPA buffer containing 0.1 mg/ml protease inhibitor. The cellular lysate was rotated for 2 h at 4°C followed by centrifugation for 10 min at 14,000*g* at 4°C. Proteins were quantified using BCA protein assay kit. For immunoblotting, 20 µg proteins were separated by SDS-polyacrylamide gels electrophoresis and transferred to PVDF membranes. Western blot analyses were performed using the antibodies described above. The level of β-actin was used as loading controls. Protein bands were detected using ECL western blot substrate and exposed on DNR MF-Chemi Bio-Imaging Systems.

LncRNA Sequencing and Analyzing

Total RNA was extracted and ribosomal RNA was removed using the Ribo-Zero Kit (Epicentre, Madison, WI, USA). Fragmented RNAs (the average length was approximately 200 bp) were subjected to the first strand and second strand cDNA synthesis followed by adaptor ligation and enrichment with a low-cycle according to instructions of NEBNext® Ultra RNA Library Prep Kit for Illumina (NEB, USA). The purified library products were evaluated using the Agilent 2200 TapeStation and Qubit®2.0 (Life Technologies, USA). The libraries were paired-end sequenced (PE150, Sequencing reads were 150 bp) at RiboBio (Guangzhou, China) using the IlluminaHiSeq 3000 platform.

For identification of new LncRNA, the raw data were first filtered to remove low-quality reads. Then, the clean data that passed repeated testing was assembled using the StringTie based on the reads mapped to the reference genome. The assembled transcripts were annotated using the GffCompare program. The unknown transcripts were used to screen for putative LncRNAs. Transcripts with lengths above 200 nucleotides with predicted ORF shorter than 300 nucleotides were selected as LncRNA candidates.

For differential expression analysis, the statistically significant DE genes were obtained by an adjusted P-value threshold of 1 using the DEGseq software. Finally, a hierarchical clustering analysis was performed using the R language package gplots according to the TPM values of differential genes in different groups. Different colors represent different cluster of information, such as the similar expression pattern in the same group, which includes similar functions or participating in the same biological process.

All differentially expressed mRNAs were selected for GO pathway analyses. GO was performed with KOBAS3.0 software. GO provides label classification of gene function and gene product attributes (http://www.geneontology.org). GO analysis covers cellular component (CC) domains.

Northern Blot Assay

The synthesis of the RNA probe used for northern blot was performed using the 5' RACE Kit following the protocol. After

TABLE 1 | The primers used are summarized.

Gene Name	Primer Orientation	Sequence
LncRNA	Forward	5'-TCAGGGACAGGGCAGTATTC-3'
Primer1	Reverse	5'-GGGCTCCATCATCTTCTCTG-3'
LncRNA	Forward	5'-GTAGGCCTCGTTCACCTTGA-3'
Primer2	Reverse	5'-GGGTCAAGTGGACTTTCCTG-3'
LncRNA	Forward	5'-GAGCCGGCTGGAACTTAAC-3'
Primer3	Reverse	5'-CCGGAAGGAGGGATCCTG-3'

first-strand cDNA synthesis from total or poly(A)$^+$ RNA using a gene-specific primer (GSP1), a homopolymeric tail was added to the 3'-end of the cDNA using TdT and dCTP. PCR amplification was accomplished using Taq DNA polymerase, a nested, gene-specific primer (GSP2) that anneals to a site located within the cDNA molecule, and a novel deoxyinosine-containing anchor primer (Abridged anchor primer) provided with the system. The sequences of GSP1 single primers: 5'-GACTCTGAGAGCAGGGCAAG-3'. The sequences of GSP2 single primers: 5'-CCGACTTAACTGACCCTCTG'.

Northern blot was performed according to the protocol described previously. In brief, a 15 μg aliquot of total RNA was resuspended in 5 μl of RNase-free H_2O, supplemented with two volumes of RNA loading buffer. RNA samples were resolved on a 0.8% formaldehyde-agarose gel, capillary transferred onto positively charged nylon transfer membrane, rinsed with H_2O and UV crosslinked at 1,200 mJ (0.1 mJ/cm^2) with 60 s. North2South® Chemiluminescent Hybridization and Detection Kit was used and the membrane was hybridized overnight to the Bio-labeled RNA probe at a final concentration of 150 ng/ml. Chemiluminescence detection was performed according to the instructions of the manufacturer.

EMSA Assay

To demonstrate a functional EMSA, the LightShift Chemiluminescent RNA EMSA Kit was used. Approximately 20 μl binding reaction contained biotin-labeled target RNA, unlabeled target RNA and protein extract. Reactions were electrophoresed, transferred, and crosslinked of binding reactions to nylon membrane according to the steps in the protocol. The biotin end-labeled RNA is detected using the Streptavidin Horseradish Peroxidase Conjugate and a highly sensitive chemiluminescent substrate.

Data Analysis

All data in the text and figures are provided as means ± S.D. The results were analyzed by a one-way analysis of variance (ANOVA), followed by Tukey *post hoc* comparisons. All analyses were performed using the Statistical Package for Social Science (SPSS) software v22.0 (IBM, Armonk, NY). P <0.05 was considered significant.

RESULTS

Chidamide Constrains Breast Cancer Cell Growth

First, we measured the pharmacological effects of Chidamide on breast cancer cell growth. According to the previous experimental results (16), MCF-7 and MDA-MB-231 cells were treated with 20 μM Chidamide for 48 h. The same concentration of DMSO was used as the positive control. Cell viability assay showed that Chidamide inhibited cell activity (**Figures 1A, G**). To further understand the mechanism of action of Chidamide, after screening positive LncRNA by high-throughput RNA sequencing (RNA-seq) in MCF-7 and MDA-MB-231 cells, we analyzed the known mRNA from the sequencing results with DEGseq (an R package used to screen the differential gene expression in different samples). From the volcano diagram of mRNA differential expression (**Figures 1B, H**), it was found that the expressions of 33 and 27 LncRNA molecules were increased in MCF-7 and MDA-MB-231 cells with Chidamide treatment respectively, accompanied by a decrease in the expressions of 28 and 15 LncRNA molecules in both cell lines, respectively. Heatmap analysis showed that an LncRNA molecule named ENST00000448869.1 (referred to as ENST869 thereafter) was consequentially produced in both cell lines (**Figures 1C, I**). Finally, we obtained the full sequence of LncRNA ENST869 in the Ensembl genome browser and designed three pairs of primers (Primer 1-3) based on different regions of the LncRNA sequence by Primer3 software to verify the software deduction. The primer sequences are listed in **Table 1**. From the results of real-time quantitative PCR, we asserted that ENST869 is over-expressed in MCF-7 (**Figures 1D–F**) and MDA-MB-231 cells (**Figures 1J–L**).

LncRNA ENST869 Promotes the Expression of Nestin mRNA

The action network of LncRNAs was established using the RNAplex software, to predict the relationship between LncRNAs and their targeted mRNAs. The results were shown in **Figures 2A, C**. We integrated the data of differential LncRNAs and its adjacent mRNAs (<10 KB) and identified a potential target, Nestin. Real-time PCR indicated that Nestin mRNA was hugely accumulated in Chidamide treated cells (**Figures 2B, D**).

In order to clarify the operation pattern of LncRNA ENST869, we designed three siRNA fragments followed in the whole sequence of LncRNA ENST869 to silence this LncRNA. The sequences of these siRNAs are as follow:

siRNA1:5'-GCTCTCCTGATCAATACAT-3'; siRNA2:5'-CCAAAGTCTCCCAGTCAAT-3'; siRNA3:5'-GGCTGGAACTTAACGCTGT-3'.

Figures 3A, B showed that siRNA3 presented an ideal inhibition on LncRNA ENST869 in both cell lines. Interestingly, Western blot demonstrated that Nestin protein was also obviously interfered along with the functional loss of LncRNA ENST869. This result indicates that there is a correlation between LncRNA ENST869 and Nestin. Cell viability and nude mice bearing tumor experiment results showed that, when LncRNA ENST869 was silenced, the number of living cells was drastically reduced, and the tumorigenicity in mice was declined, implying that the anti-cancer efficacy of Chidamide was enhanced (**Figures 3C, D**).

Silencing Nestin mRNA Does Not Affect LncRNA ENST869

To discern whether Nestin has a feedback regulation on LncRNA ENST869, we used specific siRNA to silence Nestin mRNA. **Figure 4** displayed that breast cancer cell activity was suppressive; however, LncRNA ENST869 was not affected.

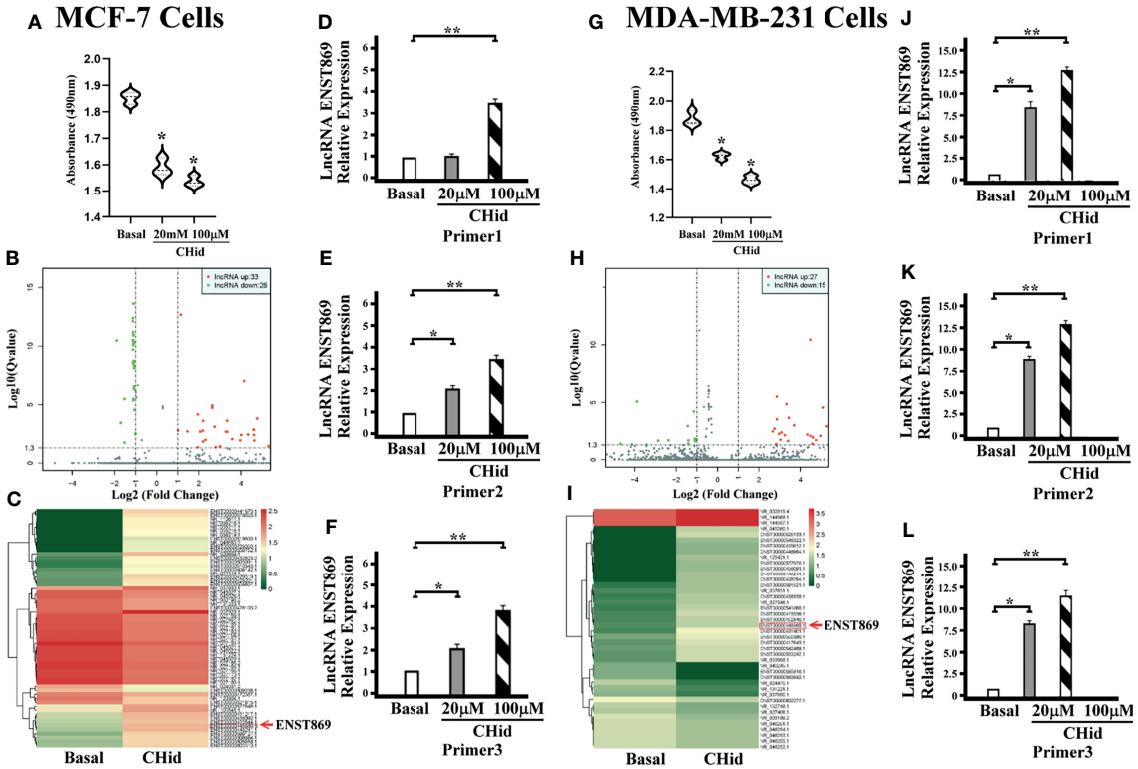

FIGURE 1 | Chidamide inhibits breast cancer cell growth. MCF-7 or MDA-MB-231 cells were cultured for 48 h in the presence of 20 or 100 μM Chidamide. The same concentrations of DMSO were used as control. The cell viability was measured by MTT assay **(A**, **G)**. The LncRNA fragments of breast cancer cells were screened by high-throughput RNA sequencing (RNAseq), and hierarchical clustering analysis was performed using the R language package gplots according to the TPM values of differential genes in different groups. The abscissa represents the fold changes of gene expression in different samples, and the ordinate represents the statistical significance of the difference in gene expression. Volcanic diagram showing the differential gene expression between samples **(B**, **H)**. Heat map of differential gene expression analysis between samples **(C**, **I)**. We designed three pairs of primers (Primers 1–3) to verify the real levels of LncRNA ENST869 in the treated cells [**(D–F)** for MCF-7, **(J–L)** for MDA-MB-231]. Data was presented as means ± S.D. for three independent experiments and analyzed using SPSS software, *20 μM Chidamide versus Basal at $p < 0.05$, **100 μM Chidamide versus Basal at $p < 0.05$.

LncRNA ENST869 Binds to the Specific Region of Nestin Transcription Promoter to Regulate Its Transcriptional Activity

Next, to explore the binding between ENST869 and Nestin mRNA, we examined the genome arrangement of LncRNA ENST869 and Nestin in the Ensembl database. As shown in **Figure 5A**, LncRNA ENST869 works in the pattern of antisense RNA. It has two exons, of which exon1 is adjacent to Nestin promoter regions, indicating that both of them have the binding possibility at the genomic level. Therefore, we designed the Nestin promoter into four regions (Named P1–P4), and synthesized those DNA sequences respectively. The primers used are listed in **Table 2**. After being subcloned into psiCHECK plasmid as shown in **Figure 5B** (Suppl. for plasmid construction), Luciferase activity was detected in cells with LncRNA ENST869 co-transfection. The results showed that the Nestin P4 promoter region showed high luciferase activity (**Figure 5C**). Furthermore, we analyzed the P4 promoter region into p4-1, p4-2 and p4-3 in detail. **Figure 5D** hinted that p4-3 possessed the highest luciferase activity. It indicates that within the 250 bp upstream of the starting point of Nestin transcription, there is a primary region of LncRNA ENST869 which affects the Nestin promoter activity.

LncRNA ENST869 Does Not Directly Bind to Nestin Protein

Finally, to find the direct evidence of the interaction between LncRNA ENST869 and Nestin, we observed the induction effect of Chidamide on LncRNA ENST869 accumulation at the RNA level. As shown in **Figure 6A**, we labeled biotin with an antisense ENST869 probe synthesized by 5'RACE and then determined the probe hybridized activity by dot blot (**Figure 6B**). Then, the probe with 100% activity was hybridized with the RNA extracted from cells on a positive nylon membrane. As shown with the Northern blot in **Figure 6C**, the expression level of LncRNA ENST869 with Chidamide treatment was notably higher than that in the control group. While we synthesized the full sequence of LncRNA ENST869 as a probe to incubate with the total

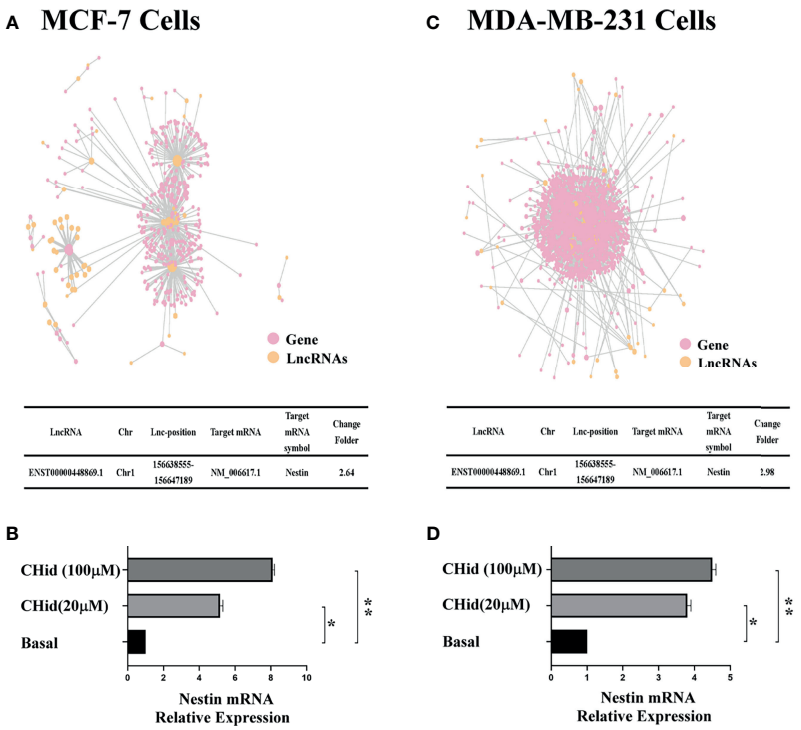

FIGURE 2 | LncRNA ENST869 promotes the expression of Nestin mRNA. The potential crosstalk between LncRNA and mRNAs was predicted through RNAplex software. Real-time PCR was used to verify the level of Nestin mRNA in Chidamide treated cells. Data was presented as means ± S.D. for three independent experiments and analyzed using SPSS software, *20 μM Chidamide versus Basal at $p < 0.05$, **100 μM Chidamide versus Basal at $p < 0.05$ [**(A, B)** for MCF-7, **(C, D)** for MDA-MB-231].

protein extracted from Chidamide treated cells. RNA-Protein Pulldown and EMSA assay showed no evidence of LncRNA ENST869 binding with any protein directly (**Figures 6D, E**). Western blot data also could not detect Nestin protein in the flow-through (data not shown).

DISCUSSION

Breast cancer is a malignant tumor occurring in the epithelia of the mammary gland (17, 18), Its occurrence and development are not only related to hereditary and endocrine factors, but also related to abnormal gene expression (19). HDACi is a family of anti-cancer drugs with great clinical application prospects. It mainly affects the corresponding target gene expression by changing the spatial structure of histone, and plays an important role in regulating cancer cell growth and cell cycle progression (20–24). Chidamide, as a new generation HDACi, has shown exceptional anti-breast cancer effects in previous experiments (25–28). In this paper, the treatment of Chidamide on MCF-7 or MDA-MB-231 breast cancer cells also confirmed that it could reduce the vitality of breast cancer cells and inhibit the growth of cancer cells.

With the increasing research on gene functions, LncRNA has attracted more attention. Its unique approach in influencing gene expression has been realized (29–32). Here, we screened the expression of LncRNA ENST869 by high-throughput sequencing combined with bioinformatics analysis and real-time PCR verification. The data showed that LncRNA ENST869 induced by Chidamide was relevant to Nestin function. Nestin is a type VI intermediate filament protein (33). There is clear evidence showing that the expression of Nestin is increased in a variety of tumor tissues including breast cancer, and is closely related to tumor malignancy. Therefore, it can be used as a biomarker to predict cancer occurrence and development (34).

Anti-cell death is an important feature of tumor cell survival (35). It enables tumor cells to withstand various challenges, including chemotherapeutic drugs (36). Nestin plays an essential role in the resistance against conventional chemotherapy of tumor stem cells (37–39). Nestin prevents tumor cell death by inducing DNA damage repair (40, 41). Nestin positive cells mark the existence of a stem cell-like population, which enables tumor cells to continue to survive and differentiate (42–44). For example, in glioma, Nestin positive cells labeled with stem cell like populations enable tumor cells to survive and proliferate when exposed to chemotherapeutic drugs (45, 46). Silencing Nestin expression with shRNA in nasopharyngeal carcinoma cells interrupted doxorubicin-induced DNA damage repair (47, 48). Studies also have shown that Nestin knockout by some LncRNAs increased cells sensitive to X-ray radiation in xenotransplantation

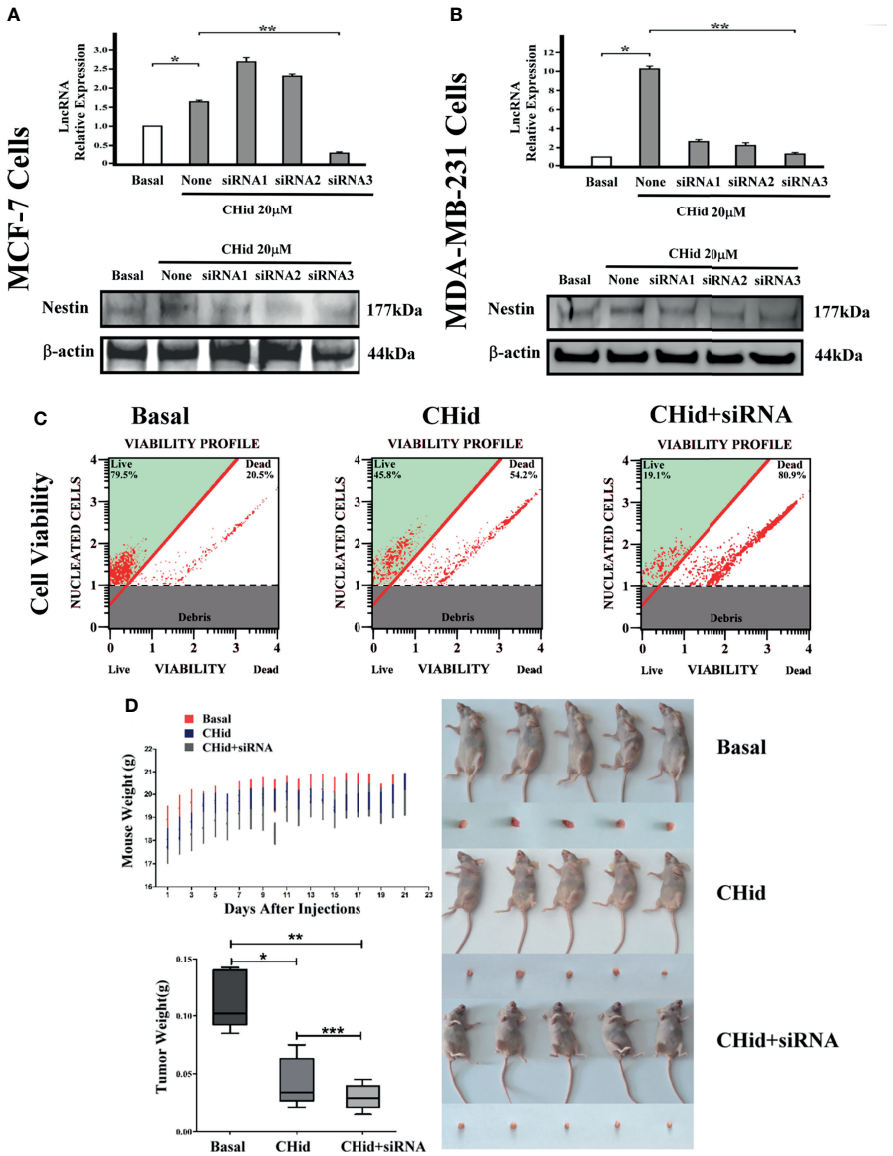

FIGURE 3 | Silencing LncRNA ENST869 increases the pharmacological effect of Chidamide. Three siRNA fragments designed for LncRNA ENST869 were screened by Real-time PCR and Western blot was done to detect the Nestin protein levels in **(A)** MCF-7 cells and **(B)** MDA-MB-231 cells. In addition, cell viability **(C)** assays and tumor xenograft models **(D)** for MDA-MB-231 cells verified the knockdown effects of LncRNA ENST869. Data was presented as means ± S.D. for three independent experiments and analyzed using SPSS software, *20 μM Chidamide versus Basal at p <0.05, **20 μM Chidamide with LncRNA siRNA versus Basal at p <0.05, ***20 μM Chidamide versus 20 μM Chidamide with LncRNA siRNA.

experiments (49). In our experiments, the anti-breast cancer drug Chidamide acts on breast cancer cells to activate Nestin expression through LncRNA ENST869, and this "inappropriate expression" is just the result of self-protection of cancer cells against drugs, suggesting that Nestin may participate in the pharmacological action against Chidamide, which may be the key in breast cancer cell drug resistance.

Bioinformatic analysis indicated that there is an interaction between LncRNA ENST869 and Nestin. We evaluated this interaction through RNA protein pull-down and other experiments. The results showed that the expression level of ENST869 RNA after Chidamide treatment was higher than that in the control group. LncRNA ENST869 did not bind directly to any protein. It is well known that LncRNA can participate in the regulation of target genes at different levels, namely, pre-transcription, transcription, and post-transcription (50–54). Luciferase assay showed that LncRNA ENST869 might regulate Nestin mRNA transcription through classical

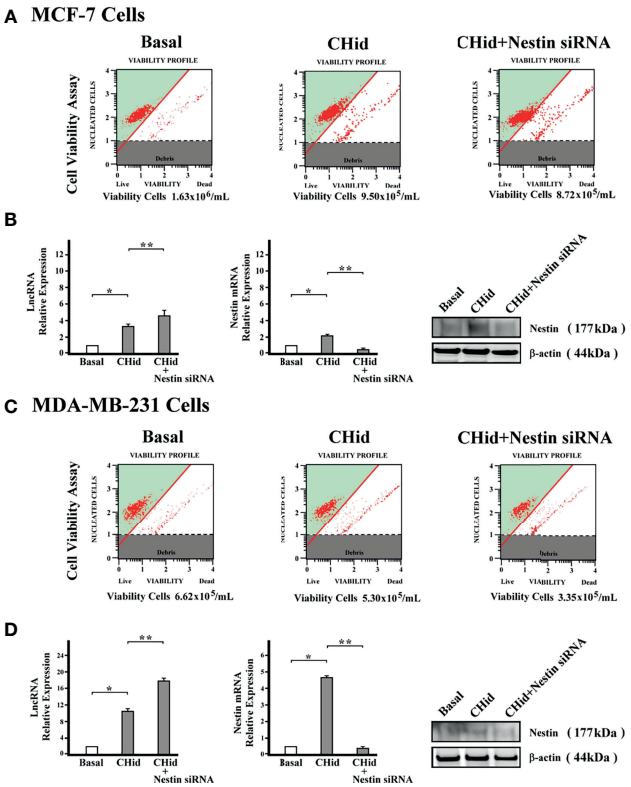

FIGURE 4 | Knockout of Nestin mRNA does not repress the expression of LncRNA ENST869. After transfecting the special Nestin siRNA and Chidamide treatment in breast cancer cells, cell viability was assessed **(A, C)**. Real-time PCR and Western blot detected the mRNA and protein level of LncRNA ENST869 and Nestin **(B, D)**. Data was presented as means±S.D. for three independent experiments and analyzed using SPSS software, * 20 mM Chidamide versus Basal at p<0.05, ** 20 mM Chidamide with Nestin siRNA versus Chidamide at p <0.05.

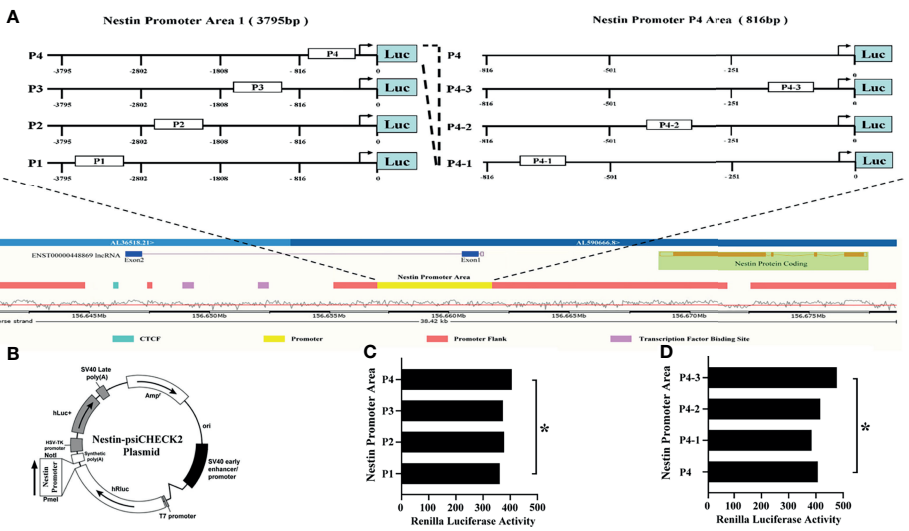

FIGURE 5 | LncRNA ENST869 binds to the specific region of the Nestin promoter to regulate its transcription activity. The Ensembl database was used to search the genomic arrangement of LncRNA ENST869 and Nestin promoter **(A)**. The sequences of Nestin promoter domains were subcloned into psiCHECK plasmid, and the activity of Luciferase was detected in cells co-transfected with LncRNA ENST869 **(B–D)**. Data was presented as mean ± S.D. for three independent experiments. **(C)** * P4 versus P1 at p<0.05, **(D)** * P4-3 versus P4 at p<0.05.

TABLE 2 | The primers used for subcloned plasmids are summarized.

Gene Name	Primer Orientation	Sequence
Nestin P1	Forward	5'-CCCTAACCTTCCCTCTCCTG-3'
	Reverse	5'-TGGCACTCACAGGTCTTCTG-3'
Nestin P2	Forward	5'-TCACCCAAATTTTCCCTCAC-3'
	Reverse	5'-CTTAGGCACTCAGGGCACTC-3'
Nestin P3	Forward	5'-AGGAGGCAGAGATGCAAGAA-3'
	Reverse	5'-TGTGGGAGGTCACACTGGTA-3'
Nestin P4	Forward	5'-CTGGGGCCAGAGTAGATCCT-3'
	Reverse	5'-AGGCAGAGGCAGACACAGAT-3'
Nestin P4-1	Forward	5'-CTGGGGCCAGAGTAGATCCT-3'
	Reverse	5'-TAAACTCCACCTCAGGGAAC-3'
Nestin P4-2	Forward	5'-GATAGTATATTGGATTCCCC-3'
	Reverse	5'-GAAACCCAACAAAGCCAGGA-3'
Nestin P4-3	Forward	5'-CTGGGGAAGGCGGAGCTGGT-3'
	Reverse	5'-AGGCAGAGGCAGACACAGAT-3'
	Reverse	5'-ACGACCAAATCCGTTGACTC-3'

anchorage of the transcriptionally active region. Because the common mode of most LncRNAs is to influence the transcription of downstream genes, it means that the direct regulation of Nestin transcription by LncRNA ENST869 might form as an integration platform, polymerizing transcription elements including transcription factors around LncRNAs to realize the transmission of upstream and downstream effector molecules. This can purposefully locate the transcription complex on the specific sequence of the promoter in an accurate pattern. Notably, studies have shown that other LncRNAs such as MALAT1 and Rik-203 may also play roles in the network affecting Nestin (55, 56).

Finally, we analyzed the target gene by the Gene Ontology (GO) enrichment function of LncRNA from Chidamide treated MDA-MB-231 breast cancer cells, and found that most LncRNAs in cells treated with Chidamide were mostly involved in autophagy initiation and the formation of secondary autophagic bodies (**Figure 7**), which is consistent with our previous experimental findings (16). That is, Chidamide exerts its pharmacological effect mainly by stimulating excessive autophagic cell death.

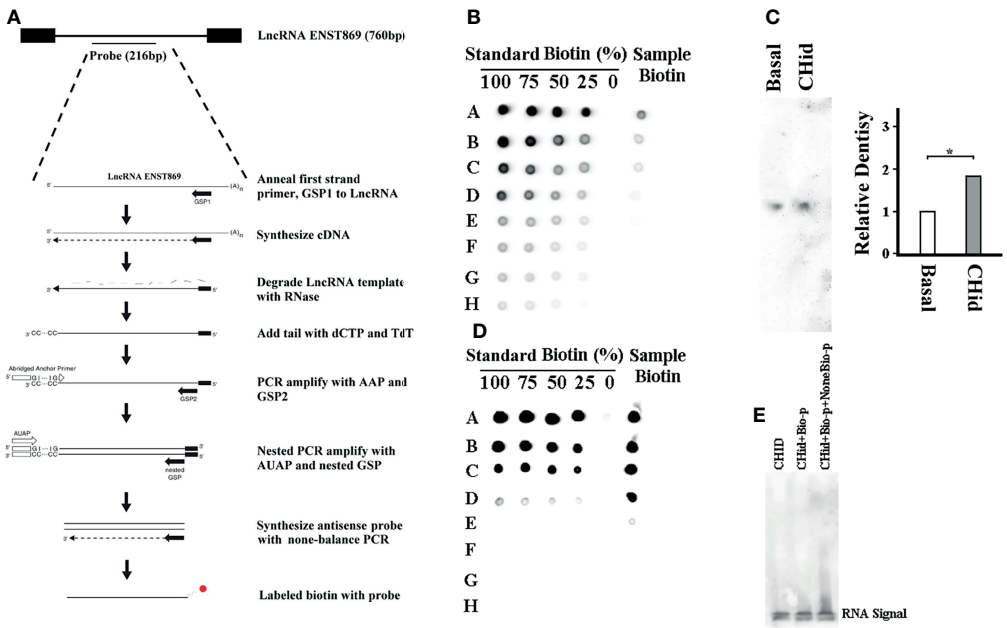

FIGURE 6 | LncRNA ENST869 does not directly bind to Nestin protein. 5'RACE was used for rapid amplification of antisense LncRNA ENST869 probe and labeled with biotin **(A)**. Dot blot hybridization was used to determine the probe activity **(B)** and Northern blot was used to detect the expression level of LncRNA ENST869 in the MDA-MB-231 cells treated with Chidamide **(C)**. The direct interaction between LncRNA and Nestin protein, RNA-Protein pulldown and EMSA assay **(D**, **E)**. Data was presented as means ± S.D. for three independent experiments and analyzed using SPSS software, *20 μM Chidamide versus Basal at p <0.05.

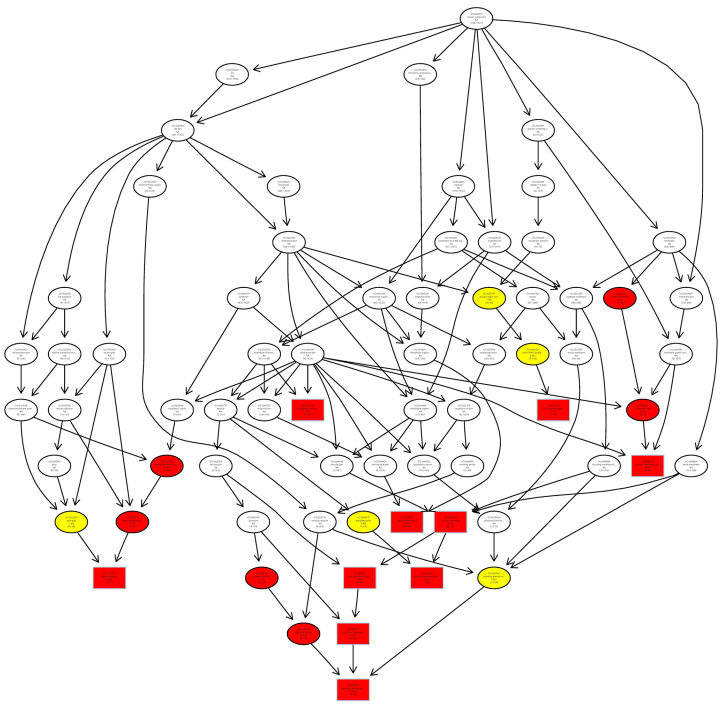

FIGURE 7 | Schematic representation of co-expression network of differentially expressed LncRNAs/mRNAs. All differentially expressed LncRNAs/mRNAs were selected for GO pathway analyses. GO was performed with KOBAS 3.0 software. GO analysis covered the cellular component (CC) domains.

CONCLUSION

Our study demonstrated that the induction of LncRNA ENST869 induced the death of breast cancer cells by regulating Nestin expression that was activated by Chidamide treatment. During this process, Nestin is involved in the pharmacological action of Chidamide against breast cancer cells. Nestin is the main factor in driving drug resistance. More detailed and specific mechanism between LncRNA ENST869 and Nestin needs further experimental verification.

DATA AVAILABILITY STATEMENT

The datasets presented in this study can be found in online repositories. The names of the repository/repositories and accession number(s) can be found below: the raw RNA-seq data is available in NCBI under the Sequence Read Archive (SRA) with accession number PRJNA807845. The data related to RNA-seq results were displayed in **Supplementary Materials**.

ETHICS STATEMENT

The animal study was reviewed and approved by the Shenyang Medical College.

AUTHOR CONTRIBUTIONS

WZ and XyF participated in the design of the study. WZ, HH, YG, and XyF performed the experiments. WZ, HH, and XyF analyzed data. WZ wrote the manuscript. All authors listed have made a substantial, direct, and intellectual contribution to the work and approved it for publication.

FUNDING

The work is supported by the Natural Science Foundation of China (81172509), the Research Foundation of Education Department of Liaoning Province (SYYX202004, 2021010620-301), the Natural Science combination Foundation for improving innovation of Liaoning Province (2022012046-301), and the Research Foundation of Shenyang Science and Technology Bureau (20-205-4-066).

SUPPLEMENTARY MATERIAL

The Supplementary Material for this article can be found online at: https://www.frontiersin.org/articles/10.3389/fonc.2022.874343/full#supplementary-material

REFERENCES

1. Sung H, Ferlay J, Siegel RL, Laversanne M, Soerjomataram I, Jemal A, et al. Global Cancer Statistics 2020: GLOBOCAN Estimates of Incidence and Mortality Worldwide for 36 Cancers in 185 Countries. *CA: Cancer J Clin* (2021) 71:209–49. doi: 10.3322/caac.21660
2. Sopik V. International Variation in Breast Cancer Incidence and Mortality in Young Women. *Breast Cancer Res Treat* (2021) 186:497–507. doi: 10.1007/s10549-020-06003-8
3. Rahman MM, Brane AC, Tollefsbol TO. MicroRNAs and Epigenetics Strategies to Reverse Breast Cancer. *Cells* (2019) 8(10):1214. doi: 10.3390/cells8101214
4. Nam HJ, Baek SH. Epigenetic Regulation in Breast Cancer. *Adv Exp Med Biol* (2021) 1187:103–19. doi: 10.1007/978-981-32-9620-6_5
5. Wu HJ, Chu PY. Epigenetic Regulation of Breast Cancer Stem Cells Contributing to Carcinogenesis and Therapeutic Implications. *Int J Mol Sci* (2021) 22(15):8113. doi: 10.3390/ijms22158113
6. You D, Richardson JR, Aleksunes LM. Epigenetic Regulation of Multidrug Resistance Protein 1 and Breast Cancer Resistance Protein Transporters by Histone Deacetylase Inhibition. *Drug Metab Disposition: Biol Fate Chemicals* (2020) 48:459–80. doi: 10.1124/dmd.119.089953
7. Meng Y, Jin J, Gong C, Miao H, Tao Z, Li T, et al. Phase II Study of Chidamide in Combination With Cisplatin in Patients With Metastatic Triple-Negative Breast Cancer. *Ann Palliative Med* (2021) 10:11255–64. doi: 10.21037/apm-21-1139
8. Zhang Q, Wang T, Geng C, Zhang Y, Zhang J, Ning Z, et al. Exploratory Clinical Study of Chidamide, an Oral Subtype-Selective Histone Deacetylase Inhibitor, in Combination With Exemestane in Hormone Receptor-Positive Advanced Breast Cancer. *Chin J Cancer Res = Chung-kuo yen cheng yen chiu* (2018) 30:605–12. doi: 10.21147/j.issn.1000-9604.2018.06.05
9. Tu K, Yu Y, Wang Y, Yang T, Hu Q, Qin X, et al. Combination of Chidamide-Mediated Epigenetic Modulation With Immunotherapy: Boosting Tumor Immunogenicity and Response to PD-1/PD-L1 Blockade. *ACS Appl Mater Interfaces* (2021) 13:39003–17. doi: 10.1021/acsami.1c08290
10. Zhou Y, Yue Y, Fan S, Jia Q, Ding X. Advances in Pathophysiology of Triple-Negative Breast Cancer: The Potential of lncRNAs for Clinical Diagnosis, Treatment, and Prognostic Monitoring. *Mol Biotechnol* (2021) 63:1093–102. doi: 10.1007/s12033-021-00368-x
11. Zhang XH, Li BF, Ding J, Shi L, Ren HM, Liu K, et al. LncRNA DANCR-miR-758-3p-PAX6 Molecular Network Regulates Apoptosis and Autophagy of Breast Cancer Cells. *Cancer Manage Res* (2020) 12:4073–84. doi: 10.2147/CMAR.S254069
12. Liang Y, Song X, Li Y, Chen B, Zhao W, Wang L, et al. LncRNA BCRT1 Promotes Breast Cancer Progression by Targeting miR-1303/PTBP3 Axis. *Mol Cancer* (2020) 19:85. doi: 10.1186/s12943-020-01206-5
13. Zhang W, Guan X, Tang J. The Long Non-Coding RNA Landscape in Triple-Negative Breast Cancer. *Cell Prolif* (2021) 54:e12966. doi: 10.1111/cpr.12966
14. Zhang H, Wang J, Yin Y, Meng Q, Lyu Y. The Role of EMT-Related lncRNA in the Process of Triple-Negative Breast Cancer Metastasis. *Bioscience Rep* (2021) 41(2):BSR20203121. doi: 10.1042/BSR20203121
15. Jin H, Du W, Huang W, Yan J, Tang Q, Chen Y, et al. lncRNA and Breast Cancer: Progress From Identifying Mechanisms to Challenges and Opportunities of Clinical Treatment. *Mol Ther Nucleic Acids* (2021) 25:613–37. doi: 10.1016/j.omtn.2021.08.005
16. Zhou W, Han H, Xu J, Sun T, Feng X. Autophagic Vacuole Secretion Triggered by Chidamide Participates in TRAIL Apoptosis Effect in Breast Cancer Cells. *Curr Pharm Design* (2021) 27:2366–80. doi: 10.2174/1381612826666200811175513
17. Cao W, Chen HD, Yu YW, Li N, Chen WQ. Changing Profiles of Cancer Burden Worldwide and in China: A Secondary Analysis of the Global Cancer Statistics 2020. *Chin Med J* (2021) 134:783–91. doi: 10.1097/CM9.0000000000001474
18. Azamjah N, Soltan-Zadeh Y, Zayeri F. Global Trend of Breast Cancer Mortality Rate: A 25-Year Study. *Asian Pacific J Cancer Prev APJCP* (2019) 20:2015–20. doi: 10.31557/APJCP.2019.20.7.2015
19. Quereda V, Bayle S, Vena F, Frydman SM, Monastyrskyi A, Roush WR, et al. Therapeutic Targeting of CDK12/CDK13 in Triple-Negative Breast Cancer. *Cancer Cell* (2019) 36:545–58.e7. doi: 10.1016/j.ccell.2019.09.004
20. Ediriweera MK, Tennekoon KH, Samarakoon SR. Emerging Role of Histone Deacetylase Inhibitors as Anti-Breast-Cancer Agents. *Drug Discov Today* (2019) 24:685–702. doi: 10.1016/j.drudis.2019.02.003
21. Kiweler N, Wünsch D, Wirth M, Mahendrarajah N, Schneider G, Stauber RH, et al. Histone Deacetylase Inhibitors Dysregulate DNA Repair Proteins and Antagonize Metastasis-Associated Processes. *J Cancer Res Clin Oncol* (2020) 146:343–56. doi: 10.1007/s00432-019-03118-4
22. Ediriweera MK, Cho SK. Targeting miRNAs by Histone Deacetylase Inhibitors (HDACi): Rationalizing Epigenetics-Based Therapies for Breast Cancer. *Pharmacol Ther* (2020) 206:107437. doi: 10.1016/j.pharmthera.2019.107437
23. Hii LW, Chung FF, Soo JS, Tan BS, Mai CW, Leong CO. Histone Deacetylase (HDAC) Inhibitors and Doxorubicin Combinations Target Both Breast Cancer Stem Cells and Non-Stem Breast Cancer Cells Simultaneously. *Breast Cancer Res Treat* (2020) 179:615–29. doi: 10.1007/s10549-019-05504-5
24. Sedky NK, Hamdan AA, Emad S, Allam AL, Ali M, Tolba MF. Insights Into the Therapeutic Potential of Histone Deacetylase Inhibitor/Immunotherapy Combination Regimens in Solid Tumors. *Clin Trans Oncol Off Publ Fed Spanish Oncol Societies Natl Cancer Institute Mexico* (2022). doi: 10.1007/s12094-022-02779-x
25. Chen X, Wang H, Sun X, Su L, Liu F, Zhao K, et al. Safety of Chidamide Plus Rituximab in Elderly Patients With Relapsed or Refractory B-Cell Lymphoma in China: A Multicenter, Single-Arm, Phase II Study. *Ann Trans Med* (2021) 9:1769. doi: 10.21037/atm-21-6019
26. Chen JS, Chou CH, Wu YH, Yang MH, Chu SH, Chao YS, et al. CC-01 (Chidamide Plus Celecoxib) Modifies the Tumor Immune Microenvironment and Reduces Tumor Progression Combined With Immune Checkpoint Inhibitor. *Sci Rep* (2022) 12:1100. doi: 10.1038/s41598-022-05055-8
27. Wang SC, Yu CY, Wu YC, Chang YC, Chen SL, Sung WW. Chidamide and Mitomycin C Exert Synergistic Cytotoxic Effects Against Bladder Cancer Cells *In Vitro* and Suppress Tumor Growth in a Rat Bladder Cancer Model. *Cancer Lett* (2022) 530:8–15. doi: 10.1016/j.canlet.2022.01.007
28. Wang BR, Wan CL, Liu SB, Qiu QC, Wu TM, Wang J, et al. A Combined Histone Deacetylases Targeting Strategy to Overcome Venetoclax Plus Azacitidine Regimen Resistance in Acute Myeloid Leukaemia: Three Case Reports. *Front Oncol* (2021) 11:797941. doi: 10.3389/fonc.2021.797941
29. Sun Z, Hu J, Ren W, Fang Y, Hu K, Yu H, et al. LncRNA SNHG3 Regulates the BMSC Osteogenic Differentiation in Bone Metastasis of Breast Cancer by Modulating the miR-1273g-3p/BMP3 Axis. *Biochem Biophys Res Commun* (2022) 594:117–23. doi: 10.1016/j.bbrc.2021.12.075
30. Deshpande RP, Sharma S, Liu Y, Pandey PR, Pei X, Wu K, et al. LncRNA IPW Inhibits Growth of Ductal Carcinoma *in Situ* by Downregulating ID2 Through miR-29c. *Breast Cancer Res BCR* (2022) 24:6. doi: 10.1186/s13058-022-01504-4
31. Di Agostino S, Vahabi M, Turco C, Fontemaggi G. Secreted Non-Coding RNAs: Functional Impact on the Tumor Microenvironment and Clinical Relevance in Triple-Negative Breast Cancer. *Non-Coding RNA* (2022) 8(1):5. doi: 10.3390/ncrna8010005
32. Fan Y, Dong X, Li M, Liu P, Zheng J, Li H, et al. LncRNA KRT19P3 Is Involved in Breast Cancer Cell Proliferation, Migration and Invasion. *Front Oncol* (2021) 11:799082. doi: 10.3389/fonc.2021.799082
33. Nouri P, Zimmer A, Brüggemann S, Friedrich R, Kühn R, Prakash N. Generation of a NES-Mscarlet Red Fluorescent Reporter Human iPSC Line for Live Cell Imaging and Flow Cytometric Analysis and Sorting Using CRISPR-Cas9-Mediated Gene Editing. *Cells* (2022) 11(2):268. doi: 10.3390/cells11020268
34. Szymańska-Chabowska A, Świątkowski F, Jankowska-Polańska B, Mazur G, Chabowski M. Nestin Expression as a Diagnostic and Prognostic Marker in Colorectal Cancer and Other Tumors. *Clin Med Insights Oncol* (2021) 15:11795549211038256. doi: 10.1177/11795549211038256
35. Yamagishi A, Susaki M, Takano Y, Mizusawa M, Mishima M, Iijima M, et al. The Structural Function of Nestin in Cell Body Softening Is Correlated With Cancer Cell Metastasis. *Int J Biol Sci* (2019) 15:1546–56. doi: 10.7150/ijbs.33423
36. Asleh K, Lyck Carstensen S, Tykjaer Jørgensen CL, Burugu S, Gao D, Won JR, et al. Basal Biomarkers Nestin and INPP4B Predict Gemcitabine Benefit in Metastatic Breast Cancer: Samples From the Phase III SBG0102 Clinical Trial. *Int J Cancer* (2019) 144:2578–86. doi: 10.1002/ijc.31969

37. Nobre AR, Risson E, Singh DK, Di Martino JS, Cheung JF, Wang J, et al. Bone Marrow NG2(+)/Nestin(+) Mesenchymal Stem Cells Drive DTC Dormancy *via* Tgfβ2. *Nat Cancer* (2021) 2:327–39. doi: 10.1038/s43018-021-00179-8
38. Nowak A, Grzegrzółka J, Kmiecik A, Piotrowska A, Matkowski R, Dzięgiel P. Role of Nestin Expression in Angiogenesis and Breast Cancer Progression. *Int J Oncol* (2018) 52:527–35. doi: 10.3892/ijo.2017.4223
39. Asleh K, Won JR, Gao D, Voduc KD, Nielsen TO. Nestin Expression in Breast Cancer: Association With Prognosis and Subtype on 3641 Cases With Long-Term Follow-Up. *Breast Cancer Res Treat* (2018) 168:107–15. doi: 10.1007/s10549-017-4583-z
40. Tampaki EC, Tampakis A, Nonni A, Kontzoglou K, Patsouris E, Kouraklis G. Nestin and Cluster of Differentiation 146 Expression in Breast Cancer: Predicting Early Recurrence by Targeting Metastasis? *Tumour Biol J Int Soc Oncodevelopmental Biol Med* (2017) 39:1010428317691181. doi: 10.1177/1010428317691181
41. Krüger K, Wik E, Knutsvik G, Nalwoga H, Klingen TA, Arnes JB, et al. Expression of Nestin Associates With BRCA1 Mutations, a Basal-Like Phenotype and Aggressive Breast Cancer. *Sci Rep* (2017) 7:1089. doi: 10.1038/s41598-017-00862-w
42. De Lara S, Nyqvist J, Werner Rönnerman E, Helou K, Kenne Sarenmalm E, Einbeigi Z, et al. The Prognostic Relevance of FOXA1 and Nestin Expression in Breast Cancer Metastases: A Retrospective Study of 164 Cases During a 10-Year Period (2004-2014). *BMC Cancer* (2019) 19:187. doi: 10.1186/s12885-019-5373-2
43. Nowak A, Grzegrzolka J, Paprocka M, Piotrowska A, Rys J, Matkowski R, et al. Nestin-Positive Microvessel Density Is an Independent Prognostic Factor in Breast Cancer. *Int J Oncol* (2017) 51:668–76. doi: 10.3892/ijo.2017.4057
44. Aglan SA, Elsammak M, Elsammak O, El-Bakoury EA, Elsheredy HG, Ahmed YS, et al. Evaluation of Serum Nestin and HOTAIR Rs12826786 C>T Polymorphism as Screening Tools for Breast Cancer in Egyptian Women. *J Med Biochem* (2021) 40:17–25. doi: 10.5937/jomb0-25295
45. Tampakis A, Tampaki EC, Trafalis D, Nonni A, Kontzoglou K, Patsouris E, et al. Nestin and CD146 Expression in Metaplastic Breast Cancer: Stem-Cell Therapy in Need? Lessons Reported From a Male Patient. *Eur Rev Med Pharmacol Sci* (2017) 21:4137–40.
46. Feng W, Liu S, Zhu R, Li B, Zhu Z, Yang J, et al. SOX10 Induced Nestin Expression Regulates Cancer Stem Cell Properties of TNBC Cells. *Biochem Biophys Res Commun* (2017) 485:522–8. doi: 10.1016/j.bbrc.2017.02.014
47. Zhang X, Xing C, Guan W, Chen L, Guo K, Yu A, et al. Clinicopathological and Prognostic Significance of Nestin Expression in Patients With Breast Cancer: A Systematic Review and Meta-Analysis. *Cancer Cell Int* (2020) 20:169. doi: 10.1186/s12935-020-01252-5
48. Nowak A, Dziegiel P. Implications of Nestin in Breast Cancer Pathogenesis (Review). *Int J Oncol* (2018) 53:477–87. doi: 10.3892/ijo.2018.4441
49. Cai YD, Zhang Q, Zhang YH, Chen L, Huang T. Identification of Genes Associated With Breast Cancer Metastasis to Bone on a Protein-Protein Interaction Network With a Shortest Path Algorithm. *J Proteome Res* (2017) 16:1027–38. doi: 10.1021/acs.jproteome.6b00950
50. Tang X, Xiao Q, Yu K. Breast Cancer Candidate Gene Detection Through Integration of Subcellular Localization Data With Protein-Protein Interaction Networks. *IEEE Trans Nanobiosci* (2020) 19:556–61. doi: 10.1109/TNB.2020.2990178
51. Tiwari S, Awasthi M, Singh S, Pandey VP, Dwivedi UN. Modulation of Interaction of Mutant TP53 and Wild Type BRCA1 by Alkaloids: A Computational Approach Towards Targeting Protein-Protein Interaction as a Futuristic Therapeutic Intervention Strategy for Breast Cancer Impediment. *J Biomol Struct Dyn* (2018) 36:3376–87. doi: 10.1080/07391102.2017.1388286
52. Li W, Bai X, Hu E, Huang H, Li Y, He Y, et al. Identification of Breast Cancer Prognostic Modules Based on Weighted Protein-Protein Interaction Networks. *Oncol Lett* (2017) 13:3935–41. doi: 10.3892/ol.2017.5917
53. Yoon HS, Choi SH, Park JH, Min JY, Hyon JY, Yang Y, et al. A Novel Protein-Protein Interaction Between RSK3 and Iκbα and a New Binding Inhibitor That Suppresses Breast Cancer Tumorigenesis. *Cancers* (2021) 13(12):2973. doi: 10.3390/cancers13122973
54. Chen N, Zhao G, Yan X, Lv Z, Yin H, Zhang S, et al. A Novel FLI1 Exonic Circular RNA Promotes Metastasis in Breast Cancer by Coordinately Regulating TET1 and DNMT1. *Genome Biol* (2018) 19:218. doi: 10.1186/s13059-018-1594-y
55. Yong H, Liang Z, Tingfeng W, Yulun H, Zhe C, Xuetao L, et al. Downregulation of lncRNA-MALAT1 Affects Proliferation and the Expression of Stemness Markers in Glioma Stem Cell Line SHG139S. *Cell Mol Neurobiol* (2016) 36:1097–107. doi: 10.1007/s10571-015-0303-6
56. Lei Z, Jia Y, Qidong L, Zhongcong X, Hong J. LncRNA Rik-203 Contributes to Anesthesia Neurotoxicity *via* microRNA-101a-3p and GSK-3β-Mediated Neural Differentiation. *Sci Rep* (2019) 9:6822. doi: 10.1038/s41598-019-42991-4

Conflict of Interest: The authors declare that the research was conducted in the absence of any commercial or financial relationships that could be construed as a potential conflict of interest.

Publisher's Note: All claims expressed in this article are solely those of the authors and do not necessarily represent those of their affiliated organizations, or those of the publisher, the editors and the reviewers. Any product that may be evaluated in this article, or claim that may be made by its manufacturer, is not guaranteed or endorsed by the publisher.

Copyright © 2022 Feng, Han, Guo, Feng, Guo and Zhou. This is an open-access article distributed under the terms of the Creative Commons Attribution License (CC BY). The use, distribution or reproduction in other forums is permitted, provided the original author(s) and the copyright owner(s) are credited and that the original publication in this journal is cited, in accordance with accepted academic practice. No use, distribution or reproduction is permitted which does not comply with these terms.

frontiers | Frontiers in Pharmacology

SYSTEMATIC REVIEW
published: 28 April 2022
doi: 10.3389/fphar.2022.895187

Efficacy and Safety Evaluation of Sintilimab for Cancer Treatment: A Systematic Review and Meta-analysis of Randomized Controlled Trials

Ziqi Ye[1†], *Wenchao Yang*[2†], *Bixia Xuan*[2], *Xiaofang Li*[2], *Jiana He*[2], *Haiyan Si*[3] *and Wenhua Ma*[2*]

[1]Department of Clinical Pharmacy, The First Affiliated Hospital, Zhejiang University School of Medicine, Hangzhou, China, [2]Department of Pharmacy, Traditional Chinese Medical Hospital of Zhuji, Zhuji, China, [3]Department of Gastroenterology, Traditional Chinese Medical Hospital of Zhuji, Zhuji, China

Objective: Meta analysis was used to explore the efficacy and safety of Sintilimab in the treatment of cancer.

Methods: The databases of CNKI, VIP, Wanfang Data, PubMed, ScienceDirect, the Cochrane Library and EMBASE were searched by computer to collect the randomized controlled trials published as of March 2022. The retrieval work was completed by two researchers alone. They screened the literature and extracted the data according to the nanodischarge standard, using Revman 5.4 software. The included studies were statistically analyzed.

Results: Six RCTs were included in this study, including 1,048 cases of Sintilimab and 711 cases of other anticancer drugs. Compared with the control group, the overall survival (HR = 1.64, 95% CI: 1.35–1.99, $p < 0.00001$) and progression free survival (HR = 1.89, 95% CI: 1.59–2.25, $p < 0.00001$) of cancer treated with Sintilimab were longer and more effective. Moreover, the risk ratio of any grade of adverse reactions (HR = 0.87, 95% CI: 0.74–1.03, $p = 0.11$) and above grade III adverse reactions (HR = 0.84, 95% CI: 0.67–1.06, $p = 0.14$) in the treatment of cancer with Sintilimab was lower and the safety was better.

Conclusion: Compared with non-Sintilimab group, Sintilimab treatment can improve the clinical efficacy of tumor patients and has a lower incidence of adverse reactions. This treatment may be a promising treatment for cancer patients.

Keywords: Sintilimab, cancer, overall survival, progression free survival, safety

Systematic Review Registration: (website), identifier (registration number).

OPEN ACCESS

Edited by:
Ting Wang,
Sichuan Cancer Hospital, China

Reviewed by:
Xun Luo,
Kerry Rehabilitation Medicine Research Institute, China
Lixing Zhuang,
Guangzhou University of Chinese Medicine, China

***Correspondence:**
Wenhua Ma
mawenhua2022@163.com

[†]*These authors have contributed equally to this work*

Specialty section:
This article was submitted to Pharmacology of Anti-Cancer Drugs, a section of the journal Frontiers in Pharmacology

Received: *13 March 2022*
Accepted: *08 April 2022*
Published: *28 April 2022*

Citation:
Ye Z, Yang W, Xuan B, Li X, He J, Si H and Ma W (2022) Efficacy and Safety Evaluation of Sintilimab for Cancer Treatment: A Systematic Review and Meta-analysis of Randomized Controlled Trials. Front. Pharmacol. 13:895187. doi: 10.3389/fphar.2022.895187

INTRODUCTION

The global epidemiological survey shows that cancer has high incidence rate and mortality rate. Clinically, traditional dual drug chemotherapy including platinum, paclitaxel and adriamycin has always been the standard first-line therapy for cancer patients (Wei et al., 2020). In recent years, immune checkpoint inhibitors (ICIs) have been more and more widely used in clinic. Multiple ICIs

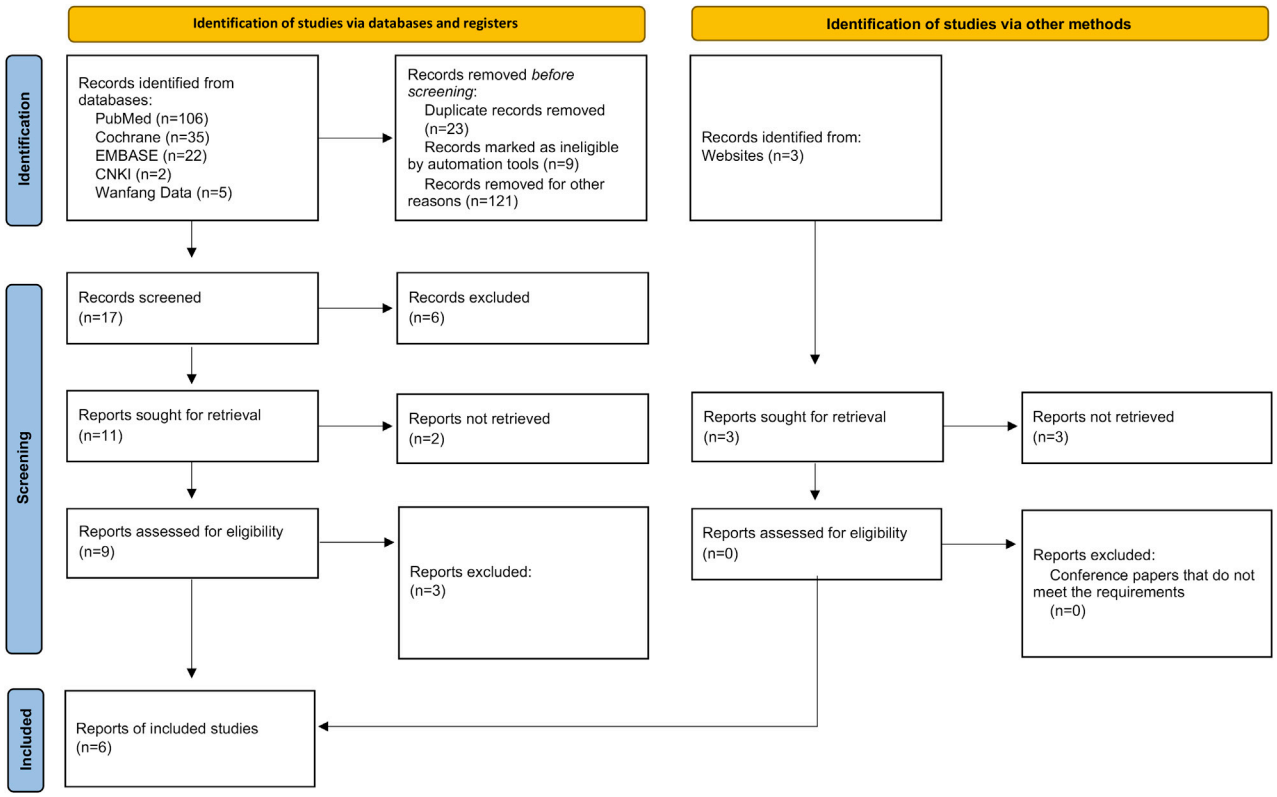

FIGURE 1 | Literature screening process and results.

have been proved to improve the survival rate of cancer patients, but the high price and high medical cost are still the main obstacles for Chinese cancer patients to obtain these treatments. For these reasons, the successful development of ICIs made in China has greatly reduced the economic burden of patients and benefited more patients. Sintilimab was officially approved by the State Drug Administration in December 2018 and was listed in the national medical insurance catalogue in November 2019 (Wang et al., 2019). Sintilimab is an inhibitor of recombinant human immunoglobulin G-type programmed death protein-1 (PD-1). It has been approved for the treatment of recurrent or refractory classical Hodgkin's lymphoma since December 2018. At present, it has carried out extensive clinical trials in solid tumors such as lung cancer, liver cancer, gastric cancer and esophageal cancer (Huang et al., 2022). This study systematically evaluated the efficacy and safety of Sintilimab in the treatment of cancer, in order to provide reference basis for clinical treatment.

MATERIALS AND METHODS

Search Strategy and Study Selection

We searched CNKI, VIP, Wanfang Data, PubMed, ScienceDirect, the Cochrane Library, EMBASE and other databases by computer. In addition, we also searched the references and meeting minutes included in the study to supplement and obtain relevant materials. Chinese key words: Sintilimab, cancer, randomized controlled trial English key words: Sintilimab, IBI308, IBI-308, cancer, randomized controlled trials, RCTs. The search time is up to March 2022.

Inclusion criteria: ① the type of study is RCTs; ② The subjects were patients diagnosed with cancer by clinicopathological examination; ③ Intervention measures: patients in the experimental group were treated with Sintilimab, and patients in the control group were treated with non Sintilimab (the treatment without Sintilimab); ④ The primary outcome measures were overall survival (OS) and progression free survival (PFS). The secondary outcome measures were adverse reactions at any level and adverse reactions above grade 3.

Exclusion criteria: ① repeatedly published literature; ② Documents that cannot obtain original data or contact the author to obtain the original text; ③ Abstract, review, meta-analysis, case report and animal experiment; ④ Non Chinese and English literature.

Bias Risk Assessment and Quality Assessment

The Newcastle Ottawa scale (NOS) was used to evaluate the quality of the included study (Bylicki et al., 2018), according to the following: 1) whether it is representative; 2)

TABLE 1 | Basic characteristics of included studies and main evaluation indicators (Shi et al., 2019; Yang et al., 2020; Ren et al., 2021; Zhou et al., 2021; Lin et al., 2022; Xu et al., 2022).

First author	Year	Clinical trial number	Phase	Type of cancer	NO. of patients with sintilimab	NO. of patients with non-sintilimab	Gender		Average age	HR for OS (95%CI)	*p*-Value for OS	HR for PFS (95%CI)	*p*-Value for PFS	Quality
							Sintilimab (M/F)	Non-sintilimab (M/F)						
Yunpeng Yang Lin et al. (2022)	2020	NCT03607539	III	NSCLC	266	131	204/62	99/32	61	0.609 (0.4,0.926)	0.01921	0.482 (0.362,0.643)	<0.00001	7
Zhenggang Ren et al. (2021)	2021	NCT03794440	II-III	HC	380	191	334/46	171/20	53–54	0.57 (0.43,0.75)	<0.0001	0.56 (0.46,0.70)	<0.0001	7
Caicun Zhou Shi et al. (2019)	2021	NCT03629925	III	NSCLC	179	178	163/16	164/14	62–64	NA	NA	0.536 (0.422,0.681)	<0.00001	8
Xinqing Lin Xu et al. (2022)	2021	NCT03629925	III	NSCLC	32	20	29/3	17/3	58–63	0.62 (0.28,1.36)	0.23	0.61 (0.30,1.25)	0.18	9
Yuankai Shi Yang et al. (2020)	2019	NCT03114683	II	Hodgkin lymphoma	96	96	56/40	56/40	33	NA	NA	NA	NA	7
Jianming Xu Zhou et al. (2021)	2022	NCT03116152	II	ESSC	95	95	88/7	84/11	60	0.70 (0.50,0.97)	0.032	NA	NA	8

Note: HC, hepatocellular carcinoma; ESSC, Esophageal squamous-cell carcinoma; HR, hazard ratio; NA, Not available; PFS, progression free survival; OS, overall survival; M, male; F, female.

Determination of blind method; 3) Whether the random method is determined; 4) Completeness of outcome events; 5) Comparability of included studies; 6) Evaluation of outcome events; 7) Whether there is follow-up; 8) Follow up integrity. High quality literature is seven to nine points, general quality literature is four to six points, and low quality literature is three points or lower. Two reviewers independently extracted data according to the specified selection criteria. Differences of opinion are resolved through discussion between authors or by obtaining opinions from a third evaluator.

Data Extraction

Two researchers independently screened the literature, extracted the data and cross checked. In case of any difference, it shall be settled through discussion or negotiation with a third party. During literature screening, first read the title. After excluding the obviously irrelevant literature, further read the abstract and full text to determine whether to be included. If necessary, contact the original study author by email or telephone to obtain information that is not determined but very important to this study. Data extraction contents include: ① basic information of the included study: first author, year of publication, sample size, outcome indicators and outcome measurement data.

Statistical Analysis

Data were processed through Revman5.4 software. Relative risk ratios (RR) and 95% confidence interval (95% CI) were used as effect indexes for counting data, and the difference was statistically significant ($p < 0.05$). I^2 is used to evaluate the heterogeneity. If the heterogeneity test result I^2 is less than 50%, it means that there is no statistical heterogeneity among the research results, and the fixed effect model is used; If the heterogeneity test result $I^2 > 50\%$, analyze the source of heterogeneity. If the heterogeneity still exists, select the random effect model to estimate the combined effect.

RESULTS

Literature Search and Characteristics of Included Studies

We searched 170 literatures (including 106 in PubMed, 35 in Cochrane, 22 in Embase, two in CNKI and five in Wangfang Data) and three conference papers by computer, and selected 17 according to the title and abstract. After full-text analysis and evaluation, we excluded 11 literatures with abnormal data, incomplete information or unavailable due to non comparative research, and finally included 6 (Shi et al., 2019; Yang et al., 2020; Ren et al., 2021; Zhou et al., 2021; Lin et al., 2022; Xu et al., 2022) literatures for systematic evaluation and meta-analysis. The process of literature screening is shown in **Figure 1**. There were 1,048 patients in the experimental group and 711 patients in the control group. The six literatures are of high quality and their basic characteristics and main evaluation indicators were shown in **Table 1**.

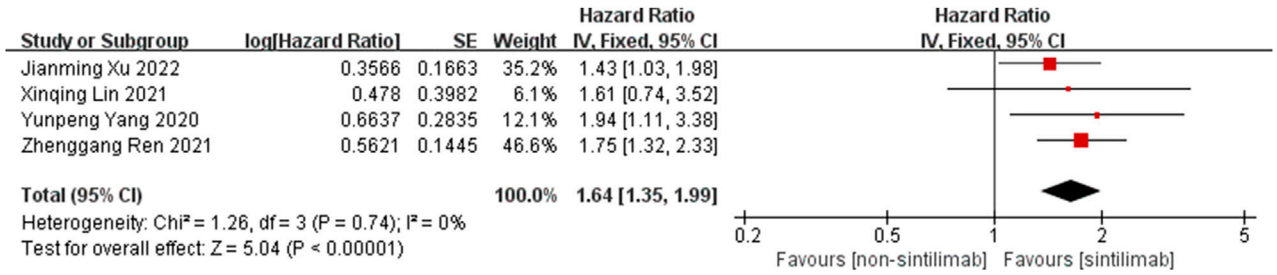

FIGURE 2 | Meta-analysis results of OS between Sintilimab group and non-Sintilimab group.

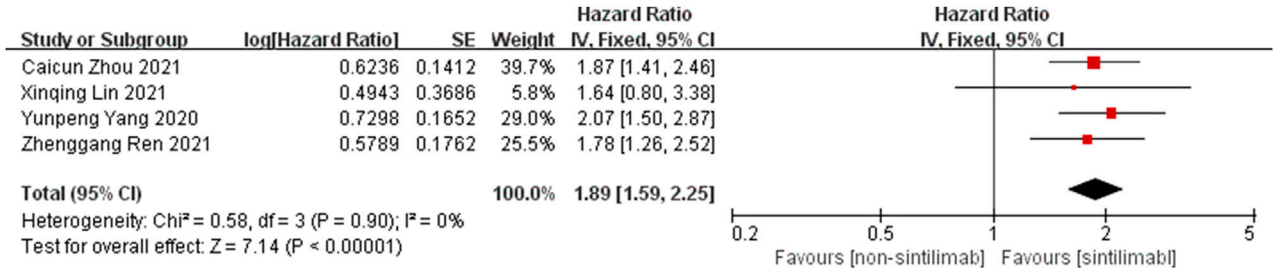

FIGURE 3 | Meta-analysis results of PFS between Sintilimab group and non-Sintilimab group.

Meta Analysis Results of Efficacy

Comparison of OS: four studies can obtain the OS data of cancer patients treated with Sintilimab. For heterogeneity analysis, I^2 = 0%, p = 0.74. There is no statistical heterogeneity among the studies. The fixed effect model is used for analysis. The results showed that HR = 1.64 (95% CI = 1.35–1.99, p < 0.00001), suggesting that Sintilimab can significantly improve the OS of cancer patients, as shown in **Figure 2**.

Comparison of PFS: the PFS data of cancer patients treated with Sintilimab can be obtained from four studies. For heterogeneity analysis, I^2 = 0%, p = 0.90. There is no statistical heterogeneity among the studies. The fixed effect model is used for analysis. The results showed that HR = 1.89 (95% CI = 1.59–2.55, p < 0.00001), suggesting that Sintilimab can significantly prolong PFS in cancer patients, as shown in **Figure 3**.

Meta Analysis Results of Safety

Comparison of adverse reactions at any level: Six studies can obtain the data of any level of adverse reactions (including nausea, ashenia, diarrhea and anemia) of cancer patients treated with Sintilimab. For heterogeneity analysis, I^2 = 77%, p < 0.00001. There is statistical heterogeneity among studies, which is analyzed by random effect model. The results showed that HR = 0.87 (95% CI = 0.74–1.03, p = 0.11), suggesting that the incidence of any level of adverse reactions in patients with Sintilimab was low, but there was no significant difference in the results, as shown in **Figure 4**.

Comparison of adverse reactions above grade III: Six studies can obtain the data of more than grade III adverse reactions (including nausea, ashenia, diarrhea and anemia) of cancer patients treated with Sintilimab. The heterogeneity analysis is carried out, with I^2 = 18%, p = 0.26. There is no statistical heterogeneity among the studies. The fixed effect model is used for analysis. The results showed that HR = 0.84 (95% CI = 0.67–1.06, p = 0.14), suggesting that the incidence of grade III and above adverse reactions in patients with Sintilimab was low, but there was no significant difference in the results, as shown in **Figure 5**.

Publication Bias Assessment and Sensitivity Analysis

The publication bias assessment of this study was performed only in OS and PFS. The funnel plot is symmetrical, indicating no significant publication bias (**Figure 6**). Sensitivity analysis was conducted on the results, and meta-analysis was conducted by ignoring each study in turn. No significant changes were found in the results, indicating that the results of this study are stable.

DISCUSSION

Sintilimab is a monoclonal antibody against programmed cell death protein 1. It can block the interaction between PD-1 and its ligand and help T cells restore their anti-tumor effect. In 2018,

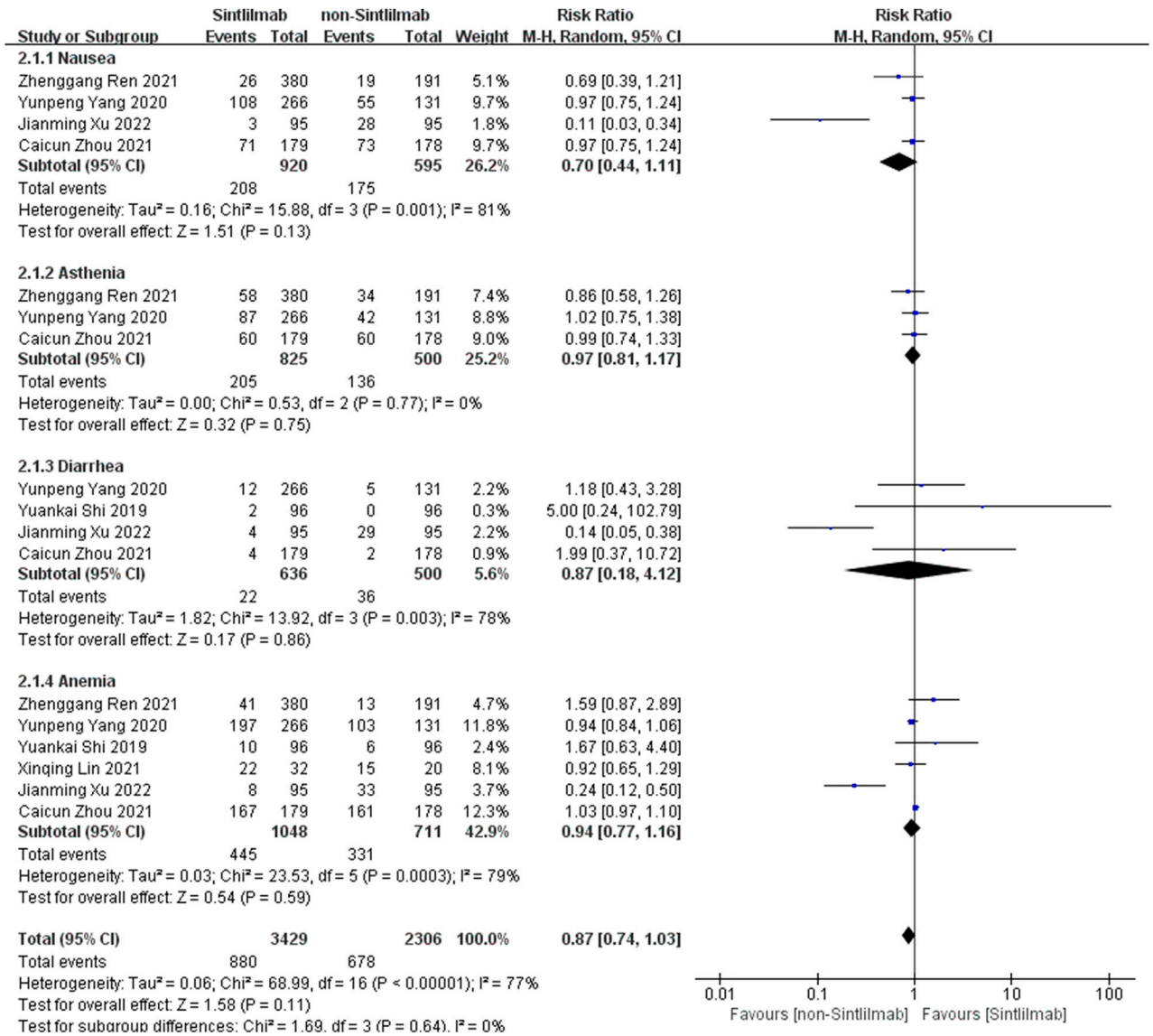

FIGURE 4 | Meta-analysis results of adverse reactions of any grade between Sintilimab group and non-Sintilimab group.

Sintilimab has been approved by the State Administration of medicine of China for the treatment of patients with recurrent or refractory classical Hodgkin's lymphoma. In recent years, a large number of studies have reported the anti-tumor effect of Sindilimab. In general, Sintilimab has similar anti-tumor effect and better safety compared with other ICIs (such as Nivolumab and Pembrolizumab) in Hodgkin's lymphoma, natural killer T-cell lymphoma and advanced non-small cell lung cancer (Zhang et al., 2020).

In phase three clinical trials, the combination of ICIs and chemotherapy is rapidly developing into a first-line treatment for many cancers. Paz-Ares et al. (Paz-Ares et al., 2018) showed that Pembrolizumab combined chemotherapy (carboplatin and paclitaxel or paclitaxel) significantly prolonged OS (median, 15.9 vs. 11.3 months, HR = 0.64, $p < 0.001$) and PFS (6.4 vs. 4.8 months, HR = 0.56, $p < 0.001$) compared with chemotherapy alone. Martin Reck et al. (Reck et al., 2016) found that the median progression free survival of Pembrolizumab combined with chemotherapy group was significantly prolonged, 10.3 vs. 6.0 months. The 6-month overall survival rate in the Pembrolizumab combined chemotherapy group was estimated to be 80.2% vs. 72.4%. The above suggests that the overall survival and progression free survival of cancer patients treated with ICIs combined with chemotherapy have been significantly improved. As an ICIs, Sintilimab has been used in combination with chemotherapeutic drugs in the treatment of cancer patients. For example, this randomized, open label, multicenter phase

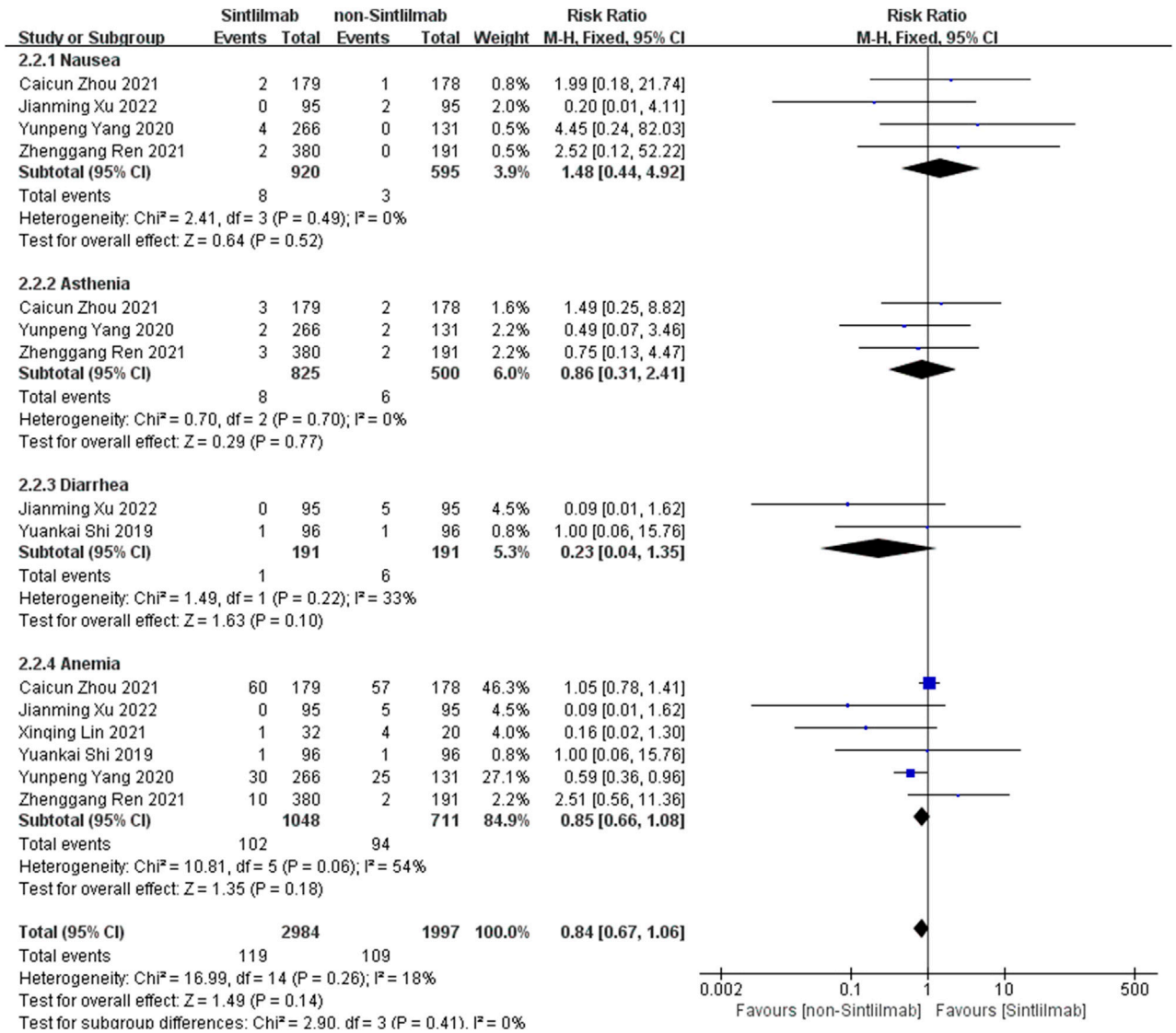

FIGURE 5 | Meta-analysis results of adverse reactions above grade 3 between Sintilimab group and non-Sintilimab group.

two trial of Jianming Xu et al. (Ren et al., 2021) evaluated the comparison of PD-1 inhibitor Sintilimab with chemotherapy in patients with esophageal squamous cell carcinoma after first-line chemotherapy. Compared with the chemotherapy group, the median OS in the Sintilimab group was significantly improved (median OS 7.2 vs. 6.2 months; p = 0.032; HR = 0.70; 95% CI, 0.50–0.97). The incidence of grade 3–5 treatment-related adverse events in the Sintilimab group was lower than that in the chemotherapy group (20.2% and 39.1%, respectively).

In this meta-analysis, we evaluated the efficacy of Sintilimab in cancer patients and selected OS and PFS as the primary outcomes. The results showed that in terms of effectiveness, Sintilimab improved the HR of OS and PFS, indicating that patients receiving immunotherapy had better OS and PFS than patients receiving ordinary chemotherapy. In terms of safety, the risk ratio of adverse reactions at any level and above in the Sintilimab treatment group is lower than that in the control group. Although there is no significant difference in the results, it also suggests that the safety of Sintilimab treatment is higher than that of ordinary chemotherapy drugs, and it is not easy to produce more common typical adverse reactions (nausea, ashenia, diarrhea, anemia). According to the above results suggest that in the process of clinical practice, especially for non-small cell lung cancer, liver cancer, non-hodgkin's lymphoma, such as cancer patients during chemotherapy, Sintilimab can be used as the preferred drug resistance. It can not only bring a higher

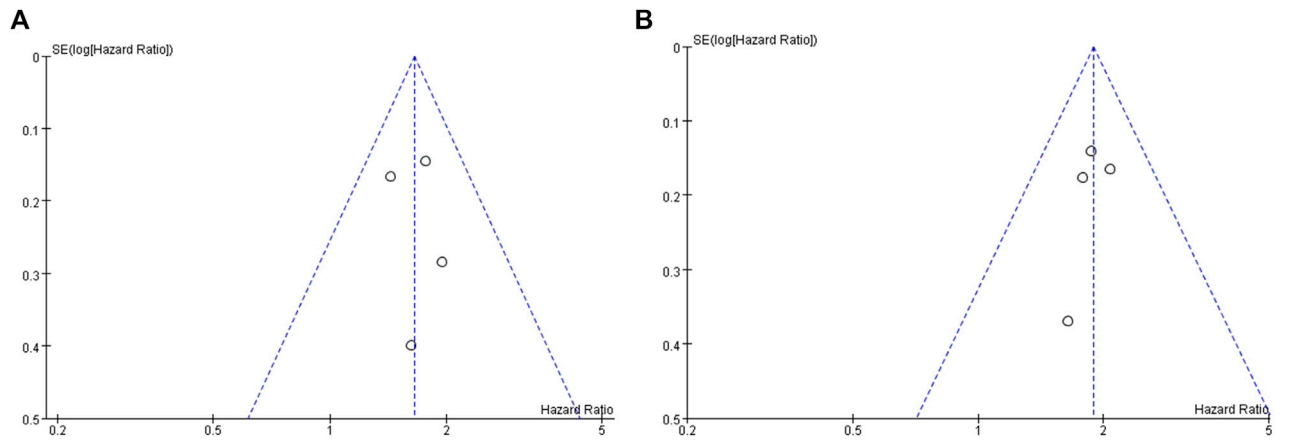

FIGURE 6 | Inverted funnel plot of OS (A) and PFS (B).

response rate, also can prolong the overall survival and disease progression, and caused most of the adverse reaction of one to two levels. With a long-lasting therapeutic response and tolerable toxicity, Sintilimab has shown promising efficacy overall.

It has to be said that this study also has some limitations: ① after systematic retrieval and screening, only six limited literatures were included for systematic evaluation and meta-analysis, resulting in a small sample size; ② The heterogeneity of individual statistical results may affect the credibility of the research results; ③ Different cancer types in different studies may increase heterogeneity and affect the reliability of results. However, in the study, in order to better reduce the above bias, when implementing retrieval and data consolidation, this study should be scientifically and objectively reported according to the Newcastle Ottawa scale as much as possible.

In conclusion, compared with non-Sintilimab group, Sintilimab can prolong the OS and PFS of patients in the treatment of cancer, with better clinical efficacy and high safety. Sintilimab may be a promising treatment for cancer patients.

DATA AVAILABILITY STATEMENT

The original contributions presented in the study are included in the article/Supplementary Material, further inquiries can be directed to the corresponding author.

AUTHORS CONTRIBUTIONS

All authors contributed to the successful completion of this study. Database search and data analysis was conducted by ZY and WY. Study selection and data extraction were performed by BX, XL, JH, and HS. The manuscript was written by ZY and WY. WM reviewed the manuscript.

FUNDING

This work was supported by the clinical fund project of Zhejiang Medical Association in 2021 (2021ZYC-A193).

REFERENCES

Bylicki, O., Paleiron, N., Rousseau-Bussac, G., and Chouaïd, C. (2018). New PDL1 Inhibitors for Non-small Cell Lung Cancer: Focus on Pembrolizumab. *Onco Targets Ther.* 11, 4051–4064. doi:10.2147/OTT.S154606

Huang, N., Zhao, C., Hu, X., Zhang, C., Xiong, F., Huang, W., et al. (2022). Safety and Efficacy of Sintilimab Combination Therapy for the Treatment of 48 Patients with Advanced Malignant Tumors. *Transl Cancer Res.* 11, 252–261. doi:10.21037/tcr-22-54

Lin, X., Deng, H., Li, S., Xie, X., Chen, C., Cai, L., et al. (2022). Sintilimab with Chemotherapy as First-Line Treatment for Locally Advanced or Metastatic Squamous Non-small-cell Lung Cancer: a Real-World Data Study. *J. Cancer Res. Clin. Oncol* Online ahead of print. doi:10.1007/s00432-021-03903-0

Paz-Ares, L., Luft, A., Vicente, D., Tafreshi, A., Gümüş, M., Mazières, J., et al. (2018). Pembrolizumab Plus Chemotherapy for Squamous Non-small-cell Lung Cancer. *N. Engl. J. Med.* 379, 2040–2051. doi:10.1056/NEJMoa1810865

Reck, M., Rodríguez-Abreu, D., Robinson, A. G., Hui, R., Csőszi, T., Fülöp, A., et al. (2016). Pembrolizumab versus Chemotherapy for PD-L1-Positive Non-small-cell Lung Cancer. *N. Engl. J. Med.* 375, 1823–1833. doi:10.1056/NEJMoa1606774

Ren, Z., Xu, J., Bai, Y., Xu, A., Cang, S., Du, C., et al. (2021). Sintilimab Plus a Bevacizumab Biosimilar (IBI305) versus Sorafenib in Unresectable Hepatocellular Carcinoma (ORIENT-32): a Randomised, Open-Label, Phase 2-3 Study. *Lancet Oncol.* 22, 977–990. doi:10.1016/s1470-2045(21)00252-7

Shi, Y., Su, H., Song, Y., Jiang, W., Sun, X., Qian, W., et al. (2019). Safety and Activity of Sintilimab in Patients with Relapsed or Refractory Classical Hodgkin Lymphoma (ORIENT-1): a Multicentre, Single-Arm, Phase 2 Trial. *Lancet Haematol.* 6, e12–e19. doi:10.1016/S2352-3026(18)30192-3

Wang, J., Fei, K., Jing, H., Wu, Z., Wu, W., Zhou, S., et al. (2019). Durable Blockade of PD-1 Signaling Links Preclinical Efficacy of Sintilimab to its Clinical Benefit. *mAbs* 11, 1443–1451. doi:10.1080/19420862.2019.1654303

Wei, W., Zeng, H., Zheng, R., Zhang, S., An, L., Chen, R., et al. (2020). Cancer Registration in China and its Role in Cancer Prevention and Control. *Lancet Oncol.* 21, e342–e349. doi:10.1016/S1470-2045(20)30073-5

Xu, J., Li, Y., Fan, Q., Shu, Y., Yang, L., Cui, T., et al. (2022). Clinical and Biomarker Analyses of Sintilimab versus Chemotherapy as Second-Line Therapy for

Advanced or Metastatic Esophageal Squamous Cell Carcinoma: a Randomized, Open-Label Phase 2 Study (ORIENT-2). *Nat. Commun.* 13, 857. doi:10.1038/s41467-022-28408-3

Yang, Y., Wang, Z., Fang, J., Yu, Q., Han, B., Cang, S., et al. (2020). Efficacy and Safety of Sintilimab Plus Pemetrexed and Platinum as First-Line Treatment for Locally Advanced or Metastatic Nonsquamous NSCLC: a Randomized, Double-Blind, Phase 3 Study (Oncology pRogram by InnovENT Anti-PD-1-11). *J. Thorac. Oncol.* 15, 1636–1646. doi:10.1016/j.jtho.2020.07.014

Zhang, L., Mai, W., Jiang, W., and Geng, Q. (2020). Sintilimab: A Promising Anti-tumor PD-1 Antibody. *Front. Oncol.* 10, 594558. doi:10.3389/fonc.2020.594558

Zhou, C., Wu, L., Fan, Y., Wang, Z., Liu, L., Chen, G., et al. (2021). Sintilimab Plus Platinum and Gemcitabine as First-Line Treatment for Advanced or Metastatic Squamous NSCLC: Results from a Randomized, Double-Blind, Phase 3 Trial (ORIENT-12). *J. Thorac. Oncol.* 16, 1501–1511. doi:10.1016/j.jtho.2021.04.011

Conflict of Interest: The authors declare that the research was conducted in the absence of any commercial or financial relationships that could be construed as a potential conflict of interest.

Publisher's Note: All claims expressed in this article are solely those of the authors and do not necessarily represent those of their affiliated organizations, or those of the publisher, the editors and the reviewers. Any product that may be evaluated in this article, or claim that may be made by its manufacturer, is not guaranteed or endorsed by the publisher.

Copyright © 2022 Ye, Yang, Xuan, Li, He, Si and Ma. This is an open-access article distributed under the terms of the Creative Commons Attribution License (CC BY). The use, distribution or reproduction in other forums is permitted, provided the original author(s) and the copyright owner(s) are credited and that the original publication in this journal is cited, in accordance with accepted academic practice. No use, distribution or reproduction is permitted which does not comply with these terms.

frontiers | Frontiers in Oncology

ORIGINAL RESEARCH
published: 29 April 2022
doi: 10.3389/fonc.2022.888922

lncRNA PRADX is a Mesenchymal Glioblastoma Biomarker for Cellular Metabolism Targeted Therapy

Can Xu[1,2†], Jixing Zhao[3,4†], Jia Song[2,5], Menglin Xiao[1,2], Xiaoteng Cui[3,4], Lei Xin[1,2], Jianglong Xu[1,2], Yuhao Zhang[1,2], Kaikai Yi[3,4], Biao Hong[3,4], Fei Tong[3,4], Shaohui Tian[1,2], Yanli Tan[2,5], Chunsheng Kang[3,4]* and Chuan Fang[1,2]**

[1] School of Clinical Medicine, Hebei University, Department of Neurosurgery, Affiliated Hospital of Hebei University, Baoding, China, [2] Hebei Key Laboratory of Precise Diagnosis and Treatment of Glioma, Baoding, China, [3] Department of Neurosurgery, Tianjin Medical University General Hospital, Laboratory of Neuro-oncology, Tianjin Neurological Institute, Tianjin, China, [4] Key Laboratory of Post-Neurotrauma Neuro-Repair and Regeneration in Central Nervous System, Ministry of Education and Tianjin City, Tianjin, China, [5] School of Basic Medical Sciences, Hebei University, Baoding, China

OPEN ACCESS

Edited by:
Zhe-Sheng Chen,
St. John's University, United States

Reviewed by:
Xiuping Zhou,
Xuzhou Medical University, China
Pengfei Ge,
Jilin University, China

***Correspondence:**
Chuan Fang
chuanfang@hbu.edu.cn
Chunsheng Kang
kang97061@tmu.edu.cn
Yanli Tan
yanlitan@hbu.edu.cn

†These authors have contributed equally to this work and share first authorship

Specialty section:
This article was submitted to Pharmacology of Anti-Cancer Drugs, a section of the journal Frontiers in Oncology

Received: *03 March 2022*
Accepted: *04 April 2022*
Published: *29 April 2022*

Citation:
Xu C, Zhao J, Song J, Xiao M, Cui X, Xin L, Xu J, Zhang Y, Yi K, Hong B, Tong F, Tian S, Tan Y, Kang C and Fang C (2022) lncRNA PRADX is a Mesenchymal Glioblastoma Biomarker for Cellular Metabolism Targeted Therapy. Front. Oncol. 12:888922. doi: 10.3389/fonc.2022.888922

Glioblastoma (GBM) is the most common and lethal type of primary malignant central nervous system (CNS) tumor with an extremely poor prognosis, and the mesenchymal subtype of GBM has the worst prognosis. Here, we found that lncRNA PRADX was overexpressed in the mesenchymal GBM and was transcriptionally regulated by RUNX1-CBFβ complex, overexpressed PRADX suppressed BLCAP expression *via* interacting with EZH2 and catalyzing trimethylation of lysine 27 on histone H3 (H3K27me3). Moreover, we showed that BLCAP interacted with STAT3 and reduced STAT3 phosphorylation, overexpressed PRADX activated STAT3 phosphorylation, and promoted ACSL1 expression *via* suppressing BLCAP expression, accelerating tumor metabolism. Finally, we determined that combined of ACSL1 and CPT1 inhibitors could reverse the accelerated cellular metabolism and tumor growth induced by PRADX overexpression *in vivo* and *in vitro*. Collectively, PRADX/PRC2 complex activated the STAT3 pathway and energy metabolism in relation to mesenchymal GBM progression. Furthermore, our findings provided a novel therapeutic strategy targeting the energy metabolism activity of GBM.

Keywords: mesenchymal GBM, lncRNA, RUNX1-CBFβ complex, STAT3 pathway, energy metabolism

INTRODUCTION

Long non-coding RNAs (lncRNAs) are defined as a versatile class of RNA transcripts, longer than 200 nucleotides, lacking protein-coding capacity (1). Accumulating evidence suggests that lncRNA dysregulation plays a pivotal role in the onset and progression of a broad spectrum of cancers, including glioblastoma (GBM) (2, 3). With the increasing appreciation of lncRNAs' indispensable mechanistic involvement and the subsequent technological advancements in biomedical research, novel lncRNAs are constantly being discovered in relation to GBM pathology. Emerging studies have shown that lncRNAs act as the key regulators of the gene expression pattern not only under the normal physiological condition but also in the pathogenesis and progression of GBM (4–6).

Furthermore, aberrant lncRNA expression profiles in GBM patients correlate with their respective cancer malignancies and molecular subtypes, which have important clinical implications in the diagnosis and progression of GBM (7–9). lncRNAs have also been reported to participate in chromatin dynamics and gene expression regulation by interacting with key epigenetic regulatory factors (10, 11). In the case of GBM, studies have shown that lncRNAs modulate chromatin remodeling in association with polycomb repressive complex 2(PRC2) (12–14). PRC2 regulates the transcriptional repression by hyper-methylating histone H3K27 through its methyltransferase activity (15, 16). Notably, PRC2 subunits encoding genes have been found dysregulated in a variety of cancers, including GBM. Hence, small-molecule inhibitors restoring PRC2 function have entered clinical trials for cancers (17, 18).

GBM is the most aggressive and frequent adult brain tumor with only a 5.1% five-years survival rate, and the mean survival time of GBM patients is about 15 months, even with multimodal therapy (19). Due to the extremely unfavorable prognosis and unknown underlying mechanism, the Cancer Genome Atlas (TCGA) has classified GBM into four major molecular subtypes- proneural, neural, mesenchymal, and classical, according to the gene expression data from three different platforms (20). Later in 2017, TCGA published the modified GBM classification based on the immune microenvironment of the tumor. After excluding the potential environmental risk factors, GBM has been reclassified into three molecular subtypes, namely proneural, mesenchymal, and classical. Interestingly, patients with mesenchymal subtypes show a tendency toward higher transcriptional heterogeneity and worse survival outcomes compared to proneural and classical subtypes (21). Sumazin et al. have exploited the TCGA GBM database to establish a post-transcriptional regulatory network involving microRNAs(miRNA) through the HERMES multivariate analysis method. The study has found that 6 genes, including runt-related transcription factor 1 (RUNX1) play a key role in the occurrence and development of GBM pathology (22). In 2018, we reported the construction of a competitive endogenous RNA (ceRNA) regulation network linking the protein-coding functional mRNA to the mechanistically related lncRNAs based on the integrated omics analysis, which has further confirmed that dysregulation of RUNX1 is a key pathological inducer of the mesenchymal GBM subtype (23). These findings have also been recapitulated in both *in vivo* and *in vitro* GBM models, including patients' samples (24).

Our previous study identified a novel lncRNA ENST00000449248.1, which we named PRADX, due to its association with PRC2 and DEAD-box helicase 5 (DDX5). We confirmed that PRADX could serve as a potential prognostic indicator of GBM and colon adenocarcinoma (COAD). Previously we have shown that the recruitment of the PRC2/DDX5 complex increases the occupancy of H3K27me3 at the UBX domain protein 1 (UBXN1) gene promoter region, thereby suppressing UBXN1 expression and promoting NF-κB activity (25). In the present study, we furthered the investigation of the transcriptional regulatory mechanism of PRADX to reveal its oncogenic role in the mesenchymal GBM *via* promoting energy metabolism.

MATERIAL AND METHODS

Cell Lines and Cell Transfection

Culture methods of the primary cell lines (N33, N9, and TBD0220) used in this study have been previously reported (26). All the cells were cultured in Dulbecco's Modified Eagle's Medium (DMEM/F12, 1:1; Gibco) containing 10% fetal bovine serum (FBS). PRADX lentiviral vector was transduced according to the manufacturer's instructions (Genechem, Shanghai, China), Small interfering RNAs (siRNAs) targeting PRADX, EZH2, RUNX1, CBFβ, and BLCAP were purchased from GenePharma (Suzhou, China), RUNX1 plasmid was purchased from Ibsbio (Shanghai, China). See **Supplementary Table S4** for details.

Cell Counting Kit 8 and Colony Formation Assays

CCK-8 (Dojindo, Japan) assay was performed to evaluate the cell viability by measuring the absorbance at 450 nm (OD450) using BioTek Gen5 Microplate Reader (BioTek Instruments, USA). A colony formation assay was performed to evaluate the colony formation ability of the specific cancer types, following the method described in our previous study (25).

Seahorse XFe Extracellular Flux Analysis (Mitochondrial Stress Test)

Extracellular flux analysis was performed to evaluate cellular metabolism indexes, including oxygen consumption rate (OCR), basal respiration, proton leak, and ATP production. The experiments were performed on a Seahorse XF24 Analyzer (Seahorse Bioscience) as described elsewhere (26).

Western Blotting and Co-Immunoprecipitation

Total cells were lysed using RIPA buffer with proteinase and phosphatase inhibitor cocktails (Selleck Chemicals, Shanghai, China). After transferring the protein bands onto the polyvinylidene fluoride (PVDF) membrane, the membrane was incubated with the respective primary antibodies at 4°C overnight, followed by horseradish peroxidase (HRP)-conjugated secondary antibody incubation for 1 h at room temperature. The protein bands were observed using a chemiluminescence reagent (ECL) (Boster, Wuhan, China). For co-IP, IP lysis buffer (Beyotime Biotechnology) was used to lyse the cells. For immunoprecipitation, 40μl of protein-A/G agarose beads (Millipore) and 5μg anti-STAT3 or anti-BLCAP antibody were incubated with the total cell lysates at 4°C overnight. The immunoblots were then washed five times with 1X phosphate-buffered saline (PBS) buffer for the downstream signal intensity detection processes.

Chromatin Immunoprecipitation

The Millipore Magna ChIP TM A/G kit (catalog # 17-10085) was used to perform the ChIP experiment. A total of 6×106 cells was cross-linked using 1% formaldehyde solution for 10 min followed by 10X glycine neutralization for 5 min at room temperature. The cell lysate was then sonicated to generate the sheared DNA fragments of 200-1000 bp in size. After that, 5μg of each of the

target antibodies were immunoprecipitated with an equal amount of chromatin fraction at 4°C overnight. The products were incubated with magnetic Protein A/G beads and quantitated by qPCR assay. The antibodies and primers are listed in **Supplementary Table S3**.

RNA Isolation and Real-Time Quantitative Reverse-Transcription PCR

TRIzol reagent (Invitrogen, USA) was used to extract the total RNA from cultured cells. 1-5ug of the total RNA was used for cDNA synthesis using the PrimeScript RT Reagent Kit (Takara, Japan). SYBR Green reaction mix (Takara, Japan) was used to perform the RT-qPCR assay with CFX96 Touch Real-Time PCR Detection System (Bio-Rad, USA). The primers are listed in **Supplementary Table S2**.

Confocal Immunofluorescence Microscopy

The cells were cultured on coverslips using 24-well plates overnight and then fixed with 4% formaldehyde. Cells were permeabilized with 0.5% Triton-X100 (ThermoFisher, USA) for 20min at room temperature followed by blocking with 5% bovine serum albumin (BSA). The primary antibodies were incubated overnight at 4°C followed by corresponding secondary antibody incubation for 1 h at room temperature. The 4'-6-diamidino-2-phenylindole (DAPI, Molecular Probes, D1306) was used to counterstain the nucleus and phalloidin for the cytoskeleton. The images were captured by Zeiss 510 META laser scanning confocal microscope.

Dual-Luciferase Report Assay

The cells were cultured in a 24-well plate for 24h followed by co-transfection of 0.5-2.0μg of PRADX plasmid and 25ng of pRL-TK (renilla luciferase reporter vector) reporter plasmids using jetPRIME kit. After 24–36 h, cells were harvested to observe the luciferase activity by the Dual-Glo Luciferase system (Promega) with the normalization to pRL-TK.

In Vivo Xenograft Mouse Models

BALB/c nude mice were purchased from Beijing Vital River Laboratory Animal Technology. PRADX overexpressed or scrambled TBD0220 cells were pre-transfused with luciferase lentiviral particles. The stereotactic injection was applied to inject the cancer cells (3×10^5 cells per mouse in 3μL PBS) into the intracranial space. The bioluminescence imaging was captured by the IVIS Lumina Imaging System (Xenogen) after 7,14,21, and 28d of injection. Intact brains were carefully extracted after euthanasia and then embedded into the paraffin section for IHC analysis.

Immunohistochemistry Staining

Tumor sections were deparaffinized in xylene followed by gradient ethanol hydration, and antigen recovery was carried out in ethylene diamine tetraacetic acid (EDTA) solution. Tumor sections were incubated with primary antibodies at 4°C overnight, followed by HRP-conjugated secondary antibody probing for 1h at room temperature. After the diaminobenzidine (DAB) staining, the sections were observed under a light microscope. The antibodies are listed in **Supplementary Table S1**.

Statistical analysis

All the statistical analyses were performed using GraphPad Prism 8. The transcriptional and clinical data were obtained from CGGA (http://www.cgga.org.cn/) and TCGA (https://tcga-data.nci.nih.gov/tcga/tcgaDownload.jsp) databases. Gene set enrichment (GSEA) analysis was performed with GSEA_4.1.0 software. Clustered heatmap analysis was performed using the online bioinformatics tools (http://bioinformatics.com.cn/). The error bars in the figures represent the mean ± standard deviation (SD) from at least three independent experiments. A P value of <0.05 was considered statistically significant.

RESULTS

PRADX is a Biomarker of Mesenchymal GBM

To investigate whether PRADX was related to the mesenchymal subtype of GBM, we searched the top 500 positively and top 500 negatively correlated genes of PRADX in the CGGA database and performed clustered heat map analysis. The results showed that the positively correlated genes were enriched in patients with the mesenchymal subtype, while the negatively correlated genes were clustered in the proneural subtype (**Figure 1A**). In addition, PRADX highly expressed patients with a high expression of mesenchymal marker genes and low expression of proneural marker genes (**Figures 1C, D**). GSEA analysis was performed using TCGA and CGGA databases by dividing the patients into high and low expression groups based on their respective PRADX expression profiles. Moreover, patients with high PRADX expression were enriched in the mesenchymal subtype (**Figure 1B**). The Pearson correlated coefficient also indicated that PRADX is positively correlated with mesenchymal GBM marker genes (**Figure 1E**). One-way ANOVA analysis revealed that PRADX expression was significantly higher in patients with mesenchymal subtype from both TCGA and CGGA databases (**Figure 1F**). Furthermore, we investigated the survival influence of PRADX in GBM according to TCGA and CGGA databases, Kaplan-Meier survival curve indicated that PRADX upregulation was associated with a shorter survival time in GBM patients (**Figure 1G**). These findings cumulatively suggest that PRADX is a potential biomarker of mesenchymal subtype, and its increased expression is correlated with the poor prognosis of GBM patients.

PRADX is Transcriptionally Upregulated by RUNX1-CBFβ Complex

RUNX1 has already been reported as a mesenchymal biomarker in the previous study and is associated with a shorter survival time in GBM patients (23, 24). Although RUNX1 is a nuclear transcription factor, the CBFβ chaperone is essential for RUNX1's transcriptional function (27, 28). To investigate if PRADX was regulated by RUNX1 and CBFβ expression, We transfected N33 and N9 cells with RUNX1 and CBFβ siRNA alone or in combination, and designed two pairs of PCR primers of PRADX, the subsequent qRT-PCR assay revealed PRADX level

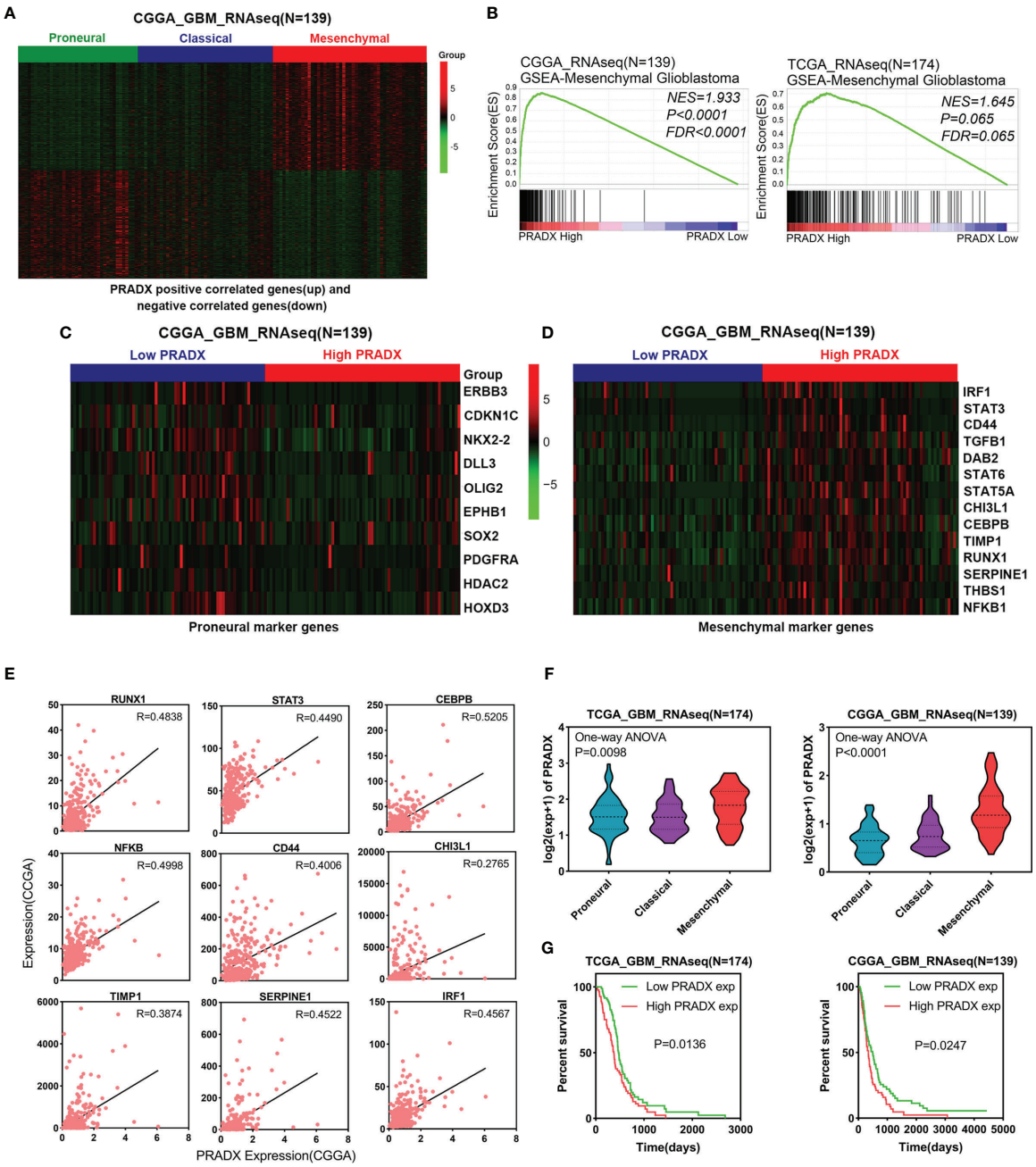

FIGURE 1 | PRADX expression correlates with mesenchymal GBM. **(A)** Clustered heat map showing that PRADX positively correlated genes (top 500) and negatively correlated genes (top 500) expression profiles in the CGGA database. **(B)** GSEA analysis of mesenchymal GBM gene expression between PRADX high and low expression groups in TCGA and CGGA databases. **(C, D)** Clustered heat map showing that proneural and mesenchymal marker genes expression profiles in PRADX high expression and low expression patients. **(E)** The correlation between PRADX and mesenchymal marker genes in the CGGA database. **(F)** Violin plots exhibiting PRADX expression in different molecular subtypes of GBM in TCGA and CGGA databases. **(G)** Kaplan-Meier curve showing patients' survival times between PRADX high expression and low expression groups.

was significantly reduced (**Figure 2A**), Consistently, N33 and N9 cells were treated with RUNX1-CBFβ binding inhibitor RO5-3335 (25μM) for 0, 6, 12, 24, and 48h, PRADX expression was reduced after RO5-3335 treatment in a time-dependent manner (**Figure 2B**). Furthermore, we constructed a luciferase reporter plasmid with a PRADX promoter region in the PGL4.10 vector. Dual-luciferase report assay consistently showed that PRADX transcription activity was significantly reduced after RUNX1 and CBFβ siRNA transfection (**Figure 2C**). In contrast, RUNX1 overexpression increased PRADX transcription activity in a

dose-dependent manner (**Figure 2D**). These findings demonstrated that PRADX was transcription regulated by the RUNX1-CBFβ complex. All the siRNAs, lentivirus, and plasmid transfection efficiency were confirmed in Supplementary Figure S1 (**Figure S1**).

Next, we sought to understand the specific mechanism of RUNX1-CBFβ-mediated transcriptional regulation of PRADX. Firstly, we predicted the RUNX1 binding site in the PRADX promoter region based on Jaspar (http://jaspar.genereg.net/) and found only one predicted forward strand sequence (**Figure 2E**). Then, we designed 3 pairs of ChIP primers based on the predicted binding sequence. The ChIP-qPCR analysis confirmed RUNX1 could bind to the predicted binding site on the PRADX promoter region (**Figures 2F, G**). To reconfirm this finding, we constructed another dual-luciferase reporter plasmid for the PRADX promoter region but with site-directed mutation of the RUNX1 binding site (**Figure 2H**). Dual-luciferase reporter assays revealed that PRADX transcriptional activity was independent of either RUNX1 overexpression or its binding inhibition to CBFβ (RO5-3335 treatment) after RUNX1 binding site mutation (**Figure 2I**). Taken together, these findings demonstrated that RUNX1-CBFβ complex-mediated transcriptional regulation of PRADX expression is modulated by the RUNX1 binding at the specific promoter sequence of PRADX.

PRADX Overexpression Suppresses BLCAP Expression *via* Interacting With EZH2 and Recruiting H3K27me3

Our previous studies have proved that PRADX mediates UBXN1 gene silencing by recruiting H3K27me3 *via* interacting with EZH2 (25). To further explore the carcinogenic mechanisms of PRADX in mesenchymal GBM, we aimed to explore new target genes and their carcinogenic pathways. We successfully overexpressed PRADX in N33 cells and performed RNA microarray analysis. Together with TCGA and CGGA cohort analysis, we found out that PRADX negatively regulated the tumor suppressor gene (TSG) BLCAP in GBM (**Figure 3A**). TSG database was downloaded from TSG (https://bioinfo.uth.edu/TSGene/) website. We then searched for an H3K27me3 binding peak in the BLCAP promoter regions of different cell lines at the UCSC (http://genome.ucsc.edu/) website (**Figure 3B**). Next, we explored if PRADX could negatively regulate BLCAP expression *via* its interaction with EZH2. To do so, we performed western blotting and qRT-PCR analyses in EZH2 siRNA transfected, PRADX siRNA transfected, and PRADX overexpressed plus EZH2 siRNA transfected N33 and N9 cells. The results demonstrated that PRADX overexpression suppressed BLCAP expression, PRADX overexpressed plus EZH2 knockdown also increased BLCAP expression (**Figures 3C, D**). Then, we conducted a ChIP experiment using primers against 3 TSG genes (PCDH10, PCDHB5, and HOXD10) (29) to verify the chromatin binding of the target proteins (**Figure 3E**). Furthermore, we designed 10 pairs of ChIP primers for BLCAP and selected 3 pairs of the most efficient primers by ChIP-PCR in N33 cells (**Figure 3F**). ChIP-qPCR analysis showed PRADX overexpression could increase the recruitment of both H3K27me3 and EZH2 at the BLCAP promoter region, whereas reduced the occupancy of RNA Polymerase II pSer2. However, there were no significant changes in total H3 levels in both N33 and N9 cells, indicating transcriptional repression (**Figures 3G, H**). In summary, these findings demonstrate that PRADX overexpression suppresses BLCAP expression *via* interacting with EZH2 and recruiting H3K27me3 at the BLCAP promoter.

PRADX overexpression Activates the Phosphorylation of STAT3 *via* Suppressing BLCAP Expression

STAT3 is an important transcription factor and is well known for its roles in cancer proliferation, survival, invasion, and immunosuppression (30, 31) is also implicated in mesenchymal GBM (27). While BLCAP is reported as a novel STAT3 interaction partner in bladder cancer (32), and A-to-I editing of BLCAP mRNA loses the inhibitory regulation of STAT3 activation in cervical cancer (33). But the mechanistic cross-talks between BLCAP and STAT3 expressions in GBM remain unclear. Pearson's correlation coefficient analysis showed PRADX expression was positively correlated with STAT3 level (R=0.4490), while BLCAP expression was negatively correlated with STAT3 (R=-0.4926) in the CGGA database (**Figure 4A**). Western blot analysis showed that tumor cells overexpressing PRADX had reduced levels of BLCAP and increased nuclear levels of phosphor(p)-STAT3. However, EZH2 knockdown with or without PRADX overexpression in tumor cells revealed increased levels of BLCAP and reduced nuclear levels of p-STAT3 (**Figure 4B**). These findings thus suggest that PRADX overexpression activates STAT3 phosphorylation *via* suppressing BLCAP expression.

To further explore whether BLCAP interacted with STAT3 and inhibited STAT3 phosphorylation in GBM cells, we performed a co-IP assay using an anti-BLCAP antibody in N33 and N9 total cell lysates. The results confirmed that BLCAP interacted with STAT3, and there was no change in total Stat3 levels in the nucleus and only the p-Stat3 levels change in response to PRADX overexpression and EZH2 knockdown overexpression of PRADX along with BLCAP knockdown increased STAT3 phosphorylation levels in the anti-STAT3 IP product (**Figure 4C**). Moreover, IF analysis revealed that BLCAP knockdown with or without PRADX overexpression increased nuclear p-STAT3 levels in N33 and N9 cells (**Figures 4D, E**), these findings indicate that BLCAP non-functionally interacts with STAT3, and PRADX overexpression induces STAT3 phosphorylation *via* suppressing BLCAP expression.

PRADX Overexpression Promotes STAT3 Downstream Genes' Expression, Including ACSL1

Recent studies have shown that the STAT3 signaling pathway promotes tumor fatty acid metabolism (34). Acyl-CoA synthetase long-chain family member 1 (ASCL1) promotes the biosynthesis of Acyl-CoA, regulates mitochondrial respiration, β-oxidation, and ATP production by regulating the activity of carnitine palmitoyltransferase 1 (CPT1), and affects fatty acid metabolism (35). Our previous study has demonstrated that ACSL1 is an important ceRNA in mesenchymal GBM (23). Pearson's correlation coefficient analysis showed ACSL1 was positively

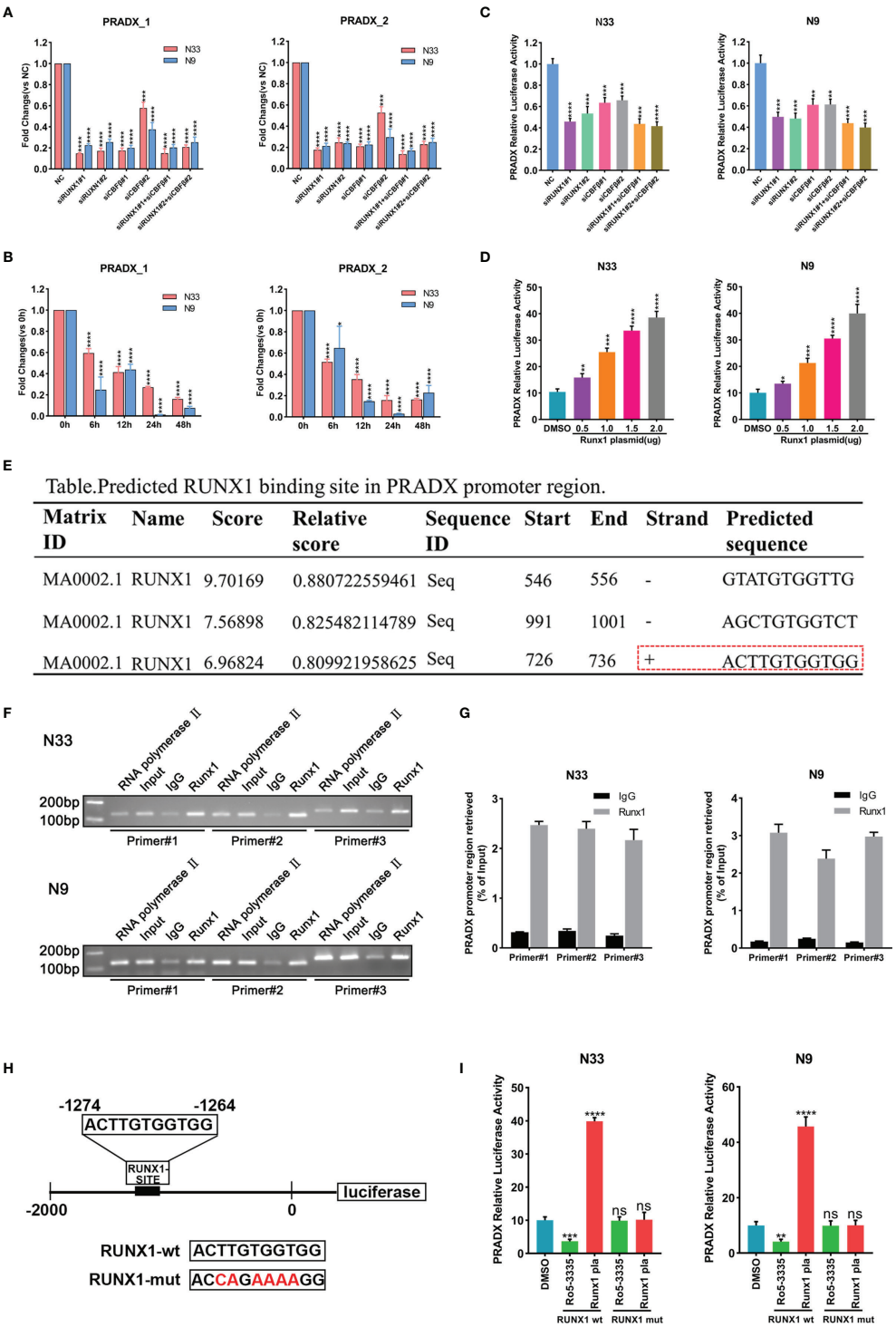

FIGURE 2 | PRADX was transcriptionally regulated by the RUNX1-CBFβ complex. **(A)** qRT-PCR assay exhibiting PRADX expressions after treating with RUNX1 and/or CBFβ siRNA. **(B)** qRT-PCR showing PRADX expressions after treating with RO5-3335 for different times. **(C, D)** Dual-luciferase report assay showing the transcriptional activity of PRADX after treating with RUNX1, CBFβ siRNA, or RUNX1 expression plasmid. **(E)** The binding site of RUNX1 in the PRADX promoter region as predicted by the JASPAR tool. **(F, G)** ChIP-PCR and ChIP-qPCR analyses show RUNX1 binds to the predicted binding site on the PRADX promoter. **(H, I)** RUNX1 binding site mutated plasmid construction for dual-luciferase reporter assay to compare PRADX transcription activities following RO5-3335 treatment or RUNX1 expression plasmid transfection in the indicated groups. Data are represented as mean ± standard deviation (SD); n = 3 independent experiments. ****P <0.00001, ***P <0.0001, **P <0.001, *P <0.05. ns: no significance.

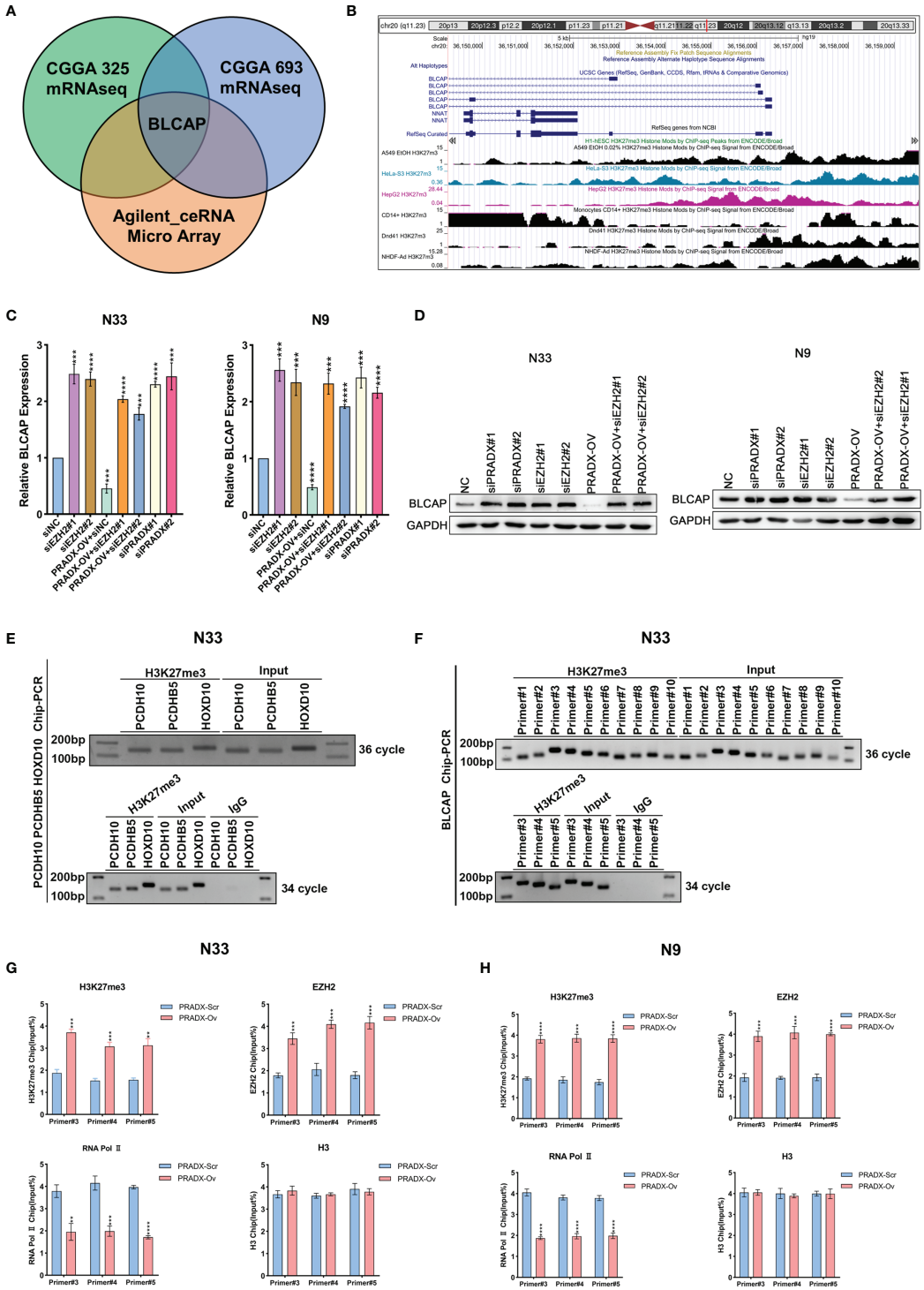

FIGURE 3 | The interaction of PRADX and EZH2 silences BLCAP expression *via* recruiting H3K27me3 at the BLCAP promoter. **(A)** BLCAP was the most negatively correlated TSG with PRADX in the CGGA database and Agilent ceRNA microarray analysis. **(B)** H3K27me3 binding peaks on the BLCAP promoter region in different cell lines as per the UCSC webtool. **(C, D)** qRT-PCR and western blotting analyses revealing BLCAP expressions after PRADX overexpression or EZH2 siRNA treatment. **(E)** Application of the ChIP primers of the three TSGs reported in the literature to verify the target protein binding at the chromatin level. **(F)** ChIP-PCR showed H3K27me3 enrichment at the BLCAP promoter region. **(G, H)** ChIP-qPCR exhibits the occupancy levels of H3K27me3, EZH2, RNA polymerase II, and H3 at the BLCAP promoter region in scrambled and PRADX overexpressed cells. The values in **(C, G, H)** are represented as mean ± SD (n = 3). **P < 0.01, ***P < 0.001, ****P <0.0001.

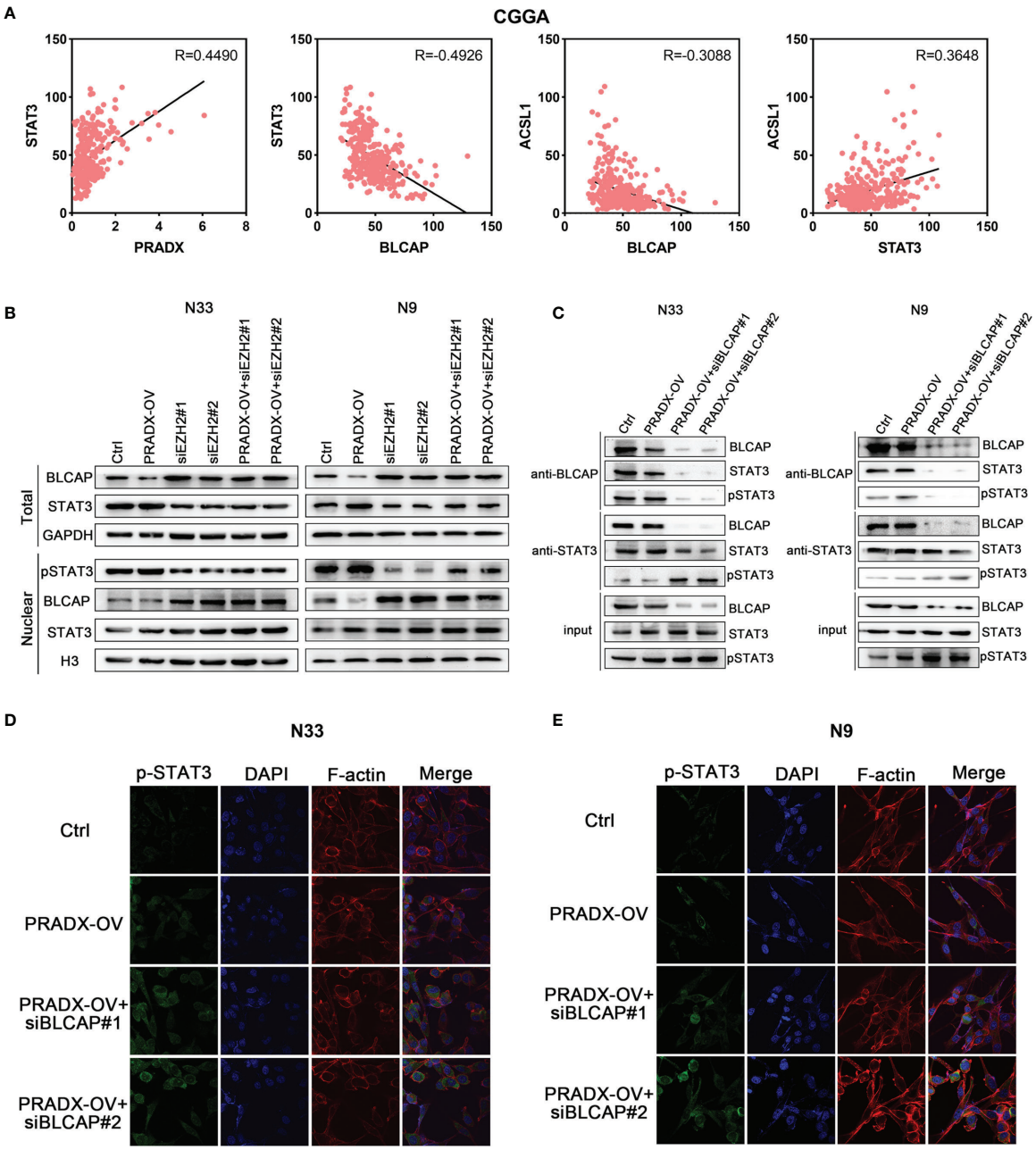

FIGURE 4 | BLCAP interacts with STAT3, and overexpression of PRADX activates the phosphorylation of STAT3 *via* suppressing BLCAP expression. **(A)** The correlation between STAT3, PRADX, ACSL1, and BLCAP mRNA expression levels in the CGGA dataset. R, Pearson r value. **(B)** Western blotting results indicate the total protein levels of BLCAP, STAT3, and GAPDH and nuclear protein levels of p-STAT3, BLCAP, STAT3, and H3 in indicated groups. **(C)** Co-IP assays were performed with anti-BLCAP or anti-STAT3 antibodies followed by immunoblotting with BLCAP, STAT3, and p-STAT3 antibodies. **(D, E)** IF staining shows p-STAT3 protein expression and localization in the indicated groups. In **(B, C)**, GAPDH and H3 served as a positive control.

correlated with STAT3 level (R=0.3648), negatively correlated with BLCAP level (R=-0.3088) (**Figure 4A**).

To determine whether ACSL1 was regulated by STAT3 expression, we observed both mRNA and protein levels of ACSL1, together with other three STAT3-downstream genes (BCL2, c-MYC, CDKN1A) (35–37) in PRADX overexpressed, PRADX overexpressed plus WP1066(5μm) or DMSO-treated groups of N33 and N9 cells. The results exhibited that ACSL1, BCL2, c-MYC, and CDKN1A mRNA and protein expressions were increased in PRADX overexpressed tumor cells, in contrast to the PRADX overexpressed plus WP1066-treated group (**Figures 5A, B**), indicating PRADX-induced activation of

STAT3 pathway and its downstream genes' expression, including ACSL1. Then, we performed western blot and qRT-PCR analyses using N33 and N9 cells treated with different doses (1,2,5,10μM) of WP1066 (STAT3 inhibitor) or DMSO for 24h. The results showed that ACSL1 protein and mRNA levels were significantly reduced by WP1066 in a dose-dependent manner (**Figures 5C, D**), Furthermore, to determine whether ACSL1, BCL2, c-MYC, and CDKN1A expressions were regulated by PRADX through BLCAP suppression, we performed western blotting and qRT-PCR analyses Using N33 and N9 cells transfected with PRADX and BLCAP siRNA alone or in combination along with the negative control (NC) group. The results showed that ACSL1, BCL2, c-MYC, and CDKN1A expressions were reduced in the PRADX knockdown group. However, their expressions were increased in BLCAP with or without PRADX knockdown groups (**Figures 5E, F**). These data indicate PRADX overexpression can activate the STAT3 signaling pathway and its downstream genes *via* suppressing BLCAP expression.

PRADX Overexpression Promotes Basal Respiration, Proton Leak, and ATP Production in GBM Cells *via* Increasing ACSL1

It has been reported that ACSL1 promotes tumorigenesis and development by regulating fatty acid metabolism (38). CPT1, located in the outer mitochondrial membrane, is the first rate-limiting factor in the mitochondrial fatty acid oxidation pathway. CPT1 plays a crucial role in transporting long-chain fatty acids and co-enzyme A into the mitochondrial matrix for β-oxidation (39). To examine whether the activation of ACSL1 by PRADX overexpression was correlated with mesenchymal GBM cell metabolism and ATP production, we explored the ACSL1 expression in TCGA and CGGA databases. One-way ANOVA analysis showed ACSL1 expression was significantly higher in the mesenchymal subtype than in proneural and classical subtypes of GBM (**Figure 6A**). Additionally, the Kaplan-Meier survival curve showed ACSL1 was associated with a shorter survival time in GBM patients (**Figure 6B**). Furthermore, we performed seahorse experiments using Triacsin C (ACSL1 inhibitor), and Etomoxir (CPT1 inhibitor) in PRADX overexpressed or scrambled N33 and N9 cells. The treated cells were divided into five groups, such as scramble plus DMSO, PRADX overexpressed, PRADX overexpressed plus Triacsin C (10μM), PRADX overexpressed plus Etomoxir (10μM), and PRADX overexpressed plus Triacsin C(10μM) plus Etomoxir(10μM). The oxygen consumption rate (OCR) represents real-time cellular respiration (**Figures 6C, D**). Basal respiration, proton leak, and ATP production were significantly increased in PRADX overexpressed groups. However, Triacsin C and Etomoxir reversed PRADX overexpression effects, as manifested by a reduction in basal respiration, proton leak, and ATP production levels in the two separate inhibitor groups. Additionally, these effects were even lower in the combination-treated groups (**Figures 6E–G**). These results demonstrated that PRADX overexpression increased cellular metabolism, and the combined application of Triacsin C and Etomoxir might be an efficient strategy to reverse PRADX-mediated metabolism acceleration.

Combination of Triacsin C and Etomoxir Reverse PRADX-Mediated Tumor Cell Growth and Tumorigenesis

Cellular metabolism and ATP production are tightly associated with cell growth and tumorigenesis (40). CCK8 assay showed overexpressed PRADX could significantly promote the viability of N33 and N9 cells. However, treatments with Triacsin C (30μM) and Etomoxir (30μM) alone or in combination significantly inhibited cell viability in PRADX overexpressed tumor cells (**Figure 7A**). Furthermore, colony formation assays also demonstrated the inhibitory effects of Triacsin C (30uM), and Etomoxir (30uM) on tumor cell growth in PRADX overexpressed N33 and N9 cells (**Figure 7B**). To seek new treatment modalities for GBM patients with a high PRADX level *in vivo*, we constructed intracranial xenograft models with PRADX overexpressed TBD0220 cells and tested the efficiency of both the monotherapies and combination therapy with Triacsin C (30mg/kg/d) and Etomoxir (30mg/kg/d). Bioluminescence images captured at 7, 14, 21, and 28d post-implantation time-points showed significantly smaller tumors sizes in the combination therapy group (**Figure 7C**). Moreover, the Kaplan-Meier survival curve showed combination therapy group had the longest survival time among the treatment groups (**Figure 7D**). The quantification of luminescence further demonstrated that the combination therapy group had the smallest tumor volume (**Figure 7E**). Additionally, the IHC staining of the tumor sections showed the tumors from the combination therapy group had the lowest expression levels of ACSL1, STAT3, p-STAT3, and Ki-67. BLCAP expression in the combination group was the highest among the 5 groups (**Figure 7F**). The schematic diagram shows the PRADX-mediated recruitment of H3K27me3 and subsequent suppression of BLCAP expression, which in turn activates STAT3 and ACSL1 expressions, promoting mesenchymal GBM energy metabolism and tumorigenesis (**Figure 7G**).

DISCUSSION

Dysregulation of lncRNAs has consistently been discovered in a variety of cancers and multiple biological functions related to cancer progression (41). Studies have shown that lncRNA-mediated chromatin modification contributes to the malignant behavior of gliomas (12, 14, 42). Our previous studies have identified a novel lncRNA PRADX, which is overexpressed in GBM and COAD and correlates with the poor prognosis of GBM patients. PRADX promotes tumorigenesis *via* interacting with the PRC2 complex and recruiting H3K27me3 at the oncogene promoters, activating the NF-κB pathway (25). To further investigate the carcinogenic role of PRADX in GBM, we demonstrated PRADX transcription was modulated by the RUNX1-CBFβ complex. PRADX overexpression activated the STAT3 pathway, promoted cell metabolism, and ATP production *via* suppressing BLCAP expression. Our results suggested that the Combination treatment of ACSL1 and CPT1 inhibitors might serve as an effective treatment regimen for GBM.

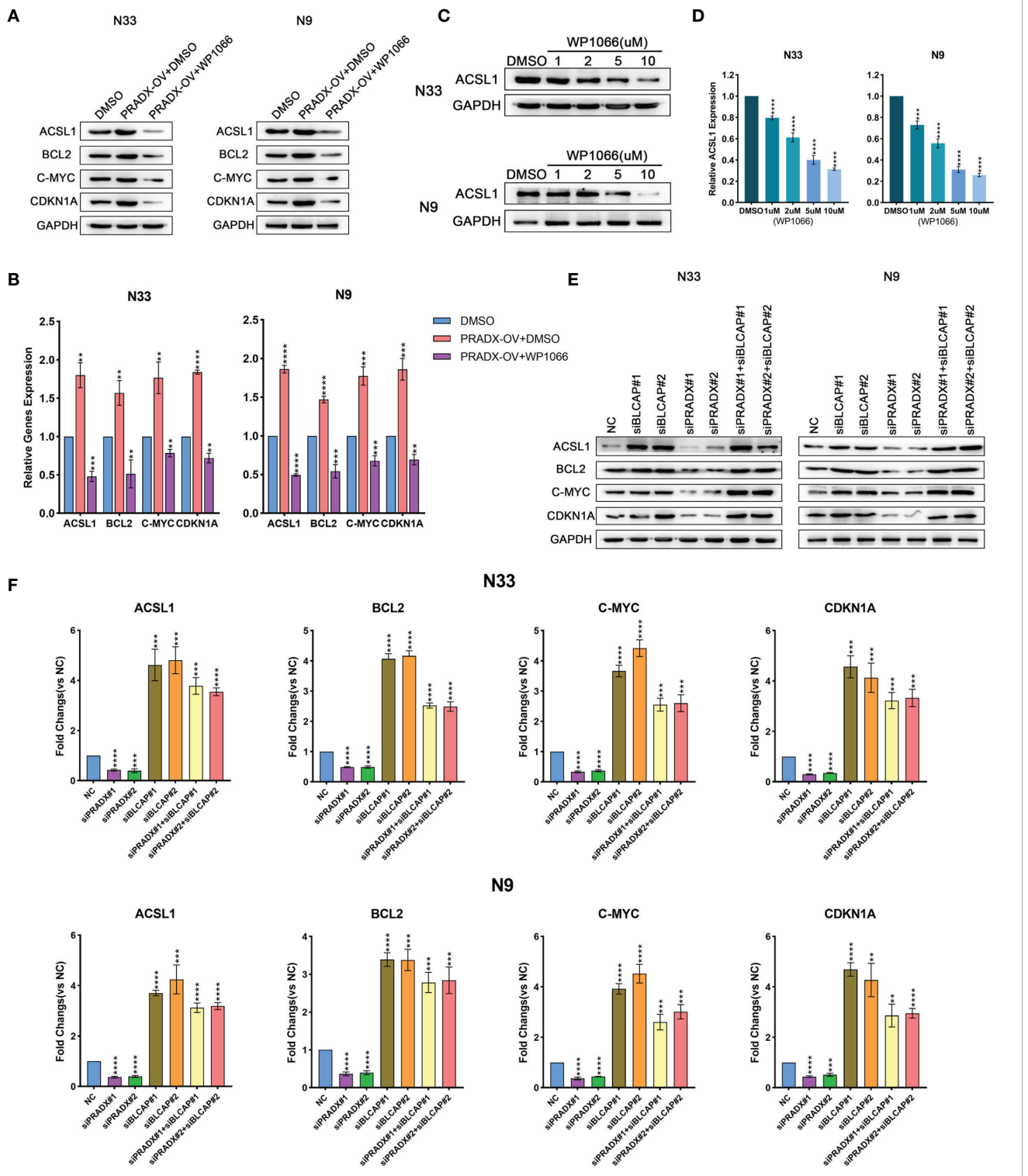

FIGURE 5 | PRADX activates the STAT3 pathway *via* suppressing BLCAP. **(A, B)** qRT-PCR and western blotting analyses showing ACSL1, BCL2, c-MYC, and CDKN1A mRNA and protein expression levels in PRADX overexpressed, PRADX overexpressed plus WP1066 and DMSO groups. **(C, D)** qRT-PCR and western blot analysis showed WP1066 treatment decreased ACSL1 mRNA and protein levels in a dose-dependent manner. GAPDH served as a positive control. **(E, F)** qRT-PCR and western blot analyses demonstrating ACSL1, BCL2, c-MYC, and CDKN1A mRNA and protein expression levels in BLCAP and/or PRADX knockdown and NC groups. The values in **(B, D, F)** are represented as mean ± SD (n = 3). **P < 0.01, ***P < 0.001, ****P <0.0001.

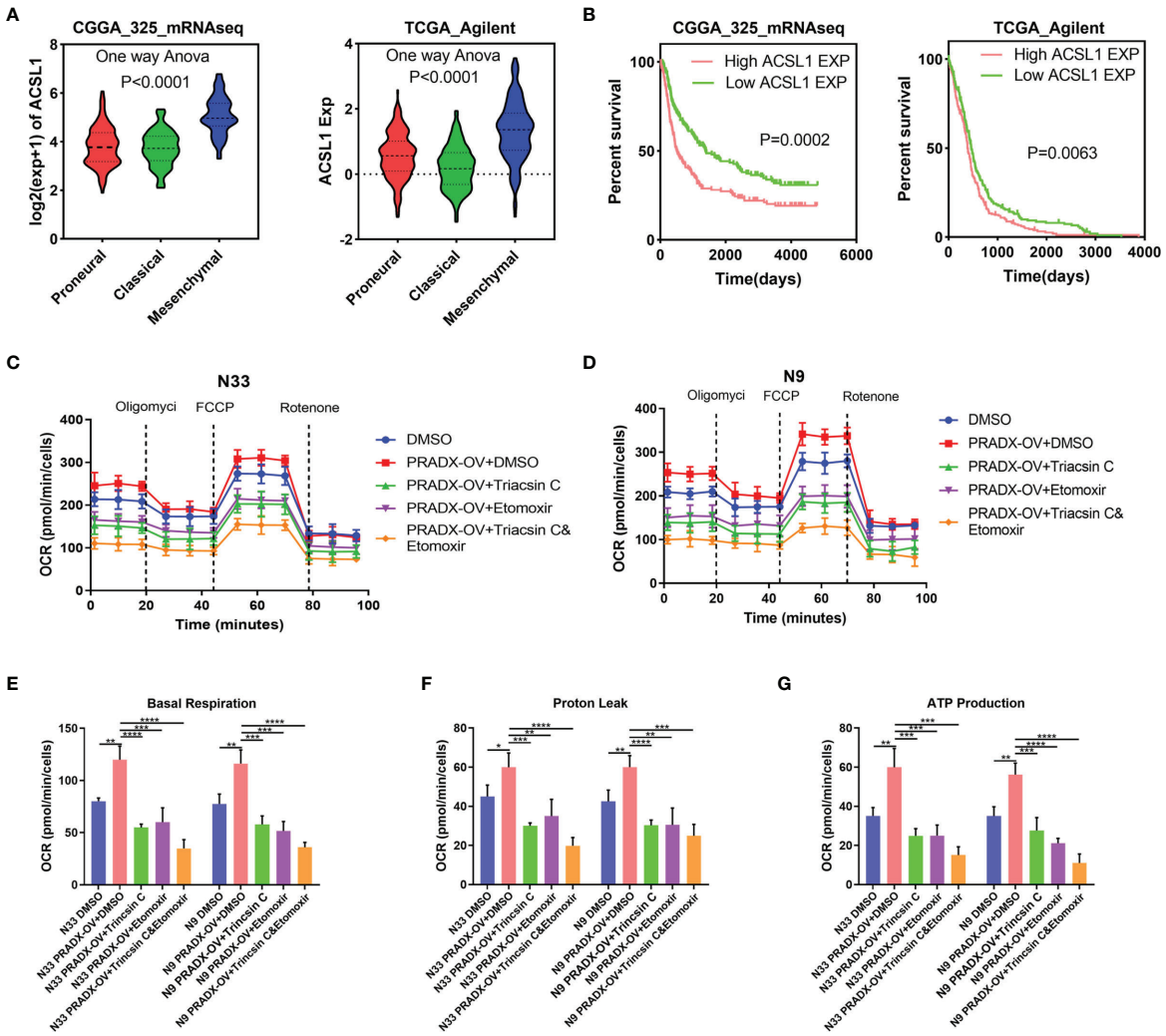

FIGURE 6 | PRADX enhances energy metabolism *via* increasing ACSL1 in glioma. **(A)** Violin plots showing ACSL1 expression in different molecular subtypes of GBM in TCGA and CGGA databases. **(B)** Kaplan-Meier curve showing patients' survival times between ACSL1 high expression and low expression groups. **(C, D)** The time series for the oxygen consumption rate (OCR) was measured by a seahorse analyzer in the indicated groups. **(E–G)** OCR measurement of basal respiration, proton leak, and ATP production for these five groups above. The values in **(C–G)** are represented as mean ± SD (n = 3). *P <0.05, **P < 0.01, ***P < 0.001, ****P <0.0001.

Genome-wide mutation analysis revealed significant heterogeneity in GBM and led to three molecular subtypes (proneural, classical, and mesenchymal) to facilitate the exploration of GBM pathomechanism. Among the 3 types, mesenchymal GBM is the most malignant and usually presents with the worst prognosis (21, 27). Revealing the mechanism of mesenchymal GBM progression is essential for drug development and targeted therapy. In this study, we showed PRADX was highly expressed in mesenchymal GBM and transcriptionally regulated by the RUNX1-CBFβ complex. RUNX1 is a nuclear transcription factor, and CBFβ is necessary for RUNX1's DNA binding affinity, but this mechanism has not been confirmed in solid tumors (28). Moreover, RUNX1 is a key mesenchymal GBM driver gene (23, 24). PARDX overexpression activates another two mesenchymal-specific genes like STAT3 and ACSL1. In addition, STAT3 also regulates PRADX mRNA expression (**Figure S2**). This might be an important regulatory feedback loop in the mesenchymal GBM development.

Several proteins function *via* interacting with other proteins. We performed co-IP and IF analyses and found out BLCAP non-functionally interacted with STAT3 and inhibited STAT3 phosphorylation. Overexpressed PRADX suppressed BLCAP expression *via* recruiting H3K27me3 at the BLCAP promoter, thus activating STAT3 phosphorylation. ACSL1 is mainly located in mitochondria, where it is involved in the biosynthesis of Acyl-COA that are channeled for subsequent β-Oxidation (43). Our results showed ACSL1 was reduced by WP1066 treatment in a dose-dependent manner, while PRADX overexpression

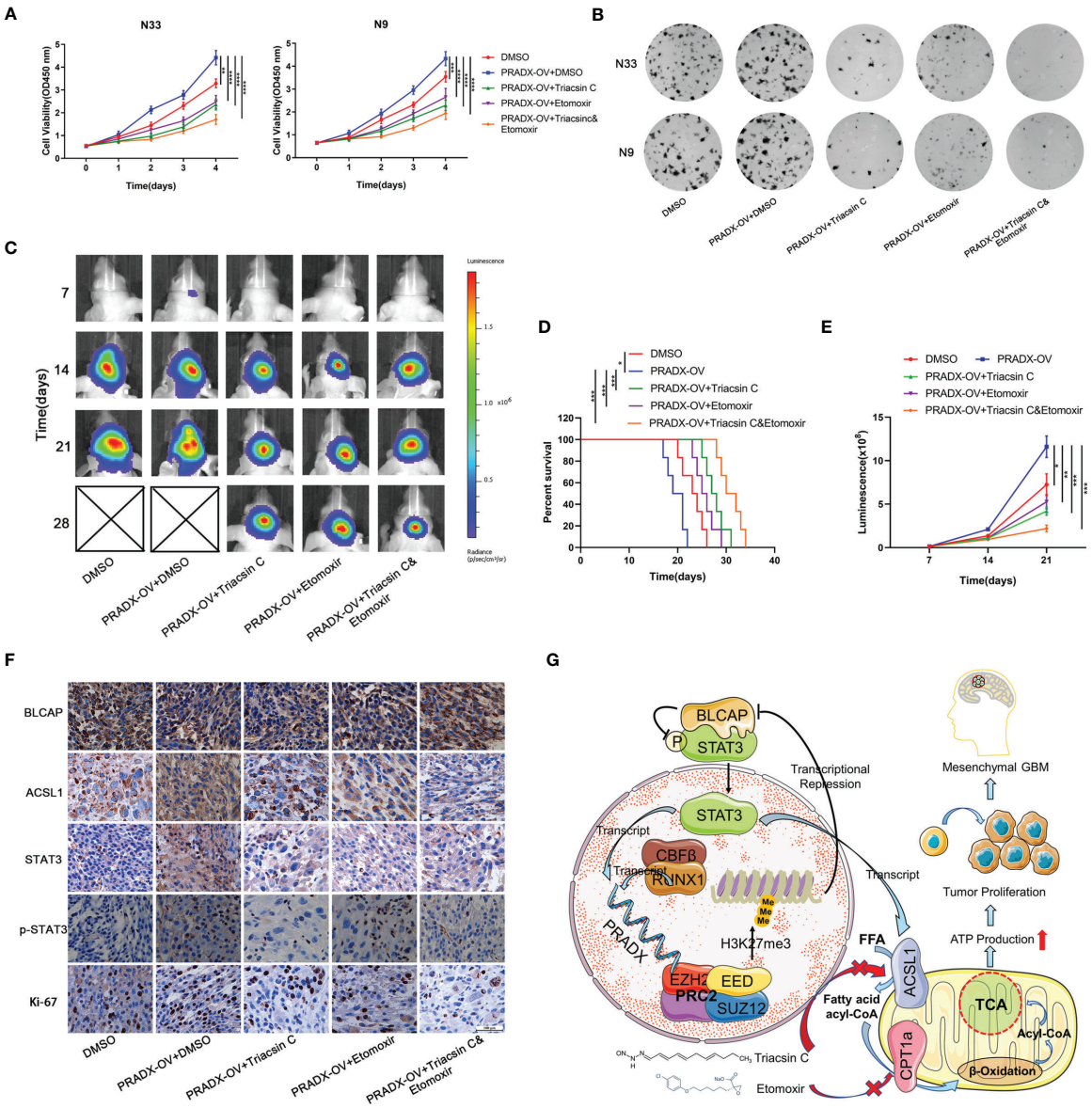

FIGURE 7 | Triacsin C and Etomoxir reduce PRADX-mediated tumorigenesis *in vitro* and *in vivo*. **(A)** CCK8 assays show the effect of PRADX overexpression and the Triacsin C and Etomoxir on cell viability. **(B)** Colony formation assays show the effect of PRADX overexpression and the Triacsin C and Etomoxir on the tumor cell growth of the indicated five groups, representative images are shown. **(C)** Nude mice were orthotopically injected with PRADX overexpression or scramble TBD0220 cells. Representative luminescence images at 7,14,21 and 28d after injection are shown. **(D, E)** Kaplan-Meier survival curve and quantification of bioluminescence signal intensities at 7,14, and 21d post-injection are shown. **(F)** IHC of tumor tissues from nude mice xenograft models showing BLCAP, ACSL1, STAT3, p-STAT3, and Ki-67 expressions in the five groups. **(G)** Scheme showing PRADX-EZH2 interaction-mediated recruitment of H3K27me3 and regulation of STAT3 activity, promoting mesenchymal GBM tumorigenesis. The values in A are represented as mean ± SD (n = 3). *P < 0.05, **P < 0.01, ***P < 0.001, ****P <0.0001.

accelerated cellular metabolism and ATP production *via* activating STAT3 phosphorylation and increasing ACSL1 expression. However, the mechanistic roles of ACSL1 in GBM energy metabolism and fatty acid production still need further exploration.

Acceleration of GBM cellular metabolic activity changes the phospholipid biosynthesis pathways, leading to energy metabolism reprogramming, which is an important feature of GBM (26, 44). Seeking clinical treatment strategies for GBM is the ultimate goal of our research. We showed that the combined use of Triacsin C and Etomoxir could reduce tumor cell metabolism and ATP production by seahorse experiment. Moreover, the combination of the ACSL1 and CPT1 inhibitors also reduced tumor growth both *in vivo* and *in vitro*. Our findings thus provide a potential therapeutic strategy for GBM treatment. However, the therapeutic efficiency of this treatment regimen in GBM patients

needs further investigation. Additionally, investigating lncRNA-Protein interaction is also a potential therapeutic target for cancer therapy (25). Previous studies have focused on discovering EZH2 inhibitors for targeted therapy (17, 18), however, our study provided a novel therapeutic avenue for developing an effective inhibitor to disrupt PRADX-EZH2 interaction, thus increasing the expression of TSGs and finally inhibiting tumor growth.

In summary, our study revealed a novel lncRNA-protein interaction-mediated positive feedback loop which was important in mesenchymal GBM proliferation. PRADX/PRC2 complex recruited H3K27me3 at BLCAP promoter, suppressing BLCAP expression and activating BLCAP binding protein STAT3 phosphorylation, promoting ACSL1 expression and energy metabolism. Taken together, PRADX is a novel mesenchymal GBM biomarker, and RUNX1-CBFβ/PRADX/BLCAP/STAT3 axis is the key carcinogenic pathway in mesenchymal GBM, targeting ACSL1 and CPT1 to reduce cellular metabolism might be a potential strategy to treat GBM patients.

CONCLUSION

We found the carcinogenic pathway of PRADX in mesenchymal GBM. PRADX was transcribed by the RUNX1-CBFβ complex. PRADX overexpression suppressed BLCAP expression *via* recruitment of H3K27me3, activating the phosphorylation of BLCAP interacting protein STAT3 and accelerating tumor metabolism and ATP production, resulting in tumor proliferation and poor survival outcomes.

DATA AVAILABILITY STATEMENT

The datasets presented in this study can be found in online repositories. The names of the repository/repositories and accession number(s) can be found in the article/**Supplementary Material**.

ETHICS STATEMENT

The animal study was reviewed and approved by Institutional Committee on Animal Care of Hebei University (Approval No. IACUC-2021XG002).

AUTHOR CONTRIBUTIONS

Developed the study concept and designed the study: CK, CF, and YT. Conducted the experiments and acquired the data: CX, JZ, YT, JS, MX, XC, LX, JX, YZ, KY, BH, FT, and ST. Analyzed the data, generated the figures, and wrote the paper: CX and JZ. Funded the work and provided overall research supervision: CF and YT. Approved the final manuscript: All authors.

FUNDING

This research was supported by grants from the National Natural Science Foundation of China (NSFC, No.82172660, No.82002657), Hebei Natural Science Foundation Precision Medicine Joint Project (No.H2020201206), Hebei provincial central leading local Science and Technology Development Fund Project (No.216Z7711G), Tianjin Key R&D Program of Tianjin Science and Technology Support Project (No.20YFZCSY00360), and the Science and Technology Project of Tianjin Municipal Health Commission (No.TJWJ2021QN003).

SUPPLEMENTARY MATERIAL

The Supplementary Material for this article can be found online at: https://www.frontiersin.org/articles/10.3389/fonc.2022.888922/full#supplementary-material

REFERENCES

1. Ulitsky I, Bartel DP. lincRNAs: Genomics, Evolution, and Mechanisms. *Cell* (2013) 154(1):26–46. doi: 10.1016/j.cell.2013.06.020
2. Deveson IW, Hardwick SA, Mercer TR, Mattick JS. The Dimensions, Dynamics, and Relevance of the Mammalian Noncoding Transcriptome. *Trends Genet* (2017) 33(7):464–78. doi: 10.1016/j.tig.2017.04.004
3. Esteller M. Non-Coding RNAs in Human Disease. *Nat Rev Genet* (2011) 12 (12):861–74. doi: 10.1038/nrg3074
4. Baspinar Y, Elmaci I, Ozpinar A, Altinoz MA. Long non-Coding RNA MALAT1 Is A Key Target in the Pathogenesis of Glioblastoma. Janus Faces or Achilles' Heal? *Gene* (2020) 739:144518. doi: 10.1016/j.gene.2020.144518
5. Tang J, Yu B, Li Y, Zhang W, Alvarez AA, Hu B, et al. TGF-Beta-Activated lncRNA LINC00115 Is A Critical Regulator of Glioma Stem-Like Cell Tumorigenicity. *EMBO Rep* (2019) 20(12):e48170. doi: 10.15252/embr.201948170
6. Zhang XZ, Liu H, Chen SR. Mechanisms of Long Non-Coding RNAs in Cancers and Their Dynamic Regulations. *Cancers (Basel)* (2020) 12(5):1245. doi: 10.3390/cancers12051245
7. Yan Y, Xu Z, Li Z, Sun L, Gong Z. An Insight Into the Increasing Role of LncRNAs in the Pathogenesis of Gliomas. *Front Mol Neurosci* (2017) 10:53. doi: 10.3389/fnmol.2017.00053
8. Wang Q, Zhang J, Liu Y, Zhang W, Zhou J, Duan R, et al. A Novel Cell Cycle-Associated lncRNA, HOXA11-AS, Is Transcribed From the 5-Prime End of the HOXA Transcript and Is A Biomarker of Progression in Glioma. *Cancer Lett* (2016) 373(2):251–9. doi: 10.1016/j.canlet.2016.01.039
9. Jing SY, Lu YY, Yang JK, Deng WY, Zhou Q, Jiao BH. Expression of Long non-Coding RNA CRNDE in Glioma and Its Correlation With Tumor Progression and Patient Survival. *Eur Rev Med Pharmacol Sci* (2016) 20 (19):3992–6.
10. Statello L, Guo CJ, Chen LL, Huarte M. Gene Regulation by Long non-Coding RNAs and Its Biological Functions. *Nat Rev Mol Cell Biol* (2021) 22(2):96–118. doi: 10.1038/s41580-020-00315-9
11. Yin Y, Lu JY, Zhang X, Shao W, Xu Y, Li P, et al. U1 snRNP Regulates Chromatin Retention of Noncoding RNAs. *Nat* (2020) 580(7801):147–50. doi: 10.1038/s41586-020-2105-3
12. Chen Q, Cai J, Wang Q, Wang Y, Liu M, Yang J, et al. Long Noncoding RNA NEAT1, Regulated by the EGFR Pathway, Contributes to Glioblastoma Progression Through the WNT/beta-Catenin Pathway by Scaffolding Ezh2. *Clin Cancer Res* (2018) 24(3):684–95. doi: 10.1158/1078-0432.CCR-17-0605
13. Zhang K, Sun X, Zhou X, Han L, Chen L, Shi Z, et al. Long non-Coding RNA HOTAIR Promotes Glioblastoma Cell Cycle Progression in an EZH2 Dependent Manner. *Oncotarget* (2015) 6(1):537–46. doi: 10.18632/oncotarget.2681

14. Katsushima K, Natsume A, Ohka F, Shinjo K, Hatanaka A, Ichimura N, et al. Targeting the Notch-Regulated Non-Coding RNA TUG1 for Glioma Treatment. *Nat Commun* (2016) 7:13616. doi: 10.1038/ncomms13616
15. Schuettengruber B, Bourbon HM, Di Croce L, Cavalli G. Genome Regulation by Polycomb and Trithorax: 70 Years and Counting. *Cell* (2017) 171(1):34–57. doi: 10.1016/j.cell.2017.08.002
16. Ciferri C, Lander GC, Maiolica A, Herzog F, Aebersold R, Nogales E. Molecular Architecture of Human Polycomb Repressive Complex 2. *Elife* (2012) 1:e00005. doi: 10.7554/eLife.00005
17. Laugesen A, Hojfeldt JW, Helin K. Role of the Polycomb Repressive Complex 2 (PRC2) in Transcriptional Regulation and Cancer. *Cold Spring Harb Perspect Med* (2016) 6(9):a026575. doi: 10.1101/cshperspect.a026575
18. Janaki Ramaiah M, Divyapriya K, Kartik Kumar S, Rajesh Y. Drug-Induced Modifications and Modulations of microRNAs and Long Non-Coding RNAs for Future Therapy Against Glioblastoma Multiforme. *Gene* (2020) 723:144126. doi: 10.1016/j.gene.2019.144126
19. Ostrom QT, Gittleman H, Xu J, Kromer C, Wolinsky Y, Kruchko C, et al. CBTRUS Statistical Report: Primary Brain and Other Central Nervous System Tumors Diagnosed in the United States in 2009-2013. *Neuro Oncol* (2016) 18 (suppl_5):v1–v75. doi: 10.1093/neuonc/now207
20. Verhaak RG, Hoadley KA, Purdom E, Wang V, Qi Y, Wilkerson MD, et al. Integrated Genomic Analysis Identifies Clinically Relevant Subtypes of Glioblastoma Characterized by Abnormalities in PDGFRA, IDH1, EGFR, and NF1. *Cancer Cell* (2010) 17(1):98–110. doi: 10.1016/j.ccr.2009.12.020
21. Wang Q, Hu B, Hu X, Kim H, Squatrito M, Scarpace L, et al. Tumor Evolution of Glioma-Intrinsic Gene Expression Subtypes Associates With Immunological Changes in the Microenvironment. *Cancer Cell* (2017) 32 (1):42–56.e6. doi: 10.1016/j.ccell.2017.06.003
22. Sumazin P, Yang X, Chiu HS, Chung WJ, Iyer A, Llobet-Navas D, et al. An Extensive microRNA-Mediated Network of RNA-RNA Interactions Regulates Established Oncogenic Pathways in Glioblastoma. *Cell* (2011) 147(2):370–81. doi: 10.1016/j.cell.2011.09.041
23. Wang Q, Cai J, Fang C, Yang C, Zhou J, Tan Y, et al. Mesenchymal Glioblastoma Constitutes a Major ceRNA Signature in the TGF-Beta Pathway. *Theranostics* (2018) 8(17):4733–49. doi: 10.7150/thno.26550
24. Zhao K, Cui X, Wang Q, Fang C, Tan Y, Wang Y, et al. RUNX1 Contributes to the Mesenchymal Subtype of Glioblastoma in a TGFbeta Pathway-Dependent Manner. *Cell Death Dis* (2019) 10(12):877. doi: 10.1038/s41419-019-2108-x
25. Li Y, Liu X, Cui X, Tan Y, Wang Q, Wang Y, et al. LncRNA PRADX-Mediated Recruitment of PRC2/DDX5 Complex Suppresses UBXN1 Expression and Activates NF-kappaB Activity, Promoting Tumorigenesis. *Theranostics* (2021) 11(9):4516–30. doi: 10.7150/thno.54549
26. Yi K, Zhan Q, Wang Q, Tan Y, Fang C, Wang Y, et al. PTRF/cavin-1 Remodels Phospholipid Metabolism to Promote Tumor Proliferation and Suppress Immune Responses in Glioblastoma by Stabilizing Cpla2. *Neuro Oncol* (2021) 23(3):387–99. doi: 10.1093/neuonc/noaa255
27. Carro MS, Lim WK, Alvarez MJ, Bollo RJ, Zhao X, Snyder EY, et al. The Transcriptional Network for Mesenchymal Transformation of Brain Tumors. *Nat* (2010) 463(7279):318–25. doi: 10.1038/nature08712
28. Zhen T, Cao Y, Ren G, Zhao L, Hyde RK, Lopez G, et al. RUNX1, and CBFbeta-SMMHC Transactivate Target Genes Together in Abnormal Myeloid Progenitors for Leukemia Development. *Blood* (2020) 136 (21):2373–85. doi: 10.1182/blood.2020007747
29. Li Y, Ren Y, Wang Y, Tan Y, Wang Q, Cai J, et al. A Compound AC1Q3QWB Selectively Disrupts HOTAIR-Mediated Recruitment of PRC2 and Enhances Cancer Therapy of DZNep. *Theranostics* (2019) 9(16):4608–23. doi: 10.7150/thno.35188
30. Priego N, Zhu L, Monteiro C, Mulders M, Wasilewski D, Bindeman W, et al. STAT3 Labels a Subpopulation of Reactive Astrocytes Required for Brain Metastasis. *Nat Med* (2018) 24(7):1024–35. doi: 10.1038/s41591-018-0044-4
31. Yu H, Lee H, Herrmann A, Buettner R, Jove R. Revisiting STAT3 Signaling in Cancer: New and Unexpected Biological Functions. *Nat Rev Cancer* (2014) 14 (11):736–46. doi: 10.1038/nrc3818
32. Gromova I, Svensson S, Gromov P, Moreira JMA. Identification of BLCAP as a Novel STAT3 Interaction Partner in Bladder Cancer. *PloS One* (2017) 12 (11):e0188827. doi: 10.1371/journal.pone.0188827
33. Chen W, He W, Cai H, Hu B, Zheng C, Ke X, et al. A-To-I RNA Editing of BLCAP Lost the Inhibition to STAT3 Activation in Cervical Cancer. *Oncotarget* (2017) 8(24):39417–29. doi: 10.18632/oncotarget.17034
34. Tse C, Warner A, Farook R, Cronin JG. Phytochemical Targeting of STAT3 Orchestrated Lipid Metabolism in Therapy-Resistant Cancers. *Biomolecules* (2020) 10(8):1118. doi: 10.3390/biom10081118
35. Koskela HL, Eldfors S, Ellonen P, van Adrichem AJ, Kuusanmaki H, Andersson EI, et al. Somatic STAT3 Mutations in Large Granular Lymphocytic Leukemia. *N Engl J Med* (2012) 366(20):1905–13. doi: 10.1056/NEJMoa1114885
36. Huang L, Liu D, Wang N, Ling S, Tang Y, Wu J, et al. Integrated Genomic Analysis Identifies Deregulated JAK/STAT-MYC-Biosynthesis Axis in Aggressive NK-Cell Leukemia. *Cell Res* (2018) 28(2):172–86. doi: 10.1038/cr.2017.146
37. Qin L, Qiao C, Sheen V, Wang Y, Lu J. DNMT3L Promotes Neural Differentiation by Enhancing STAT1 and STAT3 Phosphorylation Independent of DNA Methylation. *Prog Neurobiol* (2021) 201:102028. doi: 10.1016/j.pneurobio.2021.102028
38. Rossi Sebastiano M, Konstantinidou G. Targeting Long Chain Acyl-CoA Synthetases for Cancer Therapy. *Int J Mol Sci* (2019) 20(15):3624. doi: 10.3390/ijms20153624
39. Wang YN, Zeng ZL, Lu J, Wang Y, Liu ZX, He MM, et al. CPT1A-Mediated Fatty Acid Oxidation Promotes Colorectal Cancer Cell Metastasis by Inhibiting Anoikis. *OncoGene* (2018) 37(46):6025–40. doi: 10.1038/s41388-018-0384-z
40. Vasan K, Werner M, Chandel NS. Mitochondrial Metabolism as a Target for Cancer Therapy. *Cell Metab* (2020) 32(3):341–52. doi: 10.1016/j.cmet.2020.06.019
41. Peng Z, Liu C, Wu M. New Insights Into Long Noncoding RNAs and Their Roles in Glioma. *Mol Cancer* (2018) 17(1):61. doi: 10.1186/s12943-018-0812-2
42. Jain AK, Xi Y, McCarthy R, Allton K, Akdemir KC, Patel LR, et al. LncPRESS1 Is a P53-Regulated LncRNA That Safeguards Pluripotency by Disrupting SIRT6-Mediated De-Acetylation of Histone H3k56. *Mol Cell* (2016) 64 (5):967–81. doi: 10.1016/j.molcel.2016.10.039
43. Huh JY, Reilly SM, Abu-Odeh M, Murphy AN, Mahata SK, Zhang J, et al. TANK-Binding Kinase 1 Regulates the Localization of Acyl-CoA Synthetase ACSL1 to Control Hepatic Fatty Acid Oxidation. *Cell Metab* (2020) 32 (6):1012–27 e7. doi: 10.1016/j.cmet.2020.10.010
44. Zhou L, Wang Z, Hu C, Zhang C, Kovatcheva-Datchary P, Yu D, et al. Integrated Metabolomics and Lipidomics Analyses Reveal Metabolic Reprogramming in Human Glioma With IDH1 Mutation. *J Proteome Res* (2019) 18(3):960–9. doi: 10.1021/acs.jproteome.8b00663

Conflict of Interest: The authors declare that the research was conducted in the absence of any commercial or financial relationships that could be construed as a potential conflict of interest.

Publisher's Note: All claims expressed in this article are solely those of the authors and do not necessarily represent those of their affiliated organizations, or those of the publisher, the editors and the reviewers. Any product that may be evaluated in this article, or claim that may be made by its manufacturer, is not guaranteed or endorsed by the publisher.

Copyright © 2022 Xu, Zhao, Song, Xiao, Cui, Xin, Xu, Zhang, Yi, Hong, Tong, Tian, Tan, Kang and Fang. This is an open-access article distributed under the terms of the Creative Commons Attribution License (CC BY). The use, distribution or reproduction in other forums is permitted, provided the original author(s) and the copyright owner(s) are credited and that the original publication in this journal is cited, in accordance with accepted academic practice. No use, distribution or reproduction is permitted which does not comply with these terms.

frontiers | Frontiers in Oncology

ORIGINAL RESEARCH
published: 18 May 2022
doi: 10.3389/fonc.2022.876090

Long Noncoding RNA HAGLROS Promotes the Malignant Progression of Bladder Cancer by Regulating the miR-330-5p/SPRR1B Axis

Shiwei Xiao[1,2], Yigang Zuo[1], Yanan Li[3], Yinglong Huang[1], Shi Fu[1], Dongbo Yuan[2], Xuhua Qiao[1], Haifeng Wang[1†] and Jiansong Wang[1*†]*

[1] Department of Urology, The Second Affiliated Hospital of Kunming Medical University, Yunnan Institute of Urology, Kunming, China, [2] Department of Urology, Guizhou Provincial People's Hospital, Guiyang, China, [3] Department of Basic Chemistry, College of Pharmacy, Guizhou University of Traditional Chinese Medicine, Guiyang, China

Bladder cancer (BC) is the most common genitourinary malignancy worldwide, and its aetiology and pathogenesis remain unclear. Accumulating evidence has shown that HAGLROS is closely related to the occurrence and progression of various cancers. However, the biological functions and underlying mechanisms of HAGLROS in BC remain unknown. In the present study, the expression of HAGLROS in BC was determined by public dataset analysis, transcriptome sequencing analysis, qRT–PCR and ISH assays. Gain- or loss-of-function assays were performed to study the biological roles of HAGLROS in BC cells and nude mouse xenograft model. Bioinformatic analysis, qRT–PCR, western blot, immunohistochemistry, FISH assays, subcellular fractionation assays and luciferase reporter assays were performed to explore the underlying molecular mechanisms of HAGLROS in BC. Here, we found that HAGLROS expression is significantly upregulated in BC tissues and cells, and elevated HAGLROS expression was related to higher pathologic grade and advanced clinical stage, which is significant for BC diagnosis. HAGLROS can enhance the growth and metastasis of BC *in vitro* and *in vivo*. Furthermore, miR-330-5p downregulation reversed the BC cells proliferation, migration and invasion inhibited by silencing HAGLROS. SPRR1B silencing restored the malignant phenotypes of BC cells promoted by miR-330–5p inhibitor. Mechanistically, we found that HAGLROS functions as a microRNA sponge to positively regulate SPRR1B expression by sponging miR-330-5p. Together, these results demonstrate that HAGLROS plays an oncogenic role and may serve as a potential biomarker for the diagnosis and treatment of BC.

Keywords: bladder cancer, HAGLROS, miR-330-5p, SPRR1B, oncogene

OPEN ACCESS

Edited by:
Zhe-Sheng Chen,
St. John's University, United States

Reviewed by:
Chenyu Lin,
The Ohio State University, United States
Wei-de Zhong,
Guangzhou First People's Hospital, China

****Correspondence:***
Jiansong Wang
wangjiansong@kmmu.edu.cn
Haifeng Wang
highphone@126.com

†These authors have contributed equally to this work

Specialty section:
This article was submitted to Pharmacology of Anti-Cancer Drugs, a section of the journal Frontiers in Oncology

Received: *15 February 2022*
Accepted: *01 April 2022*
Published: *18 May 2022*

Citation:
Xiao S, Zuo Y, Li Y, Huang Y, Fu S, Yuan D, Qiao X, Wang H and Wang J (2022) Long Noncoding RNA HAGLROS Promotes the Malignant Progression of Bladder Cancer by Regulating the miR-330-5p/SPRR1B Axis. Front. Oncol. 12:876090. doi: 10.3389/fonc.2022.876090

INTRODUCTION

BC is the most common genitourinary malignancy worldwide. In the past decade, the morbidity and mortality of BC have increased significantly, showing a gradually decreasing trend in age (1). Non-muscle-invasive bladder cancer (NMIBC) can be treated with transurethral resection of the bladder tumour and postoperative adjuvant chemotherapy/immunotherapy. Of note, approximately 50-70% of patients with NMIBC will relapse, and 10-20% will eventually progress to muscle-invasive bladder cancer (MIBC) or metastasize (2). Although MIBC is mainly treated with radical cystectomy, there are many short-term and long-term complications that cause considerable pain to patients (3, 4). However, the aetiology and pathogenesis of BC remain unclear. Therefore, an in-depth understanding of the underlying mechanisms and identifying effective early detection biomarkers have great clinical significance for improving the diagnosis and therapeutic strategies of BC.

LncRNAs are noncoding RNAs greater than 200 nucleotides in length that were initially ignored as "transcription noises" due to a lack of protein-coding function (5). However, the rapid development of RNA genomics technology highlights the notion that lncRNAs are key players in gene expression regulation and significantly contribute to human disease progression, especially in cancers (6). In the past decade, growing evidence has shown that lncRNAs play a vital role in gene expression and diverse biological processes by regulating transcription, sponging miRNAs, and modifying epigenetic regulation (6, 7). Notably, enormous amounts of lncRNAs have been found to play an important role in invasion, metastasis and drug resistance in BC (8–10). For instance, lncRNA-SNHG1 promotes basal MIBC cell invasion by interacting with the PP2A catalytic subunit and inducing autophagy (11). LncRNA-SLC16A1-AS1 induces metabolic reprogramming as a target and coactivator of E2F1 in BC progression (12). HAGLR opposite strand lncRNA (HAGLROS), which is located on chromosome 2q31.1, is a 699-bp lncRNA that was first reported in 2018 (13). This study revealed that HAGLROS can promote tumorigenesis and progression *via* mTOR signal-mediated inhibition of autophagy in gastric cancer. Moreover, recent study showed that HAGLROS can promote proliferation and angiogenesis and inhibit apoptosis by activating the Erk1/2 and AKT or JNK signalling pathways in LSCC cells (14). It was reported that HAGLROS could promote osteosarcoma invasion and metastasis through the ROCK1 signalling pathway (15). Subsequently, accumulating evidence has shown that HAGLROS is closely associated with proliferation, invasion, autophagy and drug resistance, and plays a vital role in the occurrence and progression of various cancers. However, the biological functions and underlying mechanisms of HAGLROS in BC remain unknown.

In the present study, the expression level, biological function and underlying mechanism of HAGLROS in BC were initially investigated. Our findings reveal that HAGLROS was significantly upregulated in BC tissues and cells compared with adjacent normal tissues and cells, which was verified by online databases and our transcriptome sequencing dataset, qRT–PCR and *in situ* hybridization (ISH) assay. Furthermore, HAGLROS can enhance the growth and metastasis of BC *in vitro* and *in vivo*. Knockdown of miR-330-5p promotes small proline rich protein 1B (SPRR1B) expression and reverses the malignant phenotypes inhibition of BC induced by silencing HAGLROS. SPRR1B silencing restored the malignant phenotypes of BC cells promoted by decreased miR-330-3p. Mechanistically, we found that HAGLROS was mostly distributed in the cytoplasm and positively regulated SPRR1B expression by sponging miR-330-5p in a competing endogenous RNA (ceRNA)-dependent manner. Overall, our results suggest that the HAGLROS/miR-330-5p/SPRR1B axis is a promising novel biomarker that may serve as a powerful therapeutic and diagnostic target in BC.

MATERIALS AND METHODS

Clinical Samples

From June 2019 to September 2020, 43 pairs of fresh BC tissues and corresponding non-tumour tissues were collected from patients who underwent radical cystectomy. The samples were immediately cleaned with normal saline and snap-frozen in liquid nitrogen after resection. All samples were confirmed independently by two pathologists. The patients were informed of the study contents and signed informed consent forms. This study was approved and supported by the Ethics Committee of the Second Affiliated Hospital of Kunming Medical University.

Cell Culture

The BC cell lines T24 and 5637 and the normal bladder uroepithelium cell line SV-HUC-1 and human embryonic kidney (HEK) 293T were purchased from Procell Life Science & Technology Co., Ltd. (Wuhan, China). T24, SV-HUC-1 and HEK-293T cells were cultured in DMEM (Gibco, NY, USA) with 10% foetal bovine serum (Gibco, NY, USA), 5637 cells were cultured with RPMI-1640 medium (Gibco, NY, USA) and 10% foetal bovine serum (FBS). All cells were cultured at 37°C in a humidified 5% CO_2 atmosphere.

RNA Extraction and Quantitative Real-Time PCR (qRT–PCR)

Total RNA was extracted from bladder tissue and cells using TRIzol reagent (Thermo Fisher Scientific, MA, USA) according to the manufacturer's instructions. The sequence of lncRNA/mRNA primers listed in **Supplementary Table 1**. The miRNA primers were designed and synthesized by RiboBio Biotechnology (Guangzhou, China). QRT–PCR assays were performed using qRT–PCR Starter Kits (RiboBio, Guangzhou, China) and run in a LightCycler 96 sequence detection instrument (Roche, Basel, Switzerland) according to the manufacturer's instructions. Expression was normalized to GAPDH, U6 and β-actin. Each experiment was repeated at least thrice.

In Situ Hybridization (ISH)

ISH assay was used to detect the HAGLORS expression in the bladder tissue microarray. The HAGLROS probes were designed and synthesized by Boster Biological Technology (Wuhan,

China). The images were analysed by ImageScope (Leica, Mannheim, Germany) software and the expression level of HAGLORS was evaluated by histochemistry score (H-Score).

RNA Fluorescent *In Situ* Hybridization (FISH) and Subcellular Fractionation Assay

FISH was performed to detect the subcellular colocalization of HAGLROS, miR-330-5p and SPRR1B. A FISH kit was purchased from Focofish Biotechnology (Guangzhou, China). The U6 probes were purchased from Sangon (Shanghai, China). Cell nuclei were counterstained with DAPI (Sangon, Shanghai, China). The cytoplasmic and nuclear fractions of T24 and 5637 cells were extracted using nuclear and cytoplasmic extraction reagents (Thermo Fisher Scientific, MA, USA) according to the manufacturer's protocol. Then, the RNA was extracted, and qRT–PCR was performed as previously described. Each experiment was repeated at least three times.

Transcriptome Sequencing

Briefly, total RNA was extracted from three pairs of fresh bladder cancer tissues and corresponding adjacent tissues. The eligible RNAs were sent to the sequencing company for quality control, library construction and sequencing.

Cell Transfection

The plasmids of overexpressing HAGLROS (OE-HAGLROS), short hairpin (sh) HAGLROS and sh-SPRR1B were designed and synthesized by GenoMeditech Biotechnology (Shanghai, China). T24 and 5637 cells were transfected. The cells were harvested 48-72 hours. Puromycin (Solarbio, Beijing, China) was used to screen stably transfected cells. The transfection efficiency was evaluated by qRT–PCR. The miR-330-5p mimics/inhibitors were purchased from RiboBio Biotechnology (Guangzhou, China). Each experiment was repeated at least three times.

Western Blot Assay

Western blot assay was used to detect protein expression. Tissues and cells were lysed with ice-cold RIPA lysis buffer (Beyotime, Shanghai, China). The protein was quantified using a Bradford Protein Assay Kit (Beyotime, Shanghai, China), separated by sodium dodecyl sulfate–polyacrylamide gel electrophoresis (Beyotime, Shanghai, China), transferred to a polyvinylidene fluoride (PVDF) membrane (Millipore, MA, USA), blocked with bovine serum albumin (Solarbio, Beijing, China), hybridized with SPRR1B (1:1000, Abcam, MA, USA) and GAPDH (1:1000, Abmart, Shanghai, China), and incubated with a secondary antibody (1:2000, Cell Signaling Technology, MA, USA). Signals were visualized with an enhanced chemiluminescence (ECL) kit (Beyotime, Shanghai, China). Then, the bands were detected using a gel imager system and analysed by ImageJ software (NIH, Bethesda, MD, USA). Each experiment was repeated at three times.

Cell Counting Kit-8 (CCK-8) Assay

BC cell proliferation was observed using an Enhanced Cell Counting Kit-8 (Beyotime, Shanghai, China) according to the manufacturer's instructions. Briefly, 100 μl cell suspension was seeded onto 96-well plates per well. After 0 h, 24 h, 48 h and 72 h, 10 μl CCK-8 solution was added to each well, and the cells were incubated for 1 hour. Finally, the absorbance was measured at 450 nm using a microplate reader (Thermo Fisher Scientific, MA, USA). Each experiment was repeated at least three times.

Wound Healing Assay

The migration capability of cells was tested by wound healing assay. The wounds were scratched using a 200-μl pipette tip in approximately 90% confluent cells. The migration of cells was acquired using a microscope (Olympus, Tokyo, Japan). Finally, wound healing areas were measured by ImageJ software (NIH, Bethesda, MD, USA). Each experiment was repeated at least three times.

Transwell Assay

The invasive capability of cells was observed using Transwell assays. Briefly, 100 μl diluted Matrigel (Corning, MA, USA) was added to the upper chamber of the Transwell (Corning, MA, USA), and the transwells were incubated at 37°C for 1 hour. Then, 200 μl serum-free medium with 5×10^4 cells were seeded into each upper chamber. Culture medium containing 10% FBS was added to the lower chamber. The cells in the upper chamber were wiped using cotton after 48 hours of incubation, fixed with paraformaldehyde, and stained with crystal violet. The number of invaded cells was recorded under a microscope. Each experiment was repeated at least three times.

Flow Cytometry Assay

The cell cycle was determined by using a Cell Cycle Analysis Kit (Beyotime, Shanghai, China) according to the manufacturer's instructions. The cell cycle was assessed by flow cytometry. Each experiment was repeated at least three times.

Immunohistochemistry (IHC)

Protein expression levels were detected by immunohistochemical staining. The bladder tissues were prepared into paraffin sections. Then, these sections were deparaffinized, used for antigen retrieval, and incubated with a primary antibody against SPRR1B (1:150, Proteintech, Wuhan, China) overnight at 4°C. A universal two-step assay kit (Zsboi, Beijing, China) was used for IHC. The immunostaining images were detected using an optical microscope. Each experiment was repeated at least three times.

Dual-Luciferase Reporter Assays

Luciferase reporter plasmids were designed and synthesized by GenoMeditech (Shanghai, China). HEK-293T cells were cotransfected with luciferase reporter plasmids and microRNAs. A dual-luciferase reporter assay system (Promega, WI, USA) was used to determine the luciferase activity 48 h later according to the instructions. Each experiment was repeated at least three times.

Tumour Xenograft Implantation in Nude Mice

T24 cells, OE-HAGLROS and sh-HAGLROS stably transfected T24 cells (2×10^6 cells) were subcutaneously inoculated into

BALB/c nude mice (18-22 g). Then, tumour volumes were measured every 3 days. The animal experiments were approved and supported by the Ethics Committee of the Second Affiliated Hospital of Kunming Medical University. Each experiment was repeated at least three times.

Immunofluorescence

Immunofluorescence was used to detect ki67 expression levels in nude mice BC tissues, which was performed according to the standard protocol previously reported. The primary antibody against ki67 was purchased from Proteintech (1:150, Wuhan, China), and the 488-conjugated secondary antibody was purchased from KPL (1:1000, MA, USA). Sections were visualized using a fluorescence microscopy (Olympus, Tokyo, Japan). Each experiment was repeated at least three times.

Bioinformatics Analysis

The DEGseq2 R package (R version 4.0.1) was used to identify differentially expressed lncRNAs and mRNAs (DE-lncRNAs and DE-mRNAs) in RNA-sequencing data according to the thresholds |log2 (FC) |> 1.0 and P value < 0.05. A total of 408 BC samples and 19 normal samples were downloaded from TCGA database (https://portal.gdc.cancer.gov/), and the DE-lncRNAs and DE-mRNAs were identified according to the thresholds |log2 (FC) |> 0.585 and P value < 0.05. The DE-lncRNAs and DE-mRNAs were overlapped between the RNA-sequencing data and TCGA data. The differential expression of candidate genes and the relationship of their expression levels were evaluated in data retrieved from the starBase database (https://starbase.sysu.edu.cn/), the GEPIA database (http://gepia.cancer-pku.cn/), the Lnc2Cancer database (http://bio-bigdata.hrbmu.edu.cn/lnc2cancer/) and the LncBase database (https://diana.e-ce.uth.gr/lncbase/).

Statistical Analyses

The data were obtained from three independent experiments performed at least three time. All results are presented as the mean ± SD. Statistical analysis was performed with one-way ANOVA and Student's t test using GraphPad Prism 8.0 (GraphPad Software, La Jolla, CA, USA). In this study, *P-values* < 0.05 was considered statistically significant.

RESULTS

HAGLROS Expression Is Significantly Upregulated in BC

HAGLROS expression in common tumours was analysed using the GEPIA database, and the results showed that HAGLROS was highly expressed in most tumours, including BC, lung squamous cell carcinoma, and cervical squamous cell carcinoma (**Figure 1A**). To further study whether HAGLROS is significantly upregulated in BC, we retrieved and analysed data from the starBase database and the Lnc2Cancer database. The results indicated that HAGLROS was both obviously elevated in BC (**Figures 1B, C**). Meanwhile, our transcriptome sequencing analysis identified 2210 DE-lncRNAs, including 1255 upregulated DE-lncRNAs and 955 downregulated DE-lncRNAs (**Figure 1D**). There were 55 upregulated DE-lncRNAs in both the TCGA dataset and our RNA sequencing (RNA-seq) dataset (**Figure 1E**). These data also confirmed that HAGLROS was significantly overexpressed (log2FoldChange = 5.70, P<0.01) in BC tissues (**Supplementary Table 2**). Furthermore, qRT–PCR assays were used to determine the HAGLROS expression levels in BC tissues and cells. We found that HAGLROS was obviously upregulated in BC tissues and cells (**Figures 1F, G**), and increased HAGLROS expression was related to higher pathologic grade and advanced clinical stage (**Figures 1H, I**). To further validate the expression and diagnostic value of HAGLROS, ISH assay was used to detect the HAGLROS expression level of bladder tissue microarray. The results also showed that HAGLROS was significantly overexpressed in BC (**Figure 1J**). Subsequently, the adjacent normal tissues were used as a control to produce a receiver operating characteristic (ROC) curve. The data of ROC curve indicated that HAGLROS was helpful for the diagnosis of BC (**Figure 1K**). In conclusion, these results demonstrate that HAGLROS expression is significantly upregulated in BC, which is valuable for the diagnosis of BC.

HAGLROS Plays an Oncogenic Role in BC

To further study the biological functions of HAGLROS in BC, we constructed and screened HAGLROS overexpression and knockdown vectors, which were transfected into T24 and 5637 BC cells for subsequent experiments. The CCK-8 assay results indicated that HAGLROS overexpression promoted BC cell proliferation, whereas HAGLROS knockdown inhibited BC cell proliferation (**Figures 2A, B**). To investigate the role of HAGLROS in BC, wound healing assays and Transwell assays were performed. The results revealed that upregulated HAGLROS expression strengthened BC cell migration and invasion, while downregulated HAGLROS expression decreased BC cell migration and invasion (**Figures 2C–G**). Moreover, the flow cytometry data showed that knockdown of HAGLROS induced G1-phase arrest in T24 and 5637 cells (**Figures 2H–J**). Collectively, these results reveal that HAGLROS promotes the proliferation, migration and invasion of BC cells and plays an oncogenic role *in vitro*.

HAGLROS Positively Regulates SPRR1B Expression

To explore the underlying mechanism of HAGLROS in BC cells, the cytoplasmic and nuclear fractions of T24 and 5637 cells were extracted for qRT–PCR assays, and a FISH assay was performed. Both results showed that HAGLROS was mostly located in the cytoplasm of BC cells (**Figures 3A–C**). Therefore, we hypothesized that HAGLROS functioned as a microRNA sponge in BC. Then, the TCGA dataset and our transcriptional sequencing dataset were used to identify the DE-mRNAs in BC. Our transcriptome sequencing analysis identified 689 differentially upregulated mRNAs in BC (**Figure 3D**). These mRNAs were overlapped, and the top 10 mRNAs in the two datasets were intersected (**Supplementary Figures 1A, B** and **Supplementary**

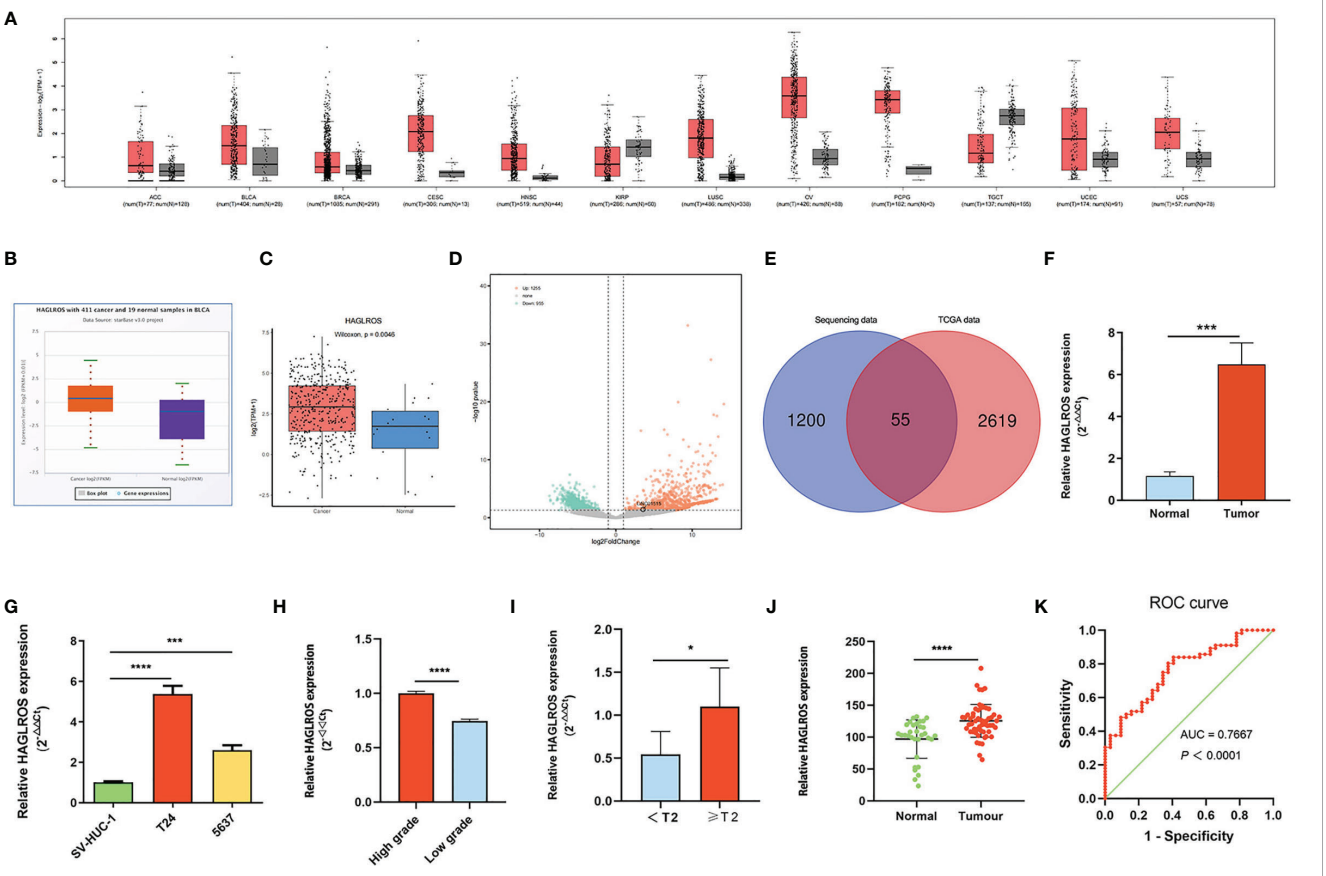

FIGURE 1 | HAGLROS expression is significantly upregulated in BC. **(A)** The expression of HAGLROS in common tumour samples and paired normal tissues was analyzed through the GEPIA database. **(B, C)** The HAGLROS expression level in BC was explored using the starBase database (P<0.0001) and the Lnc2Cancer database (P=0.0046). **(D)** Volcano plot of DE-lncRNAs in our transcriptome sequencing dataset. Each point in the plot represents a gene. Orange dots represent upregulated genes, whereas green dots represent downregulated genes. **(E)** Venn diagram of upregulated DE-lncRNAs based on the overlap between TCGA dataset and our RNA-sequencing dataset. **(F, G)** HAGLROS expression in BC samples and cells was determined using qRT–PCR assays. **(H, I)** HAGLROS expression was determined using qRT–PCR assays in different pathologic grades and clinical stages tissues. **(J)** ISH was performed to detect the expression of HAGLROS in bladder tissue microarray. **(K)** ROC curve for prediction of BC using ISH-based HAGLROS expression level. The AUC was 0.7667, *P*<0.0001. Each experiment was repeated at least three times. **P* < 0.05, ****P* < 0.001, *****P* < 0.0001.

Table 3). The data showed that six mRNAs were highly expressed in both groups, and SPRR1B was the most highly expressed in our sequencing dataset (log2FoldChange=11.83, *P*<0.01). Furthermore, qRT–PCR assay, western blot assay and IHC were used to detect SPRR1B expression levels in BC tissues and cells. The results showed that SPRR1B was highly overexpressed at both the transcriptional and protein levels in BC (**Figures 3E–I**). In addition, increasing HAGLROS expression obviously promoted SPRR1B expression, whereas decreasing HAGLROS expression inhibited SPRR1B expression in BC cells (**Figures 3J–L**). Of note, qRT-PCR results demonstrate that sh-SPRR1B can decrease HAGLROS expression (**Supplementary Figure 2**). These results suggest that HAGLROS positively regulates SPRR1B expression.

HAGLROS Regulates SPRR1B Expression by Sponging miR-330-5p

To study the regulatory mechanism of HAGLROS on SPRR1B, the potential miRNAs that shared putative binding sites with HAGLROS and SPRR1B cluster were predicted using the Lncbase database and the StarBase database. The data revealed that miR-330-5p shared putative binding sites with HAGLROS and SPRR1B cluster (**Figure 4A**). In addition, qRT–PCR assay was used to evaluate miR-330-5p expression levels in BC, and the results suggested that miR-330-5p was significantly downregulated in BC (**Figures 4B, C**). Furthermore, HAGLROS overexpression inhibited the expression of miR-330-5p, and HAGLROS knockdown increased the expression of miR-330-5p (**Figure 4D**). To further explore the relationship among HAGLROS, miR-330-5p and SPRR1B, FISH assays were performed to confirm their subcellular localizations in T24 and 5637 BC cells. The results indicate that all the above three genes are mainly located in the cytoplasm. In addition, HAGLROS may interact with miR-330-5p, and miR-330-5p could interact with SPRR1B (**Figures 4E, F**). Moreover, the dual-luciferase reporter assay data showed that HEK-293T cells cotransfected with wild-type HAGLROS and miR-330-5p mimics obviously decreased

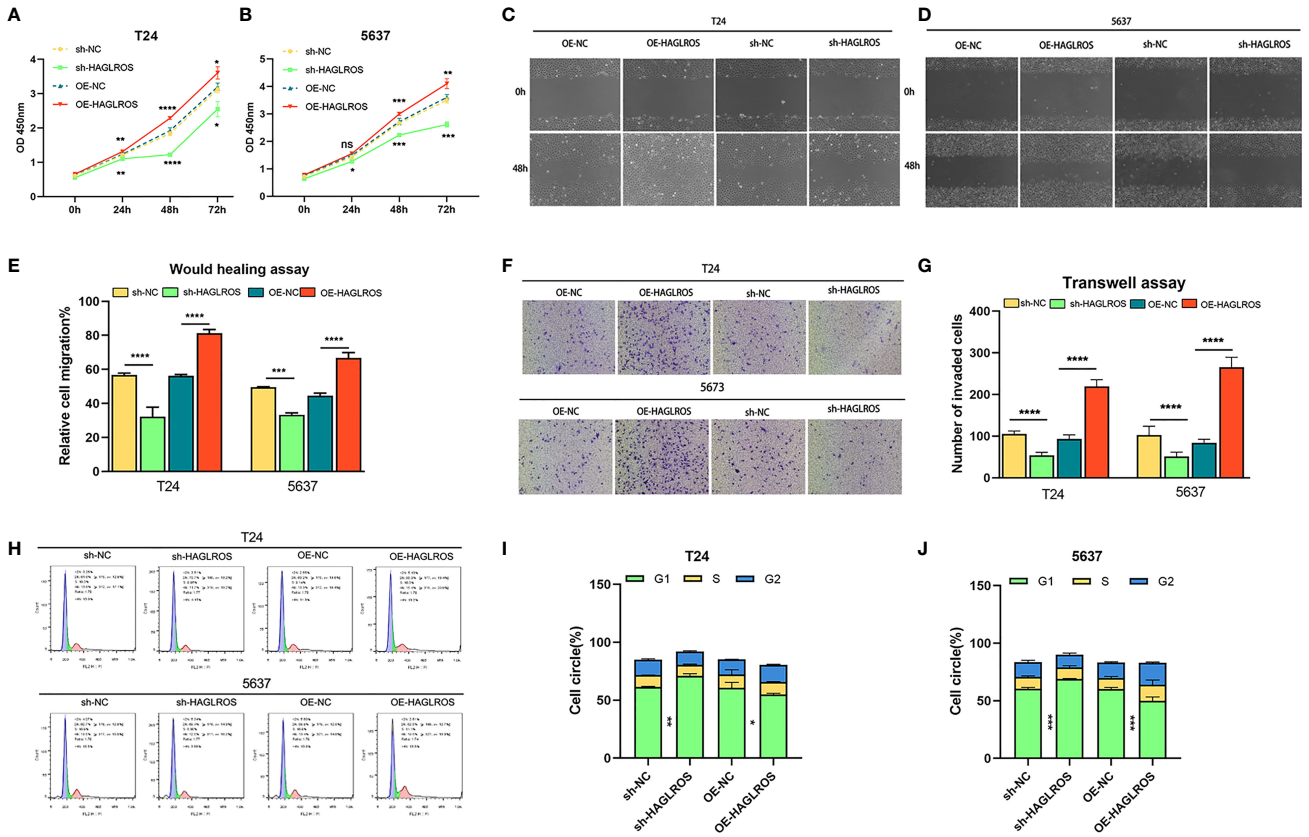

FIGURE 2 | HAGLROS promotes the proliferation, migration and invasion of BC *in vitro*. **(A, B)** Cell viability was assessed by CCK-8 assays in T24 and 5637 BC cells. **(C–E)** Cell migration was determined by wound healing assays in T24 and 5637 BC cells (magnification, x40). **(F, G)** Cell invasion was monitored by Transwell assays in T24 and 5637 BC cells (magnification, x100). **(H–J)** The cell cycle changes of T24 and 5637 BC cells were investigated using flow cytometry assays. $^{*}P < 0.05$, $^{**}P < 0.01$, $^{***}P < 0.001$, $^{****}P < 0.0001$, ns, not significant.

luciferase activity, but mut-type HAGLROS did not induce this change (**Figure 4G**). Additionally, HEK-293T cells cotransfected with wild-type SPRR1B and miR-330-5p mimics, but not mut-type SPRR1B, significantly inhibited the relative luciferase activity (**Figure 4H**). These results demonstrate that HAGLROS regulates the expression of SPRR1B by sponging miR-330-5p.

Decreasing miR-330-5p Expression Reverses Malignant Phenotypes Inhabited by Silencing HAGLROS in BC Cells

To further verify the regulatory mechanism of the HAGLROS/miR-330-5p/SPRR1B molecular axis, a series of gain- and loss-of-function assays were performed. The results showed that knockdown of miR-330-5p reversed the inhibitory effects on the proliferation, invasion and migration induced by silencing HAGLROS in BC cells (**Figures 5A–G**). In addition, the miR-330-5p inhibitor also reversed the expression of SPRR1B induced by silencing HAGLROS in BC cells (**Figures 5H, I**). Furthermore, the miR-330-5p mimic inhibited SPRR1B expression, whereas the miR-330-5p inhibitor promoted SPRR1B expression (**Figure 5J**). Notably, SPRR1B knockdown reversed the malignant phenotypes of BC cells promoted by decreasing miR-330-5p, thereby inhibiting the cancer-promoting effect of HAGLROS (**Supplementary Figure 3**). These results suggest that HAGLROS plays an important role in regulating the biological behaviour of BC by regulating the miR-330-5p/SPRR1B axis.

HAGLROS Promotes the Growth of Bladder Cancer *In Vivo*

To further validate whether HAGLROS regulates BC progression *in vivo*, T24 cells stably transfected with normal control, OE-HAGLROS and sh-HAGLROS vectors were used to establish subcutaneous xenograft mouse models. The results suggested that HAGLROS overexpression significantly promoted BC growth, while HAGLROS knockdown inhibited BC development compared with the control treatment (**Figures 6A, B**). The qRT-PCR results indicated that HAGLROS can also positively regulate SPRR1B expression and negatively regulate miR-330-5p expression *in vivo* (**Figures 6C–E**). Additionally, the expression level of ki67 was determined using an immunofluorescence assay. Consistently, the expression levels of ki-67 were dramatically increased in OE-HAGLROS group and obviously decreased in sh-HAGLROS group

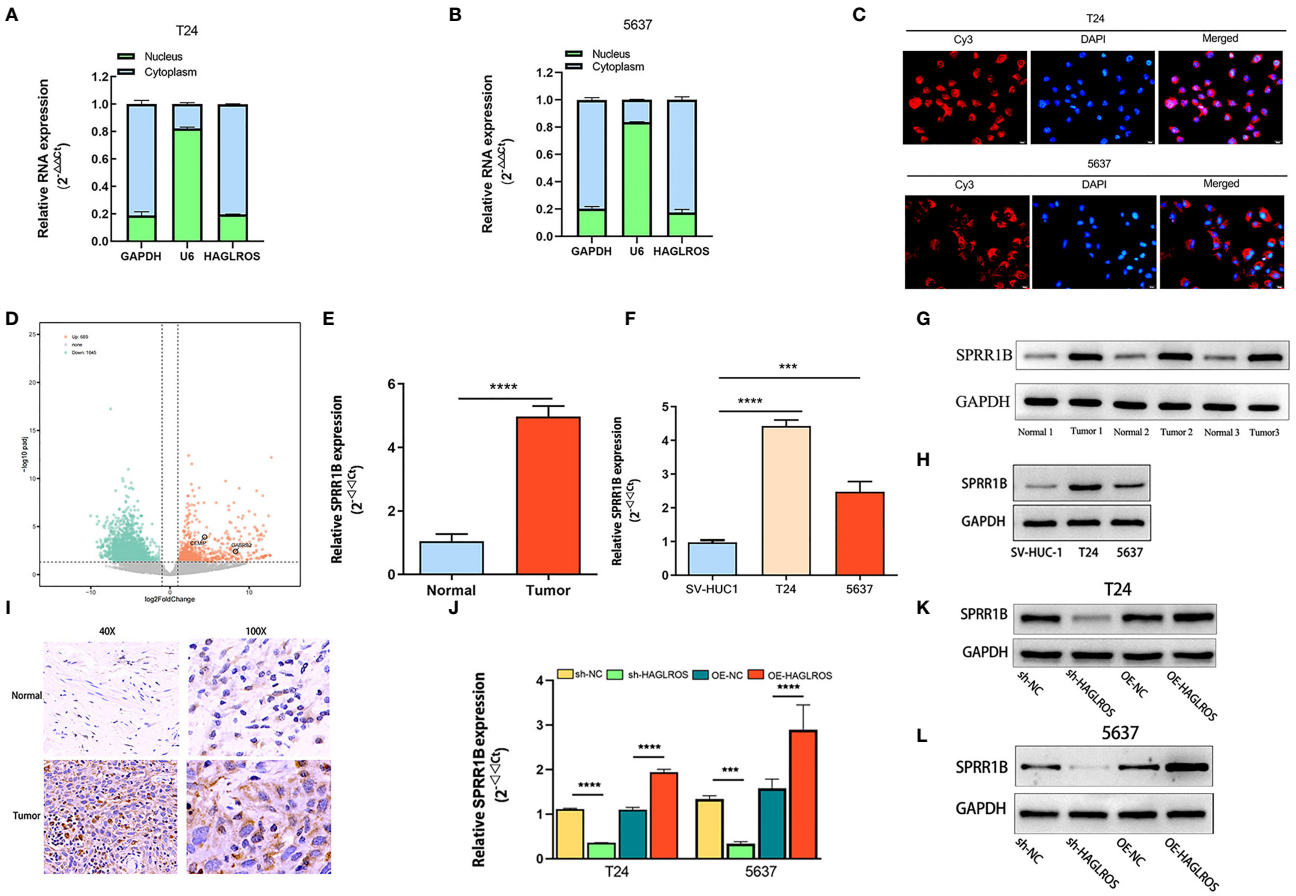

FIGURE 3 | HAGLROS positively regulates SPRR1B expression. **(A, B)** The cytoplasmic and nuclear RNA of T24 and 5637 cells were extracted for qRT–PCR assays. GAPDH was used as a cytoplasmic marker, and U6 was used as a nuclear marker. **(C)** FISH assay was performed to confirm the location of HAGLROS in T24 and 5637 cells (magnification, x 400). HAGLROS (Cy3, red), cell nuclei (DAPI, blue). **(D)** Volcano plot of DE-mRNAs in our transcriptome sequencing dataset. Each point in the plot represents a gene. Orange dots represent upregulated genes, whereas green dots represent downregulated genes. **(E–H)** SPRR1B expression was determined by qRT–PCR assays and western blot assays in bladder tissues and cells. **(I)** SPRR1B expression was analyzed by IHC assays in BC and adjacent normal samples. **(J–L)** The changes of SPRR1B expression were evaluated by qRT–PCR and western blot assays in BC cells transfected with sh-NC, sh-HAGLROS, OE-NC and OE-HAGLROS vectors. Each experiment was repeated at least three times. ***$P < 0.001$, ****$P < 0.0001$.

(**Figure 6F**). These data demonstrate HAGLROS can promote the growth of bladder tumour *in vivo*.

DISCUSSION

BC is the tenth most common malignant tumour and the fourteenth leading cause of cancer mortality worldwide and is characterized by a high recurrence rate, rapid progression and poor prognosis (1, 16). At present, the mechanisms involved in the pathogenesis and progression of BC remain unclear, and effective targets for early diagnosis and treatment of BC are urgently needed. In recent years, accumulating evidence has demonstrated that lncRNAs play an important regulatory role in cancers (6, 17, 18). Importantly, abnormal expression of lncRNAs is associated with increasing cancer-related mortality. For example, lncRNA CDKN2B-AS1 regulates progression and metastasis through the Cyclin-D pathway by interacting with miR-141 in renal cell carcinoma (19). LncRNA030, a novel lncRNA, maintains breast cancer stem cell stemness by stabilizing SQLE mRNA and increasing cholesterol synthesis (20). In addition, increasing studies have found that lncRNAs promote chemoresistance by regulating certain phase enzymes, altering drug efflux, repairing damaged DNA and inhibiting apoptosis in tumours (17). In the past decade, some of the significant lncRNAs were found to be related to BC incidence and development. For instance, UCA1 is specific and sensitive for the diagnosis of BC (21). Elevated H19 expression is associated with poor prognosis in BC (22).

HAGLROS, as a novel lncRNA, was first reported to promote the malignant phenotype of gastric cancer by sponging miR-100-5p to increase mTOR expression and interacting with mTORC1 components to activate the mTORC1 signalling pathway (13). Subsequently, numerous studies were performed to investigate

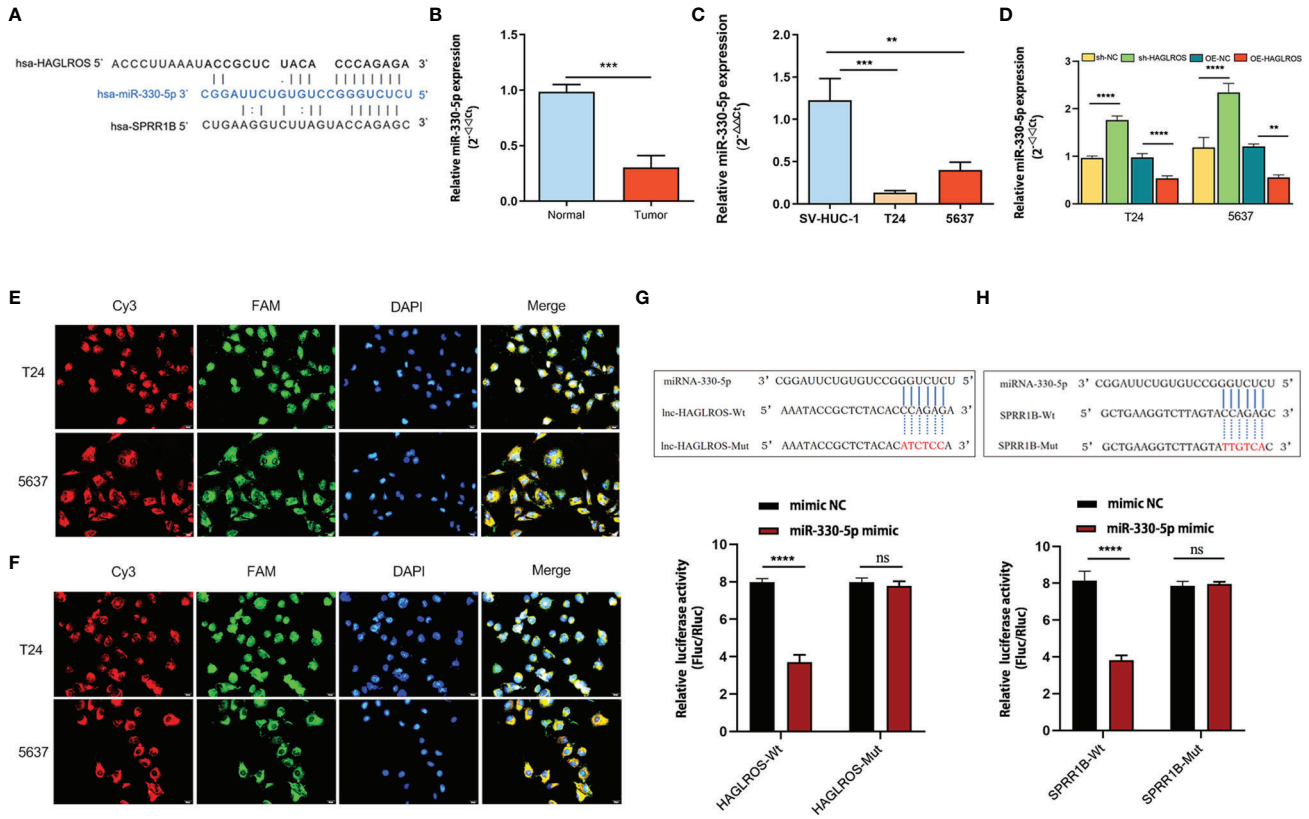

FIGURE 4 | HAGLROS regulates SPRR1B expression by sponging miR-330-5p. **(A)** The specific binding sites among HAGLROS, miR-330-5p and SPRR1B were predicted by the Lncbase database and the starBase database. **(B, C)** MiR-330-5p expression was examined in bladder tissues and cells using qRT–PCR assays. **(D)** The changes of miR-330-5p expression were determined using qRT–PCR assays. **(E)** FISH assay was used to confirm the subcellular colocalization between HAGLROS and miR-330-5p in BC cells (magnification, x 400). HAGLROS (Cy3, red), miR-330-5p (FAM, green), and cell nuclei (DAPI, blue). **(F)** FISH assay was used to confirm the subcellular colocalization between miR-330-5p and SPRR1B in BC cells (magnification, x 400). SPRR1B (Cy3, red), miR-330-5p (FAM, green), cell nuclei (DAPI, blue). **(G)** Wild-type or mutant HAGLROS was cotransfected with mimic-NC or miR-330-5p mimic into HEK-293T cells, and the relative luciferase activities were measured. **(H)** Wild-type or mutant SPRR1B was cotransfected with mimic-NC or miR-330-5p mimic into HEK-293T cells, and the relative luciferase activities were determined. Each experiment was repeated at least thrice. Ns, not significant. $^{**}P < 0.01$, $^{***}P < 0.001$, $^{****}P < 0.0001$.

the correlation between HAGLROS and cancers. For example, HAGLROS promotes proliferation, inhibits apoptosis and enhances autophagy by regulating the miR-5095/ATG12 axis and PI3K/AKT/mTOR signalling pathway in hepatocellular carcinoma (23). Lin et al. reported that knockdown HAGLROS can suppress the proliferation and promote the apoptosis of ovarian cancer cells by regulating miR-26b-5p, which affects the expression of apoptosis-related proteins (24). Notably, recent study indicated that HAGLROS was highly expressed and decreasing HAGLROS can inactivate the mTOR axis and elevate autophagy through improving lipid metabolism reprogramming in intrahepatic cholangiocarcinoma (25). In brief, growing evidence indicates that HAGLROS is closely related to apoptosis, autophagy, drug resistance and metabolic reprogramming and plays an oncogenic role in most cancers (26, 27). However, the biological functions and mechanisms of HAGLROS in BC remain unknown. In the present study, HAGLROS expression levels in BC were initially investigated using public databases, our transcriptome sequencing database, qRT–PCR and ISH assays. We found that HAGLROS is obviously increased in BC, and growing HAGLROS expression is correlated with poorer pathologic grade and clinical stage, which is significant for the diagnosis of BC. Moreover, a series of gain- and loss-of-function studies showed that HAGLROS can significantly promote proliferation, migration and invasion in BC.

The regulatory mechanism of lncRNAs depends in part on their subcellular localizations. Nuclear lncRNAs can regulate transcription by acting as enhancer RNAs (eRNAs), recruiting chromatin modifying complexes, regulating transcription factors, and cytoplasmic lncRNAs can regulate mRNA expression by regulating mRNA stability, mRNA translation, or competing microRNA binding (28). Our research shows that HAGLROS is mainly distributed in the cytoplasm of BC cells *via* subcellular fractionation assay and FISH assay. Therefore, we hypothesized that HAGLROS regulated BC growth and

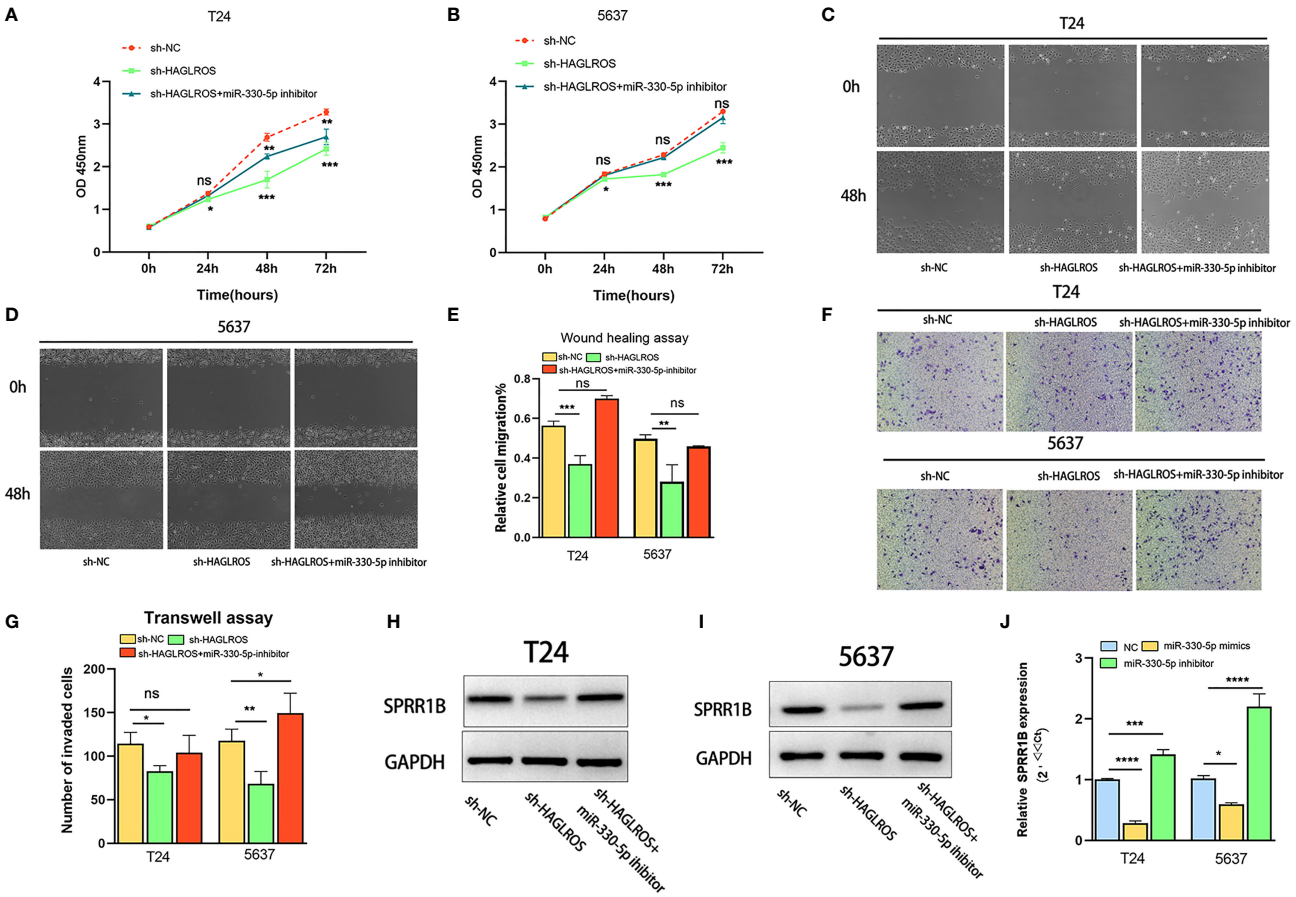

FIGURE 5 | Decreased miR-330-5p reverses malignant phenotypes induced by silencing HAGLROS in BC cells. **(A, B)** The proliferation changes of T24 and 5637 BC cells were determined by CCK-8 assays. **(C–E)** The migration ability of T24 and 5637 BC cells were observed using wound healing assays (magnification, x40). **(F, G)** The invasion changes of T24 and 5637 BC cells were monitored using Transwell assays (magnification, x100). **(H, I)** The expression levels of SPRR1B were measured using western blot assays in T24 and 5637 BC cells. **(J)** The expression levels of SPRR1B were measured using qRT–PCR assays in T24 and 5637 BC cells. Each experiment was repeated at least three times. Ns, not significant. $^{*}P < 0.05$, $^{**}P < 0.01$, $^{***}P < 0.001$, $^{****}P < 0.0001$.

metastasis in a ceRNA-dependent manner, which is the most important and extensive regulatory mechanism of lncRNAs. Through comprehensive transcriptional analysis using TCGA dataset and our transcriptome dataset, we found that SPRR1B was significantly overexpressed, which was further confirmed in BC tissues and cells. In addition, our study also demonstrated that HAGLROS can positively regulate SPRR1B expression at both transcriptional and protein levels, and aberrantly expressed SPRR1B was related to malignant phenotypes in BC. These results suggest that SPRR1B is a downstream target protein of HAGLROS. To our knowledge, the present study is the first to initially explore the correlation between SPRR1B and bladder tumour. SPRR1B is a member of the SPRR family. Related studies have revealed that the SPRR1B is closely associated with the tumorigenesis and progression of carcinoma by regulating the epithelial-mesenchymal transition (EMT) and participating in the Ras/MEKK1/MKK1 and MAPK signalling pathways (29–33). These above research indicate the direction for further study of the mechanism of SPRR1B in BC.

To explore the regulatory mechanism of HAGLROS on SPRR1B, we used public databases to predict the potential miRNAs that shared putative binding sites with HAGLROS and SPRR1B cluster. We found that miR-330-5p shared putative binding sites with HAGLROS and SPRR1B cluster, which was confirmed through further experiments. Furthermore, our study revealed that miR-330-5p was decreased and could negatively regulate SPRR1B expression in BC. More importantly, we found that HAGLROS can negatively modulate the expression of miR-330-5p in BC. Rescue assays showed that decreased miR-330-5p reversed the inhibitory effects on cellular phenotypes induced by silencing HAGLROS in BC. Remarkably, silencing SPRR1B inhibited the regulatory functions of miR-330-5p knockdown on malignant phenotype in BC cells, thereby inhibiting the tumour-promoting effect of HAGLROS. These results provide strong evidence that HAGLROS can promote the malignant progression of BC by regulating the miR-330-5p/SPRR1B axis. Of note, numerous studies have shown that upregulated miR-330-5p can inhibit

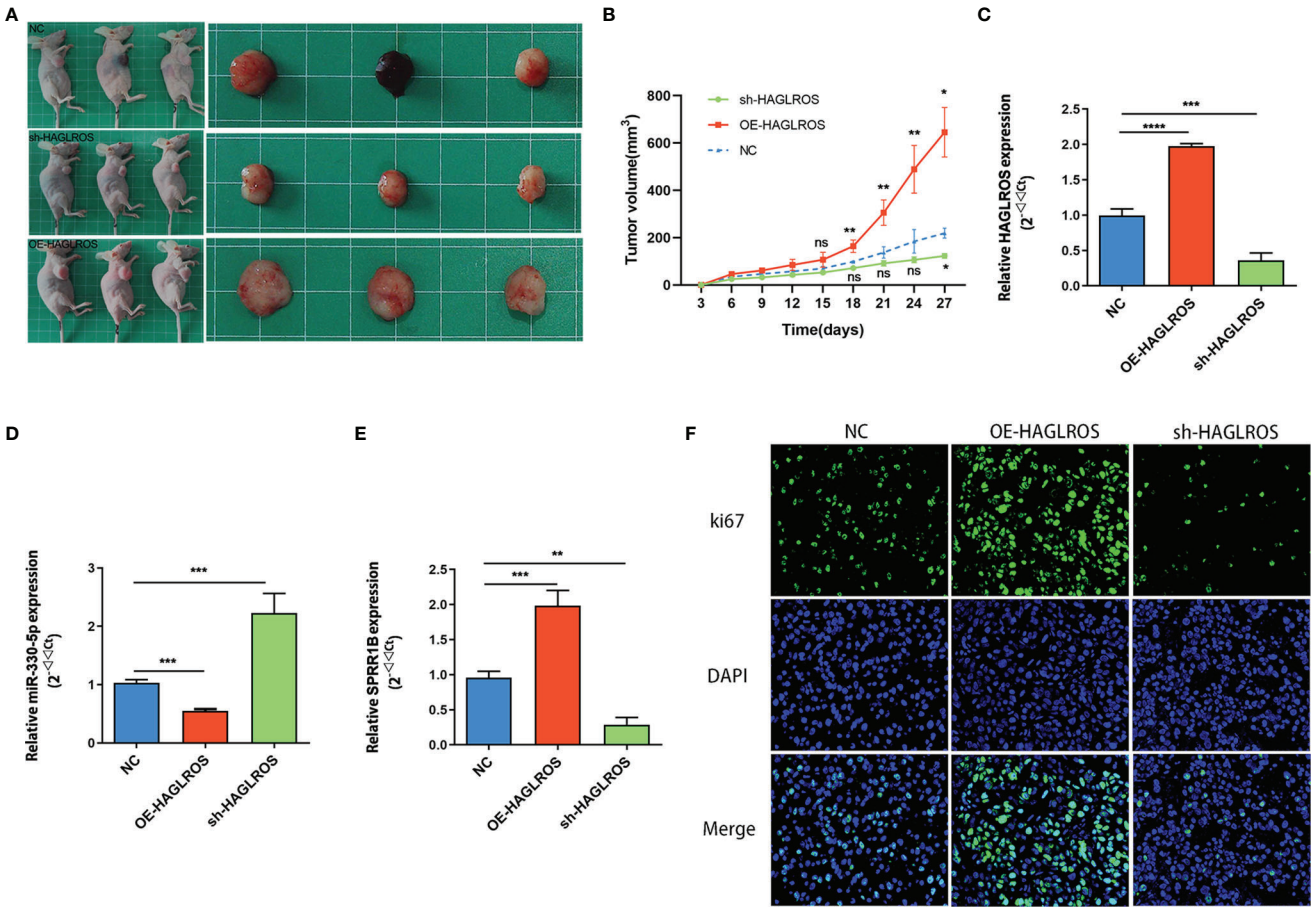

FIGURE 6 | HAGLROS promotes the growth of BC *in vivo*. **(A)** T24 cells stably transfected with normal control, OE-HAGLROS and sh-HAGLROS vectors were used to establish subcutaneous xenograft mice model and the tumours collected from mouse were exhibited. **(B)** Tumour volumes were calculated every 3 days after injection. **(C–E)** The expression levels of HAGLROS, miR-330-5p and SPRR1B were measured by qRT-PCR assays. **(F)** The ki67 expression levels of the paraffin-embedded tumour tissues from nude mice were determined through immunofluorescence assay. Each experiment was repeated at least three times. Ns, not significant, $^{*}P < 0.05$, $^{**}P < 0.01$, $^{***}P < 0.001$, $^{****}P < 0.0001$.

progression by interacting with proteins in a variety of tumours (34–37). For instance, Chen et al. found that miR-330-5p can suppress the progression of BC by inhibiting MTGR1 expression and the activity of the downstream Notch signalling pathway in BC (38). It is consistent with the results of our research. Our study also showed that miR-330-5p was significantly decreased in BC and could inhibit the proliferation, migration and invasion of BC cells by negatively regulating the expression of SPRR1B.

In summary, our study demonstrates that HAGLROS is significantly more highly expressed and plays an oncogenic role in BC. Mechanistically, we found that HAGLROS functions as a microRNA sponge to positively regulate SPRR1B expression by sponging miR-330-5p. Our findings help to elucidate the mechanism of the incidence and development of BC, and future studies will provide a powerful diagnostic and therapeutic target for BC. However, some limitations exist in the current research. For instance, we did not study the correlation between HAGLROS expression levels and BC patient prognosis due to the lack of sufficient quantities of long-term follow-up data. The regulatory mechanism of SPRR1B in BC should be investigated in further research.

DATA AVAILABILITY STATEMENT

The datasets presented in this article are not readily available because of relevant guidelines restrictions. Requests to access the datasets should be directed to the corresponding author/s.

ETHICS STATEMENT

The studies involving human participants were reviewed and approved by the Medical Ethics Committee of the Second Affiliated Hospital of Kunming Medical University. The patients/participants provided their written informed consent to participate in this study.

AUTHOR CONTRIBUTIONS

Conceptualization ideas: JW, SX, and HW. Formal analysis: SX, SF, and DY. Investigation: SX, YL, and XQ. Methodology: SX, YZ, and YH. Project administration: JW and HW. Resources: JW and HW. Supervision: JW and HW. Verification: SX and HW. Writing - original draft: SX. Writing - review and editing: SX, JW, and HW. All authors contributed to the article and approved the submitted version.

FUNDING

This work was supported by the National Natural Science Foundation of China (No. 82060464).

SUPPLEMENTARY MATERIAL

The Supplementary Material for this article can be found online at: https://www.frontiersin.org/articles/10.3389/fonc.2022.876090/full#supplementary-material

Supplementary Figure 1 | Prediction of target mRNAs of HAGLROS. **(A)** The Venn diagram of upregulated DE-mRNAs in TCGA dataset and our RNA-sequencing dataset. **(B)** The top 10 upregulated DE-mRNAs in TCGA dataset and our RNA sequencing were intersected.

Supplementary Figure 2 | Decreased SPRR1B inhibits HAGLROS expression in BC cells. **(A)** The expression levels of HAGLROS in T24 cells were measured by qRT-PCR assays. **(B)** The expression levels of HAGLROS in 5637 cells were detected through qRT-PCR assays. Ns, not significant, ****P<0.0001.

Supplementary Figure 3 | Knockdown of SPRR1B reverses the malignant phenotypes of BC cells promoted by decreasing miR-330-5p. **(A, B)** Cell proliferation was determined by CCK-8 assay in T24 and 5637 BC cells. **(C–E)** Cell migration was evaluated through wound healing assay in T24 and 5637 BC cells (magnification, x40). **(F–H)** Cell invasion was observed by transwell assays in T24 and 5637 BC cells (magnification, x100). Ns, not significant, *P<0.05, **P<0.01, ***P<0.001, ****P<0.0001.

Supplementary Table 1 | The sequence of lncRNA/mRNA primers.

Supplementary Table 2 | Upregulated DE-lncRNAs in both TCGA dataset and RNA sequencing dataset.

Supplementary Table 3 | Upregulated DE-mRNAs in both TCGA dataset and RNA sequencing dataset.

REFERENCES

1. Sung H, Ferlay J, Siegel RL, Laversanne M, Soerjomataram I, Jemal A, et al. Global Cancer Statistics 2020: GLOBOCAN Estimates of Incidence and Mortality Worldwide for 36 Cancers in 185 Countries. *CA Cancer J Clin* (2021) 71(3):209–49. doi: 10.3322/caac.21660
2. Hu X, Xiang L, He D, Zhu R, Fang J, Wang Z, et al. The Long Noncoding RNA KTN1-AS1 Promotes Bladder Cancer Tumorigenesis *via* KTN1 Cis-Activation and the Consequent Initiation of Rho GTPase-Mediated Signaling. *Clin Sci* (2021) 135(3):555–74. doi: 10.1042/CS20200908
3. Geiss R, Sebaste L, Valter R, Poisson J, Mebarki S, Conti C, et al. Complications and Discharge After Radical Cystectomy for Older Patients With Muscle-Invasive Bladder Cancer: The ELCAPA-27 Cohort Study. *Cancers* (2021) 13(23):6010. doi: 10.3390/cancers13236010
4. Reesink DJ, Gerritsen SL, Kelder H, van Melick HHE, Stijns PEF. Evaluation of Ureteroenteric Anastomotic Strictures After the Introduction of Robot-Assisted Radical Cystectomy With Intracorporeal Urinary Diversion: Results From a Large Tertiary Referral Center. *J Urol* (2021) 205(4):1119–25. doi: 10.1097/JU.0000000000001518
5. Li Y, Li G, Guo X, Yao H, Wang G, Li C. Non-Coding RNA in Bladder Cancer. *Cancer Lett* (2020) 485:38–44. doi: 10.1016/j.canlet.2020.04.023
6. Statello L, Guo CJ, Chen LL, Huarte M. Gene Regulation by Long Non-Coding RNAs and its Biological Functions. *Nat Rev Mol Cell Biol* (2021) 22 (2):96–118. doi: 10.1038/s41580-020-00315-9
7. Goodall GJ, Wickramasinghe VO. RNA in Cancer. *Nat Rev Cancer* (2021) 21 (1):22–36. doi: 10.1038/s41568-020-00306-0
8. Zhao H, Wu W, Li X, Chen W. Long Noncoding RNA UCA1 Promotes Glutamine-Driven Anaplerosis of Bladder Cancer by Interacting With hnRNP I/L to Upregulate GPT2 Expression. *Transl Oncol* (2022) 17:101340. doi: 10.1016/j.tranon.2022.101340
9. Cao Y, Tian T, Li W, Xu H, Zhan C, Wu X, et al. Long Non-Coding RNA in Bladder Cancer. *Clin Chim Acta* (2020) 503:113–21. doi: 10.1016/j.cca.2020.01.008
10. Liu Z, Xie D, Zhang H. Long Noncoding RNA Neuroblastoma-Associated Transcript 1 Gene Inhibits Malignant Cellular Phenotypes of Bladder Cancer Through miR-21/SOCS6 Axis. *Cell Death Dis* (2018) 9(10):1042. doi: 10.1038/s41419-018-1090-z
11. Xu J, Yang R, Hua X, Huang M, Tian Z, Li J. LncRNA SNHG1 Promotes Basal Bladder Cancer Invasion *via* Interaction With PP2A Catalytic Subunit and Induction of Autophagy. *Mol Ther-Nucl Acids* (2020) 21:354–66. doi: 10.1016/j.omtn.2020.06.010
12. Logotheti S, Marquardt S, Gupta S, Richter C, Edelhäuser B, Engelmann D, et al. LncRNA-SLC16A1-AS1 Induces Metabolic Reprogramming During Bladder Cancer Progression as Target and Co-Activator of E2F1. *Theranostics* (2020) 10(21):9620–43. doi: 10.7150/thno.44176
13. Chen JF, Wu P, Xia R, Yang J, Huo XY, Gu DY, et al. STAT3-Induced lncRNA HAGLROS Overexpression Contributes to the Malignant Progression of Gastric Cancer Cells *via* mTOR Signal-Mediated Inhibition of Autophagy. *Mol Cancer* (2018) 17(1):6. doi: 10.1186/s12943-017-0756-y
14. Ma Y, Zhang H, Li X, Liu Y. HAGLROS Promotes Cell Proliferation and Angiogenesis and Inhibits Apoptosis by Activating Multiple Signaling Pathways in LSCC Cells. *J Oral Pathol Med* (2021) 11. doi: 10.1111/jop.13249
15. Zhou K, Xu J, Yin X, Xia J, Huang T. Long Noncoding RNA HAGLROS Promotes Cell Invasion and Metastasis by Sponging miR-152 and Upregulating ROCK1 Expression in Osteosarcoma. *Comput Math Methods M* (2020) 2020(24):7236245. doi: 10.1155/2020/7236245
16. Siegel RL, Miller KD, Jemal A. Cancer Statistics, 2019. *CA Cancer J Clin* (2019) 69(1):7–34. doi: 10.1016/j.bj.2020.12.008
17. Liu K, Gao L, Ma X, Huang JJ, Chen J, Zeng L, et al. Long Non-Coding RNAs Regulate Drug Resistance in Cancer. *Mol Cancer* (2020) 19(1):54. doi: 10.1186/s12943-020-01162-0
18. Chen S, Shen X. Long Noncoding RNAs: Functions and Mechanisms in Colon Cancer. *Mol Cancer* (2020) 19(1):167. doi: 10.1186/s12943-020-01287-2
19. Dasgupta PA-O, Kulkarni P, Majid S, Hashimoto Y, Shiina M, Shahryari V, et al. LncRNA CDKN2B-AS1/miR-141/Cyclin D Network Regulates Tumor Progression and Metastasis of Renal Cell Carcinoma. *Cell Death Dis* (2020) 11 (8):660. doi: 10.1038/s41419-020-02877-0
20. Qin Y, Hou Y, Liu S, Zhu P, Wan X, Zhao M, et al. A Novel Long Non-Coding RNA Lnc030 Maintains Breast Cancer Stem Cell Stemness by Stabilizing SQLE mRNA and Increasing Cholesterol Synthesis. *Adv Sci* (2020) 8 (2):2002232. doi: 10.1002/advs.202002232
21. Xue M, Chen W, Xiang A, Wang R, Chen H, Pan J, et al. Hypoxic Exosomes Facilitate Bladder Tumor Growth and Development Through Transferring Long Non-Coding RNA-UCA1. *Mol Cancer* (2017) 16(1):143. doi: 10.1186/s12943-017-0714-8
22. Verhaegh G, Verkleij L, Vermeulen S, den Heijer M, Witjes J, Kiemeney L. Polymorphisms in the H19 Gene and the Risk of Bladder Cancer. *Eur Urol* (2008) 54(5):1118–26. doi: 10.1016/j.eururo.2008.01.060
23. Wei H, Hu J, Pu J, Tang Q, Li W, Ma R, et al. Long Noncoding RNA HAGLROS Promotes Cell Proliferation, Inhibits Apoptosis and Enhances Autophagy *via* Regulating miR-5095/ATG12 Axis in Hepatocellular

Carcinoma Cells. *Int Immunopharmacol* (2019) 73:72–80. doi: 10.1016/j.intimp.2019.04.049
24. Zhu L, Mei M. Interference of Long Non-Coding RNA HAGLROS Inhibits the Proliferation and Promotes the Apoptosis of Ovarian Cancer Cells by Targeting miR-26b-5p. *Exp Ther Med* (2021) 22(2):879. doi: 10.3892/etm.2021.10311
25. Jun M, Jinfeng F, Xiang Z. Long Non-Coding RNA HAGLROS Regulates Lipid Metabolism Reprogramming in Intrahepatic Cholangiocarcinoma *via* the mTOR Signaling Pathway. *Exp Mol Patho* (2020) 115:104466. doi: 10.1016/j.yexmp.2020.104466
26. Chen Y, Shen T, Ding X, Cheng L, Sheng L, Du X. HAGLROS is Overexpressed and Promotes Non-Small Cell Lung Cancer Migration and Invasion. *Jpn J Clin Oncol* (2020) 50(9):1058–67. doi: 10.1093/jjco/hyaa075
27. Li L, Hongyan Z, Xiangyang L, Yaoqi K, Shuai Y, Qingping C. Long Non-Coding RNA HAGLROS Facilitates the Malignant Phenotypes of NSCLC Cells *via* Repressing miR-100 and Up-Regulating SMARCA5. *Biomed J* (2020) S2319–4170(20):30236–5 doi: 10.1016/j.bj.2020.12.008
28. Morlando M, Ballarino M, Fatica A. Long Non-Coding RNAs: New Players in Hematopoiesis and Leukemia. *Front Med* (2015) 2:23. doi: 10.3389/fmed.2015.00023.27
29. Reddy S, Adiseshaiah P, Shapiro P, Vuong H. BMK1 (ERK5) Regulates Squamous Differentiation Marker SPRR1B Transcription in Clara-Like H441 Cells. *Am J Resp Cell Mol* (2002) 27(1):64–70. doi: 10.1165/ajrcmb.27.1.20020003oc
30. Patterson T, Vuong H, Liaw Y, Wu R, Kalvakolanu D, Reddy S. Mechanism of Repression of Squamous Differentiation Marker, SPRR1B, in Malignant Bronchial Epithelial Cells: Role of Critical TRE-Sites and its Transacting Factors. *Oncogene* (2001) 20(5):634–44. doi: 10.1038/sj.onc.1204134
31. Vuong H, Patterson T, Shapiro P, Kalvakolanu D, Wu R, Ma W, et al. Phorbol Ester-Induced Expression of Airway Squamous Cell Differentiation Marker, SPRR1B, is Regulated by Protein Kinase Cdelta /Ras/MEKK1/MKK1-Dependent/AP-1 Signal Transduction Pathway. *J Biol Chem* (2000) 275 (41):32250–9. doi: 10.1074/jbc.M005227200
32. Song Y, Pan H, Yang L, Fan Y, Zhang H, Pan M, et al. DGUOK-AS1 Promotes Cervical Squamous Cell Carcinoma Progression by Suppressing miR-499a-5p That Targets SPRR1B in Vitro. *Biochem Biophys Res Commun* (2021) 585:177–84. doi: 10.1016/j.bbrc.2021.11.003
33. Shi S, Fan Z, Liu Y, Huang C, Zhou J. Integration Analysis of M6a Related Genes in Skin Cutaneous Melanoma and the Biological Function Research of the SPRR1B. *Front Oncol* (2021) 11:729045. doi: 10.3389/fonc.2021.729045
34. Wang Y, Xu R, Zhang D, Lu T, Yu W, Wo Y, et al. Circ-ZKSCAN1 Regulates FAM83A Expression and Inactivates MAPK Signaling by Targeting miR-330-5p to Promote Non-Small Cell Lung Cancer Progression. *Transl Lung Cancer Res* (2019) 8(6):862–75. doi: 10.21037/tlcr.2019.11.04
35. Zhao G, Dai G. Hsa_circRNA_000166 Promotes Cell Proliferation, Migration and Invasion by Regulating miR-330-5p/ELK1 in Colon Cancer. *Onco Targets Ther* (2020) 13:5529–39. doi: 10.2147/OTT.S243795
36. Xu S, Lei S, Liu K, Yi S, Yang Z, Yao H. CircSFMBT1 Promotes Pancreatic Cancer Growth and Metastasis *via* Targeting miR-330-5p/PAK1 Axis. *Cancer Gene Ther* (2021) 28(3):234–49. doi: 10.1038/s41417-020-00215-2
37. Liu D, Song L, Liang Q, Hao L, Zhang Z, Han C. Long Noncoding RNA LEF1-AS1 Silencing Suppresses the Initiation and Development of Prostate Cancer by Acting as a Molecular Sponge of miR-330-5p *via* LEF1 Repression. *J Cell Physiol* (2019) 234(8):12727–44. doi: 10.1002/jcp.27893
38. Chen L, Yang X, Zhao J, Xiong M, Almaraihah R, Chen Z, et al. Circ_0008532 Promotes Bladder Cancer Progression by Regulation of the miR-155-5p/miR-330-5p/MTGR1 Axis. *J Exp Clin Cancer Res* (2020) 39(1):94. doi: 10.1186/s13046-020-01592-0

Conflict of Interest: The authors declare that the research was conducted in the absence of any commercial or financial relationships that could be construed as a potential conflict of interest.

Publisher's Note: All claims expressed in this article are solely those of the authors and do not necessarily represent those of their affiliated organizations, or those of the publisher, the editors and the reviewers. Any product that may be evaluated in this article, or claim that may be made by its manufacturer, is not guaranteed or endorsed by the publisher.

Copyright © 2022 Xiao, Zuo, Li, Huang, Fu, Yuan, Qiao, Wang and Wang. This is an open-access article distributed under the terms of the Creative Commons Attribution License (CC BY). The use, distribution or reproduction in other forums is permitted, provided the original author(s) and the copyright owner(s) are credited and that the original publication in this journal is cited, in accordance with accepted academic practice. No use, distribution or reproduction is permitted which does not comply with these terms.

frontiers | Frontiers in Pharmacology

REVIEW
published: 13 June 2022
doi: 10.3389/fphar.2022.920779

Advances in Research on the Effects and Mechanisms of Chemokines and Their Receptors in Cancer

Jing Xu[1,2†], Jing-quan Li[3†], Qi-lei Chen[4†], Elena A. Shestakova[5], Vsevolod A. Misyurin[5], Vadim S. Pokrovsky[5,6], Elena M. Tchevkina[5], Hu-biao Chen[4], Hang Song[2*] and Jian-ye Zhang[1*]*

[1]Guangzhou Municipal and Guangdong Provincial Key Laboratory of Molecular Target & Clinical Pharmacology, NMPA and State Key Laboratory of Respiratory Disease, School of Pharmaceutical Sciences and the Fifth Affiliated Hospital, Guangzhou Medical University, Guangzhou, China, [2]Department of Biochemistry and Molecular Biology, School of Integrated Chinese and Western Medicine, Anhui University of Chinese Medicine, Hefei, China, [3]The First Affiliated Hospital, Hainan Medical University, Haikou, China, [4]School of Chinese Medicine, Hong Kong Baptist University, Hong Kong, China, [5]N.N. Blokhin National Medical Research Center of Oncology of the Ministry of Health of the Russian Federation, Moscow, Russia, [6]Department of Biochemistry, People's Friendship University, Moscow, Russia

Cancer is a common and intractable disease that seriously affects quality of life of patients and imposes heavy economic burden on families and the entire society. Current medications and intervention strategies for cancer have respective shortcomings. In recent years, it has been increasingly spotlighted that chemokines and their receptors play vital roles in the pathophysiology of cancer. Chemokines are a class of structurally similar short-chain secreted proteins that initiate intracellular signaling pathways through the activation of corresponding G protein-coupled receptors and participate in physiological and pathological processes such as cell migration and proliferation. Studies have shown that chemokines and their receptors have close relationships with cancer epigenetic regulation, growth, progression, invasion, metastasis, and angiogenesis. Chemokines and their receptors may also serve as potential targets for cancer treatment. We herein summarize recent research progresses on anti-tumor effects and mechanisms of chemokines and their receptors, suggesting avenues for future studies. Perspectives for upcoming explorations, such as development of multi-targeted chemokine-based anti-tumor drugs, are also discussed in the present review.

Keywords: chemokine, chemokine receptor, epigenetic regulation, molecular mechanisms, combination medication

OPEN ACCESS

Edited by:
Hongtao Xiao,
University of Electronic Science and Technology of China, China

Reviewed by:
Qian Zhong,
Sun Yat-sen University Cancer Center (SYSUCC), China
Cihui Yan,
Tianjin Medical University Cancer Institute and Hospital, China

***Correspondence:**
Hu-biao Chen
hbchen@hkbu.edu.hk
Hang Song
tosonghang@sina.com
Jian-ye Zhang
jianyez@163.com

†These authors have contributed equally to this work.

Specialty section:
This article was submitted to Pharmacology of Anti-Cancer Drugs, a section of the journal Frontiers in Pharmacology

Received: *15 April 2022*
Accepted: *05 May 2022*
Published: *13 June 2022*

Citation:
Xu J, Li J-q, Chen Q-l, Shestakova EA, Misyurin VA, Pokrovsky VS, Tchevkina EM, Chen H-b, Song H and Zhang J-y (2022) Advances in Research on the Effects and Mechanisms of Chemokines and Their Receptors in Cancer. Front. Pharmacol. 13:920779. doi: 10.3389/fphar.2022.920779

INTRODUCTION

According to the latest statistics from American Cancer Society, the number of cancer cases and deaths remains high throughout the years, and has been even elevated due to delayed diagnosis under the COVID-19 pandemic (Siegel et al., 2022). The whirlwind growth of economy and technology have driven major development of the research on cancer, especially on the pathogenic mechanisms and relevant therapeutic strategies. Among the research topic on cancer, the study of tumor microenvironment stands out due to its close relation to the occurrence, growth, and metastasis of cancer. Tumor microenvironment not only affect the tumor cells themselves, but also the surrounding cells (fibroblasts, immune and inflammatory cells, and glial cells), as well as the interstitial cells, microvasculature, and biomolecules that penetrating into nearby tissues (Hinshaw

and Shevde 2019; Anderson and Simon 2020; DeBerardinis 2020). Recent studies have shown that the chemokine family is considered closely related to tumor microenvironment. Chemokines are a subfamily of small-molecule cytokines secreted by cells and play an essential role in transportation of immune cells and development of lymphoid tissue, with the function of inducing targeted chemotaxis of neighboring responding cells (van der Vorst et al., 2015; Hughes and Nibbs 2018). To date, 48 different chemokines have been reported, and they can be classified into four classes (C, CC, CXC and CX3C) depending on the number and location of their amino-terminal (N-terminal) pre-cysteines. They exert the biological function through selective binding to their receptors, which are G protein-coupled receptors (GPCRs) expressed on various chemotactic immune cells in tissues, organs, and circulatory system (Miller and Mayo 2017). Recent studies have shown that chemokines and their receptors also serve an important purpose in the induction of immune cells against tumors (Chow and Luster 2014; Nagarsheth et al., 2017). Based on this, the present review focuses on the study of the anti-tumor activity and mechanisms of anti-cancer effect of chemokines, with the aim of providing reference for future research.

STRUCTURE AND FUNCTION OF CHEMOKINES

Chemokines can be classified into 4 classes in accordance to the number and location of their N-terminal pre-cysteines, namely class C, CC, CXC and CX3C (Miller and Mayo 2017) (**Figure 1**). Their biological effects are exerted through their specific interactions with chemokine receptors (Baggiolini 2001). Chemokine receptors are a kind of GPCRs that are selectively located in the membranes of target cells. To date, approximately 19 different chemokine receptors have been identified, which are also divided into four families based on the chemokine types they bind: CXCR, which binds to CXC chemokines; CCR, which binds to CC chemokines; CX3CR1, which binds to chemokine CX3CL1; and XCR1, which binds to chemokines XCL1 and XCL2 (Sharma 2010; Singh et al., 2011). Detailed chemical classifications are shown in **Table 1**.

All chemokines are small proteins that are composed of 70–100 amino acids with molecular weights of 8–10 kDa, and have four site-conserved cysteine residues to ensure their tertiary structure (Fernandez and Lolis 2002; Zlotnik and Yoshie 2012). The major function of chemokines is to induce directed migration of target cells, which can be attracted to specific tissues with increased chemokine concentration. In particular, chemokines can mediate leukocyte migration to respective locations during inflammation and homeostasis *in vivo* (Baggiolini 1998; Thelen and Stein 2008; Borroni et al., 2018). In this way, new light has been shed on antitumor therapy. For example, the CC-like chemokine CCL19 expressed in T cells of secondary lymphoid tissues and organs such as spleen and lymph nodes, is chemotactic to naive T cells and mature DC cells. Its specific receptor is CCR7, which is expressed not only on mature DC cells, macrophages and T cells (Förster et al., 2008; Comerford et al., 2013), but also in many tumor cells, such as colorectal (Xu et al., 2018), lung (Zhang et al., 2017), breast (Müller et al., 2001), and ovarian (Cheng et al., 2014). It has been shown that the interplay between the chemokine and its receptor could inhibit tumor proliferation, migration and invasion (Peng et al., 2015a; Xu et al., 2017; Zhou et al., 2020).

ANTI-TUMOR EFFECT OF CHEMOKINES

Involvement in Epigenetic Regulation

Epigenetics refers to heritable changes in the function of genes without alterations in their DNA sequences, ultimately leading to

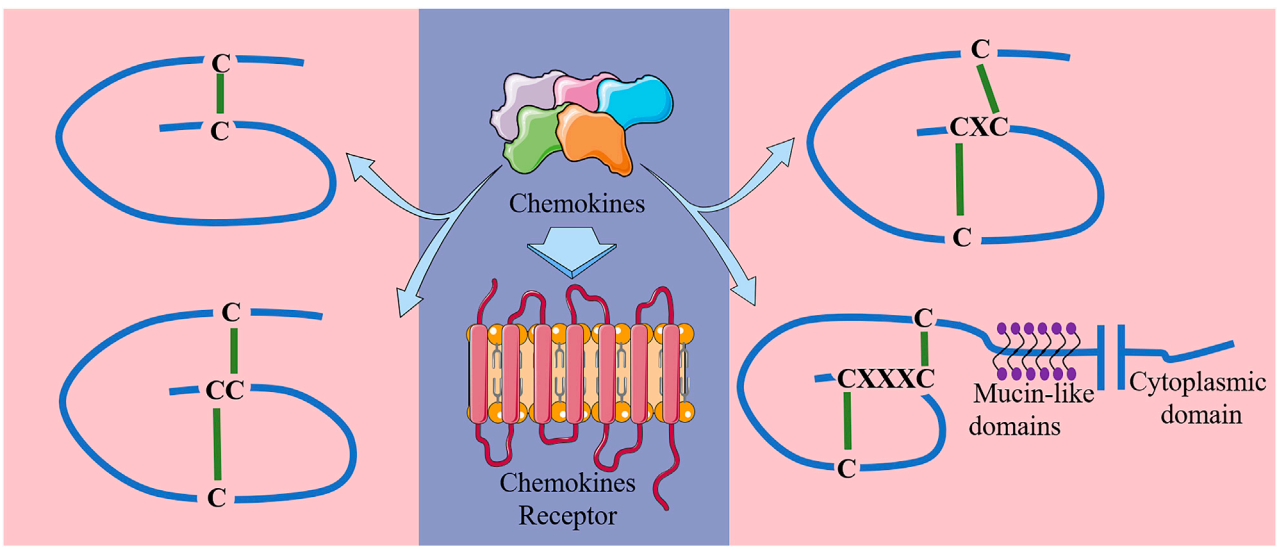

FIGURE 1 | Main structures of the four classes of chemokines.

TABLE 1 | Classification of chemokines.

Classification	Chemokines	Chemokine Receptors	Reference
CC Chemokines	CCL1~ CCL28	CCR	Singh et al. (2011)
CXC Chemokines	CXCL1~ CXCL17	CXCR	Singh et al. (2011)
XC Chemokines	XCL1、XCL2	XCR1	Singh et al. (2011)
CX3C Chemokines	CX3CL1	CX3CR1	Sharma (2010), Singh et al. (2011)

variation in the phenotype (Sapienza and Issa 2016). It is generally recognized that cancer epigenetics include modification of DNA and histones, regulation of non-coding RNA, chromatin remodeling, and nucleosome positioning (Dawson and Kouzarides 2012; Toh et al., 2017). Among the above-mentioned forms, methylation of DNA is the most well-studied epigenetic modification (Skvortsova et al., 2019). DNA methylation is a key epigenetic mechanism controlling gene expression, and in general, it inhibits gene transcription by shifting chromatin from a loose state, permissive for the active transcription, to a condensed state that prohibits the transcription (Moore et al., 2013; Zhang et al., 2014). The methylation pattern of DNA in the genome is catalyzed by DNA methyltransferases, which mainly involve DNMT1, DNMT3a, and DNMT3b. Among them, DNMT1 is the methyltransferase that plays a maintenance role, while DNMT3a and DNMT3b are mainly responsible for *de novo* methylation but also play a role in maintaining methylation (Bestor and Verdine 1994; Tajima et al., 2016).

It was shown that DNMT1-mediated DNA methylation and EZH2-mediated H3K27me3, in the enhancer region, suppressed CCL2 expression in SCLC cells, thereby enhancing tumor progression (Zheng et al., 2021). In addition, CXCL12 was down-regulated in gastric cancer tissues, accompanied by hypermethylation, and the reduced CXCL12 expression was closely associated with lymph node metastasis and histological grading, presumably playing a possible part in gastric cancer cell metastasis (Zhi et al., 2012). Similarly, upregulation of CXCR4 and downregulation of CXCL12 were observed in primary breast cancers. The hypermethylation in the CXCL12 promoter region in more than 50% of breast tumors was detected by methylation-specific PCR, and the expressions of DNMT1 and DNMT3b were distinctly higher in CXCL12-methylated breast cancers than in CXCL12-unmethylated breast cancers (Zhou et al., 2009). Additionally, studies by Ramos et al. and Dayer et al. corroborated the proposed perspective that the DNA methylation status of CXCR4 and CXCL12 genes could be used as biomarkers for breast cancer prognosis (Ramos et al., 2011; Dayer et al., 2018). The experiments of Peng et al. shown that EZH2-mediated H3K27me3 and DNMT1-mediated DNA methylation suppressed tumors and produced T helper 1 (TH1)-type chemokines CXCL9 and CXCL10, which could partially alter the T-cell landscape in cancer and may improve the clinical efficacy of cancer therapy (Peng et al., 2015b). In exploring the regulation of prostate cancer progression by hypermethylated in cancer 1 (HIC1) through epigenetic modifications, Zheng et al. were surprised to find that substantial methylation occurred within the HIC1 promoter and directly targeted the chemokine receptor CXCR7. Moreover, the CXCR7 promoter was negatively regulated by HIC1 (Zheng et al., 2013). In addition to CXCR7 studies, CXCL14 has also been well studied. Cao et al. reported that CXCL14 was frequently methylated in colorectal cancer, leading to downregulation of CXCL14 expression, and reversal of its expression inhibited the proliferation of colorectal cancer. Further experiments showed that CXCL14 inhibited the migration, infiltration and epithelial-to-mesenchymal transition (EMT) of colorectal cancer through suppressing the NF-κB signaling pathway (Cao et al., 2013). Furthermore, Tessema et al. identified that CXCL14 could be used as a typical target for epigenetic silencing in the development of lung cancer (Tessema et al., 2010). In addition, experiments of Song et al., using 5-aza-2-deoxycytidine as the demethylating agent to restore CXCL14 mRNA and protein expression, provided direct evidence for epigenetic regulation of chemokine expressions in tumor cells (Song et al., 2010).

Involvement in Tumor Growth and Progression

Numerous experimental studies have established that chemokine signaling systems are involved in tumor growth and development via different mechanisms. For instance, interactions of chemokines with their receptors can directly activate signaling pathways, such as JAK/STAT and PI3K/AKT pathways, leading to cancer progression. More involved chemokines and their receptors acting on cancer are listed in **Table 2**.

The JAK/STAT pathway is the main signal transduction mechanism of various cytokines and growth factors, and has an important role in the regulation of biological processes such as cell growth, differentiation, proliferation, migration, and apoptosis. Studies have shown that multiple chemokines exert biological effects through JAK/STAT signaling pathway. It was found that CXCL1 was a direct target of miR-302e on cell proliferation, migration, invasion, and apoptosis in colorectal cancer, and the mechanism was correlated with CXCL1 expression regulated by miR-302e and the inactivation of the JAK-STAT signaling pathway (Chen et al., 2020). CXCR1, a receptor for CXCL1, is thought to be significantly related to poor prognosis in patients with NSCLC, and its high expression is mainly involved in signaling pathways such as JAK/STAT. Yang et al. used qRT-PCR and western blot experiments to show that overexpression of CXCR1 enhanced STAT5A expression, while knockdown of CXCR1 inhibited STAT5A expression (Yang et al., 2021). In addition, the combination of FKN and CX3CR1 could also activate the JAK/STAT signaling pathway and promote pancreatic cancer cell proliferation and migration (Huang et al., 2017). Meanwhile, chemokines can

TABLE 2 | Effects on chemokines and their receptors in cancer.

Chemokine	Receptors	Tumor	Mechanism	Reference
CXCL12	CXCR4	Primary breast cancer	CXCR4 ↑, CXCL12 ↓ and the CXCL12 promoter region was hypermethylated	Zhou et al. (2009)
CXCL12	CXCR4	Breast cancer	DNA methylation	Ramos et al. (2011), Dayer et al. (2018)
CXCL13	CXCR5	Colorectal cancer	Activated a CXCL13/CXCR5/NFκB/p65/miR-934 positive feedback loop	Zhao et al. (2020)
CXCL13	CXCR5	Osteosarcoma	Regulated the phospholipase C beta, protein kinase C α, c-Src, and nuclear factor-κB signaling pathways	Liu et al. (2020)
CXCL11	CXCR3	Head and neck squamous cell carcinomas	Mediates tumor lymphatic cross-talk and inflammation-induced tumor	Kumaravel et al. (2020)
CXCL11	CXCR3	Liver tumor	Activated ERK1/2 through an autocrine signaling pathway	Zhang et al. (2019)
CXCL9	CXCR3	Tumor	Reinvigoration of CD8 T cell responses in response to PD-1 blocking tumor	Humblin and Kamphorst, (2019)
CCL2	CCR2	Hepatocellular carcinoma	Inhibits the recruitment of inflammatory monocytes, infiltration, and M2-polarisation of tumor-associated macrophages	Li et al. (2017)
CXCL1/8	CXCR2	Colorectal cancer	Recruited neutrophils to colorectal cancer tumor	Ogawa et al. (2019)
CXCL12	CXCR4	Epithelial ovarian cancer	Promote the proliferation, migration and invasion	Guo et al. (2013)
CXCL12	CXCR4	Gastrointestinal malignancies	Activation of G protein signaling kinases such as P13K/mTOR and MEK/ERK	Daniel et al. (2020)
CXCL12	CXCR7	Gastrointestinal malignancies	Activation of β-arrestin mediated signaling	Daniel et al. (2020)

cause an imbalance between pro- and anti-apoptotic proteins in tumor cells. For example, chemokines down-regulated the expression of Bcl-2 and inhibited the activation of caspase-3 and caspase-9, thereby maintaining cancer cell survival and suppressing tumor cell apoptosis (Pang et al., 2015).

The PI3K/AKT pathway is an intracellular signaling pathway that responds to various extracellular signals and regulates a series of cellular function involved in metabolism, proliferation, cell survival, growth, angiogenesis, transcription, and protein synthesis. The above process is mediated through serine or threonine phosphorylation of a series of downstream substrates, and the key genes involved are PI3K and AKT (Jafari et al., 2019; Yang et al., 2019). Some chemokines binding to their receptors can activate the PI3K/AKT pathway, which in turn promotes a variety of biological functions and plays a critical part in many cancers. In melanoma and colorectal cancer, abnormally high CXCL5 expression activates PI3K/AKT signaling pathway and promotes PD-L1 expression, thereby creating an immunosuppressive microenvironment (Li et al., 2019). In addition, CXCL12 can regulate the expression of PTEN and affect colon cancer cell proliferation and invasion through PI3K/AKT signaling pathway (Ma et al., 2019). Interaction of CXCL13 with CXCR5 could also promote the growth and metastasis of colon cancer cells via PI3K/AKT pathway (Zhu et al., 2015). Furthermore, Chen et al. revealed that the expression of CCL26 in pancreatic cancer-associated fibroblasts was obviously increased by treating pancreatic adenocarcinoma with nab-paclitaxel. They further suggested that CCL26 enhanced the invasive ability of pancreatic adenocarcinoma cells through activation of PI3K/AKT/mTOR axis (Chen et al., 2021). Shen et al. found that CXCL8 induced the process of EMT through PI3K/AKT/NF-κB signaling pathway in colon cancer cells (Shen et al., 2017). Studies of Li et al. indicated that CCL25/CCR9 inhibited the apoptosis of NSCLS cell. The mechanism involved the activation of PI3K/AKT and the downstream upregulation of the anti-apoptotic proteins Bcl-2 and Bcl-xl and downregulation of the pro-apoptotic protein Bax (Li et al., 2015). Also, Ma et al. found that CXCL12 derived from fibroblasts significantly enhanced the secretion of CXCL6, and the synergistic effect of both chemokines could regulate colon cancer metastasis via PI3K/AKT/mTOR signaling pathway (Ma et al., 2017).

Involvement in Tumor Invasion and Metastasis

A number of studies have confirmed the critical function of the chemokine axis in tumor metastasis. It has been reported that the expression of chemokine receptors on cancer cells can determine their sites of metastasis. These metastatic sites produce specific chemokines that advance the migration of moving cancer cells to "pre-metastatic ecological sites", which provides favorable circumstances for the growth of metastatic cells (Murphy 2001; Adekoya and Richardson 2020). A variety of chemokines and chemokine receptors are correlated with cancer cell metastasis, and CXCL12/CXCR4 axis is a key representative system, which participates in the metastasis of various tumor cells (Teicher and Fricker 2010; Daniel et al., 2020). Besides, increased expression of CCR7 was remarkably associated with disease stage, grade, lymph node metastasis and neurovascular infiltration in breast cancer. Therefore, Vahedi et al. suggested that this biomarker could be used as a predictor of tumor metastasis and survival in patients (Vahedi et al., 2018). Acharyya et al. concluded that chemoresistance and metastasis are inextricably linked in cancer. CXCR2 blockers can break the CXCL1/2-S100A8/9 amplification circuit that causes chemoresistance, thus enhancing the chemotherapy effect in breast neoplasms, especially in metastasis (Acharyya et al., 2012). In addition, Cheng et al. devoted a large section to detail the role of chemokines and their receptors in the advancement and metastasis of lung cancer (Cheng et al., 2016). CCL18/PITPNM3 was proved to be associated with the

migration, invasion and EMT processes in hepatocellular carcinoma by mediating the NF-κB signaling pathway (Lin et al., 2016). CCL28, a ligand for CCR3/CCR10, was also related to breast cancer growth and metastatic spread (Yang et al., 2017).

Involvement in Angiogenesis

Chemokines and their respective receptors are considered to be key regulators of the tumor vascular system with a dual role in tumor angiogenesis. CXC chemokines are divided into two categories in accordance to the presence of ELR (Glu-Leu-Arg) motifs at the N-terminal end: ELR + chemokines and ELR–chemokines. ELR + CXC chemokines, such as CXCL1, CXCL2, CXCL3, CXCL5, CXCL6, CXCL7, and CXCL8, exert angiogenic effects by activating CXCR1 and CXCR2. In contrast, ELR–CXC chemokines, such as CXCL4, CXCL9, CXCL10, CXCL11, and CXCL14, are considered as angiogenesis inhibitors (Bosisio et al., 2014).

Tumor angiogenesis plays a prominent role in the process of tumor advancement. Chemokines can interact directly with specific chemokine receptors on vascular endothelial cells and act as regulators of tumor angiogenesis through endothelial cell signaling pathways, ultimately promoting migration and proliferation as well as endothelial cell survival (Keeley et al., 2011). The *in vivo* and *in vitro* experiments of Chen et al. showed that CXCL5 enhanced the angiogenic ability of colorectal cancer tumors in a CXCR2-dependent manner by a specific mechanism of activating the AKT/NF-κB/FOXD1/VEGF-A pathway. In addition, they found that CXCL5 also increased microvessel density in a subcutaneous xenograft tumor model in nude mice by overexpression treatment of CXCL5 (Chen et al., 2019). CCR6 has also been implicated in CCR6-mediated angiogenesis in colorectal cancer. Zhu et al. proposed that CCR6 promoted the secretion of vascular endothelial growth factor A (VEGF-A) through activation of the AKT/NF-κB pathway (Zhu et al., 2018). In studies of tumor angiogenesis in colorectal cancer, CXCL11 and CXCL12 have been shown to have a reciprocal regulatory role (Rupertus et al., 2014). In addition to acting directly on vascular endothelial cells, chemokines can also induce the proliferation of vascular endothelial cells through interacting with VEGF, which in turn promotes angiogenesis (Grunewald et al., 2006). Ping et al. found that CXCL12 could promote upregulation of VEGF expression through PI3K/AKT pathway in gliomas (Skvortsova et al., 2019). Moreover, their experimental results of using the CXCR4 antagonist AMD3100 or knocking out the CXCR4 gene showed that VEGF expression was reduced and tumorigenesis and angiogenesis was inhibited in a nude mouse lotus tumor model (Ping et al., 2011). In addition, CXCL8 and CXCL12-induced upregulation of VEGF expression resulted in the stimulation of angiogenic chemokine production (Kryczek et al., 2005; Martin et al., 2009).

On the other hand, chemokines also have the function of inhibiting tumor angiogenesis and endothelial cell proliferation. For instances, CCL19 could suppress tumor angiogenesis by promoting miR-206 expression dependently on CCR7, and thereby inhibiting the Met/ERK/Elk-1/HIF-1α/VEGF-A pathway. These results were also confirmed in a mouse angiogenesis model, where enhanced CCL19 expression inhibited angiogenesis in colorectal cancer *in vivo* (Xu et al., 2018). CXCL4L1 is a natural non-allelic variant of CXCL4. Struyf et al. proposed that CXCL4L1 was an effective anti-tumor chemokine, which can prevent the progression and metastasis of various tumors by inhibiting angiogenesis (Struyf et al., 2007). Furthermore, it has been postulated that CXCL4L1 exhibited vasopressor and chemotactic activity mediated by CXCR3 (Struyf et al., 2011). The CXCL12/CXCR4 biological axis is also closely related to tumor angiogenesis, and blocking this axis can inhibit tumor angiogenesis either by inhibiting VEGF or directly. Therefore, small molecule antagonists of CXCR4, such as ALX40-4C, AMD3100, and BKT140, have been used in tumor-related treatments (Sun et al., 2013). CXCL9, CXCL10, and CXCL11/CXCR3 are anti-tumor angiogenic factors, and the inhibition of tumor angiogenesis can be achieved via upregulating the expression of CXCL9, CXCL10, and CXCL11 (Billottet et al., 2013). In a retrospective analysis of 294 NSCLC patients taking Anlotinib, Lu et al. found a downregulation of serum CCL2 levels in patients. The results suggested that changes in serum CCL2 levels could be used as a marker to monitor clinical outcomes of patients with refractory advanced NSCLC (Lu et al., 2019). Other tumor angiogenesis-related chemokines and their receptors, such as CCL21/CCR7 and CXCL4, can be used as targets for anti-tumor angiogenesis therapy (Strieter et al., 1995; Somovilla-Crespo et al., 2013). Interestingly, the CC chemokines not only inhibit pathological angiogenesis but also maintain physiological angiogenesis (Ridiandries et al., 2017).

Involvement in Tumor Microenvironment

Tumor microenvironment refers to not only the structure, function, and metabolism of tumor tissues, but also the internal environment of tumor cells themselves (Hinshaw and Shevde 2019; Vitale et al., 2019). The internal and external environment in which the tumor cells are located has a significant impact on the occurrence, growth, and metastasis of the tumor. Tumor microenvironment contains a diversity of cells and components, including lymphocytes, tumor-associated macrophages, cancer-associated fibroblasts, growth factors, cytokines, chemokines (Emon et al., 2018), which are of vital clinical significance for tumor prevention and treatment. Among them, chemokines and their receptors have attracted the attention of many researchers.

The interactions of chemokines and chemokine receptors can recruit immune cell subsets into the tumor microenvironment, and these interactions can regulate tumor progression and metastasis (Lee and Cho 2020). Marjorie et al. concluded that plasma CCL4 was positively correlated with inflammatory mediators and was associated with poor patient prognosis. They further suggested that high expression of CCL4 in colon cancer induces infiltration of tumor-associated macrophages (De la Fuente López et al., 2018). Zhang et al. observed that an increase in CCL3/6/8 led to the recruitment of myeloid cells, which restored immunosuppressive and pro-cancer effects. Further studies showed that depletion of regulatory T cells in pancreatic cancer led to differentiation of inflammatory fibroblast subpopulations, which in turn drove infiltration of bone marrow cells via CCR1, thus revealing a potential new therapeutic approach to alleviate immunosuppression in pancreatic cancer

TABLE 3 | Clinical trials involving chemokine therapy for cancer.

Molecule	Cancer	Status	Identifier	Reference
CCL2/Carlumab/CNTO 888	Ovarian and prostate cancer	Phase I	NCT00537368	Sandhu et al. (2013)
CCL2/Carlumab/CNTO 888	Metastatic prostate cancer	Phase II	NCT00992186	Pienta et al. (2013)
CCL2/Carlumab + docetaxel/gemcitabine/paclitaxel/carboplatin	Solid tumors	Phase Ib	NCT01204996	Brana et al. (2015)
CCL19 + chimeric antigen receptor (CAR)-engineered T cells + IL-7	Hepatocellular carcinoma	Phase I	NCT03198546	Pang et al. (2021)
CCR2 + FOLFIRINOX	Advanced pancreatic ductal adenocarcinoma	Phase II	NCT01413022	Nywening et al. (2016)
CCR2 + Abraxane + Gemcitabine	Metastatic pancreatic ductal adenocarcinoma	Phase Ib/II	NCT02732938	Noel et al. (2020)
CCR4/Mogamulizumab + nivolumab	Advanced/Metastatic solid tumors	Phase I	NCT02476123	Doi et al. (2019)
CCR4/Mogamulizumab	Peripheral T-cell lymphomas	phase II	NCT01192984	Ogura et al. (2014)
CCR4/Mogamulizumab + Durvalumab/Tremelimumab	Advanced solid tumors	Phase I	NCT02301130	Zamarin et al. (2020)
CCR5/Maraviroc	Refractory colorectal cancer	Phase I	NCT01736813	Halama et al. (2016)
CXCR4/Plerixafor	Refractory acute myeloid leukemia	Phase I/II	NCT00512252	Uy et al. (2012)
CXCR4/BL-8040 + Pembrolizumab	Pancreatic ductal adenocarcinoma	Phase IIa	NCT02826486	Bockorny et al. (2020)
CXCR4/Motixafortide + Pembrolizumab	Metastatic pancreatic cancer	phase II	NCT02826486	Bockorny et al. (2021)
CXCR4/Balixafortide + Eribulin	Metastatic breast cancer	Phase I	NCT01837095	Pernas et al. (2018)

(Zhang et al., 2020). In addition, CCL2 plays a role in the recruitment of tumor-associated macrophages, which promote tumor phenotype generation as well as tumor cell invasion and angiogenesis (O'Connor and Heikenwalder 2021). The same is true for CCL24/27 (Lim 2021; Martínez-Rodríguez and Monteagudo 2021). CXCL13 and the receptor CXCR5 represent an emerging example of a chemokine signaling axis that demonstrates the ability to regulate tumor growth and progression. In addition, the CXCL13-CXCR5 axis may also indirectly regulate tumor growth by modulating non-cancerous cells in the tumor microenvironment, particularly immune cells (Hussain et al., 2021). The same applies to describe the critical role of the CXCL12-CXCR4 axis and the CCL2-CCR2 axis in the tumor microenvironment (Meng et al., 2018; Kadomoto et al., 2021). Han et al. proposed that blocking the CXCL8-CXCR1/2 axis alone or in combination with other immunotherapies would be a novel immunotherapeutic strategy (Han et al., 2021).

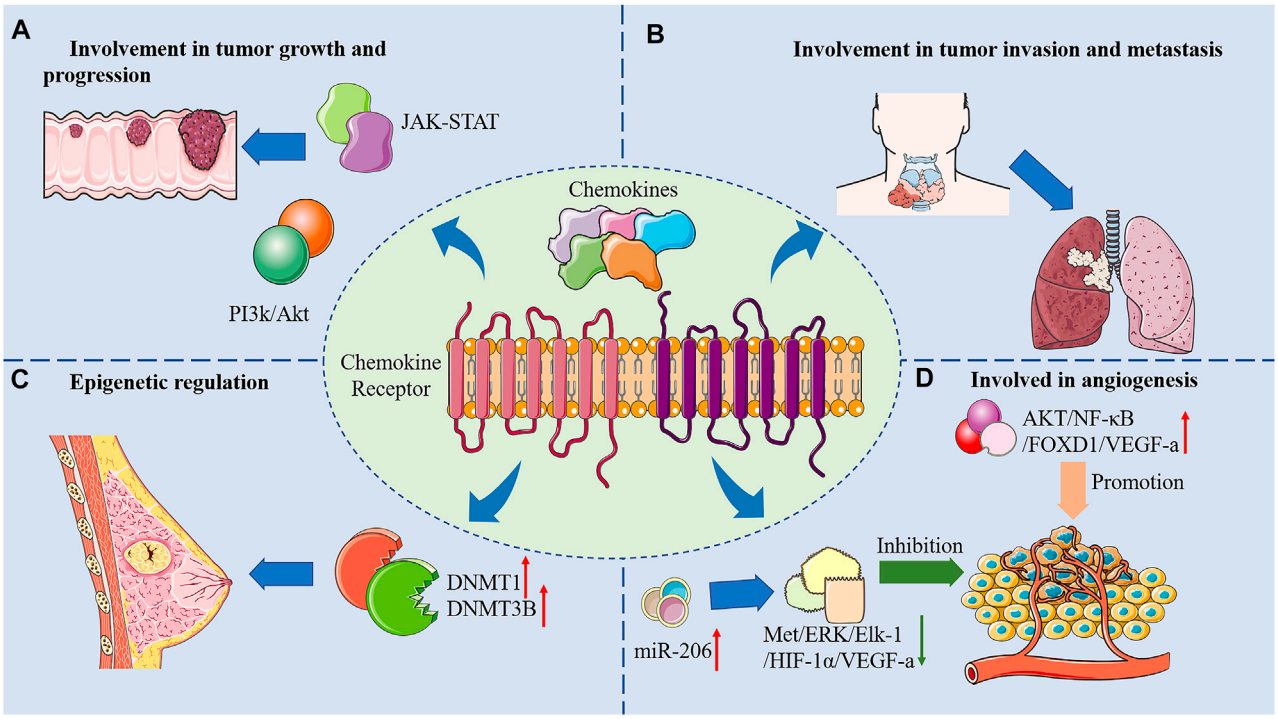

FIGURE 2 | Mechanisms of anti-tumor effects of chemokines and its receptors.

CHEMOKINES IN CLINICAL RESEARCH AND APPLICATIONS

To date, the main means of treatment for tumors are still surgical treatment, radiation therapy, chemotherapy, and targeted therapy. Surgical treatment is mainly used for diagnosis and radical treatment, which can effectively relieve symptoms and improve survival. In recent years, with the improvement of radiotherapy equipment and the development of computer science, radiotherapy has been more and more widely used in clinical practice and has become an important means of treatment for comprehensive tumors. In addition, with the occurrence of new chemotherapeutic drugs, chemotherapy has acquired therapeutic importance. Although chemotherapy has greatly improved the survival rate of patients with advanced malignancies, it still needs to be combined with other treatments to improve the efficacy. Meanwhile, targeted therapy has gradually become vital for tumor treatment due to the development of genetic testing technology and small molecule targeted drugs. Targeted therapy enables selective, targeted, patient-friendly, and safer treatment to control tumor, thereby reducing the damage to normal tissues around the tumor. Therefore, it becomes more and more prominent in tumor treatment by virtue of its specificity and less toxicity.

Currently, chemokines and their receptors exhibit positive impacts in cancer biology, such as involvement in angiogenesis, metastasis, proliferation and invasion of cancer cells. Chemokines are also considered to be key influencers on disease progression and have a great effect on patients' treatment and prognosis. In recent years, chemokines have been used as important therapeutic targets for cancer. Mogamulizumab (an anti-CCR4 antibody) and Plerixafor/AMD3100 (a CXCR4 antagonist) have been approved for the treatment of hematologic malignancies and being in clinical trials (Bule et al., 2021). In addition, Wsetermann et al. used CCL19-conjugated DNA vaccine for tumor control and showed that the combination of the two significantly inhibited tumor growth and prolonged the antitumor effect of the vaccine (Westermann et al., 2007). Subsequent studies have also confirmed that CCL19 can be used as an adjuvant for immunization with intradermal gene guns in a Her2/neu mouse tumor model, with enhanced vaccine efficacy (Nguyen-Hoai et al., 2012). Not coincidentally, the combination of CCL19/21 with CCL4 can also be used as an adjuvant for DNA vaccination in Her2/neu mouse tumor models (Nguyen-Hoai et al., 2016). In a recent clinical trial, Peng et al. found that the incorporation of CCL19 into chimeric antigen receptor (CAR)-engineered T cells dramatically improved the antitumor activity against human solid tumors, which has been in phase I clinical trial (NCT03198546) (Pang et al., 2021). CCR2 in combination with FOLFIRINOX for advanced pancreatic ductal adenocarcinoma is in clinical phase II (NCT01413022) (Nywening et al., 2016). Additionally, CCR2 combined with Abraxane and Gemcitabine for metastatic pancreatic ductal adenocarcinoma is in phase Ib/II (NCT02732938) clinical trial (Noel et al., 2020). Other chemokines and receptors, such as CCL2 (Sandhu et al., 2013), CCR5 (Doi et al., 2019), and CXCR4 (Ghobrial et al., 2020), have also been used in combination with other drugs in a variety of cancers. More clinical trials involving chemokine therapy is listed in **Table 3**.

CONCLUSION AND PROSPECT

Cancer is a life-threatening disease that imposes an economic burden on society. Due to its complexity and treatment resistance, diagnosing and curing cancer is a huge challenge. Despite recent advances in therapeutic strategies such as immunotherapy and targeted therapy, survival rates of cancer patients have not been reduced evidently. Chemokines are a large class of cytokines that coordinate the tropism of immune cell transport. They also participate in numerous cancer processes and serve as a critical part in the migration patterns of immune cells into tumors. The mechanisms of anti-tumor effects of chemokines and its receptors were briefly summarized in **Figure 2**.

The relationship between chemokines and/or chemokine receptors and tumors is complex and multifaceted, and has become a hot and difficult area in current tumor biology research. With the development of molecular biology, molecular immunology and related technologies, the role of chemokines/chemokine receptors system in tumor development and the related mechanisms have been gradually discovered. As a result, targeting these molecules may provide new strategies and means to targeted therapy of tumor. Through more in-depth research on tumor pathogenesis, more effective indicators for early diagnosis and determination of recurrence can be found, which will effectively reduce the morbidity and recurrence rate of cancer patients. A number of studies have suggested that chemokines can be involved in tumor development through a network of a variety of mechanisms. Also, chemokines are expected to become important indicators for tumor screening, diagnosis and monitoring in the future, because of the advantages of easy detection, low cost, and no surgery-related risks. Study of tumor-related chemokines has gradually turned into a research hotspot, although the specific biological properties and mechanism of action are still not fully elucidated. At present, some chemokines have been used as tumor diagnostic markers in clinical practice, and some chemokine-targeting drugs have entered various phases of clinical trial. Unfortunately, single-targeted chemokine therapeutic drugs have mostly ended up in failure. The new pathway of multicomplexer-based therapies will better help researchers discover new drugs with high effectiveness without negative impacts.

In summary, chemokines and their receptors are expected to become targets for new anti-tumor drugs and may provide a new approach to cancer therapy. As the mechanisms of interaction between chemokines and/or their receptors and cancer continue to be studied, chemokines and their receptors may also become predictors of cancer, which may then provide new strategies for targeted therapy and prevention of cancer.

AUTHOR CONTRIBUTIONS

Conceptualization HC, HS and JZ; writing—original draft preparation, JX, JL and QC; writing—review and editing, ES,

VM, VP and ET; funding acquisition, HC, HS and JZ. All authors have read and agreed to the published version of the manuscript.

FUNDING

This work is supported by National Key R&D Project of China (2021YFE0202000), Fund of Guangdong Education Department (2021ZDZX2006), the Health and Medical Research Fund in Hong Kong (16170251), the Innovation and Technology Fund in Hong Kong (PRP/036/20FX; MHP/023/20).

ACKNOWLEDGMENTS

We thank all the participants for their help.

REFERENCES

Acharyya, S., Oskarsson, T., Vanharanta, S., Malladi, S., Kim, J., Morris, P. G., et al. (2012). A CXCL1 Paracrine Network Links Cancer Chemoresistance and Metastasis. *Cell* 150 (1), 165–178. doi:10.1016/j.cell.2012.04.042

Adekoya, T. O., and Richardson, R. M. (2020). Cytokines and Chemokines as Mediators of Prostate Cancer Metastasis. *Int. J. Mol. Sci.* 21 (12). doi:10.3390/ijms21124449

Anderson, N. M., and Simon, M. C. (2020). The Tumor Microenvironment. *Curr. Biol.* 30 (16), R921–r925. doi:10.1016/j.cub.2020.06.081

Baggiolini, M. (1998). Chemokines and Leukocyte Traffic. *Nature* 392 (6676), 565–568. doi:10.1038/33340

Baggiolini, M. (2001). Chemokines in Pathology and Medicine. *J. Intern Med.* 250 (2), 91–104. doi:10.1046/j.1365-2796.2001.00867.x

Bestor, T. H., and Verdine, G. L. (1994). DNA Methyltransferases. *Curr. Opin. Cell Biol.* 6 (3), 380–389. doi:10.1016/0955-0674(94)90030-2

Billottet, C., Quemener, C., and Bikfalvi, A. (2013). CXCR3, a Double-Edged Sword in Tumor Progression and Angiogenesis. *Biochim. Biophys. Acta* 1836 (2), 287–295. doi:10.1016/j.bbcan.2013.08.002

Bockorny, B., Semenisty, V., Macarulla, T., Borazanci, E., Wolpin, B. M., Stemmer, S. M., et al. (2020). BL-8040, a CXCR4 Antagonist, in Combination with Pembrolizumab and Chemotherapy for Pancreatic Cancer: the COMBAT Trial. *Nat. Med.* 26 (6), 878–885. doi:10.1038/s41591-020-0880-x

Bockorny, B., Macarulla, T., Semenisty, V., Borazanci, E., Feliu, J., Ponz-Sarvise, M., et al. (2021). Motixafortide and Pembrolizumab Combined to Nanoliposomal Irinotecan, Fluorouracil, and Folinic Acid in Metastatic Pancreatic Cancer: The COMBAT/KEYNOTE-202 Trial. *Clin. cancer Res. official J. Am. Assoc. Cancer Res.* 27 (18), 5020–5027. doi:10.1158/1078-0432.ccr-21-0929

Borroni, E. M., Savino, B., Bonecchi, R., and Locati, M. (2018). Chemokines Sound the Alarmin: The Role of Atypical Chemokine in Inflammation and Cancer. *Seminars Immunol.* 38, 63–71. doi:10.1016/j.smim.2018.10.005

Bosisio, D., Salvi, V., Gagliostro, V., and Sozzani, S. (2014). Angiogenic and Antiangiogenic Chemokines. *Chem. Immunol. Allergy* 99, 89–104. doi:10.1159/000353317

Brana, I., Calles, A., LoRusso, P. M., Yee, L. K., Puchalski, T. A., Seetharam, S., et al. (2015). Carlumab, an Anti-C-C Chemokine Ligand 2 Monoclonal Antibody, in Combination with Four Chemotherapy Regimens for the Treatment of Patients with Solid Tumors: an Open-Label, Multicenter Phase 1b Study. *Target Oncol.* 10 (1), 111–123. doi:10.1007/s11523-014-0320-2

Bule, P., Aguiar, S. I., Aires-Da-Silva, F., and Dias, J. N. R. (2021). Chemokine-Directed Tumor Microenvironment Modulation in Cancer Immunotherapy. *Int. J. Mol. Sci.* 22 (18). doi:10.3390/ijms22189804

Cao, B., Yang, Y., Pan, Y., Jia, Y., Brock, M. V., Herman, J. G., et al. (2013). Epigenetic Silencing of CXCL14 Induced Colorectal Cancer Migration and Invasion. *Discov. Med.* 16 (88), 137–147.

Chen, C., Xu, Z. Q., Zong, Y. P., Ou, B. C., Shen, X. H., Feng, H., et al. (2019). CXCL5 Induces Tumor Angiogenesis via Enhancing the Expression of FOXD1 Mediated by the AKT/NF-κB Pathway in Colorectal Cancer. *Cell Death Dis.* 10 (3), 178. doi:10.1038/s41419-019-1431-6

Chen, B., Song, L., Nie, X., Lin, F., Yu, Z., Kong, W., et al. (2020). CXCL1 Regulated by miR-302e Is Involved in Cell Viability and Motility of Colorectal Cancer via Inhibiting JAK-STAT Signaling Pathway. *Front. Oncol.* 10, 577229. doi:10.3389/fonc.2020.577229

Chen, X., An, Y., Zhang, Y., Xu, D., Chen, T., Yang, Y., et al. (2021). CCL26 Is Upregulated by Nab-Paclitaxel in Pancreatic Cancer-Associated Fibroblasts and Promotes PDAC Invasiveness through Activation of the PI3K/AKT/mTOR Pathway. *Acta Biochim. Biophys. Sin. (Shanghai)* 53 (5), 612–619. doi:10.1093/abbs/gmab032

Cheng, S., Han, L., Guo, J., Yang, Q., Zhou, J., and Yang, X. (2014). The Essential Roles of CCR7 in Epithelial-To-Mesenchymal Transition Induced by Hypoxia in Epithelial Ovarian Carcinomas. *Tumour Biol.* 35 (12), 12293–12298. doi:10.1007/s13277-014-2540-6

Cheng, Z. H., Shi, Y. X., Yuan, M., Xiong, D., Zheng, J. H., and Zhang, Z. Y. (2016). Chemokines and Their Receptors in Lung Cancer Progression and Metastasis. *J. Zhejiang Univ. Sci. B* 17 (5), 342–351. doi:10.1631/jzus.B1500258

Chow, M. T., and Luster, A. D. (2014). Chemokines in Cancer. *Cancer Immunol. Res.* 2 (12), 1125–1131. doi:10.1158/2326-6066.CIR-14-0160

Comerford, I., Harata-Lee, Y., Bunting, M. D., Gregor, C., Kara, E. E., and McColl, S. R. (2013). A Myriad of Functions and Complex Regulation of the CCR7/CCL19/CCL21 Chemokine axis in the Adaptive Immune System. *Cytokine Growth Factor Rev.* 24 (3), 269–283. doi:10.1016/j.cytogfr.2013.03.001

Daniel, S. K., Seo, Y. D., and Pillarisetty, V. G. (2020). The CXCL12-Cxcr4/cxcr7 axis as a Mechanism of Immune Resistance in Gastrointestinal Malignancies. *Semin. Cancer Biol.* 65, 176–188. doi:10.1016/j.semcancer.2019.12.007

Dawson, M. A., and Kouzarides, T. (2012). Cancer Epigenetics: from Mechanism to Therapy. *Cell* 150 (1), 12–27. doi:10.1016/j.cell.2012.06.013

Dayer, R., Babashah, S., Jamshidi, S., and Sadeghizadeh, M. (2018). Upregulation of CXC Chemokine Receptor 4-CXC Chemokine Ligand 12 axis Ininvasive Breast Carcinoma: A Potent Biomarker Predicting Lymph Node Metastasis. *J. Cancer Res. Ther.* 14 (2), 345–350. doi:10.4103/0973-1482.177221

De la Fuente López, M., Landskron, G., Parada, D., Dubois-Camacho, K., Simian, D., Martinez, M., et al. (2018). The Relationship between Chemokines CCL2, CCL3, and CCL4 with the Tumor Microenvironment and Tumor-Associated Macrophage Markers in Colorectal Cancer. *Tumour Biol.* 40 (11), 1010428318810059. doi:10.1177/1010428318810059

DeBerardinis, R. J. (2020). Tumor Microenvironment, Metabolism, and Immunotherapy. *N. Engl. J. Med.* 382 (9), 869–871. doi:10.1056/NEJMcibr1914890

Doi, T., Muro, K., Ishii, H., Kato, T., Tsushima, T., Takenoyama, M., et al. (2019). A Phase I Study of the Anti-CC Chemokine Receptor 4 Antibody, Mogamulizumab, in Combination with Nivolumab in Patients with Advanced or Metastatic Solid Tumors. *Clin. Cancer Res.* 25 (22), 6614–6622. doi:10.1158/1078-0432.CCR-19-1090

Emon, B., Bauer, J., Jain, Y., Jung, B., and Saif, T. (2018). Biophysics of Tumor Microenvironment and Cancer Metastasis - A Mini Review. *Comput. Struct. Biotechnol. J.* 16, 279–287. doi:10.1016/j.csbj.2018.07.003

Fernandez, E. J., and Lolis, E. (2002). Structure, Function, and Inhibition of Chemokines. *Annu. Rev. Pharmacol. Toxicol.* 42, 469–499. doi:10.1146/annurev.pharmtox.42.091901.115838

Förster, R., Davalos-Misslitz, A. C., and Rot, A. (2008). CCR7 and its Ligands: Balancing Immunity and Tolerance. *Nat. Rev. Immunol.* 8 (5), 362–371. doi:10.1038/nri2297

Ghobrial, I. M., Liu, C. J., Redd, R. A., Perez, R. P., Baz, R., Zavidij, O., et al. (2020). A Phase Ib/II Trial of the First-In-Class Anti-CXCR4 Antibody Ulocuplumab in Combination with Lenalidomide or Bortezomib Plus Dexamethasone in Relapsed Multiple Myeloma. *Clin. Cancer Res.* 26 (2), 344–353. doi:10.1158/1078-0432.CCR-19-0647

Grunewald, M., Avraham, I., Dor, Y., Bachar-Lustig, E., Itin, A., Jung, S., et al. (2006). VEGF-induced Adult Neovascularization: Recruitment, Retention, and Role of Accessory Cells. *Cell* 124 (1), 175–189. doi:10.1016/j.cell.2005.10.036

Guo, Q., Wu, X. H., Lü, Y. P., Yang, B., Xu, F., and Zhang, S. J. (2013). Relationship between Chemokine axis CXCL12-CXCR4 and Epithelial Ovarian Cancer. *Zhonghua yi xue za zhi* 93 (21), 1677–1680.

Halama, N., Zoernig, I., Berthel, A., Kahlert, C., Klupp, F., Suarez-Carmona, M., et al. (2016). Tumoral Immune Cell Exploitation in Colorectal Cancer Metastases Can Be Targeted Effectively by Anti-CCR5 Therapy in Cancer Patients. *Cancer Cell* 29 (4), 587–601. doi:10.1016/j.ccell.2016.03.005

Han, Z. J., Li, Y. B., Yang, L. X., Cheng, H. J., Liu, X., and Chen, H. (2021). Roles of the CXCL8-Cxcr1/2 Axis in the Tumor Microenvironment and Immunotherapy. *Mol. (Basel, Switz.* 27 (1). doi:10.3390/molecules27010137

Hinshaw, D. C., and Shevde, L. A. (2019). The Tumor Microenvironment Innately Modulates Cancer Progression. *Cancer Res.* 79 (18), 4557–4566. doi:10.1158/0008-5472.CAN-18-3962

Huang, L., Ma, B., Ma, J., and Wang, F. (2017). Fractalkine/CX3CR1 axis Modulated the Development of Pancreatic Ductal Adenocarcinoma via JAK/STAT Signaling Pathway. *Biochem. Biophys. Res. Commun.* 493 (4), 1510–1517. doi:10.1016/j.bbrc.2017.10.006

Hughes, C. E., and Nibbs, R. J. B. (2018). A Guide to Chemokines and Their Receptors. *FEBS J.* 285 (16), 2944–2971. doi:10.1111/febs.14466

Humblin, E., and Kamphorst, A. O. (2019). CXCR3-CXCL9: It's All in the Tumor. *Immunity* 50 (6), 1347–1349. doi:10.1016/j.immuni.2019.05.013

Hussain, M., Liu, J., Wang, G. Z., and Zhou, G. B. (2021). CXCL13 Signaling in the Tumor Microenvironment. *Adv. Exp. Med. Biol.* 1302, 71–90. doi:10.1007/978-3-030-62658-7_6

Jafari, M., Ghadami, E., Dadkhah, T., and Akhavan-Niaki, H. (2019). PI3k/AKT Signaling Pathway: Erythropoiesis and beyond. *J. Cell Physiol.* 234 (3), 2373–2385. doi:10.1002/jcp.27262

Kadomoto, S., Izumi, K., and Mizokami, A. (2021). Roles of CCL2-CCR2 Axis in the Tumor Microenvironment. *Int. J. Mol. Sci.* 22 (16). doi:10.3390/ijms22168530

Keeley, E. C., Mehrad, B., and Strieter, R. M. (2011). Chemokines as Mediators of Tumor Angiogenesis and Neovascularization. *Exp. Cell Res.* 317 (5), 685–690. doi:10.1016/j.yexcr.2010.10.020

Kryczek, I., Lange, A., Mottram, P., Alvarez, X., Cheng, P., Hogan, M., et al. (2005). CXCL12 and Vascular Endothelial Growth Factor Synergistically Induce Neoangiogenesis in Human Ovarian Cancers. *Cancer Res.* 65 (2), 465–472.

Kumaravel, S., Singh, S., Roy, S., Venkatasamy, L., White, T. K., Sinha, S., et al. (2020). CXCL11-CXCR3 Axis Mediates Tumor Lymphatic Cross Talk and Inflammation-Induced Tumor, Promoting Pathways in Head and Neck Cancers. *Am. J. Pathol.* 190 (4), 900–915. doi:10.1016/j.ajpath.2019.12.004

Lee, Y. S., and Cho, Y. B. (2020). CCL7 Signaling in the Tumor Microenvironment. *Adv. Exp. Med. Biol.* 1231, 33–43. doi:10.1007/978-3-030-36667-4_4

Li, B., Wang, Z., Zhong, Y., Lan, J., Li, X., and Lin, H. (2015). CCR9-CCL25 Interaction Suppresses Apoptosis of Lung Cancer Cells by Activating the PI3K/Akt Pathway. *Med. Oncol.* 32 (3), 66. doi:10.1007/s12032-015-0531-0

Li, X., Yao, W., Yuan, Y., Chen, P., Li, B., Li, J., et al. (2017). Targeting of Tumour-Infiltrating Macrophages via CCL2/CCR2 Signalling as a Therapeutic Strategy against Hepatocellular Carcinoma. *Gut* 66 (1), 157–167. doi:10.1136/gutjnl-2015-310514

Li, Z., Zhou, J., Zhang, J., Li, S., Wang, H., and Du, J. (2019). Cancer-associated Fibroblasts Promote PD-L1 Expression in Mice Cancer Cells via Secreting CXCL5. *Int. J. Cancer* 145 (7), 1946–1957. doi:10.1002/ijc.32278

Lim, S. J. (2021). CCL24 Signaling in the Tumor Microenvironment. *Adv. Exp. Med. Biol.* 1302, 91–98. doi:10.1007/978-3-030-62658-7_7

Lin, Z., Li, W., Zhang, H., Wu, W., Peng, Y., Zeng, Y., et al. (2016). CCL18/PITPNM3 Enhances Migration, Invasion, and EMT through the NF-Kb Signaling Pathway in Hepatocellular Carcinoma. *Tumour Biol.* 37 (3), 3461–3468. doi:10.1007/s13277-015-4172-x

Liu, J. F., Lee, C. W., Lin, C. Y., Chao, C. C., Chang, T. M., Han, C. K., et al. (2020). CXCL13/CXCR5 Interaction Facilitates VCAM-1-dependent Migration in Human Osteosarcoma. *Int. J. Mol. Sci.* 21 (17). doi:10.3390/ijms21176095

Lu, J., Zhong, H., Chu, T., Zhang, X., Li, R., Sun, J., et al. (2019). Role of Anlotinib-Induced CCL2 Decrease in Anti-angiogenesis and Response Prediction for Nonsmall Cell Lung Cancer Therapy. *Eur. Respir. J.* 53 (3). doi:10.1183/13993003.01562-2018

Ma, J. C., Sun, X. W., Su, H., Chen, Q., Guo, T. K., Li, Y., et al. (2017). Fibroblast-derived CXCL12/SDF-1α Promotes CXCL6 Secretion and Co-operatively Enhances Metastatic Potential through the PI3K/Akt/mTOR Pathway in Colon Cancer. *World J. Gastroenterol.* 23 (28), 5167–5178. doi:10.3748/wjg.v23.i28.5167

Ma, J., Sun, X., Wang, Y., Chen, B., Qian, L., and Wang, Y. (2019). Fibroblast-derived CXCL12 Regulates PTEN Expression and Is Associated with the Proliferation and Invasion of Colon Cancer Cells via PI3k/Akt Signaling. *Cell Commun. Signal* 17 (1), 119. doi:10.1186/s12964-019-0432-5

Martin, D., Galisteo, R., and Gutkind, J. S. (2009). CXCL8/IL8 Stimulates Vascular Endothelial Growth Factor (VEGF) Expression and the Autocrine Activation of VEGFR2 in Endothelial Cells by Activating NFkappaB through the CBM (Carma3/Bcl10/Malt1) Complex. *J. Biol. Chem.* 284 (10), 6038–6042. doi:10.1074/jbc.C800207200

Martínez-Rodríguez, M., and Monteagudo, C. (2021). CCL27 Signaling in the Tumor Microenvironment. *Adv. Exp. Med. Biol.* 1302, 113–132. doi:10.1007/978-3-030-62658-7_9

Meng, W., Xue, S., and Chen, Y. (2018). The Role of CXCL12 in Tumor Microenvironment. *Gene* 641, 105–110. doi:10.1016/j.gene.2017.10.015

Miller, M. C., and Mayo, K. H. (2017). Chemokines from a Structural Perspective. *Int. J. Mol. Sci.* 18 (10). doi:10.3390/ijms18102088

Moore, L. D., Le, T., and Fan, G. (2013). DNA Methylation and its Basic Function. *Neuropsychopharmacology* 38 (1), 23–38. doi:10.1038/npp.2012.112

Müller, A., Homey, B., Soto, H., Ge, N., Catron, D., Buchanan, M. E., et al. (2001). Involvement of Chemokine Receptors in Breast Cancer Metastasis. *Nature* 410 (6824), 50–56. doi:10.1038/35065016

Murphy, P. M. (2001). Chemokines and the Molecular Basis of Cancer Metastasis. *N. Engl. J. Med.* 345 (11), 833–835. doi:10.1056/NEJM200109133451113

Nagarsheth, N., Wicha, M. S., and Zou, W. (2017). Chemokines in the Cancer Microenvironment and Their Relevance in Cancer Immunotherapy. *Nat. Rev. Immunol.* 17 (9), 559–572. doi:10.1038/nri.2017.49

Nguyen-Hoai, T., Hohn, O., Vu, M. D., Baldenhofer, G., Sayed Ahmed, M. S., Dörken, B., et al. (2012). CCL19 as an Adjuvant for Intradermal Gene Gun Immunization in a Her2/neu Mouse Tumor Model: Improved Vaccine Efficacy and a Role for B Cells as APC. *Cancer Gene Ther.* 19 (12), 880–887. doi:10.1038/cgt.2012.78

Nguyen-Hoai, T., Pham-Duc, M., Gries, M., Dörken, B., Pezzutto, A., and Westermann, J. (2016). CCL4 as an Adjuvant for DNA Vaccination in a Her2/neu Mouse Tumor Model. *Cancer Gene Ther.* 23 (6), 162–167. doi:10.1038/cgt.2016.9

Noel, M., O'Reilly, E. M., Wolpin, B. M., Ryan, D. P., Bullock, A. J., Britten, C. D., et al. (2020). Phase 1b Study of a Small Molecule Antagonist of Human Chemokine (C-C Motif) Receptor 2 (PF-04136309) in Combination with Nab-Paclitaxel/gemcitabine in First-Line Treatment of Metastatic Pancreatic Ductal Adenocarcinoma. *Invest. New Drugs* 38 (3), 800–811. doi:10.1007/s10637-019-00830-3

Nywening, T. M., Wang-Gillam, A., Sanford, D. E., Belt, B. A., Panni, R. Z., Cusworth, B. M., et al. (2016). Targeting Tumour-Associated Macrophages with CCR2 Inhibition in Combination with FOLFIRINOX in Patients with Borderline Resectable and Locally Advanced Pancreatic Cancer: a Single-Centre, Open-Label, Dose-Finding, Non-randomised, Phase 1b Trial. *Lancet Oncol.* 17 (5), 651–662. doi:10.1016/S1470-2045(16)00078-4

O'Connor, T., and Heikenwalder, M. (2021). CCL2 in the Tumor Microenvironment. *Adv. Exp. Med. Biol.* 1302, 1–14. doi:10.1007/978-3-030-62658-7_1

Ogawa, R., Yamamoto, T., Hirai, H., Hanada, K., Kiyasu, Y., Nishikawa, G., et al. (2019). Loss of SMAD4 Promotes Colorectal Cancer Progression by Recruiting Tumor-Associated Neutrophils via the CXCL1/8-CXCR2 Axis. *Clin. Cancer Res.* 25 (9), 2887–2899. doi:10.1158/1078-0432.CCR-18-3684

Ogura, M., Ishida, T., Hatake, K., Taniwaki, M., Ando, K., Tobinai, K., et al. (2014). Multicenter Phase II Study of Mogamulizumab (KW-0761), a Defucosylated Anti-cc Chemokine Receptor 4 Antibody, in Patients with Relapsed Peripheral T-Cell Lymphoma and Cutaneous T-Cell Lymphoma. *J. Clin. Oncol.* 32 (11), 1157–1163. doi:10.1200/JCO.2013.52.0924

Pang, X., Li, K., Wei, L., Huang, Y., Su, M., Wang, L., et al. IL-8 Inhibits the Apoptosis of MCF-7 Human Breast Cancer Cells by Up-Regulating Bcl-2 and Down-Regulating Caspase-3 = *Xi Bao Yu Fen Zi Mian Yi Xue Za Zhi*. 2015; 31(3):307–311.

Pang, N., Shi, J., Qin, L., Chen, A., Tang, Y., Yang, H., et al. (2021). IL-7 and CCL19-Secreting CAR-T Cell Therapy for Tumors with Positive Glypican-3 or Mesothelin. *J. Hematol. Oncol.* 14 (1), 118. doi:10.1186/s13045-021-01128-9

Peng, C., Zhou, K., An, S., and Yang, J. (2015). The Effect of CCL19/CCR7 on the Proliferation and Migration of Cell in Prostate Cancer. *Tumour Biol.* 36 (1), 329–335. doi:10.1007/s13277-014-2642-1

Peng, D., Kryczek, I., Nagarsheth, N., Zhao, L., Wei, S., Wang, W., et al. (2015). Epigenetic Silencing of TH1-type Chemokines Shapes Tumour Immunity and Immunotherapy. *Nature* 527 (7577), 249–253. doi:10.1038/nature15520

Pernas, S., Martin, M., Kaufman, P. A., Gil-Martin, M., Gomez Pardo, P., Lopez-Tarruella, S., et al. (2018). Balixafortide Plus Eribulin in HER2-Negative Metastatic Breast Cancer: a Phase 1, Single-Arm, Dose-Escalation Trial. *Lancet Oncol.* 19 (6), 812–824. doi:10.1016/S1470-2045(18)30147-5

Pienta, K. J., Machiels, J. P., Schrijvers, D., Alekseev, B., Shkolnik, M., Crabb, S. J., et al. (2013). Phase 2 Study of Carlumab (CNTO 888), a Human Monoclonal Antibody against CC-Chemokine Ligand 2 (CCL2), in Metastatic Castration-Resistant Prostate Cancer. *Invest. New Drugs* 31 (3), 760–768. doi:10.1007/s10637-012-9869-8

Ping, Y. F., Yao, X. H., Jiang, J. Y., Zhao, L. T., Yu, S. C., Jiang, T., et al. (2011). The Chemokine CXCL12 and its Receptor CXCR4 Promote Glioma Stem Cell-Mediated VEGF Production and Tumour Angiogenesis via PI3K/AKT Signalling. *J. Pathol.* 224 (3), 344–354. doi:10.1002/path.2908

Ramos, E. A., Grochoski, M., Braun-Prado, K., Seniski, G. G., Cavalli, I. J., Ribeiro, E. M., et al. (2011). Epigenetic Changes of CXCR4 and its Ligand CXCL12 as Prognostic Factors for Sporadic Breast Cancer. *PloS one* 6 (12), e29461. doi:10.1371/journal.pone.0029461

Ridiandries, A., Tan, J. T., Ravindran, D., Williams, H., Medbury, H. J., Lindsay, L., et al. (2017). CC-chemokine Class Inhibition Attenuates Pathological Angiogenesis while Preserving Physiological Angiogenesis. *FASEB J.* 31 (3), 1179–1192. doi:10.1096/fj.201600540R

Rupertus, K., Sinistra, J., Scheuer, C., Nickels, R. M., Schilling, M. K., Menger, M. D., et al. (2014). Interaction of the Chemokines I-TAC (CXCL11) and SDF-1 (CXCL12) in the Regulation of Tumor Angiogenesis of Colorectal Cancer. *Clin. Exp. Metastasis* 31 (4), 447–459. doi:10.1007/s10585-014-9639-4

Sandhu, S. K., Papadopoulos, K., Fong, P. C., Patnaik, A., Messiou, C., Olmos, D., et al. (2013). A First-In-Human, First-In-Class, Phase I Study of Carlumab (CNTO 888), a Human Monoclonal Antibody against CC-Chemokine Ligand 2 in Patients with Solid Tumors. *Cancer Chemother. Pharmacol.* 71 (4), 1041–1050. doi:10.1007/s00280-013-2099-8

Sapienza, C., and Issa, J. P. (2016). Diet, Nutrition, and Cancer Epigenetics. *Annu. Rev. Nutr.* 36, 665–681. doi:10.1146/annurev-nutr-121415-112634

Sharma, M. (2010). Chemokines and Their Receptors: Orchestrating a Fine Balance between Health and Disease. *Crit. Rev. Biotechnol.* 30 (1), 1–22. doi:10.1080/07388550903187418

Shen, T., Yang, Z., Cheng, X., Xiao, Y., Yu, K., Cai, X., et al. (2017). CXCL8 Induces Epithelial-Mesenchymal Transition in Colon Cancer Cells via the PI3K/Akt/NF-Kb Signaling Pathway. *Oncol. Rep.* 37 (4), 2095–2100. doi:10.3892/or.2017.5453

Siegel, R. L., Miller, K. D., Jemal, A., and Jemal, A. (2022). Cancer Statistics, 2016. *CA Cancer J. Clin.* 66 (1), 7–30. doi:10.3322/caac.21332

Singh, R., Lillard, J. W., Jr., and Singh, S. (2011). Chemokines: Key Players in Cancer Progression and Metastasis. *Front. Biosci. Sch. Ed.* 3, 1569–1582. doi:10.2741/246

Skvortsova, K., Stirzaker, C., and Taberlay, P. (2019). The DNA Methylation Landscape in Cancer. *Essays Biochem.* 63 (6), 797–811. doi:10.1042/EBC20190037

Somovilla-Crespo, B., Alfonso-Pérez, M., Cuesta-Mateos, C., Carballo-de Dios, C., Beltrán, A. E., Terrón, F., et al. (2013). Anti-CCR7 Therapy Exerts a Potent Anti-tumor Activity in a Xenograft Model of Human Mantle Cell Lymphoma. *J. Hematol. Oncol.* 6, 89. doi:10.1186/1756-8722-6-89

Song, E. Y., Shurin, M. R., Tourkova, I. L., Gutkin, D. W., and Shurin, G. V. (2010). Epigenetic Mechanisms of Promigratory Chemokine CXCL14 Regulation in Human Prostate Cancer Cells. *Cancer Res.* 70 (11), 4394–4401. doi:10.1158/0008-5472.CAN-10-0427

Strieter, R. M., Polverini, P. J., Kunkel, S. L., Arenberg, D. A., Burdick, M. D., Kasper, J., et al. (1995). The Functional Role of the ELR Motif in CXC Chemokine-Mediated Angiogenesis. *J. Biol. Chem.* 270 (45), 27348–27357. doi:10.1074/jbc.270.45.27348

Struyf, S., Burdick, M. D., Peeters, E., Van den Broeck, K., Dillen, C., Proost, P., et al. (2007). Platelet Factor-4 Variant Chemokine CXCL4L1 Inhibits Melanoma and Lung Carcinoma Growth and Metastasis by Preventing Angiogenesis. *Cancer Res.* 67 (12), 5940–5948. doi:10.1158/0008-5472.CAN-06-4682

Struyf, S., Salogni, L., Burdick, M. D., Vandercappellen, J., Gouwy, M., Noppen, S., et al. (2011). Angiostatic and Chemotactic Activities of the CXC Chemokine CXCL4L1 (Platelet Factor-4 Variant) Are Mediated by CXCR3. *Blood* 117 (2), 480–488. doi:10.1182/blood-2009-11-253591

Sun, X., Charbonneau, C., Wei, L., Yang, W., Chen, Q., and Terek, R. M. (2013). CXCR4-targeted Therapy Inhibits VEGF Expression and Chondrosarcoma Angiogenesis and Metastasis. *Mol. Cancer Ther.* 12 (7), 1163–1170. doi:10.1158/1535-7163.MCT-12-1092

Tajima, S., Suetake, I., Takeshita, K., Nakagawa, A., and Kimura, H. (2016). Domain Structure of the Dnmt1, Dnmt3a, and Dnmt3b DNA Methyltransferases. *Adv. Exp. Med. Biol.* 945, 63–86. doi:10.1007/978-3-319-43624-1_4

Teicher, B. A., and Fricker, S. P. (2010). CXCL12 (SDF-1)/CXCR4 Pathway in Cancer. *Clin. Cancer Res.* 16 (11), 2927–2931. doi:10.1158/1078-0432.CCR-09-2329

Tessema, M., Klinge, D. M., Yingling, C. M., Do, K., Van Neste, L., and Belinsky, S. A. (2010). Re-expression of CXCL14, a Common Target for Epigenetic Silencing in Lung Cancer, Induces Tumor Necrosis. *Oncogene* 29 (37), 5159–5170. doi:10.1038/onc.2010.255

Thelen, M., and Stein, J. V. (2008). How Chemokines Invite Leukocytes to Dance. *Nat. Immunol.* 9 (9), 953–959. doi:10.1038/ni.f.207

Toh, T. B., Lim, J. J., and Chow, E. K. (2017). Epigenetics in Cancer Stem Cells. *Mol. Cancer* 16 (1), 29. doi:10.1186/s12943-017-0596-9

Uy, G. L., Rettig, M. P., Motabi, I. H., McFarland, K., Trinkaus, K. M., Hladnik, L. M., et al. (2012). A Phase 1/2 Study of Chemosensitization with the CXCR4 Antagonist Plerixafor in Relapsed or Refractory Acute Myeloid Leukemia. *Blood* 119 (17), 3917–3924. doi:10.1182/blood-2011-10-383406

Vahedi, L., Ghasemi, M., Yazdani, J., Ranjbar, S., Nouri, B., Alizadeh, A., et al. (2018). Investigation of CCR7 Marker Expression Using Immunohistochemical Method and its Association with Clinicopathologic Properties in Patients with Breast Cancer. *Int. J. Hematol. Oncol. Stem Cell Res.* 12 (2), 103–110.

van der Vorst, E. P., Döring, Y., and Weber, C. (2015). *Chemokines. Arteriosclerosis, thrombosis, Vasc. Biol.* 35 (11), e52–56. doi:10.1161/atvbaha.115.306359

Vitale, I., Manic, G., Coussens, L. M., Kroemer, G., and Galluzzi, L. (2019). Macrophages and Metabolism in the Tumor Microenvironment. *Cell Metab.* 30 (1), 36–50. doi:10.1016/j.cmet.2019.06.001

Westermann, J., Nguyen-Hoai, T., Baldenhofer, G., Höpken, U. E., Lipp, M., Dörken, B., et al. (2007). CCL19 (ELC) as an Adjuvant for DNA Vaccination: Induction of a TH1-type T-Cell Response and Enhancement of Antitumor Immunity. *Cancer Gene Ther.* 14 (6), 523–532. doi:10.1038/sj.cgt.7701042

Xu, B., Zhou, M., Qiu, W., Ye, J., and Feng, Q. (2017). CCR7 Mediates Human Breast Cancer Cell Invasion, Migration by Inducing Epithelial-Mesenchymal Transition and Suppressing Apoptosis through AKT Pathway. *Cancer Med.* 6 (5), 1062–1071. doi:10.1002/cam4.1039

Xu, Z., Zhu, C., Chen, C., Zong, Y., Feng, H., Liu, D., et al. (2018). CCL19 Suppresses Angiogenesis through Promoting miR-206 and Inhibiting Met/ERK/Elk-1/HIF-1α/VEGF-A Pathway in Colorectal Cancer. *Cell Death Dis.* 9 (10), 974. doi:10.1038/s41419-018-1010-2

Yang, X. L., Liu, K. Y., Lin, F. J., Shi, H. M., and Ou, Z. L. (2017). CCL28 Promotes Breast Cancer Growth and Metastasis through MAPK-Mediated Cellular Anti-apoptosis and Pro-metastasis. *Oncol. Rep.* 38 (3), 1393–1401. doi:10.3892/or.2017.5798

Yang, Q., Jiang, W., and Hou, P. (2019). Emerging Role of PI3K/AKT in Tumor-Related Epigenetic Regulation. *Semin. Cancer Biol.* 59, 112–124. doi:10.1016/j.semcancer.2019.04.001

Yang, F., Zhang, S., Meng, Q., Zhou, F., Pan, B., Liu, F., et al. (2021). CXCR1 Correlates to Poor Outcomes of EGFR-TKI against Advanced Non-small Cell Lung Cancer by Activating Chemokine and JAK/STAT Pathway. *Pulm. Pharmacol. Ther.* 67, 102001. doi:10.1016/j.pupt.2021.102001

Zamarin, D., Hamid, O., Nayak-Kapoor, A., Sahebjam, S., Sznol, M., Collaku, A., et al. (2020). Mogamulizumab in Combination with Durvalumab or Tremelimumab in Patients with Advanced Solid Tumors: A Phase I Study. *Clin. Cancer Res.* 26 (17), 4531–4541. doi:10.1158/1078-0432.CCR-20-0328

Zhang, X., Fu, R., Yu, J., and Wu, X. (2014). DNA Demethylation: where Genetics Meets Epigenetics. *Curr. Pharm. Des.* 20 (11), 1625–1631. doi:10.2174/13816128113199990546

Zhang, L., Xiao, X., An, H., Wang, J., Ma, Y., and Qian, Y. H. (2017). Inhibition of CCR7 Promotes NF-κb-dependent Apoptosis and Suppresses Epithelial-Mesenchymal Transition in Non-small Cell Lung Cancer. *Oncol. Rep.* 37 (5), 2913–2919. doi:10.3892/or.2017.5524

Zhang, Y., Zhao, W., Li, S., Lv, M., Yang, X., Li, M., et al. (2019). CXCL11 Promotes Self-Renewal and Tumorigenicity of α2δ1+ Liver Tumor-Initiating Cells through CXCR3/ERK1/2 Signaling. *Cancer Lett.* 449, 163–171. doi:10.1016/j.canlet.2019.02.016

Zhang, Y., Lazarus, J., Steele, N. G., Yan, W., Lee, H. J., Nwosu, Z. C., et al. (2020). Regulatory T-Cell Depletion Alters the Tumor Microenvironment and Accelerates Pancreatic Carcinogenesis. *Cancer Discov.* 10 (3), 422–439. doi:10.1158/2159-8290.CD-19-0958

Zhao, S., Mi, Y., Guan, B., Zheng, B., Wei, P., Gu, Y., et al. (2020). Tumor-derived Exosomal miR-934 Induces Macrophage M2 Polarization to Promote Liver Metastasis of Colorectal Cancer. *J. Hematol. Oncol.* 13 (1), 156. doi:10.1186/s13045-020-00991-2

Zheng, J., Wang, J., Sun, X., Hao, M., Ding, T., Xiong, D., et al. (2013). HIC1 Modulates Prostate Cancer Progression by Epigenetic Modification. *Clin. Cancer Res.* 19 (6), 1400–1410. doi:10.1158/1078-0432.CCR-12-2888

Zheng, Y., Wang, Z., Wei, S., Liu, Z., and Chen, G. (2021). Epigenetic Silencing of Chemokine CCL2 Represses Macrophage Infiltration to Potentiate Tumor Development in Small Cell Lung Cancer. *Cancer Lett.* 499, 148–163. doi:10.1016/j.canlet.2020.11.034

Zhi, Y., Chen, J., Zhang, S., Chang, X., Ma, J., and Dai, D. (2012). Down-regulation of CXCL12 by DNA Hypermethylation and its Involvement in Gastric Cancer Metastatic Progression. *Dig. Dis. Sci.* 57 (3), 650–659. doi:10.1007/s10620-011-1922-5

Zhou, W., Jiang, Z., Liu, N., Xu, F., Wen, P., Liu, Y., et al. (2009). Down-regulation of CXCL12 mRNA Expression by Promoter Hypermethylation and its Association with Metastatic Progression in Human Breast Carcinomas. *J. Cancer Res. Clin. Oncol.* 135 (1), 91–102. doi:10.1007/s00432-008-0435-x

Zhou, R., Sun, J., He, C., Huang, C., and Yu, H. (2020). CCL19 Suppresses Gastric Cancer Cell Proliferation, Migration, and Invasion through the CCL19/CCR7/AIM2 Pathway. *Hum. Cell* 33 (4), 1120–1132. doi:10.1007/s13577-020-00375-1

Zhu, Z., Zhang, X., Guo, H., Fu, L., Pan, G., and Sun, Y. (2015). CXCL13-CXCR5 axis Promotes the Growth and Invasion of Colon Cancer Cells via PI3K/AKT Pathway. *Mol. Cell Biochem.* 400 (1-2), 287–295. doi:10.1007/s11010-014-2285-y

Zhu, C. C., Chen, C., Xu, Z. Q., Zhao, J. K., Ou, B. C., Sun, J., et al. (2018). CCR6 Promotes Tumor Angiogenesis via the AKT/NF-κB/VEGF Pathway in Colorectal Cancer. *Biochim. Biophys. Acta Mol. Basis Dis.* 1864 (2), 387–397. doi:10.1016/j.bbadis.2017.10.033

Zlotnik, A., and Yoshie, O. (2012). The Chemokine Superfamily Revisited. *Immunity* 36 (5), 705–716. doi:10.1016/j.immuni.2012.05.008

Conflict of Interest: The authors declare that the research was conducted in the absence of any commercial or financial relationships that could be construed as a potential conflict of interest.

Publisher's Note: All claims expressed in this article are solely those of the authors and do not necessarily represent those of their affiliated organizations, or those of the publisher, the editors and the reviewers. Any product that may be evaluated in this article, or claim that may be made by its manufacturer, is not guaranteed or endorsed by the publisher.

Copyright © 2022 Xu, Li, Chen, Shestakova, Misyurin, Pokrovsky, Tchevkina, Chen, Song and Zhang. This is an open-access article distributed under the terms of the Creative Commons Attribution License (CC BY). The use, distribution or reproduction in other forums is permitted, provided the original author(s) and the copyright owner(s) are credited and that the original publication in this journal is cited, in accordance with accepted academic practice. No use, distribution or reproduction is permitted which does not comply with these terms.

frontiers | Frontiers in Pharmacology

REVIEW
published: 16 June 2022
doi: 10.3389/fphar.2022.918709

Programmed Cell Death Protein 1/Programmed Cell Death Protein Ligand 1 Immunosuppressants in Advanced Non-Small Cell Lung Cancer Research Progress in Treatment

Feng Li[1,2], *Binchi Liao*[3], *Ting Wang*[1], *Tingting Qi*[1] *and Yixin Wang*[1]*

[1]Sichuan Cancer Hospital, Cancer Hospital Affiliate to School of Medicine, University of Electronic Science and Technology of China, Chengdu, China, [2]School of Medicine, University of Electronic Science and Technology of China, Chengdu, China, [3]National Medical Products Administration Institute of Executive Development, Beijing, China

PD-1/PD-L1 play key roles in tumor immune escape and the formation of the tumor microenvironment, and are closely related to the generation and development of tumors. Blocking the PD-1/PD-L1 pathway can reshape the tumor microenvironment or block the formation of the tumor microenvironment and enhance endogenous antitumor immune response. Clinical trials show that the treatment of non-small cell lung cancer (NSCLC) with PD-1/PD-L1 inhibitors has significant advantages. The review briefly describes these basic principles of the PD-1/PD-L1 pathway and action mechanism in the treatment of NSCLC. A summary of global PD-1/PD-L1 clinical trials and five PD-1/PD-L1 inhibitors approved by FDA, EMA and NMPA for advanced NSCLC were analyzed.

Keywords: PD-1/PD-L1 inhibitors, NSCLC, clinical trials, adverse Reactions, immunity therapy

OPEN ACCESS

Edited by:
Liang Ouyang,
Sichuan University, China

Reviewed by:
Chong Li,
Southwest University, China
Guo-Bo Li,
Sichuan University, China

***Correspondence:**
Yixin Wang
122066692@qq.com

Specialty section:
This article was submitted to Pharmacology of Anti-Cancer Drugs, a section of the journal Frontiers in Pharmacology

Received: *12 April 2022*
Accepted: *25 May 2022*
Published: *16 June 2022*

Citation:
Li F, Liao B, Wang T, Qi T and Wang Y (2022) Programmed Cell Death Protein 1/Programmed Cell Death Protein Ligand 1 Immunosuppressants in Advanced Non-Small Cell Lung Cancer Research Progress in Treatment. Front. Pharmacol. 13:918709. doi: 10.3389/fphar.2022.918709

INTRODUCTION

The incidence and death rate of cancer around the world is increasing rapidly, and it has become a major "killer" affecting people's survival and health. According to the statistics of the World Health Organization's International Cancer Research Agency (Global Cancer Observatory, IARC), the number of cancer patients in 2020 will be 19.292789 million, and the death toll was 9,958,133 (IARC Global Cancer Observatory). Lung cancer is one of the most common malignant tumors in the world. Its incidence and mortality are second only to breast cancer. It is estimated that 1,796,144 people died of lung cancer, accounting for 18.0% of the total cancer deaths (Cao and Chen, 2021). It estimates that by 2030, the number of lung cancer patients worldwide may exceed 2.2 million, and 1.1 million patients may death (Arnold et al., 2017). The non-small cell lung cancer (NSCLC) accounts for about 80%–85% of the total number of lung cancers, and most NSCLC patients are already in advanced stage at the time of diagnosis (Rosell and Karachaliou, 2016). Chemotherapy has been the main traditional treatment for advanced NSCLC in the past few decades, but chemotherapy drugs not only attack tumor cells, but also damage healthy cells. Chemotherapy is usually accompanied by a series of serious adverse reactions, such as bone marrow suppression, digestive tract reactions, hair loss, etc. Gene testing is required before using the targeted drugs. The mutation of the target gene directly affects the efficacy of the targeted drug. However, there is currently no effective method to avoid

TABLE 1 | Summary of clinical trials of PD-1/PD-L1 immunosuppressants for NSCLC registered in clinicaltrials.gov.

S/N	Drug	Type	Manufacturer	Antibody Isotype	Global Clinical Trials	Completed	Chinese Clinical Trials	Approved
1	Pembrolizumab	PD-1	MSD	IgG4	103	12	15	US (2017), China (2018)
2	Nivolumab	PD-1	Bristol-Myers Squibb	IgG4	75	13	7	US (2014), China (2018)
3	Atezolizumab	PD-L1	Roche	IgG1	51	9	6	US (2016), China (2019)
4	Durvalumab	PD-L1	AstraZeneca	IgG1	51	2	7	US (2018), China (2019)
5	Sintilimab	PD-1	Innovent Biologics	IgG4	24	0	21	US(Not),China (2020)
7	Camrelizumab	PD-1	Hengrui	IgG4	12	0	8	US(Not), China (Not)
8	Toripalimab	PD-1	Jun Real	IgG4	11	1	11	US (2021), China (2020)
9	Avelumab	PD-L1	Merck/Pfizer	IgG1	10	2	0	US (2017), China (Not)
10	Tislelizumab	PD-1	BeiGene	IgG4	10	0	8	US(Not), China (Not)
11	Cemiplimab	PD-1	Sanofi/Regeneron	IgG4	7	3	2	US (2021), China (2021)
12	Envafolimab	PD-L1	Corning Jerry	IgG1	2	0	2	US(Not), China (2020)
13	Sasanlimab	PD-1	Wuhan Costan	IgG4	2	1	1	US(Not), China (Not)
14	Dostarlimab	PD-1	TESARO/AnaptysBio	IgG4	2	0	0	US (2018), China (Not)
15	Sindelizumab	PD-1	Innovent Biologics/Eli Lilly	IgG4	1	0	1	US(Not), China (2018)

TABLE 2 | FDA/EMA/NMPA-approved NSCLC treatments of PD-1/PD-L1 blocking antibodies.

Generic	Brand	Strength	Approved	Form	Adult Dose and Treatment Endpoints
Atezolizumab	Tecentriq	60 mg/ml	US EU China	soln for IV infusion after dilution	Single agent:840 mg/2weeks、1200 mg/3weeks、1680 mg/4 weeks; In combination with platinum-based chemotherapy: 1200 mg/3 weeks; after4–6 cycles of chemotherapy completed,and if bevacizumab discontinued, give 840 mg/2 weeks、1200 mg/3 weeks、1680 mg/4 weeks Continue until disease progression or unacceptable toxicity.
Cemiplimab	Libtayo	50 mg/ml	US EU	soln for IV infusion after dilution	350 mg/3 weeks until disease progression or unacceptable toxicity.
Durvalumab	Imfinzi	50 mg/ml	US EU China	soln for IV infusion after dilution	Stage III NSCLC(<30 kg):10 mg/kg/2 weeks;(≥30 kg): 10 mg/kg/2 weeks、1500 mg/4 weeks,Continue until disease progression, unacceptable toxicity.
Nivolumab	Opdivo	10 mg/ml	US EU China	soln for IV infusion after dilution	Single agent:240 mg/2 weeks或480 mg/4 weeks,until disease progression or unacceptable toxicity.
Pembrolizumab	Keytruda	25 mg/ml	US EU China	soln for IV infusion after dilution	Single agent:200 mg/3 weeks or 400 mg/6 weeks until disease progression or unacceptable toxicity.or up to 24 months in patients without disease progression.

disease progression caused by drug resistance. Recently, researches on immunity checkpoint inhibitors (ICIs) have progressed rapidly. Various new drugs have been developed in immunotherapy. The most significant clinical improvement is programmed cell death protein 1 (PD-1) and programmed cell death protein ligand 1 (PD-L1) monoclonal antibody (Li et al., 2018a). PD-1/PD-L1 inhibitors have produced significant survival benefits in the treatment of some advanced NSCLC, bringing hope to the treatment of all NSCLC patients.

A variety of PD-1/PD-L1 inhibitors have been approved for marketing. The PD-1 inhibitor includes Nivolumab, Pembrolizumab, Cemiplimab, Sintilimab, Toripalimab, Camrelizumab, Tislelizumab, etc. PD-L1 inhibitor includes Durvalumab, Atezolizumab, etc. There are 15 PD-1/PD-L1 inhibitors for NSCLC in clinical trials registered in clinicaltrials.gov until 15 January 2022 (**Table 1**). The some of the PD-1 inhibitors (i.e., Nivolumab, Pembrolizumab, Cemiplimab), and PD-L1 inhibitors (i.e., Durvalumab and Atezolizumab) have been authorized to market at home and abroad, and have shown higher survival benefits than chemotherapy in clinical trials or clinical applications. The PD-1/PD-L1 inhibitors, approved by the European Medicines Agency (EMA) and the United States Food and Drug Administration (FDA) and the China National Medical

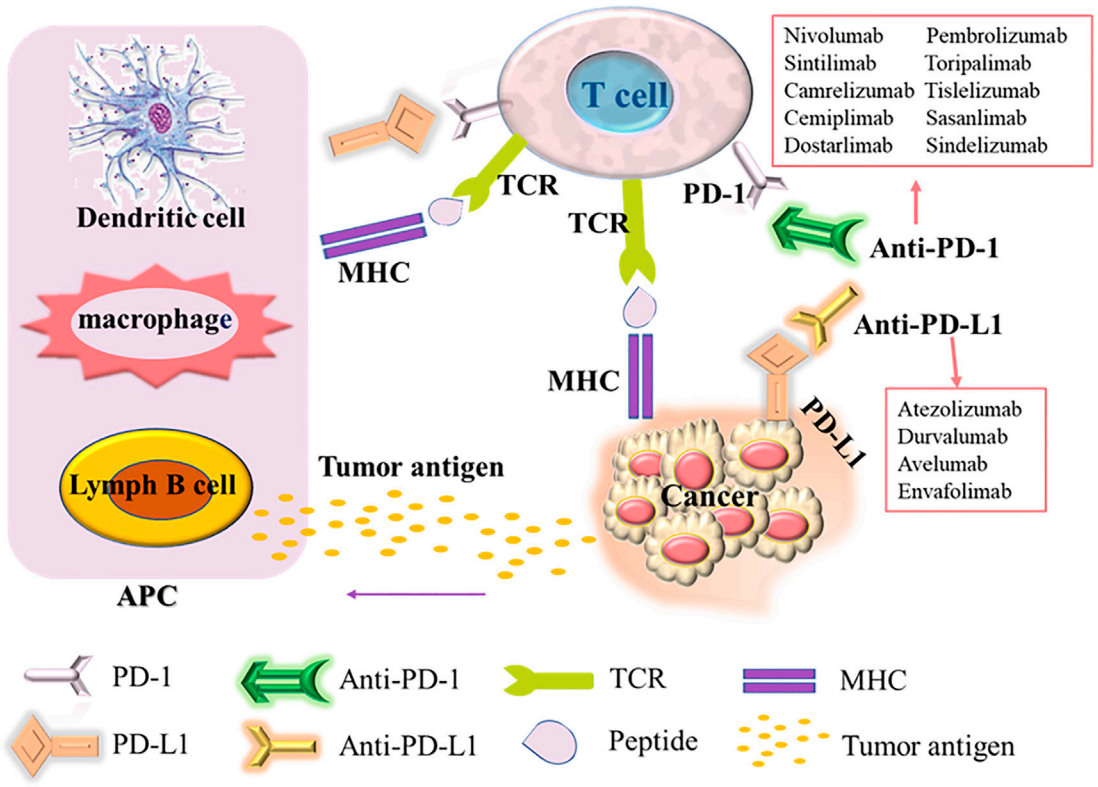

FIGURE 1 | Mechanism of action of PD-1/PD-L1 inhibitors.

Products Administration (NMPA) for the treatment of advanced NSCLC (Xu et al., 2018) (**Table 2**) domestic preparations include Sintilimab (PD-1, February 2021), Camrelizumab (PD-1, December 2021), Tislelizumab (PD-1, June 2021; approved in China for the treatment of NSCLC). The review summarizes and analyzes the clinical studies of five currently used drugs targeting PD-1/PD-L1 immune checkpoints approved by FDA, EMA, and NMPA in advanced NSCLC.

MECHANISM OF PROGRAMMED CELL DEATH PROTEIN 1/PROGRAMMED CELL DEATH PROTEIN LIGAND 1 IN NON-SMALL CELL LUNG CANCER

PD-1, also known as cluster of differentiation 279 (CD279), is a domain composed of 288 amino acid residues in the N-terminal of the immunoglobulin superfamily. It is an inhibitory protein receptor related to apoptosis. It is regarded as a sign of T cell unresponsiveness or exhaustion (Ishida et al., 1992). It is mainly expressed on the surface of T lymphocytes, B lymphocytes, dendritic cells (DC), NK cells (natural killer cells) and other cells (Calles et al., 2015), involved in autoimmune tolerance in a variety of physiological responses. As the major ligand of PD-1, PD-L1 (known as CD274 or B7-H1) is expressed in malignant tumor cells, lymphocytes, antigen presenting cells (APC), hematopoietic cells and epithelial cells. However, the expression of PD-L1 is usually low in stable state and upregulation induced by inflammatory stimulation (Yearley et al., 2017). In many cancers (including NSCLC), the PD-L1 signaling pathway is usually abnormally activated, and the interaction between PD-1 and PD-L1 inhibits the proliferation and activity of CD4+T cells and CD8+T cells, reducing their immune response to surrounding tissues and preventing the occurrence of autoimmune diseases (David et al., 2019; song et al., 2020). Thus in tumors, inflammation-induced PD-L1 expression in the tumor microenvironment causes PD-1-mediated T cell exhaustion, and suppresses anti-tumor cytotoxic T cell responses, leading to autoimmune killing of T cells in the tumor local microenvironment attenuated function. The tumor cells evade the immune system through various mechanisms, including low tumor cell immunogenicity, recognition of tumor-specific antibodies as self-antigens, tumor surface antigen modulation, tumor-induced privileged regions, tumor-induced immunosuppression, etc. Then, the tumor cells can avoid the immune system recognition and attack, achieve grow, metastasize and tumor immune escape, promoting tumor growth (Ribas, 2015; Ribas and Wolchok, 2018). Immune escape also occurs in the development of NSCLC. Tumor cells avoid the killing and elimination of the body's autoimmunity, and establish a local microenvironment in some tissues that are conducive to tumor development. The mechanism of action of PD-1 and PD-L1 immunosuppressants is to block the PD-1 and PD-L1

TABLE 3 | FDA/EMA/NMPA-approved NSCLC treatments of PD-1/PD-L1 blocking antibodies clinical trials.

Target	Drug	Study	PD-1/PD-L1 Group vs. Control Group	Inclusion Criteria	Study Type	Phase	N	OS(PD-1/PD-L1 Group vs. Control Group)
PD-1	Pembrolizumab	KEYN0TE-001 Garon et al. (2019)	Pembrolizumab/No Pembrolizumab	untreated advanced NSCLC	singlearm	I	550	22.3/10.5
		KEYNOTE-010 Herbst et al. (2016)	Pembrolizumab/Docetaxel	Previously treated NSCLC with PD-1/PD-L1 expression >50%	RCT	II/III	1,034	12.7/8.5
		KEYNOTE-021 Langer et al. (2016)	Pembrolizumab + Pemetrexed + Carboplatin/ Pemetrexed + Carboplatin	untreated advanced NSCLC	RCT	II	123	21.4/16.4
		KEYNOTE-024 Brahmer et al. (2017)	Pembrolizumab/ Carboplatin + pemetrexed or paclitaxel or cisplatin + gemcitabine	PD-1/PD-L1 expression>50%, no EGFR gene mutation	RCT	III	305	30.0/14.2
		KEYNOTE-042 Mok et al. (2019)	Pembrolizumab/platinum-based + chemotherapy	No EGFR gene mutation or ALK translocation	RCT	III	1,444	20.0/12.2
		KEYNOTE-189 Garassino et al. (2019)	Pembrolizumab + Chemo/ chemo + placebo	NSCLC patients without metastasis and without EGFR gene mutation	RCT	II/III	616	20.2/13.5
		KEYNOTE-407 Paz-Ares et al. (2020)	Pembrolizumab + Chemo/ chemo	Untreated, non-metastatic NSCLC	RCT	III	559	15.9/11.3
	Nivoliumab	CheckMate 227 Hellmann et al. (2019)	Nivoliumab or Nivoliumab + ipilimumab/chemotherapy	Squamous/non-squamous stage IV or recurrent NSCLC	RCT	III	1739	17.2/13.9
		CheckMate 9LA Paz-Ares et al. (2021)	Nivolumab + ipilimumab + chemotherapy/ chemotherapy alone	Squamous/non-squamous stage IV or recurrent NSCLC	RCT	III	719	14.1/10.7
		CheckMate 017 Horn et al. (2017)	Nivolumab/Docetaxel	Stage IIIB/IV squamous NSCLC	RCT	III	272	9.2/6.0
		CheckMate 057 Borghaei et al. (2021)	Nivolumab/Docetaxel	Stage IIIB/IV non-squamous NSCLC	RCT	III	582	[a]12.2/9.4
		NEOSTAR Cascone et al. (2021)	Nivolumab/Nivolumab + Ipilimumab	Operable NSCLC	RCT	II	44	—
		CheckMate 078 Wu et al. (2019)	Nivolumab/Docetaxel	Stage IIIB, stage IV, recurrent squamous/non-squamous NSCLC after prior chemotherapy	RCT	III	504	[a]12.3/7.9
		CheckMate 026 (Carbone et al. (2017)	Nivolumab/platinum chemotherapy	Squamous/non-squamous stage IV or recurrent NSCLC	RCT	III	530	[a]14.4/ 13.2
	Cimepritimab	MA04.01 Moreno et al. (2018)	Cimepritimab/Cimepritimab + Chemotherapy	Advanced NSCLC	RCT	I	53	—
		EMPOWER-lung1 Sezer et al. (2021)	Cimepritimab/platinum doublet chemotherapy	Stage IIIB/IV squamous/non-squamous NSCLC	RCT	III	710	[a]22.1/ 14.3
		EMPOWER-Lung2 Rizvi et al. (2018)	Cimepritimab and ipilimumab ± chemotherapy/ pembrolizumab	Advanced NSCLC with PD-L1≥50%	RCT	III	585	—
		NCT03367819 Zucali et al. (2022)	Ixatuximab + Cimipritimab	Advanced NSCLC	singlearm	I/II	20	—
		MPOWER-Lung3 Gogishvili et al. (2021)	Cimepritimab + platinum-based doublet chemotherapy/platinum-based doublet chemotherapy	Metastatic NSCLC (Stage IV)/ Locally Advanced NSCLC (Stage IIIB/C)	RCT	III	466	22/13
		EMPOWER-Lung4 Shim et al. (2020)	Cimepritimab/Cimepritimab + Ipilimumab/Ipilimumab	Advanced NSCLC	RCT	II	28	—
PD-L1	durvalumab	PACIFIC Faivre-Finn et al. (2021)	durvalumab/placebo	Unresectable Stage III NSCLC	RCT	III	709	47.5/29.1
		NCT02904954 NasserAltorki et al. (2021)	durvalumab/durvalumab + radiotherapy	Resectable early stage NSCLC	RCT	II	60	—
		ATLANTIC Garassino et al. (2018)	durvalumab	Advanced NSCLC progression after at least two prior systemic regimens	singlearm	II	444	[a]13.6

(Continued on following page)

TABLE 3 | (*Continued*) FDA/EMA/NMPA-approved NSCLC treatments of PD-1/PD-L1 blocking antibodies clinical trials.

Target	Drug	Study	PD-1/PD-L1 Group vs. Control Group	Inclusion Criteria	Study Type	Phase	N	OS(PD-1/PD-L1 Group vs. Control Group)
		NCT02125461 Antonia et al. (2017)	durvalumab/placebo	Stage III, locally advanced, unresectable NSCLC	RCT	III	713	[a]16.8/5.6
	Atezolizumab	IMpower131 Jotte et al. (2020)	Atezolizumab + chemotherapy/ chemotherapy	Chemotherapy-naïve stage IV squamous NSCLC	RCT	III	1,021	14.2/13.5
		POPLAR Fehrenbacher et al. (2016)	Atezolizumab/Docetaxel	NSCLC that has progressed after platinum-based chemotherapy	RCT	II	287	12.6/9.7
		BIRCH Peters et al. (2017)	Atezolizumab	Stage IIIB/IV or recurrent NSCLC	singlearm	II	659	[a]23.5/ 15.5/13.2
		IMpower110 Herbst et al. (2020)	Atezolizumab/ chemotherapy	Stage IV non-squamous/ squamous NSCLC	RCT	III	572	[a]20.2/ 13.1
		OAK Fehrenbacher et al. (2018)	Atezolizumab/Docetaxel	Previously treated advanced NSCLC	RCT	III	1,225	[a]13.8/9.6
		IMpower132 Nishio et al. (2021)	Atezolizumab + chemotherapy/ chemotherapy	Primary chemotherapy for stage IV non-squamous NSCLC without sensitizing EGFR or ALK gene alterations	RCT	III	578	[a]15.9/ 10.5
		IMpower150 Socinski et al. (2018)	Atezolizumab + chemotherapy/ bevacizumab + chemotherapy	Chemotherapy-naive stage IV/ recurrent metastatic non-squamous NSCLC	RCT	III	356	[a]19.2/ 14.7

OS; overall survival, Time from randomization to death (from any cause).
[a]*stands for Median Survival Time (mOS) .*
RCT, randomized controlled trial.

signaling pathways of NSCLC cells (**Figure 1**), activate the immune activity of T cells, leading to the inhibition on the growth and proliferation of tumor cells, then achieving its final apoptosis (Li et al., 2018b).

Upon T cell activation, the PD-1 receptor binds to PD-L1expressed on the surface of cancer cells and suppresses the immune response. Antigen-presenting cells (APC) process antigens released by cancer cells and present them to T cells for promoting T cell activation and high PD-1 expression. In addition, tumor cells can also present antigens directly for activating T cells in the context of the major histocompatibility complex (MHC). PD-1/PD-L1 inhibitors can enhance the body's immune response by blocking the binding of PD-1/ PD-L1.

CLINICAL STUDY OF PROGRAMMED CELL DEATH PROTEIN 1/PROGRAMMED CELL DEATH PROTEIN LIGAND 1 IMMUNOSUPPRESSANT ON ADVANCED NON-SMALL CELL LUNG CANCER TREATMENT

Table 3 is a summary of the clinical trials with PD-1/PD-L1 inhibitors that are widely used in advanced NSCLC in China and other countries. The subsequent analysis and discussion are based on the clinical trials listed in **Table 3**.

Pembrolizumab

Pembrolizumab monoclonal antibody (Keytruda; Merck, Sharp and Dohme Corp., Kenilworth, NJ) is a humanized monoclonal IgG4-κ isotype antibody. It blocks the interaction between PD-1 and PD-L1 by binding to the PD-1 receptor. In China 2018, the National Medical Products Administration (NMPA) officially approved Pembrolizumab on 28 March 2019 for: 1) a test approved by the National Medical Products Administration to evaluate the PD-L1 tumor proportion score (TPS) ≥1% epidermal growth factor receptor (EGFR) gene mutation-negative and anaplastic lymphoma kinase (ALK)-negative locally advanced or metastatic NSCLC first-line monotherapy, 2) combination with pemetrexed and platinum-based chemotherapy for the first-line treatment of epidermal growth factor receptor (EGFR) gene mutation-negative and anaplastic lymphoma kinase (ALK)-negative metastatic non-squamous NSCLC, 3) combination with carboplatin and paclitaxel for the first-line treatment of patients with metastatic squamous NSCLC. As of 15 January 2022, there are 372 clinical trials of pembrolizumab for NSCLC registered at clinicaltrials.gov, of which 35 are launched in China.

The efficacy of pembrolizumab monotherapy in patients with advanced NSCLC is showed in **Table 3**, including a phase I study

(KEYNOTE-001) in previously treated and untreated disease, a second-line or higher setting Phase II/III study (KEYNOTE-010), and two Phase III studies in the first-line setting (KEYNOTE-024 and -042). In three randomized studies (KEYNOTE-010, -024, and -042), overall survival (OS) was significantly longer with pembrolizumab than with chemotherapy (Herbst et al., 2016; Brahmer et al., 2017; Garon et al., 2019; Mok et al., 2019). Clinical trials of pembrolizumab in combination with platinum-based chemotherapy showed improved efficacy compared with platinum-based chemotherapy alone, and in squamous NSCLC (KEYNOTE-407, phase III) and two non-squamous NSCLC clinical trials demonstrated the manageable safety profile (KEYNOTE-021 (Phase II), KEYNOTE-189 (Phase III)). In the KEYNOTE-021 cohort, the objective response rate (ORR) was 55% with pembrolizumab plus chemotherapy versus 29% with chemotherapy alone (Langer et al., 2016). Primary endpoints of OS and progression-free survival (PFS) both enhanced by the combination therapy in KEYNOTE-189 and KEYNOTE-407 (Garassino et al., 2019; Paz-Ares et al., 2020).

Nivolumab

Nivolumab is a humanized monoclonal antibody (IgG4 subtype) directly against the programmed death 1 (PD-1) receptor, which is developed by Bristol-Myers Squibb. Until 15 January 2022, there are 255 clinical trials of nivolumab for NSCLC registered with clinicaltrials.gov, of which 22 are launched in China. Based on datasets from phase III randomized trials (CheckMate 017, 057) and phase II trials, FDA approved the National Comprehensive Cancer Network (NCCN) NSCLC panel recommend nivolumab as a treatment for metastatic squamous, metastatic preferred follow-up therapy for patients with non-squamous NSCLC (**Table 3**). On 15 June 2018, China approved it for the treatment of 1) epidermal growth factor receptor (EGFR) gene mutation-negative and anaplastic lymphoma kinase (ALK)-negative NSCLC; (2) previously received platinum-based chemotherapy Adult patients with locally advanced or metastatic NSCLC after disease progression or intolerance.

An OS benefit of Nivolumab over docetaxel was observed in patients with squamous NSCLC regardless of PD-1/PD-L1 expression levels. In patients with non-squamous NSCLC, higher levels of PD-L1 expression are associated with a greater OS benefit from Nivolumab, but treatment gains are also observed in patients with PD-1/PD-L1 expression <25%. Compared to docetaxel, the significant improvement in OS and tolerability of Nivolumab for NSCLC patients is progressed during or after platinum-based chemotherapy (Horn et al., 2017). The response of Nivolumab is durable and generally well-tolerated, with 14% of patients experiencing grade 3–4 treatment-related adverse events (Wu et al., 2019; Cascone et al., 2021), reflecting the unique advantage of the mechanism for the action of immunotherapy. In CheckMate 078, a Chinese-based Phase III clinical trial, compared with docetaxel in previously treated patients with advanced NSCLC, Nivolumab improves the OS. It is consistent with CheckMate 017 and 057 global trials (Horn et al., 2017; Borghaei et al., 2021).

Cimiprizumab

Cimepritimab is an IgG4 monoclonal antibody against PD-1. In 2017, Cimiprizumab was approved for the treatment of metastatic cutaneous squamous cell carcinoma and locally advanced cutaneous squamous cell carcinoma, which is not suitable for surgery or radiation. It also has shown antitumor activity in other advanced solid tumors (Papadopoulos et al., 2020). The latest results from the phase III clinical trial EMPOWER-Lung1 show that compared with platinum-based doublet chemotherapy in patients with advanced NSCLC (stage IIIB/IIIC or IV) and high PD-L1 expression (≥50%), Cimepritimab treatment significantly improved overall survival and progression-free survival (Sezer et al., 2021). In 2021, Cimepritimab is approved for first-line treatment of patients with advanced NSCLC and PD-L1 expression ≥50% in the United States. Data from the trials collated for the review (**Table 3**) suggest that the combination therapy provides a survival benefit for patients regardless of the proportion of PD-L1 expression. From the perspective of protecting patients from chemotherapy toxicity, patients with a very high proportion of PD-L1, especially those greater than 90%, may be ideal candidates for Cimepritimab monotherapy. Compared with ICI plus chemotherapy, the most favorable risk-benefit ratio was obtained in patients with high PD-L1 expression.

Durvalumab

Duvalumab is a selective, high-affinity human immunoglobulin G1 monoclonal antibody, and developed by AstraZeneca Pharmaceuticals LP. It can block the binding of PD-L1 to PD-1 and CD80, then enhance the anti-tumor T cell activity (Sezer et al., 2021). In 2017, the drug was approved by the United States Food and Drug Administration for the treatment of patients with unresectable, stage III NSCLC, who have not progressed after platinum-based chemotherapy and radiation therapy. In 2018, it was approved as consolidation immunotherapy for patients with stage III NSCLC after definitive chemoradiotherapy (CRT), and was the first drug to slow the progression of NSCLC (Aredo et al., 2021). In December 2019, it was approved for marketing in China. It is the first PD-L1 immunotherapy drug approved in China. Until 15 January 2022, there are 169 clinical trials on Nivolumab for NSCLC registered with clinicaltrials.gov, of which 19 are launched in China.

Recently, the study results from PACIFIC demonstrate that improved OS with durvalumab is widely observed regardless of PD-L1 expression (Papadopoulos et al., 2020). Compared with patients with low or no expression (PD-L1 expression <25%), the median progression-free survival was longer in EGFR−/ALK− NSCLC patients (PD-L1 expression ≥25%) (Garassino et al., 2018). A progression-free survival (PFS) benefit was also consistently observed with durvalumab in the NCT02125461 trial (Shim et al., 2020).

Atezolizumab

Atezolizumab is a humanized immunoglobulin G1 monoclonal antibody against programmed death ligand 1 (PD-L1). In December 2019, the FDA approved Atezolizumab in combination with paclitaxel and carboplatin for the first-line

TABLE 4 | Major adverse events in PD-1/PD-L1 immunotherapy.

Human Body Systems/Tissues Etc.	Adverse Reaction Symptoms
Endocrine system	Hypothyroidism, Hyperthyroidism, Hypophysis, Thyroiditis, Adrenal insufficiency
Respiratory system	Pneumonia, Difficulty breathing
Cardiovascular system	Anemia, Thrombocytopenia, Neutropenia
Digestive system	Colitis, Diarrhea, Nausea, Constipation, Decreased appetite, Hepatitis, Alanine aminotransferase increased, Aspartate aminotransferase increased
Skin related	Rash, Pruritus, Vitiligo, Cutaneous capillary hyperplasia, Lichen lichenoides, Bullous pemphigoid
Musculoskeletal System	Myalgia, Joint pain
Other	Fatigue, Fever, Chills, Hair loss, Infusion reactions
Rarely (but serious)	Immune-related encephalitis, Myasthenia gravis, Acute renal failure, Interstitial nephritis, Myocarditis

treatment of patients with metastatic non-squamous NSCLC without EGFR and ALK mutations. Until 15 January 2022, there are 150 clinical trials of nivolumab for NSCLC registered with clinicaltrials.gov, of which 17 are launched in China (Part of the clinical trial data is shown in **Table 3**). The results of clinical trials IMpower-131, -132, -150, -110 showed that the overall survival of Atezolizumab in NSCLC patients with high PD-L1 expression was significantly longer than that of platinum-based chemotherapy (Herbst et al., 2020) (Nishio et al., 2021). In phase II POPLAR trial, Atezolizumab showed significant improvement compared with docetaxel in previously treated patients with advanced NSCLC (unselected for PD-L1 expression). The improvement in overall survival increased with increased PD-L1 expression, and patients with the lowest PD-L1 expression have similar overall survival of the docetaxel group (Fehrenbacher et al., 2016). Atezolizumab monotherapy was well tolerated in PD-L1-selected patients with advanced NSCLC in BIRCH trial (Peters et al., 2017). The status of PD-L1 expression serves as a predictive biomarker to identify patients, who most likely to benefit from Atezolizumab.

Programmed Cell Death Protein 1/ Programmed Cell Death Protein Ligand 1 Combined Clinical Trial

In the tumor microenvironment, PD-1 regulates T cell function. In lymph nodes, CTLA-4 inhibits the early activation and differentiation of T cells. Therefore, the combination of anti-PD-1/PD-L1 and anti-CTLA-4 is considered as a complementary therapy to trigger immune checkpoint inhibition. On the basis of the clinical trial of PD-1/PD-L1 in combination with it in **Table 3** and clinical data from keynote-189, when Pembrolizumab combinate with platinum and pemetrexed as first-line therapy for metastatic non-squamous NSCLC, no change happens in EGFR or ALK. In the double-blind Phase III Keyn-189 study, first-line Pembrolizumab plus Pemetrexel and platinum chemotherapy significantly improved OS (HR 0.49, $p < 001$), PFS (HR 0.52, $p < 001$), and ORR (47.6% vs. 18.9%, $p < 001$). In keynote-407, compared with placebo plus chemotherapy, Pembrolizumab plus carboplatin and paclitaxel/nab-paclitaxel (chemotherapy) significantly improved overall survival (OS) and progression-free survival (PFS) in previously untreated metastatic squamous NSCLC patients. According to the CheckMate9LA study, compared to chemotherapy alone, Nivolumab plus Ipilimumab combined with two cycles of chemotherapy shows a significantly improved survival benefit. In patients with TMB≥10 mutations/Mb, compared with nivolumab plus ipilimumab, there is a significant PFS advantage (increased probability and duration of response), according to published data from CheckMate227, Part 1. Nivolumab plus Ipilimumab produces a median OS of 23.0 months versus 16.7 months for chemotherapy, and an estimated relative reduction of 23% in the risk of death (HR: 0.77; 95%CI: 0.56–1.06). In the EMPOWER-Lung 3 study, Simiprizumab plus chemotherapy showed clinically and statistically significant improvements in OS, PFS, ORR, and DOR compared with chemotherapy alone, consistently in safety with Simiprizumab monotherapy and platinum-based chemotherapy. In the Global Open-label Phase III IMpower131 study, the addition of Atezolizumab to CnP provides PFS and OS benefits in patients with metastatic squamous NSCLC, whose tumors have high PD-L1 expression. In conclusion, compared to chemotherapy, PD-1/PD-L1 combination therapy significantly prolongs OS and PFS, and has a similar risk of grade 3–4 AE. It should be notice that PD-1/PD-L1 combination therapy increases the risk of AE discontinuation or death.

Adverse Reactions of Programmed Cell Death Protein 1/Programmed Cell Death Protein Ligand 1 Inhibitors in Non-Small Cell Lung Cancer

The PD-1/PD-L1 axis acts as a brake on T cell activation and is involved in the pathogenesis of autoimmune diseases, including systemic lupus erythematosus (SLE) (Prokunina et al., 2002), rheumatoid arthritis (RA) (Wang et al., 2005), type I diabetes (TlD) (Curran and Sharon, 2017), autoimmune hepatitis (AIH) (Curran and Sharon, 2017), and multiple sclerosis(MS) (Kroner et al., 2005). Upregulation of PD-1/PD-L1 in the tumor microenvironment leads to impaired immune cell function and premature apoptosis, while autoimmune diseases are caused by excessive immunity, leading to the damage of normal tissues. The use of PD-1/PD-L1 inhibitors may cause dysregulation of the PD-1/PD-L1 signaling pathway, resulting in the loss of immune homeostasis and a strong abnormal immune

response. The loss of immune homeostasis is related to genetic factors and environmental factors, and dietary factors or other diseases are also related. PD-1 receptors need to bind their ligands for suppressing the effects of immune responses. Therefore, the number of immune cells increases dramatically, and PD-1 expression on cells is affected by cytokine or Ag receptor stimulation. It could be the main reason for serious adverse reactions of PD-1/PD-L1 inhibitors during treatment.

Immunotherapy reactivates the immune system, and the body's immune tolerance becomes unbalanced, leading to the emergence of new toxicity profiles known as immune-related adverse events (irAEs). These irAEs could affect multiple organ systems and tissues (**Table 4**), clinically manifest as autoimmune-like inflammatory side-effects, causing the damages on the skin, lungs, gastrointestinal tract, liver, endocrine glands, and skeletal muscle (Prokunina et al., 2002). Rash and pruritus are the most common cutaneous irAEs in NSCLC patients treated by anti-PD-1/PD-L1 immune checkpoint therapy. The other cutaneous tissue lesions include vitiligo, cutaneous capillary hyperplasia, lichenoid lichen, and bullous pemphigoid (Kong et al., 2005). Respiratory-related AEs also frequently occur with anti-PD-1/PD-L1 immunotherapy. Among them, immune-related pneumonia is common, including pulmonary sarcoidosis and tissue inflammatory pneumonia. The clinical symptoms are mainly dry cough, dyspnea, fever and Chest pain (Wang et al., 2005). The most common gastrointestinal toxicities during anti-PD-1/PD-L1 immunotherapy treatment are colitis and diarrhea, and the other gastrointestinal adverse reactions included decreased appetite, nausea, vomiting, and constipation (Curran and Sharon, 2017). In NSCLC patients receiving anti-PD-1/PD-L1 immunotherapy, the incidence of immune-related hepatitis is approximately 5%, whereas the incidence of severe hepatitis (grade III-IV) is <2%. The immune-mediated clinical symptoms of hepatitis include hepatomegaly, portal and periportal inflammation, lymphadenopathy, and infiltration of eosinophils, lymphocytes, and plasma cells (Kroner et al., 2005). In NSCLC patients, hypothyroidism is the most common endocrine toxicity (with an incidence of 5–15%). Hypophysitis, thyroiditis, hyperthyroidism, and adrenal insufficiency are also common immune-related endocrine diseases. The clinical symptoms are nonspecific heterosexual (common symptoms in cancer patients), such as fatigue, headache, and nausea (Naidoo et al., 2015).

DISCUSSION AND OUTLOOK

In this review, the clinical application progresses of the drug used in NSCLC was analyzed. It is found that the PD-1 inhibitors (e.g., Nivolumab, Cimipritimab and Bolizumab) and the PD-L1 inhibitors (e.g., Durvalumab and Atezolizumab) have benefited OS in clinical trials of NSCLC treatments. Although immune checkpoint inhibitors (ICIs) can improve the treatment landscape of NSCLC without EGFR, ALK or ROS1 aberrations, and reduce the proportion of chemotherapy in patients with high PD-L1 expression, leading to that these patients can avoid chemotherapy-related complications toxicity, the overall survival benefits still require to be improved by combination therapy (Huang et al., 2021). The degree of patient benefit is highly related to PD-1/PD-L1 pathway biomarkers. With the progresses of biomarker research, immunosuppressants will gain great achievements.

According to the relevant clinical trials analyzed in this review, PD-1/PD-L1 inhibitors can be considered as a class of drugs with relatively good safety, low toxicity and relatively good tolerance. The incidence and severity of immune-related adverse events (irAEs) varied widely across trials, including PD-1/PD-L1 inhibitor therapy-related adverse events. The incidence of adverse reactions, leading to the discontinuation of treatment, were significantly lower than those of docetaxel. It can be observed that PD-1/PD-L1 inhibitors are safe and can be tolerated by most patients. Combination therapy has a higher efficacy in NSCLC immunotherapy, e.g., the treatment by Ipilimumab plus Nivolumab is the first approved ICI combination therapy. However, the increased efficacy was also accompanied by higher frequency and more severe ADRs, with a greater probability of some clinically critical adverse events observed in combination therapy (Huang et al., 2021), such as diabetic ketoacidosis, thyrotoxic crisis, acute adrenal cortex insufficiency, myocarditis, non-infectious encephalitis/myelitis, Guillain-Barré syndrome, colitis, etc. Therefore, how to obtain higher efficacy and reduce or avoid serious adverse reactions in combination therapy is an important research direction in the future.

Prevention and reduction of the incidence on the adverse events can be obtained from: 1) monitoring of biomarkers can predict the occurrence of AEs during immunotherapy, such as serum thyroglobulin, thyroid autoantibodies and early changes in the levels of certain cytokines (IL-1β, increased levels of IL-2 and GM-CSF and decreased levels of IL-8, G-CSF, MCP-1), 2) comparing the changes of some biochemical indexes and imaging characteristics of tissues and organs before and after immunotherapy to assist the judgement on the possibility of irAEs (Wang et al., 2017). Routine baseline assessments include physical examination (height, weight, heart rate, blood pressure, and other general symptoms), imaging studies (chest CT, brain MRI), and laboratory tests (e.g., blood routine, blood chemistry, blood glucose, total bilirubin, TSH, free T4, LH, FSH, testosterone, cortisol, ACTH, infectious disease screening). In addition, tumor patients with different races, genders, and ages have different characteristics and severity of irAEs. Therefore, according to patients' individual conditions, precise care is beneficial to reduce the incidence of AEs. For example, older adults with NSCLC often have comorbidities and polypharmacy, thus requiring adequate clinical monitoring.

AUTHOR CONTRIBUTIONS

FL, literature review, data collection, manuscript writing; TW and TQ data proofreading, manuscript revision; BL, policy and legal support, ADR-related content review; YW, topic selection, manuscript review and revision, corresponding author.

REFERENCES

Antonia, S. J., Villegas, A., Daniel, D., Vicente, D., Murakami, S., Hui, R., et al. (2017). *N. Engl. J. Med.* 77 (20), 1919–1929. doi:10.1056/NEJMoa1709937

Aredo, J. V., Mambetsariev, I., Hellyer, J. A., Arya, A., Neal, J. W., Padda, S. K., et al. (2021). Durvalumab for Stage III EGFR-Mutated NSCLC after Definitive Chemoradiotherapy. *J. Thorac. Oncol.* 16 (6), 1030–1041. doi:10.1016/j.jtho.2021.01.1628

Arnold, M., Sierra, M. S., Laversanne, M., Soerjomataram, I., Jemal, A., and Bray, F. (2017). Global Patterns and Trends in Colorectal Cancer Incidence and Mortality. *Gut* 66 (4), 683–691. doi:10.1136/gutjnl-2015-310912

Borghaei, H., Gettinger, S., Vokes, E. E., Chow, L. Q. M., Burgio, M. A., de Castro Carpeno, J., et al. (2021). Five-Year Outcomes from the Randomized, Phase III Trials CheckMate 017 and 057: Nivolumab versus Docetaxel in Previously Treated Non-small-cell Lung Cancer. *J. Clin. Oncol.* 39 (7), 723–733. doi:10.1200/JCO.20.01605

Brahmer, J., Rodríguez-Abreu, D., Robinson, A., Hui, R., Csőszi, T., Fülöp, A., et al. (2017). Updated Analysis of KEYNOTE-024: Pembrolizumab vs Platinum-Based Chemotherapy for Advanced NSCLC with PD-L1 TPS ≥50%. *J. Thorac. Oncol.* 12 (11Suppl. 2), S1793–S1794.

Calles, A., Liao, X., Sholl, L. M., Rodig, S. J., Freeman, G. J., Butaney, M., et al. (2015). Expression of PD-1 and its Ligands, PD-L1 and PD-L2, in Smokers and Never Smokers with KRAS-Mutant Lung Cancer. *J. Thorac. Oncol.* 10 (12), 1726–1735. doi:10.1097/JTO.0000000000000687

Cao, M., and Chen, W.. Interpretation on the Global Cancer Statistics of GLOBOCAN 2020[J]. *Chin. J. Med. Front. Electron. Ed.*, 2021, 13(03):63–69. doi:10.12037/YXQY.2021.03-10

Carbone, D. P., Reck, M., Paz-Ares, L., Creelan, B., Horn, L., Steins, M., et al. (2017). A. Socinski,. For the CheckMate 026 Investigators. First-Line Nivolumab in Stage IV or Recurrent Non–small-cell Lung Cancer, *N. Engl. J. Med.*, 376, 2415–2426. doi:10.1056/NEJMoa1613493

Cascone, T., William, W. N., Weissferdt, A., Leung, C. H., Lin, H. Y., Pataer, A., et al. (2021). Neoadjuvant Nivolumab or Nivolumab Plus Ipilimumab in Operable Non-small Cell Lung Cancer: the Phase 2 Randomized NEOSTAR Trial. *Nat. Med.* 27 (3), 504–514. doi:10.1038/s41591-020-01224-2

Curran, C. S., and Sharon, E. (2017). PD-1 Immunobiology in Autoimmune Hepatitis and Hepatocellular Carcinoma. *Semin. Oncol.* 44, 428–432. doi:10.1053/j.seminoncol.2017.12.001

David, P., Megger, D. A., Kaiser, T., Werner, T., and Liu, J. The PD▪1/PD▪L1 Pathway Affects the Expansion and Function of Cytotox·1090·ic CD8(+)T Cells during an Acute Retroviral Infection [J]. *Front. Immunol.*, 2019, 10, 54.doi:10.3389/fimmu.2019.00054

Faivre-Finn, C., David, V., Kurata, T., Planchard, D., Paz-Ares, L., Vansteenkiste, J. F., et al. (2021). Antonia, Four-Year Survival with Durvalumab after Chemoradiotherapy in Stage III NSCLC—An Update from the PACIFIC Trial. *J. Thorac. Oncol.* 16 (5), 860–867. doi:10.1016/j.jtho.2020.12.015

Fehrenbacher, L., Alexander, S., Ballinger, M., Kowanetz, M., Vansteenkiste, J., Mazieres, J., et al. (2016). Atezolizumab versus Docetaxel for Patients with Previously Treated Non-small-cell Lung Cancer (POPLAR): a Multicentre, Open-Label, Phase 2 Randomised Controlled Trial. *Lancet* 387, 100301837–100301846. doi:10.1016/S0140-6736(16)00587-0

Fehrenbacher, L., von Pawel, J., Park, K., Rittmeyer, A., David, R., Gandara, S. P. A., et al. (2018). , Filippo De Marinis, Mayank Gandhi, Bradford Danner, Christina Matheny, Marcin Kowanetz, Pei He, Federico Felizzi, Hina Patel, Alan Sandler, Marcus Ballinger, Fabrice Barlesi, Updated Efficacy Analysis Including Secondary Population Results for OAK: A Randomized Phase III Study of Atezolizumab versus Docetaxel in Patients with Previously Treated Advanced Non-small Cell Lung Cancer. *J. Thorac. Oncol.* 13 (8), 1156–1170. doi:10.1016/j.jtho.2018.04.039

Garassino, M. C., Cho, B-C., and Kim etc, J. (2018). Durvalumab as Third-Line or Later Treatment for Advanced Non-small-cell Lung Cancer (ATLANTIC): an Open-Label, Single-Arm, Phase 2 Study. *Lancet Oncol.* 19 (4), 521–536. doi:10.1016/S1470-2045(18)30144-X

Garassino, M., Rodriguez-Abreu, D., Gadgeel, S., Esteban, E., Felip, E., Speranza, G., et al. (2019). OA04.06 Evaluation of TMB in KEYNOTE-189: Pembrolizumab Plus Chemotherapy vs Placebo Plus Chemotherapy for Nonsquamous NSCLC. *J. Thorac. Oncol.* 14 (10), S216–S217. doi:10.1016/j.jtho.2019.08.427

Garon, E. B., Hellmann, M. D., Rizvi, N. A., Carcereny, E., Leighl, N. B., Ahn, M. J., et al. (2019). Five-Year Overall Survival for Patients with Advanced Non–Small-Cell Lung Cancer Treated with Pembrolizumab: Results from the Phase I KEYNOTE-001 Study. *J. Clin. Oncol.* 37 (28), 2518–2527. doi:10.1200/JCO.19.00934

Gogishvili, M., Melkadze, T., Makharadze, T., Giorgadze, D., Dvorkin, M., Penkov, K. D., et al. (2021). LBA51 EMPOWER-Lung 3: Cemiplimab in Combination with Platinum Doublet Chemotherapy for First-Line (1L) Treatment of Advanced Non-small Cell Lung Cancer (NSCLC). *Ann. Oncol.* 32 (Suppl. 5S1328), 0923–7534. doi:10.1016/j.annonc.2021.08.2130

Hellmann, M. D., Paz-Ares, L., Bernabe Caro, R., Zurawski, B., Kim, S.-W., Carcereny Costa, E., et al. (2019). Nivolumab Plus Ipilimumab in Advanced Non-small-cell Lung Cancer. *N. Engl. J. Med.* 381, 2020–2031. doi:10.1056/NEJMoa1910231

Herbst, R. S., Giaccone, G., de Marinis, F., Reinmuth, N., Vergnenegre, A., Barrios, C. H., et al. (2020). Atezolizumab for First-Line Treatment of PD-L1–Selected Patients with NSCLC. *N. Engl. J. Med.* 383, 1328–1339. doi:10.1056/NEJMoa1917346

Herbst, R. S., Baas, P., Kim, D. W., Felip, E., Pérez-Gracia, J. L., Han, J. Y., et al. (2016). Pembrolizumab versus Docetaxel for Previously Treated, PD-L1-Positive, Advanced Non-small-cell Lung Cancer (KEYNOTE-010): a Randomised Controlled Trial. *Lancet* 387, 1540–1550. doi:10.1016/S0140-6736(15)01281-7

Horn, L., Spigel, D. R., Vokes, E. E., Holgado, E., Ready, N., Steins, M., et al. (2017). Nivolumab versus Docetaxel in Previously Treated Patients with Advanced Non-small-cell Lung Cancer: Two-Year Outcomes from Two Randomized, Open-Label, Phase III Trials (CheckMate 017 and CheckMate 057). *J. Clin. Oncol.* 35, 353924–353933. doi:10.1200/JCO.2017.74.3062

Huang, M-Y., Jiang, X-M., Wang, B-L., Sun, Y., and Lu, J-J. (2021). Combination Therapy with PD-1/pd-L1 Blockade in Non-small Cell Lung Cancer: Strategies and Mechanisms. *Pharmacol. Ther.* 219 (2021). 107694. doi:10.1016/j.pharmthera.2020.107694

IARC Global Cancer Observatory, World Health ORganizations. Available: https://gco.iarc.fr/.

Ishida, Y., Agata, Y., Shibahara, K., and Honjo, T. Induced Expression of PD-1, a Novel Member of the Immunoglobulin Gene Superfamily, upon Programmed Cell Death,a Novel Member of the Immunoglobulin Gene Superfamily,upon Programmed Cell Death [J]. *EMBO J.*, 1992, 11(11):3887–3895.doi:10.1002/j.1460-2075.1992.tb05481.x

Jotte, R., Cappuzzo, F., Vynnychenko, I., Stroyakovskiy, D., Rodríguez-Abreu, D., Hussein, M., et al. (2020). Atezolizumab in Combination with Carboplatin and Nab-Paclitaxel in Advanced Squamous NSCLC (IMpower131): Results from a Randomized Phase III Trial. *J. Thorac. Oncol.* 15 (8), 1351–1360. doi:10.1016/j.jtho.2020.03.028

Kong, E. K., Prokunina-Olsson, L., Wong, W. H., Lau, C. S., Chan, T. M., Alarcón-Riquelme, M., et al. (2005). A New Haplotype of PDCD1 Is Associated with Rheumatoid Arthritis in Hong Kong Chinese. *Arthritis Rheum.* 52, 1058–1062. doi:10.1002/art.20966

Kroner, A., Mehling, M., Hemmer, B., Rieckmann, P., Toyka, K. V., Mäurer, M., et al. (2005). A PD-1 Polymorphism Is Associated with Disease Progression in Multiple Sclerosis. *Ann. Neurol.* 58, 50–57. doi:10.1002/ana.20514

Langer, C. J., Gadgeel, S. M., Borghaei, H., Papadimitrakopoulou, V. A., Patnaik, A., Powell, S. F., et al. (2016). Carboplatin and Pemetrexed with or without Pembrolizumab for Advanced, Non-squamous Non-small-cell Lung Cancer: A Randomised, Phase 2 Cohort of the Open-Label KEYNOTE-021 Study. *Lancet Oncol.* 17, 1497–1508. doi:10.1016/S1470-2045(16)30498-3

Li, X., Lian, Z., Wang, S., Xing, L., and Yu, J. Interactions between EGFR and PD-1/pd-L1 Pathway:implications for Treatment of NSCLC [J]. *Cancer Lett.*, 2018. 418:1–9.doi:10.1016/j.canlet.2018.01.005

Li, X., Lian, Z., Wang, S., Xing, L., and Yu, J. Interactions between EGFR and PD-1/pd-L1 Pathway:implications for Treatment of NSCLC [J]. *Cancer Lett.*, 2018. 418:1–9.doi:10.1016/j.canlet.2018.01.005

Mok, T. S., Wu, Y., Kudaba, I., Kowalski, D. M., Cho, B. C., and Turna, H. Z. (2019). Final Analysis of the Phase 3 KEYNOTE-042 Study: Pembrolizumab (Pembro) versus Platinum-Based Chemotherapy (Chemo) as First-Line Therapy for Patients (Pts) with PD-L1-Positive

Local`y Advanced/metastatic NSCLC. *Ann. Oncol.* 30 (Suppl. 2), ii38–ii68. doi:10.1093/annonc/mdz063

Moreno, V., Gil-Martin, M., Johnson, M., Aljumaily, R., Lopez-Criado, M. P., Northfelt, D., et al. (2018). MA04.01 Cemiplimab, a Human Monoclonal Anti-PD-1, Alone or in Combination with Radiotherapy: Phase 1 NSCLC Expansion Cohorts. *J. Thorac. Oncol.* 13, 10. doi:10.1016/j.jtho.2018.08.340

Naidoo, J., Page, D. B., Li, B. T., Connell, L. C., Schindler, K., Lacouture, M. E., et al. (2015). Toxicities of the Anti-PD-1 and Anti-PD-L1 Immune Checkpoint Antibodies. *Ann. Oncol.* 26, 2375–2391. doi:10.1093/annonc/mdv383

NasserAltorki, K., McGraw, T. E., Borczuk, A. C., Saxena, A., Port, J. L., BrendonStiles, M. B. E. Lee., et al. (2021). Neoadjuvant Durvalumab with or without Stereotactic Body Radiotherapy in Patients with Early-Stage Non-small-cell Lung Cancer: a Single-Centre, Randomised Phase 2 Trial. *Lancet Oncol.* 22 (6), 824–835. doi:10.1016/S1470-2045(21)00149-2

Nishio, M., Barlesi, F., West, H., Ball, S., Bordoni, R., Cobo, M., et al. (2021). Sanborn, Zsuzsanna Szalai, Grigoriy Ursol, Diana Mendus, Lijia Wang, Xiaohui Wen, Mark McCleland, Tien Hoang, See Phan, Mark A. Socinski, Atezolizumab Plus Chemotherapy for First-Line Treatment of Nonsquamous NSCLC: Results from the Randomized Phase 3 IMpower132 Trial. *J. Thorac. Oncol.* 16 (4), 653–664. doi:10.1016/j.jtho.2020.11.025

Papadopoulos, K. P., Johnson, M. L., Lockhart, A. C., Moore, K., Falchook, G. S., and Formenti, S. C. (2020). First-in-human Study of Cemiplimab Alone or in Combination with Radiotherapy And/or Low-Dose Cyclophosphamide in Patients with Advanced Malignancies. *Clin. Cancer Res.* 26 (5), 1025–1033. doi:10.1158/1078-0432.CCR-19-2609

Paz-Ares, L., Ciuleanu, T. E., Cobo, M., Schenker, M., Zurawski, B., Menezes, J., et al. (2021). First-line Nivolumab Plus Ipilimumab Combined with Two Cycles of Chemotherapy in Patients with Non-small-cell Lung Cancer (CheckMate 9LA): an International, Randomised, Open-Label, Phase 3 Trial. *Lancet Oncol.* 22 (2), 198–211. ISSN 1470-2045. doi:10.1016/S1470-2045(20)30641-0

Paz-Ares, L., Vicente, D., Tafreshi, A., Robinson, A., Soto Parra, H., Mazières, J., et al. (2020). A Randomized, Placebo-Controlled Trial of Pembrolizumab Plus Chemotherapy in Patients with Metastatic Squamous NSCLC: Protocol-Specified Final Analysis of KEYNOTE-407. *J. Thorac. Oncol.* 15, 1657–1669. doi:10.1016/j.jtho.2020.06.015

Peters, S., Scott, G., Melissa, L., Johnson, P. A. J., Garassino, M. C., and Christoph, D. (2017). Phase II Trial of Atezolizumab as First-Line or Subsequent Therapy for Patients with Programmed Death-Ligand 1–Selected Advanced Non–small-cell Lung Cancer (BIRCH). *J. Clin. Oncol.* 35 (24), 2781–2789. doi:10.1200/JCO.2016.71.9476

Prokunina, L., Castillejo-López, C., Oberg, F., Gunnarsson, I., Berg, L., Magnusson, V., et al. (2002). A Regulatory Polymorphism in PDCD1 Is Associated with Susceptibility to Systemic Lupus Erythematosus in Humans. *Nat. Genet.* 32, 666–669. doi:10.1038/ng1020

Ribas, A. (2015). Adaptive Immune Resistance: How Cancer Protects from Immune Attack. *Cancer Discov.* 5 (9), 915–919. doi:10.1158/2159-8290.CD-15-0563

Ribas, A., and Wolchok, J. D. (2018). Cancer Immunotherapy Using Checkpoint Blockade. *Science* 359 (6382), 1350–1355. doi:10.1126/science.aar4060

Rizvi, N., Lee, S., Curtis, P., Caldwell, W., Gao, B., and Rietschel, P. (2018). EMPOWER-lung 2: Cemiplimab and Ipilimumab ± Chemotherapy vs Pembrolizumab in Advanced NSCLC with PD-L1 ≥50%, a Phase 3 Study. *J. Thorac. Oncol.* 13 (Suppl. ment), 10S931. doi:10.1016/j.jtho.2018.08.1731

Rosell, R., and Karachaliou, N. (2016). Large-scale Screening for Somatic Mutations in Lung Cancer. *Lancet* 387, 1354–1356. doi:10.1016/S0140-6736(15)01125-3

Sezer, A., Kilickap, S., Mahmut, G., Bondarenko, I., Özgüroğlu, M., Miranda, G., et al. (2021). Cemiplimab Monotherapy for First-Line Treatment of Advanced Non-small-cell Lung Cancer with PD-L1 of at Least 50%: a Multicentre, Open-Label, Global, Phase 3, Randomised, Controlled Trial. *Lancet* 397, 10274592–10274604. doi:10.1016/S0140-6736(21)00228-2

Shim, B. Y., Lee, S., de Castro Carpeño, J., Chiu, C-H., Cobo, M., Kim, H. R., et al. (2020). 1269P EMPOWER-Lung 4: Phase II, Randomized, Open-Label High Dose or Standard Dose Cemiplimab Alone/plus Ipilimumab in the Second-Line Treatment of Advanced Non-small Cell Lung Cancer (NSCLC). *Ann. Oncol.* 31 (Suppl. 4), 2020. Page S820, ISSN 0923-7534. doi:10.1016/j.annonc.2020.08.1583

Socinski, M. A., Jotte, R. M., Cappuzzo, F., Orlandi, F., Stroyakovskiy, D., Nogami, N., et al. (2018). Fabrice Barlesi, Gene Finley, Claudia Kelsch, Anthony Lee, Shelley Coleman, Yu Deng, Yijing Shen, Marcin Kowanetz, Ariel Lopez-Chavez, Alan Sandler, Martin Reck. For the IMpower150 Study Group*Atezolizumab for First-Line Treatment of Metastatic Nonsquamous NSCLC. *N. Engl. J. Med.* 378, 2288–2301. doi:10.1056/NEJMoa1716948

Song, R., Zang, A., and Jia, Y.. Research Progress on the Regulation Mechanism of PD-L1 Expression [J]. *J. Pract. Med.*, 2020, 36(10):1286–1291.

Stewart, R., Morrow, M., Hammond, S. A., Mulgrew, K., Marcus, D., and Poon, E. (2015). Identification and Characterization of MEDI4736, an Antagonistic Anti-PD-L1 Monoclonal Antibody Cancer. *Immunol. Res.* 3, 1052–1062. doi:10.1158/2326-6066.CIR-14-0191

Sul, J., Blumenthal, G. M., Jiang, X., He, K., Keegan, P., and Pazdur, R. (2016). FDA Approval Summary: Pembrolizumab for the Treatment of Patients with Metastatic Non-small Cell Lung Cancer Whose Tumors Express Programmed Death-Ligand 1. *Oncologist* 21 (5), 643–650. doi:10.1634/theoncologist.2015-0498

Wang, J., Yoshida, T., Nakaki, F., Hiai, H., Okazaki, T., and Honjo, T. (2005). Establishment of NOD-Pdcd1-/- Mice as an Efficient Animal Model of Type I Diabetes. *Proc. Natl. Acad. Sci. U. S. A.* 102, 11823–11828. doi:10.1073/pnas.0505497102

Wang, P. F., Chen, Y., Song, S. Y., Wang, T. J., Ji, W. J., Li, S. W., et al. (2017). Immune-related Adverse Events Associated with Anti-PD-1/pd-L1 Treatment for Malignancies: A Meta-Analysis. *Front. Pharmacol.* 8, 730. doi:10.3389/fphar.2017.00730

Wu, Y. L., Lu, S., Cheng, Y., Zhou, C., Wang, J., Mok, T., et al. (2019). Nivolumab versus Docetaxel in a Predominantly Chinese Patient Population with Previously Treated Advanced NSCLC: CheckMate 078 Randomized Phase III Clinical Trial. *J. Thorac. Oncol.* 14 (5), 867–875. doi:10.1016/j.jtho.2019.01.006

Xu, C., Chen, Y. P., Du, X. J., Liu, J. Q., Huang, C. L., Chen, L., et al. (2018). Comparative Safety of Immune Checkpoint Inhibitors in Cancer: Systematic Review and Network Meta-Analysis. *Bmj* 363, k4226. doi:10.1136/bmj.k4226

Yearley, J. H., Gibson, C., Yu, N., Moon, C., Murphy, E., Juco, J., et al. PD-L2 Expression in Human Tumors: Relevance to Anti-PD-1 Therapy in Cancer: relevance to anti▪PD▪1 Therapy in Cancer [J]. *Clin. Cancer Res.*, 2017, 23(12):3158–3167.doi:10.1158/1078-0432.CCR-16-1761

Zucali, PA, Lin, CC, Carthon, BC, Bauer, TM, Tucci, M, Italiano, A, et al. Targeting CD38 and PD-1 With Isatuximab Plus Cemiplimab in Patients With Advanced Solid Malignancies: Results From a Phase I/II Open-Label, Multicenter Study. *J Immunother Cancer*, 2022, 10(1):e003697.doi:10.1136/jitc-2021-003697

Conflict of Interest: The authors declare that the research was conducted in the absence of any commercial or financial relationships that could be construed as a potential conflict of interest.

Publisher's Note: All claims expressed in this article are solely those of the authors and do not necessarily represent those of their affiliated organizations, or those of the publisher, the editors and the reviewers. Any product that may be evaluated in this article, or claim that may be made by its manufacturer, is not guaranteed or endorsed by the publisher.

Copyright © 2022 Li, Liao, Wang, Qi and Wang. This is an open-access article distributed under the terms of the Creative Commons Attribution License (CC BY). The use, distribution or reproduction in other forums is permitted, provided the original author(s) and the copyright owner(s) are credited and that the original publication in this journal is cited, in accordance with accepted academic practice. No use, distribution or reproduction is permitted which does not comply with these terms.

frontiers | Frontiers in Pharmacology

SYSTEMATIC REVIEW
published: 01 July 2022
doi: 10.3389/fphar.2022.940567

Chemotherapy Combined With Immunotherapy as a First-Line Treatment Brings Benefits to Patients With Lung Squamous Cell Carcinoma but Different Risks of Adverse Reactions: A Systematic Review and Meta-Analysis

Qian Chen[1], *Zhen Zhang*[1], *Xiaoli Li*[1] *and Lingbiao Bu*[2]*

[1]Department of Pharmacy, Beijing Gaobo Boren Hospital, Beijing, China, [2]Department of Anesthesiology, Zoucheng People's Hospital, Jining, China

OPEN ACCESS

Edited by:
Ting Wang,
Sichuan Cancer Hospital, China

Reviewed by:
Mingming Wu,
Harbin Medical University, China
Ziqi Ye,
Zhejiang University, China

***Correspondence:**
Lingbiao Bu
lingbiaobu@163.com

Specialty section:
This article was submitted to Pharmacology of Anti-Cancer Drugs, a section of the journal Frontiers in Pharmacology

Received: *10 May 2022*
Accepted: *26 May 2022*
Published: *01 July 2022*

Citation:
Chen Q, Zhang Z, Li X and Bu L (2022) Chemotherapy Combined With Immunotherapy as a First-Line Treatment Brings Benefits to Patients With Lung Squamous Cell Carcinoma but Different Risks of Adverse Reactions: A Systematic Review and Meta-Analysis. Front. Pharmacol. 13:940567. doi: 10.3389/fphar.2022.940567

Objective To explore the efficacy and safety of chemotherapy combined with immunotherapy as the first-line treatment of advanced or metastatic squamous NSCLC.

Methods Two researchers independently searched PubMed, the Cochrane Library, EMBASE, CNKI, Wanfang Data, and other databases by using a computer, collected the clinical trials or randomized controlled trials published by April 2022 about immunotherapy combined with chemotherapy as the first-line treatment of advanced or metastatic squamous NSCLC, screened the literature, and extracted the data according to the nanodischarge criteria. We used Revman5.4 for statistical analysis of the included studies, and publication bias was analyzed with Egger's test in Stata12.

Results A total of seven clinical trials were included, including 1,510 cases in the chemotherapy combined with the immunotherapy group and 1,519 cases in the chemotherapy group. In terms of effectiveness, compared with the chemotherapy group, chemotherapy combined with immunotherapy for advanced or metastatic squamous NSCLC had longer overall survival (HR = 1.59, 95% CI: 1.46–1.72, $p < 0.00001$) and progression-free survival (HR = 1.84, 95% CI: 1.66–2.03, $p < 0.00001$). In terms of safety, the chemotherapy combined with immunotherapy group has a higher risk of adverse reactions at any level and above three levels of hematotoxicity, gastrointestinal abnormalities, and liver dysfunction than the chemotherapy group. Egger's test has minor publication bias.

Conclusion Chemotherapy combined with immunotherapy is effective as the first-line treatment for advanced or metastatic squamous NSCLC, but the risk of adverse reactions is relatively high. If there are adverse reactions in clinical application, it should be treated in time.

Keywords: immunotherapy, chemotherapy, squamous NSCLC, overall survival, progression-free survival, security

Clinical Trial Registration: https://Systematicreview.gov/, identifier [registration number]

INTRODUCTION

At present, the mortality rate of lung cancer is still the highest among malignant cancers in China, and the 5-year survival rate is about 20.5% (Chen et al., 2016). Lung cancer is divided into non–small cell lung cancer and small cell lung cancer. Non–small cell lung cancer accounts for more than 85% of lung cancer cases. It is the most common lung cancer. It can be divided into adenocarcinoma and squamous cell carcinoma. Squamous non–small cell lung cancer (sq-NSCLC) accounts for about 30% of NSCLC cases. It is a very serious type of lung cancer with difficult treatment and poor prognosis. In the past 20 years, many effective treatment options have been limited to non-squamous NSCLC. There are serious unmet clinical needs for sq-NSCLC, and patients with advanced sq-NSCLC urgently need more new treatment options. Because the sensitivity of sq-NSCLC to chemotherapeutic drugs is significantly lower than that of adenocarcinoma non–small cell lung cancer, some NSCLC treatment schemes (including new targeted oncogene drugs, chemotherapeutic drugs, and anti-angiogenesis therapy) have limitations in the effectiveness or safety of sq-NSCLC (American Association for Cancer Research, 2016). Therefore, at present, the first-line treatment used by the vast majority of sq-NSCLC patients is still the combined chemotherapy containing platinum drugs. However, with continuous maturity of gene detection technology, gene-targeted therapy and immunotherapy have been applied in clinics (Rossi and Di Maio, 2016).

Tumor immunotherapy is to control and kill tumor cells by mobilizing the function of the body's immune system and enhancing antitumor immunity. It is the most effective antitumor treatment after surgery, radiotherapy, chemotherapy, and targeted therapy (Seelige et al., 2018). In recent years, immune checkpoint inhibitors such as PD1/PD-L1 have become a research hotspot of immunotherapy, and they have also achieved a breakthrough in clinical treatment. At present, drugs such as sintilimab, tisliezumab, pembrolizumab, and camrelizumab combined with conventional chemotherapy in the treatment of sq-NSCLC have achieved excellent performance, but there is a lack of systematic evaluation of its clinical effect and safety. This study systematically reviewed several drugs commonly used in sq-NSCLC immunotherapy, evaluated the efficacy and safety of chemotherapy combined with immunotherapy as the first-line treatment of advanced or metastatic squamous NSCLC, and provided the basis for clinical treatment.

MATERIALS AND METHODS

We systematically searched for global clinical trials or RCTs of chemotherapy combined with immunotherapy as the first-line treatment of advanced or metastatic squamous NSCLC and systematically evaluated its efficacy and safety.

Inclusion criteria: 1) included population: patients with advanced or metastatic sq-NSCLC who received chemotherapy combined with immunotherapy; 2) literature: retrospective study and prospective study; 3) intervention measures: the treatment group was given chemotherapy combined with immunotherapy (platinum combined with paclitaxel, platinum combined with protein-bound paclitaxel, platinum combined with gemcitabine, and other conventional first-line chemotherapy drugs), and the control group was given placebo combined with chemotherapy or conventional chemotherapy; 4) OUTCOME MEASURES: the main outcome measures included progression-free survival (PFS) and overall survival (OS)–related hazard ratio (HRS) and 95% confidence interval (95% CI). Secondary outcome measures included adverse reactions at any level (hematotoxicity, gastrointestinal abnormalities, and liver dysfunction) and adverse reactions above level 3 (hematotoxicity, gastrointestinal abnormalities, and liver dysfunction).

Exclusion criteria: 1) no control group was established; 2) repeatability study; 3) non-Chinese and English literature; 4) HR literature for PFS and/or OS were not provided.

Literature Screening and Data Extraction

We used a variety of search tools to conduct a comprehensive search of the literature. 1) Retrieval of the computer literature database: ① key words include immunotherapy, sintilimab, tisliezumab, pembrolizumab, camrelizumab, sq-NSCLC, programmed cell death protein 1, programmed cell death protein ligand 1, clinical trials, RCTs, etc.,② Search PubMed, Cochrane Library, EMBASE, and CNKI in the form of keyword joint free words. Wanfang database, etc., the retrieval time limit is from the establishment of the database to April 2022. 2) manual retrieval of ASCO conference-related literature as a supplement to computer retrieval.

The extracted data mainly include the following: author's name, publication year, patient sample size, treatment methods, HRs, and 95% CI of PFS and OS.

Bias Risk Assessment

The Newcastle Ottawa scale (NOS) was used to evaluate the literature quality (Lazarus et al., 2019), and the quality of the included studies was evaluated according to the following eight criteria: 1) the representativeness of the exposure cohort; 2) selection of non-exposed cohorts; 3) determination of exposure methods; 4) there were no outcome events before the start of the study; 5) comparability between exposed and non-exposed cohorts; 6) evaluation of outcome events; 7) whether the follow-up time is long enough; 8) whether the follow-up is complete. Literature with a score of 7–9 is considered "high," 4–6 is "average," and 3 or lower is "low". The quality evaluation shall be carried out independently and cross-checked by two researchers. In case of differences, the third researcher should help solve them.

Statistical Analysis

We used Revman 5.4 software provided by the Cochrane Collaboration Network for meta-analysis. All HRs included in the study were brought together to provide the overall effect

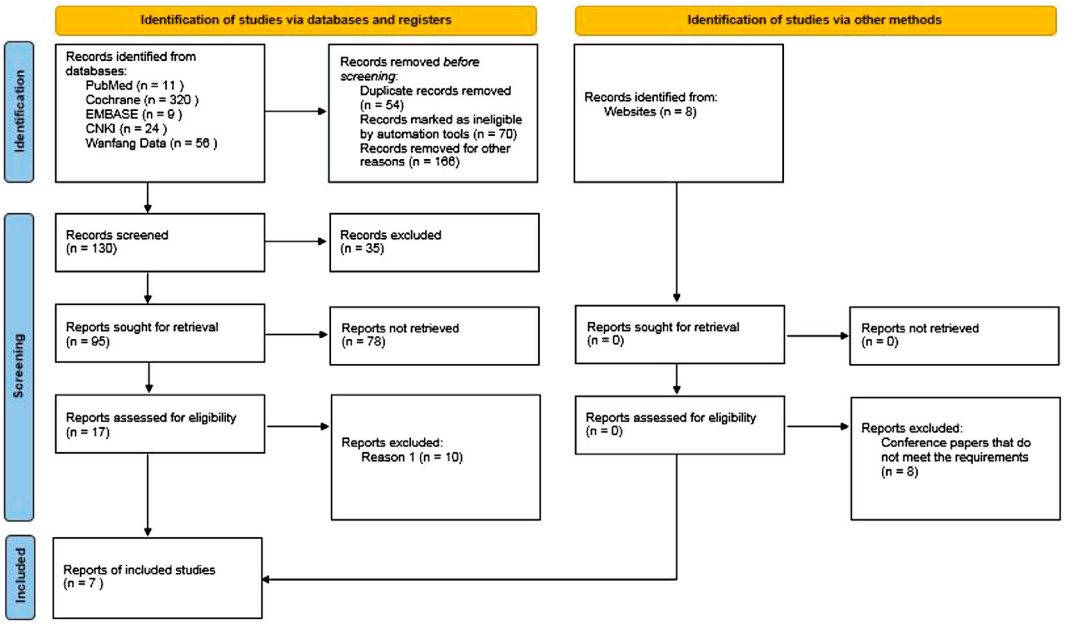

FIGURE 1 | PRISMA flow chart of article selection.

size. The Cochrane χ^2 test was used to analyze the heterogeneity among studies, and I^2 was used to evaluate the heterogeneity. When $p > 0.1$ and $I^2 < 50\%$, it indicates that there is no statistical heterogeneity in each RCTs, and the fixed-effect model is used; on the contrary, on the premise of excluding clinical heterogeneity, the random-effect model is used. The publication bias was analyzed by an inverted funnel diagram, the sensitivity of each included literature was analyzed, and the test bias of the included literature was discussed.

RESULTS

Literature Search and Screening

Through database retrieval, there were 11 literatures in PubMed, 320 literature in the Cochrane Library, nine literatures in EMBASE, 24 literatures in CNKI, and 56 literatures in Wanfang database, and a total of 420 relevant literatures and eight conference papers and abstracts were obtained. After excluding duplication, case reports, reviews and irrelevant contents, 130 literatures were screened in strict accordance with the abovementioned screening process, and finally seven (Halmos et al., 2018; Paz-Ares et al., 2018; Cheng et al., 2019; Paz-Ares et al., 2020; Wang et al., 2021; Zhou et al., 2021; Ren et al., 2022) studies were included, which met the quantitative analysis, as shown in **Figure 1**. A total of 3,029 cancer patients who met the requirements were included in the seven literatures, of which 1,510 patients received chemotherapy combined with immunotherapy and 1,519 patients received routine chemotherapy. All seven literatures are high-quality literatures, as shown in **Table 1**.

Meta-Analysis Results of Efficacy

The results of the OS analysis can be obtained from seven groups of data in the seven included studies. For heterogeneity analysis, $I^2 = 30\%$, $p = 0.20$. There is no statistical heterogeneity among the studies. The fixed-effect model is used for analysis. The results showed that HR = 1.59 (95% CI = 1.46–1.72, $p < 0.00001$), suggesting that chemotherapy combined with immunotherapy can significantly prolong the overall survival of patients in the treatment of sq-NSCLC, as shown in **Figure 2A**. PFS data were obtained from nine groups of data. Heterogeneity analysis showed that $I^2 = 28\%$, $p = 0.19$. There was no statistical heterogeneity among studies. A fixed-effect model was used for analysis. The results showed that HR = 1.84 (95% CI = 1.66–2.03, $p < 0.00001$), suggesting that immunotherapy combined with chemotherapy can significantly prolong the progression-free survival of patients in the treatment of sq-NSCLC, as shown in **Figure 2B**.

Meta-Analysis Results of Adverse Reactions at Any Level

Meta-Analysis Results of Hematological Toxin

Six studies can obtain the data of any level of adverse reactions in the blood system of sq-NSCLC patients treated with chemotherapy combined with immunotherapy (including anemia, white blood cell (WBC) discrete, neutrophil discrete, and platelet discrete). The heterogeneity analysis is carried out, with $I^2 = 35\%$, $p = 0.06$, which is analyzed by the fixed-effect model. The results showed that HR = 1.09 (95% CI = 1.05–1.13, $p < 0.00001$), suggesting that the incidence of adverse reactions at any level of the blood system using chemotherapy combined with immunotherapy is relatively high, and there are significant

TABLE 1 | Basic characteristics of included studies.

First author	Year	Phase	NO. of immune + chemo	NO. of chemo	Protocol of immune + chemo	Protocol of chemo	HR for PFS [95% CI]	*p*-Value for PFS	HR for OS [95% CI]	*p*-Value for OS	Quality
Caicun Zhou (Zhou et al., 2021)	2021	III	179	178	Sintilimab + PG	placebo + PG	0.536 [0.422.0.681]	<0.00001	0.567 [0.353.0.909]	0.01701	7
Jie Wang Wang et al. (2021)	2021	III	120	121	Tislelizumab + PC	PC	0.52 [0.37.0.74]	<0.001	NA	NA	8
	2021	III	119	121	Tislelizumab + nab-PC	nab-PC	0.48 [0.34.0.68]	<0.001	NA	NA	8
L. Paz-Ares Paz-Ares et al. (2018)	2018	III	278	281	Pembrolizumab + PC	placebo + PC	0.56 [0.45.0.70]	<0.001	0.64 [0.49.0.85]	<0.001	8
Luis Paz-Ares Paz-Ares et al. (2020)	2020	III	278	281	Pembrolizumab + PC	placebo + PC	0.57 [0.47.0.69]	<0.001	0.71 [0.58.0.88]	<0.001	7
Shengxiang Ren Ren et al. (2022)	2021	III	193	196	Camrelizumab + PC	placebo + PC	0.37 [0.29.0.47]	<0.0001	0.55 [0.40.0.75]	<0.0001	8
B. Halmos Halmos et al. (2018)	2018	III	169	167	Pembrolizumab + PC	placebo + PC	0.52 [0.40.0.68]	NA	0.67 [0.48.0.93]	NA	8
	2018	III	109	114	Pembrolizumab + nab-PC	placebo + nab-PC	0.65 [0.45.0.94]	NA	0.59 [0.36.0.98]	NA	7
Y. Cheng Cheng et al. (2019)	2019	III	65	60	Pembrolizumab + PC	placebo + PC	0.32 [0.21.0.49]	NA	0.44 [0.24.0.81]	NA	7

PFS, progression-free survival; OS, overall survival; HR, hazard ratio; NA, not available; PG, Platinum + Gemcitabine; PC, paclitaxel + carboplatin; nab, nanoparticlealbumin-bound.

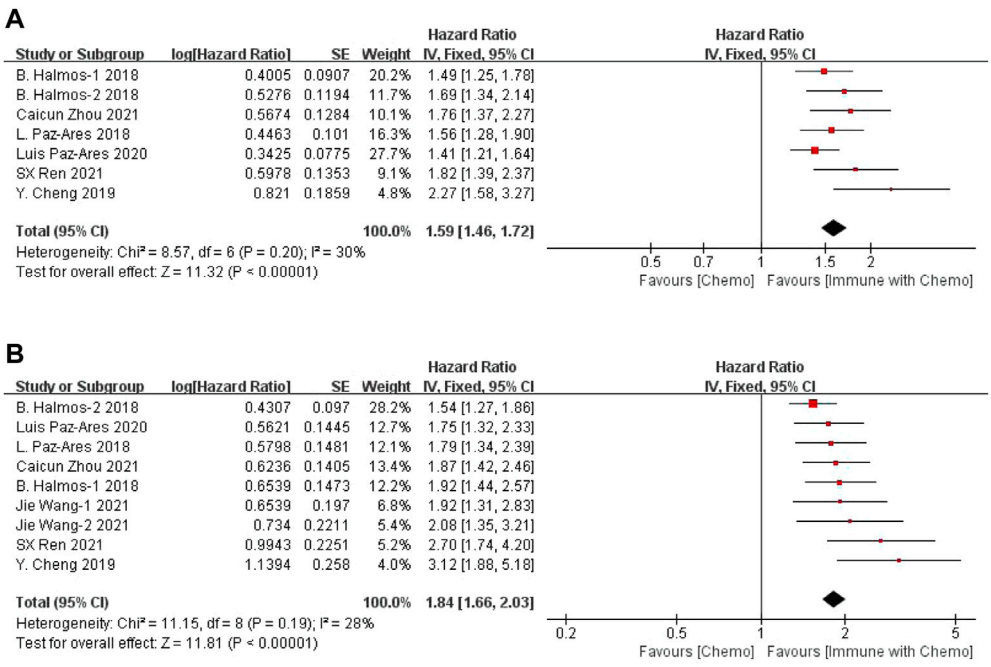

FIGURE 2 | Meta-analysis results of OS **(A)** and PFS **(B)** between the chemo with immune group and chemo group.

differences in individual results, as shown in **Figure 3**. In the subgroup analysis of this study, there was significant heterogeneity in thrombocytopenia indicators (I^2 = 67%). With factor by factor exclusion, Caicun Zhou (Zhou et al., 2021) and SX Ren (Ren et al., 2022) were found to be the sources of heterogeneity. The different medication regimens of the two experimental groups caused high heterogeneity, and I^2 was 0% after exclusion.

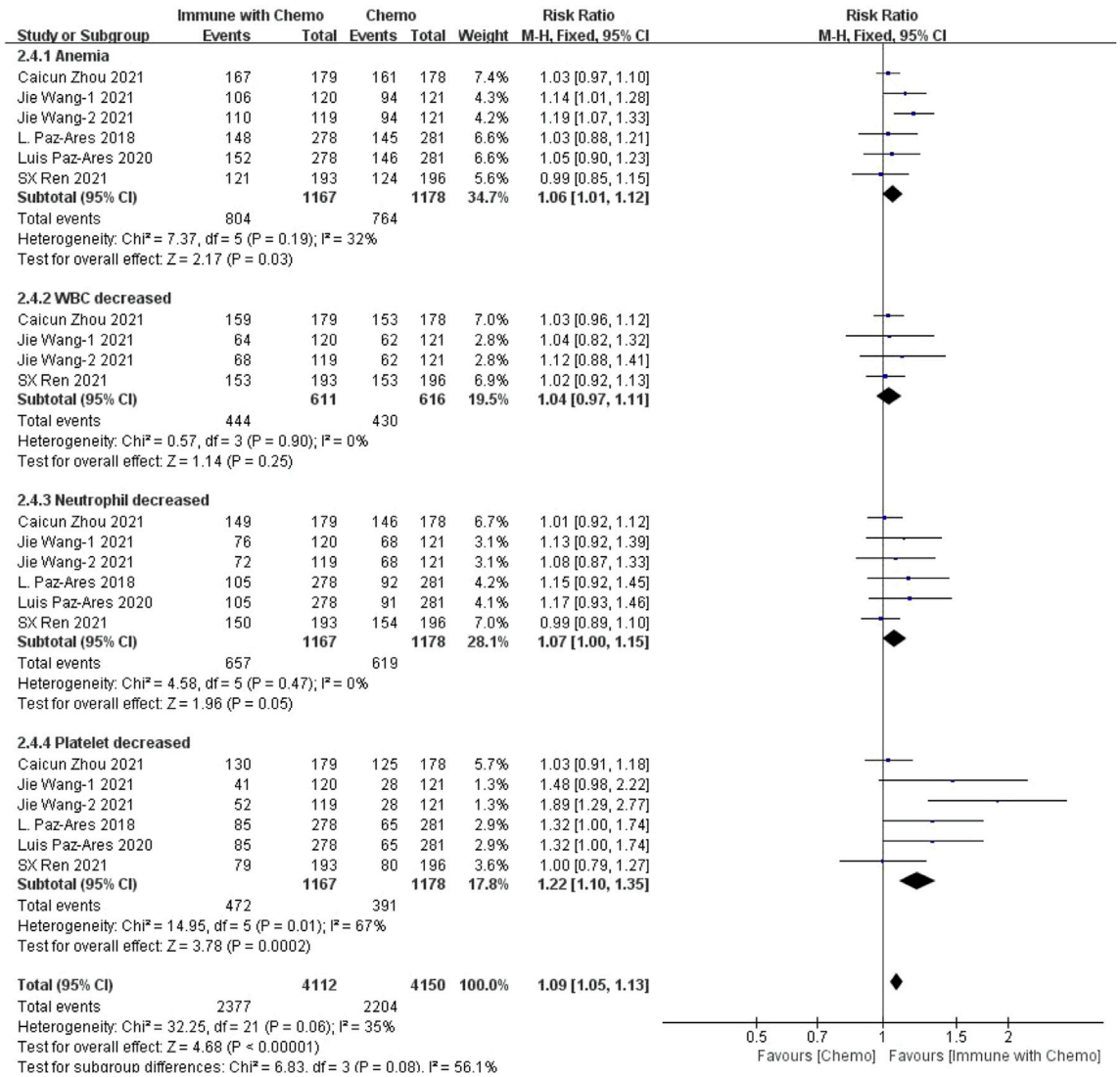

FIGURE 3 | Meta-analysis results of adverse reactions of any grade in hematological toxicity between the chemo with immune group and chemo group.

Meta-Analysis Results of Gastrointestinal Toxin

Six studies can obtain data on any level of adverse reactions in the gastrointestinal system in patients with sq-NSCLC treated by chemotherapy combined with immunotherapy (including nausea, vomiting, and appetite). The heterogeneity analysis is carried out, with I^2 = 19%, p = 0.22, which is analyzed by the fixed-effect model. The results showed that HR = 1.09 (95% CI = 1.01–1.18, p = 0.02), suggesting that the incidence of adverse reactions at any level of the gastrointestinal system caused by chemotherapy combined with immunotherapy is relatively high, but there is no significant difference in the overall results, as shown in **Figure 4**. In the subgroup analysis of this study, significant heterogeneity exists in the appetite indicator (I^2 = 52%). With factor by factor exclusion, L. Paz-Ares (Paz-Ares et al., 2018) and Luis Paz-ares (Paz-Ares et al., 2020) are the sources of heterogeneity. Compared with other studies, in both studies, adverse reactions to appetite were lower in combination with the immunochemotherapy regimen than in the control group, and I^2 heterogeneity was 6% after exclusion.

Meta Analysis Results of Hepatotoxicity

Four studies can obtain the data of any level of adverse reactions (including aspartate aminotransferase (AST) and alanine aminotransferase (ALT)) of liver function in patients with sq-NSCLC treated by chemotherapy combined with immunotherapy. The heterogeneity was analyzed, with I^2 = 70%, p = 0.002. The random-effect model is used for analysis. Four studies can obtain the data of any level of adverse reactions (including AST and ALT) of liver function in patients with sqnsclc treated by chemotherapy combined with

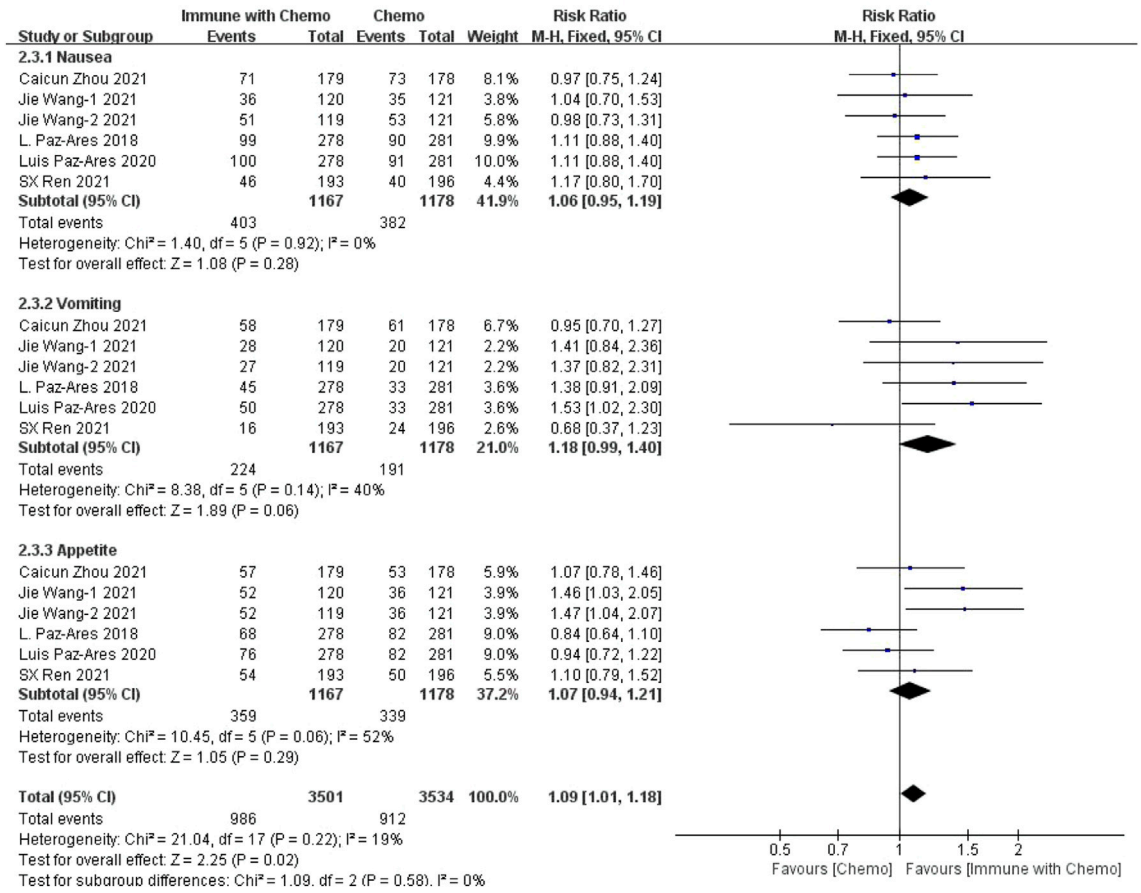

FIGURE 4 | Meta-analysis results of adverse reactions of any grade in gastrointestinal toxicity between the chemo with immune group and chemo group.

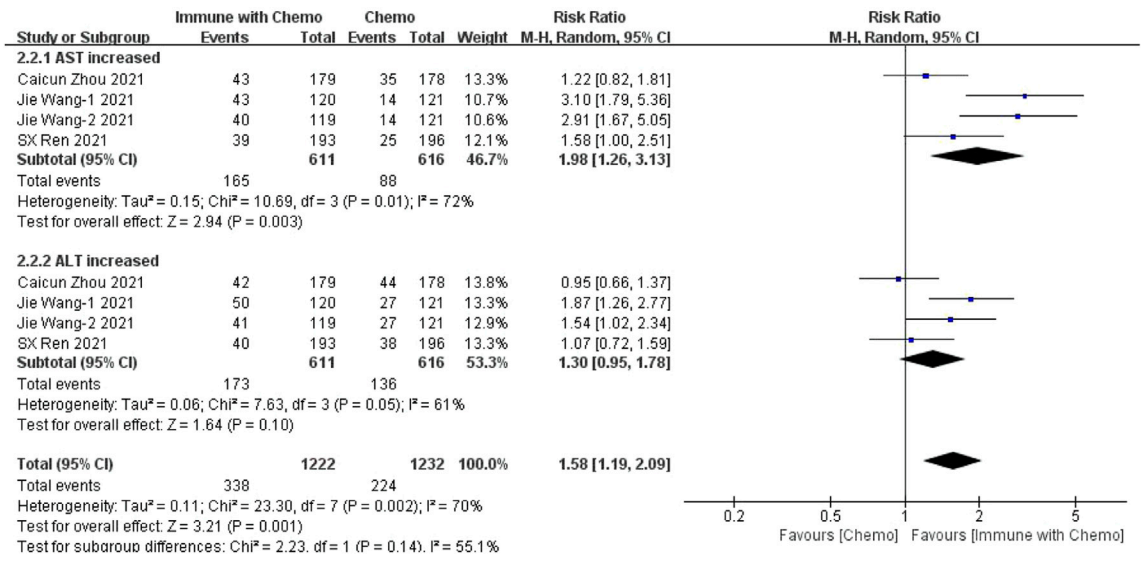

FIGURE 5 | Meta-analysis results of adverse reactions of any grade in hepatotoxicity between the chemo with immune group and chemo group.

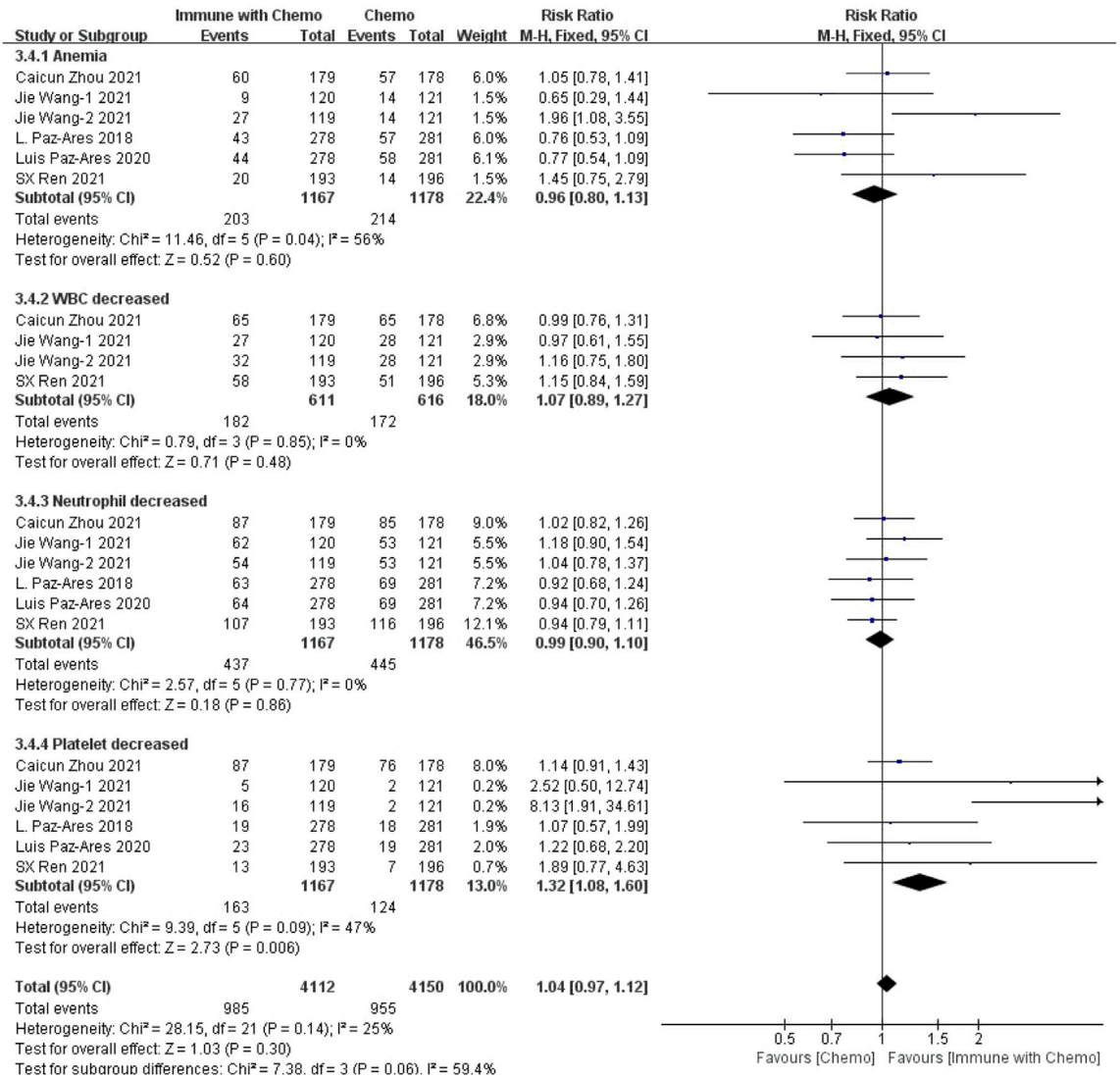

FIGURE 6 | Meta-analysis results of adverse reactions above grade 3 in hematological toxicity between the chemo with immune group and chemo group.

immunotherapy. The heterogeneity is analyzed, with I^2 = 70%, p = 0.002. The random-effect model is used for analysis. The results showed that HR = 1.58 (95% CI = 1.19–2.09, p = 0.001), suggesting that the incidence of adverse reactions at any level of liver function using chemotherapy combined with immunotherapy is relatively high, and there is a significant difference in the results, as shown in **Figure 5**. In the subgroup analysis of this study, there was significant heterogeneity in AST (I^2 = 72%) and ALT (I^2 = 61%) indexes. With factor by factor exclusion, Caicun Zhou (Zhou et al., 2021) and SX Ren (Ren et al., 2022) were found to be the sources of heterogeneity. In the two studies, different drug regimens in the experimental group caused high heterogeneity compared with other groups, and the heterogeneity I^2 of AST and ALT was 0% after exclusion.

Meta-Analysis Results of Adverse Reactions Above Grade 3

Meta-Analysis Results of Hematological Toxin

Six studies can obtain the data of hematological grade III or above adverse reactions (including anemia, WBC increase, neutrophil increase, and platelet increase) of patients with sq-NSCLC treated by chemotherapy combined with immunotherapy. The heterogeneity was analyzed with I^2 = 25%, p = 0.14, which was analyzed by the fixed-effect model. The results showed that HR = 1.04 (95% CI = 0.97–1.12, p = 0.30), suggesting that the incidence of adverse reactions above grade III in the blood system using chemotherapy combined with immunotherapy is relatively high, but there is no significant difference in the overall results, as shown in **Figure 6**. In the subgroup analysis of this study, there is significant heterogeneity

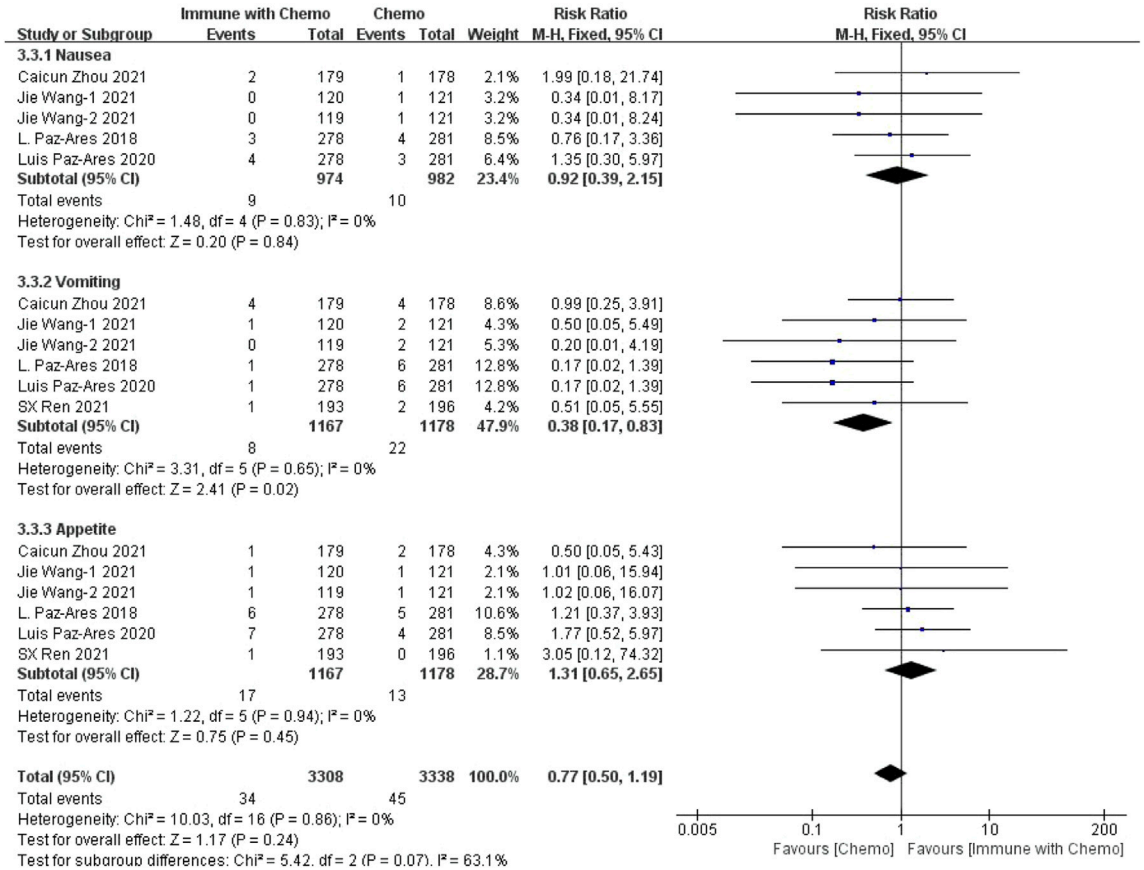

FIGURE 7 | Meta-analysis results of adverse reactions above grade 3 in gastrointestinal toxicity between the Chemo with immune group and chemo group.

in the Cia index (I^2 = 56%). Factor by factor elimination, Caicun Zhou (Zhou et al., 2021), SX Ren (Ren et al., 2022) and Jie Wang-2 (Wang et al., 2021) are the sources of heterogeneity. The immunization combined with chemotherapy in the three studies had a high indemnity compared with the control group. The heterogeneity I^2 was 0% after the exclusion.

Meta-Analysis Results of Gastrointestinal Toxin

Six studies can obtain data on gastrointestinal adverse reactions above grade III (including nausea, vomiting, and appetite) in patients with sq-NSCLC treated by chemotherapy combined with immunotherapy. The heterogeneity is analyzed, with I^2 = 0%, p = 0.86, which is analyzed by the fixed-effect model. The results showed that HR = 0.77 (95% CI = 0.50–1.19, p = 0.24), suggesting that the incidence of grade III and above adverse reactions in the digestive system using chemotherapy combined with immunotherapy is relatively high, but there is no significant difference in the overall results, as shown in **Figure 7**.

Meta-Analysis Results of Hepatotoxicity

Four studies can obtain the data of adverse reactions above grade III of liver function (including AST and ALT) in patients with sq-NSCLC treated by chemotherapy combined with immunotherapy. The heterogeneity is analyzed, with I^2 = 0%, p = 1.00, which is analyzed by the fixed-effect model. The results showed that HR = 4.18 (95% CI = 1.31–13.39, p = 0.02), suggesting that the incidence of adverse reactions at any level of liver function using immunotherapy combined with chemotherapy is relatively high, and there is a significant difference in the results, as shown in **Figure 8**.

Publication Bias Assessment and Sensitivity Analysis

Publication bias assessment was performed only in OS and PFS. The funnel plot is symmetrical, indicating no significant publication bias (**Figures 9A,B**). Sensitivity analysis was conducted on the results, and a meta-analysis was conducted by ignoring each study in turn. No significant changes were found in the results, indicating that the results of this study are stable. Quantitative analysis by Egger's test showed, Egger test in Stata12 software was used for publication bias test. In a total of nine studies with OS and PFS as outcome indicators, the results of the publication bias test indicated that there was minor publication bias in OS (p = 0.0032) and PFS (p = 0.0026), as shown in **Figures 9C,D**. The sources of publication bias in our analysis may be as follows: 1) the number of included studies in meta-analyses is small; 2)

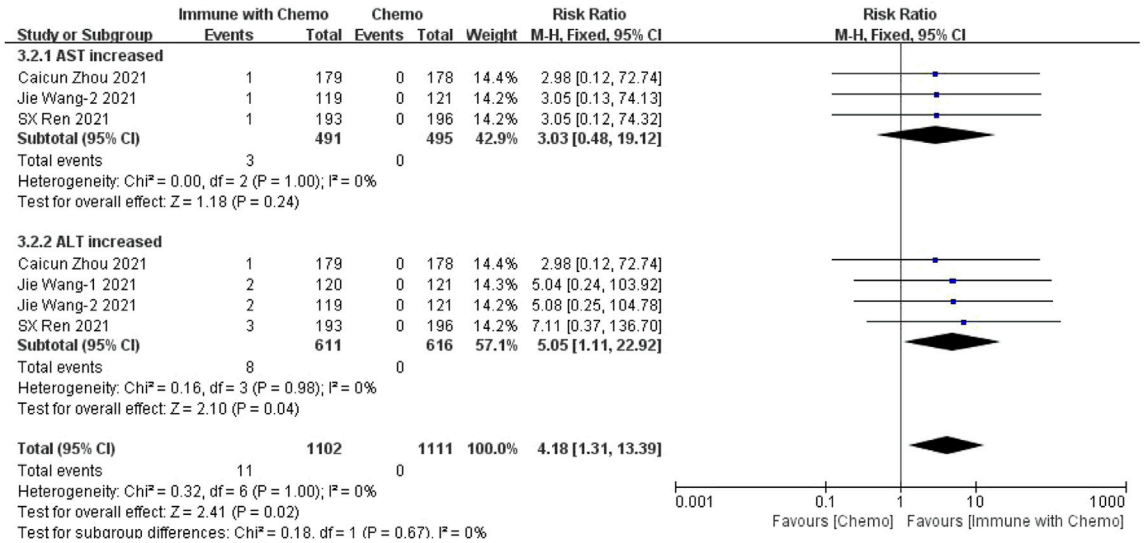

FIGURE 8 | Meta-analysis results of adverse reactions above grade 3 in hepatotoxicity between the Chemo with immune group and chemo group.

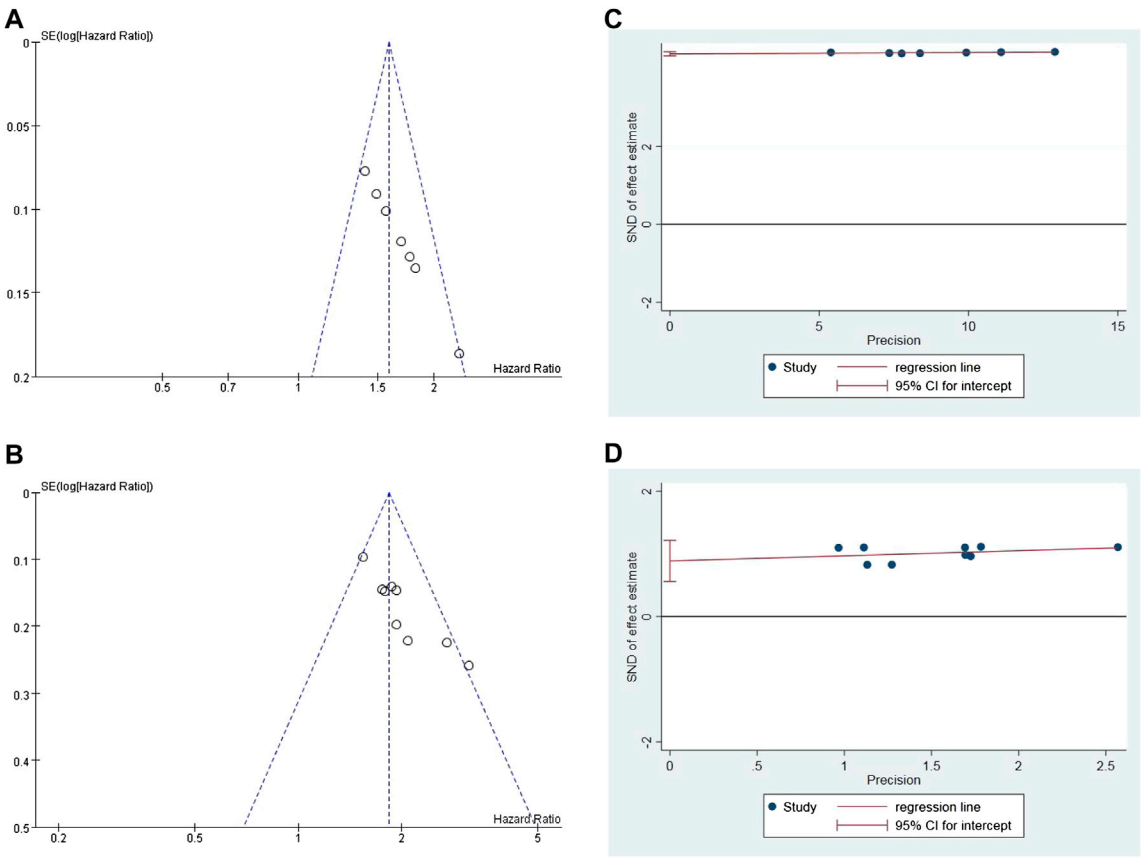

FIGURE 9 | Inverted funnel plot of OS **(A)** and PFS **(B)**. Egger test of OS **(C)** and PFS **(D)**.

the sample size was small; 3) there was heterogeneity in the analysis of individual subgroups; 4) the existence of intra-study publication bias; 5) the observation results of the same group of subjects were divided into multiple articles published by the authors, which may result in multiple publication bias of the subjects. We will continue to include more high-quality literature in the later stages to reduce publication bias.

DISCUSSION

In recent years, the treatment mode of lung cancer has changed greatly, and the prognosis has improved. The 5-year survival rate of Chinese lung cancer patients diagnosed from 2010 to 2014 has reached 20–30%. Worldwide, the survival rate of lung cancer patients has improved by 5–10% since 2000, while the survival rate of Chinese lung cancer patients has even improved by more than 10% (Allemani et al., 2018). More than 60% of lung adenocarcinomas can find driver genes (The Cancer Genome Atlas Research Network, 2014), including human epidermal growth factor receptor (EGFR), echinoderm microtubule associated protein like 4 (EML4)/anaplastic lymphoma kinase (ALK), and c-ros oncogene 1 receptor tyrosine kinase (ros1) gene fusion. Targeted drugs for the abovementioned targets are constantly updated. The survival rate of patients has significantly improved. However, for lung squamous cell carcinoma, although it accounts for 25–30% of all lung cancers (Houston et al., 2014), the incidence of common driver genes such as EGFR mutation and ALK gene rearrangement is very low, about 2.7 and 1.5–2.5%, respectively (Wang et al., 2014). Therefore, only a few patients with squamous cell carcinoma have the opportunity to receive EGFR tyrosine kinase inhibitor (EGFR-TKI) or ALK inhibitor treatment. The 5-year survival rate of lung squamous cell carcinoma was only 5%. Therefore, sq-NSCLC is a challenging disease with poor prognosis, including tumor location, more complications, and genetic complexity. At present, research shows that some treatment schemes, including new targeted oncogene drugs, chemotherapeutic drugs, and anti-angiogenesis therapy, have limitations in the effectiveness or safety of sq-NSCLC. Therefore, at present, the first-line treatment for the vast majority of sq-NSCLC patients is still platinum-containing combined chemotherapy. Clinical studies have investigated the efficacy and toxicity of cisplatin, carboplatin, and nedaplatin combined with paclitaxel in the treatment of advanced sq-NSCLC (Shukuya et al., 2015). The results showed that the efficiency of cisplatin or carboplatin combined with paclitaxel was significantly higher than that of nedaplatin combined with paclitaxel in the treatment of advanced lung squamous cell carcinoma. At the same time, according to NCCN guidelines, PD-1 inhibitor combined with chemotherapy is recommended as the first-line treatment for patients with advanced squamous NSCLC with PD-L1 > 1%, while PD-1 inhibitor alone is recommended for patients with PD-L1 > 50%. Reviewing that the expression of PD-L1 in the study population is mainly based on patients with less than 1% and more than 50%, only a small number of patients have PD-L1 expression of 1–49%. Therefore, this study does not conflict with NCCN guidelines and has certain clinical guiding significance.

At present, immunotherapy plays an excellent role in prolonging the overall survival and disease-free progression of NSCLC. PD-1/PD-L1 plays an important role in the immune escape of tumor cells. Its pathway exists in the normal immune system. PD-1 is inherently expressed on the surface of activated T lymphocytes, B lymphocytes, and natural killer cells. PD-L1, one of its ligands, is expressed on the surface of tumor cells and tumor-infiltrating immune cells. When PD-L1 is combined with PD-1, it can produce negative stimulation signals and inhibit the activation of T lymphocytes. As a result, T cells cannot engulf tumor cells, and tumor cells escape the monitoring of the immune system, that is, immune escape, which eventually leads to occurrence of tumors. Therefore, PD1/PD-L1 inhibitors activate T lymphocytes to achieve tumor inhibition. PD1/PD-L1 inhibitors commonly used in clinic include sintilimab, tisliezumab, pembrolizumab, camrelizumab, etc., Leena Gandhi et al. (Gandhi et al., 2018) showed that the overall survival rate of pembrolizumab combined with chemotherapy was 69.2% (95% CI, 64.1–73.8), while that of the placebo combined group was 49.4% (95% CI, 42.1–56.2) (HR = 0.49; 95% CI, 0.38–0.64; $p < 0.01$), and the median progression-free survival was 8.8 months (95% CI, 7.6–9.2), 4.9 months (95% CI, 4.7–5.5) in the placebo combination group (HR = 0.52; 95% CI, 0.43–0.64; $p < 0.001$). However, adverse events at level 3 or higher occurred in 67.2% of patients in the pembrolizumab-combined chemotherapy group and 65.8% in the placebo-combined treatment group. Shun Lu et al. (Lu et al., 2021) the open-label phase 3 trial (basic principle 304; nct03663205), patients with nsq-NSCLC were randomly divided into tiselizumab plus platinum (carboplatin or cisplatin) and pemetrexed. The control group was treated with platinum and pemetrexed alone. The results showed that the PFS of the tiselizumab combined chemotherapy group was significantly longer than that of the simple chemotherapy group (median PFS: 9.7 vs. 7.6 months; HR = 0.645 [95% Cl: 0.462–0.902], $p = 0.0044$). In addition, compared with chemotherapy alone, combination therapy has a higher remission rate and longer remission duration.

In this study, we evaluated the efficacy and safety of chemotherapy combined with immunotherapy as the first-line treatment for advanced or metastatic squamous NSCLC, with OS and PFS as the primary outcomes and adverse reactions as the secondary outcome. The disease was limited to the more difficult to cure sq-NSCLC. The results showed that, in terms of effectiveness, chemotherapy combined with immunotherapy improved the HR and p value of OS and PFS, indicating that patients receiving immunotherapy combined with chemotherapy had better OS and PFS than patients receiving ordinary chemotherapy. The results were similar to those of other clinical trials. However, in terms of safety, we have refined the adverse reactions into any level of adverse reactions and more than three levels of adverse reactions, mainly including hematotoxicity, hepatotoxicity, and gastrointestinal toxicity. The results showed that 1) in hematotoxicity, the risk ratio of any level of hematotoxicity in the immunotherapy combined with chemotherapy group was higher than that in the chemotherapy

group, and the results were significantly different ($p < 0.00001$). In subgroup analysis, there was a significant difference between anemia ($p = 0.03$) and decreased platelet count ($p = 0.0002$), but there was no significant difference between decreased leukocyte count ($p = 0.25$) and decreased neutrophils ($p = 0.05$). There was no significant difference in the incidence of hematotoxicity above grade 3 between the two groups ($p = 0.30$). 2) In hepatotoxicity, the risk ratio of any level of hepatotoxicity in the chemotherapy combined with immunotherapy group was higher than that in the chemotherapy group, and the results were significantly different ($p = 0.001$). Subgroup analysis showed that the increase of AST was more significant in the immune-combined chemotherapy group ($p = 0.003$), and there was no significant difference in ALT between the two groups ($p = 0.10$). For the incidence of hepatotoxicity above grade III, the increase in ALT was more significant in the immune-combined chemotherapy group ($p = 0.04$), and there was no significant difference in AST between the two groups ($p = 0.24$). 3) In gastrointestinal toxicity, the risk ratio of any level of gastrointestinal toxicity in the chemotherapy combined with the immunotherapy group was higher than that in the chemotherapy group, and the results were significantly different ($p = 0.02$). For the incidence of gastrointestinal toxicity above grade 3, there was no significant difference between the two groups ($p = 0.24$), but subgroup analysis showed that the incidence of gastrointestinal toxicity above grade 3 in the combined group was significantly higher and significant ($p = 0.02$). The abovementioned studies suggest that in clinical treatment, chemotherapy combined with immunotherapy as a first-line drug for sq-NSCLC is more effective than chemotherapy alone and can significantly prolong OS and PFS. At the same time, the incidence of adverse reactions is higher than that of chemotherapy. In clinical diagnosis and treatment, we should pay more attention to anemia, changes in platelet count, hepatotoxicity, and some conventional gastrointestinal adverse reactions to treat symptomatic treatment as soon as possible and reduce side effects.

This study also has some limitations: 1) after systematic retrieval and screening, only seven literatures were included for systematic evaluation and meta-analysis, and the sample size is too small; 2) the heterogeneity of individual statistical results may affect the credibility of the research results. This study will continue to update the clinical data and timely supplement the included literature so as to provide a scientific medication basis for the clinical treatment of sq-NSCLC.

DATA AVAILABILITY STATEMENT

The original contributions presented in the study are included in the article/Supplementary Material; further inquiries can be directed to the corresponding author.

AUTHOR CONTRIBUTIONS

The idea and topic of the manuscript were completed by QC. QC and ZZ searched the literature and analyzed the data. XL and LB sifted through the literature and extracted the data. The manuscript was written by QC and reviewed by LB. All the authors of this article have made great contributions to the manuscript.

REFERENCES

Allemani, C., Matsuda, T., Di Carlo, V., Harewood, R., Matz, M., Nikšić, M., et al. (2018). Global Surveillance of Trends in Cancer Survival 2000-14 (CONCORD-3): Analysis of Individual Records for 37 513 025 Patients Diagnosed with One of 18 Cancers from 322 Population-Based Registries in 71 Countries. *Lancet* 391, 1023–1075. doi:10.1016/S0140-6736(17)33326-3

American Association for Cancer Research. New Driver Mutations Detected in NSCLC, *Cancer Discov.*, 6 (2016) 809.doi:10.1158/2159-8290.CD-NB2016-074

Chen, W., Zheng, R., Baade, P. D., Zhang, S., Zeng, H., Bray, F., et al. (2016). Cancer Statistics in China, 2015. *CA Cancer J. Clin.* 66, 115–132. doi:10.3322/caac.21338

Cheng, Y., Zhang, L., Hu, J., Wang, D., Hu, C., Zhou, J., et al. (2019). Keynote-407 China Extension Study: Pembrolizumab (Pembro) Plus Chemotherapy in Chinese Patients with Metastatic Squamous NSCLC. *Ann. Oncol.* 30, ix201–ix202. doi:10.1093/annonc/mdz446.019

Gandhi, L., Rodríguez-Abreu, D., Gadgeel, S., Esteban, E., Felip, E., De Angelis, F., et al. (2018). Pembrolizumab Plus Chemotherapy in Metastatic Non-small-cell Lung Cancer. *N. Engl. J. Med.* 378, 2078–2092. doi:10.1056/NEJMoa1801005

Halmos, B., Luft, A., Majem, M., Hui, R., Corre, R., Gumus, M., et al. (2018). Choice of Taxane and Outcomes in the KEYNOTE-407 Study of Pembrolizumab Plus Chemotherapy for Metastatic Squamous NSCLC. *J. Thorac. Oncol.* 13, S391. doi:10.1016/j.jtho.2018.08.400

Houston, K. A., Henley, S. J., Li, J., White, M. C., and Richards, T. B. (2014). Patterns in Lung Cancer Incidence Rates and Trends by Histologic Type in the United States, 2004-2009. *Lung Cancer* 86, 22–28. doi:10.1016/j.lungcan.2014.08.001

Lazarus, G., Audrey, J., and Iskandar, A. W. B. (2019). Efficacy and Safety Profiles of Programmed Cell Death-1/programmed Cell Death Ligand-1 Inhibitors in the Treatment of Triple-Negative Breast Cancer: A Comprehensive Systematic Review. *Oncol. Rev.* 13, 425. doi:10.4081/oncol.2019.425

Lu, S., Wang, J., Yu, Y., Yu, X., Hu, Y., Ai, X., et al. (2021). Tislelizumab Plus Chemotherapy as First-Line Treatment for Locally Advanced or Metastatic Nonsquamous NSCLC (RATIONALE 304): A Randomized Phase 3 Trial. *J. Thorac. Oncol.* 16, 1512–1522. doi:10.1016/j.jtho.2021.05.005

Paz-Ares, L., Luft, A., Vicente, D., Tafreshi, A., Gümüş, M., Mazières, J., et al. (2018). Pembrolizumab Plus Chemotherapy for Squamous Non-small-cell Lung Cancer. *N. Engl. J. Med.* 379, 2040–2051. doi:10.1056/NEJMoa1810865

Paz-Ares, L., Vicente, D., Tafreshi, A., Robinson, A., Soto Parra, H., Mazières, J., et al. (2020). A Randomized, Placebo-Controlled Trial of Pembrolizumab Plus Chemotherapy in Patients with Metastatic Squamous NSCLC: Protocol-Specified Final Analysis of KEYNOTE-407. *J. Thorac. Oncol.* 15, 1657–1669. doi:10.1016/j.jtho.2020.06.015

Ren, S., Chen, J., Xu, X., Jiang, T., Cheng, Y., Chen, G., et al. (2022). Camrelizumab Plus Carboplatin and Paclitaxel as First-Line Treatment for Advanced Squamous NSCLC (CameL-Sq): A Phase 3 Trial. *J. Thorac. Oncol.* 17, 544–557. doi:10.1016/j.jtho.2021.11.018

Rossi, A., and Di Maio, M. (2016). Platinum-based Chemotherapy in Advanced Non-small-cell Lung Cancer: Optimal Number of Treatment Cycles. *Expert Rev. Anticancer Ther.* 16, 653–660. doi:10.1586/14737140.2016.1170596

Seelige, R., Searles, S., and Bui, J. D. (2018). Mechanisms Regulating Immune Surveillance of Cellular Stress in Cancer. *Cell Mol. Life Sci.* 75, 225–240. doi:10.1007/s00018-017-2597-7

Shukuya, T., Yamanaka, T., Seto, T., Daga, H., Goto, K., Saka, H., et al. (2015). Nedaplatin Plus Docetaxel versus Cisplatin Plus Docetaxel for Advanced or Relapsed Squamous Cell Carcinoma of the Lung (WJOG5208L): a Randomised,

Open-Label, Phase 3 Trial. *Lancet Oncol.* 16, 1630–1638. doi:10.1016/S1470-2045(15)00305-8

The Cancer Genome Atlas Research Network (2014). Comprehensive Molecular Profiling of Lung Adenocarcinoma. *Nature* 511, 543–550. doi:10.1038/nature13385

Wang, J., Shen, Q., Shi, Q., Yu, B., Wang, X., Cheng, K., et al. (2014). Detection of ALK Protein Expression in Lung Squamous Cell Carcinomas by Immunohistochemistry. *J. Exp. Clin. Cancer Res.* 33, 109. doi:10.1186/s13046-014-0109-2

Wang, J., Lu, S., Yu, X., Hu, Y., Sun, Y., Wang, Z., et al. (2021). Tislelizumab Plus Chemotherapy vs Chemotherapy Alone as First-Line Treatment for Advanced Squamous Non-small-cell Lung Cancer. *JAMA Oncol.* 7, 709–717. doi:10.1001/jamaoncol.2021.0366

Zhou, C., Wu, L., Fan, Y., Wang, Z., Liu, L., Chen, G., et al. (2021). Sintilimab Plus Platinum and Gemcitabine as First-Line Treatment for Advanced or Metastatic Squamous NSCLC: Results from a Randomized, Double-Blind, Phase 3 Trial (ORIENT-12). *J. Thorac. Oncol.* 16, 1501–1511. doi:10.1016/j.jtho.2021.04.011

Conflict of Interest: The authors declare that the research was conducted in the absence of any commercial or financial relationships that could be construed as a potential conflict of interest.

Publisher's Note: All claims expressed in this article are solely those of the authors and do not necessarily represent those of their affiliated organizations, or those of the publisher, the editors, and the reviewers. Any product that may be evaluated in this article, or claim that may be made by its manufacturer, is not guaranteed or endorsed by the publisher.

Copyright © 2022 Chen, Zhang, Li and Bu. This is an open-access article distributed under the terms of the Creative Commons Attribution License (CC BY). The use, distribution or reproduction in other forums is permitted, provided the original author(s) and the copyright owner(s) are credited and that the original publication in this journal is cited, in accordance with accepted academic practice. No use, distribution or reproduction is permitted which does not comply with these terms.

frontiers | Frontiers in Pharmacology

ORIGINAL RESEARCH
published: 04 July 2022
doi: 10.3389/fphar.2022.935500

Clinical Significance of Serum Haptoglobin and Protein Disulfide-Isomerase A3 in the Screening, Diagnosis, and Staging of Colorectal Cancer

Yajin Niu[1†], Jun Xue[2], Xueliang Wu[2†], Ming Qu[2], Likun Wang[2], Weizheng Liang[3] and Tian Li[4*]*

[1]Graduate School, Hebei North University, Zhangjiakou, China, [2]Department of General Surgery, The First Affiliated Hospital of Hebei North University, Zhangjiakou, China, [3]Central Laboratory, The First Affiliated Hospital of Hebei North University, Zhangjiakou, China, [4]School of Basic Medicine, Fourth Military Medical University, Xi'an, China

OPEN ACCESS

Edited by:
Hongtao Xiao,
University of Electronic Science and Technology of China, China

Reviewed by:
Botao Wang,
Tianjin Medical University, China
Chao Wang,
Peking University People's Hospital, China

***Correspondence:**
Jun Xue
xuejun@hebeinu.edu.cn
Tian Li
fmmult@foxmail.com

[†]These authors have contributed equally to this work

Specialty section:
This article was submitted to Pharmacology of Anti-Cancer Drugs, a section of the journal Frontiers in Pharmacology

Received: 04 May 2022
Accepted: 06 June 2022
Published: 04 July 2022

Citation:
Niu Y, Xue J, Wu X, Qu M, Wang L, Liang W and Li T (2022) Clinical Significance of Serum Haptoglobin and Protein Disulfide-Isomerase A3 in the Screening, Diagnosis, and Staging of Colorectal Cancer. Front. Pharmacol. 13:935500. doi: 10.3389/fphar.2022.935500

Objective: This study aims to explore the clinical significance of haptoglobin (HP) and protein disulfide-isomerase A3 (PDIA3) in human serum in the screening, diagnosis and staging of colorectal cancer (CRC), and to provide novel screening approaches featuring high specificity, sensitivity, and accuracy for early screening and diagnosis of clinical colorectal cancer.

Methods: 88, 77, and 36 blood specimens were respectively harvested from colorectal cancer patients, colorectal polyp patients, and normal subjects (the health examination) who requested medical assistance from our hospital between Oct2019 and February 2022. The serum contents of HP and PDIA3 in each sample were determined through an enzyme linked immunosorbent assay (ELISA). This step was taken to analyze the differences among different specimen groups in terms of the serum contents of HP and PDIA3, to analyze the relationships between the expression levels of HP and PDIA3 and the pathological characteristics of colorectal cancer, and to explore the critical role of HP and PDIA3 in the screening, diagnosis, and staging of colorectal cancer.

Results: Serum contents of HP and PDIA3 were higher in colorectal cancer patients, with statistical differences ($p < 0.05$), than those in the colonic polyp patients and healthy subjects. Receiver operating characteristic (ROC) curve demonstrated that the cut-offs of HP and PDIA3 serum contents indicating colorectal cancer were 149 ug/ml and 66 ng/ml respectively. The individually and jointly tested AUCs of HP (0.802) and PDIA3 (0.727) were higher than those of serum CEA and CA199, the sensitivity and specificity of HP were 64.8 and 91.2%, the sensitivity and specificity of PDIA3 were 65.9 and 71.7%. Moreover, the contents of HP and PDIA3 increased alongside disease progression, with differences ($p < 0.05$).

Abbreviations: HP, Haptoglobin; PDIA3, Protein disulfide-isomerase A3; CRC, Colorectal cancer; ELISA, Enzyme linked immunosorbent assay; ROC curve, Receiver operating characteristic curve; AUC, Area under the cure; CEA, Carcinoembryonic antigen; CA199, Carbohydrate Atigen 19–9; FIT, fecal immunochemical test.

Conclusion: Our research indicated that joint testing of HP and PDIA3 was of reference value for progressive stage and reliable biological indicators of colorectal cancer screening.

Keywords: colorectal cancer, haptoglobin, protein disulfide-isomerase A3, screening, diagnosis, staging, sequencing

INTRODUCTION

Colorectal cancer (CRC) is one of the most common malignancies worldwide (Karpiński et al., 2022; Andrei et al., 2021; Ocvirk and O'Keefe, 2021). As per the *2020 World Cancer Report* issued by the International Agency for Research on *Cancer* (IARC) in 2020, the number of new cases and deaths of colorectal cancer worldwide would exceed 1.93 million and 0.93 million respectively by 2020 (Mattiuzzi and Lippi, 2020). A statistical report on United States cases of colorectal cancer in 2020 (Siegel et al., 2020) indicated that the US predicted 147,950 new cases and 53,200 deaths in 2020xx. Since the 1970s, the incidence and mortality of colorectal cancer in the US have both experienced a sustained decline as the target group of colorectal cancer screening has gradually shifted from high-risk population to healthy subjects. In the US, the ratio of colonoscopy screening increased from 20% in 2000 to 61% in 2018. In sharp contrast to the US reality, the incidence and mortality of colorectal cancer have both surged in China. It was estimated that China would have 550,000 new cases and 280,000 deaths of colorectal cancer in 2020 (Wang, 2021). Based on the comparison of relevant data between China and the US, early screening is essential to the diagnosis and treatment of colorectal cancer. However, both early diagnosis and screening of colorectal cancer remain subpar in China.

In 90% of colorectal cancer cases, disease progression follows an established pattern, from adenoma to tumor and it usually takes five to 10 years for a benign lesion to progress into a malignant tumor, which provides a substantial window for the early screening of colorectal cancer (Dekker et al., 2019). Meanwhile, the prognosis of colorectal cancer is intricately linked to early diagnosis and treatment. The 5-years survival rate of colorectal cancer would decrease from 91% in the early stage to around 10% in the advanced stage (Siegel et al., 2020). Numerous studies suggest that the nature of colorectal cancer, as a special biological behavior, determines that the prognosis of such patients can be improved through early screening, diagnosis, and treatment. Currently, the commonly used screening methods in China include digital rectal examination, fecal occult blood test, serum tumor marker test, and other testing methods. Moreover, invasive testing includes electronic colonoscopy and other screening approaches (Shaukat et al., 2021). However, these screening methods cannot satisfactorily achieve the need for screening due to their lack of sensitivity and specificity as well as poor patient compliance and financial circumstances. Therefore, the establishment of screening methods having high sensitivity and specificity, good compliance of the screening target group, and cost acceptable to the target population is essential.

In this study, small samples were utilized to conduct date-independent acquisition (DIA), quantitative proteomics testing to select haptoglobin (HP) and protein disulfide-isomerase A3 (PDIA3) with significant differences for function enrichment. The test was followed by verification through larger samples. HP is an acute-phase protein with a role in the neutralization and clearance of free heme. Iron has tremendous potential for initiating vascular oxidation, inflammation and exacerbating coronary atherosclerosis. Hp genotype has been linked as a prognostic biomarker of acute myocardial infarction (Chapelle et al., 1982; Suleiman et al., 2005), heart failure (Holme et al., 2009; Haas et al., 2011), restenosis (Moussa et al., 2014) and cardiac transplant rejection (Shen et al., 2012; Shen et al., 2015). The increased understanding of Hp as a biomarker has provided new insights into the mechanisms of inflammation after cardiac injury and support the concept that Hp is not only an important antioxidant in vascular inflammation and atherosclerosis, but also an enhancer of inflammation in cardiac transplant (Graves and Vigerust, 2016). It is known that oxidative stress is a risk factor for cancer development. A common functional haptoglobin (Hp) polymorphism, originating from a duplication of a gene segment spanning over two exons, results in three distinct phenotypes with different anti-oxidative capacities: Hp1-1, Hp1-2, and Hp2-2 (Kaiser et al., 2020). The catalysis of disulphide (SS) bonds is the most important characteristic of protein disulphide isomerase (PDI) family. Catalysis occurs in the endoplasmic reticulum, which contains many proteins, most of which are secretory in nature and that have at least one s-s bond. Protein disulphide isomerase A3 (PDIA3) is a member of the PDI family that acts as a chaperone. PDIA3 is highly expressed in response to cellular stress, and also intercept the apoptotic cellular death related to endoplasmic reticulum (ER) stress, and protein misfolding. PDIA3 expression is elevated in almost 70% of cancers and its expression has been linked with overall low cell invasiveness, survival and metastasis (Mahmood et al., 2021). The lectin chaperones calreticulin (CALR) and calnexin (CANX), together with their co-chaperone PDIA3, are increasingly implicated in studies of human cancers in roles that extend beyond their primary function as quality control facilitators of protein folding within the endoplasmic reticulum (ER). Led by the discovery that cell surface CALR functions as an immunogen that promotes anti-tumour immunity, studies have now expanded to include their potential uses as prognostic markers for cancers, and in regulation of oncogenic signaling that regulate such diverse processes including integrin-dependent cell adhesion and migration, proliferation, cell death and chemotherapeutic resistance (Lam and Lim, 2021). **Figure 1** specifically, ELISA was adopted to determine the protein contents of HP and PDIA3 in the peripheral blood to identify the role and value of HP and PDIA3 in colorectal cancer screening, to establish statistics on relevant pathological

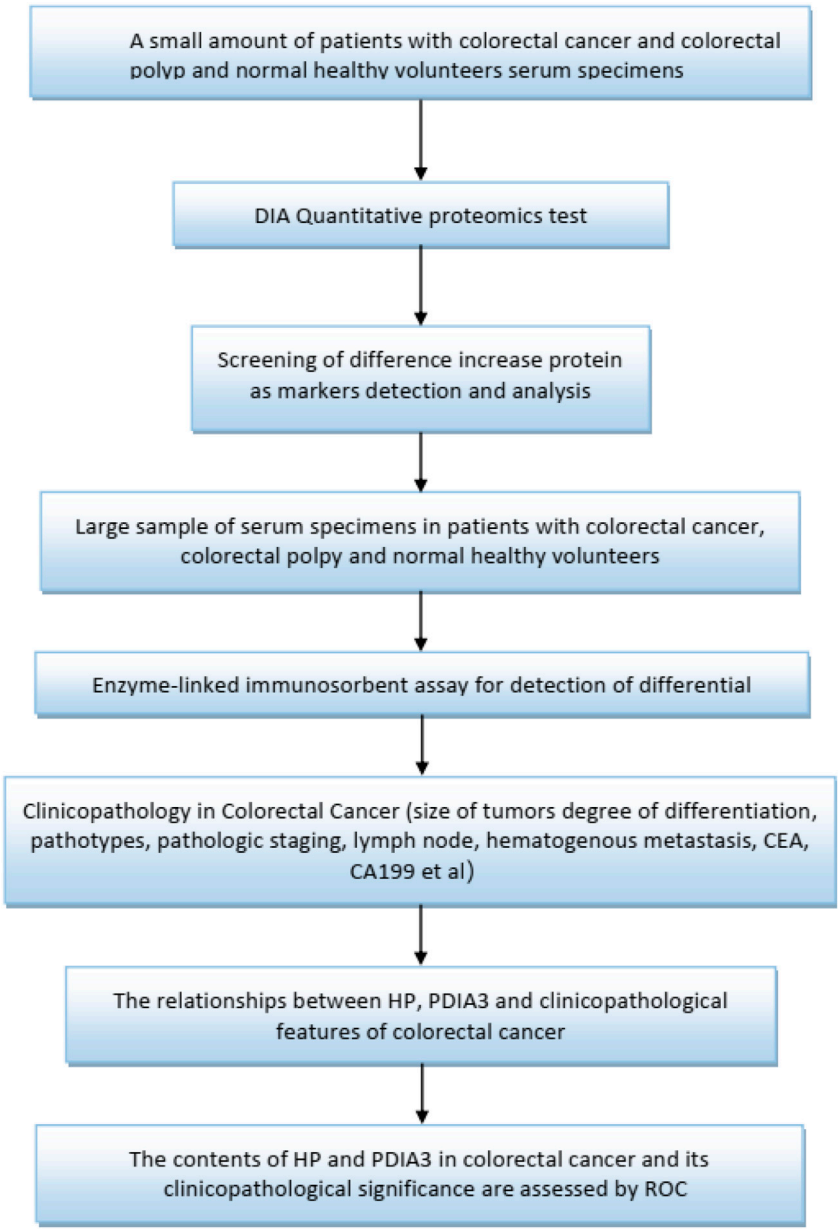

FIGURE 1 | Flow chart of study design.

characteristics, and to further verify the guiding value of the aforementioned two indicators (HP and PDIA3) in assessing colorectal cancer staging.

MATERIALS AND METHODS

General Information

A selection of colorectal cancer patients, who were treated in the First Affiliated Hospital of Hebei North University from October 2020 and January 2022, were recruited in the "cancer group". During the same period, 77 colorectal polyp patients and 36 healthy subjects were enrolled in the "polyp group" and the "group of healthy volunteers" respectively. 50 male patients and 38 female patients were included in the "cancer group", aged from 40 to 92 and the average age being 65.8 ± 10.3; 48 male patients and 29 female patients were included in the "polyp group", with the ages ranging from 32 to 79 and the average age being 60.5 ± 10.5; 18 men and 18 women were included in the "group of healthy volunteers", with the ages ranging from 16 to 85 and the average age being 59.6 ± 16.2. The differences among these three groups were not

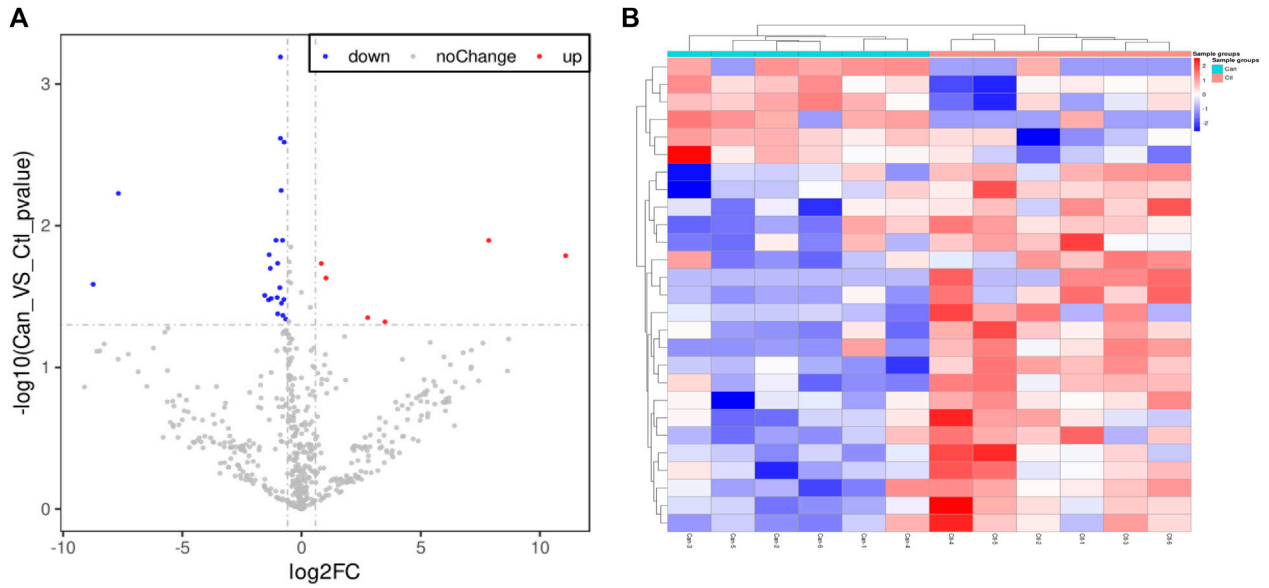

FIGURE 2 | Volcano plot and Cluster heatmap. **(A)**. The volcano plot of proteome of cancer group and group of healthy volunteers, A total of 27 differential proteins were identified; a total of six proteins with increased expressions and a total of 21 proteins with decreased expressions. **(B)**. The heatmap of proteome difference with sample clustering of cancer group and group of healthy volunteers. the abscissa are the members of "cancer group" and "group of healthy volunteers", the ordinate are the members of 27 different expressed proteins between colorectal "cancer group" and "group of healthy volunteers".

statistically significant in terms of baseline data ($p > 0.05$). The Ethics Approval No. is K2022012.

Selection Criteria

Enrollment criteria: a. The colorectal malignancy to be studied should meet the relevant diagnosis standards included in National Diagnosis and Treatment Standards for Colorectal *Cancer* (2020) (National Health Commission of the People's Republic of China, 2020); b. The colorectal polyp to be studied should meet with the relevant diagnosis standards included in Surgery; c. The patients should not have received any anti-tumor therapy prior to enrollment.

Exclusion criteria: a. The presence of neoplastic lesions in addition to those in the colon and rectum; b. The dispensing of relevant treatment regimens; c. The loss of relevant patient information, leading to the unavailability of follow-ups to collect further prognosis and survival-rate data.

Experimental Process

A total of 18 blood specimens (6 for each of the three groups: colorectal cancer patients, colorectal polyp patients, and healthy subjects) were selected for protein difference sequencing to explore proteins with different expressions. The collected whole blood samples were left to stand at room temperature for 2 hours, 3,000 g of which was subsequently centrifuged for 10 minutes. Following that, a volume of no less than 100 ul supernatant was taken and stored at −80°C, which was then delivered with dry ice to the Shanghai Origin-Gene Biomedical Technology Co., Ltd. for DIA quantitative proteomics testing. There are no statistical differences between "group of healthy volunteers" and "polyp group", so we selected difference proteins from the "colorectal cancer group"and the "group of healthy volunteers". A total of 27 differential proteins were identified; a total of 6 proteins with increased expressions and a total of 21 proteins with decreased expressions were identified in the"colorectal cancer group" and the "group of healthy volunteers". They are Tenascin-X (TN-X), Platelet glycoprotein Ib alpha chain (GPIbA), anti-leucine-rich glioma inactivated-1 (LGI1), Melanocyte protein (PMEL), Apolipoprotein M(APOM), Haptoglobin (HP), Coagulation factor X (F10), Coagulation factor XII(F12), Apolipoprotein A-I (APOA1), Fibrinogen alpha chain (FGA), Complement C1q subcomponent subunit C(C1QC), Apolipoprotein B-100 (APOB), Immunoglobulin kappa variable 2–30(IGKV2-30), Profilin-1(PFN1), Dopamine beta-hydroxylase (DBH), Lipopolysaccharide-binding protein (LBP), Protein disulfide-isomerase A3(PDIA3), Insulin-like growth factor-binding protein complex acid labile subunit (IGFALS), Cadherin-13(CDH13), Phosphatidylinositol-glycan-specific phospholipase D (GPLD1), Prolow-density lipoprotein receptor-related protein 1 (LRP1), Apolipoprotein F (APOF), Dystroglycan (DAG1), Serum paraoxonase 3(PON3), Histone H2A type 2-C(HIST2H2AC), Protocadherin-12 (PCDH12), Protein HEG homolog 1(HEG1). We did functional enrichment about the six proteins with increased expressions on uniprot, the best choice was HP and PDIA3.

The differences of these proteins were visualized to generate a volcano plot and a cluster heatmap (**Figure 2**). This study aimed to search potential biomarkers of colorectal cancer applicable to clinical use. Therefore, the focus of the study was the six proteins

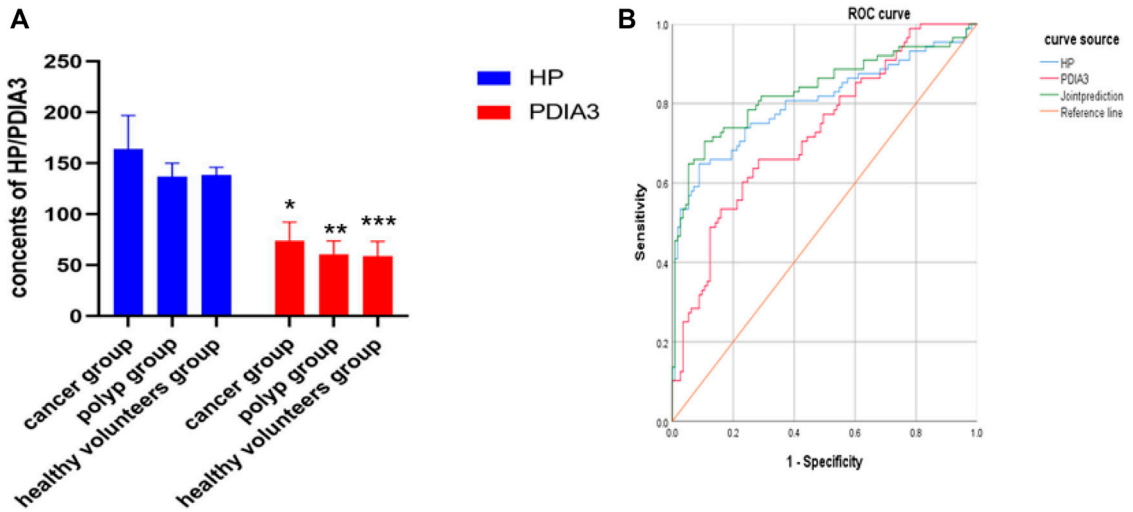

FIGURE 3 | Contents of HP and PDIA3 in each group and ROC curve in which serum levels of HP and PDIA3 indicating colorectal cancer. **(A)**. In the cancer group, the average contents of HP and PDIA3 are 164 ± 33 μl/ml and 74 ± 18 ng/ml. In the polyp group, the average contents of HP and PDIA3 are 137 ± 13 μl/ml and 61 ± 13 ng/ml. In the healthy volunteers group, the average contents of HP and PDIA3 are 138 ± 8 μl/ml and 58 ± 15 ng/ml ($p < 0.05$). **(B)**. Diagnostic value of HP and PDIA3 for colorectal cancer. *vs. cancer group ($p < 0.05$), **vs. means polyp group ($p < 0.05$), *** vs. healthy volunteers group ($p < 0.05$).

having increased expressions. Based on substantial literature review and analysis, HP and PDIA3 were selected from the six proteins for ELISA.

The above serum extraction method was utilized to extract an approximate amount of 0.6–0.8 ml of serum from the subsequently collected specimens. The serum was divided into three to four RNase-free tubes (each of capacity 1.5 ml) and stored in a refrigerator at −20°C. Human haptoglobin/haptoglobin ELISA kit (96T) and human PDIA3A3 ELISA kit (96T) (stored at 4°C), manufactured by Jiangsu Jingmei Biotechnology Co., Ltd., were used to test the levels of HP and PDIA3 in the serum. All procedures were in strict compliance with the instructions, with the specific steps delineated as follows: Preparation of relevant reagents prior to the experiment: dilution of standards as specified in **Supplementary Tables S1,2**. The specific steps are as follows: adding samples-incubation-mixing-washing-adding enzyme-incubation-washing-chromogenic reaction-stop, according to the zero setting of the blank wells, a wave of 450 nm in wavelength was adopted to measure the absorbance (OD value) of each well in the ELISA microplate. the concentration of the standard and the OD value were used to generate a quaternary linear regression equation of the standard curve; the OD value of the sample was substituted into the equation to calculate the concentration of the sample. The Figure was then multiplied by dilution multiples to yield the actual concentration of the sample. Avoid spending long time on the operation, each step is not more than 5 min.

TNM Staging Assessment

The members of colorectal cancer patients were treated by surgery. According to pathological analysis after surgery and reference *TNM Staging for Malignant Tumors* (Rosen and Sapra, 2022). TNM staging was carried out in 88 colorectal cancer patients.

Statistical Analysis

SPSS25.0 software was used for statistical analysis. The levels of HP and PDIA3 were represented as ($\bar{x} \pm s$); a *t*-test was used for comparison between two groups; enumeration data were expressed as percentages; a chi-square test was adopted for comparison between two groups; one-way analysis of variance was used to verify comparison among multiple groups; ROC curve was plotted to determine the area under curve (AUC). The diagnosis value of HP and PDIA3 levels to colorectal cancer patients were estimated: where AUC = 0.5–0.7, the diagnosis effect was poor; where AUC = 0.7–0.9, the effect was good; where AUC >0.9, the effect was excellent; the significance of all statistical comparisons was set to $p < 0.05$.

RESULTS

Levels of HP and PDIA3

In the "cancer group", the contents of HP and PDIA3 were 164 ± 33 μl/ml and 74 ± 18 ng/ml respectively; in the "polyp group", the above two contents were 137 ± 13 μl/ml and 61 ± 13 ng/ml respectively; in the "group of healthy volunteers", the two contents were 138 ± 8 μl/ml and 58 ± 15 ng/ml respectively. In the "cancer group", the average contents of HP and PDIA3 exceeded those in the "polyp group" and the "group of healthy volunteers", showcasing statistically significant differences ($p < 0.05$); whereas the differences between the average contents in the "polyp group" and the "group of healthy volunteers" were not statistically significant ($p > 0.05$) (see **Figure 3A**, **Supplementary Figure S1**, and **Table 1** for details).

TABLE 1 | Comparison of HP and PDIA3 levels in "cancer group", "polyp group" and "group of healthy volunteers" ($x \pm s$). *vs. cancer group vs. healthy volunteers ($p < 0.05$),**vs. polyp group vs. healthy volunteers ($p > 0.05$).

Group	Number of Cases	HP (μl/ml)	PDIA3 (ng/ml)
Cancer group	88	164 ± 33*	74 ± 18*
Polyp group	77	137 ± 13**	61 ± 13**
Healthy volunteers	36	138 ± 8	58 ± 15
P		0.000	0.000

Assessing the Diagnosis Value of HP and PDIA3 Levels to Colorectal Cancer Using ROC Curve

Serum levels of HP and PDIA3 were used as test variables and colorectal cancer was adopted as state variable (1 = colorectal cancer, and 0 = colorectal polyp and group of healthy volunteers). The plotted ROC curve revealed that the cut-offs of HP and PDIA3 levels indicating colorectal cancer were 149 ug/ml and 66 ng/ml respectively (see **Figure 3B** and **Table 2** for details).

TNM Staging and Pathological Characteristics of Colon Cancer Patients

Among the 88 colorectal cancer cases, 21 were at stage I (accounting for 23.9% of the total cases), 23 at stage II (accounting for 26.1%), 30 at stage III (accounting for 34.1%), and 14 at stage IV (accounting for 15.9%). The cut-offs of HP and PDIA3 served as the baseline; high expressions were defined as above the cut-offs and low expressions were defined as below the cut-offs. The relationships between clinical characteristics and pathological characteristics and the HP and PDIA3 serum contents of colorectal cancer patients at different pathological stages were subsequently analyzed (see **Table 3** for details).

HP and PDIA3 Serum Levels of Colorectal Cancer Patients at Different Pathological Stages

HP and PDIA3 levels of stage-I patients were 156 ± 29 μl/ml and 68 ± 15 ng/ml respectively; those of stage-II patients were 149 ± 26 μl/ml and 66 ± 14 ng/ml respectively; those of stage-III patients were 173 ± 23 μl/ml and 81 ± 15 ng/ml respectively; those of stage-IV patients were 183 ± 51 μl/ml and 80 ± 28 ng/ml respectively. The above figures account for the differences in the expression levels of HP and PDIA3 of patients at different stages ($p < 0.05$, **Figure 4**, **Supplementary Figure S2**, and **Table 4**).

Value of CEA and CA199 Levels to Assessment of Colorectal Cancer Patients

CEA and CA199 levels were used as test variables and colorectal cancer was adopted as state variable (1 = colorectal cancer, and 0 = colorectal polyp and group of healthy volunteers) to plot an ROC curve. The diagnosis accuracy of colorectal cancer through CEA was 69.9%, that through CA199 was 61.4%, and that through joint testing was 71% (**Figure 5** and **Table 5**).

Value of HP and PDIA Levels to the Assessment of Colorectal Cancer Stages

HP and PDIA3 levels were used as test variables and colorectal cancer was adopted as the state variable (1 = colorectal cancer (including early stage and progressive stage), and 0 = colorectal polyp and group of healthy volunteers) to plot an ROC curve. The diagnosis accuracy of early and progressive colorectal cancers through HP were 65 and 95.4% respectively, the accuracy through PDIA3 were 61.8 and 83.6% respectively, and that through joint testing were 69.3 and 97.3% respectively (see **Figure 6A**, **Figure 6B**, **Table 6**, and **Table 7**).

DISCUSSION

Colorectal cancer (CRC) alone accounts for ~10% of total new global cases and poses an over 4% lifetime risk of developing cancer (Rada et al., 2021; Saeed et al., 2021; Si et al., 2021; Weng and Goel, 2022). Presently, the common approaches for colorectal cancer screening mainly consist of invasive examinations (sigmoidoscopy, colonoscopy, barium enema, etc.), non-invasive examinations (stool examination, etc.), and radio-assay (such as fecal occult blood test, fecal immunochemical test (FIT), multi-target FIT DNA test, and tumor marker assay) (Issa and Noureddine, 2017).

Currently, fecal occult blood testing is the most extensively used screening method for colorectal cancer. However, due to its low sensitivity and specificity (specifically, its lack of specificity to the hemoglobin in the feces and its susceptibility to drugs and food containing ferrous iron) this test method is considered obsolete and has been replaced by fecal immunochemical test (FIT). Nevertheless, the presence of hysteresis arising from immune hook effect and antigen excess associated with IFT is likely to entail false negatives during clinical use. Multi-target FIT DNA testing (FIT-DNA) has good sensitivity and specificity to colorectal cancer. However, it is difficult to include in Chinese clinical practice due to the high cost screening and the low acceptability to the general population and colonoscopy remains the gold

TABLE 2 | Value of HP and PDIA3 levels to assessment of colorectal cancer patients.

Indicator	AUC	95%CI	Standard error	*P*	Specificity	Sensitivity
HP	0.802	0.736–0.868	0.034	0.000	0.912	0.648
PDIA3	0.727	0.657–0.797	0.036	0.000	0.717	0.659
Joint prediction	0.855	0.801–0.910	0.028	0.000	0.876	0.727

TABLE 3 | Relationships between HP and PDIA3 expressions and colorectal pathological characteristics.

Project Parameter	HP Expression		χ^2	*P*	PDIA3 Expression		χ^2	*P*
	Low	High			Low	High		
Size of tumor			2.343	0.126			3.751	0.097
<5 cm	23	31			22	32		
>5 cm	9	25			8	26		
Differentiation level			5.639	0.018			4.726	0.030
Low	2	17			2	17		
Medium, high	30	39			28	41		
Pathological staging			30.692	0.000			20.230	0.000
I + II	29	15			25	19		
III + IV	3	41			5	39		
Lymphatic metastasis			25.688	0.000			18.255	0.000
Yes	3	38			4	37		
None	29	18			26	21		

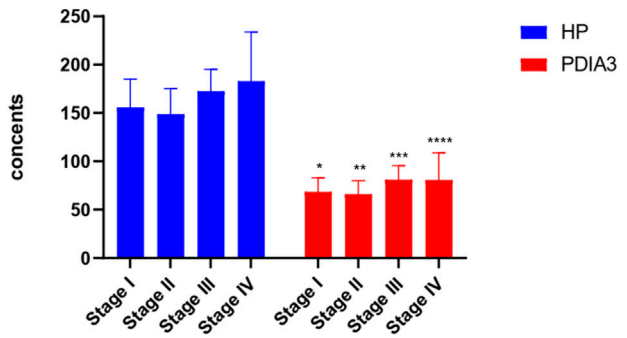

FIGURE 4 | HP and PDIA3 serum contents of patients at different pathological stages. In the Stage I, the average contents of HP and PDIA3 are 156 ± 29 μl/ml and 68 ± 15 ng/ml. In the stage II, the average contents of HP and PDIA3 are 149 ± 26 μl/ml and 66 ± 14 ng/ml. In the stage III, the average contents of HP and PDIA3 are 173 ± 23 μl/ml and 81 ± 15 ng/ml. In the stage IV, the average contents of HP and PDIA3 are 183 ± 51 μl/ml and 80 ± 28 ng/ml ($p < 0.05$). *vs. Stage I ($p < 0.05$), ** vs. Stage II ($p < 0.05$), ***vs. Stage III ($p < 0.05$), ****vs. Stage IV ($p < 0.05$).

TABLE 4 | Comparison of HP and PDIA3 levels in patients with different TNM stages of colorectal cancer ($x \pm s$). *vs. Stage I ($p > 0.05$),**vs. Stage III ($p > 0.05$).

TNM Staging	Number of Cases	HP (μl/ml)	PDIA3 (ng/ml)
Stage I	21	156 ± 29	68 ± 15
Stage II	23	149 ± 26*	66 ± 14*
Stage III	30	173 ± 23	81 ± 15
Stage IV	14	183 ± 51**	80 ± 28**
P		0.004	0.005

diagnosis standard for colorectal cancer. Previous research suggests that the early diagnosis and excision of colorectal lesions through colonoscopy can reduce the incidence of colorectal cancer. However, this investigation requires bowel cleaning thereby entailing some invasion and risks. Accordingly, the population compliance is low which substantially limits the diagnosis rate. Research reveals that the participation rates of colonoscopy and fecal immunochemical testing are 42.5 and 94.0% respectively (Chen et al., 2020). Given the current situation of the aforementioned colorectal malignancy screening methods, it is imperative to establish screening methods for colorectal cancer with high sensitivity, strong specificity, and good compliance.

Through quantitative proteomics testing and screening, two types of proteins were selected for research, namely HP and PDIA3. HP is an acid α2 glycoprotein present in the serum and body fluids of mammalian species including humans. Gene expressions of HP were successively discovered in the liver, heart, spleen, and other organs. Despite the presence of three HP genotypes: HP1-1, HP2-1, and HP2-2, all of which are associated with susceptible infectious diseases, atherosclerosis, autoimmune disorders, and vascular occlusive diseases (Goldenstein et al., 2012; Andersen et al., 2017; Simon et al., 2020). A study on HP informatics (Naryzhny and Legina, 2021) has revealed that HP is a stable hydrophilic protein, composed of 406 amino acids, with a long half-life of about 30 h. HP has two peptide chains, namely α and β, which are connected by a disulfide bond. Fucosylation, characterized by abnormal β peptide chain, is closely associated with cancer. Being an important oligosaccharide modification mode, fucosylation mainly occurs in tumor and inflammatory responses and exists in various biological processes such as origin, differentiation, and growth of cells, as well as formation and metastasis of infected tumors (Jeong et al., 2020). Previous studies demonstrate that HP expressions are higher in the serum of patients with liver cancer, lung cancer, ovarian cancer, or other cancers than in the serum of healthy subjects. Furthermore, HP expressions combined with other serum markers, would be of reference value to the early diagnosis of relevant cancers and of some guiding significance in terms of treatment and prognosis (Naryzhny et al., 2021).

PDIA3 is a member of the protein disulfide isomerase (PDI) family that is coded by genes. It serves both as an enzyme, and a chaperone. As a multifunctional protein, PDIA3 exists extensively in endoplasmic reticulums of cells. It is known that functional and viral infections (Schelhaas et al., 2007) as well as cell proliferation are connected to apoptosis (Panaretakis et al., 2008). PDIA3 exists widely in various human tissues and its expressions vary. Moreover, the expression dysregulation of PDIA3 is associated with relevant diseases. Therefore, an increasing number of studies use PDIA3 as a biomarker to assess the diagnosis and prognosis of

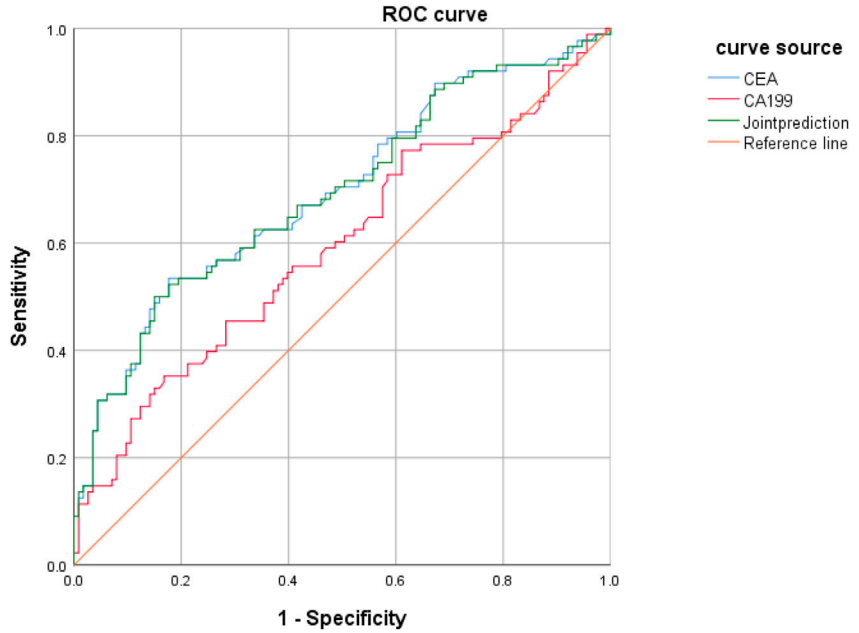

FIGURE 5 | ROC curve in which CEA and CA199 levels indicating colorectal cancer.

TABLE 5 | Value of CEA and CA199 levels to assessment of colorectal cancer patients.

Indicator	AUC	95%CI	Standard error	*P*	Specificity	Sensitivity
CEA	0.699	0.625–0.773	0.38	0.001	0.823	0.534
CA199	0.614	0.535–0.693	0.40	0.006	0.832	0.375
Joint test	0.710	0.638–0.78	0.37	0.001	0.85	0.523

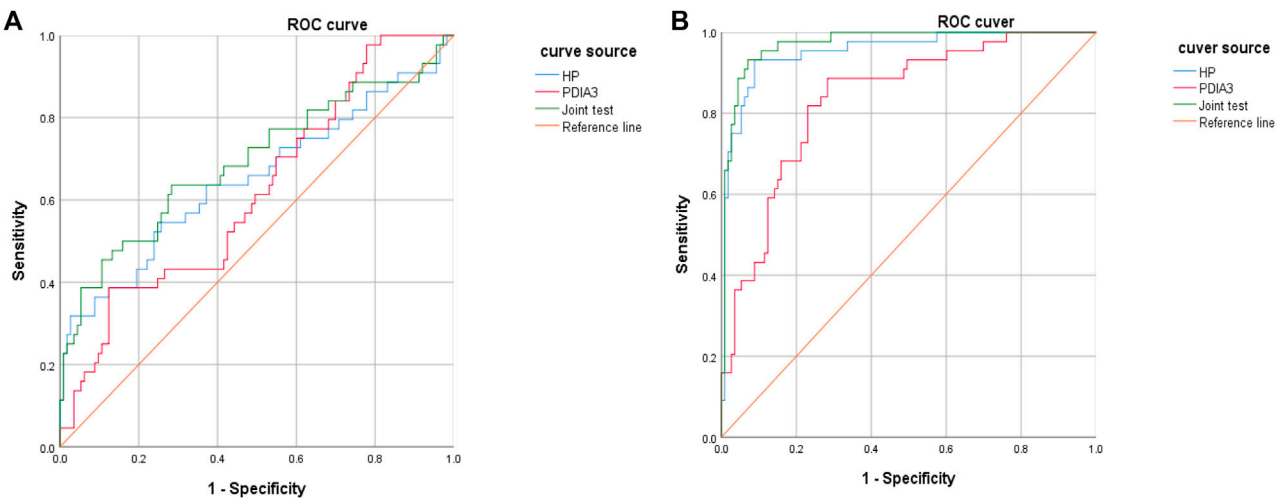

FIGURE 6 | Diagnosis value of HP and PDIA3 to early colorectal cancer and progressive stage. **(A)**. Low diagnosis accuracy of early colorectal cancer. **(B)**. Great assessment value to pathological staging of colorectal cancer.

TABLE 6 | Value of HP and PDIA3 levels to assessment of patients with early colorectal cancer.

Indicator	AUC	95%CI	Standard error	*P*	Specificity	Sensitivity
HP	0.650	0.544–0.756	0.054	0.004	0.973	0.318
PDIA3	0.618	0.521–0.714	0.049	0.022	0.876	0.386
Joint test	0.693	0.591–0.794	0.052	0.000	0.717	0.636

TABLE 7 | Value of HP and PDIA3 levels to assessment of colorectal cancer patients at progressive stage.

Indicator	AUC	95%CI	Standard error	*P*	Specificity	Sensitivity
	0.954	0.919–0.990	0.018	0.000	0.912	0.932
PDIA3	0.836	0.768–0.903	0.034	0.000	0.717	0.886
Joint test	0.973	0.951–0.995	0.011	0.000	0.929	0.932

some diseases. The expression dysregulation of PDIA3 has been assessed in several gastrointestinal cancers, and PDIA3 over-expressions in gastric carcinoma and colon cancer have been proven (Ren et al., 2006; Yang et al., 2018; Shimoda et al., 2019). Furthermore, PDIA3 can alter the chemotherapy resistance and the radiotherapy sensitivity of gastrointestinal cancers by inhibiting or activating other proteins (Choe et al., 2015). Moreover, PDIA3 features the ability to promote the proliferation of cancer cells and playing a part in cancer progression. Even though relevant mechanisms of action are still under investigation, PHIA3, as a novel anti-cancer marker, has promising application prospects.

The results of this study are as follows. Serum levels of HP and PDIA3 were significantly higher in the "cancer group" than in the "polyp group" and the "group of healthy volunteers." However, there were no significant differences between the "polyp group" and the "group of healthy volunteers". There were also significant differences in HP and PDIA3 levels between colorectal cancer patients at an early stage and those at the progressive stage, indicating that HP and PDIA3 expressions were high in malignant tumors and would continuously increase alongside disease progression. It was found through the ROC curve that the accuracy of individual or joint testing of HP and PDIA3 markedly exceeded that of traditional CEA and CA199. Further stratification analysis revealed that HP and PDIA3 contents were of great assessment value to pathological staging of colorectal cancer, particularly to the progressive stage. The diagnosis accuracy of early colorectal cancer by joint testing was 69.3% and the diagnosis accuracy of progressive colorectal cancer through this test reached a peak of 97.3%. Early lesions differ slightly from normal tissues and may account for the lower diagnosis accuracy of early colorectal cancer.

The experiment also has deficiencies such as the relatively small sample volume, the absence of comparison regarding the serum contents of these two proteins of patients before and after surgery, the absence of survival follow-ups leading to inability to probe deep the effect of the two protein contents on prognosis, and failure to further explore the mechanisms of action of HP and PDIA3. As follow-through, cooperation featuring multiple centers and large samples could be implemented to deliver authentic and accurate conclusions.

DATA AVAILABILITY STATEMENT

The original contributions presented in the study are included in the article/**Supplementary Material**, further inquiries can be directed to the corresponding authors.

ETHICS STATEMENT

The studies involving human participants were reviewed and approved by Ethic Committee of The First Affiliated Hospital of Hebei North University. The patients/participants provided their written informed consent to participate in this study.

AUTHOR CONTRIBUTIONS

YN performed the statistical analyses and wrote the manuscript. XW completed all of the data entry and provided assistance for the data analysis. MQ, LW, and WL were responsible for clinical assessment of the participants. JX designed and wrote the study.

FUNDING

This study was supportive by Hebei Funding Project for High-level Talents (A202101062), Training Project for Excellent Clinical Medical Talents of Hebei Provincial Department of Finance (361009), 2015 Key Medical Science Project of Hebei Provincial Department of Science and Technology (152777237). These fundings have no role in the study design of this article.

ACKNOWLEDGMENTS

The language is editing by First Choice Edit (www.fcedit.com).

SUPPLEMENTARY MATERIAL

The Supplementary Material for this article can be found online at: https://www.frontiersin.org/articles/10.3389/fphar.2022.935500/full#supplementary-material

REFERENCES

Andersen, C. B. F., Stødkilde, K., Sæderup, K. L., Kuhlee, A., Raunser, S., Graversen, J. H., et al. (2017). Haptoglobin. *Antioxidants Redox Signal.* 26 (14), 814–831. doi:10.1089/ars.2016.6793

Andrei, P., Battuello, P., Grasso, G., Rovera, E., Tesio, N., and Bardelli, A. (2021). Integrated Approaches for Precision Oncology in Colorectal Cancer: The More You Know, the Better. *Seminars Cancer Biol.* doi:10.1016/j.semcancer.2021.04.007

Chapelle, J. P., Albert, A., Smeets, J. P., Heusghem, C., and Kulbertus, H. E. (1982). Effect of the Haptoglobin Phenotype on the Size of a Myocardial Infarct. *N. Engl. J. Med.* 307 (8), 457–463. doi:10.1056/nejm198208193070801

Chen, H. D., Lu, M., Liu, C. C., Zhang, Y. H., Zou, S. M., Shi, J. F., et al. (2020). Rates on the Acceptance of Colonoscopy, Fecal Immunochemical Test and a Novel Risk-Adapted Screening Approach in the Screening Programs of Colorectal Cancer as Well as Related Associated Factors. *Zhonghua Liu Xing Bing Xue Za Zhi* 41 (10), 1655–1661. doi:10.3760/cma.j.cn112338-20200227-00196

Choe, M. H., Min, J. W., Jeon, H. B., Cho, D. H., Oh, J. S., Lee, H. G., et al. (2015). ERp57 Modulates STAT3 Activity in Radioresistant Laryngeal Cancer Cells and Serves as a Prognostic Marker for Laryngeal Cancer. *Oncotarget* 6 (5), 2654–2666. doi:10.18632/oncotarget.3042

Dekker, E., Tanis, P. J., Vleugels, J. L. A., Kasi, P. M., and Wallace, M. B. (2019). Colorectal Cancer. *Lancet* 394 (10207), 1467–1480. doi:10.1016/S0140-6736(19)32319-0

Goldenstein, H., Levy, N. S., and Levy, A. P. (2012). Haptoglobin Genotype and its Role in Determining Heme-Iron Mediated Vascular Disease. *Pharmacol. Res.* 66 (1), 1–6. doi:10.1016/j.phrs.2012.02.011

Graves, K. L., and Vigerust, D. J. (2016). Hp: an Inflammatory Indicator in Cardiovascular Disease. *Future Cardiol.* 12 (4), 471–481. doi:10.2217/fca-2016-0008

Haas, B., Serchi, T., Wagner, D. R., Gilson, G., Planchon, S., Renaut, J., et al. (2011). Proteomic Analysis of Plasma Samples from Patients with Acute Myocardial Infarction Identifies Haptoglobin as a Potential Prognostic Biomarker. *J. Proteomics* 75 (1), 229–236. doi:10.1016/j.jprot.2011.06.028

Holme, I., Aastveit, A. H., Hammar, N., Jungner, I., and Walldius, G. (2009). Haptoglobin and Risk of Myocardial Infarction, Stroke, and Congestive Heart Failure in 342,125 Men and Women in the Apolipoprotein MOrtality RISk Study (AMORIS). *Ann. Med.* 41 (7), 522–532. doi:10.1080/07853890903089453

Issa, I. A., and Noureddine, M. (2017). Colorectal Cancer Screening: An Updated Review of the Available Options. *World J. Gastroenterol.* 23 (28), 5086–5096. doi:10.3748/wjg.v23.i28.5086

Jeong, S., Oh, M. J., Kim, U., Lee, J., Kim, J. H., and An, H. J. (2020). Glycosylation of Serum Haptoglobin as a Marker of Gastric Cancer: an Overview for Clinicians. *Expert Rev. Proteomics* 17 (2), 109–117. doi:10.1080/14789450.2020.1740091

Kaiser, M., Thurner, E. M., Mangge, H., Herrmann, M., Semeraro, M. D., Renner, W., et al. (2020). Haptoglobin Polymorphism and Prostate Cancer Mortality. *Sci. Rep.* 10 (1), 13117. doi:10.1038/s41598-020-69333-z

Karpiński, T. M., Ożarowski, M., and Stasiewicz, M. (2022). Carcinogenic Microbiota and its Role in Colorectal Cancer Development. *Seminars Cancer Biol.* doi:10.1016/j.semcancer.2022.01.004

Lam, S. T. T., and Lim, C. J. (2021). Cancer Biology of the Endoplasmic Reticulum Lectin Chaperones Calreticulin, Calnexin and PDIA3/ERp57. *Prog. Mol. Subcell. Biol.* 59, 181–196. doi:10.1007/978-3-030-67696-4_9

Mahmood, F., Xu, R., Awan, M. U. N., Song, Y., Han, Q., Xia, X., et al. (2021). PDIA3: Structure, Functions and its Potential Role in Viral Infections. *Biomed. Pharmacother.* 143, 112110. doi:10.1016/j.biopha.2021.112110

Mattiuzzi, C., and Lippi, G. (2020). Cancer Statistics: a Comparison between World Health Organization (WHO) and Global Burden of Disease (GBD). *Eur. J. Public Health* 30 (5), 1026–1027. doi:10.1093/eurpub/ckz216

Moussa, A., Rejeb, J., Omezzine, A., Rebhi, L., Boumaiza, I., Kacem, S., et al. (2014). Association between Haptoglobin 2-2 Genotype and Coronary Artery Disease and its Severity in a Tunisian Population. *Biochem. Genet.* 52 (5-6), 269–282. doi:10.1007/s10528-014-9646-9

Naryzhny, S., Ronzhina, N., Zorina, E., Kabachenko, F., Zavialova, M., Zgoda, V., et al. (2021). Evaluation of Haptoglobin and its Proteoforms as Glioblastoma Markers. *Int. J. Mol. Sci.* 22 (12), 6533. doi:10.3390/ijms22126533

Naryzhny, S. N., and Legina, O. K. (2021). Haptoglobin as a Biomarker. *Biomed. Khim* 67 (2), 105–118. doi:10.18097/PBMC20216702105

National Health Commission of the People's Republic of China (2020). Chinese Protocol of Diagnosis and Treatment of Colorectal Cancer. *Chin. J. Pract. Surg.* doi:10.19538/j.cjps.issn1005-2208.2020.06.01

Ocvirk, S., and O'Keefe, S. J. D. (2021). Dietary Fat, Bile Acid Metabolism and Colorectal Cancer. *Semin. Cancer Biol.* 73, 347–355. doi:10.1016/j.semcancer.2020.10.003

Panaretakis, T., Joza, N., Modjtahedi, N., Tesniere, A., Vitale, I., Durchschlag, M., et al. (2008). The Co-translocation of ERp57 and Calreticulin Determines the Immunogenicity of Cell Death. *Cell Death Differ.* 15 (9), 1499–1509. doi:10.1038/cdd.2008.67

Rada, M., Lazaris, A., Kapelanski-Lamoureux, A., Mayer, T. Z., and Metrakos, P. (2021). Tumor Microenvironment Conditions that Favor Vessel Co-option in Colorectal Cancer Liver Metastases: A Theoretical Model. *Semin. Cancer Biol.* 71, 52–64. doi:10.1016/j.semcancer.2020.09.001

Ren, H., Du, N., Liu, G., Hu, H. T., Tian, W., Deng, Z. P., et al. (2006). Analysis of Variabilities of Serum Proteomic Spectra in Patients with Gastric Cancer before and after Operation. *World J. Gastroenterol.* 12 (17), 2789–2792. doi:10.3748/wjg.v12.i17.2789

Rosen, R. D., and Sapra, A. (2022). *TNM Classification*. Treasure Island (FL): StatPearls.

Saeed, M., Shoaib, A., Kandimalla, R., Javed, S., Almatroudi, A., Gupta, R., et al. (2021). Microbe-based Therapies for Colorectal Cancer: Advantages and Limitations. *Seminars Cancer Biol.* doi:10.1016/j.semcancer.2021.05.018

Schelhaas, M., Malmström, J., Pelkmans, L., Haugstetter, J., Ellgaard, L., Grünewald, K., et al. (2007). Simian Virus 40 Depends on ER Protein Folding and Quality Control Factors for Entry into Host Cells. *Cell* 131 (3), 516–529. doi:10.1016/j.cell.2007.09.038

Shaukat, A., Kahi, C. J., Burke, C. A., Rabeneck, L., Sauer, B. G., and Rex, D. K. (2021). ACG Clinical Guidelines: Colorectal Cancer Screening 2021. *Am. J. Gastroenterol.* 116 (3), 458–479. doi:10.14309/ajg.0000000000001122

Shen, H., Heuzey, E., Mori, D. N., Wong, C. K., Colangelo, C. M., Chung, L. M., et al. (2015). Haptoglobin Enhances Cardiac Transplant Rejection. *Circ. Res.* 116 (10), 1670–1679. doi:10.1161/circresaha.116.305406

Shen, H., Song, Y., Colangelo, C. M., Wu, T., Bruce, C., Scabia, G., et al. (2012). Haptoglobin Activates Innate Immunity to Enhance Acute Transplant Rejection in Mice. *J. Clin. Invest.* 122 (1), 383–387. doi:10.1172/jci58344

Shimoda, T., Wada, R., Kure, S., Ishino, K., Kudo, M., Ohashi, R., et al. (2019). Expression of Protein Disulfide Isomerase A3 and its Clinicopathological Association in Gastric Cancer. *Oncol. Rep.* 41 (4), 2265–2272. doi:10.3892/or.2019.6999

Si, H., Yang, Q., Hu, H., Ding, C., Wang, H., and Lin, X. (2021). Colorectal Cancer Occurrence and Treatment Based on Changes in Intestinal Flora. *Semin. Cancer Biol.* 70, 3–10. doi:10.1016/j.semcancer.2020.05.004

Siegel, R. L., Miller, K. D., Goding Sauer, A., Fedewa, S. A., Butterly, L. F., Anderson, J. C., et al. (2020). Colorectal Cancer Statistics, 2020. *CA Cancer J. Clin.* 70 (3), 145–164. doi:10.3322/caac.21601

Simon, A., Schneider, N., Gillery, P., and Oudart, J. B. (2020). Clinical and Biological Features of Haptoglobin Phenotypes. *Ann. Biol. Clin. Paris.* 78 (5), 493–498. doi:10.1684/abc.2020.1590

Suleiman, M., Aronson, D., Asleh, R., Kapeliovich, M. R., Roguin, A., Meisel, S. R., et al. (2005). Haptoglobin Polymorphism Predicts 30-day Mortality and Heart Failure in Patients with Diabetes and Acute Myocardial Infarction. *Diabetes* 54 (9), 2802–2806. doi:10.2337/diabetes.54.9.2802

Wang, X. (2021). Discussion of the Importance of Early Diagnosis and Treatment of Colorectal Cancer from the Epidemiological Characteristics of Colorectal

Cancer in China and United States of America. *Chin. J. Color. Dis.* 10, 26–33. doi:10.3877/cma.j.issn.2095-3224.2021.01.004

Weng, W., and Goel, A. (2022). Curcumin and Colorectal Cancer: An Update and Current Perspective on This Natural Medicine. *Semin. Cancer Biol.* 80, 73–86. doi:10.1016/j.semcancer.2020.02.011

Yang, Z., Liu, J., Shi, Q., Chao, Y., Di, Y., Sun, J., et al. (2018). Expression of Protein Disulfide Isomerase A3 Precursor in Colorectal Cancer. *Onco Targets Ther.* 11, 4159–4166. doi:10.2147/OTT.S154452

Conflict of Interest: The authors declare that the research was conducted in the absence of any commercial or financial relationships that could be construed as a potential conflict of interest.

Publisher's Note: All claims expressed in this article are solely those of the authors and do not necessarily represent those of their affiliated organizations, or those of the publisher, the editors and the reviewers. Any product that may be evaluated in this article, or claim that may be made by its manufacturer, is not guaranteed or endorsed by the publisher.

Copyright © 2022 Niu, Xue, Wu, Qu, Wang, Liang and Li. This is an open-access article distributed under the terms of the Creative Commons Attribution License (CC BY). The use, distribution or reproduction in other forums is permitted, provided the original author(s) and the copyright owner(s) are credited and that the original publication in this journal is cited, in accordance with accepted academic practice. No use, distribution or reproduction is permitted which does not comply with these terms.

frontiers | Frontiers in Pharmacology

MINI REVIEW
published: 11 July 2022
doi: 10.3389/fphar.2022.948610

Therapeutic Implications of FABP4 in Cancer: An Emerging Target to Tackle Cancer

Naihui Sun[1] *and Xing Zhao*[2]*

[1]Department of Anesthesiology, The First Affiliated Hospital of China Medical University, Shenyang, China, [2]Department of Pediatrics, The First Affiliated Hospital of China Medical University, Shenyang, China

Metabolic reprogramming is an emerging hallmark of tumor cells. In order to survive in nutrient-deprived environment, tumor cells rewire their metabolic phenotype to provide sufficient energy and build biomass to sustain their transformed state and promote malignant behaviors. Fatty acid uptake and trafficking is an essential part of lipid metabolism within tumor cells. Fatty acid-binding proteins (FABPs), which belongs to a family of intracellular lipid-binding protein, can bind hydrophobic ligands to regulate lipid trafficking and metabolism. In particular, adipocyte fatty acid binding protein (FABP4), one of the most abundant members, has been found to be upregulated in many malignant solid tumors, and correlated with poor prognosis. In multiple tumor types, FABP4 is critical for tumor proliferation, metastasis and drug resistance. More importantly, FABP4 is a crucial driver of malignancy not only by activating the oncogenic signaling pathways, but also rewiring the metabolic phenotypes of tumor cells to satisfy their enhanced energy demand for tumor development. Thus, FABP4 serves as a tumor-promoting molecule in most cancer types, and may be a promising therapeutic target for cancer treatment.

Keywords: metabolic reprogramming, fatty acid, tumor microenvironment, prognosis, cancer

OPEN ACCESS

Edited by:
Zhe-Sheng Chen,
St. John's University, United States

Reviewed by:
Khuloud Bajbouj,
University of Sharjah, United Arab Emirates

***Correspondence:**
Xing Zhao
zhaoxing_dl@126.com

Specialty section:
This article was submitted to Pharmacology of Anti-Cancer Drugs, a section of the journal Frontiers in Pharmacology

Received: *20 May 2022*
Accepted: *23 June 2022*
Published: *11 July 2022*

Citation:
Sun N and Zhao X (2022) Therapeutic Implications of FABP4 in Cancer: An Emerging Target to Tackle Cancer. Front. Pharmacol. 13:948610. doi: 10.3389/fphar.2022.948610

INTRODUCTION

Metabolic reprogramming is the capability of tumor cells to reprogram their metabolic phenotype to satisfy the energy demands and activate metabolic signaling pathways for tumorigenesis. Tumorigenesis-related metabolic alterations encompass driving the metabolite influx to endow tumor cells increased capability to acquire the necessary nutrients and preferentially assigning the nutrients to metabolic pathways to support malignant behaviors. Tumor cells reprogram their metabolic phenotype including multiple aspects, including deregulated uptake of glucose and amino acids, utilization of glycolysis and tricarboxylic acid cycle intermediates for biosynthesis and NADPH production, altered regulation of metabolite-induced gene expression as well as complex metabolic interplay with the tumor microenvironment. Altered lipid metabolism is one of the most prominent characteristic changes in tumor metabolism. Lipids are a group of hydrophobic molecules that not only sustain energy and biomass production but also activate a

Abbreviations: acute, acute myelocytic leukemia; AML, cancer-associated adipocytes; CAAs, $CD8^+$ tissue-resident memory cell; Trm, DNA methyltransferase 1; DNMT1, epithelial-mesenchymal transition; EMT, epoxy-eicosatrienoic acid; EET, fatty acid; FA, fatty acid-binding proteins; FABPs, hormone-sensitive lipase; HSL, lipid droplets; LDs, overall survival; OS, programmed death ligand 1; PD-L1, reactive oxygen species; ROS, stearoyl-CoA desaturase-1; SCD1, triple negative breast cancer; TNBC, tumor-associated macrophages; TAMs, tumor microenvironment; TME, tyrosine kinase inhibitors, TKIs.

series of oncogenic signaling pathways to participate in the regulation of tumorigenesis and progression (Currie et al., 2013). Alterations in fatty acid (FA) uptake, *de novo* synthesis, FA oxidation and storage as lipid droplets (LDs) are all considered to be critical for the survival, proliferation and metastasis of tumor cells (Snaebjornsson et al., 2020). Under metabolic stress, enzymes related to lipid metabolism are regulated due to alterations of metabolites and signaling pathways, making tumor cells increase lipids catabolic/anabolic activities, such as FA uptake, *de novo* synthesis, FA oxidation. FA synthesis and uptake supports tumorigenesis by providing necessary membrane phospholipids and signal molecules to sustain proliferation, and FA oxidation fuels tumor growth *via* production of ATP, NADPH and important intermediates. Tumor cells primarily obtain FAs through *de novo* FA synthesis or by exogenous uptake from the tumor microenvironment (TME) (Koundouros and Poulogiaanis, 2020). In terms of exogenous FA uptake, FAs require transporters to maintain solubility and efficiently mediate trafficking across the cellular membrane. Given that FA trafficking is a highly complex process and essential for many aspects of cellular function, these transporters for FA trafficking are implicated in the occurrence and development of cancer, which may open window for novel therapeutic strategies (Koundouros and Poulogiaanis, 2020).

Fatty acid-binding proteins (FABPs) belongs to a family of intracellular lipid-binding protein, binding hydrophobic ligands to regulate lipid trafficking, fluxes and metabolism (Storch and Corsico., 2008). FABP members are able to bind hydrophobic lipid ligands to function as cytoplasmic lipid chaperones to facilitate fatty acid solubilization, trafficking, and metabolism, interact with various membrane and intracellular proteins and regulate tissue and cellular specific lipid responses (Li et al., 2020). FABPs primarily participate in the regulation of uptake and trafficking of FAs from the adjacent stromal cells, regulation of specific metabolic signaling pathways and activation of metabolism-related gene expression (Furuhashi, 2019). More importantly, FABPs are essential for all aspects of FA metabolism, including promoting the trafficking of FAs for FA oxidation, regulating the transcriptional and enzymatic activity for FA *de novo* synthesis and LD storage. FABPs exhibit distinct patterns of tissue expression for the individual protein (Thumser et al., 2014). Given the importance of lipid metabolism involved in the tumorigenesis, FABPs are exploited for potential therapeutic targets in cancer management.

FABP4, also known as adipocyte fatty acid binding protein, is highly expressed in adipocytes, endothelial cells and immune cells (Furuhashi., 2019). During adipocyte differentiation, FABP4 interacts with hormone-sensitive lipase (HSL) or peroxisome PPAR-γ to regulate lipolysis, a process defined as the catabolism of triacylglycerols stored in cell lipid droplets (Garin-Shkolnik et al., 2014). FABP4 is also induced by lipopolysaccharide, advanced glycation end products and oxidized low-density lipoprotein during macrophage differentiation (Wang et al., 2011; Qiao et al., 2019). Exogenous FABP4 interacts with adipocytes to promote differentiation and facilitate p38/HSL-mediated lipolysis (Dou et al., 2020). FABP4 also mediates the maintenance and function of $CD8^+$ tissue-resident memory cells. $CD8^+$ tissue-resident memory (Trm) cells utilize exogenous FAs transported by FABP4 to sustain their oxidative metabolism for immunity (Pan et al., 2017).

FABP4 plays an important role in the pathogenesis of a series of metabolic pathologies (Furuhashi, 2019). In particular, FABP4 levels are elevated in metabolic disorders, including obesity and metabolic syndrome (Furuhashi, 2019). Notably, circulating FABP4 level serves as a potential biomarker for these metabolic disorders (Furuhashi, 2019). In addition, aberrant expression of FABP4 has been observed in multiple cancer types (Guaita-Esteruelas et al., 2018). Importantly, FABP4 contributes to the tumor transformation, proliferation, metastasis and therapy resistance by enhancing lipid transport and activating diverse oncogenic signaling pathways (Guaita-Esteruelas et al., 2018). Moreover, FABP4 functions as a link between tumor cells and the components of TME, including adipocytes, macrophages and endothelial cells. In addition, the prognostic value and targeting strategies of FABP4 in diverse tumor types are also discussed in this review (**Figure 1**).

Role of FABP4 in Tumorigenesis

FABP4 and Tumor Proliferation

Unlimited cellular proliferation is an essential hallmark of cancer (Hanahan D and Weinberg RA, 2011). In order to proliferate, tumor cells sustain increasing uptake and utilization of nutrients to support tumor growth (Hanahan D and Weinberg RA, 2011). Thus, exploring how metabolic phenotypes are intimately intertwined with rapid proliferation of tumor cells may provide novel therapeutic strategies for many types of aggressive tumors. FABP4 enhances tumor proliferation through multiple molecular mechanisms, including rewiring metabolic phenotypes, deregulating DNA methylation and upregulating oncogenic signaling pathways (Guaita-Esteruelas et al., 2017a; Yan et al., 2017; Yang et al., 2020).

FABP4 reprograms metabolic phenotypes to facilitate tumor growth. Orphan nuclear receptor Nur77 functions as a negative regulator for FA uptake and a tumor suppressor to inhibit tumor proliferation (To et al., 2012; Guan et al., 2020). Nur77 recruits SWI/SNF complex and HDAC1 to suppress the transcription of CD36 and FABP4, hampering breast cancer cells uptake of exogenous FAs and leading to the inhibition of cell proliferation (Yang et al., 2020). Proto-oncogene c-Src exerts tumor-promoting effects by activating oncogenic signaling pathways (Belli et al., 2020). Interestingly, FABP4 has shown inhibitory effects in Src-driven tumors. Src inhibition impairs LD formation by activating PPARγ-induced FABP4 expression and elevating reactive oxygen species (ROS) production, suggesting the critical role in Src/PPARγ/FABP4 axis in tumor proliferation (Hua et al., 2019).

DNA methylation is a common epigenetic modification that regulates gene expression, and aberrant DNA methylation patterns are considered a hallmark of cancer (Kulis and Esteller, 2010). Defects in DNA methylation lead to silencing of tumor suppressor genes and dysregulation of genes involved in DNA repair and chromosome stability, resulting in genome

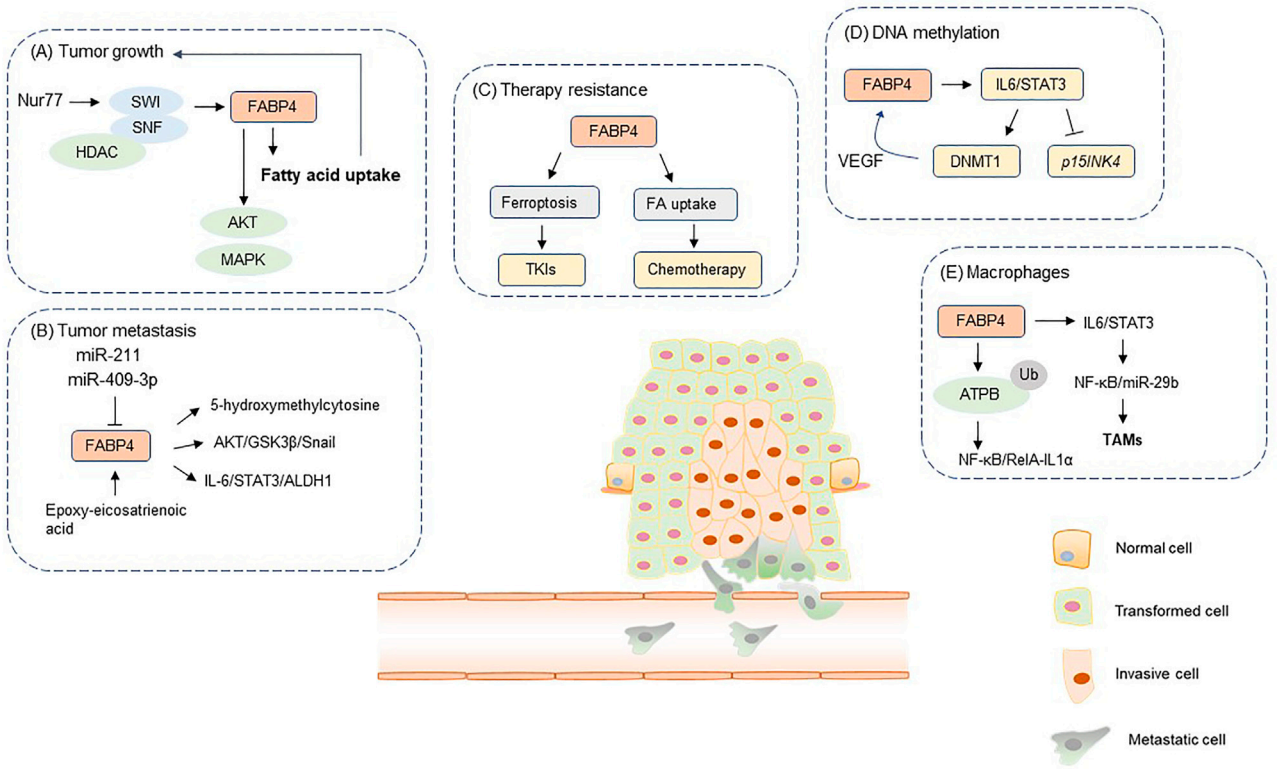

FIGURE 1 | The role of FABP4 in tumor initiation and development. FA, fatty acid; TAMs, tumor-associated macrophages; TKIs, tyrosine kinase inhibitors. FABP4 participates in the regulation of diverse tumorigenic process, including **(A)** tumor growth, **(B)** tumor metastasis, **(C)** therapy resistance, **(D)** DNA methylation, **(E)** interaction between tumor cells and macrophages.

instability in cancers (Klutstein et al., 2016). Numerous studies have pointed out that obesity or high-fat diet regulates the methylome of cancer, which was associated biomarkers involved in DNA CpG methylation in tumors (Donovan et al., 2020). Dietary fatty acids alter the expression of DNA methylation modifiers, global CpG methylation, and gene-specific CpG methylation. For instance, supplementation of omega-3 polyunsaturated fatty acids could alter DNA methylation profiles by increasing methylation of IL-6 (Tremblay et al., 2017). FABP4, as a key mediator for fatty acid trafficking, has been found to be crucial for obesity-induced acute myelocytic leukemia (AML) growth through deregulated DNA methylation. FABP4 overexpression promotes IL-6 expression and STAT3 phosphorylation, resulting in DNA methyltransferase 1 (DNMT1) upregulation and loss of the $p15^{INK4}$ tumor suppressor gene in AML cells (Yan et al., 2017). FABP4 inhibition by BMS309403 downregulated DNMT1 expression, impaired DNA methylation and rescued $p15IN^{K4B}$ tumor suppressor gene by promoter DNA hypomethylation. Moreover, DNMT1 exerts positive regulatory effect on VEGF expression, and VEGF upregulation further increases FABP4 expression to form a vicious FABP4-DNMT1 loop to promote AML progression (Yan et al., 2017). Collectively, FABP4 coordinates fatty acid metabolism and DNA methylation to modulate the development of obesity-associated cancer.

FABP4 activates a series of oncogenic signaling pathways to enhance tumor proliferation. In breast cancer cells, exogenous FABP4 activates the AKT and MAPK signaling cascades, while inhibiting these pathways could impair FABP4-induced breast tumor growth (Guaita-Esteruelas et al., 2017b). Exogenous FABP4 can also activate PI3K/Akt pathway independent of fatty acid trafficking in prostate cancer to enhance tumor growth (Uehara et al., 2014). Collectively, these studies indicate a complex role of FABP4 in the activation of oncogenic signaling pathways.

FABP4 and Tumor Metastasis

Tumor metastasis is responsible for most cancer-related deaths, and failure to limit the metastatic process is thus a huge obstacle for tumor elimination. Metastasis represents a complex multi-step process by which tumor cells disseminates from the primary tumor to a distant organ to establish the secondary metastases. FABP4 functions as a strong mediator in epithelial to mesenchymal transition, stemness, migration, invasion and metastasis (Gharpure et al., 2018; Zhao et al., 2019). The oncogenic functions of FABP4 are mediated by miRNAs in the process of regulating cell metastasis. Under hypoxia, miR-409-3p was downregulated, and FABP4 functions as a downstream target of miR-409-3p in ovarian cancer.

FABP4 substantially increases the metastatic potential of ovarian cancer cells by altering the levels of 5-hydroxymethylcytosine in the DNA and the expression of key genes involved in the metastasis-related and metabolic pathways (Gharpure et al., 2018). In colorectal cancer, miR-211 inhibits cell migration, invasion, and EMT process by targeting FABP4 (Zhao et al., 2019). A novel FABP4/epoxy-eicosatrienoic acid (EET) dynamic that induces triple negative breast cancer (TNBC) metastasis has uncovered an opportunity for TNBC intervention. EET-associated nuclear translocation of FABP4 and nuclear accumulation of SREBP-2 or PPAR-γ significantly enhances TNBC cell migratory transformation and distal metastasis priming (Apaya et al., 2020). Therefore, targeting the EET-driven signaling pathways by galactolipid dLGG can significantly impair FABP4/EET-induced TNBC relapse and metastasis.

Epithelial-mesenchymal transition (EMT) and tumor stemness are major factors contributing to the metastasis of cancer cells. Elevated levels of circulating FABP4 in obese patients increase tumor stemness and aggressiveness. FABP4 upregulation leads to the activation of the IL-6–STAT3–ALDH1 signalling pathway and an increase in levels of STAT3-activating cytokines, which enhances the stemness of tumour (Hao et al., 2018). FABP4 also induces the EMT program in various cancer types. Exogenous FABP4 promotes EMT via the activation of AKT/GSK3β/Snail pathway in cervical squamous cell carcinoma, reorganizing the actin cytoskeletons in F-Actin staining and TGF-β induced EMT assays (Jin et al., 2018). CD36, a transmembrane glycoprotein, facilitates the trafficking of Fas (Pascual et al., 2017). CD36 can directly interact with FABP4 to modulate FA import and metabolism. The positive relationship between CD36 and FABP4 expression is critical for the rates of FA import to ensure that imported FAs can be efficiently transported to subcellular locations (Gyamfi et al., 2021). CD36 inhibition in ovarian cancer impairs adipocyte-driven FABP4 expression. However, FABP4 inhibition did not affect adipocyte-mediated CD36 expression, suggesting CD36 as an upstream regulator of FABP4 (Gyamfi et al., 2021). CD36 inhibition suspends adipocyte-driven EMT and stemness. These pro-metastatic effect of CD36 may correlates with FABP4.

FABP4 and Therapy Resistance

Drug resistance is a major clinical issue that represents the principal cause of cancer-related deaths, with few targetable common pathways. The emergence of metabolic adaptation in resistance to therapeutics has paved the way to the exploration of targeting metabolic vulnerabilities of cancer cells to overcome drug resistance.

LDs have long been considered as inert depots for the storage of excess intracellular lipids. In cancer cells, LDs are often present in excessive amounts to satisfy the high demand of metabolic fuel and building blocks for membrane biosynthesis. LDs represent an underestimated organelle influencing intracellular pharmacokinetics and activity of anticancer tyrosine kinase inhibitors. For instance, LD enrichment of lung cancer cells by oleic acid supplementation potently reduces ponatinib activity, while LD depletion by the long-chain fatty acyl-CoA synthetase inhibitor triacsin C enhances the killing potential of this tyrosine kinase inhibitors (TKIs). Similarly, gefitinib-resistant NSCLC cells exhibit increased LD accumulation compared with gefitinib-sensitive NSCLC cells. Based on these findings, monitoring LD content within tumor cells may be essential for predicting therapy response to TKIs. Oxidative stress caused by hypoxia-reoxygenation exacerbated by TKIs leads to tumor reprogramming by increased lipid desaturation and transport. Ferroptosis is a new form of programmed cell death characterized by the accumulation of iron-dependent lipid peroxidation. FABP4 could enhance tumor transport for increased LD content, which coordinates with FA desaturation mediated by stearoyl-CoA desaturase-1 (SCD1), to protect tumor cells from oxidative stress-induced ferroptosis. This SCD1/FABP4 network provides tumor intrinsic antioxidant and anti-ferroptotic resources for survival and regrowth in a harsh TME (Luis et al., 2021).

Adipose tissues also play a critical role in the regulation of chemotherapeutic resistance. In the tumor microenvironment, adipose tissues survive under hypoxic and nutrient-deprived condition, which may lead to the alteration of cellular and molecular compositions. These alterations would inevitably affect chemotherapeutic responses of tumor cells growing in the neighborhood of tumor-associated adipose tissues. Adipocyte-derived conditioned medium has been found to reduce cytotoxic effects of chemotherapy to BC and PDAC cells. Besides, tumor stemness have been widely reported to be essential for mediating chemotherapy resistance and metabolic alterations in these cells might be the key to their ability to maintain stemness and drug resistance. Interestingly, adipocytes could upregulate expression levels of fatty acid transporter and fatty acid trafficking to induce tumor stemness. Co-culturing breast cancer cells with adipocytes significantly increase CD36 expression, CD36 activates STAT3 and ERK1/2 signaling pathways to induce the gene expression of EMT and stem cell traits. Recent studies have found that FABP4 specific inhibitor BMS309403 not only significantly reduces tumor burden in a syngeneic orthotopic mouse model but also increases the sensitivity of cancer cells toward carboplatin (Mukherjee et al., 2020). Taken together, targeting FABP4 may have a significant impact on the efficacy of chemotherapeutics through interactions with tumoral adipose tissues.

Interaction of FABP4 With the Tumor Microenvironment

TME contains a group of diverse cell types, including immune cells, adipocytes, and endothelial cells, alongside cancer cells. Given that tumor cells constantly interact with surrounding cells, TME has been extensively reported in tumor occurrence and development. There is a growing number of studies supporting the potential of targeting the TME in cancer therapy.

FABP4 and Adipocytes

In the TME, adipocytes have a complex interaction with tumor cells and therefore undergo a series of important phenotypic and

molecular modifications to reprogram themselves to a state of cancer-associated adipocytes (CAAs) (Cao, 2019). Compared to normal adipocytes, CAAs display a series of characteristics, including fibroblast-like phenotypes, dispersed lipid droplets, releasing more leptin, adiponectin, interleukin-6, chemokine ligand two and chemokine ligand five and other adipokines (Zhao et al., 2020). FAs released from CAAs can be transported to tumor cells for energy production relying on FA oxidation and activation of downstream signaling pathways (Nieman et al., 2011). Therefore, CAAs contribute to tumor occurrence and development. Intracellular FABP4 is the one of the most critical players implicated in CAA-tumor cell interplay. This oncogenic effect is obvious in tumor cells within CAA-rich microenvironments including the breast, or tumors metastasizing to adipocyte-enriched sites such as gastric and ovarian cancers (Nieman et al., 2011; Tan et al., 2018). Adipocyte–cancer cell coculture mediates enhanced lipolysis in CAAs and FA oxidation in tumor cells, indicating CAAs as an energy source for the tumor cells (Nieman et al., 2011).

Some tumor cells including prostate and ovarian cancer preferentially home to and proliferate in the adipocyte-rich niche (Nieman et al., 2011). In these metastatic niches, FABP4 regulates the CAA-tumor interplay by mediating the transport of FAs between tumor cells and CAAs. The adipocyte-rich niches, such as bone metastatic niche or omentum, are metabolically active components that regulate the function of neighboring cells. For instance, once the prostate tumor cells reach the skeletal sites, lipolytic signals are activated in neighboring CAAs, leading to the release of lipids. The lipid transfer between marrow adipocytes and tumor cells can further fuel the growth and invasiveness of tumor cells at the metastatic sites by upregulating FABP4. Exposure of prostate tumor cells to adipocyte-derived factors has been proved to induce PPARγ-driven FABP4 expression (Uehara et al., 2014). The FABP4 upregulation can also be induced by cytokine IL-17A secreted by IL-17A-producing cells via p-STAT3 signaling in the metastatic process of ovarian cancer to omentum (Yu et al., 2020).

FABP4 and Immune Cells

Tumor-associated macrophages (TAMs) represent one of the main tumor-infiltrating immune cell types and are generally categorized into either of two functionally contrasting subtypes, namely classical activated M1 macrophages and alternatively activated M2 macrophages. Macrophages infiltrate into solid tumor tissues and numerous evidences have pointed out that tumor-associated macrophages (TAMs) always acquire a polarized M2 phenotype to exert protumor functions, and the abundance of TAMs are correlated with poor disease prognosis (Li et al., 2019). Numerous evidences reveal that TAMs contribute to tumor progression by stimulating cell proliferation, metastasis and immune evasion (Ngambenjawong et al., 2017). Thus, eliminating TAMs may be a promising therapeutic strategy for cancer management. FABP4 was found to be significantly upregulated in a subset of TAM with a CD11b+F4/80+MHCII-Ly6C-phenotype. In these TAMs, FABP4 facilitates protumor IL6/STAT3 signaling through regulation of the NF-κB/miR-29b pathway (Hao et al., 2018). FABP4 increases FA transport and oxidation to elevate ROS generation and macrophage death (Zhang et al., 2017). In macrophages, FABP4 is critical for metabolism of excess FAs for ceramide synthesis. Ceramide is the precursor of all complex sphingolipids, which functions as a key regulator of cellular stress, senescence, and death. FABP4 inhibition in macrophage impairs FA-induced ceramide production, thus leading to suppressed cell death (Zhang et al., 2017). In neuroblastoma, FABP4 interacts with ATPB to facilitate ATPB ubiquitination in macrophages (Miao et al., 2021). The decreased ATP levels further deactivates NF-κB/RelA-IL1α pathway, contributing to the malignant phenotypes in neuroblastoma cells (Miao et al., 2021). Collectively, intracellular FABP4 is essential for the function of tumor-promoting macrophages.

CD8+Trm cells constitute the most abundant memory T cell subset. Precious studies have elucidated that the infiltration level of CD8+Trm cells are associated with antitumor immune responses, and the presence of CD8+Trm cells correlates with improved prognosis in patients with cancer. Importantly, CD8+Trm cells rely on exogenous fatty acid uptake and metabolism for cell survival. FABP4 and FABP5, the key transporters of fatty acids, have a critical role in the maintenance, longevity and function of $CD8^+$ Trm cells to mediate protective immunity. However, gastric tumor cells outcompete Trm cells for lipid uptake and thus induce apoptosis of Trm cells, which could be reversed by blocking PD-L1 on cancer cells. Tumor cells highly express programmed death ligand 1 (PD-L1), which binds to receptor PD-1 expressed on activated T cells, thus leading to immune evasion. Anti-PD-1/PD-L1 therapy inhibits the binding of PD-1/PD-L1 to activate the exhausted T cells to enhance anti-tumor immunity. PD-L1 blockade decreases FABP4 and FABP5 expression in gastric tumor cells, while increases FABP4 and FABP5 expression in Trm cells, enhancing fatty acid uptake by Trm cells and sustaining survival of Trm cells (Lin et al., 2020).

FABP4 and Angiogenesis

To increase the proliferative potential of cancer cells, complex vascular networks are required for tumor cells to sustain their malignant phenotypes (Viallard and Larrivee, 2017). Therefore, angiogenesis is a hallmark of malignant tumors and a promising therapeutic target for cancer treatment. Angiogenesis, a crucial step in tumor growth and metastasis, is regulated by various pro- or anti-angiogenic factors (De et al., 2017). Endothelial cell-FABP4, which is regulated by VEGF, mTORC1 and NOTCH1, exhibits a pro-angiogenic role by regulating expression of several key mediators of angiogenesis, including P38, eNOS, and stem cell factor/c-kit signaling to promote cell proliferation, survival, and migration, angiogenic sprouting (Elmasri et al., 2012; Harjes et al., 2017). In ovarian tumor xenografts, knockdown of endothelial FABP4 supports FA oxidation, elevates ROS and impairs angiogenesis (Harjes et al., 2017). In hepatocellular carcinoma, FABP4 promotes tumor development by upregulating the angiogenesis gene signature (Laouirem et al., 2019).

TABLE 1 | Expression patterns and clinical significance of FABP4 in diverse tumor types.

Cancer Type	Expression of FABP4	Level	Clinical Significance	References
Bladder cancer	Downregulation	Protein	Lymph node metastasis Shorter OS	Mathis et al. (2018)
Breast cancer	Upregulation	Protein	Tumor grade Short DFS	Cui et al. (2019)
	Upregulation	mRNA	N/A	Hao et al. (2018)
Cervical cancer	Upregulation	Protein	Pelvic lymph node metastasis Poor OS	Li et al. (2021)
Colon cancer	Upregulation	Protein	N/A	Tian et al. (2020)
Colorectal cancer	Upregulation	Protein	N/A	Zhang et al. (2019)
Glioblastoma	Upregulation	mRNA	N/A	Li et al. (2018)
Hepatocellular carcinoma	Downregulation	Protein	Short RFS and OS	Zhong et al. (2018)
Non-small cell lung cancer	Upregulation	Protein	Advanced TNM stage poor OS	Tang et al. (2016)
Pancreatic Ductal Adenocarcinomas	Upregulation	Protein	Lymph node metastasis Poor prognosis	Luo et al. (2017)

TABLE 2 | Therapeutic targeting of FABP4 evaluated in different cancer types.

Methods	Cancer Type	Results	References
Inhibitor BMS309403	Breast cancer	Inhibiting growth and metastasis	Uehara et al. (2014)
	Cholangiocarcinoma	Inhibiting metastasis	Yang et al. (2021)
	Colon cancer	Inhibiting metastasis	Tian et al. (2020)
	Hepatocellular carcinoma	Inhibiting growth and metastasis	Yan et al. (2018)
		Inhibiting growth and metastasis	Laouirem et al. (2019)
	Leukemia	Inhibiting growth	Yan et al. (2017)
	Liver cancer	Inhibiting growth and self-renewal	Wang et al. (2019)
	Ovarian cancer	Inhibiting growth and metastasis Increasing sensitivity to carboplatin	Mukherjee et al. (2020)
	Prostate cancer	Inhibiting metastasis	Nie et al. (2017)
Inhibitor BD62694	Ovarian cancer	Inhibiting recurrence	Tian et al. (2020)
siRNA	Hepatocellular carcinoma	Inhibiting growth and metastasis	Wang et al. (2019)
	Leukemia	Inhibiting growth	Yan et al. (2017)
	Ovarian cancer	Inhibiting metastasis	Gharpure et al. (2018)
shRNA	Triple-negative breast cancer	Inhibiting metastasis	Apaya et al. (2020)

Clinical Significance of FABP4 in Cancer

FABP4 as Prognostic Marker

Deregulated expression of FABP4 has been observed in multiple cancer types (Cui et al., 2019; Li et al., 2021). Dysregulated expression of FABP4 is associated with different clinic-parameters and prognosis, indicating FABP4 as a potential prognostic marker in different cancer types (**Table 1**). Upregulated intracellular expression of FABP4 is found in gastrointestinal stromal tumors, indicating a negative effect on the overall survival (OS) of these patients (Zang et al., 2021). Specifically, in cervical cancer, upregulated FABP4 expression in cancer tissues is associated with poor OS and pelvic lymph node metastasis, indicating the prognostic value of FABP4 in cervical cancer patients (Li et al., 2021). Among patients with non-small cell lung cancer, high expression of FABP4 is correlated with advanced tumor node metastasis stage (Tang et al., 2016). Although FABP4 has been found to be upregulated in most tumor types, FABP4 has also found to be downregulated in certain cancer. In liver cancer, FABP4 is downregulated than the adjacent normal tissue. Importantly, FABP4 was correlated with the tumor size, recurrence-free survival and OS (Zhong et al., 2018).

Recent studies pointed out that circulating FABP4 levels have great clinical implications in cancer. Breast cancer patients display higher blood concentration of FABP4, implying elevated levels of circulating FABP4 as a specific promoter of the obesity-associated breast cancer (Guaita-Esteruelas et al., 2017a; Zeng et al., 2020). Another study also revealed that serum FABP4 levels are elevated in obese breast cancer patients than in non-obese breast cancer patients (Hancke et al., 2010). Moreover, in breast cancer, serum FABP4 is positively connected with tumor size and nodal-status (Hancke et al., 2010). Interestingly, circulating FABP4 may be persistently released into the circulation and reduce after the lesion is treated. Among patients with colorectal cancer, circulating FABP4 is higher than the levels in the control groups before surgery, and remarkedly reduces after operation (Zhang et al., 2019). Moreover, patients with elevated circulating FABP4 levels indicates higher risk of colorectal cancer. Collectively, circulating FABP4 opens new diagnosis and therapy

perspectives for breast cancer, especially for obesity-associated breast cancer.

Therapeutic Targeting of FABP4

FABP4 has emerged as a critical player in tumorigenesis, thus targeting FABP4 may provide a promising therapeutic target for cancer treatment. FABP4 has been targeted using various approaches, including small molecule inhibitors, siRNAs and short hairpin RNAs (**Table 2**). Currently, no clinical trials have underwent to evaluate the efficacy of FABP4 inhibition in the clinical setting. Thus, clinical trials should be accelerated to test the therapeutic effects of FABP4 inhibitors in diverse types of cancer, which may implement the options of therapeutic strategies for cancer patients in clinical practice. BMS309403, which was first identified a drug for metabolic syndrome, can effectively impair the growth and metastases of tumor in several mouse models by targeting both tumor and stromal cells (Mukherjee et al., 2020). Further studies are required to identify the responsive tumor types. In addition, combination of FABP4 inhibitors with anti-tumor drugs like chemotherapy and TKIs could augment the anti-tumor effect of traditional (Luis et al., 2021). More studies should be focused on the oncogenic role and underlying mechanisms of FABP4 in cancer development to improve the clinical outcomes of cancer patients. In particular, deep understanding of the potential adverse effect is required to ensure the safety of combination therapies.

CONCLUSION

Collectively, FABP4 has been found to be upregulated in most cancer types, and correlated with poor prognosis. FABP4 primarily functions as a promoter for tumor proliferation, metastasis and drug resistance. More importantly, FABP4 is a crucial driver of malignancy not only by activating the oncogenic signaling pathways, but also rewiring the metabolic phenotypes of tumor cells to satisfy the increased energy demand for tumor development. Thus, FABP4 serves as a tumor-promoting molecule in most cancer types, and may be a promising therapeutic target for cancer treatment.

AUTHOR CONTRIBUTIONS

NS—writing and elaborating the figures. XZ—writing and reviewing the final version.

FUNDING

This work was supported by the Project of Liaoning Province Natural Science Foundation (2021-BS-117).

REFERENCES

Apaya, M. K., Hsiao, P. W., Yang, Y. C., and Shyur, L. F. (2020). Acid-Associated FABP4/FABP5 Signaling Network as a Therapeutic Approach for Metastatic Triple-Negative Breast Cancer. *Cancers (Basel)* 12, 199. doi:10.3390/cancers12010199

Belli, S., Esposito, D., Servetto, A., Pesapane, A., Formisano, L., Bianco, R., et al. (2020). c-Src and EGFR Inhibition in Molecular Cancer Therapy: What Else Can We Improve? *Cancers(Basel)* 12, 1489. doi:10.3390/cancers12061489

Cao, Y. (2019). Adipocyte and Lipid Metabolism in Cancer Drug Resistance. *J. Clin. Invest* 129, 3006–3017. eCollection 2019 Jul 2. doi:10.1172/JCI127201

Cui, Y., Song, M., and Kim, S. Y. (2019). Prognostic Significance of Fatty Acid Binding Protein-4 in the Invasive Ductal Carcinoma of the Breast. *Pathol. Int.* 69, 68–75. Epub 2019 Jan 29. doi:10.1111/pin.12756

Currie, E., Schulze, A., Zechner, R., Walther, T. C., and Farese, R. V., Jr. (2013). Cellular Fatty Acid Metabolism and Cancer. *Cell Metab.* 18, 153–161. doi:10.1016/j.cmet.2013.05.017

De Palma, M., Biziato, D., and Petrova, T. V. (2017). Microenvironmental Regulation of Tumour Angiogenesis. *Nat. Rev. Cancer* 17, 457–474. doi:10.1038/nrc.2017.51

Donovan, M. G., Wren, S. N., Cenker, M., Selmin, O. I., and Romagnolo, D. F. (2020). Dietary Fat and Obesity as Modulators of Breast Cancer Risk: Focus on DNA Methylation. *Br J Pharmacol.* 177, 1331–1350. doi:10.1111/bph.14891

Dou, H.-X., Wang, T., Su, H.-X., Gao, D.-D., Xu, Y.-C., Li, Y.-X., et al. (2020). Exogenous FABP4 Interferes with Differentiation, Promotes Lipolysis and Inflammation in Adipocytes. *Endocrine* 67, 587–596. doi:10.1007/s12020-019-02157-8

Elmasri, H., Ghelfi, E., Yu, C.-w., Traphagen, S., Cernadas, M., Cao, H., et al. (2012). Endothelial Cell-Fatty Acid Binding Protein 4 Promotes Angiogenesis: Role of Stem Cell Factor/c-Kit Pathway. *Angiogenesis* 15, 457–468. doi:10.1007/s10456-012-9274-0

Furuhashi, M. (2019). Fatty Acid-Binding Protein 4 in Cardiovascular and Metabolic Diseases. *Jat* 26, 216–232. doi:10.5551/jat.48710

Garin-Shkolnik, T., Rudich, A., Hotamisligil, G. S., and Rubinstein, M. (2014). FABP4 Attenuates PPARγ and Adipogenesis and Is Inversely Correlated with PPARγ in Adipose Tissues, *Diabetics.* 63, 900, 911. Doi: doi:10.2337/db13-0436

Gharpure, K. M., Pradeep, S., Sans, M., Rupaimoole, R., Ivan, C., Wu, S. Y., et al. (2018). FABP4 as a Key Determinant of Metastatic Potential of Ovarian Cancer. *Nat. Commun.* 9, 2923. doi:10.1038/s41467-018-04987-y

Guaita-Esteruelas, S., Bosquet, A., Saavedra, P., Gumà, J., Girona, J., Lam, E. W.-F., et al. (2017a). Exogenous FABP4 Increases Breast Cancer Cell Proliferation and Activates the Expression of Fatty Acid Transport Proteins. *Mol. Carcinog.* 56, 208–217. doi:10.1002/mc.22485

Guaita-Esteruelas, S., Gumà, J., Masana, L., and Borràs, J. (2018). The Peritumoural Adipose Tissue Microenvironment and Cancer. The Roles of Fatty Acid Binding Protein 4 and Fatty Acid Binding Protein 5. *Mol. Cell. Endocrinol.* 462, 107–118. Epub 2017 Feb 3. doi:10.1016/j.mce.2017.02.002

Guaita-Esteruelas, S., Saavedra-García, P., Bosquet, A., Borràs, J., Girona, J., Amiliano, K., et al. (2017b). Adipose-Derived Fatty Acid-Binding Proteins Plasma Concentrations Are Increased in Breast Cancer Patients. *Oncologist* 22, 1309–1315. doi:10.1634/theoncologist.2016-0483

Guan, Y.-f., Huang, Q.-l., Ai, Y.-l., Chen, Q.-t., Zhao, W.-x., Wang, X.-m., et al. (2020). Nur77-activated lncRNA WFDC21P Attenuates Hepatocarcinogenesis via Modulating Glycolysis. *Oncogene* 39, 2408–2423. doi:10.1038/s41388-020-1158-y

Gyamfi, J., Yeo, J. H., Kwon, D., Min, B. S., Cha, Y. J., Koo, J. S., et al. (2021). Interaction between CD36 and FABP4 Modulates Adipocyte-Induced Fatty Acid Import and Metabolism in Breast Cancer. *NPJ Breast Cancer* 7, 129. doi:10.1038/s41523-021-00324-7

Hanahan, D., and Weinberg, R. A. (2011). Hallmarks of Cancer: The Next Generation. *Cell* 144, 646–674. doi:10.1016/j.cell.2011.02.013

Hancke, K., Grubeck, D., Hauser, N., Kreienberg, R., and Weiss, J. M. (2010). Adipocyte Fatty Acid-Binding Protein as a Novel Prognostic Factor in Obese Breast Cancer Patients. *Breast Cancer Res. Treat.* 119, 367–377. doi:10.1007/s10549-009-0577-9

Hao, J., Yan, F., Zhang, Y., Triplett, A., Zhang, Y., Schultz, D. A., et al. (2018). Expression of Adipocyte/Macrophage Fatty Acid-Binding Protein in Tumor-Associated Macrophages Promotes Breast Cancer Progression. *Cancer Res.* 78, 2343–2355. Epub 2018 Feb 6. doi:10.1158/0008-5472.CAN-17-2465

Hua, T. N. M., Kim, M.-K., Vo, V. T. A., Choi, J.-W., Choi, J. H., Kim, H.-W., et al. (2019). Inhibition of Oncogenic Src Induces FABP4-Mediated Lipolysis via PPARγ Activation Exerting Cancer Growth Suppression. *EBioMedicine* 41, 134–145. doi:10.1016/j.ebiom.2019.02.015

Jin, J., Zhang, Z., Zhang, S., Chen, X., Chen, Z., Hu, P., et al. (2018). Fatty Acid Binding Protein 4 Promotes Epithelial-Mesenchymal Transition in Cervical Squamous Cell Carcinoma through AKT/GSK3β/Snail Signaling Pathway. *Mol. Cell Endocrinol.* 461, 155–164. doi:10.1016/j.mce.2017.09.005

Klutstein, M., Nejman, D., Greenfield, R., and Cedar, H. (2016). DNA Methylation in Cancer and Aging. *Cancer Res.* 76 (12), 3446–3450. Epub 2016 Jun 2. doi:10.1158/0008-5472.CAN-15-3278

Koundouros, N., and Poulogiannis, G. (2020). Reprogramming of Fatty Acid Metabolism in Cancer. *Br. J. Cancer* 122, 4–22. Epub 2019 Dec 10. doi:10.1038/s41416-019-0650-z

Kulis, M., and Esteller, M. (2010). DNA Methylation and Cancer. *Adv. Genet.* 70, 27–56. doi:10.1016/B978-0-12-380866-0.60002-2

Laouirem, S., Sannier, A., Norkowski, E., Cauchy, F., Doblas, S., Rautou, P. E., et al. (2019). Endothelial Fatty Liver Binding Protein 4: a New Targetable Mediator in Hepatocellular Carcinoma Related to Metabolic Syndrome. *Oncogene* 38, 3033–3046. doi:10.1038/s41388-018-0597-1

Li, B., Hao, J., Zeng, J., and Sauter, E. R. (2020). SnapShot: FABP Functions. *Cell* 182 (4), 1066. e1. doi:10.1016/j.cell.2020.07.027

Li, G., Wu, Q., Gong, L., Xu, X., Cai, J., Xu, L., et al. (2021). FABP4 Is an Independent Risk Factor for Lymph Node Metastasis and Poor Prognosis in Patients with Cervical Cancer. *Cancer Cell Int.* 21, 568. doi:10.1186/s12935-021-02273-4

Li, H. Y., Lv, B. B., and Bi, Y. H. (2018). FABP4 Accelerates Glioblastoma Cell Growth and Metastasis through Wnt10b Signalling. *Eur. Rev. Med. Pharmacol. Sci.* 22, 7807–7818. doi:10.26355/eurrev_201811_16405

Li, X., Liu, R., Su, X., Pan, Y., Han, X., Shao, C., et al. (2019). Harnessing Tumor Associated Macrophages as Aids for Cancer Immunotherapy. *Mol. Cancer* 18 (1), 177. doi:10.1186/s12943-019-1102-3

Lin, R., Zhang, H., Yuan, Y., He, Q., Zhou, J., Li, S., et al. (2020). Fatty Acid Oxidation Controls CD8+ Tissue-Resident Memory T-Cell Survival in Gastric Adenocarcinoma. *Cancer Immunol. Res.* 8, 479–492. doi:10.1158/2326-6066.CIR-19-0702

Luis, G., Godfroid, A., Nishiumi, S., Cimino, J., Blacher, S., Maquoi, E., et al. (2021). Tumor Resistance to Ferroptosis Driven by Stearoyl-CoA Desaturase-1 (SCD1) in Cancer Cells and Fatty Acid Biding Protein-4 (FABP4) in Tumor Microenvironment Promote Tumor Recurrence. *Redox Biol.* 43, 102006. doi:10.1016/j.redox.2021.102006

Luo, Y., Yang, Z., Li, D., Liu, Z., Yang, L., Zou, Q., et al. (2017). LDHB and FABP4 Are Associated with Progression and Poor Prognosis of Pancreatic Ductal Adenocarcinomas. *Appl. Immunohistochem. Mol. Morphol.* 25, 351–357. doi:10.1097/PAI.0000000000000306

Mathis, C., Lascombe, I., Monnien, F., Bittard, H., Kleinclauss, F., Bedgedjian, I., et al. (2018). Down-regulation of A-FABP Predicts Non-muscle Invasive Bladder Cancer Progression: Investigation with a Long Term Clinical Follow-Up. *BMC Cancer* 18, 1239. doi:10.1186/s12885-018-5137-4

Miao, L., Zhuo, Z., Tang, J., Huang, X., Liu, J., Wang, H., et al. (2021). FABP4 Deactivates NF-kappaB-IL1alpha Pathway by Ubiquitinating ATPB in Tumor-Associated Macrophages and Promotes Neuroblastoma Progression. *Clin. Transl. Med.* 11, e395. doi:10.1002/ctm2.395

Mukherjee, A., Chiang, C. Y., Daifotis, H. A., Nieman, K. M., Fahrmann, J. F., Lastra, R. R., et al. (2020). Adipocyte-Induced FABP4 Expression in Ovarian Cancer Cells Promotes Metastasis and Mediates Carboplatin Resistance. *Cancer Res.* 80, 1748–1761. CAN-19-1999. doi:10.1158/0008-5472

Ngambenjawong, C., Gustafson, H. H., and Pun, S. H. (2017). Progress in Tumor-Associated Macrophage (TAM)-targeted Therapeutics. *Adv. Drug Deliv. Rev.* 114, 206–221. Epub 2017 Apr 25. doi:10.1016/j.addr.2017.04.010

Nie, J., Zhang, J., Wang, L., Lu, L., Yuan, Q., An, F., et al. (2017). Adipocytes Promote Cholangiocarcinoma Metastasis through Fatty Acid Binding Protein 4. *J. Exp. Clin. Cancer Res.* 36, 183. doi:10.1186/s13046-017-0641-y

Nieman, K. M., Kenny, H. A., Penicka, C. V., Ladanyi, A., Buell-Gutbrod, R., Zillhardt, M. R., et al. (2011). Adipocytes Promote Ovarian Cancer Metastasis and Provide Energy for Rapid Tumor Growth. *Nat. Med.* 17, 1498–1503. doi:10.1038/nm.2492

Pan, Y., Tian, T., Park, C. O., Lofftus, S. Y., Mei, S., Liu, X., et al. (2017). Survival of Tissue-Resident Memory T Cells Requires Exogenous Lipid Uptake and Metabolism. *Nature* 543, 252–256. doi:10.1038/nature21379

Pascual, G., Avgustinova, A., Mejetta, S., Martín, M., Castellanos, A., Attolini, C. S.-O., et al. (2017). Targeting Metastasis-Initiating Cells through the Fatty Acid Receptor CD36. *Nature* 541, 41–45. doi:10.1038/nature20791

Qiao, Y., Liu, L., Yin, L., Xu, L., Tang, Z., Qi, Y., et al. (2019). RETRACTED ARTICLE: FABP4 Contributes to Renal Interstitial Fibrosis via Mediating Inflammation and Lipid Metabolism. *Cell Death Dis.* 10, 382. doi:10.1038/s41419-019-1610-5

Snaebjornsson, M. T., Janaki-Raman, S., and Schulze, A. (2020). Greasing the Wheels of the Cancer Machine: The Role of Lipid Metabolism in Cancer. *Cell Metab.* 31, 62–76. Epub2019 Dec 5. doi:10.1016/j.cmet.2019.11.010

Storch, J., and Corsico, B. (2008). The Emerging Functions and Mechanisms of Mammalian Fatty Acid-Binding Proteins. *Annu. Rev. Nutr.* 28, 73–95. doi:10.1146/annurev.nutr.27.061406

Tan, Y., Lin, K., Zhao, Y., Wu, Q., Chen, D., Wang, J., et al. (2018). Adipocytes Fuel Gastric Cancer Omental Metastasis via PITPNC1-Mediated Fatty Acid Metabolic Reprogramming. *Theranostics* 8, 5452–5468. eCollection 2018. doi:10.7150/thno.28219

Tang, Z., Shen, Q., Xie, H., Zhou, X., Li, J., Feng, J., et al. (2016). Elevated Expression of FABP3 and FABP4 Cooperatively Correlates with Poor Prognosis in Non-small Cell Lung Cancer (NSCLC). *Oncotarget* 7, 46253–46262. doi:10.18632/oncotarget.10086

Thumser, A. E., Moore, J. B., and Plant, N. J. (2014). Fatty Acid Binding Proteins. *Curr. Opin. Clin. Nutr. Metabolic Care* 17, 124–129. doi:10.1097/MCO.0000000000000031

Tian, W., Zhang, W., Zhang, Y., Zhu, T., Hua, Y., Li, H., et al. (2020). FABP4 Promotes Invasion and Metastasis of Colon Cancer by Regulating Fatty Acid Transport. *Cancer Cell Int.* 20, 512. doi:10.1186/s12935-020-01582-4

To, S. K., Zeng, J. Z., and Wong, A. S. (2012). Nur77: a Potential Therapeutic Target in Cancer. *Expert Opin. Ther. Targets* 16, 573–585. doi:10.1517/14728222.2012.680958

Tremblay, B. L., Guénard, F., Rudkowska, I., Lemieux, S., Couture, P., Vohl, M.-C., et al. (2017). Epigenetic Changes in Blood Leukocytes Following an Omega-3 Fatty Acid Supplementation. *Clin. Epigenet* 9, 43. eCollection 2017. doi:10.1186/s13148-017-0345-3

Uehara, H., Takahashi, T., Oha, M., Ogawa, H., and Izumi, K. (2014). Exogenous Fatty Acid Binding Protein 4 Promotes Human Prostate Cancer Cell Progression. *Int. J. Cancer* 135, 2558–2568. doi:10.1002/ijc.28903

Viallard, C., and Larrivée, B. (2017). Tumor Angiogenesis and Vascular Normalization: Alternative Therapeutic Targets. *Angiogenesis* 20, 409–426. Epub 2017 Jun 28. doi:10.1007/s10456-017-9562-9

Wang, S., Yao, Y., Wang, X., Zheng, G., Ouyang, W., and Chen, W. (2019). 25-HC Promotes Hepatocellular Carcinoma Metastasis through Up-Regulation of TLR4 Dependent FABP4. *Am. J. Cancer Res.* 9, 2140–2155. eCollection 2019.

Wang, X. Q., Yang, K., He, Y. S., Lu, L., and Shen, W. F. (2011). Receptor Mediated Elevation in FABP4 Levels by Advanced Glycation End Products Induces Cholesterol and Triacylglycerol Accumulation in THP-1 Macrophages. *Lipids* 46, 479–486. doi:10.1007/s11745-011-3542-4

Yan, F., Shen, N., Pang, J. X., Zhang, Y. W., Rao, E. Y., Bode, A. M., et al. (2017). Fatty Acid-Binding Protein FABP4 Mechanistically Links Obesity with Aggressive AML by Enhancing Aberrant DNA Methylation in AML Cells. *Leukemia* 31, 1434–1442. doi:10.1038/leu.2016.349

Yan, F., Shen, N., Pang, J. X., Zhao, N., Zhang, Y. W., Bode, A. M., et al. (2018). A Vicious Loop of Fatty Acid-Binding Protein 4 and DNA Methyltransferase 1 Promotes Acute Myeloid Leukemia and Acts as a Therapeutic Target. *Leukemia* 32, 865–873. doi:10.1038/leu.2017.307

Yang, H., Deng, Q., Ni, T., Liu, Y., Lu, L., Dai, H., et al. (2021). Targeted Inhibition of LPL/FABP4/CPT1 Fatty Acid Metabolic axis Can Effectively Prevent the Progression of Nonalcoholic Steatohepatitis to Liver Cancer. *Int. J. Biol. Sci.* 17, 4207–4222. doi:10.7150/ijbs.64714

Yang, P.-b., Hou, P.-p., Liu, F.-y., Hong, W.-b., Chen, H.-z., Sun, X.-y., et al. (2020). Blocking PPARγ Interaction Facilitates Nur77 Interdiction of Fatty Acid Uptake and Suppresses Breast Cancer Progression. *Proc. Natl. Acad. Sci. U.S.A.* 117, 27412–27422. doi:10.1073/pnas.2002997117

Yu, C., Niu, X., Du, Y., Chen, Y., Liu, X., Xu, L., et al. (2020). IL-17A Promotes Fatty Acid Uptake through the IL-17A/IL-17RA/p-STAT3/FABP4 axis to Fuel

Ovarian Cancer Growth in an Adipocyte-Rich Microenvironment. *Cancer Immunol. Immunother.* 69, 115–126. doi:10.1007/s00262-019-02445-2

Zang, W. J., Wang, Z. N., Hu, Y. L., Huang, H., and Ma, P. (2021). Expression of Fatty Acid-binding Protein-4 in Gastrointestinal Stromal Tumors and its Significance for Prognosis. *J. Clin. Lab. Anal.* 35, e24017. Epub 2021 Sep 24. doi:10.1002/jcla.24017

Zeng, J., Sauter, E. R., and Li, B. (2020). FABP4: A New Player in Obesity-Associated Breast Cancer. *Trends Mol. Med.* 26, 437–440. Epub 2020 Apr 8. doi:10.1016/j.molmed.2020.03.004

Zhang, Y., Zhao, X., Deng, L., Li, X., Wang, G., Li, Y., et al. (2019). High Expression of FABP4 and FABP6 in Patients with Colorectal Cancer. *World J. Surg. Oncol.* 17, 171. doi:10.1186/s12957-019-1714-5

Zhang, Y., Rao, E., Zeng, J., Hao, J., Sun, Y., Liu, S., et al. (2017). Adipose Fatty Acid Binding Protein Promotes Saturated Fatty Acid-Induced Macrophage Cell Death through Enhancing Ceramide Production. *J. Immunol.* 198, 798–807. doi:10.4049/jimmunol.1601403

Zhao, C., Wu, M., Zeng, N., Xiong, M., Hu, W., Lv, W., et al. (2020). Cancer-associated Adipocytes: Emerging Supporters in Breast Cancer. *J. Exp. Clin. Cancer Res.* 39 (1), 156. doi:10.1186/s13046-020-01666-z

Zhao, D., Ma, Y., Li, X., and Lu, X. (2019). microRNA-211 Promotes Invasion and Migration of Colorectal Cancer Cells by Targeting FABP4 via PPARgamma. *J. Cell Physiol.* 234, 15429–15437. Online ahead of print. doi:10.1002/jcp.28190

Zhong, C. Q., Zhang, X. P., Ma, N., Zhang, E. B., Li, J. J., Jiang, Y. B., et al. (2018). FABP4 Suppresses Proliferation and Invasion of Hepatocellular Carcinoma Cells and Predicts a Poor Prognosis for Hepatocellular Carcinoma. *Cancer Med.* 7, 2629–2640. Epub. doi:10.1002/cam4.1511

Conflict of Interest: The authors declare that the research was conducted in the absence of any commercial or financial relationships that could be construed as a potential conflict of interest.

Publisher's Note: All claims expressed in this article are solely those of the authors and do not necessarily represent those of their affiliated organizations, or those of the publisher, the editors and the reviewers. Any product that may be evaluated in this article, or claim that may be made by its manufacturer, is not guaranteed or endorsed by the publisher.

Copyright © 2022 Sun and Zhao. This is an open-access article distributed under the terms of the Creative Commons Attribution License (CC BY). The use, distribution or reproduction in other forums is permitted, provided the original author(s) and the copyright owner(s) are credited and that the original publication in this journal is cited, in accordance with accepted academic practice. No use, distribution or reproduction is permitted which does not comply with these terms.

frontiers | Frontiers in Pharmacology

SYSTEMATIC REVIEW
published: 13 July 2022
doi: 10.3389/fphar.2022.968163

Comparison of Adverse Reactions Caused by Olaparib for Different Indications

Yujing Zhou[1], *Shengwen Zhao*[2], *Tong Wu*[2] *and Han Zhang*[1]*

[1]Department of Nuclear Medicine, Harbin Medical University Cancer Hospital, Harbin, China, [2]Department of Radiology, Heilongjiang Academy of Traditional Chinese Medicine, Harbin, China

Objective: Meta-analysis of safety of Olaparib in the treatment of different indications.

Methods: The databases of PubMed, The Cochrane Library, EMbase, CNKI, WanFang Data and VIP were searched by computer to collect the research on the indications and the incidence of adverse reactions caused by Olaparib for different cancer types. The search time was from the establishment of the database to May 2022. After two researchers independently screened the literature, extracted the data and evaluated the bias risk included in the study, we used RevMan 5.4 software for meta-analysis.

Results: A total of 14 studies were included, with a total sample size of 5119 cases. By meta-analysis, the adverse reactions of Olaparib in the treatment of pancreatic cancer, breast cancer and ovarian cancer were compared. In adverse reactions of any grade, the results showed that fatigue (RR = 1.58, 95% CI [1.20–2.07], $p = 0.001$) was the most serious in the treatment of pancreatic cancer with Olaparib. Anemia (RR = 2.94, 95% CI [1.97–4.39], $p < 0.00001$), neutropenia (RR = 1.37, 95% CI [0.80–2.33], $p = 0.25$), nausea (RR = 1.93, 95% CI [1.61–2.32], $p < 0.00001$) and vomiting (RR = 1.96, 95% CI [1.59–2.41], $p < 0.00001$) were the most severe in ovarian cancer. In adverse reactions of grade 3 or above, fatigue (RR = 3.44, 95% CI [1.48–7.98], $p = 0.004$) and vomiting (RR = 1.09, 95% CI [0.42–2.81], $p = 0.86$) were the most serious adverse reactions in the treatment of breast cancer with Olaparib. Anemia (RR = 9.74, 95% CI [2.75–34.47], $p = 0.0004$), neutropenia (RR = 1.33, 95% CI [0.87–2.02], $p = 0.19$) and nausea (RR = 2.94, 95% CI [1.18–7.32], $p = 0.02$) were the most severe in ovarian cancer. In addition, the incidence of decreased white blood cell count and hepatotoxicity in the treatment of breast cancer, and the incidence of decreased platelet count, constipation and abdominal pain in the treatment of ovarian cancer were higher than those in pancreatic cancer.

Conclusion: Current evidence showed that the risk of adverse reactions of Olaparib in the treatment of different indications is different, and specific analysis and treatment should be carried out for different cancer types. Due to the limitation of the quantity and quality of the included studies, the above conclusions need to be verified by more high-quality studies.

Keywords: olaparib, pancreatic cancer, breast cancer, ovarian cancer, security

OPEN ACCESS

Edited by:
Hongtao Xiao,
University of Electronic Science and Technology of China, China

Reviewed by:
Kah Bik Cheong,
Southern Medical University, China
Xun Qi,
The First Affiliated Hospital of China Medical University, China

***Correspondence:**
Han Zhang
zhanghan820331@126.com

Specialty section:
This article was submitted to Pharmacology of Anti-Cancer Drugs, a section of the journal Frontiers in Pharmacology

Received: *13 June 2022*
Accepted: *24 June 2022*
Published: *13 July 2022*

Citation:
Zhou Y, Zhao S, Wu T and Zhang H (2022) Comparison of Adverse Reactions Caused by Olaparib for Different Indications. Front. Pharmacol. 13:968163. doi: 10.3389/fphar.2022.968163

1 INTRODUCTION

Since 2020, there have been nearly 19.3 million new cancer cases and nearly 10 million cancer patients died in the world, among which the most common types include lung cancer, breast cancer, pancreatic cancer, gastric cancer and colorectal cancer (Sung et al., 2021). The increasing incidence and mortality of cancer are threatening the lives and health of people all over the world. Although new anti-cancer drugs have been developed continuously, most of them have limited their curative effect due to their weak specificity, toxic and side effects and drug resistance. Therefore, it is urgent to find new anti-tumor drugs in clinic. Since Bryant put forward the concept of "synthetic lethality" in 2005, the potential anti-tumor effect of PARP inhibitors has been gradually revealed (Bryant et al., 2005; Farmer et al., 2005). With the development of genomics, people's understanding of tumor molecular level is deepening, and molecular targeted drugs related to DNA repair pathway have gradually attracted people's attention. The discovery that poly-ADP ribose polymerase (PARP) inhibitors (PARPi) selectively kill BRCA1/2 mutant cancer cells has opened up a new way for clinical treatment of tumor patients.

As one of the inhibitors of poly (ADP-ribose) polymerase (PARP), Olaparib can capture PARP at the single strand break site of DNA, prevent its repair, and produce double strand breaks that cannot be repaired accurately in tumors with defects in homologous recombination repair, such as BRCA1 or BRCA2 mutation (BRCAm), which leads to DNA damage and tumor cell death. With the continuous in-depth research of researchers, in 2018, FDA expanded the indications of Olaparib to the first-line maintenance treatment for patients with BRCA mutant ovarian cancer. Another study found that (Robson et al., 2017a; Eikesdal et al., 2021), Olaparib can significantly improve the curative effect of BRCA mutant metastatic HER2 negative breast cancer. Compared with the standard chemotherapy group, the median PFS of Olaparib group is significantly prolonged, the effective rate is significantly improved, and the side effects are less and the safety is higher. Therefore, Olaparib is the first PARPi approved for the treatment of BRCA mutant breast cancer. GOLAN (Golan et al., 2019) and other tests evaluated the role of Olaparib in patients with gBRCA1/2 mutant metastatic pancreatic cancer. Compared with placebo group, the median PFS of Olaparib group was nearly doubled, and the risk of disease progression was reduced by 47%, which opened up a new concept of pancreatic cancer maintenance treatment and promoted FDA to include BRCA mutant pancreatic cancer in the indications of Olaparib. Olaparib improves overall survival and clinical benefit, but it lacks a systematic review of its safety. In this study, the existing clinical trials of Olaparib for the above indications were searched to systematically evaluate its safety in the treatment process, in order to provide clinical evidence.

2 MATERIALS AND METHODS

The databases of PubMed, The Cochrane Library, EMbase, CNKI, WanFang Data and VIP were searched by computer to collect the research on the incidence of adverse reactions of Olaparib in treating patients with different indications. The search time was from the establishment of the database to May 2022. The retrieval is carried out by combining subject words with free words, and is adjusted according to the characteristics of each database. At the same time, the references included in the study were searched to supplement and obtain relevant information. The search terms include Olaparib, Pancreatic Cancer, Breast Cancer, Ovarian Cancer, Safety, Adverse Reactions and so on.

Inclusion criteria: ① The types of study were RCTs and Clinical trials; The language of the literature is Chinese or English; ② Patients with pancreatic, breast and ovarian cancers treated with Olaparib were studied. ③ The outcome index is the incidence of adverse reactions of any grade and above grade 3. Exclusion criteria: ① Papers such as "Non-RCT or Clinical Trial", "Short Case Report", "Review", "Review" and "Animal Experiment"; Repeated published literature; There is no report of data; The full text of the literature can not be obtained.

2.1 Literature Screening and Data Extraction

Two researchers independently screened the literatures, extracted the data and cross-checked them. If there is any disagreement, it will be resolved through discussion or consultation with a third party. When selecting documents, read the title first, and after excluding obviously irrelevant documents, read the abstract and full text further to determine whether to include them. If necessary, contact the original study author by email or telephone for unidentified information that is very important for this study. The contents of data extraction include: ① basic information included in the study, including the first author, published year, cancer types, types of intervention drugs, and total sample size; Number, grade and type of adverse reactions.

2.2 Data Extraction and Quality Assessment

The Newcastle-Ottawa scale (NOS) was used to evaluate the quality of the literature (Lazarus et al., 2019), and the quality of the included studies was evaluated according to the following eight criteria: 1) Representativeness of the exposure cohort; 2) Selection of non-exposed queues; 3) Determination of exposure method; 4) No outcome events occurred before the study began; 5) Comparability between exposed queues and non-exposed queues; 6) Evaluation of outcome events; 7) Whether the follow-up time is long enough; 8) Whether the follow-up is complete. Documents rated 7–9 are considered "high" in quality, 4–6 as "average" and 3 or less as "low". The quality evaluation is carried out independently by two researchers and cross-checked. If there is any difference, we will ask the third researcher to help solve it.

2.3 Statistical Analysis

RevMan 5.4 software was used for analysis. Cochrane χ^2 test was used to evaluate the heterogeneity, and I^2 was used to express the heterogeneity. When $p > 0.1$ and $I^2 < 50\%$, it shows that there is

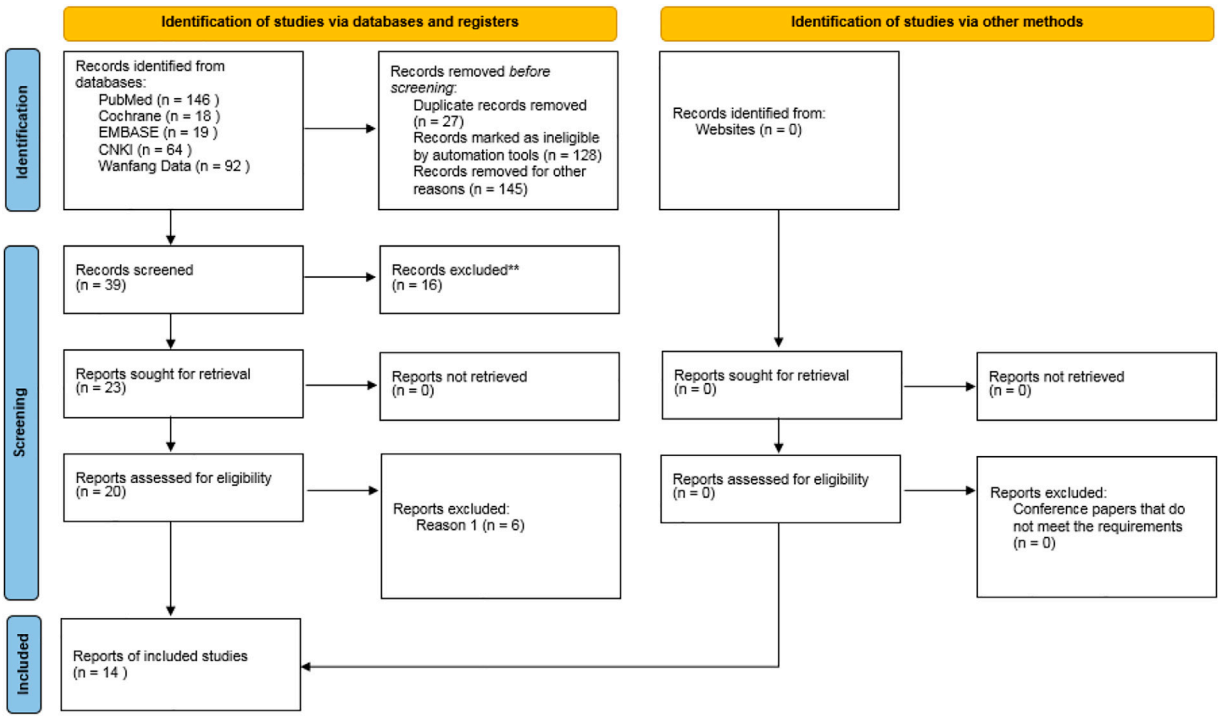

FIGURE 1 | Flow chart of literature screening process and results.

no statistical heterogeneity in each RCTs, and fixed effect model is used; On the contrary, on the premise of excluding clinical heterogeneity, the random effect model is adopted. Relative risk (RR) or odds ratio (OR) was used to describe the data of the two-class variables. Weighted mean difference (WMD) was used to describe the continuity variables. The effect variables were expressed by 95% confidence interval (95% CI). Sensitivity analysis was made for each included literature, and the bias of the included literature was discussed.

3 RESULTS

3.1 Literature Search and Screening

A total of 339 related literatures were obtained through database search, 27 duplicate literatures were eliminated, 128 inconsistent literatures were eliminated by reading titles and abstracts, and 145 literatures were eliminated by reading full texts. After strict hierarchical screening, 14 RCTs (Ledermann et al., 2012; Bendell et al., 2015; Oza et al., 2015; Robson et al., 2017b; Moore et al., 2018; Golan et al., 2019; Hammel et al., 2019; Ray-Coquard et al., 2019; Robson et al., 2019; Im et al., 2020; Penson et al., 2020; Fasching et al., 2021; Poveda et al., 2021; Tutt et al., 2021) were finally included, including 5119 patients, including 3039 cases in Olaparib group and 2080 cases in non-Olaparib group, as shown in **Figure 1**. The basic characteristics and bias risk assessment results of the 14 studies included are shown in **Table 1**.

3.2 Meta-Analysis Results

3.2.1 Major Adverse Reactions

3.2.1.1 Meta-Analysis Results of Fatigue of Any Level and Above Caused by Olaparib

Meta-analysis according to cancer types showed that: ① Among the adverse reactions of any grade in 14 studies, the risk of fatality was the highest in pancreatic cancer (RR = 1.58, 95% CI [1.20–2.07], $p = 0.001$), followed by ovarian cancer (RR = 1.48, 95% CI [1.33–1.63], $p < 0.00001$), and relatively low in breast cancer (RR = 1.41, 95% CI [1.26–1.58], $p < 0.00001$). The results were statistically significant ($p < 0.05$), as shown in **Figure 2A**. ② Among the 13 studies, the risk of severe adverse reactions above grade 3 was the highest in breast cancer (RR = 3.44, 95% CI [1.48–7.98], $p = 0.004$), followed by ovarian cancer (RR = 2.72, 95% CI [1.58–4.71], $p = 0.0003$), and relatively low in pancreatic cancer (RR = 1.79, 95% CI [0.39–8.24], $p = 0.45$). Some results were statistically significant ($p < 0.05$), as shown in **Figure 2B**. The results suggest that in the routine grade of adverse reactions, Olaparib is more likely to cause false when treating pancreatic cancer, while in the severe adverse reactions, more attention should be paid to the degree of false when treating breast cancer.

3.2.1.2 Meta-Analysis Results of Anemia of Any Level and Above Caused by Olaparib

The results of meta-analysis were as follows: ① Among the adverse reactions of any grade in 14 studies, anemia had the highest risk in ovarian cancer (RR = 2.94, 95% CI [1.97–4.39], $p < 0.00001$), followed by breast cancer (RR = 1.84, 95% CI

TABLE 1 | Basic characteristics of included studies (Ledermann et al., 2012; Bendell et al., 2015; Oza et al., 2015; Robson et al., 2017b; Moore et al., 2018; Golan et al., 2019; Hammel et al., 2019; Ray-Coquard et al., 2019; Robson et al., 2019; Im et al., 2020; Penson et al., 2020; Fasching et al., 2021; Poveda et al., 2021; Tutt et al., 2021).

First author	Year	Phase	Cancer	ID of Study	Protocol of olaparib	Protocol of Non-olaparib	No. of olaparib	No. of Non-olaparib	Quality
Bendell et al. (2015)	2015	I	PC	NCT00515866	Olaparib + Gemcitabine	Gemcitabine	15	7	7
Hammel et al. (2019)	2019	III	PC	NCT02184195	Olaparib	Placebo	89	58	7
Golan et al. (2019)	2019	NA	PC	NA	Olaparib	Placebo	91	60	8
Tutt et al. (2021)	2021	III	BC	NCT02032823	Olaparib	Placebo	921	915	8
Robson et al. (2017b)	2017	III	BC	NCT02000622	Olaparib	Standard-Therapy	205	97	8
Im et al. (2020)	2020	III	BC	NCT02000622	Olaparib	Chemotherapy TPC	59	28	7
Robson et al. (2019)	2019	III	BC	NCT02000622	Olaparib	TPC	205	97	7
Fasching et al. (2021)	2020	III	BC	NCT02789332	Olaparib + paclitaxel	carboplatinum + paclitaxel	69	37	7
Penson et al. (2020)	2020	III	OC	NCT00628251	Olaparib	chemotherapy	178	76	7
Ledermann et al. (2012)	2012	II	OC	NCT00753545	Olaparib	placebo	136	128	8
Moore et al. (2018)	2018	III	OC	NCT01844986	Olaparib	chemotherapy	260	130	8
Ray-Coquard et al. (2019)	2019	III	OC	NCT02477644	Olaparib	chemotherapy	535	267	8
Oza et al. (2015)	2014	II	OC	NCT01081951	Olaparib	chemotherapy	81	81	8
Poveda et al. (2021)	2021	III	OC	NCT01874353	Olaparib	placebo	195	99	7

PC, pancreatic cancer; BC, breast cancer; OC, ovarian cancer; TPC, treatment of physician's choice; NA, not available.

TABLE 2 | Meta-analysis of secondary adverse reactions of Olaparib for different indications.

	Pancreatic cancer		Breast cancer		Ovarian cancer	
	Any-Grade ADR	Grade 3 or Above ADR	Any-Grade ADR	Grade 3 or Above ADR	Any-Grade ADR	Grade 3 or Above ADR
WBC count decreased	NA	NA	1.11 [0.53–2.34], $p = 0.77$	0.78 [0.18–3.50], $p = 0.77$	NA	NA
Platelet count decreased	NA	NA	NA	NA	2.06 [1.46–2.92], $p < 0.0001$	1.36 [0.68–2.73], $p = 0.39$
Neutrophil count decreased	0.78 [0.25–2.37], $p = 0.66$	0.78 [0.25–2.37], $p = 0.66$	0.79 [0.42–1.48], $p = 0.46$	0.67 [0.26–1.73], $p = 0.40$	1.37 [0.80–2.33], $p = 0.25$	1.33 [0.87–2.02], $p = 0.19$
Vomiting	1.22 [0.61–2.47], $p = 0.57$	0.96 [0.13–7.17], $p = 0.97$	1.78 [1.14–2.77], $p = 0.57$	1.09 [0.42–2.81], $p = 0.86$	1.96 [1.59–2.41], $p < 0.00001$	1.02 [0.49–2.16], $p = 0.95$
Constipation	2.49 [1.54–4.02], $p = 0.0002$	NA	NA	NA	1.03 [0.85–1.26], $p = 0.74$	NA
Appetite decreased	2.29 [1.39–3.77], $p = 0.001$	NA	1.92 [1.51–2.45], $p < 0.00001$	NA	1.59 [1.20–2.12], $p = 0.001$	NA
Abdominal pain	0.99 [0.76–1.30], $p = 0.96$	0.60 [0.11–3.19], $p = 0.55$	NA	NA	1.04 [0.87–1.23], $p = 0.67$	0.83 [0.43–1.60], $p = 0.57$
AST	NA	NA	0.62 [0.46–0.82], $p = 0.0009$	2.83 [0.74–10.85], $p = 0.13$	NA	NA
ALT	NA	NA	0.74 [0.58–0.94], $p = 0.01$	0.78 [0.25–2.38], $p = 0.66$	NA	NA

WBC, white blood cell; ADR, adverse reactions; AST, aspartate aminotransferase; ALT, alanine aminotransferase; NA, not available.

[0.53–6.36], $p < 0.00001$), and relatively low risk in pancreatic cancer (RR = 1.49, 95% CI [0.82–2.72], $p < 0.00001$). Some results were statistically significant ($p < 0.05$), as shown in **Figure 3A**. ② Among the 13 studies, anemia had the highest risk in ovarian cancer (RR = 9.74, 95% CI [2.75–34.47], $p = 0.0004$), followed by breast cancer (RR = 2.57, 95% CI [0.61–10.87], $p = 0.20$), and relatively low risk in pancreatic cancer (RR = 1.69, 95% CI [0.27–10.54], $p = 0.58$). Some results were statistically significant ($p < 0.05$), as shown in **Figure 3B**. The results suggest that in the clinical application of Olaparib, compared with breast cancer, Olaparib is more likely to cause anemia in the treatment of ovarian cancer.

3.2.1.3 Meta-Analysis Results of Nausea of Any Grade and Above Caused by Olaparib

The results of meta-analysis were as follows: ① Among the 14 studies, nausea had the highest risk in ovarian cancer (RR = 1.93, 95% CI [1.61–2.32], $p < 0.00001$), followed by breast cancer (RR = 1.57, 95% CI [1.05–2.34], $p = 0.03$), and relatively low risk in pancreatic cancer (RR = 1.50, 95% CI

[0.64–3.52], $p = 0.35$). Some results were statistically significant ($p < 0.05$), as shown in **Figure 4A**. ② Among the adverse reactions above grade 3 in 13 studies, nausea has the highest risk in ovarian cancer (RR = 2.94, 95%CI [1.18–7.32], $p = 0.02$), followed by breast cancer (RR = 1.09, 95% CI [0.44–2.69], $p = 0.86$), and relatively low risk in pancreatic cancer (RR = 0.57, 95% CI [0.08–4.13], $p = 0.57$). Some results are statistically significant ($p < 0.05$), as shown in **Figure 4B**. The results suggest that in the

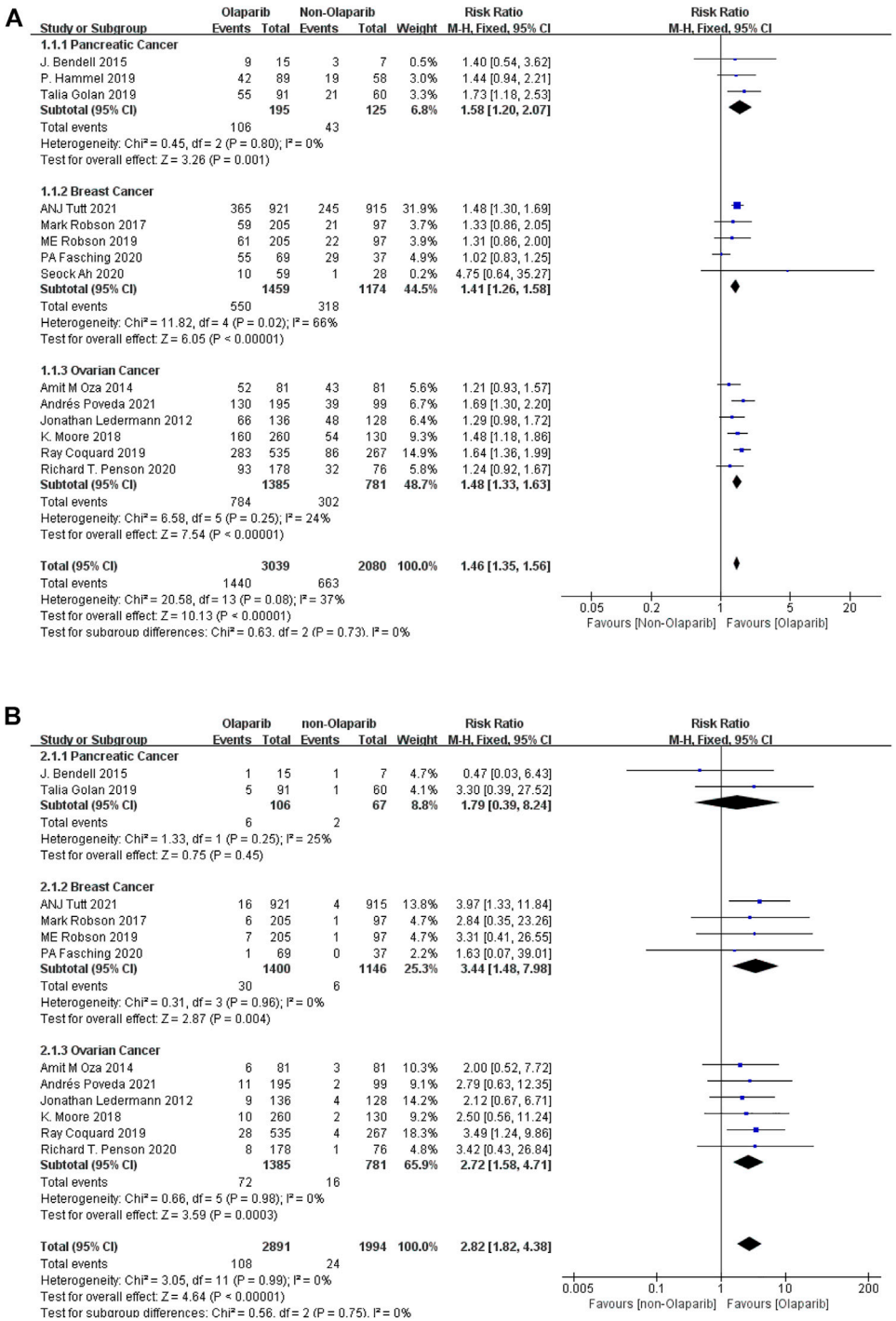

FIGURE 2 | (A) Meta-analysis of any-grade adverse reactions of fatigue caused by Olaparib for different indications. **(B)** Meta-analysis of grade 3 or above adverse reactions of fatigue caused by Olaparib for different indications.

clinical application of Olaparib, compared with the treatment of breast cancer, Olaparib is more likely to cause nausea in the treatment of ovarian cancer.

3.3 Secondary Adverse Reaction

Subgroup analysis of secondary adverse reactions was conducted according to different types of cancer, and the results of meta-

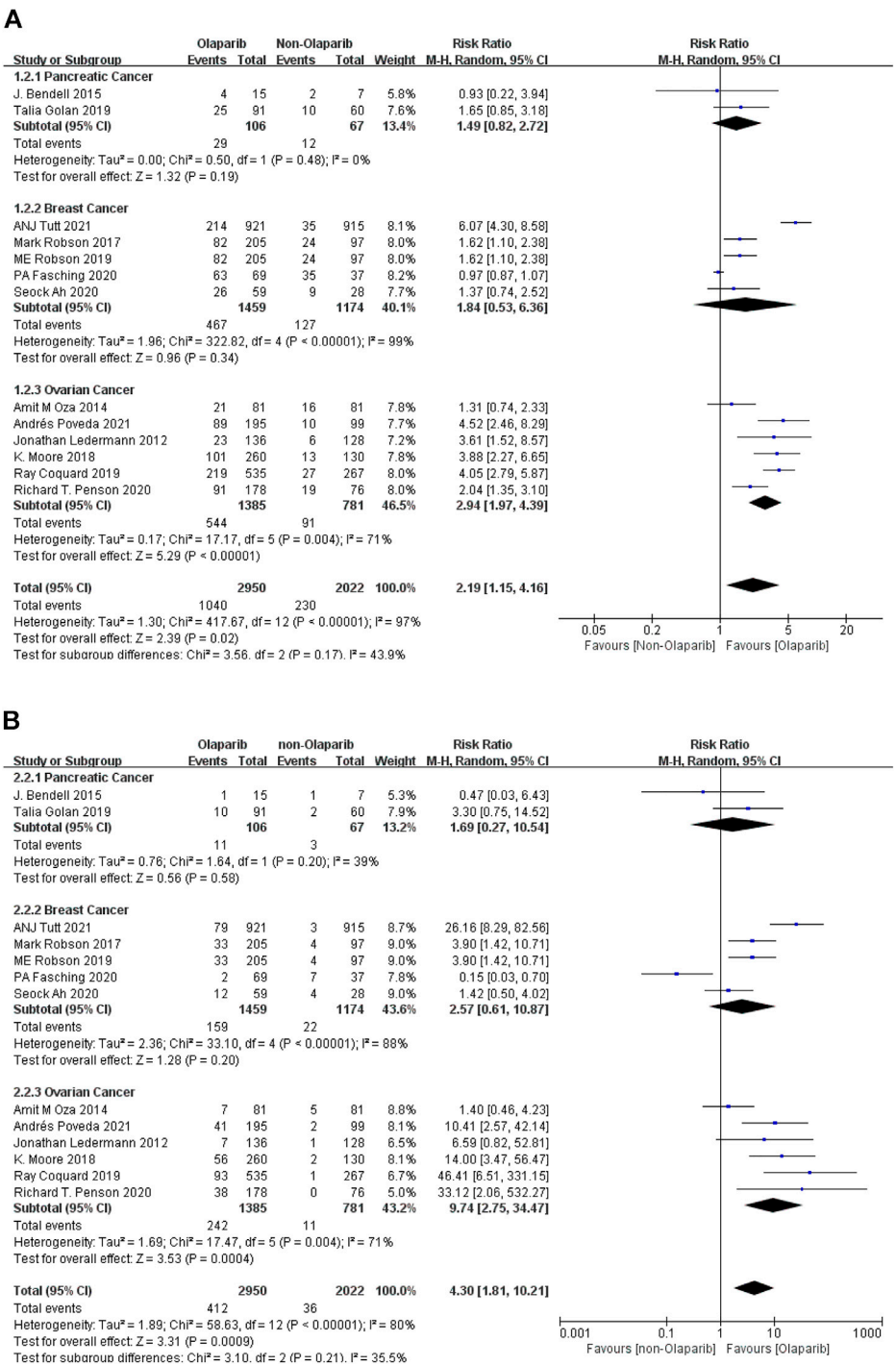

FIGURE 3 | (A) Meta-analysis of any-grade adverse reactions of anemia caused by Olaparib for different indications. **(B)** Meta-analysis of grade 3 or above adverse reactions of anemia caused by Olaparib for different indications.

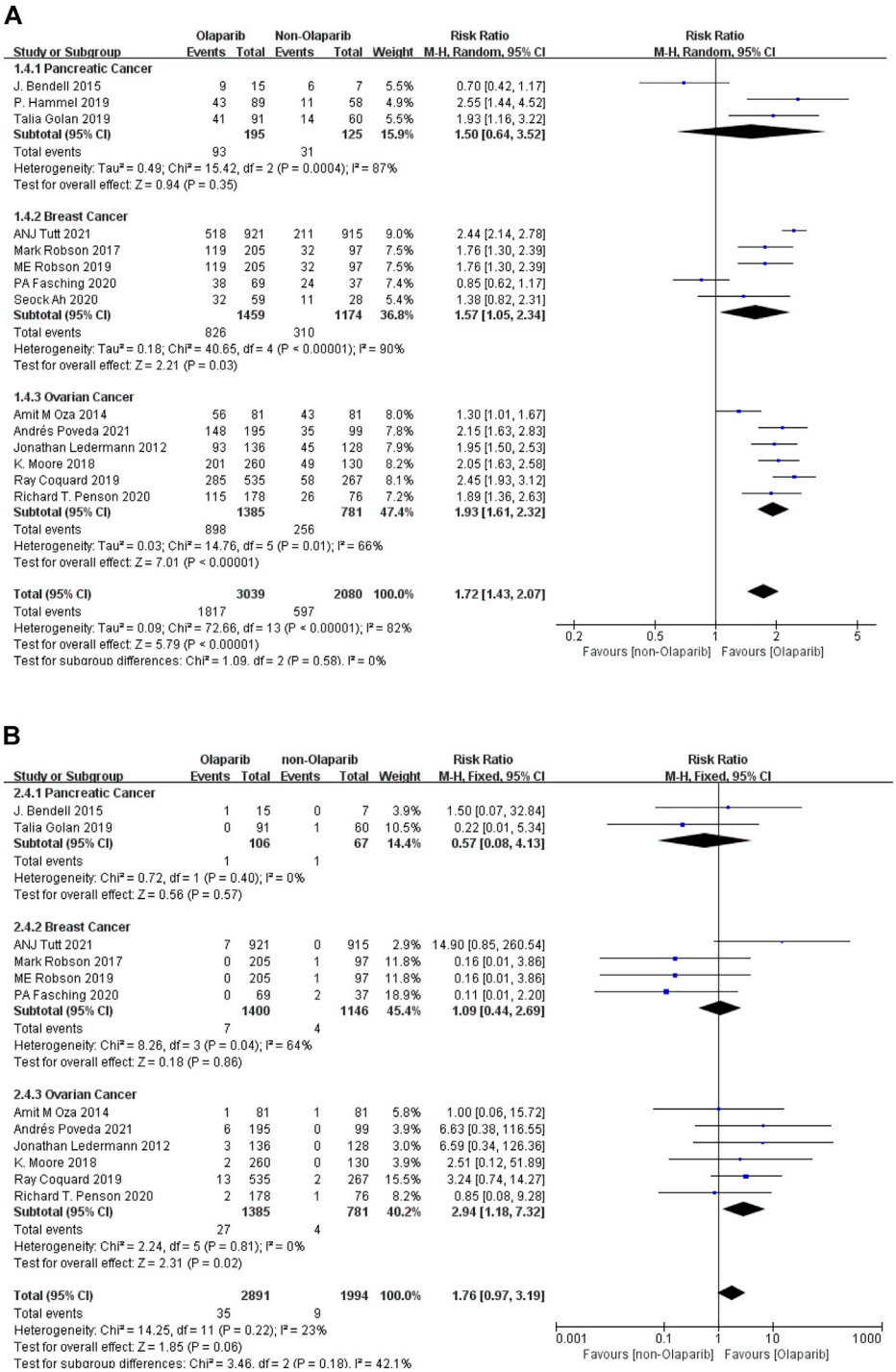

FIGURE 4 | (A) Meta-analysis of any-grade adverse reactions of nausea caused by Olaparib for different indications. **(B)** Meta-analysis of grade 3 or above adverse reactions of nausea caused by Olaparib for different indications.

analysis were as follows: ① Based on existing clinical evidence, decreased white blood cell count, hepatotoxicity (increased AST and ALT) only occurred in breast cancer, and only decreased AST (RR = 0.62, 95% CI [0.46–0.82], $p = 0.0009$) and ALT (RR = 0.74, 95% CI [0.58–0.94], $p = 0.01$) the results were statistically significant ($p < 0.05$). ② Thrombocytopenia mainly occurred in ovarian cancer, and there was statistical difference in thrombocytopenia at any grade (RR = 2.06, 95% CI [1.46–2.92], $p < 0.0001$) ($p < 0.05$). ③ Neutrophilic granulocyte reduction of any grade and above grade 3 had the

highest risk of ovarian cancer (RR = 1.37, 95% CI [0.80–2.33], p = 0.25) and (RR = 1.33, 95% CI [0.87–2.02], p = 0.19), respectively. ④ All levels of depression had the highest risk in ovarian cancer (RR = 1.96, 95% CI [1.59–2.41], $p < 0.00001$), followed by breast cancer (RR = 1.78, 95% CI [1.14–2.77], p = 0.57). The lowest risk was found in pancreatic cancer (RR = 1.22, 95% CI [0.61–2.47], p = 0.57). The risk of tertiary depression was the highest in breast cancer (RR = 1.09, 95% CI [0.42–2.81], p = 0.86). ⑤ Cases of diarrhea and Abdominal pain are only in pancreatic cancer and ovarian cancer, and the risk of both are high in pancreatic cancer (RR = 2.49, 95% CI [1.54–4.02], p = 0.0002) and (RR = 0.99, 95% CI [0.76–1.30], p = 0.96; ⑥ Appetite decreased is mainly found in pancreatic cancer, with the highest incidence (RR = 2.29, 95% CI [1.39–3.77], p = 0.001), and second in breast cancer (RR = 1.92, 95% CI [1.51–2.45], $p < 0.00001$). The incidence was lowest in ovarian cancer (RR = 1.59, 95% CI [1.20–2.12], p = 0.001) as shown in **Table 2**.

3.4 Publication Bias

In addition to meta-analysis and comparison of data indicators of adverse reactions of any grade and those above grade 3, an inverted funnel plot was also drawn for the included studies (due to the large number of outcome indicators in this study, only language description was made). The results showed that the funnel plot of outcome indicators could be symmetrical in any level of adverse reactions. In the adverse reactions above level 3, only the funnel diagram of anemia and Neutrophil indicators was asymmetric, suggesting a certain publication bias. There may be some factors, such as lack of research design and relatively poor methods, leading to a small bias.

3.5 Sensitivity Analysis

Sensitivity analysis was carried out by excluding individual studies one by one, and the results showed little change compared with the total adverse reaction rate, which indicated that the results of this study were stable.

4 DISCUSSION

Many studies have confirmed that maintenance treatment with poly ADP-ribose polymerase (PARP) inhibitors can significantly prolong the survival time of cancer patients such as breast cancer and ovarian cancer, and improve the survival benefits of patients. With the wide application of PARP inhibitors, drug-related adverse reactions have attracted much attention. The adverse reactions of PARP inhibitors include blood toxicity, digestive tract toxicity, etc. As one of PARPi, Olaparib also has corresponding adverse reactions.

Hematological adverse reactions of PARP inhibitors include anemia, thrombocytopenia, neutropenia and so on. Such adverse reactions mainly occur in the first 3 months of treatment, and sometimes it is necessary to interrupt or reduce the dose of PARP inhibitor for recovery. The whole blood cell count should be monitored weekly in the first month of PARP inhibitor treatment, monthly in the first year of treatment and regularly thereafter. In case of suspension of treatment due to grade 3 or 4 hematological adverse reactions, consider monitoring the whole blood cell count every week after resuming medication until it returns to normal level (Madariaga et al., 2020). Anemia is the most common blood adverse reaction. Studies have shown that (Farrés et al., 2013; Hopkins et al., 2019), PARP inhibitors can target PARP1, PARP2, PARP3 and PARP13. PARP1 regulates cell differentiation in bone marrow or blood system, and PARP2 plays a role in regulating erythropoiesis. The incidence of Olaparib anemia is 21 ~ 46%, the incidence of grade 3 ~ 4 anemia is about 5.1 ~ 22%, the incidence of thrombocytopenia is 16 ~ 18%, the incidence of grade 3 ~ 4 is less than 1%, the incidence of neutropenia is 16 ~ 23%, and the incidence of grade 3 ~ 4 is 3.7 ~ 9%. Non-hematological adverse reactions of PARP inhibitors include digestive tract toxicity and hepatotoxicity. Such adverse reactions generally occur in the first 4 ~ 8 weeks of treatment, which is relatively short. Most patients can pass symptom management without suspending administration or reducing dosage. Among them, nausea and vomiting are the most common digestive system adverse reactions of PARP inhibitors. The incidence of nausea is relatively high, and it mainly occurs in the early stage. The overall incidence of Olaparib is 44 ~ 73%, and the incidence of grade 3 ~ 4 is 1 ~ 2%. Fatigue is also a common adverse reaction of PARP inhibitors. The overall incidence of fatigue in Olaparib is 42 ~ 63%, and the incidence of grade 3 ~ 4 is 4.1 ~ 7.4%.

In recent years, FDA has expanded the indications of olapalil, and used it for the treatment of breast cancer and ovarian cancer before and after. Another clinical trial shows that it also has a good clinical benefit rate for pancreatic cancer. With the wide clinical use of Olaparib, its adverse reactions have attracted much attention. The innovation of this study is to evaluate the risk of adverse reactions in the treatment of pancreatic cancer, breast cancer and ovarian cancer. Subgroup analysis was carried out according to cancer types to observe which adverse reactions in different cancer types have higher risk and deserve clinical attention. This study included 14 clinical trials and RCTs, with a total of 5119 patients. Among them, there are 3 pancreatic cancer diseases, 5 breast cancer diseases and 6 ovarian cancer diseases. Subgroup analysis showed that there were significant differences in the incidence of adverse reactions among patients with different cancer types. Based on the existing clinical evidence, for the main adverse reactions, fatigue of any level has the highest risk in pancreatic cancer, followed by ovarian cancer and relatively low risk in breast cancer; Fatigue above grade three has the highest risk in breast cancer, followed by ovarian cancer and relatively low risk in pancreatic cancer. Anemia and nausea of any grade and above are at the highest risk in ovarian cancer, followed by breast cancer and relatively low risk in pancreatic cancer. The above results suggest that in clinical use, Olaparib is more prone to fatigue adverse reactions in the treatment of pancreatic cancer patients, while anemia and nausea adverse reactions should be paid more attention to in the treatment of breast cancer and ovarian cancer patients, and similar symptoms should be treated correctly in time. For minor adverse reactions, when Olaparib treats breast cancer patients, it should pay more attention to the decrease of white blood cell count and hepatotoxicity; Attention should be paid to the changes of platelet count and neutrophil count in the

treatment of ovarian cancer patients. Constipation, abdominal pain and loss of appetite often occur when treating pancreatic cancer patients.

The quality assessment of this study is shown in **Table 1**, the 14 included literatures were all high-quality literatures, of which 7 literatures scored 7 points and 7 literatures scored 8 points.

There are also some limitations in this study. Due to the short time to market of Olaparib and limited clinical data for some indications, our study is essentially a meta-analysis based on available data in published literature. Although we have made great efforts to collect as much information as possible, the number of studies included has limited our further analysis to some extent and affected our results. In the later period, the corresponding clinical trial data will be continuously supplemented to consolidate the results of this study, expecting to provide a more reliable basis for clinical medication.

In conclusion, according to the current evidence, the risk of adverse reactions of Olaparib in the treatment of different indications is different, and specific analysis and treatment should be carried out for different cancer types.

DATA AVAILABILITY STATEMENT

The original contributions presented in the study are included in the article/supplementary material, further inquiries can be directed to the corresponding author.

AUTHOR CONTRIBUTIONS

All authors contributed to the study conception and design. YZ and SZ searched and analysed the database. Study selection and data extraction were performed by SZ and TW. YZ and HZ wrote the manuscript and HZ reviewed the manuscript. These four authors have made fundamental contributions to the manuscript.

REFERENCES

Bendell, J., O'Reilly, E. M., Middleton, M. R., Chau, I., Hochster, H., Fielding, A., et al. (2015). Phase I Study of Olaparib Plus Gemcitabine in Patients with Advanced Solid Tumours and Comparison with Gemcitabine Alone in Patients with Locally Advanced/Metastatic Pancreatic Cancer. *Ann. Oncol.* 26, 804–811. doi:10.1093/annonc/mdu581

Bryant, H. E., Schultz, N., Thomas, H. D., Parker, K. M., Flower, D., Lopez, E., et al. (2005). Specific Killing of BRCA2-Deficient Tumours with Inhibitors of poly(ADP-Ribose) Polymerase. *Nature* 434, 913–917. doi:10.1038/nature03443

Eikesdal, H. P., Yndestad, S., Elzawahry, A., Llop-Guevara, A., Gilje, B., Blix, E. S., et al. (2021). Olaparib Monotherapy as Primary Treatment in Unselected Triple Negative Breast Cancer. *Ann. Oncol.* 32, 240–249. doi:10.1016/j.annonc.2020.11.009

Farmer, H., McCabe, N., Lord, C. J., Tutt, A. N., Johnson, D. A., Richardson, T. B., et al. (2005). Targeting the DNA Repair Defect in BRCA Mutant Cells as a Therapeutic Strategy. *Nature* 434, 917–921. doi:10.1038/nature03445

Farrés, J., Martín-Caballero, J., Martínez, C., Lozano, J. J., Llacuna, L., Ampurdanés, C., et al. (2013). Parp-2 Is Required to Maintain Hematopoiesis Following Sublethal γ-irradiation in Mice. *Blood* 122, 44–54. doi:10.1182/blood-2012-12-472845

Fasching, P. A., Link, T., Hauke, J., Seither, F., Jackisch, C., Klare, P., et al. (2021). Neoadjuvant Paclitaxel/olaparib in Comparison to Paclitaxel/carboplatinum in Patients with HER2-Negative Breast Cancer and Homologous Recombination Deficiency (GeparOLA Study). *Ann. Oncol.* 32, 49–57. doi:10.1016/j.annonc.2020.10.471

Golan, T., Hammel, P., Reni, M., Van Cutsem, E., Macarulla, T., Hall, M. J., et al. (2019). Maintenance Olaparib for Germline BRCA-Mutated Metastatic Pancreatic Cancer. *N. Engl. J. Med.* 381, 317–327. doi:10.1056/NEJMoa1903387

Hammel, P., Kindler, H. L., Reni, M., Van Cutsem, E., Macarulla, T., Hall, M. J., et al. (2019). Health-related Quality of Life in Patients with a Germline BRCA Mutation and Metastatic Pancreatic Cancer Receiving Maintenance Olaparib. *Ann. Oncol.* 30, 1959–1968. doi:10.1093/annonc/mdz406

Hopkins, T. A., Ainsworth, W. B., Ellis, P. A., Donawho, C. K., DiGiammarino, E. L., Panchal, S. C., et al. (2019). PARP1 Trapping by PARP Inhibitors Drives Cytotoxicity in Both Cancer Cells and Healthy Bone Marrow. *Mol. Cancer Res.* 17, 409–419. doi:10.1158/1541-7786.MCR-18-0138

Im, S. A., Xu, B., Li, W., Robson, M., Ouyang, Q., Yeh, D. C., et al. (2020). Olaparib Monotherapy for Asian Patients with a Germline BRCA Mutation and HER2-Negative Metastatic Breast Cancer: OlympiAD Randomized Trial Subgroup Analysis. *Sci. Rep.* 10, 8753. doi:10.1038/s41598-020-63033-4

Lazarus, G., Audrey, J., and Iskandar, A. W. B. (2019). Efficacy and Safety Profiles of Programmed Cell Death-1/programmed Cell Death Ligand-1 Inhibitors in the Treatment of Triple-Negative Breast Cancer: A Comprehensive Systematic Review. *Oncol. Rev.* 13, 425. doi:10.4081/oncol.2019.425

Ledermann, J., Harter, P., Gourley, C., Friedlander, M., Vergote, I., Rustin, G., et al. (2012). Olaparib Maintenance Therapy in Platinum-Sensitive Relapsed Ovarian Cancer. *N. Engl. J. Med.* 366, 1382–1392. doi:10.1056/NEJMoa1105535

Madariaga, A., Bowering, V., Ahrari, S., Oza, A. M., and Lheureux, S. (2020). Manage Wisely: Poly (ADP-Ribose) Polymerase Inhibitor (PARPi) Treatment and Adverse Events. *Int. J. Gynecol. Cancer* 30, 903–915. doi:10.1136/ijgc-2020-001288

Moore, K., Colombo, N., Scambia, G., Kim, B. G., Oaknin, A., Friedlander, M., et al. (2018). Maintenance Olaparib in Patients with Newly Diagnosed Advanced Ovarian Cancer. *N. Engl. J. Med.* 379, 2495–2505. doi:10.1056/NEJMoa1810858

Oza, A. M., Cibula, D., Benzaquen, A. O., Poole, C., Mathijssen, R. H., Sonke, G. S., et al. (2015). Olaparib Combined with Chemotherapy for Recurrent Platinum-Sensitive Ovarian Cancer: a Randomised Phase 2 Trial. *Lancet Oncol.* 16, 87–97. doi:10.1016/S1470-2045(14)71135-0

Penson, R. T., Valencia, R. V., Cibula, D., Colombo, N., Leath, C. A., 3rd, Bidziński, M., et al. (2020). Olaparib versus Nonplatinum Chemotherapy in Patients with Platinum-Sensitive Relapsed Ovarian Cancer and a Germline BRCA1/2 Mutation (SOLO3): A Randomized Phase III Trial. *J. Clin. Oncol.* 38, 1164–1174. doi:10.1200/JCO.19.02745

Poveda, A., Floquet, A., Ledermann, J. A., Asher, R., Penson, R. T., Oza, A. M., et al. (2021). Olaparib Tablets as Maintenance Therapy in Patients with Platinum-Sensitive Relapsed Ovarian Cancer and a BRCA1/2 Mutation (SOLO2/ENGOT-Ov21): a Final Analysis of a Double-Blind, Randomised, Placebo-Controlled, Phase 3 Trial. *Lancet Oncol.* 22, 620–631. doi:10.1016/S1470-2045(21)00073-5

Ray-Coquard, I., Pautier, P., Pignata, S., Pérol, D., González-Martín, A., Berger, R., et al. (2019). Olaparib Plus Bevacizumab as First-Line Maintenance in Ovarian Cancer. *N. Engl. J. Med.* 381, 2416–2428. doi:10.1056/NEJMoa1911361

Robson, M., Im, S. A., Senkus, E., Xu, B., Domchek, S. M., Masuda, N., et al. (2017a). Olaparib for Metastatic Breast Cancer in Patients with a Germline BRCA Mutation. *N. Engl. J. Med.* 377, 523–533. doi:10.1056/NEJMoa1706450

Robson, M., Im, S. A., Senkus, E., Xu, B., Domchek, S. M., Masuda, N., et al. (2017b). Olaparib for Metastatic Breast Cancer in Patients with a Germline BRCA Mutation. *N. Engl. J. Med.* 377, 1700. doi:10.1056/NEJMx170012

Robson, M. E., Tung, N., Conte, P., Im, S. A., Senkus, E., Xu, B., et al. (2019). OlympiAD Final Overall Survival and Tolerability Results: Olaparib versus Chemotherapy Treatment of Physician's Choice in Patients with a Germline

BRCA Mutation and HER2-Negative Metastatic Breast Cancer. *Ann. Oncol.* 30, 558–566. doi:10.1093/annonc/mdz012

Sung, H., Ferlay, J., Siegel, R. L., Laversanne, M., Soerjomataram, I., Jemal, A., et al. (2021). Global Cancer Statistics 2020: GLOBOCAN Estimates of Incidence and Mortality Worldwide for 36 Cancers in 185 Countries. *CA Cancer J. Clin.* 71, 209–249. doi:10.3322/caac.21660

Tutt, A. N. J., Garber, J. E., Kaufman, B., Viale, G., Fumagalli, D., Rastogi, P., et al. (2021). Adjuvant Olaparib for Patients with BRCA1- or BRCA2-Mutated Breast Cancer. *N. Engl. J. Med.* 384, 2394–2405. doi:10.1056/NEJMoa2105215

Conflict of Interest: The authors declare that the research was conducted in the absence of any commercial or financial relationships that could be construed as a potential conflict of interest.

Publisher's Note: All claims expressed in this article are solely those of the authors and do not necessarily represent those of their affiliated organizations, or those of the publisher, the editors and the reviewers. Any product that may be evaluated in this article, or claim that may be made by its manufacturer, is not guaranteed or endorsed by the publisher.

Copyright © 2022 Zhou, Zhao, Wu and Zhang. This is an open-access article distributed under the terms of the Creative Commons Attribution License (CC BY). The use, distribution or reproduction in other forums is permitted, provided the original author(s) and the copyright owner(s) are credited and that the original publication in this journal is cited, in accordance with accepted academic practice. No use, distribution or reproduction is permitted which does not comply with these terms.

frontiers | Frontiers in Pharmacology

REVIEW
published: 13 July 2022
doi: 10.3389/fphar.2022.949863

ACSL4 as a Potential Target and Biomarker for Anticancer: From Molecular Mechanisms to Clinical Therapeutics

Jun Hou[1,2†], Changqing Jiang[3†], Xudong Wen[4†], Chengming Li[5], Shiqiang Xiong[1], Tian Yue[1], Pan Long[2], Jianyou Shi[6*] and Zhen Zhang[1*]*

[1]Department of Cardiology, Chengdu Third People's Hospital/Affiliated Hospital of Southwest Jiao Tong University, Chengdu, China, [2]School of Materials Science and Engineering, Southwest Jiaotong University, Chengdu, China, [3]Department of Pharmacy, General Hospital of Western Theater Command, Chengdu, China, [4]Department of Gastroenterology and Hepatology, Chengdu First People's Hospital, Chengdu, China, [5]Clinical Medical College, Chengdu University of Traditional Chinese Medicine, Chengdu, China, [6]Personalized Drug Therapy Key Laboratory of Sichuan Province, Department of Pharmacy, Sichuan Academy of Medical Science and Sichuan Provincial People's Hospital, School of Medicine, University of Electronic Science and Technology of China, Chengdu, China

OPEN ACCESS

Edited by:
Hongtao Xiao,
University of Electronic Science and Technology of China, China

Reviewed by:
Susu Guo,
Shanghai Jiao Tong University, China
Nathchar Naowarojna,
Westlake University, China

***Correspondence:**
Pan Long
longpan1005@qq.com
Jianyou Shi
shijianyoude@126.com
Zhen Zhang
peakhell@163.com

[†]These authors have contributed equally to this work

Specialty section:
This article was submitted to Pharmacology of Anti-Cancer Drugs, a section of the journal Frontiers in Pharmacology

Received: 21 May 2022
Accepted: 23 June 2022
Published: 13 July 2022

Citation:
Hou J, Jiang C, Wen X, Li C, Xiong S, Yue T, Long P, Shi J and Zhang Z (2022) ACSL4 as a Potential Target and Biomarker for Anticancer: From Molecular Mechanisms to Clinical Therapeutics. Front. Pharmacol. 13:949863. doi: 10.3389/fphar.2022.949863

Cancer is a major public health problem around the world and the key leading cause of death in the world. It is well-known that glucolipid metabolism, immunoreaction, and growth/death pattern of cancer cells are markedly different from normal cells. Recently, acyl-CoA synthetase long-chain family 4 (ACSL4) is found be participated in the activation of long chain fatty acids metabolism, immune signaling transduction, and ferroptosis, which can be a promising potential target and biomarker for anticancer. Specifically, ACSL4 inhibits the progress of lung cancer, estrogen receptor (ER) positive breast cancer, cervical cancer and the up-regulation of ACSL4 can improve the sensitivity of cancer cells to ferroptosis by enhancing the accumulation of lipid peroxidation products and lethal reactive oxygen species (ROS). However, it is undeniable that the high expression of ACSL4 in ER negative breast cancer, hepatocellular carcinoma, colorectal cancer, and prostate cancer can also be related with tumor cell proliferation, migration, and invasion. In the present review, we provide an update on understanding the controversial roles of ACSL4 in different cancer cells.

Keywords: acyl-CoA synthetase long-chain family, anticancer biomarker, glucolipid metabolism, ferroptosis, arachidonic acid

INTRODUCTION

Cancer is a serious chronic disease which becomes the key causes of death and disability in the world. An analysis of the global burden of cancer 1990–2019 showed that more than 10 million people died of cancer in 2019, roughly double the number in 1990 (Lin et al., 2021). Using data updated in 2020 from the International Agency for Research on Cancer, it is estimated that there are 19.3 million new cancer cases and nearly 10 million cancer patients' death worldwide in 2020 (Sung et al., 2021).

It is well-known that early-prevention, early-diagnosis, and early-treatment is the most effective strategy for cancer control. Biomarkers refer to substances characterized by production or abnormal production of malignant tumor cells, or substances produced by the host in response to tumor stimulation, which can reflect the occurrence and development of tumor and monitor tumor

response to treatment. Commonly, tumor markers exist in the tissues, body fluids, and excreta of tumor patients and can be detected by immunological, biological, and chemical methods. Consequently, exploring additional molecular markers to surveil tumors emergence and metastasis has become a hot topic for scientists.

Fatty acids are one of the main energy sources in mammals and play essential roles in cell growth and metabolism. They are involved in cell membrane structure, energy metabolism, and cellular signaling pathways to maintain cellular physiological functions. The dysregulated fatty acids metabolism causes excessive synthesis and catabolism, leading to various diseases, such as type 2 diabetes, cardiovascular diseases, liver diseases, neurodegenerative diseases, and cancers (Hosseini et al., 2020). Acyl-CoA synthetase long-chain family 4 (ACSL4) is a key enzyme that catalyzes long-chain fatty acids activation, and abnormal expression of ACSL4 is closely related to various biological responses, including steroidogenesis, inflammation response, cell death, immune activation response, and so on (Liao et al., 2022). Specifically, ACSL4 participates in ferroptosis, a promising target for tumor therapeutics. Moreover, previous studies found that ACSL4 had certain effects on cancer progression, recurrence, and prognosis, and was expected to become an available tumor biomarker and therapeutic target.

This review demonstrates the latest progress in the roles of the ACSL4 in different tumors. First, we display the structure and function of the ACSL4. Second, we explore the effect of the ACSL4 in the pathological mechanisms involved with tumors. Third, we discuss the relationship between the ACSL4 and different tumors. Understanding the exact role of ACSL4 in cancer and the molecular mechanism involved would provide ideas for finding new targets for cancer diagnosis and treatment and developing new strategies for therapy.

ACYL-COA SYNTHETASE LONG-CHAIN FAMILY 4

Long chain fatty acids (carbon chain length >12) are important nutrients, which can be used as cellular fuel sources, membrane lipid components, protein post-translational modification (PTM), signal transduction pathways, energy storage within adipose tissue, and precursors of bioactive lipid mediators (Nakamura et al., 2014). Firstly, long chain fatty acids combine with fatty acid transport proteins (FATP) to transport into target cells. Then, free long chain fatty acids converted to their respective acyl-CoA forms and catalyzed by ACSL. Among the ACSL family enzymes in mammals, ACSL4 prefers to catalyze several polyunsaturated fatty acids (PUFAs), such as arachidonic acid (AA) and eicosapentaenoic acid (EPA). The PUFAs are precursors of bioactive lipid mediators, and the unique feature of ACSL4 suggests to be participated in various pathophysiological events, including lipid metabolism, ferroptosis, and immune response. Recent studies have shown that ACSL4 expression changes in a variety of cancers, and targeting at ACSL4 could affect tumor progression, suggesting that ACSL4 may be a potential tumor marker and therapeutic target.

Lipid Metabolism

Acyl-CoA synthetase long-chain family (ACSL) is a key enzyme responsible for lipid metabolism *in vivo*, mainly catalyzing the formation of 12–20 carbon chain length fatty acids (Kuwata and Hara, 2019). ACSL in mammals consists of five ACSL isoenzymes (ACSL1, ACSL3, ACSL4, ACSL5, and ACSL6), which have specific tissue localization and different functions (Wu et al., 2009; Lopes-Marques et al., 2013; Gao et al., 2016; Zhao et al., 2019; Nan et al., 2021). ACSL1 is highly expressed in major energy metabolism tissues such as fat, liver and muscle, functioning with fatty acid intake (Suzuki et al., 1990). ACSL3 is primarily located in the brain, prostate, and muscle and is responsible for activating monounsaturated fatty acids (MUFA), thereby competitively inhibiting PUFA-induced ferroptosis (Fujino et al., 1996; Teodoro et al., 2017; Ubellacker et al., 2020). ACSL5 is elevated in brown adipose tissue, small intestine and liver (Mashek et al., 2006). Moreover, ACSL6 is located in the brain and muscle tissues, which is responsible for the activation of docosahexaenoic acid (DHA) (Fernandez et al., 2018).

In 1997, a novel acyl-CoA synthase based on arachidonic and eicosatetraenoic acids was reported in PNAS (Kang et al., 1997). It was named ACSL4 and was found in adrenal gland, epididymis, brain, seminal vesicles, lungs, ovaries, liver, and many other tissues, with the adrenal gland being the most abundant. Like other mammalian ACS, ACSL4 consists of five regions: an NH2 terminus, luciferase-like regions 1 and 2, a linker connecting the two luciferase-like regions, and a COOH terminus. The amino acids at the luciferin-like region 2 and COOH terminal are highly identical in the ACS family, suggesting that these two regions are critical for the catalytic reaction of ACSL. ACSL4 lacks 50 amino acids corresponding to the NH2 which may cause the different response in fatty acids preference among ACSLs (Kang et al., 1997). The subcellular localization of ACSL4 is mainly in endosomes (Liu et al., 2014) and peroxisomes (Lewin et al., 2001) in the secretory pathway (Ansari et al., 2017). Moreover, ACSL4 transfers to the plasma membrane (Küch et al., 2014) and the endoplasmic reticulum regions in contact with the mitochondria, named mitochondrial associated membranes, which is responsible for fatty acids synthesis and β-oxidation (Tang et al., 2018).

The substrate specificities of the ACSL enzymes significantly differ among the five isozymes, and in particular, ACSL4 prefers PUFAs, such as AA and EPA as its substrate (Kang et al., 1997; Kuwata and Hara, 2019). ACSL4 mainly catalyzed the long chain PUFAs (including arachidonic acid 20:4 and adrenic acid 22:4) to CoA-PUFAs. These products are then esterized into phospholipids by multiple lysophosphatidylcholine acyltransferase (LPCAT), facilitating the incorporation of intracellular long-chain PUFAs into lipids membrane structures (Jiang et al., 2021). In cancer cells, the uptake and metabolism of fatty acids are often dysregulated. Fatty acid activation is a key step that allows these biomolecules to enter cellular metabolic pathways such as mitochondrial β-oxidation to produce ATP or adipogenesis pathways. Enhanced expression of particular ACSL4 was confirmed to be a feature of some more aggressive cancers and may contribute to the oncogenic phenotype (Radif et al., 2018).

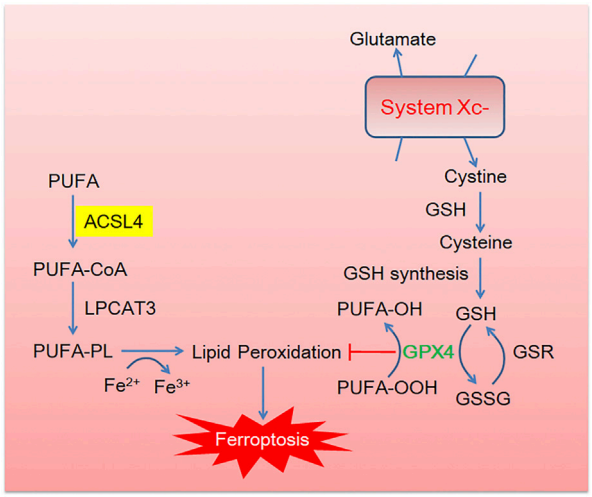

FIGURE 1 | The brief description of canonical ferroptosis pathway. Cystine enters into cells through the cystine/glutamic acid reverse transporter (System Xc-) and then reduces to cysteine in the glutathione (GSH). GSH acts as a cofactor of glutathione peroxidase 4 (GPX4) to promote the reduction of phospholipid hydroperoxides (PLOOHs) to corresponding alcohols (PLOHs) in cells. Essential lipid peroxidase acyl-CoA synthase long chain family member 4 (ACSL4) and lysophosphatidylcholine acyltransferase (LPCAT) activate PUFA into PUFA-CoA and PUFA-PL, respectively, leading to lipid peroxidation.

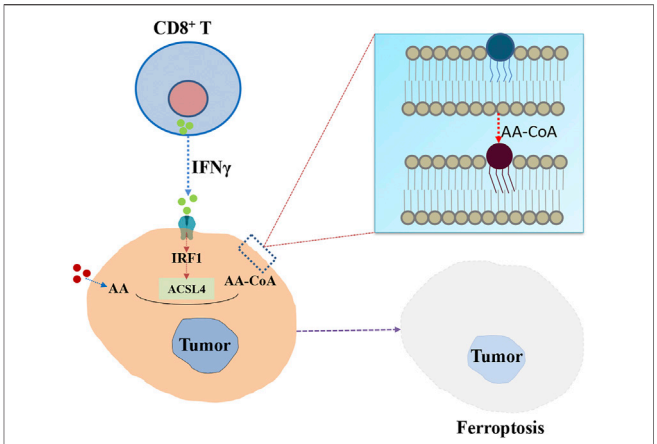

FIGURE 2 | The potential role of ACSL4 in specific immune responses mediated by $CD8^+$ T cells. IFN-γ secreted by $CD8^+$ T cells stimulates ACSL4 and alters tumor cell lipid patterns, thereby increasing the binding of AA in C16 and C18 acyl-chain phospholipids. Lipid peroxidation then leads to ferroptosis of tumor cells.

Ferroptosis

Ferroptosis is a new type of cell death characterized by a large iron-dependent accumulation of lethal lipids and reactive oxygen species (ROS), which is different from apoptosis, necrosis, and autophagy, first proposed by Dixon in 2012 (Dixon et al., 2012). Commonly, Ferroptosis is characterized by three basic features 1) Oxidation of PUFA (containing membrane phospholipids); 2) Iron utilizing related REDOX activity; 3) Loss of repair ability of lipid hydroperoxide (LOOH). Specifically, the cell death process is accompanied by the accumulation of a large number of irons, and lipid peroxidation, and changes in some genes that regulate iron homeostasis and lipid peroxidation metabolism. In the microscopic structure of cells, there are smaller mitochondria than normal cells, and the mitochondrial membrane shrinks, while the mitochondrial crest decreases or disappears, and the outer membrane is broken, but the morphological changes in the nucleus are not obvious (Lei et al., 2022). Up to now, ferroptosis has been linked to a variety of human diseases, such as ischemic organ injury, neurodegeneration and cancer (Su et al., 2020; Li and Huang, 2022).

As shown in **Figure 1**, canonical pathway of ferroptosis includes lipometabolic disturbance, glutathione (GSH)-glutathione peroxidase 4 (GPX4) exhaustion, cystine deprivation and abnormal iron metabolism. As for anti-ferroptosis pathway, ferroptosis suppressor protein 1(FSP1)- coenzyme Q (CoQ10)-Nicotinamide Adenine Dinucleotide Phosphate (NADPH) and methovalerate pathway are well-studied (Stockwell, 2019). Importantly, the phospholipid acyl chain remodeling pathway is the key process to ferroptosis. Specifically, AA and other PUFAs from lipid bilayer can be metabolized into AA-CoA and AA-PL by ACSL4 and LPCAT, respectively.

Ferroptosis is tightly associated with lipid peroxidation, in which enzymes that regulate PUFA metabolism, especially ACSL4. ACSL4 activates PUFAs and sensitizes cancer cells to ferroptosis in immunotherapy-related settings. Exogenous oxygen radicals generated by photodynamic therapy could peroxidize PUFAs (accompanied with higher expression of ACSL4) and promote ferroptosis to cancer treatment (Shui et al., 2021). Suppression ACSL4 by genetic or pharmacological inhibition could act as a specific anti-ferroptotic rescue pathway (Kagan et al., 2017). Studies showed that ionizing radiation induced ferroptosis in cancer cells by inducing ROS and activating ACSL4 (Lei et al., 2020). Therefore, ACSL4 could become a promising drug target for certain tumor treatment *via* ferroptosis pathway.

Immune Response

Commonly, ACSL4 has a wide range of biological effects, and has been reported to be involved in inflammation, steroid production, cell death, and so on. ACSL4 is found in adrenal zonulate and reticulum zonules, luteal and interstitial luteal cells of ovary, and interstitial cells of testis, participating in various immune responses.

It is well-known that ACSL4 can activate AA to initial the production processes of prostaglandin and leukotrienes synthesis. Then nonspecific immune response is activated through the release of inflammatory medium. Recently, Liao et al. (2022) demonstrated ACSL4 could play an essential role in $CD8^+$ T cell (CTL) mediated specific immune response, correlating with increased immunosurveillance and responding to checkpoint blockade (Kepp and Kroemer, 2022). Specifically, **Figure 2** shows that interferon-γ (IFN-γ) secreted by $CD8^+$ T cells, together with AA, can promote ACSL4-mediated ferroptosis, which is a mode of action for CTL-mediated tumor killing. IFN-γ stimulates ACSL4 and changes the lipid pattern of tumor cells, thereby increasing the binding of AA to C16 and C18 acyl-chain phospholipids. Common C16 and C18 fatty acids palmitic and oleic acid in blood promote

TABLE 1 | Impact of ACSL4 expression in different cancer types.

Target	Cancer type		Effect	References
ACSL4	Breast cancer	ER (+)	Overexpression is a predictor of good prognosis of breast cancer	Ragab et al. (2018), Dinarvand et al. (2020)
		ER (–)	Overexpression increases the aggressiveness of breast cancer	Maloberti et al. (2010), Monaco et al. (2010), Yu et al. (2022)
	Lung cancer		Low expression has a poor prognosis in lung adenocarcinoma	Zhang et al. (2021)
	Colorectal cancer		KRAS mutant colorectal cancer cell line shows significant upregulation of ACSL4	Park et al. (2018)
	Hepatocellular carcinoma		OS and DFS time of HCC patients with high ACSL4 expression are significantly shortened	Calvisi et al. (2011), Matter et al. (2014), Wang et al. (2020)
	Cervical cancer		High expression of ACSL4 promotes the sensitivity of cervical cancer cells to chemotherapy	Xiaofei et al. (2021)
	Prostate cancer		Downregulation of ACSL4 inhibits the proliferation, migration, invasion and growth of non-AR dependent prostate cancer cells	Baron et al. (2004), Currie et al. (2013)

ER, estrogen receptor; OS, overall survival; DFS, disease-free survival.

IFN-γ + AA induced ferroptosis of ACSL4-associated tumors. Interestingly, low doses of AA enhanced tumor ferroptosis and enhanced spontaneous and immune checkpoint blockade (ICB) -induced antitumor immunity. ACSL4 activates PUFAs and sensitizes cancer cells to ferroptosis in immunotherapy-relevant settings. Late study found genetic deletion of ACSL4 could result in an impaired antitumor $CD8^+$ T cell responses (Drijvers et al., 2021). These findings provide insights into how the metabolic and immune milieu could be used to promote ferroptosis (Friedmann Angeli et al., 2022).

ACYL-COA SYNTHETASE LONG-CHAIN FAMILY 4 AND CANCER

Recently, reprogramming of cellular energetics is a hallmark of cancer attracts researchers' attention (Pavlova and Thompson, 2016). Fatty acids, on the one hand, provide energy for cells by replacing glucose with β-oxidation (Park et al., 2016; Manley et al., 2017) and, on the other hand, drive phospholipid anabolic metabolism, which increases membrane biosynthesis and induces the production of signaling proteins in cancer cells (Röhrig and Schulze, 2016; Tan et al., 2018).

Among the five mammalian ACSL family members, ACSL1 and ACSL3 are involved in facilitating cancer progression, while ACSL5 participates in the pro-apoptotic sensing of cells, acting as a tumor suppressor (Quan et al., 2021). However, as shown in **Table 1** ACSL4 could play controversial roles being as a tumor accelerator or tumor suppressor depending on the specific cancer types and tissue environment. ACSL4 activate long chain fatty acids to initiate a number of intracellular lipid metabolic pathways (Kuwata and Hara, 2019; Rossi Sebastiano and Konstantinidou, 2019). Emerging evidences showed that dysregulated expression of ACSL4 was tightly associated with various diseases and especially with cancers (Dattilo et al., 2019; Orlando et al., 2019; Rossi Sebastiano and Konstantinidou, 2019). Mechanisms of ACSL4 involvement in tumor development may include iron-dependent, non-apoptotic, and cell death pathways (Doll et al., 2017), drug resistance caused by metabolic recombination (Orlando et al., 2019), arachidonic acid-dependent tumorigenesis (Orlando et al., 2012), steroid production (Wang et al., 2019) and activation of intracellular pro-cancer signaling pathways (Wu et al., 2015). In fact, the predictive value of ACSL4 in several cancers has been revealed by a multiple databases analysis (Yu et al., 2022). Specifically, ACSL4 is positively correlated with immune infiltration in the tumor microenvironment, which is intensively related to prognosis in breast invasive carcinoma and skin cutaneous melanoma. Additionally, ACSL4 point mutations and ACSL4-associated hypomethylation usually indicated poor prognosis in generalized carcinoma (Yu et al., 2022). Below, we would like to introduce the relationship between ACSL4 and different cancers, respectively.

Acyl-CoA Synthetase Long-Chain Family 4 and Breast Cancer

Breast cancer is one of the most dangerous diseases threatening women's/men's health. New estimates found that nearly 440,000 patients died of breast cancer each year (Wang et al., 2017). Unfortunately, breast cancer still has no effectively predictive and prognostic biomarkers. Recent evidences showed that inducing ferroptosis may enhance the efficacy of cancer therapy. ACSL4 have been well established as the positive regulator of ferroptosis and could be served as a novel predictive/prognostic breast cancer biomarker.

Recently, clinical studies demonstrated that higher ACSL4 expression was related with enhanced sensitivity to neoadjuvant chemotherapy in breast cancer, leading to a better overall survival (Sha et al., 2021). Moreover, nuclear protein Ki-67, whose function is closely related to mitosis, is considered as a marker of cell proliferation levels (Denkert et al., 2015). Several studies have shown that high expression of Ki-67 was accompanied with higher risk of recurrence, poor prognosis, and lower survival time. Interestingly, ACSL4 was found be negatively correlated with Ki-67 expression in breast cancer patients (Ragab et al., 2018). As for cell studies showed targeting ACSL4 could improve the response to irradiation and inhibit migration activities (Kwon et al., 2021). Negar Dinarvand found the prognostic significance of the expression of ACSL4 in breast cancer patients, and it was closely correlated

with tumor suppressor p53 (Dinarvand et al., 2020). In conclusion, these results suggested that higher expression of ACSL4 was a predictor of better prognosis of breast cancer.

Nevertheless, there were also evidences that ACSL4 overexpression increased the aggressiveness of breast cancer. ACSL4 expression was significantly higher in breast cancer tissues than that in adjacent tissues. ACSL4 expression was 0.386 times higher on average in p53-positive patients than in p53-negative individuals. Additionally, in both breast tumor cells and animal models, the use of PRGL493, a chemical inhibitor of ACSL4 impeding *de novo* steroid synthesis, could block cell proliferation and tumor growth, and promote the sensitivity of tumor cells to chemotherapeutic and hormonal treatment (Castillo et al., 2021). It is well-known that estrogen receptor (ER) negative breast cancer is less sensitive to chemotherapy, more likely to relapse, leading to poor prognosis. RT-PCR detections confirmed that only 2 of the 19 (10.5%) ER positive breast cancer cell lines existed ACSL4 mRNA expression, and ACSL4 mRNA was broadly expressed in 20 of 31 (64.5%) ER negative cell lines (Monaco et al., 2010). This indicated that ACSL4 mRNA expression may be correlated with more aggressive ER negative breast cancer. Moreover, Maloberti et al. (2010) found that ACSL4 was significantly upregulated in highly aggressive MDA-MB-231 breast cancer cells and played a key role in enhancing its aggressiveness. Moreover, ACSL4 was found to be more expressed in estrogen receptor (ER)-negative cancers, such as quadruple negative breast cancer (QNBC), than that in ER-positive cancers (Yen et al., 2017). ACSL4 levels were negatively correlated with hormone/growth factor receptor expression and positively correlated with the most aggressive form of QNBC (Huang et al., 2020). According to these studies, lower ACSL4 expression points more beneficial prognosis, and ACSL4 may serve as a promising prognostic biomarker for invasive breast cancer. The prognosis of breast cancer predicted by ACSL4 is related to the type of breast cancer. In ER receptor negative patients, higher ACSL4 expression could predict the poor prognosis.

ACSL4 serves not only as a prognostic biomarker but also as a therapeutic target. ACSL4, as a crucial molecule that regulates ferroptosis, is preferentially expressed in a group of basal-like breast cancer cell lines, and its expression appears to be closely associated with sensitivity to RSL3-induced ferroptosis (Doll et al., 2017). In addition, ACSL4 may be an effective therapeutic target for the regulation of multiple transporters associated with anti-cancer resistance through the mammalian target of rapamycin (mTOR) pathway, thereby restoring drug sensitivity in breast cancer with poor prognosis (Orlando et al., 2019). Thus, ACSL4 may serve as a valuable biomarker for breast cancer as well as a target for therapy in the way of promoting ferroptosis and drug sensitivity.

Acyl-CoA Synthetase Long-Chain Family 4 and Lung Cancer

Lung cancer has a high mortality rate, which is one of the common type of cancer (Siegel et al., 2017). The mechanism of lung cancer progression and the exploration of treatment strategies are still important research topics (Liu et al., 2018). Adenocarcinoma of lung is the dominant pathological types, accounting for approximately 30% of new diagnosed lung cancer worldwide (Barta et al., 2019). Due to early metastasis and recurrence, the 5-year survival rate of lung adenocarcinoma is less than 30% (Lin et al., 2019).

The Cancer Genome Atlas (TCGA) analyzing and clinical samples verification showed that ACSL4 was frequently downregulated in lung adenocarcinoma (Zhang et al., 2021). Furthermore, Kaplan-Meier survival analysis showed that patients with lower ACSL4 expression had worse progression-free survival and overall survival than patients with higher ACSL4 expression (Zhang et al., 2021). Gene set enrichment analysis found the increasing expression of ACSL4 was related with ferroptosis-related proteins. *In vivo* experiments demonstrated that knockdown of ACSL4 could improve the ability of tumor invasiveness and inhibit ferroptosis, while ACSL4 overexpression represented the opposite effects (Zhang et al., 2021). Additionally, previous studies found free fatty acid metabolism could affect ACSLs expression and cell sensitivity to ferroptosis (Magtanong et al., 2019). High-fat intervention on cancer cells could inhibit erastin-induced ferroptosis by decreasing the expression of ACSL4. It was reported that the nuclear paraspeckle assembly transcript 1 (NEAT1, a long non-coding RNA) was regarded as a novel target for diagnosis and therapy in human tumors, and higher NEAT1 expression was together with worse survival in cancer patients (Dong et al., 2018). Recent study found that the NEAT1 could target binding with ACSL4 and downregulate the expression of ACSL4, resulting in decreased sensitivity of non-small cell lung cancer (NSCLC) cells to ferroptosis (Wu and Liu, 2021). Although most studies revealed that the low expression of ACSL4 in lung cancer was a biomarker of adverse outcomes, some studies showed that the upregulation of *ACSL4* gene may be one of the causes of lung cancer. The expression of *ACSL4* gene was significantly upregulated in the tobacco exposure group compared with the non-smoking group (Xing et al., 2015).

Acyl-CoA Synthetase Long-Chain Family 4 and Colorectal Cancer

Colorectal cancer is seen with increasing frequency, being one of the most common causes of cancer mortality worldwide. The important reasons of death should be resulted from late diagnosis and recurrence or metastasis of tumor cells and new therapeutic strategies are urgently needed (Rajalingam et al., 2007; Prior et al., 2012). As we all-known that KRAS mutations were one of the most prominent oncogenes in colorectal cancer. Studies have found that mutations in KRAS were found in 30%–50% of colorectal cancers (Liu et al., 2011). In addition, patients with KRAS mutations represented a poor prognosis compared to all other patients (Inoue et al., 2012).

Here, we focus on the potential roles of ACSL4 in colorectal cancer. Dysregulated lipid metabolism resulted in cancer progression and previous studies indicated that ACSLs were essential for lipid regulation. Systematic analysis and *in vitro* experiment confirmed that high expression of ACSL4 predicted a worse prognosis in colorectal cancer and downregulating ACSL4 could reduce cell

proliferation and invasion (Chen et al., 2016). Metabolic reprogramming is a prominent feature of cancer. ACSL/stearoyl-CoA desaturase (ACSL1/ACSL4/SCD) metabolic network disorders, resulting in elevation of acylcarnitines, downregulation of polyunsaturated fatty acids (PUFA), and upregulation of monounsaturated fatty acids (MUFA), could cause invasion and poor prognosis in colorectal cancer (Sánchez-Martínez et al., 2017). Unlike the partly positive roles of ACSL4 in breast cancer, higher ACSL4 expression resulted in colorectal cancer cells proliferation and migration accompanied by a shorter survival time in colorectal cancer patients (Sánchez-Martínez et al., 2017). Moreover, Park et al. (2018) treated colorectal cancer cells with bromelain and analyzed the expression level of genes involved in cell signaling pathway. The results showed that compared with KRAS wild-type colorectal cancer cell line, KRAS mutant colorectal cancer cell line showed significant upregulation of ACSL4. Specific shRNA knockout of ACSL4 could inhibit erastin-induced ferroptosis in KRAS mutant DLD-1 cells, indicating that ACSL4 was a key regulatory molecule for bromelain to effectively inhibit KRAS mutant colorectal cancer by stimulating ferroptosis (Park et al., 2018). The result showed that bromelain could significantly inhibit the growth and proliferation of colorectal cancer cells, but the downstream molecular mechanism was unknown.

Acyl-CoA Synthetase Long-Chain Family 4 and Hepatocellular Carcinoma

Hepatocellular carcinoma (HCC) has become the second leading cause of cancer mortality worldwide, resulting in 819,000 deaths per year (Fitzmaurice et al., 2019). Furthermore, HCC is the main pathological pattern among all primary liver malignancies with 90% composition (Jemal et al., 2011). As we all-known, lipid metabolic reprogramming is tightly related with HCC proliferation, migration and invasion. Interestingly, ACSL4, a member of acyl-CoA synthetases family, is frequently upregulated in HCC and associated with poor prognosis. Furthermore, ACSL4 isoforms could be used to divided HCC, cholangiocarcinoma (CCA) and hepatic metastases (Ndiaye et al., 2020). Functionally, ACSL4 knockdown could induce decreased cell proliferation, whereas upregulation ACSL4 expression could activate tumor formation *in vitro* and *in vivo*. The molecular mechanisms could be related with microRNAs, PTMs, oncogene activation, and so on. Specifically, evidences showed that microRNAs miR-211-5p was involved in the HCC progression and prognosis, while ACSL4 was a direct downstream target of miR-211-5p. And miR-211-5p could inhibit the malignant phenotype by reducing the expression of ACSL4 protein (Qin et al., 2020). Compared with normal tissues, the relative expressions of miR-211-5p in HCC tissues and cell lines were significantly downregulated, and the upregulation of miR-211-5p *in vitro* continuously inhibited. Moreover, ACSL4 could upregulate the master lipogenesis regulator sterol regulatory element binding protein 1 (SREBP1) (Chen et al., 2021) and stabilize the oncoprotein c-Myc, resulting in HCC prognosis (Chen et al., 2020). Glycosylation was a common PTM in cancer and immunoprecipitation test demonstrated that ACSL4 protein could be O-GlcNAcylated to maintain protein stability and continuously promote cancer cell proliferation (Wang et al., 2020). Additionally, autophagy dysfunction is a crucial event in the progression of HCC, accounting for increasing cell proliferation and invasion (Calvisi et al., 2011; Ho et al., 2012; Matter et al., 2014). Specifically, the level of mTOR phosphorylation significantly increased when ACSL4 was overexpressed, and decreased when ACSL4 was downregulated. Moreover, rapamycin treatment saved the role of overexpression of ACSL4 in promoting cell growth and inhibiting cell apoptosis.

Moreover, clinical studies have shown that ACSL4 expression level was directly related to HCC prognosis (Sun and Xu, 2017). Oncomine database and TCGA databases were used to explore the relationship between the expression of ACSL4 mRNA in HCC and its prognosis. The results showed that the expression of ACSL4 mRNA in HCC tissues was significantly higher than that in normal tissues. Survival analysis showed that the overall survival and disease-free survival time of HCC patients with high ACSL4 expression were significantly shortened (Cheng et al., 2009; Iavarone et al., 2011). However, ACSL4 could play a positive role in sorafenib-resistant patients with HCC. Sorafenib is the first-line HCC treatment agent and there exists no effective biomarkers to predict sorafenib response sensitivity (Marisi et al., 2018). Recently, studies showed ACSL4 was positively correlated with the efficacy of sorafenib through cell experiment and clinical study. Cell experiments found the expression of ACSL4 protein was negatively related with half maximal inhibitory concentration (IC50) values of sorafenib in hepatoma cell line. Clinical study confirmed the expression of ACSL4 in excised HCC tissue was positively related with sorafenib reaction (Feng et al., 2021). Taken together, ACSL4 could be an essential prediction factor for sorafenib sensitivity in HCC.

Acyl-CoA Synthetase Long-Chain Family 4 and Cervical Cancer

Cervical cancer is one of the key life-threating disease among women worldwide (Schiffman et al., 2007; Crosbie et al., 2013; Manini and Montomoli, 2018). Recently, researcher found oleanolic acid (OA), a substance obtained from the leaves, fruits, and rhizomes of plants, could significantly reduce the volume of cervical cancer in mice, but the mechanism is unclear (Xiaofei et al., 2021). Interestingly, ACSL4 was highly expressed in cervical cancer cells treated with OA. Using siRNA to inhibit the expression of ACSL4 in cervical cancer cells, the suppression effect of OA on cell proliferation and viability was cancelled (Xiaofei et al., 2021). These results suggest that OA could promote ACSL4-dependent ferroptosis and may be a potential therapeutic approach for cervical cancer. Moreover, previous studies have clarified that circular RNA (circRNA) could participate in inhibiting tumorigenesis and tumor progression. Ou et al. (2022) found circular RNA (CircLMO1) could inhibit cervical cancer proliferation by activating ACSL4-induced ferroptosis, and could be a promising anti-cancer biomarker for cervical cancer. As for chemotherapy treatment of cervical cancer, ACSL4-mediated ferroptosis could play an important role in propofol synergistic anticancer effects with paclitaxel (Zhao et al., 2022).

Acyl-CoA Synthetase Long-Chain Family 4 and Prostate Cancer

Prostate cancer is one of the most frequent cancer threat to men's health (Jemal et al., 2008). Surgery or drugs that target androgen receptor (AR) signaling served as the first-line therapy (Harris et al., 2009). As is well-known that castration resistance is an essential reason for poor efficacy of prostate cancer. Studies have found that fatty acid metabolism dysregulated was highly associated with the maintenance of high proliferation rate and tumor growth of prostate cancer cells (Baron et al., 2004; Currie et al., 2013).

Recently, ACSL4, a rate-limiting enzyme, functioning as the conversion of long chain fatty acids into activated fatty acid has sparked great interests of researchers (Monaco et al., 2010; Wu et al., 2015). Studies have shown that AR, as a transcription inhibitor, could bind to the ACSL4 promoter region and inhibit its transcription. Inhibition of androgen-AR signaling, significantly increased ACSL4 levels. Downregulation of ACSL4 significantly inhibits the non-AR dependent prostate cancer cells proliferation, migration and invasion (Ma et al., 2021). Moreover, docetaxel resistance is a key problem in clinical therapy of metastatic prostate cancer and the mechanism is unclear. Researchers found lncRNAs NEAT1 could promote docetaxel-resistant prostate cancer cells proliferation and invasion by sponging miR-204-5p and miR-34a-5p, leading to an increasing expression of ACSL4 (Jiang et al., 2020). And inhibitor targeting to ACSL4 could reduce prostate cancer growth, therapeutic resistance and steroidogenesis (Castillo et al., 2021).

SUMMARIZE AND PROSPECTIVE

In this article, we introduce the cell localization, structure and function of ACSL4, and mainly summarize the evidences of ACSL4 as a potential biomarker and therapeutic target in many cancer types. ACSL4 could activate fatty acids by adding CoA and abnormal expression of ACSL4 was reported in several cancers and may affect prostaglandin biosynthesis, fatty acid β-oxidation, ferroptosis, and phosphatidyl chain remodeling. ACSL4 behaves as a crucial regulator in lipid metabolism, ferroptosis, and immune response, which contributes to its tight association with the onset and progression of various cancers. Due to different cancer types or different subtypes of the same cancer, ACSL4 showed different effects in promoting tumor proliferation or inhibiting cancer cell growth. Specifically, the expression of ACSL4 is significantly upregulated in multiple types of cancer, including breast ER negative, colorectal, and prostate, while it becomes downregulated in other cancers (breast cancer ER positive, lung cancer and cervical cancer). Commonly, in ACSL4 high expressing cancers (e.g., colon or ovarian cancer), increased expression of ACSL4 typically predicts unfavorable outcome/prognosis, while in the ACSL4 low expressing cancers (e.g., liver cancer), decreased expression of ACSL4 is corelated to unfavorable outcome/prognosis. In this context, ACSL4 may be capable of identifying abnormalities to serve as risk, diagnostic or prognostic markers as well as therapeutic targets in a wide range of cancers.

However, the Janus-faced role of ACSL4 in cancers due to the diverse pathophysiology of cancers and the heterogeneous nature of tumors, make the lack of consistency becomes a problem to evaluate the indicative effect of biomarker ACSL4. This may be associated with the different roles of ACSL4 in distinct cancers. Specifically, activation of ACSL4 may play a role in lipid metabolism reprogramming, providing an efficient supply for tumor survival, or inducing antitumor effects leading to tumor death. However, we cannot accurately evaluate whether ACSL4 has more benefits than harms in specific antitumor responses. Although ACSL4 is the activator of ferroptosis in distinct cancers, whether ferroptosis/ACSL4 benefit to improve the outcome of tumors need careful identification. On the one hand, the response to ferroptosis is regulated by a complex network of epigenetic, post-transcriptional modifications, and post-translational modifications. Targeting those pathways that regulate ferroptosis in tumor cells is an emerging antitumor strategy because malignant tumor cells often rely on oncogenic and/or survival signals, making them particularly vulnerable to ferroptosis. On the other hand, ferroptotic injury can trigger inflammation-related immunosuppression in the tumor microenvironment, thereby facilitating tumor growth. Therefore, ACSL4 could play complex roles in tumor promotion and tumor suppression when analyzing different tumors.

As we all-known each candidate biomarker has their own the limitations. Considering the tumor heterogeneity and unique micro-environment, strategy with combinatorial approaches for different tumor markers could be a more accurate way to predict tumor prognosis or therapeutic effect. Therefore, a single biomarker is not reliable for decision making, while a combination of biomarkers and/or algorithms supported by multiple methods will be more successful.

AUTHOR CONTRIBUTIONS

PL, XW, and JH wrote the review. CJ and CL designed the figures and tables. ZZ and JS collected the information. JH and JS supervised the whole work, contributed to writing, and critically revised the article.

FUNDING

This work was supported by the Natural Science Foundation of China (81900339, 82001484, and 82073311), and the Fundamental Research Funds for the Central Universities (2682021TPY031), Key Research and Development Program of Science and Technology Department of Sichuan Province (2019YFS0514), and Sichuan Provincial Science and Technology Department Application Foundation Project (2021YJ0198), Scientific Research Project of Sichuan Provincial Health Commission (20PJ196), Chengdu Science and Technology Project (2019-YF05-01161-SN), and Chengdu High-level Key Clinical Specialty Construction Project.

REFERENCES

Ansari, I. H., Longacre, M. J., Stoker, S. W., Kendrick, M. A., O'Neill, L. M., Zitur, L. J., et al. (2017). Characterization of Acyl-CoA Synthetase Isoforms in Pancreatic Beta Cells: Gene Silencing Shows Participation of ACSL3 and ACSL4 in Insulin Secretion. *Arch. Biochem. Biophys.* 618, 32–43. doi:10.1016/j.abb.2017.02.001

Baron, A., Migita, T., Tang, D., and Loda, M. (2004). Fatty Acid Synthase: A Metabolic Oncogene in Prostate Cancer? *J. Cell Biochem.* 91 (1), 47–53. doi:10.1002/jcb.10708

Barta, J. A., Powell, C. A., and Wisnivesky, J. P. (2019). Global Epidemiology of Lung Cancer. *Ann. Glob. Health* 85 (1), 8. doi:10.5334/aogh.2419

Calvisi, D. F., Wang, C., Ho, C., Ladu, S., Lee, S. A., Mattu, S., et al. (2011). Increased Lipogenesis, Induced by AKT-mTORC1-RPS6 Signaling, Promotes Development of Human Hepatocellular Carcinoma. *Gastroenterology* 140 (3), 1071–1083. doi:10.1053/j.gastro.2010.12.006

Castillo, A. F., Orlando, U. D., Maloberti, P. M., Prada, J. G., Dattilo, M. A., Solano, A. R., et al. (2021). New Inhibitor Targeting Acyl-CoA Synthetase 4 Reduces Breast and Prostate Tumor Growth, Therapeutic Resistance and Steroidogenesis. *Cell Mol. Life Sci.* 78 (6), 2893–2910. doi:10.1007/s00018-020-03679-5

Chen, W. C., Wang, C. Y., Hung, Y. H., Weng, T. Y., Yen, M. C., and Lai, M. D. (2016). Systematic Analysis of Gene Expression Alterations and Clinical Outcomes for Long-Chain Acyl-Coenzyme A Synthetase Family in Cancer. *PLoS One* 11 (5), e0155660. doi:10.1371/journal.pone.0155660

Chen, J., Ding, C., Chen, Y., Hu, W., Lu, Y., Wu, W., et al. (2020). ACSL4 Promotes Hepatocellular Carcinoma Progression via C-Myc Stability Mediated by ERK/FBW7/c-Myc axis. *Oncogenesis* 9 (4), 42. doi:10.1038/s41389-020-0226-z

Chen, J., Ding, C., Chen, Y., Hu, W., Yu, C., Peng, C., et al. (2021). ACSL4 Reprograms Fatty Acid Metabolism in Hepatocellular Carcinoma via C-Myc/SREBP1 Pathway. *Cancer Lett.* 502, 154–165. doi:10.1016/j.canlet.2020.12.019

Cheng, A. L., Kang, Y. K., Chen, Z., Tsao, C. J., Qin, S., Kim, J. S., et al. (2009). Efficacy and Safety of Sorafenib in Patients in the Asia-Pacific Region with Advanced Hepatocellular Carcinoma: A Phase III Randomised, Double-Blind, Placebo-Controlled Trial. *Lancet Oncol.* 10 (1), 25–34. doi:10.1016/S1470-2045(08)70285-7

Crosbie, E. J., Einstein, M. H., Franceschi, S., and Kitchener, H. C. (2013). Human Papillomavirus and Cervical Cancer. *Lancet* 382 (9895), 889–899. doi:10.1016/S0140-6736(13)60022-7

Currie, E., Schulze, A., Zechner, R., Walther, T. C., and Farese, R. V. (2013). Cellular Fatty Acid Metabolism and Cancer. *Cell Metab.* 18 (2), 153–161. doi:10.1016/j.cmet.2013.05.017

Dattilo, M. A., Benzo, Y., Herrera, L. M., Prada, J. G., Castillo, A. F., Orlando, U. D., et al. (2019). Regulatory Mechanisms Leading to Differential Acyl-CoA Synthetase 4 Expression in Breast Cancer Cells. *Sci. Rep.* 9 (1), 10324. doi:10.1038/s41598-019-46776-7

Denkert, C., Budczies, J., von Minckwitz, G., Wienert, S., Loibl, S., and Klauschen, F. (2015). Strategies for Developing Ki67 as a Useful Biomarker in Breast Cancer. *Breast* 24 (Suppl. 2), S67–S72. doi:10.1016/j.breast.2015.07.017

Dinarvand, N., Khanahmad, H., Hakimian, S. M., Sheikhi, A., Rashidi, B., and Pourfarzam, M. (2020). Evaluation of Long-Chain Acyl-Coenzyme A Synthetase 4 (ACSL4) Expression in Human Breast Cancer. *Res. Pharm. Sci.* 15 (1), 48–56. doi:10.4103/1735-5362.278714

Dixon, S. J., Lemberg, K. M., Lamprecht, M. R., Skouta, R., Zaitsev, E. M., Gleason, C. E., et al. (2012). Ferroptosis: An Iron-dependent Form of Nonapoptotic Cell Death. *Cell* 149 (5), 1060–1072. doi:10.1016/j.cell.2012.03.042

Doll, S., Proneth, B., Tyurina, Y. Y., Panzilius, E., Kobayashi, S., Ingold, I., et al. (2017). ACSL4 Dictates Ferroptosis Sensitivity by Shaping Cellular Lipid Composition. *Nat. Chem. Biol.* 13 (1), 91–98. doi:10.1038/nchembio.2239

Dong, P., Xiong, Y., Yue, J., Hanley, S. J. B., Kobayashi, N., Todo, Y., et al. (2018). Long Non-coding RNA NEAT1: A Novel Target for Diagnosis and Therapy in Human Tumors. *Front. Genet.* 9, 471. doi:10.3389/fgene.2018.00471

Drijvers, J. M., Gillis, J. E., Muijlwijk, T., Nguyen, T. H., Gaudiano, E. F., Harris, I. S., et al. (2021). Pharmacologic Screening Identifies Metabolic Vulnerabilities of CD8+ T Cells. *Cancer Immunol. Res.* 9 (2), 184–199. doi:10.1158/2326-6066.CIR-20-0384

Feng, J., Lu, P. Z., Zhu, G. Z., Hooi, S. C., Wu, Y., Huang, X. W., et al. (2021). ACSL4 is a Predictive Biomarker of Sorafenib Sensitivity in Hepatocellular Carcinoma. *Acta Pharmacol. Sin.* 42 (1), 160–170. doi:10.1038/s41401-020-0439-x

Fernandez, R. F., Kim, S. Q., Zhao, Y., Foguth, R. M., Weera, M. M., Counihan, J. L., et al. (2018). Acyl-CoA Synthetase 6 Enriches the Neuroprotective Omega-3 Fatty Acid DHA in the Brain. *Proc. Natl. Acad. Sci. U. S. A.* 115 (49), 12525–12530. doi:10.1073/pnas.1807958115

Fitzmaurice, C., Abate, D., Abbasi, N., Abbastabar, H., Abd-Allah, F., Abdel-Rahman, O., et al. (2019). Global, Regional, and National Cancer Incidence, Mortality, Years of Life Lost, Years Lived with Disability, and Disability-Adjusted Life-Years for 29 Cancer Groups, 1990 to 2017: A Systematic Analysis for the Global Burden of Disease Study. *JAMA Oncol.* 5 (12), 1749–1768. doi:10.1001/jamaoncol.2019.2996

Friedmann Angeli, J. P., Xavier da Silva, T. N., and Schilling, B. (2022). CD8+ T Cells PUF(A)ing the Flames of Cancer Ferroptotic Cell Death. *Cancer Cell* 40 (4), 346–348. doi:10.1016/j.ccell.2022.03.003

Fujino, T., Kang, M. J., Suzuki, H., Iijima, H., and Yamamoto, T. (1996). Molecular Characterization and Expression of Rat Acyl-CoA Synthetase 3. *J. Biol. Chem.* 271 (28), 16748–16752. doi:10.1074/jbc.271.28.16748

Gao, F., Yang, X. F., Fu, N., Hu, Y., Ouyang, Y., and Qing, K. (2016). Roles of Long-Chain Acyl Coenzyme A Synthetase in Absorption and Transport of Fatty Acid. *Chin. Med. Sci. J.* 31 (1), 62–64. doi:10.1016/s1001-9294(16)30025-6

Harris, W. P., Mostaghel, E. A., Nelson, P. S., and Montgomery, B. (2009). Androgen Deprivation Therapy: Progress in Understanding Mechanisms of Resistance and Optimizing Androgen Depletion. *Nat. Clin. Pract. Urol.* 6 (2), 76–85. doi:10.1038/ncpuro1296

Ho, C., Wang, C., Mattu, S., Destefanis, G., Ladu, S., Delogu, S., et al. (2012). AKT (V-akt Murine Thymoma Viral Oncogene Homolog 1) and N-Ras (Neuroblastoma Ras Viral Oncogene Homolog) Coactivation in the Mouse Liver Promotes Rapid Carcinogenesis by Way of mTOR (Mammalian Target of Rapamycin Complex 1), FOXM1 (Forkhead Box M1)/SKP2, and C-Myc Pathways. *Hepatology* 55 (3), 833–845. doi:10.1002/hep.24736

Hosseini, M., Poljak, A., Braidy, N., Crawford, J., and Sachdev, P. (2020). Blood Fatty Acids in Alzheimer's Disease and Mild Cognitive Impairment: A Meta-Analysis and Systematic Review. *Ageing Res. Rev.* 60, 101043. doi:10.1016/j.arr.2020.101043

Huang, M., Wu, J., Ling, R., and Li, N. (2020). Quadruple Negative Breast Cancer. *Breast Cancer* 27 (4), 527–533. doi:10.1007/s12282-020-01047-6

Iavarone, M., Cabibbo, G., Piscaglia, F., Zavaglia, C., Grieco, A., Villa, E., et al. (2011). Field-practice Study of Sorafenib Therapy for Hepatocellular Carcinoma: A Prospective Multicenter Study in Italy. *Hepatology* 54 (6), 2055–2063. doi:10.1002/hep.24644

Inoue, Y., Saigusa, S., Iwata, T., Okugawa, Y., Toiyama, Y., Tanaka, K., et al. (2012). The Prognostic Value of KRAS Mutations in Patients with Colorectal Cancer. *Oncol. Rep.* 28 (5), 1579–1584. doi:10.3892/or.2012.1974

Jemal, A., Siegel, R., Ward, E., Hao, Y., Xu, J., Murray, T., et al. (2008). Cancer Statistics, 2008. *CA Cancer J. Clin.* 58 (2), 71–96. doi:10.3322/CA.2007.0010

Jemal, A., Bray, F., Center, M. M., Ferlay, J., Ward, E., and Forman, D. (2011). Global Cancer Statistics. *CA Cancer J. Clin.* 61 (2), 69–90. doi:10.3322/caac.20107

Jiang, X., Guo, S., Zhang, Y., Zhao, Y., Li, X., Jia, Y., et al. (2020). LncRNA NEAT1 Promotes Docetaxel Resistance in Prostate Cancer by Regulating ACSL4 via Sponging miR-34a-5p and miR-204-5p. *Cell Signal* 65, 109422. doi:10.1016/j.cellsig.2019.109422

Jiang, X., Stockwell, B. R., and Conrad, M. (2021). Ferroptosis: Mechanisms, Biology and Role in Disease. *Nat. Rev. Mol. Cell Biol.* 22 (4), 266–282. doi:10.1038/s41580-020-00324-8

Kagan, V. E., Mao, G., Qu, F., Angeli, J. P., Doll, S., Croix, C. S., et al. (2017). Oxidized Arachidonic and Adrenic PEs Navigate Cells to Ferroptosis. *Nat. Chem. Biol.* 13 (1), 81–90. doi:10.1038/nchembio.2238

Kang, M. J., Fujino, T., Sasano, H., Minekura, H., Yabuki, N., Nagura, H., et al. (1997). A Novel Arachidonate-Preferring Acyl-CoA Synthetase is Present in Steroidogenic Cells of the Rat Adrenal, Ovary, and Testis. *Proc. Natl. Acad. Sci. U. S. A.* 94 (7), 2880–2884. doi:10.1073/pnas.94.7.2880

Kepp, O., and Kroemer, G. (2022). Pro-ferroptotic Fatty Acid Metabolism Renders Cancer Cells Immunogenic. *Trends Cancer* [Epub ahead of print]. doi:10.1016/j.trecan.2022.04.002

Küch, E. M., Vellaramkalayil, R., Zhang, I., Lehnen, D., Brügger, B., Sreemmel, W., et al. (2014). Differentially Localized Acyl-CoA Synthetase 4 Isoenzymes Mediate the Metabolic Channeling of Fatty Acids towards Phosphatidylinositol. *Biochim. Biophys. Acta* 1841 (2), 227–239. doi:10.1016/j.bbalip.2013.10.018

Kuwata, H., and Hara, S. (2019). Role of Acyl-CoA Synthetase ACSL4 in Arachidonic Acid Metabolism. *Prostagl. Other Lipid Mediat.* 144, 106363. doi:10.1016/j.prostaglandins.2019.106363

Kwon, Y. S., Lee, M. G., Baek, J., Kim, N. Y., Jang, H., and Kim, S. (2021). Acyl-CoA Synthetase-4 Mediates Radioresistance of Breast Cancer Cells by Regulating FOXM1. *Biochem. Pharmacol.* 192, 114718. doi:10.1016/j.bcp.2021.114718

Lei, G., Zhang, Y., Koppula, P., Liu, X., Zhang, J., Lin, S. H., et al. (2020). The Role of Ferroptosis in Ionizing Radiation-Induced Cell Death and Tumor Suppression. *Cell Res.* 30 (2), 146–162. doi:10.1038/s41422-019-0263-3

Lei, G., Zhuang, L., and Gan, B. (2022). Targeting Ferroptosis as a Vulnerability in Cancer. *Nat. Rev. Cancer* 22 (7), 381–396. doi:10.1038/s41568-022-00459-0

Lewin, T. M., Kim, J. H., Granger, D. A., Vance, J. E., and Coleman, R. A. (2001). Acyl-CoA Synthetase Isoforms 1, 4, and 5 are Present in Different Subcellular Membranes in Rat Liver and Can Be Inhibited Independently. *J. Biol. Chem.* 276 (27), 24674–24679. doi:10.1074/jbc.M102036200

Li, S., and Huang, Y. (2022). Ferroptosis: an Iron-dependent Cell Death Form Linking Metabolism, Diseases, Immune Cell and Targeted Therapy. *Clin. Transl. Oncol.* 24 (1), 1–12. doi:10.1007/s12094-021-02669-8

Liao, P., Wang, W., Wang, W., Kryczek, I., Li, X., Bian, Y., et al. (2022). CD8+ T Cells and Fatty Acids Orchestrate Tumor Ferroptosis and Immunity via ACSL4. *Cancer Cell* 40 (4), 365–e6. doi:10.1016/j.ccell.2022.02.003

Lin, H. T., Liu, F. C., Wu, C. Y., Kuo, C. F., Lan, W. C., and Yu, H. P. (2019). Epidemiology and Survival Outcomes of Lung Cancer: A Population-Based Study. *Biomed. Res. Int.* 2019, 8148156. doi:10.1155/2019/8148156

Lin, L., Li, Z., Yan, L., Liu, Y., Yang, H., and Li, H. (2021). Global, Regional, and National Cancer Incidence and Death for 29 Cancer Groups in 2019 and Trends Analysis of the Global Cancer Burden, 1990-2019. *J. Hematol. Oncol.* 14 (1), 197. doi:10.1186/s13045-021-01213-z

Liu, X., Jakubowski, M., and Hunt, J. L. (2011). KRAS Gene Mutation in Colorectal Cancer Is Correlated with Increased Proliferation and Spontaneous Apoptosis. *Am. J. Clin. Pathol.* 135 (2), 245–252. doi:10.1309/AJCP7FO2VAXIVSTP

Liu, Z., Huang, Y., Hu, W., Huang, S., Wang, Q., Han, J., et al. (2014). dAcsl, the Drosophila Ortholog of Acyl-CoA Synthetase Long-Chain Family Member 3 and 4, Inhibits Synapse Growth by Attenuating Bone Morphogenetic Protein Signaling via Endocytic Recycling. *J. Neurosci.* 34 (8), 2785–2796. doi:10.1523/JNEUROSCI.3547-13.2014

Liu, K. T., Yeh, I. J., Chou, S. K., Yen, M. C., and Kuo, P. L. (2018). Regulatory Mechanism of Fatty acid CoA Metabolic Enzymes under Endoplasmic Reticulum Stress in Lung Cancer. *Oncol. Rep.* 40 (5), 2674–2682. doi:10.3892/or.2018.6664

Lopes-Marques, M., Cunha, I., Reis-Henriques, M. A., Santos, M. M., and Castro, L. F. (2013). Diversity and History of the Long-Chain Acyl-CoA Synthetase (Acsl) Gene Family in Vertebrates. *BMC Evol. Biol.* 13, 271. doi:10.1186/1471-2148-13-271

Ma, Y., Zhang, X., Alsaidan, O. A., Yang, X., Sulejmani, E., Zha, J., et al. (2021). Long-Chain Acyl-CoA Synthetase 4-Mediated Fatty Acid Metabolism Sustains Androgen Receptor Pathway-independent Prostate Cancer. *Mol. Cancer Res.* 19 (1), 124–135. doi:10.1158/1541-7786.mcr-20-0379

Magtanong, L., Ko, P. J., To, M., Cao, J. Y., Forcina, G. C., Tarangelo, A., et al. (2019). Exogenous Monounsaturated Fatty Acids Promote a Ferroptosis-Resistant Cell State. *Cell Chem. Biol.* 26 (3), 420–e9. doi:10.1016/j.chembiol.2018.11.016

Maloberti, P. M., Duarte, A. B., Orlando, U. D., Pasqualini, M. E., Solano, A. R., López-Otín, C., et al. (2010). Functional Interaction between Acyl-CoA Synthetase 4, Lipooxygenases and Cyclooxygenase-2 in the Aggressive Phenotype of Breast Cancer Cells. *PLoS One* 5 (11), e15540. doi:10.1371/journal.pone.0015540

Manini, I., and Montomoli, E. (2018). Epidemiology and Prevention of Human Papillomavirus. *Ann. Ig.* 30 (4 Suppl. 1), 28–32. doi:10.7416/ai.2018.2231

Manley, S. J., Liu, W., and Welch, D. R. (2017). The KISS1 Metastasis Suppressor Appears to Reverse the Warburg Effect by Shifting from Glycolysis to Mitochondrial Beta-Oxidation. *J. Mol. Med. Berl.* 95 (9), 951–963. doi:10.1007/s00109-017-1552-2

Marisi, G., Cucchetti, A., Ulivi, P., Canale, M., Cabibbo, G., Solaini, L., et al. (2018). Ten Years of Sorafenib in Hepatocellular Carcinoma: Are There Any Predictive And/or Prognostic Markers? *World J. Gastroenterol.* 24 (36), 4152–4163. doi:10.3748/wjg.v24.i36.4152

Mashek, D. G., Li, L. O., and Coleman, R. A. (2006). Rat Long-Chain Acyl-CoA Synthetase mRNA, Protein, and Activity Vary in Tissue Distribution and in Response to Diet. *J. Lipid Res.* 47 (9), 2004–2010. doi:10.1194/jlr.M600150-JLR200

Matter, M. S., Decaens, T., Andersen, J. B., and Thorgeirsson, S. S. (2014). Targeting the mTOR Pathway in Hepatocellular Carcinoma: Current State and Future Trends. *J. Hepatol.* 60 (4), 855–865. doi:10.1016/j.jhep.2013.11.031

Monaco, M. E., Creighton, C. J., Lee, P., Zou, X., Topham, M. K., and Stafforini, D. M. (2010). Expression of Long-Chain Fatty Acyl-CoA Synthetase 4 in Breast and Prostate Cancers is Associated with Sex Steroid Hormone Receptor Negativity. *Transl. Oncol.* 3 (2), 91–98. doi:10.1593/tlo.09202

Nakamura, M. T., Yudell, B. E., and Loor, J. J. (2014). Regulation of Energy Metabolism by Long-Chain Fatty Acids. *Prog. Lipid Res.* 53, 124–144. doi:10.1016/j.plipres.2013.12.001

Nan, J., Lee, J. S., Lee, S. A., Lee, D. S., Park, K. S., and Chung, S. S. (2021). An Essential Role of the N-Terminal Region of ACSL1 in Linking Free Fatty Acids to Mitochondrial β-Oxidation in C2C12 Myotubes. *Mol. Cells* 44 (9), 637–646. doi:10.14348/molcells.2021.0077

Ndiaye, H., Liu, J. Y., Hall, A., Minogue, S., Morgan, M. Y., and Waugh, M. G. (2020). Immunohistochemical Staining Reveals Differential Expression of ACSL3 and ACSL4 in Hepatocellular Carcinoma and Hepatic Gastrointestinal Metastases. *Biosci. Rep.* 40 (4), BSR20200219. doi:10.1042/BSR20200219

Orlando, U. D., Garona, J., Ripoll, G. V., Maloberti, P. M., Solano, Á. R., Avagnina, A., et al. (2012). The Functional Interaction between Acyl-CoA Synthetase 4, 5-lipooxygenase and Cyclooxygenase-2 Controls Tumor Growth: A Novel Therapeutic Target. *PLoS One* 7 (7), e40794. doi:10.1371/journal.pone.0040794

Orlando, U. D., Castillo, A. F., Medrano, M. A. R., Solano, A. R., Maloberti, P. M., and Podesta, E. J. (2019). Acyl-CoA Synthetase-4 is Implicated in Drug Resistance in Breast Cancer Cell Lines Involving the Regulation of Energy-dependent Transporter Expression. *Biochem. Pharmacol.* 159, 52–63. doi:10.1016/j.bcp.2018.11.005

Ou, R., Lu, S., Wang, L., Wang, Y., Lv, M., Li, T., et al. (2022). Circular RNA circLMO1 Suppresses Cervical Cancer Growth and Metastasis by Triggering miR-4291/ACSL4-Mediated Ferroptosis. *Front. Oncol.* 12, 858598. doi:10.3389/fonc.2022.858598

Park, J. H., Vithayathil, S., Kumar, S., Sung, P. L., Dobrolecki, L. E., Putluri, V., et al. (2016). Fatty Acid Oxidation-Driven Src Links Mitochondrial Energy Reprogramming and Oncogenic Properties in Triple-Negative Breast Cancer. *Cell Rep.* 14 (9), 2154–2165. doi:10.1016/j.celrep.2016.02.004

Park, S., Oh, J., Kim, M., and Jin, E. J. (2018). Bromelain Effectively Suppresses Kras-Mutant Colorectal Cancer by Stimulating Ferroptosis. *Anim. Cells Syst. Seoul.* 22 (5), 334–340. doi:10.1080/19768354.2018.1512521

Pavlova, N. N., and Thompson, C. B. (2016). The Emerging Hallmarks of Cancer Metabolism. *Cell Metab.* 23 (1), 27–47. doi:10.1016/j.cmet.2015.12.006

Prior, I. A., Lewis, P. D., and Mattos, C. (2012). A Comprehensive Survey of Ras Mutations in Cancer. *Cancer Res.* 72 (10), 2457–2467. doi:10.1158/0008-5472.CAN-11-2612

Qin, X., Zhang, J., Lin, Y., Sun, X. M., Zhang, J. N., and Cheng, Z. Q. (2020). Identification of MiR-211-5p as a Tumor Suppressor by Targeting ACSL4 in Hepatocellular Carcinoma. *J. Transl. Med.* 18 (1), 326. doi:10.1186/s12967-020-02494-7

Quan, J., Bode, A. M., and Luo, X. (2021). ACSL Family: The Regulatory Mechanisms and Therapeutic Implications in Cancer. *Eur. J. Pharmacol.* 909, 174397. doi:10.1016/j.ejphar.2021.174397

Radif, Y., Ndiaye, H., Kalantzi, V., Jacobs, R., Hall, A., Minogue, S., et al. (2018). The Endogenous Subcellular Localisations of the Long Chain Fatty Acid-Activating Enzymes ACSL3 and ACSL4 in Sarcoma and Breast Cancer Cells. *Mol. Cell Biochem.* 448 (1-2), 275–286. doi:10.1007/s11010-018-3332-x

Ragab, H. M., Samy, N., Afify, M., El Maksoud, N. A., and Shaaban, H. M. (2018). Assessment of Ki-67 as a Potential Biomarker in Patients with Breast Cancer. *J. Genet. Eng. Biotechnol.* 16 (2), 479–484. doi:10.1016/j.jgeb.2018.03.002

Rajalingam, K., Schreck, R., Rapp, U. R., and Albert, S. (2007). Ras Oncogenes and Their Downstream Targets. *Biochim. Biophys. Acta* 1773 (8), 1177–1195. doi:10.1016/j.bbamcr.2007.01.012

Röhrig, F., and Schulze, A. (2016). The Multifaceted Roles of Fatty Acid Synthesis in Cancer. *Nat. Rev. Cancer* 16 (11), 732–749. doi:10.1038/nrc.2016.89

Rossi Sebastiano, M., and Konstantinidou, G. (2019). Targeting Long Chain Acyl-CoA Synthetases for Cancer Therapy. *Int. J. Mol. Sci.* 20 (15), 3624. doi:10.3390/ijms20153624

Sánchez-Martínez, R., Cruz-Gil, S., García-Álvarez, M. S., Reglero, G., and Ramírez de Molina, A. (2017). Complementary ACSL Isoforms Contribute to a Non-warburg Advantageous Energetic Status Characterizing Invasive Colon Cancer Cells. *Sci. Rep.* 7 (1), 11143. doi:10.1038/s41598-017-11612-3

Schiffman, M., Castle, P. E., Jeronimo, J., Rodriguez, A. C., and Wacholder, S. (2007). Human Papillomavirus and Cervical Cancer. *Lancet* 370 (9590), 890–907. doi:10.1016/S0140-6736(07)61416-0

Sha, R., Xu, Y., Yuan, C., Sheng, X., Wu, Z., Peng, J., et al. (2021). Predictive and Prognostic Impact of Ferroptosis-Related Genes ACSL4 and GPX4 on Breast Cancer Treated with Neoadjuvant Chemotherapy. *EBioMedicine* 71, 103560. doi:10.1016/j.ebiom.2021.103560

Shui, S., Zhao, Z., Wang, H., Conrad, M., and Liu, G. (2021). Non-enzymatic Lipid Peroxidation Initiated by Photodynamic Therapy Drives a Distinct Ferroptosis-like Cell Death Pathway. *Redox Biol.* 45, 102056. doi:10.1016/j.redox.2021.102056

Siegel, R. L., Miller, K. D., and Jemal, A. (2017). Cancer Statistics, 2017. *CA Cancer J. Clin.* 67 (1), 7–30. doi:10.3322/caac.21387

Stockwell, B. R. (2019). A Powerful Cell-Protection System Prevents Cell Death by Ferroptosis. *Nature* 575 (7784), 597–598. doi:10.1038/d41586-019-03145-8

Su, Y., Zhao, B., Zhou, L., Zhang, Z., Shen, Y., Lv, H., et al. (2020). Ferroptosis, a Novel Pharmacological Mechanism of Anti-cancer Drugs. *Cancer Lett.* 483, 127–136. doi:10.1016/j.canlet.2020.02.015

Sun, X. J., and Xu, G. L. (2017). Overexpression of Acyl-CoA Ligase 4 (ACSL4) in Patients with Hepatocellular Carcinoma and its Prognosis. *Med. Sci. Monit.* 23, 4343–4350. doi:10.12659/msm.906639

Sung, H., Ferlay, J., Siegel, R. L., Laversanne, M., Soerjomataram, I., Jemal, A., et al. (2021). Global Cancer Statistics 2020: GLOBOCAN Estimates of Incidence and Mortality Worldwide for 36 Cancers in 185 Countries. *CA Cancer J. Clin.* 71 (3), 209–249. doi:10.3322/caac.21660

Suzuki, H., Kawarabayasi, Y., Kondo, J., Abe, T., Nishikawa, K., Kimura, S., et al. (1990). Structure and Regulation of Rat Long-Chain Acyl-CoA Synthetase. *J. Biol. Chem.* 265 (15), 8681–8685. doi:10.1016/s0021-9258(19)38942-2

Tan, Y., Lin, K., Zhao, Y., Wu, Q., Chen, D., Wang, J., et al. (2018). Adipocytes Fuel Gastric Cancer Omental Metastasis via PITPNC1-Mediated Fatty Acid Metabolic Reprogramming. *Theranostics* 8 (19), 5452–5468. doi:10.7150/thno.28219

Tang, Y., Zhou, J., Hooi, S. C., Jiang, Y. M., and Lu, G. D. (2018). Fatty Acid Activation in Carcinogenesis and Cancer Development: Essential Roles of Long-Chain Acyl-CoA Synthetases. *Oncol. Lett.* 16 (2), 1390–1396. doi:10.3892/ol.2018.8843

Teodoro, B. G., Sampaio, I. H., Bomfim, L. H., Queiroz, A. L., Silveira, L. R., Souza, A. O., et al. (2017). Long-chain Acyl-CoA Synthetase 6 Regulates Lipid Synthesis and Mitochondrial Oxidative Capacity in Human and Rat Skeletal Muscle. *J. Physiol.* 595 (3), 677–693. doi:10.1113/JP272962

Ubellacker, J. M., Tasdogan, A., Ramesh, V., Shen, B., Mitchell, E. C., Martin-Sandoval, M. S., et al. (2020). Lymph Protects Metastasizing Melanoma Cells from Ferroptosis. *Nature* 585 (7823), 113–118. doi:10.1038/s41586-020-2623-z

Wang, D., Yin, L., Wei, J., Yang, Z., and Jiang, G. (2017). ATP Citrate Lyase is Increased in Human Breast Cancer, Depletion of Which Promotes Apoptosis. *Tumour Biol.* 39 (4), 1010428317698338. doi:10.1177/1010428317698338

Wang, W., Hao, X., Han, L., Yan, Z., Shen, W. J., Dong, D., et al. (2019). Tissue-Specific Ablation of ACSL4 Results in Disturbed Steroidogenesis. *Endocrinology* 160 (11), 2517–2528. doi:10.1210/en.2019-00464

Wang, J., Wang, Z., Yuan, J., Wang, J., and Shen, X. (2020). The Positive Feedback between ACSL4 Expression and O-GlcNAcylation Contributes to the Growth and Survival of Hepatocellular Carcinoma. *Aging (Albany NY)* 12 (9), 7786–7800. doi:10.18632/aging.103092

Wu, H., and Liu, A. (2021). Long Non-coding RNA NEAT1 Regulates Ferroptosis Sensitivity in Non-small-cell Lung Cancer. *J. Int. Med. Res.* 49 (3), 300060521996183. doi:10.1177/0300060521996183

Wu, M., Liu, H., Chen, W., Fujimoto, Y., and Liu, J. (2009). Hepatic Expression of Long-Chain Acyl-CoA Synthetase 3 is Upregulated in Hyperlipidemic Hamsters. *Lipids* 44 (11), 989–998. doi:10.1007/s11745-009-3341-3

Wu, X., Deng, F., Li, Y., Daniels, G., Du, X., Ren, Q., et al. (2015). ACSL4 Promotes Prostate Cancer Growth, Invasion and Hormonal Resistance. *Oncotarget* 6 (42), 44849–44863. doi:10.18632/oncotarget.6438

Xiaofei, J., Mingqing, S., Miao, S., Yizhen, Y., Shuang, Z., Qinhua, X., et al. (2021). Oleanolic Acid Inhibits Cervical Cancer Hela Cell Proliferation through Modulation of the ACSL4 Ferroptosis Signaling Pathway. *Biochem. Biophys. Res. Commun.* 545, 81–88. doi:10.1016/j.bbrc.2021.01.028

Xing, Y. H., Zhang, J. L., Lu, L., Li, D. G., Wang, Y. Y., Huang, S., et al. (2015). Identification of Specific Gene Modules in Mouse Lung Tissue Exposed to Cigarette Smoke. *Asian Pac J. Cancer Prev.* 16 (10), 4251–4256. doi:10.7314/apjcp.2015.16.10.4251

Yen, M. C., Kan, J. Y., Hsieh, C. J., Kuo, P. L., Hou, M. F., and Hsu, Y. L. (2017). Association of Long-Chain Acyl-Coenzyme A Synthetase 5 Expression in Human Breast Cancer by Estrogen Receptor Status and its Clinical Significance. *Oncol. Rep.* 37 (6), 3253–3260. doi:10.3892/or.2017.5610

Yu, Y., Sun, X., Chen, F., and Liu, M. (2022). Genetic Alteration, Prognostic and Immunological Role of Acyl-CoA Synthetase Long-Chain Family Member 4 in a Pan-Cancer Analysis. *Front. Genet.* 13, 812674. doi:10.3389/fgene.2022.812674

Zhang, Y., Li, S., Li, F., Lv, C., and Yang, Q. K. (2021). High-fat Diet Impairs Ferroptosis and Promotes Cancer Invasiveness via Downregulating Tumor Suppressor ACSL4 in Lung Adenocarcinoma. *Biol. Direct* 16 (1), 10. doi:10.1186/s13062-021-00294-7

Zhao, C., Liu, G., Shang, S., Wei, Q., Zhang, L., Xia, T., et al. (2019). Adaptive Evolution of the ACSL Gene Family in Carnivora. *Genetica* 147 (2), 141–148. doi:10.1007/s10709-019-00057-3

Zhao, M. Y., Liu, P., Sun, C., Pei, L. J., and Huang, Y. G. (2022). Propofol Augments Paclitaxel-Induced Cervical Cancer Cell Ferroptosis *In Vitro*. *Front. Pharmacol.* 13, 816432. doi:10.3389/fphar.2022.816432

Conflict of Interest: The authors declare that the research was conducted in the absence of any commercial or financial relationships that could be construed as a potential conflict of interest.

Publisher's Note: All claims expressed in this article are solely those of the authors and do not necessarily represent those of their affiliated organizations, or those of the publisher, the editors and the reviewers. Any product that may be evaluated in this article, or claim that may be made by its manufacturer, is not guaranteed or endorsed by the publisher.

Copyright © 2022 Hou, Jiang, Wen, Li, Xiong, Yue, Long, Shi and Zhang. This is an open-access article distributed under the terms of the Creative Commons Attribution License (CC BY). The use, distribution or reproduction in other forums is permitted, provided the original author(s) and the copyright owner(s) are credited and that the original publication in this journal is cited, in accordance with accepted academic practice. No use, distribution or reproduction is permitted which does not comply with these terms.

frontiers | Frontiers in Pharmacology

ORIGINAL RESEARCH
published: 15 July 2022
doi: 10.3389/fphar.2022.931501

RAB39B as a Chemosensitivity-Related Biomarker for Diffuse Large B-Cell Lymphoma

Cong Xu[1,2†], *Ting Liang*[3†], *Jing Liu*[1] *and Yunfeng Fu*[1,4*]

[1]Department of Hematology, The Third Xiangya Hospital of Central South University, Changsha, China, [2]Department of Hematology, The Seventh Affiliated Hospital of Sun Yat-Sen University, Shenzhen, China, [3]Department of Blood Transfusion, The Seventh Affiliated Hospital of Sun Yat-Sen University, Shenzhen, China, [4]Department of Blood Transfusion, The Third Xiangya Hospital of Central South University, Changsha, China

Background: Diffuse large B-cell lymphoma (DLBCL) is the most common aggressive lymphoma with an increased tendency to relapse or refractoriness. RAB39B, a member of the Ras-oncogene superfamily, is associated with a variety of tumors. Nevertheless, the role of RAB39B in DLBCL is still unknown. This study aimed to identify the role of RAB39B in DLBCL using integrated bioinformatics analysis.

Methods: RAB39B expression data were examined using TIMER, UCSC, and GEO databases. The LinkedOmics database was used to study the genes and signaling pathways related to RAB39B expression. A Protein–protein interaction network was performed in STRING. TIMER was used to analyze the correlation between RAB39B and infiltrating immune cells. The correlation between RAB39B and m6A-related genes in DLBCL was analyzed using TCGA data. The RAB39B ceRNA network was constructed based on starBase and miRNet2.0 databases. Drug sensitivity information was obtained from the GSCA database.

Results: RAB39B was highly expressed in multiple tumors including DLBCL. The protein–protein interaction network showed enrichment of autophagy and RAS family proteins. Functional enrichment analysis of RAB39B co-expression genes revealed that RAB39B was closely related to DNA replication, protein synthesis, cytokine–cytokine receptor interaction, JAK-STAT signaling pathway, NF-kappa B signaling pathway, and autophagy. Immune infiltrate analysis showed that the amount of RAB39B was negatively correlated with iDC, Tem, and CD8 T-cell infiltration. $CD4^+$ T cell and DC were negatively correlated with CNV of RAB39B. DLBCL cohort analysis found that RAB39B expression was related to 14 m6A modifier genes, including YTHDC1, YTHDC2, YTHDF1, YTHDF2, YTHDF3, RBMX, ZC3H13, METTL14, METTL3, RBM15, RBM15B, VIRMA, FTO, and ALKBH5. We constructed 14 possible ceRNA networks of RAB39B in DLBCL. The RAB39B expression was associated with decreased sensitivity of chemotherapy drugs such as dexamethasone, doxorubicin, etoposide, vincristine, and cytarabine and poor overall survival in DLBCL. *In vitro* experiments showed that RAB39B was associated with proliferation, apoptosis, and drug sensitivity of DLBCL cells.

OPEN ACCESS

Edited by:
Zhe-Sheng Chen,
St. John's University, United States

Reviewed by:
Shanchun Guo,
Xavier University of Louisiana, United States
Jingwen Wan,
Huazhong University of Science and Technology, China

***Correspondence:**
Yunfeng Fu
fuyunfeng@csu.edu.cn

[†]*These authors have contributed equally to this work*

Specialty section:
This article was submitted to Pharmacology of Anti-Cancer Drugs, a section of the journal Frontiers in Pharmacology

Received: *29 April 2022*
Accepted: *14 June 2022*
Published: *15 July 2022*

Citation:
Xu C, Liang T, Liu J and Fu Y (2022) RAB39B as a Chemosensitivity-Related Biomarker for Diffuse Large B-Cell Lymphoma. Front. Pharmacol. 13:931501. doi: 10.3389/fphar.2022.931501

Conclusion: RAB39B is abnormally elevated and related to drug resistance and poor OS in DLBCL, which may be due to its involvement in immune infiltration, m6A modification, and regulation by multiple non-coding RNAs. RAB39B may be used as an effective biomarker for the diagnosis and treatment of DLBCL.

Keywords: RAB39B, diffuse large B-cell lymphoma, immune infiltration, m6A modification, drug sensitivity

INTRODUCTION

Diffuse large B-cell lymphoma (DLBCL) is the most common non-Hodgkin's lymphoma, accounting for around 75% of aggressive lymphomas in adults (Teras et al., 2016). It is histologically characterized by diffuse growth, nodal architectural destruction, and extranodal infiltration with large B lymphoid cells. Although typically R-CHOP (rituximab plus cyclophosphamide, doxorubicin, vincristine, and prednisone)-based chemotherapy cures a majority of patients with DLBCL, ~40% of the patients either suffer a relapse or have primary refractory disease (Coiffier et al., 2002). Although remarkable progress has been made in understanding the pathogenesis, the precise mechanism of DLBCL remains unknown. The recently revised World Health Organization (WHO) classification of DLBCL includes the germinal center B cell–like (GCB) and non-GCB [which includes activated B cell–like (ABC) and unclassified by gene expression profiling (GEP)] cell types as new entities based on IHC staining (Swerdlow et al., 2016). Non-GCB DLBCL is associated with higher CNS relapse risk and poor prognosis (Offner et al., 2015; Klanova et al., 2019). Gaining an in-depth understanding of the mechanisms that drive DLBCL pathogenesis and response to therapy has important practical and theoretical value.

The pathogenesis of DLBCL represents a multi-factorial process. Modern genome-wide molecular analysis has uncovered significant implications of gene mutation, epigenetic remodeling, differentiation block, immune surveillance escape, immune infiltration, and the constitutive activation of several signal transduction pathways in the initiation and maintenance of the tumor clone in DLBCL (Pasqualucci and Dalla-Favera, 2018; Cheng et al., 2020; Lee et al., 2020). Similar to most cancer, several mechanisms contribute to oncogenic dysregulation in DLBCL, including gene copy number changes and somatically acquired non-silent point mutations. In addition, the genome of DLBCL is altered by chromosomal translocations and aberrant somatic hypermutation, both of which are intimately connected to the physiologic IG DNA remodeling processes operating in B lymphocytes (Pasqualucci and Dalla-Favera, 2018). Among them, the canonical cancer-related RAS/RAF/MEK/ERK pathway is considered to be associated with DLBCL cell proliferation, migration, invasion, drug sensitivity, and prognosis (Jiang et al., 2018; Yang et al., 2020; Sun et al., 2021; Wang and Sun, 2021).

RAB39B, a member of the Ras-oncogene superfamily, consists of two exons spanning 3764 bp of human genomic DNA and locates in human chromosome Xq28 (Cheng et al., 2002). RAB39B is expressed in multiple human tissues. Previous studies have mainly focused on the role of RAB39B abnormalities in X-linked neurodevelopmental defects including macrocephaly, intellectual disability, autism spectrum disorder, and Parkinson's disease (Tang, 2021). In cancer research, RAB39B is reported to be upregulated in germ cell neoplastic and gastric stromal tumors (Biermann et al., 2007; Kou et al., 2015). Studies have also shown that RAB39B is correlated with immune-infiltrating cells and poor overall survival in pancreatic adenocarcinoma (He et al., 2020). RAB39B has been considered to be involved in the regulation of autophagy and the PI3K/Akt/mTOR signaling pathway (Giannandrea et al., 2010; Tang, 2021). However, the underlying molecular mechanisms involved remain largely unknown and require detailed characterization. To date, there are no data on the expression and biological function of RAB39B in DLBCL.

In this study, we analyzed the differences in the expression of RAB39B in DLBCL from various public databases. Protein–protein interaction (PPI), co-expressed genes, immune infiltration, N6-methyladenosine (m6A) RNA methylation, and ceRNA networks were used to evaluate the potential mechanism of RAB39B in DLBCL. We also evaluated the impact of RAB39B expression on cell proliferation, apoptosis, drug sensitivity, and prognosis of DLBCL. This study provides a theoretical basis for the role of RAB39B in DLBCL.

MATERIALS AND METHODS

Tumor Immune Estimation Resource Analysis

Tumor Immune Estimation Resource (TIMER, https://cistrome.shinyapps.io/timer/) is a reliable and convenient database including comprehensive immune infiltrates and gene expression resources across diverse cancer types and TCGA gene expression profiles (Li et al., 2016; Li T. et al., 2017). In this study, we evaluated the mRNA level of RAB39B between tumor and adjacent normal tissues in pan-cancer through the DiffExp module of the TIMER database. The somatic copy number alteration (SCNA) module was used to link the genetic copy number variations (CNVs) of RAB39B with the relative abundance of immune-infiltrating cells.

UCSC Xena Data

DLBCL RNA-seq data from TCGA database and RNA-seq data of normal samples from the GTEx database were downloaded from UCSC Xena (https://xenabrowser.net/datapages/) (Goldman et al., 2020). We obtained 47 tumor samples and 444 normal samples for analysis.

Gene Expression Omnibus Data

We downloaded GSE9327 ($n = 200$) RNA-seq data from the Gene Expression Omnibus (GEO, www.ncbi.nlm.nih.gov/geo) database, which included 8 reactive lymph nodes and 36 DLBCL samples.

The Cancer Genome Atlas Data

The Cancer Genome Atlas (TCGA, https://portal.gdc.cancer.gov/) characterizes more than 20,000 samples of 33 cancer types (Tomczak et al., 2015). DLBCL RNA-seq data were downloaded from the Genomic Data Commons (GDC, https://portal.gdc.cancer.gov/) database, which included 48 tumor samples. We evaluated the correlation between RAB39B and immune-infiltrating cells using the ssGSEA algorithm in R (version 3.6.3) (Hanzelmann et al., 2013). The markers of immune cells drew on a report from Bindea et al. (2013). We also analyzed the expression level correlation between RAB39B and m6A-related genes in DLBCL samples and the differences in expression of m6A-related genes between the high and low RAB39B expression groups. M6A-related genes include YTHDC1, YTHDC2, IGF2BP1, IGF2BP2, IGF2BP3, YTHDF1, YTHDF2, YTHDF3, HNRNPA2B1, HNRNPC, RBMX, ZC3H13, METTL14, METTL3, RBM15, RBM15B, VIRMA, WTAP, FTO, and ALKBH5.

LinkedOmics Analysis

The LinkedOmics database (http://www.linkedomics.org/login.php) is a web-based portal that can provide multi-omics data analysis for TCGA database and 10 Clinical Proteomics Tumor Analysis Consortium (CPTAC) cancer cohorts (Vasaikar et al., 2018). We searched for the differentially expressed genes related to RAB39B in DLBCL ($n = 48$) in the LinkFinder module. The Pearson correlation coefficient was used for statistical analysis of RAB39B co-expression. The correlation results were visualized by volcano plots and heat maps. RAB39B co-expression genes were annotated using Gene Ontology (GO) analysis and Kyoto Encyclopedia of Genes and Genomes (KEGG) pathway enrichment analysis via the LinkInterpreter module.

STRING Analysis

STRING (https://cn.string-db.org/) is an online database that contains publicly available PPI data (Szklarczyk et al., 2019). In this study, we performed a PPI network analysis on RAB39B by STRING.

ceRNA Network Construction

starBase (https://starbase.sysu.edu.cn/) is an open-source platform for studying RNA–RNA interactions from CLIP-seq, degradome-seq, and RNA–RNA interactome data (Li et al., 2014). We used starBase to predict the target miRNAs of RAB39B. Candidate miRNAs were derived from the overlap of PITA, miRanda, and TargetScan predictions. In addition, we analyzed the correlation between the expression of these candidates and RAB39B to screen for miRNAs that were more in line with ceRNA conditions.

miRNet2.0 (www.mirnet.ca/miRNet/home.xhtml) is a platform for miRNA-centric network visual analytics (Chang et al., 2020). We used starBase and miRNet2.0 to predict the target lncRNAs of hsa-miR-144-3p and hsa-miR-381-3p. Candidate lncRNAs were obtained from the overlaps of starBase and miRNet2.0. The correlation between the expression of lncRNA candidates and miRNAs was also analyzed to screen for lncRNAs that are more in line with ceRNA conditions. miRNA–mRNA and miRNA–lncRNA with negatively correlated expression levels were screened out to construct a key lncRNA–miRNA–mRNA (RAB39B) ceRNA network for DLBCL.

Gene Set Cancer Analysis Analysis

Gene Set Cancer Analysis (GSCA, http://bioinfo.life.hust.edu.cn/GSCA/#/) integrates over 10,000 multi-dimensional genomic data from TCGA and over 750 small molecule drugs from GDSC and CTRP (Ji et al., 2016). Here, we investigated the correlation between RAB39B expression and drug response based on CTRP in the GSCA database.

Clinical Tissues and Cell Culture

Lymph node clinical specimens were obtained from patients with newly diagnosed DLBCL and healthy donors at Third Xiangya Hospital. Fresh tissues were preserved in liquid nitrogen. All patients provided informed consent. Human DLBCL cell lines U2932 and OCI-LY7 were purchased from American Type Culture Collection (ATCC; Manassas, VA, United States). Cell culture was performed according to the recommended protocols. For small interfering RNA (siRNA) transfection, DLBCL cell lines were transfected with siRNA (Niu et al., 2020) (sense: 5′-UCAUUCUUC AGAAGAGGUUTT-3'; antisense: 5′-AACCUCUUCUGA AGAAUGATT-3′) using LipofectamineTM 3000 (Invitrogen, MA, United States).

RNA Extraction and qPCR

Total RNA was extracted from clinical samples using standard TRIzol (Invitrogen, United States) RNA extraction protocol. RNA samples were quantified by NanoDrop ND-1000 (NanoDrop, United States). Reverse transcription was performed using PrimeScript RT Reagent Kit (Takara, China). Real-time qPCR was performed using Brilliant II SYBR Green RT–qPCR kit. The $2^{-\Delta\Delta Ct}$ method was used for calculating relative levels of RAB39B. Primers used were as follows (Niu et al., 2020):

For RAB39B:

forward primer: 5′-CTGGGATACAGCGGGTCAAG-3′;
reverse primer: 5′-GAAGGACCTGCGGTTGGTAA-3′.

For GAPDH:

forward primer: 5′- GGGAAACTGTGGCGTGAT-3′;
reverse primer: 5′- GAGTGGGTGTCGCTGTTGA-3′.

Cell Proliferation Assay

For cell proliferation assay, cells were incubated in 96-well plates for the required time. Cell count kit-8 reagent (Sigma-Aldrich, St

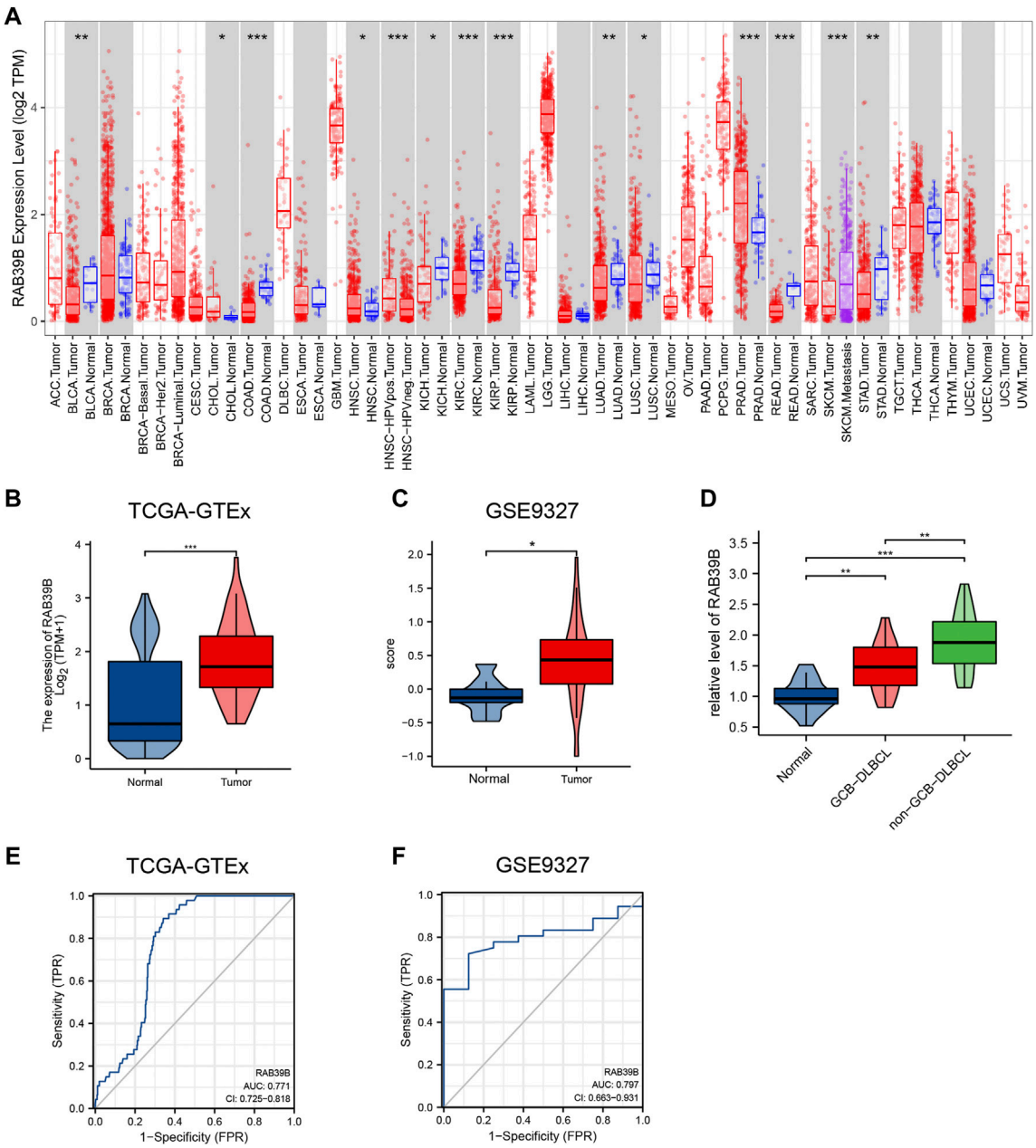

FIGURE 1 | Relationship between RAB39B expression and DLBCL. **(A)** TIMER database showed dysregulation of RAB39B in various cancers. **(B)** Expression of RAB39B between DLBCL and normal controls in TCGA–GTEx. **(C)** GSE9327 dataset was used to assess the RAB39B level between DLBCL and normal tissues. **(D)** Clinical samples showed the elevated expression of RAB39B in GCB-DLBCL, and this trend was much more pronounced in non-GCB DLBCL patients. **(E,F)** ROC analysis illustrated that RAB39B expression accurately discriminated DLBCL tumor tissues from normal tissues with an AUC of 0.771 (95% CI: 0.725–0.818) from TCGA–GTEx data and an AUC of 0.797 (95% CI: 0.663–0.931) from the GSE9327 dataset. $^{*}p < 0.05$, $^{**}p < 0.01$, and $^{***}p < 0.001$.

Louis, Missouri; 10 μL) was added to each well, followed by incubation for 4 h. The absorbance of the solution was measured at 450 nm using a microplate imaging system. For chemotherapeutic agent testing, doxorubicin (Sigma, 0.1 μM) or vincristine (MCE, 0.05 μM) was added 48 h after siRNA transfection. The cells were incubated for 72 h before monitoring the live cell rate with CCK-8.

Flow Cytometry

Cells were washed with cold PBS and resuspended at a concentration of 1×10^6 cells/ml in PBS containing 10% FBS and 1% sodium azide. For apoptosis analysis, apoptotic cells were detected using the Annexin V/PI Kit (KeyGEN BioTECH, China). Cells with the indicated transfection were collected and stained with Annexin V/PI in the dark for 15 min and

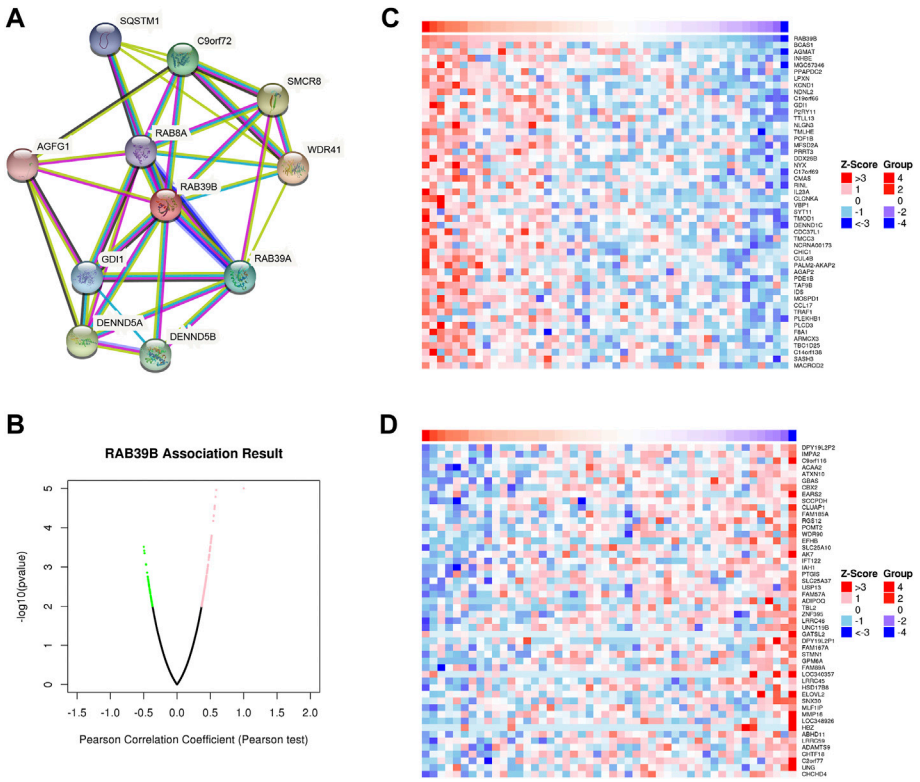

FIGURE 2 | RAB39B PPI network and co-expression genes in DLBCL. **(A)** PPI network of RAB39B. **(B)** Genes highly correlated with RAB39B identified in DLBCL by the Pearson test in the LinkedOmics database. **(C)** Top 50 genes positively related to RAB39B in DLBCL. **(D)** Top 50 genes negatively correlated with RAB39B in DLBCL.

subjected to flow cytometry. The analysis was performed with FACSVerse (BD Biosciences) and FlowJo software (Tree Star, United States).

Statistical Analysis

All statistical analyses were performed in R (v3.6.3). Shapiro–Wilk normality tests were used to assess data normality. For expression data that obeyed normal distribution, statistical significance was assessed using an independent sample *t*-test. Otherwise, data were evaluated by the Wilcoxon rank sum test. In correlation analysis, the Pearson correlation coefficient was used to evaluate the correlation between normally distributed samples; otherwise, the Spearman correlation coefficient was used. The receiver operating characteristic (ROC) curve was used to analyze the possibility of RAB39B as a diagnostic marker. The survival package (v3.2-10) was used in R (v3.6.3) for statistical analysis of survival data. A *p*-value (two-tailed) < 0.05 was considered statistically significant.

RESULTS

mRNA Levels of RAB39B in DLBCL and Pan-Cancer

The TIMER database was used to analyze the mRNA levels of RAB39B in tumors and adjacent normal tissues in pan-cancer. CHOL (cholangiocarcinoma), HNSC (head and neck squamous cell carcinoma), and PRAD (prostate adenocarcinoma) had significantly higher expression of RAB39B than adjacent normal tissues. In addition, HPV-positive HNSC had higher RAB39B than the HPV-negative subgroup. In SKCM (skin cutaneous melanoma), the RAB39B level was higher in metastases than in primaries. However, BLCA (bladder urothelial carcinoma), COAD (colon adenocarcinoma), KICH (kidney chromophobe), KIRC (kidney renal clear cell carcinoma), KIRP (kidney renal papillary cell carcinoma), LUAD (lung adenocarcinoma), LUSC (lung squamous cell carcinoma), READ (rectum adenocarcinoma), and STAD (stomach adenocarcinoma) had lower RAB39B expression than adjacent normal tissues (**Figure 1A**).

Since an adjacent normal control group of DLBCL is missing in TIMER, we analyzed TCGA-GTEx RAB39B expression data from the UCSC Xena database. The RAB39B mRNA level in DLBCL was significantly higher than that in normal tissues (**Figure 1B**). The clinical information is detailed in **Supplementary Table S1**. RAB39B mRNA levels were not associated with clinical stage, gender, extranodal involvement, and IDH level. The GSE9327 dataset from the GEO database also showed a significant increase of RAB39B in DLBCL tumor tissues compared with normal control (**Figure 1C**). For further

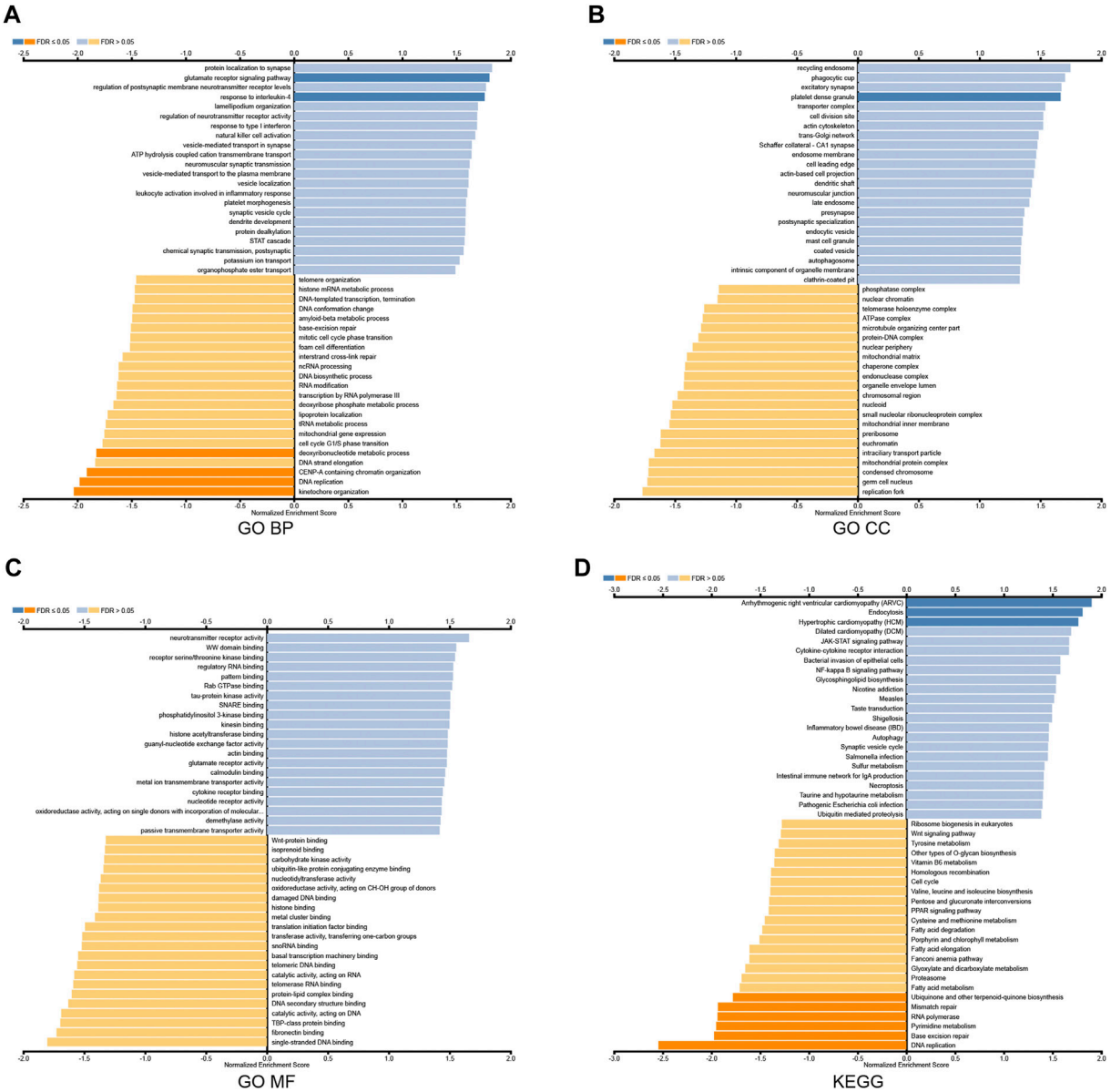

FIGURE 3 | Enrichment analysis of RAB39B co-expression genes in DLBCL. **(A–C)** RAB39B co-expression genes were annotated by GO BP **(A)**, CC **(B)**, and MF **(C)** analysis. **(D)** KEGG pathway analysis of RAB39B co-expression genes.

validation, we collected and tested the level of RAB39B in 17 healthy donors with reactive lymph nodes and 33 DLBCL patients (including 15 GCB subtypes and 18 non-GCB subtypes). We noted the elevated expression of RAB39B in GCB-DLBCL, and this trend was much more pronounced in non-GCB DLBCL patients (**Figure 1D**). ROC curve analysis was used to evaluate the diagnostic effectiveness of the RAB39B mRNA expression level, which estimated the AUC (area under the curve) at 0.771 (95% CI: 0.725–0.818, **Figure 1E**) in the TCGA–GTEx data and 0.797 (95% CI: 0.663–0.931, **Figure 1F**) in the GSE9327 dataset.

RAB39B PPI Network and Co-Expression Analysis in DLBCL

We used the STRING database to study the PPI network of RAB39B. The analysis showed that RAB39B was associated with WD repeat-containing protein 41 (WDR41), Smith–Magenis syndrome chromosome region, candidate 8 (SMCR8), DENN domain-containing protein 5A (DENND5A), C9orf72, DENN domain-containing protein 5B (DENND5B), RAB39A, Rab GDP dissociation inhibitor alpha (GDI1), sequestosome-1 (SQSTM1), RAB8A, Arf-GAP domain, and FG repeat-containing protein 1 (AGFG1) (**Figure 2A** and **Supplementary Table S2**. Among

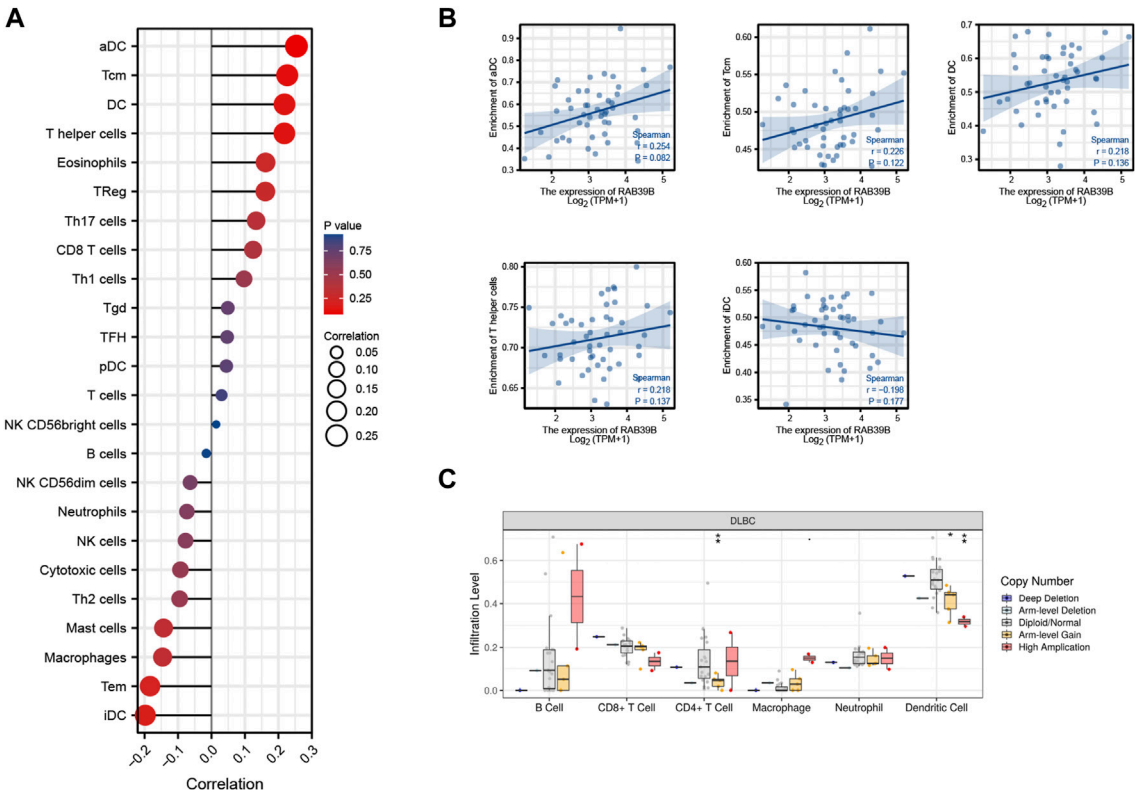

FIGURE 4 | Relationship between RAB39B and immune signatures in DLBCL. **(A)** Relationship between RAB39B expression and 24 immune cell types. **(B)** Scatter plots of E2F2 expression with the immune infiltration level of aDC, Tcm, DC, T helper cells, and iDC. **(C)** RAB39B CNV affects the infiltrating levels of $CD4^+$ T cell and DC in DLBCL.

these proteins, WDR41, SMCR8, C9orf72, SQSTM1, and RAB39A are related to autophagy, and RAB8A is a member of the Ras-oncogene family.

To further explore the biological function, we used the LinkedOmics database to analyze RAB39B co-expression in DLBCL (**Figure 2B**). The heat map shows the top 50 significant genes that were positively correlated (**Figure 2C**) and negatively correlated with RAB39B (**Figure 2D**), respectively. The LinkInterpreter module was used to perform GO and KEGG enrichment analyses of RAB39B-related genes. The GO function annotation showed that RAB39B co-expression genes were mainly involved in DNA replication and protein synthesis (**Figures 3A–C**). KEGG pathway analysis indicated an enrichment in the cytokine–cytokine receptor interaction, JAK-STAT signaling pathway, NF-kappa B signaling pathway, and autophagy (**Figure 3D**). In summary, PPI analysis and enrichment analysis of the co-expression network suggested the potential role of RAB39B in DLBCL pathological processes. Further validation of the results will require more samples.

RAB39B Was Associated With Immune Signatures in DLBCL

We used TCGA expression data to evaluate the relationship between RAB39B expression and 24 different immune cell types in DLBCL. As shown in **Figure 4A**, RAB39B showed a close positive correlation with activated dendritic cells (aDCs), T central memory (Tcm), DC, and T helper cells and a negative correlation with immature dendritic cell (iDC). Although the difference does not seem to be statistically significant (**Figure 4B**), we thought it may have been impacted by the limited sample size. In addition, we also found that RAB39B CNV had a significant correlation with the infiltration level of $CD4^+$ T cell and DC (**Figure 4C**). These results indicate that RAB39B plays an important role in the immune infiltration of DLBCL.

RAB39B Was Associated With m6A RNA Methylation Regulators in DLBCL

We tried to analyze the correlation between the expression of RAB39B and 20 m6A-related genes by using TCGA DLBCL dataset (**Figure 5A**). As shown in **Figure 5B**, the RAB39B expression was significantly positively correlated with YTHDC1, YTHDC2, YTHDF2, YTHDF3, RBMX, METTL14, VIRMA, and FTO. In addition, 48 DLBCL samples were grouped by RAB39B expression, with 24 samples in the high-expression group and 24 samples in the low-expression group. We analyzed the differential expression of 20 m6A-related genes between different RAB39B expression groups in DLBCL. Compared with the low RAB39B expression group, the expression of

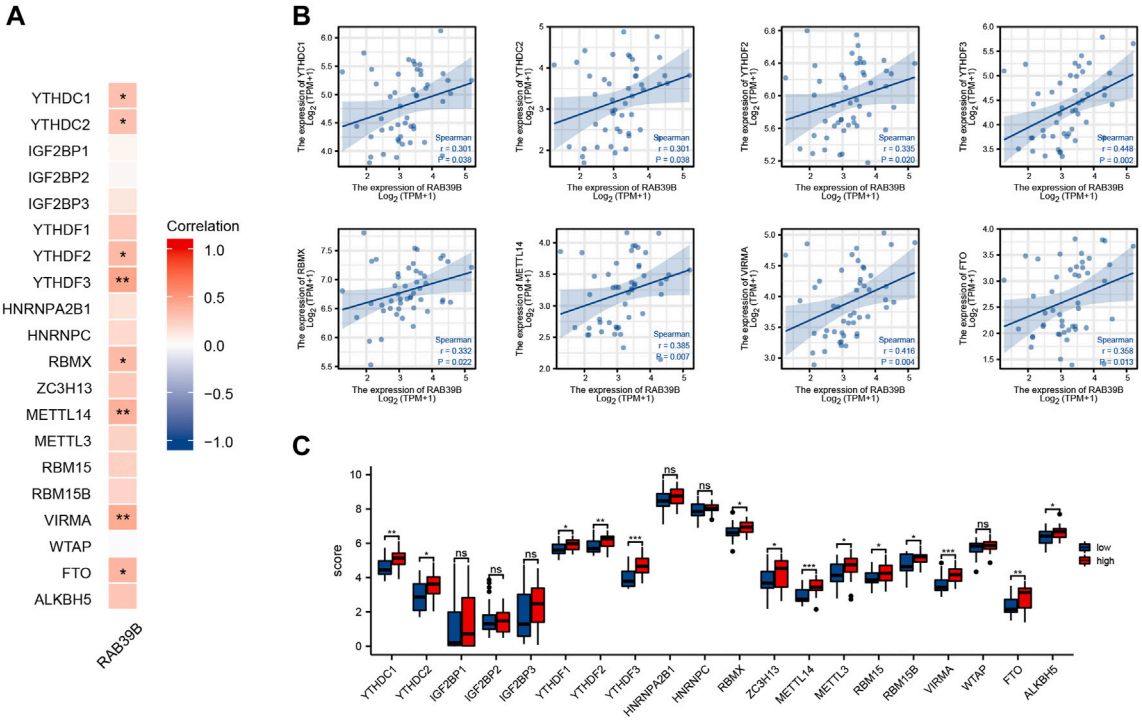

FIGURE 5 | Correlation between RAB39B and m6A-related genes in DLBCL. **(A)** Correlation between expression of RAB39B and m6A-related genes in TCGA DLBCL cohort. **(B)** Scatter plots of the correlation between RAB39B and m6A-related genes. m6A-related genes include YTHDC1, YTHDC2, YTHDF2, YTHDF3, RBMX, METTL14, VIRMA, and FTO. **(C)** Variation among m6A-related genes in the high and low RAB39B expression groups in DLBCL.

YTHDC1, YTHDC2, YTHDF1, YTHDF2, YTHDF3, RBMX, ZC3H13, METTL14, METTL3, RBM15, RBM15B, VIRMA, FTO, and ALKBH5 were significantly upregulated in the high RAB39B expression group (**Figure 5C**).

RAB39B-Related Key ceRNA Network Construction in DLBCL

We used the starBase database to predict target miRNAs of RAB39B in PITA, miRanda, and TargetScan. We obtained 49, 15, and 11 RAB39B target miRNAs, respectively. In total, eight common miRNAs were predicted in these three databases (**Figure 6A** and **Supplementary Table S3**). Since miRNAs are generally considered to negatively regulate target genes, miRNAs negatively correlated with RAB39B were screened for ceRNA construction. We found that hsa-miR-144-3p and hsa-miR-381-3p were significantly negatively correlated with the expression of RAB39B in DLBCL (**Figure 6B**).

We used starBase and miRNet databases to further predict the lncRNAs that may bind to hsa-miR-144-3p and hsa-miR-381-3p and displayed the overlaps using the Venn diagram (**Figure 6C**; **Supplementary Tables S4, S5**). In the ceRNA network hypothesis, lncRNAs are generally negatively correlated with miRNAs. We performed correlation analyses and included lncRNAs having a correlation coefficient <0.15 with miRNAs. DUXAP8 and LIFR-AS1 were negatively correlated with hsa-miR-144-3p, and ERICH3-AS1, FTX, GABPB1-AS1, LINC00472, LINC01278, NEAT1, OIP5-AS1, PSMA3-AS1, PWAR5, RBM26-AS1, RRN3P2, and TUG1 were negatively correlated with hsa-miR-381-3p (**Figure 6D**). Finally, we constructed 14 pairs of ceRNA networks (**Figure 6E**).

Effect of RAB39B Expression Level on Drug Sensitivity and Prognosis of DLBCL

To further understand the clinical significance of RAB39B expression, we predicted the relationship between RAB39B level and drug sensitivity using the GSCA database. As shown in **Figure 7A** and **Supplementary Table S6**, RAB39B was negatively correlated with the sensitivity to several chemotherapeutic drugs commonly used in DLBCL, like dexamethasone ($r = -0.20$, FDR $= 1.22 \times 10^{-6}$), doxorubicin ($r = -0.30$, FDR $= 2.36 \times 10^{-17}$), etoposide ($r = -0.33$, FDR $= 4.12 \times 10^{-21}$), vincristine ($r = -0.38$, FDR $= 2.64 \times 10^{-27}$), and cytarabine ($r = -0.34$, FDR $= 1.12 \times 10^{-21}$).

We also assessed the impact of RAB39B expression on the survival of DLBCL. Kaplan–Meier analysis demonstrated that increased expression of RAB39B was significantly associated with poor overall survival (OS) [hazard ratio (HR) = 9.28, $p = 0.041$]. High expression of RAB39B was also associated with poor disease-specific survival (DSS) and progression-free interval (PFI), but the aforementioned differences were not statistically significant, which was probably because of a partial lack of survival data (**Figure 7B**).

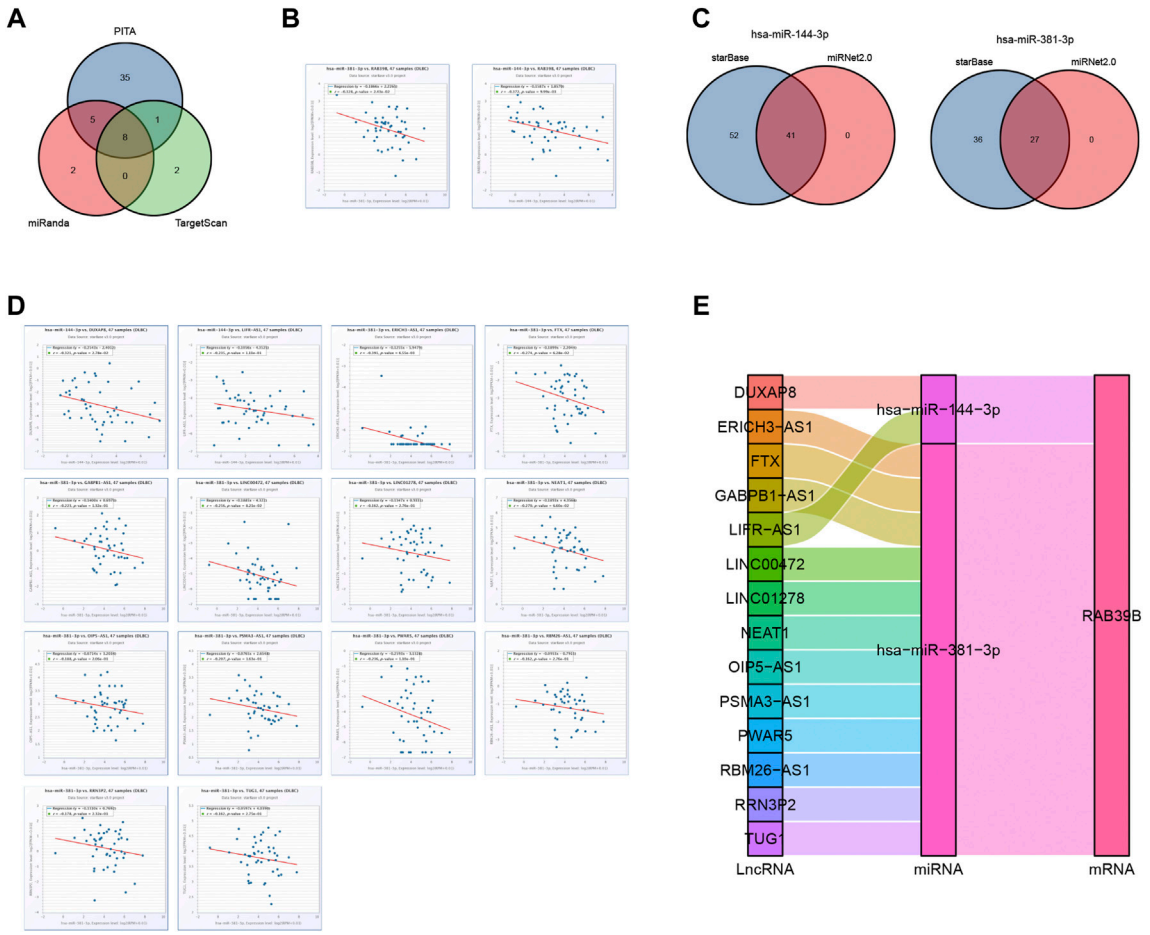

FIGURE 6 | RAB39B-related key ceRNA network construction in DLBCL. **(A)** Venn diagram of predicted RAB39B targets in PITA, miRanda, and TargetScan. **(B)** Correlation between RAB39B and the target miRNAs in scatter plots. **(C)** Venn diagram of predicted target lncRNAs of hsa-miR-144-3p and hsa-miR-381-3p in starBase and miRNet. **(D)** Correlation between hsa-miR-144-3p or hsa-miR-381-3p and the target lncRNAs in scatter plots. **(E)** lncRNA–miRNA–mRNA (RAB39B) regulatory network in line with the ceRNA hypothesis was constructed in the Sankey diagram.

RAB39B Was Associated With DLBCL Cell Proliferation, Apoptosis, and Drug Sensitivity *In Vitro*

We validated the function of RAB39B *in vitro*. First, the expression of RAB39B in DLBCL cell lines U2932 and OCI-LY7 was inhibited by siRNA transfection (**Figure 8A**). CCK-8 proliferation assay showed that treatment with RAB39B siRNA resulted in decreased proliferation of DLBCL cells (**Figure 8B**). Inhibition of RAB39B also resulted in increased apoptosis in DLBCL cells (**Figure 8C**). In addition, inhibition of RAB39B increased the sensitivity of DLBCL cells to doxorubicin and vincristine (**Figure 8D**).

DISCUSSION

Rab proteins represent the largest family of the RAS superfamily of small GTPases with 66 members identified in the human genome. As major regulators of vesicular transport, Rab and Rab-associated factors have emerged as important regulators of cell growth, differentiation, survival, and programmed cell death or apoptosis (Li and Marlin, 2015). Rab dysregulation affects the regulation of multiple signaling pathways by disrupting membrane trafficking and therefore plays a driving role in diseases such as cancer, neurological disorders, and several other genetic disorders (Menasche et al., 2000; Wasmeier et al., 2006; Giannandrea et al., 2010; Li, 2011). Multiple abnormal Rab genes have been identified as oncogenic drivers in a wide range of cancers. For example, Rab1a is upregulated in colorectal cancer, and Rab3d is overexpressed in a series of tumors including breast and lung cancer. These abnormal Rab signals are considered to be closely associated with aggressive tumor phenotypes (Thomas et al., 2014; Yang et al., 2015). As mentioned previously, RAB39B is upregulated in cancer (Biermann et al., 2007; Kou et al., 2015). In this study, we analyzed the expression level of RAB39B using TCGA–GTEX, GEO, and TIMER data. To the best of our knowledge, we are the first to report on the expression and potential diagnostic value of RAB39B in DLBCL.

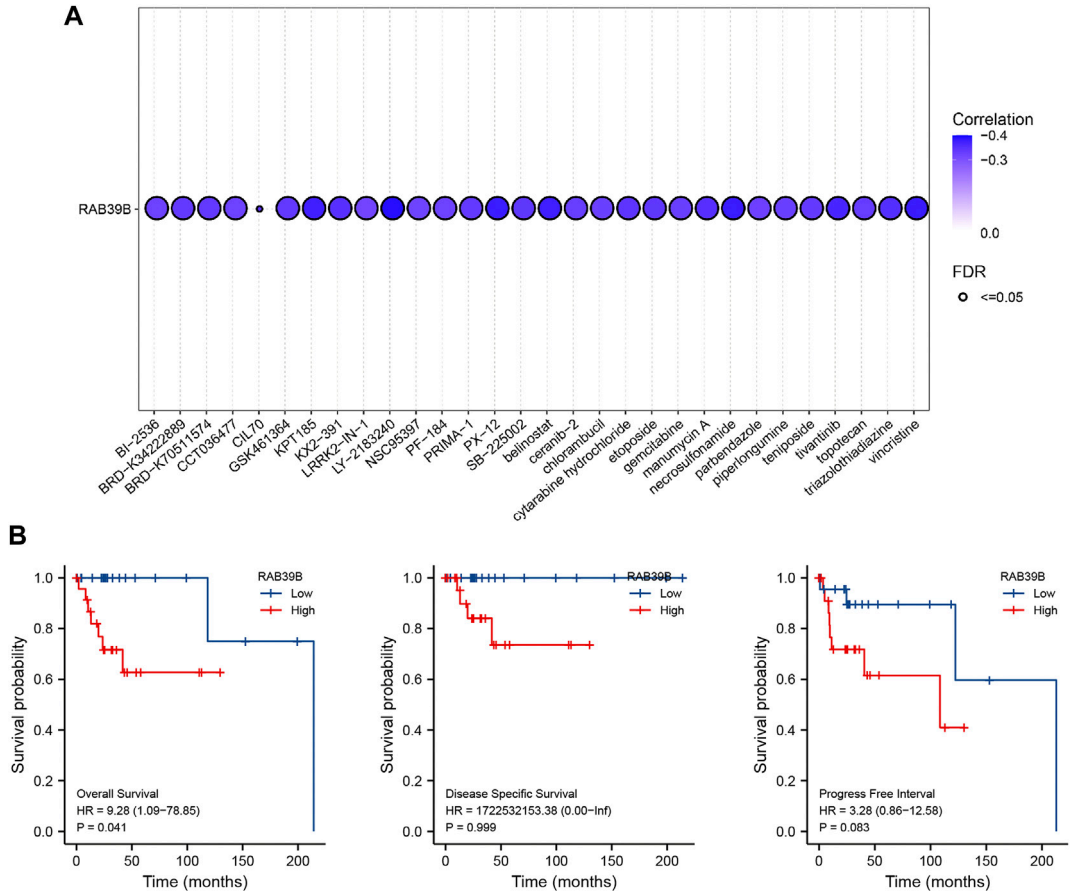

FIGURE 7 | Clinical significance of RAB39B expression. **(A)** Correlation between RAB39B expression and the sensitivity of CTRP drugs (top 30) in pan-cancer. **(B)** Relationship between RAB39B expression and OS, DSS, and PFI using Kaplan–Meier survival analysis.

A subset of Rab proteins, as well as their guanine nucleotide exchange factors or GTPase-activating proteins, are involved in autophagy regulation. For example, Rab2, Rab5, Rab6, and Rab33B have been demonstrated to participate in different steps and settings of autophagy (Ayala et al., 2018; Ding et al., 2019; Morgan et al., 2019; Zhou et al., 2019). In RAB39B-knockout mice, RAB39B deficiency compromised autophagic flux at the basal level (Niu et al., 2020). On the other hand, deregulated autophagy has been linked to proliferation, apoptosis, and drug sensitivity found in DLBCL (Li L. J. et al., 2017; Xu et al., 2021). To date, the function of RAB39B in DLBCL remains unknown. Similarly, we found that RAB39B may be involved in the regulation of DLBCL autophagy through PPI and co-expression gene enrichment analysis. We also observed the enrichment of several cancer-related pathways, like cytokine–cytokine receptor interaction, JAK-Stat signaling pathway, and NF-Kappa B signaling pathway, using the KEGG pathway enrichment analysis of RAB39B co-expressed genes. These suggest the potential role of RAB39B in the initiation and development of DLBCL.

As a major component of the tumor microenvironment, immune infiltrates have been proven to contribute to tumor progression and immunotherapy responses. Tumor-infiltrating immune cells, especially T cells, serve as the cellular underpinnings of antitumor immunity. Studies also suggest the importance of other immune cells, including myeloid cells, B cells, and NK cells in cancer immunotherapies (Zhang and Zhang, 2020). The immune infiltrates in the microenvironment have been utilized to determine the prognosis of many solid cancers (Tobin et al., 2019; Gao et al., 2020). Therefore, a better understanding of infiltrating immune cells in the tumor microenvironment of DLBCL is essential for deciphering the mechanisms of immunotherapies, defining predictive biomarkers, and identifying novel therapeutic targets. In nodal DLBCLs, memory T cells, $CD4^+$ T cells, and DC densities indicate a good prognostic value, whereas the influence of regulatory T cells (Tregs) is less clear. Immune infiltrate data for primary central nervous system DLBCL are very sparse. $CD8^+$ cytotoxic T cells seem to provide a possible immune escape mechanism and are associated with poor prognosis in all DLBCLs. From previous studies, it is known that tumor-associated macrophages are not associated with a significant prognostic value (Galand et al., 2012). Immune infiltrate analysis showed that RAB39B was negatively correlated with iDC, Tem (T effector memory), and

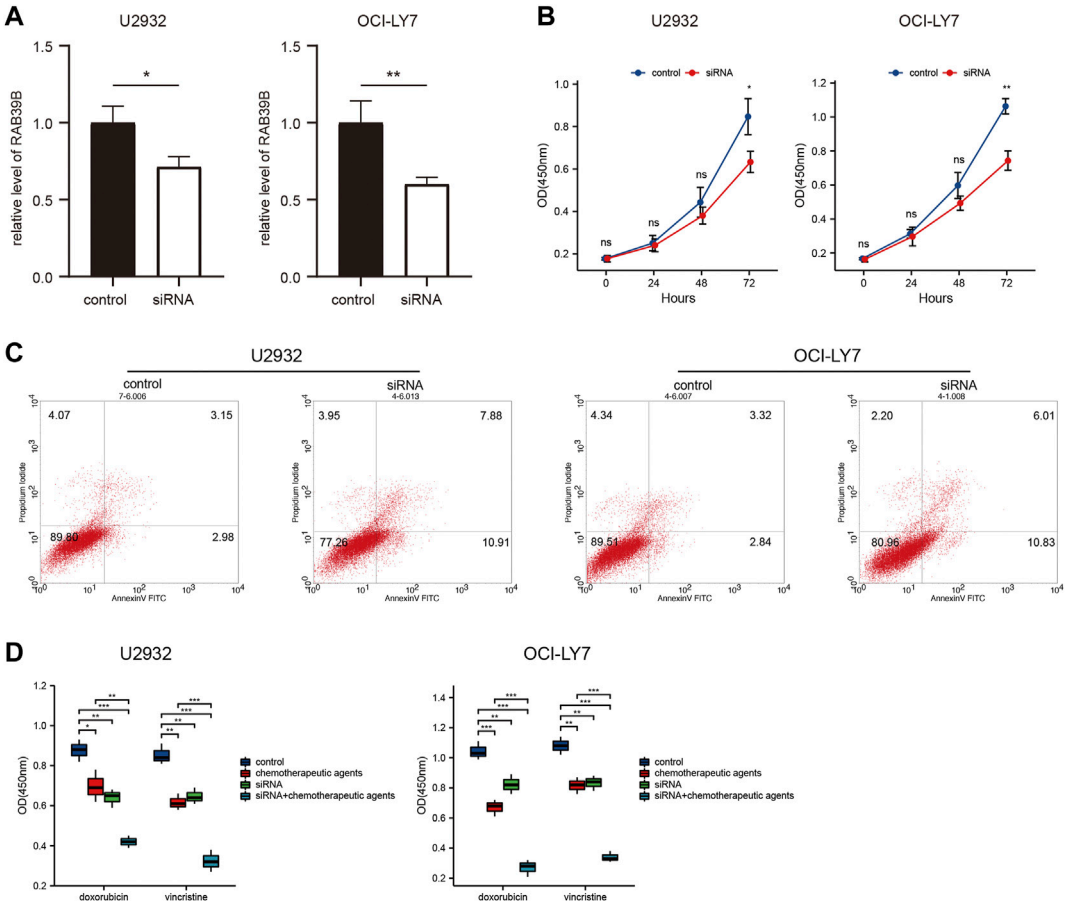

FIGURE 8 | RAB39B was associated with DLBCL cell proliferation, apoptosis, and drug sensitivity *in vitro*. **(A)** RAB39B siRNA transfection efficiency in U2932 and OCI-LY7 was measured by qPCR. **(B)** CCK-8 proliferation assay showed that RAB39B inhibition resulted in decreased proliferation of U2932 and OCI-LY7 DLBCL cells. **(C)** Inhibition of RAB39B resulted in increased apoptosis in U2932 (18.79%) and OCI-LY7 (16.84%) DLBCL cells. **(D)** Inhibition of RAB39B significantly increased the sensitivity of DLBCL cells to doxorubicin and vincristine.

CD8 T-cell infiltration but positively correlated with Tcm, aDC, and DC in this study. $CD4^+$ T cell and DC were also negatively correlated with CNV of RAB39B. These suggest that abnormality of RAB39B may lead to a poor prognosis of DLBCL by affecting immune infiltration. Further research is needed to understand alternative immune infiltration patterns.

As the most abundant eukaryotic mRNA modification, m6A is known to play a vital role in tumor initiation and progression by regulating target genes. The tumorigenic process in DLBCL is governed by both genetic and epigenetic aberrations. Previous studies have shown that m6A modifications are closely related to the occurrence and development of DLBCL. For example, Song et al. (2022) found that ALKBH5-mediated N^6-methyladenosine modification of TRERNA1 promotes DLBCL proliferation. Cheng et al. (2020) revealed that the m6A methyltransferase METTL3 promotes DLBCL progression by regulating m6A in PEDF. piRNA-30473, a PIWI-interacting RNA, has been indicated to exert its oncogenic role in DLBCL by upregulating WTAP, an m6A mRNA methylase (Han et al., 2021). The cellular machinery that regulates m6A includes proteins acting as writers, erasers, and readers of m6A. We analyzed the relationship between RAB39B expression and common m6A readers (YTHDC1, YTHDC2, IGF2BP1, IGF2BP2, IGF2BP3, YTHDF1, YTHDF2, YTHDF3, HNRNPA2B1, HNRNPC, and RBMX), writers (ZC3H13, METTL14, METTL3, RBM15, RBM15B, VIRMA, and WTAP), and erasers (FTO and ALKBH5) in DLBCL. The RAB39B expression was significantly correlated with YTHDC1, YTHDC2, YTHDF2, YTHDF3, RBMX, METTL14, VIRMA, and FTO. In addition, the level of YTHDC1, YTHDC2, YTHDF1, YTHDF2, YTHDF3, RBMX, ZC3H13, METTL14, METTL3, RBM15, RBM15B, VIRMA, FTO, and ALKBH5 increased in the high RAB39B expression group. These results suggest that the *RAB39B* gene may be modified by m6A in DLBCL.

The theory behind the regulatory ceRNA network is based on the competitive binding of lncRNA or cirRNA with miRNA to affect mRNA expression. The ceRNA regulatory mechanism is evident in DLBCL. For example, Huang et al. (2021) found that LINC00857 contributes to the proliferation and

lymphomagenesis of DLBCL by regulating the miR-370-3p/CBX3 axis. Miao et al. (2021) revealed that lncRNA GAS5 inhibits DLBCL cell proliferation by causing miR-18a-5p to upregulate RUNX1 expression. Zhu et al. (2019) illustrated that LncRNA SNHG16 promotes proliferation and inhibits apoptosis of DLBCL by targeting the miR-497-5p/PIM1 axis. In this study, we constructed an lncRNA–miRNA–mRNA (RAB39B) network based on miRNAs hsa-miR-144-3p and hsa-miR-381-3p, as well as lncRNAs DUXAP8, LIFR-AS1, ERICH3-AS1, FTX, GABPB1-AS1, LINC00472, LINC01278, NEAT1, OIP5-AS1, PSMA3-AS1, PWAR5, RBM26-AS1, RRN3P2, and TUG1. Among them, NEAT1 and TUG1 have been identified as tumor drivers in DLBCL (Cheng et al., 2019; Yuan et al., 2022). Here, we have uncovered the ceRNA network of RAB39B in DLBCL. Further experiments are required to validate this finding.

Finally, we explored the impact of the level of RAB39B expression on drug sensitivity and prognosis of DLBCL. Our results showed that increased RAB39B expression was associated with decreased sensitivity of commonly used chemotherapy drugs such as dexamethasone, doxorubicin, etoposide, vincristine, and cytarabine and poor OS in DLBCL. This trend verified the reliability of the previous functional analysis of RAB39B in DLBCL from a clinical perspective.

In summary, we are the first to analyze the relationship between RAB39B expression and tumor immune infiltrate, m6A modification, ceRNA network, drug sensitivity, and prognosis in DLBCL. RAB39B is abnormally elevated and associated with drug resistance and poor OS in DLBCL, which may be related to its involvement in immune infiltration, m6A modification, and regulation by multiple non-coding RNAs. Our study identifies RAB39B as an effective biomarker for the diagnosis and treatment of DLBCL.

DATA AVAILABILITY STATEMENT

The original contributions presented in the study are included in the article/**Supplementary Material;** further inquiries can be directed to the corresponding author.

AUTHOR CONTRIBUTIONS

JL and YF designed and performed the study. CX wrote the manuscript. TL performed the analytic calculations and statistical analysis. All authors read and approved the final manuscript.

SUPPLEMENTARY MATERIAL

The Supplementary Material for this article can be found online at: https://www.frontiersin.org/articles/10.3389/fphar.2022.931501/full#supplementary-material

REFERENCES

Ayala, C. I., Kim, J., and Neufeld, T. P. (2018). Rab6 Promotes Insulin Receptor and Cathepsin Trafficking to Regulate Autophagy Induction and Activity in Drosophila. *J. Cell Sci.* 131 (17), jcs216127. doi:10.1242/jcs.216127

Biermann, K., Heukamp, L. C., Steger, K., Zhou, H., Franke, F. E., Guetgemann, I., et al. (2007). Gene Expression Profiling Identifies New Biological Markers of Neoplastic Germ Cells. *Anticancer Res.* 27 (5A), 3091–3100.

Bindea, G., Mlecnik, B., Tosolini, M., Kirilovsky, A., Waldner, M., Obenauf, A. C., et al. (2013). Spatiotemporal Dynamics of Intratumoral Immune Cells Reveal the Immune Landscape in Human Cancer. *Immunity* 39 (4), 782–795. doi:10.1016/j.immuni.2013.10.003

Chang, L., Zhou, G., Soufan, O., and Xia, J. (2020). miRNet 2.0: Network-Based Visual Analytics for miRNA Functional Analysis and Systems Biology. *Nucleic Acids Res.* 48 (W1), W244–W251. doi:10.1093/nar/gkaa467

Cheng, H., Ma, Y., Ni, X., Jiang, M., Guo, L., Ying, K., et al. (2002). Isolation and Characterization of a Human Novel RAB (RAB39B) Gene. *Cytogenet Genome Res.* 97 (1-2), 72–75. doi:10.1159/000064047

Cheng, H., Yan, Z., Wang, X., Cao, J., Chen, W., Qi, K., et al. (2019). Downregulation of Long Non-coding RNA TUG1 Suppresses Tumor Growth by Promoting Ubiquitination of MET in Diffuse Large B-Cell Lymphoma. *Mol. Cell Biochem.* 461 (1-2), 47–56. doi:10.1007/s11010-019-03588-7

Cheng, Y., Fu, Y., Wang, Y., and Wang, J. (2020). The m6A Methyltransferase METTL3 Is Functionally Implicated in DLBCL Development by Regulating m6A Modification in PEDF. *Front. Genet.* 11, 955. doi:10.3389/fgene.2020.00955

Coiffier, B., Lepage, E., Briere, J., Herbrecht, R., Tilly, H., Bouabdallah, R., et al. (2002). CHOP Chemotherapy Plus Rituximab Compared with CHOP Alone in Elderly Patients with Diffuse Large-B-Cell Lymphoma. *N. Engl. J. Med.* 346 (4), 235–242. doi:10.1056/NEJMoa011795

Ding, X., Jiang, X., Tian, R., Zhao, P., Li, L., Wang, X., et al. (2019). RAB2 Regulates the Formation of Autophagosome and Autolysosome in Mammalian Cells. *Autophagy* 15 (10), 1774–1786. doi:10.1080/15548627.2019.1596478

Galand, C., Donnou, S., Molina, T. J., Fridman, W. H., Fisson, S., and Sautès-Fridman, C. (2012). Influence of Tumor Location on the Composition of Immune Infiltrate and its Impact on Patient Survival. Lessons from DCBCL and Animal Models. *Front. Immunol.* 3, 98. doi:10.3389/fimmu.2012.00098

Gao, Y., Chen, L., Cai, G., Xiong, X., Wu, Y., Ma, D., et al. (2020). Heterogeneity of Immune Microenvironment in Ovarian Cancer and its Clinical Significance: a Retrospective Study. *Oncoimmunology* 9 (1), 1760067. doi:10.1080/2162402X.2020.1760067

Giannandrea, M., Bianchi, V., Mignogna, M. L., Sirri, A., Carrabino, S., D'Elia, E., et al. (2010). Mutations in the Small GTPase Gene RAB39B Are Responsible for X-Linked Mental Retardation Associated with Autism, Epilepsy, and Macrocephaly. *Am. J. Hum. Genet.* 86 (2), 185–195. doi:10.1016/j.ajhg.2010.01.011

Goldman, M. J., Craft, B., Hastie, M., Repečka, K., McDade, F., Kamath, A., et al. (2020). Visualizing and Interpreting Cancer Genomics Data via the Xena Platform. *Nat. Biotechnol.* 38 (6), 675–678. doi:10.1038/s41587-020-0546-8

Han, H., Fan, G., Song, S., Jiang, Y., Qian, C., Zhang, W., et al. (2021). piRNA-30473 Contributes to Tumorigenesis and Poor Prognosis by Regulating m6A RNA Methylation in DLBCL. *Blood* 137 (12), 1603–1614. doi:10.1182/blood.2019003764

Hänzelmann, S., Castelo, R., and Guinney, J. (2013). GSVA: Gene Set Variation Analysis for Microarray and RNA-Seq Data. *BMC Bioinforma.* 14, 7. doi:10.1186/1471-2105-14-7

He, Q. L., Jiang, H. X., Zhang, X. L., and Qin, S. Y. (2020). Relationship between a 7-mRNA Signature of the Pancreatic Adenocarcinoma Microenvironment and Patient Prognosis (A STROBE-Compliant Article). *Med. Baltim.* 99 (29), e21287. doi:10.1097/MD.0000000000021287

Huang, Y., Lin, Y., Song, X., and Wu, D. (2021). LINC00857 Contributes to Proliferation and Lymphomagenesis by Regulating miR-370-3p/CBX3 axis in Diffuse Large B-Cell Lymphoma. *Carcinogenesis* 42 (5), 733–741. doi:10.1093/carcin/bgab013

Ji, Z., Vokes, S. A., Dang, C. V., and Ji, H. (2016). Turning Publicly Available Gene Expression Data into Discoveries Using Gene Set Context Analysis. *Nucleic Acids Res.* 44 (1), e8. doi:10.1093/nar/gkv873

Jiang, W., Zhou, X., Li, Z., Liu, K., Wang, W., Tan, R., et al. (2018). Prolyl 4-hydroxylase 2 Promotes B-Cell Lymphoma Progression via Hydroxylation of Carabin. *Blood* 131 (12), 1325–1336. doi:10.1182/blood-2017-07-794875

Klanova, M., Sehn, L. H., Bence-Bruckler, I., Cavallo, F., Jin, J., Martelli, M., et al. (2019). Integration of Cell of Origin into the Clinical CNS International Prognostic Index Improves CNS Relapse Prediction in DLBCL. *Blood* 133 (9), 919–926. doi:10.1182/blood-2018-07-862862

Kou, Y., Zhao, Y., Bao, C., and Wang, Q. (2015). Comparison of Gene Expression Profile between Tumor Tissue and Adjacent Non-tumor Tissue in Patients with Gastric Gastrointestinal Stromal Tumor (GIST). *Cell Biochem. Biophys.* 72 (2), 571–578. doi:10.1007/s12013-014-0504-5

Lee, C. W., Ren, Y. J., Marella, M., Wang, M., Hartke, J., and Couto, S. S. (2020). Multiplex Immunofluorescence Staining and Image Analysis Assay for Diffuse Large B Cell Lymphoma. *J. Immunol. Methods* 478, 112714. doi:10.1016/j.jim.2019.112714

Li, B., Severson, E., Pignon, J. C., Zhao, H., Li, T., Novak, J., et al. (2016). Comprehensive Analyses of Tumor Immunity: Implications for Cancer Immunotherapy. *Genome Biol.* 17 (1), 174. doi:10.1186/s13059-016-1028-7

Li, G., and Marlin, M. C. (2015). Rab Family of GTPases. *Methods Mol. Biol.* 1298, 1–15. doi:10.1007/978-1-4939-2569-8_1

Li, G. (2011). Rab GTPases, Membrane Trafficking and Diseases. *Curr. Drug Targets* 12 (8), 1188–1193. doi:10.2174/138945011795906561

Li, J. H., Liu, S., Zhou, H., Qu, L. H., and Yang, J. H. (2014). starBase v2.0: Decoding miRNA-ceRNA, miRNA-ncRNA and Protein-RNA Interaction Networks from Large-Scale CLIP-Seq Data. *Nucleic Acids Res.* 42 (Database issue), D92–D97. doi:10.1093/nar/gkt1248

Li, L. J., Chai, Y., Guo, X. J., Chu, S. L., and Zhang, L. S. (2017). The Effects of the Long Non-coding RNA MALAT-1 Regulated Autophagy-Related Signaling Pathway on Chemotherapy Resistance in Diffuse Large B-Cell Lymphoma. *Biomed. Pharmacother.* 89, 939–948. doi:10.1016/j.biopha.2017.02.011

Li, T., Fan, J., Wang, B., Traugh, N., Chen, Q., Liu, J. S., et al. (2017). TIMER: A Web Server for Comprehensive Analysis of Tumor-Infiltrating Immune Cells. *Cancer Res.* 77 (21), e108–e110. doi:10.1158/0008-5472.CAN-17-0307

Ménasché, G., Pastural, E., Feldmann, J., Certain, S., Ersoy, F., Dupuis, S., et al. (2000). Mutations in RAB27A Cause Griscelli Syndrome Associated with Haemophagocytic Syndrome. *Nat. Genet.* 25 (2), 173–176. doi:10.1038/76024

Miao, Y., Chen, X., Qin, M., Zhou, W., Wang, Y., and Ji, Y. (2021). lncRNA GAS5, as a ceRNA, Inhibits the Proliferation of Diffuse Large B-cell Lymphoma Cells by Regulating the miR-18a-5p/RUNX1 axis. *Int. J. Oncol.* 59 (5), 94. doi:10.3892/ijo.2021.5274

Morgan, N. E., Cutrona, M. B., and Simpson, J. C. (2019). Multitasking Rab Proteins in Autophagy and Membrane Trafficking: A Focus on Rab33b. *Int. J. Mol. Sci.* 20 (16), 3916. doi:10.3390/ijms20163916

Niu, M., Zheng, N., Wang, Z., Gao, Y., Luo, X., Chen, Z., et al. (2020). RAB39B Deficiency Impairs Learning and Memory Partially through Compromising Autophagy. *Front. Cell Dev. Biol.* 8, 598622. doi:10.3389/fcell.2020.598622

Offner, F., Samoilova, O., Osmanov, E., Eom, H. S., Topp, M. S., Raposo, J., et al. (2015). Frontline Rituximab, Cyclophosphamide, Doxorubicin, and Prednisone with Bortezomib (VR-CAP) or Vincristine (R-CHOP) for Non-GCB DLBCL. *Blood* 126 (16), 1893–1901. doi:10.1182/blood-2015-03-632430

Pasqualucci, L., and Dalla-Favera, R. (2018). Genetics of Diffuse Large B-Cell Lymphoma. *Blood* 131 (21), 2307–2319. doi:10.1182/blood-2017-11-764332

Song, W., Fei, F., Qiao, F., Weng, Z., Yang, Y., Cao, B., et al. (2022). ALKBH5-mediated N6-Methyladenosine Modification of TRERNA1 Promotes DLBCL Proliferation via P21 Downregulation. *Cell Death Discov.* 8 (1), 25. doi:10.1038/s41420-022-00819-7

Sun, R., Zheng, Z., Wang, L., Cheng, S., Shi, Q., Qu, B., et al. (2021). A Novel Prognostic Model Based on Four Circulating miRNA in Diffuse Large B-Cell Lymphoma: Implications for the Roles of MDSC and Th17 Cells in Lymphoma Progression. *Mol. Oncol.* 15 (1), 246–261. doi:10.1002/1878-0261.12834

Swerdlow, S. H., Campo, E., Pileri, S. A., Harris, N. L., Stein, H., Siebert, R., et al. (2016). The 2016 Revision of the World Health Organization Classification of Lymphoid Neoplasms. *Blood* 127 (20), 2375–2390. doi:10.1182/blood-2016-01-643569

Szklarczyk, D., Gable, A. L., Lyon, D., Junge, A., Wyder, S., Huerta-Cepas, J., et al. (2019). STRING V11: Protein-Protein Association Networks with Increased Coverage, Supporting Functional Discovery in Genome-wide Experimental Datasets. *Nucleic Acids Res.* 47 (D1), D607–D613. doi:10.1093/nar/gky1131

Tang, B. L. (2021). RAB39B's Role in Membrane Traffic, Autophagy, and Associated Neuropathology. *J. Cell Physiol.* 236 (3), 1579–1592. doi:10.1002/jcp.29962

Teras, L. R., DeSantis, C. E., Cerhan, J. R., Morton, L. M., Jemal, A., and Flowers, C. R. (2016). 2016 US Lymphoid Malignancy Statistics by World Health Organization Subtypes. *CA Cancer J. Clin.* 66 (6), 443–459. doi:10.3322/caac.21357

Thomas, J. D., Zhang, Y. J., Wei, Y. H., Cho, J. H., Morris, L. E., Wang, H. Y., et al. (2014). Rab1A Is an mTORC1 Activator and a Colorectal Oncogene. *Cancer Cell* 26 (5), 754–769. doi:10.1016/j.ccell.2014.09.008

Tobin, J. W. D., Keane, C., Gunawardana, J., Mollee, P., Birch, S., Hoang, T., et al. (2019). Progression of Disease within 24 Months in Follicular Lymphoma Is Associated with Reduced Intratumoral Immune Infiltration. *J. Clin. Oncol.* 37 (34), 3300–3309. doi:10.1200/JCO.18.02365

Tomczak, K., Czerwińska, P., and Wiznerowicz, M. (2015). The Cancer Genome Atlas (TCGA): an Immeasurable Source of Knowledge. *Contemp. Oncol. Pozn.* 19 (1A), A68–A77. doi:10.5114/wo.2014.47136

Vasaikar, S. V., Straub, P., Wang, J., and Zhang, B. (2018). LinkedOmics: Analyzing Multi-Omics Data within and across 32 Cancer Types. *Nucleic Acids Res.* 46 (D1), D956–D963. doi:10.1093/nar/gkx1090

Wang, S., and Sun, L. (2021). Silencing Aurora-kinase-A (AURKA) Reinforced the Sensitivity of Diffuse Large B-Cell Lymphoma Cells to Cyclophosphamide, Doxorubicin, Vincristine, and Prednisone (CHOP) via Suppressing β-Catenin and RAS-Extracellular Signal-Regulated Protein Kinase (ERK1/2) Pathway. *Bioengineered* 12 (1), 8296–8308. doi:10.1080/21655979.2021.1985346

Wasmeier, C., Romao, M., Plowright, L., Bennett, D. C., Raposo, G., and Seabra, M. C. (2006). Rab38 and Rab32 Control Post-golgi Trafficking of Melanogenic Enzymes. *J. Cell Biol.* 175 (2), 271–281. doi:10.1083/jcb.200606050

Xu, H., Yu, X., Yang, Z., Song, Q., Cheng, S., He, Z., et al. (2021). PAX5-activated lncRNA ARRDC1-AS1 Accelerates the Autophagy and Progression of DLBCL through Sponging miR-2355-5p to Regulate ATG5. *Life Sci.* 286, 119932. doi:10.1016/j.lfs.2021.119932

Yang, J., Liu, W., Lu, X., Fu, Y., Li, L., and Luo, Y. (2015). High Expression of Small GTPase Rab3D Promotes Cancer Progression and Metastasis. *Oncotarget* 6 (13), 11125–11138. doi:10.18632/oncotarget.3575

Yang, S., Yuan, L., Wang, Y., Zhu, M., Wang, J., and Ke, X. (2020). B7-H6 Promotes Cell Proliferation, Migration and Invasion of Non-hodgkin Lymphoma via Ras/MEK/ERK Pathway Based on Quantitative Phosphoproteomics Data. *Onco Targets Ther.* 13, 5795–5805. doi:10.2147/OTT.S257512

Yuan, J., Yang, J., Wang, R., Hao, H., and Li, J. (2022). LncRNA NEAT1 Regulate Diffuse Large B-Cell Lymphoma by Targeting miR-495-3p/PD-L1 axis. *Immunopharmacol. Immunotoxicol.* 44, 429–436. doi:10.1080/08923973.2022.2052896

Zhang, Y., and Zhang, Z. (2020). The History and Advances in Cancer Immunotherapy: Understanding the Characteristics of Tumor-Infiltrating Immune Cells and Their Therapeutic Implications. *Cell Mol. Immunol.* 17 (8), 807–821. doi:10.1038/s41423-020-0488-6

Zhou, F., Wu, Z., Zhao, M., Murtazina, R., Cai, J., Zhang, A., et al. (2019). Rab5-dependent Autophagosome Closure by ESCRT. *J. Cell Biol.* 218 (6), 1908–1927. doi:10.1083/jcb.201811173

Zhu, Q., Li, Y., Guo, Y., Hu, L., Xiao, Z., Liu, X., et al. (2019). Long Non-coding RNA SNHG16 Promotes Proliferation and Inhibits Apoptosis of Diffuse Large B-Cell Lymphoma Cells by Targeting miR-497-5p/PIM1 axis. *J. Cell Mol. Med.* 23 (11), 7395–7405. doi:10.1111/jcmm.14601

Conflict of Interest: The authors declare that the research was conducted in the absence of any commercial or financial relationships that could be construed as a potential conflict of interest.

Publisher's Note: All claims expressed in this article are solely those of the authors and do not necessarily represent those of their affiliated organizations, or those of the publisher, the editors, and the reviewers. Any product that may be evaluated in this article, or claim that may be made by its manufacturer, is not guaranteed or endorsed by the publisher.

Copyright © 2022 Xu, Liang, Liu and Fu. This is an open-access article distributed under the terms of the Creative Commons Attribution License (CC BY). The use, distribution or reproduction in other forums is permitted, provided the original author(s) and the copyright owner(s) are credited and that the original publication in this journal is cited, in accordance with accepted academic practice. No use, distribution or reproduction is permitted which does not comply with these terms.

frontiers | Frontiers in Pharmacology

ORIGINAL RESEARCH
published: 18 July 2022
doi: 10.3389/fphar.2022.953808

A Multicenter Study of 239 Patients Aged Over 70 Years With Diffuse Large B-Cell Lymphoma in China

*Chunli Yang[1], Qiaoer Li[2], Ke Xie[3], Yakun Zhang[4], Dania Xiang[5], Yunwei Han[6] and Liqun Zou[1,2]**

[1]State Key Laboratory of Biotherapy and Cancer Center, West China Hospital, Sichuan University, Chengdu, China, [2]Department of Oncology, West China Hospital, Sichuan University, Chengdu, China, [3]Department of Oncology, Sichuan Academy of Medical Sciences and Sichuan Provincial People's Hospital, Chengdu, China, [4]Department of Oncology, Affiliated Hospital of North Sichuan Medical College, Nanchong, China, [5]Issaquah High School, Issaquah, WA, United States, [6]Department of Oncology, Affiliated Hospital of Southwest Medical University, Luzhou, China

Background: Diffuse large B-cell lymphoma (DLBCL) is the most common aggressive lymphoma subtype worldwide and occurs frequently in the elderly population. However, there are limited data on the clinical profiles of patients with DLBCL over 70 years of age. Our objective was to summarize the clinical characteristics, treatment strategies and survival outcomes of this population in China.

Methods: This multicenter retrospective study was conducted in China from January 2012 to July 2020 to investigate the clinical characteristics and survival outcomes. A total of 239 patients with DLBCL aged over 70 years underwent pretreatment evaluations, treatment, and follow-up at local hospitals. The primary endpoints were the progression-free survival (PFS) and the overall survival (OS) rates at 2 years. Secondary endpoints included median PFS and OS, the estimated PFS and OS rates at 5 years, and adverse events during treatment.

Results: With a median follow-up of 50 months (range, 1–102 months), the 2-year PFS and OS rates were 53.0% and 65.5%, respectively. The median PFS and OS were 42.1 and 96.4 months, respectively; and the estimated 5-year PFS and OS rates were 44.7% and 56.1%, respectively. Hematological toxicities were the most common adverse effects in this study, accounting for 90.4%; and leukopenia was the most frequently observed ≥ grade 3 event. Furthermore, we found that regimens without rituximab and chemotherapy cycles < 6 were significantly associated with worse survival. Additionally, in the 70–80-year group, reduction in chemotherapy dose was associated with a significantly shorter OS, with a 2-year OS rate of 74.4% in the full dose group, compared to 67.1% for the decreased-dose group (p = 0.044).

Conclusion: Our study presents the clinical profiles and survival outcomes of elderly patients with DLBCL in China. Treatment of these patients requires careful evaluation of toxicities and benefits. To this end, a prognosis model, such as comprehensive geriatric assessment, is required in clinical practice to optimally manage elderly patients with DLBCL.

Keywords: diffuse large B-cell lymphoma, elderly, survival, prognosis, treatment

OPEN ACCESS

Edited by:
Hongtao Xiao,
University of Electronic Science and Technology of China, China

Reviewed by:
Peijie Wu,
Chengdu University of Traditional Chinese Medicine, China
Jinming Han,
Capital Medical University, China

****Correspondence:***
Liqun Zou
hxlcyxy@163.com

Specialty section:
This article was submitted to Pharmacology of Anti-Cancer Drugs, a section of the journal Frontiers in Pharmacology

Received: *26 May 2022*
Accepted: *09 June 2022*
Published: *18 July 2022*

Citation:
Yang C, Li Q, Xie K, Zhang Y, Xiang D, Han Y and Zou L (2022) A Multicenter Study of 239 Patients Aged Over 70 Years With Diffuse Large B-Cell Lymphoma in China. Front. Pharmacol. 13:953808. doi: 10.3389/fphar.2022.953808

INTRODUCTION

Diffuse large B-cell lymphoma (DLBCL) is the most common aggressive lymphoma subtype worldwide, accounting for 30–40% of non-Hodgkin lymphoma (Al- Hamadani et al., 2015). From the Surveillance, Epidemiology, and End Results Program (SEER) database, the incidence of DLBCL increases with age; the median diagnosis age is 66 years. Compared to patients with DLBCL aged younger than 60–70 years, older patients had a worse prognosis (Project TIN- HsLPF, 1993; Zhou et al., 2014; Choi et al., 2018). Moreover, most clinical trials have excluded these patients, which has led the need for elucidation of optimal treatment options and survival outcomes in the real world for patients over 70 years of age.

R-CHOP, known as combined regimen rituximab, cyclophosphamide, doxorubicin, vincristine, prednisone, is the standard regimen for initial treatment in DLBCL(Tilly et al., 2015; NCCN, 2022), reaching a cure rate of 60% for the entire cohort (Nowakowski et al., 2016). However, most elderly patients present in poor physical condition and are frequently accompanied by other diseases, which limit the use of a standard dose of the regimen and also present a worse impact on survival. Therefore, dose-reducing regimens or non-anthracycline-containing treatments have been explored in clinical trials, such as R-miniCHOP, R-GemOx (rituximab, gemcitabine, oxaliplatin), and R2 (rituximab, lenalidomide) (Peyrade et al., 2011; Shen et al., 2018; Gini et al., 2019), which achieved a balance of efficacy and tolerance in selected elderly patients with DLBCL. In China, the 5-year OS rate was reported to be 51.9% for DLBCL patients aged over 60 years between 2006 and 2012 in Beijing, including a sample of 349 patients, and 42.8% (145/349) for DLBCL patients aged over 70 years (Liu et al., 2019). To date, there have been a limited number of studies on the clinical profiles of patients with DLBCL over 70 years of age.

In this study, we enrolled 239 patients with DLBCL aged 70 years and over from five hospitals in China to summarize the clinical characteristics, analyze survival outcomes, and examine factors influencing prognosis.

MATERIALS AND METHODS

We retrospectively reviewed the records of all newly diagnosed DLBCL patients who were over 70 years old at five hospitals in China from January 2012 to July 2020, including West China Hospital, Sichuan University; Sichuan Cancer Hospital and Institute; Sichuan Provincial People's Hospital; Affiliated Hospital of North Sichuan Medical College and the Affiliated Hospitals of Southwest Medical University. For all cases, the pathological diagnosis was confirmed by expert hematopathologists in these five hospitals according to the World Health Organization classification of hematopoietic and lymphoid tumors (Swerdlow et al., 2017). Critical exclusion criteria were age less than 70 years and involvement of the central nervous system lymphoma at diagnosis.

All patients underwent pre-treatment evaluations, treatment, and follow-up at the local hospital mentioned above. The evaluations included demographics of the patients, blood tests, serum lactate dehydrogenase (LDH), and detection of bone marrow biopsy. The staging was determined according to the Ann Arbor staging system, and efficacy of the treatment was evaluated using enhanced computed tomography (CT) or positron emission tomography (PET-CT). The Hans algorithm was applied to divide patients into germinal center B cell (GCB) and non-GCB subtypes. Bulky disease was defined as any mass diameter exceeding 7 cm. The investigators also reviewed therapy regimens, cycles, and adverse events. The reduced dose chemotherapy in this study was defined by a 20–50% decrease in the standard dose.

TABLE 1 | Clinical characteristics of 239 patients with DLBCL at diagnosis.

Parameters	All patients n = 239	70–79 years n = 200	≥80 years n = 39
Median age	75.4 (70-91)	74.0 (70-79)	82.6 (80-91)
Sex			
Male	143 (59.8%)	117 (58.5%)	26 (66.7%)
Female	96 (40.2%)	83 (41.5%)	13 (33.3%)
ECOG score			
0–1	193 (80.8%)	163 (81.5%)	30 (76.9%)
≥2	46 (19.2%)	37 (18.5%)	9 (23.1%)
B symptoms			
Yes	174 (72.8%)	144 (72.0%)	30 (76.9%)
No	65 (27.2%)	56 (28.0%)	9 (23.1%)
Subtype			
GCB	52 (21.8%)	44 (22.0%)	8 (20.5%)
non-GCB	148 (61.9%)	122 (61.0%)	26 (66.7%)
Unknown	39 (16.3%)	34 (17.0%)	5 (12.8%)
Ki-67 index			
>90%	7 (2.9%)	6 (3.0%)	1 (2.6%)
≤90%	192 (80.3%)	162 (81.0%)	30 (76.9%)
Unknown	40 (16.7%)	32 (16.0%)	8 (20.5%)
Number of extra-nodal involvement			
0 or 1	174 (72.8%)	150 (75.0%)	24 (61.5%)
≥2	65 (27.2%)	50 (25.0%)	15 (38.5%)
Bone marrow Involvement			
Yes	12 (5.0%)	11 (5.5%)	1 (2.6%)
No	227 (95.0%)	189 (94.5%)	38 (97.4%)
Ann Arbor stage			
I-II	96 (40.2%)	84 (42.0%)	12 (30.8%)
III-IV	143 (59.8%)	116 (58.0%)	27 (69.2%)
Bulky disease			
Yes	38 (15.9%)	33 (16.5%)	5 (12.8%)
No	201 (84.1%)	167 (83.5%)	34 (87.2%)
Serum LDH			
Normal	102 (42.7%)	85 (42.5%)	17 (43.6%)
Elevated	137 (57.3%)	115 (57.5%)	22 (56.4%)
IPI score			
1	52 (21.8%)	44 (22.0%)	8 (20.5%)
2	61 (25.5%)	55 (27.5%)	6 (15.4%)
3	65 (27.2%)	54 (27.0%)	11 (28.2%)
4-5	61 (25.5%)	47 (23.5%)	14 (35.9%)
Comorbidities			
Yes	205 (85.8%)	171 (85.5%)	34 (87.2%)
No	34 (14.2%)	29 (14.5%)	5 (12.8%)

DLBCL, diffuse large B cell lymphoma; ECOG, eastern cooperative oncology group; GCB, germinal center B-cell like; LDH, lactate dehydrogenase; IPI, international prognostic index.

TABLE 2 | Initial treatment regimens of patients with DLBCL (n=239).

Parameters	All patients
Therapy	
Chemotherapy	219 (91.6%)
Radiotherapy/Surgery	9 (3.8%)
Untreated	11 (4.6%)
Chemotherapy dose reduction	
Yes	53 (22.2%)
No	147 (61.5%)
Unknown	39 (16.3%)

DLBCL, diffuse large B cell lymphoma.

TABLE 3 | Chemotherapy regimens adopted in patients with DLBCL (n=219).

Parameters	All patients n = 219	70–79 years n = 184	≥80 years n = 35
Rituximab			
Yes	156 (71.2%)	128 (69.6%)	28 (80.0%)
No	63 (28.8%)	56 (30.4%)	7 (20.0%)
Regimens			
CHOP	185 (84.5%)	162 (88.0%)	23 (65.7%)
CVP	15 (6.8%)	10 (5.4%)	5 (14.3%)
Others	19 (8.7%)	12 (6.5%)	7 (20.0%)
Chemotherapy dose reduction			
Yes	53 (24.2%)	37 (20.1%)	16 (45.7%)
No	147 (67.1%)	135 (73.4%)	12 (34.3%)
Unknown	19 (8.7%)	12 (6.5%)	7 (20.0%)
Therapy cycles			
<6	112 (51.1%)	95 (51.6%)	17 (48.6%)
≥6	107 (48.9%)	89 (48.4%)	18 (51.4%)
Prophylaxis with G-CSF			
Yes	44 (20.1%)	32 (17.4%)	22 (62.9%)
No	161 (73.5%)	139 (75.5%)	12 (34.2%)
Unknown	14 (6.4%)	13 (7.1%)	1 (2.9%)

DLBCL, diffuse large B cell lymphoma; CHOP, cyclophosphamide, doxorubicin, vincristine, prednisone; CVP, cyclophosphamide, vincristine, prednisone; G-CSF, granulocyte colony-stimulating factor.

The primary endpoints of this study were the PFS and the OS rates at 2 years. Secondary endpoints included median PFS and OS, 5-year PFS and OS rates, and adverse events during treatment. The PFS was calculated from diagnosis to disease progression, recurrence, any cause of death, or last follow-up; and OS was from diagnosis to death for any reason or last follow-up.

We summarized PFS and OS using the Kaplan-Meier method and compared differences by the log-rank test. Univariate logistic regression analysis evaluated the variables in predicting survival for patients with DLBCL. Parameters identified as statistically significant risk factors were assessed in multivariate logistic regression analysis. Survival data was analyzed using SPSS version 25.0 (IBM Corp., Armonk, NY), and a two-sided $p < 0.05$ was considered a statistically significant. The study was conducted in accordance with regulatory requirements and was approved by the Ethics Committee of the West China Hospital of Sichuan University.

RESULTS

Patient Characteristics

We identified 239 newly diagnosed patients with DLBCL aged over 70 years from January 2012 to July 2020. The clinical characteristics are listed in **Table 1**. The median age at diagnosis was 75.4 years (range, 70–91 years), and the ratio of males to females was 1.5:1. Stage III/IV patients accounted for 59.8% and 27.2% had extranodal involvement at more than one site. There were 200 patients who with a classified subtypes using the Hans algorithm, 21.8% for the GCB subtype, 61.9% for the non-GCB subtype, and 16.3% of the patients remained with unknown subtype. According to the IPI score (Project TIN- HsLPF, 1993), 25.5% of the cases were evaluated as belonging to the high-risk group. Approximately 85.8% of patients had other diseases.

Treatment and Response

As presented in **Table 2**, 228 patients received initial treatment, including 91.6% receiveing chemotherapy, and 3.8% radiotherapy or surgery, while 4.6% of patients

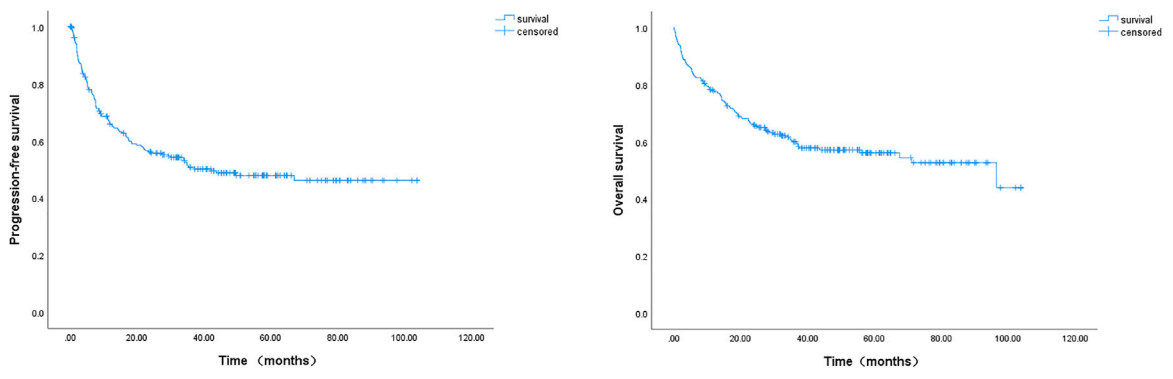

FIGURE 1 | Kaplan-Meier survival curve of progression-free survival (PFS) and overall survival (OS) of 239 DLBCL patients. The 2-year PFS and 2-year OS rates were 53.0% and 65.5%, the estimated 5-year PFS and OS rates were 44.7% and 56.1%, respectively; the median PFS and median OS were 42.1 and 96.4 months, respectively.

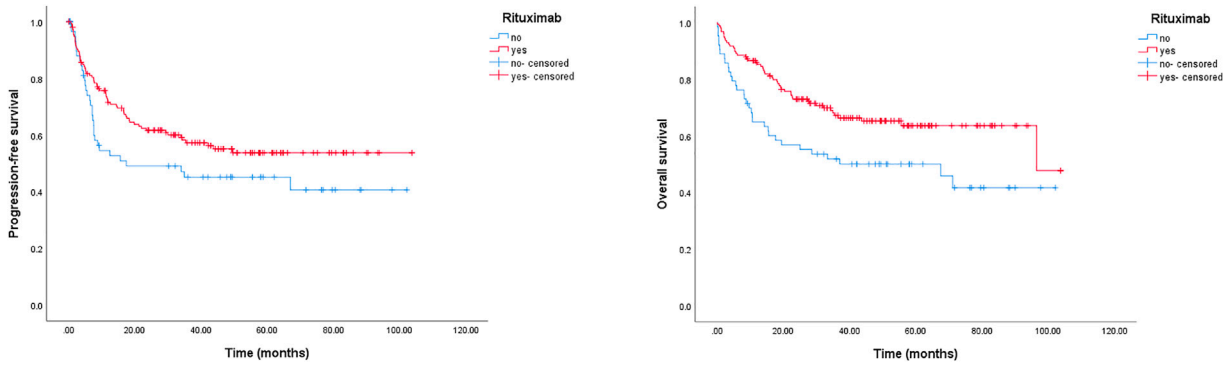

FIGURE 2 | Kaplan-Meier survival curve of PFS and OS for DLBCL patients stratified by rituximab usage. The 2-year PFS rates were 61.7% (rituximab group) and 49.1% (no rituximab group), respectively, p = 0.082; the 2-year OS rates were 72.9% (rituximab group) and 56.8% (no rituximab group), respectively, p = 0.008.

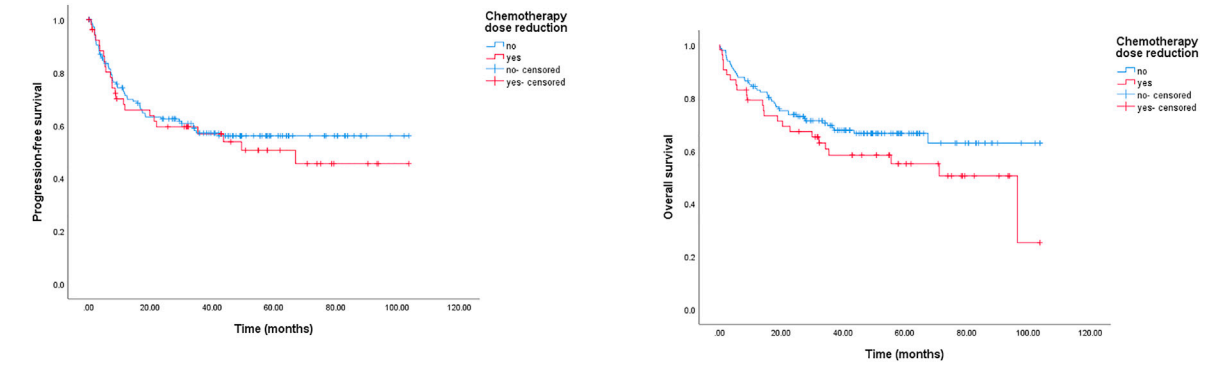

FIGURE 3 | Kaplan-Meier survival curve of PFS and OS for DLBCL patients stratified by reduction in chemotherapy dose. The 2-year PFS rates were 62.4% (chemotherapy dose reduction group) and 59.4% (standard dose group), respectively, p = 0.567; the 2-year OS rates were 67.3% (chemotherapy dose reduction group) and 73.7% (standard dose group), respectively, p = 0.139.

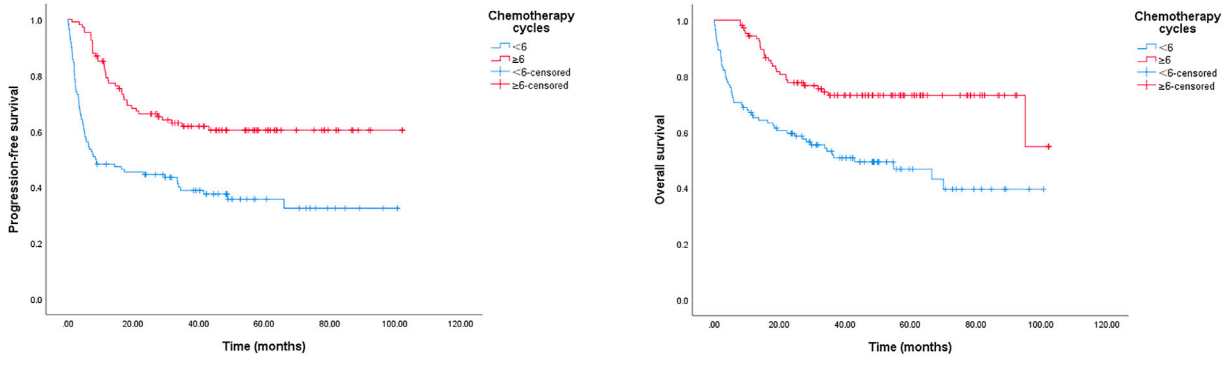

FIGURE 4 | Kaplan-Meier survival curve of PFS and OS for DLBCL patients stratified by chemotherapy cycles. The 2-year PFS rates in group of < 6 chemotherapy cycles and in group of ≥ 6 cycles were 44.5%, 66.2%, p = 0.000; the 2-year OS rates in group of < 6 chemotherapy cycles and in group of ≥ 6 cycles were 59.5%, 77.6%, p = 0.000.

received no therapy. In total, there were 219 patients received chemotherapy alone or with rituximab (**Table 3**); 1,029 total treatment cycles were administered and the median number of cycles for each patient was 4.7 (range, 1-6 cycles). The most common chemotherapy regimen applied was CHOP (cyclophosphamide, doxorubicin, vincristine, prednisone),

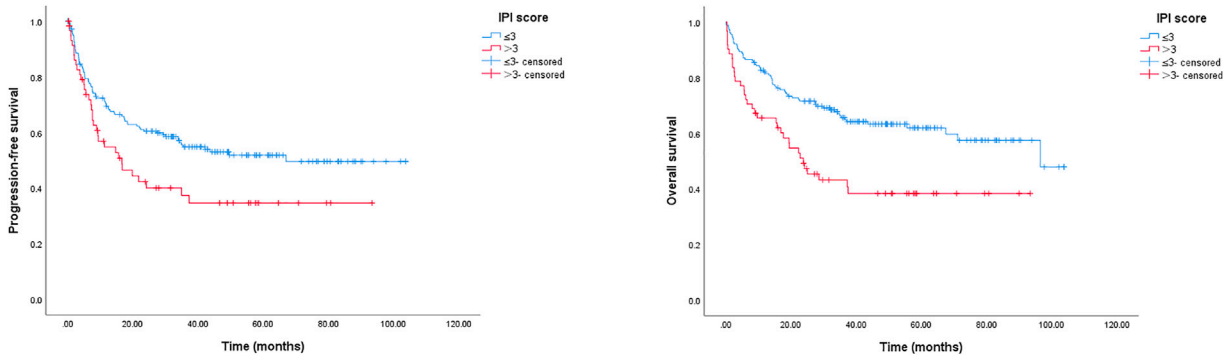

FIGURE 5 | Kaplan-Meier survival curve of PFS and OS for elderly patients with DLBCL stratified by IPI score. The 2-year PFS rates were 60.5% (IPI score ≤ 3) and 42.3% (IPI score > 3), respectively, $p = 0.021$; the 2-year OS rates were 71.5% (IPI score ≤ 3) and 49.2% (IPI score > 3), respectively, $p = 0.001$.

TABLE 4 | Multivariate analysis of PFS in patients with DLBCL (n=239).

Parameters	HR	95% CI	p value
Stage III/IV	1.640	1.031–2.610	**0.037**
ECOG score ≥2	1.261	0.760–2.092	0.369
Serum LDH >normal	1.076	0.708–1.634	0.733
Extranodal involvement > 1 site	0.980	0.616–1.557	0.931
B symptoms	1.155	0.754–1.770	0.507
Bone marrow involvement	1.137	0.466–2.774	0.777
Rituximab	0.622	0.410–0.944	**0.026**

DLBCL, diffuse large B cell lymphoma; PFS, progression-free survival;. ECO,: eastern cooperative oncology group; GCB, germinal center B-cell like; LDH, lactate dehydrogenase; HR, hazard ratio; CI, confidence intervals.

TABLE 5 | Multivariate analysis of OS in patients with DLBCL (n=239).

Parameters	HR	95% CI	*p* value
Stage III/IV	1.146	0.644–2.041	0.643
ECOG score ≥2	1.129	0.583–2.188	0.719
Serum LDH >normal	0.939	0.556–1.585	0.813
Extralnodal involvement > 1 site	1.266	0.716–2.237	0.418
B symptoms	1.440	0.842–2.463	0.183
Bone marrow involvement	1.275	0.363–4.473	0.704
Dose reduction	1.825	1.056–3.154	**0.031**
Rituximab	0.455	0.264–0.785	**0.005**

DLBCL, diffuse large B cell lymphoma; OS, overall survival; ECOG, eastern cooperative oncology group; GCB, germinal center B-cell like; LDH, lactate dehydrogenase; HR, hazard ratio; CI, confidence intervals.

accounting for 84.5%, and other regimens including CVP (cyclophosphamide, vincristine, prednisone), BR (bendamustine, rituximab), oral etoposide or cyclophosphamide. Rituximab was not administered in 28.8% of the patients. A reduction in chemotherapy dose occurred in more patients over 80 years than those aged 70–79 years (45.1% vs. 20.1%, $p < 0.001$).

Survival Outcomes

With a median follow-up of 50 months (range, 1–102 months), the median PFS and OS were 42.1 and 96.4 months, respectively

TABLE 6 | Summary of treatment-related adverse events (n=187).

Parameters	All patients
Anemia	146 (78.1%)
Leukopenia	149 (79.7%)
Neutropenia	128 (68.4%)
Febrile neutropenia	26 (13.9%)
Thrombocytopenia	59 (31.6%)
Thrombus	9 (4.8%)
Fatigue	111 (59.4%)
Nausea/vomiting	148 (79.1%)
Hypoalbumin	128 (68.4%)
Increased aspartate aminotransferase	59 (31.0%)
Elevated creatinine	13 (5.9%)
Neuro-toxicities	6 (3.2%)
Cardio-toxicities	11 (5.9%)
Death during treatment	28 (15.0%)

(**Figure 1**). The 2-year PFS and OS rates of the entire cohort were 53.0% (95% CI: 46.5–59.5%) and 65.5% (95% CI: 59.4–71.2%), respectively (**Figure 1**). The estimated 5-year PFS and OS rates were 44.7% (95% CI: 38.0–51.4%) and 56.1% (95% CI: 49.4–62.8%), respectively (**Figure 1**). Between patients younger and older than 80 years, the 2-year PFS and OS rates did not show any significant differences (data not shown): 54.5% (2-year PFS rate, 95% CI: 47.4–61.6%) and 68.0% (2-year OS rate, 95% CI: 61.5–74.5%) in the younger group; and 45.3% (2-year PFS rate, 95% CI: 29.4–61.2%) and 52.9% (2-year OS rate, 95% CI: 37.0–68.8%) in the older group, respectively.

In our study, the impact of rituximab on PFS and OS was also evaluated. We found that rituximab-included regimens could markedly improve OS for the entire cohort. The 2-year OS rates were 72.9% (95% CI: 65.9–80.1%) in the rituximab group and 56.8% (95% CI: 44.5–69.2%) in the non-rituximab group, and the 5-year OS rates were 63.6% (rituximab group, 95% CI: 55.2–72.0%) and 50.1% (no-rituximab group, 95% CI: 37.6–62.6%), respectively ($p = 0.008$) (**Figure 2**). The 2-year PFS rates were 61.7% (95% CI: 51.7–67.3%) in the rituximab-

containing treatment group, and 49.1% (95% CI: 31.9–56.5%) for chemotherapy without rituximab. The estimated 5-year PFS rates were 50.5% (rituximab group, 95% CI: 42.1–58.9%) and 40.7% (no rituximab group, 95% CI: 28.4–53.0%), respectively (p = 0.082) (**Figure 2**).

A reduction in chemotherapy dose was frequently delivered in clinical practice for elderly patients with DLBCL. In this study, we detected its role in survival outcomes. As shown in **Figure 3**, there was no significant survival difference between the standard dose group and the reduced chemotherapy dose group. However, in the group younger than 80 years, the reduced dose was associated with a significantly shorter OS, and the 2-year OS rate was 74.4% (95% CI: 67.0–81.8%) in the full dose group compared to 67.1% (95% CI: 51.8–82.4%) in the dose reduction group, p = 0.044 (data not shown). Meanwhile, we did not observe a marked deterioration in PFS or OS in the group aged older than 80 years with dose reduction (data not shown). Furthermore, treatment cycles was associated with survival outcomes in this study. As shown in **Figure 4**, patients treated with six or more cycles obtained superior OS and PFS to those treated with less than six cycles. The 2-year PFS rates were 66.2% and 44.5%, respectively (p = 0.000); and the 2-year OS rates were 77.6% and 59.5%, respectively (p = 0.000).

The IPI score is frequently applied to predict the prognosis of patients with DLBCL. Here, we used the IPI score to divide patients into IPI ≤ 3 or IPI > 3 groups; as presented in **Figure 5**, patients with IPI ≤ 3 had longer PFS and OS than those with IPI > 3, the 2-year PFS rates were 60.5% (IPI > 3 patients) and 42.3% (IPI ≤ 3 patients), respectively (p = 0.021); the 2-year OS rates were 71.5% (IPI > 3 patients) and 49.2% (IPI ≤ 3 patients), respectively (p = 0.001).

In addition, we performed univariate and multivariate analyses in this study. From the univariate analysis results (Supplementary Table S1), an ECOG score ≥ 2 (p = 0.015), Ann Arbor stage III/IV (p = 0.012), IPI score > 3 (p = 0.005), and treatment without rituximab (p = 0.002) were significantly associated with inferior PFS. And extranodal disease involvement more than 1 site (p = 0.039), ECOG score ≥ 2 (p = 0.002), IPI score > 3 (p = 0.001) and treatment without rituximab (p = 0.000) were associated with inferior OS. Regarding the impact of GCB (germinal center B-cell like) and non-GCB subtypes on survival, we found no statistical significance for PFS and OS in this cohort. In multivariate analyses, Ann Arbor stage III/IV was significantly related to worse PFS, HR 1.640 (95% CI: 1.031–2.610, p = 0.037); chemotherapy dose reduction was associated with poorer OS, HR 1.825 (95% CI: 1.056–3.154, p = 0.031); and use of rituximab was related to OS benefit, HR 0.455 (95% CI: 0.264–0.785, p = 0.005) (**Table 4, 5**).

Toxicity

A total of 187 patients were available for the analysis of treatment-related toxicity. The most common adverse effects in this study were hematological toxicities, which accounted for 90.4%, including anemia (78.1%), leukopenia (79.7%), neutropenia (68.4%), and thrombocytopenia (31.6%) (**Table 6**). Additionally, nausea, vomiting, and hypoalbumin were observed in most patients. Leukopenia was the most common ≥ grade 3 event; neutropenia and febrile neutropenia occurred also in 51.9% of the patients (**Table 6**).

DISCUSSION

To our knowledge, this is the largest case series to date reporting the clinical features and survival outcomes in patients with DLBCL aged ≥70 years in China. In this study, the 2-year PFS rate was 53.0% and 2-year OS rate was 65.5% for this population. The most common adverse effects were hematological toxicities, accounting for 90.4%, and leukopenia was the most frequently observed ≥ grade 3 event. Compared to a previous study reported in China, our data presented a significantly improved 5-year OS rate, which may attributed to the widespread use of rituximab, adoption of supportive therapy after chemotherapy, such as application of granulocyte colony-stimulating factor (G-CSF), and patient education, all together contributed to improve the survival of patients with DLBCL.

Rituximab has been reported to improve the PFS and OS in 60–80-years-old patients with DLBCL(Coiffier et al., 2002; Coiffier et al., 2010). In this cohort, we found similar results: rituximab increased survival outcomes compared to CHOP alone. Currently, rituximab is administered at 375 mg/m^2 with an interval every 3 weeks for 6–8 cycles in the standard regimen. Furthermore, some studies have investigated whether an increase in rituximab dose could improve treatment efficacy in elderly patients, showing that 500 mg/m^2 of rituximab improved PFS and OS for elderly male cases compared to standard dose (Pfreundschuh et al., 2014; Pfreundschuh et al., 2017; He et al., 2021). No patients received this maximum dose of rituximab in this study. In the future, a potential research direction involves exploring the application of rituximab intensification regimens in specific population. Furthermore, in clinical practice, eight cycles of rituximab plus six cycles of CHOP21 or six cycles of R-miniCHOP are recommended to treat DLBCL in elderly patients according to some critical study results (Coiffier et al., 2010; Pfreundschuh et al., 2008; Delarue et al., 2013; Sehn et al., 20182018; Wцsterlid et al., 2018). From our data, in contrast to ≥ 6-cycle treatment regimens, patients receving less than 6 cycles presented lower PFS and OS, suggesting that 6 or 8 cycles of treatment are necessary in clinical practice for this population.

The treatment strategy for elderly patients with DLBCL has not been well established. In comparison with R-CHOP14 applied to DLBCL patients aged 60–80 years, R-CHOP21 could achieve similar efficacy and decreased the frequency and severity of hematological adverse effects and the number of red blood cell transfusions, making R-CHOP21 a frequently administered regimen (Cunningham et al., 2013; Delarue et al., 2013). In our study, 84.5% of patients treated with R-CHOP21, 74.4% of whom achieved full dose in patients aged 70–79 years and 67.1% in those older than 80 years. R-miniCHOP is recommended in cases ≥ 80 years (Peyrade et al., 2011; Eyre et al., 2019; NCCN, 2022). Peyrade et al. reported that European patients aged 80 years treated with R-miniCHOP obtained a 2-year OS rate of 59% and a 2-year PFS rate of 47% (Peyrade et al., 2011). From our data, we observed similar results in the Chinese population with a 2-year OS rate of 52.9% and a 2-year PFS rate of 45.3% in patients treated with full-dose or reduced-dose therapy. Furthermore, in our subgroup analysis, we found that a reduced chemotherapy dose was not correlated with an improved 2-year OS rate when compared to the standard dose in the population older than

80 years (data not shown), which was comparable to the results of previously studies (Peyrade et al., 2011; Eyre et al., 2019). However, in patients aged 70–79 years, chemotherapy dose reduction (≥20%) could have a worse impact on OS than full-dose regimens. According to a previous study (Meguro et al., 2012), which reported that 70% of the standard dose would influence OS and PFS in patients over 70 years of age. Taken together, based on our data, the standard dose should be administered in 70–79-year-old patients with DLBCL in China if possible, and R-miniCHOP is reasonable for patients over 80 years of age.

DLBCL is divided into GCB, ABC and unclassified subtypes based on a gene expression profiling (GEP) (Scott et al., 2014). Furthermore, the Hans algorithm had a prognostic value based on the determination of the cell of origin (COO) (Hans et al., 2004). In our study, we applied the Hans algorithm to divide patients into GCB and non-GCB subtypes, with 21.8% of the GCB subtype and 61.9% of the non-GCB subtype. Lenz et al. reported that the GCB subtype had superior PFS and OS rates to the ABC subtype with R-CHOP(Lenz et al., 2008). Our cohort found that the GCB subtype had a similar survival outcome compared to the non-GCB subtype (data not shown). Moreover, in the univariate analyses, patients with GCB or non-GCB had similar OS and PFS.

The IPI score is a widely used prognostic model in DLBCL. Recently, a study reported that the National Comprehensive Cancer Network (NCCN)-IPI had the greatest absolute difference in OS estimates between the highest- and lowest-risk groups and the best-discriminated OS compared to the IPI score and the age-adjusted IPI (aaIPI) for the entire cohort of DLBCL(Ruppert et al., 2020). In our study, NCCN-IPI and aaIPI were not suitable to evaluate prognosis, as the included patients were all aged ≥ 70 years. According to the IPI score, there are significant differences in PFS and OS between the IPI ≤ 3 and IPI > 3 groups, suggesting that the IPI score could predict the prognosis in elderly patients. Recently, a study from Italy reported that combining the comprehensive geriatric assessment (CGA) with the IPI score could identify three risk groups with notable differences in terms of OS (Spina et al., 2019; Merli et al., 2021), which would help clinicians to evaluate the prognosis of patients with greater precisely.

This study had several limitations. First, our study was retrospective, and selection and information bias could not have been avoided. Second, patients in our study did not undergo the CGA, which could have contributed to better predict OS and assist clinicians in determining whether or not to treat patients with full-dose chemotherapy (Hamaker et al., 2014; Lin et al., 2017).

CONCLUSION

Our study presents the clinical profiles and survival outcomes of elderly patients with DLBCL in China. Treatment of these patients requires careful evaluation of toxicities and benefits. To this end, a prognosis model, such as comprehensive geriatric assessment, is required in clinical practice to optimally manage elderly patients with DLBCL.

DATA AVAILABILITY STATEMENT

The raw data supporting the conclusions of this article will be made available by the authors, without undue reservation.

ETHICS STATEMENT

The studies involving human participants were reviewed and approved by The Ethics Committee of West China Hospital of Sichuan University. The patients/participants provided their written informed consent to participate in this study. Written informed consent was obtained from the individual(s) for the publication of any potentially identifiable images or data included in this article.

AUTHOR CONTRIBUTIONS

CY, QL, and LZ: conception and design. KX, YZ, and YH: administrative support. CY, QL, and DX: collection and analysis of data. All authors: manuscript writing, final approval of the manuscript, and accountability for work.

ACKNOWLEDGMENTS

The authors thank LL to participate in patient recruitment and help gather the information of patients.

SUPPLEMENTARY MATERIAL

The Supplementary Material for this article can be found online at: https://www.frontiersin.org/articles/10.3389/fphar.2022.953808/full#supplementary-material

REFERENCES

Al-Hamadani, M., Habermann, T. M., Cerhan, J. R., Macon, W. R., Maurer, M. J., and Go, R. S. (2015). Non-Hodgkin Lymphoma Subtype Distribution, Geodemographic Patterns, and Survival in the US: A Longitudinal Analysis of the National Cancer Data Base from 1998 to 2011. *Am. J. Hematol.* 90, 790–795. doi:10.1002/ajh.24086

Choi, J. H., Kim, T. M., Kim, H. J., Koh, S. A., Mun, Y. C., Kang, H. J., et al. (2018). Multicenter Retrospective Analysis of Clinical Characteristics, Treatment Patterns, and Outcomes in Very Elderly Patients with Diffuse Large B-Cell Lymphoma: The Korean Cancer Study Group LY16-01. *Cancer Res. Treat.* 50, 590–598. doi:10.4143/crt.2017.172

Coiffier, B., Lepage, E., Briere, J., Herbrecht, R., Tilly, H., Bouabdallah, R., et al. (2002). CHOP Chemotherapy Plus Rituximab Compared with CHOP Alone in Elderly Patients with Diffuse Large-B-Cell Lymphoma. *N. Engl. J. Med.* 346 (4), 235–242. doi:10.1056/NEJMoa011795

Coiffier, B., Thieblemont, C., Van Den Neste, E., Lepeu, G., Plantier, I., Castaigne, S., et al. (2010). Long-Term Outcome of Patients in the LNH-98.5 Trial, the First Randomized Study Comparing Rituximab-CHOP to Standard CHOP Chemotherapy in DLBCL Patients: A study by the Groupe d'Etudes des

Lymphomes de l'Adulte. *Blood* 116, 2040–2045. doi:10.1182/blood-2010-03-276246

Cunningham, D., Hawkes, E. A., Jack, A., Qian, W., Smith, P., Mouncey, P., et al. (2013). Rituximab Plus Cyclophosphamide, Doxorubicin, Vincristine, and Prednisolone in Patients with Newly Diagnosed Diffuse Large B-Cell Non-Hodgkin Lymphoma: A Phase 3 Comparison of Dose Intensification with 14-day versus 21-day Cycles. *Lancet* 381, 1817–1826. doi:10.1016/S0140-6736(13)60313-X

Delarue, R., Tilly, H., Mounier, N., Petrella, T., Salles, G., Thieblemont, C., et al. (2013). Dose-Dense Rituximab-CHOP Compared with Standard Rituximab-CHOP in Elderly Patients with Diffuse Large B-Cell Lymphoma (The LNH03-6B Study): A Randomised Phase 3 Trial. *Lancet Oncol.* 14, 525–533. doi:10.1016/S1470-2045(13)70122-0

Eyre, T. A., Martinez-Calle, N., Hildyard, C., Eyre, D. W., Plaschkes, H., Griffith, J., et al. (2019). Impact of Intended and Relative Dose Intensity of R-CHOP in a Large, Consecutive Cohort of Elderly Diffuse Large B-Cell Lymphoma Patients Treated with Curative Intent: No Difference in Cumulative Incidence of Relapse Comparing Patients by Age. *J. Intern Med.* 285, 681–692. doi:10.1111/joim.12889

Gini, G., Tani, M., Tucci, A., Bassan, R., Ballerini, F., Sampaolo, M., et al. (2019). Lenalidomide and Rituximab (ReRi) as Front Line Chemo-Free Therapy of Elderly Frail Patients with Diffuse Large B-Cells Lymphoma. A Phase II Study of the Fondazione Italiana Linfomi (FIL). *Blood* 134 (Suppl. ment_1), 2880. doi:10.1182/blood-2019-126568

Hamaker, M. E., Prins, M. C., and Stauder, R. (2014). The Relevance of a Geriatric Assessment for Elderly Patients with a Haematological Malignancy-Aa Systematic Review. *Leuk. Res.* 38, 275–283. doi:10.1016/j.leukres.2013.12.018

Hans, C. P., Weisenburger, D. D., Greiner, T. C., Gascoyne, R. D., Delabie, J., Ott, G., et al. (2004). Confirmation of the Molecular Classification of Diffuse Large B-Cell Lymphoma by Immunohistochemistry Using a Tissue Microarray. *Blood* 103, 275–282. doi:10.1182/blood-2003-05-1545

He, H. X., Gao, Y., Bai, B., Wang, X-X., Li, J-B., Huang, C., et al. (2021). The Beneficial Effect of Escalated-R-CHOP-21 for the Treatment of Diffuse Large B-Cell Lymphoma in Elderly Male Patients: A Propensity-Matched Cohort Study. *Cancer Med.* 10 (21), 7650–7664. doi:10.1002/cam4.4296

Lenz, G., Wright, G., Dave, S. S., Xiao, W., Powell, J., Zhao, H., et al. (2008). Stromal Gene Signatures in Large-B-Cell Lymphomas. *N. Engl. J. Med.* 359, 2313–2323. doi:10.1056/NEJMoa0802885

Lin, R. J., Behera, M., Diefenbach, C. S., and Flowers, C. R. (2017). Role of Anthracycline and Comprehensive Geriatric Assessment for Elderly Patients with Diffuse Large B-Cell Lymphoma. *Blood* 130, 2180–2185. doi:10.1182/blood-2017-05-736975

Liu, P., Han, Y., Jiang, S. Y., He, X. H., Qin, Y., Gui, L., et al. (2019). A Retrospective Analysis of Real-World Outcomes of Elderly Chinese Patients with Diffuse Large B-Cell Lymphoma. *Chin. Med. J. Engl.* 132, 1807–1814. doi:10.1097/CM9.0000000000000354

Lugtenburg, P. J., de Nully Brown, P., van der Holt, B., D'Amore, F. A., Koene, H. R., de Jongh, E., et al. (2020). Rituximab-CHOP with Early Rituximab Intensification for Diffuse Large B-Cell Lymphoma: A Randomized Phase III Trial of the HOVON and the Nordic Lymphoma Group (HOVON-84). *J. Clin. Oncol.* 38, 3377–3387. doi:10.1200/JCO.19.03418

Meguro, A., Ozaki, K., Sato, K., Oh, I., Fujiwara, S., Hosonuma, R., et al. (2012). Rituximab Plus 70% Cyclophosphamide, Doxorubicin, Vincristine and Prednisone for Japanese Patients with Diffuse Large B-Cell Lymphoma Aged 70 Years and Older. *Leuk. Lymphoma* 53, 43–49. doi:10.3109/10428194.2011.600486

Merli, F., Luminari, S., Tucci, A., Arcari, A., Rigacci, L., Hawkes, E., et al. (2021). Simplified Geriatric Assessment in Older Patients with Diffuse Large B-Cell Lymphoma: The Prospective Elderly Project of the Fondazione Italiana Linfomi. *Jco* 39, 1214–1222. doi:10.1200/jco.20.02465

Data from NCCN (2022). National Comprehensive Cancer Network. NCCN Guidelines Version 4. https://www.nccn.org/guidelines/guidelines-detail?category=1&id=1480.

Nowakowski, G. S., Chiappella, A., Witzig, T. E., Spina, M., Gascoyne, R. D., Zhang, L., et al. (2016). ROBUST: Lenalidomide-R-CHOP versus Placebo-R-CHOP in Previously Untreated ABC-Type Diffuse Large B-Cell Lymphoma. *Future Oncol.* 12, 1553–1563. doi:10.2217/fon-2016-0130

Peyrade, F., Jardin, F., Thieblemont, C., Thyss, A., Emile, J. F., Castaigne, S., et al. (2011). Attenuated Immunochemotherapy Regimen (R-miniCHOP) in Elderly Patients Older Than 80 Years with Diffuse Large B-Cell Lymphoma: A Multicentre, Single-Arm, Phase 2 Trial. *Lancet Oncol.* 12, 460–468. doi:10.1016/S1470-2045(11)70069-9

Pfreundschuh, M., Murawski, N., Zeynalova, S., Ziepert, M., Loeffler, M., Hänel, M., et al. (2017). Optimization of Rituximab for the Treatment of DLBCL: Increasing the Dose for Elderly Male Patients. *Br. J. Haematol.* 179, 410–420. doi:10.1111/bjh.14860

Pfreundschuh, M., Poeschel, V., Zeynalova, S., Hänel, M., Held, G., Schmitz, N., et al. (2014). Optimization of Rituximab for the Treatment of Diffuse Large B-Cell Lymphoma (II): Extended Rituximab Exposure Time in the SMARTE-R-CHOP-14 Trial of the German High-Grade Non-Hodgkin Lymphoma Study Group. *J. Clin. Oncol.* 32, 4127–4133. doi:10.1200/JCO.2013.54.6861

Pfreundschuh, M., Schubert, J., Ziepert, M., Schmits, R., Mohren, M., Lengfelder, E., et al. (2008). Six versus Eight Cycles of Bi-Weekly CHOP-14 With or Without Rituximab in Elderly Patients with Aggressive CD20+ B-Cell Lymphomas: A Randomised Controlled Trial (RICOVER-60). *Lancet Oncol.* 9, 105–116. doi:10.1016/S1470-2045(08)70002-0

Project TIN-HsLPF (1993). A Predictive Model for Aggressive Non-Hodgkin's Lymphoma. *N. Engl. J. Med.* 329, 987–994. doi:10.1056/NEJM199309303291402

Ruppert, A. S., Dixon, J. G., Salles, G., Wall, A., Cunningham, D., Poeschel, V., et al. (2020). International Prognostic Indices in Diffuse Large B-Cell Lymphoma: A Comparison of IPI, R-IPI, and NCCN-IPI. *Blood* 135 (23), 2041–2048. doi:10.1182/blood.2019002729

Scott, D. W., Wright, G. W., Williams, P. M., Lih, C. J., Walsh, W., Jaffe, E. S., et al. (2014). Determining Cell-Of-Origin Subtypes of Diffuse Large B-Cell Lymphoma Using Gene Expression in Formalin-Fixed Paraffin-Embedded Tissue. *Blood* 123, 1214–1217. doi:10.1182/blood-2013-11-536433

Sehn, L. H., Congiu, A. G., Culligan, D. J., Gironella, M., Yoon, D. H., Ogura, M., et al. (20182018). No Added Benefit of Eight versus Six Cycles of CHOP When Combined with Rituximab in Previously Untreated Diffuse Large B-Cell Lymphoma Patients: Results from the International Phase III GOYA Study. *Blood* 132 (Suppl. 1), 783. doi:10.1182/blood-2018-99-116845

Shen, Q. D., Zhu, H. Y., Wang, L., Fan, L., Liang, J. H., Cao, L., et al. (2018). Gemcitabine-Oxaliplatin Plus Rituximab (R-GemOx) as First-Line Treatment in Elderly Patients with Diffuse Large B-Cell Lymphoma: A Single-Arm, Open-Label, Phase 2 Trial. *Lancet Haematol.* 5, e261–e269. doi:10.1016/S2352-3026(18)30054-1

Spina, M., Merli, F., Puccini, B., Cavallo, F., Cabras, M. G., Fabbri, A., et al. (2019). Definition and Validation of the New Elderly Prognostic Index (EPI) for Elderly Patients with Diffuse Large B-Cell Lymphoma Integrating Geriatric and Clinical Assessment: Results of the Prospective "Elderly Project" on 1353 Patients by the Fondazione Italiana Linfomi. *Blood* 134 (Suppl. 1), 398. doi:10.1182/blood-2019-123027

Swerdlow, S. H., Campo, E., Harris, N. L., Jaffe, E. S., Pileri, S. A., Stein, H., et al. (2017). *WHO Classification of Tumours of Haematopoietic and Lymphoid Tissues*. France: International Agency for Research on Cancer (IARC) 69372 Lyon Cedex 08.

Tilly, H., Gomes da Silva, M., Vitolo, U., Jack, A., Meignan, M., Lopez-Guillermo, A., et al. (2015). Diffuse Large B-Cell Lymphoma (DLBCL): ESMO Clinical Practice Guidelines for Diagnosis, Treatment and Follow-Up. *Ann. Oncol.* 26 (Suppl. 5), v116–25. doi:10.1093/annonc/mdv304

Wцπsterlid, T., Biccler, J. L., Brown, P. N., Bogsted, M., Enblad, G., Jorgenson, J. M., et al. (2018). Six Cycles of R-CHOP-21 Are Not Inferior to Eight Cycles for Treatment of Diffuse Large B-Cell Lymphoma: a Nordic Lymphoma Group Population-Based Study. *Ann. Oncol. official J. Eur. Soc. Med. Oncol.* 29, 1882–1883. doi:10.1093/annonc/mdy184

Zhou, Z., Sehn, L. H., Rademaker, A. W., Gordon, L. I., Lacasce, A. S., Crosby-Thompson, A., et al. (2014). An Enhanced International Prognostic Index

(NCCN-IPI) for Patients with Diffuse Large B-Cell Lymphoma Treated in the Rituximab Era. *Blood* 123, 837–842. doi:10.1182/blood-2013-09-524108

Conflict of Interest: The authors declare that the research was conducted in the absence of any commercial or financial relationships that could be construed as a potential conflict of interest.

Publisher's Note: All claims expressed in this article are solely those of the authors and do not necessarily represent those of their affiliated organizations, or those of the publisher, the editors and the reviewers. Any product that may be evaluated in this article, or claim that may be made by its manufacturer, is not guaranteed or endorsed by the publisher.

Copyright © 2022 Yang, Li, Xie, Zhang, Xiang, Han and Zou. This is an open-access article distributed under the terms of the Creative Commons Attribution License (CC BY). The use, distribution or reproduction in other forums is permitted, provided the original author(s) and the copyright owner(s) are credited and that the original publication in this journal is cited, in accordance with accepted academic practice. No use, distribution or reproduction is permitted which does not comply with these terms.

frontiers | Frontiers in Pharmacology

REVIEW
published: 22 July 2022
doi: 10.3389/fphar.2022.939090

A Novel Anti-Cancer Therapy: CRISPR/Cas9 Gene Editing

Xin-Zhu Chen[1,2†], Rong Guo[3†], Cong Zhao[4†], Jing Xu[5], Hang Song[5], Hua Yu[6], Christian Pilarsky[7], Firzan Nainu[8], Jing-Quan Li[2], Xin-Ke Zhou[1]* and Jian-Ye Zhang[1]**

[1]Guangzhou Municipal and Guangdong Provincial Key Laboratory of Molecular Target & Clinical Pharmacology, The NMPA and State Key Laboratory of Respiratory Disease, School of Pharmaceutical Sciences and the Fifth Affiliated Hospital, Guangzhou Medical University, Guangzhou, China, [2]The First Affiliated Hospital, Hainan Medical University, Haikou, China, [3]State Key Laboratory of Medical Molecular Biology, Department of Molecular Biology and Biochemistry, Institute of Basic Medical Sciences, Peking Union Medical College, Chinese Academy of Medical Sciences, Beijing, China, [4]Department of Cellular and Molecular Biology, Tuberculosis and Thoracic Tumor Research Institute, Beijing Chest Hospital, Beijing, China, [5]Department of Biochemistry and Molecular Biology, School of Integrated Chinese and Western Medicine, Anhui University of Chinese Medicine, Hefei, China, [6]State Key Laboratory of Quality Research in Chinese Medicine, Institute of Chinese Medical Sciences, University of Macau, Macao, China, [7]Department of Surgery, University Hospital of Erlangen, Friedrich-Alexander University of Erlangen-Nuremberg (FAU), Erlangen, Germany, [8]Faculty of Pharmacy, Hasanuddin University, Makassar, Indonesia

OPEN ACCESS

Edited by:
Liang Ouyang,
Sichuan University, China

Reviewed by:
Bing Liu,
Guangdong Pharmaceutical University, China
Xiaokun Wang,
Wayne State University, United States

***Correspondence:**
Jing-Quan Li
lijingquan2008@163.com
Xin-Ke Zhou
zxkstar@126.com
Jian-Ye Zhang
jianyez@163.com

†These authors have contributed equally to this work

Specialty section:
This article was submitted to Pharmacology of Anti-Cancer Drugs, a section of the journal Frontiers in Pharmacology

Received: *08 May 2022*
Accepted: *14 June 2022*
Published: *22 July 2022*

Citation:
Chen X-Z, Guo R, Zhao C, Xu J, Song H, Yu H, Pilarsky C, Nainu F, Li J-Q, Zhou X-K and Zhang J-Y (2022) A Novel Anti-Cancer Therapy: CRISPR/Cas9 Gene Editing. Front. Pharmacol. 13:939090. doi: 10.3389/fphar.2022.939090

Cancer becomes one of the main causes of human deaths in the world due to the high incidence and mortality rate and produces serious economic burdens. With more and more attention is paid on cancer, its therapies are getting more of a concern. Previous research has shown that the occurrence, progression, and treatment prognosis of malignant tumors are closely related to genetic and gene mutation. CRISPR/Cas9 has emerged as a powerful method for making changes to the genome, which has extensively been applied in various cell lines. Establishing the cell and animal models by CRISPR/Cas9 laid the foundation for the clinical trials which possibly treated the tumor. CRISPR-Cas9-mediated genome editing technology brings a great promise for inhibiting migration, invasion, and even treatment of tumor. However, the potential off-target effect limits its clinical application, and the effective ethical review is necessary. The article reviews the molecular mechanisms of CRISPR/Cas9 and discusses the research and the limitation related to cancer clinical trials.

Keywords: CRISPR/Cas9, gene editing technology, anti-cancer therapy, off-target effect, ethics

INTRODUCTION

The clustered regularly interspaced short palindromic repeats (CRISPR)/-CRISPR-associated nuclease (*Cas*) system is an acquired defense system to protect organisms from invading viruses and plasmids and is widespread in various bacteria and archaea (Jinek et al., 2012; Wiedenheft et al., 2012; Hsu et al., 2014). CRISPR loci are separated by a CRISPR array, comprising unique spacers consisted of short variable DNA sequences, which are flanked by diverse *cas* (CRISPR-associated) gene (Makarova et al., 2015; Koonin and Makarova, 2019). Among them, CRISPR is a series of short direct repeats interspaced with short sequences in *E. coli* that was discovered by Japanese researchers in 1987 (Ishino et al., 1987). The *Cas* gene encodes the *Cas* protein components with putative nuclease and helicase domains (Jansen et al., 2002; Haft et al., 2005). The CRISPR-Cas immune response includes three phases: adaptation; pre-CRISPR RNA (pre-crRNA) expression and processing; and interference to protect prokaryotes from succumbing to infection (Wiedenheft et al., 2012; Hille et al., 2018; and Koonin and Makarova, 2019).

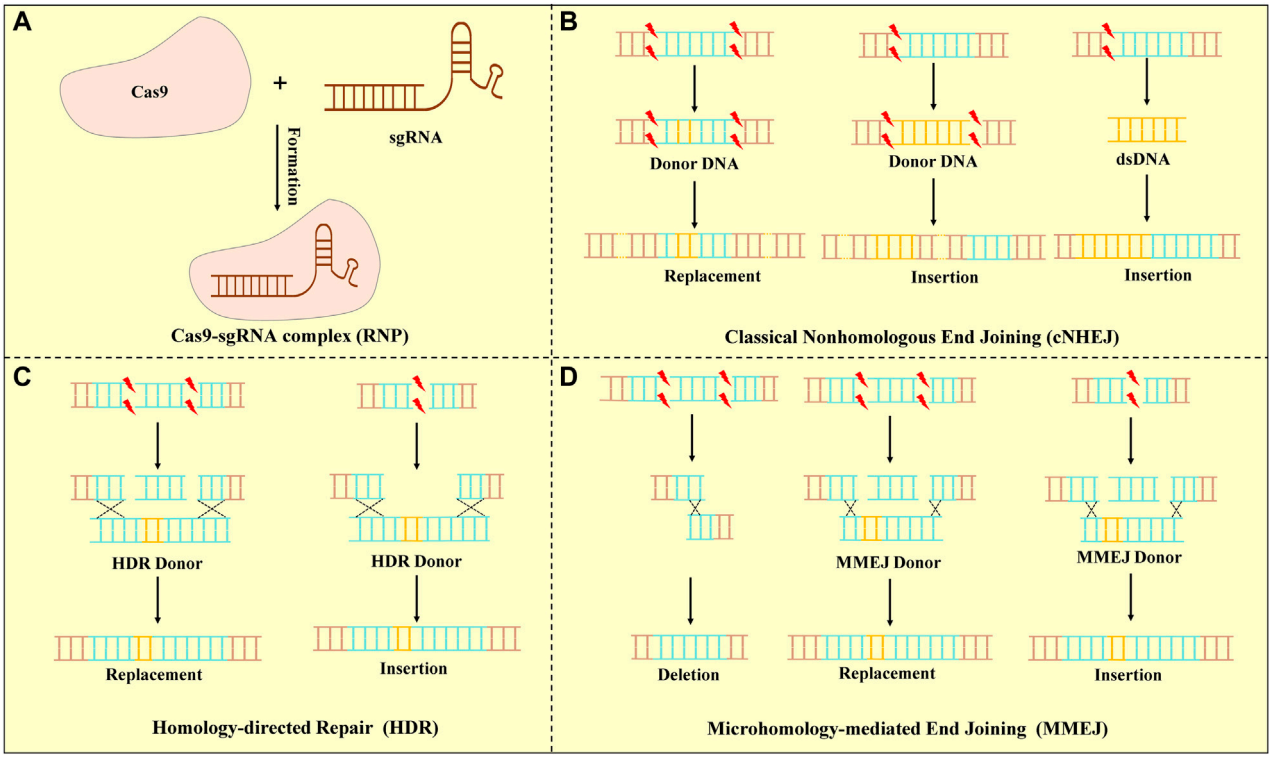

FIGURE 1 | CRISPR/Cas9 system and DSB repair. **(A)** Mechanism of the CRISPR-Cas9 system. A short guide sgRNA associates with the Cas9 endonuclease to form the Cas9-sgRNA complex. Cas9 is a targeted DNA by PAM under the sgRNA. **(B)** cNHEJ : cNHEJ was the predominant pathway for repairing DSBs and was used for re-ligating broken DNA ends. Deletions or insertion mutations lead to gene frame shift mutations or premature generation of stop codes. **(C)** HDR: HDR was used a homologous DNA template to guide DSB repair. The DNA donor templates of HDR were used to insert or replace specific sequences into the genome. **(D)** MMEJ: MMEJ-mediated repair was capable of generating precise deletions between two short micro-homologous sequences (5–25 base pairs) at target loci.

The CRISPR/Cas systems are divided into two classes, which are further classified to six types and 33 subtypes that each possess signature *cas* gene (Makarova et al., 2020). The type II CRISPR/Cas9 system is mainly used in gene editing because of its simplicity, high efficacy, and ease to use (Liu et al., 2017). Cas9 is a large multifunctional protein that has two putative nuclease domains: HNH and RuvC to cleave DNA strands (Nierzwicki et al., 2021; Shams et al., 2021). The CRISPR/Cas9 system contains three core elements: the Cas9 protein, the CRISPR RNA (crRNA), and a trans-activating CRISPR RNA (tracrRNA), of which tracrRNA bears complementarity to the repeat regions of crRNA (Deltcheva et al., 2011). The Cas9 protein associates with a mature dual RNA (tracrRNA: crRNA), as a single-guide RNA (sgRNA) to target DNA cleavage. To interfere with the expression of target genes, Cas9 identifies the viral DNA sequence through a short protospacer adjacent motif (PAM) recognition that was able to select the target DNA among the genome (Sternberg et al., 2014). After the Cas9 protein binds to the target sequence, it results in double-stranded DNA breakings (DSBs) in specific regions of the genome (Frock et al., 2015). DSBs are repaired by different DNA damage repair mechanisms in cells: homology-directed repair (HDR), classical non-homologous end joining (cNHEJ), and microhomology-mediated end joining (MMEJ) (Rassool, 2003; Brinkman et al., 2018; Schep et al., 2021). Various DNA repair pathways might be used to repair each end at a DSB leading to the potential for asymmetric repair (Nambiar et al., 2022) (**Figure 1**). In clinical practice, these repair methods are used to achieve the purpose of relieving or even curing diseases.

DSBs are generated and repaired at specific positions in CRISPR/Cas9-mediated targeted gene segments, leading to targeted mutations because the repair process is error-prone. Though editing the targeted mutation, CRISPR/Cas9 gene editing has shown tremendous potential in oncology and has attained an encouraging achievement.

THE RESEARCH OF CRISPR/CAS9 FOR ANTI-CANCER THERAPY

Cancer is the first or second leading cause of mortality and ranks as an important barrier to increasing life expectancy of the world (Bray et al., 2021; Sung et al., 2021). Tumor formation involves a variety of gene mutations and epigenetic mutations (Podlaha et al., 2012; Huang et al., 2020). Cancer genome sequencing has confirmed that there was a multitude of genes and epigenetic mutations in human tumors (Gerstung et al., 2020). At present, there are various methods to treat tumor, such as conventional

cancer therapy including operation, chemotherapy and radiotherapy, molecular targeted therapy, immunotherapy, and genetic therapy. Traditional methods pose a significant challenge to patients' tolerability and adherence due to toxicity (Mun et al., 2018). Molecular targeted drugs, one of the anti-tumor drugs, have gradually replaced traditional chemotherapeutic drugs with their advantages of high targeting and efficacy, which have made revolutionary progress in the treatment of malignant tumors. However, during the clinical application, dramatic but short-lived tumor regressions and expenses limit the benefits (Vanneman and Dranoff., 2012). Tumor immunotherapy refers to the actively or passively tumor-specific responses to suppress cancer, including immune checkpoint blocks (ICBs), adoptive cell transfer (ACT), and tumor-specific vaccines (Zhang and Zhang, 2020). Despite immunotherapy marking the beginning of a new era in cancer, it only works in a subset of cancers and a fraction of patients with cancer respond to immunotherapy (Yang, 2015). Meanwhile, the existence of immune escape makes the effect less than expected.

The gene therapy contains zinc-finger nucleases (ZFNs), transcription activator-like effector nucleases (TALENs), and the CRISPR/Cas9 system, which knockout, insert, and mutate the targeted gene to treat cancer (Knott and Doudna, 2018). ZFNs and TALENs have been applied in editing targeted gene in the body; however, they are time-consuming and complicated (Gaj et al., 2013). Compared to ZFNs and TALENs, the CRISPR/Cas9 system is the method of choice for gene editing due to its simplicity, practicability, and application diversity. Hence, the CRISPR/Cas system is used widely. For tumor and immune cells, CRISPR/Cas9 gene editing is expected to provide a new strategy for tumor therapy.

The Application of CRISPR/Cas9 Technology in Tumor Cells

CRISPR-Cas9 technology is used in tumor cells to overcome cancer. The tumor cell editing mainly has the following methods:

(1) Gene knockout is the simplest and most common approach that has tremendous potential in clinical trials, mainly for pathogenic genes. In 2012, it was confirmed that Cas9 could cut programmatically various DNA sites *in vitro* (Jinek et al., 2012). For example, through gene editing of *CCR5* in $CD4^+$ T cells from persons who have been infected with HIV helps to combat HIV infection (Hsu et al., 2014; Tebas et al., 2014; Xu et al., 2019). Similarly, disrupting the intronic erythroid-specific enhancer for the *BCL11A* gene could increase HbF protein expression to possibly cure sickle-cell anemia (SCD) and β-thalassemia (Basak and Sankaran, 2016);
(2) Targeted insertion of DNA fragments helps to correct mutation to restore the normal sequence (Mali et al., 2013). Theodore et al. applied the strategy that inserting large DNA sequences (>1 kb) helps to correct *IL2RA* mutation in cells from patients with monogenic autoimmune disease (Roth et al., 2018);
(3) Translocation of chromosomal fragment was closely associated with tumorigenesis, for instance, modeling cancer-related chromosomal translocations was able to facilitate cancer pathogenesis research (Mani and Chinnaiyan, 2010). Irina et al. have modeled the human alveolar rhabdomyosarcoma *Pax3-Foxo1* chromosome translocation in mouse myoblast by CRISPR/Cas9, which benefits researchers to explore the mechanism of the tumorigenic process (Lagutina et al., 2015);
(4) Base editing to obtain the point mutation for the purpose of various gene editing steps, such as to monitor and screen (Zhang, 2021). As we all know, the largest class of human pathogenic mutations was the point mutation (also called single nucleotide polymorphism, SNP), so that a new technology was required to change specifically an individual base pair within a vast genome (Landrum et al., 2016; Rees and Liu, 2018). Based on the CRISPR/Cas9 system, David R. Liu's group developed a CRISPR/Cas base editor (BE) technology, also known as cytosine base editors (CBEs), to replace specific base, for instance, convert cytidine (C) to thymine (T) or guanine (G) to adenine (A) (Komor et al., 2016). Later, adenine base editors (ABEs) were developed to convert an A·T base pair to a G·C base pair (Gaudelli et al., 2017). In short, ABEs and CBEs provide four possible changes to correct point mutations (Rees and Liu, 2018).

The tumor cell models were established to test *in vitro* therapeutic effects, explore the mechanisms of drug actions, and clarify pathogenesis as well by the CRISPR-Cas9-mediated genome editing technology (Augert et al., 2020). Recently, the research about CRISPR/Cas9 gene editing technology in human cells was popularly increasing (Wang et al., 2014). The Human Genome Project and International HapMap Project showed more comprehensive data and have attracted considerable interest from scientists to explain the relation between gene and disease, especially tumor (Bayarsaikhan et al., 2021). With the involvement of the CRISPR/Cas system in drug discovery, the combination contains the CRISPR/Cas9 system, and stem cells would be applied to simulate at least 75,000 diseases associated with human genetic variants (Ledford, 2019). By revealing the gene–gene interactions to synthetic lethality of genes by the CRISPR system, we could obtain the candidate drug. The researchers exposed myeloid leukemia KBM7 cells to the CRISPR/Cas9 system that carrying a library of more than 70,000 sgRNAs; thus, drug-resistant genes would be identified (Wang et al., 2014). It was not only a complicated process in drug discovery but also time-consuming. Due to the high-screening knockout by the CRISPR/Cas9 system, it was increasing to elucidate the function of gene. Meanwhile, the induced pluripotent stem cells (iPSCs) with unlimited self-renewal capability were able to differentiate into cells of any lineage attract, which owned a value in cell disease modeling (Wang et al., 2017). An immunodeficiency, centromeric region instability, and facial anomalies syndrome (ICF) model was edited efficiently in human-induced pluripotent stem cells (hPSCs) by using the CRISPR system (Horii et al., 2013). Based on the CRISPR/Cas9 system, Paquet et al. introduced mono- and biallelic sequence changes to hPSCs to establish the model with Alzheimer's disease-causing mutations in

TABLE 1 | CRISPR/Cas9 gene editing in animals.

Animal	Targeted gene	Mutation or disruption efficiency	Other	Reference
Rat	*Tet1*	36%	*Tet1* and *Tet2* with biallelic mutations in both genes with an efficiency of 80%	Li et al. (2013); Wang et al. (2013)
	Tet2	48%		
	Tet3	36%		
Goat	*MSTN*	32%	Potential off-target but no unwanted mutation occurred	Ni et al. (2014)
	MSTN/Prp	20%		
	MSTN/BLG/PrP/NUP	4%		
Rabbit	Tyrosinase *CR2*	3%	No off-target mutation	Honda et al. (2015)
	GJA8	98.7%	—	Yuan et al. (2016)
Dog	*MSTN*	Monoallelic mutation: 22.7%	Biallelic mutation: 36.4%; no mutation: 40.9%	Zou et al. (2015)
Pig	*TYR*	49.4%	Double homozygous (*PAPK2 and PINK1*): 38.1%	Zhou et al. (2015)
	PAPK2	66.7%		
	PINK1	69.9%		
Monkey	*DMD* (exon 4 and exon 46)	Mosaic mutations: 87%	—	Chen et al. (2015)
	Ppar-γ	10%–25%	No authentic mutation was detected	Niu et al. (2014)
	Rag1	23.80%		
	NrOb1	~20%		
Zebrafish	*bpt1*, *bplt4*, *C9t2*, and *C9t3*	86%, heritable	Mutation rates at potential off-target sites are 1.1~2.5%	Hruscha et al. (2013)

amyloid precursor protein and derived cortical neurons (Paquet et al., 2016). The CRISPR/Cas9 gene editing tool was combined with the *piggyBac* transposon to effectively correct the mutation of the human B hemoglobin (*HBB*) gene in the iPSC genome of patients with β-thalassemia (Xie et al., 2014). In a study, the *Lacl* gene was mutated, and several normal genes were re-expressed, which resulted in the inhibition of bladder cancer cells (Liu et al., 2014). Scientists have also cultured hPSCs *in vitro* to perfectly modify four colorectal cancer mutation genes including *APC*, *P53*, *KRAS*, and *SMAD4* and then screened the mutant cells to construct the human colorectal cancer model to explore the specific mechanism of the intestinal stem cell of colon cancer (Drost et al., 2015). In summary, the CRISPR/Cas system is typically applied for the generation of cell models.

The Application of CRISPR/Cas9 Technology in Animals

Animal tumor models have laid a foundation for revealing the molecular mechanism of tumorigenesis and development. Animal models were ideal carriers that effectively integrate basic, clinical tumor research, which have been widely used throughout cancer research. The disease animal models played a crucial role in drug development and therapeutic approaches as an *in vivo* tool. Animal tumor models can be classified into four categories: carcinogen-induced models (CIMs), spontaneous and induced models, genetically engineered models, and transplant models, in which transplant models were divided into orthotopic models, heterotopic tumor models, and primary patient-derived xenografts (PDXs) (Burtin et al., 2020). Gene knockout animal tumor models, referring to genetically engineered models, use the gene knockout method to remove genes to induce tumorigenesis (Takeda et al., 2019). This is an ideal model for understanding the role of a single gene or several genes in tumorigenesis. Compared to other gene editing technologies such as ZFNs and TALENs, CRISPR/Cas9 technology has the advantages of cost, efficiency and timesaving. Scientists have creatively applied the CRISPR system for studying malignant tumors and constructed multiple animal tumor models. Precise gene editing has been successful in various animals, including rat (Li et al., 2013; Wang et al., 2013), goat (Ni et al., 2014), rabbit (Honda et al., 2015; Yuan et al., 2016), dog (Zou et al., 2015), monkey (Niu et al., 2014; Chen et al., 2015), pig (Zhou et al., 2015), *C. elegans* (Friedland et al., 2013), and zebrafish (Hruscha et al., 2013; Varshney et al., 2015) (**Table 1**).

Traditional animal models lay on the embryonic stem cells (ESCs) and HDR techniques and succeeded to establish the transgenic animal. However, it is time-consuming, and researchers spend at least 1 year to build the model. Compared with ZFNs and TALENs, CRISPR/Cas9 technology adopted three methods to build the model:

(1) Editing gene in embryos. There are 3 steps: 1) obtain zygote, 2) deliver sgRNA and Cas9 mRNA into the zygote, and 3) embryo transfer into animals to produce generation;
(2) Editing haploid embryonic stem cells (ESCs) because the haploid ESCs easily produce homozygous mutants for the generation of transgenic model;
(3) Gene editing in spermatogonia stem cells (SSCs) would be autologous transplanted to pseudo-pregnant animals (Sato et al., 2020) (**Figure 2**).

However, editing embryos by microinjection was too time-consuming, and the microinjection required special skill, which limited the application for high-throughput genetic analysis (Hashimoto and Takemoto, 2015). On the contrary, editing in ESCs would generate multiple knockouts and large deletions at high efficiency (Safier et al., 2020). CRISPR/Cas9-mediated gene technology in SSCs did not change the paternal imprinting

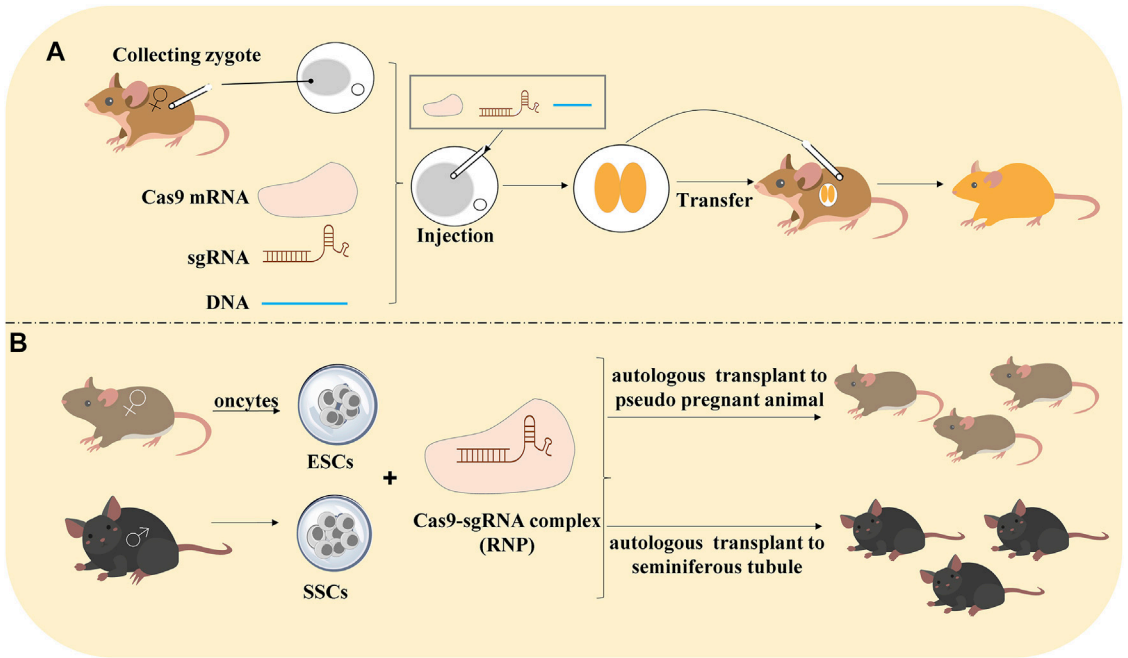

FIGURE 2 | Methods of CRISPR/Cas9 technology to construct animal models. **(A)** Editing gene in embryos. Collecting the zygote that was injected with Cas9 mRNA, sgRNA, and DNA. After the zygote develops into an embryo, it would be transferred into the animals to produce generation. **(B)** Editing gene in haploid ESCs and SSCs: haploid embryonic stem cells (ESCs) are pluripotent cells generated from oocytes. CRISPR/Cas9-mediated gene editing in ESCs and autologous transplant to pseudo-pregnant animals to produce generation. Spermatogonia stem cells (SSCs) would be transfected by RNP and autologous transplant to seminiferous tubule to produce the generation.

pattern that displayed a great promise to treat diseases (Wu et al., 2015). From the point of view of animal studies, it is more effective for the generation of transgenic animals by CRISPR/Cas9. CRISPR/Cas9 technology is integrated into tumor cell molecular biology research, allowing for accurate and quick editing of genomes, constructing animal tumor models of gene mutation and knockout to promote comprehensive research on tumor-related genes and tumor development. The CRISPR/Cas9 system was applied not only in animals but also in insects (Shirai et al., 2022). The latest research showed that "direct parental" CRISPR (DIPA-CRISPR) was defined as a method in which the RNPs were injected into the hemocoel of females to introduce the hereditary mutation in developing oocytes and successfully applied them in cockroaches and *Tribolium castaneum*. It is an exciting breakthrough to achieve the gene editing in cockroaches due to the unique reproduction system.

The Clinical Trial of CRISPR/Cas9 Technology

The purpose of developing new treatment methods is to achieve the purpose of preventing, alleviating, and even treating diseases. The emergence of CRISPR/Cas9 gene editing technology reflects the urgent need for treating diseases that are currently incurable, such as tumor. Applying this technology to the treatment of human diseases will bring hope to patients. In 2012, 2013, and 2015, CRISPR made the cut "breakthrough of the year," which achieved great success such as creating a contagious gene to fight malarial infection (Hammond et al., 2016; Macias et al., 2020).

Tumor treatment is complicated and frequently accompanied by immune escape, so that it is necessary to overcome the immune escape as a crucial treatment strategy. Chimeric antigen receptor T (CAR-T) cells have been provided with tumor cell-specific antigen chimeric domains, which can activate T cells and achieve killing effect on tumor cells (Hu et al., 2021). The signaling pathway—programmed death receptor 1 (PD-1)/programmed cell death ligand 1 (PD-L1)—led to melanoma, non-small cell lung cancer (NSCLC), colorectal cancers (CRCs), bladder cancer, and renal-cell cancer if it was activated (Ott et al., 2020; O'Neil et al., 2017; Topalian et al., 2012; Stein et al., 2021; and Yi and Li, 2016). PD-1 was encoded by the *PDCD1* gene, which blocked the binding of PD-1 to its receptor PD-L1 to enhance the activation of T cells to fight cancer by improving the IFN-γ expression (Lu et al., 2020; Stadtmauer et al., 2020). Combining CRISPR/Cas9 with CAR-T cells and PD-1, the editing *PDCD1* gene in T cells was an ideal method to cure cancer (Xu et al., 2022). In 2016, the first human phase I clinical trial of CRISPR was conducted in China to therapy metastatic NSCLC patients who did not respond to chemotherapy, radiotherapy, and other therapies (Lacey and Fraietta, 2020; Lu et al., 2020). Similarly, knocking TRAC region and *CD52* gene in CAR-T cells by CRISPR/Cas9 avoided the host immune-mediated rejection for relapsed/refractory acute lymphoblastic leukemia (r/r ALL) (Hu et al., 2021). Su et al. have confirmed that targeting PD-1 in the T cells from patient with melanoma and gastric

TABLE 2 | Clinical trials of the CRISPR/Cas9 system.

Target	Therapy	Clinicaltrials.gov number	Reference
CCR5	HIV	NCT00842634	Tebas et al. (2014)
		NCT03164135	Xu et al. (2019)
BCL11A	Sickle-cell anemia (SCD) and β-thalassemia	NCT03745287	Basak and Sankaran, (2016)
		NCT03655678	Frangoul et al. (2021)
PDCD1 (PD-1)	Non-small-cell lung cancer (NSCLC)	NCT02793856	Lu et al. (2020)
	Advanced refractory myeloma and metastatic sarcoma	NCT03399448	Stadtmauer et al. (2020)
	Relapsed/refractory acute lymphoblastic leukemia (r/r ALL)	NCT04227015	Hu et al. (2021)
	Mesothelin-positive solid tumors	NCT03545815	Wang et al. (2021)
	Metastatic colorectal cancer	NCT03174405	Stein et al. (2021)
	Prostate cancer	NCT02867345	Yi and Li, (2016)
	Bladder cancer	NCT02863913	
	Metastatic renal cell carcinoma	NCT02867332	
E6 and E7	HPV	NCT03057912	Khairkhah et al. (2022)
RPE65	Leber's congenital amaurosis type 10 (LCA10)	NCT03872479	Maeder et al. (2019)
TTR	Transthyretin amyloidosis (ATTR amyloidosis)	NCT04601051	Gillmore et al. (2021)

cancer resulted in the improvement of cytotoxicity of T cells, and the tumor cells were killed (Su et al., 2016). The successful practice of this gene therapy has laid the foundation for the clinical trial of CRISPR/Cas9 gene editing technology to inhibit tumor metastasis in human.

There are various genetic mutations in the process of tumor evolution such as proto-oncogene and tumor-suppressor gene. More and more mutated genes related to tumors have been identified by genome-sequencing technology. The efficient and specific gene editing function of the CRISPR/Cas9 system provides the possibility to directly target the mutated genes that cause cancer *in vivo*. As we all know, the epidermal growth factor receptor (EGFR) gene was changed in approximately 10%~15% of NSCLC, which played an essential role in tumor progression (Koo et al., 2017). Currently, EGFR inhibitors are the first-line drugs for curing lung cancer with EGFR mutation (Janne et al., 2022). However, the development of resistance and the efficacy of drugs were limited. It was a need to develop novel tools for EGFR-mutated NSCLC, and CRISPR/Cas9 gene editing technology maybe a promising method to correct cancer-driven mutations for cancer therapy. Experiments have shown that knocking out the EGFR mutant allele (L858R) in H1975 lung cells resulted in dying of cancer cells and decreasing tumor volume . Cervical cancer was related to human papilloma virus (HPV). After targeting E6 and E7 oncogenes, tumor growth was suppressed (Khairkhah et al., 2022). However, safety and specificity of CRISPR/Cas9 need to be optimized before executing in the clinical setting. The nuclear receptor binding SET domain-containing protein 1 (NSD1) was one of the biomarkers to participate in a variety of malignancies, and human hepatocellular carcinoma (HCC) was one of them. Knocking the NSD1 gene in HCC cells led to the function of cell proliferation, migration, and invasion that were suppressed (Zhang, et al., 2019b). Targeting the reticulon 4B (Nogo-B), a negative modulator of apoptosis, was able to inhibit the ability of cell proliferation *in vitro* and tumor growth *in vivo* (Zhu et al., 2017). Based on the CRISPR/Cas9 system, it was probable to provide individualized targeted therapy, which showed potential in tumor therapy at the gene level and rises a high level. Meanwhile, the Zhang Feng's group successfully restored vision in Leber's congenital amaurosis type 10 (LCA10) in 2019, which showed the feasibility of CRISPR-based gene editing therapy in the treatment of genetic diseases (Maeder et al., 2019) (**Table 2**).

CHALLENGES OF THE CRISPR/CAS9 SYSTEM

As only a specific nucleic acid sequence of 20 bp was provided by using CRISPR/Cas for gene editing, its construction process was simpler and faster than ZFNs and TALENs, owing to ZFNs and TALENs must depend on the Fok I enzyme to exert. In contrast, the CRISPR technology target design was simpler and efficient, making it an ideal gene editing tool. However, it may also cause "off-target" effects, and the gene sequences should not be edited to result in unpredictable consequences. This made CRISPR more secure when used *in vivo* because once off-target occurred, it cannot be checked and corrected in a timely manner like *in vitro* experiments. The new types of Cas9, such as saCas9 and Cpf1, have been developed but cannot completely get rid of the dependence on PAM (Wang et al., 2018). This year, the newest types of Cas9-Cas9TX can inhibit the occurrence of chromosomal structural abnormalities such as chromosomal translocations and large fragment deletions in the process of gene editing and greatly improve the safety of CRISPR/Cas9 gene editing (Yin et al., 2022).

In 2018, "Gene-edited Infant" event brought a lot of controversy to the application of CRISPR at the clinical level, and direct violation of the international scientific consensus that CRISPR/Cas9 technology was not ready or appropriate for making changes to humans that could be passed on through generations until the technology matures and becomes widespread (Kofler, 2019). At this time, how to define whether accepting human beings have the right to choose their own genes in place of future generations, or whether the modified human beings can enjoy the rights of ordinary people will become a problem that needs to be pondered (Zhang et al., 2019a). The effective ethical review is the proper meaning of strengthening the

ethical governance of science and technology. Therefore, it is the top priority to improve the ethical review system for human genome editing activities.

CONCLUDING REMARKS AND FUTURE PERSPECTIVES

In the past decade, CRISPR/Cas9 gene editing technology as a strategy to therapy disease successfully entered preclinical and clinical stages. With the continuous improvement of gene editing tools and the identification of new effective targets for diseases, the clinical translation and application research of gene editing technology has been expanded. Not only in insects and plants, but also in animals and even in humans, the CRISPR/Cas9 gene editing technology proves its powerful utility.

Specific gene mutation improved tumor migration, invasion, and angiogenesis, which could be reversed by targeting editing genome. At present, the *in vivo* gene-editing based on the CRISPR/Cas system is currently being used for diseases, such as tumor and immune diseases. At present, the clinical programs are being carrying out to verify the effects of CRISPR/Cas9 and have made outstanding achievements. However, the clinical trials have been developed only involving a small number of patients and a limited follow-up, for which the further in-depth *in vivo* research studies are planned (Frangoul et al., 2021). Meanwhile, long-term safety monitoring is needed to confirm the effects and unknown adverse reactions (Frangoul et al., 2021; Gillmore et al., 2021). Developing and optimizing the Cas9-based gene editing should promote the technology forward to therapeutic applications and offer a wide variety of treating strategies for human diseases, especially tumor.

In spite of the application of CRISPR/Cas9, it brings promise for tumor therapy associated with gene mutation; problems such as off-target and ethics need to resolved. Scientists must begin to observe the international consensus and strive to advance society positively by technology (Kofler, 2019). We still have a long way to go until the CRISPR/Cas9 technology is ready to treat cancer maturely.

AUTHOR CONTRIBUTIONS

X-ZC, RG, and CZ wrote the manuscript. JX and HS designed the figures. HY, CP, and FN finished the tables. J-YZ, X-KZ, and J-QL designed and revised the manuscript. All authors have read and approved the final version of the manuscript.

FUNDING

This work was supported by the National Key R&D Program of China (2021YFE0202000), the Finance Science and Technology Project of Hainan Province (ZDYF2020137), the Guangdong Basic and Applied Basic Research Foundation (2020A1515010605), and the Fund of Guangdong Education Department (2021ZDZX2006).

REFERENCES

Augert, A., Mathsyaraja, H., Ibrahim, A. H., Freie, B., Geuenich, M. J., Cheng, P. F., et al. (2020). MAX Functions as a Tumor Suppressor and Rewires Metabolism in Small Cell Lung Cancer. *Cancer Cell* 38, 97–114.e7. doi:10.1016/j.ccell.2020.04.016

Basak, A., and Sankaran, V. G. (2016). Regulation of the Fetal Hemoglobin Silencing Factor BCL11A. *Ann. N. Y. Acad. Sci.* 1368, 25–30. doi:10.1111/nyas.13024

Bayarsaikhan, D., Bayarsaikhan, G., and Lee, B. (2021). Recent Advances in Stem Cells and Gene Editing: Drug Discovery and Therapeutics. *Prog. Mol. Biol. Transl. Sci.* 181, 231–269. doi:10.1016/bs.pmbts.2021.01.019

Bray, F., Laversanne, M., Weiderpass, E., and Soerjomataram, I. (2021). The Ever-Increasing Importance of Cancer as a Leading Cause of Premature Death Worldwide. *Cancer* 127, 3029–3030. doi:10.1002/cncr.33587

Brinkman, E. K., Chen, T., de Haas, M., Holland, H. A., Akhtar, W., and van Steensel, B. (2018). Kinetics and Fidelity of the Repair of Cas9-Induced Double-Strand DNA Breaks. *Mol. Cell* 70 (5), 801–813.e6. doi:10.1016/j.molcel.2018.04.016

Bürtin, F., Mullins, C. S., and Linnebacher, M. (2020). Mouse Models of Colorectal Cancer: Past, Present and Future Perspectives. *World J. Gastroenterol.* 26, 1394–1426. doi:10.3748/wjg.v26.i13.1394

Chen, Y., Zheng, Y., Kang, Y., Yang, W., Niu, Y., Guo, X., et al. (2015). Functional Disruption of the Dystrophin Gene in Rhesus Monkey Using CRISPR/Cas9. *Hum. Mol. Genet.* 24, 3764–3774. doi:10.1093/hmg/ddv120

Deltcheva, E., Chylinski, K., Sharma, C. M., Gonzales, K., Chao, Y., Pirzada, Z. A., et al. (2011). CRISPR RNA Maturation by Trans-encoded Small RNA and Host Factor RNase III. *Nature* 471, 602–607. doi:10.1038/nature09886

Drost, J., van Jaarsveld, R. H., Ponsioen, B., Zimberlin, C., van Boxtel, R., Buijs, A., et al. (2015). Sequential Cancer Mutations in Cultured Human Intestinal Stem Cells. *Nature* 521, 43–47. doi:10.1038/nature14415

Frangoul, H., Altshuler, D., Cappellini, M. D., Chen, Y.-S., Domm, J., Eustace, B. K., et al. (2021). CRISPR-Cas9 Gene Editing for Sickle Cell Disease and β-Thalassemia. *N. Engl. J. Med.* 384, 252–260. doi:10.1056/NEJMoa2031054

Friedland, A. E., Tzur, Y. B., Esvelt, K. M., Colaiácovo, M. P., Church, G. M., and Calarco, J. A. (2013). Heritable Genome Editing in *C. elegans* via a CRISPR-Cas9 System. *Nat. Methods* 10, 741–743. doi:10.1038/nmeth.2532

Frock, R. L., Hu, J., Meyers, R. M., Ho, Y. J., Kii, E., and Alt, F. W. (2015). Genome-wide Detection of DNA Double-Stranded Breaks Induced by Engineered Nucleases. *Nat. Biotechnol.* 33, 179–186. doi:10.1038/nbt.3101

Gaj, T., Gersbach, C. A., and Barbas, C. F., 3rd. (2013). ZFN, TALEN, and CRISPR/Cas-based Methods for Genome Engineering. *Trends Biotechnol.* 31, 397–405. doi:10.1016/j.tibtech.2013.04.004

Gaudelli, N. M., Komor, A. C., Rees, H. A., Packer, M. S., Badran, A. H., Bryson, D. I., et al. (2017). Programmable Base Editing of A●T to G●C in Genomic DNA without DNA Cleavage. *Nature* 551, 464–471. doi:10.1038/nature24644

Gerstung, M., Jolly, C., Leshchiner, I., Dentro, S. C., Gonzalez, S., Rosebrock, D., et al. (2020). The Evolutionary History of 2,658 Cancers. *Nature* 578, 122–128. doi:10.1038/s41586-019-1907-7

Gillmore, J. D., Gane, E., Taubel, J., Kao, J., Fontana, M., Maitland, M. L., et al. (2021). CRISPR-Cas9 *In Vivo* Gene Editing for Transthyretin Amyloidosis. *N. Engl. J. Med.* 385, 493–502. doi:10.1056/NEJMoa2107454

Haft, D. H., Selengut, J., Mongodin, E. F., and Nelson, K. E. (2005). A Guild of 45 CRISPR-Associated (Cas) Protein Families and Multiple CRISPR/Cas Subtypes Exist in Prokaryotic Genomes. *PLoS Comput. Biol.* 1 (6), e60. doi:10.1371/journal.pcbi.0010060

Hammond, A., Galizi, R., Kyrou, K., Simoni, A., Siniscalchi, C., Katsanos, D., et al. (2016). A CRISPR-Cas9 Gene Drive System Targeting Female Reproduction in the Malaria Mosquito Vector *Anopheles gambiae*. *Nat. Biotechnol.* 34, 78–83. doi:10.1038/nbt.3439

Hashimoto, M., and Takemoto, T. (2015). Electroporation Enables the Efficient mRNA Delivery into the Mouse Zygotes and Facilitates CRISPR/Cas9-based Genome Editing. *Sci. Rep.* 5, 11315. doi:10.1038/srep11315

Hille, F., Richter, H., Wong, S. P., Bratovič, M., Ressel, S., and Charpentier, E. (2018). The Biology of CRISPR-Cas: Backward and Forward. *Cell* 172, 1239–1259. doi:10.1016/j.cell.2017.11.032

Honda, A., Hirose, M., Sankai, T., Yasmin, L., Yuzawa, K., Honsho, K., et al. (2015). Single-step Generation of Rabbits Carrying a Targeted Allele of the Tyrosinase Gene Using CRISPR/Cas9. *Exp. Anim.* 64, 31–37. doi:10.1538/expanim.14-0034

Horii, T., Tamura, D., Morita, S., Kimura, M., and Hatada, I. (2013). Generation of an ICF Syndrome Model by Efficient Genome Editing of Human Induced Pluripotent Stem Cells Using the CRISPR System. *Int. J. Mol. Sci.* 14, 19774–19781. doi:10.3390/ijms141019774

Hruscha, A., Krawitz, P., Rechenberg, A., Heinrich, V., Hecht, J., Haass, C., et al. (2013). Efficient CRISPR/Cas9 Genome Editing with Low Off-Target Effects in Zebrafish. *Development* 140, 4982–4987. doi:10.1242/dev.099085

Hsu, P. D., Lander, E. S., and Zhang, F. (2014). Development and Applications of CRISPR-Cas9 for Genome Engineering. *Cell* 157, 1262–1278. doi:10.1016/j.cell.2014.05.010

Hu, Y., Zhou, Y., Zhang, M., Ge, W., Li, Y., Yang, L., et al. (2021). CRISPR/Cas9-Engineered Universal CD19/CD22 Dual-Targeted CAR-T Cell Therapy for Relapsed/Refractory B-Cell Acute Lymphoblastic Leukemia. *Clin. Cancer Res.* 27, 2764–2772. doi:10.1158/1078-0432.CCR-20-3863

Huang, W., Yan, Y., Liu, Y., Lin, M., Ma, J., Zhang, W., et al. (2020). Exosomes with Low miR-34c-3p Expression Promote Invasion and Migration of Non-small Cell Lung Cancer by Upregulating Integrin α2β1. *Signal Transduct. Target Ther.* 5, 39. doi:10.1038/s41392-020-0133-y

Ishino, Y., Shinagawa, H., Makino, K., Amemura, M., and Nakata, A. (1987). Nucleotide Sequence of the Iap Gene, Responsible for Alkaline Phosphatase Isozyme Conversion in *Escherichia coli*, and Identification of the Gene Product. *J. Bacteriol.* 169, 5429–5433. doi:10.1128/jb.169.12.5429-5433.1987

Jänne, P. A., Baik, C., Su, W. C., Johnson, M. L., Hayashi, H., Nishio, M., et al. (2022). Efficacy and Safety of Patritumab Deruxtecan (HER3-DXd) in EGFR Inhibitor-Resistant, EGFR-Mutated Non-small Cell Lung Cancer. *Cancer Discov.* 12, 74–89. doi:10.1158/2159-8290.CD-21-0715

Jansen, R., Embden, J. D., Gaastra, W., and Schouls, L. M. (2002). Identification of Genes that Are Associated with DNA Repeats in Prokaryotes. *Mol. Microbiol.* 43, 1565–1575. doi:10.1046/j.1365-2958.2002.02839.x

Jinek, M., Chylinski, K., Fonfara, I., Hauer, M., Doudna, J. A., and Charpentier, E. (2012). A Programmable Dual-RNA-Guided DNA Endonuclease in Adaptive Bacterial Immunity. *Science* 337, 816–821. doi:10.1126/science.1225829

Khairkhah, N., Bolhassani, A., and Najafipour, R. (2022). Current and Future Direction in Treatment of HPV-Related Cervical Disease. *J. Mol. Med.* 100, 829–845. doi:10.1007/s00109-022-02199-y

Knott, G. J., and Doudna, J. A. (2018). CRISPR-cas Guides the Future of Genetic Engineering. *Science* 361, 866–869. doi:10.1126/science.aat5011

Kofler, N. (2019). Why Were Scientists Silent over Gene-Edited Babies? *Nature* 566, 427. doi:10.1038/d41586-019-00662-4

Komor, A. C., Kim, Y. B., Packer, M. S., Zuris, J. A., and Liu, D. R. (2016). Programmable Editing of a Target Base in Genomic DNA without Double-Stranded DNA Cleavage. *Nature* 533, 420–424. doi:10.1038/nature17946

Koo, T., Yoon, A. R., Cho, H. Y., Bae, S., Yun, C. O., and Kim, J. S. (2017). Selective Disruption of an Oncogenic Mutant Allele by CRISPR/Cas9 Induces Efficient Tumor Regression. *Nucleic Acids Res.* 45, 7897–7908. doi:10.1093/nar/gkx490

Koonin, E. V., and Makarova, K. S. (2019). Origins and Evolution of CRISPR-Cas Systems. *Philos. Trans. R. Soc. Lond B Biol. Sci.* 374, 20180087. doi:10.1098/rstb.2018.0087

Lacey, S. F., and Fraietta, J. A. (2020). First Trial of CRISPR-Edited T Cells in Lung Cancer. *Trends Mol. Med.* 26, 713–715. doi:10.1016/j.molmed.2020.06.001

Lagutina, I. V., Valentine, V., Picchione, F., Harwood, F., Valentine, M. B., Villarejo-Balcells, B., et al. (2015). Modeling of the Human Alveolar Rhabdomyosarcoma Pax3-Foxo1 Chromosome Translocation in Mouse Myoblasts Using CRISPR-Cas9 Nuclease. *PLoS Genet.* 11, e1004951. doi:10.1371/journal.pgen.1004951

Landrum, M. J., Lee, J. M., Benson, M., Brown, G., Chao, C., Chitipiralla, S., et al. (2016). ClinVar: Public Archive of Interpretations of Clinically Relevant Variants. *Nucleic Acids Res.* 44, D862–D868. doi:10.1093/nar/gkv1222

Ledford, H. (2019). Super-precise New CRISPR Tool Could Tackle a Plethora of Genetic Diseases. *Nature* 574, 464–465. doi:10.1038/d41586-019-03164-5

Li, W., Teng, F., Li, T., and Zhou, Q. (2013). Simultaneous Generation and Germline Transmission of Multiple Gene Mutations in Rat Using CRISPR-Cas Systems. *Nat. Biotechnol.* 31, 684–686. doi:10.1038/nbt.2652

Liu, C., Zhang, L., Liu, H., and Cheng, K. (2017). Delivery Strategies of the CRISPR-Cas9 Gene-Editing System for Therapeutic Applications. *J. Control Release* 266, 17–26. doi:10.1016/j.jconrel.2017.09.012

Liu, Y., Zeng, Y., Liu, L., Zhuang, C., Fu, X., Huang, W., et al. (2014). Synthesizing and Gate Genetic Circuits Based on CRISPR-Cas9 for Identification of Bladder Cancer Cells. *Nat. Commun.* 5, 5393. doi:10.1038/ncomms6393

Lu, Y., Xue, J., Deng, T., Zhou, X., Yu, K., Deng, L., et al. (2020). Safety and Feasibility of CRISPR-Edited T Cells in Patients with Refractory Non-small-cell Lung Cancer. *Nat. Med.* 26, 732–740. doi:10.1038/s41591-020-0840-5

Macias, V. M., McKeand, S., Chaverra-Rodriguez, D., Hughes, G. L., Fazekas, A., Pujhari, S., et al. (2020). Cas9-Mediated Gene-Editing in the Malaria Mosquito *Anopheles stephensi* by ReMOT Control. *G3 (Bethesda)* 10, 1353–1360. doi:10.1534/g3.120.401133

Maeder, M. L., Stefanidakis, M., Wilson, C. J., Baral, R., Barrera, L. A., Bounoutas, G. S., et al. (2019). Development of a Gene-Editing Approach to Restore Vision Loss in Leber Congenital Amaurosis Type 10. *Nat. Med.* 25, 229–233. doi:10.1038/s41591-018-0327-9

Makarova, K. S., Wolf, Y. I., Alkhnbashi, O. S., Costa, F., Shah, S. A., Saunders, S. J., et al. (2015). An Updated Evolutionary Classification of CRISPR-Cas Systems. *Nat. Rev. Microbiol.* 13, 722–736. doi:10.1038/nrmicro3569

Makarova, K. S., Wolf, Y. I., Iranzo, J., Shmakov, S. A., Alkhnbashi, O. S., Brouns, S. J. J., et al. (2020). Evolutionary Classification of CRISPR-Cas Systems: a Burst of Class 2 and Derived Variants. *Nat. Rev. Microbiol.* 18, 67–83. doi:10.1038/s41579-019-0299-x

Mali, P., Yang, L., Esvelt, K. M., Aach, J., Guell, M., DiCarlo, J. E., et al. (2013). RNA-guided Human Genome Engineering via Cas9. *Science* 339, 823–826. doi:10.1126/science.1232033

Mani, R. S., and Chinnaiyan, A. M. (2010). Triggers for Genomic Rearrangements: Insights into Genomic, Cellular and Environmental Influences. *Nat. Rev. Genet.* 11, 819–829. doi:10.1038/nrg2883

Mun, E. J., Babiker, H. M., Weinberg, U., Kirson, E. D., and Von Hoff, D. D. (2018). Tumor-Treating Fields: A Fourth Modality in Cancer Treatment. *Clin. Cancer Res.* 24, 266–275. doi:10.1158/1078-0432.CCR-17-1117

Nambiar, T. S., Baudrier, L., Billon, P., and Ciccia, A. (2022). CRISPR-based Genome Editing through the Lens of DNA Repair. *Mol. Cell* 82, 348–388. doi:10.1016/j.molcel.2021.12.026

Ni, W., Qiao, J., Hu, S., Zhao, X., Regouski, M., Yang, M., et al. (2014). Efficient Gene Knockout in Goats Using CRISPR/Cas9 System. *PLoS One* 9, e106718. doi:10.1371/journal.pone.0106718

Nierzwicki, Ł., Arantes, P. R., Saha, A., and Palermo, G. (2021). Establishing the Allosteric Mechanism in CRISPR-Cas9. *WIREs Comput. Mol. SciMol Sci.* 11 (3), e1503. doi:10.1002/wcms.1503

Niu, Y., Shen, B., Cui, Y., Chen, Y., Wang, J., Wang, L., et al. (2014). Generation of Gene-Modified Cynomolgus Monkey via Cas9/RNA-Mediated Gene Targeting in One-Cell Embryos. *Cell* 156, 836–843. doi:10.1016/j.cell.2014.01.027

O'Neil, B. H., Wallmark, J. M., Lorente, D., Elez, E., Raimbourg, J., Gomez-Roca, C., et al. (2017). Safety and Antitumor Activity of the Anti-PD-1 Antibody Pembrolizumab in Patients with Advanced Colorectal Carcinoma. *PLoS One* 12, e0189848. doi:10.1371/journal.pone.0189848

Ott, P. A., Hu-Lieskovan, S., Chmielowski, B., Govindan, R., Naing, A., Bhardwaj, N., et al. (2020). A Phase Ib Trial of Personalized Neoantigen Therapy Plus Anti-PD-1 in Patients with Advanced Melanoma, Non-small Cell Lung Cancer, or Bladder Cancer. *Cell* 183, 347–e24. doi:10.1016/j.cell.2020.08.053

Paquet, D., Kwart, D., Chen, A., Sproul, A., Jacob, S., Teo, S., et al. (2016). Efficient Introduction of Specific Homozygous and Heterozygous Mutations Using CRISPR/Cas9. *Nature* 533, 125–129. doi:10.1038/nature17664

Podlaha, O., Riester, M., De, S., and Michor, F. (2012). Evolution of the Cancer Genome. *Trends Genet.* 28, 155–163. doi:10.1016/j.tig.2012.01.003

Rassool, F. V. (2003). DNA Double Strand Breaks (DSB) and Non-homologous End Joining (NHEJ) Pathways in Human Leukemia. *Cancer Lett.* 193, 1–9. doi:10.1016/s0304-3835(02)00692-4

Rees, H. A., and Liu, D. R. (2018). Base Editing: Precision Chemistry on the Genome and Transcriptome of Living Cells. *Nat. Rev. Genet.* 19, 770–788. doi:10.1038/s41576-018-0059-1

Roth, T. L., Puig-Saus, C., Yu, R., Shifrut, E., Carnevale, J., Li, P. J., et al. (2018). Reprogramming Human T Cell Function and Specificity with Non-viral Genome Targeting. *Nature* 559, 405–409. doi:10.1038/s41586-018-0326-5

Safier, L. Z., Zuccaro, M. V., and Egli, D. (2020). Efficient SNP Editing in Haploid Human Pluripotent Stem Cells. *J. Assist. Reprod. Genet.* 37, 735–745. doi:10.1007/s10815-020-01723-8

Sato, M., Takabayashi, S., Akasaka, E., and Nakamura, S. (2020). Recent Advances and Future Perspectives of *In Vivo* Targeted Delivery of Genome-Editing Reagents to Germ Cells, Embryos, and Fetuses in Mice. *Cells* 9, 799. doi:10.3390/cells9040799

Schep, R., Brinkman, E. K., Leemans, C., Vergara, X., van der Weide, R. H., Morris, B., et al. (2021). Impact of Chromatin Context on Cas9-Induced DNA Double-Strand Break Repair Pathway Balance. *Mol. Cell* 81, 2216–e10. doi:10.1016/j.molcel.2021.03.032

Shams, A., Higgins, S. A., Fellmann, C., Laughlin, T. G., Oakes, B. L., Lew, R., et al. (2021). Comprehensive Deletion Landscape of CRISPR-Cas9 Identifies Minimal RNA-Guided DNA-Binding Modules. *Nat. Commun.* 12, 5664. doi:10.1038/s41467-021-25992-8

Shirai, Y., Piulachs, M. D., Belles, X., and Daimon, T. (2022). DIPA-CRISPR Is a Simple and Accessible Method for Insect Gene Editing. *Cell Rep. Methods* 2, 100215. doi:10.1016/j.crmeth.2022.100215

Stadtmauer, E. A., Fraietta, J. A., Davis, M. M., Cohen, A. D., Weber, K. L., Lancaster, E., et al. (2020). CRISPR-engineered T Cells in Patients with Refractory Cancer. *Science* 367 (6481), eaba7365. doi:10.1126/science.aba7365

Stein, A., Simnica, D., Schultheiss, C., Scholz, R., Tintelnot, J., Gökkurt, E., et al. (2021). PD-L1 Targeting and Subclonal Immune Escape Mediated by PD-L1 Mutations in Metastatic Colorectal Cancer. *J. Immunother. Cancer* 9 (7), e002844. doi:10.1136/jitc-2021-002844

Sternberg, S. H., Redding, S., Jinek, M., Greene, E. C., and Doudna, J. A. (2014). DNA Interrogation by the CRISPR RNA-Guided Endonuclease Cas9. *Nature* 507, 62–67. doi:10.1038/nature13011

Su, S., Hu, B., Shao, J., Shen, B., Du, J., Du, Y., et al. (2016). CRISPR-Cas9 Mediated Efficient PD-1 Disruption on Human Primary T Cells from Cancer Patients. *Sci. Rep.* 6, 20070. doi:10.1038/srep20070

Sung, H., Ferlay, J., Siegel, R. L., Laversanne, M., Soerjomataram, I., Jemal, A., et al. (2021). Global Cancer Statistics 2020: GLOBOCAN Estimates of Incidence and Mortality Worldwide for 36 Cancers in 185 Countries. *CA Cancer J. Clin.* 71, 209–249. doi:10.3322/caac.21660

Takeda, H., Kataoka, S., Nakayama, M., Ali, M. A. E., Oshima, H., Yamamoto, D., et al. (2019). CRISPR-Cas9-mediated Gene Knockout in Intestinal Tumor Organoids Provides Functional Validation for Colorectal Cancer Driver Genes. *Proc. Natl. Acad. Sci. U. S. A.* 116, 15635–15644. doi:10.1073/pnas.1904714116

Tebas, P., Stein, D., Tang, W. W., Frank, I., Wang, S. Q., Lee, G., et al. (2014). Gene Editing of CCR5 in Autologous CD4 T Cells of Persons Infected with HIV. *N. Engl. J. Med.* 370, 901–910. doi:10.1056/NEJMoa1300662

Topalian, S. L., Hodi, F. S., Brahmer, J. R., Gettinger, S. N., Smith, D. C., McDermott, D. F., et al. (2012). Safety, Activity, and Immune Correlates of Anti-PD-1 Antibody in Cancer. *N. Engl. J. Med.* 366, 2443–2454. doi:10.1056/NEJMoa1200690

Vanneman, M., and Dranoff, G. (2012). Combining Immunotherapy and Targeted Therapies in Cancer Treatment. *Nat. Rev. Cancer* 12, 237–251. doi:10.1038/nrc3237

Varshney, G. K., Pei, W., LaFave, M. C., Idol, J., Xu, L., Gallardo, V., et al. (2015). High-throughput Gene Targeting and Phenotyping in Zebrafish Using CRISPR/Cas9. *Genome Res.* 25, 1030–1042. doi:10.1101/gr.186379.114

Wang, H., Yang, H., Shivalila, C. S., Dawlaty, M. M., Cheng, A. W., Zhang, F., et al. (2013). One-step Generation of Mice Carrying Mutations in Multiple Genes by CRISPR/Cas-mediated Genome Engineering. *Cell* 153, 910–918. doi:10.1016/j.cell.2013.04.025

Wang, H. X., Li, M., Lee, C. M., Chakraborty, S., Kim, H. W., Bao, G., et al. (2017). CRISPR/Cas9-Based Genome Editing for Disease Modeling and Therapy: Challenges and Opportunities for Nonviral Delivery. *Chem. Rev.* 117, 9874–9906. doi:10.1021/acs.chemrev.6b00799

Wang, T., Wei, J. J., Sabatini, D. M., and Lander, E. S. (2014). Genetic Screens in Human Cells Using the CRISPR-Cas9 System. *Science* 343, 80–84. doi:10.1126/science.1246981

Wang, Y., Liu, K. I., Sutrisnoh, N. B., Srinivasan, H., Zhang, J., Li, J., et al. (2018). Systematic Evaluation of CRISPR-Cas Systems Reveals Design Principles for Genome Editing in Human Cells. *Genome Biol.* 19, 62. doi:10.1186/s13059-018-1445-x

Wang, Z., Li, N., Feng, K., Chen, M., Zhang, Y., Liu, Y., et al. (2021). Phase I Study of CAR-T Cells with PD-1 and TCR Disruption in Mesothelin-Positive Solid Tumors. *Cell Mol. Immunol.* 18, 2188–2198. doi:10.1038/s41423-021-00749-x

Wiedenheft, B., Sternberg, S. H., and Doudna, J. A. (2012). RNA-guided Genetic Silencing Systems in Bacteria and Archaea. *Nature* 482, 331–338. doi:10.1038/nature10886

Wu, Y., Zhou, H., Fan, X., Zhang, Y., Zhang, M., Wang, Y., et al. (2015). Correction of a Genetic Disease by CRISPR-Cas9-Mediated Gene Editing in Mouse Spermatogonial Stem Cells. *Cell Res.* 25, 67–79. doi:10.1038/cr.2014.160

Xie, F., Ye, L., Chang, J. C., Beyer, A. I., Wang, J., Muench, M. O., et al. (2014). Seamless Gene Correction of β-thalassemia Mutations in Patient-specific iPSCs Using CRISPR/Cas9 and piggyBac. *Genome Res.* 24, 1526–1533. doi:10.1101/gr.173427.114

Xu, L., Wang, J., Liu, Y., Xie, L., Su, B., Mou, D., et al. (2019). CRISPR-edited Stem Cells in a Patient with HIV and Acute Lymphocytic Leukemia. *N. Engl. J. Med.* 381, 1240–1247. doi:10.1056/NEJMoa1817426

Xu, Y., Chen, C., Guo, Y., Hu, S., and Sun, Z. (2022). Effect of CRISPR/Cas9-Edited PD-1/pd-L1 on Tumor Immunity and Immunotherapy. *Front. Immunol.* 13, 848327. doi:10.3389/fimmu.2022.848327

Yang, Y. (2015). Cancer Immunotherapy: Harnessing the Immune System to Battle Cancer. *J. Clin. Invest.* 125, 3335–3337. doi:10.1172/JCI83871

Yi, L., and Li, J. (2016). CRISPR-Cas9 Therapeutics in Cancer: Promising Strategies and Present Challenges. *Biochim. Biophys. Acta* 1866, 197–207. doi:10.1016/j.bbcan.2016.09.002

Yin, J., Lu, R., Xin, C., Wang, Y., Ling, X., Li, D., et al. (2022). Cas9 Exo-Endonuclease Eliminates Chromosomal Translocations during Genome Editing. *Nat. Commun.* 13, 1204. doi:10.1038/s41467-022-28900-w

Yuan, L., Sui, T., Chen, M., Deng, J., Huang, Y., Zeng, J., et al. (2016). CRISPR/Cas9-mediated GJA8 Knockout in Rabbits Recapitulates Human Congenital Cataracts. *Sci. Rep.* 6, 22024. doi:10.1038/srep22024

Zhang, B., Chen, Z., Yi, J., Tang, H., Wang, C., and Chinese Academy of, E. (2019a). Chinese Academy of Engineering Calls for Actions on the Birth of Gene-Edited Infants. *Lancet* 393, 25. doi:10.1016/S0140-6736(18)33081-2

Zhang, B. (2021). CRISPR/Cas Gene Therapy. *J. Cell Physiol.* 236, 2459–2481. doi:10.1002/jcp.30064

Zhang, S., Zhang, F., Chen, Q., Wan, C., Xiong, J., and Xu, J. (2019b). CRISPR/Cas9-mediated Knockout of NSD1 Suppresses the Hepatocellular Carcinoma Development via the NSD1/H3/Wnt10b Signaling Pathway. *J. Exp. Clin. Cancer Res.* 38, 467. doi:10.1186/s13046-019-1462-y

Zhang, Y., and Zhang, Z. (2020). The History and Advances in Cancer Immunotherapy: Understanding the Characteristics of Tumor-Infiltrating Immune Cells and Their Therapeutic Implications. *Cell Mol. Immunol.* 17, 807–821. doi:10.1038/s41423-020-0488-6

Zhou, X., Xin, J., Fan, N., Zou, Q., Huang, J., Ouyang, Z., et al. (2015). Generation of CRISPR/Cas9-mediated Gene-Targeted Pigs via Somatic Cell Nuclear Transfer. *Cell Mol. Life Sci.* 72, 1175–1184. doi:10.1007/s00018-014-1744-7

Zhu, B., Chen, S., Hu, X., Jin, X., Le, Y., Cao, L., et al. (2017). Knockout of the Nogo-B Gene Attenuates Tumor Growth and Metastasis in Hepatocellular Carcinoma. *Neoplasia* 19, 583–593. doi:10.1016/j.neo.2017.02.007

Zou, Q., Wang, X., Liu, Y., Ouyang, Z., Long, H., Wei, S., et al. (2015). Generation of Gene-Target Dogs Using CRISPR/Cas9 System. *J. Mol. Cell Biol.* 7, 580–583. doi:10.1093/jmcb/mjv061

Conflict of Interest: The authors declare that the research was conducted in the absence of any commercial or financial relationships that could be construed as a potential conflict of interest.

Publisher's Note: All claims expressed in this article are solely those of the authors and do not necessarily represent those of their affiliated organizations, or those of the publisher, the editors and the reviewers. Any product that may be evaluated in this article, or claim that may be made by its manufacturer, is not guaranteed or endorsed by the publisher.

Copyright © 2022 Chen, Guo, Zhao, Xu, Song, Yu, Pilarsky, Nainu, Li, Zhou and Zhang. This is an open-access article distributed under the terms of the Creative Commons Attribution License (CC BY). The use, distribution or reproduction in other forums is permitted, provided the original author(s) and the copyright owner(s) are credited and that the original publication in this journal is cited, in accordance with accepted academic practice. No use, distribution or reproduction is permitted which does not comply with these terms.

frontiers | Frontiers in Pharmacology

ORIGINAL RESEARCH
published: 03 August 2022
doi: 10.3389/fphar.2022.937531

Novel GIRlncRNA Signature for Predicting the Clinical Outcome and Therapeutic Response in NSCLC

Qiangzhe Zhang[1], *Xicheng Liu*[2], *Zhinan Chen*[3] *and Sihe Zhang*[4]*

[1]State Key Laboratory of Medicinal Chemical Biology and College of Pharmacy, Tianjin Key Laboratory of Molecular Drug Research, Nankai University, Tianjin, China, [2]Department of Physiology and Pathophysiology, School of Basic Medical Sciences, Capital Medical University, Beijing, China, [3]National Translational Science Center for Molecular Medicine, Department of Cell Biology, State Key Laboratory of Cancer Biology, Fourth Military Medical University, Xi'an, China, [4]Department of Cell Biology, School of Medicine, Nankai University, Tianjin, China

Background: Non–small cell lung cancer (NSCLC) is highly malignant with driver somatic mutations and genomic instability. Long non-coding RNAs (lncRNAs) play a vital role in regulating these two aspects. However, the identification of somatic mutation-derived, genomic instability-related lncRNAs (GIRlncRNAs) and their clinical significance in NSCLC remains largely unexplored.

Methods: Clinical information, gene mutation, and lncRNA expression data were extracted from TCGA database. GIRlncRNAs were screened by a mutator hypothesis-derived computational frame. Co-expression, GO, and KEGG enrichment analyses were performed to investigate the biological functions. Cox and LASSO regression analyses were performed to create a prognostic risk model based on the GIRlncRNA signature (GIRlncSig). The prediction efficiency of the model was evaluated by using correlation analyses with mutation, driver gene, immune microenvironment contexture, and therapeutic response. The prognostic performance of the model was evaluated by external datasets. A nomogram was established and validated in the testing set and TCGA dataset.

Results: A total of 1446 GIRlncRNAs were selected from the screen, and the established GIRlncSig was used to classify patients into high- and low-risk groups. Enrichment analyses showed that GIRlncRNAs were mainly associated with nucleic acid metabolism and DNA damage repair pathways. Cox analyses further identified 19 GIRlncRNAs to construct a GIRlncSig-based risk score model. According to Cox regression and stratification analyses, 14 risk lncRNAs (AC023824.3, AC013287.1, AP000829.1, LINC01611, AC097451.1, AC025419.1, AC079949.2, LINC01600, AC004862.1, AC021594.1, MYRF-AS1, LINC02434, LINC02412, and LINC00337) and five protective lncRNAs (LINC01067, AC012645.1, AL512604.3, AC008278.2, and AC089998.1) were considered powerful predictors. Analyses of the model showed that these GIRlncRNAs were correlated with somatic mutation pattern, immune microenvironment infiltration, immunotherapeutic response, drug sensitivity, and survival of NSCLC patients. The GIRlncSig risk score model demonstrated good predictive performance (AUCs of ROC for 10-year survival was 0.69) and prognostic value

OPEN ACCESS

Edited by:
Hongtao Xiao,
University of Electronic Science and Technology of China, China

Reviewed by:
Yueguo Li,
Tianjin Medical University Cancer Institute and Hospital, China
Yaojiang Huang,
Minzu University of China, China
Nishant Karadkhelkar,
The Scripps Research Institute, United States

***Correspondence:**
Sihe Zhang
sihezhang@nankai.edu.cn
https://orcid.org/0000-0002-8923-1993

Specialty section:
This article was submitted to Pharmacology of Anti-Cancer Drugs, a section of the journal Frontiers in Pharmacology

Received: *06 May 2022*
Accepted: *23 June 2022*
Published: *03 August 2022*

Citation:
Zhang Q, Liu X, Chen Z and Zhang S (2022) Novel GIRlncRNA Signature for Predicting the Clinical Outcome and Therapeutic Response in NSCLC. Front. Pharmacol. 13:937531. doi: 10.3389/fphar.2022.937531

in different NSCLC datasets. The nomogram comprising GIRlncSig and tumor stage exhibited improved robustness and feasibility for predicting NSCLC prognosis.

Conclusion: The newly identified GIRlncRNAs are powerful biomarkers for clinical outcome and prognosis of NSCLC. Our study highlights that the GIRlncSig-based score model may be a useful tool for risk stratification and management of NSCLC patients, which deserves further evaluation in future prospective studies.

Keywords: long non-coding RNA, somatic mutation, genomic instability, prognostic signature, non–small cell lung cancer

INTRODUCTION

Lung cancer is the leading cause of cancer death worldwide, with an approximate 1.8 million deaths each year (Sung et al., 2021). About 85% of lung cancer patients are diagnosed with non–small cell lung cancer (NSCLC), of which lung adenocarcinoma (LUAD) and lung squamous cell carcinoma (LUSC) are the two major subtypes (Herbst et al., 2018). Although clinical approaches have achieved significant advances in NSCLC treatment, the 5-year survival rate is only 25% in 2021 (Sung et al., 2021), and there is an urgent need for the identification of novel prognostic biomarkers for improved risk stratification and enhanced therapeutic efficiency of NSCLC (Gridelli et al., 2015; Chen and Dhahbi, 2021; Peng et al., 2021).

Genomic instability and somatic mutations are two hallmarks of cancer and contribute essentially to malignant transformation (Hanahan and Weinberg, 2011). As predicted by the "Mutator Phenotype" hypothesis, mutations of DNA repair genes, oncogenes, and tumor suppressor genes (TSG) can cause increased genomic instability, which drives cancer onset and progression (Negrini et al., 2010). Additionally, defects in genes controlling chromosome cohesion, mitotic kinetochore-microtubule attachment, centrosome copy number, checkpoint function, and cell-cycle regulation can accelerate the genomic instability. Beyond that, chromosomal instability such as translocations, deletions, insertions, amplifications, and inversions of large segments as well as gains or losses of whole chromosomes can also cause genomic instability (Thompson et al., 2010; Bastians, 2015). Furthermore, epigenetic modifications, like DNA modification, histone variants and modifications, nucleosome remodeling, and non-coding RNA, together play important roles in keeping genomic stability (Reis et al., 2016; Feng and Riddle, 2020). Moreover, an undesirable tumor microenvironment can also increase genomic instability (Rummel et al., 2012), of which hypoxia is a major factor (Sonugur and Akbulut, 2019). Notably, genomic instability contributes to the acquisition of multidrug resistance in malignancy (Lee et al., 2011; Osrodek and Wozniak, 2021), which frequently gives rise to poor therapeutic response and patient outcome (Lukow et al., 2021). Therefore, novel biomarkers correlated with genomic instability are critical for cancer diagnosis, treatment, and prognosis.

Emerging evidence indicates that long noncoding RNAs (lncRNAs) play vital roles in regulating genomic stability (Nair et al., 2020). Multiple studies have revealed that lncRNAs can preserve genomic stability in the process of DNA damage response and repair. For instance, a colorectal cancer-overexpressed oncogenic lncRNA, CRNDE, could reduce DNA damage and cell apoptosis after oxaliplatin treatment (Gao et al., 2017). Furthermore, lncRNA LINP1 could serve as a scaffold linking Ku80 and DNA-PKcs and consequently coordinate non-homologous end-joining pathways to enhance the repair of DNA double-strand breaks (Zhang et al., 2016). A poorly characterized lncRNA, NORAD, maintains genomic stability by sequestering the PUMILIO protein. Once NORAD was missing, PUMILIO induce chromosomal instability by hyperactively inhibiting mitosis, DNA replication, and DNA damage repair (Lee et al., 2016). These studies strongly suggest that genomic instability-related lncRNAs (GIRlncRNAs) may provide a vital molecular signature for predicting the malignant phenotype. Recently, Bao *et al* identified a genomic instability-related lncRNA signature (GIRlncSig) for improved predication of breast cancer outcome, which combined lncRNA expression and the somatic mutation profile (Bao et al., 2020). Geng and Peng have identified two sets of GIRlncSig in LUAD and early LUAD with the favorable prognostic outcome (Geng et al., 2021; Peng et al., 2021). Although these GIRlncSigs have been associated with the prognosis of particular subtypes of lung cancer, GIRlncSig-associated tools for NSCLC prognosis have yet to be established. More importantly, the clinical significance and biological function of GIRlncSig in NSCLC remain largely unexplored.

In this study, we identified 19 somatic mutation-derived GIRlncRNAs in NSCLC by using the mutator hypothesis-derived computational frame. A GIRlncSig-based risk score model with reliable prognostic performance was constructed, which can be a powerful indicator of genomic instability, immune microenvironment infiltration, therapeutic response, drug resistance, and patient stratification, thereby improving the personalized treatment of NSCLC.

MATERIALS AND METHODS

Data Collection and Preprocessing

The overall procedure in this study is outlined as the roadmap (**Supplementary Figure S1**). Transcriptomic and clinical information on NSCLC (LUAD and LUSC) were downloaded from The Cancer Genome Atlas (TCGA) database *via* the UCSC Xena Browser (https://xenabrowser.net/). Somatic mutation data

TABLE 1 | Clinical information of NSCLC patients.

Covariate	Type	TCGA set (n = 975)	Training set (n = 683)	Testing set (n = 292)<	*p*-value[a]
Gender	Male	584 (59.9%)	417 (61.05%)	167 (57.19%)	0.2597
	Female	391 (40.1%)	266 (38.95%)	125 (42.81%)	
Age (years)	>60	698 (71.59%)	489 (71.60%)	209 (52.74%)	0.9574
	≤60	262 (26.87%)	184 (26.93%)	78 (45.55%)	
	NA	15 (1.54%)	10 (1.46%)	5 (1.71%)	
Tumor stage	Stage I-II	772 (79.18%)	541 (79.21%)	231 (79.11%)	0.8944
	Stage III-IV	192 (19.69%)	135 (19.76%)	57 (19.52%)	
	Unknown	11 (1.13%)	7 (1.02%)	4 (1.37%)	
Pathologic M	M0	723 (74.15%)	517 (75.7%)	206 (70.55%)	0.1359
	M1	31 (3.18)	23 (3.37%)	8 (2.74%)	
	MX	221 (22.67%)	143 (20.93%)	78 (26.71%)	
Pathologic N	N0	626 (64.21%)	441 (64.57%)	185 (63.36%)	0.2510
	N1-3	333 (34.15%)	228 (33.38%)	105 (35.96%)	
	NX	16 (1.64%)	14 (2.05%)	2 (0.68%)	
Pathologic T	T1-2	821 (84.21%)	571 (83.6)	250 (85.62%)	0.4256
	T3-4	151 (15.49%)	109 (15.96%)	42 (14.38%)	
	TX	3 (0.31%)	3 (0.44%)	0 (0%)	

[a]*Chi-squared test,* p < *0.05 means significantly different.*

were downloaded from TCGA database (https://portal.gdc.cancer.gov/). Counts data were used for the transcriptome data, and the muTect version was used for the somatic mutation data. The human gtf file containing the gene symbol was downloaded from the Ensembl database (Homo_sapiens.GRCh38.99.gtf.gz; http://www.ensembl.org). Transcriptomic, somatic mutation data, and clinical information were matched according to the sample name, and samples with missing data were excluded. Finally, 975 complete samples including gene expression, mutation, patient's survival, and other clinical variables were obtained. The mRNAs and lncRNAs of 975 samples were annotated based on the gtf file containing the gene symbol. Then, these samples were randomly distributed into training and testing sets at a ratio of 7:3 using the "caret" package in R. The training set of 683 patients was used to identify the GIRlncSig and construct the prognostic risk model. The testing set of 292 patients was used to validate the performance of our risk model. The clinical information of NSCLC patients is summarized in **Table 1**.

Identification of GIRlncRNAs

The lncRNA expression profile and somatic mutation pattern of 975 patients were combined to identify GIRlncRNAs by a mutator hypothesis-derived computational frame (Bao et al., 2020) (**Supplementary Figure S2**). Briefly, NSCLC patients were ranked in increasing order according to the cumulative number of somatic mutations. The top 25% of patients with low mutation frequency were designated as the genomic stable (GS) group, and the last 25% of patients with high mutation frequency were designated as genomic unstable (GU) group. LncRNA expression profiles between the two groups were compared, and a volcano plot was made using the "edgeR" package in R. Differentially expressed (DE) lncRNAs (|Fold Change| > 1.0 and adjusted $p < 0.05$) were defined as GIRlncRNAs, and their expression levels were normalized to all patients.

Co-Expression Network, GO and KEGG Enrichments, and Alternative Splicing Analysis

The mRNA-interacting GIRlncRNAs were extracted from the RNAInter database (http://www.rna-society.org/rnainter/). Then, the co-expression network of mRNA-interacting GIRlncRNAs was visualized by Cytoscape (V3.7.2) (Chin et al., 2014). To explore the biological function of GIRlncRNAs, GO functional enrichment and KEGG pathway analyses were performed using the "clusterProfiler," "org.Hs.eg.db," "enrichplot," and "ggplot2" packages in R. Statistical significance was considered with adjusted p-value < 0.05. To determine the AS events associated with GIRlncRNAs, AS data of NSCLC were downloaded from LncAS2Cancer database (https://lncrna2as.cd120.com/), and integrated with corresponding GIRlncRNAs. Statistical histogram and Upset plot were drawn using "ggplot2" and "UpSetR" packages in R, respectively.

Hierarchical Cluster Analysis

The normalized DE-lncRNAs from 975 samples were collected for hierarchical cluster analysis using the pam method, and the spearman distances were calculated using the "ConsensusClusterPlus" package in R. All samples were divided into two clusters based on the spearman distances. One cluster with low mutation counts was assigned as GS-like subtype. The other with high mutation counts were defined as GU-like subtype (Mann–Whitney U test, $p < 0.05$). Finally, Kaplan–Meier survival curves and the expression heatmap of DE-lncRNAs in the two subtypes were plotted using "survival," "survminer," and "ComplexHeatmap" packages in R.

GIRlncRNA-Clustered Molecular Subtype and Characteristic Analyses

To estimate the differential mutation frequency between GS and GU-like subtypes of NSCLC patients, driver genes from Cancer

Gene Census (CGC) catalog in the COSMIC database (https://cancer.sanger.ac.uk/census) were downloaded. Fifty-four driver genes with corresponding MAF files were extracted and determined their mutation frequency. The landscape of mutation frequency was drawn using the "maftools" package in R. Furthermore, the differential expression of driver genes from two NSCLC subtypes was analyzed using "edgeR" package in R. The cutoff criteria were |log2 FC|>1 and adjusted $p < 0.05$. The Wilcoxon test was used to analyze the differentially expressed GIRlncRNAs. Moreover, the immune, stromal, and ESTIMATE scores for the two NSCLC subtypes were determined by the "estimate" package in R. In addition, tumor mutation burden (TMB) data were downloaded from TCGA database (https://gdc.cancer.gov/) and TMB scoring for the two NSCLC subtypes was performed. Finally, the scores for the mRNA expression-based stemness index (mRNAsi) were calculated, and NSCLC patients were stratified into different molecular subtypes by referring to the matrix in Malta et al. (2018). Boxplots for GS- and GU-like groups were drawn using the "ggpubr" package in R (Student t-test, adjusted $p<0.05$).

Identification of GIRlncSig and Performance Evaluation

To estimate the correlation of GIRlncRNA expression with overall survival (OS) of NSCLC patients, a univariate Cox proportional hazards regression analysis was performed in the training set by using "survival" and "survminer" packages in R. The candidate GIRlncRNAs were screened with $p < 0.01$. Then, the least absolute shrinkage and selection operation (LASSO) Cox regression analysis was carried out to identify the GIRlncRNAs with the most robust prognostic values. Finally, the resulting GIRlncRNAs were collected to construct a GIRlncSig based on the weighted expression level and coefficient (coef) from LASSO regression analysis. The risk score formula for GIRlncRNAs was calculated as follows:

$$\text{GIRlncSig Risk Score}_i = \sum_{j=1}^{n} \exp_{ji} \times \beta_j.$$

The "*exp*" and "*β*" represent the expression level and coefficient of each prognostic lncRNA, respectively. GIRlncSig risk score represents the sum of expression level of each prognostic lncRNA multiplied by the coef of corresponding GIRlncSig. *i* represents the sample, and *j* represents the prognostic lncRNA. Based on the risk score for all samples, high and low-risk patients were then recognized by using the median value as the cut-off point. Evaluation analyses, including the Kaplan–Meier survival curve, receiver operating characteristic curve (ROC), risk distribution, survival status of all patients, and heatmap of selected GIRlncSig expression profile were applied to test the predication performance of our risk model in training, testing, and TCGA sets.

Independent Prognostic and Clinical Stratification Analysis

To test whether the GIRlncSig risk score could be potentiated as a prognostic factor independently from other clinical variables (age, gender, and tumor stage), univariate and multivariate Cox regression analyses (UCRA and MCRA) were performed. All variables with independent prognostic values were selected from TCGA database when their *p*-values were less than 0.05. To test the prognostic stability of GIRlncSig scoring, a clinical stratification analysis was conducted. Patients were first divided into subgroups according to clinical variables, including age (≤60 and >60), gender (female and male), pathologic T (T1-T2 and T3-T4), and tumor stage (I-II and III-IV). Second, patients in each subgroup were ranked according to their GIRlncSig risk score, and assigned to high or low-risk subgroups by referring to the median value. Finally, the survival difference between high and low-risk subgroups was calculated (log-rank test, $p < 0.05$).

Correlation Analysis Between GIRlncSig and Drive Genes or the Microenvironment

Expression profiles of GIRlncSig and driver genes of NSCLC were extracted, and their correlation was calculated using "ggplot2" and "ggpubr" packages in R. The cutoff criteria were $R > 0.3$ and $p < 0.05$, respectively. Correlation between GIRlncSig score and immune, or stromal, or ESTIMATE, or mRNAsi or TMB scores were further calculated ($p < 0.05$).

Immune Cell Infiltration, Checkpoint Inhibitor-Related Genes, and Therapeutic Response

The mRNA expression matrix of each patient was converted to 22 types of immune cell matrix with cutoff criteria of $p < 0.05$. Tumor-infiltrating immune cells include naive B cells, memory B cells, plasma cells, $CD8^+$ T cells, naive $CD4^+$ T cells, resting memory $CD4^+$ T cells, activated memory $CD4^+$ T cells, follicular helper T cells, regulatory T cells (Tregs), gamma delta T cells, resting dendritic cells, activated dendritic cells, monocytes, macrophages M0, M1, M2, resting natural killer (NK) cells, activated NK cells, resting mast cells, activated mast cells, eosinophils, and neutrophils. Based on their association with clinical outcomes, NSCLC patients were classified into high- and low-risk groups using the Cell type Identification by Estimating Relative Subsets of RNA Transcript (CIBERSORT) algorithm (Chen et al., 2018). The type and distribution of infiltrating immune cells were analyzed by "ggplot2" package in R, and presented as barplots and boxplots. Subsequently, we analyzed the expression profile of immune checkpoint inhibitor genes in high and low-risk groups. A significant difference was determined by using the Wilcoxon test with *p*-value < 0.05. Based on the functional enrichment of gene expression, SubMap module from GenePattern was used to map and merge two datasets with different traits. This module can eliminate the batch effect and predict the possible traits that are not included in the original dataset. To predict the therapeutic response by checkpoint inhibitor blocking, SubMap module was used to map the high and low-risk groups based on the therapeutic information. Prediction of the response to CTLA4 and PD1 inhibitors was particularly studied in high and low-risk NSCLC patients. The

p-value was corrected by Bonferroni to increase the predictive sensitivity. Finally, we used R package "pRRophetic" to predict chemotherapeutic responses of each sample based on the genomics of drug sensitivity in the cancer (GDSC) database. The half-maximal inhibitory concentration (IC50) of each sample was calculated using ridge regression ($p < 0.001$). The Spearman correlation (Cor) between the RS score and IC50 to particular drugs was calculated and the significant correlations were cutoff with $|\text{Cor}| > 0.1$ and $p < 0.001$.

Gene Set Variation Analysis in High and Low-Risk Groups

GSVA analysis was conducted to reveal the differential pathways between high and low-risk patients. Functional enrichment analysis was conducted based on the distinct GIRlncSig patterns extracted from KEGG and MSigDB database using "GSVA" package in R. Significant differential signal pathways between high and low-risk groups were extracted by "limma" package with the threshold for adjusted $p < 0.05$ and $|\log FC| > 0.1$. Visualized heatmap of KEGG pathway was plotted using "ComplexHeatmap" package in R.

Construction and Validation of the Nomogram Score System

To develop a nomogram score system for NSCLC patients, MCRA was performed to extract the powerful OS predictors. To visualize the results of Cox regression and predict the survival of NSCLC patients, the prognostic nomogram was plotted by using "rms" and "survival" packages in R. First, the Cox proportional hazards regression model was constructed by using the cph () function, and the survival () function was used to calculate the survival probability. Finally, the nomogram () function was used to create the nomogram, time-dependent ROC, and calibration curves of OS. The predictive performance of the nomogram was validated by calibration curves, ROC, and decision curve analysis (DCA). The area under curves (AUCs) of the nomogram for predicting 1-, 3-, 5-, and 10-year OS of NSCLC patients were plotted.

Statistical Analyses

The chi-squared test, Student's t-test, Wilcoxon test, and Mann–Whitney U-test were employed to examine the differential variables from datasets or groups. Statistical significance was considered as $p < 0.05$. R (version 3.6.3) was used to perform all statistical analyses, and the results were visualized by corresponding functional packages.

RESULTS

Identification of GIRlncRNAs for NSCLC Patients

Following TCGA data collection, annotation, and preprocessing, 975 samples were obtained. These samples were subsequently ranked by their gene mutation counts. The top 25% samples ($n = 244$) with a low mutation frequency were designated as the GS group, and the last 25% samples ($n = 244$) with a high mutation frequency were designated as the GU group (**Supplementary Figure S2**; **Supplementary Table S1**). A total of 1,446 DE-lncRNAs between these two groups were identified from an expression matrix containing 10,480 lncRNAs ($|\log2\ FC| > 1$, FDR adjusted $p < 0.05$), among which 1138 lncRNAs were upregulated and 308 lncRNAs were downregulated (**Figure 1A**; **Supplementary Table S2**). Based on the expression profile of these DE-lncRNAs, all samples were clustered under an unsupervised hierarchical clustering analysis by "ConsumusClusterPlus" package. Two clusters were obtained as shown in the heatmap (**Figure 1B**; **Supplementary Table S3**). The resulting subtypes were positively correlated with the mutation frequency ($R = 1.22$; $p = 0.0001$) and the mutation frequency in cluster 2 was significantly higher than that in cluster 1 (**Figure 1C**). Therefore, cluster 1 and cluster 2 were named as GS and GU-like subtypes, respectively. As shown by the heatmap of DE-lncRNAs, a significant expression difference was observed between these two subtypes (**Figure 1D**). These results identified 1,446 lncRNAs as candidates for GIRlncRNAs of NSCLC.

Further analyses found that 60 candidate GIRlncRNAs can undergo AS events, of which all DE-lncRNAs contained skipped exon (SE), and 26 DE-lncRNAs contained mutually exclusive exons (MXE) (**Figure 1E**; **Supplementary Figure S3**; **Supplementary Table S4**). Co-expression network analyzing the interaction of DE-lncRNA with mRNA resulted in 4912 interaction pairs (**Figure 1F**; **Supplementary Table S5**), among which 3,802 (77.4%) mRNAs and 334 (6.8%) mRNAs were respectively interacting with lncRNA FENDRR and BANCR. It was also found that 38 and 5 lncRNAs were, respectively, interacting with mRNA AR and TNPO2 (**Supplementary Table S6**). GO enrichment and KEGG pathway analyses showed that these mRNA-interacting GIRlncRNAs were significantly enriched in a nucleoside or ribonucleoside binding, nuclear membranes enveloping, cell-cycle checkpoint, tumorigenesis, and virus infection signaling pathways (**Figures 1G–J**; **Supplementary Tables S7, S8)**. These results suggested that the identified mRNA-interacting GIRlncRNAs may be essential for regulating genomic stability.

Characteristics of GIRlncRNA-Clustered Molecular Subtypes in NSCLC Patients

Investigating the mutation profile of driver genes showed that GU-like subtype patients exhibited higher mutation frequency than that in GS-like subtype patients. Being the most frequent mutation genes in NSCLC, TP53 and CSMD3 were mutated in 81% and 48% of GU-like subtype patients, respectively. However, these two gene mutations only occurred respectively in 51% and 37% of GS-like subtype patients (**Figures 2A,B**). Further expression analysis of 54 driver genes showed that 16 genes were differentially expressed between GS and GU-like subtypes, among which nine genes were upregulated and seven

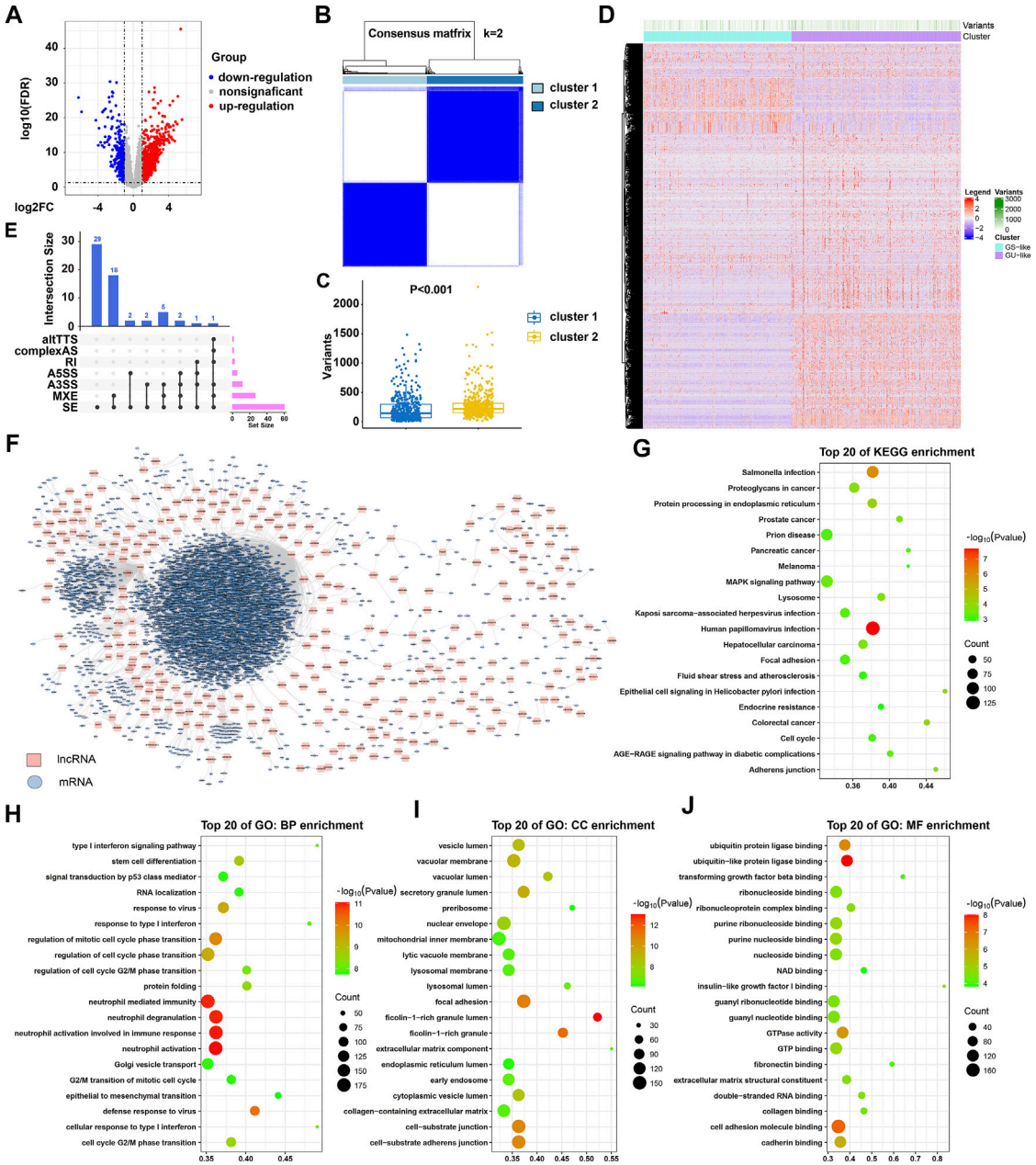

FIGURE 1 | Identification and functional analysis of GIRlncRNAs for NSCLC patients. **(A)** Volcano plot of the GIRlncRNA distribution. 1,446 DE-lncRNAs between the GU group (n = 244) and GS group (n = 244) are shown. **(B)** Unsupervised clustering of 975 NSCLC patients according to the expression pattern of identified GIRlncRNAs. Cluster 1, light blue box. Cluster 2, dark blue box. **(C)** Mutation frequency analysis of DE-lncRNAs in two clusters derived from unsupervised clustering analyses. Cluster 1, blue scatterplot. Cluster 2, orange scatterplot. **(D)** Expression heatmap of DE-lncRNAs from 975 NSCLC patients. Subtype classification was performed by unsupervised hierarchical clustering analysis. Cluster 1 (cyan box) is designated as the GS-like group, and cluster 2 (orchid box) is designated as the GU-like group. **(E)** Upset plotting the statistical AS events of 60 DE-lncRNAs. **(F)** Co-expression network of mRNA-interacting GIRlncRNAs based on Pearson correlation coefficient. **(G)** Enriched KEGG pathways for the mRNA-interacting GIRlncRNAs. **(H–J)** Enriched GO pathways for the mRNA-interacting GIRlncRNAs in three parts: BP **(H)**, CC **(I)**, and MF **(J)**.

genes were downregulated in GU-like patients (**Figure 2C**). Tumor microenvironment scoring results showed that the immune, stromal and ESTIMATE scores in GU-like subtypes were significantly lower than those in GS-like subtypes (**Figures 2D–F**). Further analysis of NSCLC tumor characteristics showed that TMB and mRNAsi scores in GU-like subtypes were significantly higher than those in GS-like subtypes (**Figures 2G,H**). Moreover, Kaplan–Meier survival analysis showed that the survival of GS-like patients was significantly better than that of GU-like patients (**Figure 2I**). These data indicated that NSCLC

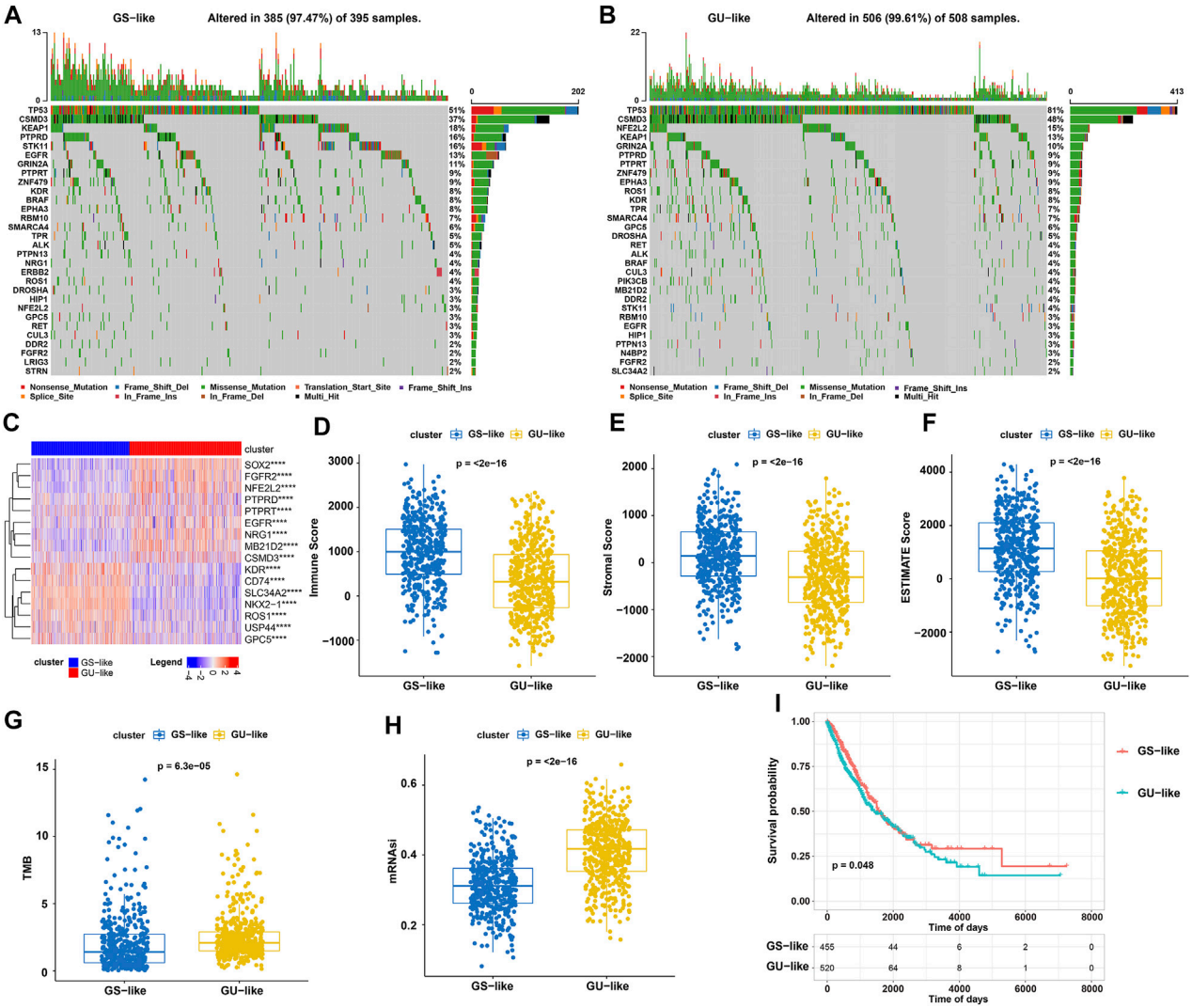

FIGURE 2 | Mutation and expression landscapes of driver genes, tumor microenvironment assessment, and Kaplan–Meier survival analyses. **(A,B)** Mutation frequency of 54 driver genes (top 30) in 395 GS-like **(A)** and 508 GU-like **(B)** NSCLC patients. Each column represents an individual patient. The upper barplot indicates TMB, and the number on the right indicates the mutation frequency for each regulator. The right barplot shows the proportion of each variant type. **(C)** Expression landscape of 17 driver genes differently expressed between GS and GU-like patients. **(D–H)** Immune **(D)**, stromal **(E)**, and ESTIMATE **(F)** score and TMB **(G)** and mRNAsi **(H)** analyses in GS and GU-like groups. **(I)** Survival analysis of GS and GU-like groups of NSCLC patients.

patients with the GU-like molecular subtype have more aggressive tumors than those with GS-like molecular subtypes.

Identification and Evaluation of GIRlncSig for NSCLC Patients

Univariate Cox proportional hazards regression analysis showed that the expressions of 23 GIRlncRNAs were significantly associated with OS of NSCLC patients in our training set ($p < 0.01$ **Figure 3A**; **Supplementary Table S9**). LASSO regression analysis was performed to identify the GIRlncRNAs with more significant associations ($p < 0.05$). When the partial likelihood deviation reached to the minimum (Log Lambda = −4.4), 19 GIRlncRNAs were screened out and used to construct a risk model for survival prediction (**Figures 3B,C**; **Supplementary Table S10**). To assess the prognostic risk of NSCLC patients, a GIRlncSig was created based on the expression level of 19 GIRlncRNAs and the coefficients from LASSO analysis. GIRlncSig score = LINC01067* (−0.1595) + AC012645.1 * (−0.1235) + AL512604.3 * (−0.0989) + AC008278.2 * (−0.0921) + AC089998.1 * (−0.0401) + AC023824.3 * 0.0050 + AC013287.1 * 0.0073 + AP000829.1 * 0.0159 + LINC01611 * 0.0177 + AC097451.1 * 0.0197 + AC025419.1 * 0.0270 + AC079949.2 * 0.0369 + LINC01600 + 0.0474 + AC004862.1 * 0.0518 + AC021594.1 * 0.0623 + (MYRF–AS1) * 0.0851 + LINC02434 * 0.0858 + LINC02412 * 0.1049 + LINC00337 * 0.1143. In the formula of GIRlncSig, 14 GIRlncRNAs (AC023824.3, AC013287.1, AP000829.1,

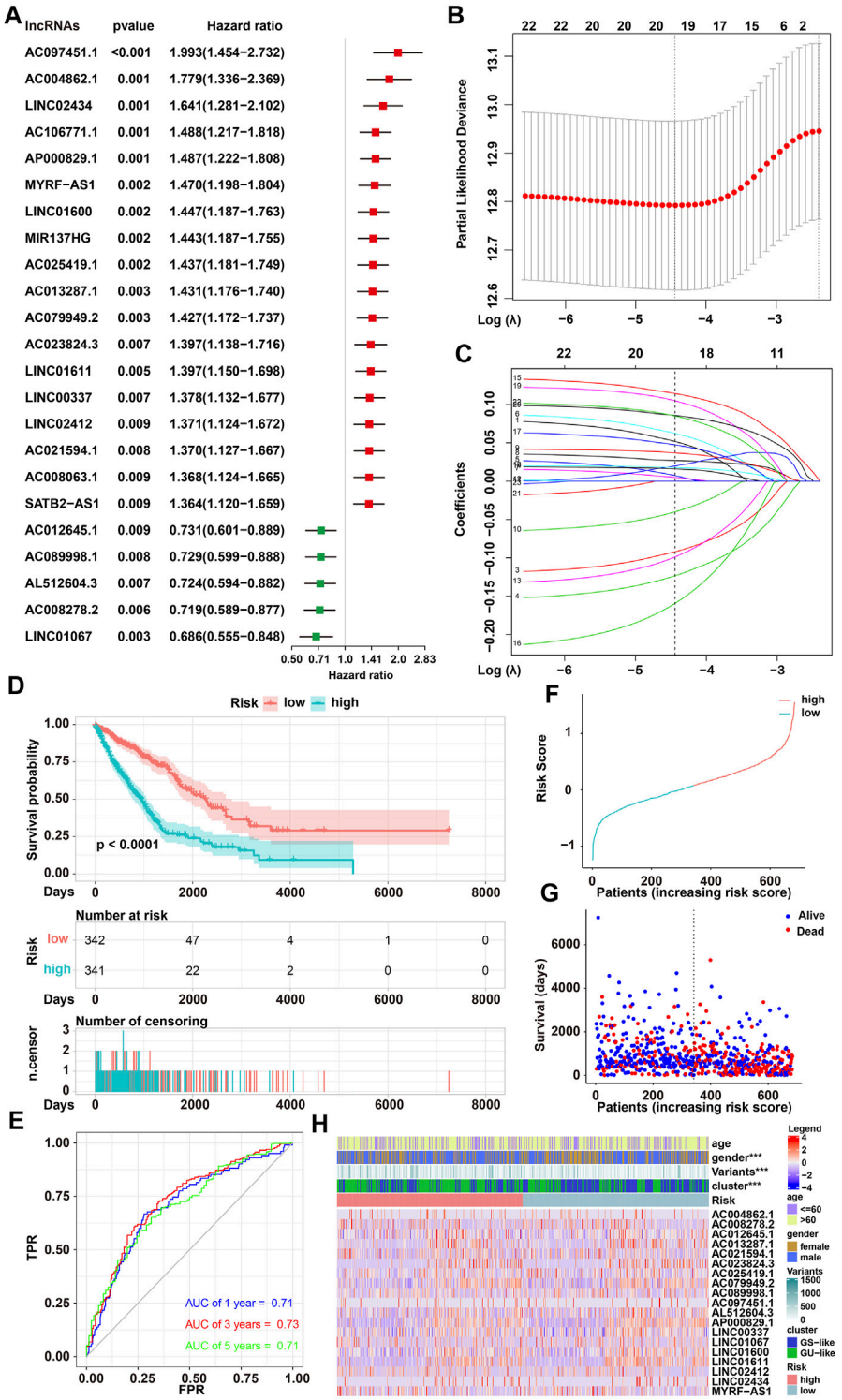

FIGURE 3 | Identification of the GIRlncSig and its predictive performance in a training set. **(A)** Forest plot of OS-associated GIRlncRNAs based on the univariate Cox proportional hazards regression analysis. Five GIRlncRNAs acted as protective risk factors for patients' survival (green), while 18 GIRlncRNAs acted as prognostic risk factors (red). **(B)** Distribution plot of partial likelihood deviation based on LASSO regression analysis. Nineteen GIRlncRNAs were selected when log lambda was equal to −4.4 (the minimum). **(C)** Distribution plot of LASSO coefficient (log lambda = −4.4). **(D)** Kaplan–Meier survival curves of low and high-risk NSCLC patients predicted by the GIRlncSig (log-rank test, $p < 0.0001$). **(E)** ROC of NSCLC patients at 1, 3, or 5 years predicted by GIRlncSig. **(F,G)** Risk distribution **(F)** and survival status **(G)** of NSCLC patients. **(H)** Expression heatmap of selected GIRlncRNAs.

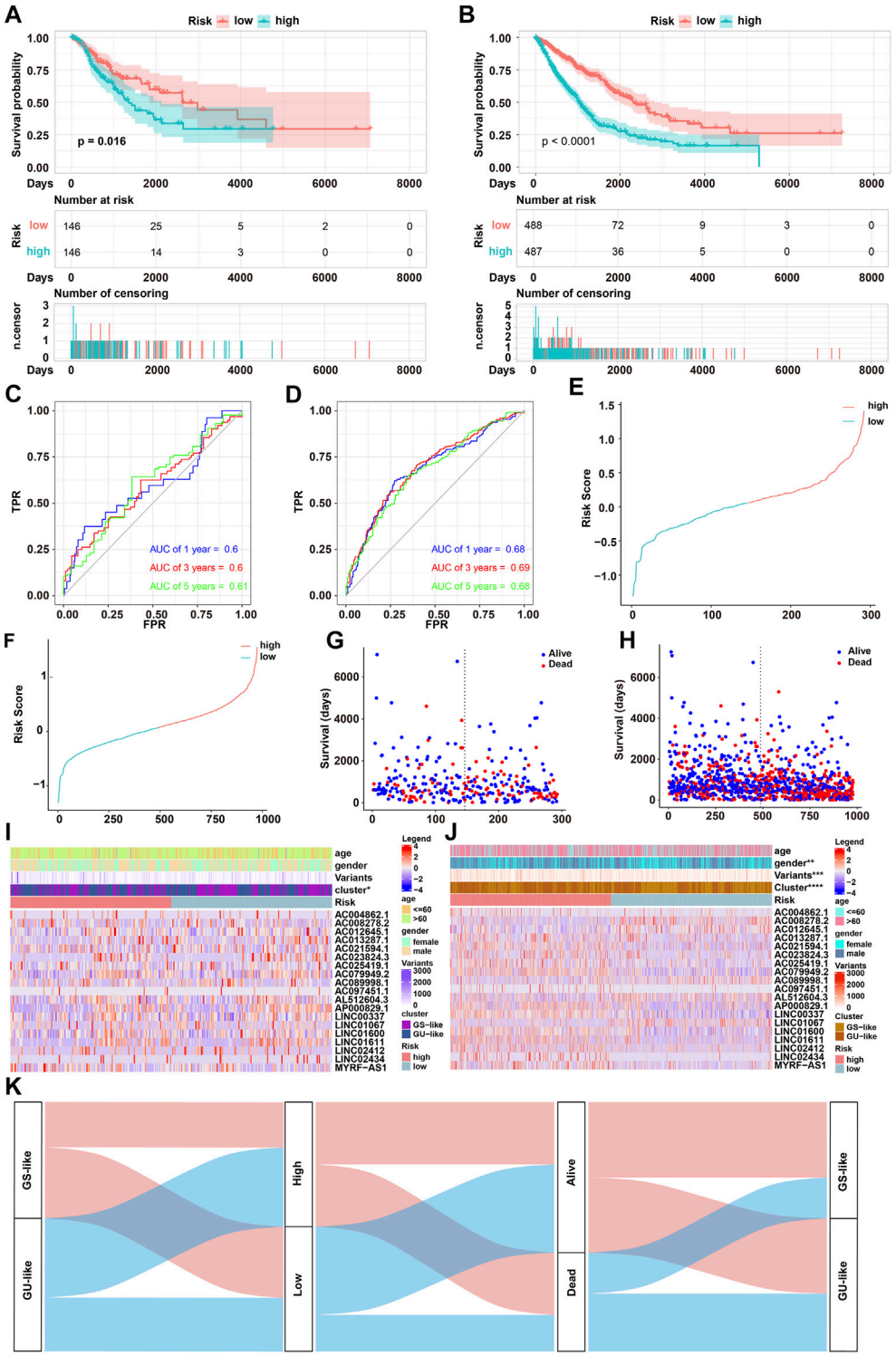

FIGURE 4 | Performance evaluation of GIRlncSig in testing and TCGA sets. **(A,B)** Kaplan–Meier survival curves of GIRlncSig-predicted low- or high-risk NSCLC patients in testing [**(A)**, log-rank test; $p < 0.05$] and TCGA [**(B)**, log-rank test, $p < 0.0001$] sets. **(C,D)** ROC of 1-, 3-, or 5- year survival predicted by GIRlncSig in testing **(C)** and TCGA **(D)** sets. **(E–J)** Risk distribution, survival status of patients, and the expression profile of GIRlncSig in testing **(E**,**G**,**I)** and TCGA **(F**,**H**,**J)** sets. **(K)** Sankey diagram for the distribution of NSCLC patients in GS or GU-like groups, low or high-risk groups, and dead or alive groups.

LINC01611, AC097451.1, AC025419.1, AC079949.2, LINC01600, AC004862.1, AC021594.1, MYRF–AS1, LINC02434, LINC02412, and LINC00337) with positive coefficients were designated as risk factors. In contrast, five lncRNAs (LINC01067, AC012645.1, AL512604.3, AC008278.2, and AC089998.1) with negative coefficients were designated as protective factors. Either upregulated expression of prognostic GIRlncRNAs or downregulated expression of protective GIRlncRNAs was significantly related to decreased OS of NSCLC patients. Based on the GIRlncSig score (cutoff = 0.075), 341 patients with a high score were classified into a high-risk group, and 342 patients with a low score were classified into a low-risk group (**Supplementary Table S11**). Kaplan–Meier survival analysis showed that the survival of low-risk NSCLC patients was significantly better than that in high-risk patients ($p < 0.0001$, log-rank test; **Figure 3D**). The AUCs of time-dependent ROC in the training set were 0.71, 0.73, 0.71 for 1-, 3-, 5-year survival, respectively, as predicted by GIRlncSig (**Figure 3E**). Finally, the risk distribution and survival status of NSCLC patients together with the expression heatmap of 19 GIRlncRNAs in the training set were plotted (**Figures 3F–H**). The results showed that high-risk-scored patients with such a GIRlncSig were mainly derived from the GU-like group and exhibited shorter survival. All these results strongly supported the utility and effectiveness of our GIRlncSig in predicting NSCLC prognosis.

To evaluate the robustness of our GIRlncSig, its prognostic performance in two independent data sets was further tested. A total of 392 NSCLC patients from the testing set and 975 NSCLC patients from the TCGA set were classified into high- and low-risk groups based on the GIRlncRNA risk score (**Supplementary Table S11**). Kaplan–Meier survival curves in the testing set ($p < 0.016$, **Figure 4A**) and entire TCGA set ($p < 0.0001$, **Figure 4B**) showed that patients from the low-risk group had better survival outcomes than patients from the high-risk group. The AUCs of time-dependent ROC in the testing set were 0.6, 0.6, and 0.61 for the 1-, 3-, and 5-year survival predicted by the GIRlncSig, respectively (**Figure 4C**). Similar results were obtained in TCGA set, where the AUCs of ROC were overall approximately 0.7 (**Figure 4D**). Furthermore, risk distribution, and survival of patients together with GIRlncSig expression heatmap in both sets showed that high-risk scored patients were mainly derived from the GU-like group and exhibited shorter survival (**Figures 4E–J**). Additionally, the Sankey diagram also showed that high-risk patients accounted for a higher proportion of mortality in the GU-like group, while these patients accounted for a less proportion of mortality in the GS-like group (**Figure 4K**). Together, these results further support that our GIRlncSig can predict the prognosis of NSCLC patients.

Correlation of GIRlncSig With the Aggressiveness of NSCLC

Since GIRlncSig possessed a robust prognostic performance, the correlation analysis between identified GIRlncRNAs and differentially expressed driver genes was further performed. Three positively correlated regulatory pairs (AC008278.2 and PTPRT, AP000829.1 and MB21D2, LINC01600 and MB21D2) were screened out by Pearson correlation analysis ($R > 0.3$ and $p < 0.05$) (**Figures 5A–C**; **Supplementary Table S12**). The expression patterns of these correlated pairs were consistent in high- and low-risk groups (**Figures 5D–F**). To determine the relationship of GIRlncSig with tumor microenvironment characteristics, Pearson correlation coefficients between GIRlncSig risk score and immune, or stromal, or ESTIMATES, or mRNAsi, or TMB scores were calculated separately. The results of correlation analysis showed that GIRlncSig-based risk scores were positively correlated with all characteristics of the tumor microenvironment (**Figures 5G–K**). Notably, the strongest correlation of the risk score with TMB was observed ($R = 0.135$; **Figure 5K**). Further correlation analyses between the GIRlncSig and infiltrating immune cells were performed. Although the resulted NSCLC-infiltrated immune cell types were different depending on algorithms, similar trends of cell distribution were as follows: high infiltrating level of B cell (especially memory B cell) and T cell (especially $CD4^+$ and $CD8^+$ memory T cells) populations were positively associated with the expression of five protective lncRNAs. By contrast, infiltrating B and T cells presented an opposite association trend for fourteen risk lncRNAs (**Supplementary Figures S4–S10**). High infiltrating levels of macrophages (especially M1 and M2), neutrophils, monocytes, and myeloid dendritic cells were positively associated with the expression of protective lncRNAs but negatively associated with the expression of risk lncRNAs (**Supplementary Figures S4–S10**). These results suggested that GIRlncSig was significantly correlated with the malignancy of NSCLC.

Risk Stratification of NSCLC Patients With GIRlncSig Score and Clinical Variables

To validate the stability of our score model, a risk stratification analysis was conducted to determine the prognostic performance of GIRlncSig. NSCLC patients were first grouped based on their clinical parameters, then stratified into subgroups by GIRlncSig-derived risk score. Kaplan–Meier survival analyses showed that patients with low-risk scores had better survival outcomes than those with high-risk scores in all stratified subgroups ($p < 0.05$; **Figures 6A–H**). The distribution of risk scores for all stratified subgroups, including age, gender, pathologic M, pathologic N, pathologic T, tumor stage, and GS/GU-like groups, was further determined. No difference in the distribution of risk score between young and old NSCLC patients was observed ($p < 0.05$; **Figure 6I**). However, the risk score distribution of male patients was significantly higher than that of female patients ($p < 0.05$; **Figure 6J**), and the risk score distribution of the GU-like group was significantly higher than that in the GS-like group ($p < 0.05$; **Figure 6O**). For the groups of pathologic N, T, and tumor stage but not pathologic M, the risk score for the primary stage was always low. Interestingly, higher risk scores were frequently observed in patients with advanced stage ($p < 0.05$; **Figures 6K–N**). These results highlight the stability of our GIRlncSig-based risk score model.

Therapeutic Evaluation of NSCLC Patients by the GIRlncSig Score

The abundance of tumor-infiltrating immune cells and the expression profile of immune checkpoint genes have a strong impact on tumor treatment, so we carried out immune cell

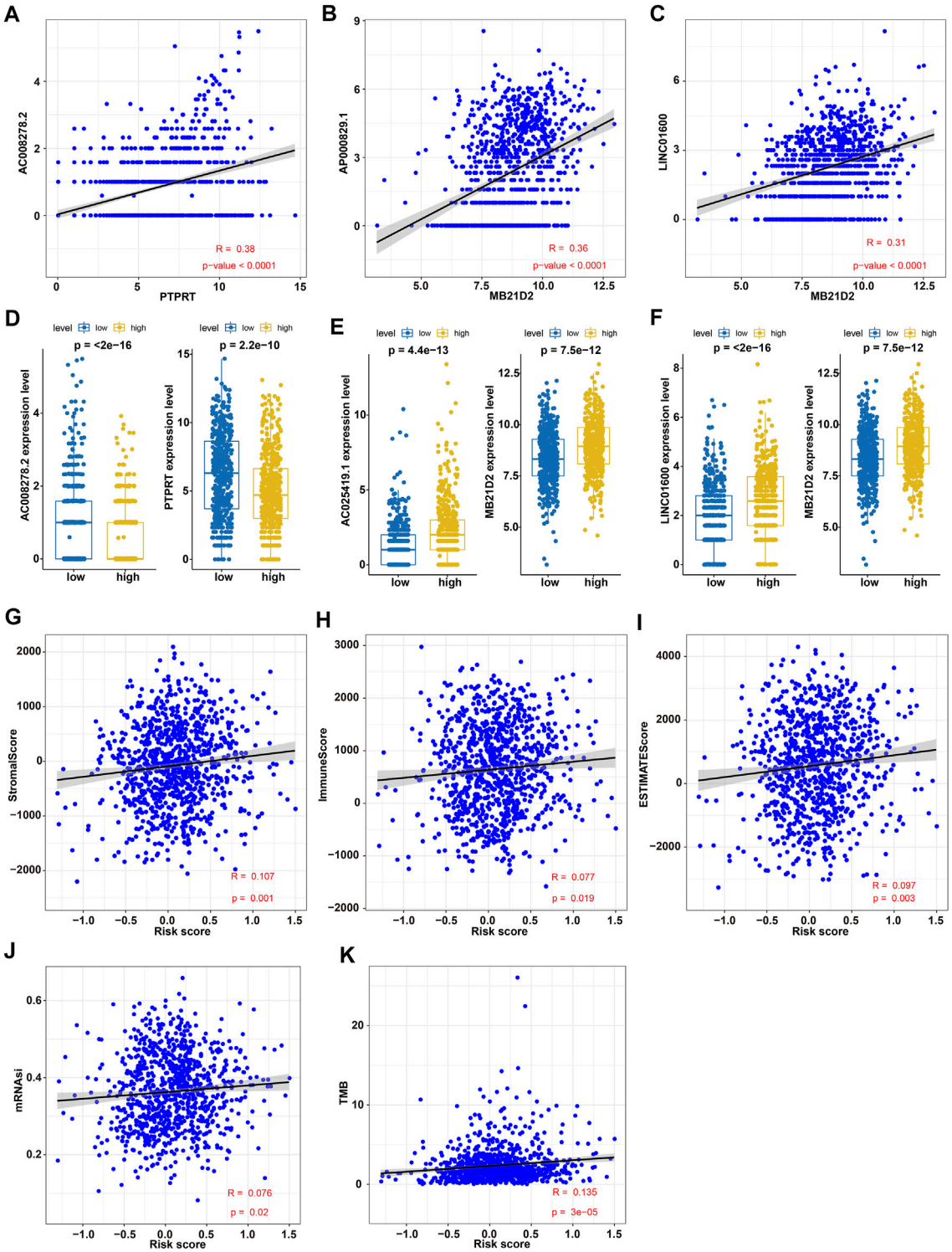

FIGURE 5 | Correlation analyses between GIRlncSig and malignant characteristics of NSCLC. **(A–C)** Pearson correlation analysis of GIRlncRNA-driver gene regulatory pairs: AC008278.2 and PTPRT **(A)**, AP000829.1 and MB21D2 **(B)**, LINC01600 and MB21D2 **(C)**; **(D–F)** Differential expression analysis of correlated regulatory pairs in different risk groups: AC008278.2 and PTPRT **(D)**, AP000829.1 and MB21D2 **(E)**, and LINC01600 and MB21D2 **(F)**. **(G–K)** Pearson correlation analysis between the risk score and immune score **(G)**, stromal score **(H)**, ESTIMATE score **(I)**, mRNAsi score **(J)**, or TMB score **(K)** in NSCLC patients.

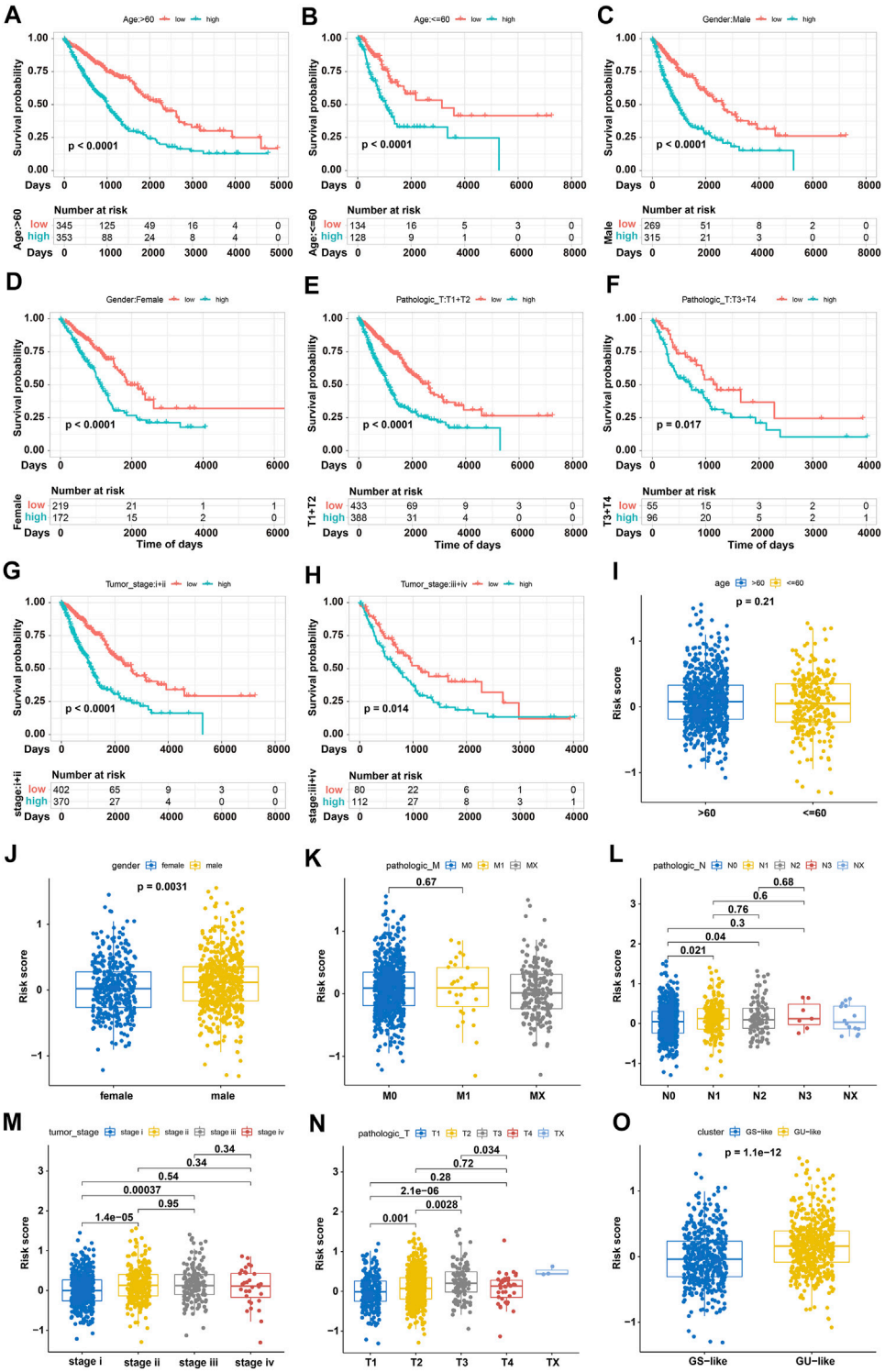

FIGURE 6 | Risk stratification analyses based on GIRlncSig score and clinical variables. **(A–H)** Kaplan–Meier survival curves of high and low-risk subgroups for old **(A)**, young **(B)**, male **(C)**, female **(D)**, T1-2 stage **(E)**, T3-4 stage **(F)**, stage I-II **(G)**, and stage III-IV **(H)** patients. **(I–N)** Boxplots showing GIRlncSig-derived risk scores stratified by age **(I)**, gender **(J)**, and pathologic M **(K)**, N **(L)**, T **(M)**, and tumor stage **(N)** in NSCLC patients. **(O)** Boxplot of GIRlncSig-derived risk scores in GS- and GU-like NSCLC groups.

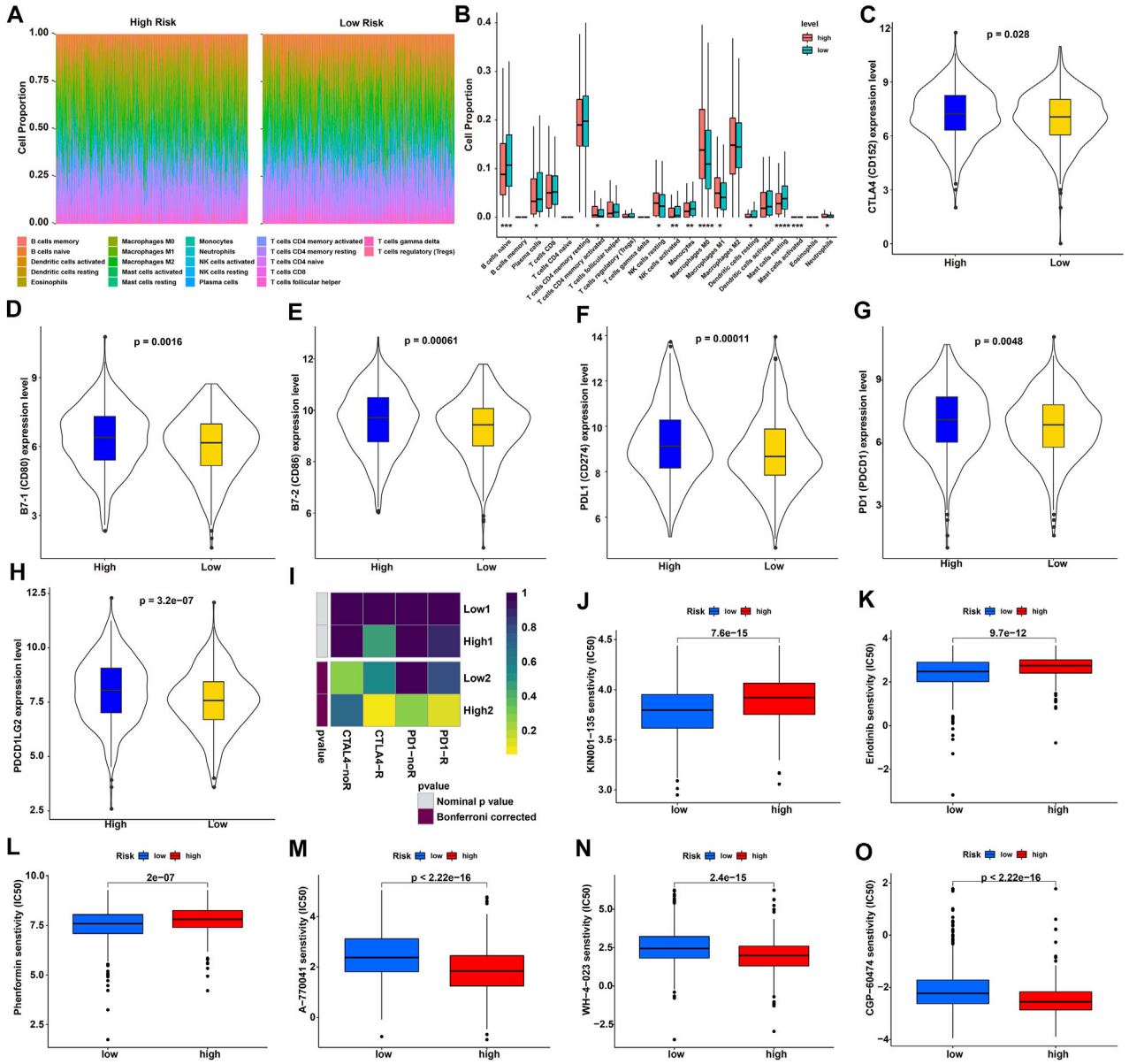

FIGURE 7 | Immune evaluation and drug resistance analyses in high- and low-risk groups of NSCLC patients. **(A)** Distribution of 22 types of immune cells in high- and low-risk groups of NSCLC patients. **(B)** Boxplot of differentially infiltrated immune cells in high- and low-risk groups of NSCLC patients ($p < 0.05$). **(C–H)** Violin plot of the differentially expressed checkpoint genes in high- and low-risk NSCLC patients. **(I)** Immunotherapy response predicted for high- and low-risk NSCLC patients by SubMap module. **(J-O)** Chemotherapeutic sensitivity predicted for high- and low-risk NSCLC patients by the pRRophetic package.

infiltration analysis with the CIBERSORT algorithm to evaluate our GIRlncSig. Abundance ratios and differential boxplots of 22 types of immune cells in high and low-risk NSCLC patients were plotted (**Figure 7A**; **Supplementary Table S13**). The abundance ratios of infiltrated M0, M1 macrophages, and resting NK cells in the high-risk score group were significantly higher than those in low-risk score group. However, naive B cells, plasma cells, monocytes, and resting mast cells in the high-risk score group were remarkably lower than those in the low-risk score group (**Figure 7B**). Subsequently, the expression profile of immune checkpoint genes, CTLA4 (CD152), B7-1 (CD80), B7-2 (CD86), PDL1 (CD274), PD1 (PDCD1) and PDL2 (PDCD1LG2), in high and low-risk groups was further analyzed (**Figures 7C–H**). The violin plots showed a significant difference in the expression levels of CTLA4, CD80, CD86, CD274, PDCD1, and PDCD1LG2 between low and high-risk groups (**Figures 7C–H**). Therefore, the SubMap module in GenePattern database was further employed to predict the risk score effect on immunotherapy of NSCLC patients. Results of the corrected Bonferroni analysis suggested that the patients in the high-risk group were slightly more sensitive to CTLA4 and PD1 inhibitors than those in the low-risk group (p = 0.0619 and 0.0739;

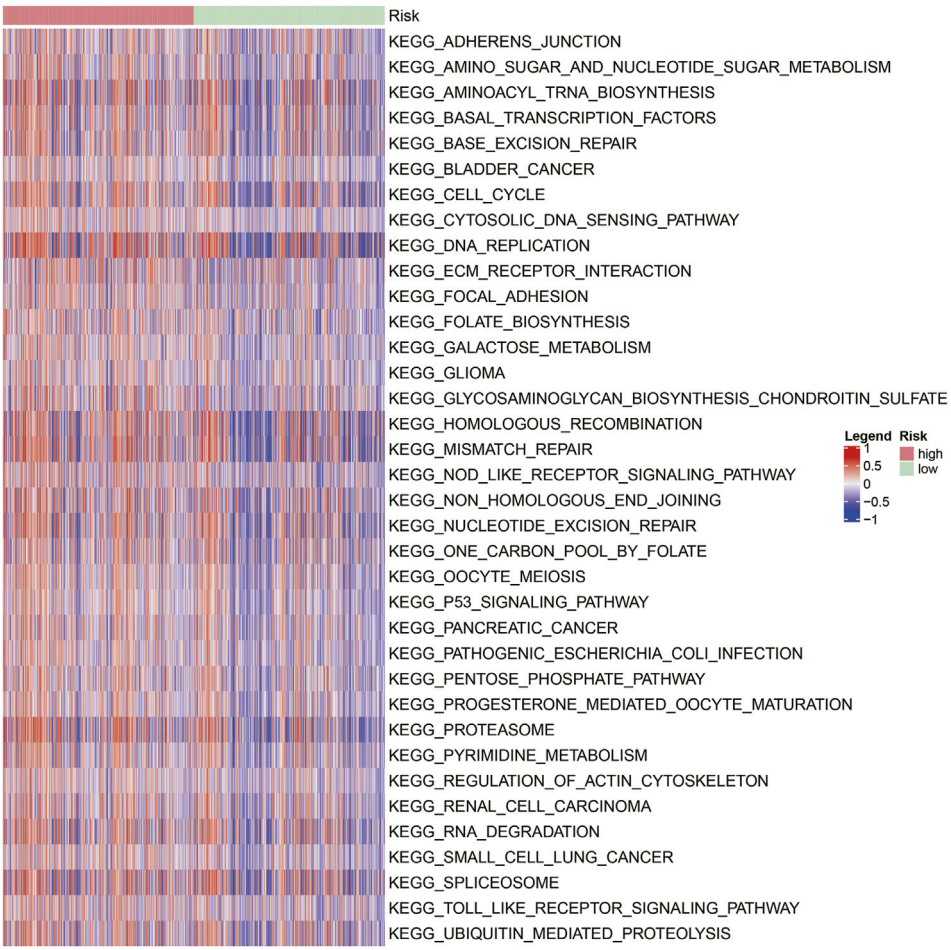

FIGURE 8 | Heatmap of KEGG pathway enrichment in high- and low-risk groups of NSCLC patients.

Figure 7I). We also evaluated the chemotherapeutics sensitivity in different risk groups predicted by pRRophetic package. It was found that a total of 76 drugs, including four resistant drugs and 72 sensitive drugs, were correlated with the RS scores (**Supplementary Figure S11**). The predicted results showed that NSCLC patients in the high-risk group were more resistant to KIN001-135, erlotinib and phenformin than those in the low-risk group. However, these high-risk NSCLC patients were more sensitive to A-770041, WH-4-023, and CGP-60474 (**Figures 7J–O**). Overall, these results suggested that GIRlncSig could be used for the evaluation of immune cell distribution and immunotherapy response in NSCLC patients.

Genomic Instability-Related Signal Pathways Were Enriched in High-Risk Patients

To explore the biological function associated with the GIRlncSig, functional enrichment analysis was conducted for high and low-risk groups of NSCLC patients using "GSVA" package. MSigDB database-based KEGG analysis revealed that 32 differentially enriched items were significantly enriched in the high-risk scored group (**Figure 8**). Notably, two types of signaling pathways were markedly enriched in the high-risk scored group. One was the nucleic acid metabolic pathway including pyrimidine metabolism, folate biosynthesis, DNA replication, and RNA degradation. The other was the DNA damage repair pathway including mismatch repair, base excision repair, nucleotide excision repair, non-homologous end joining, and homologous recombination. Notably, these two types of pathways were strongly associated with genomic stability.

Independent Prognostic Evaluation and Nomogram Construction Based on the Risk Score and Clinical Variables

To verify whether GIRlncSig was an independent prognostic factor, UCRA was conducted on variables including clinical variables and GIRlncSig-based risk score. Then, MCRA was used to evaluate the prognosis of all included variables. The UCRA and MCRA results showed that the GIRlncSig-based risk score and tumor stage exhibited good prognostic performance

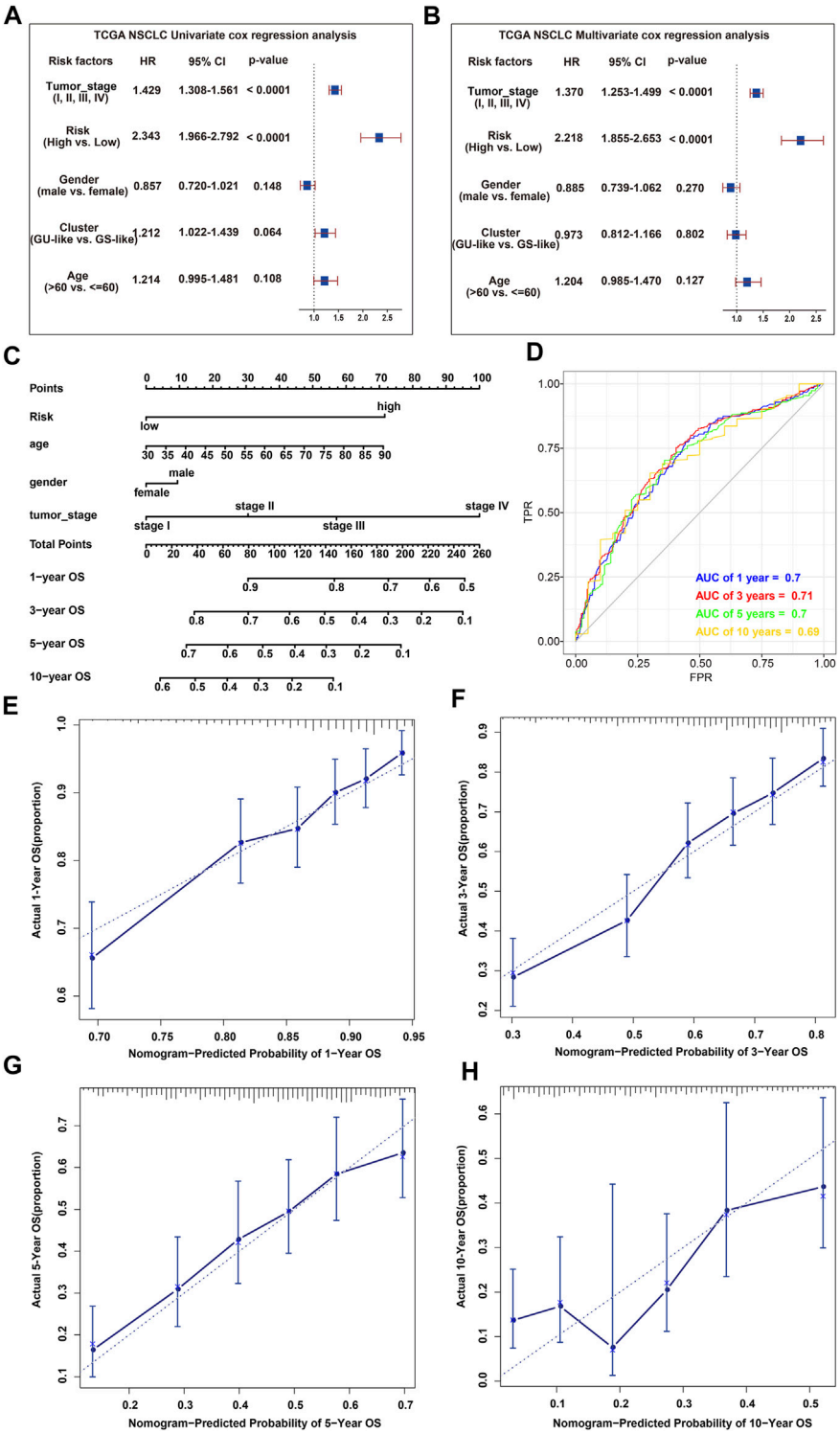

FIGURE 9 | Independent prognostic evaluation and nomogram construction. **(A,B)** UCRA **(A)** and MCRA **(B)** based on GIRlncSig-based risk scores together with clinical variables; **(C)** MCRA-developed nomogram for predicting 1-, 3-, 5-, and 10-year survival of NSCLC patients; **(D)** MCRA-developed ROC for predicting 1-, 3-, 5-, and 10-year survival of NSCLC patients; **(E–H)** Calibration curves for predicting 1- **(E)**, 3- **(F)**, 5- **(G)**, and 10- **(H)** year survival of NSCLC patients.

($p < 0.0001$; **Figures 9A,B**; **Supplementary Table S14**). Other variables, such as cluster, age, and gender, had no significant correlation with the OS of NSCLC patients ($p > 0.05$). These results suggested that the prognostic value of GIRlncSig was independent of other clinical variables. To test its clinical utility, a statistical nomogram was created by integrating GIRlncSig-based risk score with TCGA clinical information (age, gender, and tumor stage) (**Figure 9C**). The C-index of nomogram was 0.67, and the AUCs of ROC for 1-, 3-, 5-, and 10-year survival predictions were 0.69, 0.71, 0.70, and 0.69, respectively (**Figure 9D**). The calibration plots of 1-, 3-, 5-, and 10-year OS showed good agreements between the actual survival rate and the nomogram-predicted survival rate (**Figures 9E–H**). Therefore, these data suggested that the nomogram has a good prediction performance and could provide clues for clinical diagnosis of NSCLC.

DISCUSSION

Genomic instability is an evolving hallmark of most cancers (Hanahan, 2022). It is also a major driver of carcinogenesis, drug sensitivity, tumor-microenvironment-shaping, and immune contexture in NSCLC (Raynaud et al., 2018; Skoulidis and Heymach, 2019). LncRNAs play a critical role in maintaining genomic instability (Nair et al., 2020; Jianfeng et al., 2021). Increasing evidence has revealed the prognostic significance of GIRlncRNAs for cancers (Fang et al., 2021; Liang et al., 2021; Maimaiti et al., 2021; Yan et al., 2021). Since NSCLC possesses a poor survival prognosis due to limited diagnosis and treatment (Zappa and Mousa, 2016; Li C. et al., 2019), we developed a prognostic GIRlncSig to support the clinical stratification and treatment decision for NSCLC patients.

In this study, we screened out 1446 GIRlncRNAs for NSCLC by a somatic mutation burden hypothesis-derived computational frame. Functional analysis revealed that these lncRNAs were mainly enriched in nucleoside or ribonucleoside metabolism, cell-cycle checkpoint, nuclear membrane enveloping, and tumorigenesis, which are involved in maintaining genomic instability (Sieber et al., 2003; Deng, 2006; Aird and Zhang, 2015; Lim et al., 2016). TP53 and CSMD3 were the two most frequently mutated genes in NSCLC (Liu et al., 2012), and their mutation status was closely associated with high TMB causing genomic instability and poor clinical prognosis (Zhang et al., 2017; Bernard et al., 2020; Lu et al., 2021; Wen et al., 2021). We further conducted hierarchical clustering analysis and differential analysis of mutation counts and found that GIRlncRNA-clustering GU-like patients were burdened with a higher TMB than GS-like patients. The mutation frequencies of TP53 and CSMD3 genes in GS-like subtype patients were expectedly higher than those in GU-like subtype patients. The survival of GS-like subtype patients was significantly better than that of GU-like subtype patients. Furthermore, we constructed a GIRlncSig encompassing 19 lncRNAs with robust performances, which could predict prognosis independently of other clinicopathological variables and data sets. Among the 19 GIRlncRNA signature, 14 lncRNAs (AC023824.3, AC013287.1, AP000829.1, LINC01611, AC097451.1, AC025419.1, AC079949.2, LINC01600, AC004862.1, AC021594.1, MYRF-AS1, LINC02434, LINC02412, and LINC00337) were risk factors for prognosis, while the other five lncRNAs (LINC01067, AC012645.1, AL512604.3, AC008278.2, and AC089998.1) were protective factors for survival of NSCLC patients. To the best of our knowledge, most lncRNAs we identified here are novel GIRlncRNAs for NSCLC, while some GIRlncRNAs were already reported in lung adenocarcinoma (Geng et al., 2021; Peng et al., 2021; Wu G. et al., 2021). Notably, lncRNA AC023824, AC025419.1, AC079949.2, LINC02412, and LINC00337 were verified as risk factors associated with the OS of LUAD patients (Li R. et al., 2019; Song et al., 2020; Shao et al., 2021; Wu G. et al., 2021; Wu Y. et al., 2021). LINC01600 and LINC02434 were reported as predictors for the prognosis of PCa and HNSCC patients, respectively (Xu et al., 2020; Jiang et al., 2021). Importantly, we performed ROC and calibration analyses to evaluate the GIRlncSig-based risk score and found that it possessed an intact performance with good agreement between the actual survival and predicted survival in 10 years. In contrast, Wang and Geng's prognostic GIRlncSig only displayed a decreased value of AUCs in 3 years. Therefore, our novel GIRlncSig could provide robust clues for clinical diagnosis and stratification of NSCLC.

Mutations in driver genes are crucial to promoting tumorigenesis and development. NSCLC with positive driver genes possesses high mortality and metastasis risk (Wu Y. et al., 2021; Yuan et al., 2022). We found here that nine driver genes (SOX2, FGFR2, NFE2L2, PTPRD, PTPRT, EGFR, NRG1, MB21D2, and CSMD3) were upregulated. Notably, the expression levels of CSMD3, NFE2L2, and MB21D2 were substantially higher in GU-like samples than those in GS-like samples. NFE2L2 mutation, a major molecular driver of clinical radio resistance (Binkley et al., 2020), was more frequently found in advanced patients to cause a worse prognosis than in patients carrying the wild-type genotype (Sasaki et al., 2010). MB21D2, a key enzyme involved in the cGAS/STING signaling pathway, is also frequently mutated in NSCLC and HNSCC to promote tumor progression (Campbell et al., 2016; Gracilla et al., 2020). The high risk lncRNAs AP000829.1 and LINC01600 from GIRlncSig were positively correlated with MB21D2 expression, which was remarkably upregulated in the high-risk group. Another high-risk lncRNA, AP000829.1, was negatively correlated with NKX2-1. In fact, upregulated AP000829.1 was always accompanied by downregulated NKX2-1 in the high-risk group. NKX2-1 may control lung cancer progression through the induction of DUSP6, an ERK phosphatase, to decrease ERK activity (Ingram et al., 2022). The protective lncRNA, AC008278.2, was positively correlated with the driver gene PTPRT, and this pair was downregulated in the high-risk group. Because PTPRT is an endogenous inhibitor of STAT3 (Sen et al., 2020), loss-of-function mutations in PTPRT resulted in STAT3 hyperactivation to promote the malignancy of NSCLC (Wang et al., 2021). Moreover, the functional genes markedly enriched in the high-risk group mainly involve mismatch repair, base excision repair, nucleotide excision repair, non-homologous end joining, and homologous recombination. These pathways were evidenced to be strongly associated with genomic stability (Majidinia and Yousefi, 2017). Together, these findings suggested that the lncRNAs of our

GIRlncSig are remarkably modulated by the NSCLC driver genes, and that their functions are highly consistent with important biological behaviors.

The contextures of the tumor microenvironment, like infiltrated immune cells, stromal cells, cancer stem cells, and TMB, critically determine the progression of cancer (Whiteside, 2008). Hence, pursuing them can help to predict clinical outcomes, guide early diagnosis and improve the therapeutic response (Binnewies et al., 2018). We found here that the novel GIRlncSig could reflect the characteristics of the tumor microenvironment, and GIRlncSig-predicted high-risk patients exhibited features of malignancy with high levels of TMB and mRNAsi, as well as immune, stromal, and ESTIMATE scores. These results accord with the fact that genome instability contributes to neoplasia and metastasis (Bakhoum et al., 2018; Nguyen et al., 2022). Moreover, we found that NSCLC patients from high-risk groups were more sensitive to CTLA4 inhibitors than those from the low-risk group. Collectively, our GIRlncSig may guide the diagnosis and improve the clinical outcome of NSCLC by selecting a subgroup of patients that are more sensitive to this type of immunotherapy.

Two limitations are associated with this study. First, as appropriate GEO datasets were not found, some potential lncRNAs may have been excluded in our GIRlncSig. Hence, more external dataset validation is needed in future studies. Second, the biological functions of twelve newly identified GIRlncRNAs (AC013287.1, AP000829.1, LINC01611, AC097451.1, AC004862.1, AC021594.1, MYRF–AS1, LINC01067, AC012645.1, AL512604.3, AC008278.2, and AC089998.1) are not known yet. Future investigations should elucidate their functions, both *in vitro* and *in vivo*.

CONCLUSION

In summary, we constructed a GIRlncSig consisting of 19 GIRlncRNAs. This signature could predict the clinical outcome of NSCLC patients independently of other variables. Moreover, our GIRlncSig could dissect the contextures of the tumor microenvironment and driver genes to guide the diagnosis for improved stratification and individualized treatment of NSCLC patients.

DATA AVAILABILITY STATEMENT

The datasets presented in this study can be found in online repositories. The names of the repository/repositories and accession number(s) can be found in the article/ **Supplementary Material**.

AUTHOR CONTRIBUTIONS

SZ and QZ initiated the idea, designed the experiments, supervised the research, and wrote the manuscript. QZ, XL, and ZC collected, analyzed, and generated data and figures. All authors have read, edited, and approved the final version of this manuscript.

FUNDING

This work was supported by the National Natural Science Foundation of China (Nos. 81373318 and 82073233), the National Translational Science Center for Molecular Medicine Fund (F1034361), the Chinese Pharmaceutical Association-Yiling Pharmaceutical Innovation Fund (CPAYLJ202003), the Key Research Fund of Tianjin Project and Team (XB202010), the Key Research and Development Program of Tianjin (20YFZCSY00450), and the Tianjin sci-tech commissioner Fund (21YDTPJC00220).

ACKNOWLEDGMENTS

The authors greatly thank Dr. Qing Zhang (Tianjin Medical University, China) for discussion and helpful suggestion. They also thank Prof. Mattias Belting (Lund University, Sweden) for linguistic advice.

SUPPLEMENTARY MATERIAL

The Supplementary Material for this article can be found online at: https://www.frontiersin.org/articles/10.3389/fphar.2022.937531/full#supplementary-material

REFERENCES

Aird, K. M., and Zhang, R. (2015). Nucleotide Metabolism, Oncogene-Induced Senescence and Cancer. *Cancer Lett.* 356 (2 Pt A), 204–210. doi:10.1016/j.canlet.2014.01.017

Bakhoum, S. F., Ngo, B., Laughney, A. M., Cavallo, J. A., Murphy, C. J., Ly, P., et al. (2018). Chromosomal Instability Drives Metastasis through a Cytosolic DNA Response. *Nature* 553 (7689), 467–472. doi:10.1038/nature25432

Bao, S., Zhao, H., Yuan, J., Fan, D., Zhang, Z., Su, J., et al. (2020). Computational Identification of Mutator-Derived lncRNA Signatures of Genome Instability for Improving the Clinical Outcome of Cancers: a Case Study in Breast Cancer. *Brief. Bioinform* 21 (5), 1742–1755. doi:10.1093/bib/bbz118

Bastians, H. (2015). Causes of Chromosomal Instability. *Recent Results Cancer Res.* 200, 95–113. doi:10.1007/978-3-319-20291-4_5

Bernard, E., Nannya, Y., Hasserjian, R. P., Devlin, S. M., Tuechler, H., Medina-Martinez, J. S., et al. (2020). Implications of TP53 Allelic State for Genome Stability, Clinical Presentation and Outcomes in Myelodysplastic Syndromes. *Nat. Med.* 26 (10), 1549–1556. doi:10.1038/s41591-020-1008-z

Binkley, M. S., Jeon, Y. J., Nesselbush, M., Moding, E. J., Nabet, B. Y., Almanza, D., et al. (2020). KEAP1/NFE2L2 Mutations Predict Lung Cancer Radiation Resistance that Can Be Targeted by Glutaminase Inhibition. *Cancer Discov.* 10 (12), 1826–1841. doi:10.1158/2159-8290.CD-20-0282

Binnewies, M., Roberts, E. W., Kersten, K., Chan, V., Fearon, D. F., Merad, M., et al. (2018). Understanding the Tumor Immune Microenvironment (TIME) for Effective Therapy. *Nat. Med.* 24 (5), 541–550. doi:10.1038/s41591-018-0014-x

Campbell, J. D., Alexandrov, A., Kim, J., Wala, J., Berger, A. H., Pedamallu, C. S., et al. (2016). Distinct Patterns of Somatic Genome Alterations in Lung Adenocarcinomas and Squamous Cell Carcinomas. *Nat. Genet.* 48 (6), 607–616. doi:10.1038/ng.3564

Chen, J. W., and Dhahbi, J. (2021). Lung Adenocarcinoma and Lung Squamous Cell Carcinoma Cancer Classification, Biomarker Identification, and Gene Expression Analysis Using Overlapping Feature Selection Methods. *Sci. Rep.* 11 (1), 13323. doi:10.1038/s41598-021-92725-8

Chen, B., Khodadoust, M. S., Liu, C. L., Newman, A. M., and Alizadeh, A. A. (2018). Profiling Tumor Infiltrating Immune Cells with CIBERSORT. *Methods Mol. Biol.* 1711, 243–259. doi:10.1007/978-1-4939-7493-1_12

Chin, C. H., Chen, S. H., Wu, H. H., Ho, C. W., Ko, M. T., and Lin, C. Y. (2014). cytoHubba: Identifying Hub Objects and Sub-networks from Complex Interactome. *BMC Syst. Biol.* 8 Suppl 4, S11. doi:10.1186/1752-0509-8-S4-S11

Deng, C. X. (2006). BRCA1: Cell Cycle Checkpoint, Genetic Instability, DNA Damage Response and Cancer Evolution. *Nucleic Acids Res.* 34 (5), 1416–1426. doi:10.1093/nar/gkl010

Fang, X., Liu, X., Lu, L., and Liu, G. (2021). Identification of a Somatic Mutation-Derived Long Non-Coding RNA Signatures of Genomic Instability in Renal Cell Carcinoma. *Front. Oncol.* 11, 728181. doi:10.3389/fonc.2021.728181

Feng, J. X., and Riddle, N. C. (2020). Epigenetics and Genome Stability. *Mamm. Genome* 31 (5-6), 181–195. doi:10.1007/s00335-020-09836-2

Gao, H., Song, X., Kang, T., Yan, B., Feng, L., Gao, L., et al. (2017). Long Noncoding RNA CRNDE Functions as a Competing Endogenous RNA to Promote Metastasis and Oxaliplatin Resistance by Sponging miR-136 in Colorectal Cancer. *Onco Targets Ther.* 10, 205–216. doi:10.2147/OTT.S116178

Geng, W., Lv, Z., Fan, J., Xu, J., Mao, K., Yin, Z., et al. (2021). Identification of the Prognostic Significance of Somatic Mutation-Derived LncRNA Signatures of Genomic Instability in Lung Adenocarcinoma. *Front. Cell Dev. Biol.* 9, 657667. doi:10.3389/fcell.2021.657667

Gracilla, D. E., Korla, P. K., Lai, M. T., Chiang, A. J., Liou, W. S., and Sheu, J. J. (2020). Overexpression of Wild Type or a Q311E Mutant MB21D2 Promotes a Pro-oncogenic Phenotype in HNSCC. *Mol. Oncol.* 14 (12), 3065–3082. doi:10.1002/1878-0261.12806

Gridelli, C., Rossi, A., Carbone, D. P., Guarize, J., Karachaliou, N., Mok, T., et al. (2015). Non-small-cell Lung Cancer. *Nat. Rev. Dis. Prim.* 1, 15009. doi:10.1038/nrdp.2015.9

Hanahan, D., and Weinberg, R. A. (2011). Hallmarks of Cancer: the Next Generation. *Cell* 144 (5), 646–674. doi:10.1016/j.cell.2011.02.013

Hanahan, D. (2022). Hallmarks of Cancer: New Dimensions. *Cancer Discov.* 12 (1), 31–46. doi:10.1158/2159-8290.CD-21-1059

Herbst, R. S., Morgensztern, D., and Boshoff, C. (2018). The Biology and Management of Non-small Cell Lung Cancer. *Nature* 553 (7689), 446–454. doi:10.1038/nature25183

Ingram, K., Samson, S. C., Zewdu, R., Zitnay, R. G., Snyder, E. L., and Mendoza, M. C. (2022). NKX2-1 Controls Lung Cancer Progression by Inducing DUSP6 to Dampen ERK Activity. *Oncogene* 41 (2), 293–300. doi:10.1038/s41388-021-02076-x

Jianfeng, W., Yutao, W., and Jianbin, B. (2021). Long Non-Coding RNAs Correlate with Genomic Stability in Prostate Cancer: A Clinical Outcome and Survival Analysis. *Genomics* 113 (5), 3141–3151. doi:10.1016/j.ygeno.2021.06.029

Jiang, H., Ma, B., Xu, W., Luo, Y., Wang, X., Wen, S., et al. (2021). A Novel Three-lncRNA Signature Predicts the Overall Survival of HNSCC Patients. *Ann. Surg. Oncol.* 28 (6), 3396–3406. doi:10.1245/s10434-020-09210-1

Lee, A. J., Endesfelder, D., Rowan, A. J., Walther, A., Birkbak, N. J., Futreal, P. A., et al. (2011). Chromosomal Instability Confers Intrinsic Multidrug Resistance. *Cancer Res.* 71 (5), 1858–1870. doi:10.1158/0008-5472.CAN-10-3604

Lee, S., Kopp, F., Chang, T. C., Sataluri, A., Chen, B., Sivakumar, S., et al. (2016). Noncoding RNA NORAD Regulates Genomic Stability by Sequestering PUMILIO Proteins. *Cell* 164 (1-2), 69–80. doi:10.1016/j.cell.2015.12.017

Li, C., Liu, J., Lin, J., Li, Z., Shang, X., and Wang, H. (2019a). Poor Survival of Non-small-cell Lung Cancer Patients with Main Bronchus Tumor: a Large Population-Based Study. *Future Oncol.* 15 (24), 2819–2827. doi:10.2217/fon-2019-0098

Li, R., Yang, Y. E., Yin, Y. H., Zhang, M. Y., Li, H., and Qu, Y. Q. (2019b). Methylation and Transcriptome Analysis Reveal Lung Adenocarcinoma-specific Diagnostic Biomarkers. *J. Transl. Med.* 17 (1), 324. doi:10.1186/s12967-019-2068-z

Liang, Y., Ye, F., Cheng, Z., Ou, Y., Zou, L., Hu, Y., et al. (2021). Calculated Identification of Mutator-Derived lncRNA Signatures of Genomic Instability to Predict the Clinical Outcome of Muscle-Invasive Bladder Cancer. *Cancer Cell Int.* 21 (1), 476. doi:10.1186/s12935-021-02185-3

Lim, S., Quinton, R. J., and Ganem, N. J. (2016). Nuclear Envelope Rupture Drives Genome Instability in Cancer. *Mol. Biol. Cell* 27 (21), 3210–3213. doi:10.1091/mbc.E16-02-0098

Liu, P., Morrison, C., Wang, L., Xiong, D., Vedell, P., Cui, P., et al. (2012). Identification of Somatic Mutations in Non-small Cell Lung Carcinomas Using Whole-Exome Sequencing. *Carcinogenesis* 33 (7), 1270–1276. doi:10.1093/carcin/bgs148

Lu, N., Liu, J., Xu, M., Liang, J., Wang, Y., Wu, Z., et al. (2021). CSMD3 Is Associated with Tumor Mutation Burden and Immune Infiltration in Ovarian Cancer Patients. *Int. J. Gen. Med.* 14, 7647–7657. doi:10.2147/IJGM.S335592

Lukow, D. A., Sausville, E. L., Suri, P., Chunduri, N. K., Wieland, A., Leu, J., et al. (2021). Chromosomal Instability Accelerates the Evolution of Resistance to Anti-cancer Therapies. *Dev. Cell* 56, 2427–2439. doi:10.1016/j.devcel.2021.07.009

Maimaiti, A., Wang, X., Pei, Y., Nuermaimaiti, N., Tuersunniyazi, A., Abula, Y., et al. (2021). Identification and Validation of a Novel Eight Mutant-Derived Long Non-coding RNAs Signature as a Prognostic Biomarker for Genome Instability in Low-Grade Glioma. *Aging (Albany NY)* 13 (11), 15164–15192. doi:10.18632/aging.203079

Majidinia, M., and Yousefi, B. (2017). DNA Repair and Damage Pathways in Breast Cancer Development and Therapy. *DNA Repair (Amst)* 54, 22–29. doi:10.1016/j.dnarep.2017.03.009

Malta, T. M., Sokolov, A., Gentles, A. J., Burzykowski, T., Poisson, L., Weinstein, J. N., et al. (2018). Machine Learning Identifies Stemness Features Associated with Oncogenic Dedifferentiation. *Cell* 173 (2), 338–354.e15. doi:10.1016/j.cell.2018.03.034

Nair, L., Chung, H., and Basu, U. (2020). Regulation of Long Non-coding RNAs and Genome Dynamics by the RNA Surveillance Machinery. *Nat. Rev. Mol. Cell Biol.* 21 (3), 123–136. doi:10.1038/s41580-019-0209-0

Negrini, S., Gorgoulis, V. G., and Halazonetis, T. D. (2010). Genomic Instability-Aan Evolving Hallmark of Cancer. *Nat. Rev. Mol. Cell Biol.* 11 (3), 220–228. doi:10.1038/nrm2858

Nguyen, B., Fong, C., Luthra, A., Smith, S. A., DiNatale, R. G., Nandakumar, S., et al. (2022). Genomic Characterization of Metastatic Patterns from Prospective Clinical Sequencing of 25,000 Patients. *Cell* 185 (3), 563–575.e11. doi:10.1016/j.cell.2022.01.003

Osrodek, M., and Wozniak, M. (2021). Targeting Genome Stability in Melanoma-A New Approach to an Old Field. *Int. J. Mol. Sci.* 22 (7), 3485. doi:10.3390/ijms22073485

Peng, B., Li, H., Na, R., Lu, T., Li, Y., Zhao, J., et al. (2021). Identification of a Novel Prognostic Signature of Genome Instability-Related LncRNAs in Early Stage Lung Adenocarcinoma. *Front. Cell Dev. Biol.* 9, 706454. doi:10.3389/fcell.2021.706454

Raynaud, F., Mina, M., Tavernari, D., and Ciriello, G. (2018). Pan-cancer Inference of Intra-tumor Heterogeneity Reveals Associations with Different Forms of Genomic Instability. *PLoS Genet.* 14 (9), e1007669. doi:10.1371/journal.pgen.1007669

Reis, A. H., Vargas, F. R., and Lemos, B. (2016). Biomarkers of Genome Instability and Cancer Epigenetics. *Tumour Biol.* 37 (10), 13029–13038. doi:10.1007/s13277-016-5278-5

Rummel, S., Valente, A. L., Kane, J. L., Shriver, C. D., and Ellsworth, R. E. (2012). Genomic (In)stability of the Breast Tumor Microenvironment. *Mol. Cancer Res.* 10 (12), 1526–1531. doi:10.1158/1541-7786.MCR-12-0425

Sasaki, H., Hikosaka, Y., Okuda, K., Kawano, O., Moriyama, S., Yano, M., et al. (2010). NFE2L2 Gene Mutation in Male Japanese Squamous Cell Carcinoma of the Lung. *J. Thorac. Oncol.* 5 (6), 786–789. doi:10.1097/JTO.0b013e3181db3dd3

Sen, M., Kindsfather, A., Danilova, L., Zhang, F., Colombo, R., LaPorte, M. G., et al. (2020). PTPRT Epigenetic Silencing Defines Lung Cancer with STAT3 Activation and Can Direct STAT3 Targeted Therapies. *Epigenetics* 15 (6-7), 604–617. doi:10.1080/15592294.2019.1676597

Shao, J., Zhang, B., Kuai, L., and Li, Q. (2021). Integrated Analysis of Hypoxia-Associated lncRNA Signature to Predict Prognosis and Immune Microenvironment of Lung Adenocarcinoma Patients. *Bioengineered* 12 (1), 6186–6200. doi:10.1080/21655979.2021.1973874

Sieber, O. M., Heinimann, K., and Tomlinson, I. P. (2003). Genomic Instability-Tthe Engine of Tumorigenesis? *Nat. Rev. Cancer* 3 (9), 701–708. doi:10.1038/nrc1170

Skoulidis, F., and Heymach, J. V. (2019). Co-occurring Genomic Alterations in Non-small-cell Lung Cancer Biology and Therapy. *Nat. Rev. Cancer* 19 (9), 495–509. doi:10.1038/s41568-019-0179-8

Song, J. Y., Li, X. P., Qin, X. J., Zhang, J. D., Zhao, J. Y., and Wang, R. (2020). A Fourteen-lncRNA Risk Score System for Prognostic Prediction of Patients with Non-small Cell Lung Cancer. *Cancer Biomark.* 29 (4), 493–508. doi:10.3233/CBM-190505

Sonugür, F. G., and Akbulut, H. (2019). The Role of Tumor Microenvironment in Genomic Instability of Malignant Tumors. *Front. Genet.* 10, 1063. doi:10.3389/fgene.2019.01063

Sung, H., Ferlay, J., Siegel, R. L., Laversanne, M., Soerjomataram, I., Jemal, A., et al. (2021). Global Cancer Statistics 2020: GLOBOCAN Estimates of Incidence and Mortality Worldwide for 36 Cancers in 185 Countries. *CA Cancer J. Clin.* 71 (3), 209–249. doi:10.3322/caac.21660

Thompson, S. L., Bakhoum, S. F., and Compton, D. A. (2010). Mechanisms of Chromosomal Instability. *Curr. Biol.* 20 (6), R285–R295. doi:10.1016/j.cub.2010.01.034

Wang, X., Wu, B., Yan, Z., Wang, G., Chen, S., Zeng, J., et al. (2021). Association of PTPRD/PTPRT Mutation with Better Clinical Outcomes in NSCLC Patients Treated with Immune Checkpoint Blockades. *Front. Oncol.* 11, 650122. doi:10.3389/fonc.2021.650122

Wen, X. M., Xu, Z. J., Jin, Y., Xia, P. H., Ma, J. C., Qian, W., et al. (2021). Association Analyses of TP53 Mutation with Prognosis, Tumor Mutational Burden, and Immunological Features in Acute Myeloid Leukemia. *Front. Immunol.* 12, 717527. doi:10.3389/fimmu.2021.717527

Whiteside, T. L. (2008). The Tumor Microenvironment and its Role in Promoting Tumor Growth. *Oncogene* 27 (45), 5904–5912. doi:10.1038/onc.2008.271

Wu, G., Wang, Q., Zhu, T., Fu, L., Li, Z., Wu, Y., et al. (2021a). Identification and Validation of Immune-Related LncRNA Prognostic Signature for Lung Adenocarcinoma. *Front. Genet.* 12, 681277. doi:10.3389/fgene.2021.681277

Wu, Y., Ni, H., Yang, D., Niu, Y., Chen, K., Xu, J., et al. (2021b). Driver and Novel Genes Correlated with Metastasis of Non-small Cell Lung Cancer: A Comprehensive Analysis. *Pathol. Res. Pract.* 224, 153551. doi:10.1016/j.prp.2021.153551

Xu, M., Gong, S., Li, Y., Zhou, J., Du, J., Yang, C., et al. (2020). Identifying Long Non-coding RNA of Prostate Cancer Associated with Radioresponse by Comprehensive Bioinformatics Analysis. *Front. Oncol.* 10, 498. doi:10.3389/fonc.2020.00498

Yan, K., Wang, Y., Shao, Y., and Xiao, T. (2021). Gene Instability-Related lncRNA Prognostic Model of Melanoma Patients via Machine Learning Strategy. *J. Oncol.* 2021, 5582920. doi:10.1155/2021/5582920

Yuan, F., Cao, X., Zhang, Y.-H., Chen, L., Huang, T., Li, Z., et al. (2022). Identification of Novel Lung Cancer Driver Genes Connecting Different Omics Levels with a Heat Diffusion Algorithm. *Front. Cell Dev. Biol.* 10, 825272. doi:10.3389/fcell.2022.825272

Zappa, C., and Mousa, S. A. (2016). Non-small Cell Lung Cancer: Current Treatment and Future Advances. *Transl. Lung Cancer Res.* 5 (3), 288–300. doi:10.21037/tlcr.2016.06.07

Zhang, Y., He, Q., Hu, Z., Feng, Y., Fan, L., Tang, Z., et al. (2016). Long Noncoding RNA LINP1 Regulates Repair of DNA Double-Strand Breaks in Triple-Negative Breast Cancer. *Nat. Struct. Mol. Biol.* 23 (6), 522–530. doi:10.1038/nsmb.3211

Zhang, M., Zhuang, G., Sun, X., Shen, Y., Wang, W., Li, Q., et al. (2017). TP53 Mutation-Mediated Genomic Instability Induces the Evolution of Chemoresistance and Recurrence in Epithelial Ovarian Cancer. *Diagn Pathol.* 12 (1), 16. doi:10.1186/s13000-017-0605-8

Conflict of Interest: The authors declare that the research was conducted in the absence of any commercial or financial relationships that could be construed as a potential conflict of interest.

Publisher's Note: All claims expressed in this article are solely those of the authors and do not necessarily represent those of their affiliated organizations, or those of the publisher, the editors, and the reviewers. Any product that may be evaluated in this article, or claim that may be made by its manufacturer, is not guaranteed or endorsed by the publisher.

Copyright © 2022 Zhang, Liu, Chen and Zhang. This is an open-access article distributed under the terms of the Creative Commons Attribution License (CC BY). The use, distribution or reproduction in other forums is permitted, provided the original author(s) and the copyright owner(s) are credited and that the original publication in this journal is cited, in accordance with accepted academic practice. No use, distribution or reproduction is permitted which does not comply with these terms.

frontiers | Frontiers in Pharmacology

TYPE Review
PUBLISHED 10 August 2022
DOI 10.3389/fphar.2022.956619

Check for updates

OPEN ACCESS

EDITED BY
Ting Wang,
Sichuan Cancer Hospital, China

REVIEWED BY
Inamul Kabir,
Yale University, United States
Eri Saki H. Hayakawa,
Jichi Medical University, Japan

*CORRESPONDENCE
Dongming Xing,
xdm_tsinghua@163.com

†These authors share first authorship

SPECIALTY SECTION
This article was submitted to Pharmacology of Anti-Cancer Drugs, a section of the journal Frontiers in Pharmacology

RECEIVED 30 May 2022
ACCEPTED 11 July 2022
PUBLISHED 10 August 2022

CITATION
Zhang R, Zeng J, Liu W, Meng J, Wang C, Shi L, Yang S, Chang J and Xing D (2022), The role of NPC1L1 in cancer. *Front. Pharmacol.* 13:956619. doi: 10.3389/fphar.2022.956619

COPYRIGHT
© 2022 Zhang, Zeng, Liu, Meng, Wang, Shi, Yang, Chang and Xing. This is an open-access article distributed under the terms of the Creative Commons Attribution License (CC BY). The use, distribution or reproduction in other forums is permitted, provided the original author(s) and the copyright owner(s) are credited and that the original publication in this journal is cited, in accordance with accepted academic practice. No use, distribution or reproduction is permitted which does not comply with these terms.

The role of NPC1L1 in cancer

Renshuai Zhang[1†], Jun Zeng[2,1†], Wenjing Liu[2,1], Jingsen Meng[2,1], Chao Wang[1], Lingyu Shi[2,1], Shanbo Yang[2,1], Jing Chang[2,1] and Dongming Xing[1,3*]

[1]Qingdao Cancer Institute, The Affiliated Hospital of Qingdao University, Qingdao University, Qingdao, China, [2]School of Basic Medicine, Qingdao University, Qingdao, China, [3]School of Life Sciences, Tsinghua University, Beijing, China

Lipid metabolism appears to play significant roles in the development of cancer. Numerous studies have shown that the evolution of malignancies, including breast, prostate, and colorectal cancers, involves cholesterol in a profound manner. A crucial part in the intestinal absorption of cholesterol is played by Niemann–Pick C1-like 1 (NPC1L1), a cholesterol transporter protein that is widely expressed in the small intestine and liver. The importance of NPC1L1 in tumor prognosis has been demonstrated in investigations in the interim. NPC1L1 also has the potential to develop into a new therapeutic target and a cancer marker. There is, however, no comprehensive review that summarizes NPC1L1's function in cancer. To this end, we outlined NPC1L1's functions in carcinogenesis and treatment, along with resources that can be used to further comprehend the connection between NPC1L1 and tumors.

KEYWORDS

NPC1L1, tumor, cholesterol, tumor therapy, cancer marker

1 Introduction

The body needs cholesterol for many functions, but too much cholesterol can create hypercholesterolemia, which can cause atherosclerosis, stroke, and coronary heart disease (Alonso et al., 2013). Due to the additional ways in which cholesterol encourages cell division, invasion, and proliferation, it is crucial to the growth and development of tumors. Studies have revealed that the upregulation of the cholesterol synthesis level, the rise in cholesterol absorption, and the abnormal accumulation of a large number of metabolites are the main manifestations of the improper regulation of cholesterol metabolism in tumor cells. This results in improved tumor cell growth, survival, invasion, metastasis, and tumor microenvironment adaption. Tumor occurrence and growth are further encouraged (Yoshioka et al., 2000).

Niemann–Pick type C1-like 1 (NPC1L1) is a protein that is essential for intestinal cholesterol absorption and plays vital roles in dietary cholesterol absorption and biliary cholesterol resorption. With remarkable specificity, NPC1L1 mediates cholesterol entrance into small intestinal absorptive cells. A vesicular endocytosis process, as demonstrated by the studies, mediated cholesterol absorption by the NPC1L1 protein. When the extracellular cholesterol concentration was high, the plasma membrane protein NPC1L1 would endocytose the extracellular cholesterol and transfer it to the endocytic

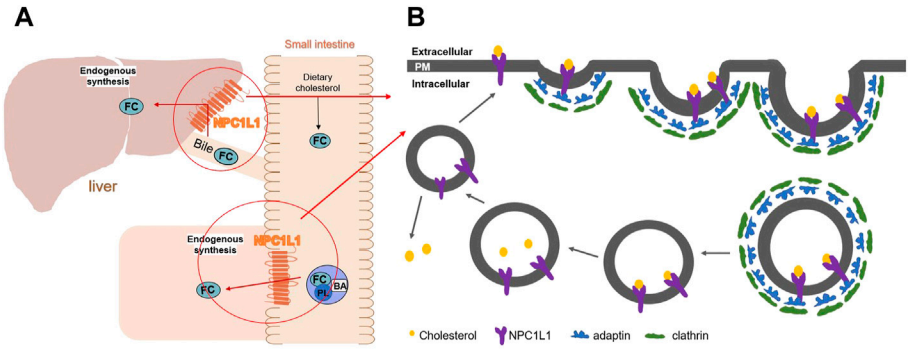

FIGURE 1
(A) Diagram of the mechanism of action of NPC1L1 in cholesterol transport in the small intestine and liver. **(B)** Working model for NPC1L1-mediated cholesterol uptake. (FC) Free cholesterol; (BA) bile acids; (PL) phospholipids; (PM) plasma membrane.

cycle (Ge et al., 2008). (Figure 1) As a specific target of NPC1L1, ezetimibe is a small molecule compound that can effectively and specifically inhibit the absorption of intestinal cholesterol. It is a medication used to treat coronary heart disease and hypercholesterolemia. According to research, it can lower plasma cholesterol by 15–20% (Bays et al., 2001; Dujovne et al., 2002). It is also a medication used to treat dyslipidemia that does not respond to statin therapy (Betters and Yu, 2010).

Obesity, hyperlipidemia, lipid storage disorders, and vascular diseases are all brought on by an abnormal cholesterol metabolism. Changes in cholesterol metabolism can significantly impact how quickly cancer develops and spreads. The current research on the association between NPC1L1 and cancer in carcinogenesis and cancer therapy is of utmost importance since NPC1L1 is a crucial member of cholesterol in intestinal absorption. First, we detailed the structure, usage, and distribution of the NPC1L1 protein in this article. Then, using the studies that were accessible, we summarized the connection between NPC1L1 and cancer for the first time.

2 Structure and function of NPC1L1

2.1 Structure of NPC1L1

NPC1L1 is a 1,332-amino acid membrane protein that is only found in primate hepatocyte tubular membranes and mammalian small intestinal brush membranes. The sequences of Niemann–Pick disease type C1 (NPC1) and NPC1L1 are comparable in 51 and 42 percent, respectively (Davies et al., 2000). A membrane protein called NPC1 performs a job in late endosomes and lysosomes (Pallottini and Pfrieger, 2020). As a homolog of NPC1, NPC1L1 likewise possesses a transmembrane domain with 13 cysteines and three major luminal structural domains in the extracellular area, the N-terminal domain (NTD), the middle domain (MLD), and the cysteine-rich domain (CTD). Thirteen molecules of membrane-embedded transmembrane helices (TM) make up the transmembrane domain (TMD) (Hu et al., 2021). The SSD domain is widely distributed in several regulatory protein substructures that are closely related to cholesterol metabolisms, such as NPC1, sterol regulatory element-binding protein cleavage activating protein (SCAP), and hydroxymethyl glutaryl-CoA reductase (HMG-CoA reductase) (Yang et al., 2012). (Figure 2)

2.2 Distribution of NPC1L1

NPC1L1 is tissue-specific in its distribution and is highly expressed in tissues connected to the digestive system. Currently, NPC1L1 is being investigated more in rodents and humans, and it has been discovered that there are small species differences in the distribution of NPC1L1 *in vivo*. The human liver and small intestine are the tissues with the highest levels of the NPC1L1 expression, followed by the stomach, ovary, lung tissues, and even minimal amounts in the brain tissues (Davies et al., 2000). However, the NPC1L1 expression in all tissues is less than 10% of that in the intestine (Davies et al., 2000). Further studies showed that NPC1L1 in small intestine tissues was mainly located in jejunal epithelial cells rather than in ileal epithelial cells. It was previously thought that the NPC1L1 protein was only expressed in cell membranes, especially in the cell membranes of the epithelial layer of the intestinal villi folds. Moreover, it was shown that NPC1L1 was dispersed in the cytoplasm and on the cell membrane (Yu et al., 2006). In rodents, NPC1L1 is highly expressed, especially in the small intestine, with minimal expression in liver tissues. Additionally, mouse testes and gallbladder tissues also showed high levels of the NPC1L1 expression (Cui et al., 2010; Wang and Song, 2012). The variety of NPC1L1 distribution among species

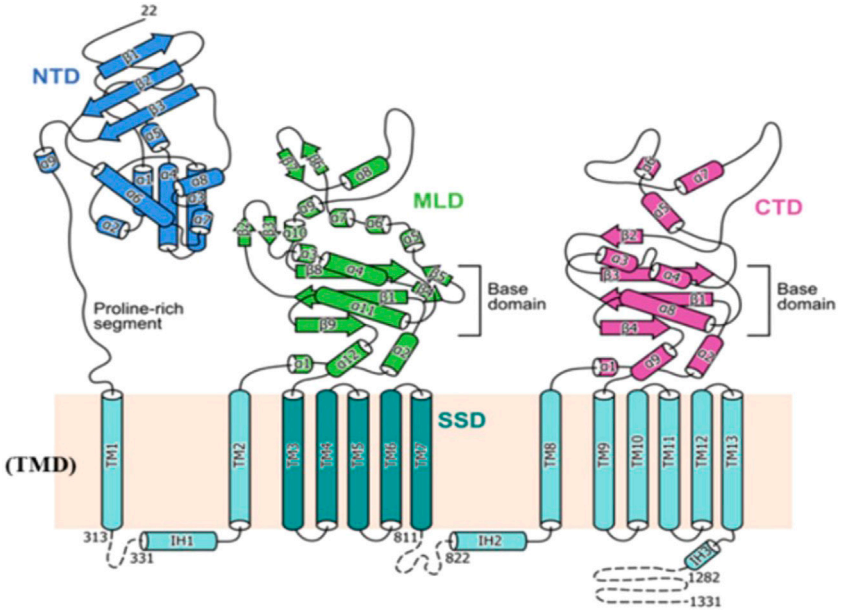

FIGURE 2
Topological representation of NPC1L1. NTD: N-terminal domain; TMD: transmembrane domain; MLD: middle luminal domain; CTD: C-terminal luminal domain; SSD: sterol-sensing domain (Huang et al., 2020).

is currently thought to be related to the degree of species evolution or possibly the outcome of long-term selection as a result of various survival settings. Cryo-EM structures of NPC1L1 were reported sequentially by three distinct research teams in the years 2020 and 2021. C.S. Huang et al. studied the structure of NPC1L1 derived from *Rattus*. Miao Qinghu et al. (Hu et al., 2021) and Long et al. (2021) studied the structure of human-derived NPC1L1. Their findings demonstrated a general similarity between the three-dimensional architecture of mouse and human NPC1L1.

2.3 Functions of NPC1L1

In humans, cholesterol is absorbed mainly in the proximal jejunum of the small intestine, where both dietary and biliary cholesterol types are absorbed (Reboul et al., 2012). Clinical investigations have demonstrated decreased membrane absorption and the subsequent transport of various lipids, as well as a 69 percent reduction in cholesterol uptake in NPC1L1-knockout mice (Iyer et al., 2005). Mice lacking NPC1L1 are resistant to hypercholesterolemia induced by a high-fat diet. Another study indicated that normal mice did not experience any significant changes in NPC1L1 or an increase in cholesterol absorption when bile acid and bile salt secretion and excretion were reduced while consuming a high-cholesterol diet (Alrefai et al., 2007). It is hypothesized that NPC1L1 may only work in the presence of diets high in cholesterol and bile acid salts.

3 Tumor suppression by NPC1L1 in cancer

3.1 Colorectal cancer

Colorectal cancer (CRC) is a malignant tumor of the colon and rectum. It is also the third most common cancer and the fourth leading cause of cancer-related deaths worldwide (Brenner et al., 2014). Due to the changes in dietary habits, the incidence of CRC is rapidly increasing in many countries, including those in Eastern Europe, South America, and Asia (Arnold et al., 2017). Age, family history, inflammatory bowel disease, hereditary colorectal cancer, obesity, and diabetes are known as the risk factors for colorectal cancer.

The development and prognosis of colorectal cancer have been shown to be associated with an altered lipid metabolism. High cholesterol intake is associated with an increased risk of colorectal cancer. Elevated serum cholesterol levels are associated with the risk of developing colorectal cancer (Jarvinen et al., 2001). Ryuk et al. (Kwon et al., 2021) explored whether alterations in the NPC1L1 expression are associated with the development and prognosis of human colorectal cancer. In comparison to normal tissues, CRC tissues showed considerably greater levels of the NPC1L1 expression (normal: mean 7.00, CRC: mean 130.09, and p 0.05) (Figure 3). This study determined whether the NPC1L1 expression had an impact on CRC patients' prognoses. NPC1L1 has an impact on colorectal cancer patients' overall survival, with patients in the NPC1L1 high-expression group having a worse OS than NPC1L1 patients, according to a KM analysis of the

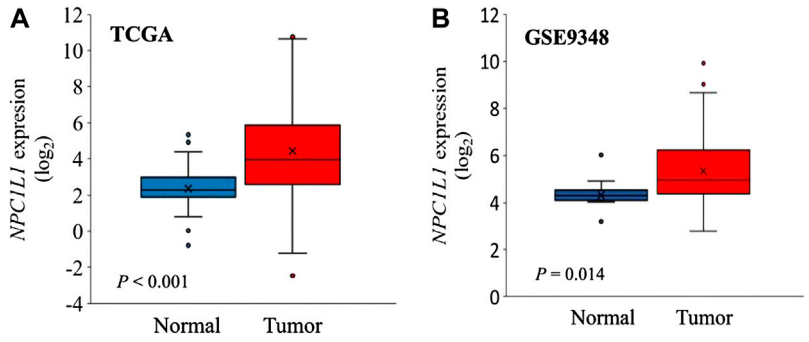

FIGURE 3
NPC1L1 expression in normal and CRC tissues. **(A)** NPC1L1 expression is higher in most CRC tissues than in normal tissues. The mean value of the NPC1L1 expression in normal tissues (blue box) is 7.00, and in CRC tissues (red box), it is 130.09. **(B)** Mean value of the NPC1L1 expression in normal tissues (blue box) is 22.69, and in CRC tissues (red box), it is 81.35 compared to normal tissues (GSE9348) (Kwon et al., 2021).

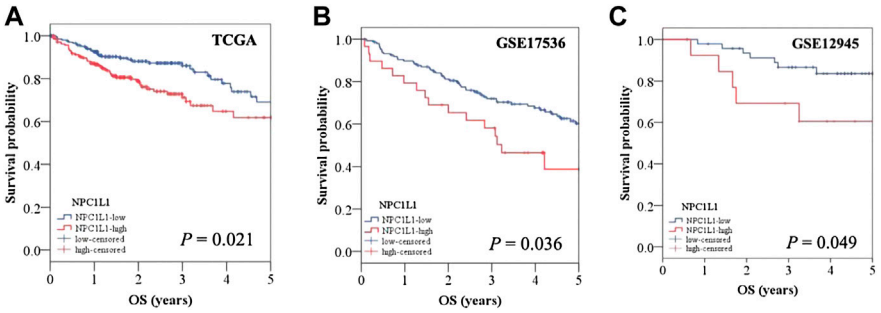

FIGURE 4
OS of CRC patients with a high NPC1L1 expression was significantly lower than that of CRC patients with a low NPC1L1 expression. The results of the two datasets (GSE17536 and GSE129451) collated in the CRC patients stratified into NPC1L1-low and NPC1L1-high groups also showed results consistent with those obtained from the analysis of TCGA dataset (Kwon et al., 2021).

NPC1L1 low-expression group and the NPC1L1 high-expression group on OS (Figure 4). It was revealed that NPC1L1 has value as a standalone prognostic factor for colorectal cancer, and it was found that the NPC1L1 expression was highly correlated with the prognosis of the disease. NPC1L1, along with other known prognostic markers, can be independent prognostic markers for colorectal cancer. Jianming H et al. (He et al., 2015) explored the role of NPC1L1 in colorectal carcinogenesis *in vivo* using transgenic mice. Their findings have shown that NPC1L1 deletion in mice reduced carcinogenesis linked to colitis. Although only expressed in the small intestine of mice, NPC1L1 mRNA was substantially elevated in the liver and small intestine of humans. Its mRNA was also present in the colon but at a very low level (Chen et al., 2018). Therefore, it is unlikely that the NPC1L1 knockdown inhibits the growth of malignancies linked to colitis. In the small intestine and liver, NPC1L1 primarily functions as a sterol transporter protein that controls lipid homeostasis. Plasma lipids, particularly cholesterol, are closely linked to colon cancer and, through inflammation, cause animals to develop tumors associated with colitis (Vinson et al., 2016). Cholesterol was evidently decreased by NPC1L1 knockdown. Additionally, the inflammatory markers pc-Jun, p-ERK, and caspase-1 p20 in colorectal cancers were considerably decreased by NPC1L1 knockdown (Figures 5, 6). Therefore, NPC1L1 knockdown decreases carcinogenesis associated with colitis, which may be brought on by the decrease in plasma lipids, particularly cholesterol, brought on by its knockdown, which lessens the sensitivity to inflammatory stimuli.

3.2 Head and neck squamous cell carcinoma

With more than 550,000 new cases and 300,000 fatalities each year, head and neck squamous cell carcinoma (HNSCC),

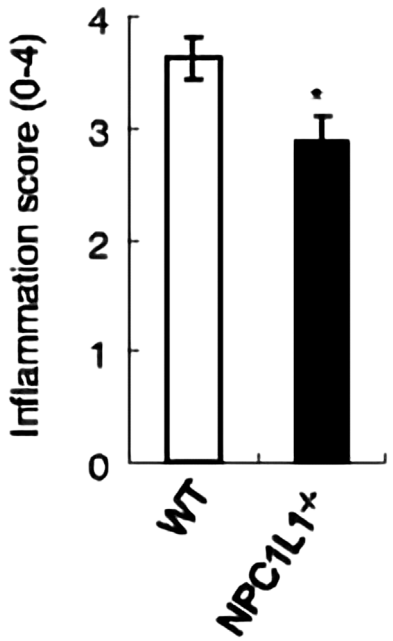

FIGURE 5
NPC1L1-knockout mice have significantly lower intestinal inflammation scores than wild-type mice (He et al., 2015).

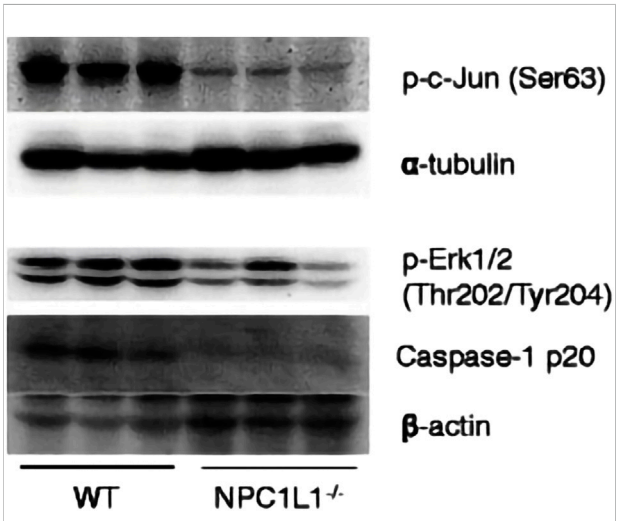

FIGURE 6
pc-Jun, p-ERK, and caspase-1 p20 protein expressions in tumors measured by protein blotting. pc-Jun, p-ERK and caspase-1 p20 were significantly reduced by NPC1L1 knockdown. pc-Jun, p-ERK, and caspase-1 p20 were also reduced by NPC1L1 knockdown (He et al., 2015).

which comprises oral cavity cancer (OC) and oropharyngeal cancer (OPC), is the sixth most prevalent cancer worldwide (Saba et al., 2011). Despite advances in HNSCC treatment, the 10-year survival rate only varies from 19 to 59 percent, and recurrence rates remain significant. Patients frequently endure a combination of radiation, chemotherapy, and surgery, which can cause severe morbidity. Smoking, drinking, and the human papillomavirus (HPV), which is primarily linked to oropharyngeal cancer (Gormley et al., 2021), have all been identified as risk factors (Warnakulasuriya, 2009).

According to several observational studies, statin use is associated negatively with cancer survival and HNSCC risk. Other research studies, however, have shown scant evidence of any impact. Using two-sample Mendelian randomization (MR), the relationship between the targets of genetically proxied cholesterol-lowering drugs and other circulating lipid profiles with OC and OPC risks was evaluated. Germline genetic variations in the genes for HMGCR, NPC1L1, CETP, PCSK9, and LDLR were utilized to simulate the effects of low-density lipoprotein cholesterol-lowering treatments in the initial analysis. There is scant evidence that inherited NPC1L1 increases the chance of developing OC and OPC (Gormley et al., 2021).

3.3 Ovarian cancer

One of the world's most dangerous malignant tumors is ovarian cancer due to the early stages of ovarian cancer's lack of visible signs. The so-called "silent killer" is frequently identified in advanced stages in patients. Based on the genetic alterations and the cell shape of epithelial ovarian cancer, type I and type II ovarian tumors can be distinguished. Low-grade plasmacytomas, endometrioid carcinomas, clear cell carcinomas, and mucinous carcinomas are examples of type I tumors. High-grade plasmacytomas and undifferentiated carcinomas are examples of type II tumors (He et al., 2021). High-grade plasmacytomas and undifferentiated carcinomas are the two main type II tumors.

When the analysis was limited to the general population or BRCA1/2 mutation carriers, there was no significant association between genetically close NPC1L1 or PCSK9 inhibition or low-density lipoprotein cholesterol levels and epithelial ovarian cancer in the Mendelian randomized analysis of 22,406 women with invasive epithelial ovarian cancer and 40,941 control individuals (Yarmolinsky et al., 2020). It is possible that circulating cholesterol is not the cause of the observed relationship between HMG-CoA reductase inhibition and ovarian cancer due to the lack of genetically close inhibition between NPC1L1 and PCSK9 inhibition and genetically close LDL cholesterol levels (Yarmolinsky et al., 2020).

3.4 Hepatocellular carcinoma

Liver cancer accounts for 8.2% of all cancer deaths globally, ranking sixth in cancer incidence. Additionally, it

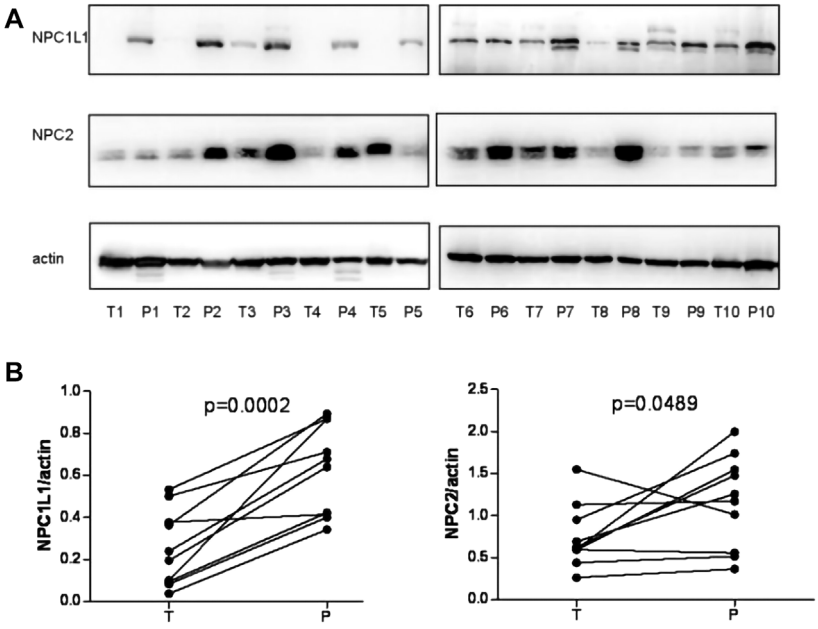

FIGURE 7
(A) NPC1L1 and NPC2 expressions were detected in 10 pairs of HCC tissues (T) and peritumoral tissues (*p*) by Western blot analysis. The expressions of NPC1L1 and NPC2 were significantly decreased in HCC tissues. Meanwhile, the mRNA expressions of NPC1L1 and NPC2 expression levels were also decreased in HCC tissues compared with peritumoral tissues. **(B)** Quantitation of proteins from Western blot analyses shows that both NPC1L1 and NPC2 expressions were significantly reduced in the HCC tissue (T) (Chen et al., 2018).

ranks third in the world for cancer-related fatalities (Siegel, Miller, and Jemal). Intrahepatic cholangiocarcinoma, hepatocellular carcinoma (HCC), fibrous lamellar carcinoma, and hepatoblastoma are several types of primary liver cancer. These classifications differ significantly in terms of their molecular, histological, and pathological traits. Of the instances of liver cancer, 85 to 90 percent are caused by HCC alone (Sia et al., 2017). Tumor removal, liver transplantation, and ablation are all forms of treatment for HCC (Llovet et al., 2004). Tumor removal, liver transplantation, and ablation are all forms of treatment for HCC. Only patients with early disease diagnoses can, however, get this treatment. Additionally, recent research has revealed that only 20% of patients receive an early diagnosis (Farinati et al., 2009).

Chen et al. (2018) investigated the prognostic value of NPC1L1 in human primary hepatocellular carcinoma (HCC). According to the findings, NPC1L1 and NPC2 are not as highly expressed in the HCC liver tissue as in the peritumoral liver tissue. There is also less NPC1L1 mRNA expression in the HCC tissue than in the peritumoral tissue (Figure 7). NPC1L1 inhibition has previously been demonstrated to protect against metabolic diseases such as fatty liver disease, obesity, diabetes, and atherosclerosis (Park, 2013). This is the first study to discuss NPC1L1's function in HCC. When matched peritumoral liver tissues were compared

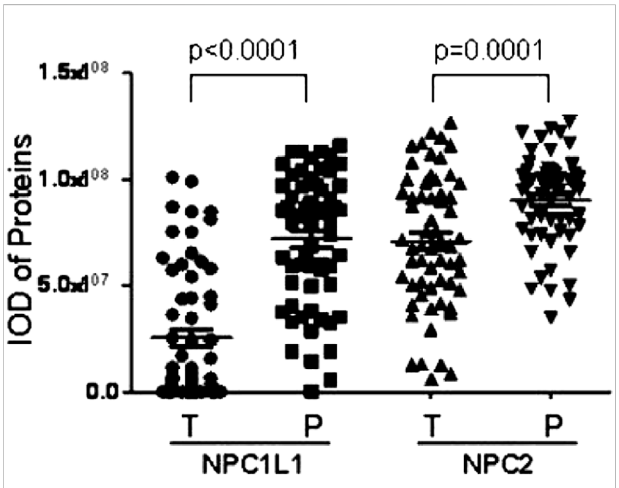

FIGURE 8
Scatter plot showing paired peritumor tissues shows that NPC1L1 and NPC2 expressions in HCC tumor tissues are usually lower than those in peritumor tissues (NPC1L1 $p < 0.0001$; NPC2 $p = 0.0001$) (Chen et al., 2018).

to HCC, NPC1L1 was shown to be lower in the latter. In postoperative HCC patients, a low NPC1L1 protein expression may be a predictor of worse OS and TTR. The

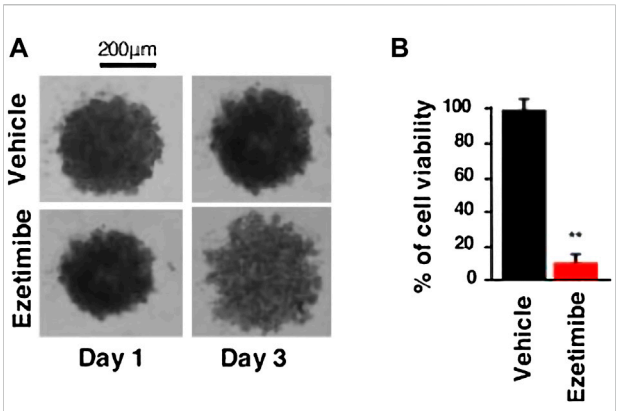

FIGURE 9
(A) Representative image of the PDAC012T-derived spheroids treated with ezetimibe (50 μM) or vehicle after 3 days. **(B)** Cell viability of spheroids was measured by CellTiter-Glo and expressed as a percentage of the vehicle-treated spheroids (**$p < 0.01$) (Nicolle et al., 2017).

expressions of NPC1L1 and NPC2 in HCC tumor tissues were often lower than those in peritumor tissues, according to the patterns of expression in tumor and peritumor tissues (Figure 8). The NPC1L1/NPC2 combination was also discovered as a separate prognostic factor for OS and TTR in postoperative HCC patients, and this study was the first to reveal the prognostic usefulness of NPC1L1 in HCC. Therefore, determining the levels of NPC1L1 and NPC2 expressions in the tissues of HCC patients may give doctors information about the risk of postoperative OS and TTR in HCC patients and may aid in the investigation of the mechanism behind the association between cholesterol and HCC disease.

3.5 Pancreatic cancer

As one of the 14 most prevalent malignancies worldwide, pancreatic cancer is the seventh most common cause of cancer-related deaths (Rawla et al., 2019). Pancreatic cancer often has a terrible prognosis, with a 5-year survival rate of fewer than 5% on average (Carter et al., 2021). More than 90% of the instances of pancreatic cancer are pancreatic ductal adenocarcinoma (PDAC). It is distinguished by an aberrant expression of mucin and nucleoside transporter proteins, as well as extensive pro-fibroproliferative stromal growth near the malignant tissue (Murthy et al., 2018). As antecedents of PDAC, three different pancreatic ductal precancerous lesions—pancreatic intraepithelial neoplasia, mucinous cystic neoplasm, and intraductal papillary mucinous neoplasm—have been found (Suh et al., 2017). The respectability of the main tumor—defined as the lack of distant metastases and topographical contacts that permit R0 resection—determines the pancreatic cancer treatment plans. In addition to chemotherapy, surgical resection is the primary treatment option for individuals who are suitable for it for curable pancreatic cancer. However, around 90% of patients have cancers that are either locally progressed or metastatic at the time of diagnosis, making them unsuitable for surgical excision. Jaundice treatment, systemic control, palliative radiation, and chemotherapy are the sole alternatives for these individuals.

Guillaumond et al. (2015) proposed that an abnormal cholesterol uptake is associated with the proliferation and survival of pancreatic cancer cells. In contrast, an overexpression of the intestinal cholesterol uptake regulator NPC1L1 is associated with extensive hypomethylation. Ezetimibe, a clinically available drug approved for FAD, is a competitor to cholesterol. Nicolle et al. (2017) investigated the specificity of NPC1L1 inhibition on PDAC survival. The outcomes demonstrated a significant impact of ezetimibe therapy on PDAC growth, following NPC1L1 knockdown, including modifications in cell viability and volume (Figure 9). It showed that NPC1L1 is a productive therapeutic target for the ezetimibe therapy of PDAC. Additionally, their findings showed that ezetimibe treatment had no impact on gemcitabine's cytotoxicity, indicating that patients could get treated with NPC1L1 transporter protein inhibitors in addition to traditional anti-cancer medications without jeopardizing the efficacy of either. Preclinical studies have demonstrated, among other things, that the use of the particular inhibitor ezetimibe or a deletion strategy dramatically impacted PDAC survivability. These lend credence to the idea that NPC1L1 might work well as a therapeutic target for pancreatic cancer.

4 Conclusion and outlook

Cholesterol aids in the proliferation, invasion, and subduction of cells and is crucial for the development and growth of tumors. As a crucial protein in intestinal cholesterol absorption, NPC1L1 plays vital functions in the development and spread of tumors. The most recent research indicates that NPC1L1 can be employed as a standalone prognostic marker in colorectal cancer. Additionally, it proved to be a reliable prognostic factor for hepatocellular carcinoma. Additionally, NPC1L1 may be a valuable therapeutic target for pancreatic cancer. The association between NPC1L1 and other malignancies has not been proven by recent investigations. The significance of NPC1L1 in carcinogenesis and cancer therapy, however, merits additional research to offer new therapeutic avenues for clinical cancers due to the role of cholesterol in tumorigenesis and development.

Overall, the current studies on the connection between NPC1L1 and cancers are deficient, however, due to the function of NPC1L1 in cholesterol uptake and the link between cholesterol and cancer. Future research examining this connection might reveal other targets to impede the progression of cholesterol-dependent cancer.

Author contributions

Conceptualization, RZ; writing—original draft preparation, RZ and JZ; writing—review and editing, RZ, JZ, and WL; supervision, DX All authors have read and agreed to the published version of the manuscript.

Conflict of interest

The authors declare that the research was conducted in the absence of any commercial or financial relationships that could be construed as a potential conflict of interest.

Publisher's note

All claims expressed in this article are solely those of the authors and do not necessarily represent those of their affiliated organizations, or those of the publisher, the editors, and the reviewers. Any product that may be evaluated in this article, or claim that may be made by its manufacturer, is not guaranteed or endorsed by the publisher.

References

Alonso, R., Mata, P., Zambon, D., Mata, N., and Fuentes-Jimenez, F. (2013). Early diagnosis and treatment of familial hypercholesterolemia: Improving patient outcomes. *Expert Rev. cardiovasc. Ther.* 11 (3), 327–342. doi:10.1586/erc.13.7

Alrefai, W. A., Annaba, F., Sarwar, Z., Dwivedi, A., Saksena, S., Singla, A., et al. (2007). Modulation of human Niemann-Pick C1-like 1 gene expression by sterol: Role of sterol regulatory element binding protein 2. *Am. J. Physiol. Gastrointest. Liver Physiol.* 292 (1), G369–G376. doi:10.1152/ajpgi.00306.2006

Arnold, M., Sierra, M. S., Laversanne, M., Soerjomataram, I., Jemal, A., Bray, F., et al. (2017). Global patterns and trends in colorectal cancer incidence and mortality. *Gut* 66 (4), 683–691. doi:10.1136/gutjnl-2015-310912

Bays, H. E., Moore, P. B., Drehobl, M. A., Rosenblatt, S., Toth, P. D., Dujovne, C. A., et al. (2001). Effectiveness and tolerability of ezetimibe in patients with primary hypercholesterolemia: Pooled analysis of two phase II studies. *Clin. Ther.* 23 (8), 1209–1230. doi:10.1016/s0149-2918(01)80102-8

Betters, J. L., and Yu, L. (2010). NPC1L1 and cholesterol transport. *FEBS Lett.* 584 (13), 2740–2747. doi:10.1016/j.febslet.2010.03.030

Brenner, H., Kloor, M., and Pox, C. P. (2014). Colorectal cancer. *Lancet* 383 (9927), 1490–1502. doi:10.1016/S0140-6736(13)61649-9

Carter, C. J., Mekkawy, A. H., and Morris, D. L. (2021). Role of human nucleoside transporters in pancreatic cancer and chemoresistance. *World J. Gastroenterol.* 27 (40), 6844–6860. doi:10.3748/wjg.v27.i40.6844

Chen, K. J., Jin, R. M., Shi, C. C., Ge, R. L., Hu, L., Zou, Q. F., et al. (2018). The prognostic value of Niemann-Pick C1-like protein 1 and Niemann-Pick disease type C2 in hepatocellular carcinoma. *J. Cancer* 9 (3), 556–563. doi:10.7150/jca.19996

Cui, W., Jiang, Z. Y., Cai, Q., Zhang, R. Y., Wu, W. Z., Wang, J. C., et al. (2010). Decreased NPC1L1 expression in the liver from Chinese female gallstone patients. *Lipids Health Dis.* 9, 17. doi:10.1186/1476-511X-9-17

Davies, J. P., Levy, B., and Ioannou, Y. A. (2000). Evidence for a niemann-pick C (NPC) gene family: Identification and characterization of NPC1L1. *Genomics* 65 (2), 137–145. doi:10.1006/geno.2000.6151

Dujovne, C. A., Ettinger, M. P., McNeer, J. F., Lipka, L. J., LeBeaut, A. P., Suresh, R., et al. (2002). Efficacy and safety of a potent new selective cholesterol absorption inhibitor, ezetimibe, in patients with primary hypercholesterolemia. *Am. J. Cardiol.* 90 (10), 1092–1097. doi:10.1016/s0002-9149(02)02798-4

Farinati, F., Sergio, A., Baldan, A., Giacomin, A., Di Nolfo, M. A., Del Poggio, P., et al. (2009). Early and very early hepatocellular carcinoma: When and how much do staging and choice of treatment really matter? A multi-center study. *BMC Cancer* 9, 33. doi:10.1186/1471-2407-9-33

Ge, L., Wang, J., Qi, W., Miao, H. H., Cao, J., Qu, Y. X., et al. (2008). The cholesterol absorption inhibitor ezetimibe acts by blocking the sterol-induced internalization of NPC1L1. *Cell Metab.* 7 (6), 508–519. doi:10.1016/j.cmet.2008.04.001

Gormley, M., Yarmolinsky, J., Dudding, T., Burrows, K., Martin, R. M., Thomas, S., et al. (2021). Using genetic variants to evaluate the causal effect of cholesterol lowering on head and neck cancer risk: A mendelian randomization study. *PLoS Genet.* 17 (4), e1009525. doi:10.1371/journal.pgen.1009525

Guillaumond, F., Bidaut, G., Ouaissi, M., Servais, S., Gouirand, V., Olivares, O., et al. (2015). Cholesterol uptake disruption, in association with chemotherapy, is a promising combined metabolic therapy for pancreatic adenocarcinoma. *Proc. Natl. Acad. Sci. U. S. A.* 112 (8), 2473–2478. doi:10.1073/pnas.1421601112

He, J., Shin, H., Wei, X., Kadegowda, A. K., Chen, R., Xie, S. K., et al. (2015). NPC1L1 knockout protects against colitis-associated tumorigenesis in mice. *BMC Cancer* 15, 189. doi:10.1186/s12885-015-1230-0

He, J., Siu, M. K. Y., Ngan, H. Y. S., and Chan, K. K. L. (2021). Aberrant cholesterol metabolism in ovarian cancer: Identification of novel therapeutic targets. *Front. Oncol.* 11, 738177. doi:10.3389/fonc.2021.738177

Hu, M., Yang, F., Huang, Y., You, X., Liu, D., Sun, S., et al. (2021). Structural insights into the mechanism of human NPC1L1-mediated cholesterol uptake. *Sci. Adv.* 7 (29), eabg3188. doi:10.1126/sciadv.abg3188

Huang, C. S., Yu, X., Fordstrom, P., Choi, K., Chung, B. C., Roh, S. H., et al. (2020). Cryo-EM structures of NPC1L1 reveal mechanisms of cholesterol transport and ezetimibe inhibition. *Sci. Adv.* 6 (25), eabb1989. doi:10.1126/sciadv.abb1989

Iyer, S. P., Yao, X., Crona, J. H., Hoos, L. M., Tetzloff, G., Davis, H. R., Jr., et al. (2005). Characterization of the putative native and recombinant rat sterol transporter Niemann-Pick C1 like 1 (NPC1L1) protein. *Biochim. Biophys. Acta* 1722 (3), 282–292. doi:10.1016/j.bbagen.2004.12.021

Jarvinen, R., Knekt, P., Hakulinen, T., Rissanen, H., and Heliovaara, M. (2001). Dietary fat, cholesterol and colorectal cancer in a prospective study. *Br. J. Cancer* 85 (3), 357–361. doi:10.1054/bjoc.2001.1906

Kwon, R. J., Park, E. J., Lee, S. Y., Lee, Y., Hwang, C., Kim, C., et al. (2021). Expression and prognostic significance of niemann-pick C1-like 1 in colorectal cancer: A retrospective cohort study. *Lipids Health Dis.* 20 (1), 104. doi:10.1186/s12944-021-01539-0

Llovet, J. M., Fuster, J., Bruix, J., and Barcelona-Clinic Liver Cancer, G. (2004). The barcelona approach: Diagnosis, staging, and treatment of hepatocellular carcinoma. *Liver Transpl.* 10 (2), S115–S120. doi:10.1002/lt.20034

Long, T., Liu, Y., Qin, Y., DeBose-Boyd, R. A., and Li, X. (2021). Structures of dimeric human NPC1L1 provide insight into mechanisms for cholesterol absorption. *Sci. Adv.* 7 (34), eabh3997. doi:10.1126/sciadv.abh3997

Murthy, D., Attri, K. S., and Singh, P. K. (2018). Phosphoinositide 3-kinase signaling pathway in pancreatic ductal adenocarcinoma progression, pathogenesis, and therapeutics. *Front. Physiol.* 9, 335. doi:10.3389/fphys.2018.00335

Nicolle, R., Blum, Y., Marisa, L., Loncle, C., Gayet, O., Moutardier, V., et al. (2017). Pancreatic adenocarcinoma therapeutic targets revealed by tumor-stroma cross-talk analyses in patient-derived xenografts. *Cell Rep.* 21 (9), 2458–2470. doi:10.1016/j.celrep.2017.11.003

Pallottini, V., and Pfrieger, F. W. (2020). Understanding and treating niemann-pick type C disease: Models matter. *Int. J. Mol. Sci.* 21 (23), E8979. doi:10.3390/ijms21238979

Park, S. W. (2013). Intestinal and hepatic niemann-pick c1-like 1. *Diabetes Metab. J.* 37 (4), 240–248. doi:10.4093/dmj.2013.37.4.240

Rawla, P., Sunkara, T., and Gaduputi, V. (2019). Epidemiology of pancreatic cancer: Global trends, etiology and risk factors. *World J. Oncol.* 10 (1), 10–27. doi:10.14740/wjon1166

Reboul, E., Soayfane, Z., Goncalves, A., Cantiello, M., Bott, R., Nauze, M., et al. (2012). Respective contributions of intestinal niemann-pick C1-like 1 and scavenger receptor class B type I to cholesterol and tocopherol uptake: *In vivo* v. *in vitro* studies. *Br. J. Nutr.* 107 (9), 1296–1304. doi:10.1017/S0007114511004405

Saba, N. F., Goodman, M., Ward, K., Flowers, C., Ramalingam, S., Owonikoko, T., et al. (2011). Gender and ethnic disparities in incidence and survival of squamous cell carcinoma of the oral tongue, base of tongue, and tonsils: A surveillance, epidemiology and end results program-based analysis. *Oncology* 81 (1), 12–20. doi:10.1159/000330807

Sia, D., Villanueva, A., Friedman, S. L., and Llovet, J. M. (2017). Liver cancer cell of origin, molecular class, and effects on patient prognosis. *Gastroenterology* 152 (4), 745–761. doi:10.1053/j.gastro.2016.11.048

Siegel, R. L., Miller, K. D., and Jemal, A. (202). Cancer statistics, 2020. *Ca. Cancer J. Clin.* 70 (1), 7–30. doi:10.3322/caac.21590

Suh, H., Pillai, K., and Morris, D. L. (2017). Mucins in pancreatic cancer: Biological role, implications in carcinogenesis and applications in diagnosis and therapy. *Am. J. Cancer Res.* 7 (6), 1372–1383.

Vinson, K. E., George, D. C., Fender, A. W., Bertrand, F. E., and Sigounas, G. (2016). The Notch pathway in colorectal cancer. *Int. J. Cancer* 138 (8), 1835–1842. doi:10.1002/ijc.29800

Wang, L. J., and Song, B. L. (2012). Niemann-Pick C1-Like 1 and cholesterol uptake. *Biochim. Biophys. Acta* 1821 (7), 964–972. doi:10.1016/j.bbalip.2012.03.004

Warnakulasuriya, S. (2009). Global epidemiology of oral and oropharyngeal cancer. *Oral Oncol.* 45 (4-5), 309–316. doi:10.1016/j.oraloncology.2008.06.002

Yang, J. Y., Hu, Y. W., Zhang, P., Zheng, L., and Wang, Q. (2012). Progress of Niemann-Pick type C1 like 1 on cholesterol metabolism. *Sheng Li Xue Bao* 64 (6), 721–728.

Yarmolinsky, J., Bull, C. J., Vincent, E. E., Robinson, J., Walther, A., Smith, G. D., et al. (2020). Association between genetically proxied inhibition of HMG-CoA reductase and epithelial ovarian cancer. *JAMA* 323 (7), 646–655. doi:10.1001/jama.2020.0150

Yoshioka, Y., Sasaki, J., Yamamoto, M., Saitoh, K., Nakaya, S., Kubokawa, M., et al. (2000). Quantitation by (1)H-NMR of dolichol, cholesterol and choline-containing lipids in extracts of normal and phathological thyroid tissue. *NMR Biomed.* 13 (7), 377–383. doi:10.1002/1099-1492(200011)13:7<377::aid-nbm658>3.0.co;2-e

Yu, L., Bharadwaj, S., Brown, J. M., Ma, Y., Du, W., Davis, M. A., et al. (2006). Cholesterol-regulated translocation of NPC1L1 to the cell surface facilitates free cholesterol uptake. *J. Biol. Chem.* 281 (10), 6616–6624. doi:10.1074/jbc.M511123200

frontiers | Frontiers in Pharmacology

TYPE Original Research
PUBLISHED 11 August 2022
DOI 10.3389/fphar.2022.949745

Check for updates

OPEN ACCESS

EDITED BY
Chen Shi,
Huazhong University of Science and Technology, China

REVIEWED BY
Arslan Ali,
University of Karachi, Pakistan
Chongru Xu,
Guangdong Provincial People's Hospital, China

*CORRESPONDENCE
Bei Xu,
xubei_jylab@sc-mch.cn

SPECIALTY SECTION
This article was submitted to Pharmacology of Anti-Cancer Drugs, a section of the journal Frontiers in Pharmacology

RECEIVED 21 May 2022
ACCEPTED 20 July 2022
PUBLISHED 11 August 2022

CITATION
Yan C, Wu D, Gan L, Wang J, Yang W and Xu B (2022), Significant metabolic alterations in non-small cell lung cancer patients by epidermal growth factor receptor-targeted therapy and PD-1/PD-L1 immunotherapy.
Front. Pharmacol. 13:949745.
doi: 10.3389/fphar.2022.949745

COPYRIGHT
© 2022 Yan, Wu, Gan, Wang, Yang and Xu. This is an open-access article distributed under the terms of the Creative Commons Attribution License (CC BY). The use, distribution or reproduction in other forums is permitted, provided the original author(s) and the copyright owner(s) are credited and that the original publication in this journal is cited, in accordance with accepted academic practice. No use, distribution or reproduction is permitted which does not comply with these terms.

Significant metabolic alterations in non-small cell lung cancer patients by epidermal growth factor receptor-targeted therapy and PD-1/PD-L1 immunotherapy

Chen Yan[1], Dan Wu[2], Lingling Gan[2], Jun Wang[3], Wenyu Yang[3] and Bei Xu[2]*

[1]Department of Clinical Pharmacy, Sichuan Cancer Hospital & Institute, Sichuan Cancer Center, School of Medicine, University of Electronic Science and Technology of China, Chengdu, China, [2]NHC Key Laboratory of Nuclear Technology Medical Transformation, Mianyang Central Hospital, School of Medicine, University of Electronic Science and Technology of China, Mianyang, China, [3]College of Medical Technology, Chengdu University of Traditional Chinese Medicine, Chengdu, China

Background: Cancer-related deaths are primarily attributable to lung cancer, of which non-small cell lung cancer (NSCLC) is the most common type. Molecular targeting therapy and antitumor immunotherapy have both made great strides in the treatment of NSCLC, but their underlying mechanisms remain unclear, especially from a metabolic perspective.

Methods: Herein, we used a nontargeted metabolomics approach based on liquid chromatography-mass spectrometry to analyze the metabolic response of NSCLC patients to epidermal growth factor receptor-tyrosine kinase inhibitors (EGFR-TKIs) or PD-1/PD-L1 inhibitors. Multiple analyses, including principal component analysis (PCA), orthogonal partial least squares-discriminant analysis (OPLS-DA) and pathway analysis, were used for metabolic data analysis. Additionally, differential metabolites were analysed and identified by publically available and integrated databases.

Results: After treatment with EGFR-TKIs or PD-1/PD-L1 inhibitors, glutamate/glutamine, phenylalanine, n-acetyl-L-leucine, n-acetyl-D-tryptophan, D-n-valine, arachidonic acid, and linoleic acid levels were significantly increased in patients with NSCLC, whereas carnitine, stearyl carnitine, palmitoyl carnitine, linoleic carnitine, and palmitic acid levels were markedly decreased. Compared with newly diagnosed, untreated patients, there were three shared metabolic pathways (phenylalanine metabolism, glycerophospholipid metabolism, and D-glutamine and D-glutamate metabolism) in the EGFR-TKIs or PD-1/PD-L1 inhibitor-treated groups, all of which were related to lipid and amino acid metabolism. Moreover,

Abbreviations: EGFR: epidermal growth factor receptor; ERK: extracellular regulated protein kinase; HC: healthy control; MEK: mitogen-activated proteinkinase kinase; mTOR: mammalian target of rapamycin; NSCLC: non-small cell lung cancer; OPLS-DA: orthogonal partial least squares-discriminant analysis; PCA: principal component analysis; PD-1: Programmed death-1; PD-L1: Programmed death ligand 1; PI3K: Phosphoinositide 3-kinases; QC: quality control; TKI: tyrosine kinase inhibitor; VIP: variable importance in projection.

there were significant differences in lipid metabolism (glycerophospholipid metabolism and phosphatidylinositol signaling) and amino acid metabolism (tryptophan metabolism) between the EGFR-TKI and PD-1/PD-L1 inhibitor groups.

Conclusion: Our results show that EGFR-TKIs and PD-1/PD-L1 inhibitors induce changes in carnitine, amino acids, fatty acids, and lipids and alter related metabolic pathways in NSCLC patients. Endogenous metabolism changes occur due to drug action and might be indicative of antitumor therapeutic effect. These findings will provide new clues for identifying the antitumor mechanism of these two treatments from the perspective of metabolism.

KEYWORDS

non-small cell lung cancer, epidermal growth factor receptor-targeted therapy, PD-1/PD-L1 immunotherapy, tumor metabolic reprogramming, untargeted metabolomics

1 Introduction

There were 19.29 million new cancer diagnoses in 2020, of which 2.2 million were lung cancers. Lung cancer accounts for 11.4% of the total cancer diagnoses, making it the second most common cancer worldwide (Sung et al., 2021). Additionally, 1.8 million people died of lung cancer in 2020, accounting for 18.0% of total cancer deaths (Sung et al., 2021). Lung cancer is the leading cause of cancer-related death. Among men, lung cancer is the most common cancer in 36 countries and the leading cause of cancer mortality in 93 countries (Sung et al., 2021). With global population growth, aging, and changing lifestyles, the burden of lung cancer is increasing.

Lung cancers are divided into two categories: non-small cell lung cancer (NSCLC) and small cell lung cancer. NSCLC is the most common type, accounting for approximately 80–85% of all lung cancer cases, and has the highest mortality rate (Singh et al., 2021). The current treatment of NSCLC is not only focused on surgical treatment, chemotherapy, radiotherapy, and comprehensive treatment but includes molecular targeted therapy and antitumor immunotherapy (Ghini et al., 2020; Wang et al., 2021). Epidermal growth factor receptor (EGFR) is the most common driver gene mutation of NSCLC, with approximately 35% of Asian patients and 60% of patients with lung adenocarcinomas (Pi et al., 2018; Yoon et al., 2020). EGFR tyrosine kinase inhibitors (EGFR-TKIs) are the most widely used targeted therapies and are remommended as first-line treatment for NSCLC patients with EGFR activating mutations (National Comprenhensive Cancer Network, 2017; He et al., 2021). These drugs improve progression-free survival and overall survival compared to conventional chemotherapy and are associated with fewer severe adverse events (Singh et al., 2021).

Antitumor immunotherapy is another effective and safe treatment for NSCLC. Immune checkpoint inhibitors are the most studied immunotherapies for NSCLC (Herzberg et al., 2017; Xiong et al., 2021). Immunotherapy differs from traditional chemotherapy and targeted therapy as it kills the tumor by overcoming immunosuppression and reactivating the patient's own immune cells (Alexander et al., 2020). The immune checkpoint molecules PD-1 and its ligands, PD-L1 and PD-L2, are key therapeutic targets (Robert, 2020).

Tumorigenesis and development are closely related to metabolism (DeBerardinis and Chandel, 2016). Metabolic reprogramming is associated with tumorigenesis and is an important hallmark of cancer. Therefore, tumors are not only genetic diseases but also metabolic diseases (Hanahan and Weinberg, 2011). Mutations in tumor-related genes cause changes in multiple signaling pathways in cells, which reshapes the metabolism of tumor cells to enhance their survival and growth ability (Nagarajan et al., 2016). EGFR-TKIs and PD-1/PD-L1 inhibitors can inhibit tumor growth through a variety of signaling pathways, but evidence of their effect on metabolic pathways is limited. Therefore, exploring the effects of EGFR-TKIs and immunotherapy on metabolic pathways in NSCLC would be useful to elucidate the mechanism of these two new therapies and provide strong evidence for clinical treatment selection from the perspective of metabolism. Metabolomics has been widely applied to quantify the changes in metabolites in cells, tissues, and entire organisms with the aim of studying the dynamic changes in endogenous metabolites and reflecting metabolic pathways and shifts in biological processes (Johnson et al., 2016). Therefore, this study aimed to clarify the metabolic changes in patients' serum after treatment with EGFR-TKIs and PD-1/PD-L1 inhibitors and identify metabolic reprogramming mechanisms, thus providing new evidence for targeted therapy and antitumor immunotherapy in NSCLC.

2 Materials and methods

2.1 Study design and participants

Between November 2020 and November 2021, 120 patients with pathologically diagnosed NSCLC were enrolled in this study: 35 patients had not yet received preoperative surgery, radiotherapy, or chemotherapy (A group), 47 patients were treated with EGFR-TKIs (B group), and 50 patients were treated with PD-1/PD-L1 inhibitors (C group). Healthy volunteers without a known chronic or major disease and who were not undergoing any treatment were matched for age, sex, and smoking status with the enrolled patients (HC group). Patients with symptoms associated with bacterial infection, such as fever, increased leukocyte and neutrophil counts, and inflammation indicated by lung imaging or microculture, were excluded from the study to avoid any influence of bacterial infection on the serum metabolome.

2.2 Sample collection and preparation for metabolomics

Blood samples in B and C groups were collected after 2–3 treatment cycles with EGFR-TKIs or PD-1/PD-L1 inhibitors. Briefly, all serum samples were collected in the morning after an overnight fast. Whole blood (5 ml) was collected in sterile coagulation BD vacuum blood collection tubes. The tubes were gently shaken and centrifuged at 3,000 rpm for 10 min at room temperature. The supernatant (serum) was collected in 1.5-ml microfuge tubes and stored at −80°C until further analyses.

After thawing on ice, small metabolites from a 100-µlaliquot of serum was extracted by vortex-mixing with 300 µl of a methanol:acetonitrile (1:1 v/v) solution. The mixture was vortexed, sonicated, and then incubated at −20°C for 30 min. After centrifugation at 13,000 ×g at 4°C for 15 min, the supernatants were filtered through a 0.22-µm microporous membrane and carefully transferred to a sample bottle for LC-MS/MS analysis. Aliquots of all serum samples (10 µl) were pooled as part of the system adjustment and quality control (QC) process to prepare QC samples. The QC samples were treated in the same manner as the analytical samples.

2.3 Metabolite detection

Metabolomics analysis was perfomed on an ultra-performance liquid chromatography (UPLC) system (Agilent1290 Infinity II; Agilent Technologies Inc., CA, United States) connecting to a high-resolution tandem mass spectrometer (TripleTOF 5,600 Plus; AB SCIEX, Framingham, MA, United States). An ACQUITY HSS T3 column (100 × 2.1 mm, i. d. 1.8 µm; Waters, Milford, United States) were equipped for reversed-phase separation. The mobile phase consisted of solvent A (water, 0.1% formic acid) and solvent B (acetonitrile, 0.1% formic acid) with a gradient as previously described (Xu et al., 2021). The column temperature was maintained at 30°C and the flow rate was 0.30 ml/min.

For MS analysis, data acquisition was performed in full scan mode combined with independent data acquisition (IDA)-based auto-MS2 mode. Parameters of mass spectrometer were set as follows: m/z range: 80–1,000 (+) and 80–1,000 (−), ionspray voltage floating: 5500 V (+) and -4500 V (-), declustering potential: 80 V (+) and -80 V (−), collision energy: 10 V (+) and -10 V (-), interface heater temperature: 550°C (+) and 550°C (−), curtain gas: 35 psi, ion source gas 1 and ion source gas 2: 55 psi (+) and 55 psi (−). The m/z range of IDA analysis was set at 50–1,000 in both positive ion mode and negative mode, the collision energy was 35 V in positive ion mode and −35 V in negative ion mode, and collision energy spread was 15 V in both positive and negative ion modes.

During the entire period, the mass accuracy was calibrated after every six samples. Additionally, the purpose of introducing QCs every 10 samples in analytical sequence is to evaluate the reliability of large-scale metabolomics analysis.

2.4 Metabolomics analysis and annotation

Analysis of raw data obtained from UPLC-TOF/MS was conducted using the qualitative analysis software Analyst TF (version 1.7.1, AB SCIEX) for peak identification and comparison. As part of the metabolomics data processing workflow, peak picking, quality assessment, missing value imputation, normalisation, transformation, and scaling were performed. The details was present as below: 1) XCMS algorithm is applied to extract peaks using One-Map/PTO software (www.5omics.com) developed by Dalian ChemDataSolution Information Technology Co. Ltd. 2) Data quality is analyzed based on QC samples' stability after peak extraction. The proportions of RSDs of mass spectrometry characteristics below 50% should account for more than 80%. QC calibration is performed using the MetNormalizer method based on support vector regression analysis. 3) The 80/20 rule is employed to eliminate metabolic features with non-zero values exceeding 20% in any category. Missing values are filled with the minimum value in the data. 4) A normalization process is required for that concentration of metabolites varies between individual organisms or during sample collection. To eliminate or reduce this heterogeneity, each metabolite is divided by the total concentration of the sample, so as to correct the influence of individual differences or other factors on the absolute concentration of metabolites. 5) In the data analysis, auto scaling and pareto scaling are used (scaling is used to

TABLE 1 The clinical characteristics of the enroled participants.

Characteristics	A (n = 35)	B (n = 47)	C (n = 50)	HC (n = 50)	χ2, P
Male/Female	25/10	30/17	40/10	38/12	5.370, 0.157
Age (years)	57.00 (52.00, 63.00)	57.00 (52.00, 66.00)	58.00 (53.00, 61.00)	54.50 (50.75, 58.00)	7.572, 0.056
Weight (Kg)	65.00 (60.00, 72.50)	61.00 (56.00, 67.00)[a]	60.00 (54.00, 67.00)[a]	67.00 (62.00, 70.00)[b,c]	17.979, <0.001
Type (n)	—	—	—	—	—
Squamous carcinoma	8	4	8	—	—
Adenocarinoma	17	27	34	—	—
Large cell carcinoma	2	2	1	—	—
NA	8	14	7	—	—
Tumor stage (n)	—	—	—	—	—
I	3	3	2	—	—
II	3	2	4	—	—
III	5	6	9	—	—
IV	14	23	26	—	—
NA	10	13	9	—	—
Metastasis (n)	19	31	39	—	—
CEA (ng/ml)	3.76 (1.27, 27.82)	3.66 (2.36, 26.82)	3.92 (1.27, 10.64)	1.25 (1.00, 1.87)[a,b,c]	20.250, <0.001
NSE (μg/L)	7.67 (5.65, 9.78)	8.62 (6.32, 10.90)	7.56 (5.41, 9.95)	5.94 (5.32, 7.67)[a,b,c]	21.682, <0.001
proGRP (ng/ml)	0.04 (0.03, 0.06)	0.06 (0.03, 0.205)	0.04 (0.03, 0.07)	0.05 (0.04, 0.06)	5.385, 0.146

Note: A, NSCLC, patients without any anticancer treatment; B, NSCLC, patients treated with EGFR-TKIs; C, NSCLC, patients treated with PD-1/PD-L1, inhibitors; HC, healthy control. [a]Compared with the A group, $p < 0.05$; [b]Compared with the B group, $p < 0.05$;[c]Compared with the C group, $p < 0.05$.

eliminate variation in metabolite concentration orders of magnitude). Auto scaling is performed on the characteristic variables during principal component analysis (PCA) and partial least squares-discriminant analysis (PLS-DA), while pareto scaling is performed on the characteristic variables during orthogonal partial least squares-discriminant analysis (OPLS-DA).

The standard database (containing information of 1,550 metabolic standards), and custom databases including METLIN (http://metlin.scripps.edu/), Kyoto Encyclopedia of Genes and Genomes (KEGG) (http://www.kegg.jp/kegg/pathway.html), LipidMaps (https://www.lipidmaps.org/), Human Metabolome DataBase (HMDB) (https://hmdb.ca/), MassBank (https://massbank.eu/), and PubChem Database (https://pubchem.ncbi.nlm.nih.gov/) were used to validate, match, and annotate the processed molecular weights of the metabolites for accurate metabolite characterization. Notably, according to the definitions of metabolite identification as described by Schrimpe-Rutledge (Schrimpe-Rutledge et al., 2016), all the metabolites determined here would be considered as putative identification (Level 2), which lack the reference standard acquisition but used MS/MS data in combination of precursor m/z and retention time to derive the structural information.

SIMCA 15.0.2 (Umetrics AB, Umea, Sweden) was used to perform multivariate analyses. An unsupervised, nontargeted PCA was conducted using LC-MS/MS data, allowing for the visualization of holistic metabolome variation among groups and monitoring of stability over time. Significantly different metabolites were identified using OPLS-DA. Model parameters R2 and Q2 were used to assess model validity and avoid overfitting by supplying information about interpretability and predictability. OPLS-DA was applied to compute variable importance in projection (VIP). In a single-dimension statistical analysis, *p*-values were estimated through paired Student's t-tests. The *t*-test, in conjunction with the OPLS-DA method, was used to determine the difference in metabolites between groups (while fulfilling VIP >1 and $p < 0.05$).

2.5 Statistical analysis

Statistics were conducted utilizing SPSS 25.0 (International Business Machines Corp., Armonk, NY, United States). Means and standard deviations of normally distributed data were calculated and reported. ANOVA was used for comparisons among multiple groups in the case of homogeneity of variance, followed by LSD *t*-test; otherwise, Welch's *t*-test and Dunnett's T3 test were adopted. A median (interquartile range) [M (P25, P75)] is calculated for non-normally distributed data. Comparing differences between groups was performed using the independent-sample Kruskal–Wallis test. A chi-square test was used to compare count data among groups Statistical significance was set at $p < 0.05$.

3 Results

3.1 Population and clinical characteristics

Characteristics of the study population are presented in Table 1. Forty-seven patients (group B) treated with EGFR-TKIs were analyzed, 29 of whom were treated with EGFR-TKIs as first-line therapy and 18 of whom were treated with EGFR-TKIs as second- and third-line therapy after cytotoxic chemotherapy. Twenty-four enrolled patients received PD-1/PD-L1 inhibitors alone as first-line treatment when their tumors had a PD-L1 expression greater than or equal to 50%, and 26 patients received PD-1/PD-L1 inhibitors as second- or third-line treatment after platinum failure regardless of the PD-L1 expression value. No significant differences in sex or age were identified among the patient groups. There were more men than women. Weight loss was observed in the EGFR-TKI and PD-1/PD-L1 inhibitor groups (B and C groups). Compared to the HC group, NSCLC patients had higher levels of CEA and NSE, whereas there was no difference in proGRP among the groups.

3.2 Multivariate statistical analysis of metabolites

Liquid chromatography-mass spectrometry is a method that is commonly used to analyze metabolomic data and generate the mass-to-charge ratio for metabolomic analysis of biological samples. Processed data comprising retention time, exact mass, and peak intensity from the three subgroups, including the untreated group (group A), the EGFR-TKI-treated group (group B), and the PD-1/PD-L1 inhibitor-treated group (group C), were subjected to multivariate statistical analysis.

PCA plots showed a clustering of QC samples (Figures 1A,B), and correlation heatmaps present strong correlations between QC samples (Figures 1C,D), indicating the satisfactory stability and repeatability of the analytical system. However, no distinct classifications were achieved for the A vs B, A vs C, or B vs C comparisons in either the positive or negative ion modes, indicating no effective separation of the principal components.

As OPLS-DA is more discriminatory than PCA, it was further used to explore the different metabolic profiles. Distinct clustering in the A vs B, A vs C, and B vs C comparisons was observed in both the positive and negative ion modes, indicating a clear separation of the three patient cohorts (Figures 1E,F and Figure 2). Model evaluation used OPLS-DA's R2X, R2Y, and Q2 (cumulative) parameters. Table 2 list these modeling parameters within each comparison. The high Q2 values of the OPLS-DA model showed its high accuracy. Overfitting of the supervised OPLS-DA models was examined by performing 200 random permutations. Positive and negative ions had

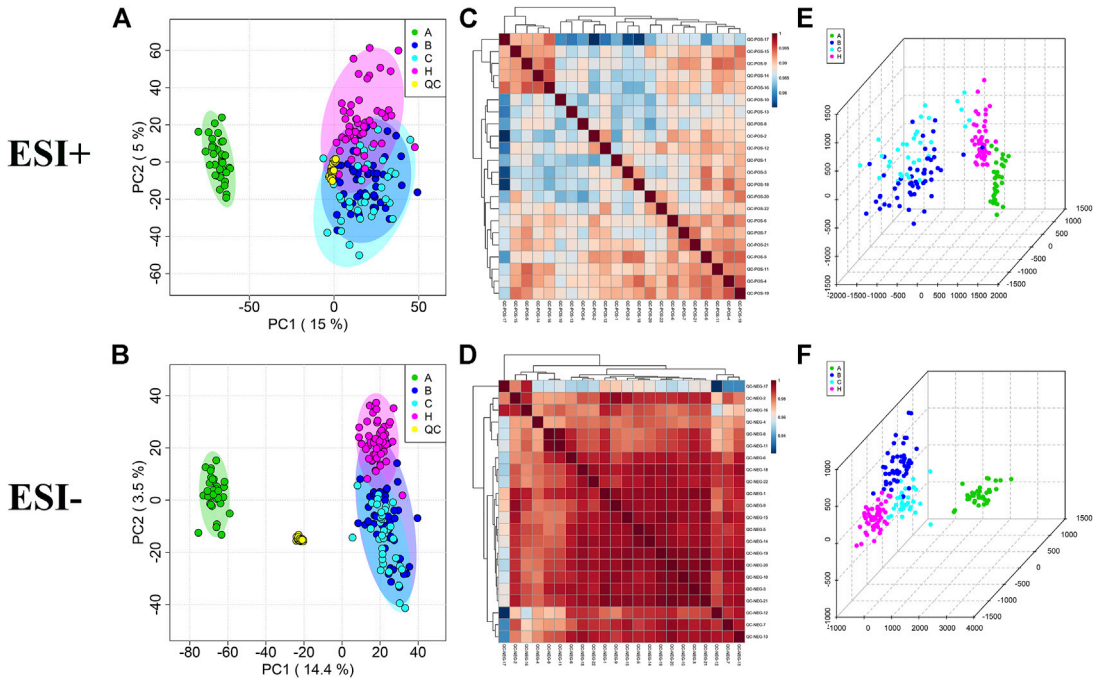

FIGURE 1
Multivariate statistical analysis in A, B, C and HC groups. **(A,B)** PCA score plots with QC samples; **(C,D)** Correlation analysis of QC samples in the ESI+ and ESI− scan modes. **(E,F)** OPLS-DA score plots of A, B, C and HC groups in the ESI+ and ESI− scan modes.

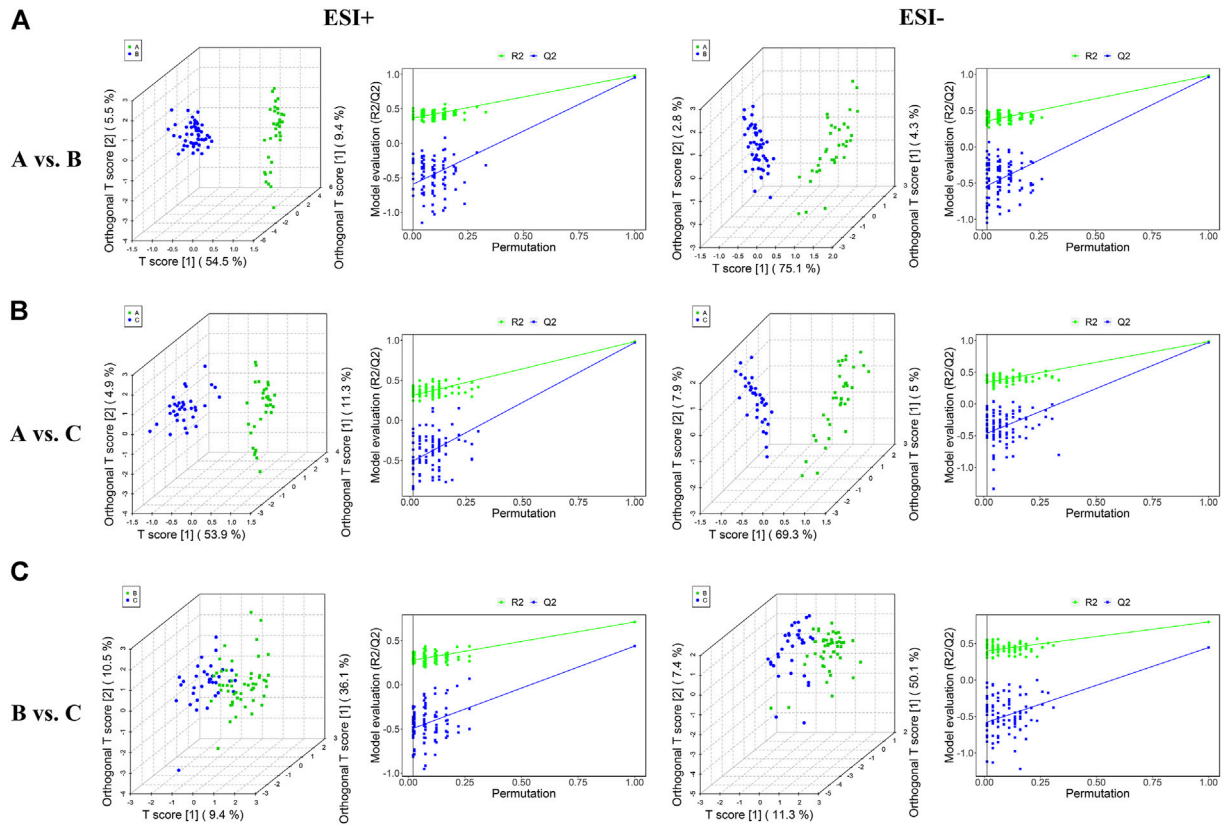

FIGURE 2
Plots of OPLS-DA score and permutation testing for A vs. B **(A)**, A vs. C **(B)**, B vs. C **(C)** comparisons in the ESI+ and ESI− scan modes. The criterion for evaluating whether there is overfitting in the OPLS-DA model is that the regression line at a blue Q2 point crosses or is less than 0 from the abscissa.

TABLE 2 Comparisons among groups under ESI+ and ESI- scan modes using PLS-DA and OPLS-DA analysis models.

Scan mode	Analysis model	Group	R2X	R2Y	Q2
ESI+	PLS-DA	4 group	0.27	0.95	0.95
	OPLS-DA	4 group	0.33	0.65	0.57
		A vs. B	0.55	0.90	0.90
		A vs. C	0.54	0.89	0.88
		B vs. C	0.36	0.42	0.31
ESI-	PLS-DA	4 group	0.23	0.99	0.99
	OPLS-DA	4 group	0.38	0.77	0.574
		A vs. B	0.75	0.96	0.96
		A vs. C	0.69	0.96	0.96
		B vs. C	0.50	0.59	0.52

Note: A, NSCLC, patients without any anticancer treatment; B, NSCLC, patients treated with EGFR-TKIs; C, NSCLC, patients treated with PD-1/PD-L1, inhibitors; HC, healthy control.

Q2 distributions with Y-intercepts lower than zero, indicating the reliability of OPLS-DA (Figure 2). Therefore, the PCA and OPLS-DA models showed significant distinctions among the A vs B, A vs C, and B vs C comparisons and were highly effective in characterizing serum metabolites.

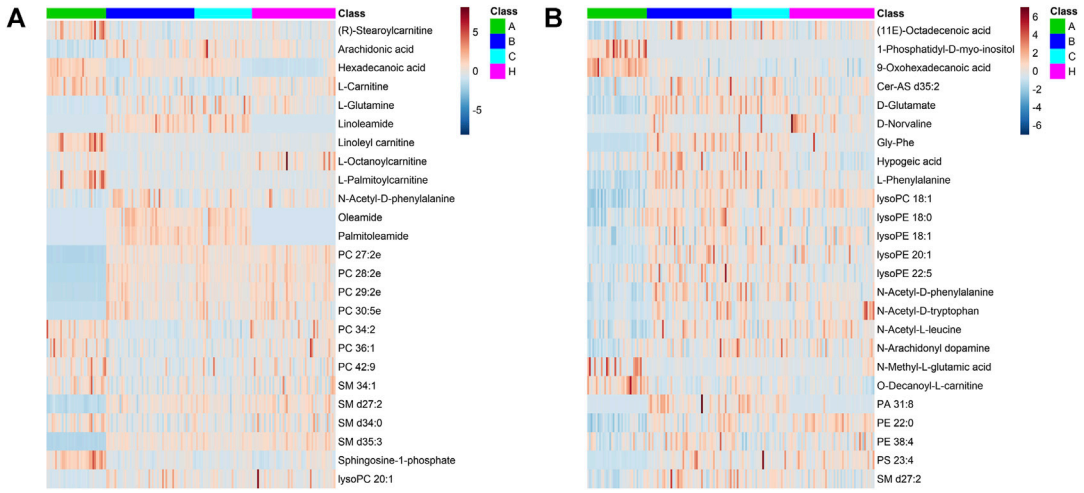

FIGURE 3
Differential metabolite heat maps in ESI+ **(A)** and ESI− **(B)** scan modes. The columns represent samples, the rows represent metabolites, and the relative content of the metabolites is displayed by color. The heat map shows differential metabolites among A, B, C, and HC groups.

TABLE 3 List of statistically significant metabolites in A vs B and A vs C comparisons.

Metabolites		B vs. A				C vs. A			
		VIP	Log2(FC)	P	Trend	VIP	Log2(FC)	P	Trend
Carnitine	L-Carnitine	1.77	-0.70	<0.001	↓	1.94	-0.89	<0.001	↓
	(R)-Stearoylcarnitine	1.55	-0.76	<0.001	↓	1.25	-0.59	<0.001	↓
	L-Palmitoylcarnitine	1.57	-1.11	<0.001	↓	1.35	-1.01	<0.001	↓
	Linoleyl carnitine	2.01	-2.05	<0.001	↓	1.80	-1.96	<0.001	↓
Amino acids	L-Glutamine	1.65	2.02	<0.001	↑	1.61	2.28	<0.001	↑
	D-Glutamate	2.00	0.81	<0.001	↑	1.90	0.83	<0.001	↑
	L-Phenylalanine	2.05	0.85	<0.001	↑	1.90	0.81	<0.001	↑
	N-Acetyl-L-leucine	1.26	0.69	<0.001	↑	1.14	0.59	<0.001	↑
	N-Acetyl-D-tryptophan	1.41	1.39	<0.001	↑	1.38	1.01	<0.001	↑
Fatty acids	Arachidonic acid	1.82	1.67	<0.001	↑	1.99	1.73	<0.001	↑
	Hypogeic acid	1.09	0.66	<0.001	↑	1.18	0.67	<0.001	↑
	9-Oxohexadecanoic acid	1.99	-0.77	<0.001	↓	2.00	-0.96	<0.001	↓
Lipids	PI 16:1	1.67	2.21	<0.001	↑	1.81	1.91	<0.001	↑
	Lyso PE 20:1	1.76	1.80	<0.001	↑	1.85	1.50	<0.001	↑
	Lyso PC 20:1	1.60	1.37	<0.001	↑	1.73	1.14	<0.001	↑
	PA 31:8	1.48	4.16	<0.001	↑	2.02	4.13	<0.001	↑
	PS 23:4	1.65	3.54	<0.001	↑	1.28	3.35	<0.001	↑
	PC 34:2	1.67	-0.82	<0.001	↓	1.17	-0.66	<0.001	↓
	PC 29:2e	2.36	4.25	<0.001	↑	2.38	4.20	<0.001	↑
	SM d35:3	2.53	5.46	<0.001	↑	2.42	5.45	<0.001	↑

Note: A, NSCLC, patients without any anticancer treatment; B, NSCLC, patients treated with EGFR-TKIs; C, NSCLC, patients treated with PD-1/PD-L1, inhibitors; HC, healthy control. VIP, variable influence on projection; FC, fold-change.

TABLE 4 List of statistically significant metabolites in B vs C comparison.

Metabolites		B vs. C			
		VIP	Log2(FC)	P	Trend
Amino acids	N-Acetyl-D-tryptophan	1.15	0.38	0.044	↑
	L-Kynurenine	1.57	-0.27	0.027	↓
	L-Isoleucine	1.26	0.96	0.045	↑
	Arachidonoyl Glycine-d8	1.45	-0.43	0.044	↓
Lipids	PI 38:3	1.38	0.35	0.018	↑
	PI 38:5	1.47	0.32	0.012	↑
	PE 38:4	2.54	0.64	<0.001	↑
	PC 38:4	1.53	0.37	0.020	↑
	LysoPE 18:0	2.38	0.33	<0.001	↑
	LysoPC 18:3	2.19	0.49	<0.001	↑

Note: A, NSCLC, patients without any anticancer treatment; B, NSCLC, patients treated with EGFR-TKIs; C, NSCLC, patients treated with PD-1/PD-L1, inhibitors; HC, healthy control. VIP, variable influence on projection; FC, fold-change.

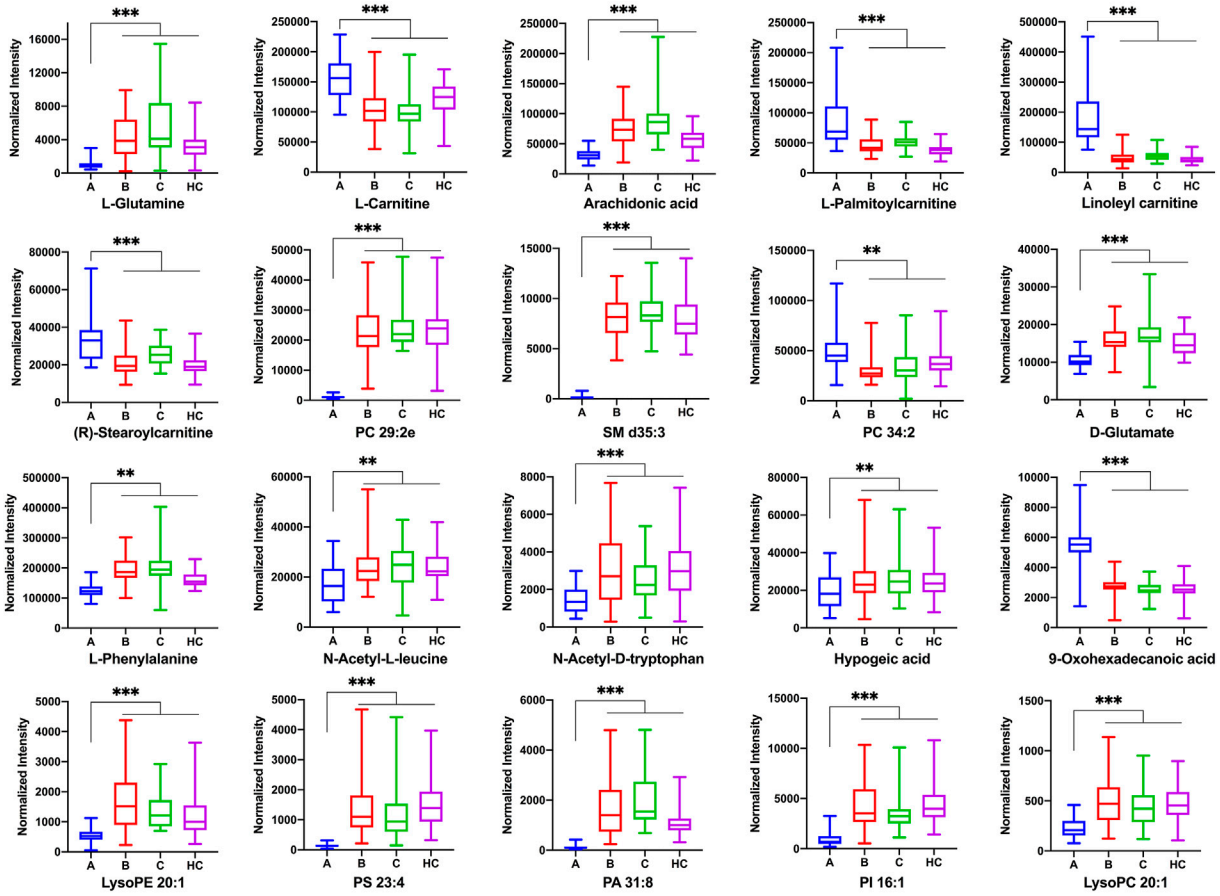

FIGURE 4
The normalized peak intensity of 20 representative differential metabolites among A, B, C, and HC groups. $p^{**} < 0.01$; $p^{***} < 0.001$.

3.3 Differential metabolite analysis and identification

Databases, publically available and integrated, were used for qualitative identification. Using the positive and negative ion modes, 754 and 697 metabolites were identified, respectively. Subsequently, 97 and 87 different metabolites in the A vs B and A vs C comparisons were selected using a fold-change threshold >1.5 or <2/3, VIP >1, and Student's t-test threshold $p < 0.05$. Thirty-four different metabolites in the B vs C comparison were selected using a fold-change threshold >1.2 or <2/3, VIP >1, and Student's t-test threshold $p < 0.05$. There was clear clustering in heat maps of 25 representative differential metabolites detected in both positive and negative modes between groups A, B, C, and HC (Figure 3), consistent with the OPLS-DA results.

The most abundant classes of metabolites for the A vs B and A vs C comparisons were carnitines, amino acids, fatty acids, and lipids (Table 3), whereas for the B vs C comparison, the most abundant classes were fatty acids and lipids (Table 4). In the A vs B and A vs C comparisons, the levels of most carnitines decreased, whereas the levels of essential amino acids increased. Fatty acids and lipids were both increased and decreased because of their wide variety. Twenty significantly altered metabolites were identified based on the screening criteria (FC > 1.5 or <2/3, VIP >1, and $p < 0.05$). Semi-quantitative analysis of these representative differential metabolites showed that after treatment with EGFR-TKIs or PD-1/PD-L1 inhibitors, the levels of the metabolites were closer to those in the HC group (Figure 4), which proved the effectiveness of the treatment. Notably, some glycerophosphatide (mainly PC and PA) levels in the treatment groups did not return to normal, and an increase of arachidonic acid in B and C groups was still observed as compared with healthy individuals (data not shown).

Ten significantly altered metabolites were identified in the B vs C comparison based on FC > 1.2 or <2/3, VIP >1, and $p < 0.05$. The main differentially regulated metabolites between the two groups were amino acids and lipids. Among them, tryptophan and its metabolite kynurenine, phosphatidylinositol, phosphatidylethanolamine, phosphatidylcholine, lysophosphatidylethanolamine, and lysophosphatidylcholine changed significantly.

3.4 Perturbed pathways identified in group comparisons

We next examined the metabolic pathways enriched among the differential metabolites. Pathway impact values refer to the cumulative percentage from the matched metabolite nodes and the maximum importance of each pathway is 1. The results of metabolic pathway analysis showed that the perturbed pathways were mainly enriched in 1) phenylalanine metabolism, glycerophospholipid metabolism, D-glutamine and D-glutamate metabolism, and phenylalanine, tyrosine, and tryptophan biosynthesis for the A vs B comparison; 2) linoleic acid metabolism, phenylalanine metabolism, glycerophospholipid metabolism, and D-glutamine and D-glutamate metabolism for the A vs C comparison; and 3) glycerophospholipid metabolism, tryptophan metabolism, and phosphatidylinositol signaling system for the B vs C comparison (Figure 5 and Table 5).

There were three shared metabolic pathways in the A vs B and A vs C comparisons, all of which were related to lipid and amino acid metabolism. The two groups shared many of the same differential metabolites and thus shared the same enriched metabolic pathways. Although both EGFR-TKIs and PD-1/PD-L1 inhibitors can regulate tumor lipid metabolism, our results suggest that the mechanisms of lipid metabolism regulation may differ, leading to significant differences in lipid metabolism between the two treatments. As expected, the enriched metabolic pathways in the B vs C comparison included the tryptophan metabolic pathway. Moreover, glycerophospholipid metabolism was the most significantly altered metabolic pathway in all three comparisons, suggesting that lipid metabolism plays an important role in tumor development.

4 Discussion

The incidence and mortality of lung cancer, especially NSCLC, are very high. Although there are many treatments for NSCLC, the underlying mechanisms of the treatment effects remain unclear. In this study, we used a nontargeted metabolomics approach based on liquid chromatography-mass spectrometry to analyze the metabolic response of NSCLC patients to EGFR-TKIs or PD-1/PD-L1 inhibitors in an attempt to provide new clues to identifying the antitumor mechanism of these two treatments from the perspective of metabolism.

Many studies have shown that EGFR-TKIs and PD-1/PD-L1 inhibitors can affect tumor metabolism (Chang et al., 2015; Zhang et al., 2021). EGFR-TKIs inhibit tumor growth by blocking the activation of EGFR in cancer cells and the downstream MAPK (RAS/RAF/MEK/ERK) and PI3K/AKT/mTOR signaling pathways. They inhibit cell proliferation and tumor-induced angiogenesis while promoting apoptosis (Singh et al., 2021). It has been reported that the overactivation of the MAPK and PI3K/AKT pathways is related to the reprogramming of specific metabolic processes, including increasing glucose uptake through glucose transporter 1, enhancing glutamine replenishment by activating glutamate pyruvate aminotransferase 2, and cellular lipid reprogramming (Koundouros and Poulogiannis, 2020). Besides, PD-1/PD-L1 inhibitors were

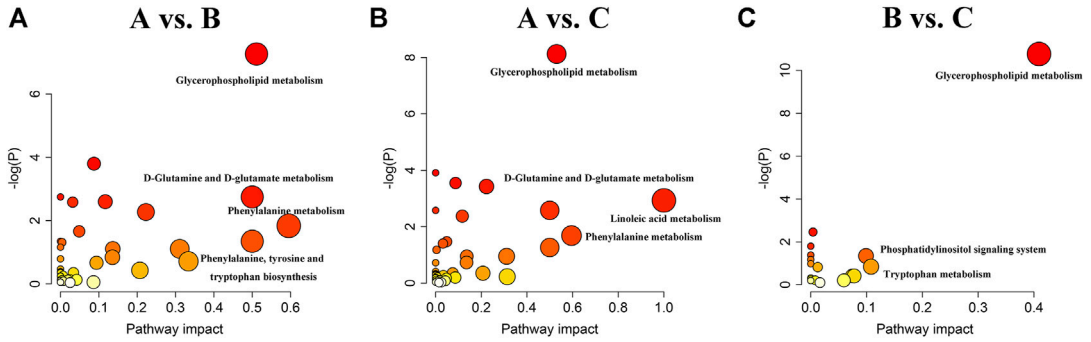

FIGURE 5
Summary of metabolic pathways analyzed in A vs. B **(A)**, A vs. C **(B)** and B vs. C **(C)** comparisons.

originally designed to reactivate the host antitumor immune response by blocking the PD-1/PD-L1 immune checkpoint. However, there is increasing evidence that immune checkpoint inhibitors can affect the metabolic fitness of tumor and T cells. For example, the expression of PD-L1 and B7-H3 (also known as CD276) in tumor cells can stimulate aerobic glycolysis in tumor cells by activating the PI3K/AKT/mTOR pathway (Li et al., 2019a; Stirling et al., 2022). Conversely, the interaction of PD-1 with PD-L1 or PD-L2 can impair the metabolic reprogramming of T cells by inhibiting the similar pathway (Wang et al., 2022). Therefore, these studies provide theoretical support for us to explore the mechanisms of these two emerging treatment methods for NSCLC from the perspective of metabolism. To the best of our knowledge, there has been no metabolomic study in NSCLC patients for comparing the EGFR-TKIs and PD-1/PD-L1 inhibitors.

Our PCA score chart showed that under the positive and negative ion modes, the clusters of the EGFR-TKI- and PD-1/PD-L1 inhibitor-treated groups tended to be close to the cluster of the HC group and were significantly separated from the cluster of the primary lung cancer group, indicating that EGFR-TKIs and PD-1/PD-L1 inhibitors have definite antitumor therapeutic effects on NSCLC. The OPLS-DA score charts showed good differentiation between the groups. Compared with the newly diagnosed, untreated lung cancer group, there were significant changes in carnitine, amino acids, fatty acids, and lipids in the EGFR-TKI- and PD-1/PD-L1 inhibitor-treated groups. The treatment groups had two similar significantly altered metabolic pathways: glutamine and D-glutamate metabolism and glycerol phospholipid metabolism. We believe that this may be related to the action of therapeutic drugs on the same signaling pathway (such as PI3K/AKT/mTOR) and the

TABLE 5 Significantly altered metabolic pathways in A vs B, A vs C and B vs C comparisons.

Comparison	Pathway name	KEGG.id	-log(P)	Impact	Hits
A vs B	Phenylalanine metabolism	hsa00360	1.84	0.60	2
	Glycerophospholipid metabolism	hsa00564	7.27	0.51	9
	D-Glutamine and D-glutamate metabolism	hsa00471	2.75	0.50	2
	Phenylalanine, tyrosine and tryptophan biosynthesis	hsa00400	1.35	0.50	1
A vs C	Linoleic acid metabolism	hsa00591	2.93	1	2
	Phenylalanine metabolism	hsa00360	1.67	0.59	2
	Glycerophospholipid metabolism	hsa00564	8.12	0.53	10
	D-Glutamine and D-glutamate metabolism	hsa00471	2.58	0.50	2
B vs C	Glycerophospholipid metabolism	hsa00564	10.77	0.41	8
	Tryptophan metabolism	hsa00380	0.84	0.11	2
	Phosphatidylinositol signaling system	hsa04070	1.34	0.10	2

Note: A, NSCLC, patients without any anticancer treatment; B, NSCLC, patients treated with EGFR-TKIs; C, NSCLC, patients treated with PD-1/PD-L1, inhibitors; HC, healthy control.

utilization of the same therapeutic drugs (such as platinum) in the early treatment stage. After treatment with EGFR-TKIs or PD-1/PD-L1 inhibitors, glutamate/glutamine, phenylalanine, n-acetyl-L-leucine, n-acetyl-D-tryptophan, D-n-valine, arachidonic acid, and linoleic acid levels were significantly increased in patients with NSCLC, whereas carnitine, stearyl carnitine, palmitoyl carnitine, linoleic carnitine, and palmitic acid levels were markedly decreased. The levels of these metabolites in the two treatment groups were similar to those in the HC group, which is consistent with the results of the PCA.

Lung cancer cells require glutamine to meet their metabolic needs. As a nitrogen source, glutamine directly or indirectly after conversion to glutamate contributes to many anabolic processes in cancer, such as the biosynthesis of amino acids, nucleotide bases, and hexosamine. It also plays an important role in redox homeostasis. In addition, in a process known as glutamine decomposition, glutamine is converted to α-ketoglutaric acid, which serves as the energy and carbon source that supplements intermediates of the tricarboxylic acid cycle (Tang et al., 2022; Vanhove et al., 2019). EGFR phosphorylates ELK1 through the MEK/ERK pathway, which can activate GDH1 transcription and glutamine degradation, providing a new perspective for changes in glutamine metabolism in tumor cells (Yang et al., 2020). In addition, as mentioned earlier, the interaction between PD-1 and PD-L1 or PD-L2 inhibits the PI3K/AKT/mTOR pathway and blocks metabolic reprogramming of T cells, including glutamine hydrolysis. In our study, EGFR-TKIs and PD-1/PD-L1 inhibitors reduced glutamine decomposition, which may be related to the inhibition of the MEK/ERK and/or PI3K/AKT/mTOR pathways. Further, the level of glutamine increased significantly in our treatment groups, indicating a reduced consumption of glutamine after treatment, which may also reflect the reduction in glutamine addiction in tumor cells after treatment (Euceda et al., 2017).

Essential amino acids (tryptophan, methionine, valine, lysine, isoleucine, phenylalanine, leucine, threonine, and histidine) not only provide raw materials for the synthesis of biological macromolecules such as proteins, lipids, and nucleic acids but can also be used as signaling molecules to induce the activation of the mTOR pathway (Hosios et al., 2016). Driven by RAS/RAF/MEK/ERK and PI3K/AKT/mTOR signaling, proliferating cells import nutrients, such as amino acids, thus activating mTORC1, inducing transcriptional reprogramming of MYC and other transcription factors, and promoting the expression of growth signal-related genes and protein and ribosome synthesis (Stine et al., 2022). We speculate that EGFR-TKIs and PD-1/PD-L1 inhibitors block PI3K/AKT/mTOR signaling, which blocks the absorption of essential amino acids by tumor cells, resulting in increased phenylalanine, n-acetyl-L-leucine, and n-acetyl-D-tryptophan. In addition, the increase in phenylalanine may be closely related to cell cycle arrest in the G1 phase. Previous studies have shown that the EGFR-TKIs gefitinib and lapatinib can block cell cycle progression (Konecny et al., 2006; Rusnak et al., 2001). This also demonstrates the effectiveness of EGFR-TKIs in EGFR-mutated NSCLC.

Arachidonic acid, linoleic acid, and palmitic acid are involved in fatty acid metabolism. Fatty acids can participate in the structural synthesis of phospholipids on the membrane of cancer cells and promote the transduction of important signals. Cancer cells also utilize ATP produced by fatty acid β-oxidation as an energy source (Koundouros and Poulogiannis, 2020). Carnitine is an essential energy substance involved in the β-oxidation of fatty acids (Longo et al., 2016); the rate-limiting step of β-oxidation is the carnitine shuttle (Li and Zhao, 2021). Our study found that carnitine levels were decreased after treatment with EGFR-TKIs or PD-1/PD-L1 inhibitors. This may inhibit the β-oxidation of fatty acids, leading to the abnormal metabolism of fatty acids (arachidonic acid, linoleic acid, and palmitic acid) and reducing the energy uptake of tumor cells. These results suggest that EGFR-TKI or PD-1/PD-L1 inhibitor treatment may improve the effect of antitumor therapy by restoring endogenous fatty acid homeostasis. The significantly differentially regulated metabolites in these patients, including arachidonic acid, linoleic acid, and glutamate, are all involved in inflammation and oxidation. It has been suggested that EGFR-TKIs or PD-1/PD-L1 inhibitors may also play a therapeutic role in NSCLC through anti-inflammatory and antioxidant mechanisms (Liao et al., 2012).

Metabolomic profiling of tumor and plasma samples from NSCLC patients has indicated alterations in the lipid composition. Lipids are used as energy sources and cellular components (in the form of phospholipids) for rapidly proliferating cancer cells (Kowalczyk et al., 2021). Glycerophospholipid metabolism is highly related to the development and progression of cancer (Yang et al., 2022). A review of 12 articles showed that the phosphatidylcholine, phosphatidylethanolamine, phosphatidylinositol, cardiolipin, phosphatidylserine, phosphatidylglycerol, ceramide, lysophosphatidylethanolamine, lysophosphatidylcholine, and lysophosphatidylglycerol levels were significantly different between NSCLC and normal tissues (Jianyong et al., 2021), which was consistent with what we observed in the serum of NSCLC patients. After treatment with EGFR-TKIs or PD-1/PD-L1 inhibitors, the levels of various glycerol phospholipids tended to decrease to levels similar to those in the HC group, indicating that these two treatments may block the dysregulation of lipid metabolism in tumor cells to a certain extent to exert antitumor therapeutic effects. In addition, changes in lipid composition can alter the

properties of the cell membrane and affect its function, including material exchange and signal transduction (Lin et al., 2017). The interference of EGFR-TKIs or PD-1/PD-L1 inhibitors on the metabolism of glycerophospholipids or glycerol esters in patients with NSCLC suggests that small-molecule targeted drugs or immunotherapies may also inhibit the malignant proliferation of tumor cells by interfering with cell membrane stability. Our results also suggest that lipid differentials may be good biomarkers for tumorigenesis, development, and prognosis.

There were significant differences in lipid metabolism (glycerophospholipid metabolism and phosphatidylinositol signaling) and amino acid metabolism (tryptophan metabolism) between the EGFR-TKI and PD-1/PD-L1 inhibitor groups. The therapeutic mechanisms of the two treatments are not identical, which leads to differences in the levels and downstream effectors of various glycerophospholipids. We also found that PD-1/PD-L1 inhibitor treatment affected phosphatidylinositol signaling more than EGFR-TKI treatment. Phosphatidylinositol is a lipid signaling molecule that is the main regulator of cell signaling (Hammond and Burke, 2020). When PD-1 binds to PD-L1, downstream T cell activation is blocked by the phosphorylation of phosphatidylinositol-3-kinase. Conversely, blocking the PD-1/PD-L1 signaling pathway can inhibit the phosphatidylinositol-3-kinase/AKT signaling pathway and promote T cell activation. Therefore, phosphatidylinositol signaling may be more related to PD-1/PD-L1 inhibitor therapy. Futhermore, the conversion of tryptophan to kynurenine can also significantly affect the response to immunotherapy in cancer (Li et al., 2019b). Tryptophan in the tumor microenvironment can be metabolized to kynurenine by indoleamine-2,3-dioxygenase. Kynurenine inhibits T cell activation, which allows tumor cells to evade immune system monitoring and clearance. In our study, the level of kynurenine was slightly increased in the PD-1/PD-L1 inhibitor group. We speculate that this might be related to PD-1/PD-L1 inhibitor resistance in some patients with NSCLC (Lei et al., 2020). This suggests that inhibiting the tryptophan-kynurenine pathway through the administration of indoleamine-2,3-dioxygenase inhibitors may benefit NSCLC patients who are resistant to PD-1/PD-L1 inhibitors (Kotecki et al., 2021).

Compared with healthy controls, patients treated with EGFR-TKIs and PD-1/PD-L1 inhibitors had abnormal glycerophosphatide metabolism. Some glycerophosphatide (mainly PC and PA) levels in the treatment groups did not return to normal, so the metabolic pathway of glycerophosphatide still differed from healthy individuals. In addition, a different metabolism of arachidonic acid was observed. Arachidonic acid metabolism is involved in inflammation and lipid oxidation processes. Tumor cells maintain their proliferation by metabolizing arachidonic acid. The arachidonic acid metabolic chain may be inhibited by EGFR-TKIs or PD-1/PD-L1 inhibitors, making it unable to produce pro-inflammatory and pro-tumor substances (such as eicosanoids) through key enzymes in the arachidonic acid metabolic network, thus causing a raise of the arachidonic acid (Koundouros et al., 2020). Consequently, treatment and healthy groups exhibit different arachidonic acid metabolic pathways. In addition, we noted that there were no significant differences in amino acid-related metabolic pathways (such as alanine, aspartic acid and glutamate metabolic pathways) between the healthy group and the treatment groups, suggesting that therapeutic drugs may restore endogenous amino acid to normal levels by regulating amino acid metabolism in NSCLC patients.

Altogether, our results show that EGFR-TKIs and PD-1/PD-L1 inhibitors induce changes in carnitine, amino acids, fatty acids, and lipids and alter related metabolic pathways in NSCLC patients. Changes in endogenous metabolism are caused by drug action and may be related to the effects of antitumor therapy. However, our research has some limitations. First, the sample size was small, so a large, multicenter study is necessary to reduce sampling error. Second, some of the included patients had different degrees of concomitant drug use in the early treatment stage, which inevitably affected metabolic pathways to some extent. Third, the types of EGFR-TKIs and PD-1/PD-L1 inhibitors were not completely consistent, which also led to slightly inconsistent results and needs to be standardized in further studies.

Data availability statement

The raw data supporting the conclusions of this article will be made available by the authors, without undue reservation.

Ethics statement

The study was approved by the Medical Ethics Committee of Sichuan Cancer Hospital & Institute, (approval no. SCCHEC-02–2017-042). All patients provided written informed consent to participate.

Author contributions

All authors contributed to the study conception and design and take responsibility for the integrity of the data and the accuracy of the data analysis. Data collection was performed by LG, DW, JW and WY; and analysis was performed by BX and YC. Material preparation and the first draft of the manuscript was written by BX and YC; and all authors commented on previous versions of the manuscript. All authors contributed to the article and approved the submitted version.

Funding

This work was financially supported by Sichuan Science and Technology Program (Nos. 2022NSFSC0792; 2022NSFSC0735; 2020YFS0417), Chengdu Key Research and Development Support Program of Science and Technology Projects (No. 2022-YF05-0159-SN), Youth Innovation Research Project of Sichuan Medical Association (No. Q21012), and Incubation Project of Mianyang Central Hospital (No. 2019FH01).

Acknowledgments

The authors thank Prof. Hongwei Zhang from Sichuan Cancer Hospital, for kindly providing the valuable clinical assistance in this study.

Conflict of interest

The authors declare that the research was conducted in the absence of any commercial or financial relationships that could be construed as a potential conflict of interest.

Publisher's note

All claims expressed in this article are solely those of the authors and do not necessarily represent those of their affiliated organizations, or those of the publisher, the editors and the reviewers. Any product that may be evaluated in this article, or claim that may be made by its manufacturer, is not guaranteed or endorsed by the publisher.

References

Alexander, M., Ko, B., Lambert, R., Gadgeel, S., and Halmos, B. (2020). The evolving use of pembrolizumab in combination treatment approaches for non-small cell lung cancer. *Expert Rev. Respir. Med.* 14 (2), 137–147. doi:10.1080/17476348.2020.1702526

Chang, C. H., Qiu, J., O'Sullivan, D., Buck, M. D., Noguchi, T., Curtis, J. D., et al. (2015). Metabolic competition in the tumor microenvironment is a driver of cancer progression. *Cell* 162 (6), 1229–1241. doi:10.1016/j.cell.2015.08.016

DeBerardinis, R. J., and Chandel, N. S. (2016). Fundamentals of cancer metabolism. *Sci. Adv.* 2 (5), e1600200. doi:10.1126/sciadv.1600200

Euceda, L. R., Hill, D. K., Stokke, E., Hatem, R., El Botty, R., Bieche, I., et al. (2017). Metabolic response to everolimus in patient-derived triple-negative breast cancer xenografts. *J. Proteome Res.* 16 (5), 1868–1879. doi:10.1021/acs.jproteome.6b00918

Ghini, V., Laera, L., Fantechi, B., Monte, F. D., Benelli, M., McCartney, A., et al. (2020). Metabolomics to assess response to immune checkpoint inhibitors in patients with non-small-cell lung cancer. *Cancers (Basel)* 12 (12), 3574. doi:10.3390/cancers12123574

Hammond, G. R. V., and Burke, J. E. (2020). Novel roles of phosphoinositides in signaling, lipid transport, and disease. *Curr. Opin. Cell Biol.* 63, 57–67. doi:10.1016/j.ceb.2019.12.007

Hanahan, D., and Weinberg, R. A. (2011). Hallmarks of cancer: the next generation. *Cell* 144 (5), 646–674. doi:10.1016/j.cell.2011.02.013

He, J., Huang, Z., Han, L., Gong, Y., and Xie, C. (2021). Mechanisms and management of 3rd-generation EGFR-TKI resistance in advanced non-small cell lung cancer (Review). *Int. J. Oncol.* 59 (5), 90. doi:10.3892/ijo.2021.5270

Herzberg, B., Campo, M. J., and Gainor, J. F. (2017). Immune checkpoint inhibitors in non-small cell lung cancer. *Oncologist* 22 (1), 81–88. doi:10.1634/theoncologist.2016-0189

Hosios, A. M., Hecht, V. C., Danai, L. V., Johnson, M. O., Rathmell, J. C., Steinhauser, M. L., et al. (2016). Amino acids rather than glucose account for the majority of cell mass in proliferating mammalian Cells. *Dev. Cell* 36 (5), 540–549. doi:10.1016/j.devcel.2016.02.012

Jianyong, Z., Yanruo, H., Xiaoju, T., Yiping, W., and Fengming, L. (2021). Roles of lipid profiles in human non-small cell lung cancer. *Technol. Cancer Res. Treat.* 20, 15330338211041472. doi:10.1177/15330338211041472

Johnson, C. H., Ivanisevic, J., and Siuzdak, G. (2016). Metabolomics: beyond biomarkers and towards mechanisms. *Nat. Rev. Mol. Cell Biol.* 17 (7), 451–459. doi:10.1038/nrm.2016.25

Konecny, G. E., Pegram, M. D., Venkatesan, N., Finn, R., Yang, G., Rahmeh, M., et al. (2006). Activity of the dual kinase inhibitor lapatinib (GW572016) against HER-2-overexpressing and trastuzumab-treated breast cancer cells. *Cancer Res.* 66 (3), 1630–1639. doi:10.1158/0008-5472.CAN-05-1182

Kotecki, N., Vuagnat, P., O'Neil, B. H., Jalal, S., Rottey, S., Prenen, H., et al. (2021). A phase I study of an IDO-1 inhibitor (LY3381916) as monotherapy and in combination with an anti-PD-L1 antibody (LY3300054) in patients with advanced cancer. *J. Immunother.* 44 (7), 264–275. doi:10.1097/CJI.0000000000000368

Koundouros, N., Karali, E., Tripp, A., Valle, A., Inglese, P., Perry, N. J. S., et al. (2020). Metabolic fingerprinting links oncogenic PIK3CA with enhanced arachidonic acid-derived eicosanoids. *Cell* 181 (7), 1596–1611. e27. doi:10.1016/j.cell.2020.05.053

Koundouros, N., and Poulogiannis, G. (2020). Reprogramming of fatty acid metabolism in cancer. *Br. J. Cancer* 122 (1), 4–22. doi:10.1038/s41416-019-0650-z

Kowalczyk, T., Kisluk, J., Pietrowska, K., Godzien, J., Kozlowski, M., Reszec, J., et al. (2021). The ability of metabolomics to discriminate non-small-cell lung cancer subtypes depends on the stage of the disease and the type of material studied. *Cancers (Basel)* 13 (13), 3314. doi:10.3390/cancers13133314

Lei, Q., Wang, D., Sun, K., Wang, L., and Zhang, Y. (2020). Resistance mechanisms of anti-PD1/PDL1 therapy in solid tumors. *Front. Cell Dev. Biol.* 8, 672. doi:10.3389/fcell.2020.00672

Li, H., Bullock, K., Gurjao, C., Braun, D., Shukla, S. A., Bosse, D., et al. (2019). Metabolomic adaptations and correlates of survival to immune checkpoint blockade. *Nat. Commun.* 10 (1), 4346. doi:10.1038/s41467-019-12361-9

Li, N., and Zhao, H. (2021). Role of carnitine in non-alcoholic fatty liver disease and other related diseases: an update. *Front. Med.* 8, 689042. doi:10.3389/fmed.2021.689042

Li, X., Wenes, M., Romero, P., Huang, S. C., Fendt, S. M., and Ho, P. C. (2019). Navigating metabolic pathways to enhance antitumour immunity and immunotherapy. *Nat. Rev. Clin. Oncol.* 16 (7), 425–441. doi:10.1038/s41571-019-0203-7

Liao, W., Wei, H., Wang, X., Qiu, Y., Gou, X., Zhang, X., et al. (2012). Metabonomic variations associated with AOM-induced precancerous colorectal lesions and resveratrol treatment. *J. Proteome Res.* 11 (6), 3436–3448. doi:10.1021/pr300284h

Lin, L., Ding, Y., Wang, Y., Wang, Z., Yin, X., Yan, G., et al. (2017). Functional lipidomics: palmitic acid impairs hepatocellular carcinoma development by modulating membrane fluidity and glucose metabolism. *Hepatology* 66 (2), 432–448. doi:10.1002/hep.29033

Longo, N., Frigeni, M., and Pasquali, M. (2016). Carnitine transport and fatty acid oxidation. *Biochim. Biophys. Acta* 1863 (10), 2422–2435. doi:10.1016/j.bbamcr.2016.01.023

Nagarajan, A., Malvi, P., and Wajapeyee, N. (2016). Oncogene-directed alterations in cancer cell metabolism. *Trends Cancer* 2 (7), 365–377. doi:10.1016/j.trecan.2016.06.002

National Comprenhensive Cancer Network (2017). Non-small cell lung cancer guidelines. Available at: https://wwwtri-kobeorg/nccn/guideline/lung/english/non_smallpdf;v17.

Pi, C., Xu, C. R., Zhang, M. F., Peng, X. X., Wei, X. W., Gao, X., et al. (2018). EGFR mutations in early-stage and advanced-stage lung adenocarcinoma: Analysis based

on large-scale data from China. *Thorac. Cancer* 9 (7), 814–819. doi:10.1111/1759-7714.12651

Robert, C. (2020). A decade of immune-checkpoint inhibitors in cancer therapy. *Nat. Commun.* 11 (1), 3801. doi:10.1038/s41467-020-17670-y

Rusnak, D. W., Lackey, K., Affleck, K., Wood, E. R., Alligood, K. J., RhodesN., et al. (2001). The effects of the novel, reversible epidermal growth factor receptor/ErbB-2 tyrosine kinase inhibitor, GW2016, on the growth of human normal and tumor-derived cell lines *in vitro* and *in vivo*. *Mol. Cancer Ther.* 1 (2), 85–94.

Schrimpe-Rutledge, A. C., Codreanu, S. G., Sherrod, S. D., and McLean, J. A. (2016). Untargeted metabolomics strategies-challenges and emerging directions. *J. Am. Soc. Mass Spectrom.* 27 (12), 1897–1905. doi:10.1007/s13361-016-1469-y

Singh, T., Fatehi Hassanabad, M., and Fatehi Hassanabad, A. (2021). Non-small cell lung cancer: Emerging molecular targeted and immunotherapeutic agents. *Biochim. Biophys. Acta. Rev. Cancer* 1876 (2), 188636. doi:10.1016/j.bbcan.2021.188636

Stine, Z. E., Schug, Z. T., Salvino, J. M., and Dang, C. V. (2022). Targeting cancer metabolism in the era of precision oncology. *Nat. Rev. Drug Discov.* 21 (2), 141–162. doi:10.1038/s41573-021-00339-6

Stirling, E. R., Bronson, S. M., Mackert, J. D., Cook, K. L., Triozzi, P. L., and Soto-Pantoja, D. R. (2022). Metabolic implications of immune checkpoint proteins in cancer. *Cells* 11 (1), 179. doi:10.3390/cells11010179

Sung, H., Ferlay, J., Siegel, R. L., Laversanne, M., Soerjomataram, I., Jemal, A., et al. (2021). Global cancer statistics 2020: GLOBOCAN estimates of incidence and mortality worldwide for 36 cancers in 185 countries. *CA. Cancer J. Clin.* 71 (3), 209–249. doi:10.3322/caac.21660

Tang, E., Liu, S., Zhang, Z., Zhang, R., Huang, D., Gao, T., et al. (2022). Therapeutic potential of glutamine pathway in lung cancer. *Front. Oncol.* 11, 835141. doi:10.3389/fonc.2021.835141

Vanhove, K., Derveaux, E., Graulus, G. J., Mesotten, L., Thomeer, M., Noben, J. P., et al. (2019). Glutamine addiction and therapeutic strategies in lung cancer. *Int. J. Mol. Sci.* 20 (2), 252. doi:10.3390/ijms20020252

Wang, M., Herbst, R. S., and Boshoff, C. (2021). Toward personalized treatment approaches for non-small-cell lung cancer. *Nat. Med.* 27 (8), 1345–1356. doi:10.1038/s41591-021-01450-2

Wang, Y., Wang, Y., Ren, Y., Zhang, Q., Yi, P., and Cheng, C. (2022). Metabolic modulation of immune checkpoints and novel therapeutic strategies in cancer. *Semin. Cancer Biol.* S1044-579X (22), 00031–1. doi:10.1016/j.semcancer.2022.02.010

Xiong, W., Zhao, Y., Du, H., and Guo, X. (2021). Current status of immune checkpoint inhibitor immunotherapy for lung cancer. *Front. Oncol.* 11, 704336. doi:10.3389/fonc.2021.704336

Xu, B., Chen, Y., Chen, X., Gan, L., Zhang, Y., Feng, J., et al. (2021). Metabolomics Profiling discriminates prostate cancer from benign prostatic hyperplasia within the prostate-specific antigen gray zone. *Front. Oncol.* 11, 730638. doi:10.3389/fonc.2021.730638

Yang, R., Li, X., Wu, Y., Zhang, G., Liu, X., Li, Y., et al. (2020). EGFR activates GDH1 transcription to promote glutamine metabolism through MEK/ERK/ELK1 pathway in glioblastoma. *Oncogene* 39 (14), 2975–2986. doi:10.1038/s41388-020-1199-2

Yang, T., Hui, R., Nouws, J., Sauler, M., Zeng, T., and Wu, Q. (2022). Untargeted metabolomics analysis of esophageal squamous cell cancer progression. *J. Transl. Med.* 20 (1), 127. doi:10.1186/s12967-022-03311-z

Yoon, H. Y., Ryu, J. S., Sim, Y. S., Kim, D., Lee, S. Y., Choi, J., et al. (2020). Clinical significance of EGFR mutation types in lung adenocarcinoma: A multi-centre Korean study. *PLoS One* 15 (2), e0228925. doi:10.1371/journal.pone.0228925

Zhang, K. R., Zhang, Y. F., Lei, H. M., Tang, Y. B., Ma, C. S., Lv, Q. M., et al. (2021). Targeting AKR1B1 inhibits glutathione de novo synthesis to overcome acquired resistance to EGFR-targeted therapy in lung cancer. *Sci. Transl. Med.* 13 (614), eabg6428. doi:10.1126/scitranslmed.abg6428

frontiers | Frontiers in Pharmacology

TYPE Original Research
PUBLISHED 19 August 2022
DOI 10.3389/fphar.2022.977025

Check for updates

OPEN ACCESS

EDITED BY
Chen Shi,
Huazhong University of Science and Technology, China

REVIEWED BY
Renfei Lu,
Nantong University, China
Wenhi Guo,
Jinzhou Medical University, China

*CORRESPONDENCE
Fengjun Sun,
fengj_sun@163.com
Jing Hu,
18219797@qq.com

†These authors have contributed equally to this work

SPECIALTY SECTION
This article was submitted to Pharmacology of Anti-Cancer Drugs, a section of the journal Frontiers in Pharmacology

RECEIVED 24 June 2022
ACCEPTED 27 July 2022
PUBLISHED 19 August 2022

CITATION
Cheng L, Weng B, Jia C, Zhang L, Hu B, Deng L, Mou N, Sun F and Hu J (2022), The expression and significance of efferocytosis and immune checkpoint related molecules in pancancer samples and the correlation of their expression with anticancer drug sensitivity. *Front. Pharmacol.* 13:977025. doi: 10.3389/fphar.2022.977025

COPYRIGHT
© 2022 Cheng, Weng, Jia, Zhang, Hu, Deng, Mou, Sun and Hu. This is an open-access article distributed under the terms of the Creative Commons Attribution License (CC BY). The use, distribution or reproduction in other forums is permitted, provided the original author(s) and the copyright owner(s) are credited and that the original publication in this journal is cited, in accordance with accepted academic practice. No use, distribution or reproduction is permitted which does not comply with these terms.

The expression and significance of efferocytosis and immune checkpoint related molecules in pancancer samples and the correlation of their expression with anticancer drug sensitivity

Lin Cheng†, Bangbi Weng†, Changsheng Jia†, Lin Zhang, Bin Hu, Li Deng, Nan Mou, Fengjun Sun* and Jing Hu*

Department of Pharmacy, The First Affiliated Hospital of Army Medical University (Third Military Medical University), Chongqing, China

Background: The efferocytosis-related molecules have been considered to be correlated with the resistance to cancer chemotherapy. The aim of this study was to investigate the expression and significance of efferocytosis-related molecules in cancers and the correlation of their expression with anticancer drug sensitivity, and provide new potential targets and treatment options for cancers.

Methods: We investigated the differential expression of 15 efferocytosis-related molecules (Axl, Tyro3, MerTK, CX3CL1, Tim-4, BAI1, Stab2, Gas6, IDO1, Rac1, MFGE8, ICAM-1, CD47, CD31, and PD-L1) and other 12 common immune checkpoint-related molecules in tumor and normal tissues, the correlation between their expression and various clinicopathological features in 16 types of cancers using publicly available pancancer datasets in The Cancer Genome Atlas. We also analyzed the correlation of the expression of efferocytosis and immune checkpoint related molecules with 126 types of anticancer drugs sensitivity using drug-RNA-seq data.

Results: There is a panel of circulating molecules among the 27 molecules. Based on the results of differential expression and correlation with various clinicopathological features of efferocytosis-related molecules in cancers, we identified new potential therapeutic targets for anticancer therapy, such as Axl for kidney renal clear cell carcinoma, Tyro3 for liver hepatocellular carcinoma, and IDO1 for renal papillary cell carcinoma. Except for BAI1, CD31, and MerTK, the enhanced expressions of Axl, Tyro3, Gas6, MFGE8, Stab2, Tim-4, CX3CL1, IDO1, Rac1, and PD-L1 were associated with decreased sensitivity of the cancer cells to many anti-cancer drugs; however, for other common immune checkpoint-related molecules, only enhanced expressions of PD-1, CD28, CTLA4, and HVEM were associated with decreased sensitivity of the cancer cells to a few drugs.

Conclusion: The efferocytosis-related molecules were significantly associated with clinical outcomes in many types of cancers and played important roles in resistance to chemotherapy. Combination therapy targeting efferocytosis-related molecules and other immune checkpoint-related molecules is necessary to reduce resistance to chemotherapy.

KEYWORDS

efferocytosis, immune checkpoint-related molecules, immunotherapy, chemotherapy resistance, cancer

Introduction

Research on the immune escape mechanism has developed a variety of antitumor immune drugs, such as immune checkpoint inhibitors and tumor vaccines, which have provided new tumor treatment methods and brought new hope to patients with advanced metastatic tumors. Cytotoxic T lymphocyte-associated antigen 4 (CTLA-4) antibody, programmed death 1 (PD-1) antibody, and its ligand PD-L1 are among the fastest-growing and most promising drug categories. They have been used in hematological malignancies, malignant melanoma, non-small cell lung cancer (NSCLC), and advanced clear cell renal cell carcinoma (ccRCC) (Galon and Bruni, 2019). The combination of checkpoint inhibitors is currently one of the most promising treatment approaches. In a phase III clinical trial, the combination treatment of PD-1 antibody nivolumab and CTLA-4 antibody ipilimumab for advanced RCC obtained a higher objective response rate as well as overall survival (OS), and the patient's quality of life was significantly improved (Motzer et al., 2018). Dual blockade of PD-1 and lymphocyte activation gene-3 (LAG-3) was also reported as a promising checkpoint blockade combination for RCC (Zelba et al., 2019). In advanced NSCLC patients treated with PD-1 axis blockers, elevated LAG-3 was significantly associated with insensitivity to PD-1 axis blockade and shorter progression-free survival (PFS) (Datar et al., 2019). Combined treatment with chemotherapy and immunotherapy has also shown clinical benefit, and the PD-1 antibody Keytruda combined with paclitaxel and platinum chemotherapy is a major advancement in chemotherapy and immunotherapy for metastatic squamous NSCLC (Pacheco, 2020). However, primary resistance occurs in the majority of patients and acquires adaptation of tumors to immune pressure in patients initially responding to therapy. Therefore, additional nonredundant actionable immunostimulatory targets need to be characterized.

Efferocytosis is a physiologic phagocytic clearance of apoptotic cells induced mainly by macrophages and dendritic cells, which modulates inflammatory responses and the immune environment and promotes the resolution of inflammation and wound healing. In the tumor microenvironment, tumor-associated macrophages (TAMs) are professional phagocytes. During efferocytosis, TAMs polarize toward an M2-like wound healing phenotype, promote the secretion of anti-inflammatory cytokines (e.g., TGF-β, IL-4, and IL-10), inhibit the secretion of inflammation-resolving cytokines (e.g., IL-1β, TNF-α, and IL-12), recruit $FOXP3^+$ regulatory T cells, and suppress the functions of $CD4^+$ and $CD8^+$ effector T cells, subsequently facilitating immune escape of cancer cells, thus promoting tumor development and progression.

The process of efferocytosis includes four steps: release of "find-me" signals by dying cells, recognition of the ligands of apoptotic cells by the phagocytes, phagocyte downstream of engagement of apoptotic cells, and production of anti-inflammatory mediators (Morioka et al., 2019). CX3CL1 is a member of the chemokine family, and is a common "find-me" signal released by lymphocytes after apoptosis and attracts macrophages to the apoptotic site. Axl, Tyro3, and MERTK bind the ligand arrest-specific protein 6 (Gas6), while Tyro3 and MERTK bind the ligand Protein S. The ligands Gas6 and Protein S bind phosphatidylserine (PS), thus Gas6 and Protein S are bridging molecules between the TAM receptors and PS. PS receptors include the T-cell immunoglobulin mucin (Tim) family members (Tim-1, Tim-3, and Tim-4), brain-specific angiogenesis inhibitor 1 (BAI1), and stabilin-2 (Stab2). The milk fat globule-EGF factor 8 (MFGE8) is the bridging molecule between PS receptors on apoptotic cells and receptors on phagocytes. Ras-related C3 botulinum toxin substrate 1 (Rac1) is a modulator of the cytoskeleton, playing important roles in phagocytosis, mesenchymal-like migration, and adhesion (Bid et al., 2013). Intercellular adhesion molecule 1 (ICAM1) is a transmembrane glycoprotein in the immunoglobulin superfamily that plays an important role in cell adhesion of tumor cells and TAMs and signal transduction (Usami et al., 2013). The most widely studied ligands of "don't-eat-me" signals are CD47 and CD31. Rac1 is a molecule that promotes apoptotic cell engulfment (Proto et al., 2018). Moreover, MerTK-driven efferocytosis also induces the expression of the PD-L1. Indoleamine-2, 3-dioxegenase (IDO) 1 is an immune regulator known for driving maternal-fetal antigen tolerance. Apoptotic and necrotic tumor cells, *via* efferocytosis and IDO1, respectively, promote tumor "homeostasis" and progression (Werfel et al., 2019).

It is generally considered that efferocytosis-related molecules and pathways are potential targets for antitumor therapy (Werfel and Cook, 2018; Zhou et al., 2020); however, their role in specific

TABLE 1 Tumor type classification and patient number.

Tumor type	Full name	Total (n)	Normal (n)	Tumor (n)
ACC	Adrenocortical carcinoma	79	0	79
BLCA	Bladder Urothelial Carcinoma	430	19	411
BRCA	Breast invasive carcinoma	1217	113	1104
CESC	Cervical squamous cell carcinoma and endocervical adenocarcinoma	309	3	306
CHOL	Cholangiocarcinoma	45	9	36
COAD	Colon adenocarcinoma	512	41	471
DLBC	Lymphoid Neoplasm Diffuse Large B-cell Lymphoma	48	0	48
ESCA	Esophageal carcinoma	173	11	162
GBM	Glioblastoma multiforme	173	5	168
HNSC	Head and Neck squamous cell carcinoma	546	44	502
KICH	Kidney Chromophobe	89	24	65
KIRC	Kidney renal clear cell carcinoma	607	72	535
KIRP	Kidney renal papillary cell carcinoma	321	32	289
LAML	Acute Myeloid Leukemia	151	0	151
LGG	Brain Lower Grade Glioma	529	0	529
LIHC	Liver hepatocellular carcinoma	424	50	374
LUAD	Lung adenocarcinoma	585	59	526
LUSC	Lung squamous cell carcinoma	550	49	501
MESO	Mesothelioma	86	0	86
OV	Ovarian serous cystadenocarcinoma	379	0	379
PAAD	Pancreatic adenocarcinoma	182	4	178
PCPG	Pheochromocytoma and Paraganglioma	186	3	183
PRAD	Prostate adenocarcinoma	551	52	499
READ	Rectum adenocarcinoma	177	10	167
SARC	Sarcoma	265	2	263
SKCM	Skin Cutaneous Melanoma	472	1	471
STAD	Stomach adenocarcinoma	407	32	375
TGCT	Testicular Germ Cell Tumors	156	0	156
THCA	Thyroid carcinoma	568	58	510
THYM	Thymoma	121	2	119
UCEC	Uterine Corpus Endometrial Carcinoma	583	35	548
UCS	Uterine Carcinosarcoma	56	0	56
UVM	Uveal Melanoma	80	0	80

cancers has not been clearly defined. To identify which molecules to target and the most promising combination of antibodies that could induce robust clinical outcomes, precise knowledge of molecular expression and co-expression on immune cells in general and their expression correlation with various clinicopathological features, including tumor TNM classification, tumor stage, and patient OS, is essential.

In the current study, we investigated the protein-protein interaction (PPI) network of efferocytosis-related molecules (Axl, Tyro3, MerTK, CX3CL1, Tim-4, BAI-1, Stab-2, Gas6, MFGE8, Rac1, ICAM-1, CD47, CD31, IDO1, and PD-L1) and other immune checkpoint-related molecules, including B- and T-lymphocyte attenuator (BTLA), glucocorticoid-induced tumor necrosis factor receptor-related protein (GITR), herpes virus entry mediator (HVEM), LAG-3, PD-1, PD-L2, Tim-3, CD28, CD80, CD137, CD27, and CTLA-4 (Wang et al., 2019). The expression of efferocytosis-related molecules in tumor and normal tissues, their roles in immune subtype, correlation with the ESTIMATE score, stromal score, and immune score, and the correlation between their expression and OS in cancers was studied using publicly available pancancer datasets from The Cancer Genome Atlas. We also analyzed the correlations of the expressions of efferocytosis-related molecules and immune checkpoint-related molecules with anticancer drugs sensitivity to provide a reference for the combined use and sequential use of drugs in each tumor treatment.

Materials and methods

Molecular protein-protein interaction network analysis

The PPI network of the 15 efferocytosis-related molecules and 12 other immune checkpoint-related molecules was constructed using the STRING database v11.0 (http://www.string-db.org/). The minimum required interaction score cutoff was set as greater than or equal to 0.400.

Study population and datasets

Patient phenotypic, survival, RNA-seq, and immune subtype data from The Cancer Genome Atlas (TCGA) were downloaded from the UCSC Xena Genomics Browser (http://xena.ucsc.edu/) on 7 July 2020. The drug sensitivity and RNA-seq data were provided by the CellMiner database v2.2 (https://discover.nci.nih.gov/cellminer/). Disease-free survival (DFS) data and graphs were obtained from the GEPIA2 website (http://gepia2.cancer-pku.cn/#index). The tumor type classification and the corresponding patient number are shown in Table 1.

Differential expression analysis

Differential expression of molecules between normal and tumor tissues in the pancancer datasets was performed in R software using the ggpubr package, and *p*-values were computed with the Wilcoxon sign-rank test when normal tissue counts were greater than or equal to 10.

Correlation with the microenvironment and immune subtype

To compute the immune and stromal cell content within the tumor microenvironment, scores were calculated using the estimate and limma packages. The corrplot package was used to assess the association of molecules with immune and stromal scores. The correlation between molecules and immune subtype was estimated with the limma, ggplot2 and reshape2 packages. The significance of the differences among immune subtypes was determined by the Kruskal-Wallis test.

Correlation with overall survival

For OS analysis, we used the Kaplan-Meier method to draw survival curves with the survival and survminer packages.

Correlation between drug sensitivity and RNA-seq analysis

Drug sensitivity and RNA-seq data analyses were implemented with R, including the limma, impute, ggplot2 and ggpubr packages. Correlation tests were computed with Pearson's correlation test. Based on the drug-RNA-seq correlation, Cytoscape v3.8.0 (http://www.cytoscape.org/) was used to visualize the network.

Results

Protein-protein interaction network of the molecules

There is a panel of circulating molecules among the 27 molecules (Figure 1), which highlights the importance of the combination therapy of efferocytosis-related molecules and other immune checkpoint-related molecules. With an interaction score greater than or equal to 0.900, CTLA4 was strongly associated with PD-L1 (CD274), CD80, and CD28; CD80 was strongly associated with CD28, PD1, PD-L2, and ICAM-1; PD-L1 was strongly associated with CD28, CD80, PD1, and PD-L2; LAG3 was strongly associated with Tim-3 (HAVCR2); MerTK was strongly associated with Tim-4; and Gas6 was strongly associated with Axl, MerTK, and Tyro3.

Expression signature in pancancer samples and correlation with overall survival

We analyzed the expression of the 15 efferocytosis-related molecules in 16 types of cancers, including bladder urothelial carcinoma (BLCA), breast invasive carcinoma (BRCA), colon adenocarcinoma (COAD), esophageal carcinoma (ESCA), head and neck squamous cell carcinoma (HNSC), kidney chromophobe (KICH), kidney renal clear cell carcinoma (KIRC), kidney renal papillary cell carcinoma (KIRP), liver hepatocellular carcinoma (LIHC), lung adenocarcinoma (LUAD), lung squamous cell carcinoma (LUSC), prostate adenocarcinoma (PRAD), rectum adenocarcinoma (READ), stomach adenocarcinoma (STAD), thyroid carcinoma (THCA), and uterine corpus endometrial carcinoma (UCEC). The expression characteristics of the molecules in tumor and normal tissues in various cancers were different (Figure 2). In different cancers, the correlation between the expression of the molecules and OS was also different (Figure 3). CX3CL1 expression was increased in tumor tissues in KIRC and KIRP, predicting better OS. Axl expression was decreased in tumor tissues in BLCA, STAD and ESCA, predicting better OS in BLCA and STAD but worse OS in ESCA; Axl expression was

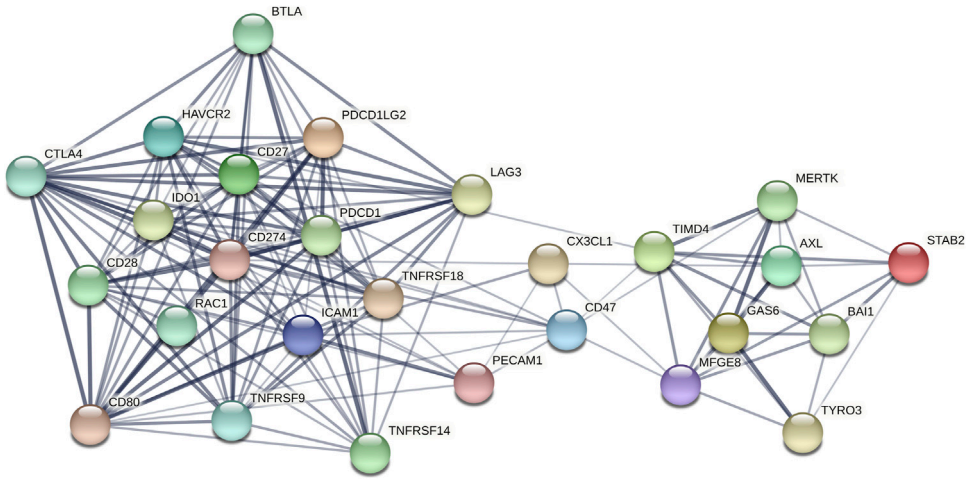

FIGURE 1
The PPI network of the 15 efferocytosis-related molecules and 12 other immune checkpoint-related molecules with confidence >0.4. The thickness of the line indicates the size of the correlation coefficient.

increased in tumor tissues in KIRC and KIRP, predicting worse OS in KIRC but better OS in KIRP. Tyro3 expression was decreased in tumor tissues in ESCA and KIRP, predicting worse OS in ESCA but better OS in KIRP; Tyro3 expression was increased in tumor tissues in LIHC and THCA, predicting worse OS in LIHC but better OS in THCA. MerTK expression was decreased in tumor tissue in BRCA and KIRC, predicting better OS in BRCA but worse OS in KIRC. Gas6 expression was decreased in tumor tissues in BLCA, LUSC, and LUAD, predicting better OS in BLCA and LUSC but worse OS in LUAD. MFGE8 expression was decreased in tumor tissues in BLCA and KIRP, predicting better OS. BAI1 expression was decreased in tumor tissues in BRCA and COAD, predicting worse OS in BRCA but better OS in COAD. Tim-4 expression was decreased in tumor tissue in READ, predicting worse OS. Stab2 expression was decreased in tumor tissues in KIRP, LUSC, and BRCA, predicting better OS in KIRP and LUSC but worse OS in BRCA. CD31 expression was increased in tumor tissues in KIRC and LIHC, predicting better OS. CD47 expression was decreased in tumor tissue in LUSC, predicting better OS; CD47 expression was increased in tumor tissue in THCA, predicting better OS. IDO1 expression was increased in tumor tissues in KIRP and HNSC, predicting worse OS in KIRP but better OS in HNSC. PD-L1 expression was decreased in tumor tissue in LIHC, predicting worse OS. Based on the results, Axl may serve as new potential therapeutic targets for KIRC, as well as Tyro3 for LIHC and IDO1 for KIRP.

The expression of the 15 molecules was also significantly associated with other tumors. Although there was no differential expression between normal and tumor tissues, we should also pay attention to their association with other clinical classifications, such as tumor size, tumor stage, and tumor metastasis.

Correlation with the tumor microenvironment

The high expressions of Axl, Tim-4, CD31, IDO1, ICAM1, and PD-L1 were associated with the high ESTIMATE score and immune score, while the high expressions of Axl, Tim-4, and CD31 were associated with the high stromal score in many types of cancers. High MerTK expression was associated with the high three scores in 3–5 types of cancers. The high expressions of Gas6 and MFGE8 were associated with the high ESTIMATE score and stromal score in certain types of cancers (Figure 4A).

According to a previous study, the C4 (lymphocyte-depleted) and C6 (TGF-β-dominant) subtypes were associated with poor OS (Thorsson et al., 2018). The expression levels of the 15 molecules in the C1-C6 subtypes were all significantly different. Tyro3, MerTK, and BAI1 were mainly expressed in the C5 (immunologically quiet) and C4 (lymphocyte-depleted) subtypes; Axl was mainly expressed in the C6 (TGF-β-dominant) and C5 (immunologically quiet) subtypes; CD31, Stab2, and Gas6 were mainly expressed in the C6 (TGF-β-dominant) and C3 (inflammatory) subtypes; CX3CL1 was mainly expressed in the C5 (immunologically quiet) and C3 (inflammatory) subtypes; Tim-4 was mainly expressed in the C3 (inflammatory) and C6 (TGF-β-dominant) subtypes; PD-L1, CD47, and IDO1 were mainly expressed in the C2 (IFN-γ-dominant) and C6 (TGF-β-dominant) subtypes; Rac1 was mainly expressed in the C6 (TGF-β-dominant) and C4 (lymphocyte-depleted) subtypes; MFGE8 was mainly expressed in the C6 (TGF-β-dominant) and C1 (low Th1/Th2 ratio) subtypes; ICAM1 was mainly expressed in the C6 (TGF-β-dominant) and C2 (IFN-γ-dominant) subtypes (Figure 4B).

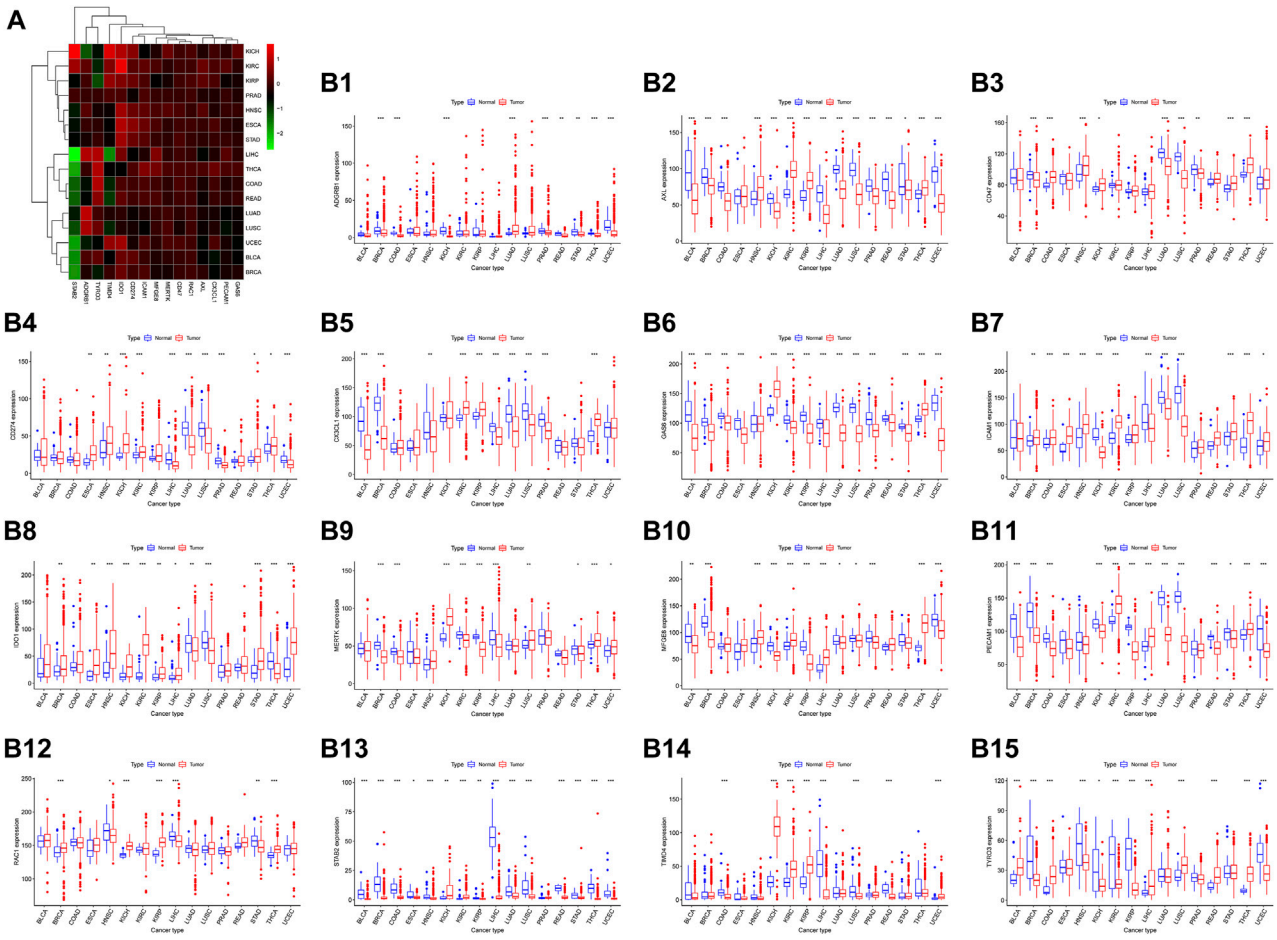

FIGURE 2
The expression level of 15 efferocytosis-related molecules in 16 types of cancers. **(A)**. Heatmap and supervised clustering of efferocytosis-related molecules with changed expression in 16 tumor tissues compared to that in normal tissues. **(B1-B15)**. The changed expression of ADGRB1 (BAI1), Axl, CD47, CD274 (PD-L1), CX3CL1, Gas6, ICAM1, IDO1, MerTK, MFGE8, PECAM1 (CD31), RAC1, STAB2, TIMD4 (Tim-4), and Tyro3 in 16 tumor tissues compared to that in normal tissues. *$p < 0.05$, **$p < 0.01$, ***$p < 0.001$ as assessed by the Wilcoxon signed-rank test.

Correlation with anticancer sensitivity

We also analyzed the associations of the expressions of the 27 molecules with sensitivity of the cancer cells to the 126 types of anti-cancer drugs (Figure 5). Except for BAI1, CD31, and MerTK, the enhanced expression of Axl, Tyro3, Gas6, MFGE8, Stab2, Tim-4, CX3CL1, IDO1, Rac1, and PD-L1 was associated with decreased sensitivity to many drugs, which may partially explain the resistance to chemotherapy in cancers.

The enhanced expression of Axl, Tyro3, Gas6, MFGE8, Tim-4, and PD-L1 was associated with increased sensitivity to 22, 10, 16, 14, 10, and 6 types of drugs, respectively. With the correlation value greater than or equal to 0.400, enhanced expression of CX3CL1 was associated with increased sensitivity to vemurafenib but decreased sensitivity to docetaxel; enhanced expression of Axl was associated with increased sensitivity to bleomycin and dasatinib but decreased sensitivity to tamoxifen, nilotinib, and raloxifene; enhanced expression of Tyro3 was associated with increased sensitivity to vemurafenib; enhanced expression of Tim-4 was associated with increased sensitivity to dasatinib, vandetanib, pentostatin, ibrutinib, gefitinib, erlotinib, and afatinib but decreased sensitivity to vinblastine, tyrothricin, and pipamperone; enhanced expression of BAI1 was associated with increased sensitivity to etoposide, thiotepa, mitomycin, and cisplatin; enhanced expression of Gas6 was associated with decreased sensitivity to trametinib and panobinostat; enhanced expression of MFGE8 was associated with decreased sensitivity to palbociclib; enhanced expression of CD47 was associated with increased sensitivity to nelarabine; enhanced expression of CD31 was associated with increased sensitivity to etoposide, triethylenemelamine, thiotepa, dexamethasone decadron, fludarabine, melphalan, uracil

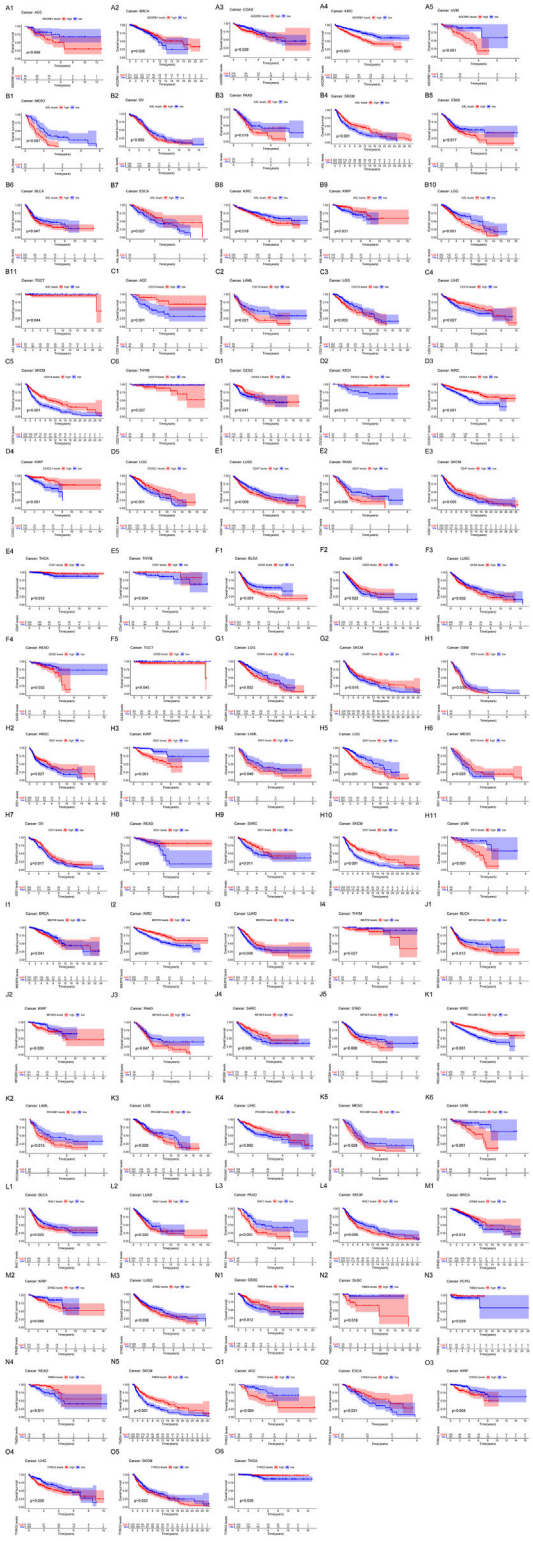

FIGURE 3
The correlation of the expression of efferocytosis-related molecules with the overall survival (OS) in 33 types of cancers. Kaplan-Meier survival curves were generated for the molecules extracted from the comparison of groups of high (red line) (*Continued*)

FIGURE 3
and low (blue line) gene expression. $p < 0.05$ in the log-rank test. **(A1–A5)** The expression of ADGRB1 (BAI1) was significantly associated with OS in ACC, BRCA, COAD, KIRC, and UVM. **(B1–B11)** The expression of Axl was significantly associated with OS in MESO, OV, PAAD, SKCM, STAD, BLCA, ESCA, KIRC, KIRP, LGG, and TGCT. **(C1–C6)** The expression of CD274 (PD-L1) was significantly associated with OS in ACC, LAML, LGG, LIHC, SKCM, and THYM. **(D1–D5)** The expression of CX3CL1 was significantly associated with OS in CESC, KICH, KIRC, KIRP, and LGG. **(E1–E5)** The expression of CD47 was significantly associated with OS in LUSC, PAAD, SKCM, THCA, and THYM. **(F1–F5)** The expression of Gas6 was significantly associated with OS in BLCA, LUAD, LUSC, READ, and TGCT. **(G1–G2)** The expression of ICAM1 was significantly associated with OS in LGG and SKCM. **(H1–H11)** The expression of IDO1 was significantly associated with OS in GBM, HNSC, KIRP, LAML, LGG, MESO, OV, READ, SARC, SKCM, and UVM. **(I1–I4)** The expression of MerTK was significantly associated with OS in BRCA, KIRC, LUAD, and THYM. **(J1–J5)** The expression of MFGE8 was significantly associated with OS in BLCA, KIRP, PAAD, SARC, and STAD. **(K1–K6)** The expression of PECAM1 (CD31) was significantly associated with OS in KIRC, LAML, LGG, LIHC, MESO, and UVM. **(L1–L4)** The expression of RAC1 was significantly associated with OS in BLCA, LUAD, PAAD, and SKCM. **(M1–M3)** The expression of STAB2 was significantly associated with OS in BRCA, KIRP, and LUSC. **(N1–N5)** The expression of TIMD4 was significantly associated with OS in CESC, DLBC, PCPG, READ, and SKCM. **(O1–O6)** The expression of Tyro3 was significantly associated with OS in ACC, ESCA, KIRP, LIHC, SKCM, and THCA.

mustard, pipobroman, ifosfamide, hydroxyurea, fluphenazine, chlorambucil, asparaginase, bendamustine, and nelarabine; enhanced expression of IDO1 was associated with decreased sensitivity to panobinostat; and enhanced expression of PD-L1 was associated with decreased sensitivity to tamoxifen.

For other immune checkpoint-related molecules, enhanced expressions of CD27, CD28, Tim-3, PD-1, and GITR were associated with increased sensitivity to many types of anticancer drugs, and only enhanced expressions of PD-1, CD28, CTLA4, and HVEM were associated with decreased sensitivity to a few drugs. In addition, enhanced expressions of Axl, PD-L1, and Rac1 were associated with decreased sensitivity to fluorouracil. Enhanced expressions of Axl, Gas6, and Tim-4 were associated with decreased sensitivity to pipamperone, eribulin mesylate, vinblastine and vinorelbine. Enhanced expressions of CX3CL1, Gas6, and Tim-4 were associated with decreased sensitivity to paclitaxel. Enhanced expressions of CTLA4, Stab2, and HVEM were associated with decreased sensitivity to everolimus. Enhanced expressions of CD28, CD80, Tim-3, PD-1, CD31, and GITR were associated with decreased sensitivity to irofulven. Enhanced expressions of Axl, PD-L1, Gas6, IDO1, and Tim-4 were associated with decreased sensitivity to tamoxifen. Enhanced expressions of CD28, CD47, Gas6, and PD-1 were associated with decreased sensitivity to trametinib. Enhanced expressions of CTLA4, PD-1, and HVEM were associated with decreased sensitivity to dasatinib. Enhanced expressions of Axl, PD-L1, and Gas6 were associated with decreased sensitivity to nilotinib.

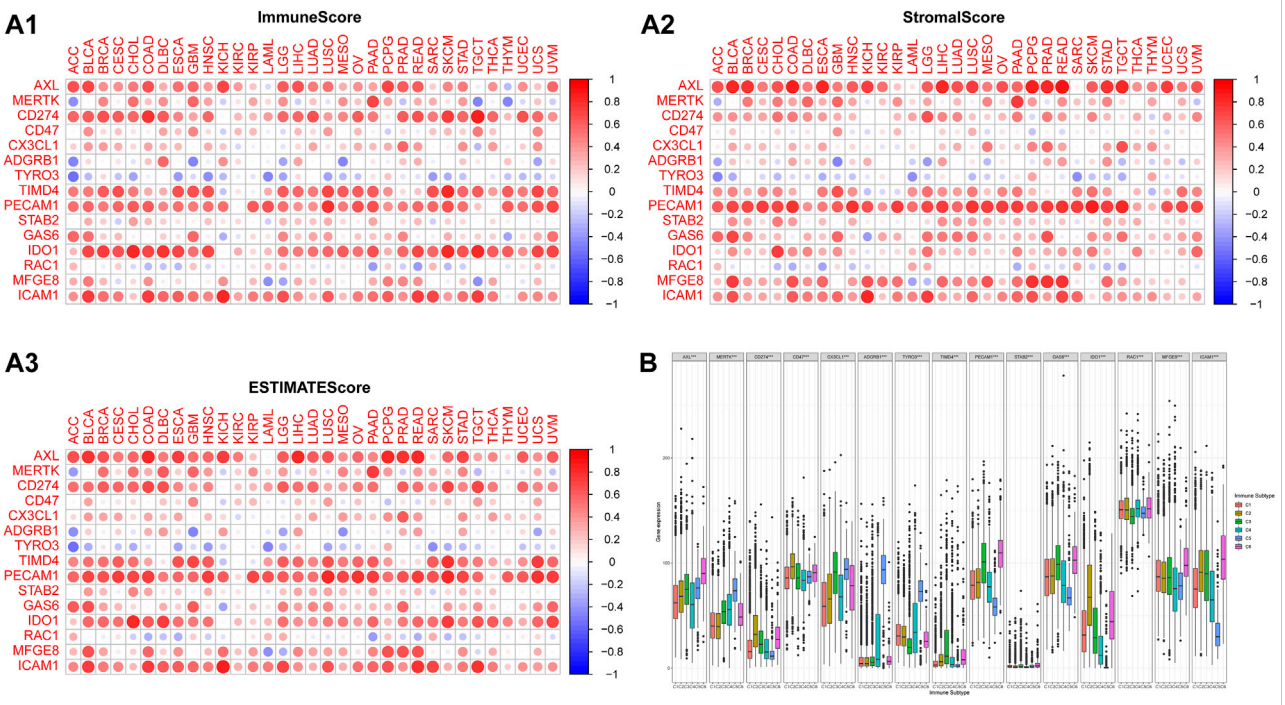

FIGURE 4
The correlations of the expressions of efferocytosis-related molecules with the microenvironment and immune subtype in 33 types of cancers. The corrplot package was used to assess the association of molecules with the immune score, stromal score, and ESTIMATE score. The color of a node reflects the log(FC) value of the Z score of gene expression, and the size of the node indicates the number of interacting proteins with the designated protein. **(A1)** The correlations of the expressions of efferocytosis-related molecules with the immune score. **(A2)** The correlations of the expressions of efferocytosis-related molecules with the stromal score. **(A3)** The correlations of the expressions of efferocytosis-related molecules with the ESTIMATE score. **(B)** Distribution of efferocytosis-related molecules in immune subtypes C1 (wound healing), C2 (IFN-γ-dominant), C3 (inflammatory), C4 (lymphocyte depleted), C5 (inflammatory) and C6 (TGF-β-dominant).

Enhanced expressions of CD28, PD-1, and HVEM were associated with decreased sensitivity to sonidegib.

The results indicate that we may choose the drugs according to the molecular expression characteristics and the correlation of their expression with anti-cancer drug sensitivity. For cancers with high expression of many types of molecules, we should choose drugs sensitive to the co-expression of the molecules or the combined use of the corresponding sensitive drugs.

Discussion

The TAM receptors Axl, Tyro3, and MerTk were a family of receptor tyrosine kinases, skew macrophage polarization towards a pro-tumor M2-like phenotype in the tumor microenvironment, and promote apoptotic cell clearance through efferocytosis (Graham et al., 2014; Myers et al., 2019). The Gas6/Axl signaling pathway has been reported to be associated with tumor metastasis, invasion, and drug resistance (Zhu et al., 2019). Inhibition of the Gas6/Axl pathway augments the efficacy of chemotherapies (Kariolis et al., 2017; Wu et al., 2018). It was reported that Gas6 expression was associated with tumor progression and patient survival in RCC, and low tumor Axl mRNA levels were independently correlated with improved survival (Gustafsson et al., 2009). In the current study, Gas6 expression was decreased in KIRC tumor tissues, and Gas6 expression was decreased with tumor grades 1–3 and tumor metastasis. Axl was overexpressed in tumor tissues, and Axl overexpression predicted poor OS. These results were consistent with those from previous studies. Gas6/Axl axis contributes to chemoresistance and metastasis in breast cancer (Wang et al., 2016). Increased expression of Axl and its ligand Gas6 was found in EGFR-mutant lung cancers obtained from individuals with acquired resistance to erlotinib (Zhang et al., 2012). We found that Gas6 expression was decreased in tumor tissues in BLCA, LUSC, and LUAD, predicting a better OS in BLCA and LUSC but worse OS in LUAD, which indicated that the specific role of Gas6 in certain cancers needs to be further investigated. Furthermore, the drug sensitivity analyses showed that enhanced expression of Gas6 was moderately associated with increased sensitivity to alectinib, olaparib, temsirolimus, zoledronate, bleomycin, and lenvatinib, and we may also consider using these drugs to target Gas6. Different therapeutic agents targeting Axl have been developed (Zhu

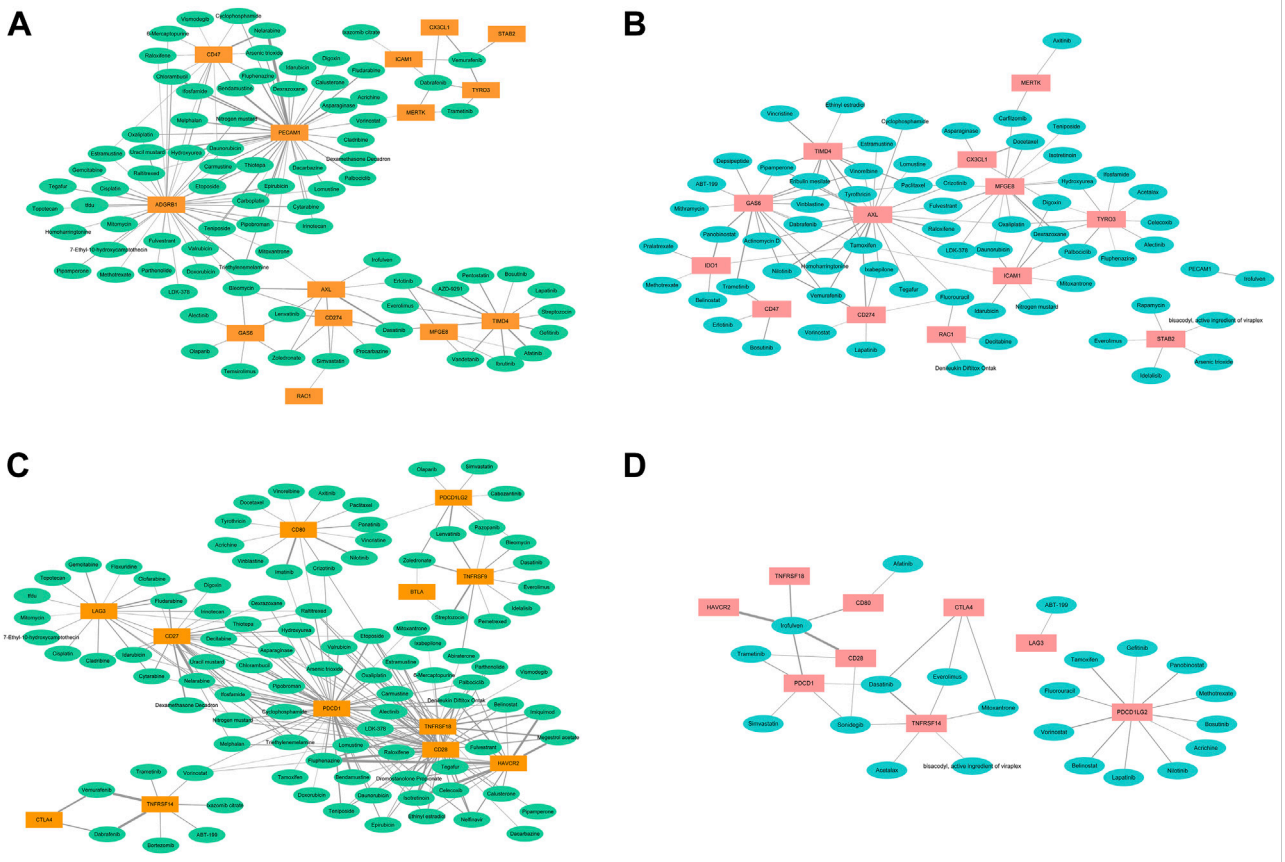

FIGURE 5
The correlations of the expressions of efferocytosis and immune checkpoint related molecules with sensitivity of the cancer cells to the 126 types of anti-cancer drugs. The thickness of the line indicates the size of the correlation coefficient. **(A)**. The correlations of the enhanced expressions of 14 efferocytosis-related molecules with increased sensitivity to anti-cancer drugs. **(B)** The correlations of the enhanced expresssions of 14 efferocytosis-related molecules with decreased sensitivity to anti-cancer drugs. **(C)** The correlations of the enhanced expressions of 12 immune checkpoint-related molecules with increased sensitivity to anti-cancer drugs. **(D)** The correlations of the enhanced expressions of 9 immune checkpoint-related molecules with decreased sensitivity to anti-cancer drugs.

et al., 2019). We also found that high expression of Axl in tumor tissues was associated with worse OS in LGG, MESO, PAAD, and TGCT, and enhanced expression of Axl was especially associated with increased sensitivity to dasatinib and bleomycin. We may consider using these drugs to treat the above cancers.

Tyro3, Axl, and MerTK control myeloid-derived suppressor cell (MDSC) functionality, regulate MDSC-mediated immune suppression and augment anti-PD-1 therapy in melanoma patients (Holtzhausen et al., 2019), which highlights the role of these molecules in antitumor therapy. In leiomyosarcoma patients, especially those whom develop metastasis, express higher levels of Tyro3 and Gas6, and crizotinib and foretinib showed effective antitumor activity in leiomyosarcoma through Tyro3 and Axl deactivation (Dantas-Barbosa et al., 2017). Based on our study, Tyro3 expression was increased in tumor tissue in LIHC, predicting worse OS. Tyro3 was reported to contribute significantly to tumor growth, aggressiveness and liver dysfunction in HCC (Duan et al., 2016) and was also considered a marker and therapeutic target for HCC with a higher hepatitis activity (Tsai et al., 2020). Sorafenib is the only approved drug for treating patients with advanced HCC. However, the therapeutic effect of sorafenib is transient, and patients invariably develop sorafenib resistance through the aberrant expression of the Tyro3/phosphoinositide 3-kinase/protein kinase B signal transduction pathway (Kabir et al., 2018). We found that enhanced expression of Tyro3 was associated with increased sensitivity to trametinib, dabrafenib, and vemurafenib, and we may consider using these drugs to target Tyro3 in HCC.

MFGE8 acts at two levels, by increasing vascular endothelial growth factor (VEGF) and ET-1 expression in mesenchymal stromal cells and by enhancing M2 polarization of macrophages, to increase melanoma tumor angiogenesis (Yamada et al., 2016). The abundant MFGE8 expression in esophageal squamous cell

carcinoma might have a negative influence on the long-term survival of patients after chemotherapy (Kanemura et al., 2018). MFGE8 also plays an important role in HCC progression (Ko et al., 2020). Our results showed that high expression of MFGE8 in tumor tissues was also associated with worse OS in PAAD and STAD, which indicated that MFGE8 may serve as a potential target in these cancers.

BAI1 expression was significantly reduced in breast cancer and higher expression was associated with better patient survival (Meisen et al., 2015). Our results were consistent with those from previous studies. BAI1 is decreased in BRCA and associated with worse OS. It was reported that BAI1 had better diagnostic efficacy than classic lung cancer biomarkers (Zhang et al., 2019). Blocking Stab2 function prevents melanoma metastasis by elevating circulating hyaluronic acid levels (Hirose et al., 2012). In our analysis, Stab2 expression was decreased in tumor tissues in KIRP, LUSC, and BRCA, predicting better OS in KIRP and LUSC but worse OS in BRCA, which indicated that the specific role of Stab2 in different cancers needs to be further investigated.

Tim-4-overexpressing cancer cells recruit TAMs, thereby accelerating cancer development. Tim-4 promotes the growth of colorectal cancer by activating angiogenesis and recruiting TAMs *via* the PI3K/AKT/mTOR signaling pathway (Tan et al., 2018). Tim-4 was also reported to promote the growth of NSCLC in an RGD motif-dependent manner (Zhang et al., 2015). In addition, IL-6 promotes metastasis of NSCLC by upregulating Tim-4 *via* NF-κB (Liu et al., 2020). In the current study, the expression level of Tim-4 in tumor tissues was significantly higher in KICH, KIRC, KIRP, and UCEC, and the specific role of Tim-4 in these cancers needs further investigation. Interestingly, Tim-3 is overexpressed in RCC tumor tissues, and overexpression of Tim-3 predicts better DFS and OS and has no significant correlation with the TNM classification and tumor grade (data not shown); this may partially explain the results that dual blockade of PD-1 and LAG-3, but not PD-1 and Tim-3, is a promising checkpoint blockade combination strategy (Zelba et al., 2019).

Rac1 plays a critical role in the progression of tumors and the development of resistance to various therapeutic modalities applied in the clinic (De et al., 2020). The overexpression of Rac1 is associated with multi-drug resistance to the neoadjuvant chemotherapy, and targeting Rac1 is a potential strategy to overcome acquired chemoresistance in breast cancer (Li et al., 2020). We found that the expression level of Rac1 in tumor tissues was significantly higher in BRCA, KICH, KIRP, and THCA, and we should also pay attention to the role of Rac1 in KICH, KIRP, and THCA.

CD47 modulates cellular phagocytosis by macrophages, transmigration of neutrophils and activation of dendritic cells, T cells and B cells. Anti-CD47 antibodies, which enhance cancer cell phagocytosis, can achieve higher anti-cancer efficacies when combined with chemotherapy and immunotherapy (Hayat et al., 2020). Our study showed that COAD, HNSC, KICH, STAD, and THCA tumor tissues expressed high levels of CD47, and high expression of CD47 in tumor tissue was associated with worse OS in PAAD. Based on this observation, CD47 may be considered a target in the above cancer therapies.

IDO1 protein is expressed in the majority of hormone receptor-positive breast cancer and is an independent negative prognostic marker (Carvajal-Hausdorf et al., 2017). IDO1 expression was associated with an unfavorable clinical outcome in esophageal cancer and colorectal cancer (Kiyozumi et al., 2019; Chen et al., 2020). IDO1 expression was also reported to correlate with PD-L1 expression, and co-expressed IDO1 and PD-L1 may be an important target for immunotherapy in lung squamous cell carcinoma (Takada et al., 2019). In the current study, IDO1 expression was increased in tumor tissue in KIRP, predicting worse OS, which suggested that IDO1 may serve as a potential target for KIRP. IDO1, LAG3, and PD-L1 expression levels in TIICs showed a better prognosis for patients with MSI-H colon cancer (Lee et al., 2018). Thus, the potential therapeutic implications of these immune checkpoint molecules should be further investigated.

PD-1 and PD-L1 are generally considered as potential targets for antitumor therapy (Balar and Weber, 2017; Constantinidou et al., 2019). Clinical trials with mAbs to PD-1 and PD-L1 have shown impressive response rates in patients, particularly for melanoma, NSCLC, RCC, and bladder cancer (Ohaegbulam et al., 2015). In a multicenter phase 1 trial, antibody-mediated blockade of PD-L1 induced durable tumor regression and prolonged stabilization of disease in patients with advanced cancers (Brahmer et al., 2012). Cancer vaccine formulation can dominantly determine synergy, or lack thereof, with CTLA-4 and PD-L1 checkpoint blockade therapy for cancer (Hailemichael et al., 2018). Based on our results, enhanced expression of PD-1 was associated with increased sensitivity to many types of drugs, and enhanced expression of CTLA4 was associated with increased sensitivity to dabrafenib and vemurafenib; however, enhanced expression of PD-L1 was associated with decreased sensitivity to vorinostat, tamoxifen, nilotinib, ixabepilone, lapatinib, and fluorouracil. In clinical use, we should pay more attention to the use of these drugs in patients with a high expression of these molecules.

The limitations of the study should be noted. Firstly, the results of our study were based on online database, and the patient number of some types of cancers was small, especially the number of normal control. We also tried to search other database to confirm our results, such as GEO DataSets (https://www.ncbi.nlm.nih.gov/geo/). However, no survival time data were available. The results need further confirmation both in clinic and experimental model. Secondly, there are data to suggest that some of the efferocytosis-related receptors are important in hematologic cancers and may have an interface with the immune checkpoint molecules in the bone marrow microenvironment. We did not perform the analysis on hematologic malignancies in the current study. Finally, not all

efferocytosis-related molecular were included in, such as other TAM receptors ligands Protein S and Galectin 3, and alpha-v/beta-5 receptor.

In summary, our results provided evidence that efferocytosis-related molecules played important roles in the invasion, metastasis, and clinical outcome of many types of cancers, and their correlation was different in each cancer. The high expression of the molecules was associated with the high ESTIMATE score, stromal score, and immune score. Except for CX3CL1, the other 14 molecules were mainly expressed in the C4 (lymphocyte-depleted) and C6 (TGF-β-dominant) subtypes, which predicted worse OS. The molecules also played important roles in resistance to chemotherapy. We may choose anticancer drugs according to the molecular expression characteristics in each tumor and the drug sensitivity results. Supplementing conventional chemotherapy, radiotherapy and other immunotherapies with efferocytosis-targeted therapy could enhance therapeutic efficacy, reduce resistance to therapy, and promote patient outcome.

Data availability statement

Publicly available datasets were analyzed in this study. These data can be found in The Cancer Genome Atlas (http://xena.ucsc.edu/), the CellMiner database v2.2 (https://discover.nci.nih.gov/cellminer/), and the GEPIA2 website (http://gepia2.cancer-pku.cn/#index).

Author contributions

LC, FS, and JH designed the study and drafted the manuscript; BW and CJ searched the data and performed the data analysis; LZ, BH, LD, and NM assisted in searched the data. All authors approved the final version of the manuscript.

Funding

This study was supported by the Key Specialty of Clinical Pharmacy of Chongqing, China (425Z2M2).

Conflict of interest

The authors declare that the research was conducted in the absence of any commercial or financial relationships that could be construed as a potential conflict of interest.

Publisher's note

All claims expressed in this article are solely those of the authors and do not necessarily represent those of their affiliated organizations, or those of the publisher, the editors and the reviewers. Any product that may be evaluated in this article, or claim that may be made by its manufacturer, is not guaranteed or endorsed by the publisher.

References

Balar, A. V., and Weber, J. S. (2017). PD-1 and PD-L1 antibodies in cancer: Current status and future directions. *Cancer Immunol. Immunother.* 66 (5), 551–564. doi:10.1007/s00262-017-1954-6

Bid, H. K., Roberts, R. D., Manchanda, P. K., and Houghton, P. J. (2013). RAC1: An emerging therapeutic option for targeting cancer angiogenesis and metastasis. *Mol. Cancer Ther.* 12 (10), 1925–1934. doi:10.1158/1535-7163.MCT-13-0164

Brahmer, J. R., Tykodi, S. S., Chow, L. Q., Hwu, W. J., Topalian, S. L., Hwu, P., et al. (2012). Safety and activity of anti-PD-L1 antibody in patients with advanced cancer. *N. Engl. J. Med.* 366 (26), 2455–2465. doi:10.1056/NEJMoa1200694

Carvajal-Hausdorf, D. E., Mani, N., Velcheti, V., Schalper, K. A., and Rimm, D. L. (2017). Objective measurement and clinical significance of Ido1 protein in hormone receptor-positive breast cancer. *J. Immunother. Cancer* 5 (1), 81. doi:10.1186/s40425-017-0285-7

Chen, B., Alvarado, D. M., Iticovici, M., Kau, N. S., Park, H., Parikh, P. J., et al. (2020). Interferon-induced Ido1 mediates radiation resistance and is a therapeutic target in colorectal cancer. *Cancer Immunol. Res.* 8 (4), 451–464. doi:10.1158/2326-6066.CIR-19-0282

Constantinidou, A., Alifieris, C., and Trafalis, D. T. (2019). Targeting programmed cell death -1 (PD-1) and ligand (PD-L1): A new era in cancer active immunotherapy. *Pharmacol. Ther.* 194, 84–106. doi:10.1016/j.pharmthera.2018.09.008

Dantas-Barbosa, C., Lesluyes, T., Loarer, F. L., Chibon, F., Treilleux, I., Coindre, J. M., et al. (2017). Expression and role of TYRO3 and AXL as potential therapeutical targets in leiomyosarcoma. *Br. J. Cancer* 117 (12), 1787–1797. doi:10.1038/bjc.2017.354

Datar, I., Sanmamed, M. F., Wang, J., Henick, B. S., Choi, J., Badri, T., et al. (2019). Expression analysis and significance of PD-1, LAG-3, and TIM-3 in human non-small cell lung cancer using spatially resolved and multiparametric single-cell analysis. *Clin. Cancer Res.* 25 (15), 4663–4673. doi:10.1158/1078-0432.CCR-18-4142

De, P., Rozeboom, B. J., Aske, J. C., and Dey, N. (2020). Active RAC1 promotes tumorigenic phenotypes and therapy resistance in solid tumors. *Cancers (Basel)* 12 (6), 1541. doi:10.3390/cancers12061541

Duan, Y., Wong, W., Chua, S. C., Wee, H. L., Lim, S. G., Chua, B. T., et al. (2016). Overexpression of Tyro3 and its implications on hepatocellular carcinoma progression. *Int. J. Oncol.* 48 (1), 358–366. doi:10.3892/ijo.2015.3244

Galon, J., and Bruni, D. (2019). Approaches to treat immune hot, altered and cold tumours with combination immunotherapies. *Nat. Rev. Drug Discov.* 18 (3), 197–218. doi:10.1038/s41573-018-0007-y

Graham, D. K., DeRyckere, D., Davies, K. D., and Earp, H. S. (2014). The TAM family: Phosphatidylserine sensing receptor tyrosine kinases gone awry in cancer. *Nat. Rev. Cancer* 14 (12), 769–785. doi:10.1038/nrc3847

Gustafsson, A., Martuszewska, D., Johansson, M., Ekman, C., Hafizi, S., Ljungberg, B., et al. (2009). Differential expression of Axl and Gas6 in renal cell carcinoma reflecting tumor advancement and survival. *Clin. Cancer Res.* 15 (14), 4742–4749. doi:10.1158/1078-0432.CCR-08-2514

Hailemichael, Y., Woods, A., Fu, T., He, Q., Nielsen, M. C., Hasan, F., et al. (2018). Cancer vaccine formulation dictates synergy with CTLA-4 and PD-L1 checkpoint blockade therapy. *J. Clin. Invest.* 128 (4), 1338–1354. doi:10.1172/JCI93303

Hayat, S. M. G., Bianconi, V., Pirro, M., Jaafari, M. R., Hatamipour, M., and Sahebkar, A. (2020). CD47: Role in the immune system and application to cancer therapy. *Cell. Oncol.* 43 (1), 19–30. doi:10.1007/s13402-019-00469-5

Hirose, Y., Saijou, E., Sugano, Y., Takeshita, F., Nishimura, S., Nonaka, H., et al. (2012). Inhibition of Stabilin-2 elevates circulating hyaluronic acid levels and prevents tumor metastasis. *Proc. Natl. Acad. Sci. U. S. A.* 109 (11), 4263–4268. doi:10.1073/pnas.1117560109

Holtzhausen, A., Harris, W., Ubil, E., Hunter, D. M., Zhao, J., Zhang, Y., et al. (2019). TAM family receptor kinase inhibition reverses MDSC-mediated suppression and augments anti-PD-1 therapy in melanoma. *Cancer Immunol. Res.* 7 (10), 1672–1686. doi:10.1158/2326-6066.CIR-19-0008

Kabir, T. D., Ganda, C., Brown, R. M., Beveridge, D. J., Richardson, K. L., Chaturvedi, V., et al. (2018). A microRNA-7/growth arrest specific 6/TYRO3 axis regulates the growth and invasiveness of sorafenib-resistant cells in human hepatocellular carcinoma. *Hepatology* 67 (1), 216–231. doi:10.1002/hep.29478

Kanemura, T., Miyata, H., Makino, T., Tanaka, K., Sugimura, K., Hamada-Uematsu, M., et al. (2018). Immunoregulatory influence of abundant MFG-E8 expression by esophageal cancer treated with chemotherapy. *Cancer Sci.* 109 (11), 3393–3402. doi:10.1111/cas.13785

Kariolis, M. S., Miao, Y. R., Diep, A., Nash, S. E., Olcina, M. M., Jiang, D., et al. (2017). Inhibition of the GAS6/AXL pathway augments the efficacy of chemotherapies. *J. Clin. Invest.* 127 (1), 183–198. doi:10.1172/JCI85610

Kiyozumi, Y., Baba, Y., Okadome, K., Yagi, T., Ishimoto, T., Iwatsuki, M., et al. (2019). Ido1 expression is associated with immune tolerance and poor prognosis in patients with surgically resected esophageal cancer. *Ann. Surg.* 269 (6), 1101–1108. doi:10.1097/SLA.0000000000002754

Ko, D. S., Kim, S. H., Park, J. Y., Lee, G., Kim, H. J., Kim, G., et al. (2020). Milk fat globule-EGF factor 8 contributes to progression of hepatocellular carcinoma. *Cancers (Basel)* 12 (2), 403. doi:10.3390/cancers12020403

Lee, S. J., Jun, S. Y., Lee, I. H., Kang, B. W., Park, S. Y., Kim, H. J., et al. (2018). CD274, LAG3, and Ido1 expressions in tumor-infiltrating immune cells as prognostic biomarker for patients with MSI-high colon cancer. *J. Cancer Res. Clin. Oncol.* 144 (6), 1005–1014. doi:10.1007/s00432-018-2620-x

Li, Q., Qin, T., Bi, Z., Hong, H., Ding, L., Chen, J., et al. (2020). Rac1 activates non-oxidative pentose phosphate pathway to induce chemoresistance of breast cancer. *Nat. Commun.* 11 (1), 1456. doi:10.1038/s41467-020-15308-7

Liu, W., Wang, H., Bai, F., Ding, L., Huang, Y., Lu, C., et al. (2020). IL-6 promotes metastasis of non-small-cell lung cancer by up-regulating TIM-4 via NF-κB. *Cell Prolif.* 53 (3), e12776. doi:10.1111/cpr.12776

Meisen, W. H., Dubin, S., Sizemore, S. T., Mathsyaraja, H., Thies, K., Lehman, N. L., et al. (2015). Changes in Bai1 and nestin expression are prognostic indicators for survival and metastases in breast cancer and provide opportunities for dual targeted therapies. *Mol. Cancer Ther.* 14 (1), 307–314. doi:10.1158/1535-7163.MCT-14-0659

Morioka, S., Maueroder, C., and Ravichandran, K. S. (2019). Living on the edge: Efferocytosis at the interface of homeostasis and pathology. *Immunity* 50 (5), 1149–1162. doi:10.1016/j.immuni.2019.04.018

Motzer, R. J., Tannir, N. M., McDermott, D. F., Aren Frontera, O., Melichar, B., Choueiri, T. K., et al. (2018). Nivolumab plus ipilimumab versus sunitinib in advanced renal-cell carcinoma. *N. Engl. J. Med.* 378 (14), 1277–1290. doi:10.1056/NEJMoa1712126

Myers, K. V., Amend, S. R., and Pienta, K. J. (2019). Targeting Tyro3, Axl and MerTK (TAM receptors): Implications for macrophages in the tumor microenvironment. *Mol. Cancer* 18 (1), 94. doi:10.1186/s12943-019-1022-2

Ohaegbulam, K. C., Assal, A., Lazar-Molnar, E., Yao, Y., and Zang, X. (2015). Human cancer immunotherapy with antibodies to the PD-1 and PD-L1 pathway. *Trends Mol. Med.* 21 (1), 24–33. doi:10.1016/j.molmed.2014.10.009

Pacheco, J. M. (2020). KEYNOTE-407: Changing the way we treat stage IV squamous non-small cell lung cancer. *Transl. Lung Cancer Res.* 9 (1), 148–153. doi:10.21037/tlcr.2020.01.12

Proto, J. D., Doran, A. C., Gusarova, G., Yurdagul, A., Jr., Sozen, E., Subramanian, M., et al. (2018). Regulatory T cells promote macrophage efferocytosis during inflammation resolution. *Immunity* 49 (4), 666–677. doi:10.1016/j.immuni.2018.07.015

Takada, K., Kohashi, K., Shimokawa, M., Haro, A., Osoegawa, A., Tagawa, T., et al. (2019). Co-expression of Ido1 and PD-L1 in lung squamous cell carcinoma: Potential targets of novel combination therapy. *Lung Cancer* 128, 26–32. doi:10.1016/j.lungcan.2018.12.008

Tan, X., Zhang, Z., Yao, H., and Shen, L. (2018). Tim-4 promotes the growth of colorectal cancer by activating angiogenesis and recruiting tumor-associated macrophages via the PI3K/AKT/mTOR signaling pathway. *Cancer Lett.* 436, 119–128. doi:10.1016/j.canlet.2018.08.012

Thorsson, V., Gibbs, D. L., Brown, S. D., Wolf, D., Bortone, D. S., Ou Yang, T. H., et al. (2018). The immune landscape of cancer. *Immunity* 48 (4), 812–830. e814. doi:10.1016/j.immuni.2018.03.023

Tsai, C. L., Chang, J. S., Yu, M. C., Lee, C. H., Chen, T. C., Chuang, W. Y., et al. (2020). Functional Genomics identifies hepatitis-induced STAT3-TYRO3-STAT3 signaling as a potential therapeutic target of hepatoma. *Clin. Cancer Res.* 26 (5), 1185–1197. doi:10.1158/1078-0432.CCR-18-3531

Usami, Y., Ishida, K., Sato, S., Kishino, M., Kiryu, M., Ogawa, Y., et al. (2013). Intercellular adhesion molecule-1 (ICAM-1) expression correlates with oral cancer progression and induces macrophage/cancer cell adhesion. *Int. J. Cancer* 133 (3), 568–578. doi:10.1002/ijc.28066

Wang, C., Jin, H., Wang, N., Fan, S., Wang, Y., Zhang, Y., et al. (2016). Gas6/Axl Axis contributes to chemoresistance and metastasis in breast cancer through akt/GSK-3β/β-catenin signaling. *Theranostics* 6 (8), 1205–1219. doi:10.7150/thno.15083

Wang, Q., Zhang, J., Tu, H., Liang, D., Chang, D. W., Ye, Y., et al. (2019). Soluble immune checkpoint-related proteins as predictors of tumor recurrence, survival, and T cell phenotypes in clear cell renal cell carcinoma patients. *J. Immunother. Cancer* 7 (1), 334. doi:10.1186/s40425-019-0810-y

Werfel, T. A., and Cook, R. S. (2018). Efferocytosis in the tumor microenvironment. *Semin. Immunopathol.* 40 (6), 545–554. doi:10.1007/s00281-018-0698-5

Werfel, T. A., Elion, D. L., Rahman, B., Hicks, D. J., Sanchez, V., Gonzales-Ericsson, P. I., et al. (2019). Treatment-induced tumor cell apoptosis and secondary necrosis drive tumor progression in the residual tumor microenvironment through MerTK and Ido1. *Cancer Res.* 79 (1), 171–182. doi:10.1158/0008-5472.CAN-18-1106

Wu, G., Ma, Z., Cheng, Y., Hu, W., Deng, C., Jiang, S., et al. (2018). Targeting Gas6/TAM in cancer cells and tumor microenvironment. *Mol. Cancer* 17 (1), 20. doi:10.1186/s12943-018-0769-1

Yamada, K., Uchiyama, A., Uehara, A., Perera, B., Ogino, S., Yokoyama, Y., et al. (2016). MFG-E8 drives melanoma growth by stimulating mesenchymal stromal cell-induced angiogenesis and M2 polarization of tumor-associated macrophages. *Cancer Res.* 76 (14), 4283–4292. doi:10.1158/0008-5472.CAN-15-2812

Zelba, H., Bedke, J., Hennenlotter, J., Mostbock, S., Zettl, M., Zichner, T., et al. (2019). PD-1 and LAG-3 dominate checkpoint receptor-mediated T-cell inhibition in renal cell carcinoma. *Cancer Immunol. Res.* 7 (11), 1891–1899. doi:10.1158/2326-6066.CIR-19-0146

Zhang, L., Pu, D., Liu, D., Wang, Y., Luo, W., Tang, H., et al. (2019). Identification and validation of novel circulating biomarkers for early diagnosis of lung cancer. *Lung Cancer* 135, 130–137. doi:10.1016/j.lungcan.2019.06.019

Zhang, Q., Wang, H., Wu, X., Liu, B., Liu, W., Wang, R., et al. (2015). TIM-4 promotes the growth of non-small-cell lung cancer in a RGD motif-dependent manner. *Br. J. Cancer* 113 (10), 1484–1492. doi:10.1038/bjc.2015.323

Zhang, Z., Lee, J. C., Lin, L., Olivas, V., Au, V., LaFramboise, T., et al. (2012). Activation of the AXL kinase causes resistance to EGFR-targeted therapy in lung cancer. *Nat. Genet.* 44 (8), 852–860. doi:10.1038/ng.2330

Zhou, Y., Yao, Y., Deng, Y., and Shao, A. (2020). Regulation of efferocytosis as a novel cancer therapy. *Cell Commun. Signal.* 18 (1), 71. doi:10.1186/s12964-020-00542-9

Zhu, C., Wei, Y., and Wei, X. (2019). AXL receptor tyrosine kinase as a promising anti-cancer approach: Functions, molecular mechanisms and clinical applications. *Mol. Cancer* 18 (1), 153. doi:10.1186/s12943-019-1090-3

frontiers | Frontiers in Pharmacology

TYPE Original Research
PUBLISHED 26 August 2022
DOI 10.3389/fphar.2022.945038

Check for updates

OPEN ACCESS

EDITED BY
Hongtao Xiao,
University of Electronic Science and Technology of China, China

REVIEWED BY
Kai Qin,
Huazhong University of Science and Technology, China
Imran Tipu,
University of Management and Technology, Pakistan

*CORRESPONDENCE
Xinwen Zhong,
xwzhong@cmu.edu.cn
Tian Li,
fmmult@foxmail.com

†These authors share first authorship

SPECIALTY SECTION
This article was submitted to Pharmacology of Anti-Cancer Drugs, a section of the journal Frontiers in Pharmacology

RECEIVED 16 May 2022
ACCEPTED 28 July 2022
PUBLISHED 26 August 2022

CITATION
Yao Y, Guan X, Bao G, Liang J, Li T and Zhong X (2022), Whole-exome sequencing and bioinformatics analysis of a case of non-alpha-fetoprotein-elevated lung hepatoid adenocarcinoma. *Front. Pharmacol.* 13:945038. doi: 10.3389/fphar.2022.945038

COPYRIGHT
© 2022 Yao, Guan, Bao, Liang, Li and Zhong. This is an open-access article distributed under the terms of the Creative Commons Attribution License (CC BY). The use, distribution or reproduction in other forums is permitted, provided the original author(s) and the copyright owner(s) are credited and that the original publication in this journal is cited, in accordance with accepted academic practice. No use, distribution or reproduction is permitted which does not comply with these terms.

Whole-exome sequencing and bioinformatics analysis of a case of non-alpha-fetoprotein-elevated lung hepatoid adenocarcinoma

Yao Yao[1†], Xiaojiao Guan[2†], Guangyao Bao[1], Jie Liang[1], Tian Li[3*] and Xinwen Zhong[1*]

[1]Department of Thoracic Surgery, First Affiliated Hospital, China Medical University, Shenyang, China, [2]Department of Pathology, Second Affiliated Hospital, China Medical University, Shenyang, China, [3]School of Basic Medicine, Fourth Military Medical University, Xi'an, China

Hepatoid adenocarcinoma of the lung (HAL) is an exceptionally rare malignant tumor with prominent hepatocellular carcinoma (HCC)-like characteristics in organs or tissues outside the liver, while there is no tumor in the liver. Most HAL cases have various degrees of serum alpha-fetoprotein (AFP) levels and exhibit a similar origin and clonal evolution process to HCC. We studied a case of HAL without elevating the AFP level by performing whole-exome sequencing (WES) and bioinformatics analyses after surgical resection. Our results showed mutations in two driver genes, NLRP3 and PBX1, and we identified HNRNPR, TP73, CFAP57, COL11A1, RUSC1, SLC6A9, DISC1, NBPF26, and OR10K1 as potential driver mutation genes in HAL. In addition, 76 significantly mutated genes (SMG) were identified after the statistical test of each mutation type on genes.

KEYWORDS

hepatoid adenocarcinoma of the lung, whole-exome sequencing, alpha-fetoprotein, lung cancer, clinical research

Introduction

Hepatoid adenocarcinoma (HAC), an exceptionally rare malignancy with prominent HCC-like characteristics in extra-hepatic organs or tissues, has been discovered in various organs, including the ovary (Mazouz et al., 2015), lung (Lin et al., 2013; Su et al., 2013; Shi et al., 2019), uterus (Kato et al., 2007), pancreas (Gardiner et al., 1992), and other sites. HAL occurs in approximately 5% of HAC cases (Haninger et al., 2014), and HAL was first reported by Ishikura et al. (1990). Although this rare disease has been identified for more than 30 years, the origin of HAC is still controversial to this date. During embryonic development, some organs like the liver, lung, stomach, and esophagus are diversified from the primitive foregut. Several abnormal differentiation processes may contribute to the development of HAC in these regions (Nakashima et al., 1987).

HAL cases are extremely rare, with less than 60 cases reported in the literature in the last 40 years (Hou et al., 2021). Usually, HAL patients exhibit chest and back pain, shoulder shooting pain, cough and breathlessness, shortness of breath, nausea, and weight loss (Sun et al., 2016). These symptoms are nonspecific and basically the same as those of other types of lung cancer, thus making accurate and timely diagnosis difficult. The main antidiastole for HAL is HCC metastases and non-small cell lung cancer. Collecting data on the patient's medical history and clinical presentation is critical to the diagnosis as HCC often occurs in cirrhosis associated with hepatitis virus infection and alcohol abuse. Meanwhile, it is insufficient to use computed tomography (CT) images alone for diagnosis; cytomorphological and immunohistochemical techniques are necessary to confirm the diagnosis (Terracciano et al., 2003). According to the literature, most HAL tumors occur mainly in the upper lobes, usually near the large blood vessels in the chest wall or mediastinal pleura, while a small proportion of HAL tumors occur in the other lobes. The incidence of HAL is much higher in middle-aged and older male smokers than in women. Because of the nonspecific symptoms and difficulty in diagnosis, most patients are diagnosed with HAL after the disease has progressed to an intermediate or advanced stage (Zhuansun et al., 2021).

A significant increase of alpha-fetoprotein (AFP) in tissues or serum is common in most HAL cases (Ishikura et al., 1990; Grossman et al., 2016). By comparison, HAL without elevated AFP levels is more challenging to diagnose and treat owing to the scarcity of clinical cases and lack of evidence-based medicine (Sun et al., 2016).

The prognosis of HAL is worse than that of other types of lung tumors; the 5-year survival rate is only 8.0%, and the 2-year survival rate is 35.3% (Hou et al., 2021). At present, the understanding of HAL is still insufficient, and the etiology and underlying mechanism of such patients are still unclear; so far, there is no unified diagnostic standard, treatment, or prevention strategy to guide clinical practice. Surgical resection, chemotherapy, and/or radiotherapy are the most common treatments for this disease (Qian et al., 2016), and recently, molecular targeted therapy has shown great promise in treating HAL (Khozin et al., 2012). Therefore, this project provides a new basis for molecular diagnosis and targeted therapy of HAL through whole-exome sequencing (WES) and bioinformatics analysis.

Materials and methods

Sample

One patient, who was diagnosed with HAL in the First Affiliated Hospital of China Medical University, was enrolled in the study. Tumor and paracancerous tissues were rapidly frozen during surgery and saved in liquid nitrogen.

DNA extraction and sequencing

DNA fragmentation was performed by NEBNext dsDNA Fragmentase (NEB, Ipswich, MA, United States), and the DNA fragments were then subjected to end-repair. In the next step, these DNA fragments were hydrolyzed and mixed with RNA library decoys and streptavidin-coated magnetic beads, followed by bead capturing, washing the beads, and RNA digestion, and finally, these DNA fragments were amplified to 150 bp. The cDNA/DNA/small RNA libraries were sequenced on the Illumina sequencing platform X Ten system (Illumina, San Diego, CA, United States) by Gene Denovo Biotechnology Co., Ltd. (Guangzhou, China).

Quality control

Quality trimming is a very important step to guarantee high confidence in variant calling. Fastp (Chen et al., 2018) was used to complete the quality trimming. The filtering criteria were: 1) unidentified nucleotides (N) in the reads >10%; 2) the number of bases >50% of the reads with a phred quality score ≤20; 3) reads aligned to the barcode adapter. If the reads met one of these three criteria, the reads would be cleared.

Variant identification and annotation

For mapping the valid sequencing reads to the reference human genome (GRCh38) and to identify SNVs and indels, the Burrows–Wheeler Aligner (BWA) (Li and Durbin, 2009) was used. Duplicate reads were marked and realigned using the Picard suite. The Genome Analysis Toolkit (GATK) (McKenna et al., 2010) Unified Genotyper was used to find variant sites on the genome, including SNV and small fragments of indels, and the base quality score recalibration. The software tool, ANNOVAR (Wang et al., 2010), was used to align and annotate SNVs or indels to the following databases: 1000 Genomes Project, HAMAP, ESP6500, dbSNP, and Kaviar.

Mutation deleteriousness prediction

SIFT (Ng and Henikoff, 2003), PolyPhen-2 (Adzhubei et al., 2010), MutationTaster (Schwarz et al., 2010), and PROVEAN (Choi et al., 2012) were used to predict whether SNVs and indels lead to changes in protein structure and function.

Driver gene identification

Driver mutation genes were identified by MuSiC (Dees et al., 2012) and OncodriveCLUST (Tamborero et al., 2013a). Comprehensively considering the preference of driver mutations in the locus distribution to form mutation clusters, we used synonymous mutations to construct a background mutation rate model with the characteristics of an unbiased distribution to find possible driver mutations by OncodriveCLUST software. MuSiC software was used to find genes with higher mutation frequency in tumor samples than control samples, and convolution tests were performed for each mutation type. The cutoff of MuSiC is FDR, 0.01 and that of OncodriveCLUST is FDR, 0.05.

Gene functional enrichment analyses

We used the clusterProfiler package on R- 4.1.2 to map the significantly mutated genes to each term of the GO database (http://www.geneontology.org/) and each pathway of the Kyoto Encyclopedia of Genes and Genomes (KEGG) database and calculated the number of genes in each term and pathway, so as to obtain a list of genes with a certain GO function and pathway of KEGG. A hypergeometric test was then applied to find GO terms and KEGG pathways that were significantly enriched in genes compared to the whole-genome background. Modified Fisher's exact test was applied, and $p < 0.05$ was considered a statistically significant difference.

Structural variation identification and analyses

SV types include translocations, inversions, and insertion events, and SVs were determined using CREST (1.0) software (Wang et al., 2011). Copy number variants (CNVs) were identified using VarScan2 (Kadalayil et al., 2015) with the following parameters: Phred base quality ≥20 and minimum coverage ≥20. Recurrent somatic CNA identification was conducted by GISTIC (Mermel et al., 2011), and CNVs were classified using Control-FREEC (10.4) (Boeva et al., 2012).

Results

Case presentation

The 63-year-old male patient was admitted to the First Affiliated Hospital of China Medical University on 5 September 2018, with intermittent dyspnea and occasional chest pain. The chest-CT scan showed a 7.5*5.5 cm^2 mass in the left upper lung with local pleural wrinkling and slightly enlarged lymph nodes in the mediastinum (Figure 1). Before the operation, no metastasis was found in brain CT or bone nuclide scan, while serum carcinoma embryonic antigen (CEA) and neuron-specific enolase (NSE) were slightly elevated, and AFP was in the normal range. On 19 September 2018, the patient underwent left upper lobe resection and mediastinal lymph node dissection. Referring to the preoperative abdominal B-ultrasound examination and postoperative abdominal B-ultrasound examination, 3 months after the surgery, there was no obvious abnormality in the liver, and the patient's status was average with no history of hepatitis, alcohol abuse, exposure to radiation, or toxins. Meanwhile, he had no symptoms of liver cirrhosis such as spider-burst, liver palms, or hepatojugular reflex. We measured the patient's plasma AFP levels 4 days before surgery, 1 day after surgery, and 3 months after surgery. The results of AFP were 11.02 ng/ml, 13.11 ng/ml, and 9.21 ng/ml, respectively. Given the patient's symptoms, personal history, physical examination, preoperative examination, and immunohistochemical staining results of postoperative pathology, the patient was diagnosed with HAL. Meanwhile, there was no metastatic lesion in the mediastinal lymph nodes or adjacent tissue or organs; thus, the post-operative staging is T4N0M0. The patient recovered well after surgery and was discharged from the hospital one week later. Subsequently, a 300 gene-panel genomic testing was conducted, which contained targeted drug-related genes and chemotherapy drug-related genes. Nevertheless, no targeted drug-matched gene mutation was found in the testing. The patient did not receive radiotherapy or chemotherapy after surgery and died of an accidental cerebral hemorrhage six months later.

Histological and immunohistochemical analysis

Hematoxylin-eosin (HE) staining of tumor tissue suggested that the typical cell clusters were flaky, trabecular, and densely arranged; the nuclei were large and deeply stained, and the nucleoplasm ratio was imbalanced. Additionally, alveolar expansion with fracture and fusion was found in the lung tissue (Figure 2). Immunohistochemistry staining demonstrated hepatocyte (+), glypican-3 (+), cytokeratin (CK) (+), Ki-67 (30% +), P40 (−), P63 (−), thyroid transcription factor-1 (TTF-1) (−), and napsin-A (−) (Figure 3).

Whole-exome sequencing and analysis of somatic mutations

To investigate the mutation in this case of HAL, we performed whole-exome sequencing of the tumor tissue. After sequencing and clean read filtering, 122 somatic SNVs and 3 somatic indels were detected using MuTect (Cibulskis et al.,

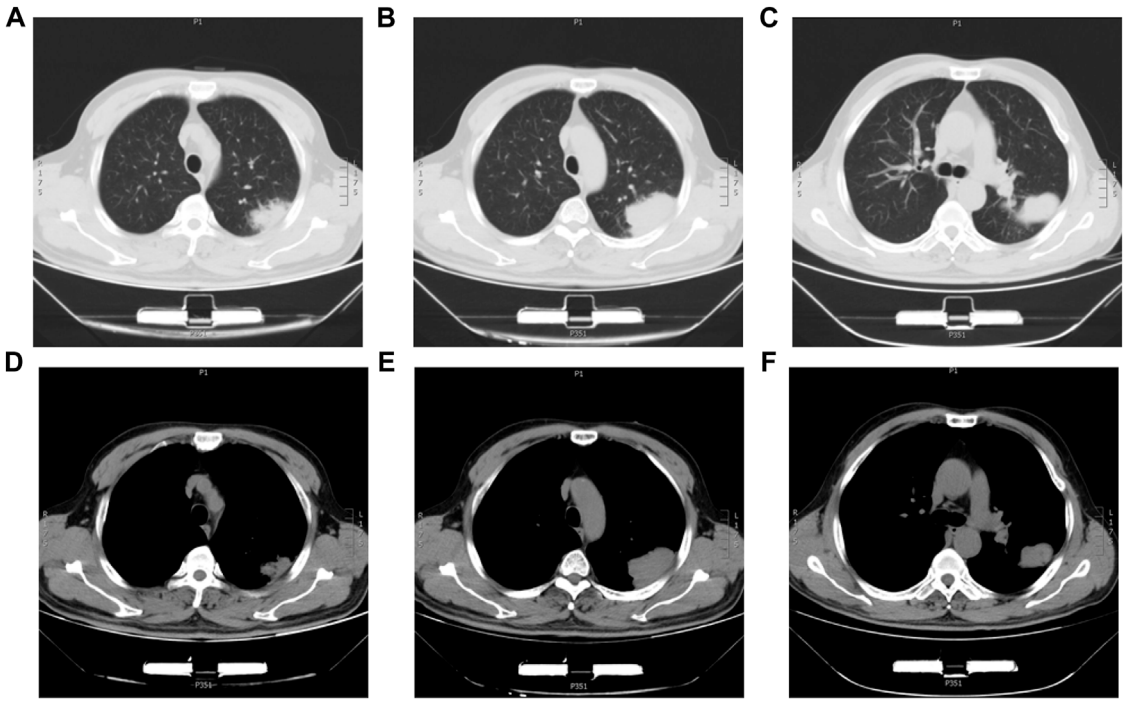

FIGURE 1
Chest CT images of the HAL patient. **(A,B,C)** CT images of the lung window with a lung mass in the left upper lobe. **(D,E,F)** CT images of the mediastinum window with a lung mass in the left upper lobe.

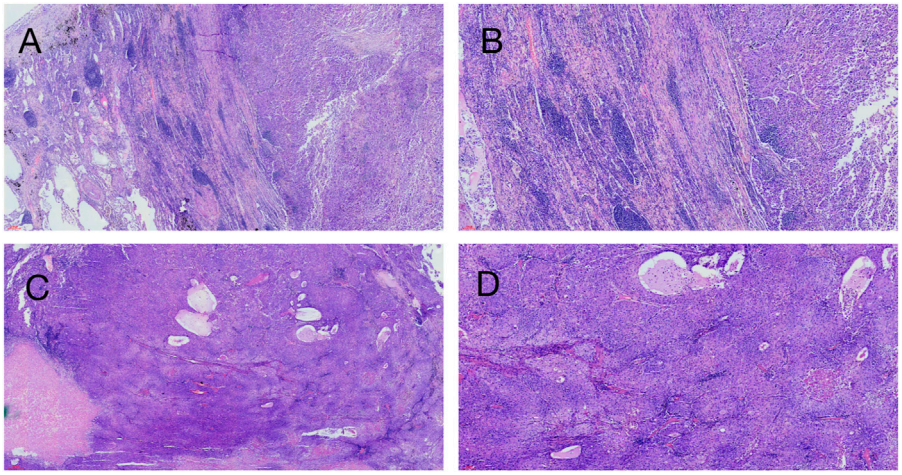

FIGURE 2
Hematoxylin-eosin staining on patient's tumor tissue. **(A)** (× 40, 200 μm), **(B)** (× 100, 100 μm) Left side of the picture is the lung tissue, and alveolar fusion and inflammatory cell infiltration can be seen; the right side is a large tumor tissue, and fibrous tissue proliferation and inflammatory cell infiltration can be seen around the tumor tissue. **(C)** (× 40, 300 μm), **(D)** (× 100, 100 μm) Tumor tissue is distributed in the form of beams and nests, with abundant cytoplasm, similar to hepatocellular carcinoma.

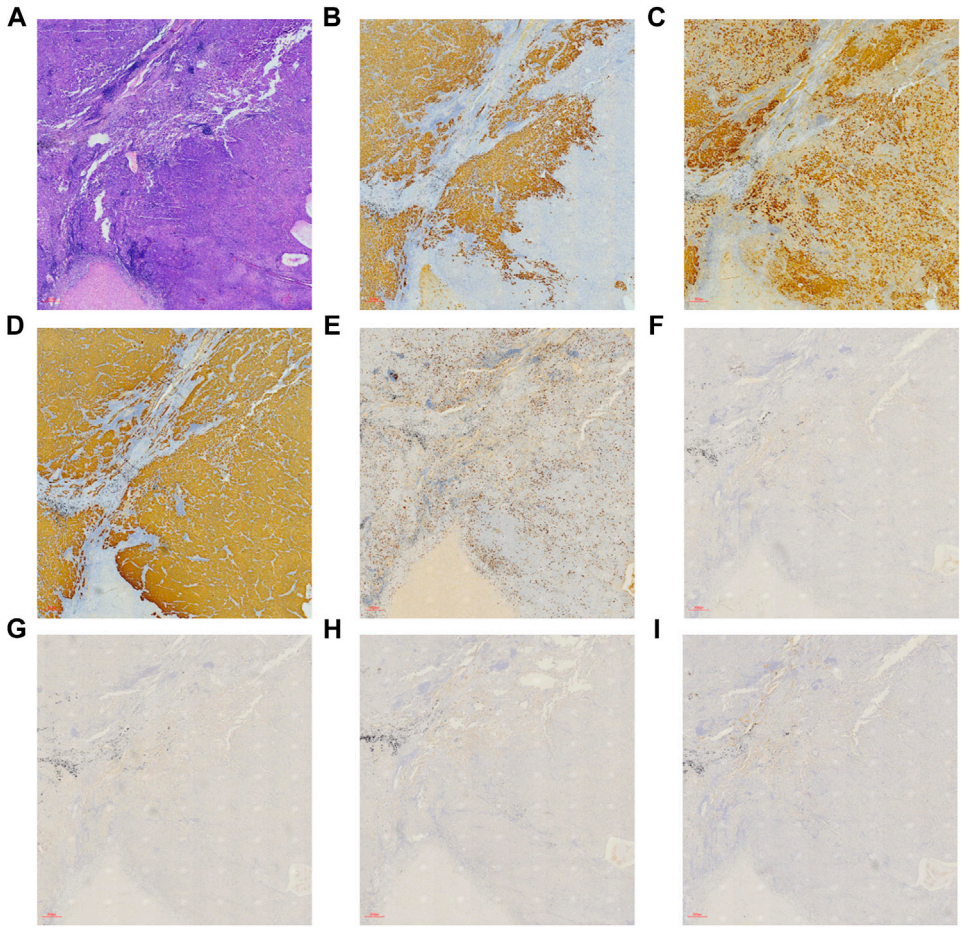

FIGURE 3
Immunohistochemical and hematoxylin-eosin staining on patient's tumor tissue (× 40, 300 μm). **(A)** HE staining, **(B)** hepatocyte (+), **(C)** glypican-3 (+), **(D)** CK (+), **(E)** Ki-67 (30% +), **(F)** P40 (–), **(G)** P63 (–), **(H)** TTF-1 (–), and **(I)** napsin-A (–).

2013), most of which were situated in the exonic parts of the genome (Figure 4). Also, we used VarScan2 (28) to filtrate the somatic CNVs. Correlation analysis revealed that most somatic mutations clustered in chromosome 1(Figure 5). Among the somatic mutations detected in the tumor samples, two alternations were found in the coding region of NLRP3, including one synonymous mutation (c.1299C>A) and one nonsynonymous mutation (c.1300 C>A). Also, one nonsynonymous mutation (c.731C>T) was detected in the exonic region of PBX1, after searching reported driver gene databases, including Cancer Gene Census, MDG125 (Vogelstein et al., 2013), SMG127 (Kandoth et al., 2013), and CDG291 (Tamborero et al., 2013b). The synonymous mutation (c.1299C>A) in NLRP3 was archived in the COSMIC database from a lung adenocarcinoma tumor sample (TCGA-50-5941-01), and the nonsynonymous mutations of neither NLRP3 nor PBX1 were archived in dbSNP, 1,000 Genomes Project, ExAC database, and COSMIC. So, we annotated the mutations with MutationTaster, SIFT, PolyPhen2, and PROVEAN to predict whether these mutations are detrimental to protein function. The PolyPhen2 predicted the variant (c.1300C>A) to be benign with a score of 0.016 and the score of the variant (c.731C>T) was 0.997, so it was determined to be probably damaging. Meanwhile, PROVEAN predicted the variant (c.1300C>A) to be neutral with a score of −1.75 and the variant (c.731C>T) to be deleterious with a score of −3.69. Although the *NLRP3* variants (c.1300C>A and c.1299C>A) and the *PBX1* variant (c.731C>T) have been identified, there are no recommended therapies for diseases caused by these genetic mutations at present.

To further verify those cancer-related mutations, we used MuSiC(25) to seek significantly mutated genes in cancer samples, and simultaneously, all the somatic alternations were statistically tested by the convolution test (Figure 6). GO and KEGG interaction analyses were conducted among the significantly mutated genes, which are shown in Figure 7. The results

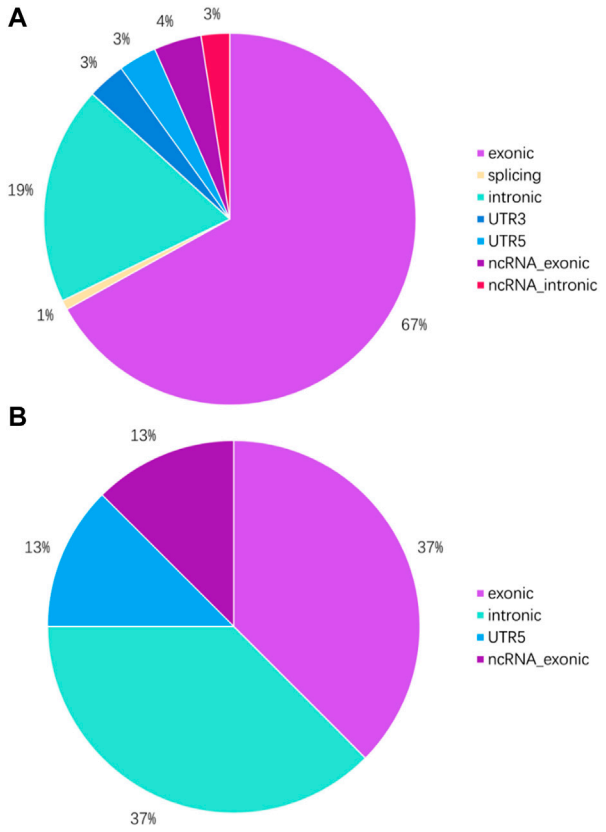

FIGURE 4
Genome location of SNVs and indels in tumor tissue. **(A)** Proportion of SNVs in different parts of the genome. **(B)** Proportion of indels in different parts of the genome.

showed that, for molecular function, these significantly mutated genes (SMGs) mainly participated in ceramide transporter activity, sphingolipid transporter activity, intermembrane lipid transfer activity, antioxidant activity, ceramide binding, and peroxidase activity (all *p*-adjusted <0.05). Additionally, "amyotrophic lateral sclerosis (ALS)" (*p*-adjusted = 0.012624) and "axon guidance" (*p*-adjusted = 0.032708) are the KEGG pathways that were mainly enriched by SMGs.

Discussion

Interpretation

The incidence of HAL is extremely low, accounting for only about 5% of HAC. Among them, smoking men above middle age are the most commonly affected individuals, and most patients have elevated AFP levels. In recent years, some patients without elevated AFP levels have occasionally appeared. Most of the lesions in patients with primary HAL appear in the upper lobe of the lung, resulting in the symptoms and imaging findings of the patients being very similar to those of other types of lung cancer, but HE and immunohistochemical staining of the tumor pathology showed HCC-like features (Zhuansun et al., 2021). Therefore, to avoid misdiagnosis, CT examination and HE and immunohistochemical staining should be conducted together to help in the diagnosis (Terracciano et al., 2003). Ishikura et al. (1990) proposed two diagnostic criteria for HAL at that time, namely, typical acinar or papillary adenocarcinoma, most of which were like HCC, and either the expression of AFP was positive or there was a significant increase of AFP in the serum content. However, the aforementioned clinical diagnostic criteria are imperfect, and occasional cases of HAL without elevated AFP had been reported over the next few years. In the first case of HAL proposed by Haninger et al. (2014), there was no increase in AFP, and the pathological manifestations were tissue neuroendocrine carcinoma and signet ring cells. Therefore, Haninger redefined the criteria for HAL diagnosis. First, the tumor can be a typical acinar or papillary adenocarcinoma, signet ring cell carcinoma, or containing neuroendocrine function. Second, if it expresses markers of liver differentiation, the abnormality in the patient should be diagnosed as HAL, no matter the AFP level is elevated or not. A thorough review of the published cases showed that patients with early diagnosis of HAL had longer postoperative survival, and the current treatment for HAL is the same as that for other lung cancers; radiotherapy and chemotherapy are effective treatments for patients with advanced HAL (Zhuansun et al., 2021). However, owing to the lack of analysis of gene mutations in HAL cases, the progress of new gene-targeted therapy has been limited. Li et al. (2019) conducted whole-genome sequencing (WGS) in a HAL patient with elevated AFP and detected a FAT1 driver gene mutation. FAT1 is one of the common mutations in malignant tumors, which inhibits tumor growth through the activation signal of Hippo signaling (Li and Guan, 2021) and promotes tumor migration by inducing actin polymerization (Katoh, 2012; Coudray et al., 2018). However, there are no effective drugs against FAT1 mutation. Chen et al. (2019) reported a case of HAL harboring an EGFR mutation and being responsive to tyrosine kinase inhibitor (TKI) therapy (Harrison et al., 2020). Also, Chen et al. (2020) reported a case of HAL with a KRAS driver mutation, but due to the lack of effective drugs against KRAS mutations, the patient experienced fifth-grade pneumonia and died after 6 months of anti-PD-1 treatment. Sun et al. (2022) performed next-generation sequencing (NGS) on three primary HAL cases and one HAS-metastatic HAL case and detected TP53 mutations in all four patients, although TP53 is a particularly common driver mutation. There have been several tumor studies targeting p53 inactivation (Chen et al., 2021; Liu et al., 2022), but there are no effective therapeutic agents for TP53 mutations currently, with only three compounds having reached phase III clinical trials: the mutant p53-reactivating drugs, APR-246 and COTI-2, and the MDM2 antagonist idasanutlin (Duffy et al., 2022). Meanwhile, CDK8, CKDN2A, CSF1R, EPHA5, PKHD1, SMARCA4, and

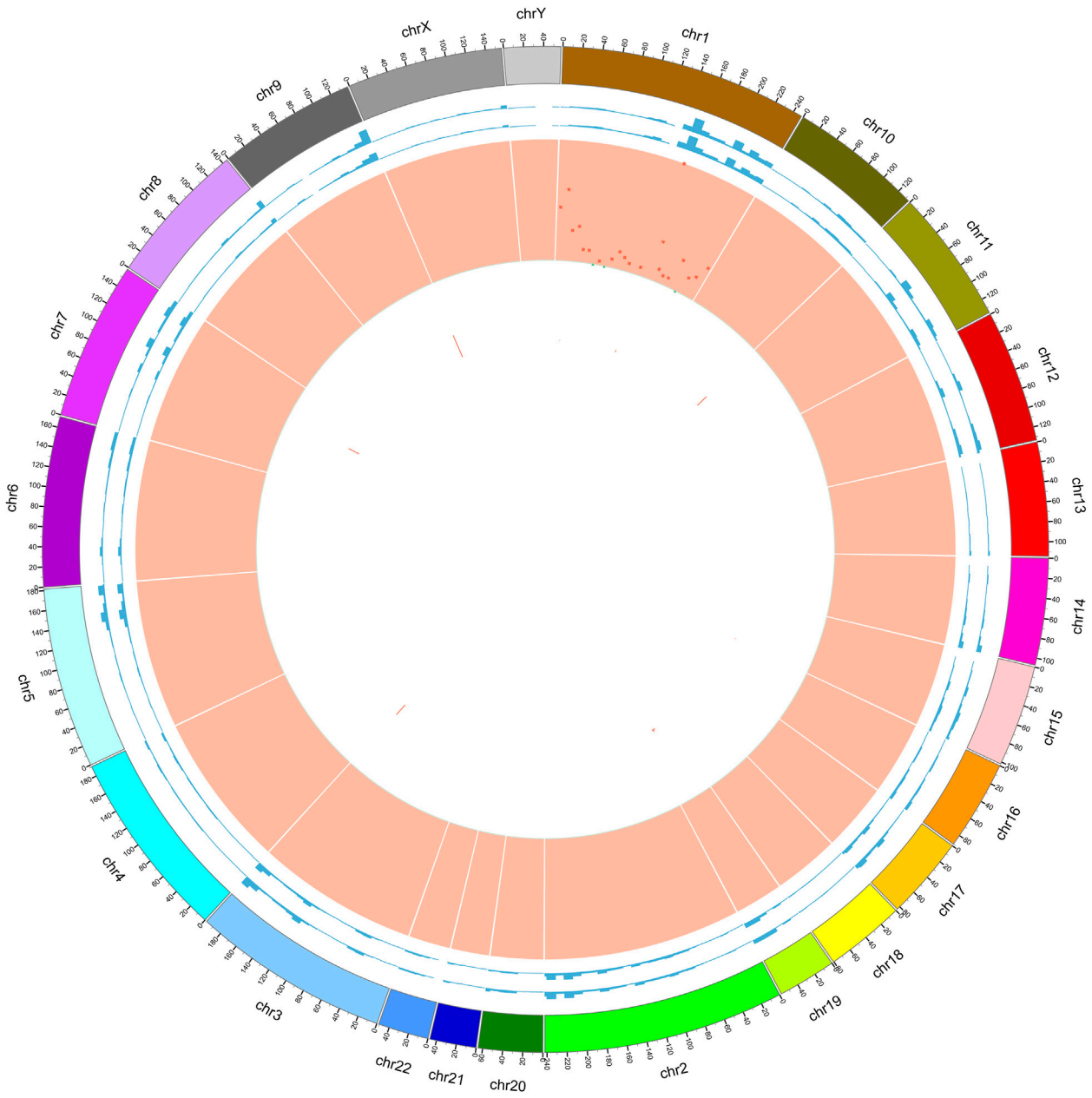

FIGURE 5
Circle graph of somatic mutations found in tumor samples. Circle 1: outer frame of the chromosome; Circle 2: sequencing coverage map of tumor samples; Circle 3: sequencing coverage map of normal samples; Circle 4: green dots indicate the density of SNP indel; Circle 5: CNV results, red indicates the copy number increase; Circle 6: CNV results, blue indicates copy number deletion; we found that by comparing with paracancerous samples, the differential mutations in tumor samples were mainly located on chromosome 1.

STK11 were detected as high-frequency mutations with a mutation rate of 50%. The expression of AFP in the immunohistochemistry of one out of four patients was also negative, and the gene mutations detected by sequencing were TP53, CDKN2A, STK11, and INPP4B, which were different from our sequencing results. In our study, only two nonsynonymous mutations, variant (c.1300C>A) in NLRP3 and variant (c.731C>T) in PBX1, were detected. NLRP3, the sensor component of the NLRP3 inflammasome, plays a crucial role in innate immunity and inflammation (Nakanishi et al., 2017). Inflammasomes can also induce pyroptosis, an inflammatory form of programmed cell death (Mitoma et al., 2013; Mishra et al., 2022). Hamarsheh summarized the therapeutic potential of targeting

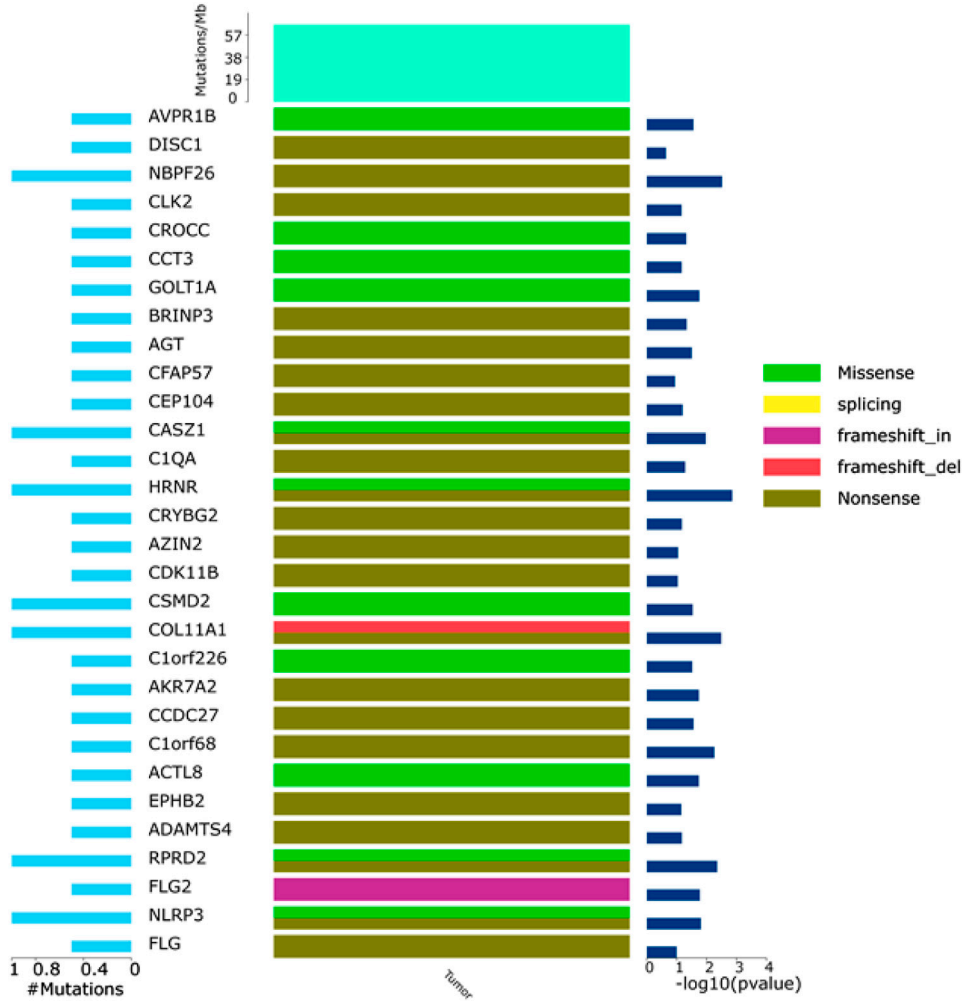

FIGURE 6
General map of high-frequency mutations. Left: percentage of genetic mutations; right: high-frequency mutant gene significance; top: mutation frequency of samples; middle: mutation types, including I. missense (green), II. splicing (yellow), III. frameshift_in (purple), IV. frameshift_del (red), and V. nonsense.

NLRP3 inflammasome in cancer (Hamarsheh and Zeiser, 2020). Moreover, some small-molecule compounds have anti-inflammatory effects that can be designed for drugs, such as thalidomide (Franks et al., 2004) and VX-765 (Wannamaker et al., 2007). PBX1 belongs to the PBX homeobox family of transcriptional factors. The *E2A-PBX1* fusion gene caused by t (McKenna et al., 2010; Mazouz et al., 2015) (q23; p13) can be found in many types of cancers, which makes it an attractive potential target for the design of new drugs (Mo et al., 2013).

Given the similar pathological features of HAL, hepatocellular carcinoma (HCC), and lung adenocarcinoma (LUAD), there may be similar disease progression among them. We compared the gene mutation information of NLRP3 and PBX1 in HCC (data from TCGA, PanCancer Atlas with 372 samples) and LUAD (data from TCGA, PanCancer Atlas with 566 samples) through the cBioPortal database (https://www.cbioportal.org/) and analyzed the relationship between HAL-related driver gene mutations. NLRP3 is altered in 11% of 566 cases in the mutation data from TCGA-LUAD samples and 2.2% of 366 cases in the mutation data from TCGA-HCC samples, and PBX1 is altered in 1.8% of 566 cases in the mutation data from TCGA-LUAD samples and 1.6% of 372 cases in the mutation data from TCGA-HCC samples. After comparing the co-expression information between mutated NLRP3, PBX1, FAT1, EGFR, KRAS, and TP53 in HCC and LUAD tissues through the cBioPortal database, we found that the samples with both NLRP3 and TP53 mutations were the most in LUAD (Figure 8).

Despite these studies showing that some gene mutations lead to the occurrence and development of HAL, its potential

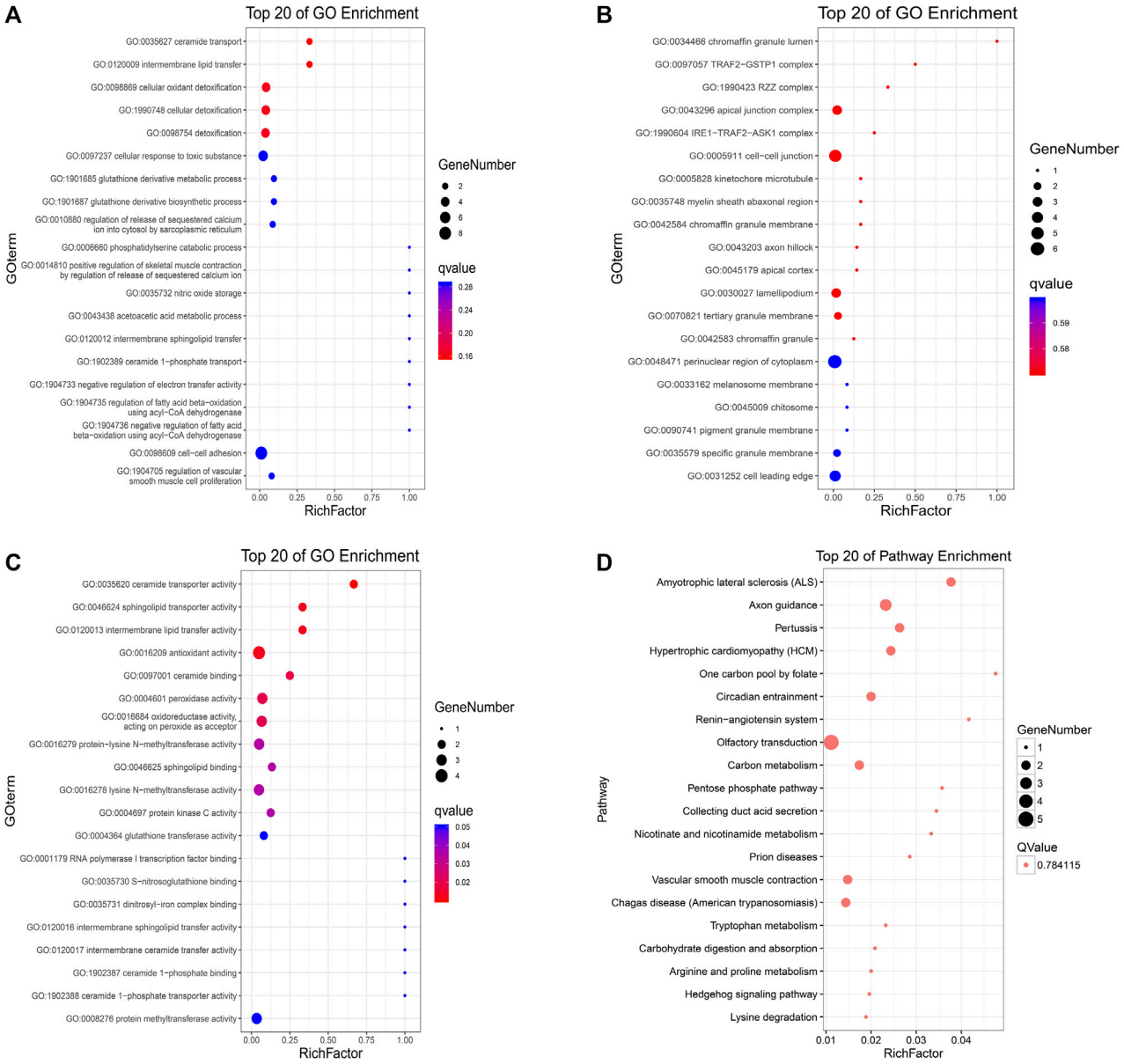

FIGURE 7
KEGG and GO analyses of identified high-frequency mutant genes. Gene Ontology **(A)** biological process, **(B)** cellular component, and **(C)** molecular function; *X*-axis: the ratio of enriched genes to the total genes; *Y*-axis: GO terms. The dot size represents the number of enriched genes, and the color represents the *p*-value. **(D)** KEGG pathway analysis; *X*-axis: the ratio of enriched genes to the total genes; *Y*-axis: the terms of pathways. The dot size represents the number of enriched genes, and the *Q*-value is 0.784115.

mechanism needs to be explored. Comprehensively considering the preference of driver mutations in the locus distribution to form mutation clusters, we used synonymous mutations to construct a background mutation rate model with the characteristics of an unbiased distribution to find possible driver mutations using OncodriveCLUST software. We identified HNRNPR, TP73, CFAP57, COL11A1, RUSC1, SLC6A9, DISC1, NBPF26, and OR10K1 as potential driver mutation genes in HAL.

HNRNPR was originally identified as a component of the heterogeneous nuclear ribonucleoproteins (hnRNPs) family, which plays a vital role in many aspects of (pre)mRNA processing (Dreyfuss et al., 2002). HNRNPR expression is altered in many malignancies, suggesting that it is associated

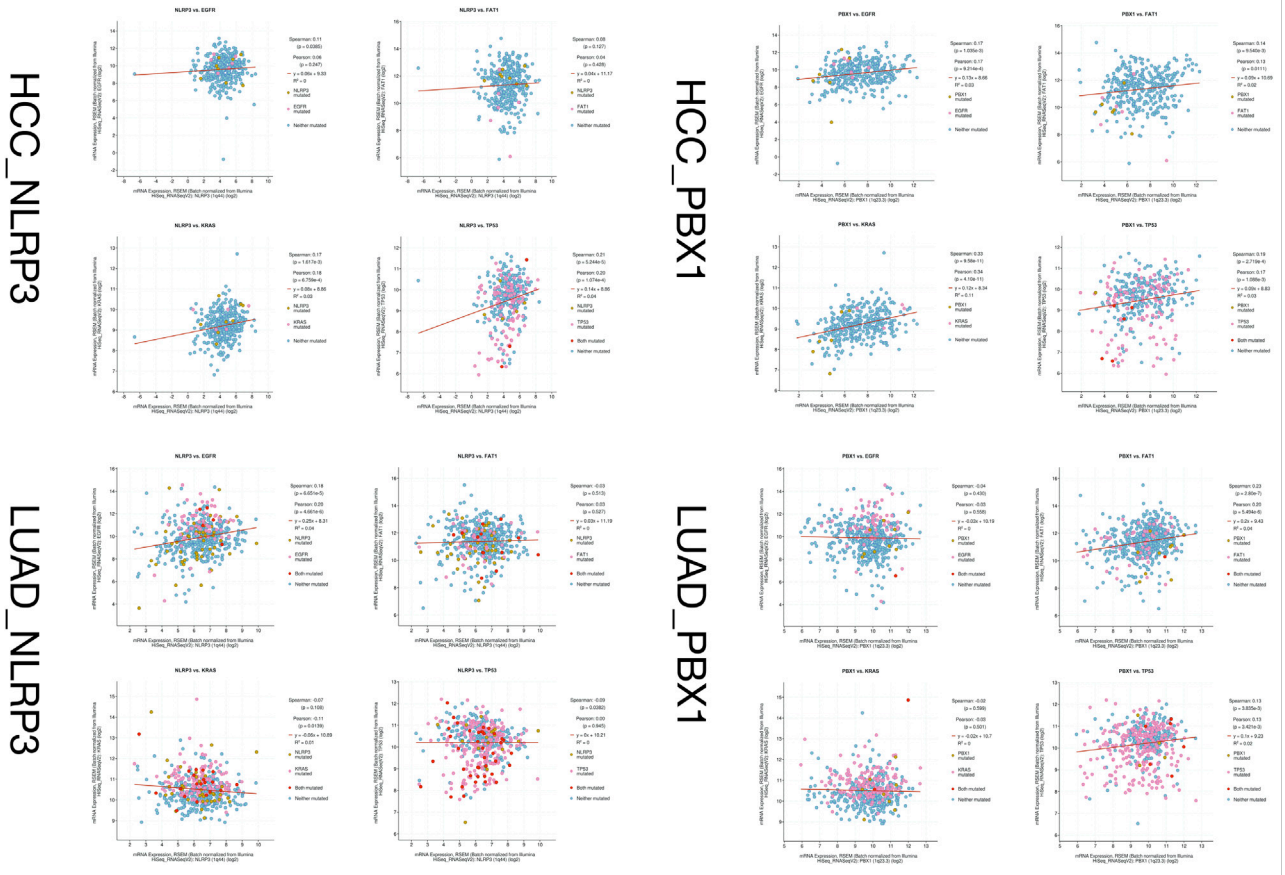

FIGURE 8
Co-expression information between mutated NLRP3, PBX1, FAT1, EGFR, KRAS, and TP53 in HCC and LUAD tissues.

with tumor formation (Pereira et al., 2017). The characteristics of HNRNPR in neurodevelopment have also been reported in many literature works (Dombert et al., 2014), which explain the occurrence of neuroendocrine differentiation in tumors of HAL. TP73 is a member of the TP53 family, mutations of which are found in many tumors and are associated with prognosis. TP73 can transform multiple variants with oncogenic and tumor-suppressive functions (Jost et al., 1997). Collagen type XI α1 (COL11A1), a minor fibrillar collagen, which plays a crucial role in cell proliferation, migration, and tumorigenesis of many malignancies, may be a valuable diagnostic marker for lung cancer. Smad signaling is activated by the overexpression of COL11A1 and promotes cell proliferation and migration (Shen et al., 2016). DISC1, an oncogene, activates the GSK3β/β-catenin signaling to promote NSCLC growth, so it could be designed to be a novel anti-NSCLC therapeutic target (Wang et al., 2017), which means that HAL has the same mutation gene and differentiation process as NSCLC does.

In this study, a comprehensive interaction analysis of GO and KEGG was performed among 76 significantly mutated genes to gain a more specific understanding of tumor genome mutation enrichment and biological functions. GO-cellular components revealed that these high-frequency mutated genes were mainly related to cell, cell part, and organelle. The GO-biological process showed these genes were related to cellular process and single-organism process, and GO-molecular function showed that these genes were related to binding function. Additionally, KEGG pathway enrichment revealed that the mutant genes mainly participated in “amyotrophic lateral sclerosis (ALS)” and “axon guidance” These findings suggest that these pathways that mutant gene aggregation enriched might play a vital role in the tumorigenesis process.

Limitation and strength

This study has several limitations, especially the small size of the sample due to the rarity of HAL, and second, there were some false-negative results caused by the inadequate sequencing coverage inevitably, despite the sequencing depth and

coverage of WES being much more improved than the Sanger sequencing. Finally, there is heterogeneity in different parts of the tumor, and the tissue obtained from the biopsy is so finite that it is impossible to cover the whole tumor genome. However, it was the first time that the WES was conducted on a non-AFP elevated HAL patient to explore the potential mechanisms of tumorigenesis. Meanwhile, the gene mutations are valuable to be the prospective candidates for gene-targeted therapy.

Further clinical guidance

Cancer is caused by abnormal cell division and differentiation due to genetic mutation (Heng and Heng, 2022); therefore, inhibiting mutations in genes related to tumor formation is the most fundamental approach for treating cancer, and with the increasing maturity of next-generation sequencing technology, more and more gene-specific research studies are being conducted in cancer diagnosis and treatment. In this study, our goal was to identify rare deleterious variants and biological pathways of HAL mutant gene enrichment that will guide future genetic and functional studies on the pathogenesis of this rare malignancy.

In the past, cancer was classified according to its morphological characteristics. To date, understanding of cancer has reached the molecular level, and based on next-generation sequencing technology, individualized precision medicine is becoming more widespread. Therefore, it is necessary to recommend targeted drugs for patients with different genetic backgrounds.

Conclusion

In summary, the rarity of HAL making large-scale trials difficult to organize, we used WES to reveal molecular patterns of HAL without an elevated AFP level. As we know, this is the first time that NLRP3 and PBX1 mutations were found in HAL without an elevated AFP level, which suggests the underlying mechanisms of tumorigenesis. Clinical treatment of HAL should not be based only on the treatments of common lung cancer or HCC; individualized and precise treatment should be implemented for its unique driver gene mutations, and our research reveals the potential mechanism of its development and provides a new potential target for treating this rare tumor.

Data availability statement

The datasets presented in this study can be found in online repositories. The names of the repository/repositories and accession number(s) can be found at: https://www.ncbi.nlm.nih.gov/, SUB11172444.

Ethics statement

The studies involving human participants were reviewed and approved by the Ethics Committee of China Medical University. The patients/participants provided their written informed consent to participate in this study. Written informed consent was obtained from the individual(s) for the publication of any potentially identifiable images or data included in this article.

Author contributions

Design of the research: XZ and YY; acquisition, analysis, and interpretation of data: YY and GB; drafting the manuscript: YY and TL; revision of the manuscript for important intellectual content: YY, JL, GB, and XZ.

Funding

This study was supported by the Jieping Wu Medical Foundation Special Fund for Clinical Research (320.6750.2020-17-7).

Acknowledgments

The authors thank Guangzhou Gene Denovo Biotechnology Co., Ltd. For assisting in sequencing and bioinformatics analyses.

Conflict of interest

The authors declare that the research was conducted in the absence of any commercial or financial relationships that could be construed as a potential conflict of interest.

Publisher's note

All claims expressed in this article are solely those of the authors and do not necessarily represent those of their affiliated organizations, or those of the publisher, the editors, and the reviewers. Any product that may be evaluated in this article, or claim that may be made by its manufacturer, is not guaranteed or endorsed by the publisher.

References

Adzhubei, I. A., Schmidt, S., Peshkin, L., Ramensky, V. E., Gerasimova, A., Bork, P., et al. (2010). A method and server for predicting damaging missense mutations. *Nat. Methods* 7 (4), 248–249. doi:10.1038/nmeth0410-248

Boeva, V., Popova, T., Bleakley, K., Chiche, P., Cappo, J., Schleiermacher, G., et al. (2012). Control-FREEC: a tool for assessing copy number and allelic content using next-generation sequencing data. *Bioinformatics* 28 (3), 423–425. doi:10.1093/bioinformatics/btr670

Chen, S., Zhou, Y., Chen, Y., and Gu, J. (2018). fastp: an ultra-fast all-in-one FASTQ preprocessor. *Bioinformatics* 34 (17), i884–i890. doi:10.1093/bioinformatics/bty560

Chen, H. F., Wang, W. X., Li, X. L., Xu, C. W., Du, K. Q., Zhu, Y. C., et al. (2019). Hepatoid adenocarcinoma of the lung with EGFR mutation and the response to tyrosine kinase inhibitors. *J. Thorac. Oncol.* 14 (10), e217–e219. doi:10.1016/j.jtho.2019.04.032

Chen, L., Han, X., Gao, Y., Zhao, Q., Wang, Y., Jiang, Y., et al. (2020). Anti-PD-1 therapy achieved disease control after multiline chemotherapy in unresectable KRAS-positive hepatoid lung adenocarcinoma: a case report and literature review. *Onco. Targets. Ther.* 13, 4359–4364. doi:10.2147/OTT.S248226

Chen, S., Thorne, R. F., Zhang, X. D., Wu, M., and Liu, L. (2021). Non-coding RNAs, guardians of the p53 galaxy. *Semin. Cancer Biol.* 75, 72–83. doi:10.1016/j.semcancer.2020.09.002

Choi, Y., Sims, G. E., Murphy, S., Miller, J. R., and Chan, A. P. (2012). Predicting the functional effect of amino acid substitutions and indels. *PLoS One* 7 (10), e46688. doi:10.1371/journal.pone.0046688

Cibulskis, K., Lawrence, M. S., Carter, S. L., Sivachenko, A., Jaffe, D., Sougnez, C., et al. (2013). Sensitive detection of somatic point mutations in impure and heterogeneous cancer samples. *Nat. Biotechnol.* 31 (3), 213–219. doi:10.1038/nbt.2514

Coudray, N., Ocampo, P. S., Sakellaropoulos, T., Narula, N., Snuderl, M., Fenyö, D., et al. (2018). Classification and mutation prediction from non-small cell lung cancer histopathology images using deep learning. *Nat. Med.* 24 (10), 1559–1567. doi:10.1038/s41591-018-0177-5

Dees, N. D., Zhang, Q., Kandoth, C., Wendl, M. C., Schierding, W., Koboldt, D. C., et al. (2012). MuSiC: identifying mutational significance in cancer genomes. *Genome Res.* 22 (8), 1589–1598. doi:10.1101/gr.134635.111

Dombert, B., Sivadasan, R., Simon, C. M., Jablonka, S., and Sendtner, M. (2014). Presynaptic localization of Smn and hnRNP R in axon terminals of embryonic and postnatal mouse motoneurons. *PLoS One* 9 (10), e110846. doi:10.1371/journal.pone.0110846

Dreyfuss, G., Kim, V. N., and Kataoka, N. (2002). Messenger-RNA-binding proteins and the messages they carry. *Nat. Rev. Mol. Cell Biol.* 3 (3), 195–205. doi:10.1038/nrm760

Duffy, M. J., Synnott, N. C., O'Grady, S., and Crown, J. (2022). Targeting p53 for the treatment of cancer. *Semin. Cancer Biol.* 79, 58–67. doi:10.1016/j.semcancer.2020.07.005

Franks, M. E., Macpherson, G. R., and Figg, W. D. (2004). Thalidomide. *Lancet* 363 (9423), 1802–1811. doi:10.1016/S0140-6736(04)16308-3

Gardiner, G. W., Lajoie, G., and Keith, R. (1992). Hepatoid adenocarcinoma of the papilla of Vater. *Histopathology* 20 (6), 541–544. doi:10.1111/j.1365-2559.1992.tb01044.x

Grossman, K., Beasley, M. B., and Braman, S. S. (2016). Hepatoid adenocarcinoma of the lung: Review of a rare form of lung cancer. *Respir. Med.* 119, 175–179. doi:10.1016/j.rmed.2016.09.003

Hamarsheh, S., and Zeiser, R. (2020). NLRP3 inflammasome activation in cancer: a double-edged sword. *Front. Immunol.* 11, 1444. doi:10.3389/fimmu.2020.01444

Haninger, D. M., Kloecker, G. H., Bousamra Ii, M., Nowacki, M. R., and Slone, S. P. (2014). Hepatoid adenocarcinoma of the lung: report of five cases and review of the literature. *Mod. Pathol.* 27 (4), 535–542. doi:10.1038/modpathol.2013.170

Harrison, P. T., Vyse, S., and Huang, P. H. (2020). Rare epidermal growth factor receptor (EGFR) mutations in non-small cell lung cancer. *Semin. Cancer Biol.* 61, 167–179. doi:10.1016/j.semcancer.2019.09.015

Heng, J., and Heng, H. H. (2022). Genome chaos: Creating new genomic information essential for cancer macroevolution. *Semin. Cancer Biol.* 81, 160–175. doi:10.1016/j.semcancer.2020.11.003

Hou, Z., Xie, J., Zhang, L., Dai, G., Chen, Y., and He, L. (2021). Hepatoid adenocarcinoma of the lung: a systematic review of the literature from 1981 to 2020. *Front. Oncol.* 11, 702216. doi:10.3389/fonc.2021.702216

Ishikura, H., Kanda, M., Ito, M., Nosaka, K., and Mizuno, K. (1990). Hepatoid adenocarcinoma: a distinctive histological subtype of alpha-fetoprotein-producing lung carcinoma. *Virchows Arch. A Pathol. Anat. Histopathol.* 417 (1), 73–80. doi:10.1007/BF01600112

Jost, C. A., Marin, M. C., and Kaelin, W. G. (1997). p73 is a simian [correction of human] p53-related protein that can induce apoptosis. *Nature* 389 (6647), 191–194. doi:10.1038/38298

Kadalayil, L., Rafiq, S., Rose-Zerilli, M. J., Pengelly, R. J., Parker, H., Oscier, D., et al. (2015). Exome sequence read depth methods for identifying copy number changes. *Brief. Bioinform.* 16 (3), 380–392. doi:10.1093/bib/bbu027

Kandoth, C., McLellan, M. D., Vandin, F., Ye, K., Niu, B., Lu, C., et al. (2013). Mutational landscape and significance across 12 major cancer types. *Nature* 502 (7471), 333–339. doi:10.1038/nature12634

Kato, K., Suzuka, K., Osaki, T., Itami, M., and Tanaka, N. (2007). Primary hepatoid adenocarcinoma of the uterine cervix. *Int. J. Gynecol. Cancer* 17 (5), 1150–1154. doi:10.1111/j.1525-1438.2007.00901.x

Katoh, M. (2012). Function and cancer genomics of FAT family genes (review). *Int. J. Oncol.* 41 (6), 1913–1918. doi:10.3892/ijo.2012.1669

Khozin, S., Roth, M. J., Rajan, A., Smith, K., Thomas, A., Berman, A., et al. (2012). Hepatoid carcinoma of the lung with anaplastic lymphoma kinase gene rearrangement. *J. Thorac. Oncol.* 7 (11), e29–31. doi:10.1097/JTO.0b013e3182697a23

Li, H., and Durbin, R. (2009). Fast and accurate short read alignment with Burrows-Wheeler transform. *Bioinformatics* 25 (14), 1754–1760. doi:10.1093/bioinformatics/btp324

Li, F. L., and Guan, K. L. (2021). The two sides of Hippo pathway in cancer. *Semin. Cancer Biol.* doi:10.1016/j.semcancer.2021.07.006

Li, J., Qi, H., Xu, B., Zhao, J., Gao, H., Ma, X., et al. (2019). Genomic profiles of a patient of pulmonary hepatoid adenocarcinoma with high AFP level: a case report. *Front. Oncol.* 9, 1360. doi:10.3389/fonc.2019.01360

Lin, S-F., Hsu, W-H., and Chou, T-Y. (2013). Primary pulmonary hepatoid carcinoma: report of a case and review of the literature. *Kaohsiung J. Med. Sci.* 29 (9), 512–516. doi:10.1016/j.kjms.2013.01.007

Liu, C., Moten, A., Ma, Z., and Lin, H. K. (2022). The foundational framework of tumors: Gametogenesis, p53, and cancer. *Semin. Cancer Biol.* 81, 193–205. doi:10.1016/j.semcancer.2021.04.018

Mazouz, A., Amaadour, L., Ameurtesse, H., Chban, L., Amarti, A., Kettani, F., et al. (2015). Primary hepatoid carcinoma of the ovary: a case report. *Pan Afr. Med. J.* 20, 93. doi:10.11604/pamj.2015.20.93.5953

McKenna, A., Hanna, M., Banks, E., Sivachenko, A., Cibulskis, K., Kernytsky, A., et al. (2010). The genome analysis Toolkit: a MapReduce framework for analyzing next-generation DNA sequencing data. *Genome Res.* 20 (9), 1297–1303. doi:10.1101/gr.107524.110

Mermel, C. H., Schumacher, S. E., Hill, B., Meyerson, M. L., Beroukhim, R., and Getz, G. (2011). GISTIC2.0 facilitates sensitive and confident localization of the targets of focal somatic copy-number alteration in human cancers. *Genome Biol.* 12 (4), R41. doi:10.1186/gb-2011-12-4-r41

Mishra, S. R., Mahapatra, K. K., Behera, B. P., Bhol, C. S., Praharaj, P. P., Panigrahi, D. P., et al. (2022). Inflammasomes in cancer: effect of epigenetic and autophagic modulations. *Semin. Cancer Biol.* 83, 399–412. doi:10.1016/j.semcancer.2020.09.013

Mitoma, H., Hanabuchi, S., Kim, T., Bao, M., Zhang, Z., Sugimoto, N., et al. (2013). The DHX33 RNA helicase senses cytosolic RNA and activates the NLRP3 inflammasome. *Immunity* 39 (1), 123–135. doi:10.1016/j.immuni.2013.07.001

Mo, M. L., Chen, Z., Zhou, H. M., Li, H., Hirata, T., Jablons, D. M., et al. (2013). Detection of E2A-PBX1 fusion transcripts in human non-small-cell lung cancer. *J. Exp. Clin. Cancer Res.* 32 (1), 29. doi:10.1186/1756-9966-32-29

Nakanishi, H., Kawashima, Y., Kurima, K., Chae, J. J., Ross, A. M., Pinto-Patarroyo, G., et al. (2017). NLRP3 mutation and cochlear autoinflammation cause syndromic and nonsyndromic hearing loss DFNA34 responsive to anakinra therapy. *Proc. Natl. Acad. Sci. U. S. A.* 114 (37), E7766–e75. doi:10.1073/pnas.1702946114

Nakashima, N., Fukatsu, T., Nagasaka, T., Sobue, M., and Takeuchi, J. (1987). The frequency and histology of hepatic tissue in germ cell tumors. *Am. J. Surg. Pathol.* 11 (9), 682–692. doi:10.1097/00000478-198709000-00004

Ng, P. C., and Henikoff, S. (2003). SIFT: predicting amino acid changes that affect protein function. *Nucleic Acids Res.* 31 (13), 3812–3814. doi:10.1093/nar/gkg509

Pereira, B., Billaud, M., and Almeida, R. (2017). RNA-binding proteins in cancer: old players and new actors. *Trends Cancer* 3 (7), 506–528. doi:10.1016/j.trecan.2017.05.003

Qian, G. Q., Yin, F. Y., Li, G. X., and Chu, J. G. (2016). Hepatoid adenocarcinoma of the lung. *QJM* 109 (9), 619–620. doi:10.1093/qjmed/hcw107

Schwarz, J. M., Rödelsperger, C., Schuelke, M., and Seelow, D. (2010). MutationTaster evaluates disease-causing potential of sequence alterations. *Nat. Methods* 7 (8), 575–576. doi:10.1038/nmeth0810-575

Shen, L., Yang, M., Lin, Q., Zhang, Z., Zhu, B., and Miao, C. (2016). COL11A1 is overexpressed in recurrent non-small cell lung cancer and promotes cell proliferation, migration, invasion and drug resistance. *Oncol. Rep.* 36 (2), 877–885. doi:10.3892/or.2016.4869

Shi, Y-F., Lu, J-G., Yang, Q-M., Duan, J., Lei, Y-M., Zhao, W., et al. (2019). Primary hepatoid adenocarcinoma of the lung in yungui plateau, China: a case report. *World J. Clin. Cases* 7 (13), 1711–1716. doi:10.12998/wjcc.v7.i13.1711

Su, J-S., Chen, Y-T., Wang, R-C., Wu, C-Y., Lee, S-W., and Lee, T-Y. (2013). Clinicopathological characteristics in the differential diagnosis of hepatoid adenocarcinoma: a literature review. *World J. Gastroenterol.* 19 (3), 321–327. doi:10.3748/wjg.v19.i3.321

Sun, J. N., Zhang, B. L., Li, L. K., Yu, H. Y., and Wang, B. (2016). Hepatoid adenocarcinoma of the lung without production of α-fetoprotein: a case report and review of the literature. *Oncol. Lett.* 12 (1), 189–194. doi:10.3892/ol.2016.4559

Sun, H., Li, X., Zhang, J., and Liu, Y. (2022). Clinicopathological features and genomic profiles of hepatoid adenocarcinoma of the lung: report of four cases. *Pathol. Res. Pract.* 229, 153652. doi:10.1016/j.prp.2021.153652

Tamborero, D., Gonzalez-Perez, A., and Lopez-Bigas, N. (2013). OncodriveCLUST: exploiting the positional clustering of somatic mutations to identify cancer genes. *Bioinformatics* 29 (18), 2238–2244. doi:10.1093/bioinformatics/btt395

Tamborero, D., Gonzalez-Perez, A., Perez-Llamas, C., Deu-Pons, J., Kandoth, C., Reimand, J., et al. (2013). Comprehensive identification of mutational cancer driver genes across 12 tumor types. *Sci. Rep.* 3, 2650. doi:10.1038/srep02650

Terracciano, L. M., Glatz, K., Mhawech, P., Vasei, M., Lehmann, F. S., Vecchione, R., et al. (2003). Hepatoid adenocarcinoma with liver metastasis mimicking hepatocellular carcinoma: an immunohistochemical and molecular study of eight cases. *Am. J. Surg. Pathol.* 27 (10), 1302–1312. doi:10.1097/00000478-200310000-00002

Vogelstein, B., Papadopoulos, N., Velculescu, V. E., Zhou, S., Diaz, L. A., and Kinzler, K. W. (2013). Cancer genome landscapes. *Science* 339 (6127), 1546–1558. doi:10.1126/science.1235122

Wang, K., Li, M., and Hakonarson, H. (2010). ANNOVAR: functional annotation of genetic variants from high-throughput sequencing data. *Nucleic Acids Res.* 38 (16), e164. doi:10.1093/nar/gkq603

Wang, J., Mullighan, C. G., Easton, J., Roberts, S., Heatley, S. L., Ma, J., et al. (2011). CREST maps somatic structural variation in cancer genomes with base-pair resolution. *Nat. Methods* 8 (8), 652–654. doi:10.1038/nmeth.1628

Wang, S., Chen, Y. Y., Li, Y. P., Gu, J., Gu, S. D., Shi, H., et al. (2017). DISC1 overexpression promotes non-small cell lung cancer cell proliferation. *Oncotarget* 8 (39), 65199–65210. doi:10.18632/oncotarget.18055

Wannamaker, W., Davies, R., Namchuk, M., Pollard, J., Ford, P., Ku, G., et al. (2007). (S)-1-((S)-2-{[1-(4-amino-3-chloro-phenyl)-methanoyl]-amino}-3, 3-dimethyl-butanoyl)-pyrrolidine-2-carboxylic acid ((2R, 3S)-2-ethoxy-5-oxo-tetrahydro-furan-3-yl)-amide (VX-765), an orally available selective interleukin (IL)-converting enzyme/caspase-1 inhibitor, exhibits potent anti-inflammatory activities by inhibiting the release of IL-1beta and IL-18. *J. Pharmacol. Exp. Ther.* 321 (2), 509–516. doi:10.1124/jpet.106.111344

Zhuansun, Y., Bian, L., Zhao, Z., Du, Y., Chen, R., Lin, L., et al. (2021). Clinical characteristics of Hepatoid adenocarcinoma of the lung: four case reports and literature review. *Cancer Treat. Res. Commun.* 29, 100474. doi:10.1016/j.ctarc.2021.100474

frontiers | Frontiers in Pharmacology

TYPE Original Research
PUBLISHED 26 August 2022
DOI 10.3389/fphar.2022.920022

Check for updates

OPEN ACCESS

EDITED BY
Chen Shi,
Huazhong University of Science and Technology, China

REVIEWED BY
Yi-Hui Wu,
Chi Mei Medical Center, Taiwan
Jiaxuan Qiu,
The First Affiliated Hospital of Nanchang University, China

*CORRESPONDENCE
Wenjuan Wang,
wangwenjuan1110@163.com
Xinyuan Ding,
aladdine@163.com
Zengyan Zhu,
zhuzengyan7676@suda.edu.cn

†These authors have contributed equally to this work

SPECIALTY SECTION
This article was submitted to Pharmacology of Anti-Cancer Drugs, a section of the journal Frontiers in Pharmacology

RECEIVED 14 April 2022
ACCEPTED 21 July 2022
PUBLISHED 26 August 2022

CITATION
Du X, Ding L, Huang S, Li F, Yan Y, Tang R, Ding X, Zhu Z and Wang W (2022), Cathepsin L promotes chemresistance to neuroblastoma by modulating serglycin.
Front. Pharmacol. 13:920022.
doi: 10.3389/fphar.2022.920022

COPYRIGHT
© 2022 Du, Ding, Huang, Li, Yan, Tang, Ding, Zhu and Wang. This is an open-access article distributed under the terms of the Creative Commons Attribution License (CC BY). The use, distribution or reproduction in other forums is permitted, provided the original author(s) and the copyright owner(s) are credited and that the original publication in this journal is cited, in accordance with accepted academic practice. No use, distribution or reproduction is permitted which does not comply with these terms.

Cathepsin L promotes chemresistance to neuroblastoma by modulating serglycin

Xiaohuan Du[1†], Leyun Ding[2†], Shungen Huang[3†], Fang Li[1], Yinghui Yan[1], Ruze Tang[3], Xinyuan Ding[2*], Zengyan Zhu[1*] and Wenjuan Wang[1*]

[1]Department of Pharmacy, Children's Hospital of Soochow University, Suzhou, China, [2]Department of Pharmacy, The Affiliated Suzhou Hospital of Nanjing Medical University, Suzhou, China, [3]Department of Oncology, Children's Hospital of Soochow University, Suzhou, China

Cathepsin L (CTSL), a lysosomal acid cysteine protease, is found to play a critical role in chemosencitivity and tumor progression. However, the potential roles and molecular mechanisms of CTSL in chemoresistance in neuroblastoma (NB) are still unclear. In this study, the correlation between clinical characteristics, survival and CTSL expression were assessed in Versteeg dataset. The chemoresistant to cisplatin or doxorubicin was detected using CCK-8 assay. Western blot was employed to detect the expression of CTSL, multi-drug resistance proteins, autophagy-related proteins and apoptosis-related proteins in NB cells while knocking down CTSL. Lysosome staining was analyzed to access the expression levels of lysosomes in NB cells. The expression of apoptosis markers was analyzed with immunofluorescence. Various datasets were analyzed to find the potential protein related to CTSL. In addition, a subcutaneous tumor xenografts model in M-NSG mice was used to assess tumor response to CTSL inhibition *in vivo*. Based on the validation dataset (Versteeg), we confirmed that CTSL served as a prognostic marker for poor clinical outcome in NB patients. We further found that the expression level of CTSL was higher in SK-N-BE (2) cells than in IMR-32 cells. Knocking down CTSL reversed the chemoresistance in SK-N-BE (2) cells. Furthermore, combination of CTSL inhibition and chemotherapy potently blocked tumor growth *in vivo*. Mechanistically, CTSL promoted chemoresistance in NB cells by up-regulating multi-drug resistance protein ABCB1 and ABCG2, inhibiting the autophagy level and cell apoptpsis. Furthermore, we observed six datasets and found that Serglycin (SRGN) expression was positively associated with CTSL expresssion. CTSL could mediate chemoresistance by up-regulating SRGN expression in NB cells and SRGN expression was positively correlated with poor prognosis of NB patients. Taken together, our findings indicate that the CTSL promotes chemoresistance to cisplatin and doxorubicin by up-regulating the expression of multi-drug resistance proteins and inhibiting the autophagy level and cell apoptosis in NB cells. Thus, CTSL may be a therapeutic target for overcoming chemoresistant to cisplatin and doxorubicin in NB patients.

KEYWORDS
chemoresistance, neuroblastoma, Cathepsin L, autophagy, apoptosis

Introduction

Neuroblastoma (NB) is the most common extracranial solid tumor in children. NB accounts for 10% of all childhood cancers and also 15% of pediatric cancer deaths (Tolbert and Matthay, 2018). Main available treatment strategy for NB patients is chemotherapy followed by surgical resection. Cisplatin (DDP) and doxorubicin (ADM) are common chemotherapeutics for NB (Jemaà et al., 2020). However, the clinical efficacy of these drugs is limited by chemoresistance, which is the main cause of the treatment failure in NB patients (Rodrigo et al., 2021). Thus, it is important to research the molecular mechanisms of chemoresistance in NB and find the potential targets to overcome it.

Various molecular mechanisms have been implicated in chemoresistance. The ATP-binding cassette transporter (ABC) family of transmembrane proteins is associated with chemoresistance by promoting drug efflux. Among these, ABC transporter B1 (ABCB1/MDR1/P-glycoprotein), ABC transporter C1 (ABCC1/MRP1) and breast cancer resistance protein (ABCG2/BCRP) are closely related to poor platinum sensitivity (Domenichini et al., 2019). Resistance to apoptosis can also cause chemoresistance. Mutations, amplifications and overexpression of the genes encoding the anti-apoptotic BCL-2 family members and inhibitor of apoptosis proteins (IAPs) have been reported associated with chemoresistance of cancers. Autophagy is another mechanism of chemoresistance by promoting cancer cell survival during metabolic stresses induced by anticancer agents. Besides, alterations in drug metabolism, DNA damage repair, epigenetic changes, mutation of drug targets and the influence of tumor microenvironment may also contribute to chemoresistance of cancers (Holohan et al., 2013).

The ability of cancer cells to maintain an internal stasis is a critical characteristic of a neoplasm (Li et al., 2017). The important role of lysosomes in cellular stasis has been identified in many studies (Yang and Wang, 2021). Lysosome is connected to chemoresistance, cellular adaptation, immune response and cell death (Hraběta et al., 2020). Lysosomes have more than 60 hydrolytic enzymes, including proteases, lipases (Davidson and Vander Heiden, 2017). Tumor stasis is a multidimensional process that is adjusted by cellular proteins, including cathepsin family of proteases, protein-protein interactions, alternative splicing and expression of miRNAs (Mijanović et al., 2019). Cathepsins play important roles in malignant tumors. Cathepsin L (CTSL) is a cysteine protease which has been reported linked to tumor occurrence, development, and metastasis (Sudhan and Siemann, 2015). CTSL up-regulation has been identified in many human malignancies including gastric (Pan et al., 2020) and lung (Wang et al., 2018) cancers. Significantly, CTSL has important roles in regulating cancer chemoresistance (Zhao et al., 2019). Our previous study found that CTSL up-regulation-induced EMT phenotype was associated with the acquisition of DDP or paclitaxel resistance in A549 cells (Han et al., 2016). However, the roles and the mechanisms of CTSL in NB chemoresistance are still unclear which need to be studied further.

In the present study, we demonstrated that CTSL was a regulator of poor DDP and ADM sensitivity in NB cells, and the regulation of chemoresistance by CTSL was mediated through its effects on ABC proteins, autophagy and cell apoptosis. These findings indicate that CTSL may represent a novel therapeutic target to overcome poor DDP and ADM sensitivity in NB patients.

Materials and methods

Validation of human datasets

Tissue array analysis results of NB patient tumor samples were obtained from the R2 Genomics Analysis and Visualization Platform (http://r2.amc.nl) using the following publicly available dataset: Versteeg (GEO: GSE16476) (Zhang H. et al., 2020), which included comprehensive information on the relevant clinical and prognostic factors selected for analysis. For Kaplan-Meier analysis, the best p value and corresponding cutoff value was selected according to the R2 Genomics Analysis and Visualization Platform.

Six datasets (including Tumor Neuroblastoma—Seeger—117—DCHIP, Westermann—144—tpm, Fischer—223—custom, Jagannathan—100—custom, Maris—101—custom and SEQC—498—custom) were observed at the same time and different colors represented different datasets in the box plot after standardization, According to $-0.6 < R < 0.6$ and $p < 0.001$ and at the top 20 of the datasets, the eligible common genes in six databases could be screened out. Then the Spearman correlation analysis between the selected gene and CTSL was performed.

Cell lines and culture

The human NB cell lines, SK-N-BE (2) and IMR-32 were obtained from the Type Culture Collection of the Chinese Academy of Sciences, Shanghai, China. SK-N-BE (2) and IMR-32 cells were cultured in a 1:1 mixture of MEM and DMEM/F-12 with 10% fetal bovine serum, 1% Penicillin-Streptomycin. These

TABLE 1 Sequences for CTSL siRNA and SRGN siRNA.

si-RNA	Base sequence	
Negative control (NC)	sense	5′-UUCUCCGAACGUGUCACGUTT-3′
	antisense	5′-ACGUGACACGUUCGGAGAATT-3′
CTSL-homo-450	sense	5′-GCGAUGCACAACAGAUUAUTT-3′
	antisense	5′-AUAAUCUGUUGUGCAUCGCTT-3′
CTSL-homo-994	sense	5′-CCAAGUAUUCUGUUGCUAATT-3′
	antisense	5′-UUAGCAACAGAAUACUUGGTT-3′
CTSL-homo-1112	sense	5′-CCUUCCUGUUCUAUAAAGATT-3′
	antisense	5′-UCUUUAUAGAACAGGAAGGTT-3′
SRGN-homo-123	sense	5′-CCUCAGUUCAAGGUUAUCCUATT-3′
	antisense	5′-UAGGAUAACCUUGAACUGAGGTT-3′
SRGN-homo-295	sense	5′-CCAGGACUUGAAUCGUAUCUUTT-3′
	antisense	5′-AAGAUACGAUUCAAGUCCUGGTT-3′
SRGN-homo-502	sense	5′-ACAUGGAUUAGAAGAGGAUUUTT-3′
	antisense	5′-AAAUCCUCUUCUAAUCCAUGUTT-3′

cells were placed in an incubator with 5% CO_2 at 37°C and passaged every 72 h.

CCK-8 assay

Cell Counting Kit-8 (CCK-8) assay was used to measure the viability and proliferation of cells. SK-N-BE (2) and IMR-32 cells in logarithmic growth phase, with the appropriate concentration of 5×10^4/ml, were inoculated into 96-well culture plates with 100 μl/well, cultured overnight in an incubator with 5% CO_2 at 37°C and treated the next day. After pretreatment with different concentrations of DDP (HY-17394, MedChemExpress, Shanghai) or ADM (HY-15142A, MedChemExpress, Shanghai) for 24 h, 10 μl CCK-8 solution was added to each well and incubated for 4 h at 37°C. The optical density was measured at 450 nm. All assays were performed in triplicate.

siRNA transfection

CTSL siRNA, SRGN siRNA, and negative control siRNA were purchased from Sangon Biotech (Shanghai, China). For transfection, siRNA was mixed with Lipofectamine® 3000 Reagent (Invitrogen) and then transfected into SK-N-BE (2) or IMR-32 cells. After 6 h, the supernatant was replaced with fresh medium containing 10% FBS and cultured for another 24 h. Three siRNA sequences were used for transfection (Table 1).

TABLE 2 Primers for CTSL and SRGN.

Gene	Primer	Primer sequence
CTSL	forward	5′-AAACTGGGAGGCTTATCTCACT-3′
	reverse	5′-GCATAATCCATTAGGCCACCAT-3′
SRGN	forward	5′-GGACTACTCTGGATCAGGCTT-3′
	reverse	5′-CAAGAGACCTAAGGTTGTCATGG-3′

Cathepsin L overexpressing cell line establishment

A lentivirus carrying CTSL gene was constructed by GeneChem (Shanghai, China). IMR-32 cells were seeded in 6-well plate and then infected with the lentivirus according to protocols as recommended by the manufacturer. After 16 h, the medium was replaced with complete medium. In order to obtain a stable CTSL overexpressing cell line, the lentivirus infected cells were selected by incubation with complete medium of 2 μg/ml puromycin. The expression of CTSL in IMR-32 cell lines stably infected with a lentivirus was examined by Western blot.

Western blot analysis

Detailed procedure was as described in a previous study (Wang et al., 2019). Primary anti-human antibody against SRGN was purchased from Santa Cruz Biotechnology. CTSL, ABCB1, ABCG2, LC3, Bax, Bcl-2, and GAPDH primary anti-human antibodies were all purchased from Cell Signaling Technology.

Real-time quantitative PCR

Detailed procedure for these steps has been previously reported (Gu et al., 2018). The primer sequences employed for the PCR analysis were listed in Table 2. All primers were synthesized by Sangon Biotech (Shanghai, China).

Immunofluorescence

Cells were cultured on glass coverslips and then fixed with 4% paraformaldehyde. After a PBS wash, the cells were permeabilized employing 0.1% Triton X-100, incubated in a blocking solution (PBS with 3% bovine serum albumin), then further incubated overnight at 4°C with the primary antibody to Bcl-2, SRGN (Santa Cruz Biotechnology) and CTSL (Abcam). The fluorescent conjugated secondary antibodies were Alexa Fluor 488 and Alexa Fluor 594 (Invitrogen, Carlsbad, California, United States), and 4′,6-diamidino-2-phenylindole (DAPI) (Sigma Aldrich, St Louis, MO) was employed as a nuclear counterstain for 10 min. The coverslips

were finally mounted onto slides with fluorescent mounting medium and instantly observed by confocal microscopy.

Lysosome staining

After removing the cell culture solution, the lysosome green fluorescent probe staining solution (Beyotime, Nantong, China) was added, and the lysosome green fluorescent probe solution and the cell culture solution were mixed at a ratio of 1/20,000, and then incubated with cells in an incubator with 5% CO_2 at 37°C for 60 min. The staining solution was discarded and new cell culture solution was added. Finally the cells were observed under the laser confocal microscope.

Apoptotic assays

Apoptotic cell death was assessed by flow cytometry using the AnnexinV-fluorescein isothiocyanate (FITC)/propidium iodide (PI) Apoptosis Detection Kit (KeyGEN). Cells were harvested and resuspended in binding buffer, then labeled with Annexin V-FITC/PI reagent for 15 min in the dark at room temperature. For each analysis, a minimum of 20,000 cells per sample were analyzed using a Beckman Coulter FACS machine. Results were analyzed and calculated by FlowJo V.10 software; the percentage of apoptosis was obtained from the sum of (Annexin V-FITC+/PI–) and (Annexin V-FITC+/PI+) cells.

Animal experiments

All mice experiments were conducted in accordance with the humane treatment of animals under institutional guidelines approved by the Ethical Committee of Children's Hospital of Soochow University. The mice were housed in individually ventilated cages in the Animal Laboratory of the Children's Hospital of Soochow University. Six-week-old male M-NSG (NOD-Prkdc^{scid}Il2rg^{em1}/Smoc) mice (Shanghai Model Organisms, Shanghai) were used in the study. Subcutaneous tumor transplantation was conducted using the SK-N-BE (2) cells. Cells ($n = 1 \times 10^7$) were resuspended in 100 μl PBS and implanted into the right flank of nude mice under sterile conditions. After the formation of palpable tumors (tumor volume reached 100 mm^3), mice were randomized into four groups (5 mice per group): control group (saline, i.p.), Z-FY-CHO (a specific CTSL inhibitor, HY-128140, MedChemExpress, Shanghai) group (5 mg/kg, i.p.), ADM group (1 mg/kg, i.p.), Z-FY-CHO (5 mg/kg, i.p.) plus ADM (1 mg/kg, i.p.) group. Mice were injected with vehicle or with drugs three times weekly. The size of the tumor and the body weight of each mouse were measured as described previously (Wang et al., 2019). Mice were sacrificed on day 15, and tumor tissues were harvested.

Statistical analysis

All measurement data were expressed as the mean ± S.D. at least three independent experiments were conducted. Differences in measured variables between the experimental and control groups were assessed by Student's *t*-test. The chi-square (χ^2) test or Fisher exact test was used to compare qualitative variables. Differences were considered statistically significant at p values of <0.05. All analyses were performed employing GraphPad Prism 5.0.

Results

High expression of cathepsin L was positively associated with poor prognosis of NB patients

To figure out the relationship between the expression of CTSL and prognosis of NB patients, we analyzed the public dataset Versteeg to examine the correlation between the mRNA expression of CTSL and the survival rates in NB. In the Versteeg dataset, patients with high CTSL mRNA levels (cut off: 615.00) showed significantly poor overall survival (OS) (22-years OS; $p = 0.0071$; Figure 1A) and poor recurrence-free survival (RFS) (22-years RFS; $p = 0.0161$; Figure 1B). Besides, increased CTSL expression was positively associated with advanced tumor stages, though there was no statistical significance (Supplementary Figure S1). In general, these results suggested that high expression of CTSL was positively correlated with poor prognosis of NB patients and CTSL might be a potential prognostic marker in NB.

The expression of cathepsin L was poorly associated with ADM and DDP sensitivity in NB cells

To determine whether CTSL expression might be related to chemoresistance in NB cells, protein and mRNA levels of CTSL in two subtypes of NB cells were analyzed. Western blot and PCR analysis showed that the protein and mRNA levels of CTSL were low in IMR-32 cells and high in SK-N-BE (2) cells (Figures 2A,B). CCK-8 assay was performed to detect the 50% inhibitory concentration (IC50) of two cell lines in the treatment of a gradient concentration of ADM and DDP at 24 h. It turned out that the IC50 of SK-N-BE (2) cells in the treatment of ADM and DDP were higher than that of IMR-32 ($p < 0.001$; Figures 2C,D). These results suggested that SK-N-BE (2) cells were more chemoresistant to ADM and DDP than IMR-32 cells and CTSL expression was poorly associated with ADM and DDP sensitivity in NB cells.

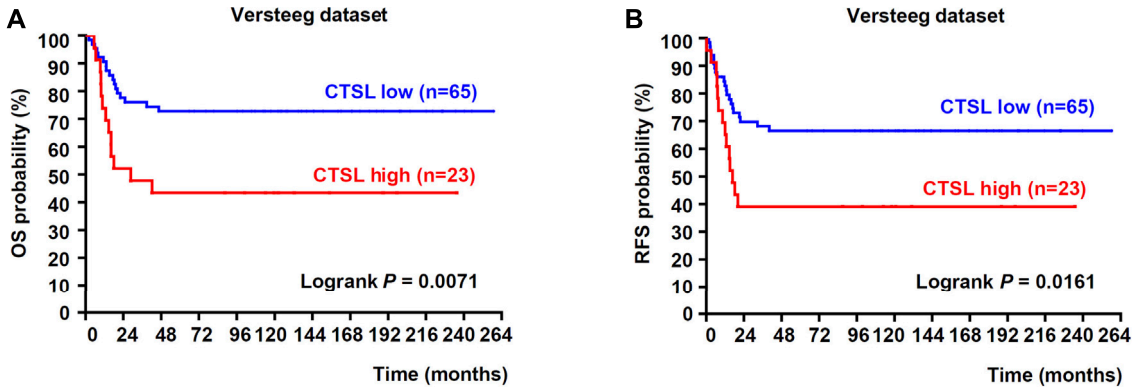

FIGURE 1
Upregulation of CTSL correlated with poor prognosis in patients with NB **(A)** Kaplan-Meier analysis of overall survival (OS) was determined according to CTSL expression in 88 NB samples from Versteeg dataset **(B)** Recurrence-free survival (RFS) was also determined according to CTSL expression from Versteeg dataset. Statistical analysis was carried out using a log-rank test.

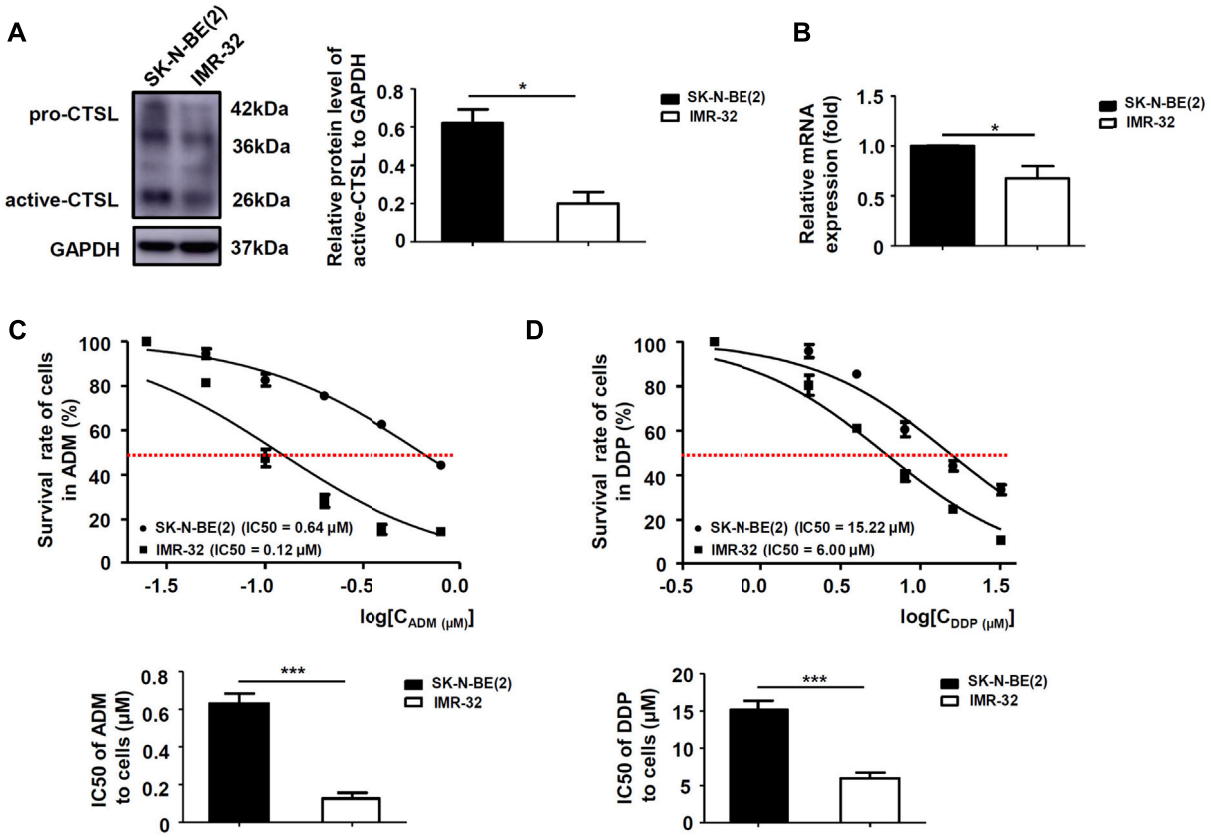

FIGURE 2
The expression of CTSL was associated with ADM and DDP sensitivity in NB cells **(A)** Western blot analysis and **(B)** real-time quantitative PCR analysis of CTSL levels in SK-N-BE (2) cells and IMR-32 cells. Cell viability curves for the two NB cell lines after ADM **(C)** and DDP **(D)** treatment were evaluated using the cell counting kit-8 assay (upper panel). The IC50 values were analyzed using the Mann-Whitney test (lower panel). *, $p < 0.05$, ***, $p < 0.001$.

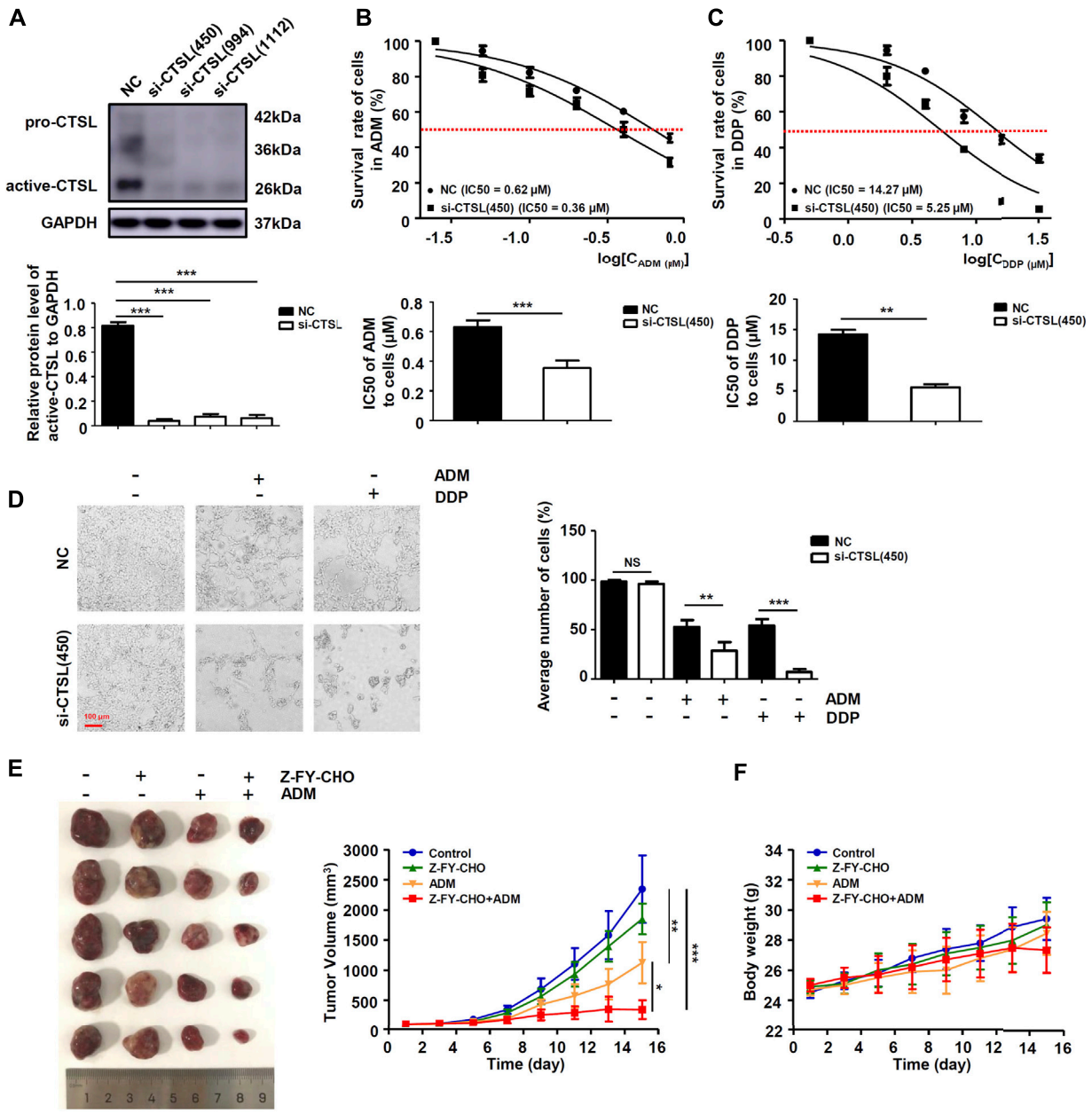

FIGURE 3
CTSL down-regulated ADM and DDP sensitivity in NB cells **(A)** Western blot showing CTSL expression in SK-N-BE (2) cells after CTSL silencing. Cell viability curves for SK-N-BE (2)/NC cells and SK-N-BE (2)/si-CTSL cells after ADM **(B)** and DDP **(C)** treatment were evaluated using the Cell Counting Kit-8 assay (upper panel). The IC50 values were analyzed using the Mann-Whitney test (lower panel) **(D)** Representative micrographs of two SK-N-BE (2)/NC cells and SK-N-BE (2)/si-CTSL cells after 50% lethal dose of ADM and DDP treatment (red bar: 100 μm) **(E)** and **(F)** Subcutaneous tumor xenograft models established using SK-N-BE (2) cells. Mice were injected with ADM or with Z-FY-CHO three times weekly. The tumor volumes were measured and the nude mice were weighed every 2 days until the mice were sacrificed. The curves were shown respectively. NS: not statistically significant, *, $p < 0.05$, **, $p < 0.01$, ***, $p < 0.001$.

Cathepsin L down-regulated ADM and DDP sensitivity in NB cells

We further researched whether chemoresistance was modulated by CTSL in NB cells. Western blot showed that all three selected si-RNAs could significantly down-regulate CTSL expression of SK-N-BE (2) cells, we chose si-CTSL (450) with the best interference effect to interfere the CTSL expression of SK-N-BE (2) cells (Figure 3A). CCK-8 assay was performed to detect the IC50 of SK-N-BE (2) cells in the treatment of a gradient concentration of ADM and DDP at

24 h in the reference of si-CTSL (450) and a specific CTSL inhibitor, Z-FY-CHO. We found that the IC50 of si-CTSL (450) group and Z-FY-CHO group under the action of ADM and DDP of various concentrations were lower than that of NC group and control group, which showed that the chemosensitivity of SK-N-BE (2) cells to ADM and DDP increased after CTSL inhibition (Figures 3B,C; Supplementary Figures S2A,B). Considering that CTSL may be closely related to the development of chemoresistance. A lentivirus carrying CTSL gene was constructed and infected into IMR-32 cells (Supplementary Figure S3A). Overexpression of CTSL rendered them resistant to ADM and DDP, as indicated by CCK-8 assay compared with LV-Vector cells, confirming the chemoresistant role of CTSL in NB cells (Supplementary Figure S3B,C). Then, the 50% lethal dose of ADM and DDP were selected to treat SK-N-BE (2) cells. The morphological changes of NC group and si-CTSL (450) group after drug treatment were observed. In NC group, the cells were inhibited to some extent, and the number of cells decreased after administration with ADM or DDP, but some cells still survived. In si-CTSL (450) group, the cell morphology changed from fusiform to round after administration with ADM or DDP, its lethality to cells also increased greatly (Figure 3D). We further investigated the effect of CTSL on chemoresistance of NB *in vivo*. The subcutaneous tumor xenograft model was established using SK-N-BE (2) cells, and then treated with Z-FY-CHO or ADM. As shown in Figure 3E, tumor volume was 2345.20 ± 561.75 mm^3 in the control group, 1850.10 ± 255.30 mm^3 in Z-FY-CHO group, 1124.80 ± 343.89 mm^3 in ADM group, and 344.60 ± 156.03 mm^3 in Z-FY-CHO plus ADM group. The average volumes of tumors were remarkably decreased in Z-FY-CHO plus ADM group compared to ADM group ($p < 0.05$), which was consistent with the results of experiments *in vitro*. The weights of mice were also recorded. As was shown, there was no significant difference among those groups in tumor weight (Figure 3F). The results of tumor xenograft experiment confirmed that CTSL inhibition down-regulated chemoresistance of NB.

Cathepsin L induced chemoresistance to ADM and DDP in NB cells by up-regulating the expression of multi-drug resistance proteins and inhibiting the autophagy level.

To explore the mechanisms of chemoresistance in NB cells with high CTSL expression, Western blot was used to detect the expression level of ABCB1 and ABCG2 in NC group and si-CTSL group. It turned out that the expression levels of ABCB1 and ABCG2 were lower in si-CTSL group than that of NC group (Figure 4A; Supplementary Figures S4A,B). The results showed that knockdown of CTSL down-regulated the expression of multi-drug resistance proteins. Further, to figure out whether CTSL expression was associated with autophagy in NB cells, we observed the expression level of lysosomes in NC group and si-CTSL (450) group and found that the green fluorescent spots in si-CTSL group were more and brighter compared with NC group (Figure 4B). This finding indicated that the autophagy level of si-CTSL group may be higher than that of NC group. Furthermore, Western blot was employed to detect the expression of autophagy-related protein LC3-II of NC group and si-CTSL group at the same concentration of ADM and DDP. It turned out that the expression of LC3-II of si-CTSL group was higher than that of NC group (Figure 4C; Supplementary Figures S4C,D). These results suggested that CTSL down-regulated ADM and DDP sensitivity in NB cells by inhibiting the autophagy level. Thus, all these findings indicated that CTSL could induce chemoresistance to ADM and DDP in NB cells by up-regulating the expression of multi-drug resistance proteins and inhibiting the autophagy level.

Cathepsin L induced chemoresistance to ADM and DDP in NB cells by inhibiting cell apoptosis

At present, it is widely accepted that anti-apoptosis is a potent inducer of chemotherapy failure. To further characterise the mechanism of underlying chemoresistance in NB, we evaluated apoptotic response with flow cytometry in SK-N-BE (2) cells with different treatments. Apoptosis levels did not significantly increase in si-CTSL (450) group compared with NC group (Supplementary Figure S5A); by contrast, a remarkable increase in the number of late apoptotic cells was observed in si-CTSL (450) plus ADM group compared with ADM group ($p < 0.001$). Then, the expression levels of Bcl-2 protein and Bax protein were detected by western blot to determine whether knockdown of CTSL could induce cell apoptosis. We found that the expression level of anti-apoptotic protein Bcl-2 in si-CTSL group under the action of ADM and DDP with the same concentrations was lower than that of NC group, and the expression level of apoptosis-related protein Bax in si-CTSL group under the action of ADM and DDP with the same concentrations was higher than that of NC group (Figure 5A; Supplementary Figures S5B,C), which indicated that knocking down CTSL induced apoptosis of SK-N-BE (2) cells. Then, we found that the fluorescence intensity of Bcl-2 protein in si-CTSL group was darker and the area was smaller than that in NC group under the action of ADM and DDP with the same concentrations using laser confocal microscope (Figure 5B). These results suggested that CTSL down-regulated ADM and DDP sensitivity in NB cells by inhibiting cell apoptosis.

Cathepsin L induced chemoresistance by up-regulating the expression of serglycin in NB cells

To further explore the downstream targets of CTSL in NB cells, six datasets were observed at the same time and showed that only

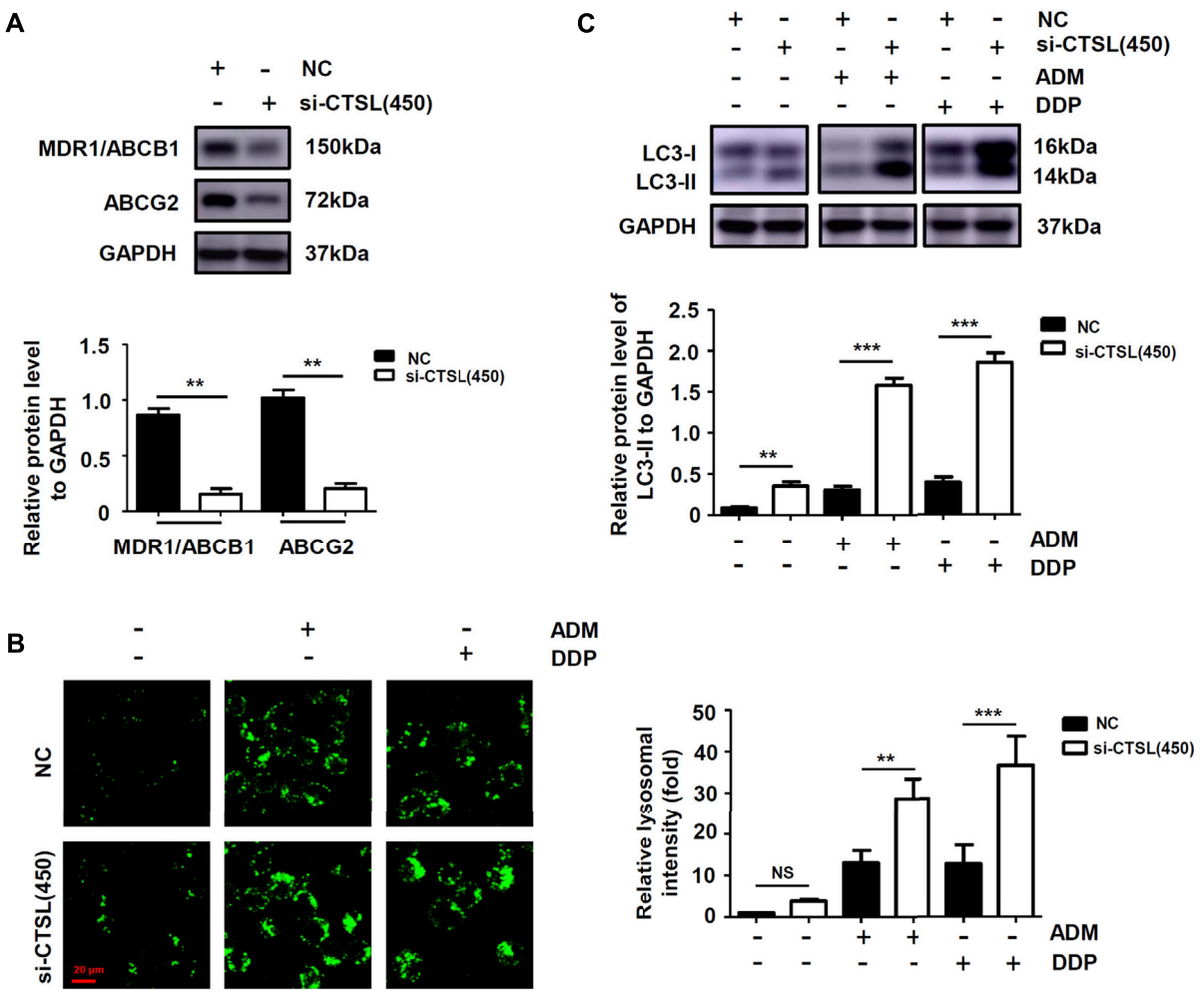

FIGURE 4
The expression of multi-drug resistance proteins and autophagy level of NB cells after knockdown of CTSL **(A)** Western blot showing multi-drug resistance proteins expression in SK-N-BE (2) cells after CTSL silencing **(B)** Lysosome staining assay showing the quantity and intracellular location of lysosome in SK-N-BE (2) cells with different treatments (red bar: 20 μm) **(C)** The expression of LC3-I and LC3-II in SK-N-BE (2) cells were analyzed using Western blot. NS: not statistically significant, **, $p < 0.01$, ***, $p < 0.001$.

Serglycin (SRGN) expression was associated with the expression levels of CTSL (−0.6 < R < 0.6 and $p < 0.001$; Figure 6A). Preliminary data analysis and outlier identification were performed using principal component analysis (PCA). PCA results before batch removal for multiple datasets showed that the three datasets were separated without any intersection, while PCA results after batch removal showed the intersection of three datasets, which could be used as a batch of data for subsequent analysis (Figure 6B). Then Spearman's correlation analysis showed that CTSL expression was positively correlated to SRGN expression (r: 0.19; *P*: 0.01577; 95% CI: 0.10–0.27; Figure 6C). Versteeg dataset also demonstrated that patients with high SRGN mRNA levels (cut off: 890.90) and high CTSL mRNA levels showed significantly poor OS (22-years OS; $p = 0.0014$; Figure 6D) and poor PFS (22-years OS; $p = 0.0430$; Figure 6E). Next we detected the expression levels of SRGN in si-CTSL NB cells to confirm our findings. The protein and mRNA levels of SRGN were lower in si-CTSL group than that in NC group (Figures 6F,G). To further investigate the potential links between CTSL and SRGN, we overexpressed CTSL in IMR-32 cells through lentivirus transduction. As shown in Figure 7A, CTSL overexpression increased SRGN expression in IMR-32/LV-Over-CTSL cells. Then, we found that high co-expression of CTSL with SRGN was shown in IMR-32/LV-Over-CTSL cells, as detected by immunofluorescence staining (Figure 7B). To further examine the effect of SRGN on CTSL induced chemoresistance, we suppressed SRGN by transfecting IMR-32/LV-Over-CTSL cells with three selected si-RNAs. Western blot results suggested that si-SRGN (295) inhibition evidently decreased the SRGN expression (Figure 7C). To elucidate the underlying mechanism, we performed

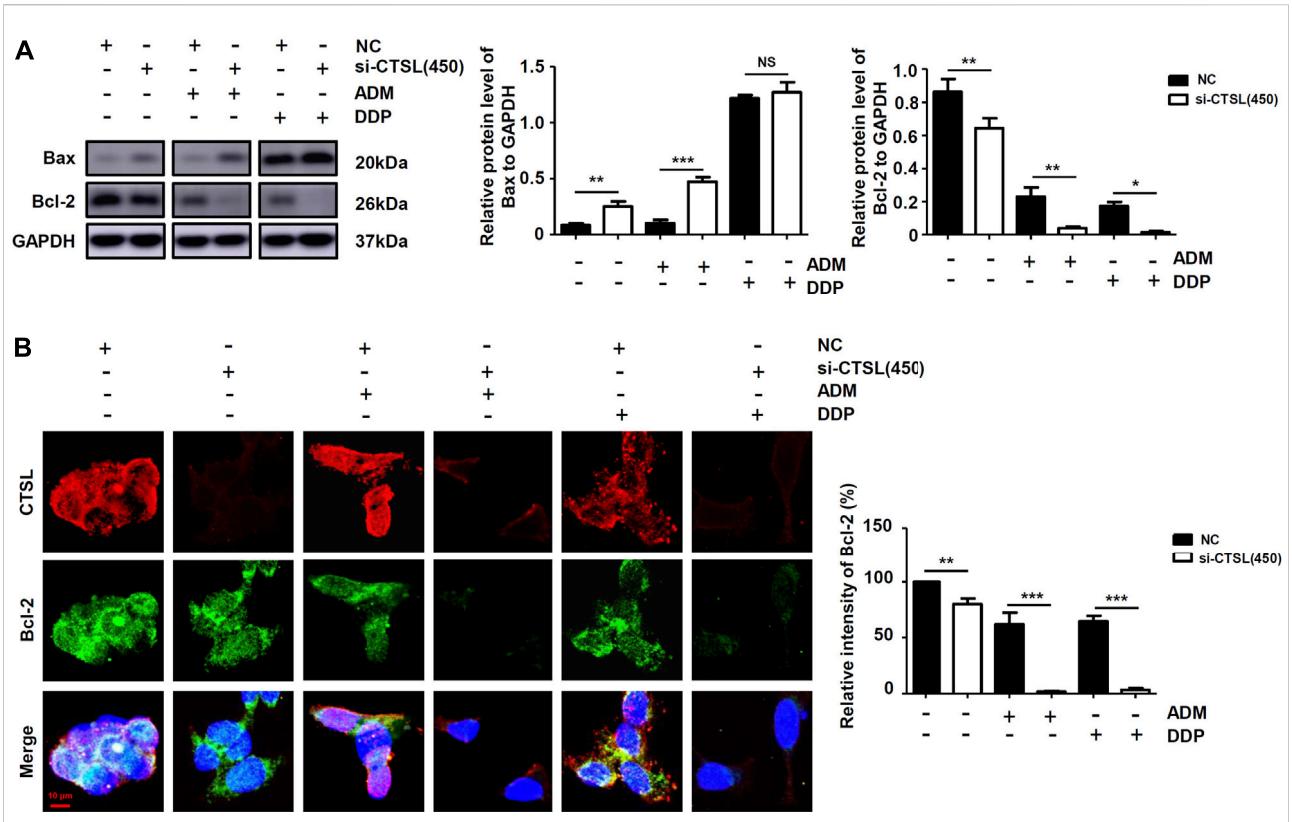

FIGURE 5
The apoptosis level of NB cells after knockdown of CTSL **(A)** Western blot showing apoptosis proteins expression in SK-N-BE (2) cells with different treatments **(B)** Immunofluorescence assay showing the expression and intracellular location of CTSL and Bcl-2 in SK-N-BE (2) cells (red bar: 10 μm). NS: not statistically significant, *, $p < 0.05$, **, $p < 0.01$, ***, $p < 0.001$.

a recovery experiment in IMR-32/LV-Over-CTSL cells which were transfected with si-SRGN (295). The results showed that the expressions of SRGN were both decreased in si-CTSL (450) group and si-SRGN (295) group compared with NC group ($p < 0.001$; Figure 7D). More importantly, we found that the IC50 of si-CTSL (450) group and si-SRGN (295) group under the treatment of ADM were significantly lower than that of NC group, which showed that the chemosensitivity of IMR-32/LV-Over-CTSL cells was mediated by CTSL-SRGN regulation (Figure 7E). All results above indicated that CTSL could mediate chemoresistance by up-regulating SRGN expression in NB cells and SRGN expression was positively correlated with poor prognosis of NB patients.

Discussion

NB is considered as the most common pediatric solid tumor (Zafar et al., 2021). DDP and ADM are two main chemotherapeutics for NB. However, the chemoresistance of NB is the most critical reason for the failure of clinical chemotherapy (Gao and Wang, 2019). Therefore, it is important to explore the molecular mechanism that affects the chemoresistance of NB and find key targets to overcome it. Our study found that the expression level of CTSL in NB patients was positively correlated with poor prognosis and poor sensitivity of DDP and ADM. Moreover, we also found that CTSL mediated the decrease of DDP and ADM sensitivity of NB cells by up-regulating the expression of multidrug resistance proteins ABCB1 and ABCG2 and inhibiting autophagy and apoptosis. In addition, we also demonstrated that CTSL might up-regulate the expression of SRGN which was positively correlated with the poor prognosis of NB patients.

CTSL is a lysosomal enzyme, which has been demonstrated to be highly expressed in many malignant tumors such as lung cancer, breast cancer and cervical cancer (Han et al., 2016; Mao et al., 2019; Parigiani et al., 2020). CTSL plays a key role in the formation, growth, invasion and migration of malignant tumors (Sudhan and Siemann, 2015). Zhang et al. discovered that CTSL was overexpressed in ovarian cancer and CTSL could induce paclitaxel resistance in ovarian cancer cells (Zhang et al., 2016). Cui et al. also found that CTSL expression was higher in NSCLC cells and overexpression of CTSL was positively

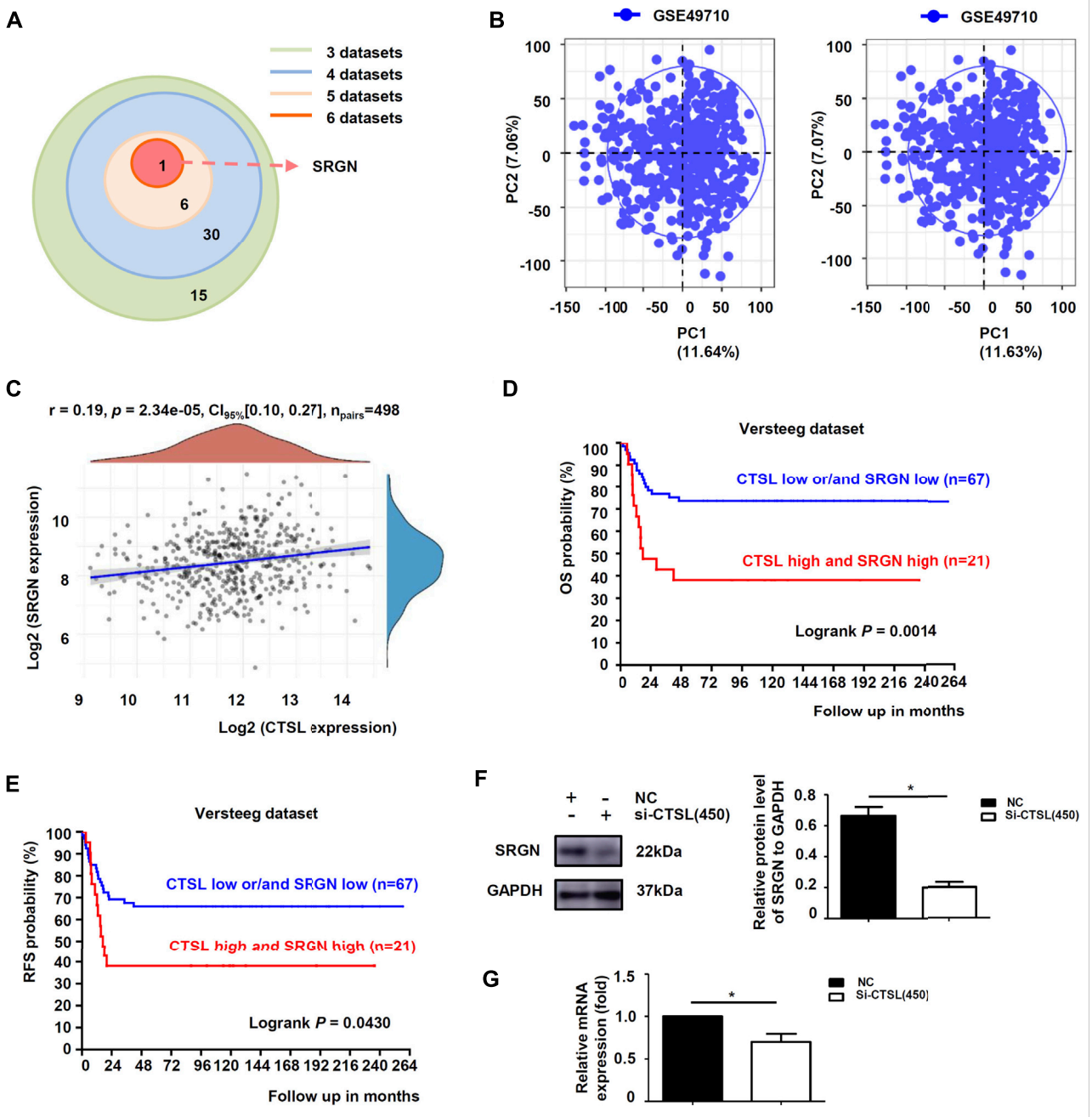

FIGURE 6
CTSL induced chemoresistance by up-regulating the expression of SRGN in NB cells **(A)** Overlap among the sets of positively-correlated genes of CTSL in NB identified by the six datasets (Tumor Neuroblastoma—Seeger—117—DCHIP; Westermann—144—tpm; Fischer—223—custom; Jagannathan—100—custom; Maris—101—custom; SEQC—498—custom) **(B)** Principal component analysis (PCA) result before batch removal for the dataset GSE49710 was show in the left, and PCA result after batch removal was show in the right **(C)** Correlation between CTSL and SRGN expression in 498 NB samples from GSE49710 dataset **(D)** Kaplan-Meier analysis of overall survival (OS) and **(E)** Recurrence-free survival (RFS) were determined according to CTSL/SRGN expression in 88 NB samples from Versteeg dataset. Statistical analysis was carried out using a log-rank test. Western blot analysis **(F)** and real-time quantitative PCR analysis **(G)** of SRGN levels in SK-N-BE (2) cells after CTSL silencing. *, $p < 0.05$.

correlated with gefitinib resistance in non-small cell lung cancer (NSCLC) (Cui et al., 2016). These results indicated that CTSL might be closely related to thechemoresistance of cancers. However, the specific role and mechanism of CTSL in chemoresistance of NB have not been studied clearly. Therefore, our study mainly researched the role and

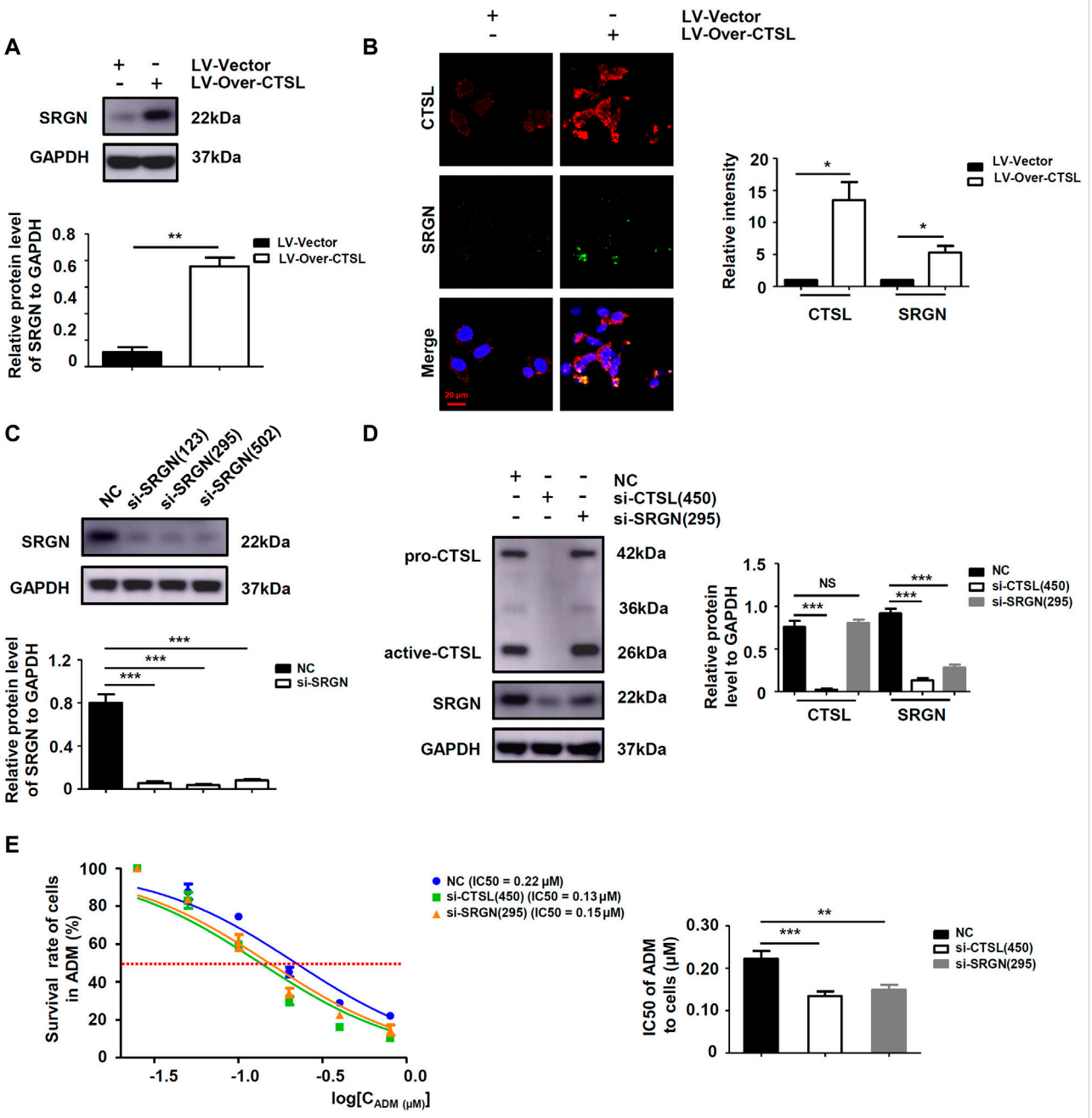

FIGURE 7
SRGN was a key protein for CTSL mediated chemoresistance in NB cells **(A)** Western blot analysis of SRGN levels in IMR-32/LV-Vector cells and IMR-32/LV-Over-CTSL cells **(B)** Immunofluorescence assay showing the expression and intracellular location of CTSL and SRGN in IMR-32/LV-Vector cells and IMR-32/LV-Over-CTSL cells. Nuclei were counterstained with DAPI (red bar: 20 μm) **(C)** and **(D)** Western blot showing SRGN expression in IMR-32/LV-Over-CTSL cells after SRGN silencing or CTSL silencing **(E)** Cell viability curves for IMR-32/LV-Over-CTSL cells after si-CTSL (450), si-SRGN (295), and ADM treatment were evaluated using the Cell Counting Kit-8 assay (left panel). The IC50 values were analyzed using the Mann-Whitney test (right panel). NS: not statistically significant, *, $p < 0.05$, **, $p < 0.01$, ***, $p < 0.001$.

molecular mechanism of CTSL in mediating chemoresistance of NB.

Firstly, we selected two different NB cells for experiments, and found that SK-N-BE (2) cells showed higher expression of CTSL and more resistant to ADM or DDP. These results indicated that CTSL might mediate the decrease of ADM and DDP sensitivity in SK-N-BE (2) cells. In order to verify the role of CTSL in mediating chemoresistance, we used CTSL targeting si-RNAs to interfere

CTSL, and the chemoresistance of SK-N-BE (2) cells to ADM decreased by about 1.7 times and that of SK-N-BE (2) cells to DDP decreased by about 2.6 times. Similarly, cotreatment with CTSL inhibition and ADM in M-NSG mice of subcutaneous tumors exhibited less tumor growth. To further verify the role of CTSL in regulating the decrease of the sensitivity to ADM and DDP, we detected the expression levels of multidrug resistance proteins ABCB1 and ABCG2 by western blot and found that ABCB1 and ABCG2 expression were decreased in si-CTSL group, which indicated that the sensitivity of SK-N-BE (2) cells to ADM and DDP were significantly increased after si-RNA interfering CTSL. According to the above results, it was demonstrated that CTSL was involved in regulating the decrease of ADM and DDP sensitivity in SK-N-BE (2) cells.

To explore the mechanisms of CTSL in the chemoresistance of SK-N-BE (2) cells, the autophagy of cells was observed from the cell morphology, and the green fluorescent spots of SK-N-BE (2) cells in si-CTSL group were brighter and more, indicating that the autophagy level was higher. With autophagy protein LC3-II as an index, we observed that the autophagy level of SK-N-BE (2) cells in si-CTSL group increased significantly under the treatment of ADM and DDP. After si-RNA interfering CTSL, the expression level of pro-apoptotic protein Bax increased and the expression level of anti-apoptotic protein Bcl-2 decreased under the treatment of ADM and DDP. The above results indicated that CTSL could mediate the chemoresistance of NB by regulating the autophagy and apoptosis of SK-N-BE (2) cells.

SRGN is a low molecular weight glycoprotein, which plays a critical role in the storage and secretion of some chemokines, cytokines and proteases, thus, it participates in lots of physiological and pathological processes (Zhu et al., 2021). SRGN has been demonstrated to be overexpressed in many cancers and is closely related to the occurrence and development of tumors (Zhang et al., 2017; Xie et al., 2021; Zhu et al., 2021). Guo et al. found that SRGN was highly expressed in NSCLC and its interaction with CD44 could promote the metastasis of NSCLC (Guo et al., 2020). Moreover, Zhang et al. discovered that the crosstalk of SRGN and the transcriptional coactivator YES-associated protein mediated the chemoresistance and stemness in breast cancer cells by regulating the expression of HDAC2 (Zhang Z. et al., 2020). We here found that CTSL could elevate SRGN expression and CTSL/SRGN axis induced the chemoresistance in NB cells.

The study still has some limitations. Since this study has not constructed NB chemoresistant cells, we have not been able to clarify the role of CTSL in NB chemothresistant cells, which needed to be further verified by more experiments. Meanwhile, the mechanism about CTSL how to regulate SRGN needed to be clarified. As reported before, CTSL could get into the nucleus, and then processes and activates certain transcription factors to perform transcription functions (Sudhan and Siemann, 2015). It was reported that SRGN could be transcriptionally regulated in the tumor cells (Xu et al., 2018). Therefore, CTSL elevated SRGN expression probably through indirect endonuclear transcription fuction.

In all, our study explored the role and molecular mechanism of CTSL in regulating the chemoresistance of ADM and DDP in NB cells, and found that CTSL could mediate the chemoresistance of NB by up-regulating the expression of SRGN. Therefore, CTSL seems to play a key role in improving the chemotherapy sensitivity of NB, and it may become an important target to improve the chemosensitivity of NB and the effect of ADM and DDP.

Data availability statement

The original contributions presented in the study are included in the article/Supplementary Material, further inquiries can be directed to the corresponding authors.

Ethics statement

The animal study was reviewed and approved by the Ethical Committee of Children's Hospital of Soochow University. Written informed consent was obtained from the owners for the participation of their animals in this study. Written informed consent was obtained from the individual(s), and minor(s)' legal guardian/next of kin, for the publication of any potentially identifiable images or data included in this article.

Author contributions

WW conceived and designed the study. XD, LD, and SH performed experiments and prepared the preliminary results of the manuscript. FL, YY, and RT performed data analysis and participated in data collection. XD and WW was a major contributor in writing the manuscript. XD and ZZ participated in data analysis and interpretation and critically reviewed the manuscript. All authors read and approved the final manuscript.

Funding

This work was supported by the grants from the National Natural Science Foundation of China (Grant No. 82172840, 81703532, and 81902320), Suzhou science and technology development plan project (SYSD2019183), and Gusu Health Talents Project of Suzhou Municipal Health Commission (GSWS2021033). The funders had no role in study design, data collection, analysis or interpretation of the data, preparation of the manuscript or decision to publish the results.

Conflict of interest

The authors declare that the research was conducted in the absence of any commercial or financial relationships that could be construed as a potential conflict of interest.

Publisher's note

All claims expressed in this article are solely those of the authors and do not necessarily represent those of their affiliated organizations, or those of the publisher, the editors and the reviewers. Any product that may be evaluated in this article, or claim that may be made by its manufacturer, is not guaranteed or endorsed by the publisher.

Supplementary material

The Supplementary Material for this article can be found online at: https://www.frontiersin.org/articles/10.3389/fphar.2022.920022/full#supplementary-material

References

Cui, F., Wang, W., Wu, D., He, X., Wu, J., and Wang, M. (2016). Overexpression of Cathepsin L is associated with gefitinib resistance in non-small cell lung cancer. *Clin. Transl. Oncol.* 18, 722–727. doi:10.1007/s12094-015-1424-6

Davidson, S. M., and Vander Heiden, M. G. (2017). Critical functions of the lysosome in cancer biology. *Annu. Rev. Pharmacol. Toxicol.* 57, 481–507. doi:10.1146/annurev-pharmtox-010715-103101

Domenichini, A., Adamska, A., and Falasca, M. (2019). ABC transporters as cancer drivers: Potential functions in cancer development. *Biochim. Biophys. Acta Gen. Subj.* 1863, 52–60. doi:10.1016/j.bbagen.2018.09.019

Gao, J., and Wang, W. (2019). Knockdown of galectin-1 facilitated cisplatin sensitivity by inhibiting autophagy in neuroblastoma cells. *Chem. Biol. Interact.* 297, 50–56. doi:10.1016/j.cbi.2018.10.014

Gu, Y., Lv, F., Xue, M., Chen, K., Cheng, C., Ding, X., et al. (2018). The deubiquitinating enzyme UCHL1 is a favorable prognostic marker in neuroblastoma as it promotes neuronal differentiation. *J. Exp. Clin. Cancer Res.* 37, 258. doi:10.1186/s13046-018-0931-z

Guo, J. Y., Chiu, C. H., Wang, M. J., Li, F. A., and Chen, J. Y. (2020). Proteoglycan serglycin promotes non-small cell lung cancer cell migration through the interaction of its glycosaminoglycans with CD44. *J. Biomed. Sci.* 27, 2. doi:10.1186/s12929-019-0600-3

Han, M.-L., Zhao, Y.-F., Tan, C.-H., Xiong, Y.-J., Wang, W.-J., Wu, F., et al. (2016). Cathepsin L upregulation-induced EMT phenotype is associated with the acquisition of cisplatin or paclitaxel resistance in A549 cells. *Acta Pharmacol. Sin.* 37, 1606–1622. doi:10.1038/aps.2016.93

Holohan, C., Van Schaeybroeck, S., Longley, D. B., and Johnston, P. G. (2013). Cancer drug resistance: An evolving paradigm. *Nat. Rev. Cancer* 13, 714–726. doi:10.1038/nrc3599

Hraběta, J., Belhajová, M., Šubrtová, H., Merlos Rodrigo, M. A., Heger, Z., and Eckschlager, T. (2020). Drug sequestration in lysosomes as one of the mechanisms of chemoresistance of cancer cells and the possibilities of its inhibition. *Ijms* 21, 4392. doi:10.3390/ijms21124392

Jemaà, M., Sime, W., Abassi, Y., Lasorsa, V. A., Bonne Køhler, J., Michaelis, M., et al. (2020). Gene expression signature of acquired chemoresistance in neuroblastoma cells. *Ijms* 21, 6811. doi:10.3390/ijms21186811

Li, X., Qian, X., and Lu, Z. (2017). Local histone acetylation by ACSS2 promotes gene transcription for lysosomal biogenesis and autophagy. *Autophagy* 13, 1790–1791. doi:10.1080/15548627.2017.1349581

Mao, Z., Sang, M. M., Chen, C., Zhu, W. T., Gong, Y. S., and Pei, D. S. (2019). CSN6 promotes the migration and invasion of cervical cancer cells by inhibiting autophagic degradation of cathepsin L. *Int. J. Biol. Sci.* 15, 1310–1324. doi:10.7150/ijbs.32987

Mijanović, O., Branković, A., Panin, A. N., Savchuk, S., Timashev, P., Ulasov, I., et al. (2019). Cathepsin B: A sellsword of cancer progression. *Cancer Lett.* 449, 207–214. doi:10.1016/j.canlet.2019.02.035

Pan, T., Jin, Z., Yu, Z., Wu, X., Chang, X., Fan, Z., et al. (2020). Cathepsin L promotes angiogenesis by regulating the CDP/Cux/VEGF-D pathway in human gastric cancer. *Gastric Cancer* 23, 974–987. doi:10.1007/s10120-020-01080-6

Parigiani, M. A., Ketscher, A., Timme, S., Bronsert, P., Schlimpert, M., Kammerer, B., et al. (2020). Conditional gene targeting reveals cell type-specific roles of the lysosomal protease cathepsin L in mammary tumor progression. *Cancers (Basel)* 12. doi:10.3390/cancers12082004

Rodrigo, M. A. M., Michalkova, H., Strmiska, V., Casar, B., Crespo, P., de Los Rios, V., et al. (2021). Metallothionein-3 promotes cisplatin chemoresistance remodelling in neuroblastoma. *Sci. Rep.* 11, 5496. doi:10.1038/s41598-021-84185-x

Sudhan, D. R., and Siemann, D. W. (2015). Cathepsin L targeting in cancer treatment. *Pharmacol. Ther.* 155, 105–116. doi:10.1016/j.pharmthera.2015.08.007

Tolbert, V. P., and Matthay, K. K. (2018). Neuroblastoma: Clinical and biological approach to risk stratification and treatment. *Cell Tissue Res.* 372, 195–209. doi:10.1007/s00441-018-2821-2

Wang, L., Zhao, Y., Xiong, Y., Wang, W., Fei, Y., Tan, C., et al. (2018). K-ras mutation promotes ionizing radiation-induced invasion and migration of lung cancer in part via the Cathepsin L/CUX1 pathway. *Exp. Cell Res.* 362, 424–435. doi:10.1016/j.yexcr.2017.12.006

Wang, W., Xiong, Y., Ding, X., Wang, L., Zhao, Y., Fei, Y., et al. (2019). Cathepsin L activated by mutant p53 and Egr-1 promotes ionizing radiation-induced EMT in human NSCLC. *J. Exp. Clin. Cancer Res.* 38, 61. doi:10.1186/s13046-019-1054-x

Xie, J., Qi, X., Wang, Y., Yin, X., Xu, W., Han, S., et al. (2021). Cancer-associated fibroblasts secrete hypoxia-induced serglycin to promote head and neck squamous cell carcinoma tumor cell growth *in vitro* and *in vivo* by activating the Wnt/β-catenin pathway. *Cell Oncol. (Dordr)* 44, 661–671. doi:10.1007/s13402-021-00592-2

Xu, Y., Xu, J., Yang, Y., Zhu, L., Li, X., and Zhao, W. (2018). SRGN promotes colorectal cancer metastasis as a critical downstream target of HIF-1α. *Cell Physiol. Biochem.* 48, 2429–2440. doi:10.1159/000492657

Yang, C., and Wang, X. (2021). Lysosome biogenesis: Regulation and functions. *J. Cell Biol.* 220, e202102001. doi:10.1083/jcb.202102001

Zafar, A., Wang, W., Liu, G., Wang, X., Xian, W., McKeon, F., et al. (2021). Molecular targeting therapies for neuroblastoma: Progress and challenges. *Med. Res. Rev.* 41, 961–1021. doi:10.1002/med.21750

Zhang, H., Zhang, J., Li, C., Xu, H., Dong, R., Chen, C. C., et al. (2020a). Survival association and cell cycle effects of B7H3 in neuroblastoma. *J. Korean Neurosurg. Soc.* 63, 707–716. doi:10.3340/jkns.2019.0255

Zhang, H., Zhang, L., Wei, L., Gao, X., Tang, L. I., Gong, W., et al. (2016). Knockdown of cathepsin L sensitizes ovarian cancer cells to chemotherapy. *Oncol. Lett.* 11, 4235–4239. doi:10.3892/ol.2016.4494

Zhang, Z., Deng, Y., Zheng, G., Jia, X., Xiong, Y., Luo, K., et al. (2017). SRGN-TGFβ2 regulatory loop confers invasion and metastasis in triple-negative breast cancer. *Oncogenesis* 6, e360. doi:10.1038/oncsis.2017.53

Zhang, Z., Qiu, N., Yin, J., Zhang, J., Liu, H., Guo, W., et al. (2020b). SRGN crosstalks with YAP to maintain chemoresistance and stemness in breast cancer cells by modulating HDAC2 expression. *Theranostics* 10, 4290–4307. doi:10.7150/thno.41008

Zhao, Y. F., Han, M. L., Xiong, Y. J., Wang, L., Fei, Y., Shen, X., et al. (2018). A miRNA-200c/cathepsin L feedback loop determines paclitaxel resistance in human lung cancer A549 cells *in vitro* through regulating epithelial-mesenchymal transition. *Acta Pharmacol. Sin.* 39, 1034–1047. doi:10.1038/aps.2017.164

Zhao, Y., Shen, X., Zhu, Y., Wang, A., Xiong, Y., Wang, L., et al. (2019). Cathepsin L-mediated resistance of paclitaxel and cisplatin is mediated by distinct regulatory mechanisms. *J. Exp. Clin. Cancer Res.* 38, 333. doi:10.1186/s13046-019-1299-4

Zhu, Y., Lam, A. K. Y., Shum, D. K. Y., Cui, D., Zhang, J., Yan, D. D., et al. (2021). Significance of serglycin and its binding partners in autocrine promotion of metastasis in esophageal cancer. *Theranostics* 11, 2722–2741. doi:10.7150/thno.49547

frontiers | Frontiers in Pharmacology

TYPE Original Research
PUBLISHED 08 September 2022
DOI 10.3389/fphar.2022.996686

Check for updates

OPEN ACCESS

EDITED BY
Hongtao Xiao,
University of Electronic Science and Technology of China, China

REVIEWED BY
Xin He,
City of Hope National Medical Center, United States
Jie Sun,
Zhejiang University, China

*CORRESPONDENCE
Jiaqiu Li,
lijq@wfmc.edu.cn

†These authors have contributed equally to this work and share first authorship

SPECIALTY SECTION
This article was submitted to Pharmacology of Anti-Cancer Drugs, a section of the journal Frontiers in Pharmacology

RECEIVED 18 July 2022
ACCEPTED 12 August 2022
PUBLISHED 08 September 2022

CITATION
Ren X, Liu J, Wang R, Liu X, Ma X, Lu Z, Hu Z, Zheng M, Ma J and Li J (2022), Exploring the oncogenic roles of LINC00857 in pan-cancer. *Front. Pharmacol.* 13:996686. doi: 10.3389/fphar.2022.996686

COPYRIGHT
© 2022 Ren, Liu, Wang, Liu, Ma, Lu, Hu, Zheng, Ma and Li. This is an open-access article distributed under the terms of the Creative Commons Attribution License (CC BY). The use, distribution or reproduction in other forums is permitted, provided the original author(s) and the copyright owner(s) are credited and that the original publication in this journal is cited, in accordance with accepted academic practice. No use, distribution or reproduction is permitted which does not comply with these terms.

Exploring the oncogenic roles of LINC00857 in pan-cancer

Xiaomin Ren[1†], Jing Liu[1†], Rui Wang[1†], Xinling Liu[2†], Xiaolin Ma[1], Zhong Lu[1], Zhenbo Hu[2], Mingzhu Zheng[1], Jingang Ma[1] and Jiaqiu Li[1*]

[1]Department of Oncology, Affiliated Hospital of Weifang Medical University, School of Clinical Medicine, Weifang Medical University, Weifang, Shandong, China, [2]Department of Hematology, Laboratory for Stem Cell and Regenerative Medicine, Clinical Research Center, Affiliated Hospital of Weifang Medical University, Weifang, Shandong, China

Although aberrant LINC00857 expression may play a key role in oncogenesis, no research has analyzed the pan-cancer oncogenic roles of LINC00857, particularly in tumor immunology. Here, we integrated data from several databases to analyze the characteristics of LINC00857 in pan-cancer. We found that LINC00857 was overexpressed and correlated with a poor prognosis in a variety of cancers. Furthermore, high-expression of LINC00857 was negatively associated with immune cell infiltration and immune checkpoint gene expression. Notably, LINC00857 expression was negatively related to microsatellite instability and tumor mutation burden in colorectal cancer, implying poor reaction to immunotherapy when LINC00857 was highly expressed. Targeting LINC00857 could dramatically impair the proliferative ability of colorectal cancer cells. After RNA-sequencing in HCT116 cells, gene set enrichment analysis showed that LINC00857 may accelerate cancer progression by inhibiting the ferroptosis pathway and promoting glycolipid metabolism in colorectal cancer. Screening by weighted gene co-expression network analysis determined PIWIL4 as a target of LINC00857, which also performed an immunosuppressive role in colorectal cancer. Based on the structure of PIWIL4, a number of small molecule drugs were screened out by virtual screening and sensitivity analysis. In summary, LINC00857 expression was closely correlated with an immunosuppressive microenvironment and may be a novel diagnostic and prognostic biomarker for diverse cancers. The LINC00857/PIWIL4 axis may be predictive biomarkers for immunotherapy and valuable molecular targets for malignant tumors.

KEYWORDS

LINC00857, biomarker, bioinformatics, tumor immunity, pan-cancer

Introduction

Cancer, a highly malignant disease, poses severe threats to human health worldwide. Despite ongoing efforts by scientists to ameliorate cancer treatment, mortality from cancer remains high (Sung et al., 2021). Conventional cancer treatments such as radiotherapy and chemotherapy have shown various limitations that can be attributed to the severe related side effects (Barazzuol et al., 2020; Bukowski et al., 2020). Consequently, with the increasing resistance to existing drugs, finding new therapeutic targets is urgently required.

In recent years, non-coding RNAs (ncRNAs) have intrigued numerous researchers. Moreover, ncRNAs may be potential therapeutic targets (Zhang et al., 2020). As emerging regulatory molecules, ncRNAs are instrumental in tumorigenesis, invasion, metastasis and drug resistance to cancer. For instance, lncRNA FEZF1-AS1 was reported to facilitate the proliferation and metastasis in colorectal cancer (Bian et al., 2018). The lncRNA GBCDRlnc1 was also found to induce chemoresistance in advanced gallbladder cancer (Cai et al., 2019). Similarly, LINC00857 was discovered to play a carcinogenic role in lung, liver, pancreatic and bladder cancers (Dudek et al., 2018; Xia et al., 2018; Han et al., 2020; Meng et al., 2021). LINC00857 likely acts as an oncogene contributing to cancer development. Nevertheless, most studies on LINC00857 have been restricted to one specific cancer type. Pan-cancer analysis has brought us to a new phase of cancer research in recent years. The commonalities and differences derived from the pan-cancer analysis help us to investigate the potential carcinogenic mechanisms and forecast the treatment results. Thus, it is valuable to delve into the oncogenic roles of LINC00857 in pan-cancer, providing novel orientations and tactics for the diagnosis and treatment of cancers.

Recently, the importance of immunotherapy in different cancer types has been highlighted. Although immunotherapy has some deficiencies, it is considered as a promising approach to combat diverse cancers (Sharma and Allison, 2015b; Kennedy and Salama, 2020). Several studies have shown that the cancer phenotype is mediated through the intrinsic activity of cancer cells and the complicated interplay of diverse cell categories in the tumor microenvironment, in particular, tumor-infiltrating immune cells (Candido and Hagemann, 2013). The most promising way to stimulate the immune system is to block immune checkpoint genes, which have displayed vigorous anti-tumor effects in the treatment of various malignant tumors (Sharma and Allison, 2015a; Postow et al., 2015). Tumor mutation burden (TMB) has been validated as a biomarker of immune checkpoint inhibition response in multiple cancers (Yarchoan et al., 2017; Yarchoan et al., 2019). Tumor genomic mutations cause the development of neoantigens (NEO) that may be effective targets for anti-tumor immunotherapy (Blass and Ott, 2021). The high reaction rate to blocking immune checkpoint genes in patients with microsatellite instability (MSI) further confirmed the effect of neoantigens in the anti-tumor immunotherapy (Schrock et al., 2019). Conversely, cancers with poor NEO, MSI and TMB may be hyposensitive to immune checkpoint blockade. Nevertheless, current reports on the association between LINC00857 expression and immunological features are scarce.

In the present analysis, we elucidated the expression, prognostic value and immune characteristics of LINC00857 in pan-cancer using bioinformatics. Our study found that LINC00857 accelerated the proliferation of colorectal cancer cells, which may offer a potential therapeutic target for colorectal cancer. We explored the possible regulatory mechanisms by RNA-sequencing analysis.

Materials and methods

Assistant for clinical bioinformatics database analysis

ACLBI tool (https://www.aclbi.com/) is an integrated online platform for bioinformatics analysis. The LINC00857 gene expression levels and correlation analysis with immune cell infiltration or immune checkpoint genes expression were discussed using the "pan-cancer single gene fast comprehensive analysis" module. Correlation was measured by Spearman analysis.

Lnc2Cancer 3.0 database analysis

Lnc2Cancer 3.0 (Gao et al., 2021) is an online database including comprehensive experimental supported lncRNAs or circRNAs in human cancers. In the "RNA-seq Web Tools" module, we selected the "Box Plot" and "Stage Plot" module to perform a search for the expression levels of LINC00857 in different cancers datasets using the Kruskal-Walli's test. "Survival" module was implemented for disease free survival (DFS) or overall survival (OS) analysis based on LINC00857 expression and the median was chosen as the group cutoff for survival curve. p value cutoff is 0.05.

StarBase V3.0 database analysis

The StarBase V3.0 (Li et al., 2014) online website was utilized to assess the expression of LINC00857 between cancers and matched normal samples. Additionally, the platform also predicted the correlation between PIWIL4 and CD274 (PD-L1, programmed cell death 1 ligand 1), PD1 (PDCD1, programmed cell death 1) and CTLA4 (cytotoxic T-lymphocyte associated protein 4) expression in COAD. p value cutoff is 0.05.

GEPIA2 database analysis

The GEPIA2 data pool (Tang et al., 2019) was utilized to probe the expression and survival status in cancers and normal tissues. Survival curves of OS and DFS for LINC00857 expression were displayed by selecting the "Survival Plot" module under the condition of group cutoff = median. In the "Expression DIY" module, we adopted box plots to exhibit the expression status of LINC00857 in diverse cancer stages. The relationship between LINC00857 and PIWIL4 expression in colorectal cancer was explored in the "Correlation Analysis" pane. p value cutoff is 0.05.

Kaplan-Meier Plotter database analysis

Pan-cancer survival analysis about recurrence-free survival (RFS) and OS for LINC00857 expression was executed using the "mRNA-RNA-seq" module in the Kaplan Meier plotter website (Nagy et al., 2021). p value cutoff is 0.05.

Sangerbox 3.0 database analysis

The Sangerbox 3.0 (http://vip.sangerbox.com/home.html) is a complimentary online platform for comprehensive bioinformatics analysis. The "Pan-cancer analysis tool" in the platform was implemented to explore the expression and immune characteristics of LINC00857 in various cancers. Concretely, the data source was set to "TCGA + GTEx" and the data transformation was set to "$\log_2$ (x+1)". The correlation between all parameters were performed using the Pearson method. Subsequently, weighted gene co-expression network analysis (WGCNA) was implemented using raw counts through the "WGCNA analysis tool". The soft threshold power of $\beta = 7$ (R2 = 0.86) was selected to assure a scale-free network. Next, the minimum number of modules was fixed at 30, the sensitivity at 2, the module merge threshold at 0.5 and other parameters were the default values for the site. Totally, 13 non-gray modules were derived. Additionally, functional enrichment analysis of 76 LINC00857-associated coding genes was implemented by the "gene ontology (GO) and kyoto encyclopedia of genes and genomes (KEGG) analysis tool". The top 10 markedly enriched pathways ($p < 0.05$) were displayed according to gene count.

CAMOIP database analysis

CAMOIP is an integrated web server for the analysis of pan-cancer immunotherapy (Lin et al., 2022). The "Immunogenicity", "Immune Infiltration" as well as "Pathway Enrichment" modules in the database were used to explore the immune characteristics and gene set enrichment analysis (GSEA) of PIWIL4 in colon cancer.

Gene set cancer analysis database analysis

GSCA is a comprehensive online tool for immunogenomic and pharmacogenomic cancer analysis (Liu et al., 2018). The "immune cell abundance" module was used to demonstrate the interrelation between PIWIL4 expression and immune cell infiltration in colon cancer by GSVA score. In addition, the relevance between PIWIL4 expression and GDSC/CTRP drug sensitivity was analyzed.

Cell miner database analysis

Through the Cell Miner database (Reinhold et al., 2012), we obtained the gene expression profile of NCI-60 human cancer cell lines and the drug data approved by FDA or clinically verified. Next, the relevance analysis between PIWIL4 expression and drug sensitivity (IC50) was conducted by R software. The correlation score was calculated by Pearson coefficient and p value < 0.05.

Molecular docking

Firstly, the 3D structure of PIWIL4 protein was obtained from Alpha Fold online platform (Jumper et al., 2021). Meanwhile, the PubChem database was used to download the chemical structure information of the drugs (Kim et al., 2021). Next, the possible small molecule binding sites on PIWIL4 protein surface were detected by GHECOM algorithm (Kawabata, 2010). The maximum pocket to cover the ligand was chosen, with a volume of 41,065 Å3. Lastly, molecular docking was performed using DOCK 6.9 software and the spatial conformation of the docking was visualized by PyMol software. The interaction between protein and small molecule drugs was calculated by ligplus. Grid_Score represented the total molecular docking score between the drug and protein. A smaller score value indicated stronger binding ability. Internal energy repulsion was usually less than 20.

Cell culture

The human colorectal cancer cell-HCT116 was purchased from the cell bank of the Chinese Academy of Sciences. HCT116 cell were incubated in McCoy's 5A medium (GNM16600, GENOM) complemented with 10% bovine serum at 37°C with 5% CO2.

SiRNA transfection

HCT116 cells was conducted in 6-well plates (1×10^5 cells) and transfected with siRNA transfection reagent (13778150,

Invitrogen). The siRNA for transient knockdown of LINC00857 was obtained from Gene Pharma (Shanghai, China). The siRNA sequence showed below:

Negative control: S: UUCUCCGAACGUGUCACGUTT, AS: ACGUGACACGUUCGGAGAATT; LINC00857-siRNA1#: S: GGCUAUGUGCUGUGAACAATT, AS: UUGUUCACAGCA CAUAGCCTT; LINC00857-siRNA2#: S: GGUAUUAGUGGG UGAAUAUTT, AS: AUAUUCACCCACUAAUACCTT.

RNA isolation and quantification

All RNA isolation was performed utilizing the Trizol (Qiagen, 1023537). Inverse transcription was accomplished with the cDNA Synthesis Kit (4375222, AB). The real-time qPCR was implemented by SYBR Green fluorescence measurement. β-actin was used as the normalized endogenous control. The primer sequences utilized were listed below:

PIWIL4-F: AAGCCCACACACACCTTTCA, R: TGGTCA GTCAGCCCTGTTAG; LINC00857-F: AGAACGCGGTGT GAAGGAAA, R: TGAGCCCTGGGAAACAATGA; actin-F: CACCAACTGGGACGACAT, R: ACAGCCTGGATA GCAACG.

RNA sequencing analysis

RNA sequencing was performed by Lianchuan Biotechnology Co. (Hangzhou, China). GSEA analysis was conducted by GSEA (v4.1.0) and MSigDB (Subramanian et al., 2005). In short, the genes were sorted using the Signal2Noise normalization method. GO terms and KEGG pathways fulfilling the conditions with |NES|>1 and NOM p-val<0.05 were deemed to be significant in the two groups. Subsequently, downstream analysis was implemented using raw counts of the genes in the selected modules. The R package "limma" was employed to perform normalized and differential expression analysis (Ritchie et al., 2015). Differentially expressed genes (DEGs) were chosen with the following screening criteria: $p < 0.05$, $\log_2$|fould change|>1. Combining the two sets of different analysis data, 76 candidate genes were finally obtained after excluding non-coding genes. The volcano plots and heatmap were created by the online data visualization platform-bioinformatics (http://www.bioinformatics.com.cn). The LINC00857-miRNA-PIWIL4 interaction network diagram was constructed using Cytoscape (v3.9.0).

Colony formation assays

Colony formation assays were determined to assess colony formation ability. 1,000 cells per well were sowed and incubated in six-well plates in triplicate. 11 days after cultivation, colonies were dyed with 0.1% crystal violet and then counted.

CCK8 assay

The effect of LINC00857 on cell viability was detected by CCK8 kit (C0038-500, Beyotime). After transfection, 3,000 cells each well were transferred into 96-well plates for 72 h, then CCK8 working solution was pipetted into every well and cultured in medium at 37°C for 30 min. Finally, absorbance (optical density, OD) was gauged at 450 nm by a microplate reader.

Fluorescence *in Situ* hybridization

FISH assays were proceeded as standard programs. The sample slides for the FISH experiments were fixed with 4% formaldehyde. Briefly, tissue or cell slides were dewaxed, dehydrated, hybridized, washed and counterstained with green fluorescence for LINC00857 expression (FAM (488)). LINC00857 FISH probe was manufactured by Servicebio (Wuhan, China) and its sequence was presented as below: 5′-FAM-TTGGGACAGGGTTTGGAACTCTTGCGG-FAM-3'.

Statistics

Student's t-test, one-way or two-way ANOVA were administered to assess statistical significance. $p < 0.05$ were indicated statistically significant.

Results

Expression levels of LINC00857 in pan-cancer

To ascertain the expression levels of LINC00857 in normal and cancers samples, we obtained data from TCGA, CCLE and GTEx datasets. We explored the expression levels of LINC00857 in 31 healthy tissues and 21 cancer cell lines through the Sangerbox database. In normal samples, the highest expression level of LINC00857 was observed in bladder tissue and the lowest in blood (Kruskal–Wallis's test $p < 0.001$) (Figure 1A). By contrast, LINC00857 was highly expressed in most cancer cell lines, which may imply its effect on the malignant phenotype of cancer cells (Figure 1B). As shown in Figures 1C,D and Supplementary Figure S1, we characterized the expression levels of LINC00857 in cancers and corresponding normal samples using the TCGA and GTEx datasets. By simultaneous analysis of four databases (Sangerbox 3.0, ACLBI, StarBase V3.0 and Lnc2Cancer 3.0), we found that the

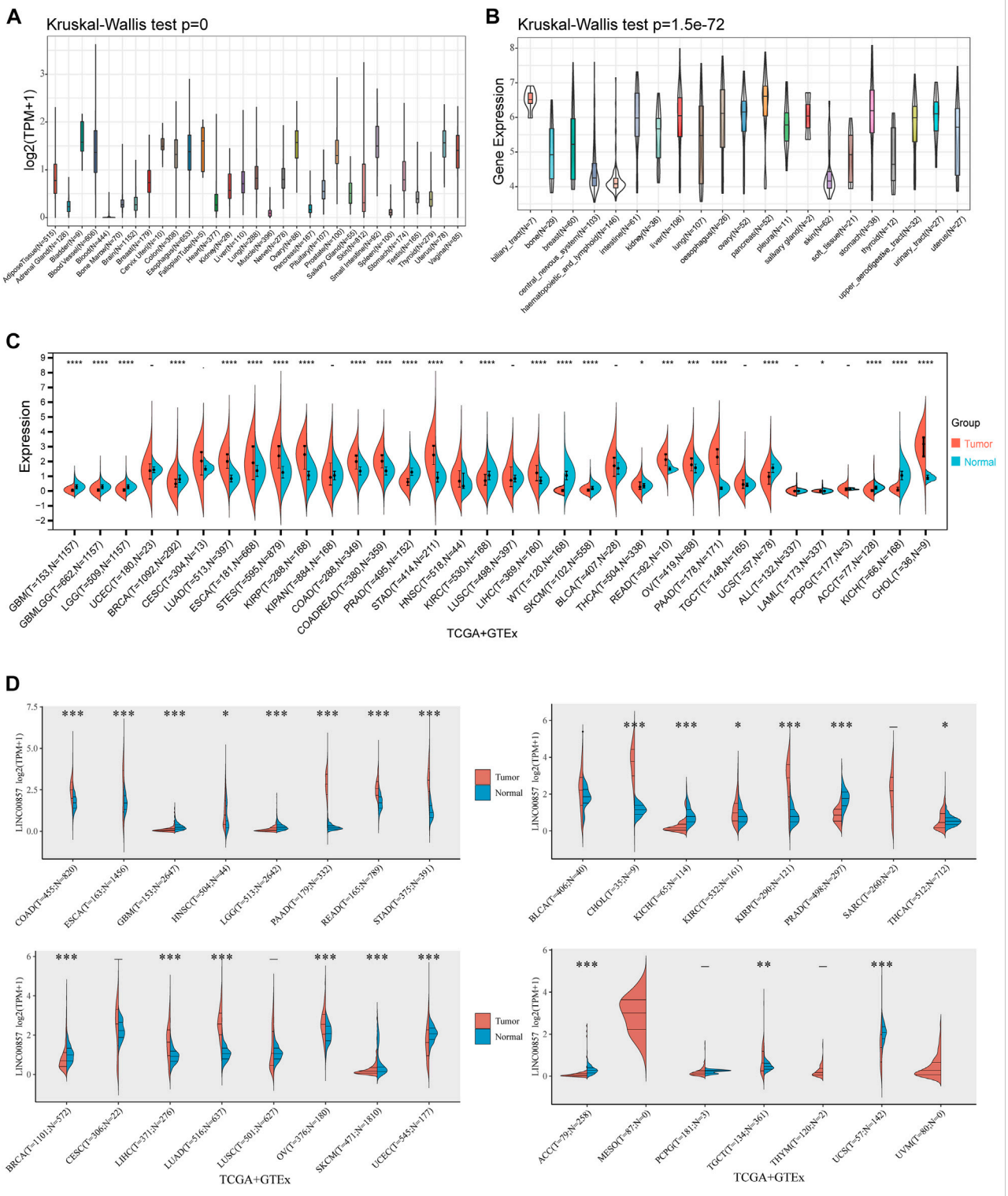

FIGURE 1
The expression levels of LINC00857 in pan-cancer. **(A)** LINC00857 expression in 31 human normal tissues from GTEx database. **(B)** LINC00857 expression in various cancer cell lines from CCLE database. **(C)** The expression levels of LINC00857 in different cancers and adjacent normal tissues were explored through Sangerbox 3.0 database. **(D)** The expression levels of LINC00857 in cancers or paired normal tissues were analyzed *via* online website ACLBI (*$p < 0.05$, **$p < 0.01$, ***$p < 0.001$).

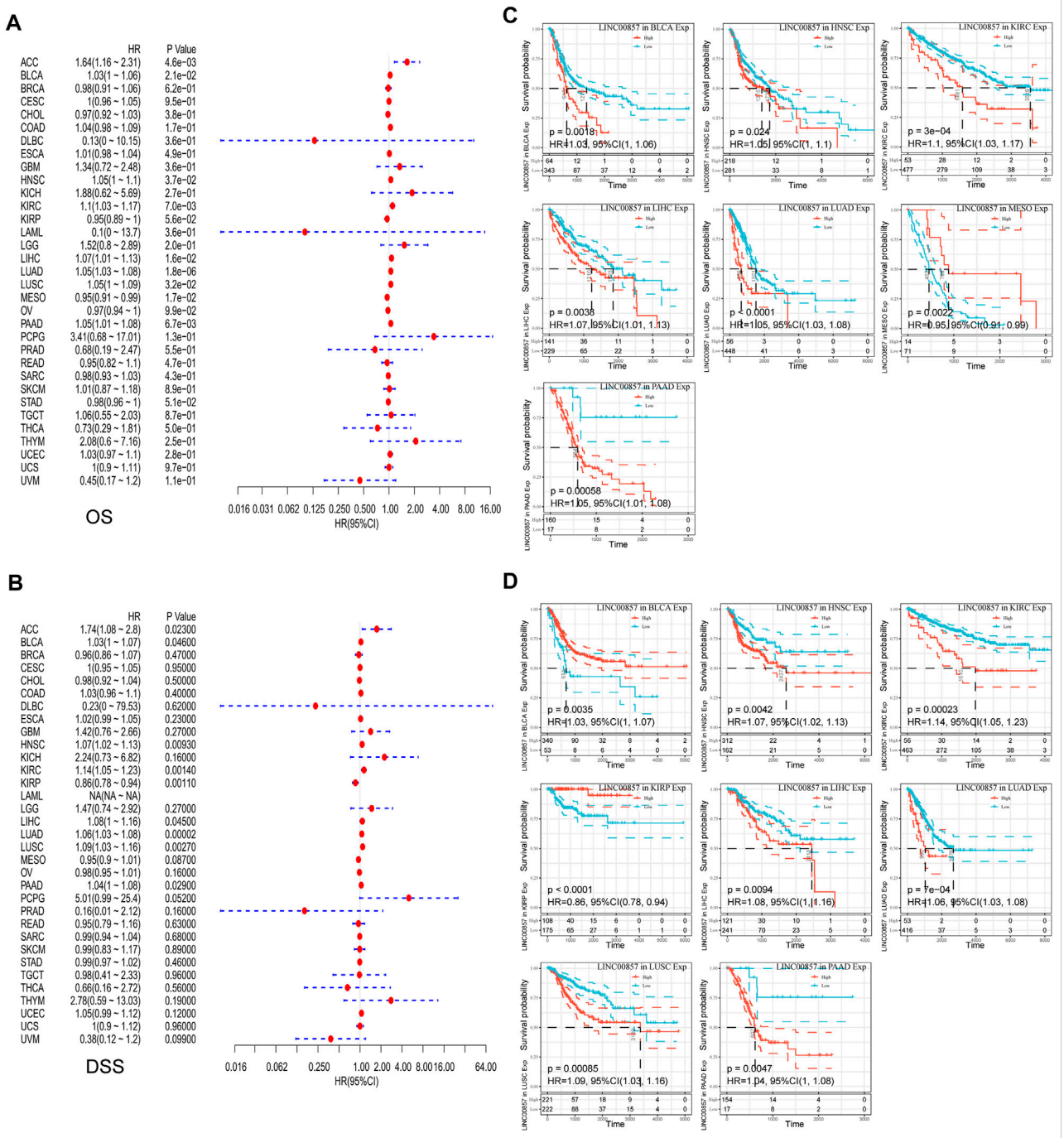

FIGURE 2
The correlation between LINC00857 expression and OS and DSS in pan-cancer. **(A,B)** Cox regression analysis of LINC00857 on OS and DSS for multiple neoplasms was depicted *via* forest diagrams. **(C,D)** Kaplan-Meier curves presented OS or DSS for patients with high and low LINCOO857 expression ($p < 0.05$).

expression levels of LINC00857 were markedly higher in eight cancers than in the adjacent normal tissues including HNSC, CHOL, COAD, KIRP, STAD, LIHC, PAAD and LUAD. LINC00857 expression was obviously decreased in BRCA, KICH, KIRC and PRAD. Furthermore, stage plot in the Lnc2Cancer 3.0 and GEPIA2 databases suggest that LINC00857 expression was strikingly correlated with the cancer pathological stages (Supplementary Figure S2).

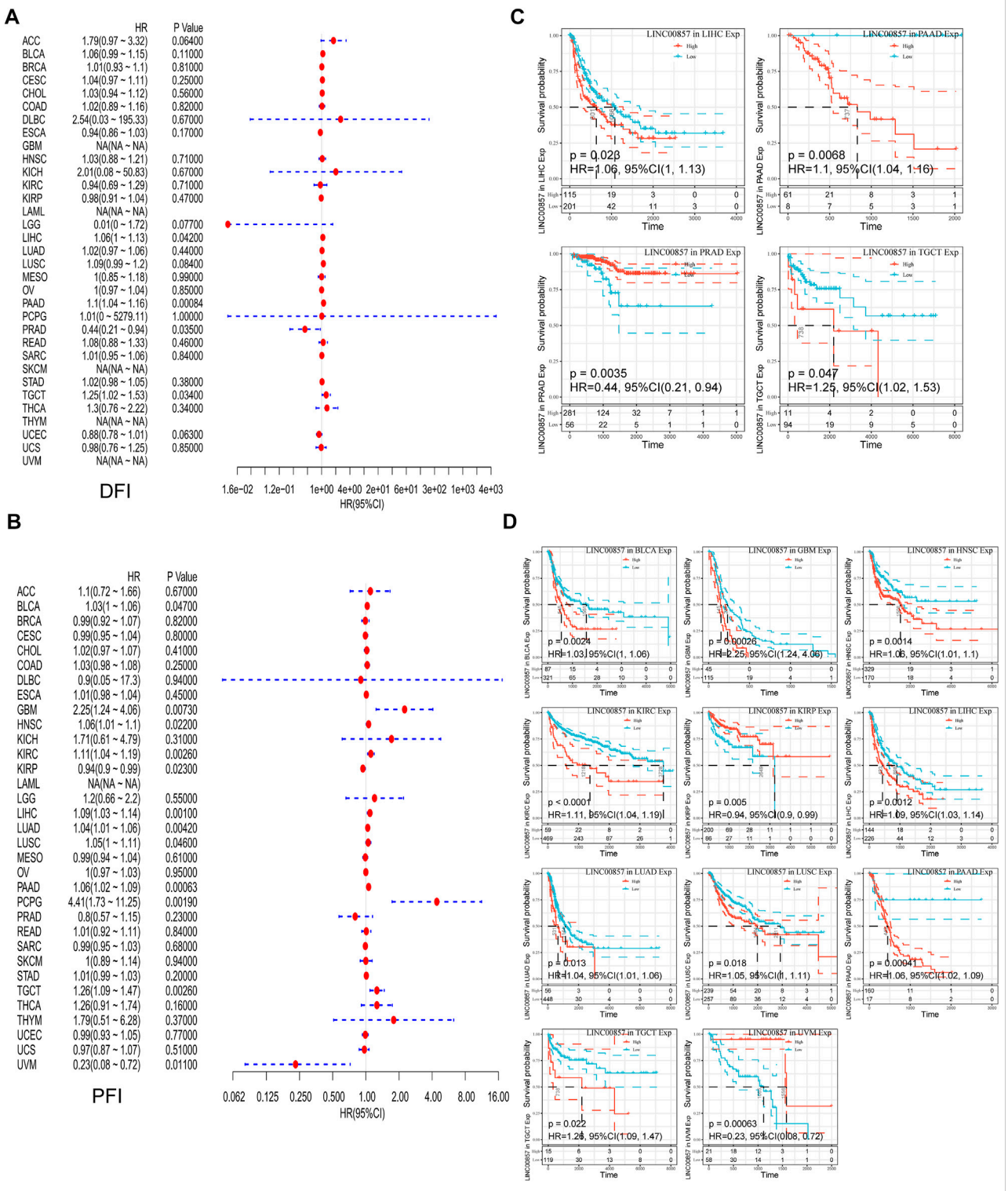

FIGURE 3
The correlation between LINC00857 expression and DFI and PFI in pan-cancer. **(A,B)** Cox regression analysis of LINC00857 on DFI and PFI for different neoplasms was depicted by forest diagrams. **(C,D)** Kaplan-Meier curves presented the prognostic value of LINC00857 for DFI or PFI ($p < 0.05$).

Consequently, these results support that LINC00857 may act as a new diagnostic biomarker for many cancer types.

The prognostic value of LINC00857 in pan-cancer

To illustrate the relevance between LINC00857 gene expression and prognosis, survival analysis for LINC00857 among different cancers was performed using Sangerbox, GEPIA2, Kaplan-Meier Plotter and Lnc2Cancer 3.0 databases. First, Cox regression analysis was implemented for 33 cancer types by TCGA datasets. The association between LINC00857 expression and OS, disease-specific survival (DSS), disease-free interval (DFI) and progression-free interval (PFI) was displayed in forest plots (Figures 2A,2B, 3A,3B). Based on these results, we further elaborated the prognostic value of LINC00857 in these cancers using Kaplan-Meier (KM) analysis (Figures 2C,D, 3C,D). We observed that higher LINC00857 expression was related to poorer OS/DSS/PFI in BLCA, HNSC, KIRC, LIHC, LUAD, PAAD, and with poorer DFI in TGCT, PAAD, LIHC. Nevertheless, patients with high LINC00857 displayed markedly longer OS in MESO, longer DSS in KIRP, longer DFI in PRAD, as well as longer PFI in KIRP and UVM. In GEPIA2 and Kaplan-Meier Plotter databases, LINC00857 hyperexpression was positively correlated with poor OS/DFS/RFS in LIHC and PAAD, but only with poor OS in LUAD (Supplementary Figures S3A,B). In the Lnc2Cancer 3.0 database, higher LINC00857 expression was related to poor OS in LUAD, poor OS/DFS in PAAD and poor DFS in LIHC and GBM (Supplementary Figure S3C). In conclusion, these data validated that LINC00857 expression was highly associated with the prognosis in multiple cancers, implicating that LINC00857 may be a reasonable biomarker to evaluate the prognosis of many cancers.

The relevance between LINC00857 expression and immune cell infiltration

Tumor-infiltrating immune cells (TIICs), a significant portion of the tumor microenvironment, are intimately linked to tumorigenesis and cancer progression (Domingues et al., 2016). Thereby, we investigated the possible relevance between LINC00857 expression and TIICs in pan-cancer by Sangerbox 3.0 and ACLBI database. The heatmap detailing the interrelation between LINC00857 expression and TIICs was shown in Figure 4A. We further analyzed the relevance between LINC00857 expression and $CD8^+$ T cells, NK cells, conventional dendritic cells (cDCs), Tregs and monocytes in eight LINC00857 high-expression cancers (Figure 4B). LINC00857 expression had a statistically inverse association with the immune cells in these eight cancers. Intriguingly, LINC00857 expression was inversely correlated with the infiltration levels of all five immune cells in COAD. In addition, the present research noticed that LINC00857 expression was negatively related to the immune score and microenvironment score in these eight cancers (Supplementary Figure S4). Overall, these findings indicated that LINC00857 expression was negatively associated with immune cell infiltration.

The relevance between LINC00857 and immune checkpoint gene expression

Cancers can elude immune response by exploiting immune checkpoint genes such as PD-1/PD-L1 and CTLA-4. A promising immunotherapeutic strategy has emerged by targeting PD-1, PD-L1 or CTLA-4 to treat various malignancies (Postow et al., 2015). We studied the major immune checkpoint genes using the ACLBI database and analyzed their relevance to LINC00857 expression (Figure 5A). We observed a positive relevance between LINC00857 and most immune checkpoint gene expression in ACC, BLCA, BRCA, GBM, PRAD, SKCM and THCA, but negative relevance in TGCT, STAD, MESO, KIRP, COAD, HNSC, and CESC. Based on the above data, we further compared the relevance of PD-1, PD-L1 and CTLA-4 with LINC00857 expression in the above eight cancers. As depicted in Figure 5B, LINC00857 expression had a significant reverse correlation with PD-1, PD-L1 and CTLA-4 expression in these cancers. In brief, LINC00857 expression was closely associated with immune checkpoint gene expression.

The relevance between LINC00857 expression and MSI, TMB or NEO

In the tumor microenvironment, MSI, TMB and NEO are correlated with anti-tumor immunity and serve as valid biomarkers of tumor immunotherapeutic response (Dudley et al., 2016; Yarchoan et al., 2017; Peng et al., 2019). To validate the significance of LINC00857 expression in immunotherapy, a pan-cancer assessment was performed for MSI, TMB and NEO (Figure 6). We discovered that LINC00857 expression was dramatically associated with MSI in seven cancers, with a positive correlation in three cancers including BRCA, LIHC, TGCT and a negative correlation in COAD, COADREAD, KICH, DLBC. LINC00857 expression was dramatically associated with TMB in ten cancers, with a positive correlation in six cancers including LUAD, KIRP, UCEC, LUSC, PCPG, UCS and a negative correlation in COAD, COADREAD, CHOL, DLBC. LINC00857 expression was positively associated with NEO in KIPAN and SKCM while was negatively correlated with in COAD and COADREAD. Intriguingly, among the eight malignancies mentioned above, LINC00857 expression was only

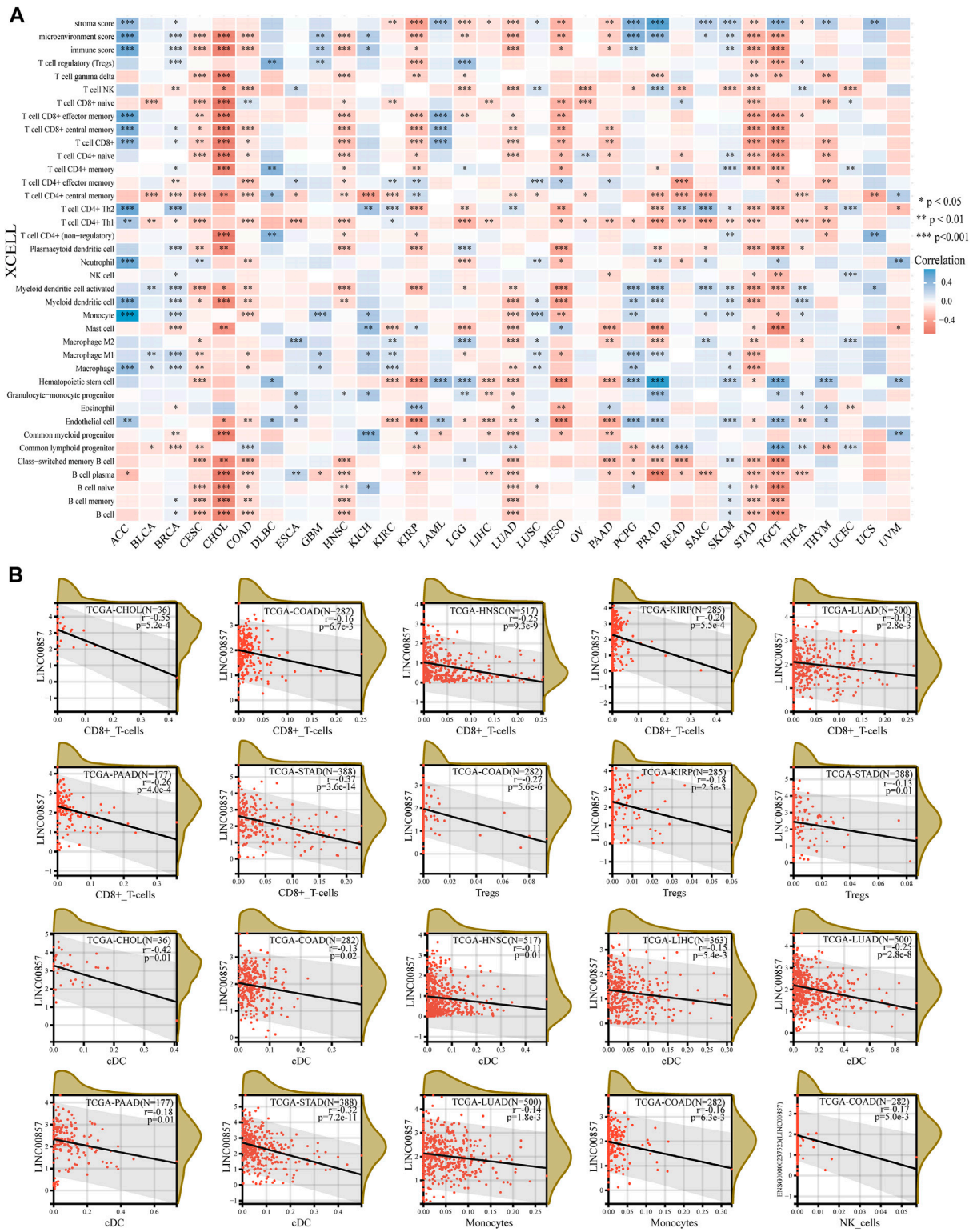

FIGURE 4
The correlation between LINC00857 expression and immune cell infiltration. **(A)** The interrelation heatmap between LINC00857 expression and immune cell infiltration levels was examined by the ACLBI database (XCELL algorithm). (*$p < 0.05$, **$p < 0.01$, ***$p < 0.001$, Spearman analysis) **(B)** Scatter plots of the pertinence between LINC00857 expression and the infiltration levels of monocyte, NK cell, conventional DC, Treg and CD8+T cell by the Sangerbox 3.0 database (XCELL algorithm) (*$p < 0.05$, **$p < 0.01$, ***$p < 0.001$, Pearson analysis).

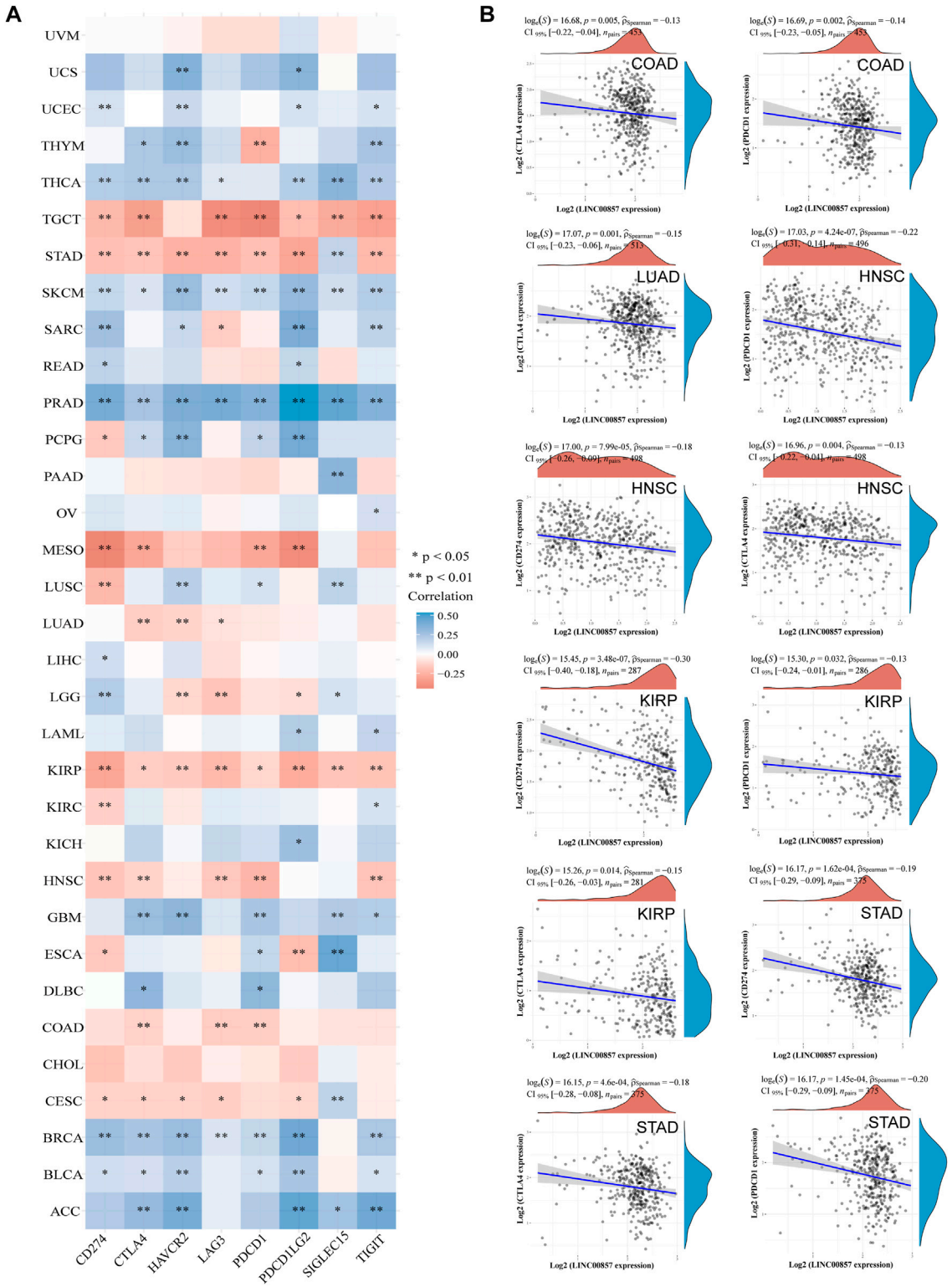

FIGURE 5
The correlation between LINC00857 and immune checkpoint genes expression. **(A)** Correlation mapping of LINC00857 expression with immune checkpoint genes in pan-cancer by the ACLBI database. **(B)** The correlation between LINC00857 and PD-L1(CD274), PD1 (PDCD1) or CTLA4 expression was shown *via* the scatter plot (*$p < 0.05$, **$p < 0.01$, ***$p < 0.001$, Spearman analysis).

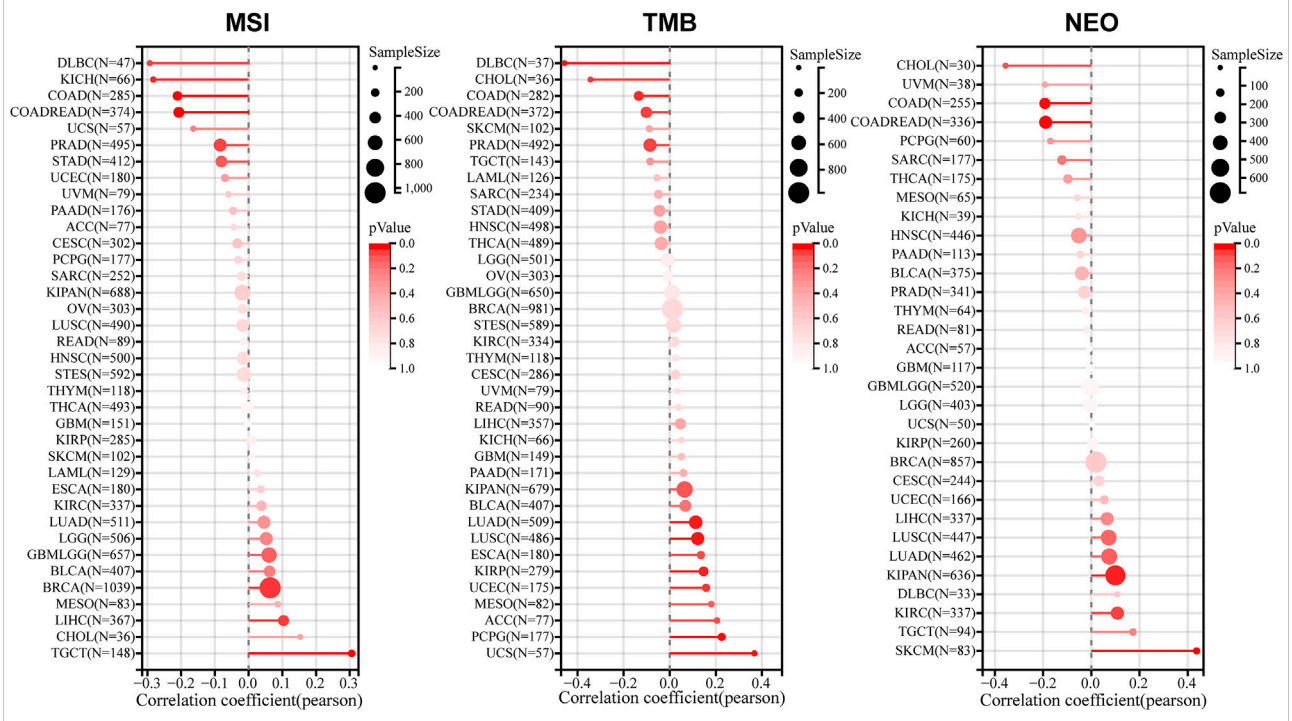

FIGURE 6
The correlation between LINC00857 expression and MSI, TMB or NEO. A stick chart displayed the connections between LINC00857 expression and MSI, TMB or NEO in diverse cancers *via* the Sangerbox 3.0 database (Pearson correlation).

simultaneously negative with TMB, MSI or NEO in colorectal cancer. In accordance with the above conclusion, it might hint a poor response to immunotherapy in colorectal cancer patients with high-expression of LINC00857.

LINC00857 promoted the proliferation of colorectal cancer cells

Considering that colorectal cancer patients with high-expression of LINC00857 may not be suitable for immune checkpoint inhibitors, targeting LINC00857 may be an ideal approach for these patients. The FISH assays confirmed that LINC00857 expression was more widely expressed in colorectal cancer than in the normal tissues (Figure 7A). In general, the action of lncRNA is prominently interrelated to its subcellular localization (Chen, 2016). We found that LINC00857 was primarily distributed in the cytoplasm as elucidated by lncLocator tool (Cao et al., 2018) and FISH assays (Figures 7B,C). Subsequently, we designed two specific siRNAs against LINC00857 and transfected them into HCT116 colorectal cancer cells. To estimate the potential influence of LINC00857 silencing on colorectal cancer cell proliferation, we performed CCK-8 and colony formation experiments. Our results validated that knockdown of LINC00857 attenuated the proliferative ability of HCT116 cells (Figures 7D–F). Thus, targeting LINC00857 may be feasible to impair the proliferation of colorectal cancer cells.

GSEA after LINC00857 knockdown

For more insight into the regulatory mechanisms of LINC00857 in colorectal cancer, we conducted a transcriptome sequencing analysis after LINC00857 knockdown with two independent siRNAs in HCT116 cells. Afterwards, we executed GSEA to investigate the possible biological function of LINC00857 in colorectal cancer. As shown in Figure 8, GSEA findings revealed that knockdown of LINC00857 triggered the ferroptosis pathway, which might account for how LINC00857 facilitated cancer growth. Interestingly, downregulated genes after LINC00857 knockdown were remarkably enriched in multiple metabolic pathways such as glycolytic process, NAD metabolic process, lipid/cholesterol/unsaturated fatty acids biosynthetic process and fatty acid binding etc. Meanwhile, silencing LINC00857 affected the activation of numerous signaling pathways including Hippo, HIF1, JAK/STAT, MAPK and PI3K/AKT signaling pathways. These findings imply that LINC00857 may affect the proliferation of cancer cells *via* multiple biological pathways.

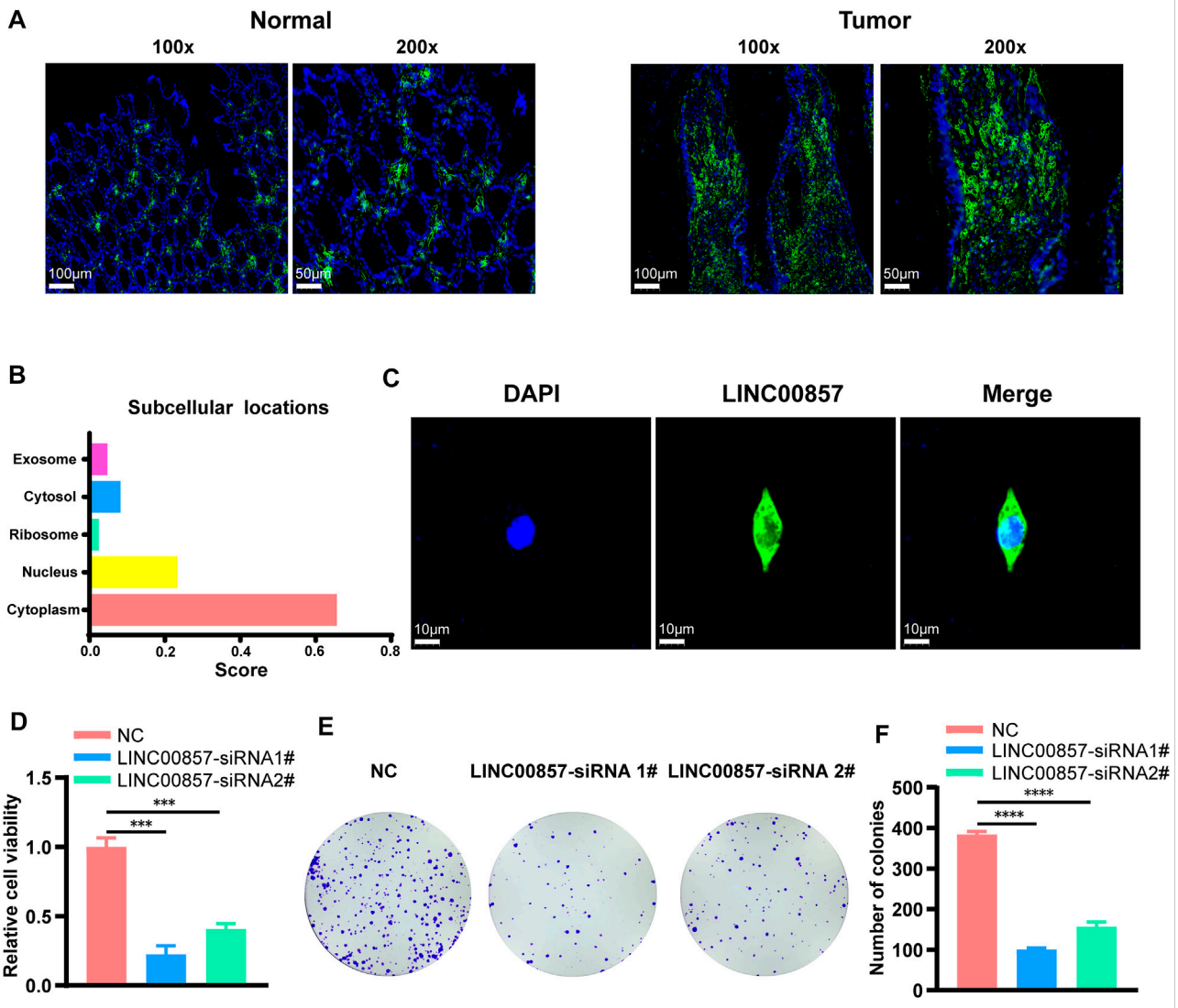

FIGURE 7
LINC00857 promoted the proliferation of colorectal cancer cells. **(A)** LINC00857 expression in colorectal cancer and corresponding normal tissues was examined by FISH assay. **(B)** The subcellular localization of LINC00857 was predicted by lncLocator tool. **(C)** The subcellular localization of LINC00857 in HCT116 cell was examined by FISH assay. **(D)** The cell viability of HCT116 cells transfected with siRNA-LINC00857 or siRNA-NC was evaluated by CCK-8 assay. **(E–F)** Colony formation experiments monitored the proliferative ability of HCT116 cells after LINC00857 silencing (*$p < 0.05$; **$p < 0.01$; ***$p < 0.001$).

Transcriptomic landscape after LINC00857 knockdown

Next, we implemented WGCNA of the abundant RNA-seq data to determine molecules underlying the regulatory mechanism of LINC00857 in colorectal cancer. To ensure connectivity between genes fulfilled the scale-free network layout, we set the soft threshold power to 7 (R2 = 0.86) (Figure 9A). As illustrated in the hierarchical clustering tree in Figure 9B, genes with analogous biological functions were categorized into the same module with the module's smallest size cutoff of 30 genes. After combining highly similar modules, we ultimately gained 13 co-expression modules with sizes ranging from 49 to 8,449 genes. The interactions between these modules were indicated in Figure 9C. Among the indicated modules, the honeydew 1, cyan and blue2 co-expression modules were most dramatically associated with the control or LINC00857 knockdown group (Figure 9D). Intriguingly, these three groups were also the modules with the highest proportion of gene counts (Figure 9E). In addition, scatter plots of interrelation between gene significance and module membership in the honeydew 1, cyan

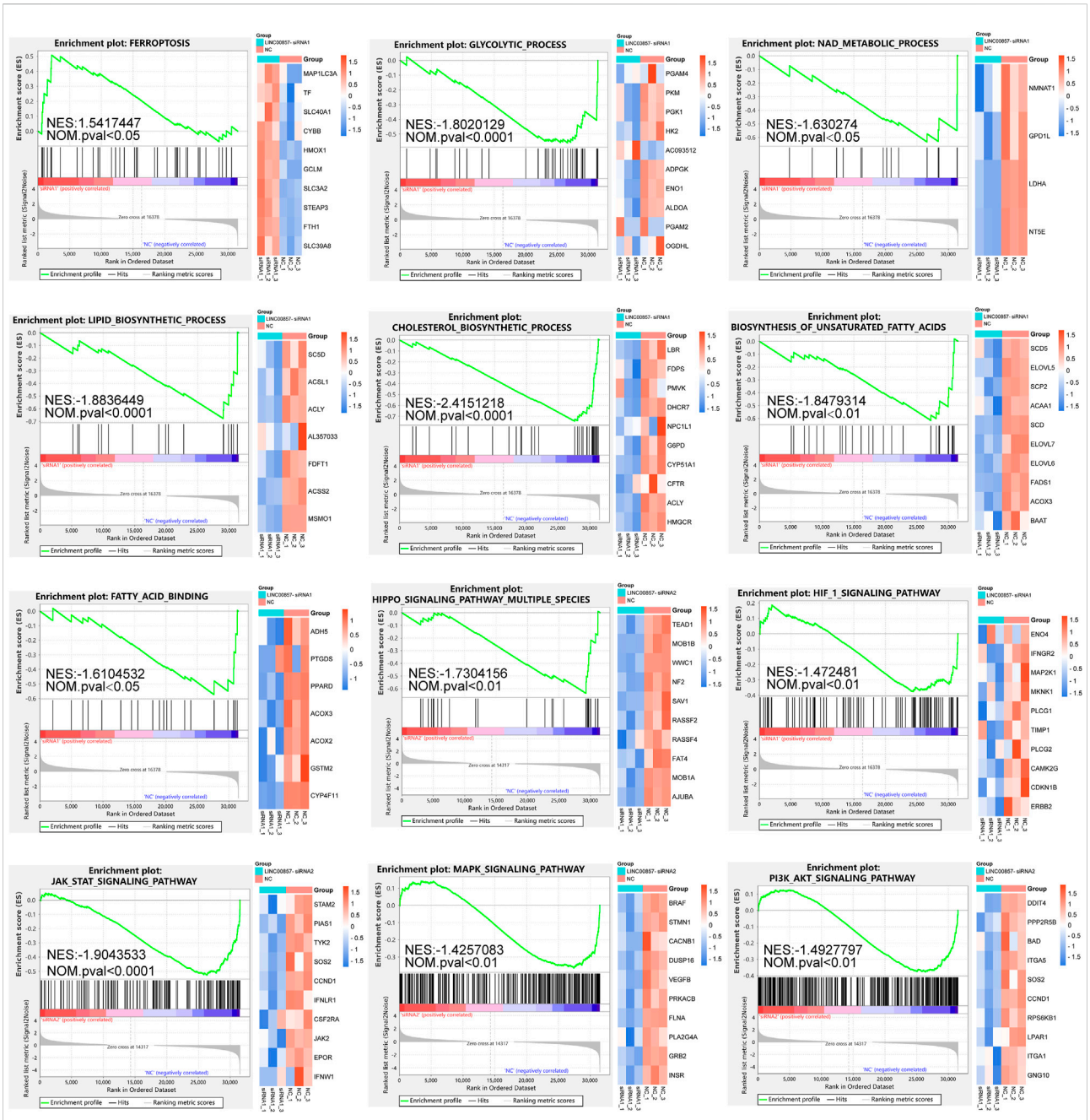

FIGURE 8
GSEA after LINC00857 silencing. Gene set enrichment analysis (GSEA) of the molecular signatures by RNA-sequencing in HCT116 cell after silencing LINC00857 (|NES|>1 and NOM $p < 0.05$).

and blue 2 modules were also presented separately (Figure 9F). Subsequently, differential expression analysis was executed on these gene datasets of the three modules. The volcanic plots preliminarily displayed the overall distribution of all differential genes (Figure 10A). As illustrated in Figure 10B, we identified 50 obviously upregulated mRNAs and 26 downregulated mRNAs. For a broader overview of LINC00857s role, we performed GO and KEGG analysis on these 76 candidate genes (Figure 10C). Cell differentiation, carbohydrate derivative binding, extracellular region and *Staphylococcus aureus* infection were remarkably enriched in biological process (BP), molecular function (MF), cellular component (CC) and KEGG pathways, respectively. These enriched pathways allowed us to better interpret the functions of LINC00857 in colorectal cancer.

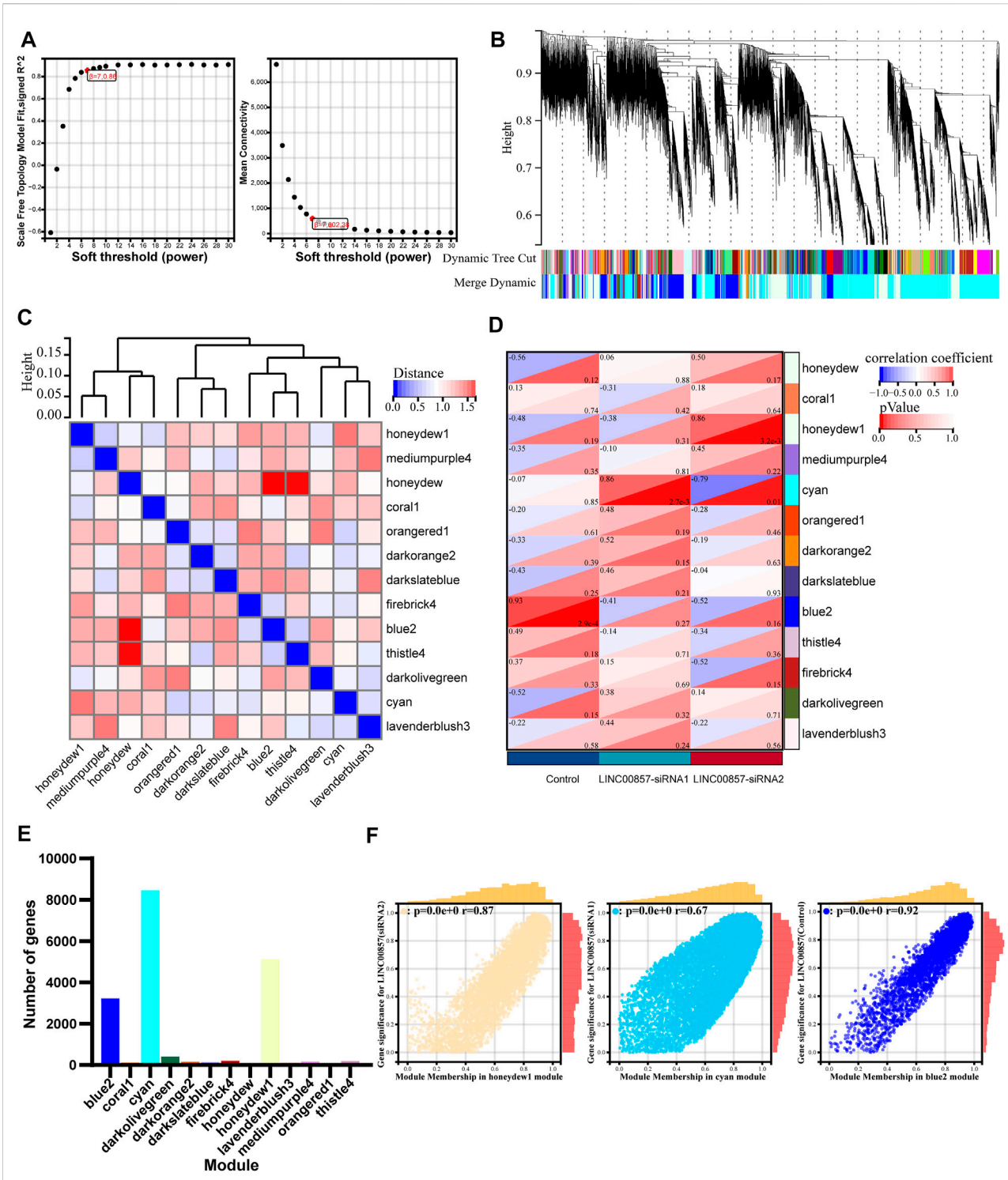

FIGURE 9
WGCNA after LINC00857 silencing. **(A)** The soft threshold of the WGCNA module. **(B)** Cluster dendrogram of LINC00857 RNA-seq expression data and functional modules were created by WGCNA. **(C)** The interaction between different modules. **(D)** Heatmap of interrelation between gene modules and sample characteristics. **(E)** The number of genes per module. **(F)** Dependence between GS and MM in honeydew 1, cyan and blue 2 modules. P< 0.05.

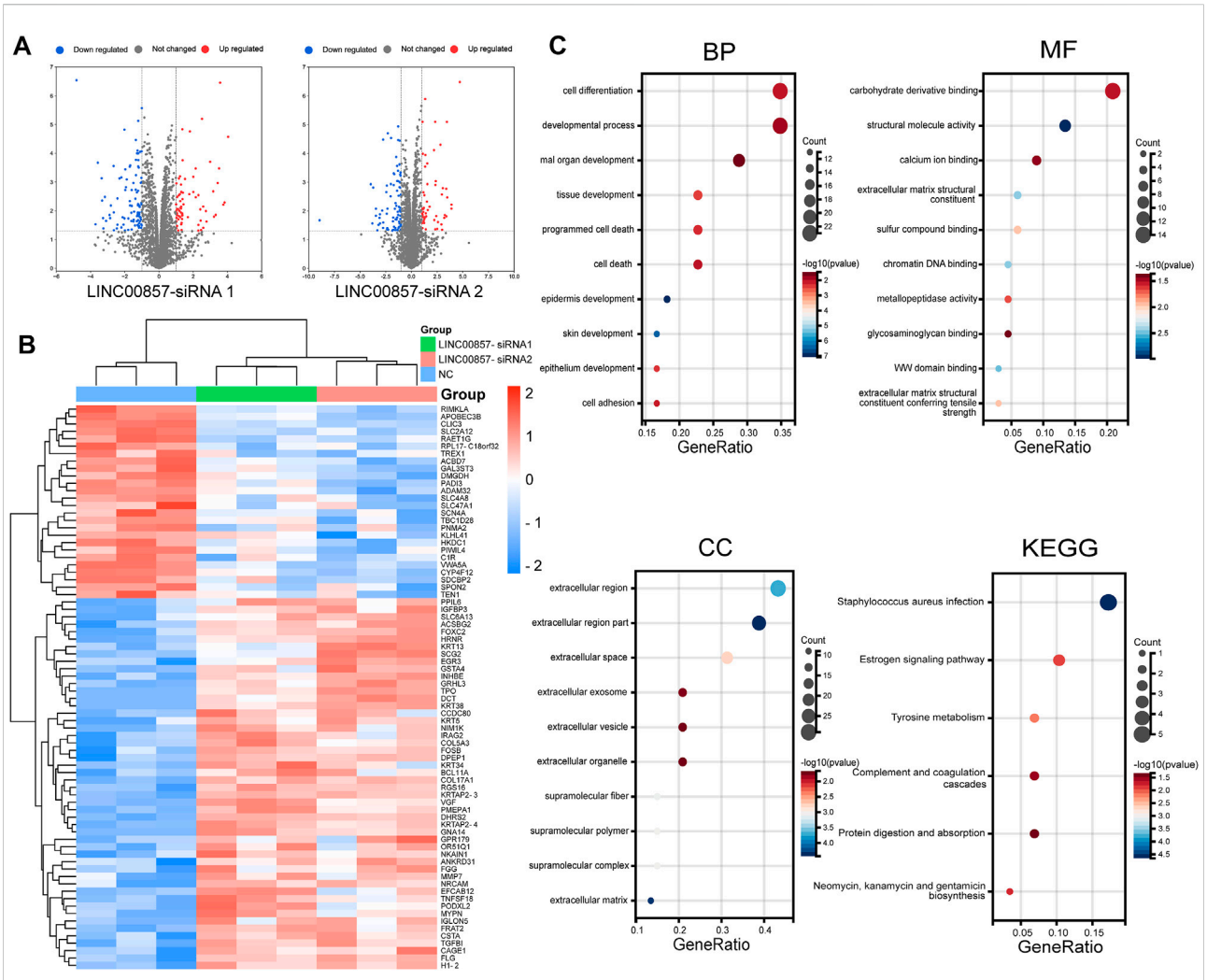

FIGURE 10
Transcriptomic landscape after LINC00857 silencing. **(A)** Volcano map depicted the distribution characteristics of all differential genes. ($p < 0.05$, $|\log_2 FC|>1$) **(B)** Heatmap displayed the expression levels of 76 differentially expressed genes (DEGs). **(C)** GO and KEGG analysis for the 76 DEGs.

LINC00857 regulated the expression of PIWIL4 in colorectal cancer

To pinpoint the downstream target genes of LINC00857, we integrated two siRNA sequencing data and screened out the top five genes with the largest fold changes among all downregulated genes: RPL17-C18orf32, TREX1, TBC1D28, TEN1 and PIWIL4 (Supplementary Figure S5A). Among them, only PIWIL4 was markedly overexpressed in colorectal cancer and positively related with LINC00857 expression by bioinformatic analysis (Figures 11A,B). In Figure 11C, qPCR analysis demonstrated the expression of PIWIL4 mRNA was dramatically decreased after LINC00857 knockdown. These data validated that PIWIL4 was a target of LINC00857 in colorectal cancer. To probe the possible roles of PIWIL4 in colorectal cancer, we implemented GSEA of TCGA datasets according to the PIWIL4 expression status in COAD tissues. As shown in Figure 11D, GSEA results revealed that immune response-related genes were predominantly enriched in the PIWIL4 hypo-expression group. These specific pathways contain immune response-activated signal transduction, positive regulation of immune response/mononuclear cell proliferation/T cell activation, macrophage/natural killer cell activation, regulation of CD8−positive, alpha−beta T cell activation and dendritic cell antigen processing and presentation. GSVA also indicated that PIWIL4 expression was negatively related to infiltration score and immune cells such as NK, DC, CD8+T cells and macrophages in COAD (Figure 11E). PIWIL4 expression in COAD was negatively correlated with immune cell infiltration and immune checkpoint gene expression such as PD1, PD-L1, CTLA4 and PD-L2 (PDCD1LG2, programmed cell death 1 ligand 2) (Figures 11F,G; Supplementary Figures S5B,C). As

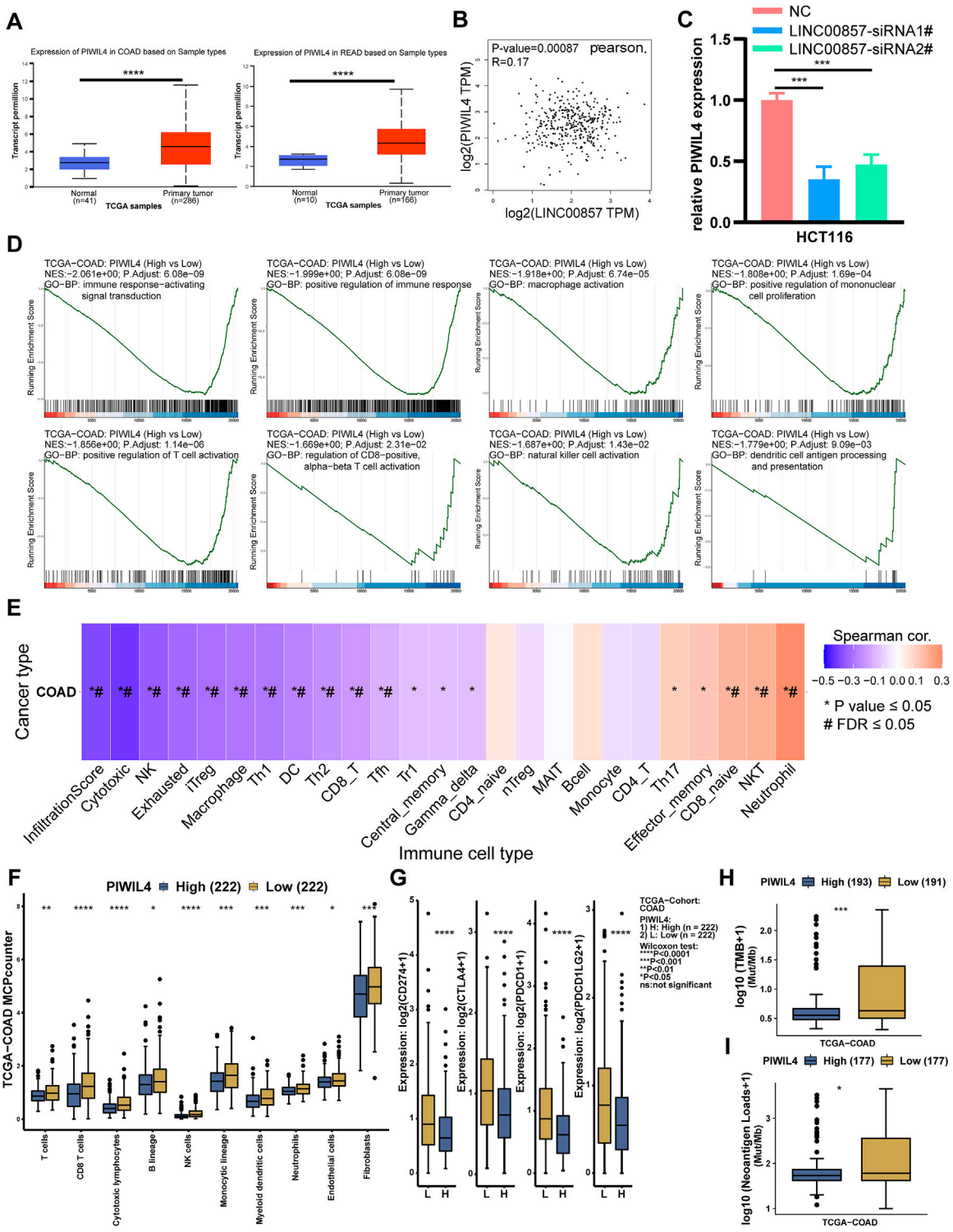

FIGURE 11
LINC00857 regulated the expression of PIWIL4 in colorectal cancer. **(A)** PIWIL4 expression in colorectal cancer samples and normal samples was explored *via* UALCAN database. **(B)** The relevance between LINC00857 and PIWIL4 expression in colorectal cancer was explored *via* GEPIA2 database. **(C)** The expression of PIWIL4 mRNA after LINC00857 silencing was determined *via* qPCR assay. **(D)** GSEA of the relevance between PIWIL4 expression and immune response pathways in COAD. (|NES|>1, *p* adjust <0.05) **(E)** The correlation between GSVA score and immune infiltration in colon cancer. (*p value < 0.05, #FDR<0.05). **(F–I)** Differences of immune cell infiltration levels, immune checkpoint genes expression levels, TMB and NEO status between PIWIL4 high and low expression group.

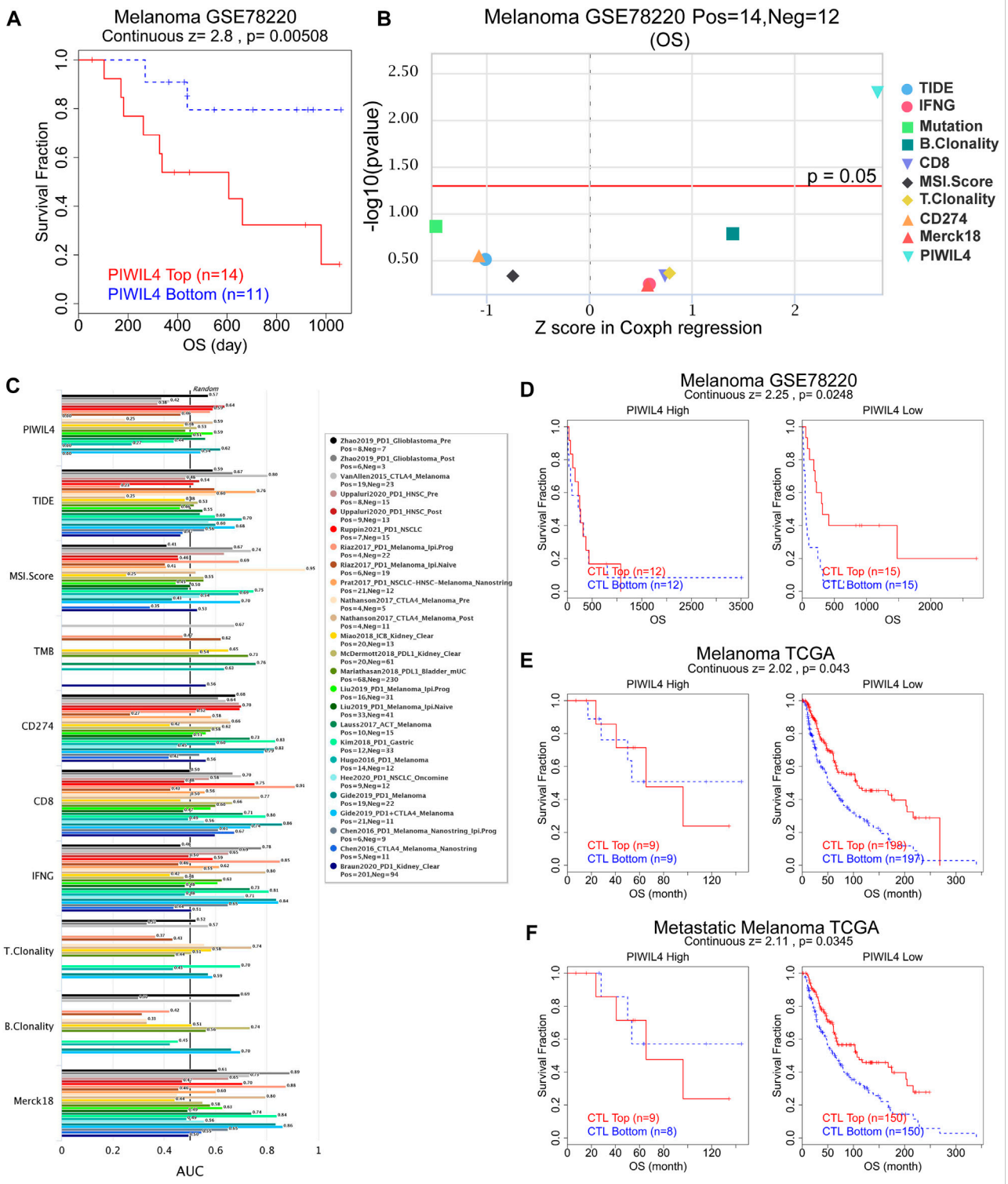

FIGURE 12
PIWIL4 predicted immunotherapy efficacy. **(A)** The overall survival analysis of patients in melanoma when receiving PD1 inhibitor. **(B)** Z score in Coxph regression analysis of different predictors of immunotherapy in melanoma. **(C)** The predictive capability of PIWIL4 for immunotherapy efficacy in multiple human immunotherapy cohorts. **(D–F)** The overall survival analysis of patients in melanoma with different PIWIL4 expression and CTL levels.

anticipated, PIWIL4 expression was also inversely correlated with TMB, MSI and neoantigen in COAD (Figures 11H,I; Supplementary Figure S5D). The foregoing analysis elucidated that LINC00857 might affect the immune characteristics of colorectal cancer by regulating PIWIL4 expression.

PIWIL4 predicted immunotherapy efficacy

Subsequently, we assessed whether PIWIL4 expression could predict the effect of cancer immunotherapy by the TIDE platform (Fu et al., 2020). Figure 12A suggested that the patients with high-expressed PIWIL4 received poorer PD1 inhibitor treatment response. We estimated the predictive value of PIWIL4 as a biomarker for cancer immunotherapy response. As illustrated in Figure 12B, PIWIL4 could independently serve as a predictor of immunotherapy response. Compared with existing biomarkers, PIWIL4 provided higher predictive power than B. clonality, T. clonality and TMB (Figure 12C) (AUC values >0.5 means that the algorithm outperformed random). Additionally, we found hypo-expressed PIWIL4 facilitated CTL (Cytotoxic T cell)-mediated anti-tumor response, implying its potential as a novel target of immunotherapy (Figures 12D–F). In summary, these data indicated that PIWIL4 could serve as a predictor for immunotherapy response and a new target for immunotherapy.

Susceptible drugs estimation for PIWIL4 protein

Lastly, based on the GDSC and CTRP databases, we predicted the drugs that possibly affect the function of PIWIL4 protein. The GDSC data set demonstrated that the sensitivity of Elesclomol, TW 37 and Temsirolimus was positively correlated with PIWIL4 expression (Figure 13A). Analogously, the results derived from the CTRP dataset elucidated that the sensitivity of PI-103, SID 26681509, YM-155 and niclosamide was positively correlated with PIWIL4 expression (Figure 13B). Significantly, the relevance between PIWIL4 expression and these drug activities could be verified by Cell Miner CDB online platform (Luna et al., 2021) (Supplementary Figure S6). In addition, molecular docking was performed to verify the binding abilities of these drugs with PIWIL4 protein. Concretely, the PIWIL4 protein spatial structure was displayed in Figure 13C. Putative binding sites and box on PIWIL4 protein were indicated in Figures 13D,E. Figures 13F–K and Supplementary Figure S7 illustrated the optimal docking space conformation and interaction force of each drug to PIWIL4 protein. The detailed docking scoring results were provided in Supplementary Table S1. Obviously, SID 26681509 had the best binding conformations to PIWIL4 protein. To further assess the influences of PIWIL4 expression on drug sensitivity, we examined the relationship between multiple drug activities and PIWIL4 expression in NCI-60 cancer cell lines (Supplementary Figures S8, S9). Apparently, as PIWIL4 expression elevated, the IC50 of INK-128, entosplenitib and Everolimus against cancer cells was lower. Therefore, we screened out several susceptible drugs targeting PIWIL4 protein.

LINC00857-miRNA-PIWIL4 ceRNA network

LncRNAs in the nucleus are mainly engaged in transcriptional regulation whereas cytoplasm lncRNAs could govern the stability and translation of mRNA *via* ceRNA mechanism (Yao et al., 2019). Since FISH assays presented that LINC00857 localized mainly in the cytoplasm, we predicted many miRNAs responsible for LINC00857-mediated PIWIL4 expression by means of online database analysis. We constructed the LINC00857-miRNA-PIWIL4 network using Cytoscape software (Supplementary Figure S10A). Concretely, we used the miRNA Walk tool (Sticht et al., 2018) with the 3′UTR (untranslated region) of PIWIL4 mRNA as the query sequence to identify miRNAs that may regulate the target genes. A total of 132 LINC00857-miRNA regulatory pairs were evaluated *via* the lncRNASNP2 platform (Miao et al., 2018). Eventually, we confirmed 7 potential microRNAs including hsa-miR-6728-3p, hsa-miR-22-5p, hsa-miR-342-5p, hsa-miR-512-5p, hsa-miR-939-3p, hsa-miR-6742-3p, hsa-miR-4433b-3p. Further analysis indicated that only hsa-miR-22-5p, hsa-miR-342-5p and hsa-miR-6728-3p had potential binding sites to both LINC00857 and PIWIL4 3′UTR (untranslated region) (Supplementary Figure S10B).

Discussion

Multiple studies have reported that LINC00857 has a high relevance with the development and progression of diverse cancers. Silencing LINC00857 alleviated the proliferative capacity and facilitated the apoptosis, autophagy and radiotherapy sensitivity of lung cancer cells, suggesting that LINC00857 could act as a potential therapeutic target for LUAD (Han et al., 2020; Su et al., 2020). Likewise, LINC00857 accelerated ovarian cancer progression and glycolysis by regulating the Hippo signaling pathway (Lin et al., 2020). So far, all studies have been limited to the effect of LINC00857 on a single cancer, but holistic analysis in multiple cancers is lacking. Pan-cancer analysis could provide insights and potential treatment strategies for cancers by comparing the similarities and differences between diverse cancers. This paper provided the first

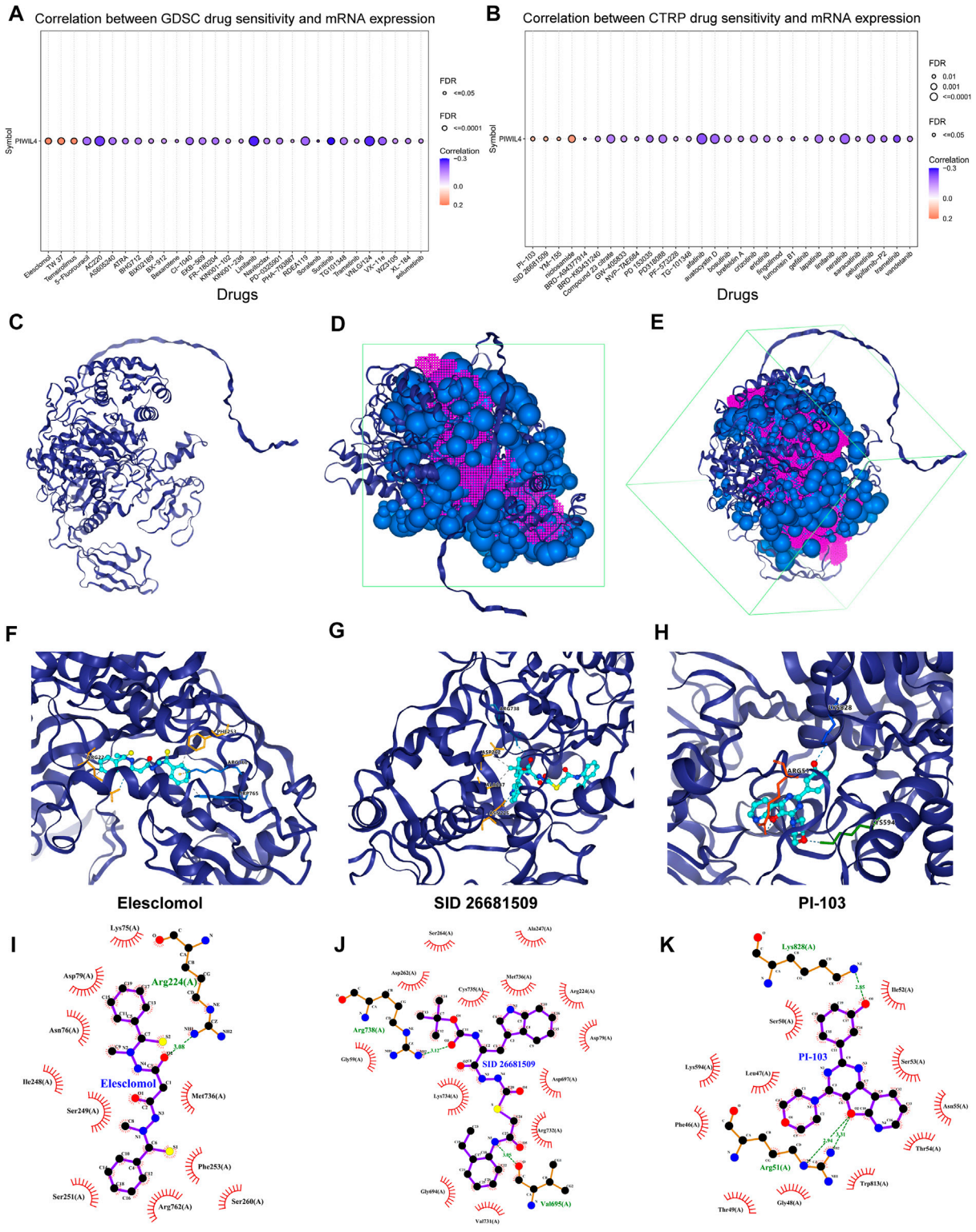

FIGURE 13
Susceptible drugs estimation for PIWIL4 protein. **(A,B)** Predicting the relevance between PIWIL4 expression and different drug sensitivities based on GDSC and CTRP databases. **(C)** The spatial structure diagram of the PIWIL4 protein. **(D,E)** Potential binding sites and box on PIWIL4 protein. **(F–H)** The optimal docking space conformation of the drug to PIWIL4 protein. (Blue dotted line: Hydrogen bond; grey dotted line: Hydrophobic interaction; yellow dotted line: Cation interaction). **(I–K)** The interaction force between PIWIL4 protein and drugs was calculated by ligplus software.

comprehensive analysis of LINC00857 expression, prognostic value as well as immune characteristics by pan-cancer datasets.

We demonstrated that LINC00857 could potentially act as a diagnostic biomarker in eight cancers, including COAD, CHOL, KIRP, HNSC, LUAD, LIHC, PAAD and STAD. Among them, LINC00857 may also serve as a prognostic biomarker in HNSC, LUAD, LIHC and PAAD. Currently, a huge challenge for cancer therapy is drug resistance, which can be greatly facilitated by the tumor microenvironment (Chatterjee and Bivona, 2019). TIICs are an integral part of the tumor microenvironment and have been shown to have a remarkable influence on the prognosis of multiple cancers (Ye et al., 2019). However, there is few research about the correlation between LINC00857 expression and tumor immunity (Mu et al., 2021). Our results suggest that LINC00857 expression was negatively associated with immune infiltrating cells in most of cancers, especially in eight LINC00857 high-expressing cancers. Similarly, our study revealed a negative correlation between LINC00857 expression and immune score in these cancers. Cancers may evade immune surveillance by utilizing immune checkpoint genes including PD-1, CTLA-4 and PD-L1 (Postow et al., 2015). Blocking these immune checkpoint genes has proven to be a valid strategy for cancer therapy (Ramagopal et al., 2017). Interestingly, our research also found that LINC00857 expression was negatively related to the expression of immune checkpoint genes including PD1, CTLA4 and PD-L1 in LINC00857 high-expressing cancers. All the data suggest that high-expression of LINC00857 was closely correlated with an immunosuppressive microenvironment.

MSI is a hypermutator phenotype due to the absence of DNA mismatch repair (Baretti and Le, 2018). Cancer patients with high microsatellite instability (MSI-H) are more likely to have a durable response to immunotherapy (Janjigian et al., 2018). MSI was found in numerous cancer types, with a high incidence in colorectal, endometrial and gastric cancer (Hause et al., 2016). Additionally, mutations in cancer cells can produce new epitopes of autoantigens, which can trigger tumor-specific T-cell response to facilitate immunotherapy (Cohen et al., 2015; Blass and Ott, 2021). At present, MSI, neoantigens (NEO) and tumor mutation burden (TMB) have become essential biomarkers for immunotherapy (Schumacher and Schreiber, 2015; Dudley et al., 2016; Yarchoan et al., 2017). Significantly, our data confirmed a negative association between LINC00857 expression and TMB/MSI/NEO in COAD, suggesting that immune checkpoint inhibitors may have poor response in those cancer patients with high-expression of LINC00857. Though LINC00857 expression was positively associated with MSI/TMB in some cancers, it may be still unsuitable for immunotherapy in consideration of the immune infiltrating cells status and immune checkpoint genes expression. In other words, the patients with high-expression of LINC00857 were not suitable for immune checkpoint inhibitors. LINC00857 may serve as a predictor for immunotherapy efficacy.

We wondered whether targeting LINC00857 could be feasible? Unsurprisingly, our data verified that LINC00857 was essential for the proliferation of colorectal cancer cells. This observation matched previous studies that LINC00857 could significantly promote the survival of cancer cells (Tang et al., 2021; Zhou et al., 2021). To further investigate the functions of LINC00857 in colorectal cancer, we conducted RNA sequencing (RNA-seq) after LINC00857 knockdown in HCT116 cells. The GSEA results hinted that LINC00857 may accelerate cancer progression by inhibiting the ferroptosis pathway in colorectal cancer. Besides, LINC00857 may also affect cancer growth by mediating lipid metabolism, glycolysis and multiple signaling pathways. The subsequent WGCNA unveiled the latent molecular mechanisms of LINC00857 in colorectal cancer. Interestingly, combining the bioinformatics and qPCR verification, we eventually discovered that LINC00857 probably exert its oncogenic effects by mediating PIWIL4 expression, which presented oncogenic potential in multiple cancer types (Su et al., 2012; Wang et al., 2016). Previous studies reported that PIWIL4 was probably a pivotal biomarker for predicting prognosis and immune landscape of cholangiocarcinoma (Zou et al., 2021). Our study further elucidated the relevance of PIWIL4 expression with the immune features of colorectal cancer, which was in accordance with the roles of LINC00857. High expression of PIWIL4 lead to poor response to immunotherapy, suggesting that PIWIL4 could also serve as a predictor of immunotherapy efficacy. Detecting the expression of LINC00857/PIWIL4 axis may contribute to screening out the exact patients suitable for immunotherapy. PIWIL4 had higher predictive power and may influence the function of CTL (Cytotoxic T cell), hinting a potential to be a new target for immunotherapy. These discoveries could likely help to illuminate the roles of LINC00857/PIWIL4 axis in colorectal tumorigenesis and development, provide a novel perspective for colorectal cancer immunotherapy, and make it possible to achieve more precise and efficient immunotherapy in the clinic. Finally, we screened out several susceptible drugs targeting PIWIL4 protein by sensitivity analysis and molecular docking analysis. This offered a powerful rationale for the clinical discovery of drugs targeting PIWIL4 for colorectal cancer treatment. Collectively, our research integrally analyzed the oncogenic roles of LINC00857 in pan-cancer. Although we have synthesized several databases for a comprehensive and systematic analysis of LINC00857, there are still some limitations and deficiencies in this research. For example, we need additional clinical data to validate our findings.

Conclusion

LINC00857 might act as a novel diagnostic and prognostic biomarker for diverse cancers. LINC00857 expression was closely

correlated with an immunosuppressive microenvironment. LINC00857/PIWIL4 axis may be predictive biomarkers for immunotherapy and valuable molecular targets for malignant tumors.

Data availability statement

The datasets presented in this study can be found in online repositories. The names of the repository/repositories and accession number(s) can be found below: Gene Expression Omnibus, GSE201069.

Author contributions

LJQ designed the project. RXM, LJ, WR, LXL, MXL, LZ, HZB, ZMZ, and MJG analyzed the data and conducted the experiments. RXM, LJ, and WR drafted the manuscript. LJQ revised the manuscript. All authors approved the final paper.

Funding

This work was supported by the National Natural Science Foundation of China (81902404), the Natural Science Foundation of Shandong Province (ZR2019BH009 and ZR2020QH096), the Project of Shandong Province medical science technology development plan (2017WS403, 2019WS601, and 202103030672) and Introduction Plan of Young Creative Talents in Colleges and Universities of Shandong Province (205).

Conflict of interest

The authors declare that the research was conducted in the absence of any commercial or financial relationships that could be construed as a potential conflict of interest.

Publisher's note

All claims expressed in this article are solely those of the authors and do not necessarily represent those of their affiliated organizations, or those of the publisher, the editors and the reviewers. Any product that may be evaluated in this article, or claim that may be made by its manufacturer, is not guaranteed or endorsed by the publisher.

Supplementary material

The Supplementary Material for this article can be found online at: https://www.frontiersin.org/articles/10.3389/fphar.2022.996686/full#supplementary-material

References

Barazzuol, L., Coppes, R. P., and Van Luijk, P. (2020). Prevention and treatment of radiotherapy-induced side effects. *Mol. Oncol.* 14 (7), 1538–1554. doi:10.1002/1878-0261.12750

Baretti, M., and Le, D. T. (2018). DNA mismatch repair in cancer. *Pharmacol. Ther.* 189, 45–62. doi:10.1016/j.pharmthera.2018.04.004

Bian, Z., Zhang, J., Li, M., Feng, Y., Wang, X., Zhang, J., et al. (2018). LncRNA-FEZF1-AS1 promotes tumor proliferation and metastasis in colorectal cancer by regulating PKM2 signaling. *Clin. Cancer Res.* 24 (19), 4808–4819. doi:10.1158/1078-0432.CCR-17-2967

Blass, E., and Ott, P. A. (2021). Advances in the development of personalized neoantigen-based therapeutic cancer vaccines. *Nat. Rev. Clin. Oncol.* 18 (4), 215–229. doi:10.1038/s41571-020-00460-2

Bukowski, K., Kciuk, M., and Kontek, R. (2020). Mechanisms of multidrug resistance in cancer chemotherapy. *Int. J. Mol. Sci.* 21 (9), E3233. doi:10.3390/ijms21093233

Cai, Q., Wang, S., Jin, L., Weng, M., Zhou, D., Wang, J., et al. (2019). Long non-coding RNA GBCDRlnc1 induces chemoresistance of gallbladder cancer cells by activating autophagy. *Mol. Cancer* 18 (1), 82. doi:10.1186/s12943-019-1016-0

Candido, J., and Hagemann, T. (2013). Cancer-related inflammation. *J. Clin. Immunol.* 33, S79. doi:10.1007/s10875-012-9847-0

Cao, Z., Pan, X., Yang, Y., Huang, Y., and Shen, H. B. (2018). The lncLocator: A subcellular localization predictor for long non-coding RNAs based on a stacked ensemble classifier. *Bioinformatics* 34 (13), 2185–2194. doi:10.1093/bioinformatics/bty085

Chatterjee, N., and Bivona, T. G. (2019). Polytherapy and targeted cancer drug resistance. *Trends Cancer* 5 (3), 170–182. doi:10.1016/j.trecan.2019.02.003

Chen, L. L. (2016). Linking long noncoding RNA localization and function. *Trends biochem. Sci.* 41 (9), 761–772. doi:10.1016/j.tibs.2016.07.003

Cohen, C. J., Gartner, J. J., Horovitz-Fried, M., Shamalov, K., Trebska-Mcgowan, K., Bliskovsky, V. V., et al. (2015). Isolation of neoantigen-specific T cells from tumor and peripheral lymphocytes. *J. Clin. Invest.* 125 (10), 3981–3991. doi:10.1172/JCI82416

Domingues, P., Gonzalez-Tablas, M., Otero, A., Pascual, D., Miranda, D., Ruiz, L., et al. (2016). Tumor infiltrating immune cells in gliomas and meningiomas. *Brain Behav. Immun.* 53, 1–15. doi:10.1016/j.bbi.2015.07.019

Dudek, A. M., Van Kampen, J. G. M., Witjes, J. A., Kiemeney, L., and Verhaegh, G. W. (2018). *<scp>LINC</scp> 00857* expression predicts and mediates the response to platinum-based chemotherapy in muscle-invasive bladder cancer. *Cancer Med.* 7, 3342–3350. doi:10.1002/cam4.1570

Dudley, J. C., Lin, M. T., Le, D. T., and Eshleman, J. R. (2016). Microsatellite instability as a biomarker for PD-1 blockade. *Clin. Cancer Res.* 22 (4), 813–820. doi:10.1158/1078-0432.CCR-15-1678

Fu, J., Li, K., Zhang, W., Wan, C., Zhang, J., Jiang, P., et al. (2020). Large-scale public data reuse to model immunotherapy response and resistance. *Genome Med.* 12 (1), 21. doi:10.1186/s13073-020-0721-z

Gao, Y., Shang, S., Guo, S., Li, X., Zhou, H., Liu, H., et al. (2021). Lnc2Cancer 3.0: An updated resource for experimentally supported lncRNA/circRNA cancer associations and web tools based on RNA-seq and scRNA-seq data. *Nucleic Acids Res.* 49 (D1), D1251–D1258. doi:10.1093/nar/gkaa1006

Han, F., Yang, S., Wang, W., Huang, X., Huang, D., and Chen, S. (2020). Silencing of lncRNA LINC00857 enhances BIRC5-dependent radio-sensitivity of lung adenocarcinoma cells by recruiting NF-κB1. *Mol. Ther. Nucleic Acids* 22, 981–993. doi:10.1016/j.omtn.2020.09.020

Hause, R. J., Pritchard, C. C., Shendure, J., and Salipante, S. J. (2016). Classification and characterization of microsatellite instability across 18 cancer types. *Nat. Med.* 22 (11), 1342–1350. doi:10.1038/nm.4191

Janjigian, Y. Y., Sanchez-Vega, F., Jonsson, P., Chatila, W. K., Hechtman, J. F., Ku, G. Y., et al. (2018). Genetic predictors of response to systemic therapy in esophagogastric cancer. *Cancer Discov.* 8 (1), 49–58. doi:10.1158/2159-8290.CD-17-0787

Jumper, J., Evans, R., Pritzel, A., Green, T., Figurnov, M., Ronneberger, O., et al. (2021). Highly accurate protein structure prediction with AlphaFold. *Nature* 596 (7873), 583–589. doi:10.1038/s41586-021-03819-2

Kawabata, T. (2010). Detection of multiscale pockets on protein surfaces using mathematical morphology. *Proteins* 78 (5), 1195–1211. doi:10.1002/prot.22639

Kennedy, L. B., and Salama, A. K. S. (2020). A review of cancer immunotherapy toxicity. *Ca. Cancer J. Clin.* 70 (2), 86–104. doi:10.3322/caac.21596

Kim, S., Chen, J., Cheng, T., Gindulyte, A., He, J., He, S., et al. (2021). PubChem in 2021: New data content and improved web interfaces. *Nucleic Acids Res.* 49 (D1), D1388–D1395. doi:10.1093/nar/gkaa971

Li, J. H., Liu, S., Zhou, H., Qu, L. H., and Yang, J. H. (2014). starBase v2.0: decoding miRNA-ceRNA, miRNA-ncRNA and protein-RNA interaction networks from large-scale CLIP-Seq data. *Nucleic Acids Res.* 42, D92–D97. doi:10.1093/nar/gkt1248

Lin, A., Qi, C., Wei, T., Li, M., Cheng, Q., Liu, Z., et al. (2022). Camoip: A web server for comprehensive analysis on multi-omics of immunotherapy in pan-cancer. *Brief. Bioinform* 23, bbac129. doi:10.1093/bib/bbac129

Lin, X., Feng, D., Li, P., and Lv, Y. (2020). LncRNA LINC00857 regulates the progression and glycolysis in ovarian cancer by modulating the Hippo signaling pathway. *Cancer Med.* 9 (21), 8122–8132. doi:10.1002/cam4.3322

Liu, C. J., Hu, F. F., Xia, M. X., Han, L., Zhang, Q., and Guo, A. Y. (2018). GSCALite: A web server for gene set cancer analysis. *Bioinformatics* 34 (21), 3771–3772. doi:10.1093/bioinformatics/bty411

Luna, A., Elloumi, F., Varma, S., Wang, Y., Rajapakse, V. N., Aladjem, M. I., et al. (2021). CellMiner Cross-Database (CellMinerCDB) version 1.2: Exploration of patient-derived cancer cell line pharmacogenomics. *Nucleic Acids Res.* 49 (D1), D1083–D1093. doi:10.1093/nar/gkaa968

Meng, X., Deng, Y., He, S., Niu, L., and Zhu, H. (2021). m(6)A-Mediated upregulation of LINC00857 promotes pancreatic cancer tumorigenesis by regulating the miR-150-5p/E2F3 Axis. *Front. Oncol.* 11, 629947. doi:10.3389/fonc.2021.629947

Miao, Y. R., Liu, W., Zhang, Q., and Guo, A. Y. (2018). lncRNASNP2: an updated database of functional SNPs and mutations in human and mouse lncRNAs. *Nucleic Acids Res.* 46 (D1), D276–D280. doi:10.1093/nar/gkx1004

Mu, L., Ding, K., Tu, R., and Yang, W. (2021). Identification of 4 immune cells and a 5-lncRNA risk signature with prognosis for early-stage lung adenocarcinoma. *J. Transl. Med.* 19 (1), 127. doi:10.1186/s12967-021-02800-x

Nagy, A., Munkacsy, G., and Gyorffy, B. (2021). Pancancer survival analysis of cancer hallmark genes. *Sci. Rep.* 11 (1), 6047. doi:10.1038/s41598-021-84787-5

Peng, M., Mo, Y., Wang, Y., Wu, P., Zhang, Y., Xiong, F., et al. (2019). Neoantigen vaccine: An emerging tumor immunotherapy. *Mol. Cancer* 18 (1), 128. doi:10.1186/s12943-019-1055-6

Postow, M. A., Callahan, M. K., and Wolchok, J. D. (2015). Immune checkpoint blockade in cancer therapy. *J. Clin. Oncol.* 33 (17), 1974–1982. doi:10.1200/JCO.2014.59.4358

Ramagopal, U. A., Liu, W., Garrett-Thomson, S. C., Bonanno, J. B., Yan, Q., Srinivasan, M., et al. (2017). Structural basis for cancer immunotherapy by the first-in-class checkpoint inhibitor ipilimumab. *Proc. Natl. Acad. Sci. U. S. A.* 114 (21), E4223–E4232. doi:10.1073/pnas.1617941114

Reinhold, W. C., Sunshine, M., Liu, H., Varma, S., Kohn, K. W., Morris, J., et al. (2012). CellMiner: A web-based suite of genomic and pharmacologic tools to explore transcript and drug patterns in the NCI-60 cell line set. *Cancer Res.* 72 (14), 3499–3511. doi:10.1158/0008-5472.CAN-12-1370

Ritchie, M. E., Phipson, B., Wu, D., Hu, Y., Law, C. W., Shi, W., et al. (2015). Limma powers differential expression analyses for RNA-sequencing and microarray studies. *Nucleic Acids Res.* 43 (7), e47. doi:10.1093/nar/gkv007

Schrock, A. B., Ouyang, C., Sandhu, J., Sokol, E., Jin, D., Ross, J. S., et al. (2019). Tumor mutational burden is predictive of response to immune checkpoint inhibitors in MSI-high metastatic colorectal cancer. *Ann. Oncol.* 30 (7), 1096–1103. doi:10.1093/annonc/mdz134

Schumacher, T. N., and Schreiber, R. D. (2015). Neoantigens in cancer immunotherapy. *Science* 348 (6230), 69–74. doi:10.1126/science.aaa4971

Sharma, P., and Allison, J. P. (2015b). Immune checkpoint targeting in cancer therapy: Toward combination strategies with curative potential. *Cell* 161 (2), 205–214. doi:10.1016/j.cell.2015.03.030

Sharma, P., and Allison, J. P. (2015a). The future of immune checkpoint therapy. *Science* 348 (6230), 56–61. doi:10.1126/science.aaa8172

Sticht, C., De La Torre, C., Parveen, A., and Gretz, N. (2018). miRWalk: An online resource for prediction of microRNA binding sites. *PLoS One* 13 (10), e0206239. doi:10.1371/journal.pone.0206239

Su, C., Ren, Z. J., Wang, F., Liu, M., Li, X., and Tang, H. (2012). PIWIL4 regulates cervical cancer cell line growth and is involved in down-regulating the expression of p14ARF and p53. *FEBS Lett.* 586 (9), 1356–1362. doi:10.1016/j.febslet.2012.03.053

Su, W., Wang, L., Zhao, H., Hu, S., Zhou, Y., Guo, C., et al. (2020). LINC00857 interacting with YBX1 to regulate apoptosis and autophagy via MET and phosphor-AMPKa signaling. *Mol. Ther. Nucleic Acids* 22, 1164–1175. doi:10.1016/j.omtn.2020.10.025

Subramanian, A., Tamayo, P., Mootha, V. K., Mukherjee, S., Ebert, B. L., Gillette, M. A., et al. (2005). Gene set enrichment analysis: A knowledge-based approach for interpreting genome-wide expression profiles. *Proc. Natl. Acad. Sci. U. S. A.* 102 (43), 15545–15550. doi:10.1073/pnas.0506580102

Sung, H., Ferlay, J., Siegel, R. L., Laversanne, M., Soerjomataram, I., Jemal, A., et al. (2021). Global cancer statistics 2020: GLOBOCAN estimates of incidence and mortality worldwide for 36 cancers in 185 countries. *Ca. Cancer J. Clin.* 71 (3), 209–249. doi:10.3322/caac.21660

Tang, S., Liu, Q., and Xu, M. (2021). LINC00857 promotes cell proliferation and migration in colorectal cancer by interacting with YTHDC1 and stabilizing SLC7A5. *Oncol. Lett.* 22 (2), 578. doi:10.3892/ol.2021.12839

Tang, Z., Kang, B., Li, C., Chen, T., and Zhang, Z. (2019). GEPIA2: An enhanced web server for large-scale expression profiling and interactive analysis. *Nucleic Acids Res.* 47 (W1), W556–W560. doi:10.1093/nar/gkz430

Wang, Z., Liu, N., Shi, S., Liu, S., and Lin, H. (2016). The role of PIWIL4, an argonaute family protein, in breast cancer. *J. Biol. Chem.* 291 (20), 10646–10658. doi:10.1074/jbc.M116.723239

Xia, C., Zhang, X. Y., Liu, W., Ju, M., Ju, Y., Bu, Y. Z., et al. (2018). LINC00857 contributes to hepatocellular carcinoma malignancy via enhancing epithelial-mesenchymal transition. *J. Cell. Biochem.* 120, 7970–7977. doi:10.1002/jcb.28074

Yao, R. W., Wang, Y., and Chen, L. L. (2019). Cellular functions of long noncoding RNAs. *Nat. Cell Biol.* 21 (5), 542–551. doi:10.1038/s41556-019-0311-8

Yarchoan, M., Albacker, L. A., Hopkins, A. C., Montesion, M., Murugesan, K., Vithayathil, T. T., et al. (2019). PD-L1 expression and tumor mutational burden are independent biomarkers in most cancers. *JCI Insight* 4 (6), 126908. doi:10.1172/jci.insight.126908

Yarchoan, M., Hopkins, A., and Jaffee, E. M. (2017). Tumor mutational burden and response rate to PD-1 inhibition. *N. Engl. J. Med.* 377 (25), 2500–2501. doi:10.1056/NEJMc1713444

Ye, L., Zhang, T., Kang, Z., Guo, G., Sun, Y., Lin, K., et al. (2019). Tumor-infiltrating immune cells act as a marker for prognosis in colorectal cancer. *Front. Immunol.* 10, 2368. doi:10.3389/fimmu.2019.02368

Zhang, X., Xie, K., Zhou, H., Wu, Y., Li, C., Liu, Y., et al. (2020). Role of non-coding RNAs and RNA modifiers in cancer therapy resistance. *Mol. Cancer* 19 (1), 47. doi:10.1186/s12943-020-01171-z

Zhou, D., He, S., Zhang, D., Lv, Z., Yu, J., Li, Q., et al. (2021). LINC00857 promotes colorectal cancer progression by sponging miR-150-5p and upregulating HMGB3 (high mobility group box 3) expression. *Bioengineered* 12 (2), 12107–12122. doi:10.1080/21655979.2021.2003941

Zou, W., Wang, Z., Zhang, X., Xu, S., Wang, F., Li, L., et al. (2021). PIWIL4 and SUPT5H combine to predict prognosis and immune landscape in intrahepatic cholangiocarcinoma. *Cancer Cell Int.* 21 (1), 657. doi:10.1186/s12935-021-02310-2

Glossary

ACC adrenocortical carcinoma

BP biological process

BLCA bladder urothelial carcinoma

BRCA breast invasive carcinoma

CC cellular component

CDCs conventional dendritic cells

CESC cervical squamous cell carcinoma and endocervical adenocarcinoma

CHOL cholangiocarcinoma

COAD colon adenocarcinoma

CTL cytotoxic T cell

DEGs differentially expressed genes

DFI disease-free interval

DFS disease free survival

DLBC lymphoid neoplasm diffuse large B-cell lymphoma

DSS disease specific survival

FISH fluorescence *in situ* hybridization

GBM glioblastoma multiforme

GO gene ontology

GSEA gene set enrichment analysis

HNSC head and neck squamous cell carcinoma

KEGG kyoto encyclopedia of genes and genomes

KICH kidney chromophobe

KIRC kidney renal clear cell carcinoma

KIRP kidney renal papillary cell carcinoma

KM Kaplan-Meier

LIHC hepatocellular carcinoma

LUAD lung adenocarcinoma

LUSC lung squamous cell carcinoma

MESO mesothelioma

MF molecular function

MSI microsatellite instability

ncRNAs non-coding RNAs

NEO neoantigen

OD optical density

OS overall survival

PAAD pancreatic adenocarcinoma

PCPG pheochromocytoma and paraganglioma

PDCD1 programmed cell death 1

PDCD1LG2 programmed cell death 1 ligand 2

PD-L1 programmed cell death 1 ligand 1

PFI progression-free interval

PRAD prostate adenocarcinoma

RFS recurrence-free survival

SKCM skin cutaneous melanoma

STAD stomach adenocarcinoma

TCGA the cancer genome atlas

TGCT testicular germ cell tumors

THCA thyroid carcinoma

TIICs tumor-infiltrating immune cells

TMB tumor mutation burden

UCEC uterine corpus endometrial carcinoma

UCS uterine carcinosarcoma

UVM uveal melanoma

WGCNA weighted gene co-expression network analysis

frontiers | Frontiers in Pharmacology

TYPE Original Research
PUBLISHED 13 September 2022
DOI 10.3389/fphar.2022.997842

Check for updates

OPEN ACCESS

EDITED BY
Ting Wang,
Sichuan Cancer Hospital, China

REVIEWED BY
Jie Fu,
The Second Xiangya Hospital of Central South University, China
Lincan Duan,
Third Affiliated Hospital of Kunming Medical University, China

*CORRESPONDENCE
Shu Yongqian,
yongqian_shu@163.com

†These authors have contributed equally to this work

SPECIALTY SECTION
This article was submitted to Pharmacology of Anti-Cancer Drugs, a section of the journal Frontiers in Pharmacology

RECEIVED 19 July 2022
ACCEPTED 22 August 2022
PUBLISHED 13 September 2022

CITATION
Mengyan X, Kun D, Xinming J, Yutian W and Yongqian S (2022), Identification and verification of hub genes associated with the progression of non-small cell lung cancer by integrated analysis. *Front. Pharmacol.* 13:997842. doi: 10.3389/fphar.2022.997842

COPYRIGHT
© 2022 Mengyan, Kun, Xinming, Yutian and Yongqian. This is an open-access article distributed under the terms of the Creative Commons Attribution License (CC BY). The use, distribution or reproduction in other forums is permitted, provided the original author(s) and the copyright owner(s) are credited and that the original publication in this journal is cited, in accordance with accepted academic practice. No use, distribution or reproduction is permitted which does not comply with these terms.

Identification and verification of hub genes associated with the progression of non-small cell lung cancer by integrated analysis

Xie Mengyan[1†], Ding Kun[2,3,4†], Jing Xinming[1†], Wei Yutian[5†] and Shu Yongqian[1,4*]

[1]Department of Oncology, The First Affiliated Hospital of Nanjing Medical University, Nanjing, China, [2]Department of Molecular Cell Biology and Toxicology, Center for Global Health, School of Public Health, Nanjing Medical University, Nanjing, China, [3]Key Laboratory of Modern Toxicology of Ministry of Education, School of Public Health, Nanjing Medical University, Nanjing, China, [4]Jiangsu Key Lab of Cancer Biomarkers, Prevention and Treatment, Collaborative Innovation Center for Cancer Personalized Medicine, Nanjing Medical University, Nanjing, China, [5]Department of Neurosurgery, The First Affiliated Hospital of Nanjing Medical University, Nanjing, Jiangsu, China

Objectives: Lung cancer is one of the most common cancers worldwide and it is the leading cause of cancer-related mortality. Despite the treatment of patients with non-small cell lung carcinoma (NSCLC) have improved, the molecular mechanisms of NSCLC are still to be further explored.

Materials and Methods: Microarray datasets from the Gene Expression Omnibus (GEO) database were selected to identify the candidate genes associated with tumorigenesis and progression of non-small cell lung carcinoma. The differentially expressed genes (DEGs) were identified by GEO2R. Protein-protein interaction network (PPI) were used to screen out hub genes. The expression levels of hub genes were verified by GEPIA, Oncomine and The Human Protein Atlas (HPA) databases. Survival analysis and receiver operating characteristic (ROC) curve analysis were performed to value the importance of hub genes in NSCLC diagnosis and prognosis. ENCODE and cBioPortal were used to explore the upstream regulatory mechanisms of hub genes. Analysis on CancerSEA Tool, CCK8 assay and colony formation assay revealed the functions of hub genes in NSCLC.

Results: A total of 426 DEGs were identified, including 93 up-regulated genes and 333 down-regulated genes. And nine hub genes (CDC6, KIAA0101, CDC20, BUB1B, CCNA2, NCAPG, KIF11, BUB1 and CDK1) were found to increase with the tumorigenesis, progression and cisplatin resistance of NSCLC, especially EGFR- or KRAS-mutation driven NSCLC. Hub genes were valuable biomarkers for NSCLC, and the overexpression of hub genes led to poor survival of NSCLC patients. Function analysis showed that hub genes played roles in cell cycle and proliferation, and knockdown of hub genes significantly inhibited A549 and SPCA1 cell growth. Further exploration demonstrated that copy number alterations (CNAs) and transcription activation may account for the up-regulation of hub genes.

Conclusion: Hub genes identified in this study provided better understanding of molecular mechanisms within tumorigenesis and progression of NSCLC, and provided potential targets for NSCLC treatment as well.

KEYWORDS

NSCLC, hub genes, bioinformatics, integrated analysis, biomarker

1 Introduction

Malignant tumors are important diseases that seriously threaten human health, among which, lung cancer occupies an important position. According to the 2020 CA reports, the global morbidity and mortality of lung cancer ranked second and first, respectively, with 2.21 million new cases and 1.80 million deaths worldwide (Sung et al., 2021). NSCLC is a subtype of lung cancer based on histopathology, including large cell carcinoma, squamous cell carcinoma (LUSC) and adenocarcinoma (LUAD). NSCLC accounts for 85% of lung cancers and the 5-year survival rate is less than 15% (Duma et al., 2019). In the past 2 decades, the investigation into NSCLC tumorigenesis has made great progress, increasing our understanding of NSCLC treatment strategy. Nowadays, the use of small molecular inhibitors and immunotherapy has brought unprecedented survival benefits to NSCLC patients (Herbst et al., 2018). However, because of individual differences and tumor heterogeneity, the problems of drug toxicities, side effects, single target and drug tolerance are still prominent, and the overall cure rates and survival rates of NSCLC are still low (Konieczkowski et al., 2018).

Overactivated oncogenes and mutated or inactivated tumor suppressor genes account for tumorigenesis. A variety of genes and signal regulatory networks are involved in tumorigenesis, leading to the occurrence and development of NSCLC (Hanahan and Weinberg, 2011). Currently, an increasing number of driver genomic alterations with potential targeted treatments have been identified in NSCLC. For example, activating gene mutations of epidermal growth factor receptor (EGFR), anaplastic lymphoma kinase (ALK), pro-oncogene receptor tyrosine kinase (ROS1) and serine/threonine protein kinase (BRAF) or fusion has now become the target of NSCLC kinase inhibitor therapy (Rotow and Bivona, 2017). However, EGFR mutations were observed in 10–20% of white patients (Dearden et al., 2013), translocations of ALK were identified in 2–7% of patients with NSCLC (Mesaros et al., 2014) and ROS1 in 1–2% of patients with NSCLC (Bergethon et al., 2012). Therefore, it is particularly important to further explore the molecular mechanism of NSCLC tumorigenesis and progression, thus identifying new biomarkers and therapeutic targets.

In this study, we reanalyzed three gene expression profiles from the GEO repository. The DEGs between NSCLC tissues and normal tissues were confirmed by the GEO2R. We also performed the GO and KEGG pathway analysis to detect the functions of DEGs in NSCLC. Through the PPI network, we found there were nine hub genes (CDC6, KIAA0101, CDC20, BUB1B, CCNA2, NCAPG, KIF11, BUB1, CDK1) in strong connection within the network. Then, the mRNA and protein expression levels in NSCLC were confirm by GEPIA, Oncomine and HPA databases. The level of protein expression was the most important as proteins were genetic products that eventually do their job. HPA collected reliable data on the protein expression of CDC6, CDC20, KIF11, CCNA2, NCAPG, CDK1. Some of these proteins showed strong positive expression in immunohistochemistry of lung cancer, making them promising markers for immunohistochemical diagnosis of NSCLC. Moreover, GEO data regarding gene-edited mouse models revealed that the expression of hub genes increased with the progression of NSCLC, and cohort study in lung cancer showed that the hub genes may be involved in EGFR- or KRAS-mutation driven NSCLC progression. The survival analysis demonstrated that the overexpression of hub genes was positively correlated with worse survival of NSCLC patients. We also validated their significance as biomarkers in NSCLC and confirmed their combined diagnostic value by ROC curve analysis. CNAs, a hallmark in the cancer genome, together with histone modifications and transcription factors, accounted for the ectopic expression of hub genes. The CancerSEA Tool indicated that the hub genes played important roles in cell cycle and cell proliferation, so we designed siRNAs targeting these hub genes to test their functions in NSCLC cell lines. CCK8 assay and colony formation assay both proved that silencing hub genes significantly inhibited A549 and SPCA1 cell growth, demonstrating the promoting abilities of hub genes in NSCLC development. The schematic representation of this study is shown in Figure 1.

2 Materials and methods

2.1 Microarray data

The GEO database (http://www.ncbi.nlm.nih.gov/geo/) is an international public repository that records and publishes microarrays, next-generation sequencing and other forms of high-throughput functional genomics data (Barrett et al., 2013). We selected the microarray datasets GSE19804, GSE43458 and GSE18842 to screen out candidate DEGs. GSE84447, GSE52248, GSE33479, GSE31210 and GSE161584 datasets were used to verify the expression of hub

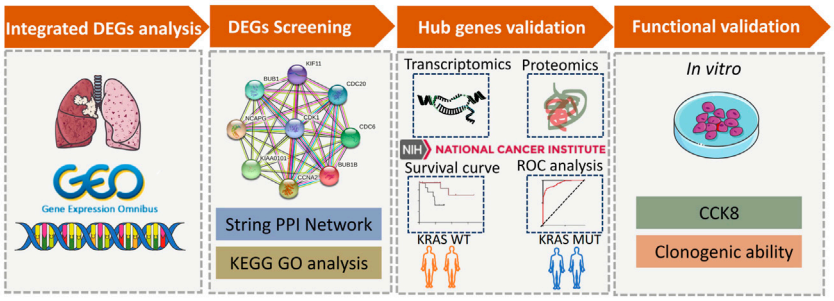

FIGURE 1
A schematic representation of the research methods. Diagram showing the four main modules in this study, including DEGs analysis, DEGs screening, hub genes validation and functional validation.

genes. Detail information of GEO profiles are shown in Supplementary Table S1.

2.2 Identification of DEGs

GEO2R is an interactive web tool that allows users to compare two or more sample groups in the GEO series to identify genes that are differentially expressed under different experimental conditions, the results are presented in the form of gene table sorted by significance. Consequently, DEGs between NSCLC tissues and normal tissues were confirmed by the GEO2R. The adjusted p values were utilized to reduce the false positive rate using the Benjamin and Hochberg false discovery rate method by default (Wei et al., 2019). We defined the cutoff value as $|\mathrm{Log_2FC}$ (fold change) $| \geq 2$ and $p < 0.05$ for further analysis. Then, Venn diagrams showing the number of overlapping DEGs in the three GEO datasets was performed by Venn package (http://bioinformatics.psb.ugent.be/webtools/Venn/). Finally, forest plots and heatmap were performed by the software GraphPad Prim 8.

2.3 GO and KEGG pathway of DEGs

The Gene Ontology (GO) is a widely used ontology in the field of bioinformatics, covering three aspects of biology: biological process (BP), cellular component (CC) and molecular function (MF) (Gene Ontology, 2015). Kyoto Encyclopedia of Genes and Genomes (KEGG) is a utility database resource for understanding advanced functions and biological systems (such as cells, organisms, and ecosystems) from the molecular level information, especially large molecular datasets generated by genome sequencing and other high-throughput experimental techniques (Kanehisa et al., 2019). Database for Annotation, Visualization and Integrated Discovery (DAVID, http://David.ncifcrf.gov/) is a bioinformatics resources that contains a large amount of integrated information and analysis tools designed to provide interpretation for large gene and protein lists (Huang Da et al., 2009). GO and KEGG pathway analyses of these DEGs were performed with DAVID.

2.4 Protein-protein interaction (PPI) network

To clarify the node molecules that play a key role in the regulation of tumorigenesis and development, we constructed a PPI network. Search Tool for the Retrieval of Interacting Genes (STRING) was used to build PPI networks (Szklarczyk et al., 2011). First, we use STRING to build a PPI network, then use Cytoscape software to visualize the results obtained from the STRING database, and finally use MCODE plugin of Cytoscape software to screen hub genes which have the highest node scores and the strongest connectivity.

2.5 Overall survival (OS) of DEGs

The Kaplan Meier plotter (https://kmplot.com/analysis/) can analyze the effect of 54,000 genes on survival in 21 cancer types. Gene expression data and OS data were obtained from GEO and TCGA(Gyorffy et al., 2013). To analyze the prognostic value of hub genes, the tumor and normal tissues were divided into two groups based on median expression (high vs. low expression) and the curves of OS were performed by the Kaplan Meier plotter with the hazard ratio (HR) with 95% confidence intervals (CIs) and log rank p value.

2.6 Receiver operating characteristic (ROC) curve

The ROC curve is a comprehensive index reflecting the continuous variables of sensitivity and specificity. Area under

the ROC curve (AUC) reflects diagnostic value of the test. In general, an AUC above 0.9 is considered a highly accurate diagnostic test. The ROC curve was conducted by Graph Pad Prism 7.0 based on the GEO chip data. The ROC curve of multi-factors was conducted by SPSS statistics 20.0 analyzed by logistic regression.

2.7 Cell culture and siRNA transfection

The A549 cell line was cultured in RPMI 1640 medium (Gibco, Carlsbad, CA, United States) and the SPCA1 cell line was cultured in Dulbecco's modified eagle medium. Cells were supplemented with 100 μg/ml streptomycin, 100 U/ml penicillin and 10% fetal bovine serum (FBS) at 37°C in a humidified atmosphere of 5% CO2. The siRNAs (Supplementary Table S2) targeting hub genes were designed and synthesized by RiboBio (Guangzhou, China). The siRNAs were transfected into the cells with Lipofectamine 3,000 (Invitrogen).

2.8 Cell counting kit-8 (CCK8) assay

After 48 h of transfection, A549 and SPCA1 cells (3×10^3) were seeded into 96-well plates (Corning). Then, 10 μL of CCK8 (Beyotime, Jiangsu, China) solution was added to each well at the point of 48 h. After 1 h of incubation at 37°C, the absorbance at 450 nm was measured using an automatic microplate reader (Synergy4; BioTek, Winooski, VT, United States).

2.9 Colony formation assay

After 48 h of transfection, A549 (300) and SPCA1 (400) cells were seeded into 6-well plates (Corning). Cells were cultured until the colony reached 2 mm wide. The cells were fixed with 1% paraformaldehyde (Beyotime) for 1 h and stained with crystal violet (Beyotime) for 12 h.

2.10 Western blot assay

Proteins in cells were extracted with RIPA lysis buffer (Thermo Fisher). Western blot assays were performed according to details previously reported (Zhou et al., 2008). The immunocomplexes were detected with ECL Western Blotting Substrate (Thermo Fisher), visualized with BIO-RAD (BIO-RAD Gel Doc XR+, United States). The following antibodies were used (1:1000): anti-α-tubulin (Beyotime, AF0001); anti-BUB1 (Proteintech, 13330-1-AP); anti-BUB1B (Proteintech, 11504-2-AP); anti-CCNA2 (Proteintech, 18202-1-AP); anti-CDC6 (Proteintech, 11640-1-AP); anti-CDC20 (Proteintech, 10252-1-AP); anti-CDK1 (Proteintech, 19532-1-AP); anti-KIF11 (Proteintech, 23333-1-AP); anti-KIAA0101 (Santa Cruz, sc-390515); anti-NCAPG (Proteintech, 24563-1-AP).

2.11 RNA preparation and quantitative real-time PCR (qRT-PCR)

Total RNA was extracted from the cells using the TRIzol reagent (Invitrogen, MA, United States). Isolated RNA was used for the reverse transcription reaction with HiScript Q RT SuperMix for qPCR (Vazyme, Jiangsu, China). Quantitative RT-PCR was carried out with SYBR Green PCR Master Mix (Vazyme) using an ABI Prism 7,900 Sequence detection system (Applied Biosystems, Canada). GAPDH was used as an internal control, and the results for each sample were normalized to GAPDH expression. The primers are listed in Supplementary Table S3.

3 Results

3.1 Identification of DEGs and hub genes in NSCLC

3.1.1 DEGs were identified *via* GEO profiles of NSCLC

Three microarray profiles (GSE19804/GSE43458/GSE18842) were obtained from GEO database. The cut-off was $|Log_2FC| \geq 2$ and p value <0.05. A total of 1280, 884 and 2,176 DEGs was observed in GSE19804, GSE43458 and GSE18842, respectively (Figures 2A–C). The Venn diagrams displayed that there were 426 genes found in all three profiles, including 93 up-regulated genes and 333 down-regulated genes in NSCLC tissues compared to normal tissues (Figures 2C, D). Twenty genes were visualized in the heatmap when the cut-off was limited to $|Log_2FC| \geq 2.5$ ($p < 0.05$) (Figures 2F).

For a deeper understanding on the selected DEGs, we performed the GO function and KEGG pathway enrichment analysis (Supplementary Figure S1). Biological process enrichment showed that up-regulated DEGs were mainly enriched in collagen fibril organization, microtubule-based movement and regulation of cell proliferation (Supplementary Figure S1A), while down-regulated DEGs were mainly enriched in transforming growth factor beta receptor signaling pathway, receptor internalization and positive regulation of angiogenesis (Supplementary Figure S1E). By KEGG pathway analysis of DEGs, we found that most of the up-regulated DEGs were enriched in cell cycle and ECM-receptor interaction (Supplementary Figure S1D), while most of the down-regulated DEGs were enriched in cell adhesion molecules and PARP signaling pathway (Supplementary Figure S1F).

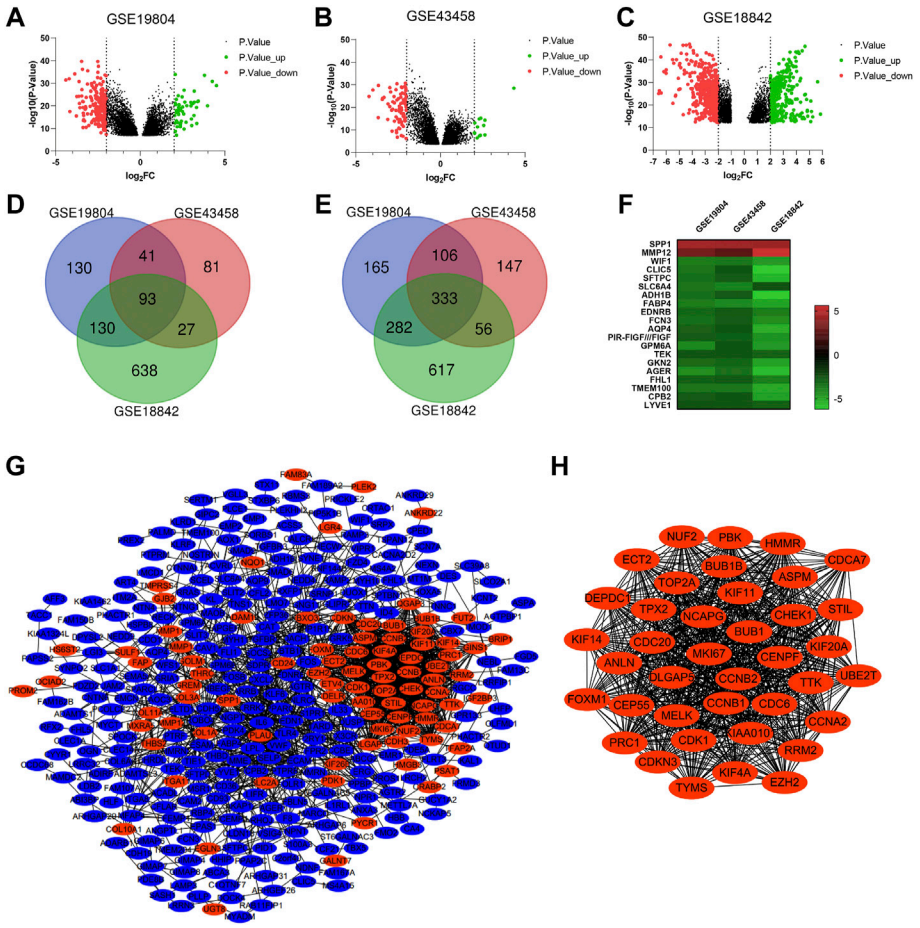

FIGURE 2
Identification of overlapping DEGs and PPI construction of DEGs. **(A-C)** Volcano plots showing DEGs in NSCLC tissues compared to normal tissues in GSE19804/GSE43458/GSE18842 ($|Log_2FC| \geq 2$ and $p < 0.05$). **(D and E)** Venn diagrams showing the number of overlapping DEGs in the three GEO datasets (D. up-regulated genes E. down-regulated genes). **(F)** Heatmap of the top representative DEGs ($|Log_2FC| \geq 2.5$ and $p < 0.05$). **(G)** PPI network of DEGs constructed by the String and Cytoscape software. **(H)** The most significant module of PPI network based on the score of each node. (Red represents up-regulated, blue represents down-regulated).

3.1.2 Hub genes were identified *via* PPI network and module analysis

To investigate the protein interactions between the screened DEGs, PPI network was constructed by the String and Cytoscape software (Figure 2G). The PPI network of DEGs consisted of 369 nodes and 1835 edges. We used the MCODE plugin to find the most significant module of the PPI network, which includes 39 nodes and 720 edges (Figure 2H). Interestingly, compared to normal tissues, the genes in the most connected module were all up-regulated in NSCLC tissues. We considered the top nine genes as the hub genes based on the score of each node: CDC6 (cell division cycle 6), NCAPG (non-SMC condensin I complex subunit G), KIF11 (kinesin family member 11), KIAA0101, CDC20 (cell division cycle 20), BUB1 (mitotic checkpoint serine/threonine kinase), CDK1 (cyclin dependent kinase 1), CCNA2 (cyclin A2), BUB1B (BUBI mitotic checkpoint serine/threonine kinase B). Go analysis of the top nine genes indicated that these hub genes were mainly associated with cell division and kinase binding (Supplementary Table S4). KEGG pathway enrichment showed that these hub genes were enriched in cell cycle, progesterone-mediated oocyte maturation, oocyte meiosis and viral carcinogenesis (Supplementary Table S4).

3.2 Verification of hub genes expression in NSCLC

3.2.1 mRNA and protein expression levels of hub genes increased in NSCLC

To further confirm the expression level of hub genes in the NSCLC tissues and normal tissues, we took advantage of the online database GEPIA (Tang et al., 2017) (Gene Expression

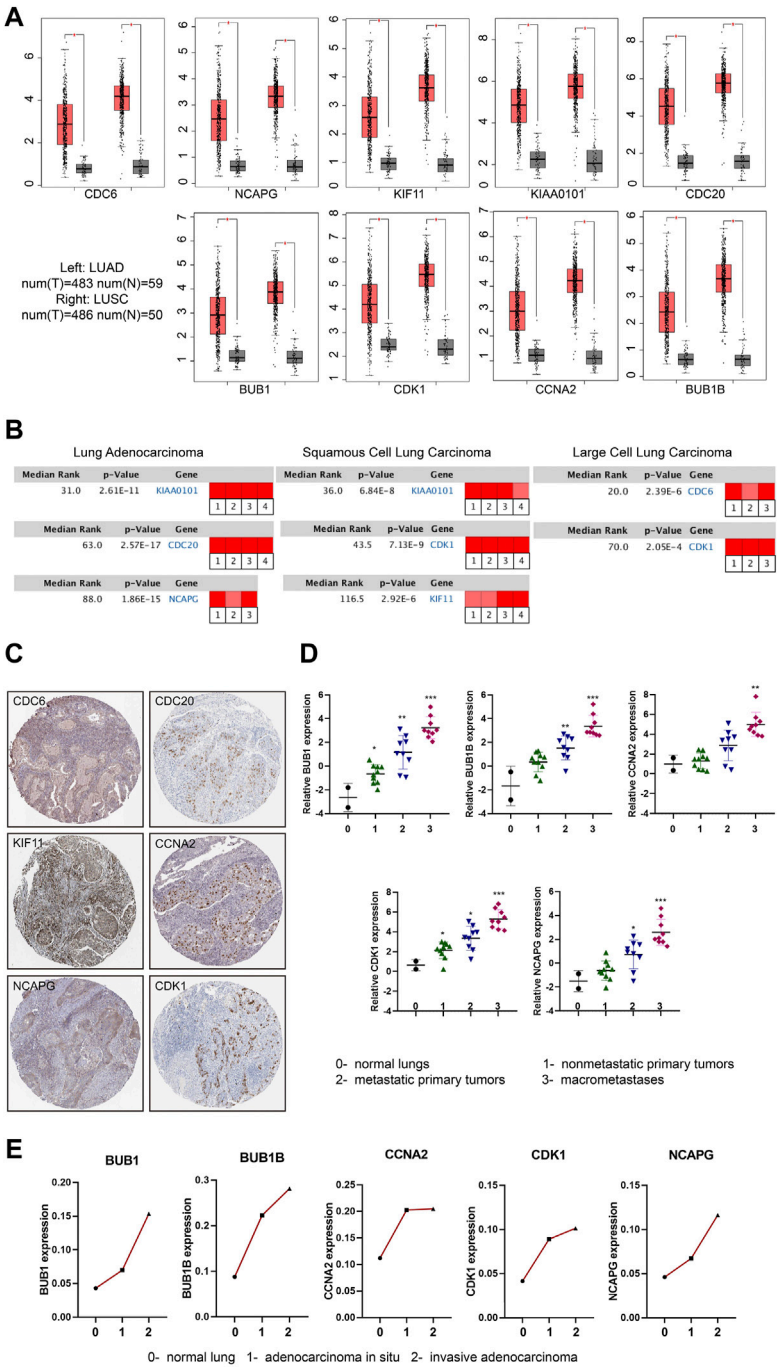

FIGURE 3
mRNA and protein expression changes of hub genes in NSCLC. **(A)** Boxplots (Red box: tumor tissue; Grey box: normal tissue) showing the expression levels of hub genes based on the TCGA database. The red and grey boxes represent NSCLC and normal tissues, respectively. $|Log_2FC|$ cutoff = 1, *p* value cutoff = 0.05. **(B)** Rank of hub genes changes in subtypes of NSCLC according to Oncomine database (Red represents up-regulated). $|Log_2FC|$ cutoff = 1, *p* value cutoff = 0.001. **(C)** Immunohistochemical staining of hub genes in NSCLC tumor cells included in HPA database. **(D)** The expression of hub genes with the progression of LUAD in GSE84447 dataset: 0- normal lungs (n = 2), one- nonmetastatic primary tumors (n = 10), two- metastatic primary tumors (n = 9),3- macrometastases (n = 9). **(E)** The expression of hub genes with the progression of LUAD in GSE52248 dataset. Each point represents the average value of the group (each group: n = 6). *p < 0.05, **p < 0.01, ***p < 0.001, ****p < 0.0001.

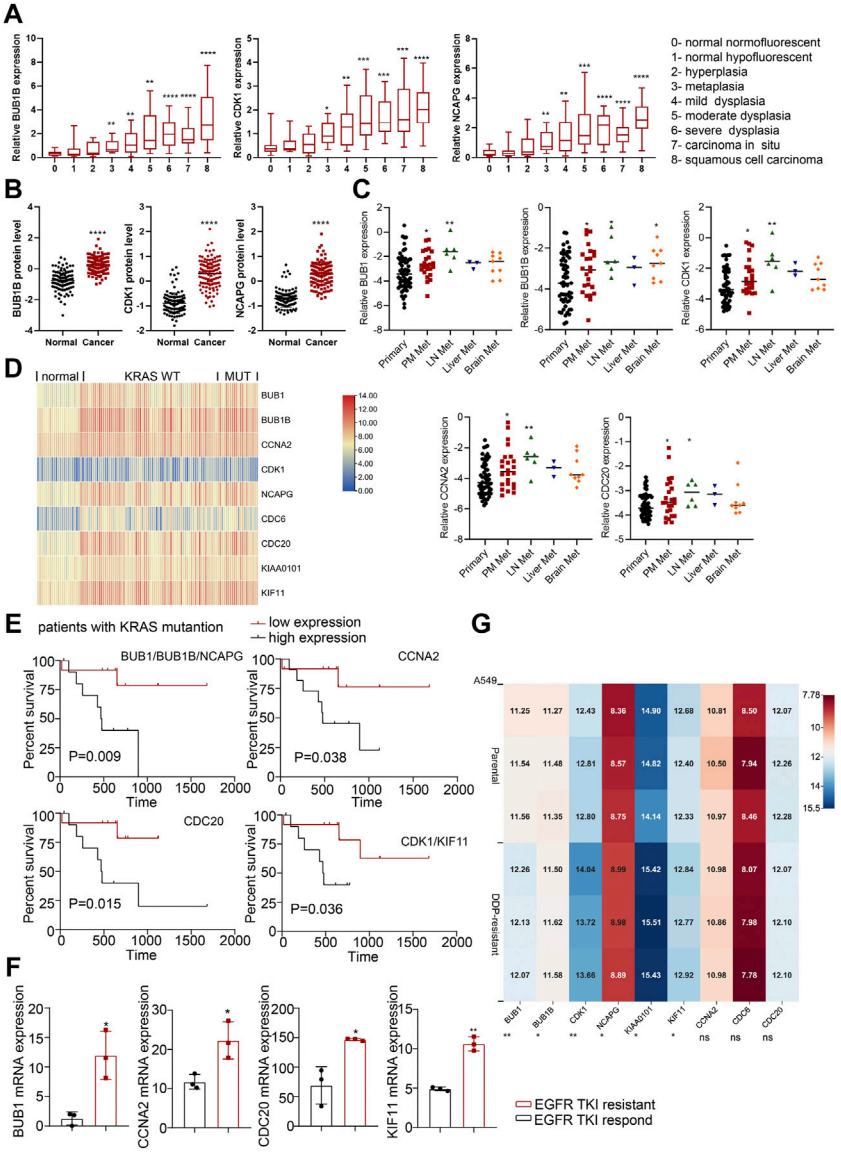

FIGURE 4
The roles of hub genes in LUSC and in EGFR- or KRAS-mutation driven NSCLC. **(A)** The expression levels of hub genes in different stages of LUSC tumorigenesis (122 samples from 77 patients). **(B)** The protein expression levels of hub genes in LUSC in CPTAC database. **(C)** The expression levels of hub genes (BUB1, BUB1B, CDK1, CCNA2 and CDC20) in lung adenocarcinomas identified patients with dismal prognosis. GSE13213: Primary lung cancer: n = 58; PM metastasis: n = 24; LN metastasis: n = 6; Liver metastasis: n = 3; Brain metastasis: n = 9. **(D)** Heatmap of hub gene expression in KRAS-mutant and KRAS-wild type lung cancer compared to normal lung tissues (GSE31210). Normal lung: n = 20, KRAS MUT: n = 20, KRAS WT: n = 68. **(E)** Kaplan-Meier analysis of hub genes in LUAD with KRAS mutation from TCGA. **(F)** Hub gene expression in EGFR-TKI-sensitive and TKI-resistant lung cancer tissues in GSE161584 dataset. **(G)** Heatmap of hub gene expression in DDP-resistant A549 cells and control cells (GSE108214). *p < 0.05, **p < 0.01, ***p < 0.001, ****p < 0.0001.

Profiling Interactive Analysis) (http://gepia.cancer-pku.cn/) and Oncomine (http://www.oncomine.org/). We found that the expression levels of the hub genes (CDC6, KIAA0101, CDC20, BUB1B, CCNA2, NCAPG, KIF11, BUB1 and CDK1) were significantly up-regulated in NSCLC tissues compared to normal tissues (Figure 3A). Interestingly, we found the expression levels of hub genes were slightly higher in LUSC than that in LUAD. Based on Oncomine database, we found that all the hub genes were related to NSCLC and were expressed differently in varied pathological types of NSCLC. The most obvious changed genes in LUAD, LUSC and large cell lung carcinoma were KIAA0101, KIAA0101 and CDC6, respectively (Figure 3B; Supplementary Table S5). Besides the expression of mRNAs, we further analyzed the protein

expression levels of the hub genes. HPA (http://www.proteinatlas.org/) includes the immunohistochemical information of CDC6, CDC20, KIF11, CCNA2, NCAPG and CDK1 proteins. According to the database, most of the hub genes were undetected or low expression in lung tissues. However, in NSCLC tissues, the positive rates of staining were over 60% (positive cases/total cases: CDC6 6/10, CDC20 11/11, KIF11 10/10, CCNA2 10/11, NCAPG 9/10, CDK1 10/12) (Figure 3C; Supplementary Table S6).

3.2.2 Hub genes expression increased with tumorigenesis, progression and chemotherapy resistance of NSCLC

We then used the GEO data regarding gene-edited mouse models (GSE84447 and GSE52248) to observe the role of hub gene expression in the occurrence and development of NSCLC. We found the expression of BUB1, BUB1B, CCNA2, CDK1 and NCAPG increased with the continuous progression of LUAD in mice (Figures 3D, E; Supplementary Figures S2A, B). Similarly, the progression data of LUSC (GSE33479) showed that these nine hub genes were highly expressed in LUSC compared with the initial stage of tumorigenesis (Figure 4A; Supplementary Figure S3A). In addition, the protein levels of hub genes (The National Cancer Institute's Clinical Proteomic Tumor Analysis Consortium, CPTAC) were also high in LUSC (Figure 4B; Supplementary Figure S3B). Considering the high metastasis rate of NSCLC, we further analyzed the relationship between hub genes and distant metastasis of lung cancer (GSE13213). Compared to primary lung cancer, all the expression of hub genes increased in lymph node metastasis samples, and the expression of BUB1, BUB1B, CDK1, CCNA2 and CDC20 were related to peritoneum metastasis (Figure 4C; Supplementary Figure S3C).

KRAS mutations and EGFR mutations are the main mutations driving the development of lung cancer. We analyzed lung cancer cohorts with KRAS mutations (GSE31210) and found that higher hub gene levels (BUB1, BUB1B, NCAPG, CDC20, CDK1, KIF11) were significantly associated with worse OS in lung cancer patients with KRAS mutations (Figures 4D, E; Supplementary Figure S3D). In addition, the expression level of main hub genes (BUB1, CCNA2, CDC20, KIF11) was significantly higher in patients with EGFR TKI-resistant lung cancer tissues (GSE161584) than EGFR TKI-sensitive lung cancer tissues (Figure 4F; Supplementary Figure S3E). Taken together, these hub genes may be involved in EGFR- or KRAS-mutation driven NSCLC progression.

Cisplatin (DDP) resistance is an important reason hindering the chemotherapy efficacy of lung cancer. We analyzed the transcriptome data of A549 cells before and after DDP resistance (GSE108214) to study the expression of hub genes in them. The results showed that BUB1, BUB1B, CDK1, NCAPG, KIAA0101 and KIF11 were highly expressed in DDP-resistant A549 cells (Figure 4G), which indicated that hub genes might promote chemoresistance in NSCLC.

3.3 Survival analysis and ROC curve analysis of hub genes in NSCLC

3.3.1 Up-regulated hub genes led to poor OS of NSCLC patients

To further confirm the correlation with the survival of clinical patients, we used the online bioinformatics tool Kaplan-Meier Plotter (http://kmplot.com/). The results showed that NSCLC patients with higher expression levels of CDC6 [HR = 1.88 (1.65–2.14), $p < 1e\text{-}16$], KIAA0101 [HR = 1.71 (1.5–1.94), $p = 2.2e\text{-}16$], CDC20 [HR = 1.82 (1.6–2.07), $p < 1e\text{-}16$], BUB1B [HR = 1.7 (1.5–1.94), $p = 2.2e\text{-}16$], CCNA2 [HR = 1.76 (1.55–2), $p < 1e\text{-}16$], NCAPG [HR = 1.59 (1.4–1.8), $p = 8.8e\text{-}13$], KIF11 [HR = 1.52 (1.34–1.73), $p = 1.1e\text{-}10$], BUB1 [HR = 1.83 (1.61–2.08), $p < 1e\text{-}16$], CDK1 [HR = 1.4 (1.23–1.59), $p = 2.3e\text{-}07$] had worse OS (Figure 5A).

3.3.2 Hub genes were valuable indicators for NSCLC

Next, we used GEO chip data (GSE19804, GSE43458 and GSE18842) to determine the feasibility of hub genes as biomarkers for NSCLC. ROC curve of independent factors showed that all nine hub genes had moderate or above diagnostic value for NSCLC (Figures 5B–F), among which CDC20, BUB1B, BUB1 and KIF11 had significant diagnostic value, and the areas under the curve were 0.9594 [95% CI: 0.9413 to 0.9775], 0.95 [95% CI: 0.9284 to 0.9716], 0.9318 [95% CI: 0.9069 to 0.9567] and 0.9111 [95% CI: 0.8816 to 0.9406], respectively ($p < 0.0001$). However, considering that the diagnosis of diseases should not rely on a single indicator, but often requires the joint diagnosis of multiple indicators, we incorporated nine hub genes into the NSCLC diagnosis system, fitted a regression equation (z = 0.031* BUB1B+ 2.666* CDC20 + 0.138* KIF11 + 0.879* BUB1+ 2.224* CDC6- 1.922* CDK1- 0.793* CCNA2+ 2.052* KIAA0101–0.983* NCAPG- 26.192) for the diagnosis score of NSCLC through logistic regression analysis, and conducted ROC analysis on the prediction probability of the regression analysis (Figure 5G). We found that the area under the curve increased to 0.9784 (95% CI: 0.966 to 0.9908, $p < 0.0001$). Compared with ROC analysis of a single indicator, multi-factor combined diagnosis has higher accuracy and application value.

3.4 Investigation into upstream regulatory mechanisms of hub genes

3.4.1 Copy number alterations

We next sought to address the correlation between CNA frequencies and expression levels of the hub genes via online cancer genomics data sets cBioPortal (http://www.cbioportal.org/). We found that there are different degrees of Hub genes changes in the genomes of 6,322 patients from 18 NSCLC studies.

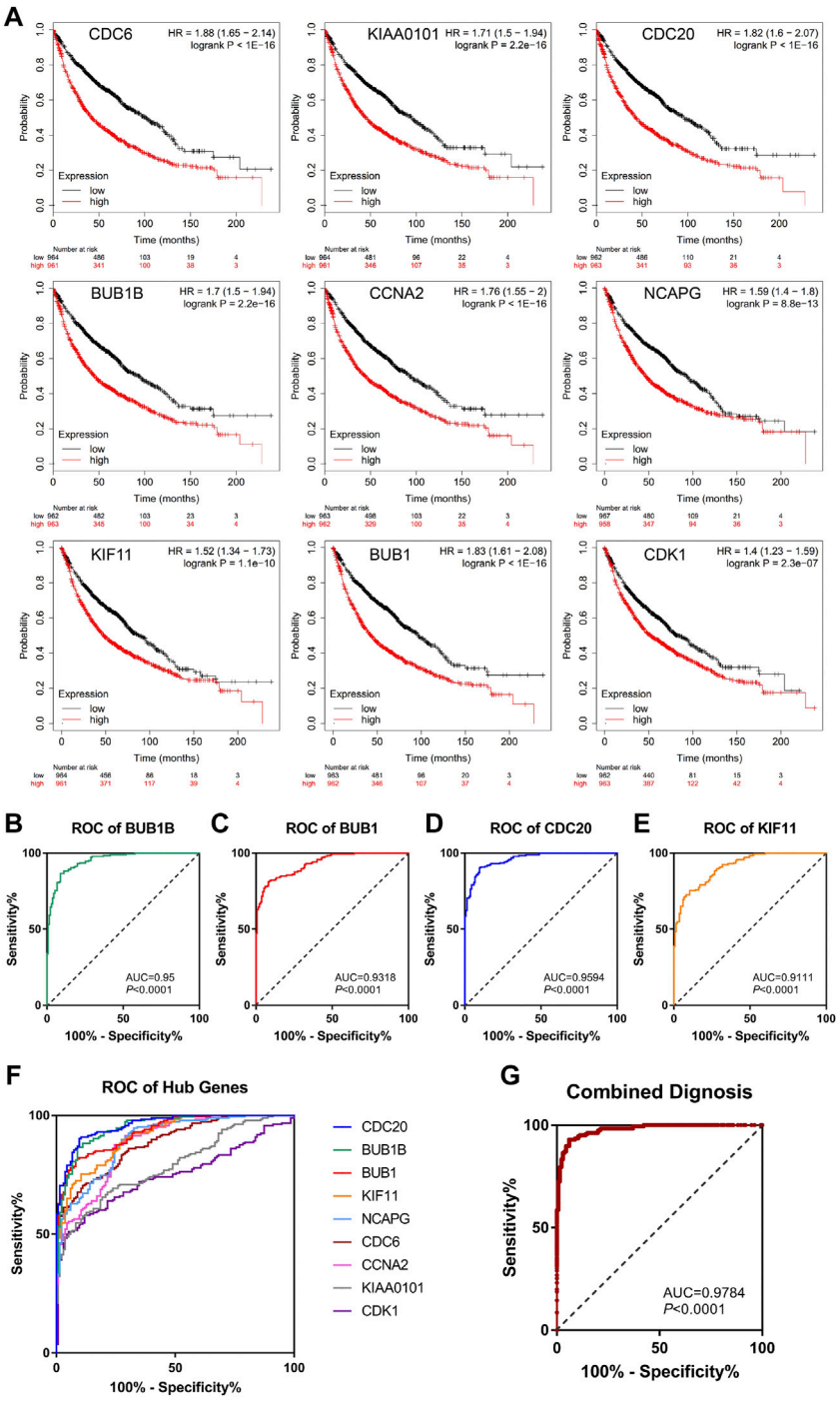

FIGURE 5
Survival analysis and ROC curve analysis of hub genes in NSCLC. **(A)** Kaplan-Meier survival curves of OS based on the hub genes (CDC6, KIAA0101, CDC20, BUB1B, CCNA2, NCAPG, KIF11, BUB1, CDK1) expression using the online bioinformatics tool Kaplan-Meier Plotter. **(B–F)** Individual ROC curve of hub genes according to the chip data of GSE19804, GSE43458 and GSE18842. **(G)** Combined ROC curve of hub genes according to the chip data of GSE19804, GSE43458 and GSE18842.

Among them, the gene alterations of hub genes were less than 2%, and the CNA types of each gene were different. While CNA events in deep depletion and amplification rarely or less occurred, most hub genes often underwent shallow depletion or copy gain (Supplementary Figures S4A–D). In addition, we also found that the alterations of CDC6 and CCNA2, KIF11 and

A

A	B	Neither	A Not B	B Not A	Both	Log2 Odds Ratio	*P*-value	Tendency
CDC6	CCNA2	3894	89	26	4	2.751	0.005	Co-occurrence
KIF11	CDK1	3900	58	51	4	2.399	0.01	Co-occurrence
CDC20	CCNA2	3914	69	27	3	2.656	0.016	Co-occurrence
CCNA2	BUB1	4055	27	90	3	2.324	0.028	Co-occurrence
CDC6	CDK1	3869	89	51	4	1.77	0.038	Co-occurrence

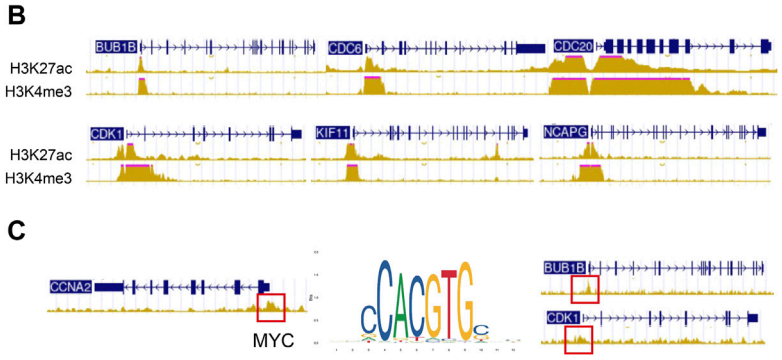

FIGURE 6
Co-occurrence of hub gene alterations in NSCLC and ChIP-seq of histone and transcription factors in A549 cells. **(A)** Five pairs of hub genes tending to have concurrent CNAs in NSCLC. **(B)** The characteristic peaks (fold change over control) of H3K4me3 and H3K27ac at the promoter region of BUB1B, CDC6, CDC20, CDK1, NCAPG and KIF11. **(C)** The characteristic peaks (fold change over control) of MYC at the promoter region of BUB1B, CDK1 and CCNA2.

CDK1, CDC20 and CCNA2, CCNA2 and BUB1, and CDC6 and CDK1 had the tendency of co-occurrence (Figure 6A).

3.4.2 Transcriptional activation

Besides CNA, chromatin immunoprecipitation (ChIP) assay of A549 (ENCSR778NQS, ENCSR000DPD) from ENCODE database verified high expression of H3K4me3 and H3K27ac at the promoter region of BUB1B, CDC6, CDC20, CDK1, NCAPG and KIF11, which may lead to the upregulation of these hub genes (Figure 6B). Some overexpressed transcription factors in lung cancer also activates the expression of hub genes. For example, characteristic peak of MYC was demonstrated by TF ChIP-seq in A549 (ENCSR000DYC) at the promoter region of BUB1B, CDK1 and CCNA2 (Figure 6C). So, transcriptional activation may partially account for the upregulation of hub genes.

3.5 The biological functions of hub genes in NSCLC

3.5.1 Hub genes were involved in cell cycle and cell proliferation

In order to detect the function of hub genes in NSCLC, we first used the CancerSEA Tool. The results showed that the single cell expression levels of hub genes were positively correlated with the progression of cell cycle, proliferation, invasion, DNA damage and EMT (Supplementary Figure S4E). Cell cycle and cell proliferation were the most relevant functions, among which KIAA0101 and CCNA2 took the first place, respectively (Figure 7A). Expression levels of hub genes were also positively correlated with the Ki-67 and PCNA expression (proliferation markers), which was in agreement with the opinion that hub genes were key factors in lung cancer cell proliferation (Figure 7B).

3.5.2 Down-regulated hub genes inhibited NSCLC cell growth

Then, we constructed two si-RNAs (si-RNA#1 and si-RNA#2) of each hub gene and transfected them into A549 and SPCA1 cells. The efficiency of si-RNAs were verified by qRT-PCR and western blot (Supplementary Figure S5). CCK8 assay revealed that silencing hub genes significantly inhibited the proliferation rate of NSCLC cells (Figures 7C, D; Supplementary Figures S6A, B). The inhibiting effect of each si-RNAs was different in 2 cell lines, but we found that the proliferation-promoting function of KIF11 was one of the most obvious in both cell lines, which was in consistent with the results in CancerSEA. We also conducted colony formation assay and the result showed that silencing hub genes remarkably decreased the numbers of colony (Figures 7E–H; Supplementary Figures S6C–F). CCK8 and colony formation assays demonstrated that the hub genes played important roles in NSCLC cell growth.

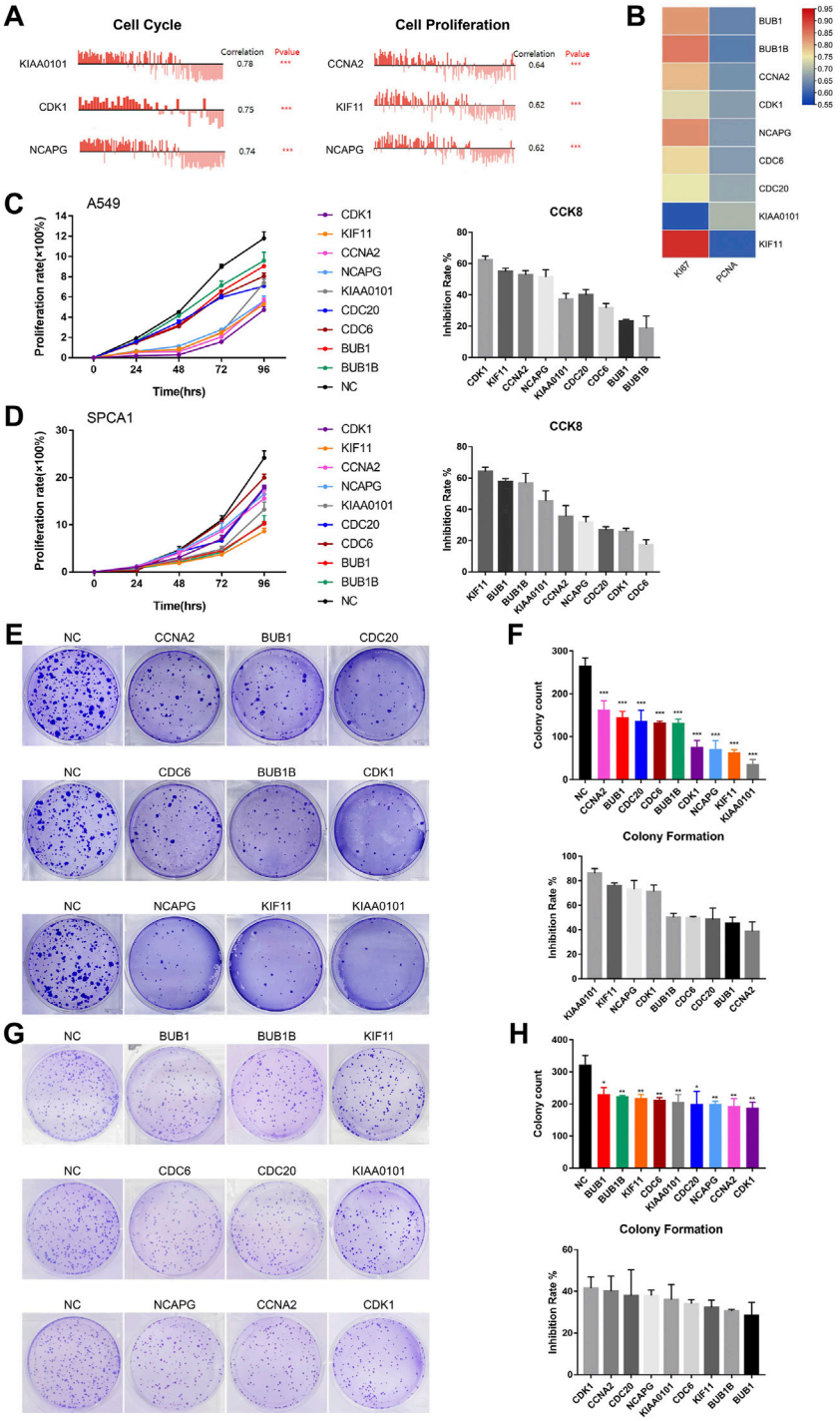

FIGURE 7
The biological functions of hub genes in NSCLC. **(A)** The correlation between cell cycle, cell proliferation and hub gene expression at single cell level in NSCLC via CancerSEA database. **(B)** Correlation between Ki-67, PCNA and hub gene expression based on TCGA-LUAD analysis, n = 526. Statistical significance was tested using Pearson's correlation coefficient. Correlation scores were analyzed by the Pearson correlation test. **(C)** Assessment of the proliferation of A549 cells transfected with siRNAs#1 targeting hub genes by CCK8 assay (Left). The inhibition rate of each siRNA#1 on cell proliferation in CCK8 assay (Right). **(D)** Assessment of the proliferation of SPCA1 cells transfected with siRNAs#1 targeting hub genes by CCK8 assay (Left). The inhibition rate of each siRNA#1 on cell proliferation in CCK8 assay (Right). **(E,F)** Assessment of the colony formation ability of A549 cells transfected with siRNAs#1 targeting hub genes by colony formation assay. The inhibition rate of each siRNA#1 on colony formation. **(G,H)** Assessment of the colony formation ability of SPCA1 cells transfected with siRNAs#1 targeting hub genes by colony formation assay. The inhibition rate of each siRNA#1 on colony formation. *p < 0.05, **p < 0.01, ***p < 0.001, ****p < 0.0001.

4 Discussion

Despite advances in targeted therapy and immunotherapy in advanced NSCLC patients, early detection and prevention can significantly improve clinical outcomes and bring economic benefits to patients. However, there are many challenges in early-stage NSCLC. About 20% early-stage lung cancer patients faced recurrence and metastasis after surgery worldwide (Hirsch et al., 2017; Herbst et al., 2018). Therefore, more comprehensive understanding of lung cancer based on transcriptomics can fill the gap between genomic abnormalities and oncogenic protein mechanisms. In this study, we screened a series of hub genes based on GEO datasets and these hub genes are associated with prognosis of NSCLC. Further pathway analysis revealed that most of the up-regulated DEGs were enriched in cell cycle and ECM-receptor interaction, which are vital events in hallmarks of tumor. In addition, combination of these genes can better predict the prognosis of NSCLC.

CDC20, CDK1, CCNA2 and CDC6 are four cyclin-related genes in screened hub genes. At the heart of the cell cycle, CDKs drive cells through different phases of the cell cycle. Importantly, CDK1 can replace other CDKs and has been found to be sufficient to drive the mammalian cell cycle (Santamaria et al., 2007; Haneke et al., 2020). CDC6 is a key replication licensing factor that plays a vital role in regulating DNA replication (Borlado and Mendez, 2008). Moreover, E6AP-low/CDC6-high/P16ink4a-low protein abundance profiles are associated with hypomethylation of the gene encoding P16ink4a (CDKN2A) and poorer prognosis in NSCLC patients (Lim and Townsend, 2020). Recent studies have shown that CDC20 promotes several types of cancer progression, including glioma and lung cancer (Wang et al., 2013; Wang et al., 2015). Aurora B phosphorylates BUB1 to facilitate spindle assembly checkpoint signaling, and target Aurora B kinase can prevent and overcome resistance to EGFR inhibitors in lung cancer (Tanaka et al., 2021; Roy et al., 2022). KIF11, known as mitotic spindle-specific protein, and its oral inhibitor 4SC-205 demonstrates anti-tumor activity and enhances targeted therapy in primary and metastatic neuroblastoma models (Masanas et al., 2021). Dysregulation of NCAPG may contribute to the progression of hepatocellular carcinoma and gastric cancer (Gong et al., 2019; Wu et al., 2021). KIAA0101 interacts with UBCH10 to regulate non-small cell lung cancer proliferation by disrupting spindle assembly checkpoint function (Lei et al., 2020). These results suggest potential therapeutic benefits of these candidates in NSCLC.

EGFR inhibitors are important targeted drugs for the treatment of lung cancer, which can significantly improve the prognosis of patients. However, the use of EGFR inhibitors will inevitably lead to mutation resistance and toxic side effects (Ercan et al., 2015; Liu et al., 2018). Acquired resistance to EGFR TKIs occurs through the selection of pre-existing resistant clones and the evolution of resistance persistence (DTP) that survives treatment through adaptive mechanisms (Hata et al., 2016). Over time, DTP can acquire resistance through mutational or non-mutational mechanisms. It is particularly vital to find drug resistance targets to improve the sensitivity of inhibitors. In this study, we found that the expression of BUB1, CCNA2, CDC20 and KIF11 increased after inhibitor resistance compared with inhibitor-sensitive lung cancer samples, and these targets were associate with cell cycle, cell proliferation, DNA damage and EMT. EMT is characterized by histological changes in a subset of EGFR-mutant NSCLC patients with acquired resistance to EGFR inhibitors, either independently or in combination with genetic resistance mechanisms such as EGFR T790M(Sequist et al., 2011; Tulchinsky et al., 2019). Therefore, targeting these gene expression may alleviate EGFR-TKI resistance to a certain extent.

Lung cancer is a molecular heterogeneous disease, extensive heterogeneity in the development hinders drug development and affects the prognosis of patients (Diaz et al., 2012; Mcgranahan et al., 2015). Given the tumor heterogeneity, targeting single molecular does not cure lung cancer patients. Therefore, multiple hub genes were screened in our study. Various studies have reported cases of multi-target sequential intervention in the treatment of various cancer types: for patients with triple-negative breast cancer expressing MYCN, the combination of BET inhibitors and MEK inhibitors can synergistically inhibit tumor growth (Schafer et al., 2020); in patients with melanoma, combined inhibition of PD-1, BRAF and MEK can significantly prolong patient survival (Dummer et al., 2020); for advanced lung cancer, combined intervention of TRA, ROS1 and ALK targets reduces brain metastasis in patients (Drilon et al., 2017). Multi-factor combined diagnosis in our screened hub genes had higher accuracy and application value, all hub genes were associated with cell proliferation and cell cycle. Knocking down these hub genes suppressed tumor growth based on colony formation and CCK8 assays. Therefore, combining these hub genes may have better predictive value for patients with NSCLC, and targeting hub genes for combination research are needed.

Our study also has some limitations that need to be noted. First, there is a lack of validation of the lung cancer cohort, as it was analyzed only by public data. Second, suitable inhibitors can be screened for intervention based on the expression of targeted genes in the future, which can be used for translational medicine research. In addition, our studies need further functional biological validations.

In conclusion, our study screened out nine hub genes associated with NSCLC progression, which make a contribution to the molecular subtyping of NSCLC. It also provides new biomarkers for the prognosis and effective targets for the treatment of NSCLC.

Data availability statement

The datasets presented in this study can be found in online repositories. The names of the repository/repositories and accession number(s) can be found in the article/ Supplementary Material.

Author contributions

XM designed the research and drafted the manuscript; DK and JX collected data and drafted the figures; WY and SY critically revised the manuscript. All authors read and approved the final manuscript.

Funding

This work was supported by the Natural Science Foundation of China [grant numbers 82172889]; Jiangsu Science and Technology Department [grant number BE2020783]; and the First Affiliated Hospital of Nanjing Medical University.

Conflict of interest

The authors declare that the research was conducted in the absence of any commercial or financial relationships that could be construed as a potential conflict of interest.

Publisher's note

All claims expressed in this article are solely those of the authors and do not necessarily represent those of their affiliated organizations, or those of the publisher, the editors and the reviewers. Any product that may be evaluated in this article, or claim that may be made by its manufacturer, is not guaranteed or endorsed by the publisher.

Supplementary material

The Supplementary Material for this article can be found online at: https://www.frontiersin.org/articles/10.3389/fphar.2022.997842/full#supplementary-material

References

Barrett, T., Wilhite, S. E., Ledoux, P., Evangelista, C., Kim, I. F., Tomashevsky, M., et al. (2013). NCBI GEO: Archive for functional genomics data sets--update. *Nucleic Acids Res.* 41, D991–D995. doi:10.1093/nar/gks1193

Bergethon, K., Shaw, A. T., Ou, S. H., Katayama, R., Lovly, C. M., Mcdonald, N. T., et al. (2012). ROS1 rearrangements define a unique molecular class of lung cancers. *J. Clin. Oncol.* 30, 863–870. doi:10.1200/JCO.2011.35.6345

Borlado, L. R., and Mendez, J. (2008). CDC6: From DNA replication to cell cycle checkpoints and oncogenesis. *Carcinogenesis* 29, 237–243. doi:10.1093/carcin/bgm268

Dearden, S., Stevens, J., Wu, Y. L., and Blowers, D. (2013). Mutation incidence and coincidence in non small-cell lung cancer: meta-analyses by ethnicity and histology (mutMap). *Ann. Oncol.* 24, 2371–2376. doi:10.1093/annonc/mdt205

Diaz, L. A., Jr., Williams, R. T., Wu, J., Kinde, I., Hecht, J. R., Berlin, J., et al. (2012). The molecular evolution of acquired resistance to targeted EGFR blockade in colorectal cancers. *Nature* 486, 537–540. doi:10.1038/nature11219

Drilon, A., Siena, S., Ou, S. I., Patel, M., Ahn, M. J., Lee, J., et al. (2017). Safety and antitumor activity of the multitargeted pan-TRK, ROS1, and ALK inhibitor entrectinib: Combined results from two phase I trials (ALKA-372-001 and STARTRK-1). *Cancer Discov.* 7, 400–409. doi:10.1158/2159-8290.CD-16-1237

Duma, N., Santana-Davila, R., and Molina, J. R. (2019). Non-small cell lung cancer: Epidemiology, screening, diagnosis, and treatment. *Mayo Clin. Proc.* 94, 1623–1640. doi:10.1016/j.mayocp.2019.01.013

Dummer, R., Lebbe, C., Atkinson, V., Mandala, M., Nathan, P. D., Arance, A., et al. (2020). Combined PD-1, BRAF and MEK inhibition in advanced BRAF-mutant melanoma: Safety run-in and biomarker cohorts of COMBI-i. *Nat. Med.* 26, 1557–1563. doi:10.1038/s41591-020-1082-2

Ercan, D., Choi, H. G., Yun, C. H., Capelletti, M., Xie, T., Eck, M. J., et al. (2015). EGFR mutations and resistance to irreversible pyrimidine-based EGFR inhibitors. *Clin. Cancer Res.* 21, 3913–3923. doi:10.1158/1078-0432.CCR-14-2789

Gene Ontology, C. (2015). Gene ontology Consortium: Going forward. *Nucleic Acids Res.* 43, D1049–D1056. doi:10.1093/nar/gku1179

Gong, C., Ai, J., Fan, Y., Gao, J., Liu, W., Feng, Q., et al. (2019). NCAPG promotes the proliferation of hepatocellular carcinoma through PI3K/AKT signaling. *Onco. Targets. Ther.* 12, 8537–8552. doi:10.2147/OTT.S217916

Gyorffy, B., Surowiak, P., Budczies, J., and Lanczky, A. (2013). Online survival analysis software to assess the prognostic value of biomarkers using transcriptomic data in non-small-cell lung cancer. *PLoS One* 8, e82241. doi:10.1371/journal.pone.0082241

Hanahan, D., and Weinberg, R. A. (2011). Hallmarks of cancer: The next generation. *Cell* 144, 646–674. doi:10.1016/j.cell.2011.02.013

Haneke, K., Schott, J., Lindner, D., Hollensen, A. K., Damgaard, C. K., Mongis, C., et al. (2020). CDK1 couples proliferation with protein synthesis. *J. Cell Biol.* 219, e201906147. doi:10.1083/jcb.201906147

Hata, A. N., Niederst, M. J., Archibald, H. L., Gomez-Caraballo, M., Siddiqui, F. M., Mulvey, H. E., et al. (2016). Tumor cells can follow distinct evolutionary paths to become resistant to epidermal growth factor receptor inhibition. *Nat. Med.* 22, 262–269. doi:10.1038/nm.4040

Herbst, R. S., Morgensztern, D., and Boshoff, C. (2018). The biology and management of non-small cell lung cancer. *Nature* 553, 446–454. doi:10.1038/nature25183

Hirsch, F. R., Scagliotti, G. V., Mulshine, J. L., Kwon, R., Curran, W. J., Jr., Wu, Y. L., et al. (2017). Lung cancer: Current therapies and new targeted treatments. *Lancet* 389, 299–311. doi:10.1016/S0140-6736(16)30958-8

Huang Da, W., Sherman, B. T., and Lempicki, R. A. (2009). Systematic and integrative analysis of large gene lists using DAVID bioinformatics resources. *Nat. Protoc.* 4, 44–57. doi:10.1038/nprot.2008.211

Kanehisa, M., Sato, Y., Furumichi, M., Morishima, K., and Tanabe, M. (2019). New approach for understanding genome variations in KEGG. *Nucleic Acids Res.* 47, D590–D595. doi:10.1093/nar/gky962

Konieczkowski, D. J., Johannessen, C. M., and Garraway, L. A. (2018). A convergence-based framework for cancer drug resistance. *Cancer Cell* 33, 801–815. doi:10.1016/j.ccell.2018.03.025

Lei, H., Wang, K., Jiang, T., Lu, J., Dong, X., Wang, F., et al. (2020). KIAA0101 and UbcH10 interact to regulate non-small cell lung cancer cell proliferation by disrupting the function of the spindle assembly checkpoint. *BMC Cancer* 20, 957. doi:10.1186/s12885-020-07463-3

Lim, N., and Townsend, P. A. (2020). Cdc6 as a novel target in cancer: Oncogenic potential, senescence and subcellular localisation. *Int. J. Cancer* 147, 1528–1534. doi:10.1002/ijc.32900

Liu, Q., Yu, S., Zhao, W., Qin, S., Chu, Q., and Wu, K. (2018). EGFR-TKIs resistance via EGFR-independent signaling pathways. *Mol. Cancer* 17, 53. doi:10.1186/s12943-018-0793-1

Masanas, M., Masia, N., Suarez-Cabrera, L., Olivan, M., Soriano, A., Majem, B., et al. (2021). The oral KIF11 inhibitor 4SC-205 exhibits antitumor activity and potentiates standard and targeted therapies in primary and metastatic neuroblastoma models. *Clin. Transl. Med.* 11, e533. doi:10.1002/ctm2.533

Mcgranahan, N., Favero, F., De Bruin, E. C., Birkbak, N. J., Szallasi, Z., and Swanton, C. (2015). Clonal status of actionable driver events and the timing of mutational processes in cancer evolution. *Sci. Transl. Med.* 7, 283ra54. doi:10.1126/scitranslmed.aaa1408

Mesaros, E. F., Ott, G. R., and Dorsey, B. D. (2014). Anaplastic lymphoma kinase inhibitors as anticancer therapeutics: A patent review. *Expert Opin. Ther. Pat.* 24, 417–442. doi:10.1517/13543776.2014.877890

Rotow, J., and Bivona, T. G. (2017). Understanding and targeting resistance mechanisms in NSCLC. *Nat. Rev. Cancer* 17, 637–658. doi:10.1038/nrc.2017.84

Roy, B., Han, S. J. Y., Fontan, A. N., Jema, S., and Joglekar, A. P. (2022). Aurora B phosphorylates Bub1 to promote spindle assembly checkpoint signaling. *Curr. Biol.* 32, 237–247. doi:10.1016/j.cub.2021.10.049

Santamaria, D., Barriere, C., Cerqueira, A., Hunt, S., Tardy, C., Newton, K., et al. (2007). Cdk1 is sufficient to drive the mammalian cell cycle. *Nature* 448, 811–815. doi:10.1038/nature06046

Schafer, J. M., Lehmann, B. D., Gonzalez-Ericsson, P. I., Marshall, C. B., Beeler, J. S., Redman, L. N., et al. (2020). Targeting MYCN-expressing triple-negative breast cancer with BET and MEK inhibitors. *Sci. Transl. Med.* 12, eaaw8275. doi:10.1126/scitranslmed.aaw8275

Sequist, L. V., Waltman, B. A., Dias-Santagata, D., Digumarthy, S., Turke, A. B., Fidias, P., et al. (2011). Genotypic and histological evolution of lung cancers acquiring resistance to EGFR inhibitors. *Sci. Transl. Med.* 3, 75ra26. doi:10.1126/scitranslmed.3002003

Sung, H., Ferlay, J., Siegel, R. L., Laversanne, M., Soerjomataram, I., Jemal, A., et al. (2021). Global cancer statistics 2020: GLOBOCAN estimates of incidence and mortality worldwide for 36 cancers in 185 countries. *Ca. Cancer J. Clin.* 71, 209–249. doi:10.3322/caac.21660

Szklarczyk, D., Franceschini, A., Kuhn, M., Simonovic, M., Roth, A., Minguez, P., et al. (2011). The STRING database in 2011: Functional interaction networks of proteins, globally integrated and scored. *Nucleic Acids Res.* 39, D561–D568. doi:10.1093/nar/gkq973

Tanaka, K., Yu, H. A., Yang, S., Han, S., Selcuklu, S. D., Kim, K., et al. (2021). Targeting Aurora B kinase prevents and overcomes resistance to EGFR inhibitors in lung cancer by enhancing BIM- and PUMA-mediated apoptosis. *Cancer Cell* 39, 1245–1261 e6. doi:10.1016/j.ccell.2021.07.006

Tang, Z., Li, C., Kang, B., Gao, G., Li, C., and Zhang, Z. (2017). Gepia: A web server for cancer and normal gene expression profiling and interactive analyses. *Nucleic Acids Res.* 45, W98–W102. doi:10.1093/nar/gkx247

Tulchinsky, E., Demidov, O., Kriajevska, M., Barlev, N. A., and Imyanitov, E. (2019). Emt: A mechanism for escape from EGFR-targeted therapy in lung cancer. *Biochim. Biophys. Acta. Rev. Cancer* 1871, 29–39. doi:10.1016/j.bbcan.2018.10.003

Wang, L., Zhang, J., Wan, L., Zhou, X., Wang, Z., and Wei, W. (2015). Targeting Cdc20 as a novel cancer therapeutic strategy. *Pharmacol. Ther.* 151, 141–151. doi:10.1016/j.pharmthera.2015.04.002

Wang, Z., Wan, L., Zhong, J., Inuzuka, H., Liu, P., Sarkar, F. H., et al. (2013). Cdc20: A potential novel therapeutic target for cancer treatment. *Curr. Pharm. Des.* 19, 3210–3214. doi:10.2174/1381612811319180005

Wei, C. Y., Zhu, M. X., Lu, N. H., Peng, R., Yang, X., Zhang, P. F., et al. (2019). Bioinformatics-based analysis reveals elevated MFSD12 as a key promoter of cell proliferation and a potential therapeutic target in melanoma. *Oncogene* 38, 1876–1891. doi:10.1038/s41388-018-0531-6

Wu, Y., Lin, Y., Pan, J., Tu, X., Xu, Y., Li, H., et al. (2021). NCAPG promotes the progression of lung adenocarcinoma via the TGF-beta signaling pathway. *Cancer Cell Int.* 21, 443. doi:10.1186/s12935-021-02138-w

Zhou, J., Ye, J., Zhao, X., Li, A., and Zhou, J. (2008). JWA is required for arsenic trioxide induced apoptosis in HeLa and MCF-7 cells via reactive oxygen species and mitochondria linked signal pathway. *Toxicol. Appl. Pharmacol.* 230, 33–40. doi:10.1016/j.taap.2008.01.041

frontiers | Frontiers in Pharmacology

TYPE Original Research
PUBLISHED 20 September 2022
DOI 10.3389/fphar.2022.950571

Check for updates

OPEN ACCESS

EDITED BY
Liang Ouyang,
Sichuan University, China

REVIEWED BY
Bo Liu,
Sichuan University, China
Yi Zhang,
Soochow University, China

*CORRESPONDENCE
Yan Cheng,
yancheng@csu.edu.cn
Zhuo Li,
xy2gcpli@163.com

†These authors have contributed equally to this work

SPECIALTY SECTION
This article was submitted to Pharmacology of Anti-Cancer Drugs, a section of the journal Frontiers in Pharmacology

RECEIVED 23 May 2022
ACCEPTED 06 July 2022
PUBLISHED 20 September 2022

CITATION
Wu H-Z, Li L-Y, Jiang S-L, Li Y-Z, Shi X-M, Sun X-Y, Li Z and Cheng Y (2022), RSK2 promotes melanoma cell proliferation and vemurafenib resistance via upregulating cyclin D1. *Front. Pharmacol.* 13:950571. doi: 10.3389/fphar.2022.950571

COPYRIGHT
© 2022 Wu, Li, Jiang, Li, Shi, Sun, Li and Cheng. This is an open-access article distributed under the terms of the Creative Commons Attribution License (CC BY). The use, distribution or reproduction in other forums is permitted, provided the original author(s) and the copyright owner(s) are credited and that the original publication in this journal is cited, in accordance with accepted academic practice. No use, distribution or reproduction is permitted which does not comply with these terms.

RSK2 promotes melanoma cell proliferation and vemurafenib resistance *via* upregulating cyclin D1

Hai-Zhou Wu[1,2†], Lan-Ya Li[1,2†], Shi-Long Jiang[1], Yi-Zhi Li[1,3], Xiao-Mei Shi[1,2], Xin-Yuan Sun[1,2], Zhuo Li[1*] and Yan Cheng[1,3*]

[1]Department of Pharmacy, The Second Xiangya Hospital, Central South University, Changsha, China, [2]Xiangya School of Pharmaceutical Sciences, Central South University, Changsha, China, [3]Hunan Provincial Engineering Research Centre of Translational Medicine and Innovative Drug, Changsha, China, [4]Department of ophthalmology, The Second Xiangya Hospital, Central South University, Changsha, China

BRAF inhibitors are commonly used in targeted therapies for melanoma patients harboring $BRAF^{V600E}$ mutant. Despite the benefit of vemurafenib therapy, acquired resistance during or after treatment remains a major obstacle in $BRAF^{V600E}$ mutant melanoma. Here we found that RSK2 is overexpressed in melanoma cells and the high expression of RSK2 indicates poor overall survival (OS) in melanoma patients. Overexpression of RSK2 leads to vemurafenib resistance, and the deletion of RSK2 inhibits cell proliferation and sensitizes melanoma cells to vemurafenib. Mechanistically, RSK2 enhances the phosphorylation of FOXO1 by interacting with FOXO1 and promoting its subsequent degradation, leading to upregulation of cyclin D1 in melanoma cells. These results not only reveal the presence of a RSK2-FOXO1-cyclin D1 signaling pathway in melanoma, but also provide a potential therapeutic strategy to enhance the efficacy of vemurafenib against cancer.

KEYWORDS

melanoma, Rsk2, vemurafenib, cyclin D1, FoxO1

Introduction

Melanoma is an aggressive skin cancer with high mortality, accounting for ~100,530 new cases in 2020 (Siegel et al., 2020). Mutations at codon 600 of BRAF gene is widespread in melanoma (mostly V600E), making it a potential therapeutic target (Holderfield et al., 2014). As a BRAF inhibitor, vemurafenib shows great clinical benefit and has been approved by the United States Food and Drug Administration (FDA) as the first-line treatment for BRAF-mutated melanoma (Kramkimel et al., 2016). However, most patients treated with vemurafenib develop resistance (acquired resistance) after a relatively short period of disease control. Vemurafenib resistance is currently a persistent clinical problem in the management of BRAF mutant melanoma. Thus, it is an urgent problem to find the mechanism of vemurafenib

resistance and effective sensitizers to prolong the survival rate of patients with malignant melanoma.

p90 ribosomal S6 kinase 2 (RSK2), belonging to the RSKs serine/threonine kinase family, is a downstream effector of the MAPK signaling cascade (Sulzmaier and Ramos, 2013). RSK2 is involved in various cellular processes, such as gene expression, cell cycle, motility, proliferation and apoptosis in various cancers by phosphorylating multiple signaling effectors (Kang and Chen, 2011). RSK2 is highly expressed in many types of cancers and promotes tumor growth and survival (Clark et al., 2005; Cho et al., 2012; Huynh et al., 2020). We previously found that RSK2 promoted autophagy under endoplasmic reticulum stress *via* phosphorylating AMPKα2 and inhibition of RSK2 enhanced the sensitivity of breast cancer cells to paclitaxel (Li et al., 2020). Furthermore, RSK2 is also associated with cisplatin resistance and lenalidomide resistance (van Jaarsveld et al., 2013; Zhu et al., 2015). Recent studies indicated that targeting RSK2 could suppress cutaneous melanoma cell proliferation and metastasis, alleviating the $BRAF^{V600E}$ inhibitor resistance (Kosnopfel et al., 2017; Zhang et al., 2019). However, the mechanism regulated by RSK2 in vemurafenib-resistant melanoma cells remains obscure.

Cyclin D1, a critical cell cycle regulator encoded by the CCND1 gene, partners with CDK4/6 to promote cell cycle progression through driving transition from G1 to S phase (Qie and Diehl, 2016; Gonzalez-Ruiz et al., 2020). CCND1 is defined as an oncogene amplified in several tumors including melanoma (Casimiro et al., 2014). Overexpression of cyclin D1 has also been found in up to 62% of primary melanomas compared with melanocytic naevi (Kaufmann et al., 2020). The main oncogenic effect of cyclin D1/CCND1 upregulation or gene amplification is to promote tumor cell proliferation (Witzel et al., 2010). Previous studies showed that cyclin D1 overexpression might be sufficient to render $BRAF^{V600E}$ melanoma cells resistant to vemurafenib (Yadav et al., 2015).

FOXO1, a multifunctional transcription factor, is one of the key substrates of PI3K/AKT signaling pathway and acts as a pivotal regulators of cell cycle progression (Wu et al., 2019). Active AKT increased the expression of cyclin D1 through promoting the phosphorylation and the degradation of FOXO1 (Cai et al., 2018; Li et al., 2019; Wu et al., 2019). Increasing evidence indicates that inhibition of FOXO1 in cancer cells promoted cell cycle transition and cell proliferation by upregulation of cyclin D1 (Sulzmaier and Ramos, 2013; Zhou et al., 2019). Thus, FOXO1/cyclin D1 signaling plays a central role in cell cycle progression and cell proliferation.

In this study, we investigated the biological role and the mechanism of RSK2 in the regulation of melanoma proliferation and vemurafenib resistance. We found that RSK2 promoted melanoma cell proliferation and vemurafenib resistance by upregulating cyclin D1 expression. Meanwhile, we also uncovered that RSK2-mediated cyclin D1 upregulation is facilitated by promoting FOXO1 degradation. Therefore, this study suggested that RSK2 was involved in acquired resistance of vemurafenib, and targeting RSK2 might be an effective way to increase the therapeutic effect of vemurafenib.

Materials and methods

Cell lines and culture

The human melanoma cell line A375 was purchased from Cell Bank of Chinese Academy of Sciences. Vemurafenib-resistant A375 cells (A375-VR) were established in our laboratory. A375 cells were cultured in DMEM/High glucose medium with 10% FBS and 1% Penicillin/Streptomycin solution. Vemurafenib-resistant A375-VR cells were maintained in DMEM/High with 10% FBS, 1% Penicillin/Streptomycin and 1.0 μM vemurafenib. All the cells above were grown at 37°C with 5% CO_2.

Reagents and antibodies

Vemurafenib and MG132 were purchased from Selleck Chemicals. Cycloheximide (CHX) was purchased from Amresco. Antibodies used in immunoblotting were purchased from Cell Signaling Technologies: RSK2 (No.5528, 1:1000), FOXO1 (No.2880,1:1000), p-FOXO1/Ser319(No.2486,1:1000) and cyclin D1 (No.55506, 1:1000). Anti-β-actin (No.60008-1-Ig,1:5000) was purchased from Proteintech.

Cell viability assay

Cells were plated at 5×10^3 cells per well in 96-well plates and were then treated with a series concentration of vemurafenib. After the treatment, cell viability was measured by Cell Counting Kit-8 assay following the manufacturer's protocol (Selleck).

EdU assay

Cells were incubated with 50 μM 5-Ethynyl-2′-deoxyuridine assay (EdU, RiboBio) for 2 h at 37°C. 4% paraformaldehyde was used to fix the cells for 30 min. After cells were treated with 2 mg/ml glycine for 5 min and incubated with 0.5% Triton X-100 for 10min. Then, cells were stained with 1× Apollo reaction cocktail for 30 min and exposed to Hoechst 33342 for 30 min at room temperature. Images were captured under a fluorescent microscope.

Clonogenicity assay

The cells were plated at 800 cells per well in six-well culture plate for 10 days. After colony formation, the cells were washed with PBS

and immobilized by 4% formaldehyde at room temperature for 30 min. Finally, the cells were dyed with 0.5% crystal violet for 30 min.

RNA isolation and RT-qPCR

Total RNA was isolated using Trizol reagent (Cwbiotech) according to the manufacturer's instruction and was reverse-transcribed by using PrimeScript RT Reagent Kit (Perfect real time) (Takara). Real time PCR was performed using iTap universal SYBR Green (Bio-rad), and was run on CFX96 system (Bio-Rad). For quantification of gene expression, the $2^{-\Delta\Delta Ct}$ method was used. GAPDH expression was used for normalization. The qPCR primer sets: cyclin D1:5′-TGCATCTACACCGACAACTCC-3′ (forward) and 5′-CGTGTTTGCGGATGATCTGTT-3′ (reverse), GAPDH: 5′-ACCACAGTCCATGCCATCAC-3′ (forward) and 5′-TCCACCACCCTGTTGCTGTA-3′ (reverse), FOXO1:forward 5' -CTTCAAGGATAAGGGCGACA-3′ (forward) and 5′ -ATT TAAGCGGTGTTAGACAG-3′ (reverse).

Immunoprecipitation assay

Cells were lysed with RIPA buffer with a protease inhibitor cocktail (Selleck). The indicated primary antibody was added to cell lysates containing protein A/G agarose beads (Santa Cruz, SC-2003) at 4°C overnight. The beads were washed four times with the cooled RIPA buffer, and the proteins were eluted by SDS-PAGE sample loading buffer and analyzed by immunoblotting.

Western blot analysis

Cells were lysed with RIPA buffer with a protease inhibitor cocktail (Selleck) following by centrifugation at 14,000 ×g for 15 min. Protein concentrations of the lysates were determined by BCA assay kit. Equivalent amounts of cellular protein (15–30 μg) were separated by SDS-PAGE and transferred to PVDF membranes. And then, the membranes were blocked with 5% skim milk in PBST. The membranes were incubated with primary antibodies overnight and then peroxidase-conjugated secondary antibodies at room temperature for 1 h. Finally, the membranes were visualized with an enhanced chemiluminescent detection kit.

Bioinformatics analysis

GPEIA2 tool were used to explore RSK2 expression between melanoma tissues and normal tissues and in different subtypes of melanoma. The Human Protein Atlas database was used to explore the protein level of RSK2 in human melanoma and normal tissues. The clinicopathological data of melanoma patients were obtained from TCGA using UCSC Xena. GSE46517, GSE22155, GSE99923, GSE15605 and GSE77940 were downloaded from the GEO database. GSE46517 was used to examine gene expression in normal tissues and melanoma tissues. The survival probability was evaluated with the Kaplan-Meier method, and the differences were determined by the log-rank test. GSE99923 was used to examine gene expression in vemurafenib sensitive and resistant cells. The gene set enrichment analysis (GSEA) was performed with GSEA-4.0 software (http://software.broad institute.org/gsea/). The correlation coefficients of RSK2 and CCND1 were determined by Spearman's correlation test. The data of RSK2 mRNA expression and sensitivity to compounds were downloaded from cell minner (https://discover.nci.nih.gov/cellminer/home.do) and converted to Z-scores. The association between RSK2 and the efficacy of different compounds were tested by Pearson's-correlation analysis.

Statistical analysis

The difference between the samples with or without silencing of RSK2 expression was analyzed using unpaired two-tailed Student's t-test. All experiments were performed at least three times. A value of $p < 0.05$ was considered to be significant. Statistical significance is displayed as $^{*}p < 0.05$, $^{**}p < 0.01$.

Results

RSK2 is highly expressed and is associated with poor prognosis in melanoma

To investigate the role of RSK2 in melanoma, we first analyzed the mRNA expression of RSK2 between melanoma and normal skin tissue using the GEPIA2 (http://gepia2.cancer-pku.cn/). The results indicate that the mRNA expression of RSK2 was significantly higher in melanoma samples than that in normal tissue (Figure 1A). We further analyzed the mRNA expression of RSK2 in different subtypes of melanoma. As shown in Figure 1B, RSK2 was highly expressed in all subtypes of melanoma compared with normal skin tissue. Compared the mRNA expression of RSK2 in the GSE46517 dataset from the GEO database (https://www.ncbi.nlm.nih.gov/geo/), it is also shown that RSK2 was highly expressed in melanoma (Figure 1C). To investigate RSK2 protein expression in human melanoma and normal skin tissue, we analyzed the immunohistochemistry results using the Human Protein Atlas database (http://www.proteinatlas.org/). We found that RSK2 protein was highly expressed in melanoma

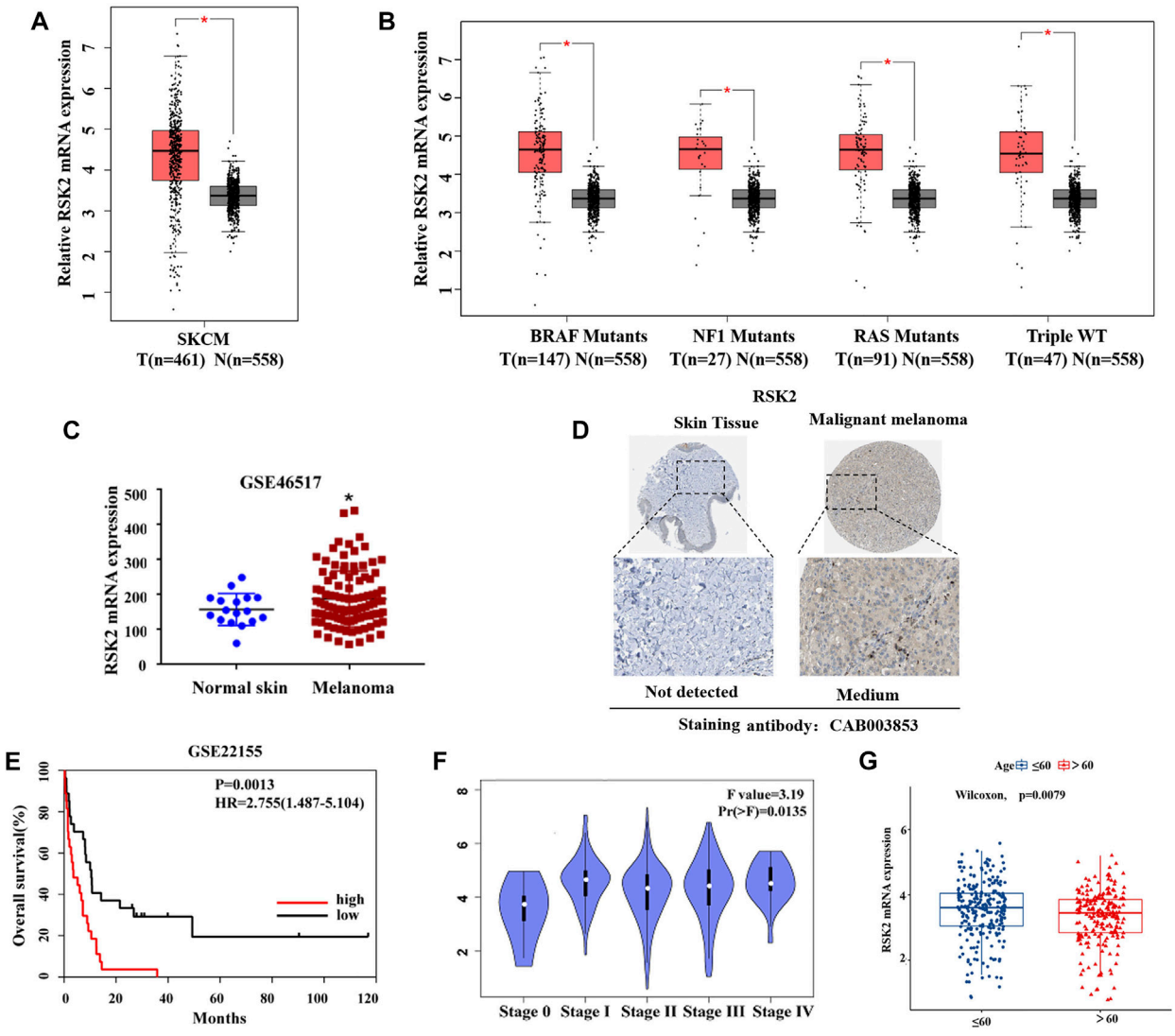

FIGURE 1
RSK2 is upregulated and is associated with poor prognosis in melanoma. **(A)** The relative expression of RSK2 mRNA in normal and melanoma tissues was analyzed by GEPIA2 database. **(B)** The relative expression of RSK2 mRNA in different subtypes of melanoma and normal skin tissues was analyzed by GEPIA2 database. **(C)** The mRNA levels of RSK2 in normal and melanoma tissues were analyzed by GEO dataset (GSE46517). **(D)** The protein levels of RSK2 in normal and melanoma tissues were analyzed by the Human Protein Altas databases. **(E)** The prognostic value of RSK2 in melanoma patients in the overall survival was analyzed by GEO dataset (GSE22155). **(F)** The association of RSK2 mRNA expression with the clinical stage of melanoma was analyzed by GEPIA2 database. **(G)** The association of RSK2 mRNA expression with the age of melanoma patients in TCGA. Values represented as mean ± SD. $*p < 0.05$, $**p < 0.01$ vs. the Con group.

tissue but not detected in normal skin tissue (Figure 1D). Importantly, we found that the high expression of RSK2 in melanoma patients was associated with poor overall survival (OS) (Figure 1E). In addition, RSK2 mRNA levels were higher in the advanced-stage melanoma relative to the early-stage ones (Figure 1F). RSK2 expression also showed a decreasing trend with the age of melanoma patients (Figure 1G). Thus, these results indicate that RSK2 expression is increased in melanoma and may be a potential biomarker for predicting the prognosis of melanoma patients.

RSK2 promotes melanoma cell proliferation

To further explore the functional role of RSK2 in melanoma cells, we knock-downed RSK2 expression in

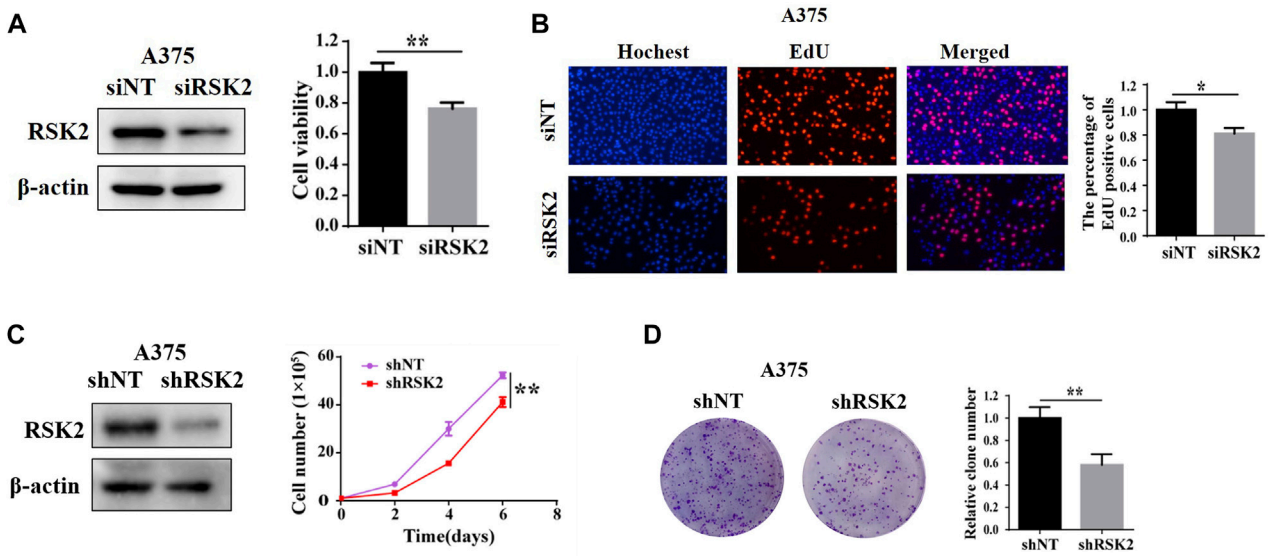

FIGURE 2
RSK2 promotes melanoma cell proliferation. **(A)** A375 cells were transfected with siNT and siRSK2, the expression of RSK2 protein was analyzed by Western blot and cell viability was measured using CCK-8 analysis. **(B)** The relative quantification of EdU-positive cells was exhibited. **(C)** A375 cells were transfected with shNT and shRSK2, the expression of RSK2 protein was analyzed by Western blot and the growth curve was determined. **(D)** The quantification of relative clone number was exhibited. $*p < 0.05$, $**p < 0.01$ vs. the Con group.

human melanoma A375 cells, and compared the cell proliferation in cells with or without RSK2 siRNA. As shown in Figure 2A, silencing of RSK2 decreased A375 cell viability as evidenced by CCK-8 assays. Silencing of RSK2 also dramatically decreased the percentage of EdU-positive A375 cells (Figure 2B). We also stably knock-downed RSK2 expression using lentiviral-mediated shRNA in A375 cells, and found that A375 cells transfected with RSK2 shRNA showed a significant reduction in cell number (Figure 2C) and colony formation (Figure 2D), compared with cells transfected with nontargeting shRNA. These results suggest that RSK2 promotes melanoma cell proliferation.

Silencing of RSK2 increases vemurafenib sensitivity in melanoma

Resistance to vemurafenib is thought to be mediated by ERK1/2 activation in some melanoma cases. As a downstream kinase of ERK1/2, we further explored whether RSK2 is involved in vemurafenib resistance in melanoma. Firstly, we downloaded the IC50 values of anti-cancer drugs and gene expression profiles in the melenoma cell lines from the Cell Miner Analysis Tool project (http://discover.nci.nih.gov/cellminer/). The IC50 values of Encorafenib, Dabrafenib and Vemurafenib were positively correlated with RSK2 expression (Figures 3A–C), indicating that patients exhibiting high RSK2 expression may be resistant to BRAF inhibitor treatment. Next, we demonstrated that silencing RSK2 increased the sensitivity of melanoma cells to vemurafenib, as evidenced by CCK-8 and colony formation (Figures 3D,E). These results suggest that silencing RSK2 increased the sensitivity of melanoma cells to vemurafenib.

RSK2 is associated with melanoma cell vemurafenib resistance

We further analyzed the role of RSK2 in vemurafenib resistance. Firstly, we found that the mRNA expression of RSK2 was significantly increased in A735-VR cells compared to the sensitive group in the GSE99923 dataset (Figure 4A). The mRNA level of RSK2 was further demonstrated higher in vemurafenib resistance A735-VR cells than that in A375 cells (Figure 4B). Furthermore, we found that the expressions of RSK2 protein were upregulated in A735-VR cells as compared to A375 cells (Figure 4C). We further investigated the potential role of RSK2 in vemurafenib resistant cells. Silencing the expression of RSK2 could increase the sensitivity of A375-VR cells to vemurafenib (Figures 4D,F). Together, these results suggested that RSK2 promotes the vemurafenib resistance in A375-VR cell line.

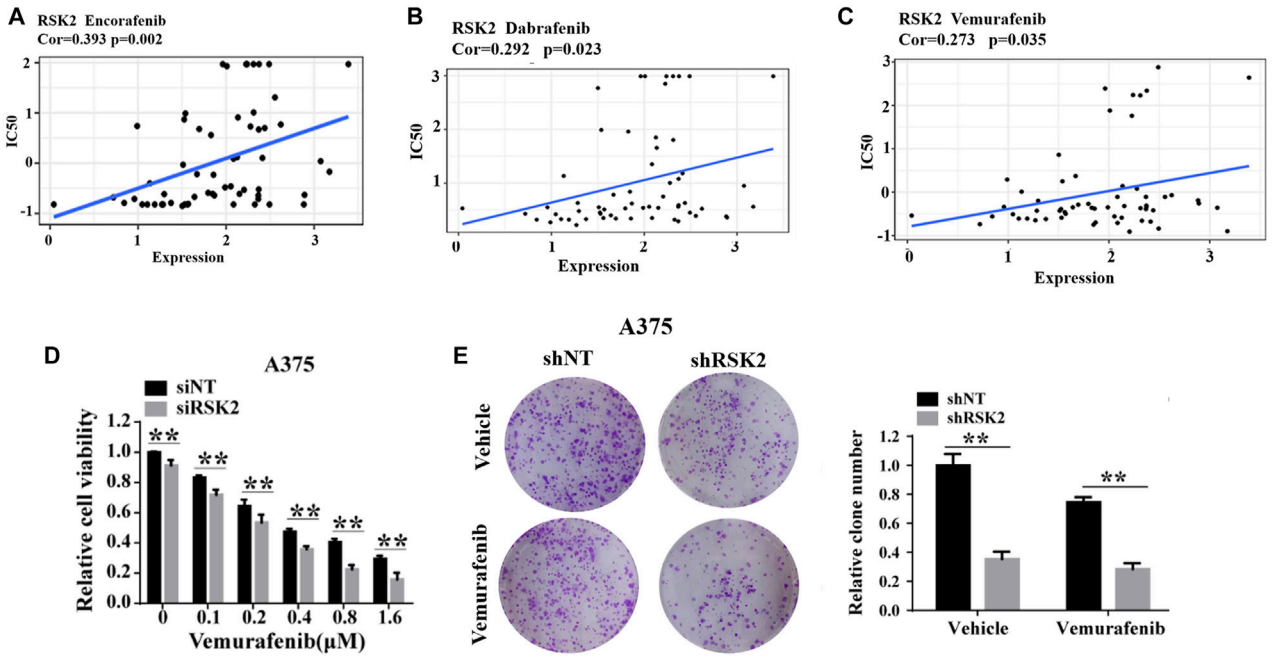

FIGURE 3
RSK2 is related with vemurafenib resistance in melanoma. The correlation between RSK2 expression and IC50 values of Encorafenib **(A)**, Dabrafenib **(B)** and Vemurafenib **(C)**. The Pearson's correlation coefficient was calculated using R software. **(D)** The cell viability of A375 cells under increasing dose of vemurafenib treatment was assessed by CCK-8 assay. **(E)** The cell proliferation of shNT or shRSK2-transfected A375 cells with vemurafenib treatment was estimated via clonogenicity assay. Values represented as mean ± SD. $*p < 0.05$, $**p < 0.01$ vs. the Con group.

RSK2 induces vemurafenib resistance through upregulating cyclin D1 expression

It has been reported that cyclin D1 elevation is associated with vemurafenib resistance. We found that the expression of cyclin D1 is indeed increased in vemurafenib-resistant A375-VR cells as reported (Figure 5A). Depletion of cyclin D1 increases the sensitivity of vemurafenib both in the vemurafenib-sensitive A375 cells and vemurafenib-resistant A375-VR cells (Figures 5B,C). To explore whether there is a regulatory relationship between RSK2 and cyclin D1, GSEA analysis shows that RSK2 is significantly enriched in the cell cycle signaling (Figure 5D). RSK2 is positively associated with CCND1 in mRNA level in a GSE77940 dataset (Figure 5E). We further transfected RSK2 siRNA and overexpression plasmid into the A375 cells, and measured the expression of cyclin D1. As shown in Figure 5F, the protein expression of cyclin D1 was decreased or increased in cells transfected with RSK2 siRNA or RSK2 plasmid. Furthermore, the mRNA level of cyclin D1 was also decreased by RSK2 knockdown (Figure 5G), indicating that RSK2 may upregulate cyclin D1 at the transcriptional level. These results indicated that RSK2 confers vemurafenib resistance in melanoma cells through regulating cyclin D1.

RSK2 upregulates cyclin D1 *via* promoting FOXO1 degradation

As the transcription factor, FOXO1 has been reported to inhibit the expression of cyclin D1 (Wu et al., 2019). We next investigated whether FOXO1 is involved in the regulation of cyclinD1 by RSK2. We found that RSK2 knockdown increased the protein expression of FOXO1, while RSK2 overexpression inhibited FOXO1 expression (Figure 6A). Depletion of RSK2 did not affect the mRNA level of FOXO1 (Figure 6B). We next investigated how RSK2 regulates FOXO1 expression in melanoma cells. The reduction of FOXO1 regulated by RSK2 overexpression was inhibited by the proteasomal inhibitor MG132, indicating that RSK2 decrease FOXO1 by promoting its proteasomal degradation (Figure 6C). In addition, depletion of RSK2 markedly enhanced the half-life of FOXO1 under CHX treatment (Figure 6D). A co-immunoprecipitation (Co-IP) experiment demonstrated that RSK2 interacted with FOXO1 (Figure 6E). The phosphorylation of FOXO1 at T24, S256, and S319 can promote FOXO1 degradation (Zhu et al., 2015). We found that silencing RSK2 decreased FOXO1 phosphorylation at Ser319, while overexpression of RSK2 increased FOXO1 phosphorylation at Ser319 (Figure 6F), suggesting that RSK2 promotes FOXO1 degradation by regulating its

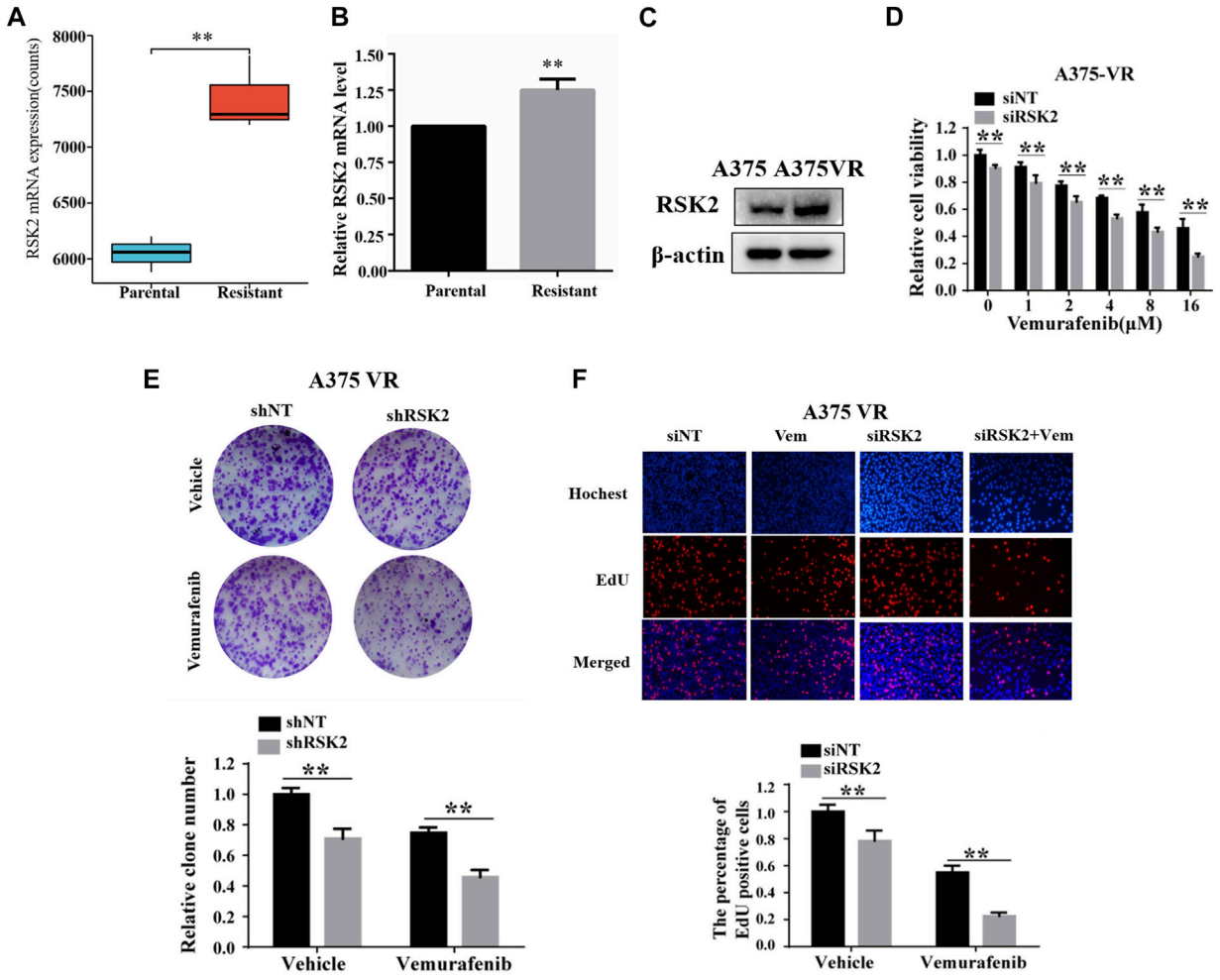

FIGURE 4
RSK2 promotes melanoma cell vemurafenib resistances. **(A)** RSK2 mRNA expression levels in A375 and A375-VR cells (GSE99923). **(B)** RT-qPCR was used to measure RSK2 mRNA expression in A375 parental cells and A375 vemurafenib resistant cells. **(C)** The protein levels of RSK2 were detected in A375 or A375-VR cells by Western blot. **(D)** Cell viability of siNT or siRSK2-transfected A375-VR cells under increasing dose of vemurafenib treatment was assessed by CCK-8 assay. **(E)** The cell proliferation of shNT or shRSK2-transfected A375-VR cells with vemurafenib treatment was estimated via clonogenicity assay. **(F)** EdU staining of indicated cells. Values represented as mean ± SD. $*p < 0.05$, $**p < 0.01$ vs. the Con group.

phosphorylation. Furthermore, the upregulation of cyclin D1 by RSK2 overexpression was inhibited by FOXO1 overexpression, indicating that FOXO1 mediates RSK2-induced increased expression of cyclin D1 (Figure 6G). Together, these results indicated that RSK2 increases cyclin D1 by promoting FOXO1 degradation in melanoma cells.

Discussion

In recent years, many studies have demonstrated that RSK2 plays a central role in the cell proliferation, metastasis and survival in various tumors and targeting it may improve the clinical efficiency of cancer therapies (Kang and Chen, 2011; Ma et al., 2018; Yoo et al., 2019). However, the molecular mechanism of RSK2 in vemurafenib resistance is not very clear. In this study, we found that RSK2 is highly expressed in melanoma tissue compared to normal skin tissue, and silencing of RSK2 inhibits melanoma cell proliferation. Furthermore, there is more expression of RSK2 in vemurafenib-resistant melanoma cells compare with vemurafenib-sensitive cells, and silencing the expression of RSK2 could increase the sensitivity of A375-VR cells to vemurafenib. Our results reveal that RSK2 not only promotes melanoma cell proliferation, but also mediates vemurafenib resistance through the upregulation of cyclin D1 mediated by accelerating the degradation of FOXO1 by phosphorylation (Figure 6H).

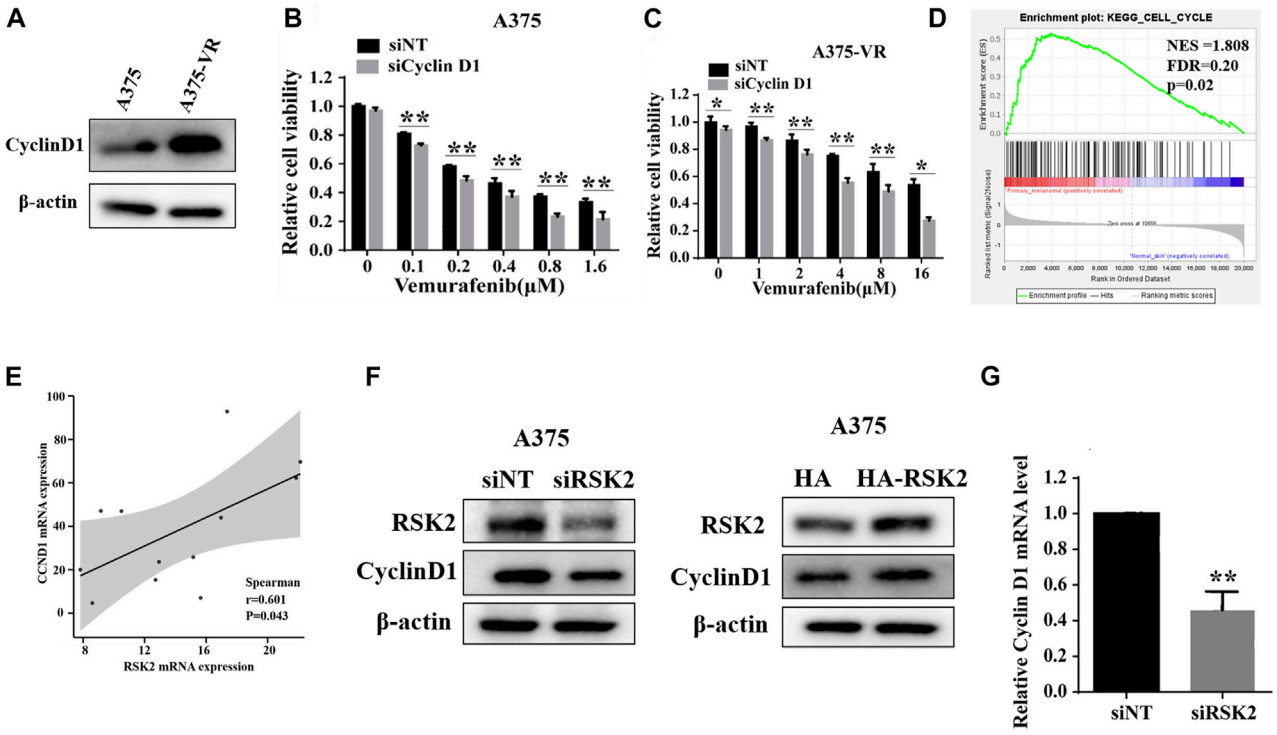

FIGURE 5
RSK2 induces vemurafenib resistance through upregulating cyclin D1 expression. **(A)** The protein levels of cyclin D1 were detected in A375 and A375-VR cells by Western blot. A375 cells **(B)** and A375-VR cells **(C)** were transfected with siNT or si CyclinD1, cell viability was assessed by CCK-8 assay. **(D)** Enrichment plots from gene set enrichment analysis (GSEA) of RSK2 in cell cycle by GEO dataset GSE15605. **(E)** The correlation between RSK2 and CCND1 predicted by GEO dataset GSE77940. **(F)** Western blot was used to measure cyclin D1 expression in A375 cells transfected with RSK2 siRNA or HA-RSK2 plasmid. **(G)** RT-qPCR was used to measure cyclin D1 expression in A375 cells transfected with RSK2 siRNA. Values represented as mean ± SD. $^{**}p < 0.01$ vs. the Con group.

Previous studies demonstrated that RSK2 is a pivotal kinase to regulate human skin cancer cell proliferation and growth by promoting the phosphorylation of LKB1 or the activation of mTORC1 in melanoma (Zheng et al., 2009; Romeo et al., 2013; Zhang et al., 2019). However, the role and regulatory mechanism of RSK2 on melanoma cell proliferation remains to be further explored. Our present results provided concrete evidences for the role of RSK2 in melanoma cell proliferation by ectopic overexpression and knockdown of RSK2. We also proved that RSK2 expression was higher in melanoma tissue compared with the normal tissue and its overexpression was associated with increased pathological stage in melanoma patients. Prior study reported that RSK2 located in nucleus could enhance breast cancer cell proliferation through upregulation of cyclin D1 mRNA and protein level (Eisinger-Mathason et al., 2008). A natural anticancer agent silybin was found to induce cell cycle arrest and attenuate melanoma cell growth. The mechanism might suppress the expression of a cell cycle regulatory protein cyclin D1 by blockading the kinase activity of MEK 1/2 and RSK2 (Lee et al., 2013). Here, we confirmed the mechanism of RSK2 in promoting melanoma cell proliferation was to elevate cyclin D1 transcription.

Transcription factor FOXO1 has been reported to be involved in the transcription of cyclin D1 (Sulzmaier and Ramos, 2013; Yang et al., 2019). Depletion of FOXO1 could promote cancer cell proliferation by enhancing cyclin D1 expression (Mao et al., 2015). In this work, we found that knockdown of RSK2 in melanoma cells did not affect FOXO1 mRNA expression but increased its protein level. We further revealed that inhibition of RSK2 improved FOXO1 protein expression by preventing its degradation. Phosphorylation at three conserved residues S319, S256, T24 by various protein kinases results in the translocation of the FOXO protein from the nucleus to the cytoplasm, thereby promoting its degradation by the 26S proteasome (Yamagata et al., 2008). In this study, we found that RSK2 interfered with FOXO1 and enhanced FOXO1 phosphorylation at S319, suggesting the mechanism of FOXO1 degradation mediated by RSK2 is due to phosphorylation. We also verified that overexpression of FOXO1 abrogated the increase of cyclin D1 induced by RSK2 overexpression. Taken together, our results revealed that FOXO1 is a novel RSK2 substrate and discovered a new RSK2–FOXO1–cyclin D1 cascade involved in melanoma cell proliferation.

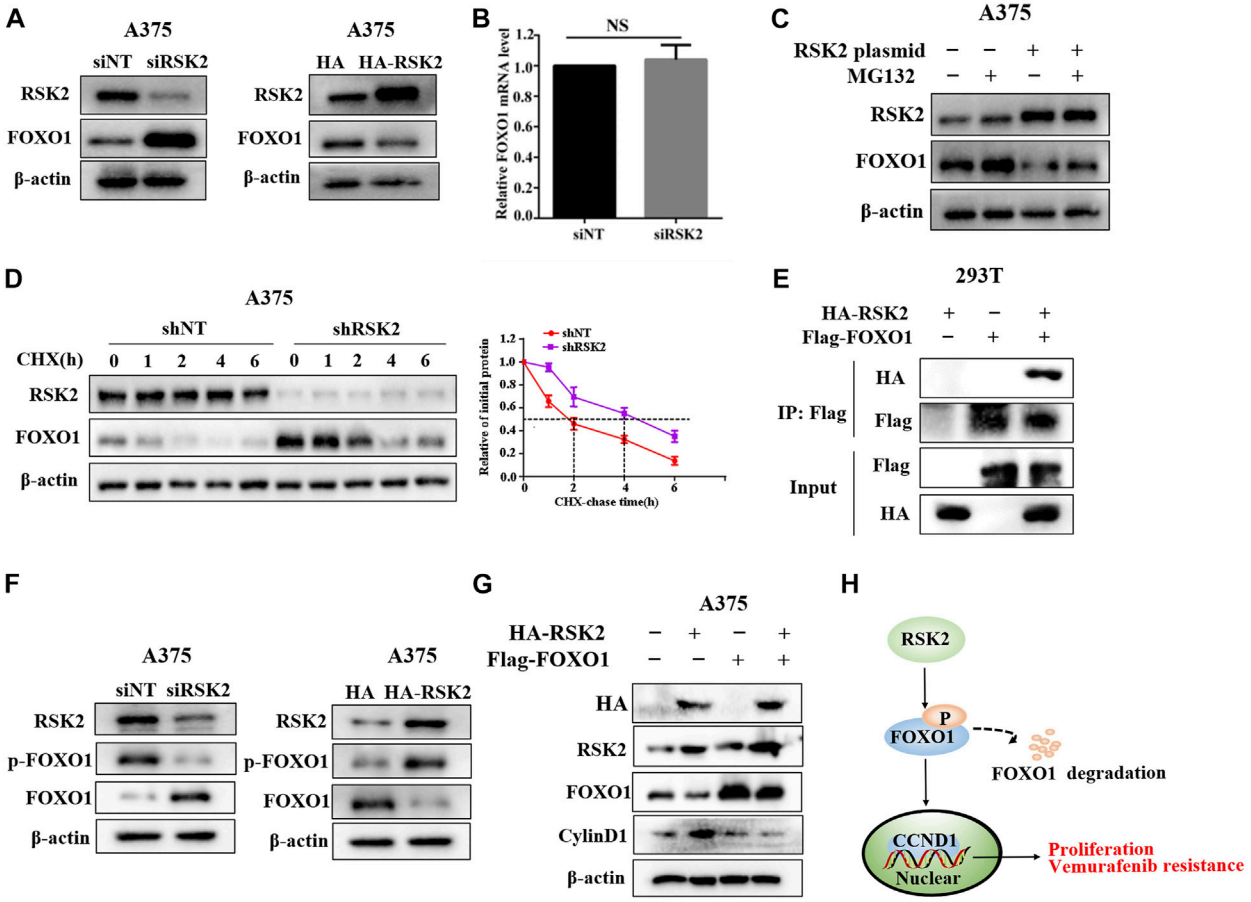

FIGURE 6
RSK2 upregulates cyclin D1 via promoting FOXO1 degradation. **(A)** Western blot was used to measure FOXO1 expression in A375 cells transfected with RSK2 siRNA or HA-RSK2 plasmid. **(B)** RT-qPCR was used to measure FOXO1 mRNA expression in A375 cells transfected with RSK2 siRNA. **(C)** The influence of RSK2 on FOXO1 degradation was estimated in A375 cells under MG132 treatment. **(D)** The effect of RSK2 on FOXO1 protein stability was evaluated in A375 cells under CHX treatment for the indicated time. **(E)** HEK293T cells were co-transfected with Flag-FOXO1 and HA-RSK2 plasmid as indicated, immunoprecipitation with anti-Flag antibody was performed. **(F)** Western blot was used to measure p-FOXO1 (S319) and FOXO1 expression in A375 cells transfected with RSK2 siRNA or HA-RSK2 plasmid. **(G)** Western blot was used to measure cyclin D1 expression in A375 cells co-transfected with Flag-FOXO1 and HA-RSK2 as indicated. **(H)** A schematic model of RSK2–FOXO1–cyclin D1 axis leading to melanoma proliferation and vemurafenib resistance.

The most common mechanism for BRAF inhibitors resistance is MAPK pathway reactivation in melanoma (Hatzivassiliou et al., 2010; Nazarian et al., 2010). Selective BRAF inhibitor Dabrafenib combined with a selective MAPK kinase (MEK) inhibitor trametinib successfully prolonged the progression-free survival of melanoma patients with $BRAF^{V600E}$ mutations in a phase I/II clinical trials (Flaherty et al., 2012). However, this effect lasted only for an average of 9.4 months, drug resistance appeared again (Wagle et al., 2014). Recent study has shown that RSK inhibitors BI-D1870 and BRD7389 significantly reduced the proliferation of BRAF mutant melanoma cells that have acquired resistance to dual BRAF and MEK inhibitor treatment (Theodosakis et al., 2017). Researchers also found that inhibition of RSK2 by CF-X9, a RSK2 inhibitor discovered by virtual screening, hindered the cell growth in BRAF inhibitor-resistant melanoma cells (Zhang et al., 2019). Consistent with these reports, we found that RSK2 silencing not only improved the sensitivity of A375 cells to vemurafenib, but also overcame vemurafenib resistance in A375-VR cells. Besides reactivating MAPK, PI3K/Akt and EGFR signaling have also been involved in BRAF inhibitor resistance in melanoma (Chi et al., 2014; Laurenzana et al., 2019).

In addition, glutamine dependence, autophagy and mitochondrial biogenesis have also been implicated in resistance to BRAF inhibitor therapy (Hernandez-Davies et al., 2015; Martin et al., 2017; Carpenter et al., 2019). Blocking a single pathway seems to be not sufficient for completely reversing drug resistance. It was reported that the increase of cyclin D1 and the reactivation of MAPK coexist in vemurafenib-resistant tumors (Yadav et al., 2014). Our study discovered that cyclin

D1 expression was upregulated in vemurafenib-resistant melanoma cells, accompanied by the increase of RSK2. Inhibition of cyclin D1 restored the sensitivity of the vemurafenib-resistant melanoma cells to vemurafenib mediated by RSK2. Together, we have uncovered a new mechanism RSK2-mediated phosphorylation and stabilization of FOXO1, thereby increasing cyclin D1 expression, is involved in promotion of melanoma cell proliferation. Inhibition of RSK2 can enhance sensitivity of BRAF mutant melanoma cells to vemurafenib and overcome vemurafenib resistance. These findings not only supported RSK2 as a critical oncoprotein in supporting cancer cell proliferation, but also provide a new mechanism by which RSK2 confers vemurafenib resistance in melanoma, suggesting that targeting RSK2 may be a potential strategy for melanoma treatment.

Data availability statement

The raw data supporting the conclusion of this article will be made available bythe authors, without undue reservation.

Author contributions

ZL, YC, H-ZW, and L-YL conceived and designed the study. H-ZW and L-YL performed the experiments. H-ZW, L-YL, S-LJ, Y-ZL, X-MS, and X-YS conducted the data analysis. L-YL drafted the manuscript. ZL and YC revised and approved the manuscript.

Funding

This work was supported by the National Natural Science Foundation of China No. 81972480.

Conflict of interest

The authors declare that the research was conducted in the absence of any commercial or financial relationships that could be construed as a potential conflict of interest.

Publisher's note

All claims expressed in this article are solely those of the authors and do not necessarily represent those of their affiliated organizations, or those of the publisher, the editors and the reviewers. Any product that may be evaluated in this article, or claim that may be made by its manufacturer, is not guaranteed or endorsed by the publisher.

References

Cai, J., Lu, W., Du, S., Guo, Z., Wang, H., Wei, W., et al. (2018). Tenascin-C modulates cell cycle progression to enhance tumour cell proliferation through AKT/FOXO1 signalling in pancreatic cancer. *J. Cancer* 9 (23), 4449–4462. doi:10.7150/jca.25926

Carpenter, E. L., Chagani, S., Nelson, D., Cassidy, P. B., Laws, M., Ganguli-Indra, G., et al. (2019). Mitochondrial complex I inhibitor deguelin induces metabolic reprogramming and sensitizes vemurafenib-resistant BRAF(V600E) mutation bearing metastatic melanoma cells. *Mol. Carcinog.* 58 (9), 1680–1690. doi:10.1002/mc.23068

Casimiro, M. C., Velasco-Velazquez, M., Aguirre-Alvarado, C., and Pestell, R. G. (2014). Overview of cyclins D1 function in cancer and the CDK inhibitor landscape: Past and present. *Expert Opin. Investig. Drugs* 23 (3), 295–304. doi:10.1517/13543784.2014.867017

Chi, M., Ye, Y., Zhang, X. D., and Chen, J. (2014). Insulin induces drug resistance in melanoma through activation of the PI3K/Akt pathway. *Drug Des. devel. Ther.* 8, 255–262. doi:10.2147/DDDT.S53568

Cho, Y. Y., Lee, M. H., Lee, C. J., Yao, K., Lee, H. S., Bode, A. M., et al. (2012). RSK2 as a key regulator in human skin cancer. *Carcinogenesis* 33 (12), 2529–2537. doi:10.1093/carcin/bgs271

Clark, D. E., Errington, T. M., Smith, J. A., Frierson, H. F., Jr., Weber, M. J., Lannigan, D. A., et al. (2005). The serine/threonine protein kinase, p90 ribosomal S6 kinase, is an important regulator of prostate cancer cell proliferation. *Cancer Res.* 65 (8), 3108–3116. doi:10.1158/0008-5472.can-04-3151

Eisinger-Mathason, T. S., Andrade, J., Groehler, A. L., Clark, D. E., Muratore-Schroeder, T. L., Pasic, L., et al. (2008). Codependent functions of RSK2 and the apoptosis-promoting factor TIA-1 in stress granule assembly and cell survival. *Mol. Cell* 31 (5), 722–736. doi:10.1016/j.molcel.2008.06.025

Flaherty, K. T., Infante, J. R., Daud, A., Gonzalez, R., Kefford, R. F., Sosman, J., et al. (2012). Combined BRAF and MEK inhibition in melanoma with BRAF V600 mutations. *N. Engl. J. Med.* 367 (18), 1694–1703. doi:10.1056/NEJMoa1210093

Gonzalez-Ruiz, L., Gonzalez-Moles, M. A., Gonzalez-Ruiz, I., Ruiz-Avila, I., Ayen, A., Ramos-Garcia, P., et al. (2020). An update on the implications of cyclin D1 in melanomas. *Pigment. Cell Melanoma Res.* 33 (6), 788–805. doi:10.1111/pcmr.12874

Hatzivassiliou, G., Song, K., Yen, I., Brandhuber, B. J., Anderson, D. J., Alvarado, R., et al. (2010). RAF inhibitors prime wild-type RAF to activate the MAPK pathway and enhance growth. *Nature* 464 (7287), 431–435. doi:10.1038/nature08833

Hernandez-Davies, J. E., Tran, T. Q., Reid, M. A., Rosales, K. R., Lowman, X. H., Pan, M., et al. (2015). Vemurafenib resistance reprograms melanoma cells towards glutamine dependence. *J. Transl. Med.* 13, 210. doi:10.1186/s12967-015-0581-2

Holderfield, M., Deuker, M. M., McCormick, F., and McMahon, M. (2014). Targeting RAF kinases for cancer therapy: BRAF-mutated melanoma and beyond. *Nat. Rev. Cancer* 14 (7), 455–467. doi:10.1038/nrc3760

Huynh, M. M., Jayanthan, A., Pambid, M. R., Los, G., and Dunn, S. E. (2020). RSK2: A promising therapeutic target for the treatment of triple-negative breast cancer. *Expert Opin. Ther. Targets* 24 (1), 1–5. doi:10.1080/14728222.2020.1709824

Kang, S., and Chen, J. (2011). Targeting RSK2 in human malignancies. *Expert Opin. Ther. Targets* 15 (1), 11–20. doi:10.1517/14728222.2010.531013

Kaufmann, C., Kempf, W., Mangana, J., Cheng, P., Emberger, M., Lang, R., et al. (2020). The role of cyclin D1 and Ki-67 in the development and prognostication of thin melanoma. *Histopathology* 77 (3), 460–470. doi:10.1111/his.14139

Kosnopfel, C., Sinnberg, T., Sauer, B., Niessner, H., Schmitt, A., Makino, E., et al. (2017). Human melanoma cells resistant to MAPK inhibitors can be effectively targeted by inhibition of the p90 ribosomal S6 kinase. *Oncotarget* 8 (22), 35761–35775. doi:10.18632/oncotarget.16204

Kramkimel, N., Thomas-Schoemann, A., Sakji, L., Golmard, J., Noe, G., Regnier-Rosencher, E., et al. (2016). Vemurafenib pharmacokinetics and its correlation with

efficacy and safety in outpatients with advanced BRAF-mutated melanoma. *Target. Oncol.* 11 (1), 59–69. doi:10.1007/s11523-015-0375-8

Laurenzana, A., Margheri, F., Biagioni, A., Chilla, A., Pimpinelli, N., Ruzzolini, J., et al. (2019). EGFR/uPAR interaction as druggable target to overcome vemurafenib acquired resistance in melanoma cells. *EBioMedicine* 39, 194–206. doi:10.1016/j.ebiom.2018.12.024

Lee, M. H., Huang, Z., Kim, D. J., Kim, S. H., Kim, M. O., Lee, S. Y., et al. (2013). Direct targeting of MEK1/2 and RSK2 by silybin induces cell-cycle arrest and inhibits melanoma cell growth. *Cancer Prev. Res.* 6 (5), 455–465. doi:10.1158/1940-6207.CAPR-12-0425

Li, L., Chen, X., Wang, K., Guan, Y., Ren, X., Cao, D., et al. (2020). RSK2 protects human breast cancer cells under endoplasmic reticulum stress through activating AMPKα2-mediated autophagy. *Oncogene* 39 (43), 6704–6718. doi:10.1038/s41388-020-01447-0

Li, Y., Deng, S., Peng, J., Wang, X., Essandoh, K., Mu, X., et al. (2019). MicroRNA-223 is essential for maintaining functional beta-cell mass during diabetes through inhibiting both FOXO1 and SOX6 pathways. *J. Biol. Chem.* 294 (27), 10438–10448. doi:10.1074/jbc.RA119.007755

Ma, J., Lu, Y., Zhang, S., Li, Y., Huang, J., Yin, Z., et al. (2018). β-Trcp ubiquitin ligase and RSK2 kinase-mediated degradation of FOXN2 promotes tumorigenesis and radioresistance in lung cancer. *Cell Death Differ.* 25 (8), 1473–1485. doi:10.1038/s41418-017-0055-6

Mao, X. P., Zhang, L. S., Huang, B., Zhou, S. Y., Liao, J., Chen, L. W., et al. (2015). Mir-135a enhances cellular proliferation through post-transcriptionally regulating PHLPP2 and FOXO1 in human bladder cancer. *J. Transl. Med.* 13, 86. doi:10.1186/s12967-015-0438-8

Martin, S., Dudek-Peric, A. M., Garg, A. D., Roose, H., Demirsoy, S., Van Eygen, S., et al. (2017). An autophagy-driven pathway of ATP secretion supports the aggressive phenotype of BRAF(V600E) inhibitor-resistant metastatic melanoma cells. *Autophagy* 13 (9), 1512–1527. doi:10.1080/15548627.2017.1332550

Nazarian, R., Shi, H., Wang, Q., Kong, X., Koya, R. C., Lee, H., et al. (2010). Melanomas acquire resistance to B-RAF(V600E) inhibition by RTK or N-RAS upregulation. *Nature* 468 (7326), 973–977. doi:10.1038/nature09626

Qie, S., and Diehl, J. A. (2016). Cyclin D1, cancer progression, and opportunities in cancer treatment. *J. Mol. Med.* 94 (12), 1313–1326. doi:10.1007/s00109-016-1475-3

Romeo, Y., Moreau, J., Zindy, P. J., Saba-El-Leil, M., Lavoie, G., Dandachi, F., et al. (2013). RSK regulates activated BRAF signalling to mTORC1 and promotes melanoma growth. *Oncogene* 32 (24), 2917–2926. doi:10.1038/onc.2012.312

Siegel, R. L., Miller, K. D., and Jemal, A. (2020). Cancer statistics, 2020. *Ca. Cancer J. Clin.* 70 (1), 7–30. doi:10.3322/caac.21590

Sulzmaier, F. J., and Ramos, J. W. (2013). RSK isoforms in cancer cell invasion and metastasis. *Cancer Res.* 73 (20), 6099–6105. doi:10.1158/0008-5472.CAN-13-1087

Theodosakis, N., Micevic, G., Langdon, C. G., Ventura, A., Means, R., Stern, D. F., et al. (2017). p90RSK blockade inhibits dual BRAF and MEK inhibitor-resistant melanoma by targeting protein synthesis. *J. Invest. Dermatol.* 137 (10), 2187–2196. doi:10.1016/j.jid.2016.12.033

van Jaarsveld, M. T., Blijdorp, I. C., Boersma, A. W., Pothof, J., Mathijssen, R. H., Verweij, J., et al. (2013). The kinase RSK2 modulates the sensitivity of ovarian cancer cells to cisplatin. *Eur. J. Cancer* 49 (2), 345–351. doi:10.1016/j.ejca.2012.08.024

Wagle, N., Van Allen, E. M., Treacy, D. J., Frederick, D. T., Cooper, Z. A., Taylor-Weiner, A., et al. (2014). MAP kinase pathway alterations in BRAF-mutant melanoma patients with acquired resistance to combined RAF/MEK inhibition. *Cancer Discov.* 4 (1), 61–68. doi:10.1158/2159-8290.CD-13-0631

Witzel, I. I., Koh, L. F., and Perkins, N. D. (2010). Regulation of cyclin D1 gene expression. *Biochem. Soc. Trans.* 38 (1), 217–222. doi:10.1042/BST0380217

Wu, Z., Qiu, M., Mi, Z., Meng, M., Guo, Y., Jiang, X., et al. (2019). WT1-interacting protein inhibits cell proliferation and tumorigenicity in non-small-cell lung cancer via the AKT/FOXO1 axis. *Mol. Oncol.* 13 (5), 1059–1074. doi:10.1002/1878-0261.12462

Yadav, V., Burke, T. F., Huber, L., Van Horn, R. D., Zhang, Y., Buchanan, S. G., et al. (2014). The CDK4/6 inhibitor LY2835219 overcomes vemurafenib resistance resulting from MAPK reactivation and cyclin D1 upregulation. *Mol. Cancer Ther.* 13 (10), 2253–2263. doi:10.1158/1535-7163.MCT-14-0257

Yadav, V., Chen, S. H., Yue, Y. G., Buchanan, S., Beckmann, R. P., Peng, S. B., et al. (2015). Co-targeting BRAF and cyclin dependent kinases 4/6 for BRAF mutant cancers. *Pharmacol. Ther.* 149, 139–149. doi:10.1016/j.pharmthera.2014.12.003

Yamagata, K., Daitoku, H., Takahashi, Y., Namiki, K., Hisatake, K., Kako, K., et al. (2008). Arginine methylation of FOXO transcription factors inhibits their phosphorylation by Akt. *Mol. Cell* 32 (2), 221–231. doi:10.1016/j.molcel.2008.09.013

Yang, L., Yang, F., Zhao, H., Wang, M., and Zhang, Y. (2019). Circular RNA circCHFR facilitates the proliferation and migration of vascular smooth muscle via miR-370/FOXO1/cyclin D1 pathway. *Mol. Ther. Nucleic Acids* 16, 434–441. doi:10.1016/j.omtn.2019.02.028

Yoo, S. M., Lee, C. J., An, H. J., Lee, J. Y., Lee, H. S., Kang, H. C., et al. (2019). RSK2-Mediated ELK3 activation enhances cell transformation and breast cancer cell growth by regulation of c-fos promoter activity. *Int. J. Mol. Sci.* 20 (8), E1994. doi:10.3390/ijms20081994

Zhang, X., Cai, L., Zhao, S., Long, J., Li, J., Wu, L., et al. (2019). CX-F9, a novel RSK2 inhibitor, suppresses cutaneous melanoma cells proliferation and metastasis through regulating autophagy. *Biochem. Pharmacol.* 168, 14–25. doi:10.1016/j.bcp.2019.06.014

Zheng, B., Jeong, J. H., Asara, J. M., Yuan, Y. Y., Granter, S. R., Chin, L., et al. (2009). Oncogenic B-RAF negatively regulates the tumor suppressor LKB1 to promote melanoma cell proliferation. *Mol. Cell* 33 (2), 237–247. doi:10.1016/j.molcel.2008.12.026

Zhou, Z. H., Chen, G., Deng, C., Tang, J. M., Xie, L., Zhou, H. Y., et al. (2019). TCF19 contributes to cell proliferation of non-small cell lung cancer by inhibiting FOXO1. *Cell Biol. Int.* 43, 1416–1424. doi:10.1002/cbin.11189

Zhu, Y. X., Yin, H., Bruins, L. A., Shi, C. X., Jedlowski, P., Aziz, M., et al. (2015). RNA interference screening identifies lenalidomide sensitizers in multiple myeloma, including RSK2. *Blood* 125 (3), 483–491. doi:10.1182/blood-2014-05-577130

frontiers | Frontiers in Pharmacology

TYPE Original Research
PUBLISHED 21 September 2022
DOI 10.3389/fphar.2022.998199

Check for updates

OPEN ACCESS

EDITED BY
Chen Shi,
Huazhong University of Science and Technology, China

REVIEWED BY
Xiaoyan Huang,
Shaanxi Provincial People's Hospital, China
Dmitry A. Khochenkov,
Russian *Cancer* Research Center NN Blokhin, Russia

*CORRESPONDENCE
Luoting Yu,
yuluot@scu.edu.cn
Zhihao Liu,
liuzhihao@scu.edu.cn
Yongxia Zhu,
zhuyongxia0409@163.com

†These authors contributed equally to this work and share first authorship

SPECIALTY SECTION
This article was submitted to Pharmacology of Anti-Cancer Drugs, a section of the journal Frontiers in Pharmacology

RECEIVED 19 July 2022
ACCEPTED 30 August 2022
PUBLISHED 21 September 2022

CITATION
Zeng J, Ran K, Li X, Tao L, Wang Q, Ren J, Hu R, Zhu Y, Liu Z and Yu L (2022), A novel small molecule RK-019 inhibits FGFR2-amplification gastric cancer cell proliferation and induces apoptosis in vitro and in vivo.
Front. Pharmacol. 13:998199.
doi: 10.3389/fphar.2022.998199

COPYRIGHT
© 2022 Zeng, Ran, Li, Tao, Wang, Ren, Hu, Zhu, Liu and Yu. This is an open-access article distributed under the terms of the Creative Commons Attribution License (CC BY). The use, distribution or reproduction in other forums is permitted, provided the original author(s) and the copyright owner(s) are credited and that the original publication in this journal is cited, in accordance with accepted academic practice. No use, distribution or reproduction is permitted which does not comply with these terms.

A novel small molecule RK-019 inhibits *FGFR2*-amplification gastric cancer cell proliferation and induces apoptosis *in vitro* and *in vivo*

Jun Zeng[1†], Kai Ran[2†], Xinyue Li[1†], Longyue Tao[1], Qiwei Wang[1], Jiangtao Ren[1], Rong Hu[1], Yongxia Zhu[3]*, Zhihao Liu[4]* and Luoting Yu[1]*

[1]State Key Laboratory of Biotherapy and Cancer Center, Sichuan University and Collaborative Innovation Center for Biotherapy, West China Hospital, Sichuan University, Chengdu, China, [2]College of Pharmacy, National and Local Joint Engineering Research Center of Targeted and Innovative Therapeutics, Chongqing Key Laboratory of Kinase Modulators as Innovative Medicine, Chongqing University of Arts and Sciences, Chongqing, China, [3]Department of Clinical Pharmacy, Sichuan Cancer Hospital and Institute, Sichuan Cancer Center, School of Medicine, University of Electronic Science and Technology of China, Chengdu, China, [4]Research Laboratory of Emergency Medicine, Department of Emergency Medicine, West China Hospital, Sichuan University, Chengdu, China

Gastric cancer (GC) is one of the most malignant cancers and is estimated to be fifth in incidence ratio and the third leading cause of cancer death worldwide. Despite advances in GC treatment, poor prognosis and low survival rate necessitate the development of novel treatment options. Fibroblast growth factor receptors (FGFRs) have been suggested to be potential targets for GC treatment. In this study, we report a novel selective FGFR inhibitor, RK-019, with a pyrido [1, 2-a] pyrimidinone skeleton. *In vitro*, RK-019 showed excellent FGFR1-4 inhibitory activities and strong anti-proliferative effects against *FGFR2*-amplification (*FGFR2*-amp) GC cells, including SNU-16 and KATO III cells. Treatment with RK-019 suppressed phosphorylation of FGFR and its downstream pathway proteins, such as FRS2, PLCγ, AKT, and Erk, resulting in cell cycle arrest and induction of apoptosis. Furthermore, daily oral administration of RK-019 could attenuate tumor xenograft growth with no adverse effects. Here, we reported a novel specific FGFR inhibitor, RK-019, with potent anti-FGFR2-amp GC activity both *in vitro* and *in vivo*.

KEYWORDS

gastric cancer, receptor tyrosine kinase, antineoplastic agents, FGFRs, cell apoptosis

Introduction

Gastric cancer (GC) is one of the most malignant cancers and is estimated to be fifth in incidence ratio and the third leading cause of cancer death worldwide (Sung et al., 2021). Patients with early-stage GC are mostly asymptomatic, and most diagnoses are made at the medium or advanced stage (Takahashi et al., 2013). However, at these stages, chemotherapy, radiotherapy, and surgical treatment efficacies are very low (Van Cutsem et al., 2016). Hence, developing new therapeutic strategies with high efficacy and low toxicity for the treatment of advanced GC is crucial.

Fibroblast growth factor receptors (FGFR1-4) belong to the receptor tyrosine kinase family that bind to numerous fibroblast growth factor (FGF) members (Ornitz and Itoh, 2001; Beenken and Mohammadi, 2009; Belov and Mohammadi, 2013). Extracellular ligand FGFs bind to FGFRs and induce FGFR dimerization and then initiate downstream intracellular signaling cascade pathways, including those involving Ras-Raf-Erk, PI3K-AKT-mTOR, and PLCγ/Ca^{2+} (Sarabipour and Hristova, 2016). Moreover, the JAK2-STAT pathway can be activated by FGFRs in certain cellular contexts (Deo et al., 2002; Cerliani et al., 2011; Li et al., 2019). Furthermore, by regulating signaling cascade pathways, FGFRs mediate physiological processes, such as development progress, cell proliferation, differentiation, and angiogenesis (Eswarakumar et al., 2005; Fukumoto, 2008; Brooks et al., 2012). Anomalously activated FGFR signaling due to FGFR mutations, amplifications, and translocations is involved in tumorigenesis and progression of cancers, including breast cancer, prostate cancer, GC, urothelial cancer, and cholangiocarcinoma (Grose and Dickson, 2005; Katoh, 2010; Lamont et al., 2011; Jain et al., 2018).

Studies indicated that FGFR1 overexpression facilitates peritoneal diffusion *via* epithelial-to-mesenchymal transition (EMT) in GC (Shimizu et al., 2018). Overexpression of FGFR1 in GC tissue samples was correlated with EphA4 protein expression whose synergy promoted GC development (Oki et al., 2008). In addition, FGFR2 is considered to play an important role in GC, especially in GC with chromosomal instability (Network, 2014). FGFR2 overexpression was identified in 60% of patients with GC, and *FGFR2*-amplification (*FGFR2*-amp) was found to occur in approximately 2–15% of these patients (Matsumoto et al., 2012; Su et al., 2014; Han et al., 2015; Ahn et al., 2016; Jia et al., 2016; Kim et al., 2019b). *FGFR2* expression level, amplification, and mutations are associated with drug resistance and prognosis (Matsumoto et al., 2012; Tokunaga et al., 2016; Hosoda et al., 2017). Furthermore, *FGFR2*-amp is an adverse prognostic factor in GC patients. Compared to *FGFR2*-unamplified GC, *FGFR2*-amp is significantly associated with lymph node metastasis and worse survival rate (Kim et al., 2019a). Besides, FGFR3 and FGFR4 expression levels and mutations are associated with poor prognosis and drug resistance, inhibition of cell proliferation signals, and induction of apoptosis (Jang et al., 2001; Ye et al., 2012; Ye et al., 2013; Piro et al., 2016). Evidence suggests that *FGFR* knockdown or inhibition selectively inhibits GC cell line growth (Katoh, 2010; Jang et al., 2017; Zhang et al., 2019). Hence, pharmacological targeting of FGF/FGFRs signaling pathways may be effective for the treatment of FGFRs-altered GC.

Based on biochemistry and cell-based screening from our laboratory's bioactive compound library, we found a novel FGFR inhibitor RK-019. In this study, we evaluated the anti-neoplastic activity of RK-019 both *in vitro* and *in vivo*. RK-019 showed excellent inhibition and great selectivity against FGFR family kinases, strong anti-proliferative effects, and anti-metastasis on *FGFR2*-amp GC cells. Therefore, RK-019 might be an effective treatment agent against *FGFR2*-amp GC, making it a candidate drug for GC treatment.

Materials and methods

Materials

RK-019 was synthesized in our laboratory (State Key Laboratory of Biotherapy, Sichuan University, Chengdu, China). RK-019 was dissolved in dimethyl sulfoxide (DMSO) from Sigma (D8418, St Louis, Mo, United States) at a stock concentration of 40 mM and stored in a -80°C refrigerator. The working solution was diluted to 100 nM, 10 nM, 5 nM, 1 nM, and 0.1 nM by DMSO and stored in a -20°C refrigerator. 3-(4,5-Dimethyl-2-thiazolyl)-2,5-diphenyl-2-H-tetra-zolium bromide (MTT) was purchased from CSNpharm (CSN12440, Shanghai, China). A PE Annexin V Apoptosis Detection Kit was purchased from BD Biosciences (559763, Franklin, NJ, United States). Antibodies: FGFR2 (23328), p-FRS2 (3864), PLCγ (5690), p-PLCγ (14008), AKT (4691), p-AKT (4060), Erk (4695), p-Erk (4370), CDK 2 (18048), CDK 4 (12790), CDK 6 (13331), Cyclin D1 (55506), Cyclin E (4136), p27 (3686), Caspase 3 (9662), and Cleaved-caspase 3 (9661) were purchased from Cell Signaling Technology (Beverly, MA, United States). p-$FGFR2^{T653/T654}$ (AF8210), JAK2 (AF6022), p-$JAK2^{T1007}$ (AF3022), STAT3 (AF6294), and p-$STAT3^{T705}$ (AF3293) were purchased from Affinity Biosciences (Changzhou, China). MMP-2 (CY7164) and MMP-9 (CY5205) were purchased from Abways (Shanghai, China). FRS2 (R26776) and β-actin (200068-8F10) are from Zen-bio (Chengdu, China).

Synthesis of RK-019

Synthesis route diagrammed in Figure 1C

Step i: (*E*)-5-(((5-bromopyridin-2-yl)imino)methyl)-2,2-dimethyl-1,3-dioxane-4,6-dione (2). A mixture of triethyl

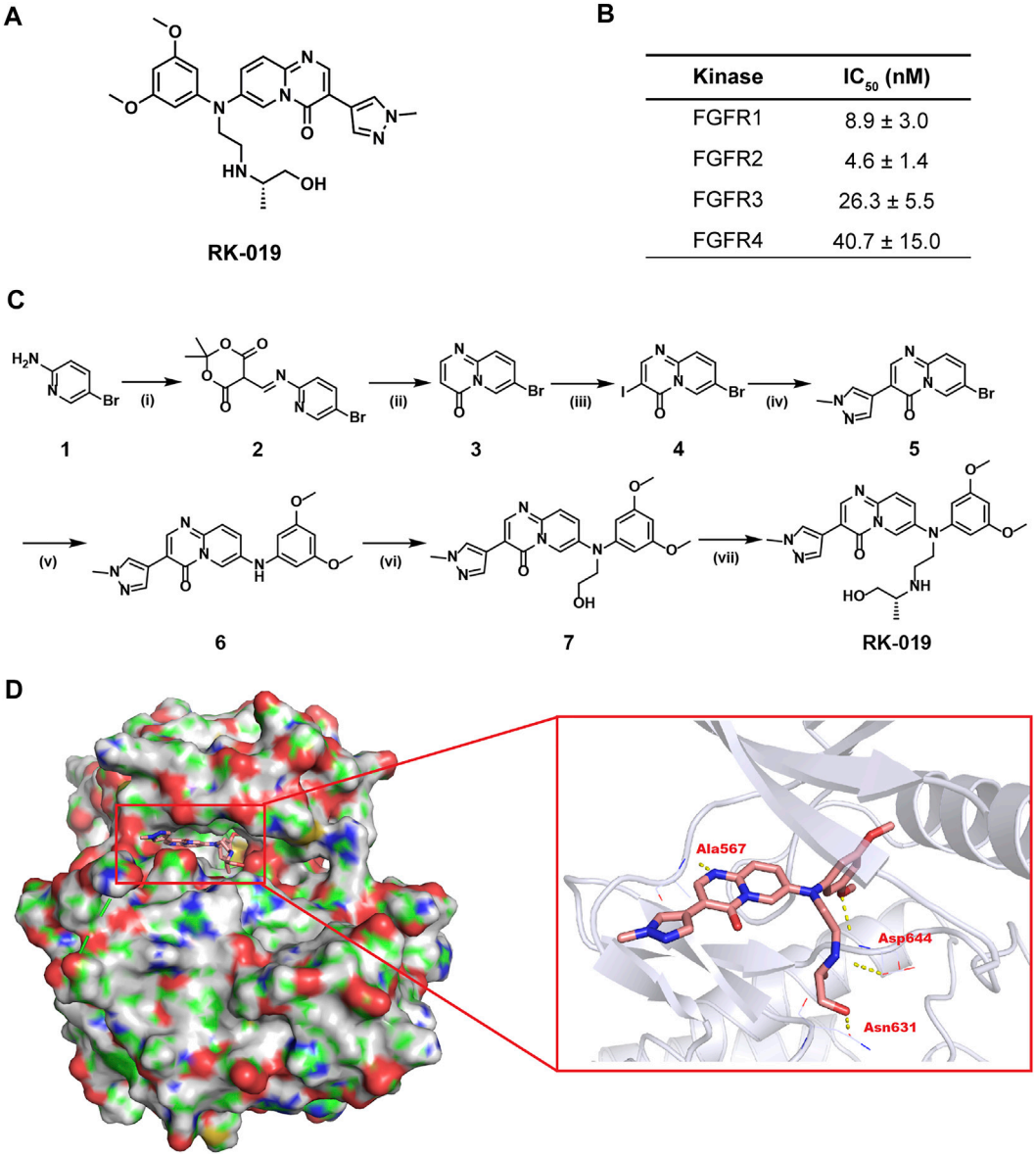

FIGURE 1
Development of RK-019. **(A)** Chemical structure of RK-019. **(B)** IC_{50} values of RK-019 against kinases FGFR 1–4. **(C)** Synthesis route of RK-019. Reagents and conditions: (i) Triethyl orthoformate, 2,2-dimethyl-1,3-dioxane-4,6-dione, EtOH, reflux; (ii) Diphenyl oxide, 220°C; (iii) NIS, DMF, 80°C; (iv) Boronic acids or boronate esters, Pd $(dppf)_2Cl_2$, K_2CO_3, dioxane, H_2O, 100°C; (v) 3,5-Dimethoxyaniline, Pd_2 $(dba)_3$, 2,2′-bis(diphenylphosphino)-1,1′-dinaphthalene, Cs_2CO_3, toluene, 100°C; (vi) (a) 2-(tert-Butyldimethylsilyloxy)bromoethane, NaH, DMF, 5°C–r.t.; **(b)** TBAF, THF, r. t.; and (vii) (a) MsCl, Et_3N, CH_2Cl_2, 0°C; (b) (R)-1-(aminomethyl)ethanol, CH_3CN, 100°C. **(D)** Docking results of RK-019 on FGFR2 protein (PDB ID: 6AGX).

orthoformate (8.5 g, 80 mmol) and 2,2-dimethyl-1,3-dioxane-4,6-dione (11.5 g, 80 mmol) was heated at 60°C for 2 h. Then, a solution of 5-bromopyridin-2-amine (1, 13.8 g, 80 mmol) in EtOH (80 ml) was added slowly and the resulting reaction mixture was stirred at 60°C for additional 2 h. Upon completion of the reaction, the mixture was cooled to room temperature. The precipitate was filtered and the filter cake was washed with a small amount of EtOH and dried in a vacuum oven to afford 2 as white solid (16.6g, 64%). ^{1}H NMR (400 MHz, $CDCl_3$): δ 11.39–11.24 (m, 1 H), 9.38–9.28 (m, 1 H), 8.47 (d, J = 2.4 Hz, 1H), 7.86 (dd, J = 8.5, 2.4 Hz, 1H), 6.95 (d, J = 8.5 Hz, 1H), and 1.76 (s, 6H). ESI-MS: $C_{12}H_{11}BrN_2O_4$, MS (ESI) *m/z* 327.1 $[M + H]^+$.

Step ii: 7-bromo-4*H*-pyrido [1,2-a]pyrimidin-4-one (3). Ph_2O (200 ml) was heated to 220°C, then 2 (16.6 g, 51 mmol) was slowly added into the solution. The mixture was stirred at

220°C for 30 min. TLC detected that the reaction was completed. The mixture was cooled and purified by column chromatography with petroleum ether/ethyl acetate (4:1) to afford 3 (10.7g, 93%). ^{1}H NMR (400 MHz, DMSO-d_6): δ 9.03 (d, J = 2.2 Hz, 1H), 8.32 (d, J = 6.4 Hz, 1H), 8.08 (dd, J = 9.4, 2.2 Hz, 1H), 7.65 (d, J = 9.4 Hz, 1H), and 6.46 (d, J = 6.4 Hz, 1H). ESI-MS: $C_8H_5BrN_2O$, MS (ESI) m/z 225.2 $[M + H]^+$.

Step iii: 7-bromo-3-iodo-4*H*-pyrido [1,2-a]pyrimidin-4-one (4). To a stirred solution of 3 (10.2 g, 45 mmol) in DMF (50 ml) was added NIS (13.6g, 60 mmol), the mixture was stirred at 80°C for 5 h. Upon completion of the reaction, the reaction mixture was cooled to room temperature, and then added with H_2O (50 ml) under stirring. The precipitate was collected by filtration, washed with water dried to a constant weight to afford 4 (15.0 g, 95%).^{1}H NMR (400 MHz, DMSO-d_6): δ 9.02 (d, J = 2.0 Hz, 1H), 8.75 (s, 1H), 8.13 (dd, J = 9.4, 2.0 Hz, 1H), 7.67 (d, J = 9.4 Hz, 1H). MS (ESI) m/z 351.0 $[M + H]^+$.

Step iv: 7-bromo-3-(1-methyl-1H-pyrazol-4-yl)-4H-pyrido [1,2-a]pyrimidin-4-one (5). 4 (14.1 g, 40 mmol) and 1-methyl-4-(4,4,5,5-tetramethyl-1,3,2-dioxaborolan-2-yl)-1H-pyrazole (8.3 g, 40 mmol), Na_2CO_3 (8.5 g, 80 mmol) were dissolved in dioxane (100 ml) and H_2O (25 ml). The suspension was degassed under nitrogen bubbling for 10 min before Pd $(dppf)_2Cl_2$ (2.9 g, 4 mmol) was added. The reaction mixture was heated to 100°C for 5 h, and then diluted with ethyl acetate. The solution was washed with water and brine successively, dried over anhydrous sodium sulfate, and concentrated in vacuum. The residue was purified *via* silica gel chromatography with petroleum ether/ethyl acetate (2:1) to afford 5 (8.1 g, 66%). ^{1}H NMR (400 MHz, DMSO-d_6): δ 8.79–8.68 (m, 2H), 8.32 (s, 1H), 8.10 (s, 1H), 7.78 (dd, J = 9.6, 2.6 Hz, 1H), 7.69 (d, J = 9.6 Hz, 1H).

Step v: 7-((3,5-dimethoxyphenyl)amino)-3-(1-methyl-1*H*-pyrazol-4-yl)-4*H*-pyrido [1,2-a]pyrimidin-4-one (6). A mixture of 5 (8.1 g, 26.3 mmol), 3,5-dimethoxyaniline (4.8 g, 31.6 mmol), Pd_2 $(dba)_3$ (2.4 g, 2.63 mmol), (±)-BINAP (2.5 g, 3.95 mmol), and cesium carbonate (12.9 g, 39.5 mmol) in anhydrous toluene (120 ml) was degassed with N_2 for 10 min. The reaction was heated to 100°C overnight under N_2, and then cooled to room temperature. The mixture was filtrated through a Celite and the filter cake was washed with DCM/MeOH (10/1). After concentration of the filtrate, the residue was purified by column chromatography with methyl allylchloride/methanol (20:1) to give 6 (7.1 g, 56%).^{1}H NMR (400 MHz, DMSO-d_6): δ 10.70 (s, 1H), 8.67 (d, J = 2.6 Hz, 1H), 8.48 (s, 1H), 8.23 (s, 1H), 7.89 (s, 1H), 7.36 (d, J = 9.6 Hz, 1H), 7.25 (dd, J = 9.6, 2.6 Hz, 1H), 6.28–6.16 (m, 3H), 3.86 (s, 3H), and 3.74 (s, 6H).

Step vi: 7-((3,5-dimethoxyphenyl) (2-hydroxyethyl)amino)-3-(1-methyl-1*H*-pyrazol-4-yl)-4*H*-pyrido [1,2-a]pyrimidin-4-one (7). To a solution of 6 (4.0 g, 10.6 mmol) in DMF (60 ml) was added sodium hydride (60% dispersion in mineral oil, 933 mg, 23.32 mmol) slowly at 0 °C under argon. After being stirred at this temperature for 30 min, (2-bromoethoxy) (tert-butyl)dimethylsilane (4.6 ml, 21.2 mmol) was added and then the reaction mixture was stirred at room temperature overnight. Following this time, the reaction mixture was diluted with water and then extracted with ethyl acetate twice. The combined extracts were washed with water and brine, dried over anhydrous Na_2SO_4, and concentrated under reduced pressure. The residue was dissolved in tetrahydrofuran (20 ml) and tetrabutylammonium fluoride (1 M in tetrahydrofuran, 21.2 ml, 21.2 mmol) was added. The reaction mixture was stirred at room temperature overnight. Following this time, the reaction mixture was concentrated under vacuum and the resulting residue was purified by column chromatography with methyl allylchloride/methanol (10:1) to give the title compound 7 as yellow solid (2.5g, 56%). ^{1}H NMR (400 MHz, DMSO-d_6): δ 8.77–8.71 (m, 2H), 8.38 (s, 1H), 8.12 (s, 1H), 7.68 (dd, J = 9.6, 2.6 Hz, 1H), 7.61 (d, J = 9.6 Hz, 1H), 6.43–6.32 (m, 3H), 4.96 (t, J = 5.0 Hz, 1H), 3.93–3.83 (m, 5H), 3.71 (s, 6H), and 3.68–3.61 (m, 2H). HRMS: calculated for $C_{22}H_{23}N_5O_4$ $[(M + H)^+]$, 422.1824; found 422.1821.

Step vii: (*R*)-7-((3,5-dimethoxyphenyl) (2-((1-hydroxypropan-2-yl)amino)ethyl)amino)-3-(1-methyl-1*H*-pyrazol-4-yl)-4*H*-pyrido [1,2-a]pyrimidin-4-one (RK-019). To a mixture of 7 (2.5 g, 5.9 mmol) and Et_3N (2.1 ml, 14.75 mmol) in DCM (30 ml) was added methanesulfonyl chloride (0.917 ml, 11.8 mmol) dropwise at 0°C under argon. The reaction mixture was stirred at room temperature for 2 h. After completion (monitored by TLC), the reaction mixture was quenched with water, then extracted with DCM twice. The combined extracts were washed with water and brine successively, dried over anhydrous Na_2SO_4, and concentrated under vacuum. The residue was purified by column chromatography to give the intermediate (2.2 g). A mixture of the intermediate (2.2 g, 4.4 mmol) and (*R*)-1-(aminomethyl) ethanol (3.3 g, 44 mmol) in acetonitrile (44 ml) was heated at 100°C overnight. After completion (monitored by TLC), the reaction mixture was concentrated under vacuum and the residue was purified on TLC-preparative plates with methyl allylchloride/methanol (10:1) to afford the desired product RK-019 as light-yellow solid (366 mg, 18%), mp.144–150°C. ^{1}H NMR (400 MHz, DMSO-d6): δ 8.73 (s, 1H), 8.66 (d, J = 2.5 Hz, 1H), 8.38 (s, 1H), 8.12 (s, 1H), 7.66 (dd, J = 9.6, 2.5 Hz, 1H), 7.61 (d, J = 9.6 Hz, 1H), 6.38 (d, J = 2.1 Hz, 2H), 6.31 (d, J = 2.1 Hz, 1H), 4.51–4.43 (m, 1H), 3.89 (s, 3H), 3.84 (t, J = 6.5 Hz, 2H), 3.72 (s, 6H), 3.29–3.20 (m, 3H), 2.86–2.75 (m, 2H), 2.63–2.57 (m, 1H), and 0.90 (d, J = 6.2 Hz, 3H). ^{13}C NMR (101 MHz, DMSO-d_6) δ 161.88, 149.53, 148.44, 147.50, 143.96, 140.08, 138.25, 135.93, 131.16, 129.47, 121.78, 120.85, 109.54, 104.32, 97.49, 55.76, 52.78, 48.55, 44.28, and 23.31. HRMS: calculated for $C_{25}H_{30}N_6O_4$ $[(M + H)^+]$, 479.2403; found 479.2405.

Molecular docking

The 3D structure of FGFR2 was downloaded from the PDB (http://www.rcsb.org/, PDB ID: FGFR1: 5EW8, FGFR2: 6AGX, FGFR3: 6LVM, and FGFR4: 6NVK). The protein was prepared

with discovery studio 3.1. Molecule RK-019 was built with ChemBio3D and optimized at the molecular mechanical level. Then, RK-019 was docked to the binding site of JNJ42756493 by employing a protein-ligand docking program GOLD 2.5, respectively. Scoring function GOLDSCORE was used for exhaustive searching, solid body optimizing, and interaction scoring. The final results for molecular docking were visualized by using the PyMol program.

Kinase inhibition and selectivity assay

Median-inhibitory concentration (IC_{50}) and inhibition ratio of kinases by RK-019 was assessed by Eurofins Discovery Services (Dundee, United Kingdom) using the ATP-site competition binding assay *in vitro*. Firstly, gradient concentration of RK-019 against FGFRs, including FGFR1, FGFR2, FGFR3, and FGFR4, were tested. IC_{50} value was calculate by the GraphPad Prism software (v8.4.3, GraphPad Software, California, United States). Then, to measure the selectivity prolife of RK-019, a panel of 422 recombinant human kinases was screened at a concentration of 1 μM RK-019. Kinase MAP was drawn by webtools from Cell Signaling Technology, Inc. (www.cellsignal.com).

Cell lines

SNU-16, KATO III, AZ 521, MGC 80–3, HGC 27, N87, AGS, NUGC-4, GT 39, MKN 45, BGC823, and GES-1 were purchased from BeNa Culture Collection (Beijing, China). HGC27, AGS, NUGC-4, and GT39 cell lines were cultured in DMEM (L110KJ, BasalMedia, Shanghai, China) with 10% of fetal bovine serum (900–108, Gemini, California, USA). SNU-16, AZ521, MGC 80–3, N87, MKN45, BGC823, and GES-1cell lines were cultured in RPMI-1640 medium (L210KJ, BasalMedia) with 10% of fetal bovine serum. KATO III cell was cultured in IMDM medium (L610KJ, BasalMedia) with 20% of fetal bovine serum. All the culture medium was contained with 1% antibiotic (30–002-CI, Corning, Corning, NY, United States). All the cell lines were maintained in 5% CO_2 condition at 37 °C.

Cell viability assay

For suspension and mixed suspension adherent cells, the cells were seeded in 96-well plate with different cell density, 0.5×10^4 per well for 96 h treatment, 1×10^4 per well for 72 h treatment, 2×10^4 per well for 48 h treatment, and 5×10^4 per well for 24 h treatment. Different doses of RK-019 were treated as soon as the cell seeded in 96-well plates. For adherent cells, the cells were seeded in a 96-well plate with 3×10^3 per well and cultured overnight followed by administrated different doses of RK-019. After indicated time treatment, MTT solution at a final concentration of 0.5 mg/ml was added and incubated 2–4 h at 37°C. Formazan formed by the living cells was dissolved with DMSO and the absorbance was measured using a microplate spectrophotometer (MultiskanFC, ThermoFisher, Waltham, MA, United States) at 570 nm. IC_{50} value of RK-019 was calculated by the Graphpad Prism software.

Quantitative reverse transcription PCR (qRT-PCR)

The GC cell total RNAs were extracted by TRIzol (15596026, ThermoFisher). RNA was reversed transcribed into cDNA by using HiScript III RT SuperMix for qPCR (R323-01, Vazyme, Nanjing, China) according to the manufacturer's protocol. qRT-PCR for *FGFR2* gene expression was carried out by ChamQ universal SYBR qPCR Master Mix (Q711-02, Vazyme) on Bio-Rad CFX96 Realtime PCR system. The PCR primer for *FGFR1*: forward 5'- GCTACAAGGTCCGTTATGC -3' and reverse 5′- CAATGCAGGTGTAGTTGCC -3', *FGFR2*: forward 5'- GGT GGCTGAAAAACGGGAAG -3' and reverse 5′- AGATGGGAC CACACTTTCCATA -3', *FGFR3*: forward 5'- TGCGTCGTG GAGAACAAGTTT -3' and reverse 5′- GCACGGTAACGT AGGGTGTG -3', *FGFR4*: forward 5'- CCATAGGGACCCCTC GAATAG -3' and reverse 5′- CAGCGGAACTTGACGGTGT -3', and *ACTB*: forward 5'- CACCATTGGCAATGAGCGGTTC -3' and reverse 5′- AGGTCTTTGCGGATGTCCACGT -3'. The gene expression analysis was conducted by the ΔΔCq method.

Cell counting assay

SNU-16 and KATO III were seeded in 6-well plated with 1×10^5 per well. RK-019 was treated as soon as the cells seeded in the 6-well plates. After indicated time, the images were captured using an inverted microscope. Then, the cells in the captured well were resuspended and live cell numbers were determined by the trypan blue (BL627A, Biosharp, Hefei, China) method.

Edu staining assay

For Edu staining assay, 1×10^5 cells were seeded in 24-well plates. RK-019 and DMSO were treated as soon as the cells seeded into the plates. After 24 h, the cells were incubated with the medium contained 10 μM Edu for 2 h. After that, the cells were collected and fixated to slide, and then stained with the Cell-Light EdU Apollo488 *In Vitro* Kit (C10310, Ribobio, Guangzhou, China). After staining, the samples were photographed and analyzed by the ImageJ software (v1.53a, Wayne Rasband, United States).

Cell cycle and apoptosis analysis

Cell cycle and apoptosis assay were both measured by flow cytometry (FCM). The data were analyzed by the NovoExpress software (v1.4.0, Agilent, Santa Clara, CA, United States). For cell cycle assay, the cells were treated by different concentrations of RK-019 for 24 h, then were harvested and washed twice with cold phosphate buffered solution (PBS), followed by fixed with 75% ethanol overnight. Before test, the cells were washed twice with cold PBS and stained with PI stanning solution using cell cycle detecting kit (KGA512, KeyGEN, Nanjing, China), and then measured by FCM. For apoptosis assay, the cells were harvested after treated with different concentrations of RK-019 for 24 h, and stained with a PE Annexin V Apoptosis Detection Kit according to the manufacturer's protocol followed by detected using FCM.

Transwell migration and invasion assay

In the migration assay, 1×10^5 cells were resuspended in a serum-free medium, then added into the upper chamber, meanwhile the medium containing 10% FBS was added at the bottom with 100 nM RK-019. After 24 h incubation, the migration cells on the filters were fixed with 4% paraformldehyde and washed with PBS, then stained with crystal violet solution for 20 min. In the invasion assay, the upper surface of the transwell was coated with Matrigel (356234, Corning) for 30 min at 37°C until Matrigel was solidified. 1×10^5 cells were resuspended in a serum-free medium, then added into the upper chamber, meanwhile the medium containing 10% FBS was added at the bottom with 100 nM RK-019.After 24 h , the invasion cells on the filters were hatched and fixed, then stained with crystal violet.

Western blot analysis

The cells treated with RK-019 at indicated concentration for 24 h were harvested and lysed in 1× RIPA buffer (20e188, MilliporeSigma, Burlington, MA, United States), which contained protease inhibitor cocktail (B14001, Bimake, Houston, TX, United States) and phosphatase inhibitor cocktail (B15001, Bimake), for 30 min and equalized by concentration of the total protein before loading. Using sodium dodecyl sulphate - polyacrylamide gel electrophoresis (SDS-PAGE) to separate the protein sample and transfer to PVDF membranes (ISEQ00010, MilliporeSigma). The membranes were incubated with relevant primary antibody and corresponding HRP-labeled secondary antibody. Then, chemiluminescence was used to detect target bands. ImageJ software were used to make the gradation analysis.

In western blot, results analysis of relative expression quantification level, data were firstly calculated according to the following formular: Protein Relative expression data = G_t/G_i. G_t means the gradation level of target protein band and G_i means the gradation level of internal reference protein band. Then, the relative expression level can be calculated by the following formular: Protein Relative expression level = $D_t/D_c \times100\%$. D_t means the protein relative expression data of target group and D_c means the protein relative expression data of control group.

In western blot, results analysis of relative phosphorylation quantification level, data were firstly calculated according to the following formular: Protein Relative phosphorylation data = G_p/G_{up}. G_p means the gradation level of target phosphorylation protein band and G_{up} means the gradation level of target total protein band. Then, the relative phosphorylation level can be calculated by the following formular: Protein Relative expression level = $P_t/P_c \times100\%$. P_t means the relative phosphorylation data or target group and P_c means the relative phosphorylation data of control group.

In vivo PK assay

All animal experiments in this study have been approved by the Institutional Animal Care and Treatment Committee of Sichuan University in China and were carried out in accordance with the approved guidelines. Sprague-Dawley rats (weight 180–200 g, Beijing HJF bioscience, Beijing, China) were used in this experiment and maintained in a specific-pathogen-free (SPF) condition facility. RK-019 was dissolve in ethanol first, followed by mixed with Kolliphor EL, then filled with saline to the calculated volume. The formula was 12.5% ethanol, 12.5% Kolliphor EL, and 75% saline. RK-019 was administrated *via* i. v. 3 mg/kg or p. o. 30 mg/kg. After 5, 10, 15, 30, 60, 120, 240, 360, 600, and 1,440 min of administration, the blood samples were collected. Plasma fraction was obtained by centrifuged blood, then deproteinized with methanol containing an internal standard. The compound concentrations of the target compound in the supernatant were measured by liquid chromatography–mass spectrometry/mass spectrometry (LC-MS/MS).

Subcutaneous xenograft model

NOD/SCID mice (6-week-old, weight 18–20 g, Beijing HJF bioscience) were used in this experiment and maintained in a specific-pathogen-free (SPF) condition facility. SNU-16 Cells were resuspended in PBS mixed with Matrigel (1:1) and adjust the density to 1×10^7 per mice (100 μL). The cell suspensions were inoculated subcutaneously on the right flank of the mice. When the mean tumor volume reached approximately 200 mm^3, the mice were divided into four groups (five mice each group): i. Vehicle group, ii. RK-019 15 mg/kg group, iii. RK-019 30 mg/kg group, and iv. RK-

019 45 mg/kg group. RK-019 was dissolved in same formula as the *in vivo* PK study. RK-019 was administrated once *per* day by oral gavage for 21 days. Tumor volumes were measured three times *per* week. The tumor volume was measured by a caliper and calculated according to the following formula:

$$\text{Tumor volume} = \frac{\text{Major axis} \times \text{Miner axis}^2}{2}.$$

At the end of administration, the mice were executed euthanasia, then tumors, blood, and organs were extracted. The complete blood count (CBC), serum phosphorus analysis, and blood biochemical analysis were completed by West China Frontier Pharma Tech (Chengdu, China). The pathological section and IHC stanning was completed by Servicebio (Wuhan, China). The tumor growth inhibition (TGI) values were calculated with the following formula:

$$\text{TGI} = \left(1 - \frac{T_n - T_0}{C_n - C_0}\right) \times 100\%.$$

T_n and T_0 represent average tumor volume before treatment and that of day n after treatment in the treatment group. C_n and C_0 represent average tumor volume before treatment and that of day n after treatment in the vehicle group. In this study, n is 21st day.

Statistical analyses

All data were analyzed by the GraphPad Prism 8.4.3 (GraphPad Software, California, United States), and was shown as mean value ±SD or SEM, details will be illustrated in the figure legends. Dose-effect curve analysis (IC_{50} calculation) was performed by the Graphpad Prism software. First, concentration value was converted to log value, followed by non-linear regression analyze which is l*og(inhibitor)* vs. *normalized response—Variable slope*, was performed to calculate the IC_{50} values. The statistically significant p values were calculated by student's t-test or two-way ANOVA and were shown in graphics which were labeled as follows: $^*p < 0.05$; $^{**}p < 0.01$; $^{***}p < 0.001$.

Result

Development of RK-019

In this study, we identified a novel small molecule pan-FGFR inhibitor, RK-019, whose chemical structure was named as (*R*)-7-((3,5-dimethoxyphenyl) (2-((1-hydroxypropan-2-yl)amino)ethyl) amino)-3-(1-methyl-1*H*-pyrazol-4-yl)-4*H*-pyrido [1,2-a] pyrimidin-4-one (Figure 1A). The method of synthesis of RK-019 is described in detail in the materials and methods section (Figure 1C). Briefly, RK-019 was synthesized from 5-bromopyridin-2-amine 1) with imidization, cyclization, iodination, and Suzuki coupling of 4 with 1-methyl-4-pyrazole boronic acid pinacol ester, followed by Buchwald coupling to get 6. Finally, nucleophilic substitution with 6 and 2-isopropylaminoethylchloride and deprotection by hydrochloric acid produced RK-019. ^{1}H-NMR, ^{13}C-NMR, and HRMS spectrometry results were shown in Supplementary Figure S3.

Molecular docking was conducted to model the binding of RK-019 in the ATP pocket using a reported crystal structure of FGFR kinase domain (PDB ID: 6AGX). As shown in Figure 1D, RK-019 could fit well in the ATP pocket of FGFR2 and the *N*-methyl pyrazole group could extend into the solvent region. RK-019 maintained H-bond interactions with FGFR2 at the backbone NH of Ala567 in the hinge region. The methoxyphenyl motif occupied the hydrophobic region in the ATP pocket and its methoxy group formed a H-bond with the NH of Asp644. The 2-amino-propanol group can interact with the main carbonyl group of Asp644 and Asn631 to form two hydrogen bonds. Overall, RK-019 could fit well into the ATP pocket of FGFR2. Similarity, RK-019 could also fit well in FGFR1 (PDB ID: 5EW8), FGFR3 (PDB ID: 6LVM), and FGFR4 (PDB ID: 6NVK) ATP binding pocket (Supplementary Figure S1). Then, the ATP-based kinase activity assay provided by kinase profile service (Eurofins Discovery) revealed that RK-019 was sufficient to inhibit the FGFR family kinase activity, with the IC_{50} of 9.1 nM (FGFR1), 4.6 nM (FGFR2), 26.3 nM (FGFR3), and 40.7 nM (FGFR4) (Figure 1B).

Kinase selectivity profile of RK-019

To further investigate the kinase selectivity, the kinase inhibitory profile of RK-019 was determined against a diverse panel of 422 recombinant human kinases from Eurofins Discovery by the ATP-site competition binding assay at a concentration of 1 μM (Supplementary Table S1). The kinase inhibition results were depicted in a kinase MAP at a 35% activity cutoff of the DMSO control (Figure 2). Of these, only seven hits (FGFR1, FGFR2, FGFR3, FGFR4, FLT4, RET, and LYN) showed over 90% of inhibition. A further enzyme activity assay was performed to determine the IC_{50} values of these seven hits. As results shown, RK-019 showed a great selectivity to the FGFRs family kinase, which indicated that the molecule was a potent and selective pan-FGFR inhibitor.

Anti-proliferation effects of RK-019 against *FGFR2*-amp GC cell lines

Different GC cell lines were used to verify the biological activity of RK-019, including SNU-16, KATO III, AZ 521, MGC 80–3, HGC 27, N87, AGS, NUGC-4, GT 39, MKN 45, BGC823, and gastric epithelial cell line GES-1. The

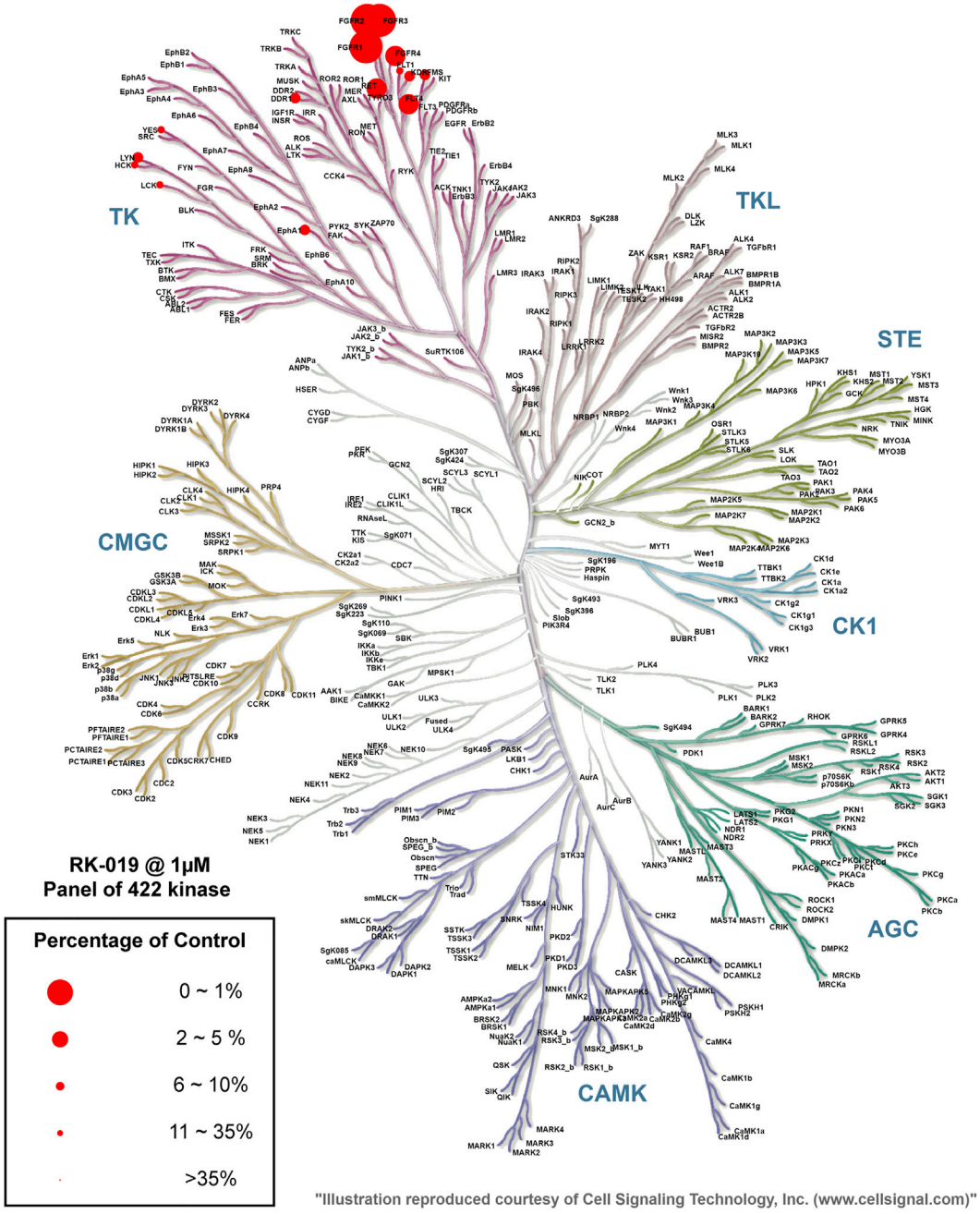

FIGURE 2
Kinase selectivity profile of RK-019. Measurement of 422 kinases was performed at 1 μM of RK-019. Each kinase was measured once. Data were cutoff on 35% kinase activity compared to the DMSO group. The TREE spot image was mapped with the KinMap software tool provided by Cell Signaling Technology, Inc. (www.cellsignal.com). The percentage of control means remaining active kinase percentage.

FGFR2 expression level is relevant to poor pathological features and prognostic, and anti-FGFR2 agents could provide potential effectiveness in GC treatment [22, 31, 32]. Firstly, we measured the *FGFRs* mRNA expression levels in these GC cell lines by qRT-PCR. By comparing the expression data, we have found that *FGFR2*-amp cell lines, SNU-16, and KATO III exhibited the highest mRNA expression level of *FGFR2* (Figure 3A, Supplementary Figure S2). Then, MTT assay was performed to test the viability of GC cell lines following treatment with RK-019.

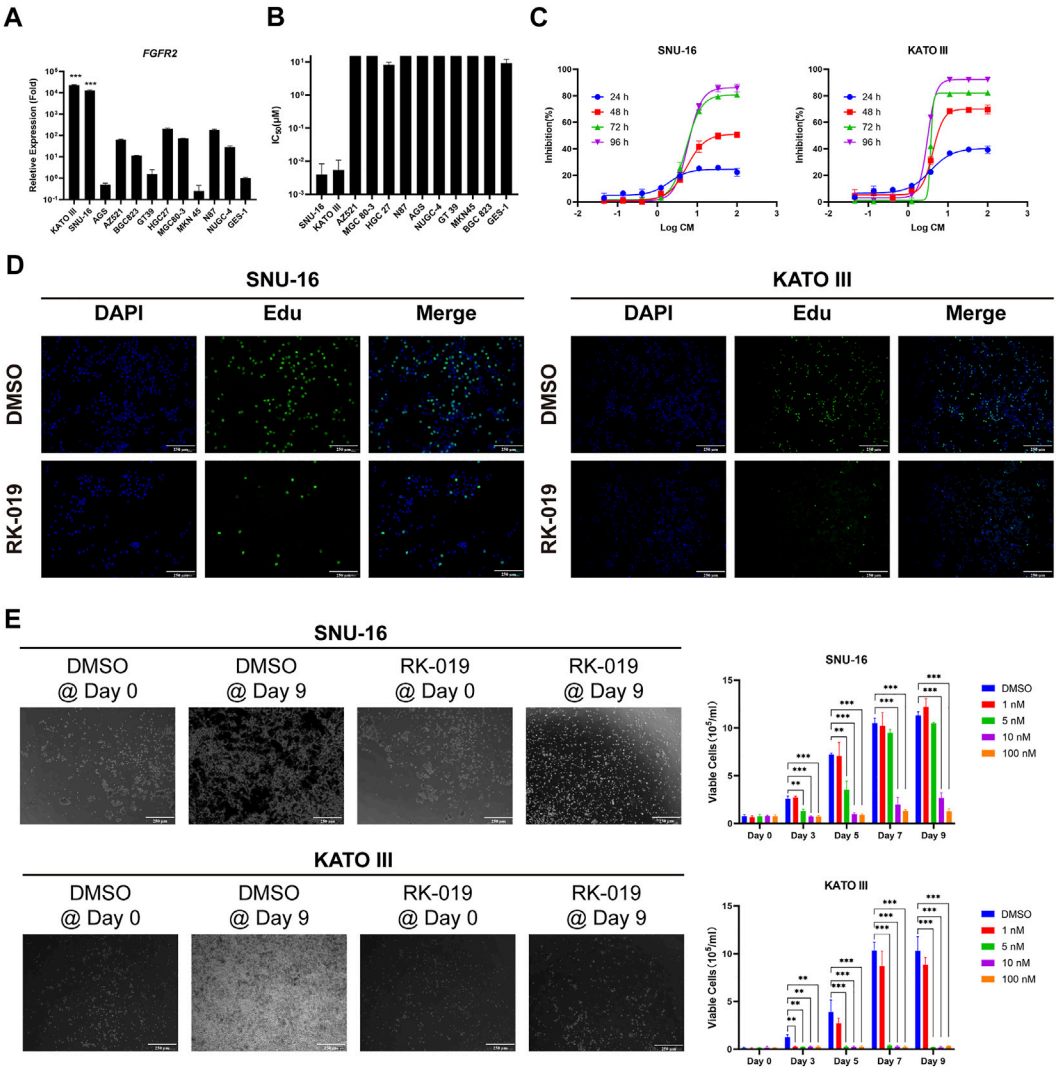

FIGURE 3
Anti-proliferative action of RK-019. **(A)** qRT-PCR analysis of the *FGFR2* relative expression level on different types of gastric cancer cell lines. GES-1 was used as control. Data were shown in mean ± SEM. **(B)** IC_{50} of RK-019 measured by MTT assay on different types of gastric cancer cell lines. Data were shown in mean ± SD. **(C)** SNU-16 and KATO III cell lines were treated with different concentrations of RK-019 for 24, 48, 72 and 96 h, respectively. The inhibition ratio indexes by MTT assay were the percentage of cells contrast to DMSO-treated group at respect time. Data were shown in mean ± SD. **(D)** Edu staining was used to detect the cell proliferation phenotype with 100 nM RK-019 treatment for 24 h **(E)** SNU-16 and KATO III were treated with RK-019 for 9 days in different concentrations, cells were counted by trypan blue and took pictures every 2 day. The picture only shows the 100 nM RK-019 treatment group on Day 0 and Day 9. Data were shown in mean ± SD. All the data were compiled from three independently repeat experiments. The significance was determined by Student's t-test, $*p < 0.05$; $**p < 0.01$; $***p < 0.001$, for the designated treatment group vs. the DMSO group.

As shown in Figure 3B, SNU-16 and KATO III cell lines were demonstrated to be the most sensitive cell lines to RK-019, with the IC_{50} values of SNU-16 and KATO III cell lines were 3.96 ± 4.4 nM and 5.45 ± 5.3 nM, respectively.

Furthermore, SNU-16 and KATO III cells were exposed to graded concentrations of RK-019 for 24, 48, 72, and 96 h to evaluate the dose- and time-dependent relationships. As shown in Figure 3C, RK-019 showed limited suppression effect after 24 h treatment and obvious suppression effect after 48 and 72 h, but did not significantly increase after 96 h. Moreover, Edu staining was used to verify the changes in cell proliferation. After 24 h of RK-019 administration, the number of Edu-positive stained cells significantly decreased in SNU-16 and KATO III (Figure 3D). The results demonstrated that the inhibition of cell proliferation by RK-019 occurred in a time- and dose-dependent manner. In addition, a prolonged drug

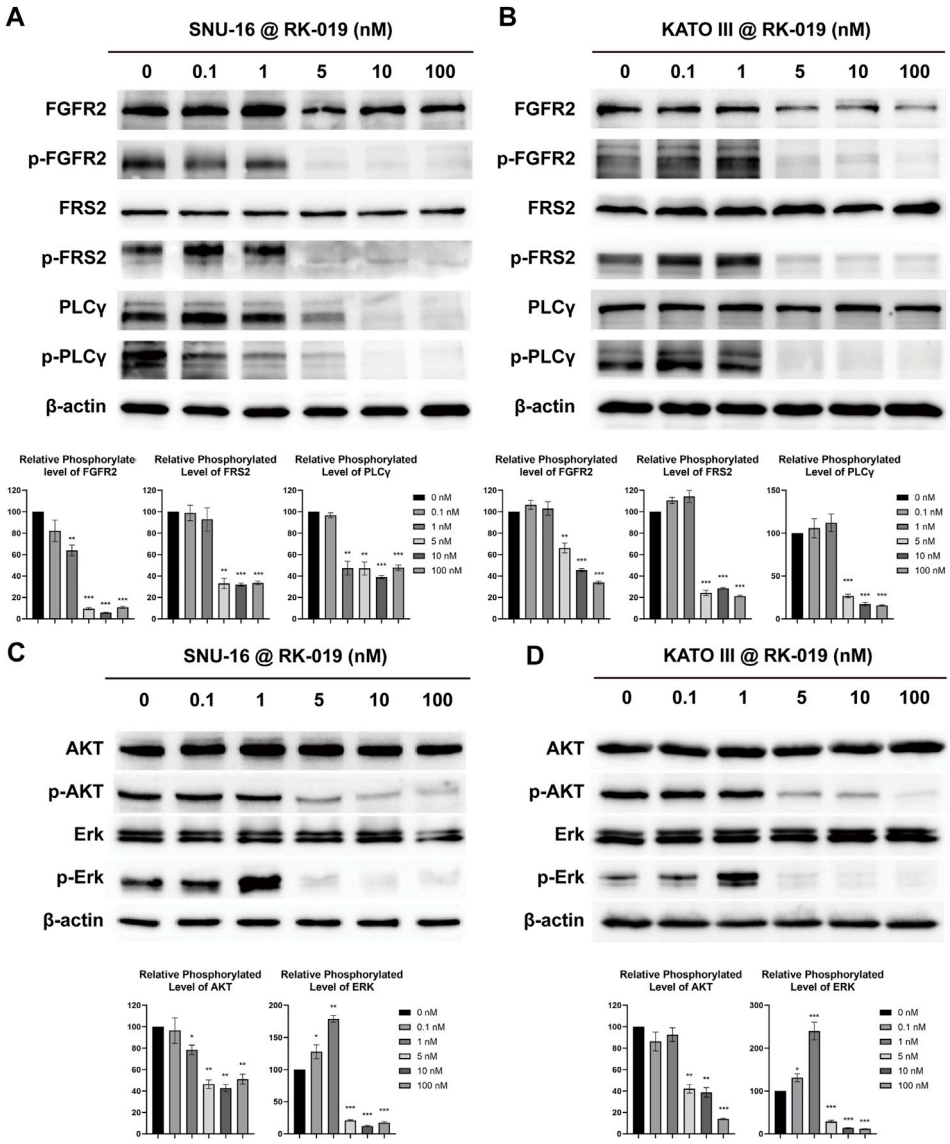

FIGURE 4
RK-019 effectively inhibits the phosphorylation of FGFR2 and the downstream protein in SNU-16 and KATO III cells. SNU-16 and KATO III cells were treated with different concentrations of RK-019 for 24 h. Then, the cells were harvested and lysed with RIPA, then western blot analyses were performed. Western blot results of FGFR signal related proteins in SNU-16 **(A)** and KATO III **(B)**. Western blot results of downstream of FGFR signal in SNU-16 **(C)** and KATO III **(D)**. Each experiment was repeated for three times independently. ImageJ software was used to quantify the analysis of image profile. Quantification data are performed in mean value ±SD. The significance was determined by Student's t-test, $*p < 0.05$; $**p < 0.01$; $***p < 0.001$, for the designated treatment group vs. the DMSO group.

administration experiment was performed. SNU-16 and KATO III were treated with 1, 5, 10, and 100 nM of RK-019 for 9 days. Live cell numbers were determined by trypan blue staining and photos were taken every 2 days to verify the RK-019 anti-proliferation activity. As shown in Figure 3E, SNU-16 cells were inhibited by treatment with 10 and 100 nM of RK-019, and KATO III cells was suppressed by treatment with 5, 10, and 100 nM of RK-019.

RK-019 inhibited FGFR2 phosphorylation and the downstream signal pathway in SNU-16 and KATO III cells

When FGFR is bound to its ligand, auto-phosphorylation at T653/T654 site occurs, which is important for the FGFR kinase activity (Zou et al., 2012). Activated FGFR can phosphorylate downstream proteins, such as FRS2 and PLCγ (Xu et al., 1998;

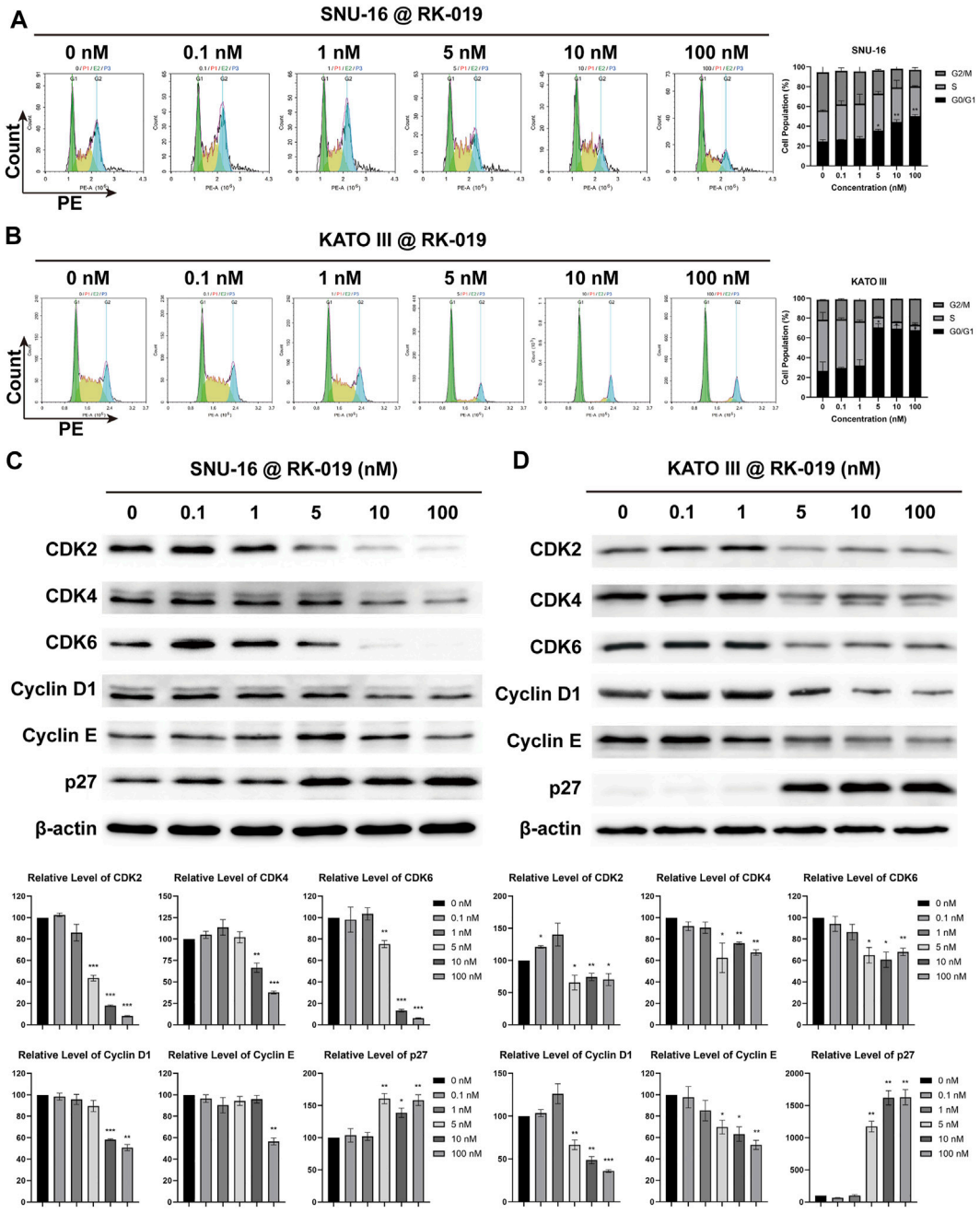

FIGURE 5
RK-019 induced G0/G1 phase arrest. SNU-16 and KATO III cells were treated with different concentrations of RK-019 for 24 h **(A)**, **(B)** FCM analysis cell cycle distribution by PI staining. Cell cycle distribution was analyzed and quantified by the NovoExpress software. Values were shown by mean ± SD. **(C)**, **(D)** Western blot of cell cycle related proteins and quantification analysis. ImageJ software was used to quantify the analysis of image profile. Quantification data were performed in mean value ±SD. Each experiment was repeated for three times independently. Significance was determined by Student's t-test $*p < 0.05$; $**p < 0.01$; $***p < 0.001$, for the designated treatment group vs. the DMSO group.

Goetz and Mohammadi, 2013), and further activate PI3K-AKT-mTOR and Ras-Raf-Erk pathways (Cailliau et al., 2001; Kamata et al., 2002; Tsang and Dawid, 2004). FGFR signaling activation could induce cell proliferation and survival through the signaling cascade. Thus, western blot analysis was used to study the molecular mechanisms underlying the anti-tumor effects of RK-019 and phosphorylation levels of FGFR2, and downstream proteins were determined and analyzed in SNU-16 and KATO III cells.

As shown in Figures 4A and B, after treated with 0.1, 1, 5, 10, and 100 nM of RK-019 for 24 h in SNU-16 and KATO III cells, the protein expression level of phosphorylated $FGFR2^{T653/T654}$ was decreased. Furthermore, the FRS2 and PLCγ phosphorylation levels were also significantly decreased, indicating that RK-019 could suppress the FGFR signaling activity by inhibiting its auto-phosphorylation ability. In addition, we observed that the AKT and Erk phosphorylation levels were also decreased (Figures 4C and D). The AKT and Erk phosphorylation levels reflect the activities of the PI3K-AKT-mTOR and Ras-Raf-Erk pathways, which play an important role in cell proliferation and survival (Lawlor and Alessi, 2001; Zhang and Liu, 2002). Overall, our results suggested that RK-019 could inhibit the auto-phosphorylation of FGFR2, affect the activities of downstream proteins, such as FRS2 and PLCγ, and deactivate the PI3K-AKT-mTOR and Ras-Raf-Erk pathways, resulting in cell proliferation inhibition.

RK-019 induced G0/G1 phase arrest

The FCM analysis was performed to detect the cell cycle distribution. As shown in Figure 5A and B, RK-019 induced G0/G1 arrest after 24 h treatment of RK-019 in SNU-16 and KATO III cells. The G0/G1 proportion was raised from 24.75% to 26.81%–50.29% and 67.88% in SNU-16 and KATO III cells, respectively, after 100 nM RK-019 administration.

We also examined the cell cycle related protein expression levels in cells by western blot analysis. As shown in Figures 5C and D, the G0/G1 cell cycle protein expression levels, including CDK2, 4, and 6, and Cyclin D1 and E, were obviously decreased in KATO III and SNU-16 cells, respectively. Meanwhile, the protein expression level of cell cycle suppression factor p27 was both increased in SNU-16 and KATO III cells. The protein expression levels of CDK2, 4, 6, and Cyclin D1 and E are related with G0/G1 arrest, and p27 can mediate the inhibition of cyclin-CDK2 complex function and result in cell cycle arrest (Massagué, 2004). Therefore, we conclude that RK-019 might induce G0/G1 arrest by inhibited the expression levels of cyclin-CDK complex.

RK-019 induced apoptosis

FGFR signal activation in different types of cancer can lead to the apoptosis resistance (Acevedo et al., 2009). Here, we used the Annexin V-PE/7-AAD dual-labeling method to evaluate the apoptosis levels. SNU-16 and KATO III cells were treated with different concentrations of RK-019 for 72 h and analyzed by FCM. The population of apoptotic cells (early and late apoptotic cells) was increased significantly in SNU-16 (45.5%) and KATO III (32.7%) cells (Figures 6A and B), indicating that apoptosis was induced by RK-019. Further, western blot analysis showed that the amount of cleaved caspase-3 in SNU-16 and KATO III was significantly increased after administering RK-019. In addition, the presence of activated caspase-3 and the cleaved version of poly (ADP-ribose) polymerase (PARP) verified the induction of apoptosis (Figures 6C,D).

RK-019 inhibits cell migration and invasion

Peritoneal metastasis is one of the leading causes of death in patients with GC (Yao et al., 2020) and FGFRs can phosphorylate STAT to promote cancer cell metastasis (Babina and Turner, 2017). As shown in transwell assays, RK-019 could significantly suppress the migration and invasion ability in SNU-16 and KATO III cells (Figures 7A,B). Furthermore, western blot analysis for migration and invasion-related protein confirmed the effect of RK-019 (Figure 7C). The proteins expression levels of MMP-2 and MMP-9 were reduced obviously after RK-019 treatment. The phosphorylation levels of JAK2 and STAT3, which are FGFRs-related downstream proteins, were decreased. As the STAT signaling pathway can regulate the expression levels of MMP-2 and MMP-9 directly (Xie et al., 2004; Jia et al., 2017), we speculated that RK-019 may suppress the migration and invasion of GC cells by blocking the JAK2-STAT signal axis.

In vivo efficacy of RK-019

Pharmacokinetic profile of RK-019 was conducted in Sprague-Dawley rats (*i.v.*,3 mg/kg; oral, 30 mg/kg). The pharmacokinetic parameters are listed in Table 1. After a single oral administration, RK-019 showed slow absorption (T_{max} = 2.67), the peak plasma concentration (C_{max}) was 234.65 ng/ml, the area under the plasma concentration time curve (AUC) was 1,448.41 ng h/mL, the biological half-life ($T_{1/2}$) was 2.83 h, and the oral relative bioavailability was 19.00%.

To investigate the anti-tumor effect of RK-019 *in vivo*, we established a xenograft model using SNU-16 cells. RK-019 was administered at doses of 15, 30, and 45 mg/kg once a day and after 21 days of treatment, the TGI values were 34.3, 85.9, and 83.5%, respectively (Figure 8A). Meanwhile, a significant decrease in tumor weight in the RK-019-treated group was observed compared to that in the vehicle group (Figure 8B).

To validate the results of the *in vivo* assay, we conducted IHC analyses using Ki67 as a cell proliferation marker, cleaved caspase-3 as an apoptotic cell marker, and p-FGFR2 as a FGFR2 signaling activity marker. As shown in Figure 8D, the number of p-FGFR2-positive and

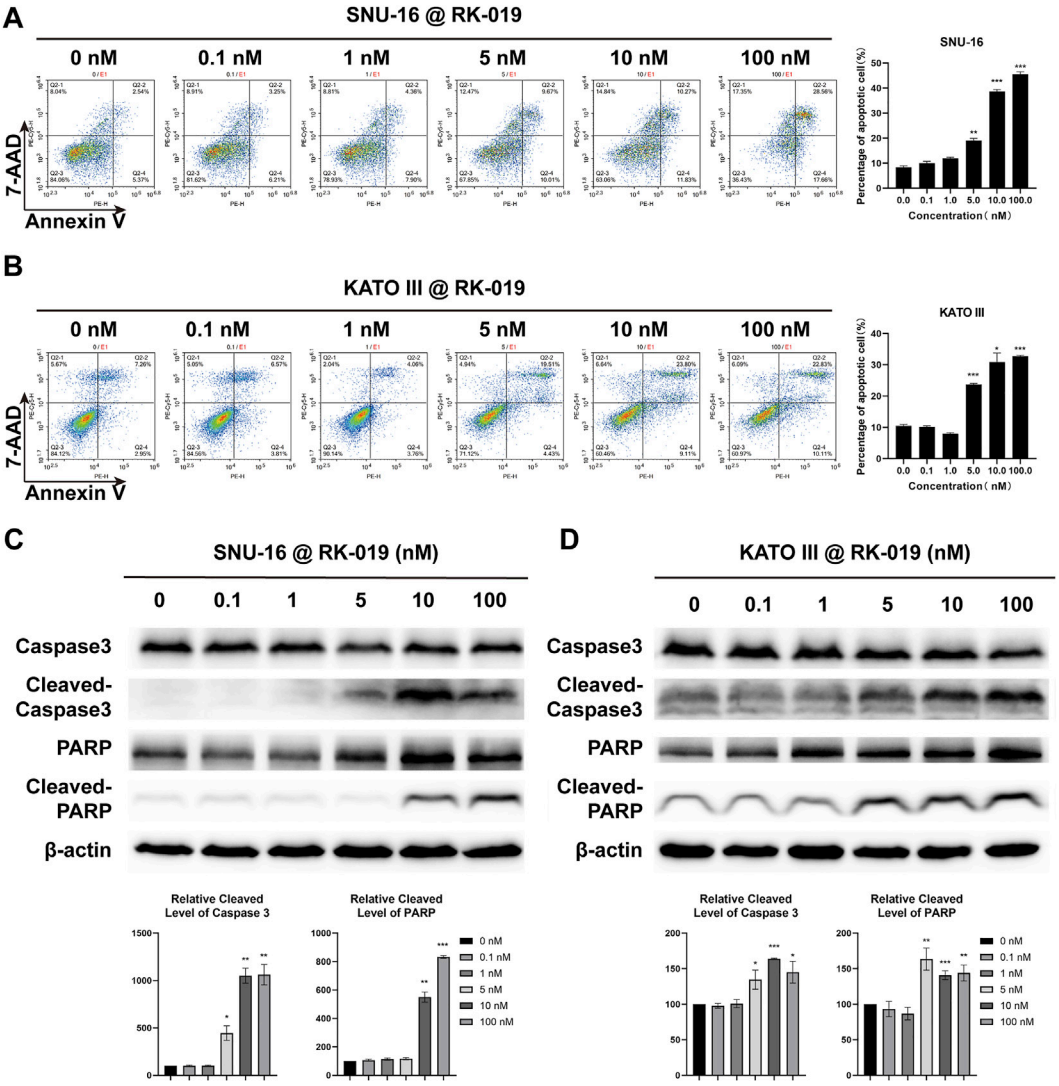

FIGURE 6
RK-019 induced cell apoptosis. SNU-16 and KATO III cells were treated with different concentrations of RK-019 for 72 h **(A)**, **(B)** FCM analysis cell apoptosis by 7-AAD and Annexin V-PE duel staining and quantified FCM apoptosis analysis data. Values were shown the total number of Q2-2 (early apoptotic) and Q2-4 (late apoptotic) by mean ± SD. **(C)**, **(D)** Western blot of apoptosis related proteins and quantification analysis, data were shown by mean ± SD. Each experiment was repeated for three times independently. Significance was determined by Student's t-test $*p < 0.05$; $**p < 0.01$; $***p < 0.001$, for the designated treatment group vs. the DMSO group.

Ki67-positive cells decreased, while the number of cleaved-caspase 3-positive cells increased significantly. Moreover, western blot analysis was performed to detecting the influence of RK-019 on JAK2-STAT signal axis *in vivo* (Figure 8D). Although the changes of relative phosphorylation level of JAK2 and STAT3 are not significant, the JAK2 and STAT3 phosphorylation level decreased remarkably in 30 and 45 mg/kg RK-019 treatment groups. The downstream proteins expression of this axis, MMP2 and MMP9, have also decreased after RK-019 treatment. These results suggested that RK-019 could block the FGFR signaling pathway *in vivo*, and result in proliferation arrest and cell apoptosis induction, corroborating the *in vitro* observations.

In the meantime, RK-019 exhibit the potential ability, suppress the migration, and invasion of GC cells *in vivo*.

Meanwhile, preliminary toxicity of RK-019 was evaluated. During the treatment, no significant body weight change occurred (Figure 8C). Moreover, no pathological changes were observed in the harvested organs of the RK-019-treated group (Figure 9D), and hematopoietic toxicity was absent (Figures 9A–C) at the end of treatment, suggesting that the mice were tolerant to RK-019 treatment. Taken together, RK-019 inhibited tumor growth in the SNU-16 xenograft model by inhibiting cell proliferation and inducing cell apoptosis.

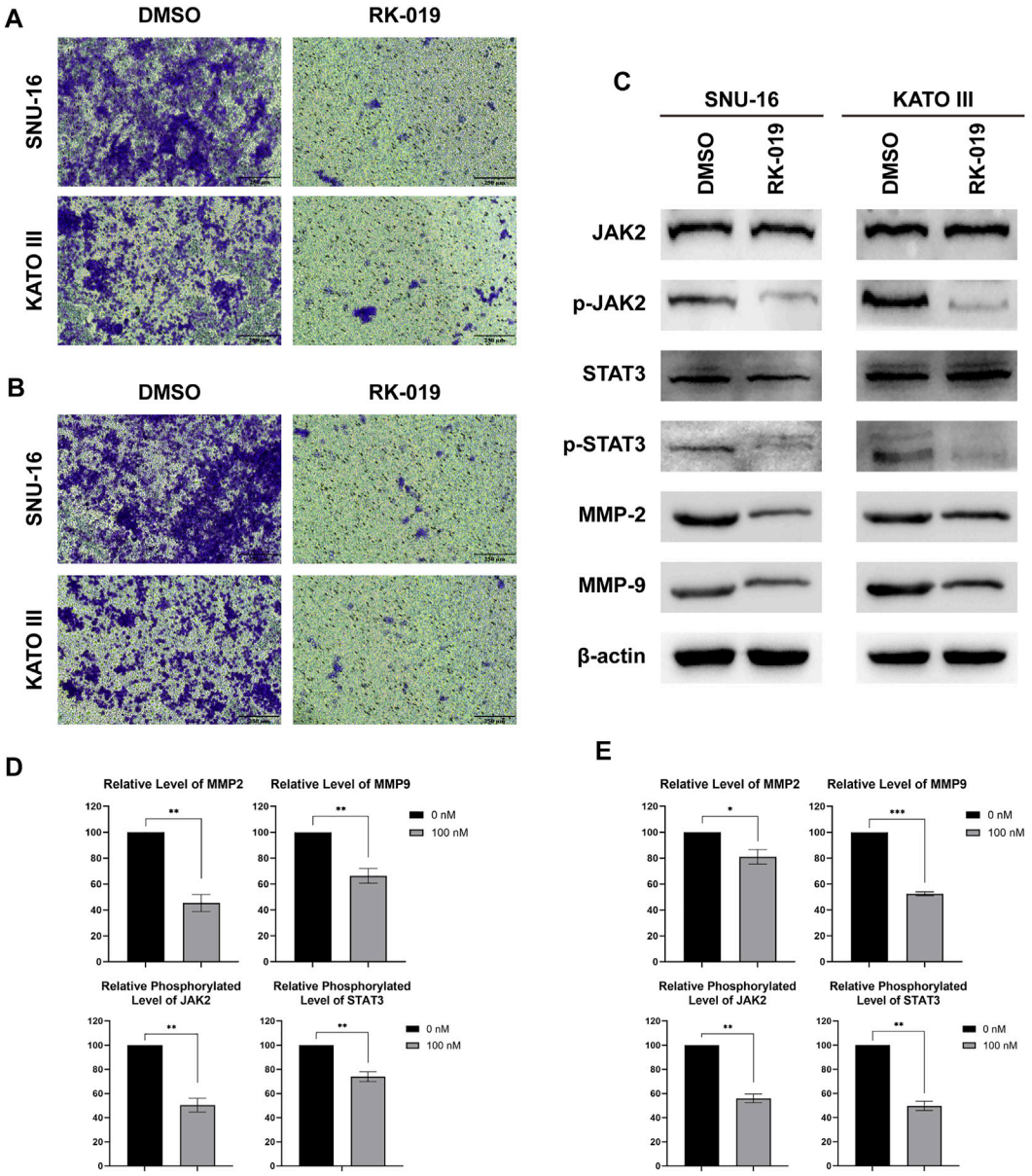

FIGURE 7
RK-019 inhibit SNU-16 and KATO III migration and invasion. Migration and invasion assay, cells (1×10^5) were seeded in the top chamber of transwell with serum-free medium and treated with RK-019 100 nM for 24 h, then the cells were stained with crystal violet. **(A)** Photographs of migration assay. **(B)** Photographs of invasion assay. **(C)** Western blot of FGFR downstream protein, including JAK2, p-JAK2, STAT3 and p-STAT3, and migration and invasion proteins, MMP-2 and MMP-9. **(D)**, **(E)** Quantification analysis by the ImageJ software of western blot results, data were performed by mean ± SD. Each experiment was repeated for three times independently. Significance was determined by Student's t-test $^*p < 0.05$; $^{**}p < 0.01$; $^{***}p < 0.001$, for the designated treatment group vs. the DMSO group.

TABLE 1 Pharmacokinetic profiles of RK-019 in rats.

	Dose (mg/kg)	C_{max} (ng/ml)	T_{max} (h)	AUC_{0-t} (ng·h/ml)	MRT (h)	T1/2 (h)	F%
RK-019	3 mg/kg i.v	461.40 ± 47.84	-	762.51 ± 50.79	1.64 ± 0.19	1.58 ± 0.29	-
	30 mg/kg p.o	234.65 ± 77.76	2.67 ± 2.89	1,448.41 ± 313.4	4.49 ± 1.19	2.83 ± 0.37	19.00

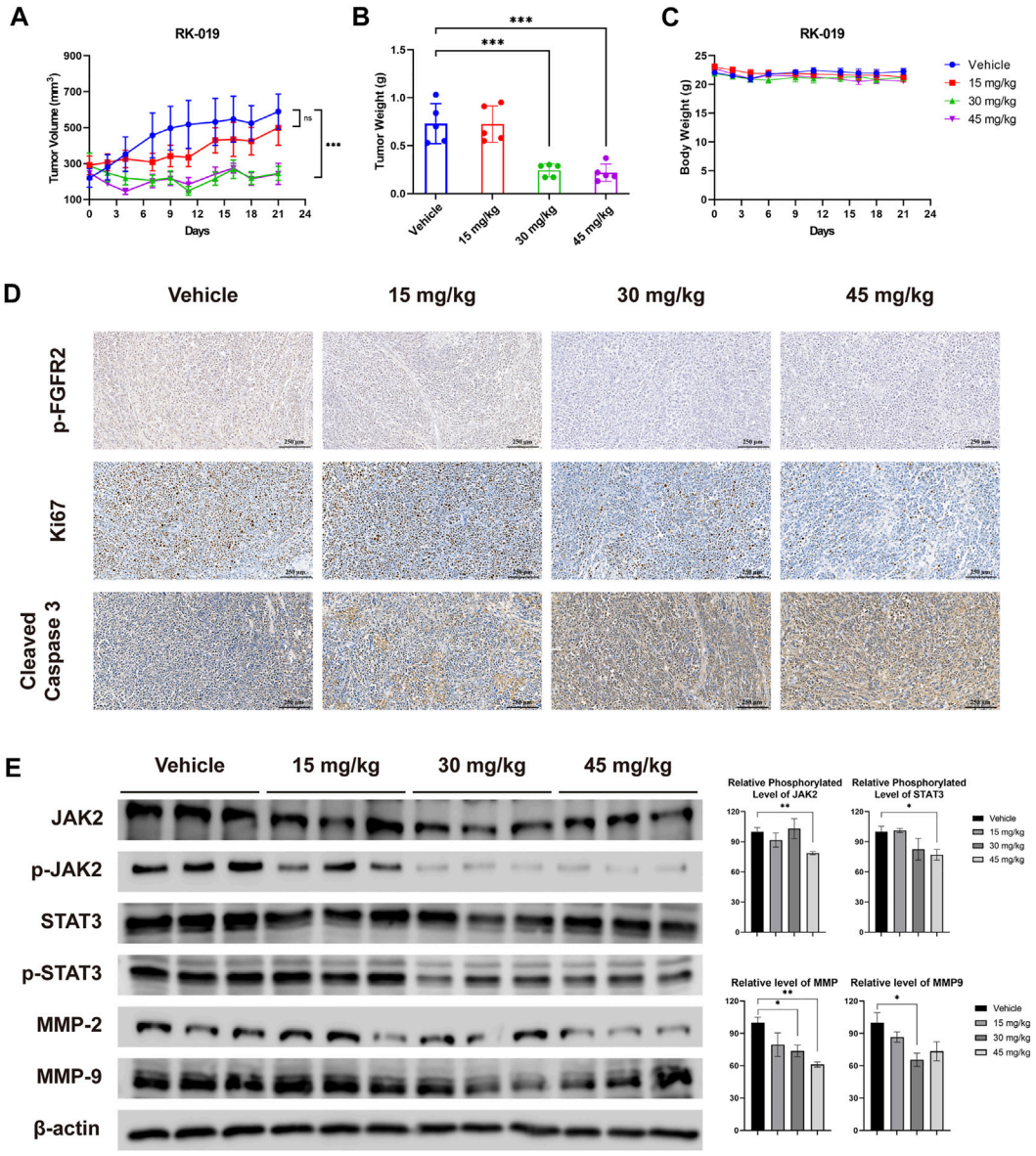

FIGURE 8
Anti-tumor efficacy of RK-019 in the SNU-16 xenograft model. NOD/SCID mice bearing SNU-16 were orally treated with vehicle or RK-019 once a day for 21 days. Tumor volume and body weight were measured three times *per* week. After 21 days of administration, mice were euthanasia and tumor tissue were collected, and were immunohistochemically analyzed with anti-Ki-67, anti-cleaved caspase-3, and anti p-FGFR2 antibodies. **(A)** Tumor growth curve, data were performed by mean ± SEM. (n = 5) **(B)** Tumor weight, data were performed by mean ± SD. (n = 5) Significance was determined by two-way ANNOVA $*p < 0.05$; $**p < 0.01$; $***p < 0.001$, for the designated treatment group vs. the Vehicle group. **(C)** Mice body weight curve, data were performed by mean ± SD. (n = 5) **(D)** IHC results of tumor tissue after treatment. **(E)** Western blot analysis of FGFR downstream protein and migration and invasion proteins, including JAK2, p-JAK2, STAT3, p-STAT3, MMP-2, and MMP-9. Each group was randomly selected three tumor tissues, followed by lysis and western blot analysis was performed. Results were quantified by the ImageJ software, and data was performed by mean ± SD. Significance was determined by Student's t-test $*p < 0.05$; $**p < 0.01$; $***p < 0.001$, for the designated treatment group vs. the vehicle group.

Discussion

FGFR signaling is an important regulatory pathway. However, FGFR signaling disorder is closely related to many diseases, such as cancer and fibrosis (Robertson et al., 2000). Abnormally activated FGFR signaling in cancer activates a series of signaling pathways, such as PI3K-AKT-mTOR, Ras-Raf-Erk, and JAK-STAT, which results in uncontrolled cell proliferation, metastasis, and avoidance of cell death (Gschwind et al., 2004). Preclinical

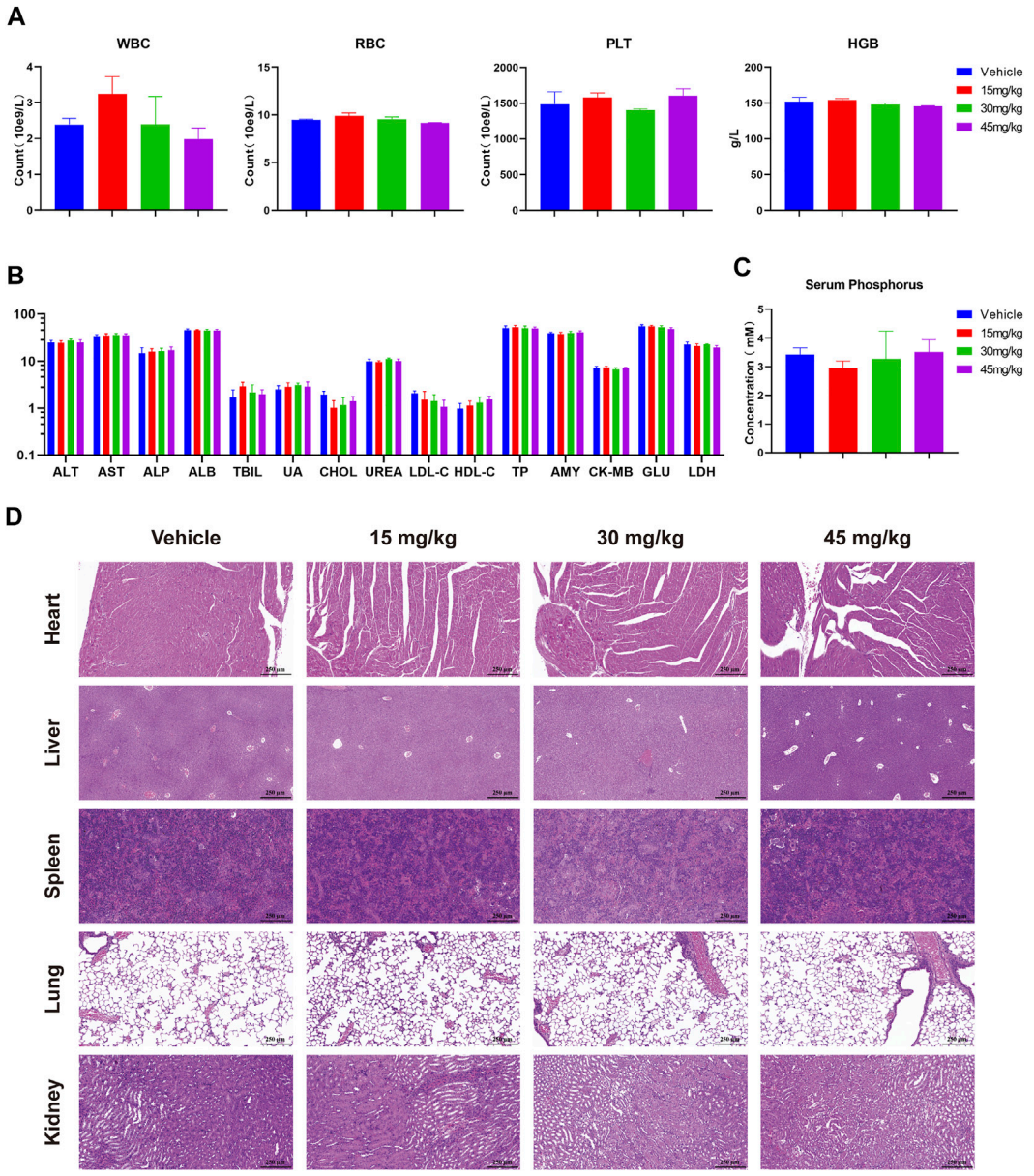

FIGURE 9
Safety profile of RK-019 in the xenograft mice model. After 21 days of RK-019 treatment, the mice were euthanasia, then blood and organs were extracted and analysis. Values in graphics were plotted as mean ± SD (n = 5). **(A)** Complete blood count data. **(B)** Blood biochemical analysis. **(C)** Serum phosphorus analysis. **(D)** H&E staining of pathological section in the heart, liver, spleen, lungs, and kidneys.

studies have identified FGFRs as a potential therapeutic target in many types of cancers, including lung, breast, gastric, and hematologic cancers. Excitingly, FGFR inhibitors, including Erdafitinib (JNJ-42756493) and Infigratinib (BGJ-398), have been approved for urothelial carcinoma and cholangiocarcinoma treatment (Markham, 2019; Montazeri and Bellmunt, 2020; Botrus et al., 2021).

GC is a highly heterogeneous disease from morphological and molecular standpoints (Gullo et al., 2018). This results in heterogeneity of treatment effect and makes the GC treatment development more difficult than other types of cancers. Until now, therapeutic schedules for GC are very limited. Traditional chemotherapy drugs, such as anti-tumor platinum drugs, docetaxel, and 5-Fu, still are the most common drugs in gastric cancer treatment (Smyth et al., 2020). Compared to the chemotherapy, targeted therapy exhibited more advantages in efficacy and safety. However, targeted drugs for GC treatment are very limited. Studies have revealed FGFR2 as a potential

target for GC treatment (Lengyel et al., 2022). Therefore, discovery targeted therapy for FGFR2 is very significant.

However, FGFRs inhibitors still are face many challenges. Firstly, although regulation of FGFR signaling cascades has been widely investigated, their unique function and drug resistance mechanisms remain unclear (Babina and Turner, 2017; Simons, 2021). Use of FGFRs inhibitors might cause a series of problems such as mutations conferring resistance to FGFR-targeting drugs and side-effects (Yue et al., 2021). On the other hand, due to the patient heterogeneity, FGFRs kinase inhibitors and anti-body drug conjugates had shown lower efficacy than expected, and drug toxicity, multiple GC treatment clinical trials targeted on FGFRs have not made any progress (Repetto et al., 2021; Lengyel et al., 2022). Hence, the discovery of novel FGFRs inhibitors is necessary.

In our present study, we demonstrated a novel small molecule RK-019 by screening our library of pharmacologically active compounds. In the following research, we found RK-019 exhibited great inhibitory capacity and selectivity against the FGFRs family kinases, the IC_{50} were 9.1 nM (FGFR1), 4.6 nM (FGFR2), 26.3 nM (FGFR3), and 40.7 nM (FGFR4), respectively. This indicated RK-019 is a pan-FGFR inhibitor with great kinase inhibitory activity.

Then, we tested the anti-proliferative effect of RK-019 on multiple GC cell lines and found that it could efficiently inhibit the proliferation of *FGFR2*-amp GC cell lines, SNU-16 and KATO III, with average IC_{50} values of 3.96 ± 4.4 nM and 5.45 ± 5.3 nM, respectively. These IC_{50} values were significantly different from that of the gastric epithelial cells GES-1 or other types of GC cell lines, indicating that RK-019 could inhibit *FGFR2*-amp GC cells. However, prolonged treatment of SNU-16 cells with RK-019 (5 and 10 nM) showed contrasting results, likely due to the activation of drug resistance pathways. Thus, in the future, we will focus on identifying the mechanism of drug resistance and developing anti-drug resistance strategies to enhance the anti-tumor effect.

Our results verified that RK-019 could inhibit $FGFR2^{T653/T654}$ auto-phosphorylation, which is the critical modification for the FGFR2 kinase activity and could prevent the phosphorylation of downstream proteins, including FRS2 and PLCγ. Phosphorylated FRS2 and PLCγ play a central role in the FGFR pathway activity, triggering PI3K-AKT-mTOR and Ras-Raf-Erk pathways (Katoh and Katoh, 2006; Acevedo et al., 2009; Ahmad et al., 2012; Ornitz and Itoh, 2015). In our study, we observed a decrease in the phosphorylation of AKT and Erk, which are known regulators of cell proliferation and survival. Furthermore, FCM and western blot results revealed G0/G1 phase arrest, validating our speculation about the inhibitory effects on the FGFR signaling.

Interestingly, although cell cycle arrest occurred immediately after RK-019 treatment, apoptosis was delayed. Apoptosis occurred after 72 h treatment, indicating that apoptosis might not be directly triggered by the inhibition of FGFR signaling. In addition, we found that apoptosis induced by RK-019 was not mediated by mitochondria. Mitochondrial membrane potential was increased, while the expression levels of mitochondrial apoptosis-related proteins did not change as expected after RK-019 treatment (Data not shown). Thus, we presume that RK-019 induced apoptosis *via* non-classic pathways.

Furthermore, we found that RK-019 could inhibit cell migration and invasion in SNU-16 and KATO III cells. Peritoneal metastasis is a leading cause of death in patients with gastric carcinoma. However, there are limited treatment options and no targeted therapy or immunotherapy for gastric carcinoma (Yao et al., 2020). RK-019 could inhibit the FGFR2 activity and repress JAK2 phosphorylation, thus mediating the STAT3 activity and decreasing the MMP-2 and MMP-9 levels. These findings demonstrate the ability of RK-019 to control cancer cell metastasis, which is crucial in GC therapy.

Finally, we verified the anti-tumor activity *in vivo* using the SNU-16 xenograft model. The results showed that RK-019 (30 mg/kg, daily oral administration for 21 days) could remarkably suppress SNU-16 tumor growth, with an inhibitory ratio of 85.9%. Furthermore, IHC revealed that RK-019 could prevent FGFR2 phosphorylation, induce apoptosis, and inhibit cell proliferation in the tumor sections.

Taken together, we have reported here a novel pan-FGFR inhibitor, RK-019, which exhibited excellent anti-tumorigenic activity against *FGFR2*-amp GC *in vitro* and *in vivo*.

Data availability statement

The original contributions presented in the study are included in the article/Supplementary Material; further inquiries can be directed to the corresponding authors.

Ethics statement

The animal study was reviewed and approved by the Institutional Animal Care and Treatment Committee of Sichuan University.

Author contributions

LY is the project administrator. JZ, KR, YZ, ZL, and LY contributed to conception and design of the study. JZ, KR, XL, LT, and QW performed the experiments in this article. JZ, KR, and XL organized and validated the experiment results. JR gave material and resource support. JZ wrote the first draft of the manuscript. YZ, ZL, and LY performed reviewing and editing. All authors contributed to manuscript revision and read and approved the submitted version.

Funding

This study was supported by the National S&T Major Special Project on Major New Drug Innovations of China (2018ZX09201018), the Science and Technology Program of Sichuan Province (2021YFH0145), and the Scientific Research Project of the Health Planning Committee of Sichuan (20PJ108).

Conflict of interest

The authors declare that the research was conducted in the absence of any commercial or financial relationships that could be construed as a potential conflict of interest.

Publisher's note

All claims expressed in this article are solely those of the authors and do not necessarily represent those of their affiliated organizations, or those of the publisher, the editors, and the reviewers. Any product that may be evaluated in this article, or claim that may be made by its manufacturer, is not guaranteed or endorsed by the publisher.

Supplementary material

The Supplementary Material for this article can be found online at: https://www.frontiersin.org/articles/10.3389/fphar.2022.998199/full#supplementary-material

References

Acevedo, V. D., Ittmann, M., and Spencer, D. M. (2009). Paths of FGFR-driven tumorigenesis. *Cell Cycle* 8 (4), 580–588. doi:10.4161/cc.8.4.7657

Ahmad, I., Iwata, T., and Leung, H. Y. (2012). Mechanisms of FGFR-mediated carcinogenesis. *Biochim. Biophys. Acta* 1823 (4), 850–860. doi:10.1016/j.bbamcr.2012.01.004

Ahn, S., Lee, J., Hong, M., Kim, S. T., Park, S. H., Choi, M. G., et al. (2016). FGFR2 in gastric cancer: Protein overexpression predicts gene amplification and high H-index predicts poor survival. *Mod. Pathol.* 29 (9), 1095–1103. doi:10.1038/modpathol.2016.96

Babina, I. S., and Turner, N. C. (2017). Advances and challenges in targeting FGFR signalling in cancer. *Nat. Rev. Cancer* 17 (5), 318–332. doi:10.1038/nrc.2017.8

Beenken, A., and Mohammadi, M. (2009). The FGF family: Biology, pathophysiology and therapy. *Nat. Rev. Drug Discov.* 8 (3), 235–253. doi:10.1038/nrd2792

Belov, A. A., and Mohammadi, M. (2013). Molecular mechanisms of fibroblast growth factor signaling in physiology and pathology. *Cold Spring Harb. Perspect. Biol.* 5 (6), a015958. doi:10.1101/cshperspect.a015958

Botrus, G., Raman, P., Oliver, T., and Bekaii-Saab, T. (2021). Infigratinib (BGJ398): An investigational agent for the treatment of FGFR-altered intrahepatic cholangiocarcinoma. *Expert Opin. Investig. Drugs* 30 (4), 309–316. doi:10.1080/13543784.2021.1864320

Brooks, A. N., Kilgour, E., and Smith, P. D. (2012). Molecular pathways: Fibroblast growth factor signaling: A new therapeutic opportunity in cancer. *Clin. Cancer Res.* 18 (7), 1855–1862. doi:10.1158/1078-0432.CCR-11-0699

Cailliau, K., Browaeys-Poly, E., and Vilain, J. P. (2001). Fibroblast growth factors 1 and 2 differently activate MAP kinase in Xenopus oocytes expressing fibroblast growth factor receptors 1 and 4. *Biochim. Biophys. Acta* 1538 (2-3), 228–233. doi:10.1016/s0167-4889(01)00074-x

Cerliani, J. P., Guillardoy, T., Giulianelli, S., Vaque, J. P., Gutkind, J. S., Vanzulli, S. I., et al. (2011). Interaction between FGFR-2, STAT5, and progesterone receptors in breast cancer. *Cancer Res.* 71 (10), 3720–3731. doi:10.1158/0008-5472.CAN-10-3074

Deo, D. D., Axelrad, T. W., Robert, E. G., Marcheselli, V., Bazan, N. G., and Hunt, J. D. (2002). Phosphorylation of STAT-3 in response to basic fibroblast growth factor occurs through a mechanism involving platelet-activating factor, JAK-2, and src in human umbilical vein endothelial cells: Evidence for a dual kinase mechanism. *J. Biol. Chem.* 277 (24), 21237–21245. doi:10.1074/jbc.M110955200

Eswarakumar, V. P., Lax, I., and Schlessinger, J. (2005). Cellular signaling by fibroblast growth factor receptors. *Cytokine Growth Factor Rev.* 16 (2), 139–149. doi:10.1016/j.cytogfr.2005.01.001

Fukumoto, S. (2008). Actions and mode of actions of FGF19 subfamily members. *Endocr. J.* 55 (1), 23–31. doi:10.1507/endocrj.kr07e-002

Goetz, R., and Mohammadi, M. (2013). Exploring mechanisms of FGF signalling through the lens of structural biology. *Nat. Rev. Mol. Cell Biol.* 14 (3), 166–180. doi:10.1038/nrm3528

Grose, R., and Dickson, C. (2005). Fibroblast growth factor signaling in tumorigenesis. *Cytokine Growth Factor Rev.* 16 (2), 179–186. doi:10.1016/j.cytogfr.2005.01.003

Gschwind, A., Fischer, O. M., and Ullrich, A. (2004). The discovery of receptor tyrosine kinases: Targets for cancer therapy. *Nat. Rev. Cancer* 4 (5), 361–370. doi:10.1038/nrc1360

Gullo, I., Carneiro, F., Oliveira, C., and Almeida, G. M. (2018). Heterogeneity in gastric cancer: From pure morphology to molecular classifications. *Pathobiology* 85 (1-2), 50–63. doi:10.1159/000473881

Han, N., Kim, M. A., Lee, H. S., and Kim, W. H. (2015). Evaluation of fibroblast growth factor receptor 2 expression, heterogeneity and clinical significance in gastric cancer. *Pathobiology* 82 (6), 269–279. doi:10.1159/000441149

Hosoda, K., Yamashita, K., Ushiku, H., Ema, A., Moriya, H., Mieno, H., et al. (2017). Prognostic relevance of FGFR2 expression in stage II/III gastric cancer with curative resection and S-1 chemotherapy. *Oncol. Lett.* 15, 1853–1860. doi:10.3892/ol.2017.7515

Jain, A., Borad, M. J., Kelley, R. K., Wang, Y., Abdel-Wahab, R., Meric-Bernstam, F., et al. (2018). Cholangiocarcinoma with FGFR genetic aberrations: A unique clinical phenotype. *JCO Precis. Oncol.* 2, 1–12. doi:10.1200/PO.17.00080

Jang, J.-H., Shin, K.-H., and Park, J.-G. (2001). Mutations in fibroblast growth factor receptor 2 and fibroblast growth factor receptor 3 genes associated with human gastric and colorectal cancers. *Cancer Res.* 61 (9), 3541. https://aacrjournals.org/cancerres/article/61/9/3541/508688/Mutations-in-Fibroblast-Growth-Factor-Receptor-2

Jang, J., Kim, H. K., Bang, H., Kim, S. T., Kim, S. Y., Park, S. H., et al. (2017). Antitumor effect of AZD4547 in a fibroblast growth factor receptor 2-amplified gastric cancer patient-derived cell model. *Transl. Oncol.* 10 (4), 469–475. doi:10.1016/j.tranon.2017.03.001

Jia, Y.-X., Li, T.-F., Zhang, D.-D., Fan, Z.-M., Fan, H.-J., Yan, J., et al. (2016). The coexpression and prognostic significance of c-MET, fibroblast growth factor receptor 2, and human epidermal growth factor receptor 2 in resected gastric cancer: A retrospective study. *Onco. Targets. Ther.* 9, 5919–5929. doi:10.2147/OTT.S111778

Jia, Z.-H., Jia, Y., Guo, F.-J., Chen, J., Zhang, X.-W., and Cui, M.-H. (2017). Phosphorylation of STAT3 at Tyr705 regulates MMP-9 production in epithelial ovarian cancer. *Plos One* 12 (8), e0183622. doi:10.1371/journal.pone.0183622

Kamata, T., Hattori, Y., Hamada, H., Kizaki, M., Terada, M., and Ikeda, Y. (2002). Keratinocyte growth factor regulates proliferation and differentiation of hematopoietic cells expressing the receptor gene K-sam. *Exp. Hematol.* 30 (4), 297–305. doi:10.1016/s0301-472x(01)00800-1

Katoh, M. (2010). Genetic alterations of FGF receptors: An emerging field in clinical cancer diagnostics and therapeutics. *Expert Rev. Anticancer Ther.* 10 (9), 1375–1379. doi:10.1586/era.10.128

Katoh, M., and Katoh, M. (2006). FGF signaling network in the gastrointestinal tract (review). *Int. J. Oncol.* 29 (1), 163–168. doi:10.3892/ijo.29.1.163

Kim, H. S., Kim, J. H., Jang, H. J., Han, B., and Zang, D. Y. (2019b). Pathological and prognostic impacts of FGFR2 overexpression in gastric cancer: A meta-analysis. *J. Cancer* 10 (1), 20–27. doi:10.7150/jca.28204

Kim, H. S., Kim, J. H., and Jang, H. J. (2019a). Pathologic and prognostic impacts of FGFR2 amplification in gastric cancer: A meta-analysis and systemic review. *J. Cancer* 10 (11), 2560–2567. doi:10.7150/jca.29184

Lamont, F., Tomlinson, D., Cooper, P. A., Shnyder, S. D., Chester, J. D., and Knowles, M. (2011). Small molecule FGF receptor inhibitors block FGFR-dependent urothelial carcinoma growth *in vitro* and *in vivo*. *Br. J. Cancer* 104 (1), 75–82. doi:10.1038/sj.bjc.6606016

Lawlor, M. A., and Alessi, D. R. (2001). PKB/Akt: A key mediator of cell proliferation, survival and insulin responses? *J. Cell Sci.* 114 (16), 2903–2910. doi:10.1242/jcs.114.16.2903

Lengyel, C. G., Hussain, S., Seeber, A., Jamil Nidhamalddin, S., Trapani, D., Habeeb, B. S., et al. (2022). FGFR pathway inhibition in gastric cancer: The golden era of an old target? *Life* 12 (1), 81. doi:10.3390/life12010081

Li, P., Huang, T., Zou, Q., Liu, D., Wang, Y., Tan, X., et al. (2019). FGFR2 promotes expression of PD-L1 in colorectal cancer via the JAK/STAT3 signaling pathway. *J. Immunol.* 202 (10), 3065–3075. doi:10.4049/jimmunol.1801199

Markham, A. (2019). Erdafitinib: First global approval. *Drugs* 79 (9), 1017–1021. doi:10.1007/s40265-019-01142-9

Massagué, J. (2004). G1 cell-cycle control and cancer. *Nature* 432 (7015), 298–306. doi:10.1038/nature03094

Matsumoto, K., Arao, T., Hamaguchi, T., Shimada, Y., Kato, K., Oda, I., et al. (2012). FGFR2 gene amplification and clinicopathological features in gastric cancer. *Br. J. Cancer* 106 (4), 727–732. doi:10.1038/bjc.2011.603

Montazeri, K., and Bellmunt, J. (2020). Erdafitinib for the treatment of metastatic bladder cancer. *Expert Rev. Clin. Pharmacol.* 13 (1), 1–6. doi:10.1080/17512433.2020.1702025

Network, C. G. A. R. (2014). Comprehensive molecular characterization of gastric adenocarcinoma. *Nature* 513 (7517), 202–209. doi:10.1038/nature13480

Oki, M., Yamamoto, H., Taniguchi, H., Adachi, Y., Imai, K., and Shinomura, Y. (2008). Overexpression of the receptor tyrosine kinase EphA4 in human gastric cancers. *World J. Gastroenterol.* 14 (37), 5650–5656. doi:10.3748/wjg.14.5650

Ornitz, D. M., and Itoh, N. (2001). Fibroblast growth factors. *Genome Biol.* 2 (3),S3005. doi:10.1186/gb-2001-2-3-reviews3005

Ornitz, D. M., and Itoh, N. (2015). The fibroblast growth factor signaling pathway. *Wiley Interdiscip. Rev. Dev. Biol.* 4 (3), 215–266. doi:10.1002/wdev.176

Piro, G., Carbone, C., Cataldo, I., Di Nicolantonio, F., Giacopuzzi, S., Aprile, G., et al. (2016). An FGFR3 autocrine loop sustains acquired resistance to trastuzumab in gastric cancer patients. *Clin. Cancer Res.* 22 (24), 6164–6175. doi:10.1158/1078-0432.ccr-16-0178

Repetto, M., Crimini, E., Giugliano, F., Morganti, S., Belli, C., and Curigliano, G. (2021). Selective FGFR/FGF pathway inhibitors: Inhibition strategies, clinical activities, resistance mutations, and future directions. *Expert Rev. Clin. Pharmacol.* 14 (10), 1233–1252. doi:10.1080/17512433.2021.1947246

Robertson, S. C., Tynan, J. A., and Donoghue, D. J. (2000). RTK mutations and human syndromes: When good receptors turn bad. *Trends Genet.* 16 (6), 265–271. doi:10.1016/s0168-9525(00)02021-7

Sarabipour, S., and Hristova, K. (2016). Mechanism of FGF receptor dimerization and activation. *Nat. Commun.* 7 (1), 10262–10312. doi:10.1038/ncomms10262

Shimizu, D., Saito, T., Ito, S., Masuda, T., Kurashige, J., Kuroda, Y., et al. (2018). Overexpression of FGFR1 promotes peritoneal dissemination via epithelial-to-mesenchymal transition in gastric cancer. *Cancer Genomics Proteomics* 15 (4), 313–320. doi:10.21873/cgp.20089

Simons, M. (2021). Fibroblast growth factors: The keepers of endothelial normalcy. *J. Clin. Invest.* 131 (17), e152716. doi:10.1172/jci152716

Smyth, E. C., Nilsson, M., Grabsch, H. I., van Grieken, N. C., and Lordick, F. (2020). Gastric cancer. *Lancet* 396 (10251), 635–648. doi:10.1016/S0140-6736(20)31288-5

Su, X., Zhan, P., Gavine, P., Morgan, S., Womack, C., Ni, X., et al. (2014). FGFR2 amplification has prognostic significance in gastric cancer: Results from a large international multicentre study. *Br. J. Cancer* 110 (4), 967–975. doi:10.1038/bjc.2013.802

Sung, H., Ferlay, J., Siegel, R. L., Laversanne, M., Soerjomataram, I., Jemal, A., et al. (2021). Global cancer statistics 2020: GLOBOCAN estimates of incidence and mortality worldwide for 36 cancers in 185 countries. *Ca. Cancer J. Clin.* 71 (3), 209–249. doi:10.3322/caac.21660

Takahashi, T., Saikawa, Y., and Kitagawa, Y. (2013). Gastric cancer: Current status of diagnosis and treatment. *Cancers* 5 (4), 48–63. doi:10.3390/cancers5010048

Tokunaga, R., Imamura, Y., Nakamura, K., Ishimoto, T., Nakagawa, S., Miyake, K., et al. (2016). Fibroblast growth factor receptor 2 expression, but not its genetic amplification, is associated with tumor growth and worse survival in esophagogastric junction adenocarcinoma. *Oncotarget* 7 (15), 19748–19761. doi:10.18632/oncotarget.7782

Tsang, M., and Dawid, I. B. (2004). Promotion and attenuation of FGF signaling through the Ras-MAPK pathway. *Sci. STKE* 2004 (228), pe17. doi:10.1126/stke.2282004pe17

Van Cutsem, E., Sagaert, X., Topal, B., Haustermans, K., and Prenen, H. (2016). Gastric cancer. *Lancet* 388 (10060), 2654–2664. doi:10.1016/S0140-6736(16)30354-3

Xie, T.-X., Wei, D., Liu, M., Gao, A. C., Ali-Osman, F., Sawaya, R., et al. (2004). Stat3 activation regulates the expression of matrix metalloproteinase-2 and tumor invasion and metastasis. *Oncogene* 23 (20), 3550–3560. doi:10.1038/sj.onc.1207383

Xu, H., Lee, K. W., and Goldfarb, M. (1998). Novel recognition motif on fibroblast growth factor receptor mediates direct association and activation of SNT adapter proteins. *J. Biol. Chem.* 273 (29), 17987–17990. doi:10.1074/jbc.273.29.17987

Yao, X., Ajani, J. A., and Song, S. (2020). Molecular biology and immunology of gastric cancer peritoneal metastasis. *Transl. Gastroenterol. Hepatol.* 5, 57. doi:10.21037/tgh.2020.02.08

Ye, Y.-W., Hu, S., Shi, Y.-Q., Zhang, X.-F., Zhou, Y., Zhao, C.-L., et al. (2013). Combination of the FGFR4 inhibitor PD173074 and 5-fluorouracil reduces proliferation and promotes apoptosis in gastric cancer. *Oncol. Rep.* 30 (6), 2777–2784. doi:10.3892/or.2013.2796

Ye, Y. W., Zhang, X., Zhou, Y., Wu, J., Zhao, C., Yuan, L., et al. (2012). The correlations between the expression of FGFR4 protein and clinicopathological parameters as well as prognosis of gastric cancer patients. *J. Surg. Oncol.* 106 (7), 872–879. doi:10.1002/jso.23153

Yue, S., Li, Y., Chen, X., Wang, J., Li, M., Chen, Y., et al. (2021). FGFR-TKI resistance in cancer: Current status and perspectives. *J. Hematol. Oncol.* 14 (1), 23. doi:10.1186/s13045-021-01040-2

Zhang, J., Tang, P. M. K., Zhou, Y., Cheng, A. S. L., Yu, J., Kang, W., et al. (2019). Targeting the oncogenic FGF-FGFR Axis in gastric carcinogenesis. *Cells* 8 (6), E637. doi:10.3390/cells8060637

Zhang, W., and Liu, H. T. (2002). MAPK signal pathways in the regulation of cell proliferation in mammalian cells. *Cell Res.* 12 (1), 9–18. doi:10.1038/sj.cr.7290105

Zou, L., Cao, S., Kang, N., Huebert, R. C., and Shah, V. H. (2012). Fibronectin induces endothelial cell migration through β1 integrin and Src-dependent phosphorylation of fibroblast growth factor receptor-1 at tyrosines 653/654 and 766. *J. Biol. Chem.* 287 (10), 7190–7202. doi:10.1074/jbc.M111.304972

Glossary

GC Gastric cancer

FGFR Fibroblast growth factor receptor

FGF Fibroblast growth factor

EMT Epithelial-to-mesenchymal transition

MTT 3-(4,5-Dimethyl-2-thiazolyl)-2,5-diphenyl-2-H-tetrazolium bromide

DMSO Dimethyl sulfoxide

qRT-PCR Quantitative reverse transcription PCR

FCM Flow cytometryFlow cytometry

PBS Phosphate buffered solution

SDS-PAGE Sodium dodecyl sulphate-polyacrylamide gel electrophoresis

PVDF Polyvinylidene difluoride

SPF Specific-pathogen free

LC-MS/MS Liquid chromatography–mass spectrometry/mass spectrometry

PK Pharmacokinetics

FCM Flow cytometryFlow cytometry

PI Propidium iodide

PARP Poly (ADP-ribose) polymerase

CBC Complete blood count

TGI Tumor growth inhibition

IC50 Median-inhibitory concentration

ATP Adenosine triphosphate

AUC Area under the plasma concentration time curve

IHC Immunohistochemistry

FRS2 Fibroblast growth factor receptor substrate 2

PLCγ Phosphoinositide phospholipase C gamma

Erk Extracellular signal-regulated kinase

JAK Janus kinase

STAT Signal transducer and activator of transcription

CDK Cyclin-dependent kinases

MMP Matrix metalloproteinases

PI3K Phosphatidylinositol 3 kinase.

frontiers | Frontiers in Pharmacology

TYPE Original Research
PUBLISHED 26 September 2022
DOI 10.3389/fphar.2022.1018411

Check for updates

OPEN ACCESS

EDITED BY
Chen Shi,
Huazhong University of Science and Technology, China

REVIEWED BY
Takafumi Yanagisawa,
School of Medicine, Jikei University, Japan
Sha Li,
Shanghai Jiao Tong University, China

*CORRESPONDENCE
Wenhong Deng,
wenhongdeng@whu.edu.cn
Weixing Wang,
sate.llite@163.com

†These authors have contributed equally to this work

SPECIALTY SECTION
This article was submitted to Pharmacology of Anti-Cancer Drugs, a section of the journal Frontiers in Pharmacology

RECEIVED 13 August 2022
ACCEPTED 07 September 2022
PUBLISHED 26 September 2022

CITATION
Zhang L, Chen C, Chai D, Li C, Kuang T, Liu L, Dong K, Deng W and Wang W (2022), Effects of PPIs use on clinical outcomes of urothelial cancer patients receiving immune checkpoint inhibitor therapy.
Front. Pharmacol. 13:1018411.
doi: 10.3389/fphar.2022.1018411

COPYRIGHT
© 2022 Zhang, Chen, Chai, Li, Kuang, Liu, Dong, Deng and Wang. This is an open-access article distributed under the terms of the Creative Commons Attribution License (CC BY). The use, distribution or reproduction in other forums is permitted, provided the original author(s) and the copyright owner(s) are credited and that the original publication in this journal is cited, in accordance with accepted academic practice. No use, distribution or reproduction is permitted which does not comply with these terms.

Effects of PPIs use on clinical outcomes of urothelial cancer patients receiving immune checkpoint inhibitor therapy

Lilong Zhang†, Chen Chen†, Dongqi Chai, Chunlei Li, Tianrui Kuang, Li Liu, Keshuai Dong, Wenhong Deng* and Weixing Wang*

Department of General Surgery, Renmin Hospital of Wuhan University, Wuhan, China

Objective: Immune checkpoint inhibitors (ICIs) have recently demonstrated promising performance in improving the prognosis of urological cancer patients. The goal of this meta-analysis was to determine the impact of PPI use on the clinical outcomes of urological cancer patients receiving ICI therapy.

Methods: Before 6 May 2022, the eligible literature was searched using PubMed, EMBASE, Cochrane Library, and Google Scholar. The clinical outcomes were overall survival (OS), progression-free survival (PFS), and objective response rate (ORR).

Results: A total of six articles met the inclusion criteria, and of the 1980 patients with advanced or metastatic urothelial cancers (UC) included. The meta-analysis displayed that PPI use could increase the risk of progression by 50.7% (HR: 1.507, 95% CI: 1.327–1.711, $p < 0.001$) and death by 58.7% (HR: 1.587, 95% CI: 1.367–1.842, $p < 0.001$), and reduce the ORR (OR: 0.503, 95% CI: 0.360–0.703, $p < 0.001$) in UC patients receiving ICIs. No significant heterogeneity and publication bias existed. Sensitivity analysis proved that the results were stable and reliable.

Conclusion: The meta-analysis indicated that concomitant PPI use was significantly associated with low clinical benefit in UC patients.

KEYWORDS

immune checkpoint inhibitors, proton pump inhibitors, urothelial cancer, clinical outcomes, meta-analysis

1 Introduction

Urological cancers, mostly including renal cell carcinoma (RCC), prostate cancer (PC), and urothelial cancer (UC), are the common public health concerns worldwide (Sung et al., 2021). Despite the advances in treatments and techniques for tumors, such as chemotherapy and molecular targeted therapy, the clinical prognosis of urological cancers has not improved considerably over the last 2 decades (Niu et al., 2021). The introduction

of immune checkpoint inhibitors (ICIs) has transformed the treatment of a variety of cancers, including urological malignancies. These antibodies act by blocking the checkpoint pathways, which are physiologic mechanisms established to switch off the immune response and prevent autoimmunity (Bimbatti et al., 2022).

UC has the fourth highest rate of mutations of all cancers and is known to be highly antigenic (Kim et al., 2020), whereas RCC has a moderate tumor mutation load but a high frequency of deletion and clonal insertion mutations, which may be linked to neoantigen abundance and $CD8^+$ T cell activation (Carretero-González et al., 2020). These characteristics make the theme appropriate for ICI therapy. In contrast, PC immunogenicity is hampered by a low mutation burden and a highly immunosuppressive microenvironment. As a result, it is deemed a "cold tumor" that is difficult to treat with ICIs (Kim and Koo, 2020). ICIs have been approved for RCC and UC and have been shown to improve patient survival when compared to traditional treatments (Pierantoni et al., 2019; Xu et al., 2020). However, the clinical efficacy of ICIs varies widely amongst sufferers, with only a tiny percentage of the population benefiting from treatment. Furthermore, primary resistance to ICIs is still frequent, and a significant number of patients continue to worsen or relapse as a result of ICI resistance (Sharma et al., 2017; Seto et al., 2019). Regrettably, no perfect biomarker for predicting the efficacy of ICIs exists at this time. Thus, the search for prospective biomarkers that predict its efficacy as well as factors that influence its efficacy is critical for a more targeted selection of treatment populations in clinical practice.

Antacid agents such as proton pump inhibitors (PPIs) and histamine-2-receptor antagonists (H2RAs) are commonly prescribed for extended periods in urological cancer patients. Recent evidence also suggested that PPI usage in patients with advanced NSCLC receiving ICI therapy was associated with an increased mortality risk (Qin et al., 2021; Rizzo et al., 2022; Wei et al., 2022). However, the relationship between antacid use and ICI outcomes in urological cancer patients remains controversial due to a lack of comprehensive evaluations. Therefore, we conducted the first systematic review and meta-analysis to elucidate whether antacid use affects the efficacy of ICI therapy for urological cancer. This will provide evidence for future clinical use of antacids in urological cancers treated with ICIs, thereby maximizing the clinical benefit to patients.

2 Materials and methods

2.1 Literature search strategies

This meta-analysis accompanied the Preferred Reporting Items for Systematic Reviews and Meta-Analyses (PRISMA) guidelines (Page et al., 2021). The protocol for this meta-analysis is available in PROSPERO (CRD42022332633). On 6 May 2022, PubMed (https://pubmed.ncbi.nlm.nih.gov/), EMBASE (https://www.embase.com/), and Cochrane Library (https://www.cochranelibrary.com/) were retrieved. The following Medical Subject Headings (MeSH) terms and their entry terms: "Immune Checkpoint Inhibitors" [Mesh], "Antacids" [Mesh], "Proton Pump Inhibitors" [Mesh], "Histamine H2 Antagonists" [Mesh], as well as the following terms: "omeprazole," "pantoprazole," "lansoprazole," "esomeprazole," "dexlansoprazole," "rabeprazole," "ranitidine" were searched in [All Fields]. Detailed search strategies were shown in Supplementary Table S1. We also searched Google Scholar to uncover gray literature that was not indexed in the previously listed databases, such as presentations and unpublished research data. Furthermore, we also manually retrieved the reference lists of eligible papers.

2.2 Study selection criteria

If articles matched all the following criteria, they were included (Sung et al., 2021). patients diagnosed with urological cancers (Niu et al., 2021); patients treated with ICIs (Bimbatti et al., 2022); patients separated into the antacid use group and non-antacid use group (Kim et al., 2020); provided at least one of the outcomes of interest [multivariable/adjusted overall survival (OS), progression-free survival (PFS), and objective response rate (ORR)]. For retrospective studies, the results of univariable analysis are vulnerable to confounding factors, so we included studies that provided multivariable analysis. Only the article with the most comprehensive data and rigorous methods was chosen when studies reported overlapping patient populations. Meanwhile, the following exclusion criteria were employed: abstract, comments, and case report.

2.3 Data extraction and quality assessment

Data extraction mainly focused on the author, publication year, study region, study period, study type, cancer type, the number of patients, the age of patients, the number of male patients, timing of antacid use, types of ICI treatment, types of antacids, and the outcomes of interest (OS, PFS, and ORR). Response Evaluation Criteria in Solid Tumors (RECIST) version 1.1 was used to estimate the ORR. The Newcastle-Ottawa Scale (NOS) score was used to estimate the quality of the retrospective studies (Wells et al., 2019). Literature with a score ≥7 was considered to be of high quality. Two authors independently cross-checked all the above steps, and the

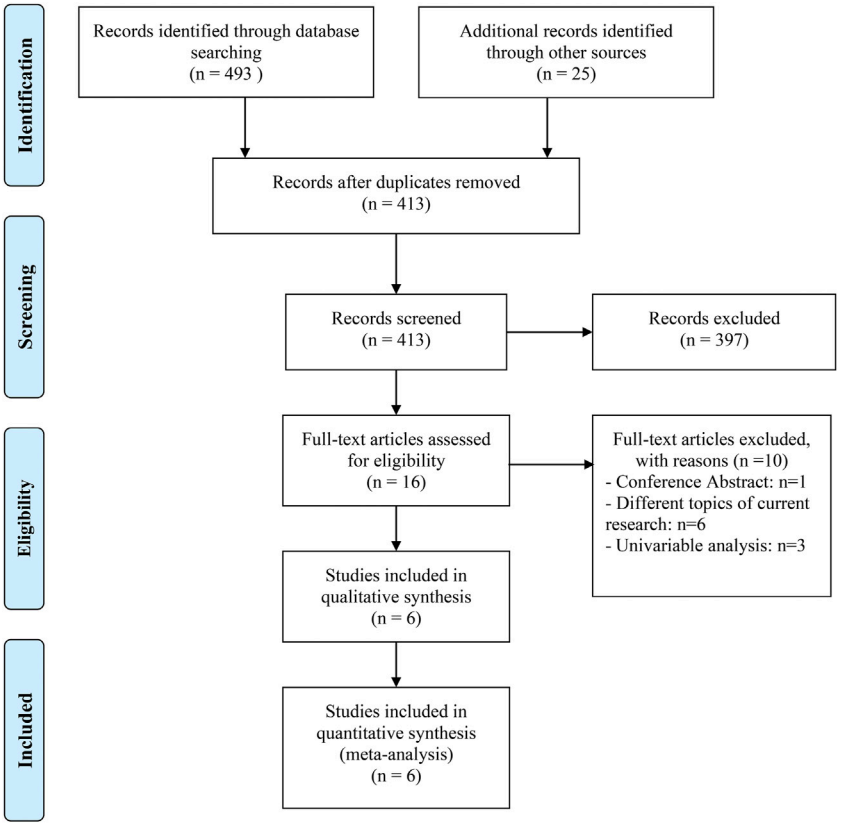

FIGURE 1
The flow diagram of identifying eligible studies.

senior authors (Wenhong Deng and Wang Weixing) addressed any disparities.

2.4 Statistical methods

Stata MP16.0 was used for the statistical analysis. The HR and its 95% CI were used to calculate the influence of antacid use on the risk of survival in cancer patients. The association between ICI efficacy and antacid usage was expressed as an odds ratio (OR) with a 95% CI. The statistical heterogeneity among the studies was determined using the chi-squared test. $p > 0.1$ and $I^2 < 50\%$ indicated low heterogeneity where a fixed-effect model was used; otherwise, the random-effect model was adopted. To reduce the influence of heterogeneity on the meta-analysis, a subgroup analysis was performed. Begg's and Egger's tests were implemented to assess publication bias. Sensitivity analysis by the leave-one-out method was conducted to estimate the stability of the results. All p values were two-sided with significance set at $p < 0.05$.

3 Results

3.1 Studies retrieved and characteristics

We gathered 518 potentially eligible records and assessed their titles and abstracts to see if they were suitable for inclusion. We discovered that six articles (Hopkins et al., 2020; Ruiz-Bañobre et al., 2021; Fukuokaya et al., 2022; Kunimitsu et al., 2022; Okuyama et al., 2022; Tomisaki et al., 2022) met our criteria for inclusion after carefully reading the full texts of 16 records. The studies on RCC by Peng et al. (2022), Mollica et al. (2022), Kostine et al. (2021) only provided the results of univariate analysis, so they were excluded. Figure 1 depicts the flow diagram for identifying eligible studies. All six articles explored the effects of PPIs on ICI efficacy in patients with advanced or metastatic UC. A total of 1980 patients were included. Of the six retrospective studies, five articles were awarded seven or eight points and were regarded as high quality; one article was awarded six points and was deemed as medium quality. Table 1 shows the baseline characteristics of the included studies as well as the quality evaluation.

TABLE 1 Baseline characteristics of included studies.

Author, year	Study region	Study period	Study type	Cancer type	Antacids/Non-antacids			Timing of antacid use	Types of ICI treatment	Types of antacids	Quality
					No. of patients	Man	Age[a]				
Tomisaki, (2022)	Japan	03/2018–03/2021	R	Advanced UC	15/25	10/20	72/72	Within 60 days before and after beginning ICIs	Pembrolizumab	PPI	7
Ruiz-Bañobre, (2021), Peng et al. (2022)	Europe	06/2016–02/2020	R	Advanced or metastatic UC	54/65	45/51	70/68	Within 30 days before beginning ICIs	Pembrolizumab, Nivolumab, Atezolizumab, Durvalumab	PPI	7
Okuyama, (2022), Kunimitsu et al. (2022)	Japan	08/2015–04/2021	R	Advanced UC	99/56	75/43	71/73	Within 30 days before ICI initiation and during ICI therapy	Pembrolizumab, Nivolumab, Atezolizumab, Durvalumab	PPI	6
Kunimitsu et al. (2022), Ruiz-Bañobre et al. (2021)	Japan	05/2017–12/2020	R	Metastatic or Unresectable UC	34/45	24/35	72/71	Within 60 days before and 30 days after beginning ICIs	Pembrolizumab	PPI	7
Hopkins et al. (2020), Kostine et al. (2021)	Worldwide	—	R	Advanced or metastatic UC	471/889	359/696	67/67	Within 30 days before and after beginning ICIs	Atezolizumab	PPI	8
Fukuokaya et al. (2022), Hopkins et al. (2020)	Japan	04/2018–04/2021	R	Metastatic UC	86/141	62/103	70/71	Within 30 days before and after beginning ICIs	Pembrolizumab	PPI	7

[a]median/mean age; UC, urothelial carcinoma; R, retrospective study; PPI, proton pump inhibitor; ICI, immune checkpoint inhibitor; CTLA-4, the cytotoxic T-lymphocyte antigen-4; PD-(L)-1, programmed cell death protein (ligand)-1

3.2 Progression-free survival

Six studies (Hopkins et al., 2020; Ruiz-Bañobre et al., 2021; Fukuokaya et al., 2022; Kunimitsu et al., 2022; Okuyama et al., 2022; Tomisaki et al., 2022), involving 1980 participants (759 who received PPIs and 1221 who did not), explored the impact of concomitant PPI usage on adjusted PFS among UC cancers receiving ICI treatment. As shown in Figure 2A, there was no significant heterogeneity among studies (I^2 = 7.4%, p = 0.369), so a fixed-effects model was utilized. Compared with patients without PPI usage, the meta-analysis showed that PPI use could increase the risk of progression by 50.7% (Figure 2A, HR: 1.507, 95% CI: 1.327-1.711, $p < 0.001$).

3.3 Overall survival

\The meta-analysis of adjusted OS was performed on six studies (Hopkins et al., 2020; Ruiz-Bañobre et al., 2021; Fukuokaya et al., 2022; Kunimitsu et al., 2022; Okuyama et al., 2022; Tomisaki et al., 2022) with a total of 1980 participants (759 with PPIs and 1221 without PPIs). Since there was no significant heterogeneity (Figure 2B, I^2 = 37.4%, p = 0.157), we applied a fixed-effects model. The meta-analysis revealed that PPI use was related to a shorter OS of UC patients receiving ICIs. PPI usage increased the risk of death by 58.7% (Figure 2B, HR: 1.587, 95% CI: 1.367–1.842, $p < 0.001$).

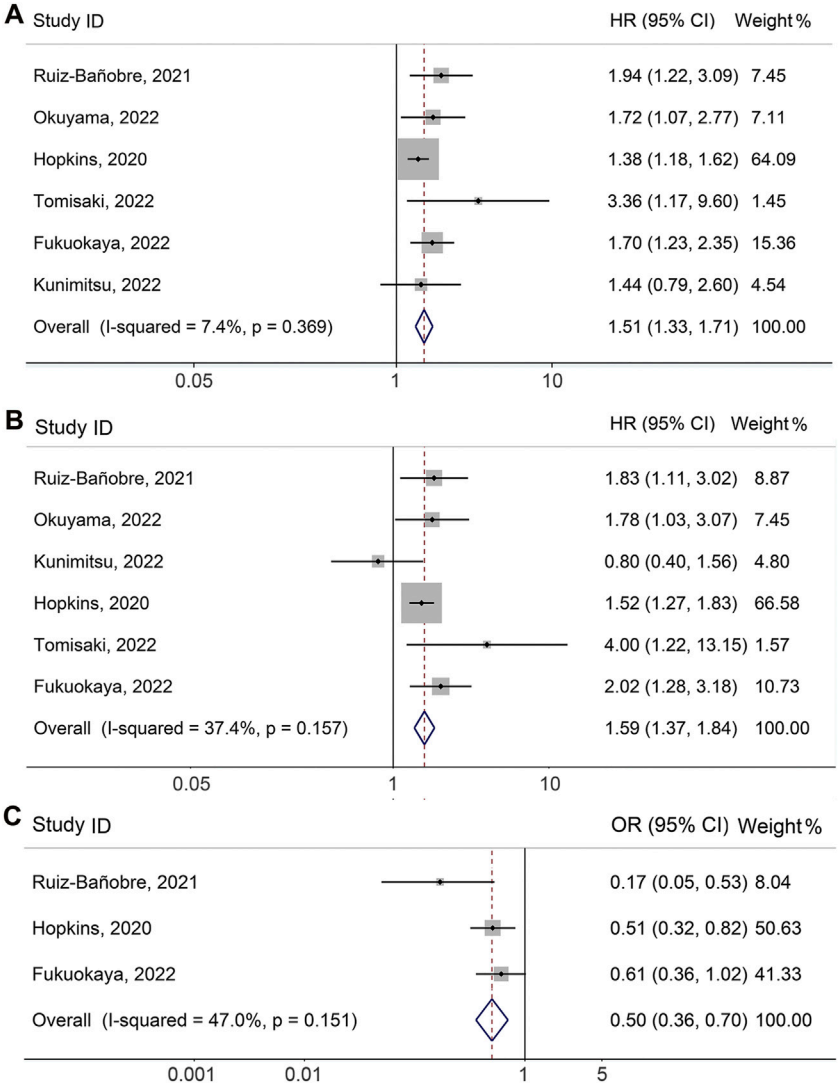

FIGURE 2
Forest plots of HR for correlation of proton pump inhibitor use with adjusted progression-free survival **(A)** and overall survival **(B)**. Forest plots of OR for correlation of proton pump inhibitor use with adjusted objective response rate **(C)**. OR, odds ratio; HR, hazard ratio; CL, confidence interval.

3.4 Objective response rate

As shown in Figure 2C, the pooled meta-analysis for multivariable analysis of the ORR included three studies (Hopkins et al., 2020; Ruiz-Bañobre et al., 2021; Fukuokaya et al., 2022) with 1706 urological cancer patients (611 with PPIs and 1095 without PPIs). No significant heterogeneity existed, so a fixed-effects model was implemented (I^2 = 47.0%, p = 0.151). The results were consistent with the above finding that concomitant PPI use was associated with lower ORR in patients (OR: 0.503, 95% CI: 0.360–0.703, $p < 0.001$).

3.5 Publication bias

The Begg's and Egger's tests were then performed to investigate publication bias, with the results indicating that there was no evidence of publication bias for adjusted OS (Egger's test: p = 0.574, Begg's test: p = 1.000) and adjusted ORR (Egger's test: p = 0.247, Begg's test: p = 1.000) across the studies. However, Egger's test showed a publication bias in adjusted PFS (Egger's test: p = 0.032, Begg's test: p = 0.452). Next, the number of missing studies in adjusted PFS was calculated using the trim and fill method. The combined HR was recalculated by including those missing hypothesis studies,

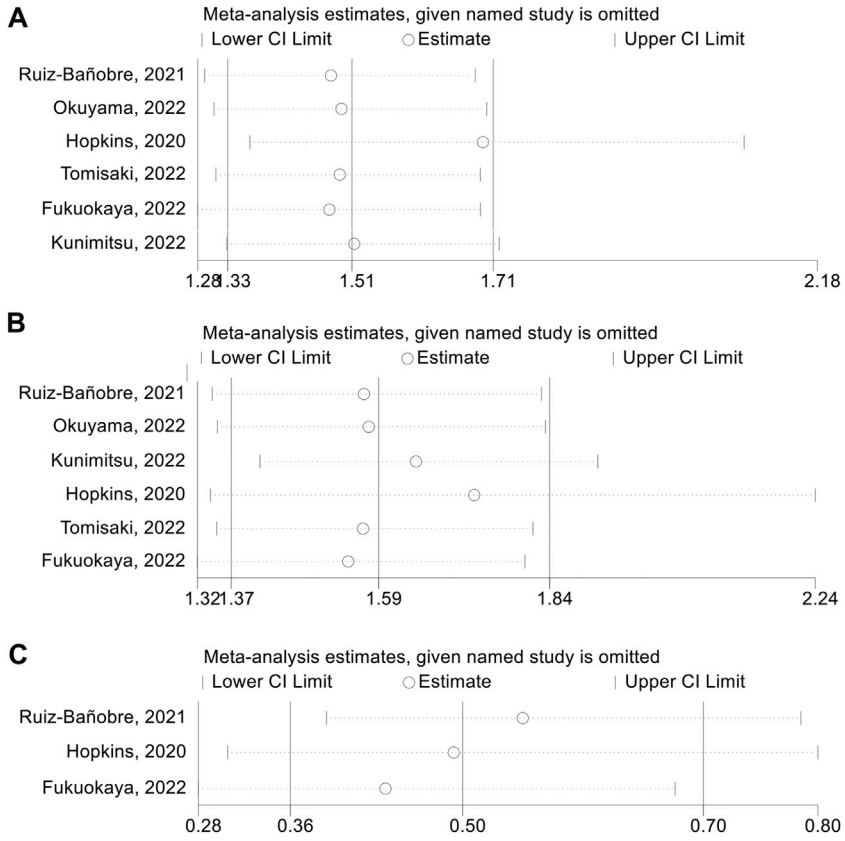

FIGURE 3
Sensitivity analysis of adjusted progression-free survival **(A)**, overall survival **(B)** and objective response rate **(C)**. CL, confidence interval.

which were not found to be significantly altered (HR:1.437, 95% CI: 1.277–1.617; $p < 0.001$). Thus, the publication bias had little effect, and the result was relatively stable.

3.6 Sensitivity analysis

We also performed a sensitivity analysis via the leave-one-out method to assess the impact of each study on the overall meta-analysis. As shown in Figure 3A, the pooled HR for adjusted PFS was not significantly changed after excluding one study at a time, ranging from 1.489 (95% CI: 1.311–1.692, after omitting Tomisaki, 2022) to 1.697 (95% CI: 1.359–2.076, after omitting Hopkins, 2020). Besides, the pooled HR for adjusted OS also did not significantly differ in the sensitivity analysis. The overall HR ranged from 1.542 (95% CI: 1.317–1.805, after omitting Fukuokaya et al., 2022) to 1.730 (95% CI: 1.336–2.238, after omitting Hopkins et al., 2020) (Figure 3B). Similarly, the pooled OR for adjusted ORR was not significantly different in the sensitivity analysis. The overall OR ranged from 0.439 (95% CI: 0.283–0.679, after omitting Fukuokaya et al., 2022) to 0.553 (95% CI: 0.390–0.784, after omitting Ruiz-Bañobre et al., 2021) (Figure 3C).

4 Discussion

With the increased use of ICIs in urological tumor therapy, tremendous effort has been made to uncover possible factors that affect its efficacy. Whether PPIs can impact the response to ICIs in UC patients is still being debated. For all we know, this is the first meta-analysis to investigate the relationship between PPIs and ICI efficacy in patients with UC. We synthesized all the available evidence and found concomitant PPI use was significantly associated with low clinical benefit in UC patients treated with ICIs. Our publication bias and sensitivity analyses verified the dependability of our conclusions. Consequently, our study is essential and hopes to provide novel insights into the precise management of PPIs in clinical practice. PPIs should be used with caution before and after ICI treatment in patients with UC.

PPIs were not only used to treat gastrointestinal adverse effects (nausea and vomiting) caused by systemic antineoplastic therapy; they were also used prophylactically for cancer patients taking high-dose glucocorticoids as an antiemetic regimen and with concomitant non-steroidal anti-inflammatory drugs as analgesics. Besides, tumor patients with a history of peptic ulcers or bleeding used PPI prophylaxis to reduce the incidence of stress ulcers (Triadafilopoulos et al., 2013). PPIs have been demonstrated to impact the intestinal microbiota, owing to both altered stomach acidity and direct compounds effects (Imhann et al., 2016; Le Bastard et al., 2018; Maier et al., 2018; Reveles et al., 2018). A significant decrease in bacterial richness and specific bacteria, such as the *Bifidobacteriaceae* and *Ruminococcaceae*, as well as a remarkable increase in pathogenic bacteria, were found among PPI users compared to non-users in a study of 1,815 people (Imhann et al., 2016; Reveles et al., 2018). Currently, the impact of microbiota on the response to ICI treatment is receiving increasing attention. Two landmark studies in mice provided the first evidence that the microbiome had a direct impact on ICI effectiveness (Sivan et al., 2015; Vétizou et al., 2015). Prospective studies have also revealed that microbiome diversity and composition were strongly associated with the efficacy of ICIs in patients with RCC (Derosa et al., 2020; Salgia et al., 2020) and NSCLC (Huemer et al., 2019; Hakozaki et al., 2020), among others. Dysbiosis of the gut microbiota reduces the activity of ICIs (Sivan et al., 2015; Vétizou et al., 2015; Huemer et al., 2019; Derosa et al., 2020; Hakozaki et al., 2020; Salgia et al., 2020). Furthermore, several preclinical studies have revealed that PPIs could impair the physiological function of natural killer cells, cytotoxic T-lymphocytes, and polymorphonuclear neutrophils, all of which are implicated in the efficacy of ICIs (Aybay et al., 1995; Zedtwitz-Liebenstein et al., 2002). Thus, PPIs may reduce the efficacy of ICIs by altering the intestinal flora and affecting innate immune cell function.

However, there is also evidence that PPIs not only inhibit tumor growth and enhance chemosensitivity by modulating the acidic environment, but also promote immune responses and prevent tumor immune escape (Peppicelli et al., 2015; Spugnini and Fais, 2017). Esomeprazole has also been shown to inhibit melanoma growth by inactivating NF-κB to downregulate vascular endothelial growth factor-C (VEGF-C) expression (Peppicelli et al., 2013). Notably, no basic research has been conducted on the role of PPI in the development of UC. In the context of ICI treatment, the underlying mechanisms of the effects of PPI on UC are completely unknown and need to be investigated in subsequent experiments.

This article has some inherent restrictions, to be sure. To begin with, this study was essentially a meta-analysis that relied on previously published articles. We did not have sufficient data to perform subgroup analyses based on different types, and doses of PPIs and ICIs, the PPI window respective to ICIs start, etc. Secondly, all included articles in this meta-analysis are retrospective studies with intrinsic limitations of reporting and selection bias. Thus, a larger prospective study should be performed to better understand the relationship between PPI use and ICI efficacy.

5 Conclusion

The meta-analysis suggested that concomitant PPI use was significantly associated with low clinical benefit in UC patients.

Data availability statement

The original contributions presented in the study are included in the article/Supplementary Material, further inquiries can be directed to the corresponding authors.

Author contributions

LZ, CC, WD, and WW conceived and designed the study. LZ, CC, DC, TK, KD, and CL were responsible for the collection and assembly of data, data analysis, and interpretation. LZ, CC, and LL were involved in writing the manuscript. LZ, CC, DC, WD, and WW revised the manuscript. All the work was performed under WD instruction. All authors read and approved the final manuscript.

Funding

This work was supported by grants from National Natural Science Foundation of China (No. 82172855, 81870442, 82003063)), and Natural Science Foundation of Hubei Province, China (No. 2021CFB365, 2020CFB213).

Acknowledgments

The authors thank all the medical staff who contributed to the maintenance of the medical record database.

Conflict of interest

The authors declare that the research was conducted in the absence of any commercial or financial relationships that could be construed as a potential conflict of interest.

Publisher's note

All claims expressed in this article are solely those of the authors and do not necessarily represent those of their affiliated organizations, or those of the publisher, the editors and the reviewers. Any product that may be evaluated in this article, or claim that may be made by its manufacturer, is not guaranteed or endorsed by the publisher.

Supplementary material

The Supplementary Material for this article can be found online at: https://www.frontiersin.org/articles/10.3389/fphar.2022.1018411/full#supplementary-material

References

Aybay, C., Imir, T., and Okur, H. (1995). The effect of omeprazole on human natural killer cell activity. *Gen. Pharmacol.* 26 (6), 1413–1418. doi:10.1016/0306-3623(94)00301-3

Bimbatti, D., Maruzzo, M., Pierantoni, F., Diminutto, A., Dionese, M., Deppieri, F. M., et al. (2022). Immune checkpoint inhibitors rechallenge in urological tumors: An extensive review of the literature. *Crit. Rev. Oncol. Hematol.* 170, 103579. doi:10.1016/j.critrevonc.2022.103579

Carretero-González, A., Lora, D., Martín Sobrino, I., Sáez Sanz, I., Bourlon, M. T., Anido Herranz, U., et al. (2020). The value of PD-L1 expression as predictive biomarker in metastatic renal cell carcinoma patients: A meta-analysis of randomized clinical trials. *Cancers (Basel)* 12 (7), E1945. doi:10.3390/cancers12071945

Derosa, L., Routy, B., Fidelle, M., Iebba, V., Alla, L., Pasolli, E., et al. (2020). Gut bacteria composition drives primary resistance to cancer immunotherapy in renal cell carcinoma patients. *Eur. Urol.* 78 (2), 195–206. doi:10.1016/j.eururo.2020.04.044

Fukuokaya, W., Kimura, T., Komura, K., Uchimoto, T., Nishimura, K., Yanagisawa, T., et al. (2022). Effectiveness of pembrolizumab in patients with urothelial carcinoma receiving proton pump inhibitors. *Urol. Oncol.* 12, 346.e1–346346.e8. doi:10.1016/j.urolonc.2022.02.020

Hakozaki, T., Richard, C., Elkrief, A., Hosomi, Y., Benlaïfaoui, M., Mimpen, I., et al. (2020). The gut microbiome associates with immune checkpoint inhibition outcomes in patients with advanced non-small cell lung cancer. *Cancer Immunol. Res.* 8 (10), 1243–1250. doi:10.1158/2326-6066.CIR-20-0196

Hopkins, A. M., Kichenadasse, G., Karapetis, C. S., Rowland, A., and Sorich, M. J. (2020). Concomitant proton pump inhibitor use and survival in urothelial carcinoma treated with atezolizumab. *Clin. Cancer Res.* 26 (20), 5487–5493. doi:10.1158/1078-0432.CCR-20-1876

Huemer, F., Rinnerthaler, G., Lang, D., Hackl, H., Lamprecht, B., and Greil, R. (2019). Association between antibiotics use and outcome in patients with NSCLC treated with immunotherapeutics. *Ann. Oncol.* 30 (4), 652–653. doi:10.1093/annonc/mdz021

Imhann, F., Bonder, M. J., Vich Vila, A., Fu, J., Mujagic, Z., Vork, L., et al. (2016). Proton pump inhibitors affect the gut microbiome. *Gut* 65 (5), 740–748. doi:10.1136/gutjnl-2015-310376

Kim, T. J., Cho, K. S., and Koo, K. C. (2020). Current status and future perspectives of immunotherapy for locally advanced or metastatic urothelial carcinoma: A comprehensive review. *Cancers* 12 (1), E192. doi:10.3390/cancers12010192

Kim, T. J., and Koo, K. C. (2020). Current status and future perspectives of checkpoint inhibitor immunotherapy for prostate cancer: A comprehensive review. *Int. J. Mol. Sci.* 21 (15), E5484. doi:10.3390/ijms21155484

Kostine, M., Mauric, E., Tison, A., Barnetche, T., Barre, A., Nikolski, M., et al. (2021). Baseline co-medications may alter the anti-tumoural effect of checkpoint inhibitors as well as the risk of immune-related adverse events. *Eur. J. Cancer* 157, 474–484. doi:10.1016/j.ejca.2021.08.036

Kunimitsu, Y., Morio, K., Hirata, S., Yamamoto, K., Omura, T., Hara, T., et al. (2022). Effects of proton pump inhibitors on survival outcomes in patients with metastatic or unresectable urothelial carcinoma treated with pembrolizumab. *Biol. Pharm. Bull.* 45 (5), 590–595. doi:10.1248/bpb.b21-00939

Le Bastard, Q., Al-Ghalith, G. A., Grégoire, M., Chapelet, G., Javaudin, F., Dailly, E., et al. (2018). Systematic review: Human gut dysbiosis induced by non-antibiotic prescription medications. *Aliment. Pharmacol. Ther.* 47 (3), 332–345. doi:10.1111/apt.14451

Maier, L., Pruteanu, M., Kuhn, M., Zeller, G., Telzerow, A., Anderson, E. E., et al. (2018). Extensive impact of non-antibiotic drugs on human gut bacteria. *Nature* 555 (7698), 623–628. doi:10.1038/nature25979

Mollica, V., Santoni, M., Matrana, M. R., Basso, U., De Giorgi, U., Rizzo, A., et al. (2022). Concomitant proton pump inhibitors and outcome of patients treated with nivolumab alone or plus ipilimumab for advanced renal cell carcinoma. *Target. Oncol.* 17 (1), 61–68. doi:10.1007/s11523-021-00861-y

Niu, X., Zhu, Z., and Bao, J. (2021). Prognostic significance of pretreatment controlling nutritional status score in urological cancers: A systematic review and meta-analysis. *Cancer Cell Int.* 21 (1), 126. doi:10.1186/s12935-021-01813-2

Okuyama, Y., Hatakeyama, S., Numakura, K., Narita, T., Tanaka, T., Miura, Y., et al. (2022). Prognostic impact of proton pump inhibitors for immunotherapy in advanced urothelial carcinoma. *BJUI Compass* 3 (2), 154–161. doi:10.1002/bco2.118

Page, M. J., McKenzie, J. E., Bossuyt, P. M., Boutron, I., Hoffmann, T. C., Mulrow, C. D., et al. (2021). The PRISMA 2020 statement: An updated guideline for reporting systematic reviews. *Bmj* 372, n71. doi:10.1136/bmj.n71

Peng, K., Chen, K., Teply, B. A., Yee, G. C., Farazi, P. A., and Lyden, E. R. (2022). Impact of proton pump inhibitor use on the effectiveness of immune checkpoint inhibitors in advanced cancer patients. *Ann. Pharmacother.* 56 (4), 377–386. doi:10.1177/10600280211033938

Peppicelli, S., Bianchini, F., Contena, C., Tombaccini, D., and Calorini, L. (2013). Acidic pH via NF-κB favours VEGF-C expression in human melanoma cells. *Clin. Exp. Metastasis* 30 (8), 957–967. doi:10.1007/s10585-013-9595-4

Peppicelli, S., Bianchini, F., Toti, A., Laurenzana, A., Fibbi, G., and Calorini, L. (2015). Extracellular acidity strengthens mesenchymal stem cells to promote melanoma progression. *Cell Cycle* 14 (19), 3088–3100. doi:10.1080/15384101.2015.1078032

Pierantoni, F., Maruzzo, M., Gardi, M., Bezzon, E., Gardiman, M. P., Porreca, A., et al. (2019). Immunotherapy and urothelial carcinoma: An overview and future prospectives. *Crit. Rev. Oncol. Hematol.* 143, 46–55. doi:10.1016/j.critrevonc.2019.08.005

Qin, B. D., Jiao, X. D., Zhou, X. C., Shi, B., Wang, J., Liu, K., et al. (2021). Effects of concomitant proton pump inhibitor use on immune checkpoint inhibitor efficacy among patients with advanced cancer. *Oncoimmunology* 10 (1), 1929727. doi:10.1080/2162402X.2021.1929727

Reveles, K. R., Ryan, C. N., Chan, L., Cosimi, R. A., and Haynes, W. L. (2018). Proton pump inhibitor use associated with changes in gut microbiota composition. *Gut* 67 (7), 1369–1370. doi:10.1136/gutjnl-2017-315306

Rizzo, A., Cusmai, A., Giovannelli, F., Acquafredda, S., Rinaldi, L., Misino, A., et al. (2022). Impact of proton pump inhibitors and histamine-2-receptor antagonists on non-small cell lung cancer immunotherapy: A systematic review and meta-analysis. *Cancers (Basel)* 14 (6), 1404. doi:10.3390/cancers14061404

Ruiz-Bañobre, J., Molina-Díaz, A., Fernández-Calvo, O., Fernández-Núñez, N., Medina-Colmenero, A., Santomé, L., et al. (2021). Rethinking prognostic factors in locally advanced or metastatic urothelial carcinoma in the immune checkpoint blockade era: A multicenter retrospective study. *ESMO Open* 6 (2), 100090. doi:10.1016/j.esmoop.2021.100090

Salgia, N. J., Bergerot, P. G., Maia, M. C., Dizman, N., Hsu, J., Gillece, J. D., et al. (2020). Stool microbiome profiling of patients with metastatic renal cell carcinoma

receiving anti-PD-1 immune checkpoint inhibitors. *Eur. Urol.* 78 (4), 498–502. doi:10.1016/j.eururo.2020.07.011

Seto, T., Sam, D., and Pan, M. (2019). Mechanisms of primary and secondary resistance to immune checkpoint inhibitors in cancer. *Med. Sci.* 7 (2), E14. doi:10.3390/medsci7020014

Sharma, P., Hu-Lieskovan, S., Wargo, J. A., and Ribas, A. (2017). Primary, adaptive, and acquired resistance to cancer immunotherapy. *Cell* 168 (4), 707–723. doi:10.1016/j.cell.2017.01.017

Sivan, A., Corrales, L., Hubert, N., Williams, J. B., Aquino-Michaels, K., Earley, Z. M., et al. (2015). Commensal Bifidobacterium promotes antitumor immunity and facilitates anti-PD-L1 efficacy. *Science* 350 (6264), 1084–1089. doi:10.1126/science.aac4255

Spugnini, E., and Fais, S. (2017). Proton pump inhibition and cancer therapeutics: A specific tumor targeting or it is a phenomenon secondary to a systemic buffering? *Semin. Cancer Biol.* 43, 111–118. doi:10.1016/j.semcancer.2017.01.003

Sung, H., Ferlay, J., Siegel, R. L., Laversanne, M., Soerjomataram, I., Jemal, A., et al. (2021). Global cancer statistics 2020: GLOBOCAN estimates of incidence and mortality worldwide for 36 cancers in 185 countries. *Ca. Cancer J. Clin.* 71 (3), 209–249. doi:10.3322/caac.21660

Tomisaki, I., Harada, M., Minato, A., Nagata, Y., Kimuro, R., Higashijima, K., et al. (2022). Impact of the use of proton pump inhibitors on pembrolizumab effectiveness for advanced urothelial carcinoma. *Anticancer Res.* 42 (3), 1629–1634. doi:10.21873/anticanres.15638

Triadafilopoulos, G., Roorda, A. K., and Akiyama, J. (2013). Indications and safety of proton pump inhibitor drug use in patients with cancer. *Expert Opin. Drug Saf.* 12 (5), 659–672. doi:10.1517/14740338.2013.797961

Vétizou, M., Pitt, J. M., Daillère, R., Lepage, P., Waldschmitt, N., Flament, C., et al. (2015). Anticancer immunotherapy by CTLA-4 blockade relies on the gut microbiota. *Science* 350 (6264), 1079–1084. doi:10.1126/science.aad1329

Wei, N., Zheng, B., Que, W., Zhang, J., and Liu, M. (2022). The association between proton pump inhibitor use and systemic anti-tumour therapy on survival outcomes in patients with advanced non-small cell lung cancer: A systematic review and meta-analysis. *Br. J. Clin. Pharmacol.* 88, 3052–3063. doi:10.1111/bcp.15276

Wells, G., Shea, B., and O'Connell, D. (2019). The newcastle-ottawa Scale (NOS) for assessing the quality if nonrandomizes studies in meta-analyses. AvaliableAt: http://wwwohrica/programs/clinical_ epidemiology/oxfordasp.

Xu, W., Atkins, M. B., and McDermott, D. F. (2020). Checkpoint inhibitor immunotherapy in kidney cancer. *Nat. Rev. Urol.* 17 (3), 137–150. doi:10.1038/s41585-020-0282-3

Zedtwitz-Liebenstein, K., Wenisch, C., Patruta, S., Parschalk, B., Daxböck, F., and Graninger, W. (2002). Omeprazole treatment diminishes intra- and extracellular neutrophil reactive oxygen production and bactericidal activity. *Crit. Care Med.* 30 (5), 1118–1122. doi:10.1097/00003246-200205000-00026

frontiers | Frontiers in Pharmacology

TYPE Original Research
PUBLISHED 29 September 2022
DOI 10.3389/fphar.2022.972934

Check for updates

OPEN ACCESS

EDITED BY
Ting Wang,
Sichuan Cancer Hospital, China

REVIEWED BY
Chen Xue,
Zhejiang University, China
Yingxue Zhang,
Wayne State University, United States

*CORRESPONDENCE
Shengtian Zhao,
zhaoshengtian@sdu.edu.cn

SPECIALTY SECTION
This article was submitted to Pharmacology of Anti-Cancer Drugs, a section of the journal Frontiers in Pharmacology

RECEIVED 19 June 2022
ACCEPTED 12 September 2022
PUBLISHED 29 September 2022

CITATION
Wang G, Wang Z, Lu H, Zhao Z, Guo L, Kong F, Wang A and Zhao S (2022), Comprehensive analysis of FRAS1/FREM family as potential biomarkers and therapeutic targets in renal clear cell carcinoma.
Front. Pharmacol. 13:972934.
doi: 10.3389/fphar.2022.972934

COPYRIGHT
© 2022 Wang, Wang, Lu, Zhao, Guo, Kong, Wang and Zhao. This is an open-access article distributed under the terms of the Creative Commons Attribution License (CC BY). The use, distribution or reproduction in other forums is permitted, provided the original author(s) and the copyright owner(s) are credited and that the original publication in this journal is cited, in accordance with accepted academic practice. No use, distribution or reproduction is permitted which does not comply with these terms.

Comprehensive analysis of FRAS1/FREM family as potential biomarkers and therapeutic targets in renal clear cell carcinoma

Ganggang Wang[1,2], Zheng Wang[1], Haiquan Lu[3], Zhiqun Zhao[3], Liqiang Guo[4], Feng Kong[1], Aizhen Wang[1] and Shengtian Zhao[1,5]*

[1]Department of Urology, Shandong Provincial Hospital, Shandong University, Jinan, Shandong, China, [2]Department of Urology, Maternal and Child Health Care Hospital of Shandong Province, Shandong University, Jinan, Shandong, China, [3]Advanced Medical Research Institute and Key Laboratory for Experimental Teratology of the Ministry of Education, Cheeloo College of Medicine, Shandong University, Jinan, Shandong, China, [4]Department of Urology, Qilu Hospital, Shandong University, Jinan, Shandong, China, [5]Binzhou Medical University, Binzhou, Shandong, China

Background: FRAS1 (Fraser syndrome protein 1), together with FREM1 (the Fras1-related extracellular matrix proteins 1) and FREM2, belonging to the FRAS1/FREM extracellular matrix protein family, are considered to play essential roles in renal organogenesis and cancer progression. However, their roles in kidney renal clear cell carcinoma (KIRC) remain to be elucidated.

Methods: FRAS1/FREM RNA expression analysis was performed using TCGA/GTEx databases, and valided using GEO databases and real-time PCR. Protein expression was peformed using CPTAC databases. Herein, we employed an array of bioinformatics methods and online databases to explore the potential oncogenic roles of FRAS1/FREM in KIRC.

Results: We found that FRAS1, FREM1 and FREM2 genes and proteins expression levels were significantly decreased in KIRC tissues than in normal tissues. Decreased FRAS1/FREM expression levels were significantly associated with advanced clinicopathological parameters (pathological stage, grade and tumor metastasis status). Notably, the patients with decreased FRAS1/FREM2 expression showed a high propensity for metastasis and poor prognosis. FRAS1/FREM were correlated with various immune infiltrating cells, especially $CD4^+$ T cells and its corresponding subsets (Th1, Th2, Tfh and Tregs). FRAS1 and FREM2 had association with DNA methylation and their single CpG methylation levels were associated with prognosis. Moreover, FRAS1/FREM might exert antitumor effects by functioning in key oncogenic signalling pathways and metabolic pathways. Drug sensitivity analysis indicated that high FRAS1 and FREM2 expression can be a reliable predictor of targeted therapeutic drug response, highlighting the potential as anticancer drug targets.

Conclusion: Together, our results indicated that FRAS1/FREM family members could be potential therapeutic targets and valuable prognostic biomarkers of KIRC.

KEYWORDS

renal clear cell carcinoma, prognosis, biomarker, therapeutic target, tumor immune infiltrating, DNA methylation

Introduction

Renal cell carcinoma (RCC) is one of the common urinary system tumors, which affects over 400,000 individuals worldwide and its incidence continues to increase in both men and women per year (Siegel et al., 2021). There are several subvariants of RCC, the most common pathological type is kidney renal clear cell carcinoma (KIRC), which accounts for approximately 70%–80% of RCC. Although nephrectomy remains the standard care for patients with locally advanced RCC, recurrence occurs in up to 50%–80% of patients, ultimately causing death from the disease. Moreover, up to a third of KIRC at initial diagnosis will present with or develop metastases, which state is almost uniformly lethal with a poor prognosis (Diaz-Montero et al., 2020; Jonasch et al., 2021). Therefore, screening effective biomarkers for the diagnosis, treatment and prognostic evaluation of KIRC is of great clinical significance (Choueiri et al., 2022).

As one of the major components of the tumor microenvironment (TME), the extracellular matrix (ECM), which comprises proteins and polysaccharides, plays multiple crucial roles during the development of cancer (Huang et al., 2021). Moreover, the interplay between TME and malignant cells contribute to ECM stiffness, and, the stiffened ECM can also cause the changes of cancer cells (Nazemi and Rainero, 2020; Romani et al., 2021). The basement membrane (BM), a specialized type of ECM in direct contact with cells, constitutes architecturally complex ECM protein networks of great structural and regulatory importance (Stuelten et al., 2018; Reuten et al., 2021). FRAS1 (Fraser syndrome protein 1), together with FREM1 (the Fras1-related extracellular matrix proteins 1) and FREM2, belonging to the FRAS1/FREM extracellular matrix protein family, are located in the sublamina densa of basement membranes (Pavlakis et al., 2011). They can form an independent ternary complex, in which each component is necessary for stabilization of the entire complex (Pavlakis et al., 2011; Kiyozumi et al., 2012).

FRAS1, FREM1 and FREM2 are linked to human disorders. Recessive mutations in FRAS1 and FREM2 are shown to be able to cause fraser syndrome, which is a rare, hereditary, autosomal, recessive, multisystem disorder characterized by cryptophthalmos, syndactyly, renal agenesis, and a variety of morphogenetic defects (Jadeja et al., 2005; Pavlakis et al., 2011). Mutation of FREM1 can also cause another rare autosomal-recessive human disorder namely, bifid nose, renal agenesis and anorectal malformations syndrome (BNAR) (Alazami et al., 2009). Notably, the mutation of any one of FRAS1, FREM1 and FREM2 can cause congenital anomalies of the kidneys and urinary tract (CAKUT), which means that FRAS1/FREM genes and proteins play essential roles in renal organogenesis (Pavlakis et al., 2011; Al-Hamed et al., 2021). FRAS1/FREM are also found to be involved in the progression of several cancers, such as lung cancer (Zhan et al., 2014), gastric cancer (Umeda et al., 2020), breast carcinoma (Li H. N. et al., 2020) and isocitrate dehydrogenase (IDH)- wild-type glioblastoma (Jovcevska et al., 2019). However, up to now, the roles of FRAS1/FREM family in KIRC have yet been fully elucidated.

We herein conducted a comprehensive analysis to illustrate the FRAS1/FREM profiles in KIRC including expression patterns, potential functions, prognostic value, immune infiltrating levels, as well as DNA methylation levels using the TCGA project and GEO databases. Biological interaction networks and relevant cellular pathway were also analyzed to investigate the potential molecular mechanism of FRAS1/FREM in KIRC.

Materials and methods

Differentially expressed FRAS1/FREM at the transcriptional level

First, the mRNA expressions of FRAS1, FREM1, and FREM2 in KIRC tissues with those in normal controls were analyzed by the Oncomine database (https://www.oncomine.org, an integrated online cancer microarray database and data-mining platform), using a Student *t* test. The cut-off *p*-value and fold change were as following: p-value < 0.001, fold change = 1.5, gene rank = 10%.

Then TIMER 2 (tumor immune estimation resource, version 2, http://timer.cistrome.org) was used for the analysis the expression profiling of FRAS1, FREM1, and FREM2 between cancers and normal tissues. Considering that there are limited normal samples in TCGA, we have integrated data from normal tissues in the GTEx database and data from TCGA tumor tissues. RNA sequencing and related clinical data were downloaded from TCGA (http://cancergenome.nih.gov) using UCSC Xena (https://xena.ucsc.edu/), Gene expression data from normal tissues were downloaded from GTEx (https://commonfund.

nih.gov/GTEx). Data analysis was conducted using R software (Version 4.0.3), and the R package "ggpubr" was used to draw box plots, *$p < 0.05$, **$p < 0.01$, ***$p < 0.001$).

We used the data of GEO (Gene Expression Omnibus, https://www.ncbi.nlm.nih.gov/geo) to further verify the differential expression levels of FRAS1, FREM1, and FREM2 between cancer and normal tissues in KIRC. The datasets [GSE40435 (Wozniak et al., 2013) and GSE53757 (von Roemeling et al., 2014)] used were from GEO database, and the download data format was MINIML. Box plots were drawn by boxplot; PCA graphs were drawn by R software package ggord; The box plot was implemented by the R software package ggplot2; the heat map was displayed by the R software package pheatmap.

Differentially expressed FRAS1/FREM at protein level in KIRC

The CPTAC (Clinical proteomic tumor analysis consortium, https://proteomics.cancer.gov/programs/cptac) was used for proteomics research of various tumors. We used UALCAN tool (http://ualcan.path.uab.edu/analysisprot.html) to conduct protein expression analysis of the CPTAC dataset. Expression levels of the total protein of FRAS1, FREM1, and FREM2 had been compared between KIRC and normal tissues, respectively.

HPA (Human Protein Atlas, http://www.proteinatlas.org) is a platform that contains representative immunohistochemistry (IHC) based protein expression data for near 20 highly common kinds of cancers. To evaluate differences in FRAS/FREM protein expression, IHC images of FRAS1 and FREM2 protein expression in KIRC tissues and normal tissues, were directly visualized by HPA.

Participants and reverse transcription PCR

The surgically resected KIRC tissue and paired normal adjacent kidney tissue were collected from 35 patients with KIRC in the department of urology in shandong provincial hospital from February to August 2022. All patients did not receive radiotherapy or chemotherapy before operation. After operation, they were pathologically diagnosed as kidney renal clear cell carcinoma and signed the informed consent. Total mRNA was isolated from frozen human tissues using the RNA-Quick Purification Kit (eSUN Bio Material Co., Ltd.) according to the manufacturer's instruction, and mRNA levels were analyzed using real-time quantitative RT-PCR with the Bio-Rad iCycler sysytem. The sequences of the specific primers for the target genes were listed below: FRAS1, forward primer: 5′-AATAGCTGCCAACCAATGCTG -3′, Reverse Primer: 5′- CAA GAGCACACACTACATGGAG -3′; FREM1, forward primer: 5′- GCCTGTGGTAACCAGGAACAA -3′, Reverse Primer: 5′-CGCAGGTGTATCAGGGTCG -3′; FREM2, forward primer: 5′-GAGGGGCAGTAGTGCTACCA -3′, Reverse Primer: 5′- GAC CAGAGGCAAGTTCCGA -3′; 18 s, forward primer: 5′- CGG CGACGACCCATTCGAAC -3′, Reverse Primer: 5′- GAATCG AACCCTGATTCCCCGTC -3′. The data of real-time PCR were analyzed using the value 2-Δct. 18 s rRNA was used as the internal control. The continuous data were represented by Mean, SED. *$p < 0.05$, **$p < 0.01$, ***$p < 0.001$, and ****$p < 0.0001$. The paired t test was used to analyze the correlation between the paired tissues of the normal distribution. The wilcoxon test was used to analyze the correlation between the paired tissues of the non-normal distribution.

Correlation between FRAS1/FREM and clinical phenotype in KIRC

Raw counts of RNA-sequencing data of FRAS1, FREM1 and FREM2 and corresponding clinical information such as pathological stage, grade and prognosis from 530 KIRC samples were obtained from TCGA. Sanguini diagram was built based on the R software package ggalluval. All the above analysis methods and R package were implemented by R foundation. $p < 0.05$.

The expression distribution of FRAS1, FREM1 and FREM2 genes in different pathological stage (stage I, stage II, stage III and stage IV and normal tissues), different pathological grade (grade I, grade II, grade III and grade IV and normal tissues) and different state (with and without metastasis) were implemented by R foundation and ggplot2 (v3.3.2). *$p < 0.05$, **$p < 0.01$, ***$p < 0.001$. When the number of groups greater than or equal to 3, Kruskal–Wallis test was used, otherwise, Wilcoxon test was used.

We used GEO database to further verify the expression distribution of FRAS1, FREM1 and FREM2 genes in different pathological stage (Stage I + II, Stage III + IV) and different pathological grade (Grade I + II, Grade III + IV) in KIRC. The pathological stage data was from GSE73731 and GSE53757, while, the pathological grade was from GSE 40435 and GSE73731. Box plots are drawn by boxplot; PCA graphs are drawn by R software package ggord; the box plot was implemented by the R software package ggplot2.

The UALCAN tool was also applied to analyse the correlation between FRAS1/FREM proteins expression and pathological stage and grade with the date from CPTAC.

As the TCGA dateset didn't include metastatic tumor tissues, we also used GEO database [GSE105261 (Nam et al., 2019) and GSE22541 (Wuttig et al., 2012)] to compare the expression distribution of FRAS1, FREM1 and FREM2 genes in primary KIRC and metastatic KIRC. What's more, we further divided the patients from GSE22541 in three groups: The low matestasis risk primary RCC ($n = 16$, eight patients with distant or lymph node metastases within one year after the nephrectomy were

excluded); pulmonary metastasis of KIRC, No. (the number of matastases) < 10; pulmonary metastasis of KIRC, No. (the number of matastases) > = 10. The differential expression of FRAS1, FREM1 and FREM2 genes in these groups were compared. It is worth noting that, GSE155209 was used to verify the diagnostic value of FRAS1, FREM1 and FREM2 genes for metastatic progression in stage I and stage II KIRC. Box plots were drawn by boxplot; the box plot was implemented by the R software package ggplot2. *$p < 0.05$, **$p < 0.01$, ***$p < 0.001$, ****$p < 0.0001$. When the number of groups greater than or equal to 3, Kruskal–Wallis test was used, otherwise, Wilcoxon test was used.

Correlation between FRAS1/FREM and survival analysis in KIRC

Raw counts of RNA-sequencing data of the FRAS1, FREM1 and FREM2 and corresponding clinical information from 530 KIRC patients were obtained from TCGA. We performed survival analysis to search for relationships between gene expression and patient prognosis, such as OS, DSS and PFS, computed the log-rank p value and hazard ratio (HR) with 95% confidence intervals (95% CI) using "survival" package in R. The results were displayed as forestplots (using "forestplot" package in R) and survival curves. For Kaplan–Meier curves, p-values and HR with 95% CI were generated by log-rank tests and univariate Cox proportional hazards regression.

Multivariate cox regression analysis was performed to evaluate the utility of FRAS1, FREM1 and FREM2 expression in predicting cancer patient prognosis. The forest was used to show the p value, HR and 95% CI of each variable through "forestplot" R package. HR and p value of constituents involved in multivariate Cox regression and some parameters (age, gender, race, TNM stage and grade).

Correlation analysis between FRAS1/FREM and immune infiltrating levels

Pearson analysis was performed to assess the correlations between FRAS1/FREM gene expression and quantitative variables such as immune checkpoints, TMB, MSI as well as MMR proteins. A p-value of less than 0.05 was considered statistically significant. The results were displayed as heatmaps using "pheatmap" package in R.

The relationship between FRAS1/FREM gene expression and Tumor-infiltrating immune cell profiles across TCGA pan-cancer cohort was analyzed by TIMER 2. The TIMER, TIDE, CIBERSORT, CIBERSORT-ABS, QUANTISEQ, XCELL, MCPCOUNTER and EPIC algorithms were applied for estimations. Furthermore, the immune cell subsets associated with $CD4^+$ T cells including Th1, Th2, T cell follicular helper, T cell regulatory (Tregs) were selected for detailed analysis.

Correlation between FRAS1/FREM expression and DNA methylation

The UALCAN tool was applied to analyse the correlation between FRAS1/FREM gene expression and the gene promoter methylation level for KIRC. Then we analysed the assciation between FRAS1/FREM gene expression and four DNA methyltransferases (DNMT1: red, DNMT2: blue, DNMT3A: green, DNMT3B: purple) for each tumor, and visualization were performed as follows.

MethSurv (https://biit.cs.ut.ee/methsurv/), a web tool for survival analysis based on CpG methylation patterns, was applied to explore the prognostic value of single CpG methylation of FRAS1 and FREM2 in KIRC patients ($p < 0.05$ as significant).

Function enrichment of FRAS1/FREM in KIRC

GeneMANIA 3.6.0 (http://www.genemania.org) is a website for generating hypotheses about gene function using available genomics and proteomics data. In our study, the FRAS1, FREM1 and FREM2 genes were submitted to the GeneMANIA to illustrate the functional association network among FRAS1/FREM and their related genes. Protein–protein interaction (PPI) network construction Search Tool for the Retrieval of Interacting Genes (STRING; http://string-db.org) online database was used to predict PPI network of co-regulated hub genes and analyse the functional interactions between proteins.

Gene set enrichment analysis (GSEA) was performed to explore the potential mechanisms involved in the effect of risk score on KIRC using transcriptional sequences in TCGA database. The enrichment analysis was performed using the Molecular Signatures Database (MSigDB) of H (hallmark), C2 (C2:CP:KEGG) and C5 (C5:GO:BP, CC, MF). The enriched gene sets in the GSEA that reached a nominal significance level of $p < 0.05$ and normalized Enrichment Score (NES) > 1.5 were considered significant. The top 20 sets of each phenotype associated with genes were listed to reflect the role of FRAS1, FREM1 and FREM2.

Drug sensitivity analysis

The data of gene expression level and corresponding clinical information were downloaded from the TCGA dataset. The largest publicly available pharmacogenomics database [the

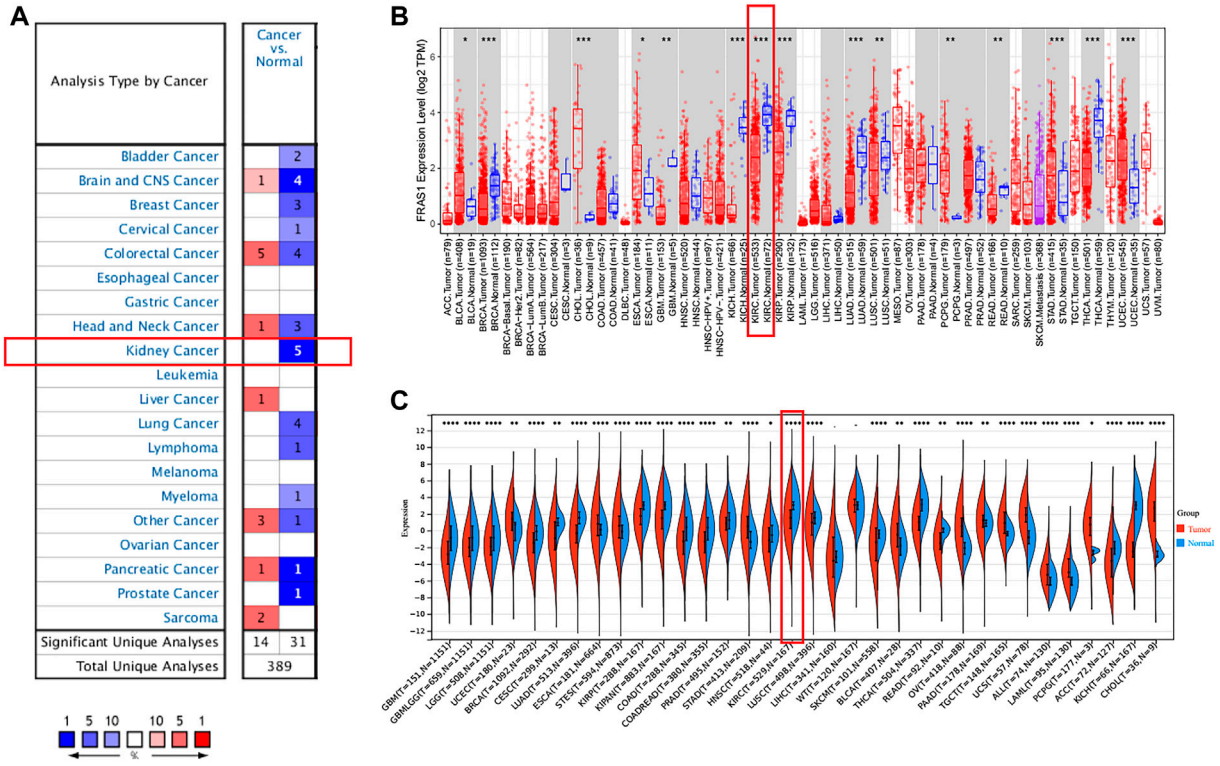

FIGURE 1
Pan-cancer expression analysis of FRAS1 mRNA in human tumors vs. normal tissues. **(A)** Differential expression of FRAS1 in the Oncomine database. **(B)** The expression profile of FRAS1 in pan-cancer analysis by TIMER2.0. **(C)** The expression profile of FRAS1 in pan-cancer analysis from TCGA database and GTEx database. (*$p < 0.05$, **$p < 0.01$, ***$p < 0.001$).

TABLE 1 Differential expression of FRAS1/FREM family members in KIRC tissues and normal kidney tissues in the Oncomine database.

	Types of KIRC VS. Normal	Fold change	*p*-value	*t*-test	Ref
FRAS1					
	Clear Cell Renal Cell Carcinoma	-3.812	2.98E-05	-7.000	Higgins Renal
	Clear Cell Renal Cell Carcinoma	-5.118	6.19E-05	-4.933	Yusenko Renal
	Non-Hereditary Clear Cell Renal Cell Carcinoma	-2.205	5.10E-05	-5.495	Beroukhim Renal
FREM1					
	Clear Cell Renal Cell Carcinoma	-1.664	2.35E-06	-7.279	Lenburg Renal
	Clear Cell Renal Cell Carcinoma	-20.647	2.05E-04	-6.737	Yusenko Renal
FREM2					
	Clear Cell Renal Cell Carcinoma	-5.168	1.27E-04	-4.257	Yusenko Renal

Genomics of Drug Sensitivity in Cancer (GDSC), https://www.cancerrxgene.org/] was used to predict the targeted therapeutic response for each sample. The prediction process was implemented by R package "pRRopheticm". The samples' half-maximal inhibitory concentration (IC50) was estimated by ridge regression. Spearman's-correlation analysis was used to explore the correlation between drug sensitivity and FRAS1, FREM1 and FREM2 gene expression in KIRC.

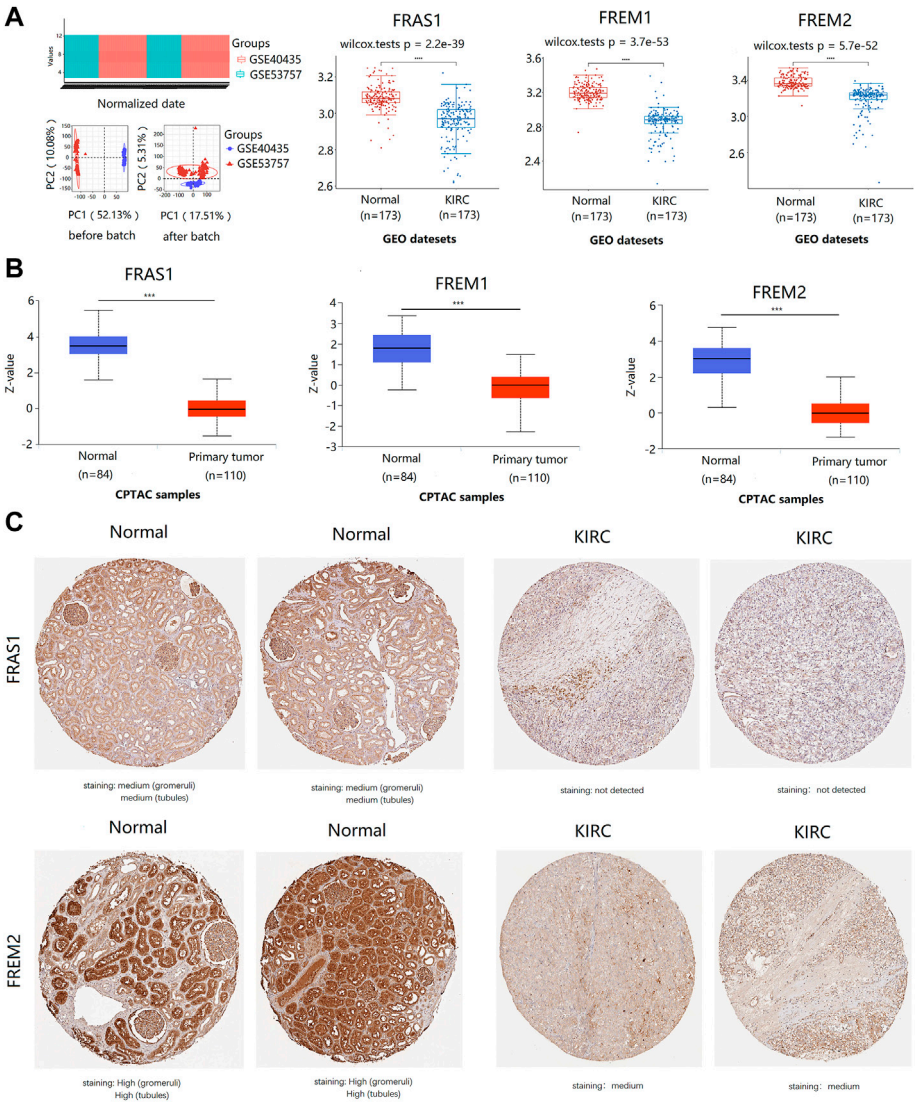

FIGURE 2
The expression profile of FRAS1/FREM family members in KIRC tissues and normal kidney tissues with datesets from GEO and CPTAC datebase. **(A)** the expression profile of FRAS1/FREM mRNA in KIRC samples and paired normal samples with datesets from the GEO database (GSE40435 and GSE53757) (****$p < 0.0001$). **(B)** Protein expression of FRAS1/FREM in KIRC tissues and normal kidney tissues with datesets from CPTAC datebase. ***$p < 0.001$. **(C)** Representative immunohistochemistry images of FRAS1 and FREM2 in normal kidney tissues and KIRC tissues (HPA database).

Results

Transcriptional levels and protein levels of FRAS1/FREM in KIRC

The mRNA expression levels of FRAS1, FREM1 and FREM2 were analyzed in Oncomine over a cancer-wide range. As shown in Figure 1A, Supplementary Figure S1A,2A, FRAS1 expression was lower in most cancer groups compared with the respective normal groups. The mRNA expression levels of FRAS1, FREM1 and FREM2 were significantly downregulated in KIRC, the detailed results were summarized in Table 1. The mRNA expression level of FRAS1 was significantly downregulated in patients with KIRC in three datasets (with a fold change of -3.812 in Higgins Renal dateset, -5.118 in Yusenko Renal dateset and -2.205 in Beroukhim Renal dateset). Similarly, the mRNA expression level of FREM1 was also downregulated in patients with KIRC in two datasets (with a fold change of -1.664 in Lenburg Renal dateset and -20.647 in Yusenko Renal dateset). The mRNA expression level of FREM2 was

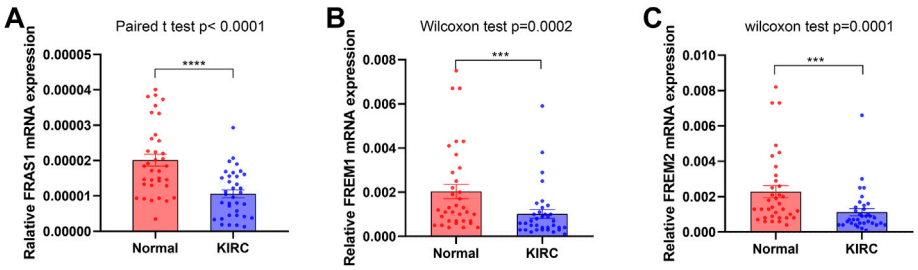

FIGURE 3
FRAS1/FREM expression in cancer and adjacent normal kidney tissues of KIRC patients by RT-PCR. **(A)**FRAS1 expression in cancer and adjacent normal kidney tissues of KIRC patients. **(B)** FREM1 expression in cancer and adjacent normal kidney tissues of KIRC patients. **(C)** FREM2 expression in cancer and adjacent normal kidney tissues of KIRC patients.

also downregulated with a fold change of -5.168 in Yusenko Renal dateset.

Next, we compared the FRAS1, FREM1 and FREM2 expression levels across all TCGA tumors using TIMER 2.0 (as shown in Figure 1B; Supplementary Figures S1B, 2B). Considering the number size of normal tissue in the TCGA database is small, we further matched the GTEx normal tissues with the TCGA cancer tissues to reflect the gene expression landscape in a more convincing manner (as shown in Figure 1C; Supplementary Figures S1C, 2C). Consistent from the Oncomine database, the mRNA expression levels of FRAS1, FREM1 and FREM2 were still significantly down-regulated in KIRC tissues compared to normal samples ($p < 0.001$).

Furthermore, we used datasets GSE40435 (Wozniak et al., 2013) (101 KIRC vs. 101 normal) and GSE53757 (von Roemeling et al., 2014) (72 KIRC vs. 72 normal) from GEO database to further validate this conclusion, As shown in Figure 2A, the mRNA expression levels of FRAS1, FREM1 and FREM2 were also significantly downregulated in the 173 KIRC tissues included compared to matched normal tissues ($p < 0.0001$).

In addition to transcription, we explored the protein expression of FRAS/FREM family members in KIRC by CPTAC and the Human Protein Atlas. The protein expression levels of FRAS1, FREM1 and FREM2 were lower in KIRC tissues than in normal tissues using the CPTAC dataset (Figure 2B, $p < 0.001$). Similar results appeared by CPTAC analysis, We found that KIRC tissues had negative or medium IHC staining, while normal kidney tissues had medium or high staining by HPA. Negative expression of FRAS1 protein was observed in KIRC tissues, while medium protein expression was observed in normal kidney tissues. Medium protein expression of FREM2 was observed in KIRC tissues, while high protein expression was observed in normal kidney tissues (Figure 2C).

The expression levels of FRAS1, FREM1 and FREM2 in both KIRC and non-tumor tissues were also measured by qRT-PCR verification, which confirmed the expression profiles of FRAS1/FREM family. Compared with normal tissues, the expression levels of FRAS1 (Figure 3A, $p < 0.0001$), FREM1 (Figure 3B, $p = 0.0002$) and FREM2 (Figure 3C, $p = 0.0001$) were significantly decreased in KIRC tissues.

Taken together, all the results above showed that the expression levels of FRAS1, FREM1 and FREM2 were downregulated in KIRC both in the transcriptional and protein expressions.

Correlation of FRAS1/FREM expression with clinical phenotypes in KIRC

Sanguini diagram was built to show the relevance of FRAS1/FREM expression levels and corresponding clinical information such as pathological stage, grade and prognosis. Notably, we found a significant correlation between them, as KIRC progressed, the low expression levels of FRAS1, FREM1, FREM2 were associated with the advanced pathological stage, the advanced pathological grade and poor prognosis (Figures 4A,E,I). Next, we verified this tendency by Kruskal–Wallis test and Wilcoxon test. The low expression level of FRAS1 gene was significantly correlated with advanced clinical stage ($p = 7.1E-10$, Figure 4C), high pathological grade ($p = 1.2E-10$, Figure 4D) and tumor metastasis status ($p = 0.016$, Figure 4E). The low expression level of FREM1 gene was significantly correlated with advanced clinical stage ($p = 4.1E-65$, Figure 4F), high pathological grade ($p = 4.6E-66$, Figure 4G) and tumor metastasis status ($p = 0.00066$, Figure 4H). The low expression level of FREM2 gene was also significantly correlated with advanced pathological stage (p = 2E-17, Figure 4J), high pathological grade ($p = 2.1E-20$, Figure 4K) and tumor metastasis status ($p = 5.9E-06$, Figure 4L).

Furthermore, we validated the association of FRAS1/FREM mRNA expression levels and pathological stage using GSE53757 (43 Stage I + II vs. 29 Stage III + IV) and GSE73731 (Wei et al., 2017) (52 Stage I + II vs. 71 Stage III + IV). We found that the low expression levels of FRAS1 ($p = 0.048$), FREM1 ($p = 8.2E-05$),

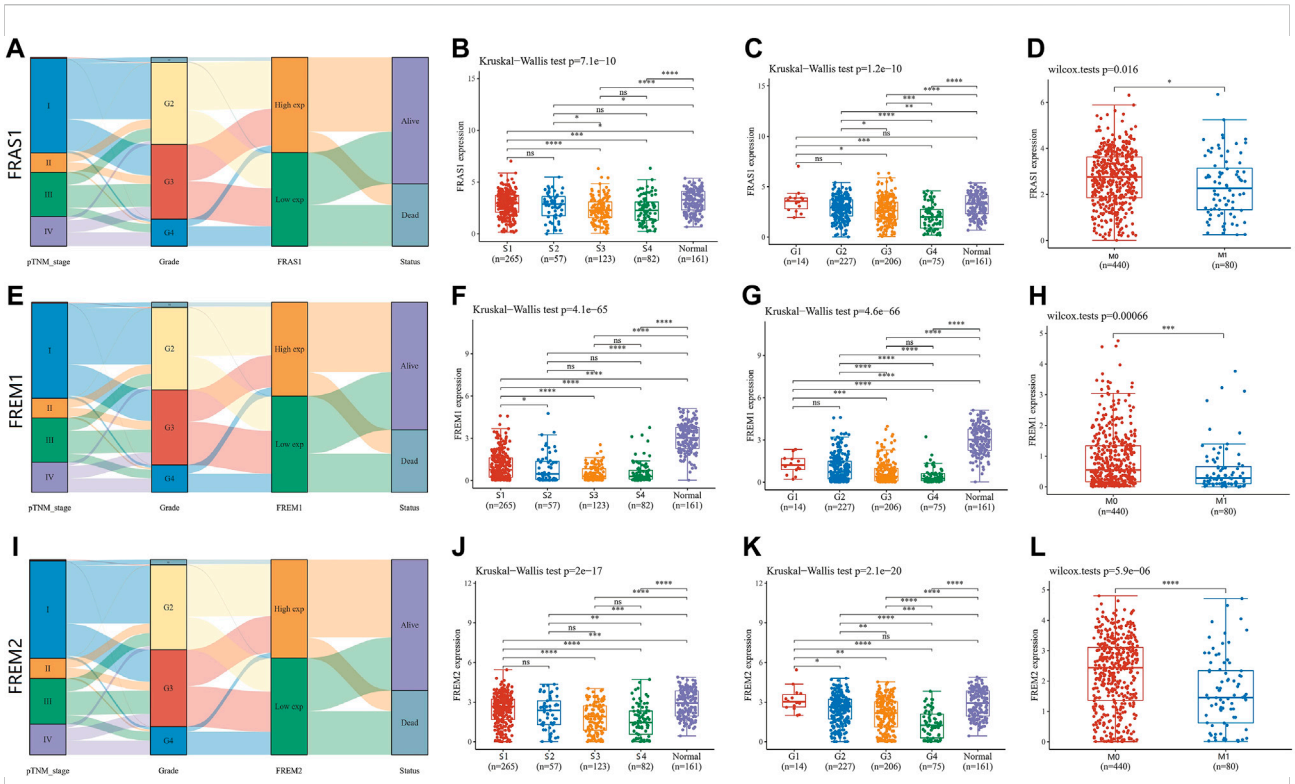

FIGURE 4
Correlation of FRAS1/FREM mRNA expression with clinicopathological parameters (such as pathological stage, grade, tumor metastasis status and prognosis) in KIRC with datesets from TCGA datebase (*$p < 0.05$, **$p < 0.01$, ***$p < 0.001$, ****$p < 0.0001$). **(A)**Sanguini diagram of the relevance of FRAS1 and corresponding clinical information. **(B)** The relevance of FRAS1 and pathological stage. **(C)** The relevance of FRAS1 and pathological grade. **(D)** The relevance of FRAS1 and tumor metastasis status. **(E)** Sanguini diagram of the relevance of FREM1 and corresponding clinical information. **(F)** The relevance of FREM1 and pathological stage. **(G)** The relevance of FREM1 and pathological grade. **(H)** The relevance of FREM1 and tumor metastasis status. **(I)** Sanguini diagram of the relevance of FREM2 and corresponding clinical information. **(J)** The relevance of FREM2 and pathological stage. **(K)** The relevance of FREM2 and pathological grade. **(L)** The relevance of FREM2 and tumor metastasis status.

and FREM2 (p = 0.016) mRNA expression levels were significantly correlated with advanced pathological stage (Figure 5A). Then, we validated the association of FRAS1/FREM expression levels and pathological grade using GSE40435 (69 Grade I + II vs. 32 Grade III + IV) and GSE73731 (112 Grade I + II vs. 144 Grade III + IV). We also found that the low expression levels of FRAS1 (p = 0.00082), FREM1 (p = 1.4E-05), and FREM2 (p = 0.003) mRNA expression levels were significantly correlated with advanced pathological grade (Figure 5B). The low expression levels of FRAS1, FREM1 and FREM2 proteins were also correlated with advanced pathological stage and pathological grade by CPTAC, due to the limited sample size (Figure 5C,D). These data above indicated that FRAS1, FREM1 and FREM2 played significant roles in the progression of KIRC.

Notably, we used datasets GSE105261 (9 primary KIRC vs. 26 matestasis of KIRC) and GSE22541 (24 primary KIRC vs. 24 matestasis of KIRC) from GEO database to study whether FRAS1/FREM could be tumor metastasis markers. As shown in Figure 6A, the mRNA expression levels of FRAS1 and FREM2 were also significantly downregulated in the matestasis of KIRC tissues included compared to matched normal tissues ($p < 0.05$). What's more, the expression level of FRAS1 was significantly correlated with the number of pulmonary matastases (Figure 6B). Interesting that FRAS1 and FREM2 expression decreased in 23 stage I and stage II patients who developed metastasis within 5 years of nephrectomy, compared to 21 patients who remained disease free ($p < 0.05$, Figure 6C).

Correlation of FRAS1/FREM expression with patient prognosis in KIRC

To further evaluate the value of FRAS1/FREM in predicting the prognosis of KIRC cancer patients, the association between FRAS1, FREM1 and FREM2 expression and overall survival (OS), disease-specific survival (DSS) and progression-free survival (PFS) was analyzed using TCGA. Elevated FRAS1 expression was significantly related to a better

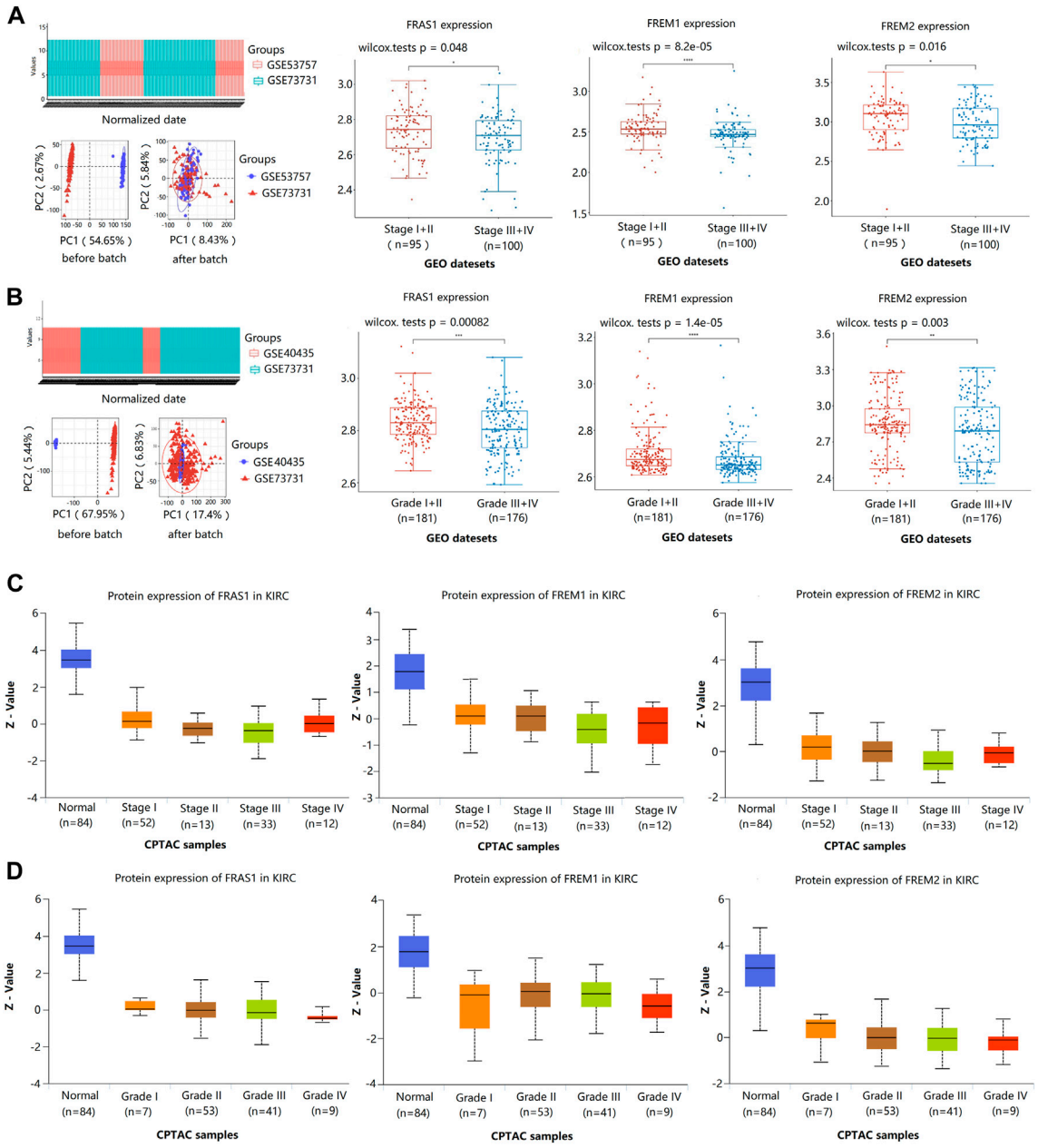

FIGURE 5
Correlation of FRAS1/FREM mRNA expression with clinical phenotypes in KIRC with datesets from GEO and CPTAC datebase. **(A)** Correlation of FRAS1/FREM mRNA expression with pathological stage in KIRC with datesets from GEO datebase (GSE53757 and GSE73731) (*$p < 0.05$, ****$p < 0.0001$). **(B)** Correlation of FRAS1/FREM expression with pathological grade in KIRC with datesets from GEO datebase (GSE40435 and GSE73731) (*$p < 0.05$, ****$p < 0.0001$). **(C)** Correlation of FRAS1/FREM protein expression with pathological stage in KIRC with datesets from CPTAC datebase. **(D)** Correlation of FRAS1/FREM protein expression with pathological grade in KIRC with datesets from CPTAC datebase.

OS (HR = 0.513, 95% CI = 0.376–0.701, p = 2.82E-05), DSS (HR = 0.48, 95% CI = 0.322–0.716, p = 0.000325) and PFS (HR = 0.577, 95% CI = 0.418–0.795, p = 0.000762) in KIRC. Similarly, high expression of FREM1 was significantly associated with a better OS (HR = 0.586, 95% CI = 0.432–0.794, p = 0.000566), DSS (HR = 0.393, 95% CI = 0.262–0.591, p = 6.94E-06) and PFS (HR = 0.484, 95% CI = 0.35–0.67, p = 1.23E-05) in KIRC. High expression of FREM2 was also significantly associated with a better OS (HR = 0.458, 95% CI = 0.334–0.628, p = 1.16E-06), DSS

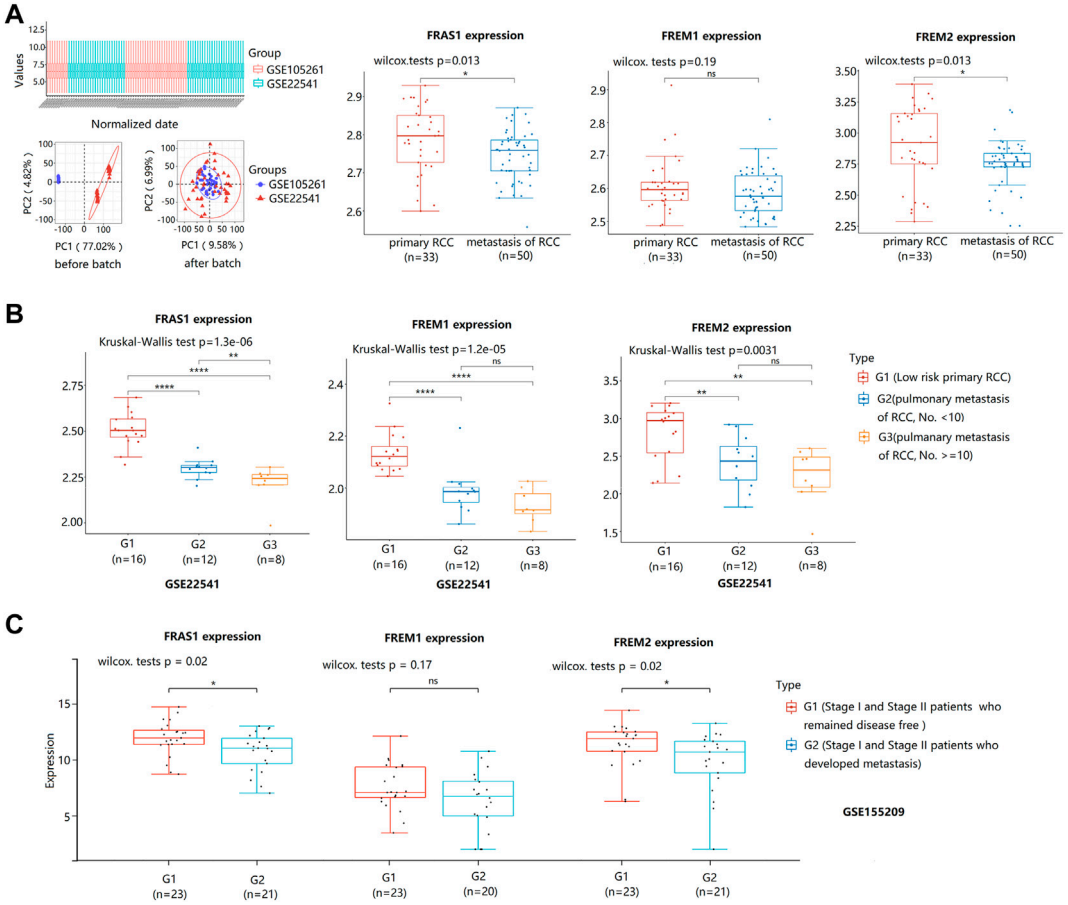

FIGURE 6
FRAS1/FREM mRNA expression between primary KIRC and matestasis of KIRC with datesets from GEO datebase. **(A)**FRAS1/FREM mRNA expression between primary KIRC and matestasis of KIRC with datesets from GEO datebase (GSE105261 and GSE22541) (*p < 0.05, ns, not statistically significant). **(B)** FRAS1/FREM mRNA expression in three groups: The low matestasis risk primary RCC (n = 16), pulmonary metastasis of KIRC, the number of matastases <10 (n = 12), pulmonary metastasis of KIRC, the number of matastases > = 10 (n = 8) in KIRC from GSE22541. (**p < 0.01, ****p < 0.0001). **(C)** FRAS1/FREM mRNA expression between stage I and stage II patients who developed metastasis within 5 years of nephrectomy and patients who remained disease free (*p < 0.05, ns, not statistically significant).

(HR = 0.241, 95% CI = 0.152–0.382, p = 1.42E-09) and PFS (HR = 0.336, 95% CI = 0.238–0.474, p = 5.1E-10) in KIRC. The survival curves were displayed as Figure 7A.

As above, pathological stage and grade were assiociated with FRAS1/FREM expression levels and were also highly associated with prognosis. As shown in Figure 7B, multivariate Cox proportional-hazards regression adjusted for clinical parameters (age, gender, race, TNM stage and grade) still suggested that FRAS1 expression was an independent risk factor for better prognosis (OS: HR = 0.83746, 95% CI = 0.73762–0.95082, p = 0.00617; DSS: HR = 0.82321, 95% CI = 0.69615–0.97346, p = 0.02294; PFS: HR = 0.88171, 95% CI = 0.77386–1.0046, p = 0.05861). FREM2 expression was also an independent risk factor for better prognosis (OS: HR = 0.79093, 95% CI = 0.68556–0.9125, p = 0.0013; DSS: HR = 0.69109, 95% CI = 0.57167–0.83547; PFS: HR = 0.7908, 95% CI = 0.68308–0.91551, p = 0.00168).

Correlation of FRAS1/FREM expression with immune infiltrating levels in KIRC

Mismatch repair (MMR), microsatellite instability (MSI) and tumor mutation burden (TMB) are responsible for tumor initiation and regard as independent predictors of immune checkpoint blockade efficacy (Baretti and Le, 2018; Jardim et al., 2021). Here we examined the correlation between FRAS1/FREM expression and several essential MMR signatures. As shown in Supplementary Figure S3A, FRAS1 expression was positively correlated with MutL homolog 1 (MLH1), MutS homolog 2 (MSH2), MutS

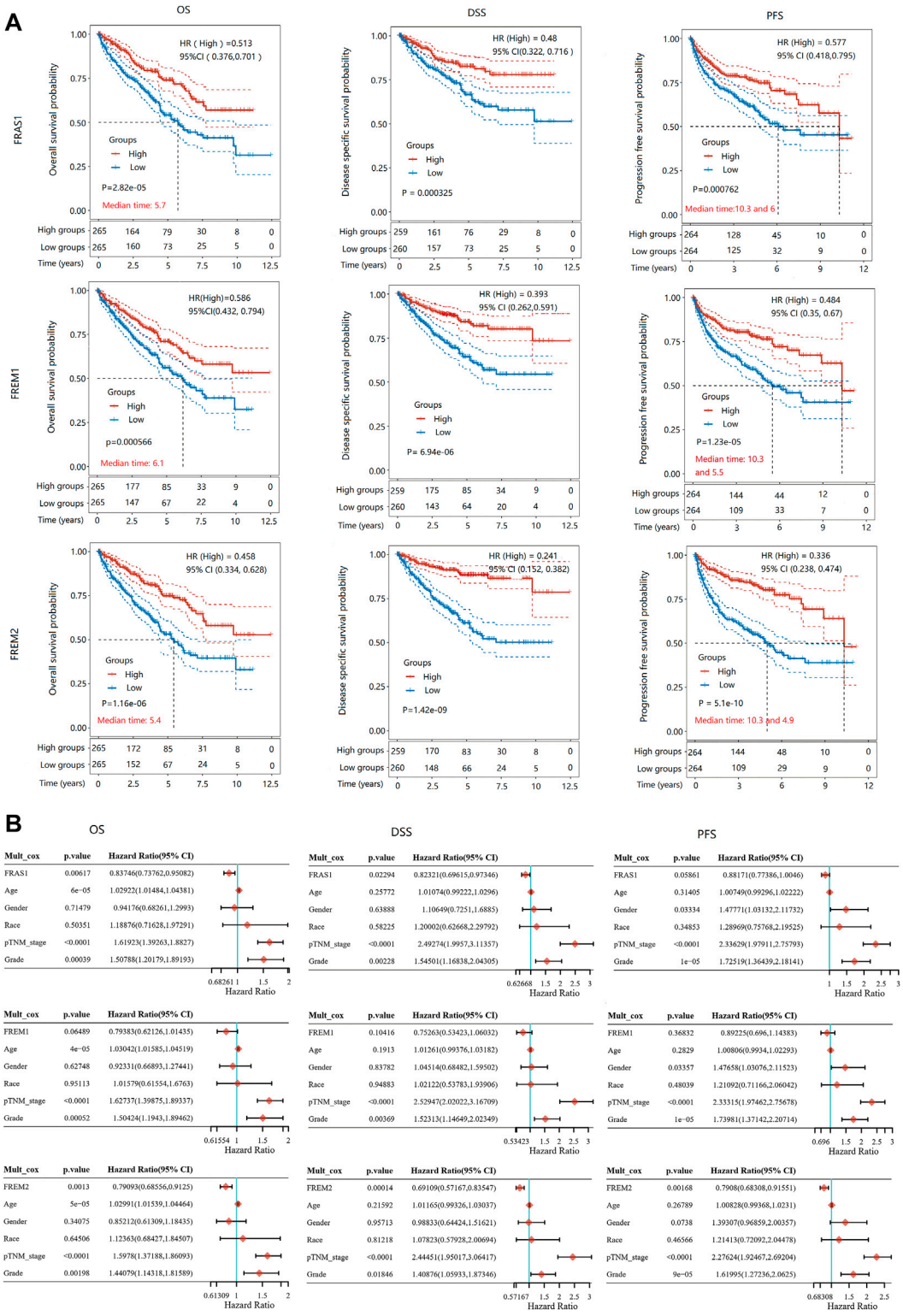

FIGURE 7
The prognostic value of mRNA level of FRAS1/FREM family members in KIRC patients. **(A)** Survival curves comparing the high and low expression of FRAS1, FREM1 and FREM2. (Kaplan-Meier survival analysis). **(B)** Hazard ratio and *p* value of constituents involved in multivariate Cox regression adjusted for clinical parameters (age, gender, race, TNM stage and grade).

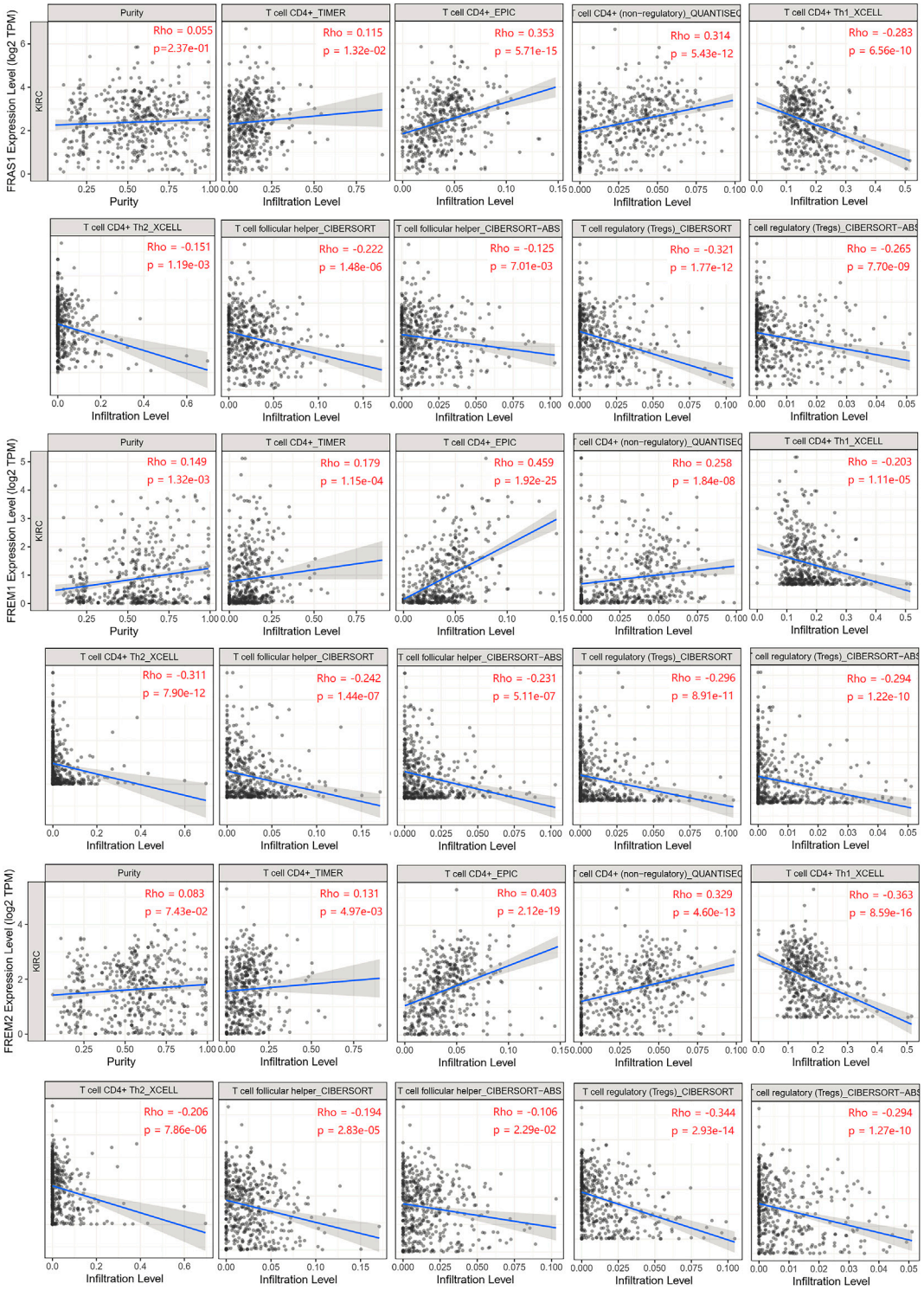

FIGURE 8
Relationship between FRAS1/FREM expression and CD4$^+$ T cells, its corresponding subsets (Th1, Th2, Tfh, and Tregs) in KIRC.

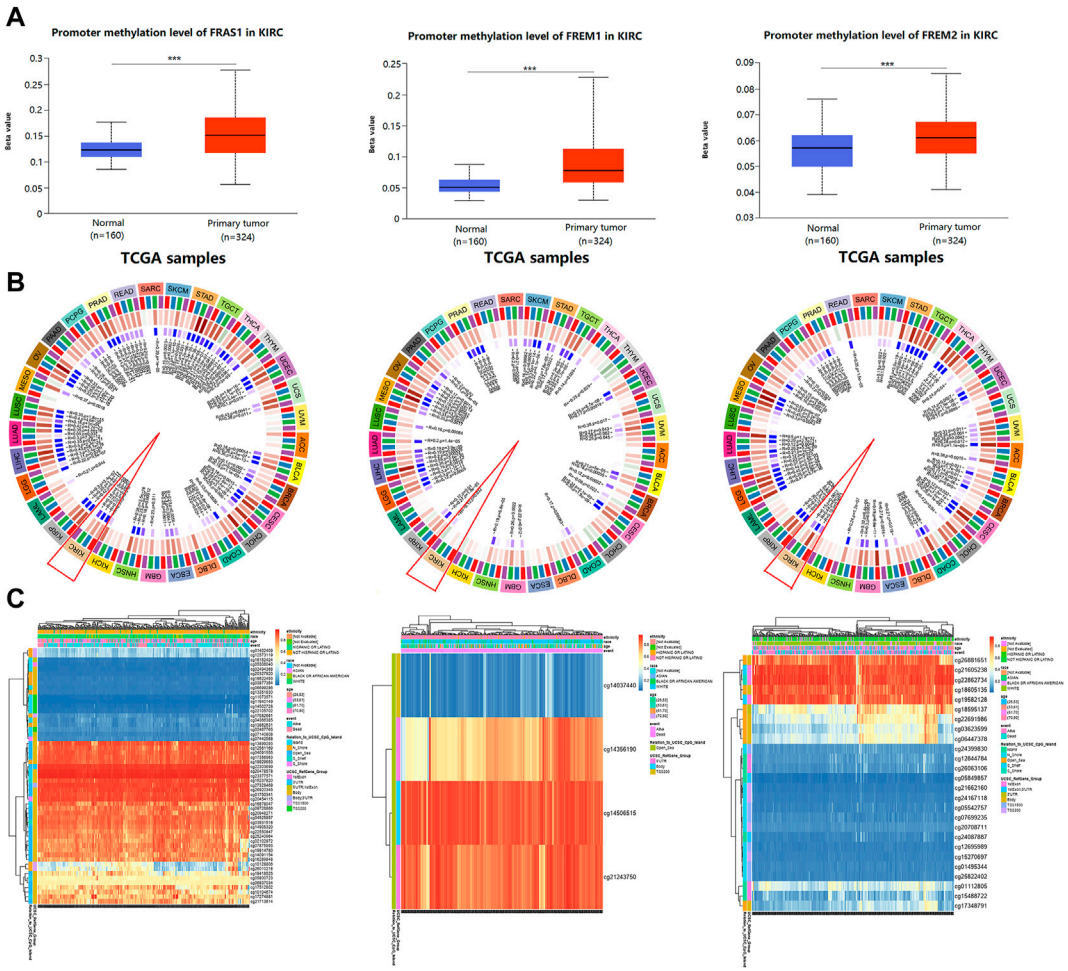

FIGURE 9
The correlation between FRAS/FREM expression and DNA methylation. **(A)** The promoter methylation levels of FRAS1, FREM1 and FREM2 in KIRC tissues vs. normal tissues. **(B)** The correlations between FRAS1, FREM1, FREM2 expression and three DNA methyltransferases (DNMT1, DNMT2 and DNMT3A). **(C)** The heat map of DNA methylation of FRAS1, FREM1, FREM2 in KIRC.

homolog 6 (MSH6) and PMS1 homolog 2 (PMS2) in KIRC. FREM1 expression was positively correlated with MLH1, PMS2 and epithelial cell adhesion molecule (EpCAM) in KIRC (Supplementary Figure S3B). FREM2 expression was positively correlated with MLH1, MSH2, MSH6, PMS2 and EpCAM in KIRC (Supplementary Figure S3C). In addition, as shown in Supplementary Figure S4, FRAS1 and FREM2 expression were positively correlated with MSI (p = 6E-04 and p = 0.024, respectively), while FREM1 expression was negatively correlated with TMB (p = 2E-05) in KIRC.

To explore whether FRAS1, FREM1 and FREM2 were involved in the process of immune infiltration in KIRC, we employed TIMER 2.0 to exhibit the landscape of FRAS1/FREM correlating with tumor purity and various immune infiltrates in human cancers. As Supplementary Figure S5 indicated, the expression levels of FRAS1, FREM1 and FREM2 were positively correlated with immune infiltrating levels of multiple infiltrates including $CD4^+$ T cells ($p < 0.05$) and macrophages ($p < 0.05$). Th1, Th2, induced or natural regulatory T cells (iTregs and nTregs), and Tfh (T cell follicular helper) cells are the main $CD4^+$ T cell subsets (Oh and Fong, 2021). Herein, we used the TIMER, CIBERSORT, CIBERSORT-ABS, QUANTISEQ, XCELL, MCPCOUNTER and EPIC algorithms to investigate the potential relationship between the infiltration level of $CD4^+$ T cells subsets and FRAS1/FREM gene expression in KIRC. The FRAS1 expression level in KIRC is positively correlated with the infiltration level of $CD4^+$ T cells and negatively correlated with the infiltration level of Th1, Tfh and Tregs. Likewise, the same trend goes as FREM1 and FREM2 unfolds (Figure 8).

TABLE 2 The prognostic value of single CpG of FRAS1 and FREM2 in KIRC by MethSurv ($p < 0.05$).

Gene	Relation to island	Genomic region	CpG site	Best_split	HR	CI	LR test *p* value
FRAS1							
	Open_Sea	Body	cg20948271	q25	0.41	(0.276; 0.611)	2.95E-05
	Open_Sea	Body	cg17512,802	mean	2.544	(1.65; 3.922)	7.49E-06
	Island	Body	cg02494368	mean	0.441	(0.286; 0.681)	0.000104156
	Open_Sea	Body	cg14091154	q25	0.47	(0.314; 0.704)	0.000486185
	Open_Sea	Body	cg04091555	q25	0.51	(0.341; 0.764)	0.001728597
	N_Shore	Body	cg03877364	median	1.856	(1.253; 2.75)	0.001735773
	Island	TSS200	cg11073571	q75	0.423	(0.244; 0.733)	0.000734126
	Island	TSS200	cg11940149	q75	0.428	(0.247; 0.741)	0.000872463
	Island	Body	cg16678047	q25	2.328	(1.341; 4.041)	0.000980456
	Island	Body	cg04366385	q75	0.435	(0.251; 0.752)	0.001079704
FREM2							
	Open_Sea	Body	cg26881651	mean	0.489	(0.333; 0.719)	0.000342
	Open_Sea	3′UTR	cg18595137	q25	2.426	(1.38; 4.265)	0.000642
	N_Shore	TSS1500	cg05542757	q75	1.877	(1.257; 2.804)	0.003037
	Island	1stExon	cg12844784	q25	2.383	(1.306; 4.348)	0.001604
	Open_Sea	Body	cg03623599	q25	1.926	(1.171; 3.17)	0.00591
	N_Shore	TSS200	cg21662160	q75	1.607	(1.067; 2.419)	0.02758
	Island	1stExon	cg26063106	q75	1.597	(1.063; 2.398)	0.028575
	N_Shore	TSS1500	cg25822402	q75	0.575	(0.352; 0.941)	0.020161
	S_Shelf	1stExon	cg19582,128	mean	0.647	(0.436; 0.96)	0.034219
	Island	1stExon; 5′UTR	cg24087887	q25	1.668	(1.024; 2.715)	0.030612

Abbreviations: KIRC, kidney renal clear cell carcinoma; HR, hazard ratio; LR, test, likelihoodratio test.

Correlation between FRAS1/FREM expression and DNA methylation

DNA methylation has been recognized as an important biological process of tumorigenesis and cancer development (Koch et al., 2018). We calculated the levels of correlation between FRAS1/FREM gene expression and their promoter methylation using UALCAN. As Figure 9A indicated, the promoter methylation levels of FRAS1, FREM1 and FREM2 were significantly higher in KIRC than normal tissues ($p < 0.001$). Moreover, there were positive correlations between FRAS1/FREM2 expression and three DNA methyltransferases (DNMT1, DNMT2 and DNMT3A) (Figure 9B). The heat map of DNA methylation results of FRAS1, FREM1 and FREM2 in KIRC via the MethSurv platform were displayed in Figure 9C. Further, we conducted Kaplan-Meier survival analysis based on CpG methylation patterns to explore the prognostic value of single CpG methylation of FRAS1 and FREM2. We found that single CpG methylation levels of FRAS1 and FREM2 were associated with prognosis in KIRC. Among them, the top ten significant prognostic values of FRAS1 and FREM2 single CpG methylation were displayed in Supplementary Figure S6 and summarized in Table 2.

Function enrichment of FRAS1/FREM in KIRC

Finally, to further investigate the molecular mechanism of the FRAS1, FREM1 and FREM2 in tumorigenesis, we filtered out the known FRAS1/FREM-interacting proteins and the FRAS1/FREM expression correlated genes for a series of pathway enrichment analyses. PPI network analysis of FRAS1/FREM family members and their 20 related genes was conducted by GeneMANIA (Figure 10A). In addition, using the STRING tool, we acquired a total of eight, experimentally detected FRAS1/FREM-binding proteins. Figure 10B shows the interaction network of these 11 proteins.

To investigate the biological significance of FRAS1, FREM1 and FREM2 expression in KIRC, we conducted GESA. The top 20 items of GO functional annotation (BP: biological process, MF: molecular function), the Kyoto Encyclopedia of Genes and Genomes (KEGG) and Hallmark were shown in Supplementary Figure S7; Figure 10C. The results of BP revealed that FRAS1, FREM1 and FREM2 were mainly enriched in regulation of mRNA, protein stabilization, transport, catabolic and methylation (Supplementary Figure S7A). The results of MF revealed that FRAS1, FREM1 and FREM2 were mainly enriched in regulation of expression, transport activity

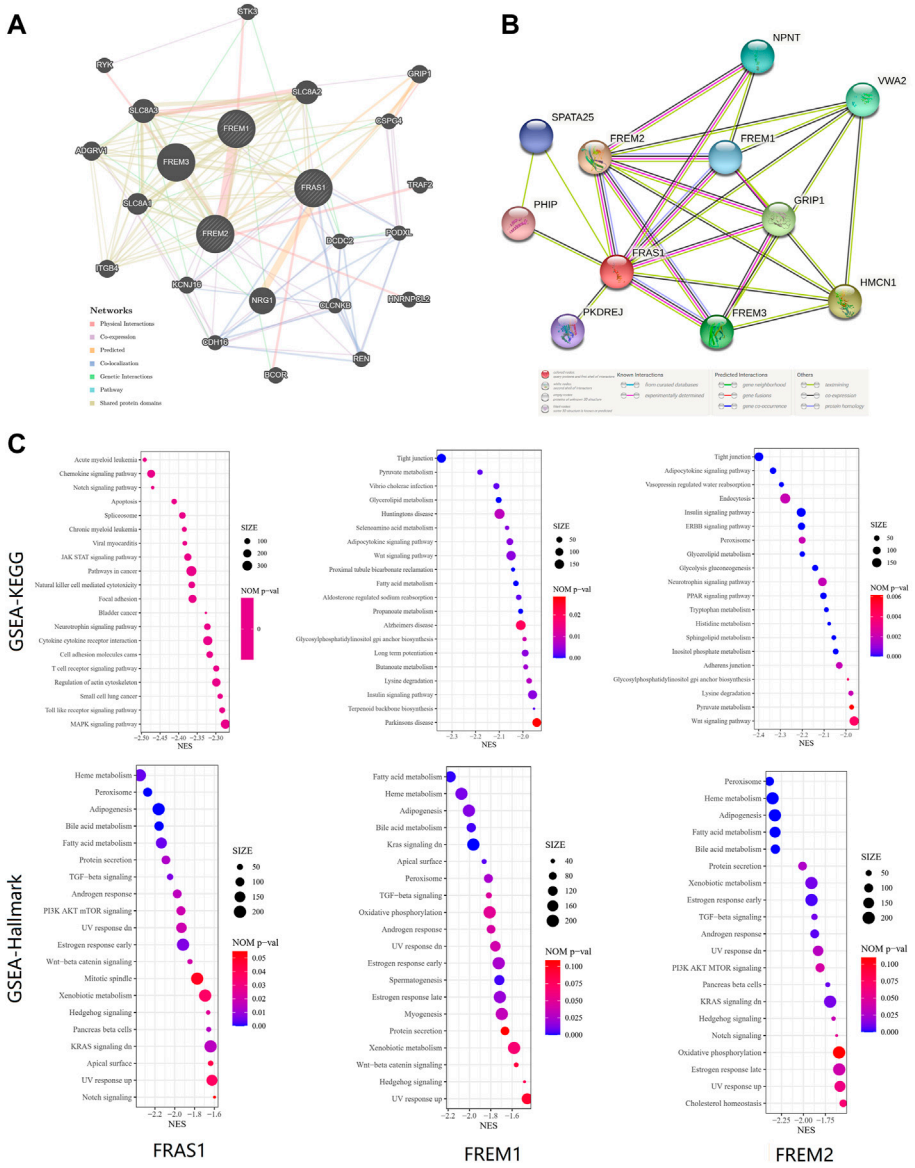

FIGURE 10
FRAS1/FREM-related gene enrichment, pathway analysis and function profiles. **(A)**PPI network analysis of FRAS1/FREM family members and their 20 co-regulated hub genes conducted by GeneMANIA. **(B)** STRING protein network map of experimentally determined FRAS1/FREM-binding proteins. **(C)** Significant gene set enrichment analysis (GSEA) results of FRAS1, FREM1 and FREM2 including KEGG pathways and Hallmark pathways.

and specific epigenetic modification enzymatic activities (Supplementary Figure S7B). The results of KEGG and Hallmark revealed that FRAS1, FREM1 and FREM2 were mainly enriched in several signalling pathways (TGF-beta signaling, PI3K AKT mTOR signaling, Wnt-beta catenin signaling, Kras signaling, Hedgehog signaling and Notch signaling) and metabolic pathways (Heme metabolism, Fatty acid metabolism, Bile acid metabolism, Xenobiotic metabolism) (Figure 10C).

Relationship between FRAS1/FREM expression and drug sensitivity

Genetic alterations affect the drug sensitivity of cancer to clinical treatment and therefore are potential biomarkers for drug screening (Kim and Cho, 2022; Li et al., 2022). Therefore, we question the association between mRNA expression levels of FRAS1, FREM1 and FREM2 and patient sensitivity to four common targeted therapeutic

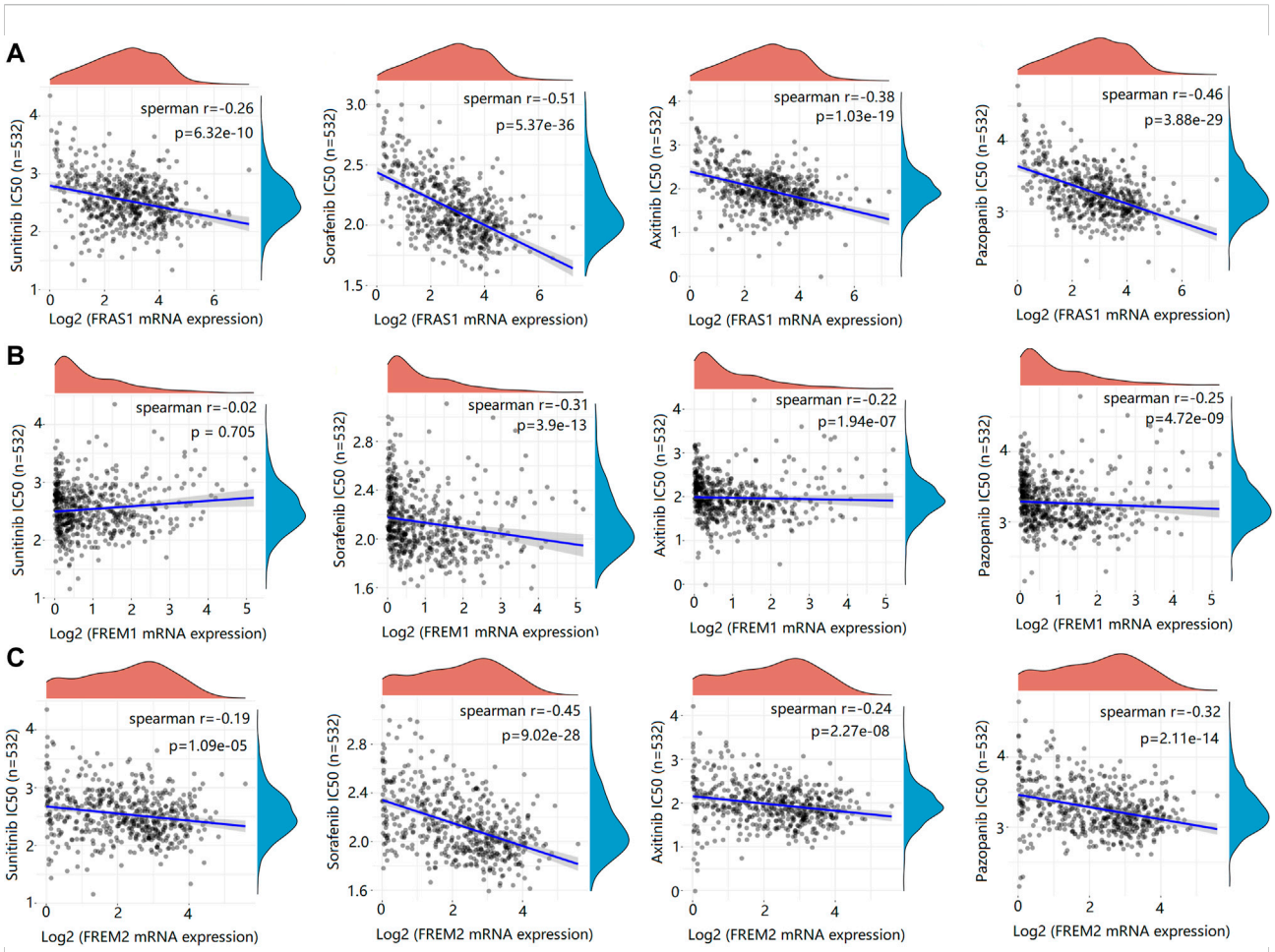

FIGURE 11
Drug sensitivity analysis of IC50 score and FRAS1/FREM expression. **(A)** Spearman correlation analysis of IC50 score and FRAS1 expression including four common targeted therapeutic drugs (sunitinib, sorafenib, axitinib and pazopanib) in KIRC. **(B)** Spearman correlation analysis of IC50 score and FREM1 expression. **(C)** Spearman correlation analysis of IC50 score and FREM2 expression.

drugs (sunitinib, sorafenib, axitinib and pazopanib). Based on the GDSC database, we performed a correlation analysis between gene expression level and drug sensitivity of the above four drugs in KIRC. We found that the IC50s of sunitinib (r = −0.26, p = 6.32e-10), sorafenib (r = −0.51, p = 5.37e-36), axitinib (r = −0.38, p = 1.03e-19) and pazopanib (r = −0.46, p = 3.88e-29) were significantly negatively correlated with FRAS1 expression (Figures 10A–D). Similarly, the IC50s of sunitinib (r = −0.19, p = 1.09e-05), sorafenib (r = −0.45, p = 9.02e-28), axitinib (r = −0.24, p = 2.27e-08) and pazopanib (r = −0.32, p = 2.11e-14) were also significantly negatively correlated with FRAS1 expression (Figures 11A–D). These results indicated that the expression level of FRAS1 and FREM2 interact with the sensitivity of targeted therapeutic drugs.

Discussion

As one of the major components of TME, the ECM plays multiple crucial roles during tumorigenesis. The dysregulation of ECM is a remarkable feature of cancer. Growing studies have shown that ECM-related proteins may modulate the migration and invasion of cancer cells through related signaling pathways (Huang et al., 2021; Romani et al., 2021). More importantly, the deposition, reconstruction, and cross-linking of ECM can reprogram the local microenvironment and regulate the pro- and antitumor immune responses upon the stimulation of different ECM-related proteins, leading to aberrant mechanotransduction and further malignant transformation (Koliaraki et al., 2020; Nazemi and Rainero, 2020; Huang et al., 2021). As a special type of ECM, BM also presents the major barrier cancer cells have to overcome multiple times to form

metastases (Stuelten et al., 2018; Reuten et al., 2021). Therefore, a comprehensive understanding of the dysregulation of the BM in the TME would contribute to the discovery of promising therapeutic targets for cancer treatment.

FRAS1, comprising 4,010 amino acids, is encoded by the FRAS1 gene located at the chromosome 4q21.21. FREM1 comprises 2,197 residues and resides on chromosome 9p22.3. In between, FREM2 consists of 3,160 amino acids and is encoded by the FREM2 gene located at the chromosome 13q13.3. FRAS1 and FREM2 are produced by epithelial cells as membrane proteins, while FREM1 is produced by mesenchymal cells as a secreted protein (Kiyozumi et al., 2012). These three proteins meet together at BM and form an independent ternary complex, supposedly having a similar function to collagen VII. FRAS1/FREM share common polypeptide repetitive motifs with possible interactive and organizing functions, and contribute to embryonic epithelial–mesenchymal integrity (Pavlakis et al., 2011; Kiyozumi et al., 2012).

FRAS1/FREM family are involved in the progression of several cancers. Zhan et al. (2014) reported that FRAS1 knockdown reduced non-small cell lung cancer A549 cells migration and invasion ability and Umeda et al. (2020) reported that knockout of FRAS1 inhibited liver metastasis of gastric cancer. The analysis of a xenograft model of human endometrial cancer found that FRAS1 might also serve as a potential diagnostic marker (Xu et al., 2012). FREM1 was reported to be associated with the favorable prognosis of breast carcinoma patients and negatively correlated with tumor stages in KIRC, while FREM2 was reported to be associated with favorable prognosis of patients with isocitrate dehydrogenase (IDH)- wild-type glioblastoma (Jovcevska et al., 2019; Li H. N. et al., 2020; Luo et al., 2020). Additionally, the polymorphism of FRAS1 was involved in various malignancies. For example, miR-1 targeting FRAS1 was downregulated in sunitinib resistance renal cancer cell (Butz et al., 2018). The rs1910301, the promoter region of FRAS1, was found to be a candidate SNP associated with lethal prostate cancer (Wang et al., 2021). The rs150303591, the nearby genomic loci of FRAS1 was also involved in drug resistance of ovarian cancer to carboplatin (Fridley et al., 2016). Yet, none of them in KIRC has been systematically studied.

Our study revealed that the mRNA and protein expression levels of FRAS1/FREM1 were significantly downregulated in KIRC tissues than in normal tissues. Besides, FRAS1, FREM1 and FREM2 mRNA and protein expressions were correlated with the clinicopathological characteristics (pathological stage, grade and tumor metastasis status) of the patients with KIRC. The expression levels of FRAS1 and FREM2 were low in the matestasis of KIRC tissues and might be associated with the number of pulmonary matastases. Interestingly, FRAS1 and FREM2 expression decreased in the stage I and stage II patients who had a high *propensity* to metastasise, which means FRAS1 and FREM2 could be tumor metastasis markers of KIRC. In addition, we report that FRAS1/FREM expression correlated with the prognosis of KIRC. Elevated FRAS1, FREM1 and FREM2 expression levels were found to be significantly related to a better OS, DSS and PFS in KIRC. Multivariate Cox proportional-hazards regression adjusted for clinical parameters (age, gender, race, TNM stage and grade) still suggested that FRAS1 and FREM2 could be independent risk factors for better prognosis. Thus, these results above indicated that FRAS1 and FREM2 might be used as potential biomarkers of diagnosis and prognosis in KIRC.

TMB is a potential pan-cancer predictive biomarker of immune checkpoint inhibitor response in most cancers (Jardim et al., 2021). MSI and MMR deficiency could also serve as an potential biomarker and predict the efficacy of immune-checkpoint inhibitors (ICI) (Baretti and Le, 2018). Our results show that FRAS1/FREM expression were positively correlated with essential MMR signatures in KIRC. In addation, FRAS1 and FREM2 expression were positively correlated with high MSI in KIRC, while FREM1 expression was negatively correlated with low TMB in KIRC. However, the correlation coefficients between FRAS1/FREM and TMB, as well as MSI, were below 0.5, suggesting that they were not sufficient to independently predict the patient's response to immune checkpoint blockade efficacy.

Tumor immune infiltrating cells migrate from blood to tumor tissues and can antagonize or promote tumor occurrence and development. Cancer immunotherapy activates the immune system to specifically target malignant cells (Garner and de Visser, 2020). Previous research has often focused on $CD8^+$ cytotoxic T cells, however, $CD4^+$ T cells have gained attention in the field, as they are not only essential to promote help to $CD8^+$ T cells, but are also able to kill tumor cells. Therefore, immunotherapy approaches have shifted from only stimulating $CD8^+$ T cells to targeting and assessing $CD4^+$ subsets and increasing numbers of clinical studies have demonstrated that targeting $CD4^+$ T cells is safe and effective (Li T. et al., 2020; Cachot et al., 2021; Oh and Fong, 2021). Our study revealed that the FRAS1/FREM genes expression levels in KIRC were positively correlated with the infiltration level of $CD4^+$ T cells and negatively correlated with the infiltration level of $CD4^+$ T cell subsets (such as Th1, Tfh and Tregs). $CD4^+$ T cells are now recognized as essential and pleiotropic effectors in the antitumor immune response, while various $CD4^+$ T cell subsets play an antagonistic role in the antitumor immune response. Thus FRAS1/FREM might play an important part in recruitment and regulation of immune infiltrating cells, especially $CD4^+$ T cells and its corresponding subsets (Th1, Th2, Tfh and Tregs) and macrophages. It will be interesting to investigate whether FRAS1/FREM might serve as new targets for the development of various cancer immunotherapies.

Another main finding of our study is that multiple factors such as genetic changes, epigenetic regulation, transcriptional regulation and translation regulation can synergistically be the potential mechanisms through which FRAS1/FREM exerts antitumor effects. As an a central epigenetic modification of the human genome, the changes of DNA methylation in cancer have been heralded as promising targets for the development of powerful diagnostic, prognostic, and predictive biomarkers (Dor and

Cedar, 2018; Koch et al., 2018; Pan et al., 2021). Our study explored the relationship between FRAS1, FREM1 and FREM2 promoter methylation and cancer for the first time. We found that FRAS1 and FREM2 gene expression levels were significantly correlated with DNA promoter methylation and three DNA methyltransferases (DNMT1, DNMT2 and DNMT3A). This may partially explain the differential mRNA expression of FRAS1/FREM between tumor tissues and normal tissues, while the somatic mutation rates of them in KIRC were low. More importantly, the correlations of FRAS1 and FREM2 single CpG methylation levels with clinical prognosis revealed that they could serve as biomarkers of prognosis in patients with KIRC. Consistent with the conclusion stated above, the results of BP and MF by GSEA also revealed that FRAS1, FREM1 and FREM2 were mainly enriched in the process of transcriptional regulation, post-transcriptional regulation, and regulation of specific epigenetic modification enzymatic activities.

The oncogenic developmental signalling pathways such as the Notch, WNT, Hedgehog and Hippo are crucial for the development Cancer stem cells (CSC), which have important roles in tumour development, relapse and metastasis. As such, therapeutics targeting the above pathways are prime targets for anti-CSC therapy—with some success in certain tumors (Saygin et al., 2019; Clara et al., 2020). The crosstalk between the above pathways and other tumorigenic pathways (e.g., NF-κB, KRAS–RAF–MAPK and PI3K–AKT–mTOR) have also hinted at their profoundly complex roles in cancer (Pelullo et al., 2019; Clara et al., 2020). Moreover, the tumor microenvironment and the ECM can regulate cell metabolism, such as glucose metabolism and lipid synthesis (Nazemi and Rainero, 2020; Romani et al., 2021). Indeed, aberrant activation of PI3K/AKT and Ras signaling pathways can facilitate constant glucose uptake, mTOR can also induce anabolic processes such as protein, nucleotide, and lipid biosynthesis (Nazemi and Rainero, 2020). Our results of KEGG and Hallmark by GSEA revealed that FRAS1, FREM1 and FREM2 can potentially impact cancer etiology or pathogenesis by functioning in oncogenic signalling pathways (TGF-β signaling, PI3K AKT mTOR signaling, Wnt-β catenin signaling, Kras signaling, Hedgehog signaling and Notch signaling) and metabolic pathways (Heme metabolism, Fatty acid metabolism, Bile acid metabolism, Xenobiotic metabolism). It will be very interesting to find the potential targets that are involved in these signaling and potentially interact with FRAS1/FREM in future studies. A better understanding of the interplay between FRAS1/FREM and the tumor microenvironment might be the key to unlock a new era of oncological treatments and proposes new therapeutic targets for KIRC.

Through drug sensitivity analysis, we found that high FRAS1 and FREM2 expression were negatively correlated with IC50 values of four common targeted therapeutic drugs (sunitinib, sorafenib, axitinib and pazopanib) which indicated that the measurement of FRAS1 and FREM2 expression level can be a reliable predictor of targeted therapeutic drug response, highlighting the potential as an anticancer drug target. These results will help us better understand how the ECM protein in TME can benefit cancer treatment, and guide the drug selection in patients with multiline treatment resistance.

However, there are limitations to our study. First, while bioinformatics has the advantages of large sample size, simplicity and low cost, the biases caused by the confounders might exist. Second, our analyses are mainly based on TCGA database and some results are further validated by GEO database, CPTAC database and RT-PCR results. Even so, further experiments *in vivo* and *in vitro* should be still needed. Third, although a serious of function annotations and enrichment analysis were investigated in our study, the detailed molecular biological mechanisms of FRAS1/FREM in KIRC need to be further validated.

In summary, our first pan-cancer analyses indicated that the FRAS1/FREM genes and proteins were differentially expressed between tumor and normal tissues. Moreover, elevated FRAS1/FREM expression levels were significantly correlated with cancer progression (pathological stage, pathological grade and tumor metastasis status), poor survival (OS, DSS and PFS), immune infiltrations (MMR, TMB, MSI and $CD4^+$ T cells subsets) and DNA methylation in KIRC patients, sharing the potential as efficient markers of the prognostic value of KIRC and potential targets in the development of anti-KIRC therapeutics.

Data availability statement

The original contributions presented in the study are included in the article/Supplementary Material, further inquiries can be directed to the corresponding author.

Author contributions

GW, ZW, and SZ designed the research study. GW, ZW, ZZ, SZ, LG, and FK performed the experiments, acquired data and performed database analyses. GW, HL, and SZ wrote the manuscript. GW, FK, ZZ, and AW edited the manuscript. SZ supervised the study.

Funding

This study was funded by the National Natural Science Funds of China (81670686, 81970578), and Engineering laboratory of urinary organ and functional reconstruction of Shandong Province.

Acknowledgments

Preprint statement: this manuscript has been preprinted by research square at [https://doi.org/10.21203/rs.3.rs-1733569/v1] (Wang et al., 2022). We acknowledge TCGA, GEO, HPA, GDSC and CPTAC database for providing their platforms and contributors for uploading their meaningful datasets.

Conflict of interest

The authors declare that the research was conducted in the absence of any commercial or financial relationships that could be construed as a potential conflict of interest.

Publisher's note

All claims expressed in this article are solely those of the authors and do not necessarily represent those of their affiliated organizations, or those of the publisher, the editors and the reviewers. Any product that may be evaluated in this article, or claim that may be made by its manufacturer, is not guaranteed or endorsed by the publisher.

Supplementary material

The Supplementary Material for this article can be found online at: https://www.frontiersin.org/articles/10.3389/fphar.2022.972934/full#supplementary-material.

References

Alazami, A., Shaheen, R., Alzahrani, F., Snape, K., Saggar, A., Brinkmann, B., et al. (2009). FREM1 mutations cause bifid nose, renal agenesis, and anorectal malformations syndrome. *Am. J. Hum. Genet.* 85, 414–418. doi:10.1016/j.ajhg.2009.08.010

Al-Hamed, M. H., Sayer, J. A., Alsahan, N., Tulbah, M., Kurdi, W., Ambusaidi, Q., et al. (2021). Novel loss of function variants in FRAS1 AND FREM2 underlie renal agenesis in consanguineous families. *J. Nephrol.* 34, 893–900. doi:10.1007/s40620-020-00795-0

Baretti, M., and Le, D. (2018). DNA mismatch repair in cancer. *Pharmacol. Ther.* 189, 45–62. doi:10.1016/j.pharmthera.2018.04.004

Butz, H., Ding, Q., Nofech-Mozes, R., Lichner, Z., Ni, H., and Yousef, G. (2018). Elucidating mechanisms of sunitinib resistance in renal cancer: an integrated pathological-molecular analysis. *Oncotarget* 9, 4661–4674. doi:10.18632/oncotarget.23163

Cachot, A., Bilous, M., Liu, Y., Li, X., Saillard, M., Cenerenti, M., et al. (2021). Tumor-specific cytolytic CD4 T cells mediate immunity against human cancer. *Sci. Adv.* 7, eabe3348. doi:10.1126/sciadv.abe3348

Choueiri, T., Albiges, L., Atkins, M., Bakouny, Z., Bratslavsky, G., Braun, D., et al. (2022). From basic science to clinical translation in kidney cancer: a report from the second kidney cancer research summit. *Clin. Cancer Res.* 28, 831–839. doi:10.1158/1078-0432.CCR-21-3238

Clara, J. A., Monge, C., Yang, Y., and Takebe, N. (2020). Targeting signalling pathways and the immune microenvironment of cancer stem cells - a clinical update. *Nat. Rev. Clin. Oncol.* 17, 204–232. doi:10.1038/s41571-019-0293-2

Diaz-Montero, C. M., Rini, B. I., and Finke, J. H. (2020). The immunology of renal cell carcinoma. *Nat. Rev. Nephrol.* 16, 721–735. doi:10.1038/s41581-020-0316-3

Dor, Y., and Cedar, H. (2018). Principles of DNA methylation and their implications for biology and medicine. *Lancet* 392, 777–786. doi:10.1016/S0140-6736(18)31268-6

Fridley, B., Ghosh, T., Wang, A., Raghavan, R., Dai, J., Goode, E., et al. (2016). Genome-wide study of response to platinum, taxane, and combination therapy in ovarian cancer: *In vitro* phenotypes, inherited variation, and disease recurrence. *Front. Genet.* 7, 37. doi:10.3389/fgene.2016.00037

Garner, H., and de Visser, K. E. (2020). Immune crosstalk in cancer progression and metastatic spread: a complex conversation. *Nat. Rev. Immunol.* 20, 483–497. doi:10.1038/s41577-019-0271-z

Huang, J., Zhang, L., Wan, D., Zhou, L., Zheng, S., Lin, S., et al. (2021). Extracellular matrix and its therapeutic potential for cancer treatment. *Signal Transduct. Target. Ther.* 6, 153. doi:10.1038/s41392-021-00544-0

Jadeja, S., Smyth, I., Pitera, J. E., Taylor, M. S., van Haelst, M., Bentley, E., et al. (2005). Identification of a new gene mutated in Fraser syndrome and mouse myelencephalic blebs. *Nat. Genet.* 37, 520–525. doi:10.1038/ng1549

Jardim, D., Goodman, A., de Melo Gagliato, D., and Kurzrock, R. (2021). The challenges of tumor mutational burden as an immunotherapy biomarker. *Cancer Cell* 39, 154–173. doi:10.1016/j.ccell.2020.10.001

Jonasch, E., Walker, C. L., and Rathmell, W. K. (2021). Clear cell renal cell carcinoma ontogeny and mechanisms of lethality. *Nat. Rev. Nephrol.* 17, 245–261. doi:10.1038/s41581-020-00359-2

Jovcevska, I., Zottel, A., Samec, N., Mlakar, J., Sorokin, M., Nikitin, D., et al. (2019). High FREM2 gene and protein expression are associated with favorable prognosis of IDH-WT glioblastomas. *Cancers (Basel)* 11, E1060. doi:10.3390/cancers11081060

Kim, S., and Cho, S. (2022). The evasion mechanisms of cancer immunity and drug intervention in the tumor microenvironment. *Front. Pharmacol.* 13, 868695. doi:10.3389/fphar.2022.868695

Kiyozumi, D., Takeichi, M., Nakano, I., Sato, Y., Fukuda, T., and Sekiguchi, K. (2012). Basement membrane assembly of the integrin α8β1 ligand nephronectin requires Fraser syndrome-associated proteins. *J. Cell Biol.* 197, 677–689. doi:10.1083/jcb.201203065

Koch, A., Joosten, S. C., Feng, Z., de Ruijter, T. C., Draht, M. X., Melotte, V., et al. (2018). Analysis of DNA methylation in cancer: Location revisited. *Nat. Rev. Clin. Oncol.* 15, 459–466. doi:10.1038/s41571-018-0004-4

Koliaraki, V., Prados, A., Armaka, M., and Kollias, G. (2020). The mesenchymal context in inflammation, immunity and cancer. *Nat. Immunol.* 21, 974–982. doi:10.1038/s41590-020-0741-2

Li, L., Huang, Z., Du, K., Liu, X., Li, C., Wang, D., et al. (2022). Integrative pan-cancer analysis confirmed that FCGR3A is a candidate biomarker associated with tumor immunity. *Front. Pharmacol.* 13, 900699. doi:10.3389/fphar.2022.900699

Li, H. N., Li, X. R., Lv, Z. T., Cai, M. M., Wang, G., and Yang, Z. F. (2020). Elevated expression of FREM1 in breast cancer indicates favorable prognosis and high-level immune infiltration status. *Cancer Med.* 9, 9554–9570. doi:10.1002/cam4.3543

Li, T., Wu, B., Yang, T., Zhang, L., and Jin, K. (2020). The outstanding antitumor capacity of CD4(+) T helper lymphocytes. *Biochim. Biophys. Acta. Rev. Cancer* 1874, 188439. doi:10.1016/j.bbcan.2020.188439

Luo, J., Xie, Y., Zheng, Y., Wang, C., Qi, F., Hu, J., et al. (2020). Comprehensive insights on pivotal prognostic signature involved in clear cell renal cell carcinoma microenvironment using the ESTIMATE algorithm. *Cancer Med.* 9, 4310–4323. doi:10.1002/cam4.2983

Nam, H. Y., Chandrashekar, D. S., Kundu, A., Shelar, S., Kho, E. Y., Sonpavde, G., et al. (2019). Integrative epigenetic and gene expression analysis of renal tumor progression to metastasis. *Mol. Cancer Res.* 17, 84–96. doi:10.1158/1541-7786.MCR-17-0636

Nazemi, M., and Rainero, E. (2020). Cross-talk between the tumor microenvironment, extracellular matrix, and cell metabolism in cancer. *Front. Oncol.* 10, 239. doi:10.3389/fonc.2020.00239

Oh, D. Y., and Fong, L. (2021). Cytotoxic CD4(+) T cells in cancer: Expanding the immune effector toolbox. *Immunity* 54, 2701–2711. doi:10.1016/j.immuni.2021.11.015

Pan, H., Renaud, L., Chaligne, R., Bloehdorn, J., Tausch, E., Mertens, D., et al. (2021). Discovery of candidate DNA methylation cancer driver genes. *Cancer Discov.* 11, 2266–2281. doi:10.1158/2159-8290.CD-20-1334

Pavlakis, E., Chiotaki, R., and Chalepakis, G. (2011). The role of Fras1/Frem proteins in the structure and function of basement membrane. *Int. J. Biochem. Cell Biol.* 43, 487–495. doi:10.1016/j.biocel.2010.12.016

Pelullo, M., Zema, S., Nardozza, F., Checquolo, S., Screpanti, I., and Bellavia, D. (2019). Wnt, Notch, and TGF-β pathways impinge on Hedgehog signaling complexity: an open window on cancer. *Front. Genet.* 10, 711. doi:10.3389/fgene.2019.00711

Reuten, R., Zendehroud, S., Nicolau, M., Fleischhauer, L., Laitala, A., Kiderlen, S., et al. (2021). Basement membrane stiffness determines metastases formation. *Nat. Mater.* 20, 892–903. doi:10.1038/s41563-020-00894-0

Romani, P., Valcarcel-Jimenez, L., Frezza, C., and Dupont, S. (2021). Crosstalk between mechanotransduction and metabolism. *Nat. Rev. Mol. Cell Biol.* 22, 22–38. doi:10.1038/s41580-020-00306-w

Saygin, C., Matei, D., Majeti, R., Reizes, O., and Lathia, J. (2019). Targeting cancer stemness in the clinic: From hype to hope. *Cell stem Cell* 24, 25–40. doi:10.1016/j.stem.2018.11.017

Siegel, R. L., Miller, K. D., Fuchs, H. E., and Jemal, A. (2021). Cancer statistics, 2021. *CA. A Cancer J. Clin.* 71, 7–33. doi:10.3322/caac.21654

Stuelten, C. H., Parent, C. A., and Montell, D. J. (2018). Cell motility in cancer invasion and metastasis: insights from simple model organisms. *Nat. Rev. Cancer* 18, 296–312. doi:10.1038/nrc.2018.15

Umeda, S., Kanda, M., Miwa, T., Tanaka, H., Tanaka, C., Kobayashi, D., et al. (2020). Fraser extracellular matrix complex subunit 1 promotes liver metastasis of gastric cancer. *Int. J. Cancer* 146, 2865–2876. doi:10.1002/ijc.32705

von Roemeling, C., Radisky, D., Marlow, L., Cooper, S., Grebe, S., Anastasiadis, P., et al. (2014). Neuronal pentraxin 2 supports clear cell renal cell carcinoma by activating the AMPA-selective glutamate receptor-4. *Cancer Res.* 74, 4796–4810. doi:10.1158/0008-5472.CAN-14-0210

Wang, V., Geybels, M., Jordahl, K., Gerke, T., Hamid, A., Penney, K., et al. (2021). A polymorphism in the promoter of FRAS1 is a candidate SNP associated with metastatic prostate cancer. *Prostate* 81, 683–693. doi:10.1002/pros.24148

Wang, G. G., Wang, Z., Lu, H. Q., Guo, L. Q., Kong, F., Wang, A., et al. (2022). Comprehensive analysis of FRAS1/FREM family as potential biomarkers and therapeutic targets in renal clear cell carcinoma. *Res. Square*. Preprinted. doi:10.21203/rs.3.rs-1733569/v1

Wei, X., Choudhury, Y., Lim, W., Anema, J., Kahnoski, R., Lane, B., et al. (2017). Recognizing the continuous nature of expression heterogeneity and clinical outcomes in clear cell renal cell carcinoma. *Sci. Rep.* 7, 7342. doi:10.1038/s41598-017-07191-y

Wozniak, M., Le Calvez-Kelm, F., Abedi-Ardekani, B., Byrnes, G., Durand, G., Carreira, C., et al. (2013). Integrative genome-wide gene expression profiling of clear cell renal cell carcinoma in Czech Republic and in the United States. *PloS one* 8, e57886. doi:10.1371/journal.pone.0057886

Wuttig, D., Zastrow, S., Füssel, S., Toma, M., Meinhardt, M., Kalman, K., et al. (2012). CD31, EDNRB and TSPAN7 are promising prognostic markers in clear-cell renal cell carcinoma revealed by genome-wide expression analyses of primary tumors and metastases. *Int. J. Cancer* 131, E693–E704. doi:10.1002/ijc.27419

Xu, J., Min, W., Liu, X., Xie, C., Tang, J., Yi, T., et al. (2012). Identification of FRAS1 as a human endometrial carcinoma-derived protein in serum of xenograft model. *Gynecol. Oncol.* 127, 406–411. doi:10.1016/j.ygyno.2012.07.109

Zhan, Q., Huang, R., Liang, X., Ge, M., Jiang, J., Lin, H., et al. (2014). FRAS1 knockdown reduces A549 cells migration and invasion through downregulation of FAK signaling. *Int. J. Clin. Exp. Med.* 7, 1692–1697.

frontiers | Frontiers in Pharmacology

TYPE Original Research
PUBLISHED 12 October 2022
DOI 10.3389/fphar.2022.1005855

Check for updates

OPEN ACCESS

EDITED BY
Ting Wang,
Sichuan Cancer Hospital, China

REVIEWED BY
Yu H. Sun,
University of Rochester, United States
Ebru Temiz,
Harran University, Turkey
Milad Shirvaliloo,
Tabriz University of Medical Sciences, Iran

*CORRESPONDENCE
Wenshan Liu,
liuwenshan@wfmc.edu.cn
Zhong Lu,
luzhong@wfmc.edu.cn
Jiaqiu Li,
lijq@wfmc.edu.cn

†These authors have contributed equally to this work and share first authorship

SPECIALTY SECTION
This article was submitted to Pharmacology of Anti-Cancer Drugs, a section of the journal Frontiers in Pharmacology

RECEIVED 28 July 2022
ACCEPTED 28 September 2022
PUBLISHED 12 October 2022

CITATION
Ma J, Song P, Liu X, Ma C, Zheng M, Ren X, Wang R, Liu W, Lu Z and Li J (2022), Insights into the roles and driving forces of CCT3 in human tumors. *Front. Pharmacol.* 13:1005855. doi: 10.3389/fphar.2022.1005855

COPYRIGHT
© 2022 Ma, Song, Liu, Ma, Zheng, Ren, Wang, Liu, Lu and Li. This is an open-access article distributed under the terms of the Creative Commons Attribution License (CC BY). The use, distribution or reproduction in other forums is permitted, provided the original author(s) and the copyright owner(s) are credited and that the original publication in this journal is cited, in accordance with accepted academic practice. No use, distribution or reproduction is permitted which does not comply with these terms.

Insights into the roles and driving forces of CCT3 in human tumors

Jingang Ma[1†], Ping Song[2†], Xinling Liu[3†], Changgeng Ma[4], Mingzhu Zheng[1], Xiaomin Ren[1], Rui Wang[1], Wenshan Liu[5]*, Zhong Lu[1]* and Jiaqiu Li[1]*

[1]Department of Oncology, Affiliated Hospital of Weifang Medical University, School of Clinical Medicine, Weifang Medical University, Weifang, China, [2]Department of Gastroenterology, Affiliated Hangzhou First People's Hospital, Medical School of Zhejiang University, Hangzhou, China, [3]Department of Hematology, Laboratory for Stem Cell and Regenerative Medicine, Clinical Research Center, Affiliated Hospital of Weifang Medical University, Weifang, China, [4]Department of Radiotherapy, Affiliated Hospital of Weifang Medical University, Weifang, China, [5]Shandong Key Laboratory of Clinical Applied Pharmacology, Department of Pharmacy, Affiliated Hospital of Weifang Medical University, Weifang, China

CCT3 played a key role in many cancers. This study aimed to further explore the characteristics of CCT3 from a pan-cancer perspective and reveal the driving forces for CCT3. By bioinformatic analysis, we found that the mRNA and protein levels of CCT3 were abnormally elevated in most tumor types and were correlated with poor prognosis. Single-cell sequencing data indicated an abnormal increase of CCT3 expression in both malignant cells and multiple immune cells. In the tumor microenvironment, CCT3 expression was negatively relevant with immune cell infiltration and immune checkpoint genes expression. In colon cancer, knockdown of CCT3 inhibited cell proliferation. Gene set enrichment analysis showed that CCT3 may be oncogenic by regulating amino acid metabolism. Furthermore, we predicted sensitive drugs for CCT3 by virtual screening and sensitivity analysis. Many driver genes such as TP53 and KRAS were essential for CCT3 overexpression. Epigenetic factors, enhancers in particular, were also critical for CCT3 expression. Additionally, we constructed the lncRNA/circRNA-miRNA-CCT3 regulatory network. Collectively, CCT3 had the potential to be a diagnostic and prognostic biomarker for multiple tumor types. CCT3 expression was relevant with an immunosuppressive tumor microenvironment. CCT3 could be a new molecular target for colon cancer. Both genetic and epigenetic factors were responsible for CCT3 expression in tumors.

KEYWORDS

CCT3, pan-cancer, biomarker, immune microenvironment, enhancers

Introduction

In 2020, the International Agency for Research on Cancer (IARC) reported that there were about 19.3 million new cancer cases and 10.2 million cancer deaths worldwide (Sung et al., 2021). Cancer remains one of the main diseases that cause human death worldwide. Despite the research on cancer has made great breakthroughs, finding new molecular therapeutic targets are still a requirement for tumor patients.

With the continuous development of many open bioinformatic databases such as TCGA (The Cancer Genome Atlas) and GEO (Gene Expression Omnibus) (Clough and Barrett, 2016; Blum et al., 2018), it has become an essential and important research method to use bioinformatics to explore medical questions. Chaperonin-containing TCP-1 (CCT) and HSP60 are the two main types of the chaperone system (Dong et al., 2020). CCT can promote the folding of a fraction of newly synthesized proteins such as KRAS, STAT3 and p53 (Liu et al., 2022a). CCT3 is one of the 8 subunits of CCT (Stoldt et al., 1996; Valpuesta et al., 2002; Macario and Conway de Macario, 2021) and has been explored its central roles in some tumors. For instance, CCT3 inhibitor inhibited the proliferation and migration in breast cancer (Xu et al., 2020). Abnormal expression of CCT3 significantly reduced the overall survival (OS) of hepatocellular carcinoma (HCC) patients (Cui et al., 2015). CCT3 knockdown blocked the proliferation of gastric cancer (GC) cells (Li et al., 2017). Meanwhile, the high expression of CCT3 also contributed to the progression of head and neck squamous cell carcinoma (HNSCC) (Wang et al., 2021). Interestingly, recent study showed that CCT3 is an RNA-binding protein (RBP) and could regulate lipid metabolism by LINC00326 in HCC (Sondergaard et al., 2022). In agreement with this study, CCT3 suppression led to oxidative stress and energy deficiency in breast and prostate cancer (Temiz et al., 2021). Moreover, CCT3 promotes cisplatin resistance by JAK2/STAT3 pathway in lung cancer (Danni et al., 2021). And CCT3 is responsible for castration-resistant prostate cancer (Lin et al., 2021a). Collectively, CCT3 plays a key role in cancer cell division, proliferation, metabolism and drug resistance. However, the roles of CCT3 in pan-cancer are not compared, especially from the immune aspect. And the upstream regulatory mechanisms for CCT3 overexpression in tumors are unclear.

In this study, a systematic pan-cancer analysis of CCT3 was performed by bioinformatics and experiments. We explored the characteristics of CCT3 in different tumors including expression levels, prognostic value and gene function. Meanwhile, we also analyzed the correlation between CCT3 expression and immune microenvironment. Furthermore, we predicted sensitive drugs for CCT3 by virtual screening and sensitivity analysis. Finally, the upstream regulatory mechanisms for CCT3 overexpression in tumors were elucidated. In summary, our results implied CCT3 as a potential biomarker for many tumors and CCT3 could be a new molecular target for colon cancer.

Materials and methods

The expression analysis of CCT3

The expression levels of CCT3 in normal tissues and tumor tissues were analyzed by SangerBox based on the Genotype Tissue Expression (GTEx) and the Cancer Cell Line Encyclopedia (CCLE) datasets. All abbreviations are showed in Supplementary Table S1. The TCGA and GTEx combination cohorts were used for statistical analysis by ACLBI database (https://www.aclbi.com/static/index.html#/). The gene expression RNA-seq data in 8 cancer types (BRCA, CHOL, COAD, LIHC, LUAD, LUSC, STAD and UCEC) were downloaded from UCSC Xena (https://xenabrowser.net/datapages/). The counts data were analyzed for upregulate differential genes using the R package 'DESeq2'. In addition, we analyzed CCT3 expression differences between cancerous and adjacent tissues by TIMER, GEPIA2 and UANLCAN databases.

Immunohistochemistry analysis of CCT3 protein

The Human Protein Atlas (HPA) (Karlsson et al., 2021) database provides pathological information on protein expression datasets from 17 different forms of human cancers. We downloaded IHC images of 5 tumor types-BRCA, LIHC, LUAD, LUSC and UCEC to identify the protein levels of CCT3 in cancerous and adjacent tissues.

Analysis of the diagnostic value of CCT3

Gene Expression Profiling Interactive Analysis 2.0 (GEPIA2) (Li et al., 2021) is a web server that can be used for gene expression analysis. We explored the relevance between CCT3 expression and tumor clinicopathology through the "Stage plot" module. Besides, we calculated the relevance between CCT3 expression and tumor grades by using the TISIDB database (Ru et al., 2019).

Prognostic value analysis of CCT3

The relevance between CCT3 expression and OS, DSS, DFI and PFI in 33 tumor types was analyzed by SangerBox. Based on the GEO, EGA, and TCGA datasets, survival data of CCT3 was evaluated by Kaplan-Meier Plotter (Lanczky and Gyorffy, 2021). In addition, we also calculated the correlation between the expression of CCT3 and overall survival by the "Survival Analysis" module of GEPIA2.

Analysis of the single-cell sequencing data

The Tumor Immune Single Cell Center (TISCH) (Sun et al., 2021), the single cell RNA-seq database, can provide cell type annotation at the single-cell level for different cancer types. We obtained single-cell sequencing datasets through the TISCH database-BRCA (GSE114727), CHOL (GSE 125449), COAD

(GSE146771), LIHC (GSE140228), NSCLC (GSE117570), STAD (GSE134520), UCEC (GSE154763), and quantified CCT3 expression levels by UMAP and violin plots.

Analysis of the immunological features of CCT3

We explored the immune correlation using pan-cancer datasets from TCGA which integrates six algorithms including TIMER, xCell, MCP-counter, CIBERSORT, EPIC and quanTIseq. We calculated the relevance between CCT3 expression and immune cell infiltration by SangerBox. SIGLEC15, IDO1, CD274, HAVCR2, PDCD1, CTLA4, LAG3 and PDCD1LG2 are the immune checkpoint genes. We compared the relevance between CCT3 and these genes expression.

Enrichment analysis of the CCT3-related genes

Through the STRING database (https://string-db.org/) (Szklarczyk et al., 2019), CCT3 was retrieved in the "Protein Names" module to get the CCT3 interaction proteins and the species were selected as homo species. We set the parameters as follows: the meaning of the network edge is "evidence", the active interaction source is "Textmining" and "Experiment" and the minimum requirement interaction score is "high confidence (0. 700)". The associated genes for CCT3 were obtained by the GENEMANIA database (Warde-Farley et al., 2010). The two groups of genes were combined for GO and KEGG enrichment analysis by DAVID database (Sherman et al., 2022).

Analysis of genetic and epigenetic alteration for CCT3

The mutational characteristics of CCT3, including mutation type and frequency, were explored through the cBioPortal database (Cerami et al., 2012). The effect of driver genes on CCT3 expression in cancers was showed by the TCGA portal database (Xu et al., 2019). The effect of the TP53 mutation on the CCT3 expression in the tumors was analyzed by the UALCAN database. The CpG islands in the CCT3 promoter region were observed by Methprimer database (Li and Dahiya, 2002). And the effect of DNA methylation on CCT3 expression in the pan-cancer was analyzed by DiseaseMeth database (Xiong et al., 2017). Finally, we analyzed the enrichment of H3K27ac signals in CCT3 gene loci by WashU Epigenome Browser (http://epigenomegateway.wustl.edu/browser/).

Sensitive drugs and molecular docking

We obtained RNA expression and drug data for NCI-60 cell lines from the CELLMiner database (Reinhold et al., 2012). CCT3 expression and drug sensitivity (IC50) was calculated and visualized by R software. The spatial structure of the CCT3 protein was obtained from the Protein Data Bank (PDB) and the drug molecular structure was obtained from the Pubchem database. The GHECOM algorithm was used to identify the CCT3 protein-binding sites. The UCSF DOCK 6.9 software was used for molecular docking. And it was visualized by PyMol. Finally, Ligplus was used to analyze the interaction forces.

CeRNA regulatory network analysis

The miRNAs targetingCCT3 were predicted by 5 databases including StarBase (Li et al., 2014), Targetsacn (McGeary et al., 2019), MiRDB (Chen and Wang, 2020), MiRWalk (Dweep and Gretz, 2015) and DIANA (Paraskevopoulou et al., 2013). Then we compared and obtained the intersection. Then, the upstream lncRNAs/circRNAs were predicted by StarBase database. Finally, the lncRNA/circRNA-miRNA-CCT3 regulatory network was visualized by Cytoscape software.

Cells

All cells were obtained from cell bank of the Chinese Academy of Sciences. HCT116 was cultured in 10 cm dish containing McCoy's 5A medium supplemented with 10% FBS. DLD1, SGC7901 and BGC823 were cultured in 10 cm dish containing RPMI 1640 medium supplemented with 10% FBS. The culture conditions were 37°C, 5% CO2 and 95% humidity.

Cell transfection

1×10^5cells in 6-well plates were transfected with siRNA by RNAiMAX (Invitrogen, 13778150) or added JQ1-1uM and I-BET-762-2uM (Selleck, S7110 and S7189) for 24h. The siRNA was purchased from Gene Pharma (Shanghai, China). The siRNA sequences used were listed below:

CCT3-siRNA-1#: S: GCUGUGAAGCUGCAGACUUTT, AS: AAGUCUGCAGCUUCACAGCTT; CCT3-siRNA-2#: S: GCAAGGCAUUGGAUGAUAUTT, AS: AUAUCAUCCAAU GCCUUGCTT; BRD4-siRNA-1#: S: CCGUGAUGCUCAGGA GUUUTT, AS: AAACUCCUGAGCAUCACGGTT; BRD4-siRNA-2#: S: AGCUGAACCUCCCUGAUUATT, AS: UAA UCAGGGAGGUUCAGCUTT.

Quantitative real-time PCR

The qPCR assays were performed as reported previously (Li et al., 2018). Briefly, the extraction of total RNA from cells was performed by Trizol following the manufacturer's instructions. And after RNA quantification, cDNA was synthesized. Next, mRNA expression was detected by qPCR using UltraSYBR Mixture (CW0957M, cwbiotech). The primer sequences used were listed below:

CCT3-F: TTTGGACCCAATGGGAGGC, R: ACAGCATTTCCCCTGCAAGAAT; Tubulin-F: GAAGCAGCAACCATGCGTGA, R: AAGGAATCATCTCCTCCCCCA.

CCK-8 assay

3×10^3 cells were seeded in the 96-well plate and were incubated in an incubator for 72 h 10ul CCK8 reagent (Beyotime, C0038) and 100ul culture medium were then added to each well and incubated for 30min. Finally, the absorbance at 490 nm in each well was measured using a microplate reader.

Colony formation assay

1×10^5 cells were uniformly spread in 6-well plates overnight and then were treated for CCT3 knockdown with the corresponding siRNA. After 3 days, 1000 cells per well were reseeded in 6-well plates and cultured for 2 weeks. Then the medium was taken away and the cells were washed with PBS to remove impurities. Cells were fixed with paraformaldehyde (4% concentration, 20 min, room temperature). Finally, cells were stained with 0.1% crystal violet solution and then counted.

Chromatin immunoprecipitation

The ChIP assay was performed as reported previously (Song et al., 2020). Anti-H3K27ac antibody was purchased from Abcam (ab177178). Anti-BRD4 antibody was purchased from Bethyl Laboratories (A301-985A100). The purified DNA was analyzed by qPCR. The primer sequences used were listed below: CCT3-H3K27ac-CHIP-F: GCCTCTCTAGTCCACCTGTTG, R: ACTGTGTATTGCGACTCGGC.

Statistical analysis

Two-sided student's t-test was used to assess statistical significance by using GraphPad Prism seven software and the results were presented as mean ± SD. All the experiments were repeated in triplicate. If the results do not have the same SD, then we used *t*-test with Welch's correction. The p value < 0.05 was considered statistically significant. $^*p < 0.05$; $^{**}p < 0.01$; $^{***}p < 0.001$; $^{****}p < 0.0001$.

Results

CCT3 expression in pan-cancer

First, we analyzed the mutation status of CCT3 in tumors by the cBioportal database (Supplemenrtary Figure S1A,B). The results showed the mutation frequency of CCT3 was rare in pan-cancer. To obtain a detailed understanding of CCT3 expression in normal and tumor tissues, CCT3-related expression was specifically analyzed by SangerBox. First, we calculated the expression levels of CCT3 in normal tissues by analyzing the GTEx datasets (Figure 1A). Next, we calculated CCT3 expression levels in different tumor tissues by analyzing the CCLE datasets (Figure 1B). Moreover, based on the TCGA datasets, we analyzed the CCT3 differential expression levels between carcinomas and adjacent tissues (Figure 1C). The results showed that CCT3 expression was up-regulated in 20 cancer types and down-regulated in three cancer types. To take a closer step into the aberrant expression of CCT3 in pan-cancer, we analyzed CCT3 expression using a combined cohort of TCGA and GTEx in ACLBI. In the 33 cancer types, we found abnormal high expression of CCT3 in 27 of these cancer types (Figure 1D). In addition, 8 cancer types including BRCA, CHOL, COAD, LIHC, LUAD, LUSC, STAD and UCEC, showed abnormal high expression of CCT3 in other three databases-TIEMR, GEPIA and UALCAN (Supplementary Figure S2A–C). Then we calculated the ranking of CCT3 expression among the differentially expressed genes in the 8 high-expressed cancer types (Supplementary Table S1). Notably, in BRCA, COAD, LIHC, LUAD and LUSC, CCT3 belongs to the top 10% differentially expressed genes. Besides, we found a close correlation between CCT3 expression and pathological stages of multiple cancer types, including KICH, KIRP, LIHC, LUAD, LUSC and STAD (Supplementary Figure S3A). And we observed a close link between CCT3 expression and tumor grades of multiple cancer types, including CESC, KIRC, LIHC, STAD and UCEC (Supplementary Figure S3B). Finally, we explored the protein expression levels of CCT3 in the above 8 tumors by immunohistochemistry analysis and found that the protein expression levels of CCT3 were obvious higher in BRCA, COAD, LIHC, LUAD and UCEC than the corresponding normal tissues (Figures 2A–E). In summary, the above results imply a potential of CCT3 as a diagnostic biomarker for many tumor types.

Prognostic value of CCT3

Whether the high-expressed CCT3 has a key prognostic value in tumors? Then we calculated the relevance between CCT3 expression and the prognosis in 33 cancer types. The

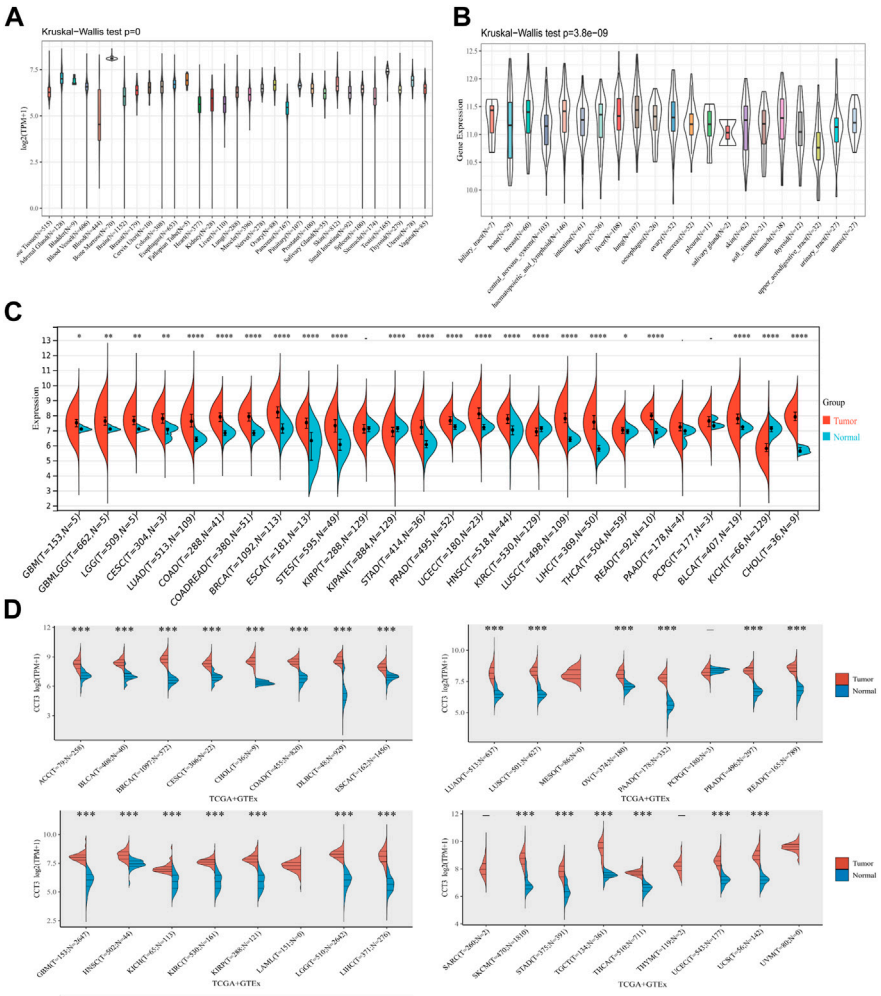

FIGURE 1
Expression levels of CCT3 in pan-cancer. **(A)** The expression levels of CCT3 in normal tissues were analyzed using the GTEx datasets. **(B)** The expression levels of CCT3 in different tumor tissues were analyzed using the CCLE datasets. **(C)** Differential expression levels of CCT3 in tumor and corresponding normal tissues were analyzed using the TCGA datasets. **(D)** Differential expression levels of CCT3 in tumor and corresponding normal tissues were analyzed using the TCGA and GETx datasets. *$p < 0.05$, **$p < 0.01$, ***$p < 0.001$.

prognosis contains overall survival (OS), disease-specific survival (DSS), disease-free interval (DFI) and progression-free interval (PFI). The forest plot showed that CCT3 acted as a risk factor for OS in 12 cancer types (Figure 3A). In addition, the KM curves showed that high CCT3 expression was associated with poor OS in 11 cancer types (Figure 3B). And CCT3 expression was significantly relevant with DSS in 14 tumors (Figure 3C). Among them, the high expression of CCT3 resulted in poor DSS in 13 tumors (Figure 3D). Meanwhile, abnormal high expression of CCT3 was related with DFI and PFI in six cancers and 9cancers, respectively (Figures 4A–D). Furthermore, based on TCGA or GEO datasets, we found a negative correlation between CCT3 high expression and the OS of multiple tumor types by Kaplan-Meier Plotter and GEPIA2 databases (Supplementary Figure S4A,B). All the data suggest CCT3 might be a prognostic biomarker for a number of tumor types.

Immune characteristics of CCT3

Single-cell sequencing was used to reveal the specific characteristics of genes in cancer cells, as well as in tumor microenvironment (Zhang et al., 2022). Interestingly, among the CCT3 high-expressed 8 tumors, other than in malignant cells, we also found an abnormal increase of CCT3 expression in multiple immune cells of the tumor microenvironment in CHOL, COAD, NSCLC and STAD (Figure 5 and Supplementary Figure S5). Particularly, the highest cancer type of CCT3 expression in the tumor microenvironment was

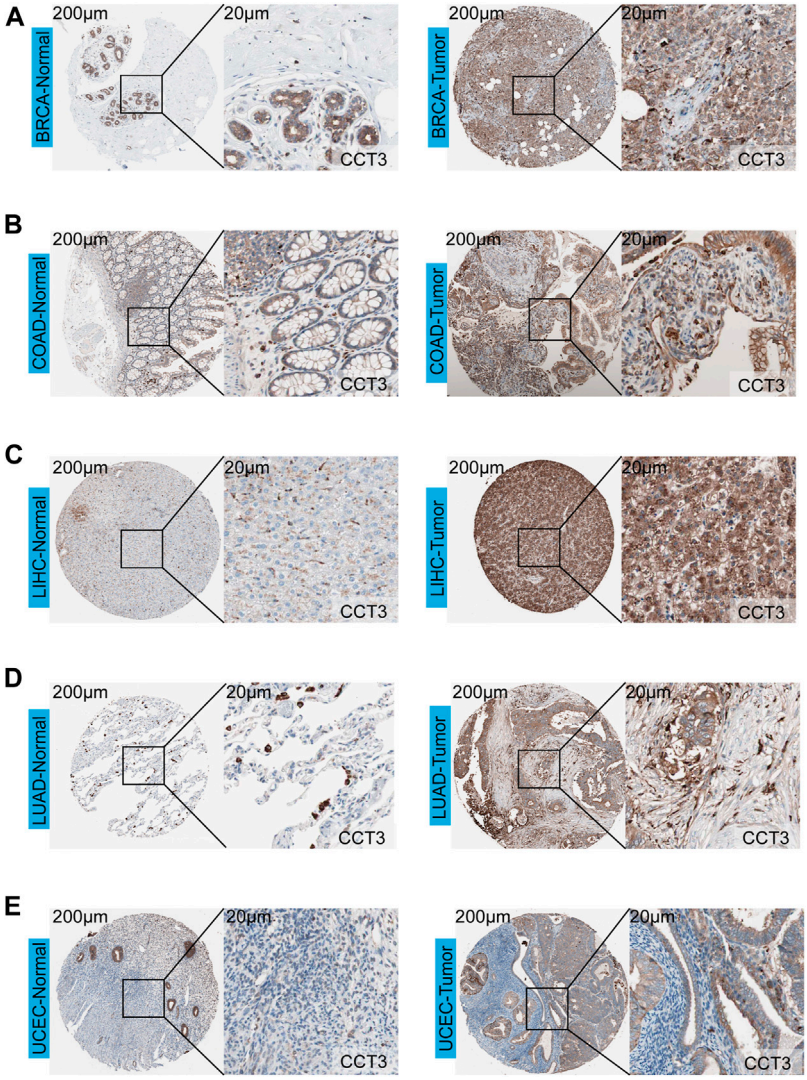

FIGURE 2
Immunohistochemistry analysis of CCT3 protein. The protein levels of CCT3 were analyzed by IHC in several cancer types: **(A)** BRCA, **(B)** COAD, **(C)** LIHC, **(D)** LUAD, **(E)** UCEC.

COAD. As is known to all, the immune cells in tumor microenvironment play a central part in the immunotherapy (Uyanik et al., 2021). Therefore, we wondered the relevance between CCT3 expression and immune characteristics. We discovered that CCT3 expression was negatively relevant with immune cell infiltration in most of tumor types (Figure 6A and Supplementary Figure S6). Moreover, our findings revealed that CCT3 expression was negatively relevant with immune scores including ESTIMATE Score, Stromal Score and Immune Score (Figures 6B–D). Besides, we identified that the immune checkpoint genes expression including CD274, PDCD1 and CTLA4, was negatively relevant withCCT3 expression (Figures 7A,B). Interestingly, we found that CCT3 expression was negatively relevant with the roles of cytotoxic T lymphocyte (CTL) (Figures 7C,D). In conclusion, CCT3 expression was relevant with immunosuppressive tumor microenvironment. And CCT3 may be a novel target of immunotherapy.

Functional enrichment analysis of CCT3

Considering that CCT3 showed higher expression levels in both cancer cells and tumor microenvironment in COAD and STAD than other tumors, we wondered whether targeting CCT3 was feasible in gastrointestinal tumor. Previous study suggested that CCT3 was critical for gastric cancer cell growth

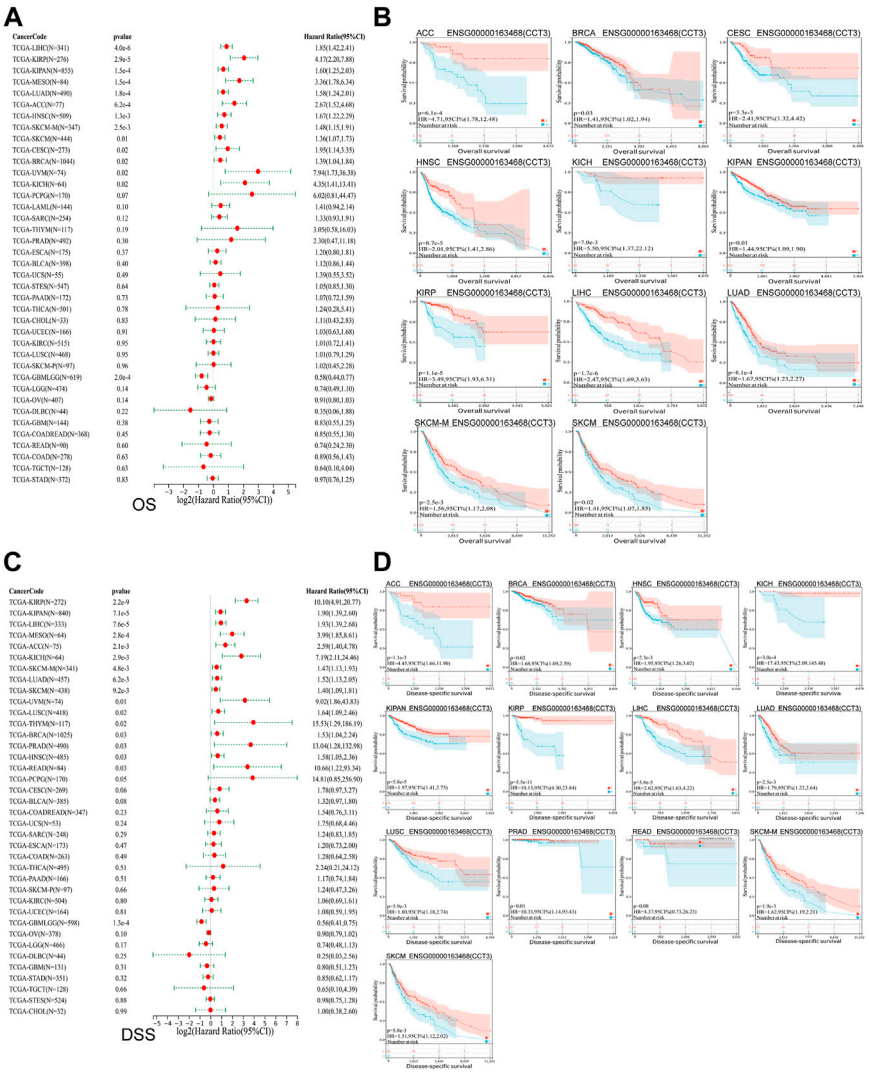

FIGURE 3
Prognostic value of CCT3 for overall survival (OS) and disease-specific survival (DSS) in pan-cancer. **(A)** Forest plots showed the correlation between CCT3 expression and OS in 33 cancer types. **(B)** The KM curves showed the correlation between CCT3 expression and OS in pan-cancer. **(C)** Forest plots showed the correlation between CCT3 expression and DSS in 33 cancer types. **(D)** The KM curves showed the correlation between CCT3 expression and DSS in pan-cancer.

(Li et al., 2017). Now we explored CCT3's function in colon cancer cells. QPCR assay validated that CCT3 mRNA levels in the colon normal cell line-FHC was lower than those in the COAD tumor cell lines (Figure 8A). Knockdown of CCT3 expression in the COAD cell lines inhibited the cell viability and colony formation ability (Figures 8B,C). Next, gene set enrichment analysis (GSEA) showed that amino acid active, regulation of cellular amino acid metabolic process, oxidative phosphorylation and cell cycle were mainly enriched in the CCT3 high-expressed group. However, response to lipid, positive regulation of lipid localization, natural killer cell mediated cytotoxicity and B cell receptor signaling pathway were enriched in the CCT3 low-expressed group (Figure 8D). This is consistent with the above findings that CCT3 expression was negative relevant with tumor immune process. To further explore the functions of CCT3 in cancers, we obtained the CCT3-related genes through the online analysis tools String and GENEMANIA (Figures 9A,B). Then we performed GO and KEGG enrichment analysis for these genes. The results showed that the main functional enrichment of biological processes (BP) is protein folding (Figure 9C). The cellular component (CC) is mainly chaperonin−containing T−complex (Figure 9D). Molecular function (MF) is mainly involved in the unfolded protein binding (Figure 9E). KEGG enrichment

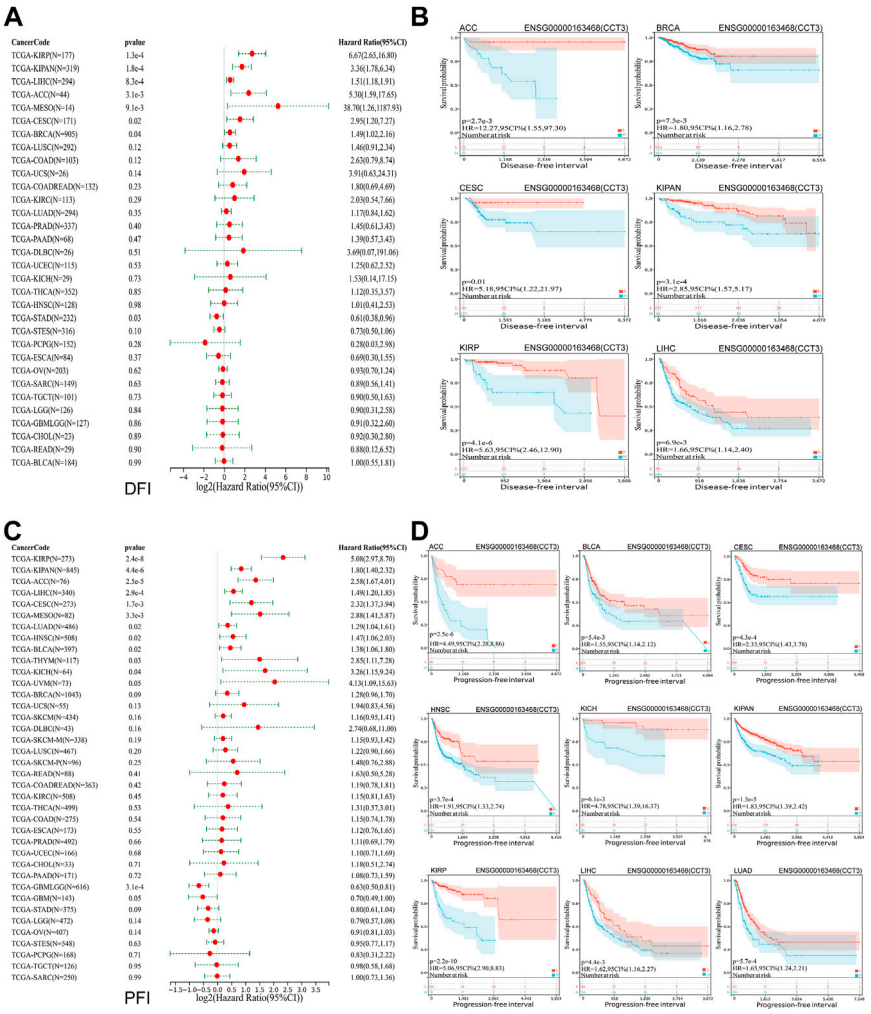

FIGURE 4
Prognostic value of CCT3 for disease-free interval (DFI) and progression-free interval (PFI) in pan-cancer. **(A)** Forest plots showed the correlation between CCT3 expression and DFI in 33 cancer types. **(B)** The KM curves showed the correlation between CCT3 expression and DFI in pan-cancer. **(C)** Forest plots showed the correlation between CCT3 expression and PFI in 33 cancer types. **(D)** The KM curves showed the correlation between CCT3 expression and PFI in pan-cancer.

analysis revealed that CCT3-related genes were enriched in Sphingolipid signaling pathway, mRNA surveillance pathway, AMPK signaling pathway and Hippo signaling pathway (Figure 9F). In summary, our results revealed the important functions of CCT3 in tumorigenesis.

Predicting sensitive drugs for CCT3 protein

Subsequently, we wanted to predict sensitive drugs for targeting CCT3 protein. First, the FDA-approved clinical trial drugs were screened through the CellMiner database to obtain the CCT3-related susceptible drugs (Supplementary Figure S7A,B). Among them, A1210477, LY-3023414, PKI-587, AT-7519, Kahalide F and AZD-3147 were screened out according to the correlation. Meanwhile, the spatial structure of the CCT3 protein was obtained by the PDB database (Figure 10A). The binding sites and boxes for the CCT3 protein were obtained by the GHECOM algorithm (Figure 10B). Compound structures of the six drugs were obtained through the PubChem database (Supplementary Figure S7C). Next, we used AutoDock for molecular docking and obtained the free binding energies (Supplementary Table S2). We used the PyMol software to visualize the interaction between 5 sensitive drugs and CCT3 protein (Figure 10C). Finally, we

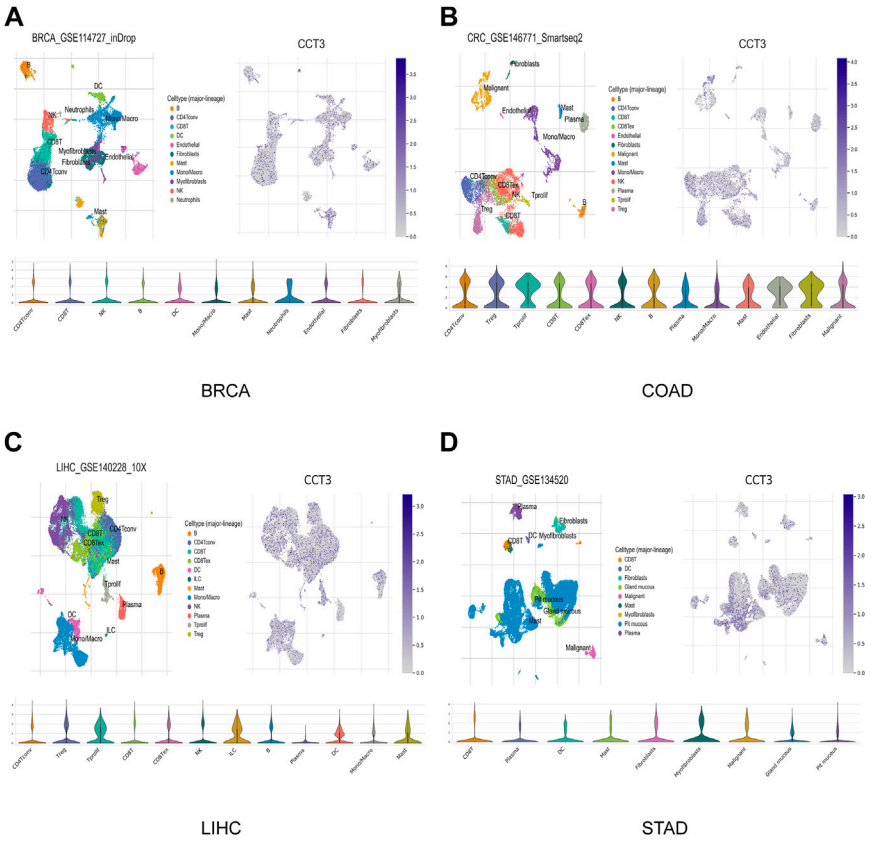

FIGURE 5
CCT3 expression based on the single-cell sequencing data. CCT3 expression in various cell types was investigated by single-cell sequencing data in **(A)** BRCA, **(B)** COAD, **(C)** LIHC and **(D)** STAD.

calculated the interaction force of the docking conformation by Ligplus (Figure 10D). In conclusion, we predicted several sensitive drugs for CCT3 protein.

The effect of genetic and epigenetic factors on CCT3 expression

For better targeting CCT3 to treat tumors, it should reveal the mechanisms for the abnormal expression of CCT3. Through the TCGA portal database, we discovered that CCT3 expression may be subject to many driver genes such as APC, TP53 and KRAS in multiple tumors (Figure 11A). In particular, TP53 mutation status showed a significant correlation with CCT3 expression (Figure 11B). Other than genetic factors, epigenetic factors including DNA methylation, histone modification and non-coding RNA are also critical for gene expression (Moore et al., 2013; Audia and Campbell, 2016; Boulos et al., 2020). We observed the presence of CpG islands in the CCT3 promoter region by the Methprimer database (Supplementary Figure S8A). Furthermore, the DNA methylation levels of CCT3 were lower in tumor tissues than normal tissues (Supplementary Figure S8B). In addition, the SangerBox data showed a significant correlation between CCT3 and the methyltransferases (Supplementary Figure S8C). Histone H3K27ac modification is necessary for enhancer to activate the transcription of target genes (Kang et al., 2021). We found a strong H3K27ac signal in CCT3 promoter region by the WashU database in various tumor cells (Figure 12A). BRD4, the H3K27ac signal reader, was positively relevant with CCT3 expression in gastric cancer (Supplementary Figure S8D). Our ChIP assay confirmed the occupancy of H3K27ac and BRD4 in CCT3 promoter region (Figures 12B,C). More importantly, enhancer inhibitors (JQ1 and I-BET-762) or BRD4 knockdown attenuated CCT3 expression in gastrointestinal tumor cells (Figures 12D,E). It is well known that microRNA can regulate gene expression by depressing the translation of the mRNA or by inducing its degradation. Next, we screened the potential miRNAs for CCT3 by using the StarBase, Targetscan, MiRDB, MiWALK and DIANA database, resulting in six common members (Figures 13A,B). Finally, we predicted the lncRNAs and circRNAs for the above six miRNAs through the StarBase database (Figure 13C).

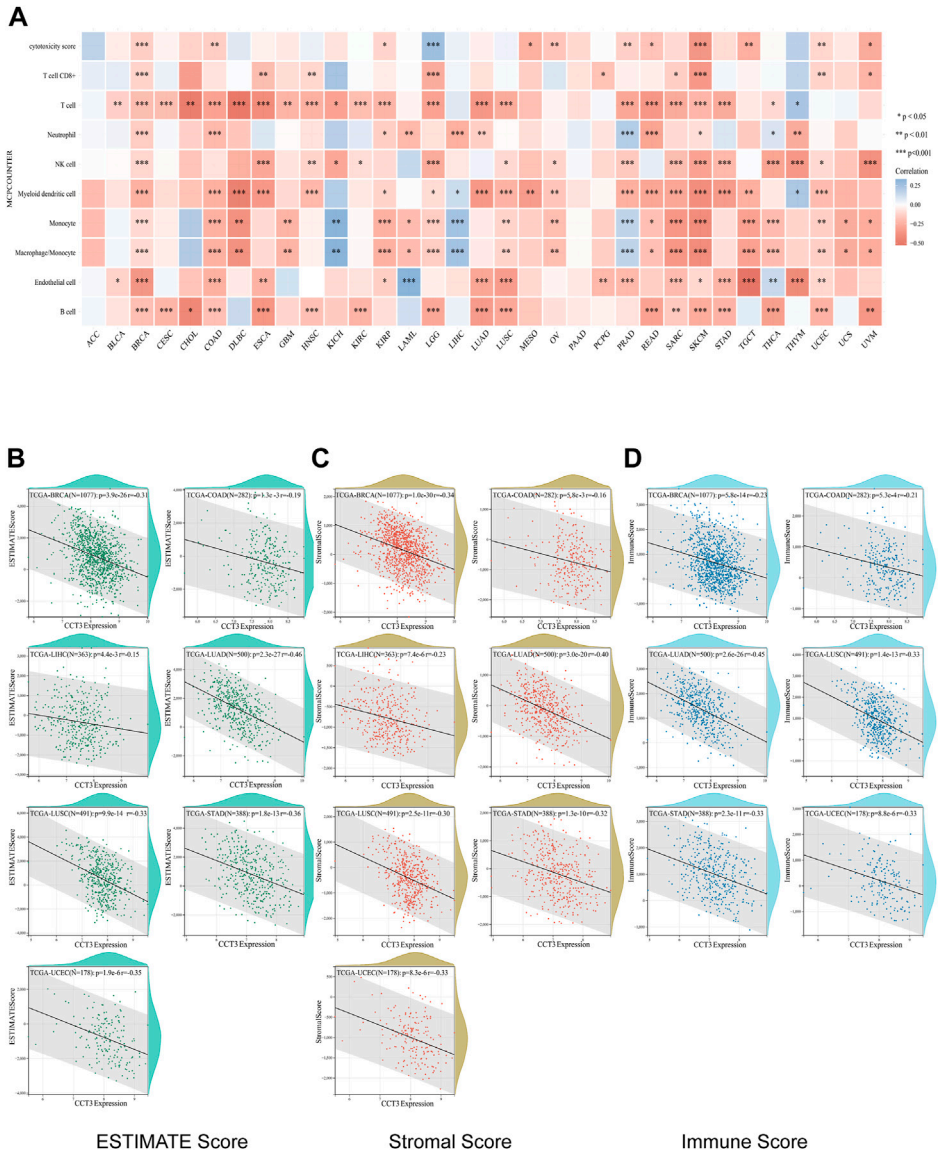

FIGURE 6
Correlation between CCT3 expression and immune cell infiltration. **(A)** Correlation between CCT3 expression and immune cell infiltration was analyzed using the MCP-counter algorithm in the R package "immunedeconv". **(B–D)** Estimate Immune-infiltration score in 8 tumors (BRCA, CHOL, COAD, LIHC, LUAD, LUSC, STAD and UCEC) based on CCT3 expression using the R package 'ESTIMATE'.

Collectively, we revealed various genetic and epigenetic factors responsible for CCT3 expression.

Discussion

Molecular chaperone CCT played a central role in tumorigenesis (Narayanan et al., 2016). As one of the significant subunits of CCT, CCT3 regulated the folding process of 7% cytosolic proteins such as VHL, tubulin, actin and cyclin E (Sternlicht et al., 1993; Willison, 2018; Manna et al., 2019). As a chaperon protein, CCT3 was critical for cancer pathogenesis by regulating cell apoptosis, proliferation and energy metabolism. CCT3 has been studied in multiple tumor types. This study wanted to further explore CCT3's roles through a comprehensive pan-cancer analysis workflow, contributing to revealing the similarity and difference among different tumors. Our study showed a widespread high expression of CCT3 in pan-cancer, especially in 8 cancer types, suggesting that CCT3 may function as an oncogene in tumors. Given its correlation with tumor stages and grades, CCT3 may act as a new diagnostic biomarker. CCT3 has been identified as a prognostic factor in

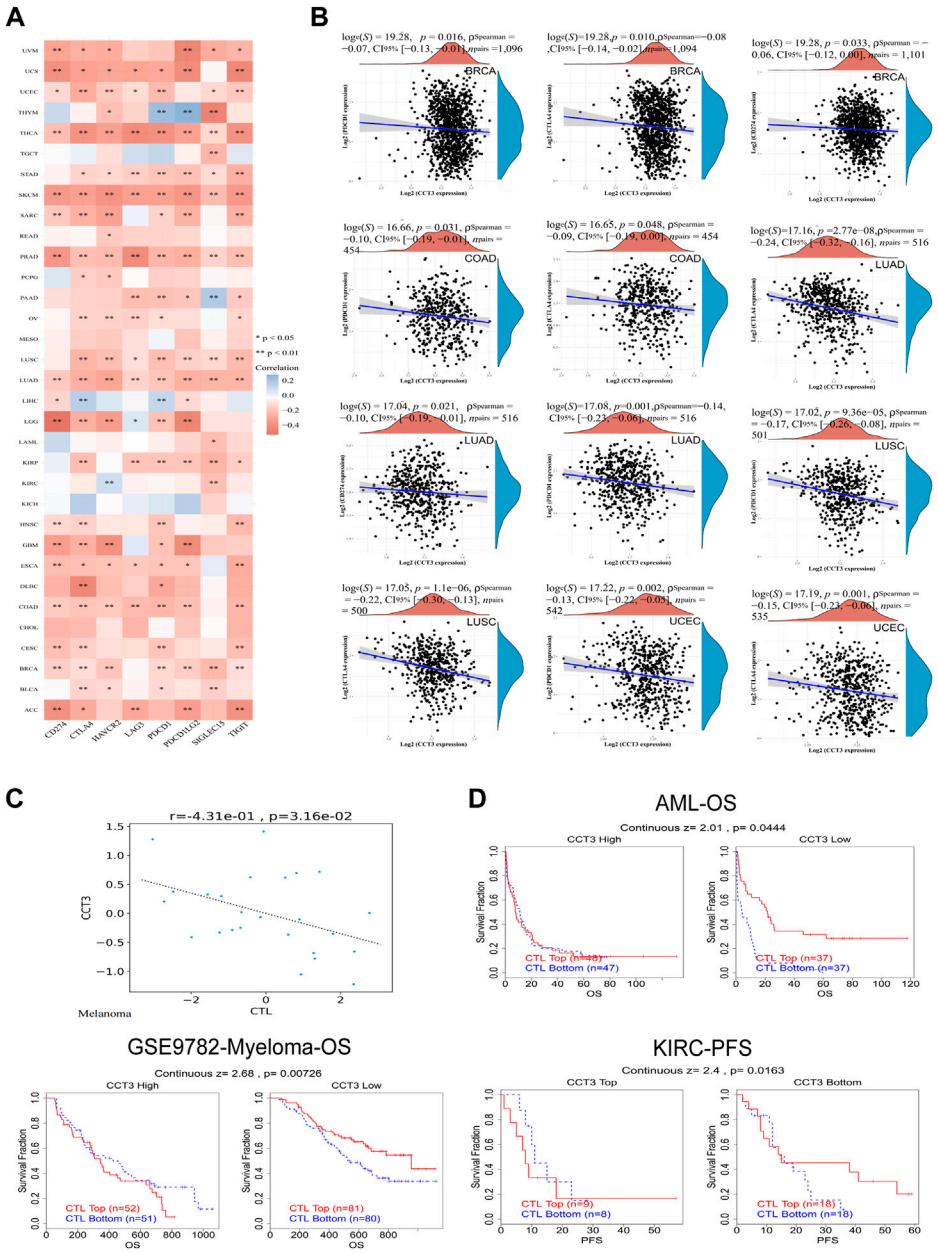

FIGURE 7
Correlation between CCT3 and immune checkpoint gene expression. **(A)** Heatmap showed the correlation between CCT3 and immune checkpoint gene expression in pan-cancer. **(B)** The correlation between CCT3 and CD274, CTLA4 and PDCD1 expression in ACLBI database. **(C)** The correlation between CCT3 and cytotoxic T lymphocyte (CTL). **(D)** The prognosis of tumor patients with different CCT3 expression and CTL levels. *$p < 0.05$, **$p < 0.01$, ***$p < 0.001$.

HNSC and HCC (Cui et al., 2015; Wang et al., 2021). Similarly, we affirmed that the tumor patients with high-expressed CCT3 showed poor prognosis, demonstrating its potential as a prognostic biomarker for multiple tumor types.

As an emerging treatment for tumors, immunotherapy has showed significant improvement in the survival time and the quality of life (Esfahani et al., 2020). Extraordinarily, immune checkpoint inhibitors (ICI) have been applicated in a variety of cancers. However, the adverse effects and high cost pose an obstacle to its application. Therefore, screening out the patients who are really suitable for immunotherapy is required (Hou et al., 2021). Owing to

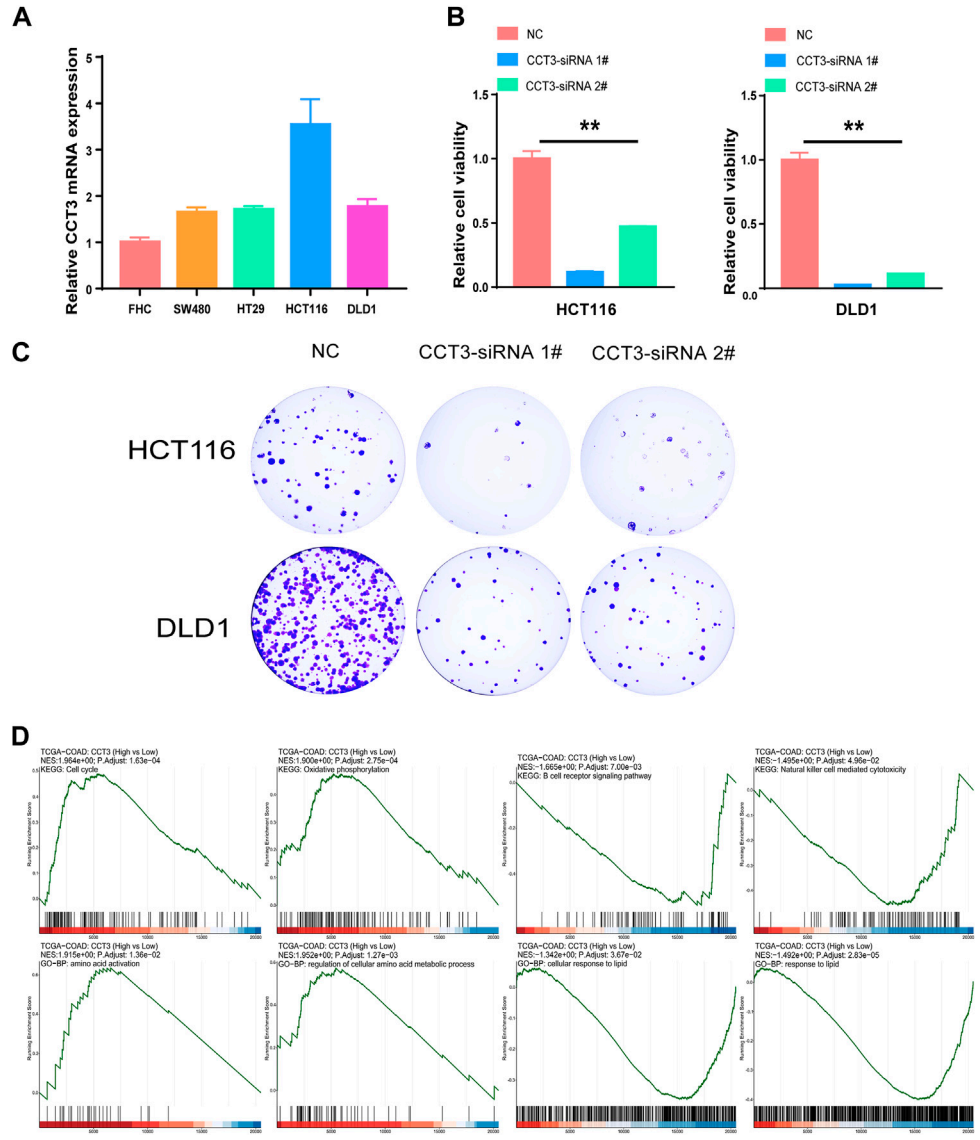

FIGURE 8
The effect of targeting CCT3 in COAD. **(A)** The expression levels of CCT3 in COAD cell lines were detected by qPCR assay. **(B)** The effect of CCT3 knockdown on the cell viability was determined by CCK-8 assay. **(C)** Colony formation assay was conducted after CCT3 knockdown. **(D)** Gene set enrichment analysis (GSEA) for CCT3 in COAD.

the heterogeneity of tumors, single-cell sequencing analysis is becoming popular. Our study observed an abnormal increase of CCT3 expression in multiple immune cells of the tumor microenvironment based on single-cell sequencing data. Moreover, we found a significant negative correlation of CCT3 expression with a variety of immune cells in various carcinomas. Additionally, CCT3 expression was negatively relevant with the immune checkpoint genes expression including CD274, PDCD1 and CTLA4. That means that the tumor patients with high CCT3 expression may not be suitable for immune checkpoint inhibitors, contributing to selecting the exact patients. Considering that CCT3 was relevant with an immunosuppressive tumor microenvironment, we assumed whether CCT3 overexpression lead to immune escape? Indeed, our results found CCT3 expression was negatively correlated with the function of cytotoxic T lymphocyte, B cell receptor signaling pathway and NK cell mediated cytotoxicity. How does CCT3 regulate tumor microenvironment? This may be attributed to CCT3's key roles in regulating amino acid

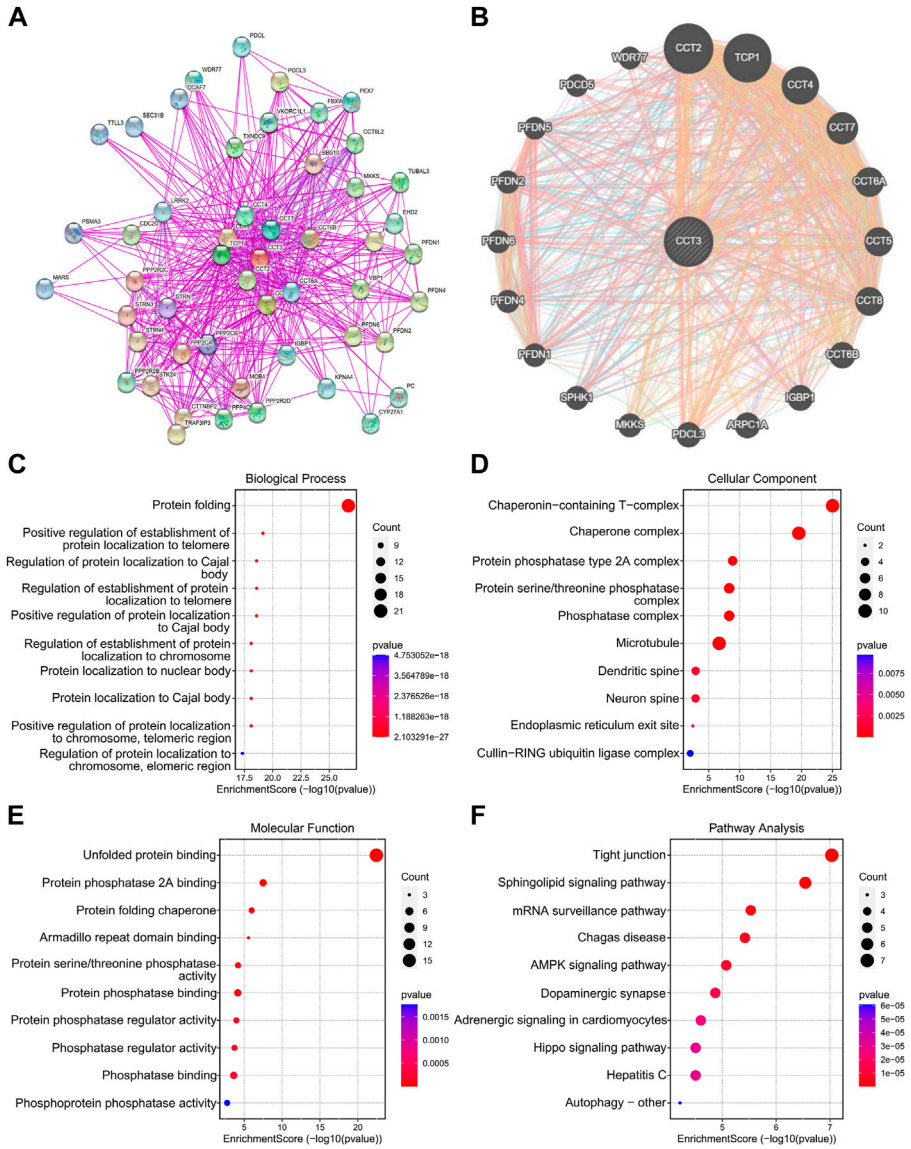

FIGURE 9
Functional enrichment analysis of CCT3. **(A)** The protein-protein interaction (PPI) networks for CCT3 were obtained by the STRING tool. **(B)** The top 20 CCT3-related genes were displayed using the GeneMANIA tool. **(C–F)** GO and KEGG analysis for CCT3-related genes. *$p < 0.05$, **$p < 0.01$, ***$p < 0.001$.

metabolic process. Amino acid metabolism is essential for driving drug resistance including immunotherapy (Yoo and Han, 2022). In addition to energy generation, amino acid metabolism could also support cancer cells by maintaining redox homeostasis. For example, reactive oxygen species (ROS) produced by amino acid metabolism, are associated with immunosuppression by acting as signaling messengers (Chen et al., 2016). ROS elevated in the tumor microenvironment, could suppress T cell activation, apoptosis, and hyporesponsiveness. Growing evidences suggest that targeting amino acid metabolism is effective in simulating anti-tumor immune response (Ananieva, 2015; Sosnowska et al., 2021). Thus, we hypothesize that CCT3 may regulate amino acid metabolism to inhibit the functions of immune cells in COAD, contributing to immune escape.

We further explored the oncogenic roles of CCT3 in colon cancer by vitro assay. Here, we were the first study

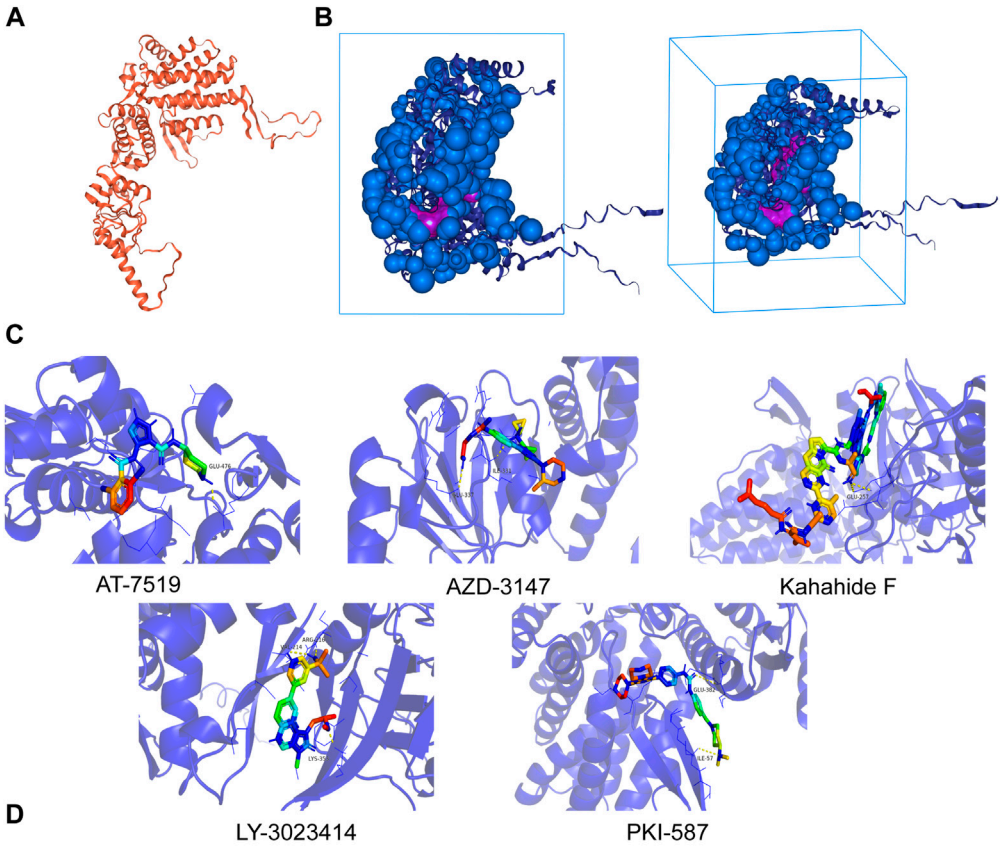

FIGURE 10
Predicting sensitive drugs for CCT3 protein. **(A)** Three-dimensional structure of CCT3 protein. **(B)** Predicted binding sites and box of CCT3 protein. **(C)** The interaction between sensitive drugs and CCT3 protein by PyMol software. **(D)** The two-dimensional structure of the interaction force between the compound (middle) and the amino acid residues of CCT3 protein (green dotted lines represents the hydrogen bonds).

to report that targeting CCT3 significantly inhibited colon cancer cells proliferation. GSEA analysis indicated that CCT3 promoted cell growth by means of regulating cell cycle, which was consist with the results in cervical cancer (Dou and Zhang, 2021). Previous studies elucidated that CCT3 promoted tumor cell proliferation by mediating YAP activity (Liu et al., 2019; Shi et al., 2022). Our functional enrichment analysis showed that CCT3 may be oncogenic by regulating multiple pathways such as AMPK and Hippo signaling pathway. All these data implied that CCT3 could be a new molecular target. Of course, more *in vivo* and vitro assays are needed to validate our conclusion. Subsequently, our study screened out sensitive drugs for CCT3 protein by sensitivity analysis and virtual screening. We obtained 5 drugs derived from the FDA-approved clinical trials, which provided a rationale for targeting CCT3. Among

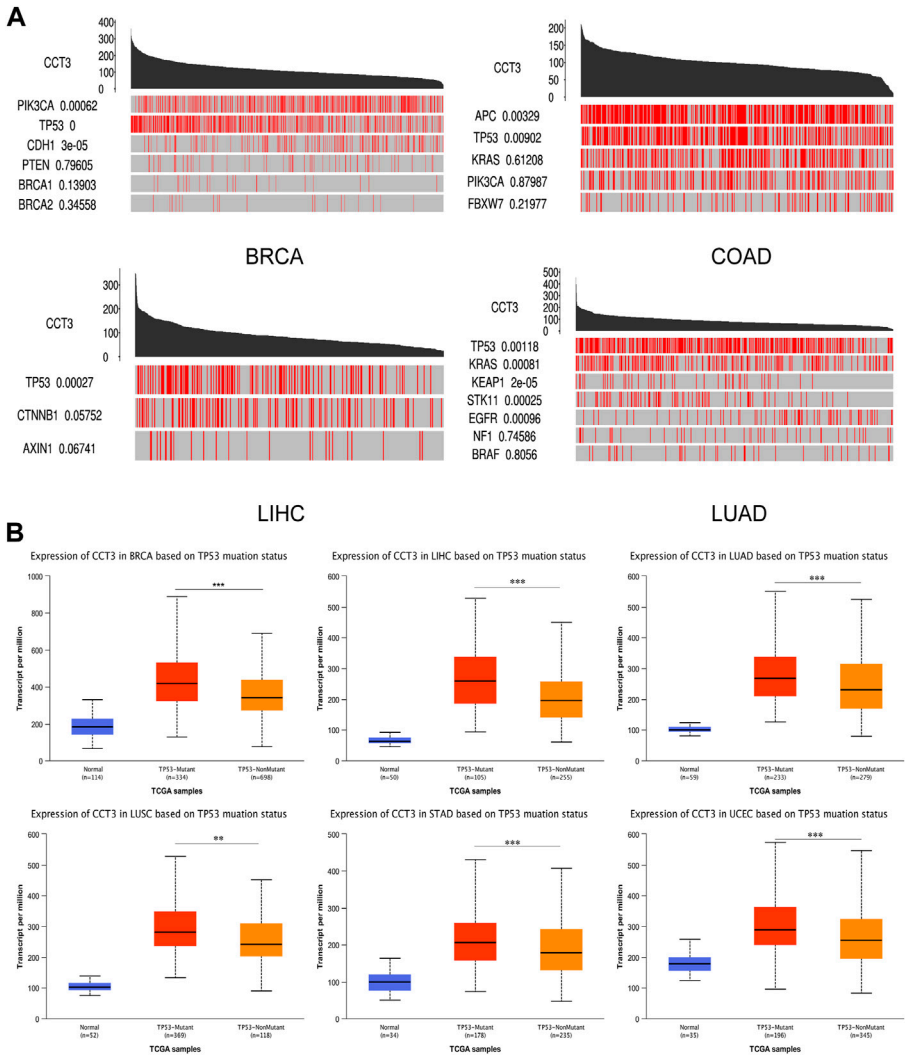

FIGURE 11
The effect of driver genes on CCT3 expression. **(A)** The correlation between CCT3 expression and driver genes in four cancers (BRCA, COAD, LIHC, LUAD) was analyzed using the TCGA portal database. **(B)** The correlation between CCT3 expression and TP53 mutation status was analyzed using the UALCAN database. *$p < 0.05$, **$p < 0.01$, ***$p < 0.001$.

them, AT-7519 has showed a therapeutic efficacy for non-small cell lung cancer patients with concurrent chemo-radiotherapy resistance (Liu et al., 2022b). And AT-7529 could be also noticed as potential drugs for HER2-positive breast cancer (Khanjani et al., 2021). PKI-587 enhanced chemosensitivity and radiosensitization of HCC by inhibiting PI3K/AKT/mTOR pathway (Zhang et al., 2019; Xie et al., 2021). Moreover, PKI-587 demonstrated anti-tumor activity in ovarian cancer xenograft models (Langdon et al., 2019). Whether these two drugs play their roles of anti-tumor by targeting CCT3? This needs further experiments to validate. However, there is still no research about the effect of AZD-3147, Kahahide F and LY-3023414 on cancers. The safety and effectiveness of these drugs needs to be further verified by *in vitro* and *in vivo* assays.

Meanwhile, we also investigated the regulatory mechanisms for CCT3 overexpression in tumors. We discovered that CCT3 mutation was seldom. However, many driver genes, TP53 in particular, were responsible for CCT3 overexpression. TP53 depressed tumor growth and promoted cell cycle arrest, apoptosis and senescence in response to diverse forms of cellular stress (Levine and Oren, 2009; Pope et al., 2021). Certainly, how mutant TP53 affected CCT3 expression needs further exploration. Besides, epigenetic factors were indispensable for CCT3 overexpression. The epigenetic factors contain DNA methylation, histone modification and non-coding RNA.

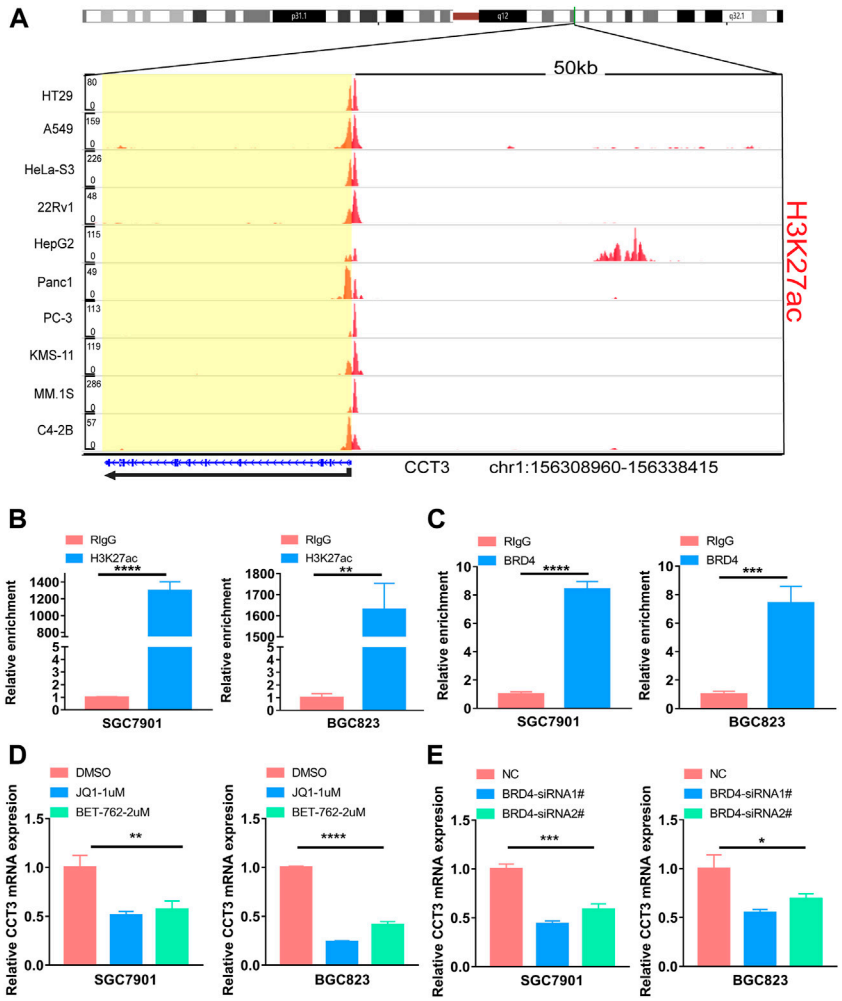

FIGURE 12
The effect of enhancers on CCT3 expression. **(A)** The H3K27ac signal of the CCT3 gene loci in different tumor cell lines was showed by WashU Epigenome Browser. **(B–C)** The relative enrichment levels of H3K27ac or BRD4 to CCT3 gene loci by ChIP-qPCR in gastric cancer cells. **(D–E)** The relative CCT3 expression after the treatment with enhancer inhibitors (JQ1 and I-BET-762) or BRD4 siRNAs.

Among them, histone acetylation, especially histone three lysine 27 acetylation (H3K27ac), has intrigued more attention. H3K27ac modification is used as the best marker to identify enhancers. Enhancers play important roles in controlling cellular states in human cancers, which provides novel therapeutic targets for cancer treatment (Ye et al., 2021). Unexpectedly, our study shed light on the effect of enhancers on CCT3 expression by a series of *in vitro* assays. Therefore, our research provided another proof for the crucial roles of enhancers in cancers. It is well known that miRNA can regulate gene expression by regulating the translation efficiency of mRNA, as well as its degradation (Guo et al., 2010). While lncRNA or circRNA could influence gene expression by acting as molecular "sponges" (Dai et al., 2015). Therefore, we predicted and constructed the lncRNA/circRNA-miRNA-CCT3 regulatory network. Similarly, Qu et al. discovered that CCT3 was a direct target of miR-223 (Qu et al., 2020). Interestingly, they also found CCT3 could regulate Wnt/β-catenin signaling pathway activity by miR-223. A positive regulatory loop may exist between CCT3 and miR-223 in breast cancer. Among the predicted lncRNA/circRNA, KCNQ1OT1 was involved in the regulation of tumor microenvironment in colon cancer by regulating CD155 expression (Lin et al., 2021b; Liu et al., 2021). Even exosome-derived KCNQ1OT1 could mediate immune escape by regulating PD-L1 ubiquitination in colon cancer (Xian et al., 2021). Of course, specific assays are needed to validate the regulatory relationship between KCNQ1OT1 and CCT3. The regulatory network could not only be used to explain the reasons for CCT3 overexpression, but also provide potential therapeutic

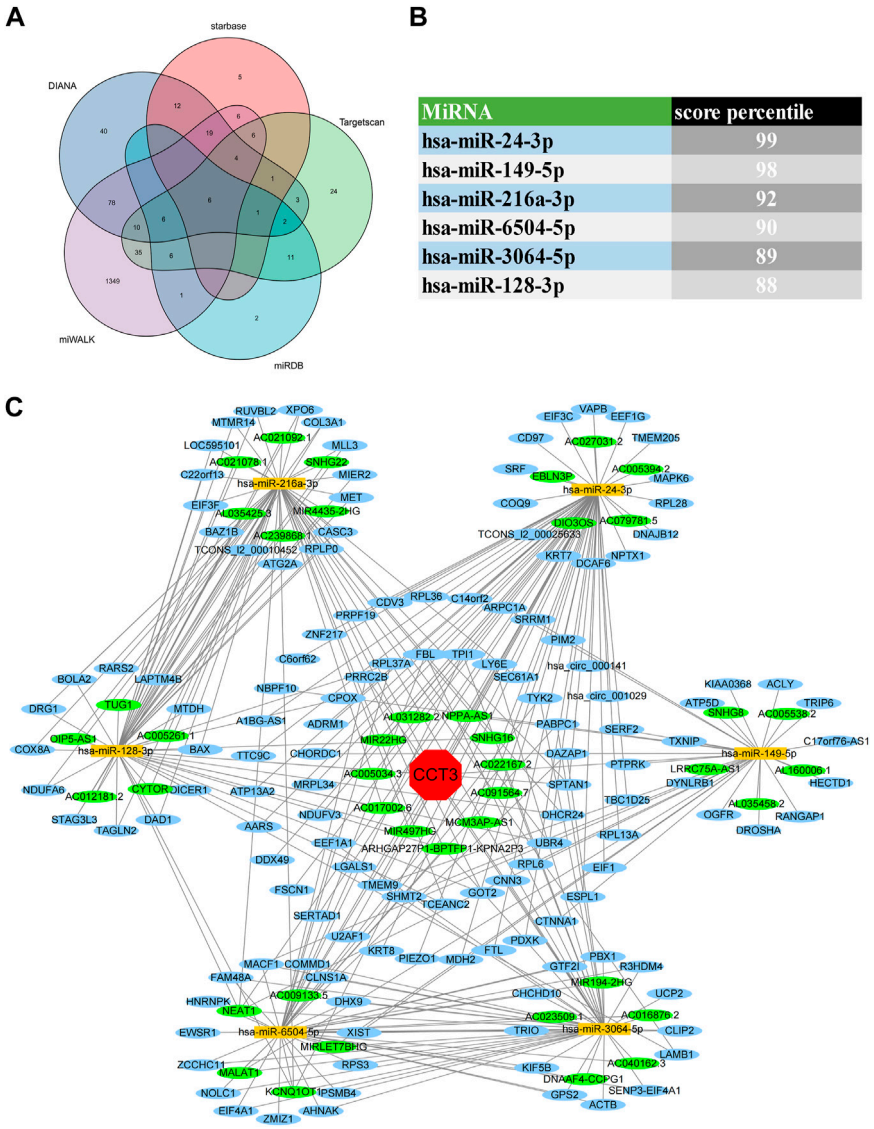

FIGURE 13
CeRNA regulatory network analysis for CCT3. **(A)** The Venn diagrams showed the predicted miRNAs complementary to CCT3 3′UTR region. **(B)** Targetscan database showed the score percentile of the predicted six miRNAs. **(C)** The ceRNA regulatory network for CCT3 was constructed by Cytoscape.

targets for tumors. In summary, CCT3 expression was subject to genetic and epigenetic factors in tumors. Our results revealed the oncogenic roles and driving forces of CCT3 in tumors, providing clues for the research of targeting CCT3 in human tumors.

Conclusion

CCT3 had the potential to be a diagnostic and prognostic biomarker for multiple tumor types. CCT3 expression was relevant with an immunosuppressive tumor microenvironment. CCT3 could be a new molecular target for colon cancer. Both genetic and epigenetic factors were responsible for CCT3 expression in tumors.

Data availability statement

The datasets presented in this study can be found in online repositories. The names of the repository/repositories and accession number(s) can be found in the article/Supplementary Material.

Author contributions

Conceptualization, JL; Methodology, JM, PS and XL; Software, JM and MZ; Validation, CM; Formal Analysis, XR; Investigation, RW; Writing–Original Draft Preparation, JM; Writing–Review and Editing, JL; Supervision, JL; Project Administration, JL, ZL and WL; Funding Acquisition, JL, XL.

Funding

This work was supported by the National Natural Science Foundation of China (81902404), the Natural Science Foundation of Shandong Province (ZR2019BH009, ZR2020QH096) and the Project of Shandong Province medical science technology development plan (2017WS403, 2019WS601).

Conflict of interest

The authors declare that the research was conducted in the absence of any commercial or financial relationships that could be construed as a potential conflict of interest.

Publisher's note

All claims expressed in this article are solely those of the authors and do not necessarily represent those of their affiliated organizations, or those of the publisher, the editors and the reviewers. Any product that may be evaluated in this article, or claim that may be made by its manufacturer, is not guaranteed or endorsed by the publisher.

Supplementary material

The Supplementary Material for this article can be found online at: https://www.frontiersin.org/articles/10.3389/fphar.2022.1005855/full#supplementary-material

References

Ananieva, E. (2015). Targeting amino acid metabolism in cancer growth and anti-tumor immune response. *World J. Biol. Chem.* 6 (4), 281–289. doi:10.4331/wjbc.v6.i4.281

Audia, J. E., and Campbell, R. M. (2016). Histone modifications and cancer. *Cold Spring Harb. Perspect. Biol.* 8 (4), a019521. doi:10.1101/cshperspect.a019521

Blum, A., Wang, P., and Zenklusen, J. C. (2018). SnapShot: TCGA-analyzed tumors. *Cell* 173 (2), 530. doi:10.1016/j.cell.2018.03.059

Boulos, J. C., Yousof Idres, M. R., and Efferth, T. (2020). Investigation of cancer drug resistance mechanisms by phosphoproteomics. *Pharmacol. Res.* 160, 105091. doi:10.1016/j.phrs.2020.105091

Cerami, E., Gao, J., Dogrusoz, U., Gross, B. E., Sumer, S. O., Aksoy, B. A., et al. (2012). The cBio cancer genomics portal: An open platform for exploring multidimensional cancer genomics data. *Cancer Discov.* 2 (5), 401–404. doi:10.1158/2159-8290.CD-12-0095

Chen, X., Song, M., Zhang, B., and Zhang, Y. (2016). Reactive oxygen species regulate T cell immune response in the tumor microenvironment. *Oxid. Med. Cell. Longev.* 2016, 1580967. doi:10.1155/2016/1580967

Chen, Y., and Wang, X. (2020). miRDB: an online database for prediction of functional microRNA targets. *Nucleic Acids Res.* 48 (D1), D127–D31. doi:10.1093/nar/gkz757

Clough, E., and Barrett, T. (2016). The gene expression Omnibus database. *Methods Mol. Biol.* 1418, 93–110. doi:10.1007/978-1-4939-3578-9_5

Cui, X., Hu, Z. P., Li, Z., Gao, P. J., and Zhu, J. Y. (2015). Overexpression of chaperonin containing TCP1, subunit 3 predicts poor prognosis in hepatocellular carcinoma. *World J. Gastroenterol.* 21 (28), 8588–8604. doi:10.3748/wjg.v21.i28.8588

Dai, Q., Li, J., Zhou, K., and Liang, T. (2015). Competing endogenous RNA: A novel posttranscriptional regulatory dimension associated with the progression of cancer. *Oncol. Lett.* 10 (5), 2683–2690. doi:10.3892/ol.2015.3698

Danni, X., Jiangzheng, Z., Huamao, S., Yinglian, P., Changcheng, Y., and Yanda, L. (2021). Chaperonin containing TCP1 subunit 3 (CCT3) promotes cisplatin resistance of lung adenocarcinoma cells through targeting the Janus kinase 2/signal transducers and activators of transcription 3 (JAK2/STAT3) pathway. *Bioengineered* 12 (1), 7335–7347. doi:10.1080/21655979.2021.1971030

Dong, Y., Lu, S., Wang, Z., and Liu, L. (2020). CCTs as new biomarkers for the prognosis of head and neck squamous cancer. *Open Med.* 15 (1), 672–688. doi:10.1515/med-2020-0114

Dou, L., and Zhang, X. (2021). Upregulation of CCT3 promotes cervical cancer progression through FN1. *Mol. Med. Rep.* 24 (6), 856. doi:10.3892/mmr.2021.12496

Dweep, H., and Gretz, N. (2015). miRWalk2.0: a comprehensive atlas of microRNA-target interactions. *Nat. Methods* 12 (8), 697. doi:10.1038/nmeth.3485

Esfahani, K., Roudaia, L., Buhlaiga, N., Del Rincon, S. V., Papneja, N., and Miller, W. H., Jr (2020). A review of cancer immunotherapy: From the past, to the present, to the future. *Curr. Oncol.* 27 (2), S87–S97. doi:10.3747/co.27.5223

Guo, H., Ingolia, N. T., Weissman, J. S., and Bartel, D. P. (2010). Mammalian microRNAs predominantly act to decrease target mRNA levels. *Nature* 466 (7308), 835–840. doi:10.1038/nature09267

Hou, W., Zhou, X., Yi, C., and Zhu, H. (2021). Immune check point inhibitors and immune-related adverse events in small cell lung cancer. *Front. Oncol.* 11, 604227. doi:10.3389/fonc.2021.604227

Kang, Y., Kim, Y. W., Kang, J., and Kim, A. (2021). Histone H3K4me1 and H3K27ac play roles in nucleosome eviction and eRNA transcription, respectively, at enhancers. *FASEB J.* 35 (8), e21781. doi:10.1096/fj.202100488R

Karlsson, M., Zhang, C., Mear, L., Zhong, W., Digre, A., Katona, B., et al. (2021). A single-cell type transcriptomics map of human tissues. *Sci. Adv.* 7 (31), eabh2169. doi:10.1126/sciadv.abh2169

Khanjani, F., Jafari, L., Azadiyan, S., Roozbehi, S., Moradian, C., Zahiri, J., et al. (2021). Drug repositioning based on gene expression data for human HER2-positive breast cancer. *Arch. Biochem. Biophys.* 712, 109043. doi:10.1016/j.abb.2021.109043

Lanczky, A., and Gyorffy, B. (2021). Web-based survival analysis tool tailored for medical research (KMplot): Development and implementation. *J. Med. Internet Res.* 23 (7), e27633. doi:10.2196/27633

Langdon, S. P., Kay, C., Um, I. H., Dodds, M., Muir, M., Sellar, G., et al. (2019). Evaluation of the dual mTOR/PI3K inhibitors Gedatolisib (PF-05212384) and PF-04691502 against ovarian cancer xenograft models. *Sci. Rep.* 9 (1), 18742. doi:10.1038/s41598-019-55096-9

Levine, A. J., and Oren, M. (2009). The first 30 years of p53: Growing ever more complex. *Nat. Rev. Cancer* 9 (10), 749–758. doi:10.1038/nrc2723

Li, C., Tang, Z., Zhang, W., Ye, Z., and Liu, F. (2021). GEPIA2021: Integrating multiple deconvolution-based analysis into GEPIA. *Nucleic Acids Res.* 49 (W1), W242–W246. doi:10.1093/nar/gkab418

Li, J., Song, P., Jiang, T., Dai, D., Wang, H., Sun, J., et al. (2018). Heat shock factor 1 epigenetically stimulates glutaminase-1-dependent mTOR activation to promote colorectal carcinogenesis. *Mol. Ther.* 26 (7), 1828–1839. doi:10.1016/j.ymthe.2018.04.014

Li, J. H., Liu, S., Zhou, H., Qu, L. H., and Yang, J. H. (2014). starBase v2.0: decoding miRNA-ceRNA, miRNA-ncRNA and protein-RNA interaction networks from large-scale CLIP-Seq data. *Nucleic Acids Res.* 42, D92–D97. doi:10.1093/nar/gkt1248

Li, L. C., and Dahiya, R. (2002). MethPrimer: Designing primers for methylation PCRs. *Bioinformatics* 18 (11), 1427–1431. doi:10.1093/bioinformatics/18.11.1427

Li, L. J., Zhang, L. S., Han, Z. J., He, Z. Y., Chen, H., and Li, Y. M. (2017). Chaperonin containing TCP-1 subunit 3 is critical for gastric cancer growth. *Oncotarget* 8 (67), 111470–111481. doi:10.18632/oncotarget.22838

Lin, X. D., Lin, N., Lin, T. T., Wu, Y. P., Huang, P., Ke, Z. B., et al. (2021). Identification of marker genes and cell subtypes in castration-resistant prostate cancer cells. *J. Cancer* 12 (4), 1249–1257. doi:10.7150/jca.49409

Lin, Z. B., Long, P., Zhao, Z., Zhang, Y. R., Chu, X. D., Zhao, X. X., et al. (2021). Long noncoding RNA KCNQ1OT1 is a prognostic biomarker and mediates CD8(+) T cell exhaustion by regulating CD155 expression in colorectal cancer. *Int. J. Biol. Sci.* 17 (7), 1757–1768. doi:10.7150/ijbs.59001

Liu, J., Lv, W., Li, S., and Deng, J. (2021). Regulation of long non-coding RNA KCNQ1OT1 network in colorectal cancer immunity. *Front. Genet.* 12, 684002. doi:10.3389/fgene.2021.684002

Liu, W., Zhang, X., Chen, C., Li, Y., Yang, C., Han, Z., et al. (2022). Suppression of CCT3 inhibits melanoma cell proliferation by downregulating CDK1 expression. *J. Cancer* 13 (6), 1958–1971. doi:10.7150/jca.69497

Liu, Y., Qi, H., Wang, C., Deng, J., Tan, Y., Lin, L., et al. (2022). Predicting chemo-radiotherapy sensitivity with concordant survival benefit in non-small cell lung cancer via computed tomography derived radiomic features. *Front. Oncol.* 12, 832343. doi:10.3389/fonc.2022.832343

Liu, Y., Zhang, X., Lin, J., Chen, Y., Qiao, Y., Guo, S., et al. (2019). CCT3 acts upstream of YAP and TFCP2 as a potential target and tumour biomarker in liver cancer. *Cell Death Dis.* 10 (9), 644. doi:10.1038/s41419-019-1894-5

Macario, A. J. L., and Conway de Macario, E. (2021). Chaperonins in cancer: Expression, function, and migration in extracellular vesicles. *Semin. Cancer Biol.* doi:10.1016/j.semcancer.2021.05.029

Manna, P. R., Ahmed, A. U., Yang, S., Narasimhan, M., Cohen-Tannoudji, J., Slominski, A. T., et al. (2019). Genomic profiling of the steroidogenic acute regulatory protein in breast cancer: *In silico* assessments and a mechanistic perspective. *Cancers (Basel)* 11 (5), 623. doi:10.3390/cancers11050623

McGeary, S. E., Lin, K. S., Shi, C. Y., Pham, T. M., Bisaria, N., Kelley, G. M., et al. (2019). The biochemical basis of microRNA targeting efficacy. *Science* 366 (6472), 366eaav1741. doi:10.1126/science.aav1741

Moore, L. D., Le, T., and Fan, G. (2013). DNA methylation and its basic function. *Neuropsychopharmacology* 38 (1), 23–38. doi:10.1038/npp.2012.112

Narayanan, A., Pullepu, D., and Kabir, M. A. (2016). The interactome of CCT complex - a computational analysis. *Comput. Biol. Chem.* 64, 396–402. doi:10.1016/j.compbiolchem.2016.09.002

Paraskevopoulou, M. D., Georgakilas, G., Kostoulas, N., Reczko, M., Maragkakis, M., Dalamagas, T. M., et al. (2013). DIANA-LncBase: Experimentally verified and computationally predicted microRNA targets on long non-coding RNAs. *Nucleic Acids Res.* 41 , D239–D245. doi:10.1093/nar/gks1246

Pope, B. J., Clendenning, M., Rosty, C., Mahmood, K., Georgeson, P., Joo, J. E., et al. (2021). Germline and tumor sequencing as a diagnostic tool to resolve suspected lynch syndrome. *J. Mol. Diagn.* 23 (3), 358–371. doi:10.1016/j.jmoldx.2020.12.003

Qu, H., Zhu, F., Dong, H., Hu, X., and Han, M. (2020). Upregulation of CCT-3 induces breast cancer cell proliferation through miR-223 competition and wnt/β-catenin signaling pathway activation. *Front. Oncol.* 10, 533176. doi:10.3389/fonc.2020.533176

Reinhold, W. C., Sunshine, M., Liu, H., Varma, S., Kohn, K. W., Morris, J., et al. (2012). CellMiner: A web-based suite of genomic and pharmacologic tools to explore transcript and drug patterns in the NCI-60 cell line set. *Cancer Res.* 72 (14), 3499–3511. doi:10.1158/0008-5472.CAN-12-1370

Ru, B., Wong, C. N., Tong, Y., Zhong, J. Y., Zhong, S. S. W., Wu, W. C., et al. (2019). Tisidb: An integrated repository portal for tumor-immune system interactions. *Bioinformatics* 35 (20), 4200–4202. doi:10.1093/bioinformatics/btz210

Sherman, B. T., Hao, M., Qiu, J., Jiao, X., Baseler, M. W., Lane, H. C., et al. (2022). David: A web server for functional enrichment analysis and functional annotation of gene lists (2021 update). *Nucleic Acids Res.* 50, W216–W221. doi:10.1093/nar/gkac194

Shi, H., Zhang, Y., Wang, Y., Fang, P., Liu, Y., and Li, W. (2022). Restraint of chaperonin containing T-complex protein-1 subunit 3 has antitumor roles in non-small cell lung cancer via affection of YAP1. *Toxicol. Appl. Phar acol.* 439, 115926. doi:10.1016/j.taap.2022.115926

Sondergaard, J. N., Sommerauer, C., Atanasoai, I., Hinte, L. C., Geng, K., Guiducci, G., et al. (2022). CCT3-LINC00326 axis regulates hepatocarcinogenic lipid metabolism. *Gut* 71 (10), 2081–2092. doi:10.1136/gutjnl-2021-325109

Song, P., Feng, L., Li, J., Dai, D., Zhu, L., Wang, C., et al. (2020). β-catenin represses miR455-3p to stimulate m6A modification of HSF1 mRNA and promote its translation in colorectal cancer. *Mol. Cancer* 19 (1), 129. doi:10.1186/s12943-020-01244-z

Sosnowska, A., Chlebowska-Tuz, J., Matryba, P., Pilch, Z., Greig, A., Wolny, A., et al. (2021). Inhibition of arginase modulates T-cell response in the tumor microenvironment of lung carcinoma. *Oncoimmunology* 10 (1), 1956143. doi:10.1080/2162402X.2021.1956143

Sternlicht, H., Farr, G. W., Sternlicht, M. L., Driscoll, J. K., Willison, K., and Yaffe, M. B. (1993). The t-complex polypeptide 1 complex is a chaperonin for tubulin and actin *in vivo*. *Proc. Natl. Acad. Sci. U. S. A.* 90 (20), 9422–9426. doi:10.1073/pnas.90.20.9422

Stoldt, V., Rademacher, F., Kehren, V., Ernst, J. F., Pearce, D. A., and Sherman, F. (1996). Review: The cct eukaryotic chaperonin subunits of *Saccharomyces cerevisiae* and other yeasts. *Yeast* 12 (6), 523–529. doi:10.1002/(SICI)1097-0061(199605)12:6%3C523::AID-YEA962%3E3.0.CO;2-C

Sun, D., Wang, J., Han, Y., Dong, X., Ge, J., Zheng, R., et al. (2021). Tisch: A comprehensive web resource enabling interactive single-cell transcriptome visualization of tumor microenvironment. *Nucleic Acids Res.* 49 (D1), D1420–D1430. doi:10.1093/nar/gkaa1020

Sung, H., Ferlay, J., Siegel, R. L., Laversanne, M., Soerjomataram, I., Jemal, A., et al. (2021). Global cancer statistics 2020: GLOBOCAN estimates of incidence and mortality worldwide for 36 cancers in 185 countries. *Ca. Cancer J. Clin.* 71 (3), 209–249. doi:10.3322/caac.21660

Szklarczyk, D., Gable, A. L., Lyon, D., Junge, A., Wyder, S., Huerta-Cepas, J., et al. (2019). STRING v11: Protein-protein association networks with increased coverage, supporting functional discovery in genome-wide experimental datasets. *Nucleic Acids Res.* 47 (D1), D607–D13. doi:10.1093/nar/gky1131

Temiz, E., Koyuncu, I., and Sahin, E. (2021). CCT3 suppression prompts apoptotic machinery through oxidative stress and energy deprivation in breast and prostate cancers. *Free Radic. Biol. Med.* 165, 88–99. doi:10.1016/j.freeradbiomed.2021.01.016

Uyanik, B., Goloudina, A. R., Akbarali, A., Grigorash, B. B., Petukhov, A. V., Singhal, S., et al. (2021). Inhibition of the DNA damage response phosphatase PPM1D reprograms neutrophils to enhance anti-tumor immune responses. *Nat. Commun.* 12 (1), 3622. doi:10.1038/s41467-021-23330-6

Valpuesta, J. M., Martin-Benito, J., Gomez-Puertas, P., Carrascosa, J. L., and Willison, K. R. (2002). Structure and function of a protein folding machine: The eukaryotic cytosolic chaperonin CCT. *FEBS Lett.* 529 (1), 11–16. doi:10.1016/s0014-5793(02)03180-0

Wang, Y., Liu, P., Zhang, Z., Wang, J., Cheng, Z., and Fan, C. (2021). Identification of CCT3 as a prognostic factor and correlates with cell survival and invasion of head and neck squamous cell carcinoma. *Biosci. Rep.* 41 (10), BSR20211137. doi:10.1042/BSR20211137

Warde-Farley, D., Donaldson, S. L., Comes, O., Zuberi, K., Badrawi, R., Chao, P., et al. (2010). The GeneMANIA prediction server: Biological network integration for gene prioritization and predicting gene function. *Nucleic Acids Res.* 38, W214–W220. Web Server issue). doi:10.1093/nar/gkq537

Willison, K. R. (2018). The substrate specificity of eukaryotic cytosolic chaperonin CCT. *Philos. Trans. R. Soc. Lond. B Biol. Sci.* 373, 37320170192. doi:10.1098/rstb.2017.0192

Xian, D., Niu, L., Zeng, J., and Wang, L. (2021). LncRNA KCNQ1OT1 secreted by tumor cell-derived exosomes mediates immune escape in colorectal cancer by regulating PD-L1 ubiquitination via MiR-30a-5p/USP22. *Front. Cell Dev. Biol.* 9, 653808. doi:10.3389/fcell.2021.653808

Xie, Y., Liu, C., Zhang, Y., Li, A., Sun, C., Li, R., et al. (2021). PKI-587 enhances radiosensitization of hepatocellular carcinoma by inhibiting the PI3K/AKT/mTOR pathways and DNA damage repair. *PLoS One* 16 (10), e0258817. doi:10.1371/journal.pone.0258817

Xiong, Y., Wei, Y., Gu, Y., Zhang, S., Lyu, J., Zhang, B., et al. (2017). DiseaseMeth version 2.0: A major expansion and update of the human disease methylation database. *Nucleic Acids Res.* 45 (D1), D888–D95. doi:10.1093/nar/gkw1123

Xu, G., Bu, S., Wang, X., Zhang, H., and Ge, H. (2020). Suppression of CCT3 inhibits the proliferation and migration in breast cancer cells. *Cancer Cell Int.* 20, 218. doi:10.1186/s12935-020-01314-8

Xu, S., Feng, Y., and Zhao, S. (2019). Proteins with evolutionarily hypervariable domains are associated with immune response and better survival of basal-like breast cancer patients. *Comput. Struct. Biotechnol. J.* 17, 430–440. doi:10.1016/j.csbj.2019.03.008

Ye, B., Fan, D., Xiong, W., Li, M., Yuan, J., Jiang, Q., et al. (2021). Oncogenic enhancers drive esophageal squamous cell carcinogenesis and metastasis. *Nat. Commun.* 12 (1), 4457. doi:10.1038/s41467-021-24813-2

Yoo, H. C., and Han, J. M. (2022). Amino acid metabolism in cancer drug resistance. *Cells* 11 (1), 140. doi:10.3390/cells11010140

Zhang, J., Wang, Z., Zhang, X., Dai, Z., Zhi-Peng, W., Yu, J., et al. (2022). Large-Scale single-cell and bulk sequencing analyses reveal the prognostic value and immune aspects of CD147 in pan-cancer. *Front. Immunol.* 13, 810471. doi:10.3389/fimmu.2022.810471

Zhang, Y., Xie, C., Li, A., Liu, X., Xing, Y., Shen, J., et al. (2019). PKI-587 enhances chemosensitivity of oxaliplatin in hepatocellular carcinoma through suppressing DNA damage repair pathway (NHEJ and HR) and PI3K/AKT/mTOR pathway. *Am. J. Transl. Res.* 11 (8), 5134–5149.

frontiers | Frontiers in Pharmacology

TYPE Review
PUBLISHED 14 October 2022
DOI 10.3389/fphar.2022.1019312

Check for updates

OPEN ACCESS

EDITED BY
Ting Wang,
Sichuan Cancer Hospital, China

REVIEWED BY
Shiv K. Sah-Teli,
University of Oulu, Finland
Jinhua Zhou,
The First Affiliated Hospital of Soochow University, China

*CORRESPONDENCE
Yongsheng Yang,
yyswxt@126.com
Ranji Cui,
cuiranji@jlu.edu.cn

SPECIALTY SECTION
This article was submitted to Pharmacology of Anti-Cancer Drugs, a section of the journal Frontiers in Pharmacology

RECEIVED 15 August 2022
ACCEPTED 23 September 2022
PUBLISHED 14 October 2022

CITATION
Fang H, Li H, Zhang H, Wang S, Xu S, Chang L, Yang Y and Cui R (2022), Short-chain L-3-hydroxyacyl-CoA dehydrogenase: A novel vital oncogene or tumor suppressor gene in cancers. *Front. Pharmacol.* 13:1019312. doi: 10.3389/fphar.2022.1019312

COPYRIGHT
© 2022 Fang, Li, Zhang, Wang, Xu, Chang, Yang and Cui. This is an open-access article distributed under the terms of the Creative Commons Attribution License (CC BY). The use, distribution or reproduction in other forums is permitted, provided the original author(s) and the copyright owner(s) are credited and that the original publication in this journal is cited, in accordance with accepted academic practice. No use, distribution or reproduction is permitted which does not comply with these terms.

Short-chain L-3-hydroxyacyl-CoA dehydrogenase: A novel vital oncogene or tumor suppressor gene in cancers

He Fang[1], Hanyang Li[2], Hang Zhang[1], Shu Wang[3], Shuang Xu[4], Li Chang[5], Yongsheng Yang[1]* and Ranji Cui[6]*

[1]Department of Hepatobiliary and Pancreatic Surgery, The Second Hospital of Jilin University, Changchun, China, [2]Department of Thyroid Surgery, The Second Hospital of Jilin University, Changchun, China, [3]Department of Radiotherapy, The Second Hospital of Jilin University, Changchun, China, [4]Department of Anesthesiology, The Second Hospital of Jilin University, Changchun, China, [5]Department of Pathology, The Second Hospital of Jilin University, Changchun, China, [6]Jilin Provincial Key Laboratory on Molecular and Chemical Genetic, The Second Hospital of Jilin University, Changchun, China

The reprogramming of cellular metabolism is frequently linked to tumorigenesis. Glucose, fatty acids, and amino acids are the specific substrates involved in how an organism maintains metabolic equilibrium. The *HADH* gene codes for the short-chain L-3-hydroxyacyl-CoA dehydrogenase (HADH), a crucial enzyme in fatty acid oxidation that catalyzes the third phase of fatty acid oxidation in mitochondria. Increasing data suggest that HADH is differentially expressed in various types of malignancies and is linked to cancer development and progression. The significance of HADH expression in tumors and its potential mechanisms of action in the onset and progression of certain cancers are summarized in this article. The possible roles of HADH as a target and/or biomarker for the detection and treatment of various malignancies is also described here.

KEYWORDS

HADH, oncogene, tumor suppressor gene, differential expression, tumor microenvironment, tumor-infiltrating immune cells

Abbreviations: HADH, short-chain-L-3-hydroxyacyl-CoA dehydrogenase; TME, tumor microenvironment; FAO, fatty acid oxidation; TIICs, tumor-infiltrating immune cells; PTEN, phosphatase and tensin homolog; AKT, serine threonine kinase; EMT, epithelial-mesenchymal transition; TNF- α, tumor necrosis factor-α; IL-6, interleukin 6; JAK, Janus kinase; STAT3, signal transducer and activator of transcription 3; ROR2, receptor tyrosine kinase like orphan receptor 2; Dvl2, disheveled segment polarity protein 2; ATF2, activating transcription factor 2; ATF4, activating transcription factor 4; GPX-7, glutathione peroxidase 7; Rpp40, ribonuclease p protein subunit p40; OS, overall survival; DFS, disease-free survival; HCC, hepatocellular carcinoma

1 Introduction

Cancer is a major public health problem worldwide and has been identified as the biggest obstacle to improving life expectancy in the 21st century, making it a continuous focus of scientific attention (Fitzgerald et al., 2021). Cancer remains one of the leading causes of death (Galván Morales et al., 2020), and by 2018, approximately more than 11 million people have been diagnosed with cancer (Wang et al., 2018). The American Cancer Society expects that number to increase further, with an estimated 1,918,030 new cases and 609,360 cancer-related deaths occurring in the United States in 2022 (Siegel et al., 2022). More than 4 million new cancer patients and more than 2 million cancer-related mortalities are reported every year in China. Although cancer is treated in a variety of ways, such as surgery, chemotherapy, radiation therapy, and targeted therapy, 3- and 5-year cancer-specific survival rates remain poor (Kim and Kim, 2015; Vijayvergia et al., 2015; Koinis et al., 2016; Miller et al., 2016; Nakashima, 2018; Zhang and Zhang, 2018; Wen et al., 2019). Despite cancer-related deaths having declined overall (Henley et al., 2020), it is important to note that this decrease is mainly a result of early detection and prevention rather than better treatments (Etzioni et al., 2003; Chabner et al., 2005; Huff et al., 2006; Buskwofie et al., 2020). The vast majority of cancers are asymptomatic in their early stages of development (Smith et al., 2007; Zheng et al., 2020). Therefore, it is very important to explore the mechanisms of tumorigenesis and development, search for new diagnostic and prognostic markers, and develop effective and novel therapeutic methods. Further advancements will have a major impact on improving cancer patient survival rates.

Numerous studies have strongly demonstrated that specific genes, such as oncogenes and tumor suppressor genes, are risk factors for certain malignancies (Khan et al., 2018; Elek et al., 2020; Shareefi et al., 2020; Vysotskaia et al., 2020; Xiong et al., 2020). Oncogenes can promote tumor growth when they are activated, whereas tumor suppressor genes hinder tumor growth and development. Oncogene-directed metabolic reprogramming (Ward and Thompson, 2012), which appears to be a common hallmark of highly malignant tumors (Hanahan and Weinberg, 2011) regardless of their carcinogenic origin (Bustamante et al., 1981), is the most prevalent cause of metabolic alterations.

The tumor microenvironment (TME) is involved with carcinogenesis in a complex manner and can influence cancer incidence and progression (Arneth, 2019). The non-malignant cells in the TME frequently play a key role in all phases of tumorigenesis by stimulating and promoting uncontrolled cell proliferation (Balkwill et al., 2012; Hanahan and Coussens, 2012). The extracellular matrix (ECM), blood vessels, fibroblasts, lymphocytes, signaling chemicals and bone marrow-derived inflammatory cells make up the TME (Spill et al., 2016; Del Prete et al., 2017). Immune cells, such as lymphocytes, macrophages, and granulocytes, are a very significant component and can impact the formation, growth, and development of tumor cells in patients with various forms of cancer (Mantovani et al., 2008; Grivennikov et al., 2010; Hanahan and Weinberg, 2011; Lebleu, 2015; Spill et al., 2016; Del Prete et al., 2017). The TME homeostasis is the result of numerous complex interactions, many of which involve cell metabolism (Nieman et al., 2011; Colegio et al., 2014; Chang et al., 2015; Sousa et al., 2016; Chen P. et al., 2017; Angelin et al., 2017; Buck et al., 2017; Bantug et al., 2018; Zhang et al., 2018; Vitale et al., 2019a; Vitale et al., 2019b). Under normal circumstances, an organism's metabolism is in equilibrium. The reprogramming of cellular metabolism is a hallmark of tumorigenesis (Hanahan and Weinberg, 2011; Wettersten et al., 2017) and aids in the conversion of large amounts of nutrients into cellular building blocks such as nucleotides, amino acids, and lipids (Ren et al., 2020), resulting in an excess of the antioxidant glutathione to produce new cells (Gao et al., 2009; Hirschhaeuser et al., 2011). Glucose, fatty acids, and amino acids are the substrates that keep metabolic homeostasis in check (Heslegrave and Hussain, 2013). Fatty acid metabolism is often altered in cancer cells to sustain cell proliferation, meet energy needs, and produce metabolites for anabolic activities (Currie et al., 2013; Sanchez and Simon, 2018). Several reports have shown that the enzymes involved in fatty acid β-oxidation are reduced in individuals with malignancies (Tanaka et al., 2013; Enjoji et al., 2016). β-oxidation in mitochondria breaks down fatty acids (Bartlett and Eaton, 2004), and this is a crucial metabolic process for energy balance in organs such the liver, heart, and skeletal muscle (Heslegrave and Hussain, 2013). Enoyl-CoA hydratase, acyl-CoA dehydrogenase, ketoacyl-CoA thiolase, and hydroxyacyl-CoA dehydrogenase are four main enzymes involved in the breakdown of fatty acids (Shen et al., 2017). The role of fatty acids in the breakdown of cancer cells, however, is still debated. Additional research is required to further understand how fatty acid metabolism reprogramming influences the formation and development of cancers.

The human HADH gene, which has 10 exons and is expressed in most tissues, is found on chromosome 4q25 (Heslegrave and Hussain, 2013). The gene encodes the intramitochondrial homodimer enzyme short-chain-L-3-hydroxyacyl-CoA dehydrogenase (HADH), which is a key enzyme in the third step of fatty acid β-oxidation (Vredendaal et al., 1996; Eaton et al., 2000; Yang et al., 2005; Kapoor et al., 2010; Schulz et al., 2011; Popa et al., 2012; Arya et al., 2014; Jiang et al., 2021). During extended fasting, HADH transforms short- and medium-chain fatty acids into ketones to fuel the liver, heart, muscles, and pancreas (Shen et al., 2017), with enzyme activity being highest in the pancreas and especially in the islets of Langerhans (Agren et al., 1977). Several investigations have shown that HADH plays an important role in controlling insulin secretion from the β-cell (Hardy et al., 2007; Martens et al., 2007; Filling et al., 2008; Li et al., 2010; Heslegrave et al.,

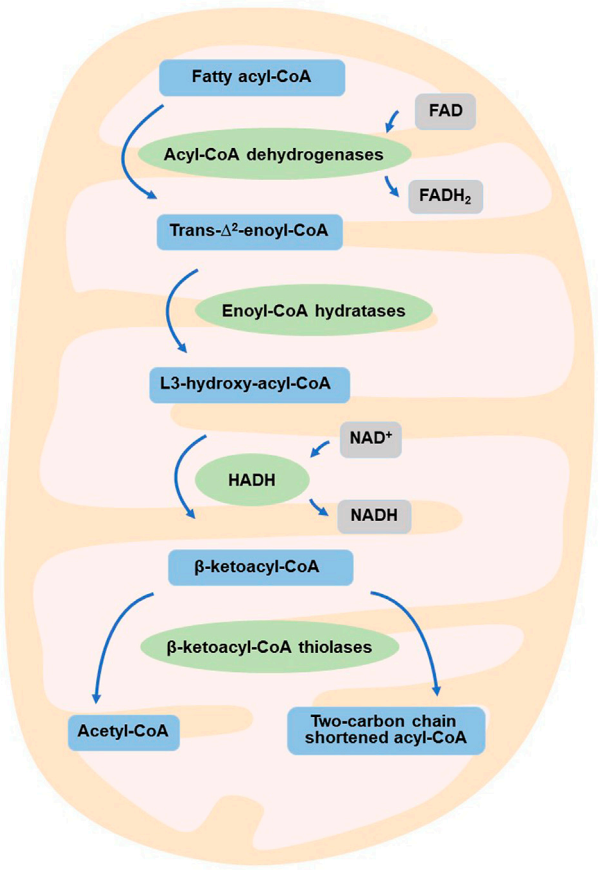

FIGURE 1
HADH is involved in fatty acid β-oxidation.

2012) and that inhibiting its activity results in a considerable increase in insulin secretion (Kapoor et al., 2009; Heslegrave et al., 2012; Heslegrave and Hussain, 2013).

Reprogramming of energy metabolism is a well-known feature of malignancies (Hanahan and Weinberg, 2011; Wettersten et al., 2017), and fatty acid metabolism is also thought to be a crucial contributor to cancer cell proliferation (Currie et al., 2013). HADH is a crucial enzyme in the oxidation of fatty acids (Flanagan et al., 2013; Babiker et al., 2015; Çamtosun et al., 2015; Satapathy et al., 2016; Boerrigter-Eenling et al., 2017). Dehydrogenation, hydration, dehydrogenation again, and thiolytic cleavage are the four enzymatic processes that make up fatty acid oxidation (FAO) (Wanders et al., 1999). HADH is a component of the enzymatic reaction mentioned above (Houten and Wanders, 2010). In the mitochondrial matrix, HADH catalyzes the penultimate process in the β-oxidation of fatty acids (Vredendaal et al., 1998), dehydroxylating medium- and short-chain NAD^+-dependent L3-hydroxy-acyl-CoA to produce β-ketoacyl-CoA and NADH, respectively (Figure 1) (Houten et al., 2016). The expression levels of HADH are also higher than those of other fatty acid β oxidases, such as acyl-CoA dehydrogenase and acetyl-CoA acyltransferase 2. Additionally, HADH enzymatic activity is the most effective for metabolizing medium-chain length fatty acids (Pepin et al., 2010). Reduced HADH expression can impede β-oxidation and stimulate fatty acid buildup, which leads to fatty acid metabolism reprogramming and promotes tumor development (Wettersten et al., 2017). Growing evidence has recently shown its importance in the occurrence and progression of several malignancies (Shen et al., 2017; Wilkins et al., 2017; Nwosu et al., 2018; Voloshanenko et al., 2018; Ren et al., 2020; Jiang et al., 2021; Sun et al., 2022). HADH has been identified as a possible target for the diagnosis and therapeutic treatment of many malignancies because of this apparent influence on carcinogenesis (Figure 2). The specific functions and molecular details of HADH in the incidence and progression of various cancers are summarized in this article, with an emphasis on gastric cancer, kidney renal clear cell carcinoma, liver cancer, colon cancer, and acute myeloid leukemia.

2 Short-chain L-3-hydroxyacyl-CoA dehydrogenase in cancers

HADH expression is upregulated or downregulated in different types of cancers, including gastric cancer, kidney renal clear cell carcinoma, liver cancer, colon cancer, and acute myeloid leukemia. The relevant clinicopathological features and molecular mechanisms of HADH in these cancers are summarized in Table 1 and detailed in the rest of this section.

2.1 Gastric cancer

2.1.1 Functional characteristics and clinical features of short-chain L-3-hydroxyacyl-CoA dehydrogenase in gastric cancer

HADH is expressed at lower levels in gastric cancer tissues compared with that in normal gastric tissues. Shen et al. (2017) showed that downregulation of HADH was significantly correlated with advanced clinical stage, low overall survival (OS), low disease-free survival (DFS), and poor clinical prognosis. Hence, HADH expression has been proposed as an independent prognostic factor that affects patient survival rates. Mechanistically, reduced HADH expression significantly promoted cell proliferation and increased migration and invasion of tumor cells *in vitro*; in contrast, overexpression of HADH inhibited the proliferation of gastric cancer cells (Shen et al., 2017).

In summary, HADH is a potential novel tumor suppressor gene in gastric cancer that can inhibit cell proliferation, migration, and invasion of gastric cancer cells. Furthermore, its expression levels are correlated with cancer progression and patient survival.

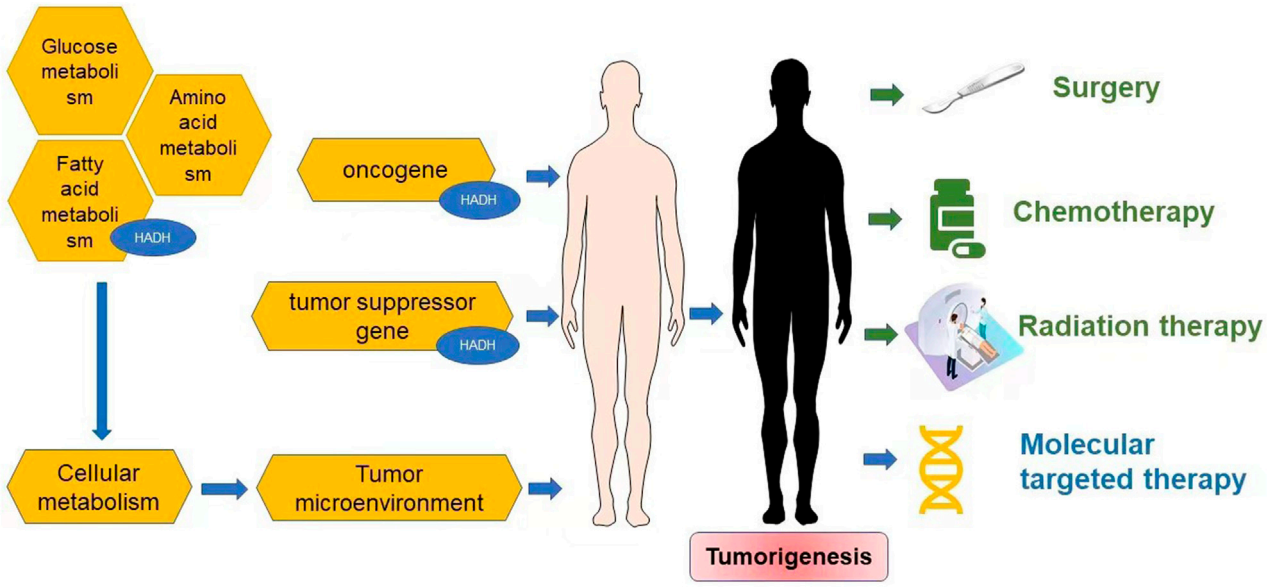

FIGURE 2
Cancer progression and therapy.

TABLE 1 Functional characteristics and clinical features of HADH in human cancers.

Cancer types	Expression	Role	Functional role	Related genes	Clinical features	References
Gastric cancer	Downregulated	Tumor suppressor gene	Inhibits proliferation, migration, and invasion	PTEN, AKT	Early clinical stage, long OS and DFS, and good clinical prognosis	(Shen et al., 2017; Du et al., 2021)
Kidney renal clear cell carcinoma	Downregulated	Tumor suppressor gene	No studies have been reported	genes in EMT, TNF- α, IL-6-JAK-STAT3, and interferon-γ signaling pathway	Early clinical stage, low histologic grade, long OS and DFS, low distant metastasis, good prognosis, and immune infiltration	(Zhang et al., 2019; Jiang et al., 2021; Sun et al., 2022)
Liver cancer	Downregulated	Tumor suppressor gene	No studies have been reported	No studies have been reported	No studies have been reported	Nwosu et al. (2018)
Colon cancer	Upregulated	Oncogene	Promotes proliferation	Wnt5a/b, Evi/Wls, RoR2, Dvl2, ATF2 and ATF4	Poor clinical outcome	(Voloshanenko et al., 2018; Ren et al., 2020)
Acute myeloid leukemia	Upregulated	Oncogene	No studies have been reported	GPX-7 and RPP40	Poor OS	Wei et al. (2020)

PTEN, phosphatase and tensin homolog; AKT, serine threonine kinase; EMT, epithelial-mesenchymal transition; TNF- α, tumor necrosis factor- α; IL-6, interleukin 6; JAK, janus kinase; STAT3, signal transducer and activator of transcription 3; ROR2, receptor tyrosine kinase like orphan receptor 2; Dvl2, disheveled segment polarity protein 2; ATF2, activating transcription factor 2; ATF4, activating transcription factor 4; GPX-7, glutathione peroxidase 7; Rpp40, ribonuclease *p* protein subunit p40; OS, overall survival; DFS, disease-free survival.

2.1.2 Signaling pathways influenced by short-chain L-3-hydroxyacyl-CoA dehydrogenase in gastric cancer

The AKT signaling pathway is required for HADH to regulate cell proliferation, migration, and invasion, according to Shen et al. (Shen et al., 2017). AKT signaling is a growth-regulating biological pathway that has been shown to improve tumor cell survival, proliferation, and motility in a variety of tumor types (Chan et al., 2014; Bao et al., 2021; Junaid et al., 2021; Tsai et al., 2021). AKT, also known as protein kinase B (PKB), is a critical node in many signaling pathways, as well as one of the most essential and flexible protein kinases in human physiology and illness (Meier and Hemmings, 1999; Manning and Cantley, 2007; Revathidevi and Munirajan, 2019). Many interesting advancements in the mechanism controlling AKT activity have been achieved since its identification as an oncogene homologue of murine leukemia virus AKT8 (Staal, 1987; Bellacosa et al., 1991) and protein kinase C (Jones et al.,

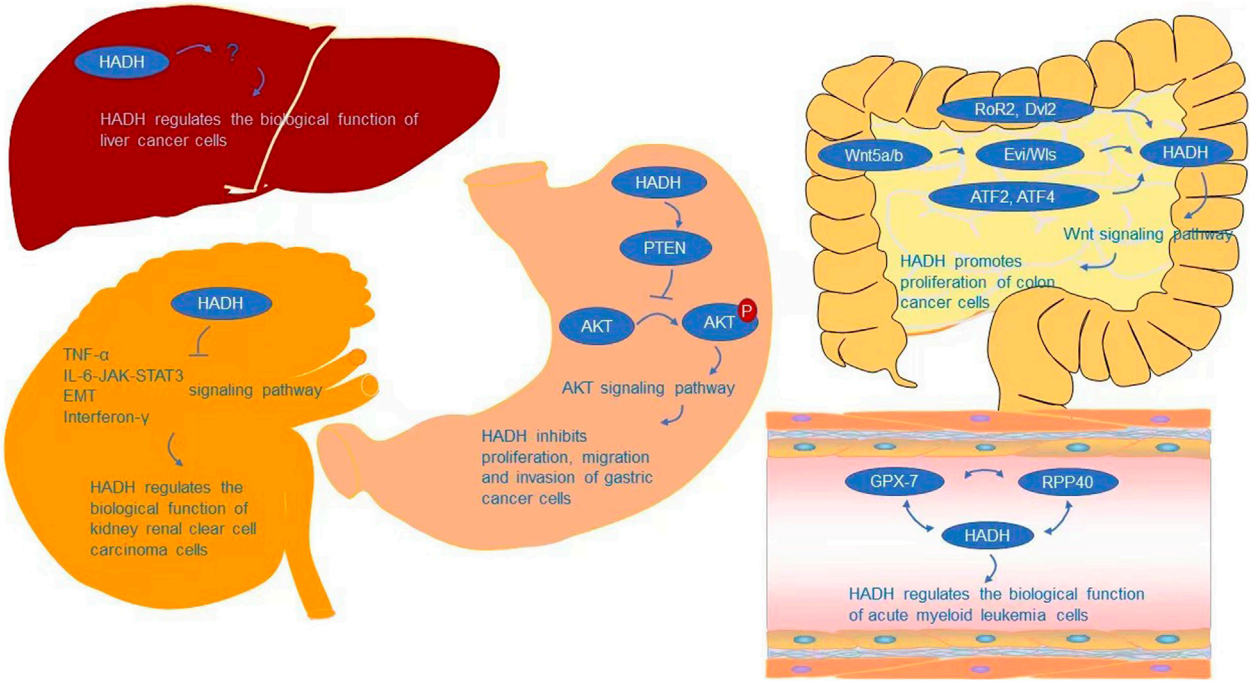

FIGURE 3
Underlying molecular mechanisms of HADH in cancers.

1991). As a critical regulatory protein of cell growth, survival, proliferation, and metabolism (Kennedy et al., 1997; Sun et al., 2001; Vivanco and Sawyers, 2002; Bellacosa et al., 2005; Manning and Cantley, 2007; Broustas et al., 2012; Sanidas et al., 2014; Fan et al., 2018; Li et al., 2021), AKT crosses multiple signaling pathways (Gao and Pan, 2001; Ward et al., 2011; Yecies et al., 2011; Yin et al., 2017) and participates in a range of physiological activities. AKT is involved in the development of a variety of human malignancies (Manning and Cantley, 2007; Revathidevi and Munirajan, 2019). AKT gene mutations are uncommon, while AKT gene amplification and overexpression are widespread in malignancies such as gastric, colon, liver, thyroid, and ovarian tumors (Staal, 1987; Bellacosa et al., 1995; Cheng et al., 1996; Nakatani et al., 1999; Roy et al., 2002; Knobbe and Reifenberger, 2003; Xu et al., 2004; Altomare and Testa, 2005; Parsons et al., 2005; Carpten et al., 2007; Malanga et al., 2008; Mohamedali et al., 2008; Shoji et al., 2009; Zilberman et al., 2009; Askham et al., 2010; Mundi et al., 2016; Manning and Toker, 2017). Overexpression and activation of AKT have been linked to the initiation or progression of a number of human malignancies (Samuels et al., 2004; Cully et al., 2006; Cerami et al., 2012; Fruman and Rommel, 2014). AKT has a role in several physiological processes and, once activated, can affect the activity of several downstream proteins that control cell growth, survival, proliferation, and metabolism (Kennedy et al., 1997; Sun et al., 2001; Vivanco and Sawyers, 2002; Bellacosa et al., 2005; Hay, 2005; Manning and Cantley, 2007; Broustas et al., 2012; Sanidas et al., 2014; Liu H. W. et al., 2018; Fan et al., 2018). An abnormal loss or increase of AKT activation underpins the pathogenesis of a variety of complicated illnesses, including type 2 diabetes and cancers (Manning and Cantley, 2007). AKT also affects cell survival by phosphorylating and activating a number of oncoproteins implicated in cell cycle progression and carcinogenesis, including murine double minute (MDM2), S-phase kinase-associated protein 2 (Skp2), IKKα, and E3 ligase (Datta et al., 1999; Ozes et al., 1999; Mayo and Donner, 2001; Zhou et al., 2001; Chan et al., 2012; Chan et al., 2014). PTEN is a tumor suppressor that causes a significant reduction in cell proliferation by arresting the cell cycle in the G1 phase. PTEN and PHLPP2 are the most important negative regulators of AKT (Stambolic et al., 1998; Meng et al., 2007). Therefore, PTEN inactivation can potentially activate AKT by promoting AKT's phosphorylation ability, leading to a cell survival advantage and uncontrolled cell proliferation (Downward, 2003; Gomes et al., 2014; Liu J. et al., 2018). Shen et al. (Shen et al., 2017) showed that downregulation of HADH could inhibit the expression of PTEN and promote the phosphorylation of AKT, further stimulating the proliferation, migration, and invasion of gastric cancer cells by activating the AKT pathway (Figure 3).

2.2 Kidney renal clear cell carcinoma

2.2.1 Functional characteristics and clinical features of short-chain L-3-hydroxyacyl-CoA dehydrogenase in kidney renal clear cell carcinoma

Similar to gastric cancer tissues, HADH expression was markedly downregulated in kidney renal clear cell carcinoma tissues compared with that in adjacent non-cancerous tissues (Zhang et al., 2019; Jiang et al., 2021; Sun et al., 2022). Additionally, similarly to gastric cancer, HADH downregulation was significantly associated with poor OS, DFS, and poor prognosis in kidney renal clear cell carcinoma (Zhang et al., 2019; Jiang et al., 2021; Sun et al., 2022). It was positively correlated with the early clinical stage of disease and low histologic grade (Jiang et al., 2021; Sun et al., 2022). Moreover, HADH expression was also associated with tumor-infiltrating immune cells (TIICs) in kidney renal clear cell carcinoma (Jiang et al., 2021). Levels of M2 macrophages, naïve B cells, resting mast cells, and resting dendritic cells were positively correlated with HADH expression, while amounts of follicular helper T cells, plasma cells, regulatory T cells (Tregs), and neutrophils were negatively correlated with HADH expression (Jiang et al., 2021). These results suggest that HADH has an important role in the regulation of the immune microenvironment in kidney renal clear cell carcinoma.

In conclusion, HADH may be a novel tumor suppressor gene in kidney renal clear cell carcinoma, and its reduced expression is associated with immune cell infiltration and poor prognosis.

2.2.2 Signaling pathways influenced by short-chain L-3-hydroxyacyl-CoA dehydrogenase in kidney renal clear cell carcinoma

Analyses of biological processes have indicated that HADH is associated with cell cycle arrest and negative regulation of the cell cycle (Zhang et al., 2019). Jiang et al. (2021) further analyzed this using GSEA, finding that the inflammatory response, TNF-α, IL-6-JAK-STAT3, epithelial-mesenchymal transition (EMT), and interferon-γ signaling pathways were activated in the HADH-low expression group, while fatty acid metabolism and protein secretion were inhibited (Figure 3). However, the specific molecular mechanism of how HADH can inhibit kidney renal clear cell carcinoma progression requires further study.

2.3 Liver cancer

Nwosu et al. (2018) found that HADH involved in fatty acid β-oxidation was expressed at lower levels in poorly differentiated hepatocellular carcinoma (HCC) cells compared with that in well differentiated HCC cells. However, whether the higher proliferation and migration rates of these poorly differentiated HCC cells are directly related to metabolic changes, including fatty acid β-oxidation, is still unknown. Further research is needed on the biological function of HADH and its signaling pathways in HCC (Figure 3).

2.4 Colon cancer

2.4.1 Functional characteristics and clinical features of short-chain L-3-hydroxyacyl-CoA dehydrogenase in colon cancer

Unlike gastric, kidney, and liver cancers, HADH is highly expressed in colon cancer cells (Ren et al., 2020). High HADH levels can promote colon cancer cell proliferation and are significantly associated with poor clinical outcomes (Voloshanenko et al., 2018; Ren et al., 2020). Thus, HADH potentially functions as an oncogene in colon cancer.

2.4.2 Signaling pathways influenced by short-chain L-3-hydroxyacyl-CoA dehydrogenase in colon cancer

In colon cancer cells, the Wnt signaling pathway is required for HADH-mediated regulation of cell proliferation (Voloshanenko et al., 2018). Wnt signaling is involved in a variety of events throughout embryonic development and tissue homeostasis, and has also been linked to cancer (Mao et al., 2014; Kahn, 2014; Morin et al., 1997; Clevers and Nusse, 2012; Roelink et al., 1992; Clements et al., 2002; van't Veer et al., 1984; Cleary et al., 2014). β-catenin-dependent (canonical) and independent (non-canonical) signaling are two types of Wnt signaling (Zhan et al., 2017). Multiple intracellular signal cascades can be triggered by Wnt ligands, which can orchestrate complicated context-dependent responses. With the aid of Porcupine (Porcn) and Evi/Wls/GRP177, cells can release Wnt ligands in an autocrine or paracrine manner (Kadowaki et al., 1996; Herr and Basler, 2012). Wnt5a/b has been demonstrated to regulate HADH expression, with HADH relying on Evi/Wls secretion to act on the β-catenin-independent Wnt signaling pathway for regulation of colon cancer cell growth and proliferation (Voloshanenko et al., 2018). Dvl2 and RoR2 are also involved in the regulation of HADH, which is consistent with existing knowledge of the participation of RoR2/Dvl2 in β-catenin-independent Wnt signaling (Boutros et al., 1998; Nishita et al., 2010; Ishida-Takagishi et al., 2012) (Figure 3). ATF2 and ATF4 transcription factors are also involved in regulating HADH.

2.5 Acute myeloid leukemia

2.5.1 Functional characteristics and clinical features of short-chain L-3-hydroxyacyl-CoA dehydrogenase in acute myeloid leukemia

Similar to colon cancer tissues, HADH expression was markedly upregulated in acute myeloid leukemia patient

samples. Wei et al. showed that HADH upregulation was significantly associated with poor OS (Wei et al., 2020).

2.5.2 Signaling pathways influenced by short-chain L-3-hydroxyacyl-CoA dehydrogenase in acute myeloid leukemia

Glutathione peroxidases (GPXs) are peroxidase enzymes that reduce lipid hydroperoxide and free hydrogen peroxide levels to protect organisms from oxidative damage (Takebe et al., 2002). In mammals, eight GPX sub-members have been discovered (Margis et al., 2008), which have been reported to play key roles in repairing reactive oxygen species (ROS)-induced damage, shielding DNA, proteins, and lipids from oxidative damage (Brigelius-Flohé and Maiorino, 2013), and carcinogenesis (Peng et al., 2014; Yang et al., 2014; Nalkiran et al., 2015; Chen Z. et al., 2017; Hangauer et al., 2017; Jiao et al., 2017; Liu et al., 2017; Viswanathan et al., 2017; An et al., 2018; Metere et al., 2018; Naiki et al., 2018; Zhu et al., 2018; Zhou et al., 2019a; Zhou et al., 2019b; Cai et al., 2019; Cheng et al., 2019; Lin et al., 2019; Wang et al., 2019; Yi et al., 2019; Li et al., 2020). Wei et al. discovered that HADH expression was linked to GPX-7 and RPP40 (Figure 3). However, the precise molecular mechanism by which HADH acts in acute myeloid leukemia is unknown, and more research is needed.

3 Conclusion and future perspectives

Around the world, cancer incidence and mortality are quickly rising. High-throughput gene expression profiling technologies allow for the simultaneous screening of expression levels of thousands of genes. Identifying variations in gene expression patterns between tumor and control samples is one of the key goals of gene expression profiling in cancer (Feten et al., 2007). Technological advancements and less expensive DNA sequencing procedures have fueled global efforts to identify relevant differentially expressed genes. In various human cancers, including gastric cancer, kidney renal clear cell carcinoma, liver cancer, colon cancer, and acute myeloid leukemia, the recently discovered gene HADH was found to be widely elevated or downregulated depending on the disease. Extensive therapeutics that target HADH have yet to be produced, leading to potential future developments. Multiple clinicopathological characteristics and patient prognoses were significantly associated with HADH expression levels, including clinical stage, histologic grade, immune cell infiltration, OS, DFS, and distant metastases. *In vitro* investigations have demonstrated that HADH can influence tumor cell proliferation, migration, and invasion rates in numerous malignancies, supporting its role in carcinogenesis and tumor progression. Preliminary findings reveal that HADH can impact multiple signaling pathways that promote carcinogenesis and cancer progression, including AKT, Wnt, EMT, TNF-α, IL-6-JAK-STAT3, and interferon signaling pathways.

Although HADH is a potential therapeutic target, several questions still remain to be addressed. Firstly, the molecular mechanisms of HADH in different types of cancers are not completely understood. Previous studies have suggested that HADH serves as a tumor suppressor gene in gastric cancer, kidney renal clear cell carcinoma, and liver cancer by inhibiting cell proliferation, migration, and invasion, as well as being associated with cancer progression and patient survival. However, it can also exist as an oncogene in colon cancer and acute myeloid leukemia, where it promotes cell proliferation and is associated with poor patient outcomes. Pathway analyses of HADH activity have only been conducted in kidney renal clear cell carcinoma, liver cancer, colon cancer, and acute myeloid leukemia, but the specific molecular mechanisms were not explained in detail. Furthermore, while the functions of HADH in gastric cancer, kidney renal clear cell carcinoma, liver cancer, colon cancer, and acute myeloid leukemia have been studied to some extent, its potential role in other cancers, such as cancers associated with the respiratory and reproductive systems, remain unexplored. Secondly, the search for diagnostic biomarkers or therapeutic targets is a promising direction for cancer diagnosis and treatment. HADH can be upregulated or downregulated in certain tumor tissues, but it is currently not known if HADH is also upregulated or downregulated in body fluids such as urine and plasma. Next, we will focus on whether the levels of upstream and downstream factors in the HADH pathway are changed in urine and serum, as well as further analyze whether expression of HADH itself changes in these body fluids. If HADH is detected in urine or plasma, a simple non-invasive test can possibly be performed to use HADH as a cancer-specific molecular biomarker to facilitate early detection and prognostic assessment of specific cancers. Thirdly, whether HADH can play a role in cancer diagnosis as a tumor-associated antigen is still unknown and requires further evaluation. Lastly, HADH is an immune system-associated gene, but whether it can play a role in clinical trials and individualized treatment of various immune modulators remains to be seen. Therefore, more attention should be paid to the clinical value of HADH in cancer diagnosis and treatment.

In summary, various studies have shown that HADH can have oncogenic or tumor suppressive functions in cancer development and progression and may serve as a potential cancer-specific molecular biomarker in the diagnosis, treatment, and prognosis of different types of cancers. Some progress has been made in studying the mechanism of HADH, but this work is currently in early stages. Future investigations should focus on exploring the precise molecular mechanism of

how HADH is regulated in carcinogenesis and tumor progression to support its potential clinical application.

Author contributions

HF and YY contributed to the conception and design of the review. HF wrote the first draft of the manuscript. YY revised the manuscript. All authors contributed to the article and approved the submitted version.

Funding

This work was supported by Jilin Province Financial and Health Project (Research on the mechanism of Mir-23A-27A-24-2 cluster promoting invasion and metastasis of hepatocellular carcinoma by regulating WNT signaling pathway, 2018GDYYZ001); Jilin Province Medical and Health Talent Special Project (Application of ICG fluorescence imaging combined with intraoperative ultrasound in laparoscopic precision hepatectomy, 2019SCZT009).

Acknowledgments

We want to thank colleagues for their critical discussion regarding this manuscript.

Conflict of interest

The authors declare that the research was conducted in the absence of any commercial or financial relationships that could be construed as a potential conflict of interest.

Publisher's note

All claims expressed in this article are solely those of the authors and do not necessarily represent those of their affiliated organizations, or those of the publisher, the editors and the reviewers. Any product that may be evaluated in this article, or claim that may be made by its manufacturer, is not guaranteed or endorsed by the publisher.

References

Agren, A., Borg, K., Brolin, S. E., Carlman, J., and Lundqvist, G. (1977). Hydroxyacyl CoA dehydrogenase, an enzyme important in fat metabolism in different cell types in the islets of Langerhans. *Diabete Metab.* 3, 169–172.

Altomare, D. A., and Testa, J. R. (2005). Perturbations of the AKT signaling pathway in human cancer. *Oncogene* 24, 7455–7464. doi:10.1038/sj.onc.1209085

An, B. C., Choi, Y. D., Oh, I. J., Kim, J. H., Park, J. I., and Lee, S. W. (2018). GPx3-mediated redox signaling arrests the cell cycle and acts as a tumor suppressor in lung cancer cell lines. *PLoS One* 13, e0204170. doi:10.1371/journal.pone.0204170

Angelin, A., Gil-De-GóMEZ, L., Dahiya, S., Jiao, J., Guo, L., Levine, M. H., et al. (2017). Foxp3 reprograms T cell metabolism to function in low-glucose, high-lactate environments. *Cell Metab.* 25, 1282–1293. e7. doi:10.1016/j.cmet.2016.12.018

Arneth, B. (2019). *Tumor microenvironment*. Medicina (Kaunas), 56.

Arya, V. B., Mohammed, Z., Blankenstein, O., De Lonlay, P., and Hussain, K. (2014). Hyperinsulinaemic hypoglycaemia. *Horm. Metab. Res.* 46, 157–170. doi:10.1055/s-0034-1367063

Askham, J. M., Platt, F., Chambers, P. A., Snowden, H., Taylor, C. F., and Knowles, M. A. (2010). AKT1 mutations in bladder cancer: Identification of a novel oncogenic mutation that can co-operate with E17K. *Oncogene* 29, 150–155. doi:10.1038/onc.2009.315

Babiker, O., Flanagan, S. E., Ellard, S., Al Girim, H., Hussain, K., and Senniappan, S. (2015). Protein-induced hyperinsulinaemic hypoglycaemia due to a homozygous HADH mutation in three siblings of a Saudi family. *J. Pediatr. Endocrinol. Metab.* 28, 1073–1077. doi:10.1515/jpem-2015-0033

Balkwill, F. R., Capasso, M., and Hagemann, T. (2012). The tumor microenvironment at a glance. *J. Cell Sci.* 125, 5591–5596. doi:10.1242/jcs.116392

Bantug, G. R., Galluzzi, L., Kroemer, G., and Hess, C. (2018). The spectrum of T cell metabolism in health and disease. *Nat. Rev. Immunol.* 18, 19–34. doi:10.1038/nri.2017.99

Bao, F., Hao, P., An, S., Yang, Y., Liu, Y., Hao, Q., et al. (2021). Akt scaffold proteins: The key to controlling specificity of akt signaling. *Am. J. Physiol. Cell Physiol.* 321, C429–c442. doi:10.1152/ajpcell.00146.2020

Bartlett, K., and Eaton, S. (2004). Mitochondrial beta-oxidation. *Eur. J. Biochem.* 271, 462–469. doi:10.1046/j.1432-1033.2003.03947.x

Bellacosa, A., Testa, J. R., Staal, S. P., and Tsichlis, P. N. (1991). A retroviral oncogene, akt, encoding a serine-threonine kinase containing an SH2-like region. *Science* 254, 274–277. doi:10.1126/science.1833819

Bellacosa, A., De Feo, D., Godwin, A. K., Bell, D. W., Cheng, J. Q., Altomare, D. A., et al. (1995). Molecular alterations of the AKT2 oncogene in ovarian and breast carcinomas. *Int. J. Cancer* 64, 280–285. doi:10.1002/ijc.2910640412

Bellacosa, A., Kumar, C. C., Di Cristofano, A., and Testa, J. R. (2005). Activation of AKT kinases in cancer: Implications for therapeutic targeting. *Adv. Cancer Res.* 94, 29–86. doi:10.1016/S0065-230X(05)94002-5

Boerrigter-Eenling, R., Alewijn, M., Weesepoel, Y., and Van Ruth, S. (2017). New approaches towards discrimination of fresh/chilled and frozen/thawed chicken breasts by HADH activity determination: Customized slope fitting and chemometrics. *Meat Sci.* 126, 43–49. doi:10.1016/j.meatsci.2016.12.009

Boutros, M., Paricio, N., Strutt, D. I., and Mlodzik, M. (1998). Dishevelled activates JNK and discriminates between JNK pathways in planar polarity and wingless signaling. *Cell* 94, 109–118. doi:10.1016/s0092-8674(00)81226-x

Brigelius-Flohé, R., and Maiorino, M. (2013). Glutathione peroxidases. *Biochim. Biophys. Acta* 1830, 3289–3303. doi:10.1016/j.bbagen.2012.11.020

Broustas, C. G., Zhu, A., and Lieberman, H. B. (2012). Rad9 protein contributes to prostate tumor progression by promoting cell migration and anoikis resistance. *J. Biol. Chem.* 287, 41324–41333. doi:10.1074/jbc.M112.402784

Buck, M. D., Sowell, R. T., Kaech, S. M., and Pearce, E. L. (2017). Metabolic instruction of immunity. *Cell* 169, 570–586. doi:10.1016/j.cell.2017.04.004

Buskwofie, A., David-West, G., and Clare, C. A. (2020). A review of cervical cancer: Incidence and disparities. *J. Natl. Med. Assoc.* 112, 229–232. doi:10.1016/j.jnma.2020.03.002

Bustamante, E., Morris, H. P., and Pedersen, P. L. (1981). Energy metabolism of tumor cells. Requirement for a form of hexokinase with a propensity for mitochondrial binding. *J. Biol. Chem.* 256, 8699–8704. doi:10.1016/s0021-9258(19)68900-3

Cai, M., Sikong, Y., Wang, Q., Zhu, S., Pang, F., and Cui, X. (2019). Gpx3 prevents migration and invasion in gastric cancer by targeting NFκB/Wnt5a/JNK signaling. *Int. J. Clin. Exp. Pathol.* 12, 1194–1203.

Çamtosun, E., Flanagan, S. E., Ellard, S., ŞıKLAR, Z., Hussain, K., Kocaay, P., et al. (2015). A deep intronic HADH splicing mutation (c.636+471G>T) in a congenital

hyperinsulinemic hypoglycemia case: Long term clinical course. *J. Clin. Res. Pediatr. Endocrinol.* 7, 144–147. doi:10.4274/jcrpe.1963

Carpten, J. D., Faber, A. L., Horn, C., Donoho, G. P., Briggs, S. L., Robbins, C. M., et al. (2007). A transforming mutation in the pleckstrin homology domain of AKT1 in cancer. *Nature* 448, 439–444. doi:10.1038/nature05933

Cerami, E., Gao, J., Dogrusoz, U., Gross, B. E., Sumer, S. O., Aksoy, B. A., et al. (2012). The cBio cancer genomics portal: An open platform for exploring multidimensional cancer genomics data. *Cancer Discov.* 2, 401–404. doi:10.1158/2159-8290.CD-12-0095

Chabner, B. A., and Roberts, T. G., JR (2005). Timeline: Chemotherapy and the war on cancer. *Nat. Rev. Cancer* 5, 65–72. doi:10.1038/nrc1529

Chan, C. H., Li, C. F., Yang, W. L., Gao, Y., Lee, S. W., Feng, Z., et al. (2012). The Skp2-SCF E3 ligase regulates Akt ubiquitination, glycolysis, herceptin sensitivity, and tumorigenesis. *Cell* 149, 1098–1111. doi:10.1016/j.cell.2012.02.065

Chan, C. H., Jo, U., Kohrman, A., Rezaeian, A. H., Chou, P. C., Logothetis, C., et al. (2014). Posttranslational regulation of Akt in human cancer. *Cell Biosci.* 4, 59. doi:10.1186/2045-3701-4-59

Chang, C. H., Qiu, J., O'Sullivan, D., Buck, M. D., Noguchi, T., Curtis, J. D., et al. (2015). Metabolic competition in the tumor microenvironment is a driver of cancer progression. *Cell* 162, 1229–1241. doi:10.1016/j.cell.2015.08.016

Chen, P., Zuo, H., Xiong, H., Kolar, M. J., Chu, Q., Saghatelian, A., et al. (2017a). Gpr132 sensing of lactate mediates tumor-macrophage interplay to promote breast cancer metastasis. *Proc. Natl. Acad. Sci. U. S. A.* 114, 580–585. doi:10.1073/pnas.1614035114

Chen, Z., Hu, T., Zhu, S., Mukaisho, K., El-Rifai, W., and Peng, D. F. (2017b). Glutathione peroxidase 7 suppresses cancer cell growth and is hypermethylated in gastric cancer. *Oncotarget* 8, 54345–54356. doi:10.18632/oncotarget.17527

Cheng, J. Q., Ruggeri, B., Klein, W. M., Sonoda, G., Altomare, D. A., Watson, D. K., et al. (1996). Amplification of AKT2 in human pancreatic cells and inhibition of AKT2 expression and tumorigenicity by antisense RNA. *Proc. Natl. Acad. Sci. U. S. A.* 93, 3636–3641. doi:10.1073/pnas.93.8.3636

Cheng, Y., Xu, T., Li, S., and Ruan, H. (2019). GPX1, a biomarker for the diagnosis and prognosis of kidney cancer, promotes the progression of kidney cancer. *Aging (Albany NY)* 11, 12165–12176. doi:10.18632/aging.102555

Cleary, A. S., Leonard, T. L., Gestl, S. A., and Gunther, E. J. (2014). Tumour cell heterogeneity maintained by cooperating subclones in Wnt-driven mammary cancers. *Nature* 508, 113–117. doi:10.1038/nature13187

Clements, W. M., Wang, J., Sarnaik, A., Kim, O. J., Macdonald, J., Fenoglio-Preiser, C., et al. (2002). beta-Catenin mutation is a frequent cause of Wnt pathway activation in gastric cancer. *Cancer Res.* 62, 3503–3506.

Clevers, H., and Nusse, R. (2012). Wnt/β-catenin signaling and disease. *Cell* 149, 1192–1205. doi:10.1016/j.cell.2012.05.012

Colegio, O. R., Chu, N. Q., Szabo, A. L., Chu, T., Rhebergen, A. M., Jairam, V., et al. (2014). Functional polarization of tumour-associated macrophages by tumour-derived lactic acid. *Nature* 513, 559–563. doi:10.1038/nature13490

Cully, M., You, H., Levine, A. J., and Mak, T. W. (2006). Beyond PTEN mutations: The PI3K pathway as an integrator of multiple inputs during tumorigenesis. *Nat. Rev. Cancer* 6, 184–192. doi:10.1038/nrc1819

Currie, E., Schulze, A., Zechner, R., Walther, T. C., and Farese, R. V., JR. (2013). Cellular fatty acid metabolism and cancer. *Cell Metab.* 18, 153–161. doi:10.1016/j.cmet.2013.05.017

Datta, S. R., Brunet, A., and Greenberg, M. E. (1999). Cellular survival: A play in three akts. *Genes Dev.* 13, 2905–2927. doi:10.1101/gad.13.22.2905

Del Prete, A., Schioppa, T., Tiberio, L., Stabile, H., and Sozzani, S. (2017). Leukocyte trafficking in tumor microenvironment. *Curr. Opin. Pharmacol.* 35, 40–47. doi:10.1016/j.coph.2017.05.004

Downward, J. (2003). Targeting RAS signalling pathways in cancer therapy. *Nat. Rev. Cancer* 3, 11–22. doi:10.1038/nrc969

Du, Z., Zhang, X., Gao, W., and Yang, J. (2021). Differentially expressed genes PCCA, ECHS1, and HADH are potential prognostic biomarkers for gastric cancer. *Sci. Prog.* 104, 368504211011344. doi:10.1177/00368504211011344

Eaton, S., Bursby, T., Middleton, B., Pourfarzam, M., Mills, K., Johnson, A. W., et al. (2000). The mitochondrial trifunctional protein: Centre of a beta-oxidation metabolon? *Biochem. Soc. Trans.* 28, 177–182. doi:10.1042/bst0280177

Elek, Z., KováCS, Z., Keszler, G., Szabó, M., Csanky, E., Luo, J., et al. (2020). High throughput multiplex SNP-analysis in chronic obstructive pulmonary disease and lung cancer. *Curr. Mol. Med.* 20, 185–193. doi:10.2174/1566524019666191017123446

Enjoji, M., Kohjima, M., Ohtsu, K., Matsunaga, K., Murata, Y., Nakamuta, M., et al. (2016). Intracellular mechanisms underlying lipid accumulation (white opaque substance) in gastric epithelial neoplasms: A pilot study of expression profiles of lipid-metabolism-associated genes. *J. Gastroenterol. Hepatol.* 31, 776–781. doi:10.1111/jgh.13216

Etzioni, R., Urban, N., Ramsey, S., Mcintosh, M., Schwartz, S., Reid, B., et al. (2003). The case for early detection. *Nat. Rev. Cancer* 3, 243–252. doi:10.1038/nrc1041

Fan, T. C., Yeo, H. L., Hsu, H. M., Yu, J. C., Ho, M. Y., Lin, W. D., et al. (2018). Reciprocal feedback regulation of ST3GAL1 and GFRA1 signaling in breast cancer cells. *Cancer Lett.* 434, 184–195. doi:10.1016/j.canlet.2018.07.026

Feten, G., Aastveit, A. H., Snipen, L., and AlmøY, T. (2007). A discussion concerning the inclusion of variety effect when analysis of variance is used to detect differentially expressed genes. *Gene Regul. Syst. Bio.* 1, 117762500700100–117762500700107. doi:10.1177/117762500700100005

Filling, C., Keller, B., Hirschberg, D., Marschall, H. U., JöRNVALL, H., Bennett, M. J., et al. (2008). Role of short-chain hydroxyacyl CoA dehydrogenases in SCHAD deficiency. *Biochem. Biophys. Res. Commun.* 368, 6–11. doi:10.1016/j.bbrc.2007.10.188

Fitzgerald, J., Higgins, D., Mazo Vargas, C., Watson, W., Mooney, C., Rahman, A., et al. (2021). Future of biomarker evaluation in the realm of artificial intelligence algorithms: Application in improved therapeutic stratification of patients with breast and prostate cancer. *J. Clin. Pathol.* 74, 429–434. doi:10.1136/jclinpath-2020-207351

Flanagan, S. E., Xie, W., Caswell, R., Damhuis, A., Vianey-Saban, C., Akcay, T., et al. (2013). Next-generation sequencing reveals deep intronic cryptic ABCC8 and HADH splicing founder mutations causing hyperinsulinism by pseudoexon activation. *Am. J. Hum. Genet.* 92, 131–136. doi:10.1016/j.ajhg.2012.11.017

Fruman, D. A., and Rommel, C. (2014). PI3K and cancer: Lessons, challenges and opportunities. *Nat. Rev. Drug Discov.* 13, 140–156. doi:10.1038/nrd4204

Galván Morales, M. A., Barrera RodríGUEZ, R., Santiago Cruz, J. R., and Teran, L. M. (2020). Overview of new treatments with immunotherapy for breast cancer and a proposal of a combination therapy. *Molecules* 25, E5686. doi:10.3390/molecules25235686

Gao, P., Tchernyshyov, I., Chang, T. C., Lee, Y. S., Kita, K., Ochi, T., et al. (2009). c-Myc suppression of miR-23a/b enhances mitochondrial glutaminase expression and glutamine metabolism. *Nature* 458, 762–765. doi:10.1038/nature07823

Gao, X., and Pan, D. (2001). TSC1 and TSC2 tumor suppressors antagonize insulin signaling in cell growth. *Genes Dev.* 15, 1383–1392. doi:10.1101/gad.901101

Gomes, A. M., Soares, M. V., Ribeiro, P., Caldas, J., PóVOA, V., Martins, L. R., et al. (2014). Adult B-cell acute lymphoblastic leukemia cells display decreased PTEN activity and constitutive hyperactivation of PI3K/Akt pathway despite high PTEN protein levels. *Haematologica* 99, 1062–1068. doi:10.3324/haematol.2013.096438

Grivennikov, S. I., Greten, F. R., and Karin, M. (2010). Immunity, inflammation, and cancer. *Cell* 140, 883–899. doi:10.1016/j.cell.2010.01.025

Hanahan, D., and Coussens, L. M. (2012). Accessories to the crime: Functions of cells recruited to the tumor microenvironment. *Cancer Cell* 21, 309–322. doi:10.1016/j.ccr.2012.02.022

Hanahan, D., and Weinberg, R. A. (2011). Hallmarks of cancer: The next generation. *Cell* 144, 646–674. doi:10.1016/j.cell.2011.02.013

Hangauer, M. J., Viswanathan, V. S., Ryan, M. J., Bole, D., Eaton, J. K., Matov, A., et al. (2017). Drug-tolerant persister cancer cells are vulnerable to GPX4 inhibition. *Nature* 551, 247–250. doi:10.1038/nature24297

Hardy, O. T., Hohmeier, H. E., Becker, T. C., Manduchi, E., Doliba, N. M., Gupta, R. K., et al. (2007). Functional genomics of the beta-cell: Short-chain 3-hydroxyacyl-coenzyme A dehydrogenase regulates insulin secretion independent of K+ currents. *Mol. Endocrinol.* 21, 765–773. doi:10.1210/me.2006-0411

Hay, N. (2005). The Akt-mTOR tango and its relevance to cancer. *Cancer Cell* 8, 179–183. doi:10.1016/j.ccr.2005.08.008

Henley, S. J., Ward, E. M., Scott, S., Ma, J., Anderson, R. N., Firth, A. U., et al. (2020). Annual report to the nation on the status of cancer, part I: National cancer statistics. *Cancer* 126, 2225–2249. doi:10.1002/cncr.32802

Herr, P., and Basler, K. (2012). Porcupine-mediated lipidation is required for Wnt recognition by Wls. *Dev. Biol.* 361, 392–402. doi:10.1016/j.ydbio.2011.11.003

Heslegrave, A. J., and Hussain, K. (2013). Novel insights into fatty acid oxidation, amino acid metabolism, and insulin secretion from studying patients with loss of function mutations in 3-hydroxyacyl-CoA dehydrogenase. *J. Clin. Endocrinol. Metab.* 98, 496–501. doi:10.1210/jc.2012-3134

Heslegrave, A. J., Kapoor, R. R., Eaton, S., Chadefaux, B., Akcay, T., Simsek, E., et al. (2012). Leucine-sensitive hyperinsulinaemic hypoglycaemia in patients with loss of function mutations in 3-Hydroxyacyl-CoA Dehydrogenase. *Orphanet J. Rare Dis.* 7, 25. doi:10.1186/1750-1172-7-25

Hirschhaeuser, F., Sattler, U. G., and Mueller-Klieser, W. (2011). Lactate: A metabolic key player in cancer. *Cancer Res.* 71, 6921–6925. doi:10.1158/0008-5472.CAN-11-1457

Houten, S. M., Violante, S., Ventura, F. V., and Wanders, R. J. (2016). The biochemistry and physiology of mitochondrial fatty acid β-oxidation and its genetic disorders. *Annu. Rev. Physiol.* 78, 23–44. doi:10.1146/annurev-physiol-021115-105045

Houten, S. M., and Wanders, R. J. (2010). A general introduction to the biochemistry of mitochondrial fatty acid β-oxidation. *J. Inherit. Metab. Dis.* 33, 469–477. doi:10.1007/s10545-010-9061-2

Huff, C. A., Matsui, W., Smith, B. D., and Jones, R. J. (2006). The paradox of response and survival in cancer therapeutics. *Blood* 107, 431–434. doi:10.1182/blood-2005-06-2517

Ishida-Takagishi, M., Enomoto, A., Asai, N., Ushida, K., Watanabe, T., Hashimoto, T., et al. (2012). The Dishevelled-associating protein Daple controls the non-canonical Wnt/Rac pathway and cell motility. *Nat. Commun.* 3, 859. doi:10.1038/ncomms1861

Jiang, H., Chen, H., Wan, P., and Chen, N. (2021). Decreased expression of HADH is related to poor prognosis and immune infiltration in kidney renal clear cell carcinoma. *Genomics* 113, 3556–3564. doi:10.1016/j.ygeno.2021.08.008

Jiao, Y., Wang, Y., Guo, S., and Wang, G. (2017). Glutathione peroxidases as oncotargets. *Oncotarget* 8, 80093–80102. doi:10.18632/oncotarget.20278

Jones, P. F., Jakubowicz, T., Pitossi, F. J., Maurer, F., and Hemmings, B. A. (1991). Molecular cloning and identification of a serine/threonine protein kinase of the second-messenger subfamily. *Proc. Natl. Acad. Sci. U. S. A.* 88, 4171–4175. doi:10.1073/pnas.88.10.4171

Junaid, M., Akter, Y., Afrose, S. S., Tania, M., and Khan, M. A. (2021). Biological role of AKT and regulation of AKT signaling pathway by thymoquinone: Perspectives in cancer therapeutics. *Mini Rev. Med. Chem.* 21, 288–301. doi:10.2174/1389557520666201005143818

Kadowaki, T., Wilder, E., Klingensmith, J., Zachary, K., and Perrimon, N. (1996). The segment polarity gene porcupine encodes a putative multitransmembrane protein involved in Wingless processing. *Genes Dev.* 10, 3116–3128. doi:10.1101/gad.10.24.3116

Kahn, M. (2014). Can we safely target the WNT pathway? *Nat. Rev. Drug Discov.* 13, 513–532. doi:10.1038/nrd4233

Kapoor, R. R., James, C., Flanagan, S. E., Ellard, S., Eaton, S., and Hussain, K. (2009). 3-Hydroxyacyl-coenzyme A dehydrogenase deficiency and hyperinsulinemic hypoglycemia: Characterization of a novel mutation and severe dietary protein sensitivity. *J. Clin. Endocrinol. Metab.* 94, 2221–2225. doi:10.1210/jc.2009-0423

Kapoor, R. R., Heslegrave, A., and Hussain, K. (2010). Congenital hyperinsulinism due to mutations in HNF4A and HADH. *Rev. Endocr. Metab. Disord.* 11, 185–191. doi:10.1007/s11154-010-9148-y

Kennedy, S. G., Wagner, A. J., Conzen, S. D., JordáN, J., Bellacosa, A., Tsichlis, P. N., et al. (1997). The PI 3-kinase/Akt signaling pathway delivers an anti-apoptotic signal. *Genes Dev.* 11, 701–713. doi:10.1101/gad.11.6.701

Khan, R. T., Siddique, A., Shahid, N., Khokher, S., and Fatima, W. (2018). Breast cancer risk associated with genes encoding DNA repair MRN complex: A study from Punjab, Pakistan. *Breast Cancer* 25, 350–355. doi:10.1007/s12282-018-0837-9

Kim, Y., and Kim, D. H. (2015). CpG island hypermethylation as a biomarker for the early detection of lung cancer. *Methods Mol. Biol.* 1238, 141–171. doi:10.1007/978-1-4939-1804-1_8

Knobbe, C. B., and Reifenberger, G. (2003). Genetic alterations and aberrant expression of genes related to the phosphatidyl-inositol-3'-kinase/protein kinase B (Akt) signal transduction pathway in glioblastomas. *Brain Pathol.* 13, 507–518. doi:10.1111/j.1750-3639.2003.tb00481.x

Koinis, F., Kotsakis, A., and Georgoulias, V. (2016). Small cell lung cancer (SCLC): No treatment advances in recent years. *Transl. Lung Cancer Res.* 5, 39–50. doi:10.3978/j.issn.2218-6751.2016.01.03

Lebleu, V. S. (2015). Imaging the tumor microenvironment. *Cancer J.* 21, 174–178. doi:10.1097/PPO.0000000000000118

Li, C., Chen, P., Palladino, A., Narayan, S., Russell, L. K., Sayed, S., et al. (2010). Mechanism of hyperinsulinism in short-chain 3-hydroxyacyl-CoA dehydrogenase deficiency involves activation of glutamate dehydrogenase. *J. Biol. Chem.* 285, 31806–31818. doi:10.1074/jbc.M110.123638

Li, F., Dai, L., and Niu, J. (2020). GPX2 silencing relieves epithelial-mesenchymal transition, invasion, and metastasis in pancreatic cancer by downregulating Wnt pathway. *J. Cell. Physiol.* 235, 7780–7790. doi:10.1002/jcp.29391

Li, H., Fang, H., Chang, L., Qiu, S., Ren, X., Cao, L., et al. (2021). TC2N: A novel vital oncogene or tumor suppressor gene in cancers. *Front. Immunol.* 12, 764749. doi:10.3389/fimmu.2021.764749

Lin, Y., Zhang, Y., Chen, Y., and Liu, Z. (2019). Promoter methylation and clinical significance of GPX3 in esophageal squamous cell carcinoma. *Pathol. Res. Pract.* 215, 152676. doi:10.1016/j.prp.2019.152676

Liu, C., He, X., Wu, X., Wang, Z., Zuo, W., and Hu, G. (2017). Clinicopathological and prognostic significance of GPx2 protein expression in nasopharyngeal carcinoma. *Cancer Biomark.* 19, 335–340. doi:10.3233/CBM-160542

Liu, H. W., Bi, W. T., Huang, H. T., Li, R. X., XI, Q., Feng, L., et al. (2018a). Satb1 promotes Schwann cell viability and migration via activation of PI3K/AKT pathway. *Eur. Rev. Med. Pharmacol. Sci.* 22, 4268–4277. doi:10.26355/eurrev_201807_15423

Liu, J., Eckert, M. A., Harada, B. T., Liu, S. M., Lu, Z., Yu, K., et al. (2018b). m(6)A mRNA methylation regulates AKT activity to promote the proliferation and tumorigenicity of endometrial cancer. *Nat. Cell Biol.* 20, 1074–1083. doi:10.1038/s41556-018-0174-4

Malanga, D., Scrima, M., De Marco, C., Fabiani, F., De Rosa, N., De Gisi, S., et al. (2008). Activating E17K mutation in the gene encoding the protein kinase AKT1 in a subset of squamous cell carcinoma of the lung. *Cell Cycle* 7, 665–669. doi:10.4161/cc.7.5.5485

Manning, B. D., and Cantley, L. C. (2007). AKT/PKB signaling: Navigating downstream. *Cell* 129, 1261–1274. doi:10.1016/j.cell.2007.06.009

Manning, B. D., and Toker, A. (2017). AKT/PKB signaling: Navigating the network. *Cell* 169, 381–405. doi:10.1016/j.cell.2017.04.001

Mantovani, A., Allavena, P., Sica, A., and Balkwill, F. (2008). Cancer-related inflammation. *Nature* 454, 436–444. doi:10.1038/nature07205

Mao, J., Fan, S., Ma, W., Fan, P., Wang, B., Zhang, J., et al. (2014). Roles of Wnt/β-catenin signaling in the gastric cancer stem cells proliferation and salinomycin treatment. *Cell Death Dis.* 5, e1039. doi:10.1038/cddis.2013.515

Margis, R., Dunand, C., Teixeira, F. K., and Margis-Pinheiro, M. (2008). Glutathione peroxidase family - an evolutionary overview. *Febs J.* 275, 3959–3970. doi:10.1111/j.1742-4658.2008.06542.x

Martens, G. A., Vervoort, A., Van De Casteele, M., Stangé, G., Hellemans, K., Van Thi, H. V., et al. (2007). Specificity in beta cell expression of L-3-hydroxyacyl-CoA dehydrogenase, short chain, and potential role in down-regulating insulin release. *J. Biol. Chem.* 282, 21134–21144. doi:10.1074/jbc.M700083200

Mayo, L. D., and Donner, D. B. (2001). A phosphatidylinositol 3-kinase/Akt pathway promotes translocation of Mdm2 from the cytoplasm to the nucleus. *Proc. Natl. Acad. Sci. U. S. A.* 98, 11598–11603. doi:10.1073/pnas.181181198

Meier, R., and Hemmings, B. A. (1999). Regulation of protein kinase B. *J. Recept. Signal Transduct. Res.* 19, 121–128. doi:10.3109/10799899909036639

Meng, F., Henson, R., Wehbe-Janek, H., Ghoshal, K., Jacob, S. T., and Patel, T. (2007). MicroRNA-21 regulates expression of the PTEN tumor suppressor gene in human hepatocellular cancer. *Gastroenterology* 133, 647–658. doi:10.1053/j.gastro.2007.05.022

Metere, A., Frezzotti, F., Graves, C. E., Vergine, M., De Luca, A., Pietraforte, D., et al. (2018). A possible role for selenoprotein glutathione peroxidase (GPx1) and thioredoxin reductases (TrxR1) in thyroid cancer: Our experience in thyroid surgery. *Cancer Cell Int.* 18, 7. doi:10.1186/s12935-018-0504-4

Miller, K. D., Siegel, R. L., Lin, C. C., Mariotto, A. B., Kramer, J. L., Rowland, J. H., et al. (2016). Cancer treatment and survivorship statistics, 2016. *Ca. Cancer J. Clin.* 66, 271–289. doi:10.3322/caac.21349

Mohamedali, A., Lea, N. C., Feakins, R. M., Raj, K., Mufti, G. J., and Kocher, H. M. (2008). AKT1 (E17K) mutation in pancreatic cancer. *Technol. Cancer Res. Treat.* 7, 407–408. doi:10.1177/153303460800700509

Morin, P. J., Sparks, A. B., Korinek, V., Barker, N., Clevers, H., Vogelstein, B., et al. (1997). Activation of beta-catenin-Tcf signaling in colon cancer by mutations in beta-catenin or APC. *Science* 275, 1787–1790. doi:10.1126/science.275.5307.1787

Mundi, P. S., Sachdev, J., Mccourt, C., and Kalinsky, K. (2016). AKT in cancer: New molecular insights and advances in drug development. *Br. J. Clin. Pharmacol.* 82, 943–956. doi:10.1111/bcp.13021

Naiki, T., Naiki-Ito, A., Iida, K., Etani, T., Kato, H., Suzuki, S., et al. (2018). GPX2 promotes development of bladder cancer with squamous cell differentiation through the control of apoptosis. *Oncotarget* 9, 15847–15859. doi:10.18632/oncotarget.24627

Nakashima, L. (2018). Evolution of cancer treatment and evolving challenges. *Healthc. Manage. Forum* 31, 26–28. doi:10.1177/0840470417722568

Nakatani, K., Thompson, D. A., Barthel, A., Sakaue, H., Liu, W., Weigel, R. J., et al. (1999). Up-regulation of Akt3 in estrogen receptor-deficient breast cancers and androgen-independent prostate cancer lines. *J. Biol. Chem.* 274, 21528–21532. doi:10.1074/jbc.274.31.21528

Nalkiran, I., Turan, S., Arikan, S., Kahraman Ö, T., Acar, L., Yaylim, I., et al. (2015). Determination of gene expression and serum levels of MnSOD and GPX1 in colorectal cancer. *Anticancer Res.* 35, 255–259.

Nieman, K. M., Kenny, H. A., Penicka, C. V., Ladanyi, A., Buell-Gutbrod, R., Zillhardt, M. R., et al. (2011). Adipocytes promote ovarian cancer metastasis and provide energy for rapid tumor growth. *Nat. Med.* 17, 1498–1503. doi:10.1038/nm.2492

Nishita, M., Enomoto, M., Yamagata, K., and Minami, Y. (2010). Cell/tissue-tropic functions of Wnt5a signaling in normal and cancer cells. *Trends Cell Biol.* 20, 346–354. doi:10.1016/j.tcb.2010.03.001

Nwosu, Z. C., Battello, N., Rothley, M., Piorońska, W., Sitek, B., Ebert, M. P., et al. (2018). Liver cancer cell lines distinctly mimic the metabolic gene expression pattern of the corresponding human tumours. *J. Exp. Clin. Cancer Res.* 37, 211. doi:10.1186/s13046-018-0872-6

Ozes, O. N., Mayo, L. D., Gustin, J. A., Pfeffer, S. R., Pfeffer, L. M., and Donner, D. B. (1999). NF-kappaB activation by tumour necrosis factor requires the Akt serine-threonine kinase. *Nature* 401, 82–85. doi:10.1038/43466

Parsons, D. W., Wang, T. L., Samuels, Y., Bardelli, A., Cummins, J. M., Delong, L., et al. (2005). Colorectal cancer: Mutations in a signalling pathway. *Nature* 436, 792. doi:10.1038/436792a

Peng, D., Hu, T., Soutto, M., Belkhiri, A., Zaika, A., and El-Rifai, W. (2014). Glutathione peroxidase 7 has potential tumour suppressor functions that are silenced by location-specific methylation in oesophageal adenocarcinoma. *Gut* 63, 540–551. doi:10.1136/gutjnl-2013-304612

Pepin, E., Guay, C., Delghingaro-Augusto, V., Joly, E., Madiraju, S. R., and Prentki, M. (2010). Short-chain 3-hydroxyacyl-CoA dehydrogenase is a negative regulator of insulin secretion in response to fuel and non-fuel stimuli in INS832/13 β-cells. *J. Diabetes* 2, 157–167. doi:10.1111/j.1753-0407.2010.00076.x

Popa, F. I., Perlini, S., Teofoli, F., Degani, D., Funghini, S., La Marca, G., et al. (2012). 3-hydroxyacyl-coenzyme a dehydrogenase deficiency: Identification of a new mutation causing hyperinsulinemic hypoketotic hypoglycemia, altered organic acids and acylcarnitines concentrations. *JIMD Rep.* 2, 71–77. doi:10.1007/8904_2011_50

Ren, J., Feng, J., Song, W., Wang, C., Ge, Y., and Fu, T. (2020). Development and validation of a metabolic gene signature for predicting overall survival in patients with colon cancer. *Clin. Exp. Med.* 20, 535–544. doi:10.1007/s10238-020-00652-1

Revathidevi, S., and Munirajan, A. K. (2019). Akt in cancer: Mediator and more. *Semin. Cancer Biol.* 59, 80–91. doi:10.1016/j.semcancer.2019.06.002

Roelink, H., Wagenaar, E., and Nusse, R. (1992). Amplification and proviral activation of several Wnt genes during progression and clonal variation of mouse mammary tumors. *Oncogene* 7, 487–492.

Roy, H. K., Olusola, B. F., Clemens, D. L., Karolski, W. J., Ratashak, A., Lynch, H. T., et al. (2002). AKT proto-oncogene overexpression is an early event during sporadic colon carcinogenesis. *Carcinogenesis* 23, 201–205. doi:10.1093/carcin/23.1.201

Samuels, Y., Wang, Z., Bardelli, A., Silliman, N., Ptak, J., Szabo, S., et al. (2004). High frequency of mutations of the PIK3CA gene in human cancers. *Science* 304, 554. doi:10.1126/science.1096502

Sanchez, D. J., and Simon, M. C. (2018). Genetic and metabolic hallmarks of clear cell renal cell carcinoma. *Biochim. Biophys. Acta. Rev. Cancer* 1870, 23–31. doi:10.1016/j.bbcan.2018.06.003

Sanidas, I., Polytarchou, C., Hatziapostolou, M., Ezell, S. A., Kottakis, F., Hu, L., et al. (2014). Phosphoproteomics screen reveals akt isoform-specific signals linking RNA processing to lung cancer. *Mol. Cell* 53, 577–590. doi:10.1016/j.molcel.2013.12.018

Satapathy, A. K., Jain, V., Ellard, S., and Flanagan, S. E. (2016). Hyperinsulinemic hypoglycemia of infancy due to novel HADH mutation in two siblings. *Indian Pediatr.* 53, 912–913. doi:10.1007/s13312-016-0958-1

Schulz, N., Himmelbauer, H., Rath, M., Van Weeghel, M., Houten, S., Kulik, W., et al. (2011). Role of medium- and short-chain L-3-hydroxyacyl-CoA dehydrogenase in the regulation of body weight and thermogenesis. *Endocrinology* 152, 4641–4651. doi:10.1210/en.2011-1547

Shareefi, G., Turkistani, A. N., Alsayyah, A., Kussaibi, H., Abdel Hadi, M., and Alkharsah, K. R. (2020). Pathway-affecting single nucleotide polymorphisms (SNPs) in RPS6KA1 and MBIP genes are associated with breast cancer risk. *Asian pac. J. Cancer Prev.* 21, 2163–2168. doi:10.31557/APJCP.2020.21.7.2163

Shen, C., Song, Y. H., Xie, Y., Wang, X., Wang, Y., Wang, C., et al. (2017). Downregulation of HADH promotes gastric cancer progression via Akt signaling pathway. *Oncotarget* 8, 76279–76289. doi:10.18632/oncotarget.19348

Shoji, K., Oda, K., Nakagawa, S., Hosokawa, S., Nagae, G., Uehara, Y., et al. (2009). The oncogenic mutation in the pleckstrin homology domain of AKT1 in endometrial carcinomas. *Br. J. Cancer* 101, 145–148. doi:10.1038/sj.bjc.6605109

Siegel, R. L., Miller, K. D., Fuchs, H. E., and Jemal, A. (2022). Cancer statistics, 2022. *Ca. Cancer J. Clin.* 72, 7–33. doi:10.3322/caac.21708

Smith, J. S., Lindsay, L., Hoots, B., Keys, J., Franceschi, S., Winer, R., et al. (2007). Human papillomavirus type distribution in invasive cervical cancer and high-grade cervical lesions: A meta-analysis update. *Int. J. Cancer* 121, 621–632. doi:10.1002/ijc.22527

Sousa, C. M., Biancur, D. E., Wang, X., Halbrook, C. J., Sherman, M. H., Zhang, L., et al. (2016). Pancreatic stellate cells support tumour metabolism through autophagic alanine secretion. *Nature* 536, 479–483. doi:10.1038/nature19084

Spill, F., Reynolds, D. S., Kamm, R. D., and Zaman, M. H. (2016). Impact of the physical microenvironment on tumor progression and metastasis. *Curr. Opin. Biotechnol.* 40, 41–48. doi:10.1016/j.copbio.2016.02.007

Staal, S. P. (1987). Molecular cloning of the akt oncogene and its human homologues AKT1 and AKT2: Amplification of AKT1 in a primary human gastric adenocarcinoma. *Proc. Natl. Acad. Sci. U. S. A.* 84, 5034–5037. doi:10.1073/pnas.84.14.5034

Stambolic, V., Suzuki, A., De La Pompa, J. L., Brothers, G. M., Mirtsos, C., Sasaki, T., et al. (1998). Negative regulation of PKB/Akt-dependent cell survival by the tumor suppressor PTEN. *Cell* 95, 29–39. doi:10.1016/s0092-8674(00)81780-8

Sun, M., Wang, G., Paciga, J. E., Feldman, R. I., Yuan, Z. Q., Ma, X. L., et al. (2001). AKT1/PKBalpha kinase is frequently elevated in human cancers and its constitutive activation is required for oncogenic transformation in NIH3T3 cells. *Am. J. Pathol.* 159, 431–437. doi:10.1016/s0002-9440(10)61714-2

Sun, Z., Tao, W., Guo, X., Jing, C., Zhang, M., Wang, Z., et al. (2022). Construction of a lactate-related prognostic signature for predicting prognosis, tumor microenvironment, and immune response in kidney renal clear cell carcinoma. *Front. Immunol.* 13, 818984. doi:10.3389/fimmu.2022.818984

Takebe, G., Yarimizu, J., Saito, Y., Hayashi, T., Nakamura, H., Yodoi, J., et al. (2002). A comparative study on the hydroperoxide and thiol specificity of the glutathione peroxidase family and selenoprotein P. *J. Biol. Chem.* 277, 41254–41258. doi:10.1074/jbc.M202773200

Tanaka, M., Masaki, Y., Tanaka, K., Miyazaki, M., Kato, M., Sugimoto, R., et al. (2013). Reduction of fatty acid oxidation and responses to hypoxia correlate with the progression of de-differentiation in HCC. *Mol. Med. Rep.* 7, 365–370. doi:10.3892/mmr.2012.1201

Tsai, Y. T., Kuo, P. H., Kuo, H. P., Hsu, C. Y., Lee, Y. J., Kuo, C. L., et al. (2021). Ganoderma tsugae suppresses the proliferation of endometrial carcinoma cells via Akt signaling pathway. *Environ. Toxicol.* 36, 320–327. doi:10.1002/tox.23037

Van't Veer, L. J., Van Kessel, A. G., Van Heerikhuizen, H., Van Ooyen, A., Nusse, R., and vAn Ooyen, A. (1984). Molecular cloning and chromosomal assignment of the human homolog of int-1, a mouse gene implicated in mammary tumorigenesis. *Mol. Cell. Biol.* 4, 2532–2534. doi:10.1128/mcb.4.11.2532

Vijayvergia, N., Shah, P. C., and Denlinger, C. S. (2015). Survivorship in non-small cell lung cancer: Challenges faced and steps forward. *J. Natl. Compr. Canc. Netw.* 13, 1151–1161. doi:10.6004/jnccn.2015.0140

Viswanathan, V. S., Ryan, M. J., Dhruv, H. D., Gill, S., Eichhoff, O. M., Seashore-Ludlow, B., et al. (2017). Dependency of a therapy-resistant state of cancer cells on a lipid peroxidase pathway. *Nature* 547, 453–457. doi:10.1038/nature23007

Vitale, I., Manic, G., Coussens, L. M., Kroemer, G., and Galluzzi, L. (2019a). Macrophages and metabolism in the tumor microenvironment. *Cell Metab.* 30, 36–50. doi:10.1016/j.cmet.2019.06.001

Vitale, I., Manic, G., Galassi, C., and Galluzzi, L. (2019b). Stress responses in stromal cells and tumor homeostasis. *Pharmacol. Ther.* 200, 55–68. doi:10.1016/j.pharmthera.2019.04.004

Vivanco, I., and Sawyers, C. L. (2002). The phosphatidylinositol 3-Kinase AKT pathway in human cancer. *Nat. Rev. Cancer* 2, 489–501. doi:10.1038/nrc839

Voloshanenko, O., Schwartz, U., Kranz, D., Rauscher, B., Linnebacher, M., Augustin, I., et al. (2018). β-catenin-independent regulation of Wnt target genes by RoR2 and ATF2/ATF4 in colon cancer cells. *Sci. Rep.* 8, 3178. doi:10.1038/s41598-018-20641-5

Vredendaal, P. J., Van Den Berg, I. E., Malingré, H. E., Stroobants, A. K., Olde Weghuis, D. E., and Berger, R. (1996). Human short-chain L-3-hydroxyacyl-CoA dehydrogenase: Cloning and characterization of the coding sequence. *Biochem. Biophys. Res. Commun.* 223, 718–723. doi:10.1006/bbrc.1996.0961

Vredendaal, P. J., Van Den Berg, I. E., Stroobants, A. K., Van Der, A. D., Malingré, H. E., and Berger, R. (1998). Structural organization of the human short-chain L-3-hydroxyacyl-CoA dehydrogenase gene. *Mamm. Genome* 9, 763–768. doi:10.1007/s003359900860

Vysotskaia, V., Kaseniit, K. E., Bucheit, L., Ready, K., Price, K., and Johansen Taber, K. (2020). Clinical utility of hereditary cancer panel testing: Impact of PALB2, ATM, CHEK2, NBN, BRIP1, RAD51C, and RAD51D results on patient

management and adherence to provider recommendations. *Cancer* 126, 549–558. doi:10.1002/cncr.32572

Wanders, R. J., Vreken, P., Den Boer, M. E., Wijburg, F. A., Van Gennip, A. H., and Ijlst, L. (1999). Disorders of mitochondrial fatty acyl-CoA beta-oxidation. *J. Inherit. Metab. Dis.* 22, 442–487. doi:10.1023/a:1005504223140

Wang, J. J., Lei, K. F., and Han, F. (2018). Tumor microenvironment: Recent advances in various cancer treatments. *Eur. Rev. Med. Pharmacol. Sci.* 22, 3855–3864. doi:10.26355/eurrev_201806_15270

Wang, Y., Cao, P., Alshwmi, M., Jiang, N., Xiao, Z., Jiang, F., et al. (2019). GPX2 suppression of H(2)O(2) stress regulates cervical cancer metastasis and apoptosis via activation of the β-catenin-WNT pathway. *Onco. Targets. Ther.* 12, 6639–6651. doi:10.2147/OTT.S208781

Ward, P. S., and Thompson, C. B. (2012). Metabolic reprogramming: A cancer hallmark even warburg did not anticipate. *Cancer Cell* 21, 297–308. doi:10.1016/j.ccr.2012.02.014

Ward, S. G., Westwick, J., and Harris, S. (2011). Sat-Nav for T cells: Role of PI3K isoforms and lipid phosphatases in migration of T lymphocytes. *Immunol. Lett.* 138, 15–18. doi:10.1016/j.imlet.2011.02.007

Wei, J., Xie, Q., Liu, X., Wan, C., Wu, W., Fang, K., et al. (2020). Identification the prognostic value of glutathione peroxidases expression levels in acute myeloid leukemia. *Ann. Transl. Med.* 8, 678. doi:10.21037/atm-20-3296

Wen, J., Liu, D., Chen, D., Chen, J., Xu, X., Chen, C., et al. (2019). Treatment of clinical T4 stage superior sulcus non-small cell lung cancer: A propensity-matched analysis of the surveillance, epidemiology, and end results database. *Biosci. Rep.* 39, BSR20181545. doi:10.1042/BSR20181545

Wettersten, H. I., Aboud, O. A., Lara, P. N., JR, and Weiss, R. H. (2017). Metabolic reprogramming in clear cell renal cell carcinoma. *Nat. Rev. Nephrol.* 13, 410–419. doi:10.1038/nrneph.2017.59

Wilkins, O. M., Titus, A. J., Gui, J., Eliot, M., Butler, R. A., Sturgis, E. M., et al. (2017). Genome-scale identification of microRNA-related SNPs associated with risk of head and neck squamous cell carcinoma. *Carcinogenesis* 38, 986–993. doi:10.1093/carcin/bgx056

Xiong, Z., Wu, J., Sun, Y., Bai, M., Niu, F., and Jin, T. (2020). Variants in multiple genes are associated with esophageal cancer risk in a Chinese han population: A case-control study. *J. Gene Med.* 22, e3266. doi:10.1002/jgm.3266

Xu, X., Sakon, M., Nagano, H., Hiraoka, N., Yamamoto, H., Hayashi, N., et al. (2004). Akt2 expression correlates with prognosis of human hepatocellular carcinoma. *Oncol. Rep.* 11, 25–32. doi:10.3892/or.11.1.25

Yang, S. Y., He, X. Y., and Schulz, H. (2005). 3-Hydroxyacyl-CoA dehydrogenase and short chain 3-hydroxyacyl-CoA dehydrogenase in human health and disease. *Febs J.* 272, 4874–4883. doi:10.1111/j.1742-4658.2005.04911.x

Yang, W. S., Sriramaratnam, R., Welsch, M. E., Shimada, K., Skouta, R., Viswanathan, V. S., et al. (2014). Regulation of ferroptotic cancer cell death by GPX4. *Cell* 156, 317–331. doi:10.1016/j.cell.2013.12.010

Yecies, J. L., Zhang, H. H., Menon, S., Liu, S., Yecies, D., Lipovsky, A. I., et al. (2011). Akt stimulates hepatic SREBP1c and lipogenesis through parallel mTORC1-dependent and independent pathways. *Cell Metab.* 14, 21–32. doi:10.1016/j.cmet.2011.06.002

Yi, Z., Jiang, L., Zhao, L., Zhou, M., Ni, Y., Yang, Y., et al. (2019). Glutathione peroxidase 3 (GPX3) suppresses the growth of melanoma cells through reactive oxygen species (ROS)-dependent stabilization of hypoxia-inducible factor 1-α and 2-α. *J. Cell. Biochem.* 120, 19124–19136. doi:10.1002/jcb.29240

Yin, F., Sharen, G., Yuan, F., Peng, Y., Chen, R., Zhou, X., et al. (2017). TIP30 regulates lipid metabolism in hepatocellular carcinoma by regulating SREBP1 through the Akt/mTOR signaling pathway. *Oncogenesis* 6, e347. doi:10.1038/oncsis.2017.49

Zhan, T., Rindtorff, N., and Boutros, M. (2017). Wnt signaling in cancer. *Oncogene* 36, 1461–1473. doi:10.1038/onc.2016.304

Zhang, M., Di Martino, J. S., Bowman, R. L., Campbell, N. R., Baksh, S. C., Simon-Vermot, T., et al. (2018). Adipocyte-derived lipids mediate melanoma progression via FATP proteins. *Cancer Discov.* 8, 1006–1025. doi:10.1158/2159-8290.CD-17-1371

Zhang, B., Wu, Q., Wang, Z., Xu, R., Hu, X., Sun, Y., et al. (2019). The promising novel biomarkers and candidate small molecule drugs in kidney renal clear cell carcinoma: Evidence from bioinformatics analysis of high-throughput data. *Mol. Genet. Genomic Med.* 7, e607. doi:10.1002/mgg3.607

Zhang, Y., and Zhang, X. (2018). Controlling nutritional status score, a promising prognostic marker in patients with gastrointestinal cancers after surgery: A systematic review and meta-analysis. *Int. J. Surg.* 55, 39–45. doi:10.1016/j.ijsu.2018.05.018

Zheng, X., Li, X., and Wang, X. (2020). Extracellular vesicle-based liquid biopsy holds great promise for the management of ovarian cancer. *Biochim. Biophys. Acta. Rev. Cancer* 1874, 188395. doi:10.1016/j.bbcan.2020.188395

Zhou, B. P., Liao, Y., Xia, W., Spohn, B., Lee, M. H., and Hung, M. C. (2001). Cytoplasmic localization of p21Cip1/WAF1 by Akt-induced phosphorylation in HER-2/neu-overexpressing cells. *Nat. Cell Biol.* 3, 245–252. doi:10.1038/35060032

Zhou, C., Hu, H., Zheng, Z., Chen, C., Li, Y., Li, B., et al. (2019a). Association between GPX3 promoter methylation and malignant tumors: A meta-analysis. *Pathol. Res. Pract.* 215, 152443. doi:10.1016/j.prp.2019.152443

Zhou, C., Pan, R., Li, B., Huang, T., Zhao, J., Ying, J., et al. (2019b). GPX3 hypermethylation in gastric cancer and its prognostic value in patients aged over 60. *Future Oncol.* 15, 1279–1289. doi:10.2217/fon-2018-0674

Zhu, X., Wang, J., Li, L., Deng, L., Wang, J., Liu, L., et al. (2018). GPX3 suppresses tumor migration and invasion via the FAK/AKT pathway in esophageal squamous cell carcinoma. *Am. J. Transl. Res.* 10, 1908–1920.

Zilberman, D. E., Cohen, Y., Amariglio, N., Fridman, E., Ramon, J., and Rechavi, G. (2009). AKT1 E17 K pleckstrin homology domain mutation in urothelial carcinoma. *Cancer Genet. cytogenet.* 191, 34–37. doi:10.1016/j.cancergencyto.2009.01.009

frontiers | Frontiers in Pharmacology

TYPE Original Research
PUBLISHED 25 October 2022
DOI 10.3389/fphar.2022.949126

Check for updates

OPEN ACCESS

EDITED BY
Chen Shi,
Huazhong University of Science and Technology, China

REVIEWED BY
Kai Yu,
Sun Yat-sen University Cancer Center (SYSUCC), China
Zhuoyuan Xin,
Jilin University, China

*CORRESPONDENCE
Rongsheng Tong,
tongrs@126.com

SPECIALTY SECTION
This article was submitted to Pharmacology of Anti-Cancer Drugs, a section of the journal Frontiers in Pharmacology

RECEIVED 20 May 2022
ACCEPTED 11 October 2022
PUBLISHED 25 October 2022

CITATION
Liu Y, Du S, Yuan M, He X, Zhu C, Han K, Zhu Y, Yang Q and Tong R (2022), Identification of a novel ferroptosis-related gene signature associated with prognosis, the immune landscape, and biomarkers for immunotherapy in ovarian cancer.
Front. Pharmacol. 13:949126.
doi: 10.3389/fphar.2022.949126

COPYRIGHT
© 2022 Liu, Du, Yuan, He, Zhu, Han, Zhu, Yang and Tong. This is an open-access article distributed under the terms of the Creative Commons Attribution License (CC BY). The use, distribution or reproduction in other forums is permitted, provided the original author(s) and the copyright owner(s) are credited and that the original publication in this journal is cited, in accordance with accepted academic practice. No use, distribution or reproduction is permitted which does not comply with these terms.

Identification of a novel ferroptosis-related gene signature associated with prognosis, the immune landscape, and biomarkers for immunotherapy in ovarian cancer

Yilong Liu[1], Suya Du[2], Mengying Yuan[1], Xia He[1,3], Changyu Zhu[1,3], Ke Han[1], Yuyan Zhu[1], Qianwen Yang[1] and Rongsheng Tong[1,3]*

[1]Department of Pharmacy, Sichuan Academy of Medical Science and Sichuan Provincial People's Hospital, School of Medicine, University of Electronic Science and Technology of China, Chengdu, China, [2]Department of Clinical Pharmacy, Sichuan Cancer Hospital and Institute, Sichuan Cancer Center, School of Medicine, University of Electronic Science and Technology of China, Chengdu, China, [3]Personalized Drug Therapy Key Laboratory of Sichuan Province, School of Medicine, University of Electronic Science and Technology of China, Chengdu, China

Ferroptosis has been implicated in tumor progression and immunoregulation. Identification of ferroptosis-related prognostic gene is important for immunotherapy and prognosis in ovarian cancer (OV). We assessed the potential predictive power of a novel ferroptosis-related gene (FRG) signature for prognosis and immunotherapy in Asian and Caucasian OV populations. We collected gene expression profiles and clinicopathological data from public databases. The least absolute shrinkage and selection operator Cox regression algorithm was used to construct the FRG signature. Receiver operating characteristic (ROC) curve, Kaplan-Meier method, Cox regression model were used to evaluate the clinical benefits of FRG signature. Gene functional and gene set enrichment analyses were used for functional annotation and immune landscape analysis. A 15-FRG signature was constructed and used to stratify patients into two risk groups. Patients in the high-risk group had significantly worse survival. The risk score was a significant independent risk factor for OS. The area under the ROC curve indicated the good prediction performance of the FRG signature. Notably, the low-risk group showed a significant enrichment in immune-related pathways and a "hot" immune status. The risk score was found to be an efficient and robust predictor of response to immunotherapy. In conclusion, our study identified a novel 15-FRG prognostic signature that can be used for prognostic prediction and precision immunotherapy in Asian and Caucasian OV populations.

KEYWORDS
ovarian cancer, ferroptosis, biomarker, prognosis, immunotherapy

Introduction

Ovarian cancer (OV), the third most common gynecologic malignancy and the second leading cause of cancer-related deaths (Bray et al., 2018), is frequently diagnosed late due to hidden and nonspecific symptoms in the early stage, resulting in a 5-year survival rate of only 47% after diagnosis, which is low in comparison with the 85% survival rate of breast cancer (Lheureux et al., 2019). The standard therapy for OV relies heavily on upfront surgical debulking followed by platinum-based chemotherapy (Lheureux et al., 2019), with a favorable early response observed in approximately 80% of patients. However, unfortunately, the disease soon recurs in most of these patients. Meanwhile, OV is a highly heterogeneous disease that comprises multiple histological subtypes and different microenvironmental features (Chen et al., 2018; Geistlinger et al., 2020). Studies have shown that there are huge differences in the treatment effect and prognosis of individuals with OV (Morand et al., 2021), which make the prediction of tumor treatment response and prognosis challenging. Therefore, considering the high recurrence rate and cellular heterogeneity of OV, the development of innovative treatments and refinement of prognostic prediction are urgently needed.

Ferroptosis is a novel iron-dependent form of non-apoptotic regulated cell death, with distinct features of overaccumulation of reactive oxygen species (ROS) and lipid peroxidation (Yu et al., 2017; Tang et al., 2019). Recently, ferroptosis induction has been demonstrated as a potential prevention or therapeutic modality in various diseases (Tang et al., 2018; Qiu et al., 2020), especially for anticancer treatments (Xu et al., 2019; Wang et al., 2020). In addition to small-molecule inhibitors and agonists, various ferroptosis-related genes (FRGs) have been identified as drivers, suppressors, and markers in OV, including *CYBB* and *TAZ* (Yang W. et al., 2020), which have been confirmed as ferroptosis-driving factors that contribute to the sensitization of OV cells to ferroptosis. In contrast, *GPX4*, *GCH1*, and *FSP1* (Li et al., 2021) mediate three distinct mechanisms of ferroptosis protection to ensure tumor cellular homeostasis. And, a previous study has indicated that inducing ferroptosis is correlated with prolonged progression free survival in patients with platinum-resistant ovarian cancer (Chekerov et al., 2018). Taken together, these compelling findings demonstrate that OV may be highly sensitive to ferroptosis, and targeting ferroptosis may be helpful to improve the prognosis of OV. However, the underlying ferroptosis-related prognostic biomarkers in OV remain largely unknown. Hence, it is important to excavate more ferroptosis-related biomarkers for treatment and prognosis in OV. Up to now, several studies have extensively explored the relationship between FRGs and tumor prognosis, and constructed a prognostic signature for a variety of tumor types, such as a novel 10-FRG prognostic signature in liver cancer, a novel 9-FRG prognostic signature in breast cancer (Liang et al., 2020; Wang D. et al., 2021). Regretfully, most previous studies have failed to verify these relationships across multiple regions and races, which may lead to weak generalization ability of research results among different races.

Thus, in the present study, the prognostic capacity of FRGs in patients with OV was comprehensively analyzed using publicly available gene expression profiles obtained from the Asian and Caucasian populations. Besides, a prognostic signature was constructed and its potential associations with the immune landscape and immunotherapy were explored. Notably, our results revealed the prognostic value of a novel 15-FRG signature and provided a promising predictor of response to immunotherapy and chemotherapy.

Materials and methods

Public data collection

The GSE32062 microarray dataset, comprising the data and clinical information of 260 OV patients, was obtained from the Gene Expression Omnibus (GEO) website (http://www.ncbi.nlm.nih.gov/geo) for use as a training cohort. The raw expression data were background-corrected by applying the "normexp" method (with an offset of 1) and were subjected to quantile normalization using the "limma" R package. When genes were mapped to more than one probe, the gene with the mean fold-change value was selected.

International Cancer Genome Consortium (ICGC) (OV-AU) RNA-sequencing (RNA-seq) data of 93 OV patients and their clinical information were obtained from the ICGC data portal (https://dcc.icgc.org/projects/OV-AU) for use as an external validation cohort. RNA-seq datasets of 41 patients treated with anti-PD-1 monotherapy (Gide et al., 2019) and 42 patients treated with anti-CTLA4 monotherapy (Van Allen et al., 2015) were obtained from the Tumor Immune Dysfunction and Exclusion (TIDE) website (http://tide.dfci.harvard.edu/download/) for use as an external validation cohort. All the datasets used for analysis are freely and publicly available, hence local ethical approval was exempted.

FRGs were retrieved from a public ferroptosis database (FerrDb; http://www.zhounan.org/ferrdb/) (Zhou and Bao, 2020) and were limited to published human studies. Immune-related genes (IRGs) were retrieved from a public immunology database (ImmPort; https://www.immport.org/shared/genelists) (Bhattacharya et al., 2018). A comprehensive gene list is provided in Supplementary Tables S1A, S1B.

Ferroptosis-related gene signature construction and validation

Univariate analyses for identifying overall survival (OS)-related FRGs were performed using Cox regression analysis, with adjusted (adj.) $p < 0.05$ considered significant. The STRING v11.0 database (Szklarczyk et al., 2010) (https://string-db.org/) was used for protein-protein interaction (PPI) analysis. The least absolute shrinkage and selection operator (LASSO) algorithm was used to penalize the risk of overfitting and to construct a Cox regression model with an optimal penalty parameter λ selected based on a 10-fold cross validation (Simon et al., 2011). The FRG signature was constructed as follows: the risk score = $\sum (\beta \times m)$, where β is the Cox coefficient and m is the z-score standardized expression value of the corresponding gene. According to the median risk score value, patients were categorized into high- and low-risk groups. Kaplan–Meier (KM) survival curve analysis was conducted in combination with a log-rank test, using the "survival" and "survminer" packages. The predictive performance of the risk score was determined with a time-dependent receiver operating characteristic (ROC) curve, using the R package "timeROC." The prognostic value was validated in the external Caucasian validation cohort.

Validation of independent prognostic role

The risk score and other available clinical variables were included for univariate analyses using the Cox proportional hazard model. Variables that were significant ($p < 0.05$) in univariate analyses were considered for multivariate analyses.

Construction and validation of a predictive nomogram

Nomograms are widely applied to simplify statistical prediction models into an objective and operational graphical tool (Iasonos et al., 2008). All available prognostic factors were selected to build a nomogram to investigate the probability of 2-, 4-, and 6-year OS of patients with OV. Subsequently, the nomogram was validated by discrimination and calibration. Discrimination was measured with the concordance index (C-index), using the R package "survcomp." Calibration was evaluated graphically by plotting the nomogram prediction probabilities against the actual proportion. Overlap with the slash diagonal indicates that the model is completely consistent.

Functional enrichment analysis

To investigate the underlying biological functions of the FRG signature, 15 FRGs and differentially expressed genes (DEGs) with adj. $p < 0.05$ and $|\log2FC| > 0.5$ between the high- and low-risk samples were selected separately for Gene Ontology (GO) classification and Kyoto Encyclopedia of Genes and Genomes (KEGG) pathway analyses, using the R packages "limma" and "clusterProfiler." Gene set enrichment analysis (GSEA) of the high- and low-risk samples was conducted using the GSEA software (Subramanian et al., 2005) (http://www.broadinstitute.org/gsea).

Immune infiltration landscape analysis

The enrichment scores of various immune cells represented by 16 gene sets and immune-related functions represented by 13 gene sets were quantified using single-sample gene (ss)GSEA in the Bioconductor package "GSVA" (Barbie et al., 2009; Rooney et al., 2015). The annotated immune-related gene sets are provided in Supplementary Table S1C. Enrichment scores for seven steps of the cancer-immunity cycle were calculated with the Tracking Tumor Immunophenotype (TIP) meta-server tool (http://biocc.hrbmu.edu.cn/TIP/) (Xu et al., 2018). The Estimation of STromal and Immune cells in MAlignant Tumor tissues using Expression data (ESTIMATE) immune score was computed to analyze the infiltration levels of immune cells using the "ESTIMATE" R package. The expression correlation between the key immune checkpoint molecules and risk score were further analyzed.

Validation of the predictive power of the risk score in immunotherapy and chemotherapy

SubMap method from GeneParttern was applied to predict the response to immunotherapy in OV patients with high- and low-risk groups (Hoshida et al., 2007). Besides, the anti-PD-1 and anti-CTLA4 cohorts were used as the independent external validation cohorts, which were also used on other predictors to compare with our signature in terms of performance. Fourteen published predictors of clinical response to immune checkpoint blockade (ICB), such as the TIDE score, microsatellite instability score (MSI), and T-cell exclusion score, were integrated into TIDE computational framework (Fu et al., 2020) (http://tide.dfci.harvard.edu). Prediction scores were calculated and downloaded for each patient in the anti-PD-1 and anti-CTLA4 cohorts after uploading the normalized gene expression profiles to TIDE. Furthermore, the pRRophetic algorithm was utilized to calculate the half-maximal inhibitory concentration (IC50) values for monitoring the response of chemotherapy to the ovarian cancer patients (Geeleher et al., 2014).

Statistical analysis

All statistical analyses were carried out using the R programming software (version 3.6.3). Two-sided Pearson's

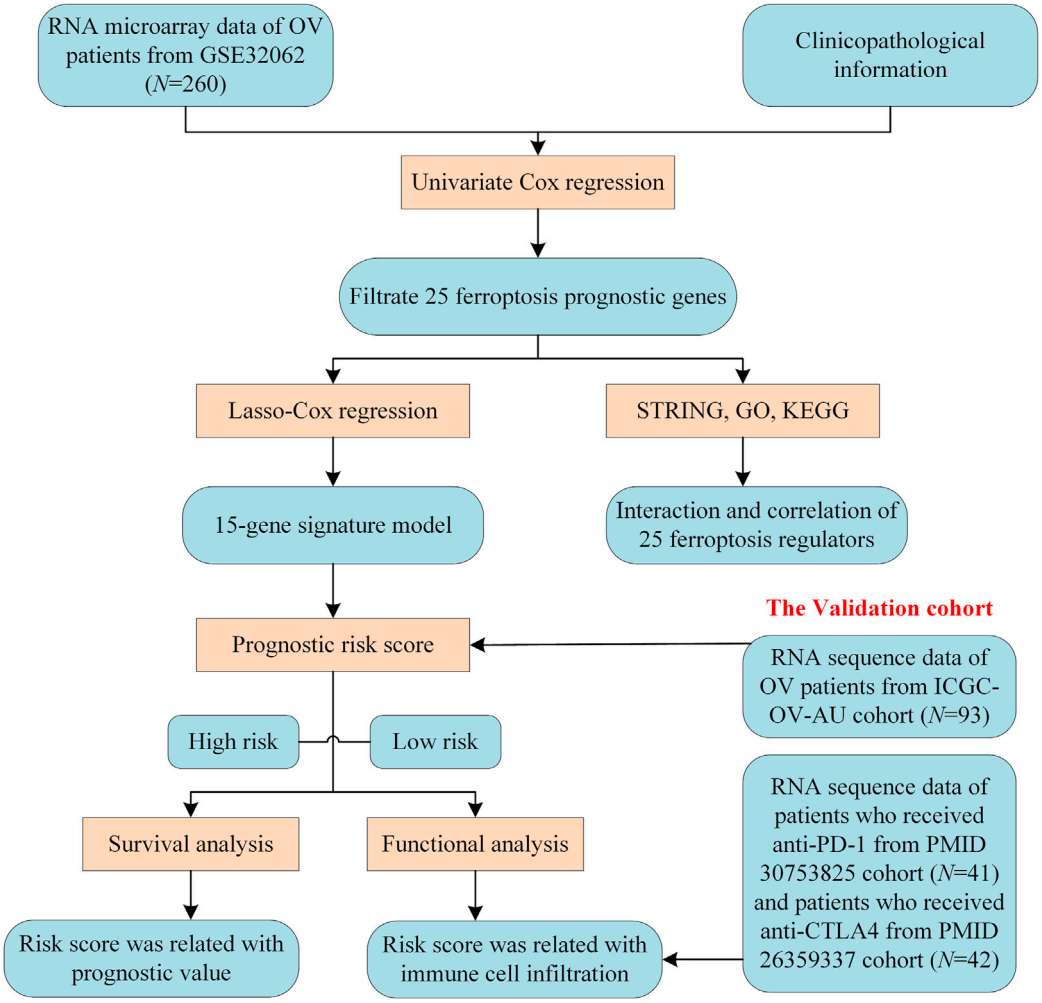

FIGURE 1
Flow chart for cohort collection and bioinformatics analysis.

chi-squared test or Fisher's exact test was used for categorical data, and the non-parametric Wilcoxon test was applied for quantitative data. KM analysis with the log-rank test for OS was conducted using the auto-select best threshold or the median value. Correlations between variables were determined using Spearman or Pearson correlation. Significant differences between two correlated ROC curves were analyzed using DeLong's test. Unless noted otherwise, $p < 0.05$ was considered statistically significant.

Results

A methodology flow chart for the present study is shown in Figure 1. In total, 260 Asian OV samples from the GSE32062 cohort and 93 Caucasian OV samples from the ICGC (OV-AU) cohort with complete clinical information were included. Detailed clinical information for these samples is provided in Supplementary Table S2A.

Identification of prognostic ferroptosis-related genes in the GSE32062 cohort

We analyzed 213 well-defined FRGs in this study, namely 75 ferroptosis driver genes, 58 ferroptosis suppressor genes, and 80 ferroptosis marker genes. Detailed information on these FRGs is provided in Supplementary Table S1A. The relationship between FRG expression levels and the OS of patients in the GSE32062 cohort was evaluated using univariate Cox proportional hazards regression analysis. Twenty-five FRGs were significantly correlated with OS ($p < 0.05$, Figure 2A). Among the 25 prognostic FRGs, seven genes (*IDH1*, *NRAS*, *STMN1*, *ELAVL1*, *VDAC2*,

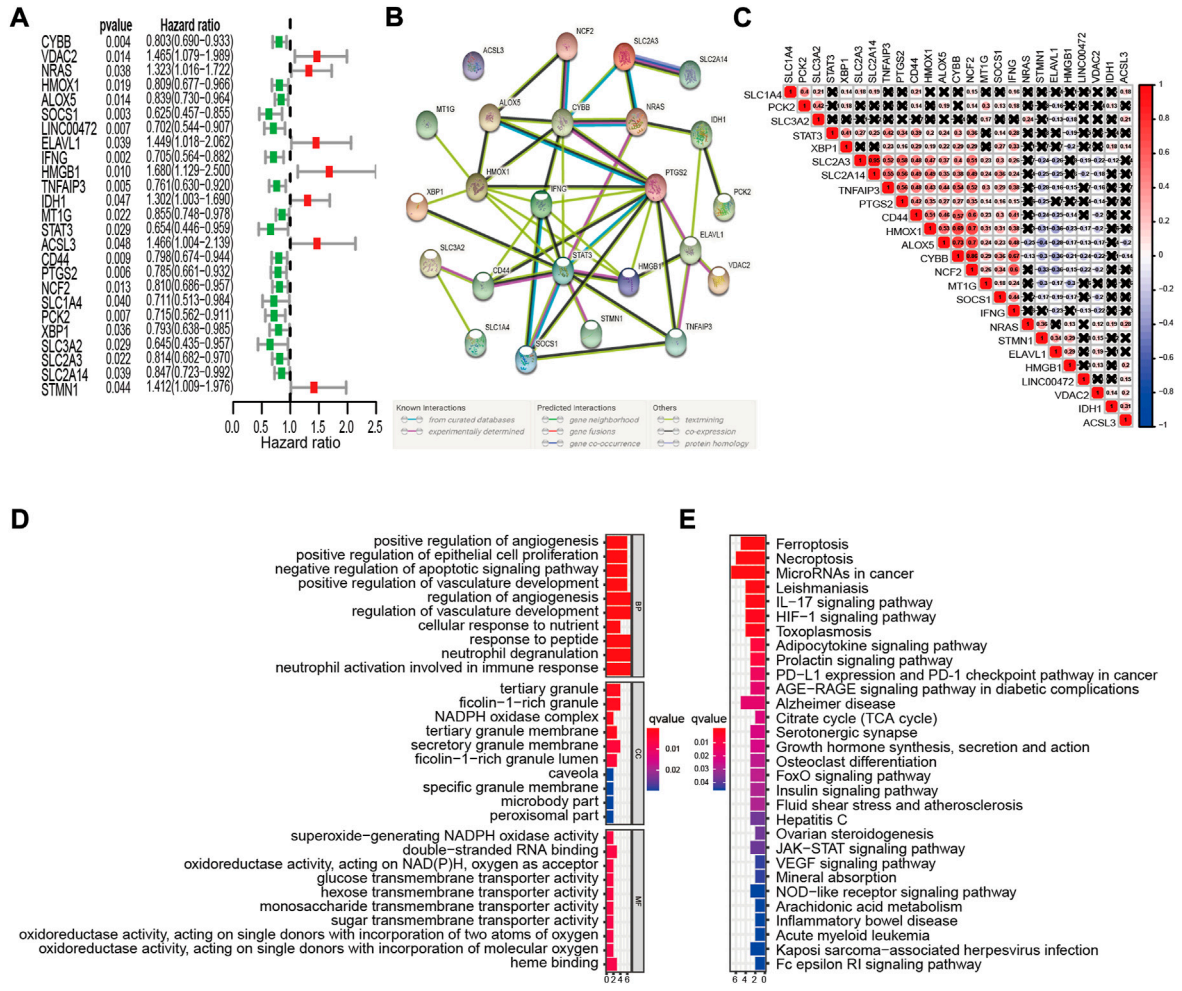

FIGURE 2
Identification of prognostic FRGs in the GSE32062 cohort. **(A)** Forest plots of HRs and 95% CIs of the association between FRGs expression and OS. **(B)** A PPI network showing the interactions among the prognostic FRGs. **(C)** FRGs correlation network. **(D,E)** The most significantly enriched GO terms **(D)** and KEGG pathways **(E)** are displayed. FRG, ferroptosis-related gene; HR, hazard ratio; CI, confidence interval; OS, overall survival; PPI, protein-protein interaction; GO, Gene Ontology; KEGG, Kyoto Encyclopedia of Genes and Genomes.

ACSL3, and *HMGB1*) were identified as risk factors, with hazard ratios (HRs) > 1. The remaining 18 genes (*SOCS1*, *SLC3A2*, *STAT3*, *LINC00472*, *IFNG*, *SLC1A4*, *PCK2*, *TNFAIP3*, *PTGS2*, *XBP1*, *CD44*, *CYBB*, *HMOX1*, *NCF2*, *SLC2A3*, *ALOX5*, *SLC2A14*, and *MT1G*) were identified as protective factors, with HRs < 1. In a PPI network of the prognostic FRGs, *PTGS2*, *STAT3*, *HMOX1*, *IFNG*, and *CYBB* were hub genes (Figure 2B). Furthermore, most of the protective factors were strongly positively correlated with each other ($p < 0.05$, Figure 2C). GO enrichment analysis revealed that the 25 FRGs were primarily involved in the biological process of tumor progression, including "positive regulation of angiogenesis," "epithelial cell proliferation," "negative regulation of apoptotic signaling pathway," and other immune-specific processes, including "neutrophil degranulation" and "neutrophil activation involved in immune response" (adj. $p < 0.05$, Figure 2D). KEGG analysis results suggested that these genes were correlated with ferroptosis and necroptosis (adj. $p < 0.05$, Figure 2E).

Construction of a novel 15-ferroptosis-related gene prognostic signature in the GSE32062 cohort

Genes without prognostic significance were filtered out, leaving 25 genes for further analysis. It is well known that the more genes the signature included, the more complex it became. Hence, the LASSO algorithm was employed to shrink the variables and to optimize the signature. A 15-

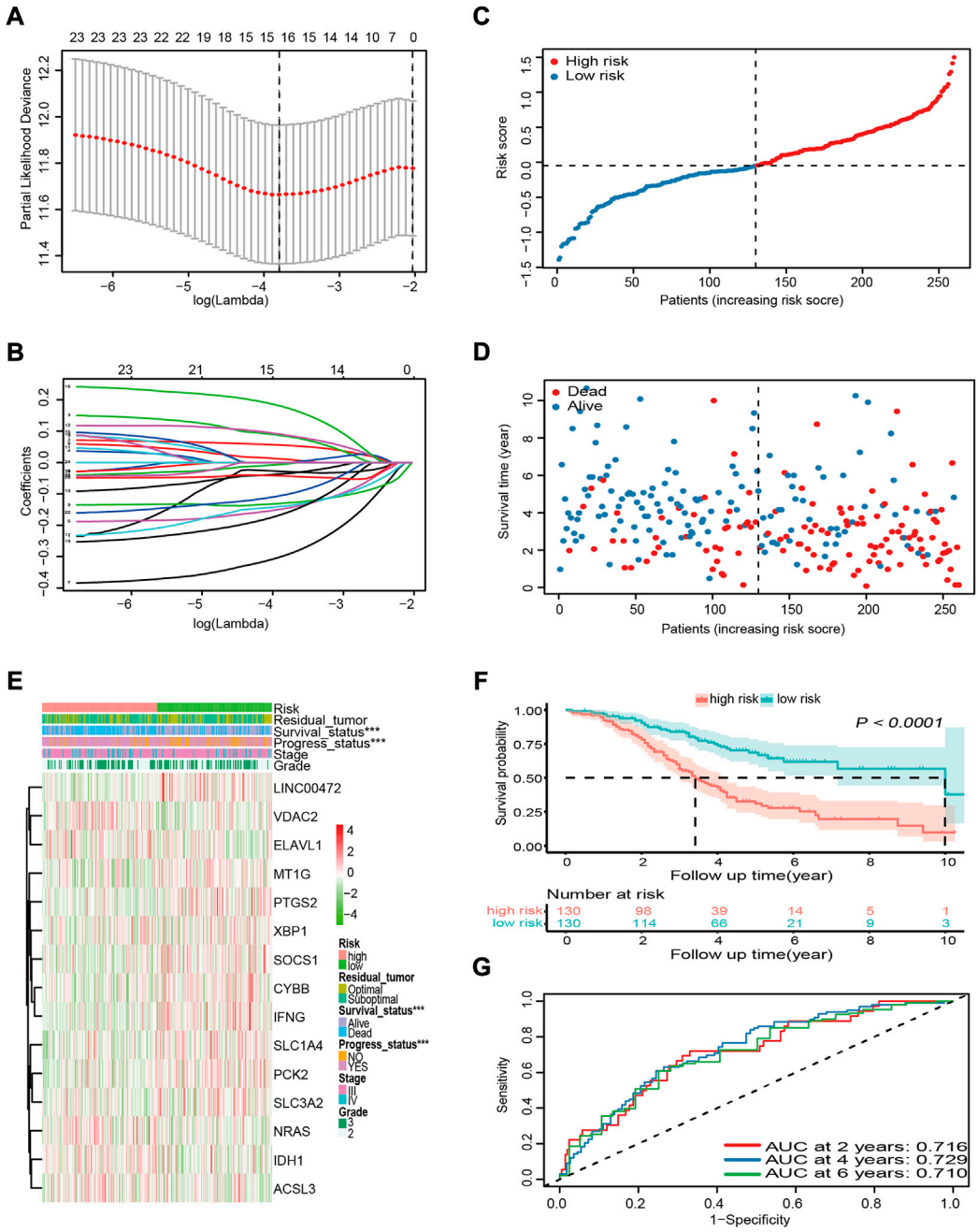

FIGURE 3
Construction and prognostic analysis of the 15-FRG prognostic signature based on the GSE32062 cohort data. **(A)** Penalty parameter λ optimization using the LASSO algorithm, with 10-fold cross validation. The optimal values using minimum criteria (left) and the one standard error of the minimum criteria (right) are indicated by dotted vertical lines. **(B)** LASSO coefficient profiles of the 25 candidate genes. **(C)** Distribution and median values of the risk scores. **(D)** Distributions of survival time, survival status, and risk score. **(E)** Distributions of risk score, clinical characteristics, and gene expression panels. *$p < 0.05$; **$p < 0.01$; ***$p < 0.001$. **(F)** Kaplan–Meier curves for OS in the different groups. **(G)** Time-dependent ROC curves and their AUCs verifying the prediction efficacy of the risk score. FRG, ferroptosis-related gene; LASSO, least absolute shrinkage and selection operator; OS, overall survival; ROC, receiver operating characteristic; AUC, area under the curve.

FRG signature was constructed based on the optimal λ value (Figures 3A,B). Based on the expression levels of the 15 FRGs and the corresponding regression coefficients, the following signature formula was built: risk score = −0.0291 × *CYBB* + 0.0548 × *VDAC2* + 0.0836 × *NRAS* − 0.1457 × *SOCS1* − 0.2943 × *LINC00472* + 0.0101 ×

ELAVL1 − 0.1289 × *IFNG* + 0.0873 × *IDH1* − 0.0351 × *MT1G* + 0.1742 × *ACSL3* − 0.1379 × *PTGS2* − 0.1599 × *SLC1A4* − 0.0432 × *PCK2* − 0.0044 × *XBP1* − 0.1017 × *SLC3A2*. To evaluate the prognostic prediction performance of the 15-FRG signature, the risk score of each sample was calculated according to the signature formula above. The OV patients were classified into a high-risk group (n = 130) and a low-risk group (n = 130) based on median risk score (Figure 3C). Patients with a high risk of the disease tended to suffer from earlier disease progression and worse survival status than their low-risk counterparts (p < 0.001, Figures 3D,E). Meanwhile, KM survival analysis revealed that the OS rate was significantly worse in the high-risk group compared with the low-risk group (p < 0.0001, Figure 3F). To exclude the influence of confounding clinical characteristics on the risk score, we further stratified patients by clinical variables to evaluate the prognostic prediction performance of the risk score on OS. The results reconfirmed that the risk score could classify the patients into high- and low-risk groups with significantly different OS rate (Supplementary Figures S1A–C). The prognostic performances of the 15 ferroptosis-related genes were also further confirmed by using Kaplan Meier plotter online tool. The results revealed that, apart from ELAVL1 and LINC00472, the other 13 FRGs were also significantly associated with patient OS (Supplementary Figure S2). Based on our findings above, time-dependent ROC curves were constructed to further evaluate the accuracy of the risk score for predicting prognosis. The area under the ROC curve (AUC) of the risk score for OS reached 0.716, 0.729, 0.710 at 2, 4, 6 years respectively, which suggested that the risk score had adequate prediction efficiency (Figure 3G).

Validation of the 15-ferroptosis-related gene prognostic signature in the international cancer genome consortium cohort

To validate the robustness and reproducibility of the signature constructed using Asian cohort data for predicting OS in Caucasian cohort data, we first calculated the risk score for each Caucasian OV sample in the ICGC cohort with the formula used in the GSE32062 cohort. Based on the median risk score of the GSE32062 cohort, patients from the ICGC cohort were divided into high- and low-risk groups (Figure 4A). As expected, similar results were obtained in Caucasian OV patients. In the high-risk group, patients were more likely to die earlier (Figure 4B) and the risk of mortality was higher (p = 0.0019, Figures 4C,D). Comparison of OS stratified by age, tumor stage, and disease status also further confirmed these results (Supplementary Figures S1D–F). Further, the AUC of the risk score for OS was 0.627 at 2 years, 0.726 at 4 years, and 0.801 at 6 years in the Caucasian cohort, suggesting that the risk score had adequate generalization performance between different races (Figure 4E).

To illustrate the advantages of established 15-FRG signature, we further compared the performance of our prediction model with that reported previously (Wang H. et al., 2021; Yu et al., 2021) in the ICGC cohort. The results showed that our novel 15-FRG model (Model3) outperformed the 3-gene model (Model1; PMID: 35071242) and 6-gene model (Model2; PMID: 34075060) in predicting overall survival of an individual patient (adj. p < 0.05, Figures 5A–C), especially in predicting the long-term survival outcome (OS > 2 years) (Figure 5D).

Independent prognostic value of the 15-ferroptosis-related gene prognostic signature

More importantly, we conducted univariate and multivariate Cox regression analyses to explore the independence of the risk score as a prognostic factor of OS. The risk score was found to be obviously related to OS in both the GSE32062 and the ICGC cohorts by univariate Cox regression analysis (HR = 3.634, 95% CI = 2.547–5.185, p < 0.001; HR = 2.538, 95% CI = 1.593–4.044, p < 0.001, respectively, Figures 6A,B). Furthermore, after the adjustment of the potential confounding factors by multivariate Cox regression analysis, the risk score was validated as an independent prognostic factor of OS in both the GSE32062 and ICGC cohorts (HR = 3.532, 95% CI = 2.451–5.091, p < 0.001; HR = 2.320, 95% CI = 1.455–3.699, p < 0.001, respectively, Figures 6C,D).

Prognostic nomogram establishment for predicting the overall survival of ovarian cancer patients

We integrated the available clinical characteristics and risk score into a prediction system to create a novel nomogram system for predicting OS. Statistically significant variables were residual tumor (p < 0.01) and risk score (p < 0.001) in the GSE32062 cohort model (Figure 7A), and disease status (p < 0.01) and risk score (p < 0.001) in the ICGC cohort model (Figure 7B). The nomogram demonstrated good predictive accuracy with a C-index of 0.71 (95% CI = 0.66–0.75) in the GSE32062 cohort and 0.65 (95% CI = 0.57–0.72) in the ICGC cohort. Bootstrap validation was performed for calibration of 6-year OS, and the calibration curve indicated excellent agreement between actual and nomogram-predicted outcomes across the spectrum of predictions (Figures 7C,D). Taken together, these results revealed that the nomogram based on 15-FRG signature could efficiently predict patient survival outcome and showed a significant clinical practical value for OV patients.

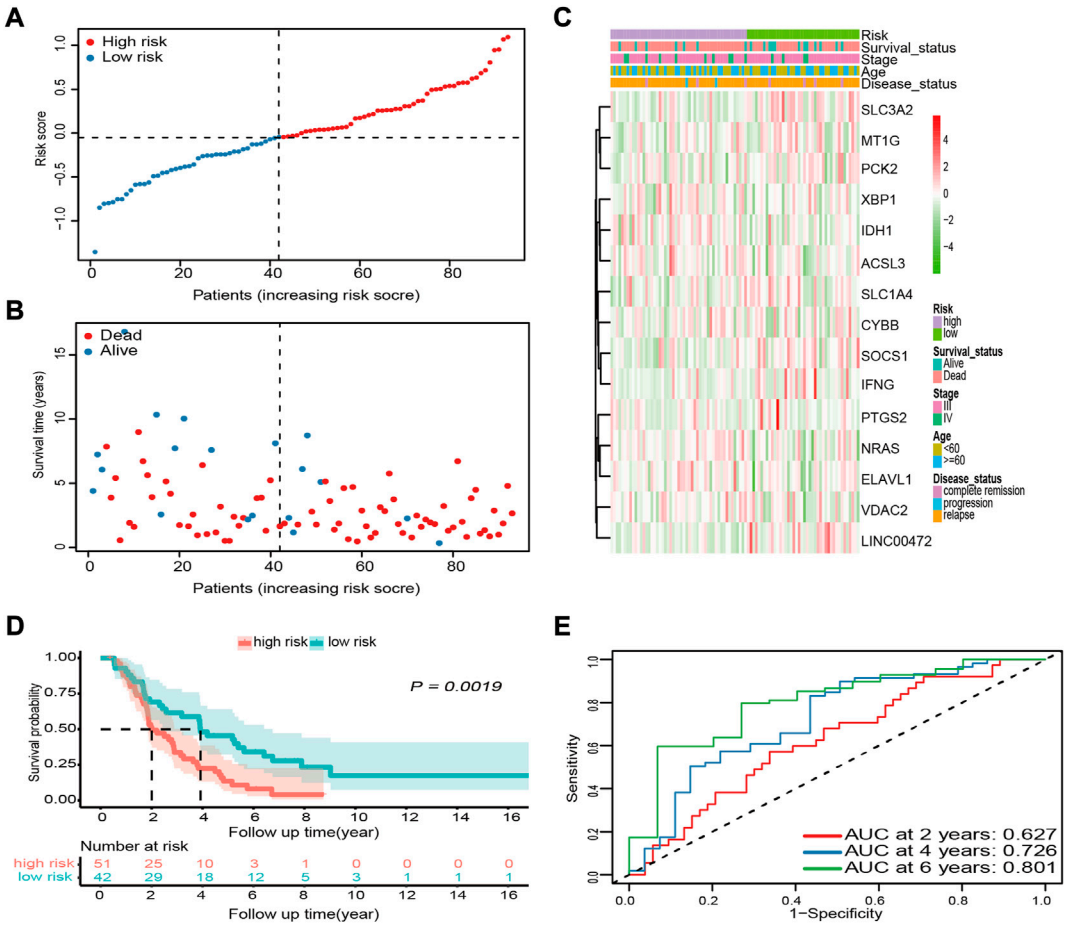

FIGURE 4
External validation of the prognostic performance of the 15-FRG signature in the ICGC cohort. **(A)** Distribution and median values of the risk scores. **(B)** Distributions of survival status, survival time, and risk score. **(C)** Distributions of risk score, clinical characteristics, and gene expression panels. **(D)** Kaplan–Meier curves for OS in the different groups based on the cut-off point determined for the GSE32062 cohort. **(E)** Time-dependent ROC curves and their AUCs. FRG, ferroptosis-related gene; ICGC, International Cancer Genome Consortium; OS, overall survival; ROC, receiver operating characteristic; AUC, area under the curve.

Functional analysis of 15-ferroptosis-related gene prognostic signature

To investigate the 15-FRG prognostic signature in terms of underlying biological functions and pathways. GO and KEGG pathway enrichment analyses were performed first for 15 ferroptosis-related genes. The GO and KEGG analysis results indicated that the 15 ferroptosis-related genes were enriched in ferroptosis pathway and lipid-related biologic process, including "regulation of lipid metabolic process" and "regulation of lipid biosynthetic process." Interestingly, those FRGs were also enriched for immune-related terms, including "positive regulation of MHC class II biosynthetic process," "positive regulation of T cell differentiation" and "IL−17 signaling pathway" (adj. $p < 0.05$, Supplementary Figures S3A, S3B). In parallel, 560 DEGs were detected between high- and low-risk samples (Figure 8A), and then the GO and KEGG pathway enrichment analyses of 560 DEGs were also performed. As expected, DEGs were also significantly enriched in several iron-related molecular functions, such as "cellular divalent inorganic cation homeostasis," "response to metal ion," "divalent inorganic cation transport" and "regulation of reactive oxygen species biosynthetic process" (adj. $p < 0.05$, Supplementary Tables S3A, S3B). Interestingly, among the top 30 GO terms, the DEGs were also obviously enriched in various immune-related GO terms, such as "T-cell activation," "leukocyte migration," "regulation of lymphocyte activation," "leukocyte cell–cell adhesion," "response to interferon-gamma (IFN-γ)," "major histocompatibility complex (MHC) protein complex," "cytokine activity" and "antigen binding" (adj. $p < 0.05$, Figure 8C). Meanwhile, some immune-related pathways

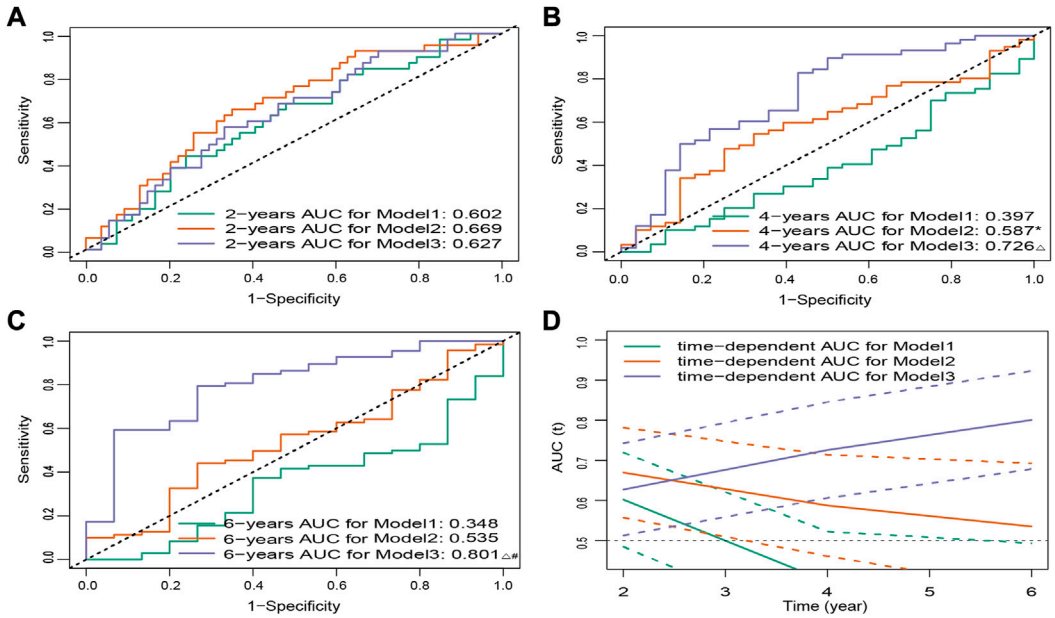

FIGURE 5
ROC curves for three models of predicting 2- **(A)**, 4- **(B)**, and 6-year **(C)** OS. *$p < 0.05$ versus Model1, △ $p < 0.001$ versus Model1, #$p < 0.05$ versus Model2. **(D)** Time-dependent ROC curves for three models in the ICGC cohort. Dashed lines represent 95% CIs. ROC, receiver operating characteristic; OS, overall survival; ICGC, International Cancer Genome Consortium; CI, confidence interval.

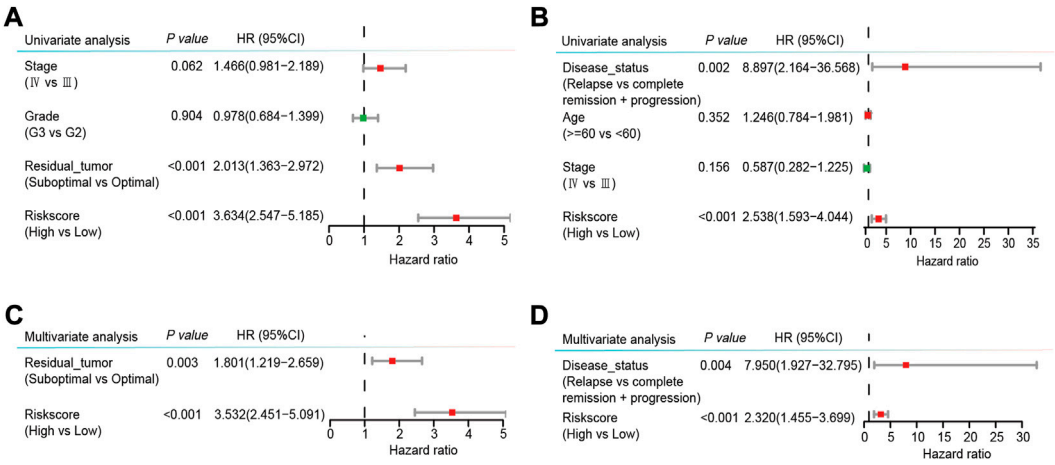

FIGURE 6
Forest plots of univariable **(A,B)** and multivariable **(C,D)** Cox regression analyses with HRs and 95% CIs in the GSE32062 cohort **(A,C)** and the ICGC cohort **(B,D)**. HR, hazard ratio; CI, confidence interval; ICGC, International Cancer Genome Consortium.

were also found in the KEGG pathway analysis, including "Cytokine–cytokine receptor interaction," "Phagosome," "Antigen processing and presentation," "Th17 cell differentiation," "Natural killer cell-mediated cytotoxicity" and "Th1 and Th2 cell differentiation" (adj. $p < 0.05$, Figure 8D).

To further investigate the relationship between the DEGs and immune status, an intersection analysis between the 560 DEGs and

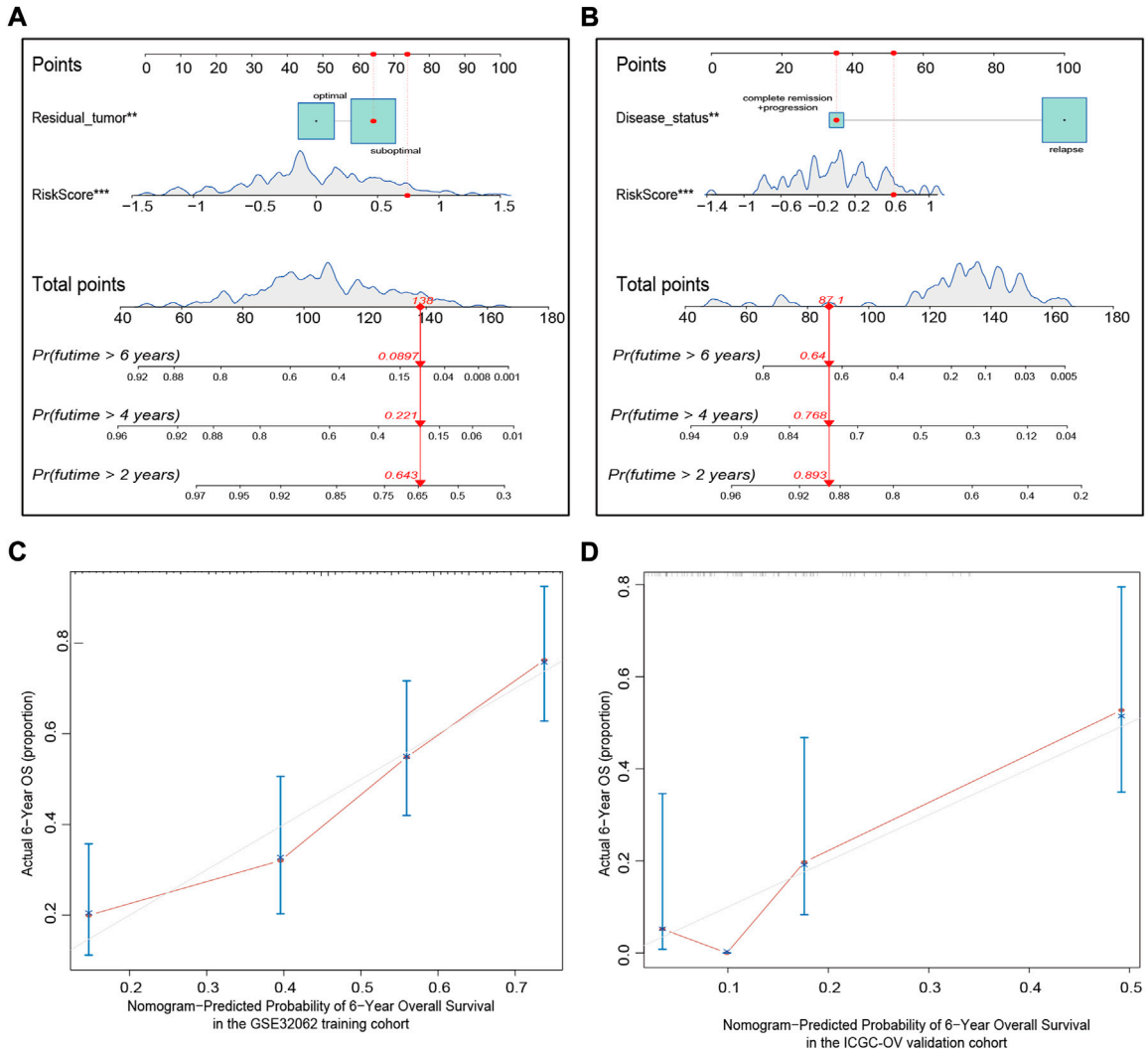

FIGURE 7
Nomogram establishment for predicting the 2-, 4-, and 6-year OS of OV patients in the GSE32062 **(A)** and ICGC **(B)** cohorts. An example demonstrating the percentage of survival according to the nomogram score is marked in red. To use the nomogram, first find the position of a variable on the variable axis, and then, draw a vertical line upward to find the point number of the variable. The sum of these point numbers is presented on the total points axis, and a vertical line is drawn downward to determine the differential OS probabilities. $^{**}p < 0.01$; $^{***}p < 0.001$. Calibration curves of the nomogram predictive performance in the GSE32062 **(C)** and ICGC **(D)** cohorts. Distributions of the predicted probabilities of 6-year OS are shown at the top of the graphs, the brownish red solid line indicates the performance of the nomogram; the closer the line to the gray line, the better the consistency between predicted and actual outcomes. OS, overall survival; OV, ovarian cancer; ICGC, International Cancer Genome Consortium.

1793 IRGs was performed, revealing 158 immune-related DEGs (Figure 8B). Next, for the high- and low-risk samples, we further conducted GSEA using the molecular signatures database (MSigDB) to elucidate the association between the risk score and immune regulation. GSEA revealed that highly similar immune-related GO terms and KEGG pathways were enriched in the low-risk group (adj. $p < 0.05$, FDR < 0.25, Figures 8E,F), including antigen ("KEGG_ANTIGEN_PROCESSING_AND_PRESENTATION"), cytokine ("KEGG_CYTOKINE_CYTOKINE_RECEPTOR_INTERACTION"), chemokines ("GO_CHEMOKINE_BINDING"), immune cells ("KEGG_T_CELL_RECEPTOR_SIGNALING_PATHWAY"), damage-associated molecular patterns ("KEGG_NOD_LIKE_RECEPTOR_SIGNALING_PATHWAY"; "KEGG_TOLL_LIKE_RECEPTOR_SIGNALING_PATHWAY"), and other immune-regulatory processes. Collectively, these findings suggested that the 15 FRGs and ferroptosis-based risk score were largely associated with immune-related biological processes, and patients in the high- and low-risk group might have different immune landscape.

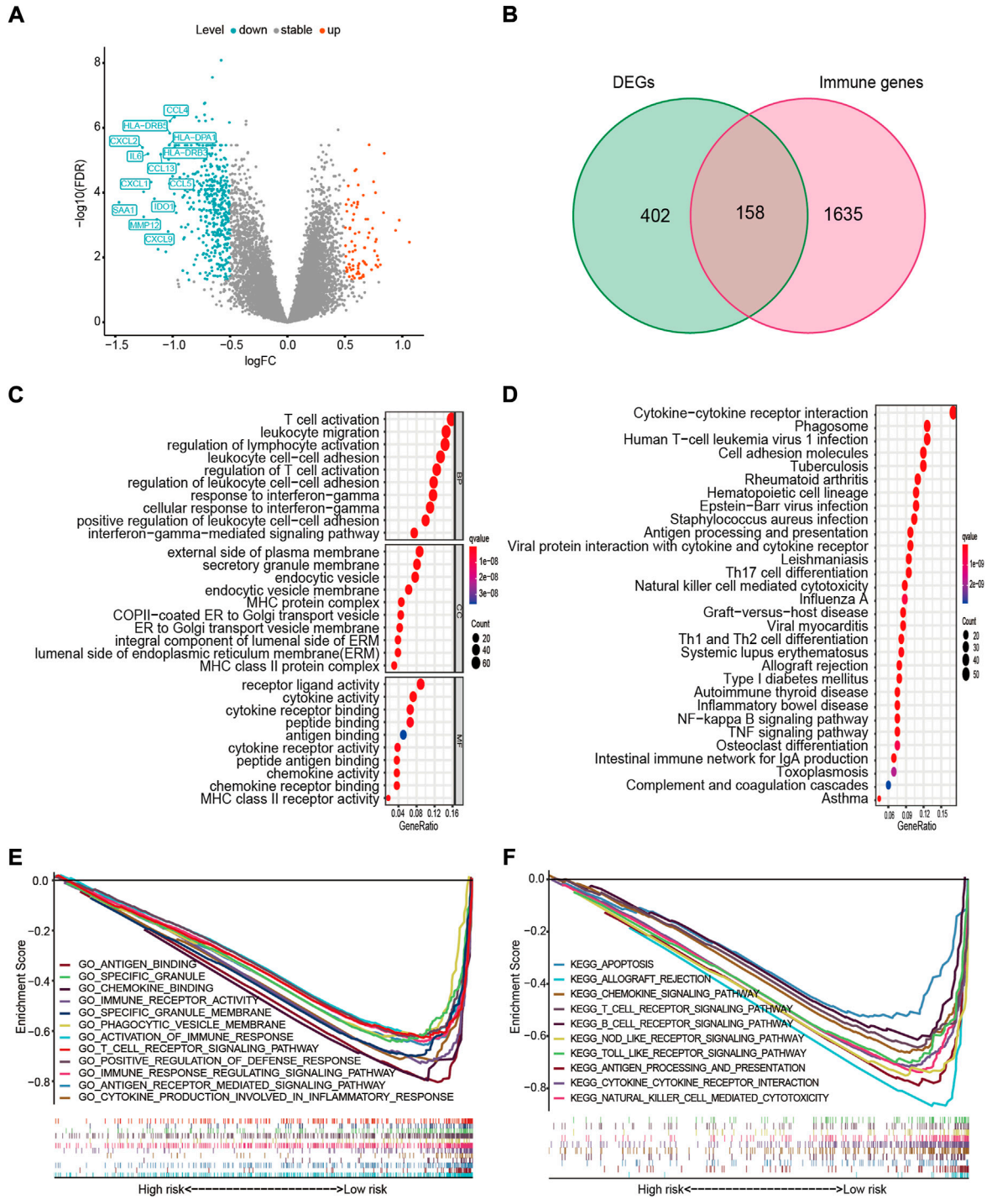

FIGURE 8
Functional enrichment and pathway analyses. **(A)** Volcano plot of 560 DEGs. Upregulated immune-related DEGs with $p < 0.05$ and $|log2FC| > 1$ in the low-risk group are presented (left). **(B)** Venn diagram of DEGs and IRGs. **(C)** The top 10 GO terms in molecular function (MF), cellular component (CC), and biological process (BP). **(D)** The top 30 enriched KEGG pathways. **(E)** Most significant GSEA sets, from GO-related MSigDB, associated with the low-risk group. **(F)** Most significant GSEA sets, from KEGG-related MSigDB, associated with the low-risk group. DEG, differentially expressed gene; FC, fold change; IRG, immune-related gene; GO, Gene Ontology; KEGG, Kyoto Encyclopedia of Genes and Genomes; GSEA, gene set enrichment analysis; MSigDB, The Molecular Signatures Database.

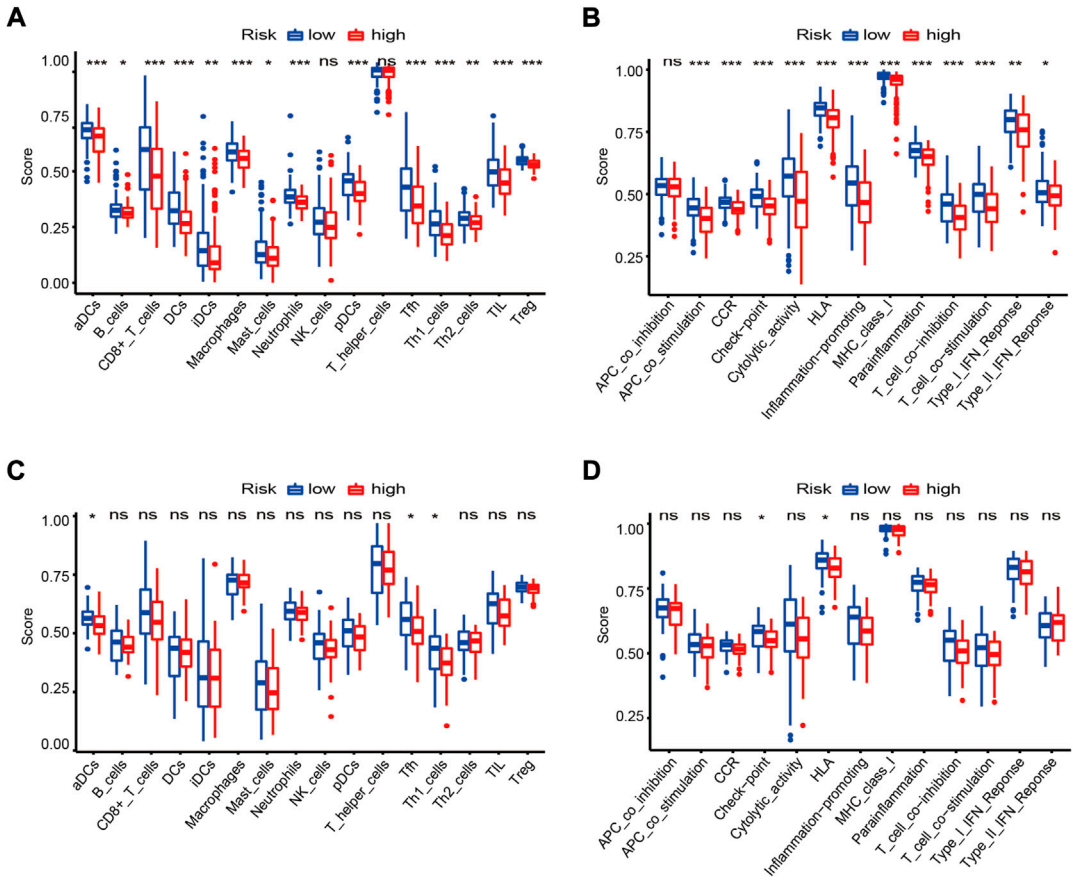

FIGURE 9
Landscapes of immune cell infiltration and immune-related functions between risk groups in the GSE32062 **(A,B)** and ICGC **(C,D)** cohorts. Boxplots of ssGSEA scores in 16 types of immune cells **(A,C)** and 13 immune-related functions **(B,D)** are presented. *adj. $p < 0.05$; **adj. $p < 0.01$; ***adj. $p < 0.001$; ns, not significant. ICGC, International Cancer Genome Consortium; GSEA, gene set enrichment analysis; CCR, cytokine-cytokine receptor; HLA, human leukocyte antigen.

Differences in the immune landscape among risk groups

Given the high correlation between the ferroptosis-based risk score and immune-related biological processes, the relationships among the risk score, immune cell infiltration, and immune-related functions were analyzed in more detail. First, we used the ssGSEA algorithm to assess immune infiltration and immune-related functions in each OV sample in the GSE32062 cohort. The infiltration levels of 14 out of 16 immune cell subpopulations and 12 out of 13 immune-related functions were higher in the low-risk group than in the high-risk group (adj. $p < 0.05$, Figures 9A,B). And then, based on ICGC cohort data, the significant enrichment of three immune cell subpopulations were reconfirmed in the low-risk group, namely antigen-processing and presenting cells subpopulations ("aDCs") and helper T-cell subpopulations ("Tfh", "Th1_cells") (adj. $p < 0.05$, Figure 9C), which were also enriched in the above KEGG analysis. In parallel, the significant enrichment of two immune-related functions were reconfirmed in the low-risk group, namely checkpoint molecules ("Check-point") and human leukocyte antigen ("HLA") functions (adj. $p < 0.05$, Figure 9D), corresponding to the GO term "MHC protein complex."

As the complex antitumor immune response comprises a series of stepwise events (termed cancer-immunity cycle). We determined enrichment scores for the seven-step cancer-immunity cycle using the TIP meta-server tool in both cohorts. The results revealed that antigen release and presentation cycles ("Step 1" and "Step 2") and immune cells recruitment cycles ("Step 4. CD4 T-cell. recruiting, and Macrophage. Recruiting") were significantly enriched in the low-risk group (adj. $p < 0.05$, Figures 10A,B). The same trend was also observed for the overall immune activity score of cancer-immunity cycle (by summating the normalized scores of all seven steps) in both cohorts (adj. $p < 0.05$, Figures 10C,D).

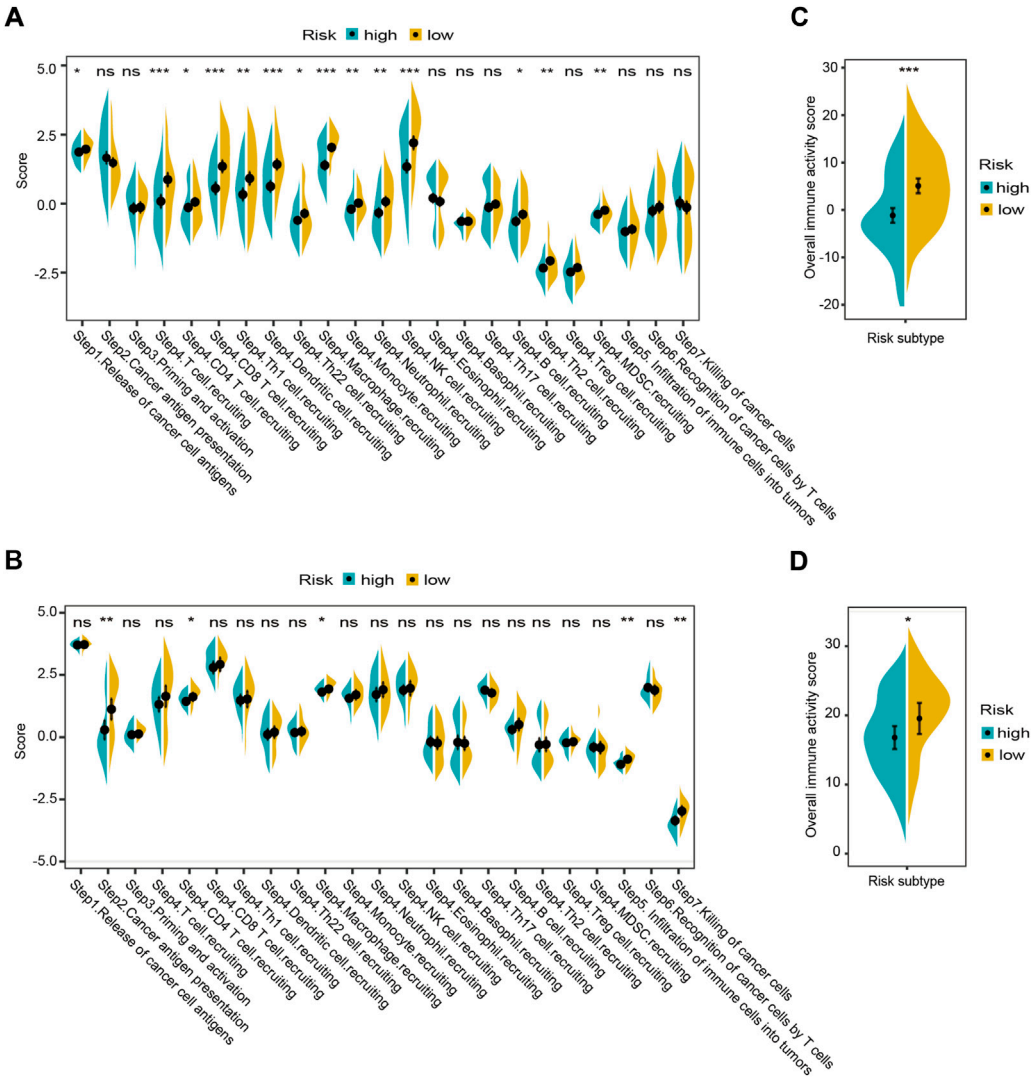

FIGURE 10
Landscapes of the seven-step cancer-immunity cycle between different risk groups in the GSE32062 **(A,C)** and ICGC **(B,D)** cohorts. Enrichment scores in the seven-step cancer-immunity cycle **(A,B)** and an overall immune activity score **(C,D)** are shown in violin plots. *adj. $p < 0.05$; ** adj. $p < 0.01$; ***adj. $p < 0.001$; ns, not significant. ICGC, International Cancer Genome Consortium.

A high degree of immune cell infiltration is usually accompanied by high expression levels of immune checkpoint molecules (Galon and Bruni, 2019). It is generally recognized that patients with a high immune score or immune checkpoint expression levels may achieve a higher objective response rate to immunotherapy (Taube et al., 2018). Therefore, the immune score and immune checkpoint molecules have been shown to be predictors of response to various tumor immunotherapies. In this study, we observed a significant negative correlation between the risk score and the immune score in the GSE32062 and ICGC cohorts (Spearman correlation: r = −0.39, $p < 0.001$; r = −0.28, $p = 0.007$, respectively, Figures 11A,B). In addition, we also conducted a correlation analysis between mRNA levels of seven checkpoint molecules and the risk score. The results indicated that most checkpoint molecules were strongly positively correlated with each other, while the mRNA expression levels of CTLA4, PD-1, PD-L1, LAG3, TIGIT, and VISTA were significantly negatively correlated with the risk score in both cohorts (Pearson correlation: r < −0.2, $p < 0.05$, Figures 11C,D). Taken together, the results indicated that patients in the low-risk group had an immune "hot" status, which was characterized by a high degree of immune cell infiltration and multiple checkpoint activation (Galon and Bruni, 2019), and might be more likely to benefit from immunotherapy.

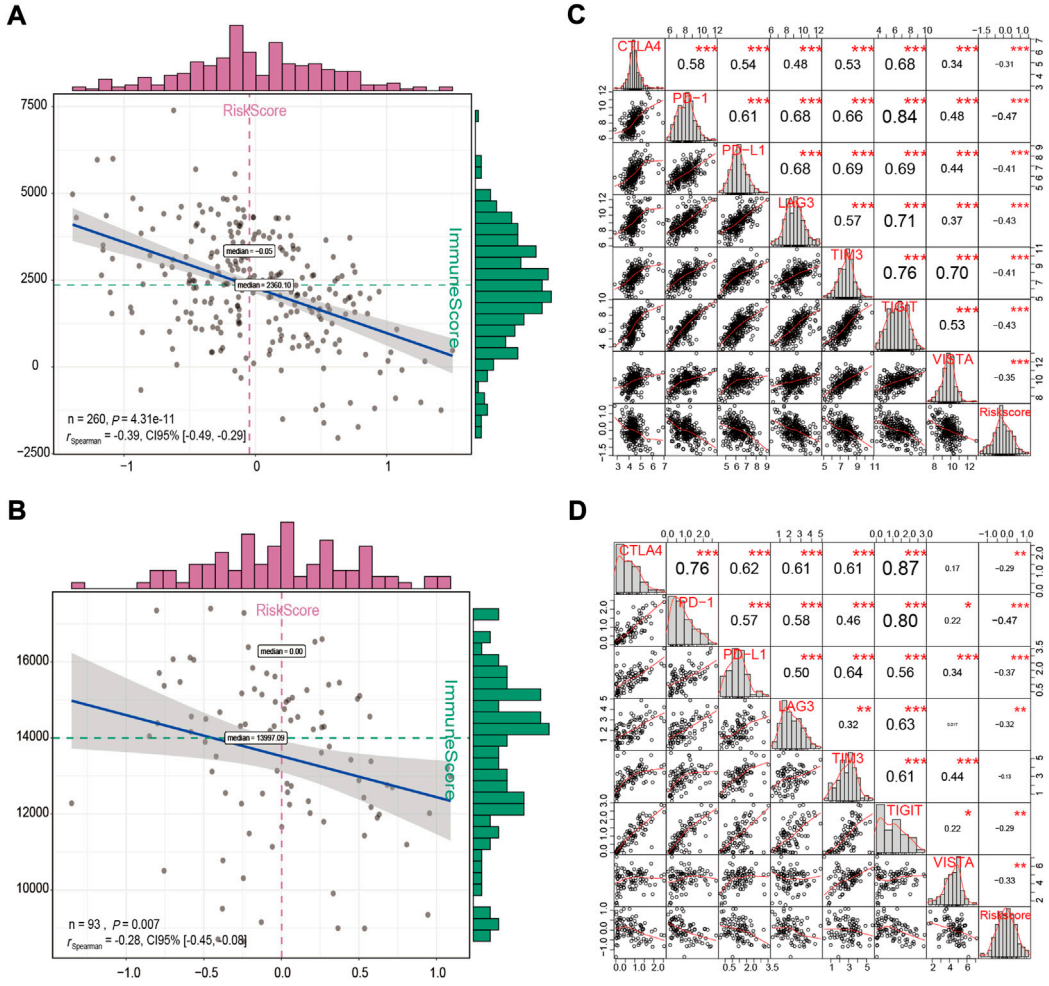

FIGURE 11
Correlation analysis between the immune score and the risk score **(A,B)**, and between the risk score and the expression levels of immune checkpoint molecules **(C,D)** in the GSE32062 **(A,C)** and ICGC **(B,D)** cohorts. *$p < 0.05$; **$p < 0.01$; ***$p < 0.001$. ICGC, International Cancer Genome Consortium.

Prediction performance of the risk score in immunotherapy and chemotherapy

In spite of the fact that immune checkpoint inhibitors have not yet been approved as routine drugs for patients with OV. We therefore utilized the SubMap algorithm to predict the likelihood of response to immunotherapy in patients with OV. We were very delighted to see that patients with low risk showed a greater likelihood of responding to anti-PD-1 treatment in both OV cohorts (Bonferroni corrected $p = 0$ 0.008, Supplementary Figures S3C, S3D). In addition, RNA-seq data and the related clinical information from previous studies, including 42 samples following anti-CTLA4 immunotherapy and 41 samples following anti-PD-1 immunotherapy, were used for external validation. Detailed clinical information for these samples is provided in Supplementary Table S2B. The risk score was calculated for each patients using the 15-FRG risk score formula. First, we observed that the non-responders had a significantly higher risk score than the responders in both external cohorts ($p = 0.012$; $p = 0.024$, respectively, Figures 12A,B). A Kaplan–Meier curve demonstrated that high-risk patients had a significantly lower survival rate than their low-risk counterparts in immunotherapy (Figures 12C,D, $p < 0.01$). Consistently, after adjustment for available confounding factors by multivariate Cox regression, the risk score was still an independent prognostic factor for OS in the anti-CTLA4 cohort and for progression-free survival (PFS) in the anti-PD-1 cohort (HR = 3.842, 95% CI = 1.495–9.877, $p = 0.005$; HR = 4.023, 95% CI = 1.061–15.247, $p = 0.041$, respectively) (Figures 12E,F). Then, we compared the prediction efficiency of the risk score to that of 15 published predictors in both immunotherapy cohorts. Based on sibling comparison between 15 published predictors (Figures 12G,H), we found

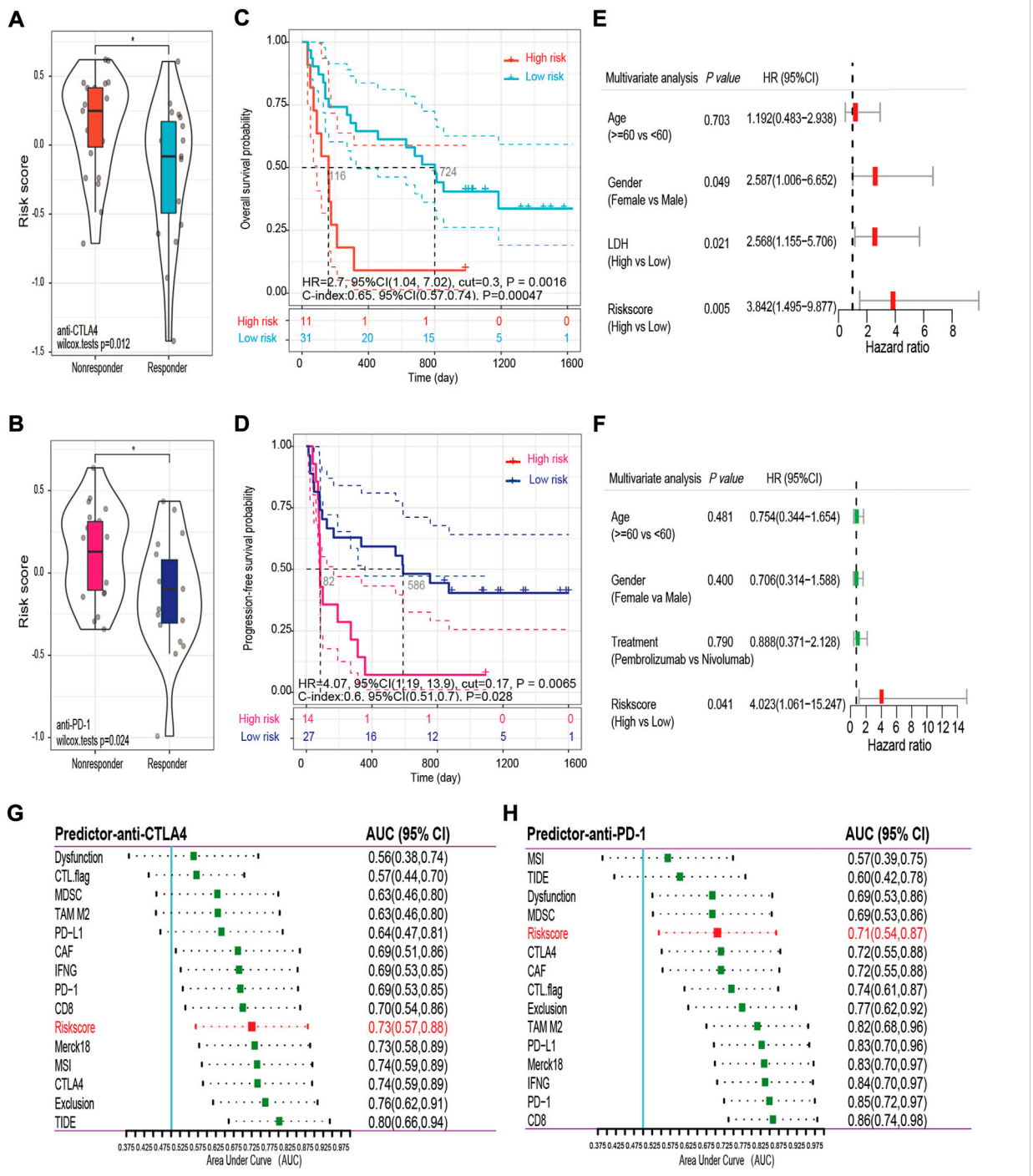

FIGURE 12
Validation and comparison of the predictive performance of the risk score in the anti-CTLA4 **(A,C,E,G)** and anti-PD-1 **(B,D,F,H)** cohorts. Distributions of the risk scores in the non-responder and responder groups are displayed in violin plots **(A,B)**. Kaplan–Meier curves for OS **(C)** and PFS **(D)** in the different groups. Forest plots of the multivariable Cox regression analysis with HR and 95% CIs **(E,F)**. AUC values and 95% CIs for the 15 predictors are shown in the forest plots **(G,H)**. OS, overall survival; PFS, progression-free survival; HR, hazard ratio; CI, confidence interval; AUC, area under the curve; TIDE: tumor immune dysfunction and exclusion score; IFNG: normalized average expression of IFN-γ response biomarkers, including HLA-DRA, CXCL10, IDO1, STAT1, and IFNG; MSI: microsatellite instability score predicted from gene expression through ridge regression; Merck18: T cell-inflamed signature (PMID: 28650338); PD-L1, PD-1, CTLA4: gene expression values of CD274, PDCD1 and CTLA4; CD8: average expression value of CD8A and CD8B; CTL flag: flag indicator for whether gene expression values are all positive for five cytotoxic T lymphocyte markers, including PRF1, GZMB, GZMA, CD8B, and CD8A; Dysfunction, Exclusion: enrichment scores based on the gene expression signatures of T-cell dysfunction and T-cell exclusion; TAM M2, MDSC, CAF: Pearson correlation coefficients between expression profile and M2 tumor-associated macrophages, myeloid-derived suppressor cells, and cancer-associated fibroblasts.

no significant differences in AUC values among these predictors ($p > 0.05$), the risk score had an AUC value > 0.7 in both immunotherapy cohorts and correlated well with the prediction scores of most predictors (Supplementary Figures S4A, S4B). In contrast, several recently published predictors, such as the TIDE score and MSI, showed significantly performance variations in different immunotherapy regimens (anti-CTLA4 vs. anti-PD-1: 0.80 vs. 0.60; 0.74 vs. 0.57; respectively). In general, these results indicated that the 15-FRG risk score has excellent robustness and generalization ability in predicting the response to different immunotherapy.

In addition to immunotherapy, we also aimed to further understand the chemotherapy comprehensively, the pRRophetic algorithm was used to predict the IC50 of common chemotherapeutic agents in high- and low-risk groups. According to our findings, the estimated IC50 of 45 chemotherapy drugs varied significantly between the high- and low-risk groups, and patients in the low-risk group were more sensitive to the commonly used chemotherapeutic agents, including camptothecin, cytarabine, dasatinib, erlotinib, mitomycin.C and vinblastine ($p < 0.05$, Supplementary Figures S5A–F), which demonstrated that the risk score might serve as a potential predicter of response to chemosensitivity in OV.

Discussion

In recent years, ferroptosis has attracted much attention, particularly in the area of oncology. Several studies aimed to elucidate the relationship between the ferroptosis-related signature and tumor prognosis, and some progress has been made (Liang et al., 2020; Wang H. et al., 2021). Regretfully, the vast majority of studies have failed to verify these relationships across multiple regions and races, which may lead to weak generalization ability of research results among different races. Therefore, we specifically selected both Asian and Caucasian population datasets as study subjects since the beginning, and then constructed a novel 15-FRG prognostic signature based on the Asian population dataset, which was externally validated for accuracy and robustness based on the Caucasian population. We confirmed that the risk score calculated by the 15-FRG signature was significantly associated with patient overall survival, and could be an independent risk factor for OV prognosis, and showed good prognostic predictive performance in both races. Moreover, the 15-FRG signature was superior to the other two models. Functional analyses indicated that the risk score was closely related to the tumor immunity, and that patients in the high- and low-risk groups exhibited opposite immune landscape. Notably, the risk score might serve as a good predictor of response to immunotherapy and chemotherapy. We supposed that this 15-FRG signature can better assess prognosis and facilitates patient stratification and precision drug treatment in OV.

Previous studies showed that tumor was provoked by multiple genetic mechanisms and key genes. Therefore, using the signature comprised by multiple genes to predict treatment response and prognosis of cancer showed a good clinical application prospect. In our study, we set up a 15-gene prognostic signature with genes screened from ferroptosis in OV. Previous studies regarding other diseases have indicated that these FRGs could be roughly classified into three categories: ferroptosis drivers (CYBB, VDAC2, SOCS1, LINC00472, ELAVL1, IFNG, IDH1), ferroptosis suppressors (NRAS, MT1G, ACSL3, SLC3A2), and ferroptosis markers (PTGS2, SLC1A4, PCK2, XBP1). It has been reported that these 15 genes involve tumorigenesis and tumor development in a variety of cancers. A recent study found that CYBB knockdown decreases ferroptosis and induces chemoresistance *via* the TAZ-ANGPTL4-NOX2 signaling axis in OV (Yang W. et al., 2020). Conversely, CYBB overexpression led to poor prognosis of osteosarcoma (Lin et al., 2021). VDAC2 as a voltage-dependent anion channel was widely explored in multiple FRG prognostic models (Ren et al., 2021; Yi et al., 2021) and bound directly with the ferroptosis activator erastin for increasing the sensitivity of cancer cells to ferroptosis *via* a FOXM1-Nedd4-VDAC2/3 negative feedback loop in melanoma, (Yang Y. et al., 2020). It was well known that the tumor suppressor protein p53 (TP53) was the guardian of the genome that regulated cell survival and death by apoptosis, autophagy, or ferroptosis (Gnanapradeepan et al., 2018). Some FRGs played a p53 context-dependent role in the regulation of ferroptosis. On the one hand, there are FRGs functioning upstream of p53 in ferroptosis, such as SOCS1, which has been found to be sufficient for p53 activation and to reduce SLC7A11 expression and glutathione levels, explaining in part its ability to sensitize cells to a ferroptosis inducer (Saint-Germain et al., 2017). Interestingly, SOCS1 could reduce PD-L1 expression and restore the activation of tumor-infiltrating $CD8^+$ T cells, which highlighted its potential as an immune checkpoint inhibitor in OV (Nakagawa et al., 2018). Another p53 upstream molecule was LINC00472, which was significantly correlated with better survival in patients with breast and ovarian cancers (Fu et al., 2016). It mediated apoptosis and ferroptosis in a p53-dependent manner to suppress cancer progression by interacting with Ras GTPase-activating protein-binding protein 1 (Mao et al., 2018). On the other hand, there are FRGs functioning downstream of p53 in ferroptosis. For example, ELAVL1, which was negatively regulated by miR-139-3p (Xue et al., 2019), was associated with poor prognosis and contributes to invasion, migration, and cell proliferation in OV (Huang et al., 2016). PTGS2, which encoded cyclooxygenase-2 (COX-2), was upregulated by the

ferroptosis agonist erastin only in p53 wild-type cells, suggesting that its regulation was p53-dependent. Meanwhile, prognostic analysis suggested that higher PTGS2 expression may be associated with poor OS in OV, but the results of different studies were somewhat conflicting (Steffensen et al., 2007). Moreover, SLC1A4, PCK2 and XBP1 were upregulated by 2-fold in erastin-treated HT-1080 cells (Dixon et al., 2014) and could be used as powerful prognostic markers in hepatobiliary cancer (Liu et al., 2020; Peng et al., 2021; Wang et al., 2022). As the key genes of ferroptosis, SLC3A2, MT1G and ACSL3 have also been widely explored in multiple FRG prognostic models. SLC3A2 was suppressed by IFN-γ that produced by activated $CD8^+$ T cells, which resulted in a restriction of cystine uptake and then enhanced tumor lipid peroxidation and ferroptosis, and improved tumor control (Lang et al., 2019; Wang W. et al., 2019). MT1G as a critical regulator of sorafenib resistance could inhibit sorafenib-induced ferroptosis in hepatocellular carcinoma through decreased glutathione depletion and lipid peroxidation (Sun et al., 2016). ACSL3, which was required for exogenous monounsaturated fatty acid activation, promoted a ferroptosis-resistant cell state (Magtanong et al., 2019). It is well known that gene mutation may cause splicing changes, resulting in altered gene function or altered pathways. Therefore, mutant FRGs may play a dual role in ferroptosis. Oncogenic mutant NRAS protected cells from oxidative stress-induced ferroptosis in primary rhabdomyosarcoma (Schott et al., 2015), whereas wild-type NRAS appeared to do the opposite. Wild-type IDH1 was an NADP + -dependent protein that catalyzed the production of NADPH from NADP+, which in turn sustained lipid biosynthesis and redox homeostasis in the TCA cycle (Sonego and Baldassarre, 2020). Conversely, mutant IDH1 could break the homeostasis and promote ROS accumulation, and sensitize cells to ferroptosis through a reduction in glutathione peroxidase 4 (GPX4), a core enzyme in lipid ROS scavenging and ferroptosis (Wang T. et al., 2019). In addition, through the literature review, we found that except CYBB, VDAC2, IDH1, MT1G, SLC1A4, PCK2, SLC3A2, the prognostic value of other FRGs in ovarian cancer has been reported, which provided a possibility for constructing a prognostic model. Meanwhile, our study reconfirmed that these genes were closely related to OS in OV, and used these 15 FRGs to construct a novel prognostic signature. The predictive power of the risk score calculated by the signature was proved to be reliable in different ethnic groups, and the performance was even superior to some of the reported prognostic risk models. Moreover, the risk score was an independent risk factor for OV patients, and patients in the low-risk group showed longer OS and better prognosis. We believed that these results could help to implement stratified management of ovarian cancer patients.

Notably, functional analysis revealed a broad immune-related functional spectrum based on DEGs between the high- and low- risk groups. It was reasonable to assume that there was a close correlation between the risk score and tumor immunity. Therefore, we used various immune profile-relevant analytical methods to gain additional insights into the immune landscape. The results indicated that patients with a high-risk score were in an immune "cold" phenotypic state, with low levels of immune cell infiltration (e.g., $CD4^+$) and cancer-immunity cycle steps as well as reduced antigen-presenting capacity (e.g., aDCs). One possible hypothesis was that activated immune infiltrating cells enhanced ferroptosis-specific lipid peroxidation in OV cells, and that, in turn, the increased numbers of ferroptotic cells released distinct tumor-associated antigens to further attract immune cell infiltration. This interaction network between ferroptosis and immune infiltrating cells, analogous to damage-associated molecular patterns (DAMPs) (Garg and Agostinis, 2017), may ultimately contribute to the antitumor efficacy of ferroptosis (Wang W. et al., 2019). Therefore, the immune "cold" state in patients with a high-risk score may explain their poor prognosis. Based on this assumption, it can be envisaged that strategies that combine immunotherapies with classical chemotherapies promoting ferroptosis may turn immune "cold" (high-risk) tumors into "hot" (low-risk) tumors, which will help to improve patient prognosis.

Up to this point, treatment options remain limited in OV with high rates of recurrence and chemoresistance. Immunotherapy, as one of the frontiers of tumor therapy, has been receiving increasing attention from gynecologists. Despite this, clinical research on anti-PD-1 and PD-L1 immune checkpoint blockade has shown that only a limited percentage of patients exhibit a durable clinical benefit (Matulonis et al., 2019). Therefore, early identification of patients with potential response to the immunotherapy was crucial to improving their prognosis. Regrettably, predictors of the response to immunotherapy were scarce. It was reported that immune checkpoint molecules and immune score might be potential predictive biomarkers for the efficacy of immunotherapy (Fu et al., 2020). Interestingly, we found that the ferroptosis-based risk score was negatively related with various immune checkpoint biomarkers and the immune score, highlighting that risk score could be a predictor and low-risk patients might more specifically benefit from immune checkpoint blockade-based immunotherapies. The submap results also suggested that patients with low risk might have a high likelihood of responding to anti-PD1 immunotherapy. Meanwhile, multiple immune checkpoint biomarkers were positively correlated with each other, suggesting that multi-target immunotherapy may overcome the resistance to single-target immunotherapy. Moreover, by comparing with 14 well-validated predictors (Fu et al., 2020), including the classical biomarkers PD1, PDL-1, TIDE, and MSI, we validated that

the prediction accuracy and robustness of the risk score performed well. However, these findings were made in melanoma datasets and further clinical verification is required in patients with OV. Ovarian cancer is usually treated with platinum-based chemotherapy. Using the pRRophetic algorithm, we imputed that patients with low risk could be more sensitive to some commonly used chemotherapeutic agents. These results indicated that the risk score might improve our understanding of immunotherapy and facilitate a precise application of immunotherapy and chemotherapy in cancer patients.

There are several key limitations of our analyses. First, the signature was built and validated using retrospective samples, validation using prospective real-world samples was also required. In addition, the hallmark genes evaluated in our study were restricted to FRGs. Hence, the intrinsic weakness of predictive power was inevitable. Further, the associations between the risk score and the immune landscape were estimated by bioinformatics analysis, and we did not conduct further experimental verification.

Conclusion

In conclusion, our study constructed a novel 15-FRG prognostic signature that performed well in Asian and Caucasian populations, and might serve as an effective predictor of response to immunotherapy. Our findings may provide a better insight into OV prognostic management and may serve as a basis to facilitate a precise application of immunotherapy in OV. The underlying mechanisms between FRGs and the immune microenvironment in OV remained to be investigated.

Data availability statement

Publicly available datasets were analyzed in this study. This data can be found here: http://tide.dfci.harvard.edu/, https://dcc.icgc.org/, https://www.ncbi.nlm.nih.gov/geo/query/acc.cgi?acc=GSE32062.

Author contributions

YL, RT conceived of and designed the study. YL performed the data acquisition. YL, SD drafted the manuscript, conducted data analysis and prepared the figures. MY managed the raw data. XH, CZ, KH, YZ, QY were responsible for revising the research. All authors were involved in data interpretation and discussion of the results. The final version of the manuscript was approved by all authors. All authors agree to be accountable for the content of the work.

Funding

This study was supported by grants from the National Key Research and Development Program of China (2020YFC2005500, 2020YFC2005506) and by grants from the Key Research and Development Program of Science and Technology Department of Sichuan Province (2019YFS0514, 2022YFS0272) and by grants from the Research Subject of Health Commission of Sichuan Province (18PJ557) and by grants from the Key Science and Technology Program of Leshan (18SZD113).

Acknowledgments

We sincerely thank Kosuke Yoshihara, et al., Tuba Gide, et al., and Eliezer Van Allen, et al. for sharing, donating, and authorizing the use of their high-throughput sequencing datasets.

Conflict of interest

The authors declare that the research was conducted in the absence of any commercial or financial relationships that could be construed as a potential conflict of interest.

Publisher's note

All claims expressed in this article are solely those of the authors and do not necessarily represent those of their affiliated organizations, or those of the publisher, the editors and the reviewers. Any product that may be evaluated in this article, or claim that may be made by its manufacturer, is not guaranteed or endorsed by the publisher.

Supplementary material

The Supplementary Material for this article can be found online at: https://www.frontiersin.org/articles/10.3389/fphar.2022.949126/full#supplementary-material

SUPPLEMENTARY FIGURE S1
Stratified Kaplan–Meier survival curves. Kaplan–Meier survival curves stratified by tumor stage **(A)**, tumor grade **(B)**, and residual tumor **(C)** in the GSE32062 cohort. Kaplan–Meier survival curves stratified by age **(D)**, tumor stage **(E)**, and disease status **(F)** in the ICGC cohort.

SUPPLEMENTARY FIGURE S2
Kaplan–Meier survival curves of 15 FRGs constructed using a Kaplan–Meier plotter tool (http://www.kmplot.com). Auto select best cutoff was chosen in the analysis. FRG, ferroptosis-related gene.

SUPPLEMENTARY FIGURE S3
The top 10 enriched GO terms related to 15-FRGs in molecular function (MF), cellular component (CC), and biological process (BP) **(A)**. The top 14 enriched KEGG pathways related to 15-FRGs **(B)**.

Immunotherapeutic responses to anti-CTLA-4 and anti-PD-1 treatments in the GSE32062 **(C)** and ICGC **(D)** cohorts. GO, Gene Ontology; KEGG, Kyoto Encyclopedia of Genes and Genomes. FRG, ferroptosis-related gene.

SUPPLEMENTARY FIGURE S4
Correlations between the risk score and other predictor scores in the anti-CTLA4 **(A)** and anti-PD-1 **(B)** cohorts. $*p < 0.05$; $**p < 0.01$; $***p < 0.001$. TIDE: tumor immune dysfunction and exclusion score; IFNG: normalized average expression of IFN-γ response biomarkers, including HLA-DRA, CXCL10, IDO1, STAT1, and IFNG; MSI: microsatellite instability score predicted from gene expression through ridge regression; Merck18: T cell-inflamed signature (PMID: 28650338); PD-L1, PD-1, CTLA4: gene expression values of CD274, PDCD1 and CTLA4; CD8: average expression value of CD8A and CD8B; CTL flag: flag indicator for whether gene expression values are all positive for five cytotoxic T lymphocyte markers, including PRF1, GZMB, GZMA, CD8B, and CD8A; Dysfunction, Exclusion: enrichment scores based on the gene expression signatures of T-cell dysfunction and T-cell exclusion; TAM M2, MDSC, CAF: Pearson correlation coefficients between expression profile and M2 tumor-associated macrophages, myeloid-derived suppressor cells, and cancer-associated fibroblasts.

SUPPLEMENTARY FIGURE S5
Estimated IC_{50} values of six commonly used chemotherapeutic agents for high- and low-risk groups in the GSE32062 cohort **(A–F)**.

SUPPLEMENTARY TABLE S1
List of the ferroptosis-related genes (A) immune-related genes (B) immune infiltration annotated gene sets (C).

SUPPLEMENTARY TABLE S2
Characteristics of patients in the GSE32062 and ICGC-OV-AU cohorts (A) and the anti-CTLA4 and anti-PD-1 cohorts (B).

SUPPLEMENTARY TABLE S3
Table of GO terms (A) and KEGG pathways (B) significantly enriched in 15 ferroptosis-related genes.

References

Barbie, D. A., Tamayo, P., Boehm, J. S., Kim, S. Y., Moody, S. E., Dunn, I. F., et al. (2009). Systematic RNA interference reveals that oncogenic KRAS-driven cancers require TBK1. *Nature* 462 (7269), 108–112. doi:10.1038/nature08460

Bhattacharya, S., Dunn, P., Thomas, C. G., Smith, B., Schaefer, H., Chen, J., et al. (2018). ImmPort, toward repurposing of open access immunological assay data for translational and clinical research. *Sci. Data* 5 (1), 180015. doi:10.1038/sdata.2018.15

Bray, F., Ferlay, J., Soerjomataram, I., Siegel, R. L., Torre, L. A., and Jemal, A. (2018). Global cancer statistics 2018: GLOBOCAN estimates of incidence and mortality worldwide for 36 cancers in 185 countries. *CA. Cancer J. Clin.* 68 (6), 394–424. doi:10.3322/caac.21492

Chekerov, R., Hilpert, F., Mahner, S., El-Balat, A., Harter, P., De Gregorio, N., et al. (2018). Sorafenib plus topotecan versus placebo plus topotecan for platinum-resistant ovarian cancer (TRIAS): a multicentre, randomised, double-blind, placebo-controlled, phase 2 trial. *Lancet Oncol.* 19, 1247–1258. doi:10.1016/S1470-2045(18)30372-3

Chen, G. M., Kannan, L., Geistlinger, L., Kofia, V., Safikhani, Z., Gendoo, D. M. A., et al. (2018). Consensus on molecular subtypes of high-grade serous ovarian carcinoma. *Clin. Cancer Res.* 24 (20), 5037–5047. doi:10.1158/1078-0432.CCR-18-0784

Dixon, S. J., Patel, D. N., Welsch, M., Skouta, R., Lee, E. D., Hayano, M., et al. (2014). Pharmacological inhibition of cystine–glutamate exchange induces endoplasmic reticulum stress and ferroptosis. *eLife* 3, e02523. doi:10.7554/eLife.02523

Fu, Y., Biglia, N., Wang, Z., Shen, Y., Risch, H. A., Lu, L., et al. (2016). Long non-coding RNAs, ASAP1-IT1, FAM215A, and LINC00472, in epithelial ovarian cancer. *Gynecol. Oncol.* 143 (3), 642–649. doi:10.1016/j.ygyno.2016.09.021

Fu, J., Li, K., Zhang, W., Wan, C., Zhang, J., Jiang, P., et al. (2020). Large-scale public data reuse to model immunotherapy response and resistance. *Genome Med.* 12 (1), 21. doi:10.1186/s13073-020-0721-z

Galon, J., and Bruni, D. (2019). Approaches to treat immune hot, altered and cold tumours with combination immunotherapies. *Nat. Rev. Drug Discov.* 18 (3), 197–218. doi:10.1038/s41573-018-0007-y

Garg, A. D., and Agostinis, P. (2017). Cell death and immunity in cancer: From danger signals to mimicry of pathogen defense responses. *Immunol. Rev.* 280 (1), 126–148. doi:10.1111/imr.12574

Geeleher, P., Cox, N., and Huang, R. S. (2014). pRRophetic: an R package for prediction of clinical chemotherapeutic response from tumor gene expression levels. *PLoS One* 9 (9), e107468. doi:10.1371/journal.pone.0107468

Geistlinger, L., Oh, S., Ramos, M., Schiffer, L., Larue, R. S., Henzler, C. M., et al. (2020). Multiomic analysis of subtype evolution and heterogeneity in high-grade serous ovarian carcinoma. *Cancer Res.* 80 (20), 4335–4345. doi:10.1158/0008-5472.CAN-20-0521

Gide, T. N., Quek, C., Menzies, A. M., Tasker, A. T., Shang, P., Holst, J., et al. (2019). Distinct immune cell populations define response to anti-PD-1 monotherapy and anti-PD-1/anti-CTLA-4 combined therapy. *Cancer Cell* 35 (2), 238–255.e6. doi:10.1016/j.ccell.2019.01.003

Gnanapradeepan, K., Basu, S., Barnoud, T., Budina-Kolomets, A., Kung, C. P., and Murphy, M. E. (2018). The p53 tumor suppressor in the control of metabolism and ferroptosis. *Front. Endocrinol.* 9, 124. doi:10.3389/fendo.2018.00124

Hoshida, Y., Brunet, J., Tamayo, P., Golub, T. R., and Mesirov, J. P. (2007). Subclass mapping: identifying common subtypes in independent disease data sets. *PLoS One* 2 (11), e1195. doi:10.1371/journal.pone.0001195

Huang, Y., Peng, W., Furuuchi, N., Gerhart, J., Rhodes, K., Mukherjee, N., et al. (2016). Delivery of therapeutics targeting the mRNA-binding protein HuR using 3DNA nanocarriers suppresses ovarian tumor growth. *Cancer Res.* 76 (6), 1549–1559. doi:10.1158/0008-5472.CAN-15-2073

Iasonos, A., Schrag, D., Raj, G. V., and Panageas, K. S. (2008). How to build and interpret a nomogram for cancer prognosis. *J. Clin. Oncol.* 26 (8), 1364–1370. doi:10.1200/JCO.2007.12.9791

Lang, X., Green, M. D., Wang, W., Yu, J., Choi, J. E., Jiang, L., et al. (2019). Radiotherapy and immunotherapy promote tumoral lipid oxidation and ferroptosis via synergistic repression of SLC7A11. *Cancer Discov.* 9 (12), 1673–1685. doi:10.1158/2159-8290.CD-19-0338

Lheureux, S., Braunstein, M., and Oza, A. M. (2019). Epithelial ovarian cancer: Evolution of management in the era of precision medicine. *CA. Cancer J. Clin.* 69 (4), 280–304. doi:10.3322/caac.21559

Li, L., Qiu, C., Hou, M., Wang, X., Huang, C., Zou, J., et al. (2021). Ferroptosis in ovarian cancer: A novel therapeutic strategy. *Front. Oncol.* 11, 665945. doi:10.3389/fonc.2021.665945

Liang, J., Wang, D., Lin, H., Chen, X., Yang, H., Zheng, Y., et al. (2020). A novel ferroptosis-related gene signature for overall survival prediction in patients with hepatocellular carcinoma. *Int. J. Biol. Sci.* 16 (13), 2430–2441. doi:10.7150/ijbs.45050

Lin, R., Huang, Z., Wang, S., Chen, H., Wei, H., Shen, R., et al. (2021). Clinicopathological and prognostic value of NADPH oxidase 2 (NOX2) in primary osteosarcoma. *J. Orthop. Sci.* 26 (3), 466–472. doi:10.1016/j.jos.2020.04.002

Liu, R., Wu, Z., Zhang, Y., Miao, X., Zou, Q., Yuan, Y., et al. (2020). Prognostic and clinicopathological significance of X-box-binding protein 1 and N-acetyltransferase 1 in gallbladder cancer. *Front. Oncol.* 10, 1124. doi:10.3389/fonc.2020.01124

Magtanong, L., Ko, P., To, M., Cao, J. Y., Forcina, G. C., Tarangelo, A., et al. (2019). Exogenous monounsaturated fatty acids promote a ferroptosis-resistant cell state. *Cell Chem. Biol.* 26 (3), 420–432.e9. doi:10.1016/j.chembiol.2018.11.016

Mao, C., Wang, X., Liu, Y., Wang, M., Yan, B., Jiang, Y., et al. (2018). A G3BP1-interacting lncRNA promotes ferroptosis and apoptosis in cancer via nuclear sequestration of p53. *Cancer Res.* 78 (13), 3484–3496. doi:10.1158/0008-5472.CAN-17-3454

Matulonis, U. A., Shapira-Frommer, R., Santin, A. D., Lisyanskaya, A. S., Pignata, S., Vergote, I., et al. (2019). Antitumor activity and safety of pembrolizumab in patients with advanced recurrent ovarian cancer: results from the phase II KEYNOTE-100 study. *Ann. Oncol.* 30 (7), 1080–1087. doi:10.1093/annonc/mdz135

Morand, S., Devanaboyina, M., Staats, H., Stanbery, L., and Nemunaitis, J. (2021). Ovarian cancer immunotherapy and personalized medicine. *Int. J. Mol. Sci.* 22 (12), 6532. doi:10.3390/ijms22126532

Nakagawa, S., Serada, S., Kakubari, R., Hiramatsu, K., Sugase, T., Matsuzaki, S., et al. (2018). Intratumoral delivery of an adenoviral vector carrying the SOCS-1 gene enhances T-cell–mediated antitumor immunity by suppressing PD-L1. *Mol. Cancer Ther.* 17 (9), 1941–1950. doi:10.1158/1535-7163.MCT-17-0822

Peng, X., Chen, R., Cai, S., Lu, S., and Zhang, Y. (2021). SLC1A4: A powerful prognostic marker and promising therapeutic target for HCC. *Front. Oncol.* 11, 650355. doi:10.3389/fonc.2021.650355

Qiu, Y., Cao, Y., Cao, W., Jia, Y., and Lu, N. (2020). The application of ferroptosis in diseases. *Pharmacol. Res.* 159, 104919. doi:10.1016/j.phrs.2020.104919

Ren, Z., Hu, M., Wang, Z., Ge, J., Zhou, X., Zhang, G., et al. (2021). Ferroptosis-related genes in lung adenocarcinoma: Prognostic signature and immune, drug resistance, mutation analysis. *Front. Genet.* 12, 672904. doi:10.3389/fgene.2021.672904

Rooney, M. S., Shukla, S. A., Wu, C. J., Getz, G., and Hacohen, N. (2015). Molecular and genetic properties of tumors associated with local immune cytolytic activity. *Cell* 160 (1-2), 48–61. doi:10.1016/j.cell.2014.12.033

Saint-Germain, E., Mignacca, L., Vernier, M., Bobbala, D., Ilangumaran, S., and Ferbeyre, G. (2017). SOCS1 regulates senescence and ferroptosis by modulating the expression of p53 target genes. *Aging* 9 (10), 2137–2162. doi:10.18632/aging.101306

Schott, C., Graab, U., Cuvelier, N., Hahn, H., and Fulda, S. (2015). Oncogenic RAS mutants confer resistance of RMS13 rhabdomyosarcoma cells to oxidative stress-induced ferroptotic cell death. *Front. Oncol.* 5, 131. doi:10.3389/fonc.2015.00131

Simon, N., Friedman, J., Hastie, T., and Tibshirani, R. (2011). Regularization paths for cox's proportional hazards model via coordinate descent. *J. Stat. Softw.* 39 (5), 1–13. doi:10.18637/jss.v039.i05

Sonego, M., and Baldassarre, G. (2020). A new role for IDH1 in the control of ovarian cancer cells metabolism and senescence. *Ann. Transl. Med.* 8 (12), 780. doi:10.21037/atm.2020.02.62

Steffensen, K. D., Waldstrøm, M., Jeppesen, U., Jakobsen, E., Brandslund, I., Jakobsen, A., et al. (2007). The prognostic importance of cyclooxygenase 2 and HER2 expression in epithelial ovarian cancer. *Int. J. Gynecol. Cancer* 17 (4), 798–807. doi:10.1111/j.1525-1438.2006.00855.x

Subramanian, A., Tamayo, P., Mootha, V. K., Mukherjee, S., Ebert, B. L., Gillette, M. A., et al. (2005). Gene set enrichment analysis: A knowledge-based approach for interpreting genome-wide expression profiles. *Proc. Natl. Acad. Sci. U. S. A.* 102 (43), 15545–15550. doi:10.1073/pnas.0506580102

Sun, X., Niu, X., Chen, R., He, W., Chen, D., Kang, R., et al. (2016). Metallothionein-1G facilitates sorafenib resistance through inhibition of ferroptosis. *Hepatology* 64 (2), 488–500. doi:10.1002/hep.28574

Szklarczyk, D., Franceschini, A., Kuhn, M., Simonovic, M., Roth, A., Minguez, P., et al. (2010). The STRING database in 2011: functional interaction networks of proteins, globally integrated and scored. *Nucleic Acids Res.* 39, D561–D568. doi:10.1093/nar/gkq973

Tang, M., Chen, Z., Wu, D., and Chen, L. (2018). Ferritinophagy/ferroptosis: Iron-related newcomers in human diseases. *J. Cell. Physiol.* 233 (12), 9179–9190. doi:10.1002/jcp.26954

Tang, D., Kang, R., Berghe, T. V., Vandenabeele, P., and Kroemer, G. (2019). The molecular machinery of regulated cell death. *Cell Res.* 29 (5), 347–364. doi:10.1038/s41422-019-0164-5

Taube, J. M., Galon, J., Sholl, L. M., Rodig, S. J., Cottrell, T. R., Giraldo, N. A., et al. (2018). Implications of the tumor immune microenvironment for staging and therapeutics. *Mod. Pathol.* 31 (2), 214–234. doi:10.1038/modpathol.2017.156

Van Allen, E. M., Miao, D., Schilling, B., Shukla, S. A., Blank, C., Zimmer, L., et al. (2015). Genomic correlates of response to CTLA-4 blockade in metastatic melanoma. *Science* 350 (6257), 207–211. doi:10.1126/science.aad0095

Wang, T., Liang, J., Zhang, C., Xiong, Y., Guan, K., and Yuan, H. (2019). The oncometabolite 2-hydroxyglutarate produced by mutant IDH1 sensitizes cells to ferroptosis. *Cell Death Dis.* 10 (10), 755. doi:10.1038/s41419-019-1984-4

Wang, W., Green, M., Choi, J. E., Gijón, M., Kennedy, P. D., Johnson, J. K., et al. (2019). CD8+ T cells regulate tumour ferroptosis during cancer immunotherapy. *Nature* 569 (7755), 270–274. doi:10.1038/s41586-019-1170-y

Wang, Y., Wei, Z., Pan, K., Li, J., and Chen, Q. (2020). The function and mechanism of ferroptosis in cancer. *Apoptosis* 25, 786–798. doi:10.1007/s10495-020-01638-w

Wang, D., Wei, G., Ma, J., Cheng, S., Jia, L., Song, X., et al. (2021). Identification of the prognostic value of ferroptosis-related gene signature in breast cancer patients. *BMC Cancer* 21 (1), 645. doi:10.1186/s12885-021-08341-2

Wang, H., Cheng, Q., Chang, K., Bao, L., and Yi, X. (2021). Integrated analysis of ferroptosis-related biomarker signatures to improve the diagnosis and prognosis prediction of ovarian cancer. *Front. Cell Dev. Biol.* 9, 807862. doi:10.3389/fcell.2021.807862

Wang, H., Yang, C., Jiang, Y., Hu, H., Fang, J., and Yang, F. (2022). A novel ferroptosis-related gene signature for clinically predicting recurrence after hepatectomy of hepatocellular carcinoma patients. *Am. J. Cancer Res.* 12 (5), 1995–2011.

Xu, L., Deng, C., Pang, B., Zhang, X., Liu, W., Liao, G., et al. (2018). TIP: A web server for resolving tumor Immunophenotype profiling. *Cancer Res.* 78 (23), 6575–6580. doi:10.1158/0008-5472.CAN-18-0689

Xu, T., Ding, W., Ji, X., Ao, X., Liu, Y., Yu, W., et al. (2019). Molecular mechanisms of ferroptosis and its role in cancer therapy. *J. Cell. Mol. Med.* 23 (8), 4900–4912. doi:10.1111/jcmm.14511

Xue, F., Li, Q. R., Xu, Y. H., and Zhou, H. B. (2019). MicroRNA-139-3p inhibits the growth and metastasis of ovarian cancer by inhibiting ELAVL1. *Onco. Targets. Ther.* 12, 8935–8945. doi:10.2147/OTT.S210739

Yang, W., Huang, Z., Wu, J., Ding, C. C., Murphy, S. K., and Chi, J. (2020). A TAZ-ANGPTL4-NOX2 Axis regulates ferroptotic cell death and chemoresistance in epithelial ovarian cancer. *Mol. Cancer Res.* 18 (1), 79–90. doi:10.1158/1541-7786.MCR-19-0691

Yang, Y., Luo, M., Zhang, K., Zhang, J., Gao, T., Connell, D. O., et al. (2020). Nedd4 ubiquitylates VDAC2/3 to suppress erastin-induced ferroptosis in melanoma. *Nat. Commun.* 11 (1), 433. doi:10.1038/s41467-020-14324-x

Yi, K., Liu, J., Rong, Y., Wang, C., Tang, X., Zhang, X., et al. (2021). Biological functions and prognostic value of ferroptosis-related genes in bladder cancer. *Front. Mol. Biosci.* 8, 631152. doi:10.3389/fmolb.2021.631152

Yu, H., Guo, P., Xie, X., Wang, Y., and Chen, G. (2017). Ferroptosis, a new form of cell death, and its relationships with tumourous diseases. *J. Cell. Mol. Med.* 21 (4), 648–657. doi:10.1111/jcmm.13008

Yu, Z., He, H., Chen, Y., Ji, Q., and Sun, M. (2021). A novel ferroptosis related gene signature is associated with prognosis in patients with ovarian serous cystadenocarcinoma. *Sci. Rep.-UK.* 11 (1), 11486. doi:10.1038/s41598-021-90126-5

Zhou, N., and Bao, J. (2020). FerrDb: a manually curated resource for regulators and markers of ferroptosis and ferroptosis-disease associations. *Database.* 2020, baaa021–8. doi:10.1093/database/baaa021

frontiers | Frontiers in Pharmacology

TYPE Review
PUBLISHED 25 October 2022
DOI 10.3389/fphar.2022.949566

Check for updates

OPEN ACCESS

EDITED BY
Hongtao Xiao,
University of Electronic Science and Technology of China, China

REVIEWED BY
Liyun Liu,
Chinese Center for Disease Control and Prevention, China
Po-Fu Yueh,
National Yang Ming Chiao Tung University, Taiwan

*CORRESPONDENCE
Yunhe Zhu,
yunhezhu2008@126.com
Haining Zhou,
haining_zhou@zmu.edu.cn

†These authors have contributed equally to this work and share first authorship

SPECIALTY SECTION
This article was submitted to Pharmacology of Anti-Cancer Drugs, a section of the journal Frontiers in Pharmacology

RECEIVED 21 May 2022
ACCEPTED 12 September 2022
PUBLISHED 25 October 2022

CITATION
Yan H, Tang S, Tang S, Zhang J, Guo H, Qin C, Hu H, Zhong C, Yang L, Zhu Y and Zhou H (2022), miRNAs in anti-cancer drug resistance of non-small cell lung cancer: Recent advances and future potential.
Front. Pharmacol. 13:949566.
doi: 10.3389/fphar.2022.949566

COPYRIGHT
© 2022 Yan, Tang, Tang, Zhang, Guo, Qin, Hu, Zhong, Yang, Zhu and Zhou. This is an open-access article distributed under the terms of the Creative Commons Attribution License (CC BY). The use, distribution or reproduction in other forums is permitted, provided the original author(s) and the copyright owner(s) are credited and that the original publication in this journal is cited, in accordance with accepted academic practice. No use, distribution or reproduction is permitted which does not comply with these terms.

miRNAs in anti-cancer drug resistance of non-small cell lung cancer: Recent advances and future potential

Hang Yan[1,2†], Shengjie Tang[1†], Shoujun Tang[1†], Jun Zhang[1,2], Haiyang Guo[1,3], Chao Qin[1,2], Haiyang Hu[1,2], Chuan Zhong[1], Li Yang[1], Yunhe Zhu[1*] and Haining Zhou[1,2,3*]

[1]Department of Thoracic Surgery, Suining Central Hospital, An Affiliated Hospital of Chongqing Medical University, Suining, China, [2]Graduate School, Institute of Surgery, Zunyi Medical University, Zunyi, China, [3]Graduate School, Institute of Surgery, Chengdu University of TCM, Chengdu, China

Non-small cell lung cancer (NSCLC) is one of the most common malignant tumors worldwide. Clinical success is suboptimal owing to late diagnosis, limited treatment options, high recurrence rates, and the development of drug resistance. MicroRNAs (miRNAs), a range of small endogenous non-coding RNAs that are 22 nucleotides in length, have emerged as one of the most important players in cancer initiation and progression in recent decades. Current evidence has revealed the pivotal roles of miRNAs in regulating cell proliferation, migration, invasion, and metastasis in NSCLC. Recently, several studies have demonstrated that miRNAs are strongly associated with resistance to anti-cancer drugs, ranging from traditional chemotherapeutic and immunotherapy drugs to anti-vascular drugs, and even during radiotherapy. In this review, we briefly introduce the mechanism of miRNA dysregulation and resistance to anti-tumor therapy in NSCLC, and summarize the role of miRNAs in the malignant process of NSCLC. We then discuss studies of resistance-related miRNAs in chemotherapy, radiotherapy, targeted therapy, immunotherapy, and anti-vascular therapy in NSCLC. Finally, we will explore the application prospects of miRNA, an emerging small molecule, for future anti-tumor therapy. This review is the first to summarize the latest research progress on miRNAs in anti-cancer drug resistance based on drug classification, and to discuss their potential clinical applications.

KEYWORDS

drug resistance, miRNA, NSCLC, therapy, biomarker

Introduction

Lung cancer is the most frequent cause of cancer-related death worldwide, with 2.09 million new cases and 1.76 million deaths estimated in the GLOBOCAN 2018 databases (Siegel et al., 2019; Siegel et al., 2021). It has been pathologically subdivided into two subsets: small-cell lung cancer (SCLC) and non-small cell lung

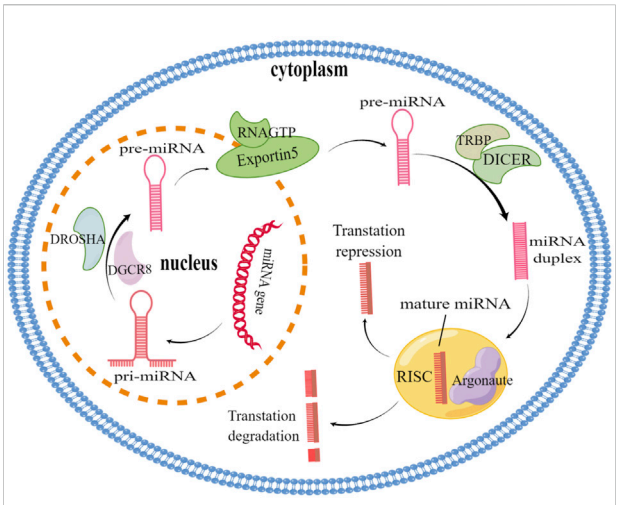

FIGURE 1
miRNA biogenesis and action. miRNA genes are transcribed by RNA polymerase II to produce primary miRNA (Pri-miRNA), Pri-miRNA is further processed by Drosha-Dgcr8 in the nucleus to form pre-miRNA, which is then exported to the cytoplasm *via* Exportin5/Ran GTP. TRBP, and DICER in the cytoplasm further process the pre-miRNA into mature short double strand RNA fragments. One mature miRNA is associated with the Argonaute protein (AGO2) and binds to the 3′UTR of the complementary site target mRNA of RISC leading to translation inhibition while the other strand is degraded.

cancer (NSCLC). NSCLC accounts for approximately 85% of all lung cancer cases, of which the most common types are lung adenocarcinoma (LUAD) and lung squamous cell carcinoma (LUSC) (Herbst et al., 2018). Generally, NSCLC is not detected and diagnosed until advanced-stage disease or symptomatic is present (Siegel et al., 2021). Cough is the most common symptom in 50–75 percent of patients, and is sometimes accompanied by chest pain, hemoptysis and dyspnea (Kocher et al., 2015). Surgery, radiotherapy, and chemotherapy are the three main treatments for lung cancer (Duma et al., 2019). In recent years, molecular targeted therapies and immunotherapy have become increasingly popular for the treatment of lung cancer (Hirsch et al., 2017). Research has shown that anti-angiogenic therapy has become a critical treatment method for NSCLC (Hu et al., 2020). Despite the clinical availability of multiple treatments for NSCLC, the 5-year survival rate remains dismal, largely owing to the emergence of resistance to therapies (Siegel et al., 2021). Drug resistance presents a significant obstacle in the treatment of NSCLC and conduce to disease progression, tumor recurrence, and greatly increased cancer mortality (Sarkar et al., 2010). The development of new therapeutic regimens for NSCLC has been restricted by a lack of reliable diagnostic and prognostic biomarkers and limited research on mechanisms that promote rapid cancer progression, early metastatic spread, and drug resistance.

MicroRNAs (miRNAs) are 18–25 nucleotides in length and function in gene expression and post-transcriptional regulation (Bartel, 2004). They are transcribed under the function of RNA polymerase II to generate miRNA primary miRNA (Pri-miRNA), which is processed by Drosha protein in the nucleus as precursor miRNA (pre-miRNA). The pre-miRNAs are subsequently transported to the cytoplasm in exportin-5 mediated, and further processed by Dicer enzyme into mature miRNAs in the cytoplasm. Then, a mature miRNA strand is incorporated into the RNA-induced silencing complex (RISC) (Figure 1). By this way, the protein complex can complement the target mRNA; Binding to the complementary sequence in the 3′ untranslated region (3′-UTR) of the target mRNA and the target gene was silenced by either degrading mRNA or blocking the translation of mRNA (Bartel, 2004; Kim, 2005; Winter et al., 2009; Krol et al., 2010; Jonas and Izaurralde, 2015). Through the post-transcriptional regulation of gene expression, miRNAs are participate in all kinds of cellular processes, including proliferation of cell or apoptosis, tumorigenesis or invasion–metastasis, angiogenesis and cancer progression (Lu et al., 2005; Shivdasani, 2006; Lin and Gregory, 2015). In recent years, miRNAs have been shown to have tremendous effects on tumor progression (Croce, 2009). Interestingly, miRNAs are refer to drug resistance in many cancers, and their dysregulation has been highlighted as an emerging mechanism of drug resistance (Zhang and Wang, 2017; Wei et al., 2019a). Understanding the relationship between miRNAs regulation and drug resistance mechanism is a new direction of anti-tumor drug resistance.

The effect and expression status of miRNAs have been extensively studied in lung cancer tissues and cell lines (Iqbal et al., 2019). MiRNAs in lung cancer tissues and tumor cells and their mechanisms of action in tumorigenesis (include invasion, metastasis, recurrence, drug resistance, etc.) are hotly reported. In this review, we briefly summarize the current understanding of the miRNAs link with the progression of NSCLC, discussing their potential in the treatment of NSCLC.

Function of MicroRNAs in progression of NSCLC

Sustained cell proliferation is a fundamental characteristic of cancer, which is regulated by miRNAs bioactivities. For example, decreased expression of the let -7 miRNA family is common in lung cancer patients because let -7 directly or indirectly inhibits multiple target genes involved in cell cycle and cell division (Osada and Takahashi, 2011). Johnson and colleagues reported evidence that let-7 expression is associated with lung cancer proliferation, suggesting that let-7 deletion significantly enhances cell division in the S-phase of the A549 cell cycle (Johnson et al., 2007). Moreover, NSCLC tissues are markedly up-regulated by miR-196b-5p, which directly targets the tumor suppressors GATA6 and TSPAN12 to promote lung cancer cell proliferation and cell cycle (Liang et al., 2020). In contrast,

Harel et al. reported that exosome miR-512 stopped the proliferation of lung tumor cells by targeting member four of the TEA domain family (TEAD4), indicating that miR-512 has the function of tumor inhibition (Adi Harel et al., 2015). Additionally, the upstream Ras signaling pathway molecule SOS2 was inhibited by miR-148A-3p *in vitro*, leading to inhibition of NSCLC cell proliferation (Xie et al., 2019). Besides, it has been reported that miR-520A-3p is involved in the downstream PI3K/Akt/mTOR pathway, thereby affecting cell proliferation (Lv et al., 2018). To further understand the important relationship between miRNA and lung cancer cell proliferation is still the focus of current experimental studies.

Evasion of programmed cell death (apoptosis) is another essential hallmark of cancer, with external and internal pathways predominating. Similarly, studies have shown that miRNAs can take part in the regulation of lung cancer cell apoptosis through acting on transcription factors involved in endogenous and exogenous pathways. The intrinsic pathway is apoptosis caused by dysfunction of some members of the BCL-2 family. Wang et al. reported that miR-16–1 induces apoptosis by downregulating Bcl-2 (Wang et al., 2016). Tian et al. showed that miR-130b indirectly upregulates Bcl-2 *via* the peroxisome proliferator-activated receptor gamma (PPAR-γ)/VEGF pathway and suppresses lung cancer cell apoptosis (Tian et al., 2016). The extrinsic pathway refers to apoptosis that initiated start with extracellular death-inducing signals *via* cell surface receptors (e.g., TNF family receptors). Garofalo et al. reported that a trail-targeted molecular signaling cascade initiated by Mir-221/222 resulted in loss of PTEN signaling, which in turn activated the PI3K/AKT/mTOR pathway, showing a strong inhibitory effect on TRAIL-mediated apoptosis (Garofalo et al., 2009). Subsequently, the researchers also found that miR-760 was detected to play a key role in TRAIL-induced apoptosis of lung cancer cells (Zhang X.et al., 2018). Overall, much remains to be learned about the potential role of miRNAs in apoptosis activity of lung cancer cells.

The invasion–metastasis cascade is a distinct cancer behavior, and miRNAs are not absent from the process. Recent studies have verify that miR-31-3p have the function of facilitates proliferation, invasion, and migration of NSCLC cells by targeting FOXO1 (Zeng et al., 2022). In addition, the study of Yang et al. showed that miR-1246 modulates the Wnt/β-catenin pathway by targeting GSK-3β/β-catenin which promotes the invasion and metastasis of lung cancer tumors (Yang et al., 2019). Epithelial-to-mesenchymal transition (EMT) is the central process to cancer metastasis, whose feature are the loss of E-cadherin-mediated cell adhesion, increase in cell viability and promoting tumor aggressiveness and metastasis (Du and Pertsemlidis, 2010). However, miR-200 targets zinc finger E-box-binding homeobox (ZEB)1 and ZEB2, and also encode transcriptional repressors of E-cadherin. Therefore, the increased expression of E-cadherin is caused by the up-regulation of miR-200, resulting in decreased vitality of lung cancer cells and inhibition of tumor metastasis (Chen L.et al., 2014). Additionally, the miR-183–96–182 cluster also inhibits invasion and metastasis of lung cancer by targeting Foxf2 (Kundu et al., 2016). Therefore, the study of the association between miRNAs and lung cancer metastasis may be a meaningful focus for clinical prediction of lung cancer recurrence.

Neovascularization is an essential condition for cancer survival and the effect of vascular endothelial growth factor (VEGF) on angiogenesis induction is irreplaceable (Hanahan and Weinberg, 2011; Nowak-Sliwinska et al., 2018). Many miRNAs have been reported to be involved in regulating angiogenesis in various cancer cell lines (Wang et al., 2018). Coincidentally, inhibition of angiogenesis by targeting VEGF by members of the miR-200 family has been reported (Pecot et al., 2013). Hu et al. (2014) agreed that upregulation of miR-126 and miR-128 could directly targeting VEGF-A and VEGF-C showed the capacity of inhibiting angiogenesis in lung tumor cell lines. In contrast, exosome miR-25-3p regulates the VEGFR2 and ZO-1 expression of endothelial cells by targeting KLF2 and KLF4, thereby promoting vascular permeability and accelerating angiogenesis (Zeng et al., 2018). In hypoxia, miR-23a expression in lung-derived exosomes induces HIF-1 α by targeting prolyl hydroxylase 1 and 2 (PHD1 and 2), thereby activating the VEGF pathway and promoting angiogenesis (Hsu et al., 2017). Moreover, through RT-qPCR analysis, Chen et al. revealed that silencing miR-511-5p increases the mRNA expression levels of VEGF-A, which promotes the proliferation of vascular endothelial cells (Chen et al., 2020a).

The examples mentioned above are sufficient to prove that miRNAs can be used as new regulatory factors in tumor genesis and development. In-depth study on the relationship between miRNAs and proliferation, apoptosis and metastasis of lung cancer cells is expected to become a new biomarker for diagnosis, treatment and prognosis of lung cancer.

MicroRNAs and drug resistance in NSCLC

Although a variety of therapeutic approaches like chemotherapy, targeted therapy and radiotherapy have been used clinically, drug resistance remains a major impediment to effective NSCLC therapy. However, the expression of miRNAs has also been implicated with the booming of drug resistance in NSCLC, such as controlling cell proliferation, inhibiting apoptosis and activating autophagy (Lampis et al., 2020). Many studies have reported an association between miRNAs and drug resistance in NSCLC. For example, platinum-based therapy is the preferred regimen for NSCLC, and cisplatin sensitivity is increased at an unstoppable speed in NSCLC cell lines with miR-106b upregulation (Yu et al., 2017).

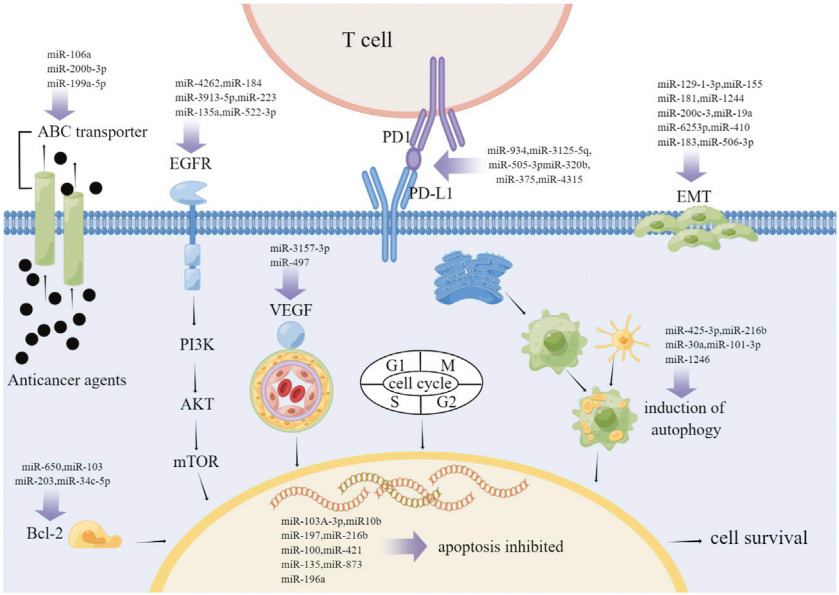

FIGURE 2
Drug resistance in non-small cell lung cancer. The mechanisms of drug resistance in NSCLC are complex and diverse, including ABC transporter activity, anti-apoptosis, autophagy induction, EGFR mutation, EMT promotion, angiogenesis promotion and checkpoint changes. The figure shows the mechanism of miRNA involved in different drug resistance processes of NSCLC. Abbreviations: ABC, ATP-binding cassette; EMT, epithelial–mesenchymal transition; EGFR, epidermal growth factor receptor; VEGF, vascular endothelial growth factor.

Both miR-146b and miR-218 decreased the resistance of NSCLC cells to cisplatin (Shi et al., 2017; Han et al., 2019). In contrast, miR-15b enhances cisplatin-resistant by targeting PEBP4- and RKIP-mediated EMT, as to miR-27a (Zhao et al., 2015; Yin et al., 2017). Interestingly, down-regulation of miR-199a-5p induces autophagy and re-sensitizes cells to multiple chemotherapeutic agents, nevertheless overexpression of miR-199a-5p inhibits autophagy and desensitizes cells to various chemotherapeutic agents (Zeng et al., 2021). In contrast, many miRNAs, such as miR-133a-3p, are regulates drug resistance in lung cancer patients by working with EGFR signaling networks (Li et al., 2021a). Upregulation of miR-762 induced by the IL-6 signaling pathway significantly increased cell survival and rendered NSCLC cells unresponsive to gefitinib-induced cell death (Ge et al., 2019). In addition, exosome miR-96 levels were not only significantly elevated in patients with radioresistant NSCLC, but were also significantly intimated with vascular invasion and poor overall survival (Zheng et al., 2021). In addition, microRNA-3127-5P can upregulate PD-L1, and the upregulation of PD-L1 induces immune escape and leads to chemotherapy resistance in lung cancer (Tang et al., 2018). These studies reflect the important role of miRNAs in drug resistance in NSCLC. A detailed study of the mechanism of miRNA drug resistance in NSCLC may provide new therapeutic targets. Next, we review the role of miRNA regulation in drug resistance in NSCLC (Figure 2).

miRNA and drug resistance in NSCLC chemotherapy

Conventional chemotherapy remains the leading treatment for NSCLC patients, especially those with advanced stages. However, the rapidly development of resistance to chemotherapeutic drugs has greatly reduced the therapeutic efficacy of NSCLC patients. Numerous studies have identified several common signaling pathways, such as phosphoinositide 3-kinase (PI3K)/Akt/mTOR, MDM2/p53 and mitogen-activated protein kinase (MAPK)/Slug signaling, which are implicated in lung cancer chemoresistance (Xing et al., 2018; Li et al., 2021c). In addition to these pathways, some important mechanisms are also involved in chemotherapeutic resistance, such as 1) overexpression of efflux transporters (ATP binding box (ABC) transporter) (Choi and Yu, 2014), 2) defects in the apoptotic machinery (An et al., 2017), 3) activation of the EMT program (Erin et al., 2020), and 4) hypoxic environment and autophagy (Shahverdi et al., 2022). However, the mechanism of drug resistance is so intricacy that it has not been fully elucidated, and the interactions between these complicated mechanisms and their regulatory mechanisms remain largely unknown. To our interest, miRNAs play key roles in these biological processes. In terms of the role of miRNAs in chemotherapy resistance among these mechanisms, we describe the regulation of cisplatin, paclitaxel, and other chemotherapeutic agents (Table 1).

TABLE 1 Summary of miRNAs involved in drug resistance in chemotherapy of NSCLC.

MiRNAs	Drugs	Target	Mechanisms	References
miR-103A-3p	cisplatin	Bak1	inhibit apoptosis	Wang et al. (2021)
miR-10b	cisplatin	p53		Lin et al. (2021)
miR-197	cisplatin	Bcl-2, c-Myc, cyclin D1		Fujita et al. (2015)
miR-216b	cisplatin	Bcl-2		Vu et al. (2020)
miR-106a	cisplatin	ABCA1	increased efflux of drug and (or)	Ma et al. (2015)
miR-200b-3p	cisplatin	ABCA1	decreased drug intake	Liu et al. (2019)
miR-425-3p	cisplatin	AKT1	activate autophagy by negatively regulating the AKT/mTOR pathway	Ma et al. (2019)
miR-216b	cisplatin	PVT1	regulating apoptosis and autophagy through the Mir-216b/Beclin-1 pathway	Chen et al. (2019)
miR-19a	cisplatin	PTEN/Akt	inhibits CP and Akt by down-regulating PTEN	Xing et al. (2019)
miR-100	docetaxel	Plk1	influences cell proliferation, apoptosis, cell cycle distribution, and docetaxel sensitivity of LUAD cells	Feng et al. (2012)
miR-650	docetaxel	Bcl-2, Bax	Spc-a1 or H1299 cell colony formation was enhanced, which promoted cell growth	Huang et al. (2013)
miR-34c-5p	paclitaxel	Bcl-2	inhibit apoptosis	Catuogno et al. (2013)
miR-4262	paclitaxel	PTEN	through targeting PTEN and activating the PI3 K/Akt signalling pathway	Sun et al. (2019)
miR-421	paclitaxel	KEAP1 3′UTR	promoted the migration and invasion of lung cancer cells and inhibited apoptosis *in vivo* and *in vitro*	Duan et al. (2019)
miR-4443	epirubicin	INPP4A	regulating the activation of JAK2/STAT3 pathway	Zhang et al. (2018)
miR-199a-5p	doxorubicin	ABCC1, HIF-1α	increased efflux of drug and (or) decreased drug intake	Jin et al. (2020)

Platinum resistance

Systemic therapy with cytotoxic drugs remains one of the primary treatment methods for NSCLC. Cisplatin is a commonly used chemotherapeutic drug and is an effective treatment for NSCLC when used in combination with other drugs (Teng et al., 2018). However, effective cancer treatment is hampered by patients' resistance to cisplatin. Defects in the apoptotic machinery refer to cancer cells that can escape apoptosis and continue to survive either by overexpressing of anti-apoptotic proteins or underexpressing of pro-apoptotic proteins, and contribute to the development of drug resistance in NSCLC cells (An et al., 2017). However, miRNAs command the cell cycle by regulating proteins involved in DNA damage or inhibiting apoptosis-mediated cell death (Zang et al., 2017). Wang et al. found that cancer-associated fibroblast (CAFs)-derived exosomes miR-103A-3p promote cisplatin resistance by targeting Bak1 to inhibit apoptosis (Wang et al., 2021). One of the key regulators of apoptosis is the intrinsic mitochondrial pathway mediated by p53 (Hafner et al., 2019). As an upstream regulator of p53 signaling pathway, ectopic expression of miR-10b reduces the expression of p53 and its downstream effector factors and inhibits apoptosis, thus leading to cisplatin resistance (Lin et al., 2021). Bcl-2 family members, important anti-apoptotic proteins, are the most concerned miRNAs target molecules that promote cisplatin resistance in NSCLC through anti-apoptotic pathways (Su et al., 2014). Fujita et al. confirmed that an miR-197 was down-regulated in platinum-resistant NSCLC samples, leading to activation of various oncogenes (Bcl-2, C-myc and Cyclin D1), promoting chemotherapy resistance, tumorigenicity and lung metastasis (Fujita et al., 2015). Subsequently, it was reported that miR-216b increased the expression of Bcl-2 by reducing apoptosis and promoting chemotherapy resistance in NSCLC cells (Vu et al., 2020).

Epithelial-mesenchymal transformation (EMT) plays a momentous role in chemotherapy resistance in NSCLC (Adachi et al., 2020). Studies have shown that microspherule protein 1 (MCRS1) is negatively regulated by miR-129-1-3 p, and MCRS1 can induce EMT and cisplatin resistance by increasing the expression of miR-155 (Liu et al., 2014). In addition, downregulation of miR-181 and miR-1244 was observed in cisplatin-resistant NSCLC cells, on the one hand promoting the occurrence of EMT, and on the other hand promoting the growth, migration and metastasis of cancer cells (Li et al., 2015; Li et al., 2016).

The escape of tumor cell from chemotherapy can be achieved by regulating the expression of the number of transporter molecules for drug influx and efflux. Adenosine triphosphate (ATP)-binding cassette (ABC) multidrug transporters confer drug resistance (Balzer et al., 2022). Several studies have confirmed that miRNAs can take part in chemoresistance by upregulating the levels of ABC membrane transporters. Experiments have shown that in NSCLC cell lines, miR-106a

targets the ABCA1 transporter, which induces cisplatin resistance (Ma et al., 2015). miR-200b-3p is another miRNA that targets the ABCA1 transporter, and its expression is upregulated in lung cancer tumor cells, thus driving cell drug resistance (Liu et al., 2019).

There are abundant studies have reflected the important roles of miRNAs and autophagy in the evolve and drug resistance of lung cancer (Jing et al., 2020). For example, AKT1 can be targeted by exosome Mir-425-3p, and Mir-425-3p activate autophagy by negatively regulating and controlling the AKT/mTOR pathway, ultimately give rise to resistance to cisplatin-induced apoptosis (Ma et al., 2019). PVT1 may act as a competitive endogenous RNA of miR-216b, regulating apoptosis and autophagy through the miR-216b/Beclin-1 pathway and inhibiting the sensitivity of cisplatin in NSCLC (Chen et al., 2019). In addition, inducing resistance to both Akt and CP *via* downregulation of PTEN is demonstrated by miR-19a (Xing et al., 2019). However, studies have found that intentional upregulation of miR-30a can improve the prognosis of NSCLC after neoadjuvant chemotherapy and inhibit drug-induced autophagy and drug resistance (Lin et al., 2021). So, miR-30a could be a target for effective chemotherapy and a monitoring marker. Direct targeting of miR-101-3p at ATG4D can upregulate the sensitivity of NSCLC cells to cisplatin, induce cell apoptosis, and inhibit autophagy (Cui et al., 2021). Therefore, miR-101-3p may also be a potential therapeutic target molecular for NSCLC treatment.

Taxanes resistance

Taxanes, a first-line treatment for NSCLC, are commonly used in combination with other anticancer drugs for lung cancer (Long and Suresh, 2020). Resistance to paclitaxel is common in NSCLC patients. In Feng's study, miR-100 downregulation was first reported in the docetaxel-resistant LUAD line SPC-A1/DTX compared with the sensitive parent cells SpC-A1 (Feng et al., 2012). It has also been proved that miR-100 directly targets Plk1 in SPC-A1/DTX cells, and low expression of Mir-100 can lead to overexpression of Plk1 and ultimately lead to chemotherapy resistance of docetaxel in human LUAD (Feng et al., 2012). Subsequently, Huang et al. (2013) believed that miR-650 caused docetaxel chemotherapy resistance in lung adenocarcinoma cells by regulating the expression of Bcl-2/Bax. In addition, miR-34c-5p confers paclitaxel resistance in NSCLC cells by working with the Bcl-2 modifying factor (Catuogno et al., 2013). miR-4262 enhances paclitaxel resistance in NSCLC cells by targeting PTEN and motivating the PI3 K/Akt signaling pathway (Sun et al., 2019). The high expression of miR-421 may at least partially explain paclitaxel resistance in lung cancer patients, and miR-421 induces paclitaxel resistance in the way of binding to KEAP1 3′UTR (Duan et al., 2019). Interestingly, the overexpression of miR-221-3p regulates the MDM2/p53 signaling pathway. Down-regulation of miR-221-3p decreased the sensitivity of A549 cells to paclitaxel, while up-regulation of miR-221-3p partially reversed the resistance of A549 cells to paclitaxel (Ni et al., 2021). Therefore, miR-221-3p may serve as an effective therapeutic target for paclitaxel treatment. Besides, miR-379-5p potentiated paclitaxel sensitivity through targeting TRIM65 in NSCLC (Guo et al., 2022). There is potential for miRNAs to be markers of taxanes resistance or response, and by using these markers, treatment decisions can be guided and the sensitivity of cells to taxanes can be restored.

Resistance to other chemotherapy drugs

Other chemotherapeutic agents have also developed resistance to NSCLC treatment. For instance, miR-363-3p expression enhances gemcitabine resistance in NSCLC cells (Bian et al., 2021). Liang et al. (2019) believed that gemcitabine resistance in NSCLC is caused by the interaction of several miRNAs, such as LET-7D-5P, LET-7I-5p, miR-17-5p, and miR-23b-3p. Furthermore, overexpression of miR-4443 generated the resistance to epirubicin of NSCLC cells in the manner of targeting INPP4A and adjusting the activation of the JAK2/STAT3 pathway (Zhang W.et al., 2018). Among a variety of miR-199a-5p targets, chemotherapy resistance increases the expression of ABCC1 and HIF-1α. miR-199a-5p is participate in chemotherapy resistance of NSCLC *via* regulating the expression of ABCC1 and HIF-1α (Jin et al., 2020). However, miR-451A mitigated resistance of doxorubicin in lung cancer by targeting c-MYC and inhibiting EMT (Tao et al., 2020). These miRNAs mentioned above can be regarded as potential biomarkers for the predict of drug resistance in patients with NSCLC.

miRNA and drug resistance in NSCLC target therapy

NSCLC patients with epidermal growth factor receptor (EGFR) -activated mutations are clinically common and often benefit from EGFR tyrosine kinase inhibitors (TKIs). Unfortunately, more than 50% of first—and second-generation TKIs clinical trial resistance cases are caused by secondary mutations (T790M) or tertiary mutation (C797S) (Sequist et al., 2011). Aside from the T790M mutation, a more common event is EGFR amplification, which occurs in10% of NSCLC patients who develop drugs resistance to these therapies (Sigismund et al., 2018). Similar to chemotherapy, both epithelial-mesenchymal transformation (EMT) regulates and interferes with apoptosis induced by EGFR-TKIs are also cause EGFR-TKIs resistance. In addition, activation of several signaling pathways, for instance PI3K/AKT/mTOR constitute key transduction cascades responsible for

TABLE 2 Summary of miRNAs involved in drug resistance in targeted therapy of NSCLC.

dslrMiRNAs	Drugs	Target	Mechanisms	References
miR-135a	gefitinib	PI3K/Akt	promoted cell growth and metastasis and activated the PI3K/AKT signaling pathway	Zhang and Wang. (2018)
miR-522-3p	gefitinib	PI3K/AKT	activating PI3K/AKT signaling pathway	Liu et al. (2020)
miR-200c-3p	gefitinib	c-Met	promotes EMT and inhibit apoptosis	Wang et al. (2020)
miR-103	gefitinib	Bcl-2	inhibit apoptosis and promote epithelial-mesenchymal transformation	Garofalo et al. (2011)
miR-203	gefitinib	Bcl-2		
miR-19a	gefitinib	c-Met	through targeting c-Met 3′UTR regulation and c-Met protein dependence	Cao et al. (2017)
miR-506-3p	gefitinib	EMT	inhibiting EMT	Haque et al. (2020)
miR-630	gefitinib	miR-630/YAP1/ERK feedback loop	persistent activation of ERK signaling *via* the miR-630/YAP1/ERK feedback loop	Wu et al. (2018)
miR-135	gefitinib	TRIM16	by targeting TRIM16 as a tumor promoter, it is involved in the inherent mitochondrial apoptosis, caspase and JAK/STAT pathways in NSCLC cells	Wang and Zhang. (2018)
miR-223	erlotinib	FBXW7	activation of Akt and Notch signaling pathways	Zhang et al. (2017)
miR-873	gefitinib	GLI1	induced cell proliferation	Jin et al. (2018)
mir-6253p	gefitinib	AXL	*via* activation of the TGF-β/Smad pathway and EMT in EGFR-mutant non-small cell lung cancer	Du et al. (2020)
miR-196a	gefitinib	GLTP	inducing cell proliferation and inhibiting cell apoptosis	Liu et al. (2022)
miR-326	gefitinib	IFNAR2	prostate cancer-associated transcription 6 (PCAT6) activates the miR-326/IFNAR2 axis	Zheng et al. (2022)
miR-323-3p	oximitinib	PI3K/Ak	PI3K-Akt signaling pathway	Janpipatkul et al. (2021)
miR-1468-3p				
miR-5189-5p				
miR-6513-5p				
let-7c	osimertinib	WNT1, TCF-4	reduced proliferation and invasion	Li et al. (2020)
miR-210	osimertinib	E-cadherin	promote vimentin expression	Hisakane et al. (2021)
miR-184/miR-3913-5p	osimertinib	RAS-MAPK/PI3K	ctivation or abnormal regulation by bypass pathways	Li et al. (2021b)

tumor cell survival, proliferation, invasion and metastasis. (Fumarola et al., 2014). Thus, in NSCLC with EGFR mutation, miRNAs mediate drug resistance of TKIs by activating PI3K/AKT/mTOR signaling pathway (Table 2).

Resistance of first-generation EGFR-TKIs

The first-generation EGFR-TKIs (include Gefitinib and erlotinib) are applied to the treatment of lung cancer. What cannot be ignored, however, is the blossom of resistance to these agent treatments, and several studies have shown that miRNAs are involved. For instance, miR-135a is associated with the lack of PI3K/Akt pathway activation and is involved in gefitinib resistance (Zhang and Wang, 2018). Liu et al. reveal that exosomes released from H1975 could induce resistance of gefitinib to PC9 *in vivo* and *in vitro* by activating the PI3K/AKT signaling pathway. However, up-regulation of miR-522-3p can enhance drug resistance in PC9 cells to gefitinib (Liu et al., 2020). Among patients treated with EGFR-TKI, those with high expression of miR-200c-3p had significantly longer progression-free survival (PFS) than those with miR-200C-3p in low expression. Silencing of miR-200C-3p in EGFR TKI highly sensitive cell lines increases drug gefitinib resistance (Wang et al., 2020). An evidence-based study reports that activation or overexpression of c-MET reduced the levels of miR-103 and miR-203 *in vitro*, which typically function as oncosuppressor miRNAs. Hence, these two miRNAs could cause acquired resistance to EGFR-TKIs in cases of c-MET gene amplification or overexpression (Garofalo et al., 2011). miR-19a downregulation promoted gefitinib resistance and EMT in gefitinib-sensitive NSCLC cells (Cao et al., 2017). Down-regulation of miR-506-3p promotes EGFR-TKI resistance by inhibiting EMT in NSCLC cell line (Haque et al., 2020). The miR-630/YAP1/ERK axis has also been reported to promotes TKI resistance in EGFR-mutated lung tumor cells. miR-630 downregulation promoted ERK activation through YAP1 upregulation, resulting in TKI resistance (Wu et al., 2018), and miR-135 down-regulates CDH1 and β-catenin and upregulates PD-L1 by targeting TRIM16, promoting drug resistance of NSCLC cells to gefitinib (Wang and Zhang, 2018). The AKT and Notch signaling pathways in erlotinib-

resistant cells were stimulated and activated by up-regulated miR-223, and mir-223 was highly expressed in erlotinib-resistant HCC827 cells compared to that in parental cells (Zhang et al., 2017). It was found that inhibition of miRr-873 not only enhanced angiogenesis of NSCLC cells but also led to gefitinib resistance, because down-regulation of miR-873 dramatically trigger proliferation of gefitinib-treated PC9 cells, up-regulation of GLI1 subsequently (Jin et al., 2018). Recent data suggest that TGF-β1-induced EMT may be associated with gefitinib resistance mediated by the miR-6253p/AXL axis, which contributes to gefitinib-acquired resistance (Du et al., 2020). Recent studies have found that glycolipid transfer protein (GLTP) is a direct functional target of miR-196a, which can down-regulate GLTP and lead to gefitinib resistance. moreover, forced expression of miR-196a can also increases gefitinib resistance in NSCLC tumor cells by inducing cell proliferation and inhibiting cell apoptosis (Liu et al., 2022). In addition, IFN-α receptor 2 (IFNAR2) was identified as a downstream target of miR-326, reducing gefitinib resistance by inhibiting IFNAR2 expression. However, prostate cancer-associated transcription 6 (PCAT6) enhances gefitinib resistance in NSCLC *via* the miR-326/IFNAR2 axis (Zheng et al., 2022). Numerous studies have confirmed the important role of miRNAs in acquired gefitinib and erlotinib resistance and targeting these miRNAs may be an effective treatment option for lung cancer patients with first-generation EGFR-TKI-resistant.

Resistance of second-generation EGFR-TKIs

Second-generation EGFR-TKIs is the preferred choice after the developed resistance to first-generation EGFR-TKIs in NSCLC. At present, afatinib is the most commonly used second-generation EGFR-tkis clinically, followed by nalatinib and dacomitinib (Tripathi et al., 2020). Afatinib is an efficient TKI that acts similarly to first-generation EGFR-Tkis, targeting EGFR mutations as well as secondary mutations, such as T790M (Tripathi et al., 2020). However, acquired afatinib resistance has also been observed in clinical use. Hashida et al. (2015) established an afatinib-resistant cell line, HCC827-ACR, from MET-amplified cell lines. Several kinds of afatinib-resistant cell lines like HCC827-ACR, show EMT characteristics, and epigenetic silencing of miR-200c and miR-200c promoter region methylation was observed in these cell lines (Hashida et al., 2015). Subsequent studies have shown that miR-34a mimics act synergistically with afatinib, rociletinib, or osimertinib in all EFGR mutant cells (Zhao et al., 2017). Optimal and consistently strong synergies were observed in a cellular model of acquired resistance (Zhao et al., 2017). Although miRNAs are rarely reported to be involved in drug resistance to second-generation EGFR-TKIs, some miRNA changes have been observed when afatinib is used to treat NSCLC cancer.

Resistance of third-generation EGFR-TKIs

To date, third-generation EGFR-TKIs represented by osimertinib have been prescribed usually for T790M-positive patient (Cross et al., 2014). Unfortunately, patients typically develop resistance to osimertinib after 6–17 months treatment (Walter et al., 2013). Coincidentally, miR-147b was discovered to be the most upregulated miRNA in lung cancer cells resistant to osimertinib and EGFR mutations (Zhang et al., 2019). Janpipatkul et al. (2021) showed that four exosomal miRNAs (miR-323-3p, miR-1468-3p, miR-5189-5p, and miR-6513-5p) can not only be used as molecular biomarkers for the detection of oximitinib resistance in NSCLC patients, but also have the potential to distinguish oximitinib-resistant and oximitinib-sensitive NSCLC patients. In addition, in NSCLC cells with EGFR T790M mutation, leT-7C-mediated EMT leads to osimertinib resistance (Li et al., 2020). Exosome miR-210 may play a crucial part in the development of osimertinib resistance in the tumor microenvironment, and work as a therapeutic target to overcome this resistance in EGFR-mutant NSCLC. According to reports, exosomes from EGFR-mutated NSCLC cells induce EMT and drug resistance in osimertinib-sensitive cells *via* miR-210 delivery (Hisakane et al., 2021). In patients with EGFR mutations and T790m positivity, elevated expression levels of miR-184 and miR-3913-5p in serum exosomes are resistant to oximitinib by activating the RAS-MAPK/PI3K pathway (Li et al., 2021b). These studies also confirmed the important role of miRNAs in osimertinib resistance; therefore, targeting them may improve and restore the sensitivity of NSCLC patients with inherent and acquired resistance to third-generation EGFR-TKIs. The interactions between various miRNAs and complex signaling pathways during the process of third-generation EGFR-TKIs resistance in lung tumor cells are summarized above, paving the way for the introduction of miRNA-based biomarkers to detect the third-generation EGFR-TKIs response in lung cancer patients.

miRNA and drug resistance in NSCLC immunotherapy

Immunotherapy (IO) has revolutionized the treatment landscape of NSCLC, particularly immune checkpoint inhibitors (ICI), including the T lymphocyte receptor CTLA-4 (cytotoxic T lymphocyte antigen 4), programmed death receptor 1 (PD-1), and PD-ligand 1 (PD-L1) inhibitors (Horvath et al., 2020). Despite striking clinical improvements, most patients end up responding poorly to ICI treatment because of the emergence of primary or secondary resistance. Currently, immunotherapy against the PD-1/PD-L1 axis is the first-line or subsequent treatment option for NSCLC patients and PD-1/PD-L1 antibodies, including pembrolizumab, nivolumab,

atezolizumab, and durvalumab (Herbst et al., 2020). Similarly, the development of resistance to the PD-1/PD-L1 blockade is inevitable. The PD-1/PD-L1 blockade is intended to reinvigorate exhausted tumor-specific CD8 + T-cells, and the expression of CD8 + T cells is required for therapeutic response (Kurtulus et al., 2019). Some studies have indicated that Mir-934 can interact with circUSP7 in CD8+T cells, and the activity levels of Mir-934 will be inhibited by circUSP7, which finally caused the function of CD8+T cells be impaired so that immune escape in NSCLC (Chen et al., 2021). A key requirement for the PD-1/PD-L1 blocking response is that tumor-specific T cells in the patient are inhibited by PD-1, and PD-L1 expression in the tumor inhibits PD-1+ T cells at sites that require antitumor activity (Poggio et al., 2019). miR-3127-5p promotes the expression of PSTAT3 induced PD-L1, and immune escape induced by increased PD-L1 expression in lung cancer (Tang et al., 2018). A necessary condition for tumor cells to prevent immune escape is sensitivity to cytotoxic molecules produced by T cells. In a study by Zhu et al. (2020), the miR-505-3p axis can affect the primary functions of CD8+T cells, including cytokine secretion and cytotoxicity. The introduction of miR-505-3p may provide a new direction for immune resistance in NSCLC.

Nivolumab, however, which targets PD-1 for its function, is preferentially propitious to NSCLC patients with high tumor mutation burden (TMB). In short, upregulation of miR-320b and miR-375 was related to resistance in nivolumab treatment whereas the upregulation of some miRNAs predicted responsiveness to nivolumab treatment, such as miR-93, miR-138-5p, miR-200, miR-27a, miR-424, miR-34a, miR-28, miR-106b, miR-193a-3p, miR-181A and so on. (Costantini et al., 2018; Fan et al., 2020a). However, it has been found that anti-PD1 exposure of T cells promotes the aggregation of exosomal miRNA-4315. And miR-4315 can be used to determine the time cycle in which ABT263 therapy can effectively accelerate tumor cell death and bypass anti-PD1 resistance. Therefore, miRNA-4315 could be used as a biomarker for the development of anti-PD1 antibody treatment resistance (Guyon et al., 2020). Research on the resistance of miRNAs against PD-1/PD-L1 in lung cancer will contribute to the development of personalized combined immunotherapy.

miRNA and drug resistance in NSCLC anti-angiogenesis therapy

Neovascularization is a prerequisite for tumor proliferation and metastasis; thus, anti-angiogenic agents are indispensable in treating NSCLC (Assoun et al., 2017). However, the emergence of impedance towards angiogenic blockers has been regarded as the main challenge in cancer treatment using the anti-angiogenesis strategy. VEGF is a major regulator of any kind of blood vessel growth in the human body and plays a role in angiogenesis (Altorki et al., 2019). Alterations in VEGF-dependent, non-VEGF pathways, and the interactions of stromal cell are the mechanisms of anti-angiogenesis therapy resistance (Haibe et al., 2020). However, the major angiogenic factors are regulated by miRNAs. Shi et al. (2018) suggested that up-regulation of miR-126 down-regulates VEGF-A and VEGFR2 through inactivation of VEGF-A/VEGFR2/ERK signaling pathway, demonstrating its significance in regulating angiogenesis in lung cancer. Exosome miR-3157-3p regulates the expression of VEGF/MMP2/MMP9 from endothelial cells *via* target TIMP/KLF2, therefore, promoting angiogenesis and increasing vascular permeability, leading to drug resistance (Ma et al., 2021). In A549 cells, exosome miR-497 can effectively inhibit the expression of tumor-related genes, such as VEGF-A, suggesting that exosome miR-497 may be involved in the regulation of anti-vascular resistance (Jeong et al., 2020). Currently, there are few reports on the anti-angiogenic treatment resistance of miRNAs in NSCLC. Due to the important role of miRNAs in angiogenesis, further research on the anti-angiogenic treatment resistance of miRNAs is needed to provide a new direction for the treatment of NSCLC.

miRNA and radioresistance in NSCLC

Radiotherapy, a widely used and effective therapy in clinics, can help improve the 5-year survival rate of NSCLC patients. However, radiation therapy is not as effective as it could be due to the complicated genetic cellular responses to radiation. To date, there have been many reports on the relationship between miRNAs and radiotherapy resistance in NSCLC. Previously, upregulation of miR-95 was shown to promote radiation resistance in NSCLC cells by directly targeting Nexin1 (SNX1) (Chen X.et al., 2014). Yuan et al. (2020) showed that miR-410 was a vital regulator of EMT and radiation resistance in NSCLC, and induced EMT promoted the enhancement of radiation resistance by targeting the PTEN/PI3K/mTOR axis. MiR-22 is downregulated in NCI-466 SCLC cells and inhibits radiosensitivity *via* targeting Werner helicase-interacting protein-1 (WRNIP1) (Jiang W.et al., 2019). It has been reported that miR-183 expression could give rise to radiation-resistant in lung adenocarcinoma cell lines (H1299R cells), and miR-183 promotes EMT and radiation tolerance in H1299 cells (Huang et al., 2021). Fan et al. found that mTOR is a direct target gene of miR-1246 that mediates miR-1246-induced autophagy activation. MiR-1246 of intracellular and extracellular were found to be upregulated in a time-dependent manner after irradiation, giving rise to radioresistance in NSCLC cells (Fan et al., 2020b). Moreover, it was observed in Chen's experiment, apoptosis induced by radiotherapy in the miR-181a mimic group was markedly inhibited in comparison with that of the miR-181a inhibitor group. also reported that miR-181A inhibits PTEN in non-small cell lung cancer and reduces radiosensitivity (Chen et al., 2020b). However, some miRNAs strengthen the sensitivity

of NSCLC cells to radiation. For example, miR-9 can make cancer cells die by inhibiting the activity and migration of A549 cells and enhancing the radiosensitivity of A549 cells. This effect is highly regulated by the methylation state of its promoter, so the overexpression of miR-9 enhances the radiosensitivity of NSCLC (Wei et al., 2019b). In A549-R and H1299-R cells, miR-129-5p expression was markedly decreased, whereas SOX4 and RUNX1 expression was increased. MiR-129-5p was then transfected into NSCLC cell lines to caused cell apoptosis, DNA damage and cell cycle arrest, therewith restrain cell proliferation and colony formation by targeting RUNX1 and SOX, making A549-R and H1299-R cells sensitive to radiation (Xue et al., 2021). Potassium voltage-gated channel subfamily Q member 1 opposite strand 1 (KCNQ1OT1), is an imprinted antisense lncRNA located in the KCNQ1 locus on human chromosome 11p15.510, working in several human cancers (Sachani et al., 2018). In a study by HE (He et al., 2020), KCNQ1OT1 upregulation induced ATG5/ATG12-mediated autophagy through miR-372-3p, thereby promoting radiotherapy resistance in lung cancer. Therefore, miR-372-3p may also plays an important role in radiation resistance. Besides, using lung cancer cells, Sun et al. (2020) demonstrated that miR-125a-5p enhanced the radiosensitivity of these cells by upregulating SIRT7 and further increasing apoptosis. Taken together, using these findings, new directions can be taken to improve the radiosensitivity of malignant lung tumors.

MicroRNAs delivery method in the treatment of NSCLC

MiRNAs have been the subject of several research studies since Lee et al. (1993) discovered them in 1993, and their function continues to be unraveled as they are discovered. It has become increasingly interesting to examine the way miRNAs are delivered in cancer therapy. The trial of Orellana et al. (2017) that the microRNAs are attached directly to folate (FolamiR), which allows them to be delivered directly into cells overexpressing the folate receptor, and using an autochthonous lung cancer model, they demonstrate that FolamiR-34a, a tumor-suppressor, is rapidly taken up by tumors and slows tumor growth. Afterwards, Perepelyuk et al., 2018 demonstrated that using MUC1-aptamer-functionalized hybrid nanoparticles, miRNA-29b could be efficiently delivered to NSCLC patients for downregulating target oncogenes. An early-stage lung cancer metastasis model showed significant tumor inhibition and survival enhancement with CL-PVAX-Mir-143 systemically delivered. It is important to note that the same results were obtained in advanced mouse models that had metastases. And there was no obvious acute toxicity associated with Cl-pvax-mir-143 treatment (Jiang Q.et al., 2019). Therefore, the delivery of Mir-143 is likely to be a breakthrough point in the treatment of NSCLC. According to two studies published recently, lung cancer development is suppressed by UTMD-mediated delivery of miR-216bM and miR-21-5p inhibitors (Wang et al., 2022; Zhou et al., 2022). Taking these examples into account, Deep dissection of miRNA delivery patterns will be a breakthrough in the journey of lung cancer treatment and a focus of scientists' future research.

Potential of miRNAs in the treatment of NSCLC

Among the benefits of miRNAs for clinical use include high stability in serum, fast noninvasive testing, and easy detection in tissues, blood, or other body fluids (Li and Sarkar, 2016). The similarities between miRNAs and their target genes, as well as the fact that a single miRNA can regulate multiple miRNAs, make miRNAs more likely to become biomarkers than mRNAs alone. Also, miRNAs regulate cancer cell proliferation, apoptosis, migration and tumor progression, making new lung cancer therapies possible. We also summarized the clinical trials for lung cancer treatment (Table 3).

Cancer cells use miRNAs for various functions, with some of them specifically targeting cancer-related pathways, posing a potential therapeutic opportunity. As part of the phase I MesomiR-1 study, TargomiRs, a miR-16-based microRNA mimic, was tested in those with malignant pleural mesothelioma or NSCLC at advanced stages in 2017. A newly developed anti-EGFR antibody, targeting EDVTM nanocells, was used in this trial to deliver MESOMir-1 to patients with EDVTM-targeted nanocells, and the first five patients were exposed to 1.5g of the phase 1 dose, which had an acceptable safety profile. In general, there has been a good tolerance and safety record for TargomiR treatment among patients (Van Zandwijk et al., 2017). Subsequently, in this phase 1 trial of microRNA-based cancer therapy, MRX34 (RP2D), a liposome analog (miR-34a), was identified and evaluated. Patients treated with MRX34 receiving premedication with dexamethasone showed manageable side effects and some clinical response. As a result of severe immune-mediated adverse events (AEs) that resulted in the deaths of four patients, the trial was closed early (Hong et al., 2020). Additionally, as the mechanisms by which they function are clarified, miR-200 and let-7 have been extensively used as therapeutic targets in animal studies, and they have been validated (Pecot et al., 2013; Stahlhut and Slack, 2015). It is important to note that miRNA-based therapies are still in the early stages of phase I clinical trials, but dose-dependent modulation of relevant target genes is proving that miRNA-based cancer treatments are feasible.

It might be possible to predict cancer response to chemotherapy or other therapeutic interventions using microRNAs. According to the study, 148 LUAD patients who had received pemetrexed maintenance therapy were negative for mutations in the EGFR or translocations of the

TABLE 3 NSCLC clinical trials with miRNA-based therapy.

miRNA	drug	Population	Number	Toxicities	Safety (≥G3,%)	Efficacy	Status	References
miR-16	TargomiRs, MesomiR-1 trial (NCT02369198)	NSCLC,MPM	27	Infusion-related inflammatory symptoms, coronary ischemia, anaphylaxis, cardiomyopathy, non-cardiac pain	lymphopenia (42), increased AST or ALT (19), temporal hypophosphatemia (15), infusion-related inflammatory symptoms (8), cardiomyopathy (4)	ORR: 5%, SD: 68%, DOR: 32 weeks	Completed	Van Zandwijk et al. (2017)
miR-34	MRX34 (NCT01829971)	NSCLC,SCL,HCC,RCC,GIST, Melanoma	85	Hypoxia, neutropenia, thrombocytopenia	SAEs (35), lymphopenia (18), chills (14), deaths (9), fatigue (9), neutropenia (8), thrombocytopenia (6), back/neck pain (5), dyspnea (5)	ORR: 4%, SD for ≥4 cycles: 24%	Early closed	Hong et al. (2020)

HCC, hepatocellular carcinoma; RCC, renal cell carcinoma; GIST, gastrointestinal stromal tumor; SAEs, severe adverse events; ORR, objective response rate; SD, stable disease; MPM, malignant pleural mesothelioma; AST, aspartate aminotransferase; ALT, alanine aminotransferase; DOR, duration of the objective response.

ALK, compared with patients who were treated with pemetrexed, patients who expressed the levels differ of miR-25, miR-145, and miR-210 had significantly shorter progression-free survival times, this suggests that these three miRNAs can predict maintenance treatment efficacy (Mok et al., 2019). In addition, miR-125b-5p levels in partial response-post samples were significantly lower, monitoring miR-125b-5p levels in response to anti-PD-1/PD-L1 therapy might be useful (Liang et al., 2020).

There is growing evidence that miRNAs having a significant impact on predicting lung cancer outcomes. For example, identified miR-374a and miR-374b, two EMT-related miRNAs that may be associated with poor survival, after profiling miRNA expression levels in NSCLC patient samples (Kim et al., 2020). An analysis conducted recently found, the expression of miR-2355-3p in LUAD is upregulated, and this overexpression allows us to distinguish LUAD serum from normal serum. Additionally, the prognosis of patients with high miR-2355-3p levels is unfavorable. By targeting ZCCHC14, miR-2355-3p can be inhibited to suppress the progression of LUAD (Zhao et al., 2021). As such, miR-2355-3p may prove to be an effective noninvasive diagnostic and prognostic factor as well as a potential therapeutic target for lung cancer.

Conclusion and prospects

In conclusion, the death rate of lung cancer is increasing year by year, and the existence of drug resistance is a major cause of treatment failure. A number of important roles that miRNAs play in cancer biology have been recognized in recent years, and they are one of the most exciting discoveries in the field of NSCLC. As oncogenes or tumor suppressor genes, miRNAs have been implicated in proliferation, apoptosis, angiogenesis, invasion, and migration of lung cancer cells. Drug resistance in lung cancer is also influenced by miRNAs in a variety of ways, but many miRNAs involved in drug resistance remain unknown. In addition, the analysis of miRNAs is potentially useful for lung cancer diagnosis, prognosis, and predictability, may provide a reliable, non-invasive biomarker for monitoring relapse and individual response to treatment. Therapeutic potential of miRNA mimics or miRNA inhibitors (such as anticancer drugs) could be achieved by mimicking tumor suppression of miRNAs. Despite this, certain challenges cannot be ignored. To start with, miRNAs are expressed heterogeneously, and their interactions with other miRNAs and effects on cell function are significant. It is essential to study the network of interactions between miRNAs and whether these molecules are complementary or antagonistic. A second point is that we still have very little knowledge about the mechanisms of miRNA secretion and uptake, and we need to further explore the specific molecules and mechanisms of novel miRNA delivery systems. In the third place, there is uncertainty about miRNA target selection and drug delivery accuracy. There is an urgent need for larger, more comprehensive studies to further optimize existing miRNA-targeted therapies and provide better therapeutic alternatives. Finally, there are few large-scale studies on the safety and

efficacy of miRNA-based drugs, and reproducible results require studies involving stratified patients at large scale and ensure the clinical safety and efficacy of miRNAs as therapeutics. Overall further research on miRNA and its regulatory function will provide new ideas for preventing, monitoring, and treating lung cancer. To gain a deeper understanding of miRNA-based cancer treatments, future research is necessary.

Author contributions

Conceptualization, HZ and YZ; methodology, HY and SET; software, YZ; validation, HY, CQ, and HH; formal analysis, HG; investigation, SOT, CZ, YZ, and JZ; resources, HZ and SOT; data curation, YZ; writing—original draft preparation, HY and SET; writing—review and editing, HY, SET, and HG; visualization, LY and YZ; supervision, HZ and YZ; project administration, HZ and SET; funding acquisition, HZ and YZ. All authors have read and agreed to the published version of the manuscript.

Funding

The research was supported by Chengdu University of Traditional Chinese Medicine (YYZX2020093) and Health Department of Sichuan Province (21PJ188).

Conflict of interest

The authors declare that the research was conducted in the absence of any commercial or financial relationships that could be construed as a potential conflict of interest.

Publisher's note

All claims expressed in this article are solely those of the authors and do not necessarily represent those of their affiliated organizations, or those of the publisher, the editors and the reviewers. Any product that may be evaluated in this article, or claim that may be made by its manufacturer, is not guaranteed or endorsed by the publisher.

References

Adachi, Y., Ito, K., Hayashi, Y., Kimura, R., Tan, T. Z., Yamaguchi, R., et al. (2020). Epithelial-to-Mesenchymal transition is a cause of both intrinsic and acquired resistance to KRAS G12C inhibitor in KRAS G12C-mutant non-small cell lung cancer. *Clin. Cancer Res.* 26 (22), 5962–5973. doi:10.1158/1078-0432.CCR-20-2077

Adi Harel, S., Bossel Ben-Moshe, N., Aylon, Y., Bublik, D. R., Moskovits, N., Toperoff, G., et al. (2015). Reactivation of epigenetically silenced miR-512 and miR-373 sensitizes lung cancer cells to cisplatin and restricts tumor growth. *Cell Death Differ.* 22 (8), 1328–1340. doi:10.1038/cdd.2014.221

Altorki, N. K., Markowitz, G. J., Gao, D., Port, J. L., Saxena, A., Stiles, B., et al. (2019). The lung microenvironment: An important regulator of tumour growth and metastasis. *Nat. Rev. Cancer* 19 (1), 9–31. doi:10.1038/s41568-018-0081-9

An, X., Sarmiento, C., Tan, T., and Zhu, H. (2017). Regulation of multidrug resistance by microRNAs in anti-cancer therapy. *Acta Pharm. Sin. B* 7 (1), 38–51. doi:10.1016/j.apsb.2016.09.002

Assoun, S., Brosseau, S., Steinmetz, C., Gounant, V., and Zalcman, G. J. F. (2017). Bevacizumab in advanced lung cancer: State of the art. *Future Oncol.* 13 (28), 2515–2535. doi:10.2217/fon-2017-0302

Balzer, V., Poc, P., Puris, E., Martin, S., Aliasgari, M., Auriola, S., et al. (2022). Re-evaluation of the hCMEC/D3 based *in vitro* BBB model for ABC transporter studies. *Eur. J. Pharm. Biopharm.* 173, 12–21. doi:10.1016/j.ejpb.2022.02.017

Bartel, D. J. C. (2004). MicroRNAs: Genomics, biogenesis, mechanism, and function. *Cell* 116 (2), 281–297. doi:10.1016/s0092-8674(04)00045-5

Bian, W., Zhou, X., Song, S., Chen, H., Shen, Y., Chen, P. J. E., et al. (2021). Reduced miR-363-3p expression in non-small cell lung cancer is associated with gemcitabine resistance via targeting of CUL4A. *Eur. Rev. Med. Pharmacol. Sci.* 25 (21), 6444. doi:10.26355/eurrev_202111_27133

Cao, X., Lai, S., Hu, F., Li, G., Wang, G., Luo, X., et al. (2017). miR-19a contributes to gefitinib resistance and epithelial mesenchymal transition in non-small cell lung cancer cells by targeting c-Met. *Sci. Rep.* 7 (1), 2939. doi:10.1038/s41598-017-01153-0

Catuogno, S., Cerchia, L., Romano, G., Pognonec, P., Condorelli, G., and de Franciscis, V. (2013). miR-34c may protect lung cancer cells from paclitaxel-induced apoptosis. *Oncogene* 32 (3), 341–351. doi:10.1038/onc.2012.51

Chen, J., Liu, A., Wang, Z., Wang, B., Chai, X., Lu, W., et al. (2020a). LINC00173.v1 promotes angiogenesis and progression of lung squamous cell carcinoma by sponging miR-511-5p to regulate VEGFA expression. *Mol. Cancer* 19 (1), 98. doi:10.1186/s12943-020-01217-2

Chen, L., Gibbons, D., Goswami, S., Cortez, M., Ahn, Y., Byers, L., et al. (2014). Metastasis is regulated via microRNA-200/ZEB1 axis control of tumour cell PD-L1 expression and intratumoral immunosuppression. *Nat. Commun.* 5, 5241. doi:10.1038/ncomms6241

Chen, L., Han, X., Hu, Z., and Chen, L. (2019). The PVT1/miR-216b/Beclin-1 regulates cisplatin sensitivity of NSCLC cells via modulating autophagy and apoptosis. *Cancer Chemother. Pharmacol.* 83 (5), 921–931. doi:10.1007/s00280-019-03808-3

Chen, S. W., Zhu, S. Q., Pei, X., Qiu, B. Q., Xiong, D., Long, X., et al. (2021). Cancer cell-derived exosomal circUSP7 induces CD8(+) T cell dysfunction and anti-PD1 resistance by regulating the miR-934/SHP2 axis in NSCLC. *Mol. Cancer* 20 (1), 144. doi:10.1186/s12943-021-01448-x

Chen, X., Chen, S., Hang, W., Huang, H., and Ma, H. (2014). MiR-95 induces proliferation and chemo- or radioresistance through directly targeting sorting nexin1 (SNX1) in non-small cell lung cancer. *Biomed. Pharmacother.* 68 (5), 589–595. doi:10.1016/j.biopha.2014.04.008

Chen, Y., Liao, W., Yuan, A., Xu, H., Yuan, R., and Cao, J. (2020b). MiR-181a reduces radiosensitivity of non-small cell lung cancer via inhibiting PTEN. *Panminerva Med.* 64 (3), 374–383. doi:10.23736/s0031-0808.20.03976-2

Choi, Y., and Yu, A. (2014). ABC transporters in multidrug resistance and pharmacokinetics, and strategies for drug development. *Curr. Pharm. Des.* 20 (5), 793–807. doi:10.2174/13816128005140214165212

Costantini, A., Julie, C., Dumenil, C., Hélias-Rodzewicz, Z., Tisserand, J., Dumoulin, J., et al. (2018). Predictive role of plasmatic biomarkers in advanced non-small cell lung cancer treated by nivolumab. *Oncoimmunology* 7 (8), e1452581. doi:10.1080/2162402x.2018.1452581

Croce, C. M. (2009). Causes and consequences of microRNA dysregulation in cancer. *Nat. Rev. Genet.* 10 (10), 704–714. doi:10.1038/nrg2634

Cross, D. A. E., Ashton, S. E., Ghiorghiu, S., Eberlein, C., Nebhan, C. A., Spitzler, P. J., et al. (2014). AZD9291, an irreversible EGFR TKI, overcomes t790m-mediated resistance to EGFR inhibitors in lung cancer. *Cancer Discov.* 4 (9), 1046–1061. doi:10.1158/2159-8290.Cd-14-0337

Cui, D., Feng, Y., and Qian, R. J. B. (2021). Up-regulation of microRNA miR-101-3p enhances sensitivity to cisplatin via regulation of small interfering RNA (siRNA) anti-human AGT4D and autophagy in non-small-cell lung carcinoma (NSCLC). *Bioengineered.* 12 (1), 8435–8446. doi:10.1080/21655979.2021.1982274

Du, L., and Pertsemlidis, A. J. C. (2010). microRNAs and lung cancer: tumors and 22-mers. *Cancer Metastasis Rev.* 29 (1), 109–122. doi:10.1007/s10555-010-9204-9

Du, W., Sun, L., Liu, T., Zhu, J., Zeng, Y., Zhang, Y., et al. (2020). The miR-625-3p/AXL axis induces non-T790M acquired resistance to EGFR-TKI via activation of the TGF-β/Smad pathway and EMT in EGFR-mutant non-small cell lung cancer. *Oncol. Rep.* 44 (1), 185–195. doi:10.3892/or.2020.7579

Duan, F.-G., Wang, M.-F., Cao, Y.-B., Dan, L., Li, R.-Z., Fan, X.-X., et al. (2019). MicroRNA-421 confers paclitaxel resistance by binding to the KEAP1 3′UTR and predicts poor survival in non-small cell lung cancer. *Cell Death Dis.* 10 (11), 821. doi:10.1038/s41419-019-2031-1

Duma, N., Santana-Davila, R., and Molina, J. R. (2019). Non-small cell lung cancer: Epidemiology, screening, diagnosis, and treatment. *Mayo Clin. Proc.* 94 (8), 1623–1640. doi:10.1016/j.mayocp.2019.01.013

Erin, N., Grahovac, J., Brozovic, A., and Efferth, T. (2020). Tumor microenvironment and epithelial mesenchymal transition as targets to overcome tumor multidrug resistance. *Drug resist. updat.* 53, 100715. doi:10.1016/j.drup.2020.100715

Fan, J., Yin, Z., Xu, J., Wu, F., Huang, Q., Yang, L., et al. (2020a). Circulating microRNAs predict the response to anti-PD-1 therapy in non-small cell lung cancer. *Genomics* 112 (2), 2063–2071. doi:10.1016/j.ygeno.2019.11.019

Fan, L., Wang, J., Cao, Q., Ding, X., and Li, B. J. A. J. O. C. R. (2020b). Aberrant miR-1246 expression promotes radioresistance in non-small cell lung cancer: A potential prognostic biomarker and radiotherapy sensitization target. *Am. J. Cancer Res.* 10 (1), 314–335.

Feng, B., Wang, R., and Chen, L. B. (2012). MiR-100 resensitizes docetaxel-resistant human lung adenocarcinoma cells (SPC-A1) to docetaxel by targeting Plk1. *Cancer Lett.* 317 (2), 184–191. doi:10.1016/j.canlet.2011.11.024

Fujita, Y., Yagishita, S., Hagiwara, K., Yoshioka, Y., Kosaka, N., Takeshita, F., et al. (2015). The clinical relevance of the miR-197/CKS1B/STAT3-mediated PD-L1 network in chemoresistant non-small-cell lung cancer. *Mol. Ther.* 23 (4), 717–727. doi:10.1038/mt.2015.10

Fumarola, C., Bonelli, M., Petronini, P., and Alfieri, R. J. B. P. (2014). Targeting PI3K/AKT/mTOR pathway in non small cell lung cancer. *Biochem Pharmacol.* 90 (3), 197–207. doi:10.1016/j.bcp.2014.05.011

Garofalo, M., Di Leva, G., Romano, G., Nuovo, G., Suh, S., Ngankeu, A., et al. (2009). miR-221&222 regulate TRAIL resistance and enhance tumorigenicity through PTEN and TIMP3 downregulation. *Cancer Cell* 16 (6), 498–509. doi:10.1016/j.ccr.2009.10.014

Garofalo, M., Romano, G., Di Leva, G., Nuovo, G., Jeon, Y., Ngankeu, A., et al. (2011). EGFR and MET receptor tyrosine kinase-altered microRNA expression induces tumorigenesis and gefitinib resistance in lung cancers. *Nat. Med.* 18 (1), 74–82. doi:10.1038/nm.2577

Ge, P., Cao, L., Chen, X., Jing, R., and Yue, W. (2019). miR-762 activation confers acquired resistance to gefitinib in non-small cell lung cancer. *BMC Cancer* 19 (1), 1203. doi:10.1186/s12885-019-6416-4

Guo, C., Wang, H., Jiang, H., Qiao, L., and Wang, X. (2022). Circ_0011292 enhances paclitaxel resistance in non-small cell lung cancer by regulating miR-379-5p/TRIM65 Axis. *Cancer biother. Radiopharm.* 37 (2), 84–95. doi:10.1089/cbr.2019.3546

Guyon, N., Garnier, D., Briand, J., Nadaradjane, A., Bougras-Cartron, G., Raimbourg, J., et al. (2020). Anti-PD1 therapy induces lymphocyte-derived exosomal miRNA-4315 release inhibiting Bim-mediated apoptosis of tumor cells. *Cell Death Dis.* 11 (12), 1048. doi:10.1038/s41419-020-03224-z

Hafner, A., Bulyk, M. L., Jambhekar, A., and Lahav, G. (2019). The multiple mechanisms that regulate p53 activity and cell fate. *Nat. Rev. Mol. Cell Biol.* 20 (4), 199–210. doi:10.1038/s41580-019-0110-x

Haibe, Y., Kreidieh, M., El Hajj, H., Khalifeh, I., Mukherji, D., Temraz, S., et al. (2020). Resistance mechanisms to anti-angiogenic therapies in cancer. *Front. Oncol.* 10, 221. doi:10.3389/fonc.2020.00221

Han, Q., Cheng, P., Yang, H., Liang, H., and Lin, F. (2019). miR-146b Reverses epithelial-mesenchymal transition via targeting PTP1B in cisplatin-resistance human lung adenocarcinoma cells. *J. Cell. Biochem.* 121, 3901–3912. doi:10.1002/jcb.29554

Hanahan, D., and Weinberg, R. J. C. (2011). Hallmarks of cancer: The next generation. *Cell* 144 (5), 646–674. doi:10.1016/j.cell.2011.02.013

Haque, I., Kawsar, H., Motes, H., Sharma, M., Banerjee, S., Banerjee, S., et al. (2020). Downregulation of miR-506-3p facilitates EGFR-TKI resistance through induction of sonic hedgehog signaling in non-small-cell lung cancer cell lines. *Int. J. Mol. Sci.* 21 (23), E9307. doi:10.3390/ijms21239307

Hashida, S., Yamamoto, H., Shien, K., Miyoshi, Y., Ohtsuka, T., Suzawa, K., et al. (2015). Acquisition of cancer stem cell-like properties in non-small cell lung cancer with acquired resistance to afatinib. *Cancer Sci.* 106 (10), 1377–1384. doi:10.1111/cas.12749

He, H., Song, X., Yang, Z., Mao, Y., Zhang, K., Wang, Y., et al. (2020). Upregulation of KCNQ1OT1 promotes resistance to stereotactic body radiotherapy in lung adenocarcinoma by inducing ATG5/ATG12-mediated autophagy via miR-372-3p. *Cell Death Dis.* 11 (10), 883. doi:10.1038/s41419-020-03083-8

Herbst, R. S., Giaccone, G., de Marinis, F., Reinmuth, N., Vergnenegre, A., Barrios, C. H., et al. (2020). Atezolizumab for first-line treatment of PD-L1-selected patients with NSCLC. *N. Engl. J. Med.* 383 (14), 1328–1339. doi:10.1056/NEJMoa1917346

Herbst, R. S., Morgensztern, D., and Boshoff, C. (2018). The biology and management of non-small cell lung cancer. *Nature* 553 (7689), 446–454. doi:10.1038/nature25183

Hirsch, F. R., Scagliotti, G. V., Mulshine, J. L., Kwon, R., Curran, W. J., Wu, Y.-L., et al. (2017). Lung cancer: Current therapies and new targeted treatments. *Lancet* 389 (10066), 299–311. doi:10.1016/s0140-6736(16)30958-8

Hisakane, K., Seike, M., Sugano, T., Yoshikawa, A., Matsuda, K., Takano, N., et al. (2021). Exosome-derived miR-210 involved in resistance to osimertinib and epithelial-mesenchymal transition in EGFR mutant non-small cell lung cancer cells. *Thorac. Cancer* 12 (11), 1690–1698. doi:10.1111/1759-7714.13943

Hong, D. S., Kang, Y. K., Borad, M., Sachdev, J., Ejadi, S., Lim, H. Y., et al. (2020). Phase 1 study of MRX34, a liposomal miR-34a mimic, in patients with advanced solid tumours. *Br. J. Cancer* 122 (11), 1630–1637. doi:10.1038/s41416-020-0802-1

Horvath, L., Thienpont, B., Zhao, L., Wolf, D., and Pircher, A. (2020). Overcoming immunotherapy resistance in non-small cell lung cancer (NSCLC) - novel approaches and future outlook. *Mol. Cancer* 19 (1), 141. doi:10.1186/s12943-020-01260-z

Hsu, Y., Hung, J., Chang, W., Lin, Y., Pan, Y., Tsai, P., et al. (2017). Hypoxic lung cancer-secreted exosomal miR-23a increased angiogenesis and vascular permeability by targeting prolyl hydroxylase and tight junction protein ZO-1. *Oncogene* 36 (34), 4929–4942. doi:10.1038/onc.2017.105

Hu, C., Hui, K., and Jiang, X. (2020). Effects of microRNA regulation on antiangiogenic therapy resistance in non-small cell lung cancer. *Biomed. Pharmacother.* 131, 110557. doi:10.1016/j.biopha.2020.110557

Hu, J., Cheng, Y., Li, Y., Jin, Z., Pan, Y., Liu, G., et al. (2014). microRNA-128 plays a critical role in human non-small cell lung cancer tumourigenesis, angiogenesis and lymphangiogenesis by directly targeting vascular endothelial growth factor-C. *Eur. J. Cancer* 50 (13), 2336–2350. doi:10.1016/j.ejca.2014.06.005

Huang, J. Y., Cui, S. Y., Chen, Y. T., Song, H. Z., Huang, G. C., Feng, B., et al. (2013). MicroRNA-650 was a prognostic factor in human lung adenocarcinoma and confers the docetaxel chemoresistance of lung adenocarcinoma cells via regulating Bcl-2/Bax expression. *PLoS One* 8 (8), e72615. doi:10.1371/journal.pone.0072615

Huang, Y., Zhang, M., Li, Y., Luo, J., Wang, Y., Geng, W., et al. (2021). miR-183 promotes radioresistance of lung adenocarcinoma H1299 cells via epithelial-mesenchymal transition. *Braz J. Med. Biol. Res.* 54 (5), e9700. doi:10.1590/1414-431x20209700

Iqbal, M., Arora, S., Prakasam, G., Calin, G., and Syed, M. J. M. (2019). MicroRNA in lung cancer: Role, mechanisms, pathways and therapeutic relevance. *Mol. Asp. Med.* 70, 3–20. doi:10.1016/j.mam.2018.07.003

Janpipatkul, K., Trachu, N., Watcharenwong, P., Panvongsa, W., Worakitchanon, W., Metheetrairut, C., et al. (2021). Exosomal microRNAs as potential biomarkers for osimertinib resistance of non-small cell lung cancer patients. *Cancer Biomark.* 31 (3), 281–294. doi:10.3233/CBM-203075

Jeong, K., Yu, Y. J., You, J. Y., Rhee, W. J., and Kim, J. A. (2020). Exosome-mediated microRNA-497 delivery for anti-cancer therapy in a microfluidic 3D lung cancer model. *Lab. Chip* 20 (3), 548–557. doi:10.1039/c9lc00958b

Jiang, Q., Yuan, Y., Gong, Y., Luo, X., Su, X., Hu, X., et al. (2019). Therapeutic delivery of microRNA-143 by cationic lipoplexes for non-small cell lung cancer treatment *in vivo*. *J. Cancer Res. Clin. Oncol.* 145 (12), 2951–2967. doi:10.1007/s00432-019-03051-6

Jiang, W., Han, X., Wang, J., Wang, L., Xu, Z., Wei, Q., et al. (2019). miR-22 enhances the radiosensitivity of small-cell lung cancer by targeting the WRNIP1. *J. Cell. Biochem.* 120 (10), 17650–17661. doi:10.1002/jcb.29032

Jin, S., He, J., Li, J., Guo, R., Shu, Y., and Liu, P. J. T. C. (2018). MiR-873 inhibition enhances gefitinib resistance in non-small cell lung cancer cells by targeting glioma-associated oncogene homolog 1. *Thorac. Cancer* 9 (10), 1262–1270. doi:10.1111/1759-7714.12830

Jin, Y., Wang, H., Zhu, Y., Feng, H., Wang, G., and Wang, S. (2020). miR-199a-5p is involved in doxorubicin resistance of non-small cell lung cancer (NSCLC) cells. *Eur. J. Pharmacol.* 878, 173105. doi:10.1016/j.ejphar.2020.173105

Jing, Y., Liang, W., Liu, J., Zhang, L., Wei, J., Yang, J., et al. (2020). Autophagy-mediating microRNAs in cancer chemoresistance. *Cell Biol. Toxicol.* 36 (6), 517–536. doi:10.1007/s10565-020-09553-1

Johnson, C. D., Esquela-Kerscher, A., Stefani, G., Byrom, M., Kelnar, K., Ovcharenko, D., et al. (2007). The let-7 microRNA represses cell proliferation pathways in human cells. *Cancer Res.* 67 (16), 7713–7722. doi:10.1158/0008-5472.CAN-07-1083

Jonas, S., and Izaurralde, E. (2015). Towards a molecular understanding of microRNA-mediated gene silencing. *Nat. Rev. Genet.* 16 (7), 421–433. doi:10.1038/nrg3965

Kim, J. S., Chun, S. H., Park, S., Lee, S., Kim, S. E., Hong, J. H., et al. (2020). Identification of novel microRNA prognostic markers using cascaded wx, a neural network-based framework, in lung adenocarcinoma patients. *Cancers (Basel)* 12 (7), E1890. doi:10.3390/cancers12071890

Kim, V. N. (2005). MicroRNA biogenesis: Coordinated cropping and dicing. *Nat. Rev. Mol. Cell Biol.* 6 (5), 376–385. doi:10.1038/nrm1644

Kocher, F., Hilbe, W., Seeber, A., Pircher, A., Schmid, T., Greil, R., et al. (2015). Longitudinal analysis of 2293 NSCLC patients: A comprehensive study from the TYROL registry. *Lung Cancer* 87 (2), 193–200. doi:10.1016/j.lungcan.2014.12.006

Krol, J., Loedige, I., and Filipowicz, W. (2010). The widespread regulation of microRNA biogenesis, function and decay. *Nat. Rev. Genet.* 11 (9), 597–610. doi:10.1038/nrg2843

Kundu, S. T., Byers, L. A., Peng, D. H., Roybal, J. D., Diao, L., Wang, J., et al. (2016). The miR-200 family and the miR-183~96~182 cluster target Foxf2 to inhibit invasion and metastasis in lung cancers. *Oncogene* 35 (2), 173–186. doi:10.1038/onc.2015.71

Kurtulus, S., Madi, A., Escobar, G., Klapholz, M., Nyman, J., Christian, E., et al. (2019). Checkpoint blockade immunotherapy induces dynamic changes in PD-1(-) CD8(+) tumor-infiltrating T cells. *Immunity* 50 (1), 181–194. doi:10.1016/j.immuni.2018.11.014

Lampis, A., Hahne, J., Hedayat, S., and Valeri, N. J. (2020). MicroRNAs as mediators of drug resistance mechanisms. *Curr. Opin. Pharmacol.* 54, 44–50. doi:10.1016/j.coph.2020.08.004

Lee, R., Feinbaum, R., and Ambros, V. J. C. (1993). The *C. elegans* heterochronic gene lin-4 encodes small RNAs with antisense complementarity to lin-14. *Cell* 75 (5), 843–854. to lin-14. doi:10.1016/0092-8674(93)90529-y

Li, H., Zhang, P., Sun, X., Sun, Y., Shi, C., Liu, H., et al. (2015). MicroRNA-181a regulates epithelial-mesenchymal transition by targeting PTEN in drug-resistant lung adenocarcinoma cells. *Int. J. Oncol.* 47 (4), 1379–1392. doi:10.3892/ijo.2015.3144

Li, Q., Wang, Y., and He, J. (2021a). MiR-133a-3p attenuates resistance of non-small cell lung cancer cells to gefitinib by targeting SPAG5. *J. Clin. Lab. Anal.* 35 (7), e23853. doi:10.1002/jcla.23853

Li, W., Wang, W., Ding, M., Zheng, X., Ma, S., and Wang, X. (2016). MiR-1244 sensitizes the resistance of non-small cell lung cancer A549 cell to cisplatin. *Cancer Cell Int.* 16, 30. doi:10.1186/s12935-016-0305-6

Li, X., Chen, C., Wang, Z., Liu, J., Sun, W., Shen, K., et al. (2021b). Elevated exosome-derived miRNAs predict osimertinib resistance in non-small cell lung cancer. *Cancer Cell Int.* 21 (1), 428. doi:10.1186/s12935-021-02075-8

Li, X. F., Shen, W. Z., Jin, X., Ren, P., and Zhang, J. (2020). Let-7c regulated epithelial-mesenchymal transition leads to osimertinib resistance in NSCLC cells with EGFR T790M mutations. *Sci. Rep.* 10 (1), 11236. doi:10.1038/s41598-020-67908-4

Li, X., Li, C., Guo, C., Zhao, Q., Cao, J., Huang, H., et al. (2021c). PI3K/Akt/mTOR signaling orchestrates the phenotypic transition and chemo-resistance of small cell lung cancer. *J. Genet. Genomics* 48 (7), 640–651. doi:10.1016/j.jgg.2021.04.001

Li, Y., and Sarkar, F. H. (2016). MicroRNA targeted therapeutic approach for pancreatic cancer. *Int. J. Biol. Sci.* 12 (3), 326–337. doi:10.7150/ijbs.15017

Liang, A., Du, S., Zhang, B., Zhang, J., Ma, X., Wu, C., et al. (2019). Screening miRNAs associated with resistance gemcitabine from exosomes in A549 lung cancer cells. *Cancer Manag. Res.* 11, 6311–6321. doi:10.2147/cmar.S209149

Liang, G., Meng, W., Huang, X., Zhu, W., Yin, C., Wang, C., et al. (2020). miR-196b-5p-mediated downregulation of TSPAN12 and GATA6 promotes tumor progression in non-small cell lung cancer. *Proc. Natl. Acad. Sci. U. S. A.* 117 (8), 4347–4357. doi:10.1073/pnas.1917531117

Lin, C., Liao, W., Yang, T., Lu, H., Hsu, S., and Wu, C. (2021). MicroRNA-10b modulates cisplatin tolerance by targeting p53 directly in lung cancer cells. *Oncol. Rep.* 46 (2), 167. doi:10.3892/or.2021.8118

Lin, S., and Gregory, R. I. (2015). MicroRNA biogenesis pathways in cancer. *Nat. Rev. Cancer* 15 (6), 321–333. doi:10.1038/nrc3932

Liu, B., Li, F., Xie, Y., Fan, C., Liu, W., Qiu, J., et al. (2022). miR-196a upregulation contributes to gefitinib resistance through inhibiting GLTP expression. *Int. J. Mol. Sci.* 23 (3), 1785. doi:10.3390/ijms23031785

Liu, K., Zhang, W., Tan, J., Ma, J., and Zhao, J. (2019). MiR-200b-3p functions as an oncogene by targeting ABCA1 in lung adenocarcinoma. *Technol. Cancer Res. Treat.* 18, 1533033819892590. doi:10.1177/1533033819892590

Liu, M., Zhou, K., and Cao, Y. J. M. c. (2014). MCRS1 overexpression, which is specifically inhibited by miR-129*, promotes the epithelial-mesenchymal transition and metastasis in non-small cell lung cancer. *Mol. Cancer* 13, 245. doi:10.1186/1476-4598-13-245

Liu, X., Jiang, T., Li, X., Zhao, C., Li, J., Zhou, F., et al. (2020). Exosomes transmit T790M mutation-induced resistance in EGFR-mutant NSCLC by activating PI3K/AKT signalling pathway. *J. Cell. Mol. Med.* 24 (2), 1529–1540. doi:10.1111/jcmm.14838

Long, K., and Suresh, K. (2020). Pulmonary toxicity of systemic lung cancer therapy. *Respirology* 25 (2), 72–79. doi:10.1111/resp.13915

Lu, J., Getz, G., Miska, E., Alvarez-Saavedra, E., Lamb, J., Peck, D., et al. (2005). MicroRNA expression profiles classify human cancers. *Nature* 435 (7043), 834–838. doi:10.1038/nature03702

Lv, X., Li, C., Han, P., and Xu, X. (2018). MicroRNA-520a-3p inhibits cell growth and metastasis of non-small cell lung cancer through PI3K/AKT/mTOR signaling pathway. *Eur. Rev. Med. Pharmacol. Sci.* 22 (8), 2321–2327. doi:10.26355/eurrev_201804_14822

Ma, Y., Li, X., Cheng, S., Wei, W., and Li, Y. (2015). MicroRNA-106a confers cisplatin resistance in non-small cell lung cancer A549 cells by targeting adenosine triphosphatase-binding cassette A1. *Mol. Med. Rep.* 11 (1), 625–632. doi:10.3892/mmr.2014.2688

Ma, Y., Yuwen, D., Chen, J., Zheng, B., Gao, J., Fan, M., et al. (2019). Exosomal transfer of cisplatin-induced miR-425-3p confers cisplatin resistance in NSCLC through activating autophagy. *Int. J. Nanomedicine* 14, 8121–8132. doi:10.2147/ijn.S221383

Ma, Z., Wei, K., Yang, F., Guo, Z., Pan, C., He, Y., et al. (2021). Tumor-derived exosomal miR-3157-3p promotes angiogenesis, vascular permeability and metastasis by targeting TIMP/KLF2 in non-small cell lung cancer. *Cell Death Dis.* 12 (9), 840. doi:10.1038/s41419-021-04037-4

Mok, T., Wu, Y., Kudaba, I., Kowalski, D., Cho, B., Turna, H., et al. (2019). Pembrolizumab versus chemotherapy for previously untreated, PD-L1-expressing, locally advanced or metastatic non-small-cell lung cancer (KEYNOTE-042): A randomised, open-label, controlled, phase 3 trial. *Lancet* 393 (10183), 1819–1830. doi:10.1016/s0140-6736(18)32409-7

Ni, L., Xu, J., Zhao, F., Dai, X., Tao, J., Pan, J., et al. (2021). MiR-221-3p-mediated downregulation of MDM2 reverses the paclitaxel resistance of non-small cell lung cancer *in vitro* and *in vivo*. *Eur. J. Pharmacol.* 899, 174054. doi:10.1016/j.ejphar.2021.174054

Nowak-Sliwinska, P., Alitalo, K., Allen, E., Anisimov, A., Aplin, A. C., Auerbach, R., et al. (2018). Consensus guidelines for the use and interpretation of angiogenesis assays. *Angiogenesis* 21 (3), 425–532. doi:10.1007/s10456-018-9613-x

Orellana, E., Tenneti, S., Rangasamy, L., Lyle, L., Low, P., and Kasinski, A. (2017). FolamiRs: Ligand-targeted, vehicle-free delivery of microRNAs for the treatment of cancer. *Sci. Transl. Med.* 9 (401), eaam9327. doi:10.1126/scitranslmed.aam9327

Osada, H., and Takahashi, T. (2011). let-7 and miR-17-92: small-sized major players in lung cancer development. *Cancer Sci.* 102 (1), 9–17. doi:10.1111/j.1349-7006.2010.01707.x

Pecot, C., Rupaimoole, R., Yang, D., Akbani, R., Ivan, C., Lu, C., et al. (2013). Tumour angiogenesis regulation by the miR-200 family. *Nat. Commun.* 4, 2427. doi:10.1038/ncomms3427

Perepelyuk, M., Sacko, K., Thangavel, K., and Shoyele, S. (2018). Evaluation of MUC1-aptamer functionalized hybrid nanoparticles for targeted delivery of miRNA-29b to nonsmall cell lung cancer. *Mol. Pharm.* 15 (3), 985–993. doi:10.1021/acs.molpharmaceut.7b00900

Poggio, M., Hu, T., Pai, C., Chu, B., Belair, C., Chang, A., et al. (2019). Suppression of exosomal PD-L1 induces systemic anti-tumor immunity and memory. *Cell* 177 (2), 414–427. e413. doi:10.1016/j.cell.2019.02.016

Sachani, S. S., Landschoot, L. S., Zhang, L., White, C. R., MacDonald, W. A., Golding, M. C., et al. (2018). Nucleoporin 107, 62 and 153 mediate Kcnq1ot1 imprinted domain regulation in extraembryonic endoderm stem cells. *Nat. Commun.* 9 (1), 2795. doi:10.1038/s41467-018-05208-2

Sarkar, F. H., Li, Y., Wang, Z., Kong, D., and Ali, S. (2010). Implication of microRNAs in drug resistance for designing novel cancer therapy. *Drug resist. updat.* 13 (3), 57–66. doi:10.1016/j.drup.2010.02.001

Sequist, L., Waltman, B., Dias-Santagata, D., Digumarthy, S., Turke, A., Fidias, P., et al. (2011). Genotypic and histological evolution of lung cancers acquiring

resistance to EGFR inhibitors. *Sci. Transl. Med.* 3 (75), 75ra26. doi:10.1126/scitranslmed.3002003

Shahverdi, M., Hajiasgharzadeh, K., Sorkhabi, A. D., Jafarlou, M., Shojaee, M., Jalili Tabrizi, N., et al. (2022). The regulatory role of autophagy-related miRNAs in lung cancer drug resistance. *Biomed. Pharmacother.* 148, 112735. doi:10.1016/j.biopha.2022.112735

Shi, H., Bi, H., Sun, X., Dong, H., Jiang, Y., Mu, H., et al. (2018). Antitumor effects of Tubeimoside-1 in NCI-H1299 cells are mediated by microRNA-126-5p-induced inactivation of VEGF-A/VEGFR-2/ERK signaling pathway. *Mol. Med. Rep.* 17 (3), 4327–4336. doi:10.3892/mmr.2018.8459

Shi, Z. M., Wang, L., Shen, H., Jiang, C. F., Ge, X., Li, D. M., et al. (2017). Downregulation of miR-218 contributes to epithelial-mesenchymal transition and tumor metastasis in lung cancer by targeting Slug/ZEB2 signaling. *Oncogene* 36 (18), 2577–2588. doi:10.1038/onc.2016.414

Shivdasani, R. A. (2006). MicroRNAs: Regulators of gene expression and cell differentiation. *Blood* 108 (12), 3646–3653. doi:10.1182/blood-2006-01-030015

Siegel, R. L., Miller, K. D., Fuchs, H. E., and Jemal, A. (2021). Cancer statistics, 2021. *Ca. Cancer J. Clin.* 71 (1), 7–33. doi:10.3322/caac.21654

Siegel, R. L., Miller, K. D., and Jemal, A. (2019). Cancer statistics, 2019. *Ca. Cancer J. Clin.* 69 (1), 7–34. doi:10.3322/caac.21551

Sigismund, S., Avanzato, D., and Lanzetti, L. (2018). Emerging functions of the EGFR in cancer. *Mol. Oncol.* 12 (1), 3–20. doi:10.1002/1878-0261.12155

Stahlhut, C., and Slack, F. J. (2015). Combinatorial action of MicroRNAs let-7 and miR-34 effectively synergizes with erlotinib to suppress non-small cell lung cancer cell proliferation. *Cell Cycle* 14 (13), 2171–2180. doi:10.1080/15384101.2014.1003008

Su, J., Zhou, L., Xia, M. H., Xu, Y., Xiang, X. Y., and Sun, L. K. (2014). Bcl-2 family proteins are involved in the signal crosstalk between endoplasmic reticulum stress and mitochondrial dysfunction in tumor chemotherapy resistance. *Biomed. Res. Int.* 2014, 234370. doi:10.1155/2014/234370

Sun, C., Zeng, X., Guo, H., Wang, T., Wei, L., Zhang, Y., et al. (2020). MicroRNA-125a-5p modulates radioresistance in LTEP-a2 non-small cell lung cancer cells by targeting SIRT7. *Cancer Biomark.* 27 (1), 39–49. doi:10.3233/cbm-190381

Sun, H., Zhou, X., Bao, Y., Xiong, G., Cui, Y., and Zhou, H. (2019). Involvement of miR-4262 in paclitaxel resistance through the regulation of PTEN in non-small cell lung cancer. *Open Biol.* 9 (7), 180227. doi:10.1098/rsob.180227

Tang, D., Zhao, D., Wu, Y., Yao, R., Zhou, L., Lu, L., et al. (2018). The miR-3127-5p/p-STAT3 axis up-regulates PD-L1 inducing chemoresistance in non-small-cell lung cancer. *J. Cell. Mol. Med.* 22 (8), 3847–3856. doi:10.1111/jcmm.13657

Tao, L., Shu-Ling, W., Jing-Bo, H., Ying, Z., Rong, H., Xiang-Qun, L., et al. (2020). MiR-451a attenuates doxorubicin resistance in lung cancer via suppressing epithelialmesenchymal transition (EMT) through targeting c-Myc. *Biomed. Pharmacother.* 125, 109962. doi:10.1016/j.biopha.2020.109962

Teng, J., Yang, Z., Zhu, Y., Ni, D., Zhu, Z., Li, X., et al. (2018). Gemcitabine and cisplatin for treatment of lung cancer *in vitro* and vivo. *Eur. Rev. Med. Pharmacol. Sci.* 22 (12), 3819–3825. doi:10.26355/eurrev_201806_15266

Tian, J., Hu, L., Li, X., Geng, J., Dai, M., Bai, X., et al. (2016). MicroRNA-130b promotes lung cancer progression via PPARγ/VEGF-A/BCL-2-mediated suppression of apoptosis. *J. Exp. Clin. Cancer Res.* 35 (1), 105. doi:10.1186/s13046-016-0382-3

Tripathi, S. K., Pandey, K., Rengasamy, K. R. R., and Biswal, B. K. (2020). Recent updates on the resistance mechanisms to epidermal growth factor receptor tyrosine kinase inhibitors and resistance reversion strategies in lung cancer. *Med. Res. Rev.* 40 (6), 2132–2176. doi:10.1002/med.21700

Van Zandwijk, N., Pavlakis, N., Kao, S. C., Linton, A., Boyer, M. J., Clarke, S., et al. (2017). Safety and activity of microRNA-loaded minicells in patients with recurrent malignant pleural mesothelioma: A first-in-man, phase 1, open-label, dose-escalation study. *Lancet. Oncol.* 18 (10), 1386–1396. doi:10.1016/s1470-2045(17)30621-6

Vu, T., Yang, S., and Datta, P. K. (2020). MiR-216b/Smad3/BCL-2 Axis is involved in smoking-mediated drug resistance in non-small cell lung cancer. *Cancers (Basel)* 12 (7), E1879. doi:10.3390/cancers12071879

Walter, A. O., Sjin, R. T., Haringsma, H. J., Ohashi, K., Sun, J., Lee, K., et al. (2013). Discovery of a mutant-selective covalent inhibitor of EGFR that overcomes T790M-mediated resistance in NSCLC. *Cancer Discov.* 3 (12), 1404–1415. doi:10.1158/2159-8290.CD-13-0314

Wang, H., Huang, H., Wang, L., Liu, Y., Wang, M., Zhao, S., et al. (2021). Cancer-associated fibroblasts secreted miR-103a-3p suppresses apoptosis and promotes cisplatin resistance in non-small cell lung cancer. *Aging* 13 (10), 14456–14468. doi:10.18632/aging.103556

Wang, H. Y., Liu, Y. N., Wu, S. G., Hsu, C. L., Chang, T. H., Tsai, M. F., et al. (2020). MiR-200c-3p suppression is associated with development of acquired resistance to epidermal growth factor receptor (EGFR) tyrosine kinase inhibitors in EGFR mutant non-small cell lung cancer via a mediating epithelial-to-mesenchymal transition (EMT) process. *Cancer Biomark.* 28 (3), 351–363. doi:10.3233/CBM-191119

Wang, J., Mo, J., Xie, Y., and Wang, C. J. T. (2022). Ultrasound microbubbles-mediated miR-216b affects MALAT1-miRNA axis in non-small cell lung cancer cells. *Tissue Cell* 74, 101703. doi:10.1016/j.tice.2021.101703

Wang, N., and Zhang, T. (2018). Downregulation of MicroRNA-135 promotes sensitivity of non-small cell lung cancer to gefitinib by targeting TRIM16. *Oncol. Res.* 26 (7), 1005–1014. doi:10.3727/096504017x15144755633680

Wang, W., Chen, J., Dai, J., Zhang, B., Wang, F., and Sun, Y. (2016). [ARTICLE WITHDRAWN] MicroRNA-16-1 inhibits tumor cell proliferation and induces apoptosis in A549 non-small cell lung carcinoma cells. *Oncol. Res.* 24 (5), 345–351. doi:10.3727/096504016X14685034103194

Wang, Y., Wang, L., Chen, C., and Chu, X. (2018). New insights into the regulatory role of microRNA in tumor angiogenesis and clinical implications. *Mol. Cancer* 17 (1), 22. doi:10.1186/s12943-018-0766-4

Wei, L., Wang, X., Lv, L., Liu, J., Xing, H., Song, Y., et al. (2019a). The emerging role of microRNAs and long noncoding RNAs in drug resistance of hepatocellular carcinoma. *Mol. Cancer* 18 (1), 147. doi:10.1186/s12943-019-1086-z

Wei, W., Dong, Z., Gao, H., Zhang, Y. Y., Shao, L. H., Jin, L. L., et al. (2019b). MicroRNA-9 enhanced radiosensitivity and its mechanism of DNA methylation in non-small cell lung cancer. *Gene* 710, 178–185. doi:10.1016/j.gene.2019.05.050

Winter, J., Jung, S., Keller, S., Gregory, R., and Diederichs, S. (2009). Many roads to maturity: microRNA biogenesis pathways and their regulation. *Nat. Cell Biol.* 11 (3), 228–234. doi:10.1038/ncb0309-228

Wu, D. W., Wang, Y. C., Wang, L., Chen, C. Y., and Lee, H. (2018). A low microRNA-630 expression confers resistance to tyrosine kinase inhibitors in EGFR-mutated lung adenocarcinomas via miR-630/YAP1/ERK feedback loop. *Theranostics* 8 (5), 1256–1269. doi:10.7150/thno.22048

Xie, Q., Yu, Z., Lu, Y., Fan, J., Ni, Y., and Ma, L. J. (2019). microRNA-148a-3p inhibited the proliferation and epithelial-mesenchymal transition progression of non-small-cell lung cancer via modulating Ras/MAPK/Erk signaling. *J. Cell. Physiol.* 234 (8), 12786–12799. doi:10.1002/jcp.27899

Xing, S., Qu, Y., Li, C., Huang, A., Tong, S., Wu, C., et al. (2019). Deregulation of lncRNA-AC078883.3 and microRNA-19a is involved in the development of chemoresistance to cisplatin via modulating signaling pathway of PTEN/AKT. *J. Cell. Physiol.* 234 (12), 22657–22665. doi:10.1002/jcp.28832

Xing, Y., Liu, Y., Liu, T., Meng, Q., Lu, H., Liu, W., et al. (2018). TNFAIP8 promotes the proliferation and cisplatin chemoresistance of non-small cell lung cancer through MDM2/p53 pathway. *Cell Commun. Signal.* 16 (1), 43. doi:10.1186/s12964-018-0254-x

Xue, T., Yin, G., Yang, W., Chen, X., Liu, C., Yang, W., et al. (2021). MiR-129-5p promotes radio-sensitivity of NSCLC cells by targeting SOX4 and RUNX1. *Curr. Cancer Drug Targets* 21 (8), 702–712. doi:10.2174/1568009621666210415094350

Yang, F., Xiong, H., Duan, L., Li, Q., Li, X., Zhou, Y., et al. (2019). MiR-1246 promotes metastasis and invasion of A549 cells by targeting GSK-3β–mediated wnt/β-catenin pathway. *Cancer Res. Treat.* 51 (4), 1420–1429. doi:10.4143/crt.2018.638

Yin, J., Zhao, J., Hu, W., Yang, G., Yu, H., Wang, R., et al. (2017). Disturbance of the let-7/LIN28 double-negative feedback loop is associated with radio- and chemo-resistance in non-small cell lung cancer. *PLoS One* 12 (2), e0172787. doi:10.1371/journal.pone.0172787

Yu, S., Qin, X., Chen, T., Zhou, L., Xu, X., and Feng, J. (2017). MicroRNA-106b-5p regulates cisplatin chemosensitivity by targeting polycystic kidney disease-2 in non-small-cell lung cancer. *Anticancer. Drugs* 28 (8), 852–860. doi:10.1097/CAD.0000000000000524

Yuan, Y., Liao, H., Pu, Q., Ke, X., Hu, X., Ma, Y., et al. (2020). miR-410 induces both epithelial-mesenchymal transition and radioresistance through activation of the PI3K/mTOR pathway in non-small cell lung cancer. *Signal Transduct. Target. Ther.* 5 (1), 85. doi:10.1038/s41392-020-0182-2

Zang, H., Peng, J., Wang, W., and Fan, S. (2017). Roles of microRNAs in the resistance to platinum based chemotherapy in the non-small cell lung cancer. *J. Cancer* 8 (18), 3856–3861. doi:10.7150/jca.21267

Zeng, T., Xu, M., Zhang, W., Gu, X., Zhao, F., Liu, X., et al. (2021). Autophagy inhibition and microRNA-199a-5p upregulation in paclitaxel-resistant A549/T lung cancer cells. *Oncol. Rep.* 46 (1), 149. doi:10.3892/or.2021.8100

Zeng, X., Liu, D., Peng, G., Liu, J., and Yang, H. J. C. (2022). MiroRNA-31-3p promotes the invasion and metastasis of non-small-cell lung cancer cells by targeting forkhead box 1 (FOXO1). *Comput. Math. Methods Med.* 2022, 4597087. doi:10.1155/2022/4597087

Zeng, Z., Li, Y., Pan, Y., Lan, X., Song, F., Sun, J., et al. (2018). Cancer-derived exosomal miR-25-3p promotes pre-metastatic niche formation by inducing vascular permeability and angiogenesis. *Nat. Commun.* 9 (1), 5395. doi:10.1038/s41467-018-07810-w

Zhang, H., Chen, F., He, Y., Yi, L., Ge, C., Shi, X., et al. (2017). Sensitivity of non-small cell lung cancer to erlotinib is regulated by the Notch/miR-223/FBXW7 pathway. *Biosci. Rep.* 37 (3), BSR20160478. doi:10.1042/bsr20160478

Zhang, T., and Wang, N. (2018). miR-135a confers resistance to gefitinib in non-small cell lung cancer cells by upregulation of RAC1. *Oncol. Res.* 26 (8), 1191–1200. doi:10.3727/096504018X15166204902353

Zhang, W. C., Wells, J. M., Chow, K. H., Huang, H., Yuan, M., Saxena, T., et al. (2019). miR-147b-mediated TCA cycle dysfunction and pseudohypoxia initiate drug tolerance to EGFR inhibitors in lung adenocarcinoma. *Nat. Metab.* 1 (4), 460–474. doi:10.1038/s42255-019-0052-9

Zhang, W., Qiao, B., and Fan, J. (2018). Overexpression of miR-4443 promotes the resistance of non-small cell lung cancer cells to epirubicin by targeting INPP4A and regulating the activation of JAK2/STAT3 pathway. *Pharmazie* 73 (7), 386–392. doi:10.1691/ph.2018.8313

Zhang, Y., and Wang, J. (2017). MicroRNAs are important regulators of drug resistance in colorectal cancer. *Biol. Chem.* 398 (8), 929–938. doi:10.1515/hsz-2016-0308

Zhang, X., Wang, L., Liu, Y., Huang, W., and Cheng, D. (2018). MiR-760 enhances TRAIL sensitivity in non-small cell lung cancer via targeting the protein FOXA1. *Biomed. Pharmacother.* 99, 523–529. doi:10.1016/j.biopha.2018.01.076

Zhao, J., Guerrero, A., Kelnar, K., Peltier, H. J., and Bader, A. G. (2017). Synergy between next generation EGFR tyrosine kinase inhibitors and miR-34a in the inhibition of non-small cell lung cancer. *Lung Cancer* 108, 96–102. doi:10.1016/j.lungcan.2017.02.020

Zhao, Y., Zhang, W., Yang, Y., Dai, E., and Bai, Y. (2021). Diagnostic and prognostic value of microRNA-2355-3p and contribution to the progression in lung adenocarcinoma. *Bioengineered* 12 (1), 4747–4756. doi:10.1080/21655979.2021.1952367

Zhao, Z., Zhang, L., Yao, Q., and Tao, Z. (2015). miR-15b regulates cisplatin resistance and metastasis by targeting PEBP4 in human lung adenocarcinoma cells. *Cancer Gene Ther.* 22 (3), 108–114. doi:10.1038/cgt.2014.73

Zheng, Q., Ding, H., Wang, L., Yan, Y., Wan, Y., Yi, Y., et al. (2021). Circulating exosomal miR-96 as a novel biomarker for radioresistant non-small-cell lung cancer. *J. Oncol.* 2021, 5893981. doi:10.1155/2021/5893981

Zheng, Y., Guo, Z., and Li, Y. J. B. (2022). Long non-coding RNA prostate cancer-associated transcript 6 inhibited gefitinib sensitivity of non-small cell lung cancer by serving as a competing endogenous RNA of miR-326 to up-regulate interferon-alpha receptor 2. *Bioengineered* 13 (2), 3785–3796. doi:10.1080/21655979.2022.2031416

Zhou, X., Liu, H., Pang, Y., Wang, M., and Liu, S. J. T. (2022). UTMD-mediated delivery of miR-21-5p inhibitor suppresses the development of lung cancer. *Tissue Cell* 74, 101719. doi:10.1016/j.tice.2021.101719

Zhu, P., Liu, Z., Huang, H., Zhong, C., and Zhou, Y. (2020). MiRNA505/NET1 Axis Acts as a CD8(+) T-TIL regulator in non-small cell lung cancer. *Onco. Targets. Ther.* 13, 9785–9795. doi:10.2147/OTT.S265859

frontiers | Frontiers in Pharmacology

TYPE Original Research
PUBLISHED 09 November 2022
DOI 10.3389/fphar.2022.984555

Check for updates

OPEN ACCESS

EDITED BY
Zhe-Sheng Chen,
St. John's University, United States

REVIEWED BY
Jiang Chen,
Zhejiang University, China
Alexander T. Sougiannis,
Medical University of South Carolina, United States

*CORRESPONDENCE
Jingdong Zhang,
jdzhang@cancerhosp-ln-cmu.com

SPECIALTY SECTION
This article was submitted to Pharmacology of Anti-Cancer Drugs, a section of the journal Frontiers in Pharmacology

RECEIVED 02 July 2022
ACCEPTED 20 October 2022
PUBLISHED 09 November 2022

CITATION
Ma Y, Zhan L, Yang J and Zhang J (2022), SLC11A1 associated with tumor microenvironment is a potential biomarker of prognosis and immunotherapy efficacy for colorectal cancer.
Front. Pharmacol. 13:984555.
doi: 10.3389/fphar.2022.984555

COPYRIGHT
© 2022 Ma, Zhan, Yang and Zhang. This is an open-access article distributed under the terms of the Creative Commons Attribution License (CC BY). The use, distribution or reproduction in other forums is permitted, provided the original author(s) and the copyright owner(s) are credited and that the original publication in this journal is cited, in accordance with accepted academic practice. No use, distribution or reproduction is permitted which does not comply with these terms.

SLC11A1 associated with tumor microenvironment is a potential biomarker of prognosis and immunotherapy efficacy for colorectal cancer

Yiming Ma[1], Lei Zhan[1], Jun Yang[2] and Jingdong Zhang[1]*

[1]Medical Oncology Department of Gastrointestinal Tumors, Cancer Hospital of China Medical University, Liaoning Cancer Hospital and Institute, Shenyang, China, [2]Medical Oncology Department of Breast Tumors, Cancer Hospital of China Medical University, Liaoning Cancer Hospital and Institute, Shenyang, China

Colorectal cancer (CRC) is one of the most lethal cancers of the digestive system. The tumor microenvironment (TME) plays a central role in the initiation and development of CRC. However, little is known about the modulation mechanism of the TME in CRC. In our study, we attempted to identify a biomarker related to the TME modulation that could serve as a potential prognostic biomarker for CRC. We identified differentially expressed genes between the ImmuneScore high/low and StromalScore high/low groups. Using univariate COX regression analysis and hub gene analysis (cytoHubba), SLC11A1 was identified as the only candidate gene for subsequent analysis. CIBERSORT, EPIC, MCPcounter, and immunogenic cell death were performed to evaluate the effect of SLC11A1 on the TME. We also collected samples and performed Real-time quantitative PCR to verify the expression levels of SLC11A1 in CRC and adjacent normal tissues. The IMvigor210 cohort, TIDE score, and immunophenoscore (IPS) were used to analyze the association between SLC11A1 and immunotherapy efficacy. SLC11A1 was highly expressed in CRC tissues compared with its expression in normal colorectal tissues and was associated with poor prognosis and advanced clinicopathological stages. Gene set enrichment analysis showed that TGF-β pathways, JAK-STAT pathways, and angiogenesis were significantly enriched in the high-SLC11A1 group. Single-cell analysis validated the correlation between SLC11A1 and the TME. Using CIBERSORT, EPIC, and MCPcounter algorithms, we found that there was more macrophage and fibroblast infiltration in the SLC11A1 high-expression group. Meanwhile, high-SLC11A1 patients had lower IPS scores, higher TIDE scores, and fewer immunotherapy benefits than those of low-SLC11A1 patients. In conclusion, SLC11A1 plays a crucial role in the TME and could serve as a potential biomarker for poor prognosis and immunotherapy efficacy in CRC.

KEYWORDS

tumor microenvironment, CRC, immunotherapy, prognosis, SLC11A1

Introduction

Colorectal cancer (CRC) is one of the most common gastrointestinal cancers worldwide, with high mortality rates (Siegel et al., 2018; Solano-Iturri et al., 2020; Sung et al., 2021). Currently, the incidence of CRC is increasing, and it is predicted that more than two million new cases will occur by the year 2030 (Arnold et al., 2017). Several factors related to carcinogenesis have been identified, including smoking, obesity, alcohol intake, and physical activity (Jayasekara et al., 2018). However, the precise molecular mechanisms underlying CRC development remain unclear. Colorectal adenocarcinoma is the most common type of CRC (Luo et al., 2019). CRC formation takes place through a multi-stage process, from normal mucosa to adenoma, and finally to cancer tissue (Strum, 2016; Hauptman et al., 2018). Due to the lack of early indications and specific biomarkers, most CRC patients are diagnosed at advanced stages, which leads to poor prognosis. Although treatment methods for CRC have recently improved, the mortality rate remains high. Immune checkpoint inhibitors (ICIs) are novel antitumor drugs that have shown promising therapeutic efficacy in some types of cancers, such as melanoma, non-small-cell lung cancer, and urinary system cancers (Hamid et al., 2013; Sharma and Allison, 2015). However, the clinical benefits of immunotherapy vary widely among patients and conventional ICIs do not offer optimal clinical efficacy for most patients with advanced CRC (Morse et al., 2020). Potential indicators for predicting immunotherapy response, such as expression levels of immune checkpoints, tumor mutation burden (TMB), and neoantigens, are limited by tumor heterogeneity (Liu et al., 2022). Therefore, it is essential to develop a novel biomarker to predict the prognosis and immunotherapy benefits for patients with CRC.

The tumor microenvironment (TME), which is composed of tumor cells, immune cells, blood vessels, extracellular matrix, and fibroblasts, is considered to play a central role in tumorigenesis and tumor progression (Zhang et al., 2018; Schürch et al., 2020). TME may promote cancer progression by affecting immune surveillance and diminish the ability of chemotherapy to target tumor cells (Laplane et al., 2019). Recent research has shown that the initiation of CRC depends on the interaction between tumor cells and the TME (Ziegler et al., 2018). However, the interaction between CRC and the TME remains unknown. Therefore, it would be in the best interest of the medical field to further investigate the TME of CRC and identify factors related to TME modulation.

SLC11A1, also known as natural resistance-associated macrophage protein-1, is a member of the solute-carrier family. SLC11A1 was initially reported to fight several types of pathogens, and some studies have shown that SLC11A1 plays a role in innate immunity, autoimmune diseases, and infection (Stewart et al., 2010; Li et al., 2011; Neves et al., 2011; Cunrath and Bumann, 2019). In tuberculosis patients, the low expression and variation of SLC11A1 may impair immunologic response to tuberculosis (Shahzad et al., 2022). However, the roles of SLC11A1 in CRC have not been reported.

In the present study, we applied the ESTIMATE (Estimation of STromal and Immune cells in MAlignant Tumor tissues using Expression data) algorithm, hub gene analysis, and univariate COX regression and identified a TME-related factor in CRC, solute carrier family 11 member 1 (SLC11A1). The prognostic value of SLC11A1 has been evaluated in CRC and other digestive tract cancers. CIBERSORT, EPIC, MCPcounter, gene set enrichment analysis (GSEA), and single-cell analysis were used to further assess the potential effects of SLC11A1 in the TME and immunotherapy. Our findings provide a potential prognostic biomarker and may help in the individual selection of immunotherapy for patients with CRC.

Materials and methods

Raw data collection

The transcriptome profiles and corresponding clinical data on primary colon adenocarcinoma (COAD) and rectal adenocarcinoma (READ) were collected from TCGA database using TCGAbiolinks (Colaprico et al., 2016) (Supplementary Table S1). This study enrolled 612 patients with complete prognostic information. We also collected TCGA pan-cancer RNA-seq data in the TPM format processed by Toil from UCSC Xena (Vivian et al., 2017) (https://xenabrowser.net/datapages). Microarray data from GSE17536, including 177 patients, were downloaded from the GEO database (Smith et al., 2010). Moreover, we also downloaded data from the immunotherapy-related dataset (IMvigor210) using IMvigor210CoreBiologies (Mariathasan et al., 2018). In the IMvigor210 cohort, 298 advanced urothelial cancer patients with complete clinical data were included in our study.

Identification of differentially expressed genes related with tumor microenvironment

A previous study has shown the application of ESTIMATE algorithm to microarray and RNA-sequencing data might help to clarify the role of the TME and provide novel insights into genomic alterations (Yoshihara et al., 2013). ESTIMATE algorithm is an efficacy method to screen TME-related genes (Cheng et al., 2021; Guo et al., 2021; Wu et al., 2021). In our study, ImmuneScore, StromalScore, and ESTIMATEScore were calculated using the ESTIMATE R package, based on the transcriptome data of TCGA-CRC patients. These scores were assessed in patients at different pathological stages: T stage, N stage, and M stage.

We used the DEseq2 R package to analyze differentially expressed genes (DEGs) between patients with high and low ImmuneScores to identify genes associated with immune cells (Love et al., 2014). Moreover, we used the DEseq2 R package to analyze DEGs between patients with high and low StromalScores to identify genes associated with stromal cells. The DEGs were defined as genes with $|Log2FC| > 1.5$ and adjusted $p < 0.01$. The overlapping DEGs in the StromalScore and ImmuneScore groups were considered TME-related genes. Kyoto Encyclopedia of Genes and Genomes (KEGG) and Gene Ontology (GO) enrichment analyses were performed using the DEGs associated with TME using the R package clusterProfiler (Yu et al., 2012). The enrichment terms were considered significant with a p-value < 0.05.

CytoHubba and univariate COX regression analyses

We used the STRING database to construct a protein–protein interaction (PPI) network (confidence score > 0.9) based on the common DEGs in both the StromalScore and ImmuneScore groups (Szklarczyk et al., 2019). To identify hub genes, we used the cytoHubba plugin and acquired the top 30 hub genes using the multi-network clustering (MNC) algorithm (Chin et al., 2014). Univariate COX regression analysis was performed to screen for DEGs associated with overall survival (OS) time. Genes with $p < 0.05$ were shown in the plot.

Gene set enrichment analysis

The expression differences between low-SLC11A1 and high-SLC11A1 groups were identified using DESeq2. To identify key pathways and biological processes associated with SLC11A1, GSEA was performed using KEGG and Hallmark gene sets as target sets.

Tumor microenvironment-related analyses of SLC11A1

The Immuno-Oncology-Biological-Research (IOBR) R package integrates common algorithms for estimating the TME cells (Zeng et al., 2021). The TME of CRC samples was estimated using three different algorithms, including the CIBERSORT, EPIC, and MCPcounter algorithms, using the IOBR R package. We extracted immunogenic cell death (ICD)-related genes from a previous study and found differences in the expression of ICD-related genes between low-SLC11A1 and high-SLC11A1 groups (Garg et al., 2016). To further investigate SLC11A1 expression in the TME of CRC, we used the Tumor Immune Single Cell Hub database, which contains single-cell transcriptome profiles of 27 types of cancer (Sun et al., 2021). The cell location of SLC11A1 was determined using single-cell data in GSE146771.

Evaluation of SLC11A1 expression and immunotherapy response

A previous study on LUAD has shown that TIDE and IPS scores are valid scoring schemes to predict immunotherapy response. TIDE is one of the most effective methods for assessing the immune escape of tumors by analyzing their expression profiles (Jiang et al., 2018). Higher TIDE scores indicate that tumor cells are more likely to escape from immune surveillance, which means lower immunotherapy efficacy. Therefore, we calculated the TIDE scores based on RNA-seq of TCGA-CRC to analyze the relationship between SLC11A1 expression and immunotherapy response. The immunophenoscore (IPS) is also defined as a crucial factor in predicting the efficacy of ICIs (Charoentong et al., 2017). Patients with a higher IPS indicated a higher efficacy of ICIs. The IPS data of TCGA-CRC patients were downloaded from the TCIA database (https://tcia.at/home) to identify the relationship between IPS and SLC11A1 expression.

Real-time quantitative PCR

We collected 15 paired CRC tissues and adjacent normal colorectal tissues from the Liaoning Cancer Hospital. Total RNA was extracted from the tissue specimens using TRIzol reagent. Total RNA was treated with kits from Takara (Shiga, Japan) to remove genomic DNA and to conduct reverse transcription. Real-time quantitative PCR (RT-qPCR) was performed using TB GREEN Premix Ex Taq (Takara). The primer sequences were: *GAPDH*-F, 5′ GGAAGCTTGTCATCAATGGAAATC 3′; *GAPDH*-R 5′ TGATGACCCTTTTGGCTCCC 3′; *SLC11A1*-F 5′ GTCCGTCTCCTTTATCATCAACCT 3′; *SLC11A1*-R 5′ GAAGCCCTCCATCACGAACTG 3′.

Statistical analyses

All statistical analyses were conducted using R software (version 4.1.0). Kaplan–Meier (KM) curves were constructed to evaluate the relationship between OS rates and SLC11A1 expression. The survminer R package was used to identify the optimum cutoff point of SLC11A1 expression to classify CRC patients into low-SLC11A1 and high-SLC11A1 groups. The Wilcoxon test was used to compare differences between the two groups. The Kruskal–Wallis test was used to compare the differences between multiple groups. Univariate COX regression was performed to screen the prognostic factors

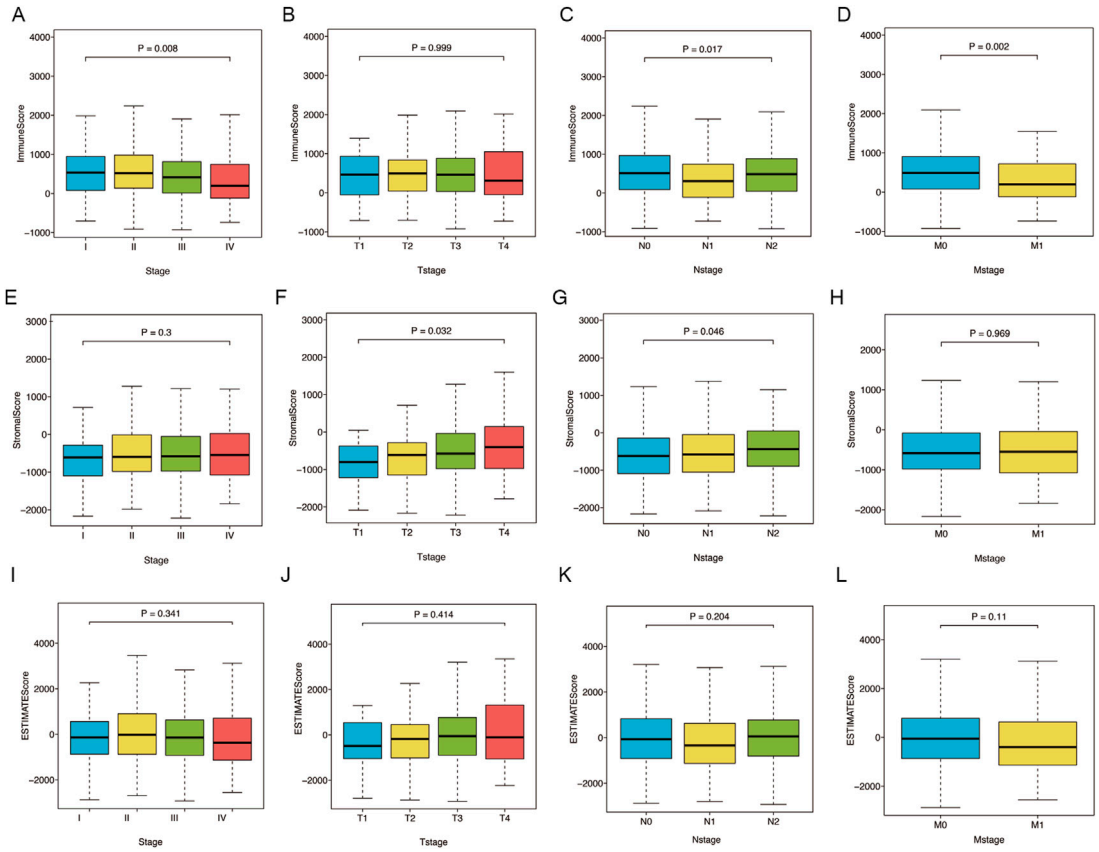

FIGURE 1
Relations of ImmuneScore, StromalScore, and ESTIMATEScore with clinicopathological stages. **(A–D)** Relations of ImmuneScore with pathological stage (p = 0.008), T stage (p = 0.999), N stage (p = 0.017) and M stage (p = 0.002). **(E–H)** Relations of StromalScore with pathological stage (p = 0.3), T stage (p = 0.032), N stage (p = 0.046) and M stage (p = 0.969). **(I–L)** Relations of ESTIMATEScore with pathological stage (p = 0.341), T stage (p = 0.414), N stage (p = 0.204) and M stage (p = 0.11). Statistical difference of four groups was compared by the Kruskal–Wallis test.

of CRC using the survival R package. Statistical significance was set to p-value < 0.05.

Results

Relationship of ImmuneScore, StromalScore, and ESTIMATEScore with clinicopathological features

First, we analyzed the ImmuneScore, StromalScore, and ESTIMATEScore of TCGA-CRC patients with different clinicopathological characteristics (Figure 1). The ImmuneScore was significantly associated with pathological stage (p = 0.008), N stage (p = 0.017), and M stage (p = 0.002) (Figures 1A,C,D). Additionally, the StromalScore increased significantly in patients with advanced T stage (p = 0.032) and N stage (p = 0.046) (Figures 1F,G). However, ESTIMATEScore was not significantly associated with pathological stage, T stage, N stage, or M stage (Figures 1I–L). These results indicate that the immune and stromal components of CRC tissues may affect tumor proliferation and metastasis.

Identification of genes related with tumor microenvironment

A comparison between the high/low ImmuneScore and StromalScore groups was performed to identify genes related to the TME. In total, there were 586 DEGs between the high/low-ImmuneScore groups and 676 DEGs between the high- and low-StromalScore groups (Figures 2A,B). In total, there were 241 DEGs in both the ImmuneScore and StromalScore groups (Figure 2C), and 241 DEGs were considered TME-related genes. In addition, we analyzed the related functions and pathways of the genes using GO and KEGG enrichment analyses. The genes were mainly enriched in immune-related GO terms, such as chemokine activity, complement C3b binding, immunoglobulin

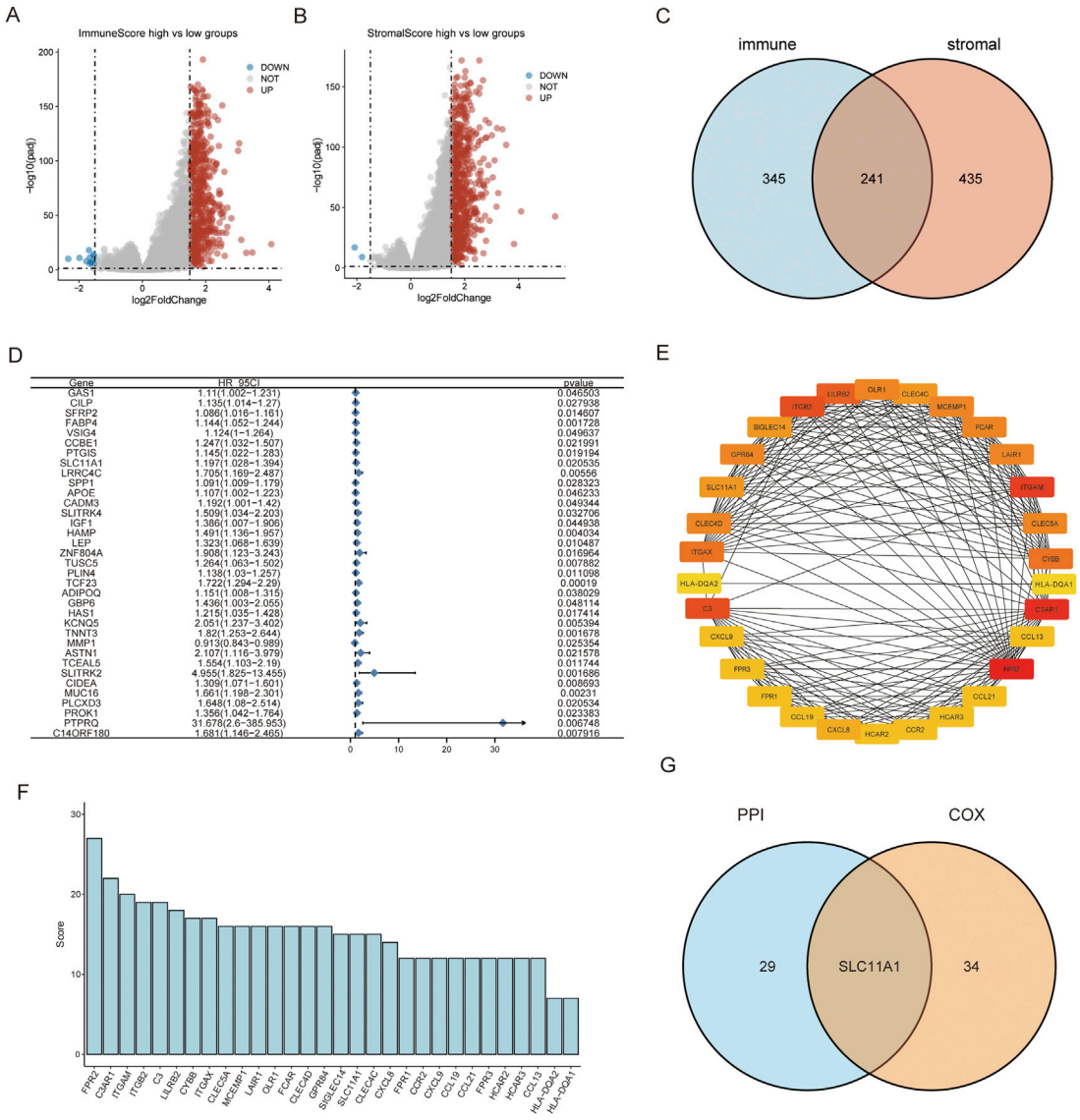

FIGURE 2
SLC11A1 was identified as the hub gene for TME. **(A,B)** Volcano plots for DEGs identified by comparison of high-ImmuneScore vs. low-ImmuneScore groups and high-StromalScore vs. low-StromalScore groups. **(C)** Venn plot showed 241 common factors with the DEGs from ImmuneScore and StromalScore analyses. **(D)** Thirty-five factors with p-value < 0.05 by univariate Cox analysis. **(E)** Thirty genes with the screened with MNC algorithm. **(F)** The bar chart showed MNC scores of the 30 genes. **(G)** SLC11A1 was identified in the intersection of the two modules.

binding, immune receptor activity, regulation of T cell adhesion, and leukocyte cell-cell adhesion (Supplementary Figure 1A). KEGG enrichment analysis indicated that the enriched genes were related to immune pathways, such as neutrophil extracellular trap formation, cytokine-cytokine receptor interaction, chemokines, IL-17, and antigen processing and presentation pathways Supplementary Figure 1B). The results of the enrichment analysis illustrated that these genes seemed to be associated with immune-related functions and might play predominant roles in the TME (Supplementary Tables S2, S3).

We conducted a univariate COX regression analysis to identify the prognostic factors of CRC among the 241 TME-related genes. Then, 35 significant genes were acquired and are shown in the forest plot ($p < 0.05$) (Figure 2D). We identified the top 30 hub genes amongst these using the MNC algorithm and identified the hub genes ranked by the MNC score (Figures 2E,F). We performed an intersection analysis between the top 30 hub genes in the PPI network and 35 significant genes associated with prognosis using univariate COX regression. SLC11A1 was the only gene that overlapped between the two groups (Figure 2G).

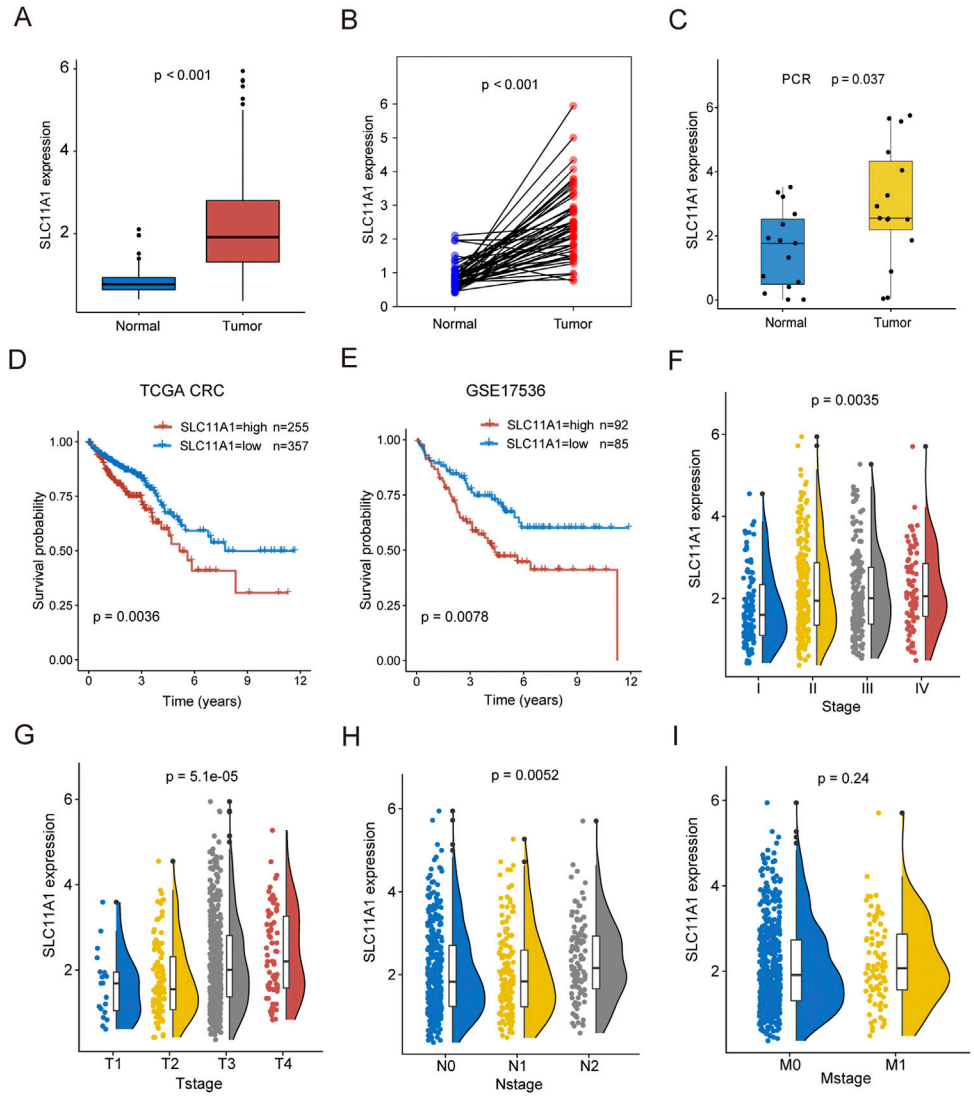

FIGURE 3
High expression of SLC11A1 indicated poor prognosis of CRC patients. **(A)** Expression differences of SLC11A1 between CRC and adjacent normal samples. **(B)** Expression differences of SLC11A1 between paired CRC and adjacent normal samples. **(C)** RTq-PCR demonstrated that the high expression of SLC11A1 in CRC. **(D,E)** KM curves showed different outcomes of overall survival between high- and low-SLC11A1 groups by using TCGA-CRC and GSE17536. **(F–I)** The associations between SLC11A1 and clinicopathological stages (Stage, T stage, N stage and M stage). ns, $p \geq 0.05$; *, $p < 0.05$; **$p < 0.01$; ***$p < 0.001$. Statistical difference of two groups was compared by the Wilcoxon test and statistical difference of four groups was compared by the Kruskal–Wallis test.

Survival and clinical features analyses of SLC11A1

SLC11A1 expression was higher in CRC tissues than that in normal tissues (Figures 3A,B). Similarly, the RT-qPCR results also validated that SLC11A1 expression was upregulated in tumor tissues (Figure 3C). According to the KM plots from TCGA and GSE17536, the high-SLC11A1 group had a worse prognosis than the low-SLC11A1 group (p = 0.0036 and p = 0.0078, respectively) (Figures 3D,E). We also evaluated the relationship between SLC11A1 mRNA levels and clinicopathological stages. Higher SLC11A1 expression was observed in the progression of pathological stage, T stage, and N stage (Figures 3F–H). There was no significant difference between SLC11A1 expression and the M stage (Figure 3I). These results suggest that CRC with high SLC11A1 mRNA expression is closely related to advanced clinicopathological cancer stages and poor prognosis.

We also investigated the prognostic value of SLC11A1 using pan-cancer data from TCGA. In other digestive tract cancers,

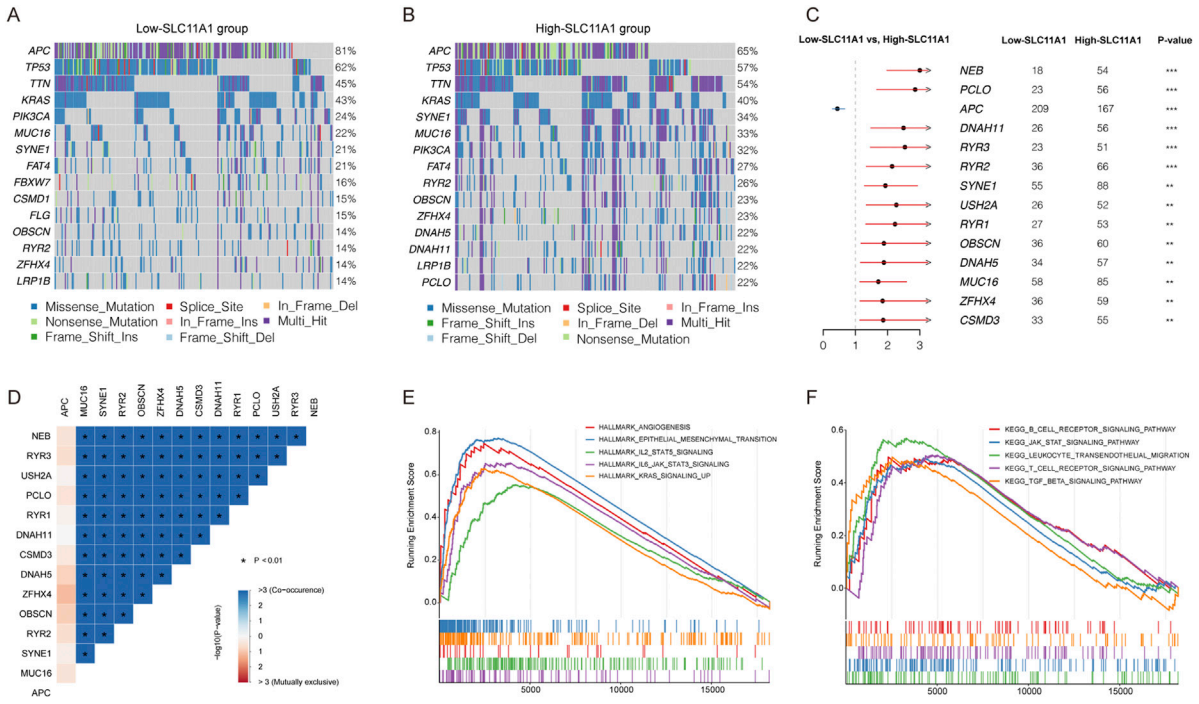

FIGURE 4
SLC11A1 expression was related with CRC mutation status. **(A,B)** Top 15 genes with the highest mutation frequency in the low- and high-SLC11A1 groups. **(C)** The forest plot illustrated the differently mutational genes between the two groups ($p < 0.01$) **(D)** Mutation correlations of differently mutational genes. **(E,F)** GSEA of SLC11A1.

such as STAD, PAAD, and LIHC, high expression of SLC11A1 was also associated with poor prognosis (Supplementary Figures S2A–C). Similar results were found in KIRC, BLCA, LAML, HNSC, UCEC, and LGG/GBM patients (Supplementary Figures S2D–J).

Mutation landscapes between high-SLC11A1 and low-SLC11A1 groups

To explore the potential mechanism between low-SLC11A1 and high-SLC11A1 groups, we analyzed the mutation profiles of the two groups. Fifteen genes with the highest mutational frequencies were observed in waterfall plots (Figures 4A,B). Among the mutated genes, TP53 and KRAS were mostly observed to have missense mutations. We then identified the differentially mutated genes using Fisher's exact test ($p < 0.01$). APC showed a higher mutational frequency in the low-SLC11A1 group, and NER, PCI, DNAH11, RYR3, RYR2, SYME1, USH2A, RYR1, OBSCN, DNAH5, MUC16, ZFHX4, and CSM3 showed a higher mutational frequency in the high-SLC11A1 group (Figure 4C). Mutational correlations were also analyzed with the differentially mutated genes, which revealed that all genes except APC showed mutational co-occurrence with each other (Figure 4D).

Correlation between SLC11A1 expression and immune cell infiltration

To identify key pathways and biological functions associated with SLC11A1, GSEA was performed in the high/low SLC11A1 groups. Angiogenesis, epithelial-mesenchymal transition, and JAK-STAT were enriched in the high-SLC11A1 group in the Hallmark collection (Figure 4E). KEGG pathways such as the B cell receptor, JAK-STAT, and T cell receptor pathways were enriched in the high-SLC11A1 group (Figure 4F). GSEA results indicated that SLC11A1 might play a crucial role in the TME of CRC.

Immune and stromal cells of CRC samples were estimated using CIBERSORT, EPIC, and MCPcounter (Figure 5A). Our results indicated that fibroblasts, cancer-associated fibroblasts (CAFs), and macrophages (M0, M1, and M2) infiltrated more in the high-SLC11A1 group (Figures 5B,D). However, the proportion of activated dendritic cells was higher in the low-SLC11A1 group (Figure 5C). We also analyzed ICD-related gene expression in the two groups and found that 26 genes showed significant differences (Figure 5E). IL-10, IL-6 (immunosuppressive cytokines), and FOXP3 (a significant marker of Treg cells) were expressed at higher levels in the high-SLC11A1 group. Using single-cell transcriptomic analysis,

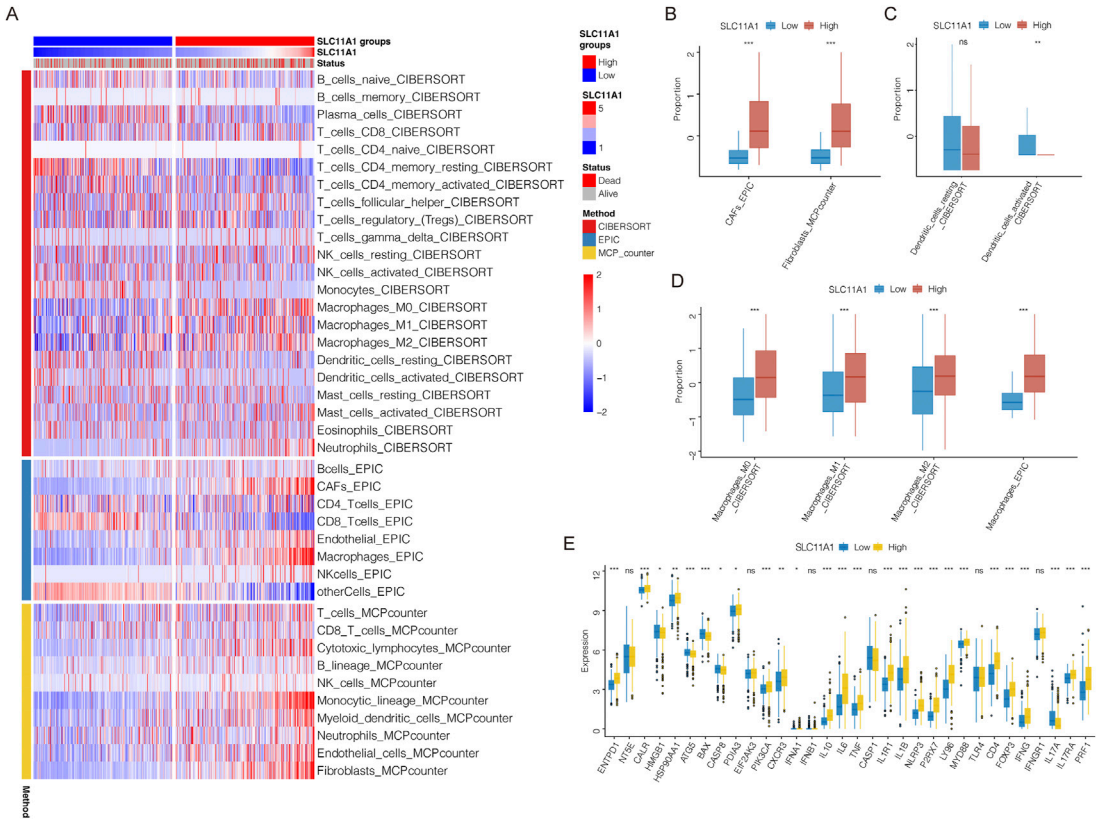

FIGURE 5
TME landscape in the low/high-SLC11A1 groups. **(A)** The heatmap showed the infiltration of immune and stromal cells. **(B–D)** Difference analyses of infiltration levels of CAFs, fibroblasts, dendritic cells and macrophages between the low/high-SLC11A1 groups. **(E)** Expression differences of ICD-related genes between the low/high-SLC11A1 groups. Statistical difference was compared by the Wilcoxon test.

we investigated the localization of SLC11A1 in CRC cells. The expression of cell markers in the TME is shown in the bubble chart (Figure 6A). The distribution and proportion of the 12 types of TME-related cells in samples from GSE146771 are shown in Figures 6B,C. In this dataset, SLC11A1 expression was mainly distributed in monocytes and macrophages (Figures 6D,E). These results demonstrated that SLC11A1, mainly expressed in macrophages and monocytes, might have an immunosuppressive effect in the CRC TME.

Immunotherapy-related analyses

We examined the relationship between SLC11A1 expression and immunotherapy response. In the immunotherapeutic IMvigor210 cohort, patients with higher *SLC11A1* expression had longer OS (p = 0.0028) (Figure 7A). Similarly, the high-SLC11A1 group yielded a lower response rate than the low-SLC11A1 group (Figure 7B). Patients with high SLC11A1 expression had lower TMB than that of patients with low SLC11A1 expression (Figure 7C). We evaluated the TIDE scores of TCGA-CRC samples to predict the immunotherapy response of the patients. The high-SLC11A1 group had higher TIDE scores, which indicated that high-SLC11A1 patients with enhanced immune evasion might have had a poor response to immunotherapy (Figure 7D). Moreover, we evaluated the association between SLC11A1 and the IPS (Figures 7E–H). IPS, IPS-PD1/PD-L1/PD-L2, and IPS-CTLA4 levels were significantly increased in the SLC11A1-low group. These findings demonstrate that SLC11A1 might mediate cancer immune escape and inhibit the sensitivity to immunotherapy.

Discussion

In this study, we screened TME-related prognostic biomarkers for CRC patients. Through multiple bioinformatics analysis methods, we demonstrated that SLC11A1 could serve as a significant indicator in the TME for predicting prognosis and immunotherapy resistance in CRC. First, we calculated the ImmuneScore and StromalScore

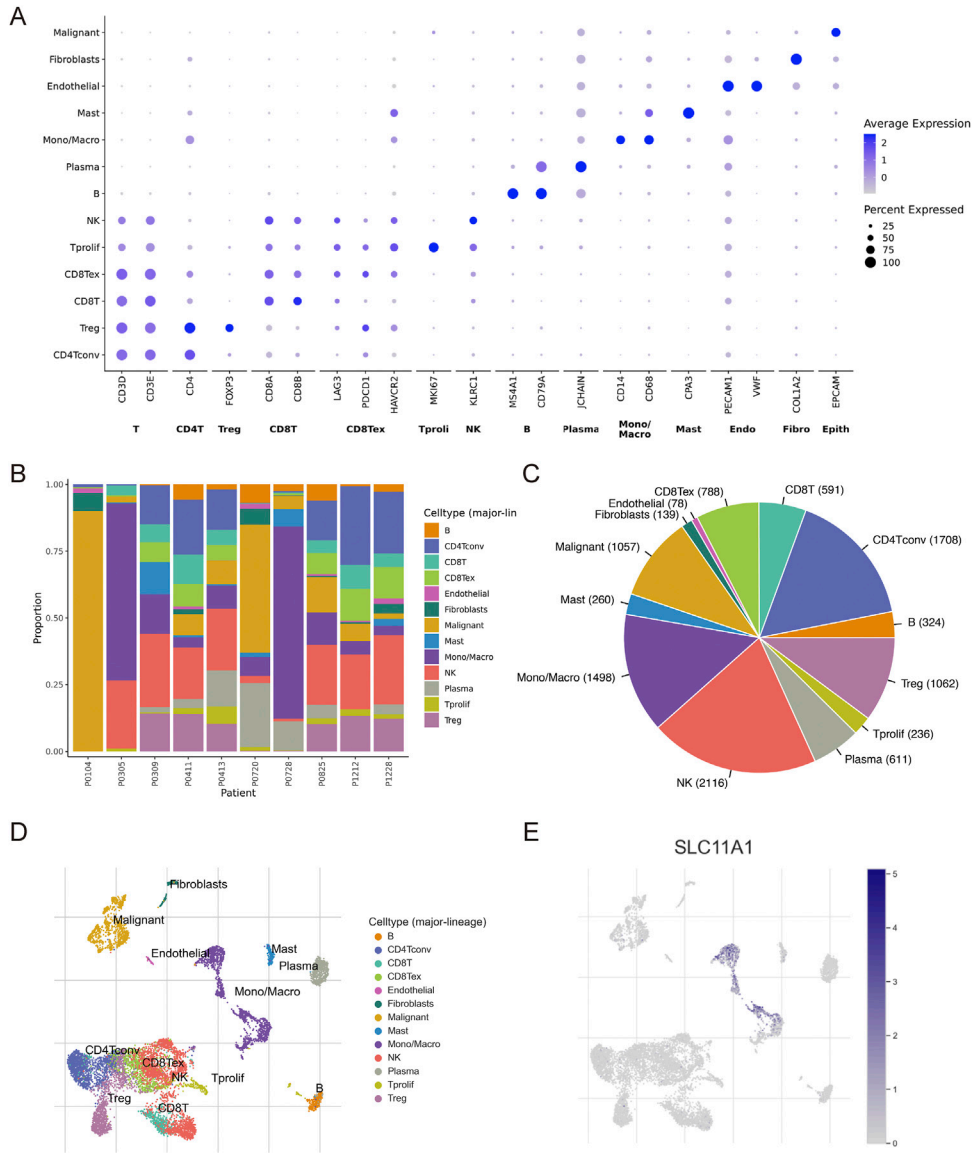

FIGURE 6
Single-cell analysis to explore the cell location of SLC11A1. **(A)** The bubble chart showed the expression markers of cells in TME with GSE146771. **(B,C)** Proportion of 12 types of TME-related cells. **(D,E)** SLC11A1 expression was mainly distributed in monocytes and macrophages.

of TCGA-CRC patients using the ESTIMATE algorithm and found that the ImmuneScore and StromalScore were closely related to clinicopathological stages. To identify genes associated with TME, DEGs were identified between the ImmuneScore high/low groups and the StromalScore high/low groups. In total, 241 DEGs associated with TME were identified, and SLC11A1 was identified as a hub prognostic gene.

We demonstrated that SLC11A1 was highly expressed in CRC tissues compared to that in normal tissues, and high-SLC11A1 patients had poor prognosis in CRC as well as other digestive cancers. Meanwhile, higher expression of SLC11A1 was associated with more fibroblast, CAF, and macrophage infiltration and less activated dendritic cell infiltration. Finally, our findings also revealed that increased SLC11A1 levels were correlated with decreased immunotherapy efficacy and poor prognosis in patients treated with immunotherapy. SLC11A1 was identified as a metabolism-related gene involved in predicting the prognosis of hepatocellular cancer (Zhu et al., 2021). Mutations in SLC11A1 could help estimate PD-L1 expression and predict responses to anti-PD-1 therapy in patients with gastric cancer

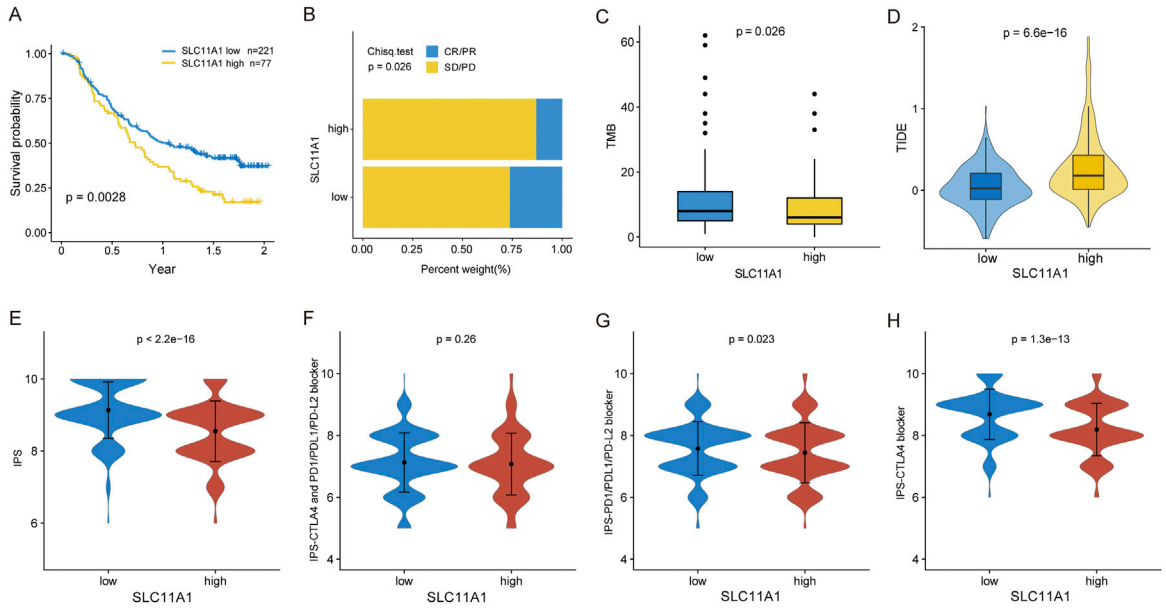

FIGURE 7
High SLC11A1 expression was related with immunotherapy resistance. **(A)** KM plot for the low- and high-SLC11A1 groups in IMvigor210 cohort. **(B)** Bar plot showed immunotherapy efficacy of the two groups. **(C)** Box plot showed the TMB difference of the two groups by the Wilcoxon test. **(D)** TIDE scores of TCGA-CRC patients with higher SLC11A1 and lower SLC11A1 expression by the Wilcoxon test. **(E–H)** Evaluation of IPS differences between the low- and high-SLC11A1 groups with TCIA database by the Wilcoxon test.

(Menyhárt et al., 2018). At present, little is known about the function of SLC11A1 in CRC. In our study, we found that SLC11A1 was highly expressed in CRC tissues compared to that in normal colorectal tissues in TCGA, and similar results were demonstrated by RT-qPCR. Upregulated SLC11A1 expression in CRC is associated with poor prognosis and advanced clinicopathological stages (pathological, T, and N stages), which indicates that SLC11A1 tends to be an unfavorable factor in CRC patients. We also demonstrated that SLC11A1 is associated with poor prognosis in other common cancers of the digestive system, such as STAD, PAAD, and LIHC. The potential implications of SLC11A1 in the prognosis of patients with digestive tract cancers warrant further investigation.

In the TME, immune cell, blood vessel, and stromal components play crucial roles in the carcinogenesis and progression of cancer (Yao et al., 2020). Angiogenesis plays a key role in the proliferation and metastasis of primary CRC, and increased angiogenesis is associated with poor prognosis and recurrence (Liu et al., 2013; Kantola et al., 2014). Changes in immune function are among the most significant causes of CRC initiation. The tumor immune microenvironment is defined as the density, type, and location of tumor-infiltrating immune cells, which have a great influence on the development of CRC (Amicarella et al., 2017). An increasing number of studies have recognized the specific functions of macrophages and CAFs in CRC development (Peng et al., 2022; Yi et al., 2022). Activated fibroblast-derived CAFs are the most abundant cell type in the TME. CAFs, a popular topic of oncological research, have been reported to be involved in tumor progression. Increasing evidence has indicated that CAFs are related to resistance to chemotherapy, targeted treatment, and immunotherapy, and specific treatment for CAFs is expected to be an important adjunct of immunotherapy (Marusyk et al., 2016). In our study, we identified SLC11A1 as the key TME-related biomarker using the ESTIMATE algorithm, and the GSEA results further illustrated that SLC11A1 was correlated with angiogenesis and the JAK-STAT and TGF-β pathways. Higher SLC11A1 expression was associated with increased infiltration of CAFs and fibroblasts and less infiltration of activated dendritic cells. TGF-β has been proposed to induce activation of CAFs, which promotes the proliferation and metastasis of tumors (Chandra Jena et al., 2021). Therefore, we inferred that SLC11A1 could activate the TGF-β pathway to enhance the infiltration of CAFs in CRC. Myeloid dendritic cells are innate immune cells derived from bone marrow with the function of linking and activating adaptive immunity (Collin and Bigley, 2018). Both CD4 T and dendritic cells play significant roles in anti-tumor immunity.

In a data analysis of thyroid cancer, SLC11A1 is associated with macrophages and participates in the

construction of a risk model for evaluating the prognosis of thyroid cancer patients (Zhuang et al., 2020). SLC11A1 modulates iron metabolism in macrophages and plays a crucial role in the activation of early-stage macrophages (Wyllie et al., 2002). A previous study also showed that SLC11A1 is expressed in macrophages in mice (Xu et al., 2005). In our study, SLC11A1 expression was related to high infiltration of macrophages (M0, M1, and M2) in the CRC TME. Furthermore, we also elucidated SLC11A1 expression in the TME by single-cell transcriptomic analysis. SLC11A1 is primarily expressed in monocytes and macrophages in the CRC TME. These results are consistent with those form previous studies. Macrophages play an important role in tumorigenesis and progression. In CRC, TME-related stimulation that induces the polarization of macrophages can modulate the growth and metastasis of tumor cells (Zhang et al., 2020). M1 macrophages overexpressing CD80 and CD86 are considered antineoplastic macrophages with immune promotion functions in the TME (Yunna et al., 2020). M2 macrophages, exhibiting an anti-inflammatory phenotype, play immunosuppressive roles and promote tumor progression (Murray et al., 2014). M1 and M2 macrophages show distinct phenotypes for tumor immunity and the polarization of macrophages from M2 to M1 phenotype could improve the immunotherapy effect (Xia et al., 2020). Therefore, based on all the results of the TME, we preliminarily considered that SLC11A1 regulates the TME in many ways, resulting in immunosuppression and the progression of CRC. Further experimental studies are warranted to demonstrate the relationship between SLC11A1 and macrophage in CRC and investigate how SLC11A1 impacts the efficacy of immunotherapy.

In various cancer types, immunosuppressive TME can inhibit the activity and anti-tumor ability of immunocytes (Mahata et al., 2020). Immune checkpoints expressed in tumor cells are associated with immune evasion and inhibition of anti-tumor immunity (Liu et al., 2020). In the CRC microenvironment, the expression levels of immune checkpoints in tumor cells can suppress the anti-tumor immunity of T cells (Masugi et al., 2017; Zhou et al., 2018). Nowadays ICD, as a novel type of regulated cell death, has been reported as an adjuvant strategy for ICIs (Rizvi and Gores, 2017; Irvine and Dane, 2020). Among ICD-related genes, IL-6, IL-10, and FOXP3 are significant markers associated with the suppression of the immune response (Harshyne et al., 2016; Layman et al., 2017; Smith et al., 2020). Our findings also showed that SLC11A1 was related to 26 ICD-related genes, and high-SLC11A1 patients had higher expression of IL-6, IL-10, and FOXP3 than that in low-SLC11A1 patients. Moreover, through three different methods, including the TIDE, IPS, and IMvigor210 datasets, we obtained consistent results. We found that high SLC11A1 expression was associated with immunotherapy resistance. Thus, these consistent results further demonstrate that SLC11A1 plays a crucial role in the suppression of anti-tumor immunity and is a potential therapeutic target for CRC.

Here, we propose SLC11A1 as a potential biomarker for prognosis and immunotherapy efficacy in patients with CRC. However, this study had some limitations. Independent CRC patients treated with immunotherapy are required, to evaluate the accuracy of SLC11A1 in predicting immunotherapy response. Although RT-qPCR was performed to examine the higher expression of SLC11A1 in CRC, other experimental methods are required to explore the specific functions of SLC11A1 *in vitro* or *in vitro*. Our research group is currently collecting more clinical samples from CRC patients. In future study, immunohistochemistry would be performed to further evaluate the expression levels and clinical values of SLC11A1 in CRC. We would use immunostaining to validate the relationship between SLC11A1 and immune cells, such as fibroblasts, cancer-associated fibroblasts (CAFs) and macrophages (M1 and M2). Further experimental studies are planned to explore roles of SLC11A1 in modulating CRC TME.

In conclusion, we revealed that SLC11A1 was associated with poor prognosis and immunotherapy resistance in CRC for the first time. SLC11A1 may be a potential biomarker for predicting prognosis and immunotherapy efficacy in CRC.

Data availability statement

The datasets presented in this study can be found in online repositories. The names of the repository/repositories and accession number(s) can be found in the article/ Supplementary Material.

Ethics statement

The studies involving human participants were reviewed and approved by the Ethics Committee of Liaoning Cancer Hospital (No. 202206126). Written informed consent for participation was not required for this study in accordance with the national legislation and the institutional requirements.

Author contributions

YM conceived the study, analyzed the data and performed experimental operation. LZ and JY collected data from public databases. JZ supervised the study and reviewed the manuscript. All authors contributed to the study and approved the submitted version.

Funding

This research was supported by Science and Technology Planning Project of Shenyang (No. 19-112-4-088), Science and Technology Planning Project of Liaoning Province of China (No. 201800449), National Key R&D Program of China (Grant #2018YFC1311600), Scientific research foundation for the introduction of talents, Liaoning Cancer Hospital and Institute (No. Z1702), and the National Natural Science Foundation of China (No. 81372532).

Acknowledgments

We thanked for the free use of TCGA, GEO database and other available data from public databases.

Conflict of interest

The authors declare that the research was conducted in the absence of any commercial or financial relationships that could be construed as a potential conflict of interest.

Publisher's note

All claims expressed in this article are solely those of the authors and do not necessarily represent those of their affiliated organizations, or those of the publisher, the editors and the reviewers. Any product that may be evaluated in this article, or claim that may be made by its manufacturer, is not guaranteed or endorsed by the publisher.

Supplementary material

The Supplementary Material for this article can be found online at: https://www.frontiersin.org/articles/10.3389/fphar.2022.984555/full#supplementary-material

SUPPLEMENTARY FIGURE S1
GO **(A)** and KEGG **(B)** enrichment analyses for the overlapping DEGs of ImmuneScore and StromalScore groups.

SUPPLEMENTARY FIGURE S2
Prognostic value of SLC11A1 for other digestive system tumors. **(A–C)** In STAD, PAAD and LIHC, high expression of SLC11A1 was associated with poor outcomes of OS. **(D–I)** In KIRC, BLCA, LAML, HNSC, UCEC and LGG/GBM patients, high-SLC11A1 groups had lower survival rates than low-SLC11A1 groups.

References

Amicarella, F., Muraro, M. G., Hirt, C., Cremonesi, E., Padovan, E., Mele, V., et al. (2017). Dual role of tumour-infiltrating T helper 17 cells in human colorectal cancer. *Gut* 66 (4), 692–704. doi:10.1136/gutjnl-2015-310016

Arnold, M., Sierra, M. S., Laversanne, M., Soerjomataram, I., Jemal, A., and Bray, F. (2017). Global patterns and trends in colorectal cancer incidence and mortality. *Gut* 66 (4), 683–691. doi:10.1136/gutjnl-2015-310912

Chandra Jena, B., Sarkar, S., Rout, L., and Mandal, M. (2021). The transformation of cancer-associated fibroblasts: Current perspectives on the role of TGF-β in CAF mediated tumor progression and therapeutic resistance. *Cancer Lett.* 520, 222–232. doi:10.1016/j.canlet.2021.08.002

Charoentong, P., Finotello, F., Angelova, M., Mayer, C., Efremova, M., Rieder, D., et al. (2017). Pan-cancer immunogenomic analyses reveal genotype-immunophenotype relationships and predictors of response to checkpoint blockade. *Cell Rep.* 18 (1), 248–262. doi:10.1016/j.celrep.2016.12.019

Cheng, Y., Wang, X., Qi, P., Liu, C., Wang, S., Wan, Q., et al. (2021). Tumor microenvironmental competitive endogenous RNA network and immune cells act as robust prognostic predictor of acute myeloid leukemia. *Front. Oncol.* 11, 584884. doi:10.3389/fonc.2021.584884

Chin, C. H., Chen, S. H., Wu, H. H., Ho, C. W., Ko, M. T., and Lin, C. Y. (2014). cytoHubba: identifying hub objects and sub-networks from complex interactome. *BMC Syst. Biol.* 8 (4), S11. doi:10.1186/1752-0509-8-S4-S11

Colaprico, A., Silva, T. C., Olsen, C., Garofano, L., Cava, C., Garolini, D., et al. (2016). TCGAbiolinks: An R/bioconductor package for integrative analysis of TCGA data. *Nucleic Acids Res.* 44 (8), e71. doi:10.1093/nar/gkv1507

Collin, M., and Bigley, V. (2018). Human dendritic cell subsets: An update. *Immunology* 154 (1), 3–20. doi:10.1111/imm.12888

Cunrath, O., and Bumann, D. (2019). Host resistance factor SLC11A1 restricts Salmonella growth through magnesium deprivation. *Sci. (New York, NY)* 366 (6468), 995–999. doi:10.1126/science.aax7898

Garg, A. D., De Ruysscher, D., and Agostinis, P. (2016). Immunological metagene signatures derived from immunogenic cancer cell death associate with improved survival of patients with lung, breast or ovarian malignancies: A large-scale meta-analysis. *Oncoimmunology* 5 (2), e1069938. doi:10.1080/2162402X.2015.1069938

Guo, Q., Xiao, X., and Zhang, J. (2021). MYD88 is a potential prognostic gene and immune signature of tumor microenvironment for gliomas. *Front. Oncol.* 11, 654388. doi:10.3389/fonc.2021.654388

Hamid, O., Robert, C., Daud, A., Hodi, F. S., Hwu, W. J., Kefford, R., et al. (2013). Safety and tumor responses with lambrolizumab (anti-PD-1) in melanoma. *N. Engl. J. Med.* 369 (2), 134–144. doi:10.1056/NEJMoa1305133

Harshyne, L. A., Nasca, B. J., Kenyon, L. C., Andrews, D. W., and Hooper, D. C. (2016). Serum exosomes and cytokines promote a T-helper cell type 2 environment in the peripheral blood of glioblastoma patients. *Neuro. Oncol.* 18 (2), 206–215. doi:10.1093/neuonc/nov107

Hauptman, N., Boštjančič, E., Žlajpah, M., Ranković, B., and Zidar, N. (2018). Bioinformatics analysis reveals most prominent gene candidates to distinguish colorectal adenoma from adenocarcinoma. *Biomed. Res. Int.* 2018, 9416515. doi:10.1155/2018/9416515

Irvine, D. J., and Dane, E. L. (2020). Enhancing cancer immunotherapy with nanomedicine. *Nat. Rev. Immunol.* 20 (5), 321–334. doi:10.1038/s41577-019-0269-6

Jayasekara, H., English, D. R., Haydon, A., Hodge, A. M., Lynch, B. M., Rosty, C., et al. (2018). Associations of alcohol intake, smoking, physical activity and obesity with survival following colorectal cancer diagnosis by stage, anatomic site and tumor molecular subtype. *Int. J. Cancer* 142 (2), 238–250. doi:10.1002/ijc.31049

Jiang, P., Gu, S., Pan, D., Fu, J., Sahu, A., Hu, X., et al. (2018). Signatures of T cell dysfunction and exclusion predict cancer immunotherapy response. *Nat. Med.* 24 (10), 1550–1558. doi:10.1038/s41591-018-0136-1

Kantola, T., Väyrynen, J. P., Klintrup, K., Mäkelä, J., Karppinen, S. M., Pihlajaniemi, T., et al. (2014). Serum endostatin levels are elevated in colorectal cancer and correlate with invasion and systemic inflammatory markers. *Br. J. Cancer* 111 (8), 1605–1613. doi:10.1038/bjc.2014.456

Laplane, L., Duluc, D., Bikfalvi, A., Larmonier, N., and Pradeu, T. (2019). Beyond the tumour microenvironment. *Int. J. Cancer* 145 (10), 2611–2618. doi:10.1002/ijc.32343

Layman, A. A. K., Deng, G., O'Leary, C. E., Tadros, S., Thomas, R. M., Dybas, J. M., et al. (2017). Ndfip1 restricts mTORC1 signalling and glycolysis in regulatory T cells to prevent autoinflammatory disease. *Nat. Commun.* 8, 15677. doi:10.1038/ncomms15677

Li, X., Yang, Y., Zhou, F., Zhang, Y., Lu, H., Jin, Q., et al. (2011). SLC11A1 (NRAMP1) polymorphisms and tuberculosis susceptibility: Updated systematic review and meta-analysis. *PloS one* 6 (1), e15831. doi:10.1371/journal.pone.0015831

Liu, Y., Starr, M. D., Bulusu, A., Pang, H., Wong, N. S., Honeycutt, W., et al. (2013). Correlation of angiogenic biomarker signatures with clinical outcomes in metastatic colorectal cancer patients receiving capecitabine, oxaliplatin, and bevacizumab. *Cancer Med.* 2 (2), 234–242. doi:10.1002/cam4.71

Liu, Y., Zugazagoitia, J., Ahmed, F. S., Henick, B. S., Gettinger, S. N., Herbst, R. S., et al. (2020). Immune cell PD-L1 colocalizes with macrophages and is associated with outcome in PD-1 pathway blockade therapy. *Clin. Cancer Res.* 26 (4), 970–977. doi:10.1158/1078-0432.CCR-19-1040

Liu, Z., Liu, L., Weng, S., Guo, C., Dang, Q., Xu, H., et al. (2022). Machine learning-based integration develops an immune-derived lncRNA signature for improving outcomes in colorectal cancer. *Nat. Commun.* 13 (1), 816. doi:10.1038/s41467-022-28421-6

Love, M. I., Huber, W., and Anders, S. J. G. B. (2014). Moderated estimation of fold change and dispersion for RNA-seq data with DESeq2. *Genome Biol.* 15 (12), 550–621. doi:10.1186/s13059-014-0550-8

Luo, C., Cen, S., Ding, G., and Wu, W. (2019). Mucinous colorectal adenocarcinoma: Clinical pathology and treatment options. *Cancer Commun.* 39 (1), 13. doi:10.1186/s40880-019-0361-0

Mahata, B., Pramanik, J., van der Weyden, L., Polanski, K., Kar, G., Riedel, A., et al. (2020). Tumors induce de novo steroid biosynthesis in T cells to evade immunity. *Nat. Commun.* 11 (1), 3588. doi:10.1038/s41467-020-17339-6

Mariathasan, S., Turley, S. J., Nickles, D., Castiglioni, A., Yuen, K., Wang, Y., et al. (2018). TGFβ attenuates tumour response to PD-L1 blockade by contributing to exclusion of T cells. *Nature* 554 (7693), 544–548. doi:10.1038/nature25501

Marusyk, A., Tabassum, D. P., Janiszewska, M., Place, A. E., Trinh, A., Rozhok, A. I., et al. (2016). Spatial proximity to fibroblasts impacts molecular features and therapeutic sensitivity of breast cancer cells influencing clinical outcomes. *Cancer Res.* 76 (22), 6495–6506. doi:10.1158/0008-5472.CAN-16-1457

Masugi, Y., Nishihara, R., Yang, J., Mima, K., da Silva, A., Shi, Y., et al. (2017). Tumour CD274 (PD-L1) expression and T cells in colorectal cancer. *Gut* 66 (8), 1463–1473. doi:10.1136/gutjnl-2016-311421

Menyhárt, O., Pongor, L. S., and Győrffy, B. (2018). Mutations defining patient cohorts with elevated PD-L1 expression in gastric cancer. *Front. Pharmacol.* 9, 1522. doi:10.3389/fphar.2018.01522

Morse, M. A., Hochster, H., and Benson, A. (2020). Perspectives on treatment of metastatic colorectal cancer with immune checkpoint inhibitor therapy. *Oncologist* 25 (1), 33–45. doi:10.1634/theoncologist.2019-0176

Murray, P. J., Allen, J. E., Biswas, S. K., Fisher, E. A., Gilroy, D. W., Goerdt, S., et al. (2014). Macrophage activation and polarization: Nomenclature and experimental guidelines. *Immunity* 41 (1), 14–20. doi:10.1016/j.immuni.2014.06.008

Neves, J. V., Wilson, J. M., Kuhl, H., Reinhardt, R., Castro, L. F., and Rodrigues, P. N. (2011). Natural history of SLC11 genes in vertebrates: Tales from the fish world. *BMC Evol. Biol.* 11, 106. doi:10.1186/1471-2148-11-106

Peng, S., Li, Y., Huang, M., Tang, G., Xie, Y., Chen, D., et al. (2022). Metabolomics reveals that CAF-derived lipids promote colorectal cancer peritoneal metastasis by enhancing membrane fluidity. *Int. J. Biol. Sci.* 18 (5), 1912–1932. doi:10.7150/ijbs.68484

Rizvi, S., and Gores, G. J. (2017). Emerging molecular therapeutic targets for cholangiocarcinoma. *J. Hepatol.* 67 (3), 632–644. doi:10.1016/j.jhep.2017.03.026

Schürch, C. M., Bhate, S. S., Barlow, G. L., Phillips, D. J., Noti, L., Zlobec, I., et al. (2020). Coordinated cellular neighborhoods orchestrate antitumoral immunity at the colorectal cancer invasive front. *Cell* 183 (3), 1341–1359. doi:10.1016/j.cell.2020.07.005

Shahzad, F., Bashir, N., Ali, A., Nadeem, A., Ammar, A., Kashif, M., et al. (2022). SLC11A1 genetic variation and low expression may cause immune response impairment in TB patients. *Genes Immun.* 23 (2), 85–92. doi:10.1038/s41435-022-00165-9

Sharma, P., and Allison, J. P. (2015). The future of immune checkpoint therapy. *Sci. (New York, NY)* 348 (6230), 56–61. doi:10.1126/science.aaa8172

Siegel, R. L., Miller, K. D., and Jemal, A. (2018). Cancer statistics. *Ca. Cancer J. Clin.* 68 (1), 7–30. doi:10.3322/caac.21442

Smith, A. D., Lu, C., Payne, D., Paschall, A. V., Klement, J. D., Redd, P. S., et al. (2020). Autocrine IL6-mediated activation of the STAT3-DNMT Axis silences the tnfα-RIP1 necroptosis pathway to sustain survival and accumulation of myeloid-derived suppressor cells. *Cancer Res.* 80 (15), 3145–3156. doi:10.1158/0008-5472.CAN-19-3670

Smith, J. J., Deane, N. G., Wu, F., Merchant, N. B., Zhang, B., Jiang, A., et al. (2010). Experimentally derived metastasis gene expression profile predicts recurrence and death in patients with colon cancer. *Gastroenterology* 138 (3), 958–968. doi:10.1053/j.gastro.2009.11.005

Solano-Iturri, J. D., Beitia, M., Errarte, P., Calvete-Candenas, J., Etxezarraga, M. C., Loizate, A., et al. (2020). Altered expression of fibroblast activation protein-α (FAP) in colorectal adenoma-carcinoma sequence and in lymph node and liver metastases. *Aging* 12 (11), 10337–10358. doi:10.18632/aging.103261

Stewart, L. C., Day, A. S., Pearson, J., Barclay, M. L., Gearry, R. B., Roberts, R. L., et al. (2010). SLC11A1 polymorphisms in inflammatory bowel disease and *Mycobacterium avium* subspecies paratuberculosis status. *World J. Gastroenterol.* 16 (45), 5727–5731. doi:10.3748/wjg.v16.i45.5727

Strum, W. B. (2016). Colorectal adenomas. *N. Engl. J. Med.* 374 (11), 1065–1075. doi:10.1056/NEJMra1513581

Sun, D., Wang, J., Han, Y., Dong, X., Ge, J., Zheng, R., et al. (2021). Tisch: A comprehensive web resource enabling interactive single-cell transcriptome visualization of tumor microenvironment. *Nucleic Acids Res.* 49 (D1), D1420–d1430. doi:10.1093/nar/gkaa1020

Sung, H., Ferlay, J., Siegel, R. L., Laversanne, M., Soerjomataram, I., Jemal, A., et al. (2021). Global cancer statistics 2020: GLOBOCAN estimates of incidence and mortality worldwide for 36 cancers in 185 countries. *Ca. Cancer J. Clin.* 71 (3), 209–249. doi:10.3322/caac.21660

Szklarczyk, D., Gable, A. L., Lyon, D., Junge, A., Wyder, S., Huerta-Cepas, J., et al. (2019). STRING v11: Protein-protein association networks with increased coverage, supporting functional discovery in genome-wide experimental datasets. *Nucleic Acids Res.* 47 (D1), D607–D613. doi:10.1093/nar/gky1131

Vivian, J., Rao, A. A., Nothaft, F. A., Ketchum, C., Armstrong, J., Novak, A., et al. (2017). Toil enables reproducible, open source, big biomedical data analyses. *Nat. Biotechnol.* 35 (4), 314–316. doi:10.1038/nbt.3772

Wu, P., Shi, J., Sun, W., and Zhang, H. (2021). The prognostic value of plasma complement factor B (CFB) in thyroid carcinoma. *Bioengineered* 12 (2), 12854–12866. doi:10.1080/21655979.2021.2005745

Wyllie, S., Seu, P., and Goss, J. A. (2002). The natural resistance-associated macrophage protein 1 Slc11a1 (formerly Nramp1) and iron metabolism in macrophages. *Microbes Infect.* 4 (3), 351–359. doi:10.1016/s1286-4579(02)01548-4

Xia, Y., Rao, L., Yao, H., Wang, Z., Ning, P., and Chen, X. (2020). Engineering macrophages for cancer immunotherapy and drug delivery. *Adv. Mater.* 32 (40), e2002054. doi:10.1002/adma.202002054

Xu, Y. Z., Di Marco, S., Gallouzi, I., Rola-Pleszczynski, M., and Radzioch, D. (2005). RNA-binding protein HuR is required for stabilization of SLC11A1 mRNA and SLC11A1 protein expression. *Mol. Cell. Biol.* 25 (18), 8139–8149. doi:10.1128/MCB.25.18.8139-8149.2005

Yao, M., Ventura, P. B., Jiang, Y., Rodriguez, F. J., Wang, L., Perry, J. S. A., et al. (2020). Astrocytic trans-differentiation completes a multicellular paracrine feedback loop required for medulloblastoma tumor growth. *Cell* 180 (3), 502–520. e519. doi:10.1016/j.cell.2019.12.024

Yi, B., Dai, K., Yan, Z., and Yin, Z. (2022). Circular RNA PLCE1 promotes epithelial mesenchymal transformation, glycolysis in colorectal cancer and M2 polarization of tumor-associated macrophages. *Bioengineered* 13 (3), 6243–6256. doi:10.1080/21655979.2021.2003929

Yoshihara, K., Shahmoradgoli, M., Martínez, E., Vegesna, R., Kim, H., Torres-Garcia, W., et al. (2013). Levine DAJNc: Inferring tumour purity and stromal and immune cell admixture from expression data. *Nat. Commun.* 4 (1), 2612–2711. doi:10.1038/ncomms3612

Yu, G., Wang, L. G., Han, Y., and He, Q. Y. (2012). clusterProfiler: an R package for comparing biological themes among gene clusters. *Omics a J. Integr. Biol.* 16 (5), 284–287. doi:10.1089/omi.2011.0118

Yunna, C., Mengru, H., Lei, W., and Weidong, C. (2020). Macrophage M1/M2 polarization. *Eur. J. Pharmacol.* 877, 173090. doi:10.1016/j.ejphar.2020.173090

Zeng, D., Ye, Z., Shen, R., Yu, G., Wu, J., Xiong, Y., et al. (2021). Iobr: Multi-Omics immuno-oncology biological research to decode tumor microenvironment and signatures. *Front. Immunol.* 12, 687975. doi:10.3389/fimmu.2021.687975

Zhang, M., Di Martino, J. S., Bowman, R. L., Campbell, N. R., Baksh, S. C., Simon-Vermot, T., et al. (2018). Adipocyte-derived lipids mediate melanoma progression via FATP proteins. *Cancer Discov.* 8 (8), 1006–1025. doi:10.1158/2159-8290.CD-17-1371

Zhang, W. L., Liu, Y., Jiang, J., Tang, Y. J., Tang, Y. L., and Liang, X. H. (2020). Extracellular vesicle long non-coding RNA-mediated crosstalk in the tumor microenvironment: Tiny molecules, huge roles. *Cancer Sci.* 111 (8), 2726–2735. doi:10.1111/cas.14494

Zhou, G., Noordam, L., Sprengers, D., Doukas, M., Boor, P. P. C., van Beek, A. A., et al. (2018). Blockade of LAG3 enhances responses of tumor-infiltrating T cells in mismatch repair-proficient liver metastases of colorectal cancer. *Oncoimmunology* 7 (7), e1448332. doi:10.1080/2162402X.2018.1448332

Zhu, P., Li, F. F., Zeng, J., Tang, D. G., Chen, W. B., and Guo, C. C. (2021). Integrative analysis of the characteristics of lipid metabolism-related genes as prognostic prediction markers for hepatocellular carcinoma. *Eur. Rev. Med. Pharmacol. Sci.* 25 (1), 116–126. doi:10.26355/eurrev_202101_24355

Zhuang, G., Zeng, Y., Tang, Q., He, Q., and Luo, G. (2020). Identifying M1 macrophage-related genes through a Co-expression network to construct a four-gene risk-scoring model for predicting thyroid cancer prognosis. *Front. Genet.* 11, 591079. doi:10.3389/fgene.2020.591079

Ziegler, P. K., Bollrath, J., Pallangyo, C. K., Matsutani, T., Canli, O., De Oliveira, T., et al. (2018). Mitophagy in intestinal epithelial cells triggers adaptive immunity during tumorigenesis. *Cell* 174 (1), 88–101. e116. doi:10.1016/j.cell.2018.05.028

Frontiers in Pharmacology

Explores the interactions between chemicals and living beings

The most cited journal in its field, which advances access to pharmacological discoveries to prevent and treat human disease.

Discover the latest Research Topics

See more →

Frontiers

Avenue du Tribunal-Fédéral 34
1005 Lausanne, Switzerland
frontiersin.org

Contact us

+41 (0)21 510 17 00
frontiersin.org/about/contact